Coastal Research Library 6

Charles W. Finkl *Editor*

Coastal Hazards

Springer

Coastal Hazards

Coastal Research Library

VOLUME 6

Series Editor:

Charles W. Finkl
Department of Geosciences
Florida Atlantic University
Boca Raton, FL 33431
USA

The aim of this book series is to disseminate information to the coastal research community. The Series covers all aspects of coastal research including but not limited to relevant aspects of geological sciences, biology (incl. ecology and coastal marine ecosystems), geomorphology (physical geography), climate, littoral oceanography, coastal hydraulics, environmental (resource) management, engineering, and remote sensing. Policy, coastal law, and relevant issues such as conflict resolution and risk management would also be covered by the Series. The scope of the Series is broad and with a unique crossdisciplinary nature. The Series would tend to focus on topics that are of current interest and which carry some import as opposed to traditional titles that are esoteric and non-controversial. Monographs as well as contributed volumes are welcomed.

For further volumes:
http://www.springer.com/series/8795

Charles W. Finkl
Editor

Coastal Hazards

Springer

Editor
Charles W. Finkl
Department of Geosciences
Florida Atlantic University
Boca Raton, FL, USA

ISSN 2211-0577 ISSN 2211-0585 (electronic)
ISBN 978-94-007-5233-7 ISBN 978-94-007-5234-4 (eBook)
DOI 10.1007/978-94-007-5234-4
Springer Dordrecht Heidelberg New York London

Library of Congress Control Number: 2012954679

Printed on acid-free paper

Springer is part of Springer Science+Business Media (www.springer.com)

Preface

With increasing coastal populations worldwide, a greater number of people and infrastructure lie at risk from a wide range of potential hazards. Many coastal environments are salubrious places to live and this fact has not gone unnoticed by people wishing to improve their standard of living and general wellbeing. However, even though enticing sand, sea, and sun may prompt the hoards migrating to coastal realms, there lay many hazards that are seen but soon forgotten. Smith (1994), for example, reports that many coastal dwellers forget the trauma of a severe coastal impact between 100 and 500 days. Then it is business as usual. Perhaps still more risky are coastal hazards that are unseen by the general public because they are not aware of hidden dangers lurking in polluted waters or the repercussions of exotic, invasive species that are beautiful to the eye but deadly to the environment, such as the lionfish along Florida's southeast coast. Still more menacing are deadly reptiles (*e.g.* cobras, green mambas, Burmese pythons) in the Florida Everglades that go unnoticed by the public until they have an unfortunate encounter.

In short, the coastal zone is home to many different kinds of potential hazards, and this book, intended as an update to *Coastal Hazards: Perception, Susceptibility and Mitigation* (Finkl 1994), provides a wide array of chapters to that fact. Much has changed in the last couple of decades since *Coastal Hazards: Perception, Susceptibility and Mitigation* (Finkl 1994) was published, mostly in the area of technological advances for sensing environmental conditions, which have brought a better understanding of the processes and triggers for both high-energy events and incipient exposures to risk. In an edited work of this sort, it is difficult to arrange the topical coverage, as no categorization is truly perfect. Complicating matters is the fact that many coastal hazards partly overlap, are multifaceted, and often reinforced by other processes; as is the case of coastal flooding and erosion, where many contributing factors can be present, such as storm surge, tsunamis, subsidence, high rainfall events, sea-level rise, and so on. Many different types of coastal environments are affected by short-term super-elevations of sea level and long-term inundation. Further complicating the picture are attempts to project phases of storminess and future sea-level rise in many different kinds of probabilistic scenarios. This uncertain future makes it difficult to assess risk, vulnerability,

and the best course for planning remediation of impacts that may or may not occur. With these overlapping problems in mind and for convenience of presentation and discussion, chapters in this book have been grouped under very generalized topical headings in an attempt to highlight the predominant hazard that is discussed with the proviso that ancillary hazards are additionally associated. Knowing that it is impossible to discretize the subject matter into ultimate units, the following parts nevertheless have been identified as a guide for study: Part I: Environmental and Human-Induced Hazards; Part II: Remote Sensing of Coastal Hazards (platforms, methods, and procedures); Part III: Flood Hazards (storm surge, sea-level rise, and populations from risk of coastal flood hazards); Part IV: Hydrologic (groundwater, saltwater intrusion) Hazards; Part V: Coastal Erosion and Sedimentation (detection and measurement of shoreline retreat); Part VI: Coastal Dune Hazards (erosion and management); Part VII: Coastal Storms (tropical cyclones and extra-tropical winter storms); Part VIII: Wave Hazards (extreme coastal waves, storm surge, and runup); Part IX: Coastal Marine Pollution (beach litter and oil spills); and Part X: Beach Safety.

The single chapter in **Part I (Environmental and Human-Induced Hazards)** starts out with an introductory chapter by Charlie Finkl and Chris Makowski that embraces a gamut of hazards in the exemplar of the Southeast Florida Coastal Zone (SFCZ). The highly urbanized SFCZ is susceptible to many different kinds of coastal hazards that often combine into a cascade of risks that now threaten millions of people who are partly aware of obvious dangers, but almost completely oblivious to incipient and mostly unseen hazards.

In **Part II (Remote Sensing of Coastal Hazards)**, Vic Klemas' chapter provides an overview of remote sensing methods that are used to acquire near real-time information to monitor high-energy events and assist in the assembly of post-storm reports that assess damage and plan implementation for recovery. Vic's chapter mostly concentrates on space-borne ocean sensing techniques for a wide variety of hazards. The chapter features by Elif Sertel and Dursun Seker human-induced coastal changes along the Black Sea coast of Turkey. The impacts of intense coastal urbanization are investigated by integrated remote sensing, geographic information systems, and geostatistics in attempts to determine and examine coastal changes that are in effect hazardous to the environment. The main types of change included road construction and urbanization that resulted in coastal erosion and damage to local ecological systems.

Part III (Flood Hazards) features aspects of impacts from storm surge, sea-level rise, and populations at risk of coastal flooding. The seven chapters in this part cover reports of coastal populations at risk from flooding, public perception of flood risks, impacts of storm surges, and a review of sea-level rise. The chapter by Michael Kearney starts out by considering the distinction between vulnerability and risk, a consideration that is often not clearly defined in coastal hazard research. Mike specifically examines how amenable the natural hazard components of coastal disasters are to risk analysis. A broad continental-scale overview of sea-level rise impacts is provided by Sally Brown and colleagues. This perspective considers the age-old problem of how much will sea levels rise in the future as well as discussion

of projected or potential impacts to sandy environments, wetlands and low-lying coasts, developed shorelines, and impacts on infrastructure such as transportation networks and energy production facilities. Mark Crowell and colleagues provide an interesting investigation of 8.6 million permanent residents, about 2.8% of the US population based on the 2010 census, that live in areas subject to the 1% annual chance of flood as defined by FEMA. Consideration of tourists and people working in these areas would increase the number of people whose property and jobs would be affected by the 1% annual chance flood. Lee Lindner and Charles Cockcroft surveyed 200 residents in Charleston, South Carolina, and found some surprising statistics *viz*. over half of the respondents did not realize that the main threat from hurricanes was from storm surge and the majority were not able to translate a standard National Hurricane Center projection of storm surge depth into a realistic appreciation of the risk posed to their lives. Understanding of the risk from storm surge was far higher when a graphic-filled advisory instead of a text-based advisory was used. Nick Coch provides an interesting case study of the amplification of storm surge by viaducts of the Florida East Coast Railway extension to Key West. The 1935 Labor Day hurricane made landfall in the middle section of the Florida Keys with the storm surge killing many people and causing much damage to infrastructure. Nick also reports on how coastal development has increased risk from storm surge by reducing natural flow patterns with the construction of causeways, placement of viaducts, reduction of mangrove areas in favor of canal-type developments, and so on. In another chapter Sotiris Lycourghiotis and Strathos Stiros compare the flooding hazards along low-tidal and high-tidal amplitude coasts, particularly along the north Aegean coast. They found smaller risks of flooding events along high-tidal amplitude coasts because the threat existed only for a few hours a day during high water periods as a result of meteorological events. Threats of flooding are higher along Aegean microtidal coasts because surge amplitudes are not dissipated by astronomic sea-level oscillations. Finally, Jim Houston reviews fluctuations of sea-level over long- and short-term intervals with an emphasis on threats from projected future sea-level rise. In this chapter, Jim considers coastal hazards from future sea-level rise in terms of permanent and episodic inundation, increase shore erosion, and saltwater intrusion. He also summarizes adaptation strategies that should be part of an integrated coastal zone management approach.

Part IV (Hydrologic Hazards) contains two chapters, the first dealing with saltwater intrusion, a hazard along many developed shores and in low-lying islands, and the second with the problem of brine disposal from desalinization plants. The first chapter by Ahmad Aris and Sarva Praveena describes a geochemical modeling approach that can be used for small islands where groundwater is the sole option to meet the water demand. Because groundwater exists as freshwater lenses floating over transition zones, grading into seawater in small islands presents an innate hazard from over use of limited supplies. It is thus necessary to monitor groundwater supplies and create models that can predict future demands and availability of potable water. This study shows how groundwater geochemical modeling assists stakeholders, governmental bodies, and the public to improve the sustainability of groundwater resources that are necessary for survival. The second chapter by

Adrian Ciocanea and colleagues deals with an interesting problem that is increasing along coasts where groundwaters are contaminated by saltwater intrusion. Here, desalinization of seawater provides an alternative to aquifer withdrawal but disposal of waste products from the plants is concerning because of the release of concentrated salt brine, residual chlorine levels, antiscalant and anti-foaming additives, and coagulants. Many desalination plants are located in the Middle East where there is an adequate fuel supply to run the plants. This chapter discusses possible ways to mitigate the concentrate and chemical discharges to the marine environment because they may have adverse effects on water and sediment quality, and impair marine life and the functioning of coastal ecosystems.

Part V (Coastal Erosion and Sedimentation) starts out with an introduction to the worldwide problem of coastal erosion where Robert Dean and colleagues discuss natural and human-induced causes of beach erosion as well as different kinds of remediation efforts. Dean et al. highlight the most pervasive natural causes of beach erosion as being due to sea-level rise, and trapping of sand by natural inlets and migration of inlets. Human-induced causes of erosion are related to the construction of littoral barriers that ironically may include beach renourishment projects. They conclude that it may be possible to maintain some highly developed coastal areas for a century or so with available technology and resources, but some areas will require probably abandonment. Other chapters in this part deal with modern methods of detection and measurement of shoreline retreat that include, for example, the use of aerial photography (photogrammetry), satellite imagery, global positioning system (GPS) ground surveys, and laser scanning. In the chapter by Jay Gao, various geo-informatic means of detecting coastal change are compared and evaluated by reference to different types of coastal morphologies. Here, Gao carefully explains the pros and cons of photogrammetric methods, GPS (combined with RTK), and laser scanning (*e.g.* LiDAR-derived DEM). Combinations of methodologies such as the use of RTK GPS for accurate ground control for photogrammetry enables the changing coastal environment to be monitored at an unprecedented frequency and accuracy. The chapter by Kwasi Appeaning-Addo and Emmanuel Lamptey mirrors concepts advanced in the preceding chapter by providing an actual case study in Accra, Ghana, where shoreline status assessment was studied via an innovative technique that combined dated historic maps, aerial photography, satellite imagery, conventional and global positioning system (GPS) ground surveys, and laser altimetry data. Using these data sets, Appeaning-Addo and Lamptey were able to show that the generic technique involving linear regression was suitable for estimating historic rates of shoreline change. The methodology was also used for long-term forecasting to obtain estimates of the average recession rate of change for Accra and other data-sparse coastal regions in developing countries. The penultimate chapter by Jarba Bonetti and colleagues in this part considers the development of different methodological alternatives to assess and predict coastal risk. The need for new approaches is stimulated by increasing human occupation of the coastal zone and the anticipated intensification in the frequency of meteohydrological events due to global change. Critical hazard areas are identified using this methodology and a numerical index of coastal vulnerability established. Erosional hot spots were identified by calculating longshore sediment

transport rates. The beach erosion model, which quantified the sediment transport rate through simulations, was corroborated field data.

Part V concludes with the chapter by Giovanni Randazzo, Jordi Raventos, and Lanza Stefania that deals with increasing demands on coastal resources and the hazards associated with shore erosion in the European Union (EU). Of the 27 Member States, 22 open directly onto five different seas. At present, the total coastal area lost to marine erosion is estimated to be about 15 km^2/year. Many countries attempt to 'hold the line' and avoid realignment. Cross-border shore protection programs are difficult to implement without a cohesive coastal management plan.

Part VI (Coastal Dune Hazards) primarily deals with aspects of erosion and management. The chapter by Sara Muñoz Vallés and Jesús Cambrollé identifies the main current threats to coastal dunes as expansion of invasive species, anthropogenic impacts associated with development and tourism, and climate change. The decline in frequency of occurrence of coastal dunes is itself a hazard because they form protective coastal barriers, help prevent contamination of fresh groundwater by intrusion of seawater, and preserve natural areas and human settlements from the effects of storm waves, high tides, and wind damage. The chapter by Silvia Cristina Marcomini and Ruben Alvaro López features a summary of the unique and complex systems of dune environments, hazard remediation, and examples from dunes in Buenos Aires, Argentina. Considered here are examples of dune hazards (*e.g.* dune migration, flooding of inter-dunal swales, wave erosion) associated with minor climate change in response to El Niño–La Niña cycles. Examples that are presented here show the benefits of dune stabilization by afforestation. Together both chapters provide a good overview of dune hazards and mitigation measures.

Part VII (Coastal Storms) highlights the impacts of coastal storms (tropical cyclones, extra-tropical winter storms, and flooding). The chapter by S. M. May and colleagues deals with coastal hazards that are derived from impacts of tropical cyclones (tropical storms, hurricanes, typhoons). May et al. take an interesting look at trying to figure out the potential number of prior storms in the Holocene that can be interpreted from storm signatures in landforms and sediments. Although there is a problem of correlating of paleo-events with strong cycles in modern times, these authors point out the advantages of attempting numerical dating along beach ridge systems and in other geo-bioarchives. Such efforts provide a degree of insight into interpretation of present cycles by reference to deduced paleo-event frequencies. The chapter by Paul Komar, Jonathon Allan, and Peter Ruggiero focuses on the US Pacific Northwest coast (Washington, Oregon, and northern California) and deals with meteohydrological events and tectonic processes. The main thrust here is impacts from storms, mostly those that lead to storm-surge flooding, inundation from eustatic sea-level rise, shore (beach, cliff) erosion, and potential tsunamis. Cycles of El Niño, climatic controls on storm surge levels, and increasing storm-generated wave heights since the 1970s constitute a range of coastal hazards for this section of coast. The convergence of geological (subduction earthquakes) and atmospheric phenomena along this coast make for hazardous conditions that must be paid attention to for preparation, prevention, and remediation where feasible.

Part VIII (Wave Hazards) deals with extreme coastal waves (including tsunamis), storm surge, and runup. The chapter by Zai-Jin (Bob) You and Peter

Nielsen focuses on the authors' research experience with extreme waves and elevated water levels along the New South Wales (Australia) coast. These authors consider short-term wave analysis to determine wave heights in deep waters and long-term wave analysis to estimate extreme wave heights from an historical time-series record. The chapter is filled out by discussions of oceanic surges, swash hydrodynamics, wave runup, and extreme wave runup. The chapter by Monzur Imteaz, Fatemeh Mekanik, and Amimul Ahsan deals with tsunamis. They discuss the advantages of an efficient tsunami warning system and then explain the importance of the numerical simulations that are used, providing a newly developed 'stratification number'. They report that as this dimensionless number increases in magnitude, the wave surface and amplitude decrease.

Part IX (Coastal Marine Pollution) contains two chapters that respectively deal with beach litter and oil spills. Both coastal pollution problems are significant and locally important but of entirely different scope and magnitude. Beach litter hazards are discussed by Allan Williams and colleagues, who collectively focus on litter sources, types and composition of litter, and methods for evaluating the impacts of beach litter. This is a growing problem with multifaceted hazards that affect not only humans but wildlife as well. Also considered here are regional variations in sources and densities of litter as well as avoidance procedures. The chapter on hazards from oil spills by Erich Gundlach in a tour de force that considers many aspects of the problem. Legion here are discussions of spill source, risk, and size as they relate to shoreline oiling and impacts. Also highlighted are aspects of oil spill cleanup, biological effects, economic losses and compensation, damages to natural resources, psychological and social impacts, and human health effects.

Part X: Beach Safety deals mostly with rip currents and the hazards associated therewith. The chapter by Stephen Leatherman focuses on beach safety concerns as related to the development, recognition, and response to rip currents. These cross-shore currents are a danger to beachgoers who need to be aware of the hazard before they get jetted offshore by some of these powerful currents. Leatherman recommends public education about the dangers of rip currents through outreach programs. Learning how to recognize the presence of rips and what to do if caught in one can be lifesavers for swimmers.

Although this collection of chapters does not cover all aspects of coastal hazards, it represents an honest attempt to consider most of the major types of coastal hazards as part of disaster research in general. Perhaps the most difficult part of coastal hazard research is to project future courses of human action when natural cycles are incompletely understood, especially as they are affected by anthropogenic activities that further complicate our predictive capabilities. Taking that into consideration, this volume covers the gamut of coastal hazards from various points of view and should provide the interested reader with a base of understanding for the dangers that face coastal dwellers, tourists, and those who work in the coastal zone.

Florida Atlantic University
Boca Raton, Florida, USA

Charles W. Finkl

References

Finkl CW (ed) (1994) Coastal hazards: perception, susceptibility and mitigation. J Coast Res 12 (Special Issue): 372

Smith AWS (1994) Response of beachfront residents to coastal erosion along the Queensland Gold Coast, Australia. In: Finkl CW (ed) Coastal hazards: perception, susceptibility and mitigation. J Coast Res 12 (Special Issue):17–25

Contents

Contributors

L. Absalonsen Department of Civil and Coastal Engineering, University of Florida, Gainesville, FL, USA

Amimul Ahsan Faculty of Engineering and Industrial Sciences, Swinburne University of Technology, Hawthorn, Melbourne, VIC, Australia; University Putra Malaysia, Kuala Lumpur, Malaysia

Jonathan C. Allan Coastal Field Office, Oregon Department of Geology and Mineral Industries, Newport, OR, USA

Kwasi Appeaning-Addo Department of Oceanography & Fisheries, University of Ghana, Legon, Ghana

Ahmad Zaharin Aris Department of Environmental Sciences, Faculty of Environmental Studies, Universiti Putra Malaysia, Serdang, Selangor Darul Ehsan, Malaysia

Viorel Badescu Candida Oancea Institute, Polytechnic University of Bucharest, Bucharest, Romania; Romanian Academy, Bucharest, Romania

Doug Bellomo Federal Emergency Management Agency, Arlington, VA, USA

Jarbas Bonetti Coastal Oceanography Laboratory, Department of Geosciences, Federal University of Santa Catarina, Florianópolis, SC, Brazil

D. Brill Institute of Geography, University of Cologne, Cologne, Germany

Sally Brown Faculty of Engineering and the Environment and the Tyndall Centre for Climate Change Research, University of Southampton, Highfield, Southampton, UK

Jesús Cambrollé Departamento de Biología Vegetal y Ecología, Universidad de Sevilla, Seville, Spain

Richard B. Cathcart Geographos, Burbank, CA, USA

Adrian Ciocanea Department of Hydraulics, Polytechnic University of Bucharest, Bucharest, Romania

Nicholas K. Coch School of Earth and Environmental Sciences, Queens College of C.U.N.Y., Flushing, NY, USA

Charles Cockcroft Physics and Astronomy Department, College of Charleston, Charleston, SC, USA

Kevin Coulton AECOM, Portland, OR, USA

Mark Crowell Federal Emergency Management Agency, Arlington, VA, USA

M.J. Cullis Built Environment, Swansea Metropolitan University, Swansea, Wales, UK

R.G. Dean Department of Civil and Coastal Engineering, University of Florida, Gainesville, FL, USA

M. Engel Institute of Geography, University of Cologne, Cologne, Germany

A. Ergin Civil Engineering Department, Middle East Technical Univeristy, Ankara, Turkey

Charles W. Finkl Department of Geosciences, Charles E. Schmidt College of Science, Florida Atlantic University, Boca Raton, FL, USA; Coastal Education & Research Foundation (CERF), Coconut Creek, FL, USA

Jay Gao School of Environmental, University of Auckland, Auckland, New Zealand

Mauricio González Instituto de Hidráulica Ambiental "IH Cantabria", Universidad de Cantabria, Santander, España, Spain

Erich R. Gundlach E-Tech International, Inc., New Paltz, NY, USA

Susan Hanson Faculty of Engineering and the Environment and the Tyndall Centre for Climate Change Research, University of Southampton, Highfield, Southampton, UK

Jochen Hinkel Global Climate Forum e.V. (GCF), Adaptation and Social Learning, Berlin, Germany; Potsdam Institute for Climate Impact Research (PIK), Transdisciplinary Concepts and Methods, Potsdam, Germany

James R. Houston US Army Engineer Research Center, Vicksburg, MS, USA

Monzur A. Imteaz Faculty of Engineering and Industrial Sciences, Swinburne University of Technology, Hawthorn, Melbourne, VIC, Australia

Michael S. Kearney Department of Environmental Science and Technology, University of Maryland, College Park, MD, USA

Abiy S. Kebede Faculty of Engineering and the Environment and the Tyndall Centre for Climate Change Research, University of Southampton, Highfield, Southampton, UK

D. Kelletat Institute of Geography, University of Cologne, Cologne, Germany

Antonio Henrique da Fontoura Klein Coastal Oceanography Laboratory, Department of Geosciences, Federal University of Santa Catarina, Florianópolis, SC, Brazil

Victor V. Klemas School of Marine Science and Policy, University of Delaware, Newark, DE, USA

Paul D. Komar College of Earth, Oceanic & Atmospheric Sciences, Oregon State University, Corvallis, OR, USA

Emmanuel Lamptey Dept. of Oceanography & Fisheries, University of Ghana, Legon, Ghana

Lanza Stefania Dipartimento di Scienze della Terra, Università degli Studi di Messina, Messina, Italy

Stephen P. Leatherman Laboratory for Coastal Research and Department of Earth & Environment, Florida International University, Miami, FL, USA

Bernhard Lee Lindner Physics and Astronomy Department, College of Charleston, Charleston, SC, USA

Rubén Alvaro López Departamento de Geología, Facultad de Ciencias Exactas y Naturales, Universidad de Buenos Aires, Buenos Aires, Argentina

Clarissa Brelinger De Luca Coastal & Port Engineering Master Program, University of Cantabria, Santander - Cantabria, Spain

Sotiris A. Lycourghiotis Geodesy & Geodetic Applications Lab, Department of Civil Engineering, Patras University, Patras, Greece

Tucker Mahoney Federal Emergency Management Agency, Region IV, Atlanta, GA, USA

Christopher Makowski Department of Geosciences, Charles E. Schmidt College of Science, Florida Atlantic University, Boca Raton, FL, USA; Coastal Education & Research Foundation (CERF), West Palm Beach, FL, USA

Silvia Cristina Marcomini Departamento de Geología, Facultad de Ciencias Exactas y Naturales, Universidad de Buenos Aires, Buenos Aires, Argentina

S.M. May Institute of Geography, University of Cologne, Cologne, Germany

Fatemeh Mekanik Faculty of Engineering and Industrial Sciences, Swinburne University of Technology, Hawthorn, Melbourne, VIC, Australia

Mariela Muler Coastal Oceanography Laboratory, Department of Geosciences, Federal University of Santa Catarina, Florianópolis, SC, Brazil

Barbara Neumann Coastal Risks and Sea-Level Rise Research Group, Future Ocean Excellence Cluster, Institute of Geography, Christian-Albrechts-University Kiel, Kiel, Germany

Robert J. Nicholls Faculty of Engineering and the Environment and the Tyndall Centre for Climate Change Research, University of Southampton, Highfield, Southampton, UK

Peter Nielsen School of Civil Engineering, University of Queensland, St Lucia, Australia

Susan Phelps AECOM, Greensboro, NC, USA

K. Pond Centre for Public and Environmental Health, University of Surrey, Guildford, UK

Sarva Mangala Praveena Department of Environmental Sciences, Faculty of Environmental Studies, Universiti Putra Malaysia, Serdang, Selangor Darul Ehsan, Malaysia

Giovanni Randazzo Dipartimento di Scienze della Terra, Università degli Studi di Messina, Messina, Italy

Jordi Serra Raventos Department d'Estratigrafia, Paleontologia i Geociències Marines, Universitat de Barcelona, Barcelona, Spain

J.D. Rosati Engineer Research and Development Center, U. S. Army Corps of Engineers, Vicksburg, MS, USA

Peter Ruggiero College of Earth, Oceanic and Atmospheric Sciences, Oregon State University, Corvallis, OR, USA

Vanda Claudino Sales Departamento de Geografia, Universidade Federal do Ceará, Fortaleza, CE, Brazil

Anja Scheffers Southern Cross GeoScience, Southern Cross University, Lismore, NSW, Australia

Dursun Zafer Seker Geomatics Engineering Department, Istanbul Technical University, Maslak, Istanbul, Turkey

Elif Sertel Geomatics Engineering Department, ITU-CSCRS Istanbul Technical University Center for Satellite Communications and Remote Sensing, Istanbul Technical University, Maslak, Istanbul, Turkey

Guilherme Vieira da Silva Centro de Estudos de Geologia Costeira e Oceânica - CECO, Instituto de Geociências – IG, Universidade Federal do Rio Grande do Sul – UFRGS, Porto Alegre, RS Brazil

Peter Squire Southern Cross GeoScience, Southern Cross University, Lismore, NSW, Australia

Stathis C. Stiros Geodesy & Geodetic Applications Lab, Department of Civil Engineering, Patras University, Patras, Greece

Elírio E. Toldo Jr Centro de Estudos de Geologia Costeira e Oceânica – CECO, Instituto de Geociências – IG, Universidade Federal do Rio Grande do Sul – UFRGS, Porto Alegre, RS, Brazil

Zai-Jin You Coastal and Marine Science Unit, Science Division, Office of Environment and Heritage, Dangar, NSW, Australia

Athanasios T. Vafeidis Coastal Risks and Sea-level Rise Research Group, Future Ocean Excellence Cluster, Institute of Geography, Christian-Albrechts-University Kiel, Kiel, Germany

Sara Muñoz Vallés Departamento de Biología Vegetal y Ecología, Universidad de Sevilla, Sevilla, Spain

T.L. Walton Beaches and Shores Resource Center, Florida State University, Tallahassee, FL, USA

Jonathan Westcott Federal Emergency Management Agency, Arlington, VA, USA

A.T. Williams Built & Natural Environment, Swansea Metropolitan University, Swansea, Wales, UK; e-GEO Centro de Estudos de Geografia e Planeamento Regional, Faculdade de Ciências Sociais e Humanas, Universidade Nova de Lisboa, Lisbon, Portugal

Colin D. Woodroffe School of Earth and Environmental Sciences, University of Wollongong, Wollongong, NSW, Australia

Part I
Environmental and Human-Induced Hazards

Chapter 1
The Southeast Florida Coastal Zone (SFCZ): A Cascade of Natural, Biological, and Human-Induced Hazards

Charles W. Finkl and Christopher Makowski

Abstract The Southeast Florida Coastal Zone (SFCZ), the southern part of the South Atlantic Coastal Zone (SACZ), is an exemplar of a developed, low-lying coastal zone that is prone to a wide range of coastal hazards. Threats to environmental integrity, infrastructure, and human wellbeing include both the frequent occurrence of natural meteohydrological disturbances, hazardous marine life interactions, and human-induced events. Natural hazards are mainly centered on storms and impacts from wind damage, shore erosion, flooding, and rip currents. Anthropogenic hazards, aside from dramatic or obvious events such as ship groundings, are caused by human endeavors that are regarded as normal day-to-day activities but which invisibly lead to land degradation in agricultural areas and urban settings, as well as the pollution of coastal marine environments through nutrient loading and sewage outfall dumping. Additionally, managerial positionalities that defeat sustainable development contribute to human-induced coastal hazards. Furthermore, increased human interaction with the coastal marine environment now leads to hazardous contact with biological fauna along coastal environments on both land and in the water. Release of non-native, invasive species in this subtropical coastal zone also poses a whole new range of potential hazards ranging from the loss of native species to a coastal population threatened by dangerous animals. These examples from the SFCZ also apply to many sensitive coastal marine environments around the world where increasing population densities multiply risks that eventually cascade into definable potential disaster zones.

C.W. Finkl (✉) • C. Makowski
Department of Geosciences, Charles E. Schmidt College of Science, Florida Atlantic University, Boca Raton, FL 33431, USA

Coastal Education & Research Foundation (CERF), Coconut Creek, FL 33073, USA
e-mail: cfinkl@cerf-jcr.com; cfinkl@fau.edu; cmakowski@cerf-jcr.com

C.W. Finkl (ed.), *Coastal Hazards*, Coastal Research Library 6,
DOI 10.1007/978-94-007-5234-4_1,

1.1 Introduction

Developed coasts the world over are characterized by urban sprawl and industrial-commercial complexes that are situated in sensitive ecological environments or dynamic high-energy settings. Development and its supporting infrastructure impinges on surrounding habitats that becomes compromised by pollution, over use, or fractionation into ever smaller natural parcels that eventually cannot function as a viable ecosystem. This scenario is the same throughout the world where populations multiply in coastal zones. The South Atlantic Coastal Zone (SACZ) (Finkl 1983) and its subset, the subtropical southeast Florida coastal zone (SFCZ), is no exception and is perhaps an example par excellence of where many coastal regions are headed.

Developed shores threaten local and regional ecologies and the natural environment in turn can be hazardous to infrastructure and those who live there. The coastal conurbation of the SFCZ illustrates the perils of a burgeoning population living, working, and recreating on the shore (Pilkey et al. 1985). For ease of discussion, the coastal hazards in this region are identified as those occurring mainly on land and those in the water, realizing of course that there is a transition zone between land and water. Attempts to study and manage this composite battle space (Finkl 1997) have been met with mixed results, as regulation tends to focus on the most egregious human behaviors that threaten or despoil coastal marine environments or which put populations at risk. Natural processes such as storms and coastal erosion, which can be exacerbated by engineering works, and as well as, human induced activities that result in pollution receive a majority of the attention from scientists, engineers, and the media because they are visible hazards with often dramatic results. However, other non-point, human-induced coastal hazards, such as offshore sewage outfalls and soil amendments, contribute to the overall risk assessment of the SFCZ. Additionally, with increased use of these coastal marine environments, residents and tourists more often come in contact with biological hazards that can pose serious threats to human wellbeing. The flip side of the coin points to adverse impacts on the local ecology when exotics are released unintentionally, for example, when there is structural failure of cages and pens during storms or by deliberate release by pet owners when the animal becomes difficult to handle or keep. As a result, this region is now beset by a multitude of coastal hazards that are emblematic of management practices that have gone wrong for a host of reasons. Initially there was too little oversight by environmental agencies, but now there is an overreaction in a multi-pronged attack on activities that attempt sustainable development (e.g. Finkl 1983; Finkl and Charlier 2003; Finkl et al. 2005a; Finkl and Kruempel 2005). In this kind of hazardous environment, sustainability may not be sustainable as the population density continues to increase.

1.1.1 Purpose, Goals and Objectives

The purpose of this chapter is to highlight the development of coastal hazards that multiply with increasing population densities. Many obvious coastal hazards, such as beach erosion and related impacts, garner scientific inquiry as well as media attention. Although urban sprawl is usually not seen as a coastal hazard in itself, the effects of more intense land use and water visitations, combined with wastewater disposal techniques, create adverse pressures on fragile coastal marine ecosystems and calls for a greater recognition and study of the specific hazards. In addition to derivatives of well-known, high-energy meteohydrological events, are hazards that are generally marginalized or little discussed because they generally do not impact many people. For example, human contact with hazardous marine life is not widely accepted by researchers or the public as valid risks, but they nevertheless deserve greater recognition for the threats they pose to human wellbeing within the coastal zone. Among generally unseen coastal hazards are threats to the environment that result from release of non-native, invasive species. Dramatic and insipient hazards are thus briefly considered here to emphasize the precarious nature of the subtropical southeast Florida coastal zone and by inference or example, many other similar coastal regions the world over.

1.1.2 Study Area

Described in general by Fenneman (1938) and later delineated by NOAA (2006) using coastal counties on land and the continental shelf break in water (Fig. 1.1a), the South Atlantic Coastal Zone (SACZ) serves as one of the major physiographic divisions of the United States by occupying the southern seaward portion of the Atlantic Coastal Plain and continental shelf. The SACZ thus encompasses coastal plains and continental shelf areas, both zones color differentiated in Fig. 1.1 for clarity; one zone in two parts, terrestrial and marine. The area of investigation for this study constitutes the Eastern Florida Section of the SACZ (Finkl 1994a), which technically extends northward from Biscayne Bay to the St. John's River near Jacksonville; however, for purposes of this discussion the most highly developed section is conveniently referred to as the Southeast Florida Coastal Zone (SFCZ). The SFCZ extends from the southern shores of Lake Okeechobee and the Everglades Agricultural Area (EAA) in northwest Palm Beach County to the southern part of Miami-Dade County along Biscayne Bay and to the northern-most Florida Keys (Fig. 1.1b). Occupying a land area (excluding Lake Okeechobee, Biscayne Bay, and the continental shelf) of about 12,730 km^2, the study area embraces numerous types of coastal wetlands (Everglades, marshes, swamps, galleria forests), upland sandplains and flatlands, limestone ridges, lagoons, lakes, estuaries, coastal barriers,

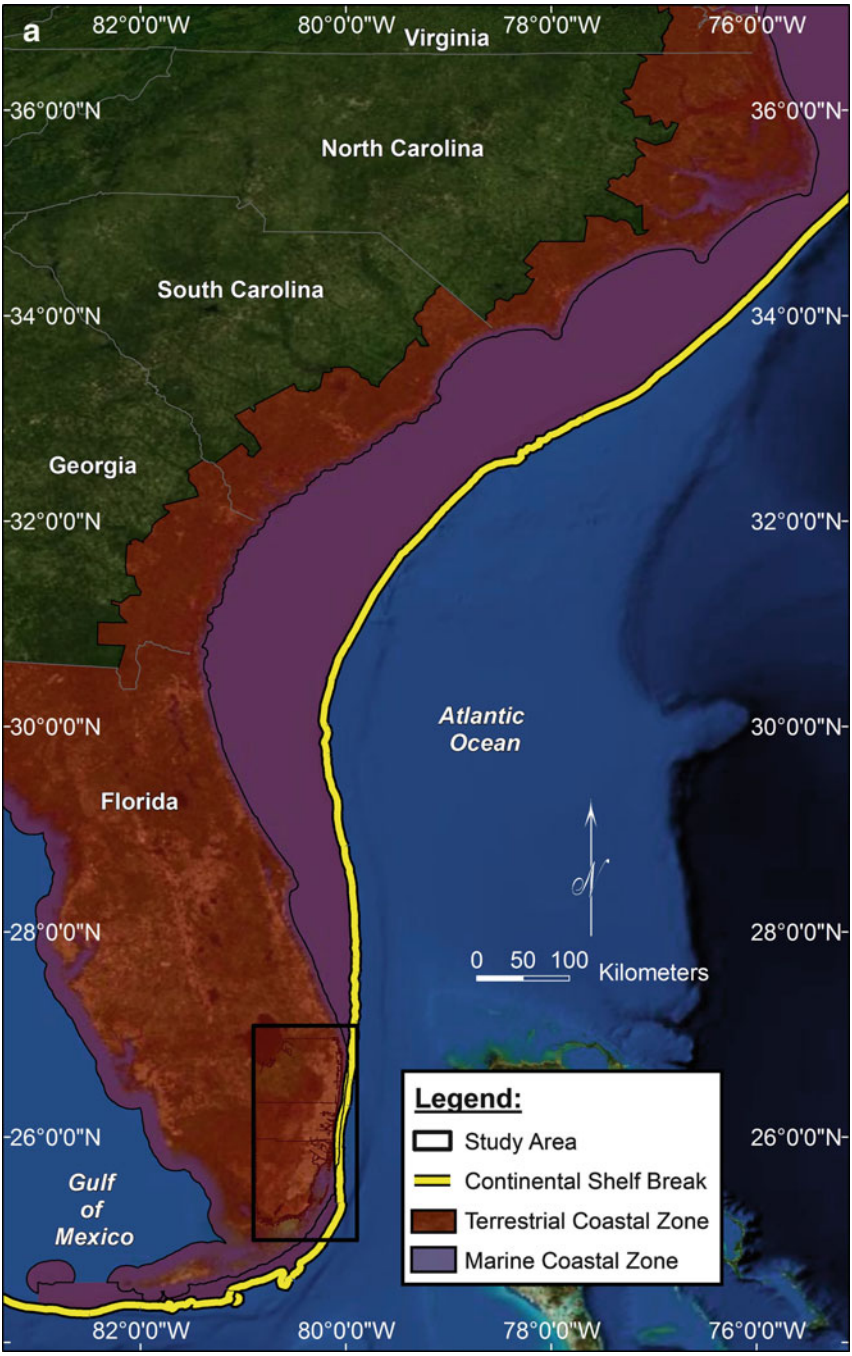

Fig. 1.1 (**a**) Composite image of the South Atlantic Coastal Zone (SACZ) showing the overall extent of terrestrial and coastal marine components. The SACZ extends from the continental shelf break to the western boundaries of coastal counties and the whole of the Florida Peninsula. The study area is here defined as the Southeast Florida Coastal Zone (SFCZ). (Image Background: ESRI ArcGIS Online and data partners, including imagery from agencies supplied via the Content Sharing Program. Continental Shelf break: Continental Shelf Boundary for the Southeast U.S. – 1998, NOAA Coastal Services Center. Coastal Zone: Coastal Zone Management Act, Department of Commerce (DOC), National Oceanic and Atmospheric Administration (NOAA), National Ocean Service (NOS), Coastal Services Center (CSC), published: 24 May 2006).

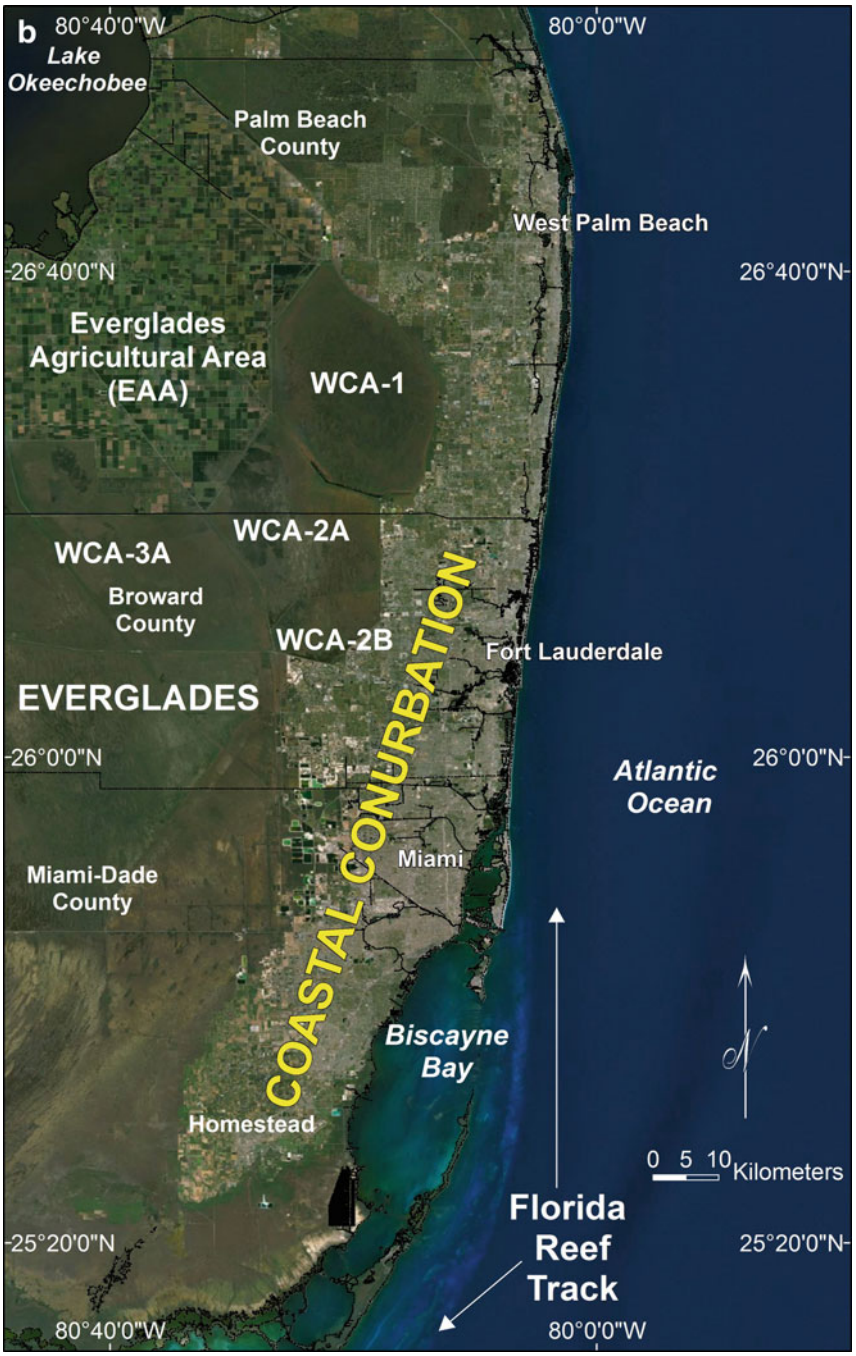

Fig. 1.1 (continued) (**b**) Southeast Florida Coastal Zone (SFCZ) subsection of the South Atlantic Coastal Zone (SACZ) (Fig. 1.1a) showing the coastal conurbation in relation to major biophysical features such as Lake Okeechobee, Florida Everglades (and its water conservation areas), the Everglades Agricultural Area (EAA), Biscayne Bay, and the Florida Reef Tract

and a shallow-narrow continental shelf (e.g. Myers and Ewel 1990; White 1970). The terrestrial part is a nearly level plain with a general elevation from sea level to about 8 m above mean sea level. On average, the general elevation of the Everglades is about 3 m in the western part of the SFCZ. The narrow continental shelf averages about 2.5–3.5 km in width and extends to the shelf break at about 40–50 m depth, covering an area of about 600 km^2.

The southern tip of the Florida (Miami) peninsula contains the only tropical climate in North America (Corcoran and Johnson 2005). Southern Florida's climate is transitional between tropical wet-and-dry (savanna) and humid subtropical (McKnight and Hess 2000). There is a summer wet season and a winter dry season. Thunderstorms are the major source of rainfall, although erratically occurring tropical cyclones (May through October) and winter frontal systems can contribute significantly in some years (Duever et al. 1994). Although the average annual rainfall is approximately 1,320 mm, droughts periodically affect the entire region.

Florida, the most populated state in the southeast, is also one of the fastest growing of the 50 states. In 2002, Florida had the fourth-largest population of all 50 states, with an estimated 16,713,150 people, a 4.6% increase since 2000. By 2025, Florida is expected to be the third most populous state, with a population of approximately 20.7 million. The southeast Florida Metropolitan Statistical Area (MSA) (Palm Beach, Broward, and Miami-Dade counties) is the sixth largest in the United States and by 2030, 7.4 million people are projected to live in this MSA. If the water conservation areas of Everglades National Park and the Everglades Agricultural Area are not included in population density calculations, that is, just including the areas where people live, population density averages about 800 persons per km^2 making it the third most densely settled MSA in the United States (US Census Bureau 2000). Population densities in the southeast Florida MSA are exceeded only by the New York – Newark – Edison MSA in New York and the Los Angeles – Long Beach – Santa Ana MSA in California. Coastal strips such as Galt Ocean Mile in Fort Lauderdale are characterized by high-rise condominiums on the beach with population densities >2,500 persons per km^2 (OnBoard LLC 2007).

1.2 Natural and Human-Induced Threats to Coastal Integrity

Coastal hazards contain pervasive themes that are related to human perception of potential dangers. Whether an incipient or accelerated process is perceived as hazardous depends on many factors (e.g. Kennish 2002), but it is only those events that tend to occur rather quickly (within hours or days) with dramatic consequences

that garner people's attention to a level that they relate in some way to personal or institutional risk management. With this thought in mind, it is perhaps instructive to consider that coastal hazards are normally thought of in terms of extreme high-energy events that have potential for causing damage to life, limb, and property. However, these kinds of hazards are relatively easy to mentally accommodate because the threat is apparent, if not ominous. More difficult to comprehend are natural and human-induced processes that are invisible or at least not easily observed because they operate on decadal scales (e.g. land subsidence in the Everglades or secular erosion that results in coastal land loss, coastal pollution). Extended linkages that impose hazardous conditions along the coast are of themselves relatively innocuous in their upland environs, but they exert deleterious impacts along the coast via complex biophysical pathways (e.g. Finkl et al. 2005a). These threats, however, are also compounded with *psychological barriers* to comprehension of intermittent biological hazards that are associated with shark attacks, influx of Portuguese man-o-war, sea lice, and dangerous invasive species, which are described subsequently.

Classes of coastal hazards can be categorized as *apparent or obvious* (undeniably in the public's eye), *incipient or cryptic* (unseen to the public eye and intermittent in frequency), and *misunderstood or uncomprehended* (public is unaware through a low level of consciousness) (e.g. Finkl 2000; Finkl and Kruempel 2005). Apparent and obvious hazards (clear and present danger), such as an oncoming hurricane or a ship grounding on a coral reef, elicit the public's attention which demands governmental planning for risk reduction. However, coastal hazards that impose a more cryptic or uncomprehended nature, pose a new bevy of complications. For example, how does a coastal community formulate a strategy against incipient hazards such as land subsidence or soil degradation, when the threat itself is unseen, invisible, or intermittent? Furthermore, coastal hazards that are uncomprehended hardly receive media coverage, like the half-century lag time it takes the agricultural nutrients from the Everglades Agricultural Area (EAA) to pollute waters in the SFCZ, and consequently these hazards remain a mystery to most of the coastal population.

The problem of detection (i.e. perception at lower levels of consciousness) is further complicated by the fact that these more or less hidden biophysical hazards are secular; although the processes are incipient, they are cumulative and often culminate by convergence in crescendo events, as described for physical processes by Fairbridge (1989) but which is germane to the discussion here. Examples include oxidation of organic soils due to dredge and drain policies (e.g. Finkl 1995; Stephens 1984; Stephens et al. 1984), degradation (pollution) of surface and groundwater quality by coastal marine and upland activities (e.g. Finkl and Krupa 2003; Finkl et al. 2005a; Sonenshein 1995), and population pressures associated with over-use of resources such as visitations to coastal and marine parks (Klee 1998). The following sections describe a range of natural and human-induced hazards in the SFCZ that are obvious, incipient, or uncomprehended.

1.2.1 Coastal Erosion

The SFCZ is known for its beautiful sandy beaches that are a major tourist attraction and a source of income for the State of Florida (Houston 2002). Estimates of gross sandy beach length in Florida vary, but the Florida Department of Environmental Protection sets the total length of oceanfront beaches at about 1,600 km. But there is trouble in paradise, as according to Bernd-Cohen and M. Gordon (1999), approximately 5% of Florida's shoreline is critically eroding. The problem arose when settlement in the SFCZ originally took place too close to the shore as population started increasing after World War II. As a result of the erosion progressing, oceanfront properties, often built on bulldozed sand dunes to provide better views of the water, became threatened by narrowing beaches. With development came the opening of tidal inlets that supported a burgeoning tourist industry and local demands for access to coastal marine waters for sport fishing and other activities. With increased use, it became necessary to stabilize the dredged inlets and provide safe navigation by installing jetties. The jetties, however, interrupted the natural north to south longshore drift of sand, incrementally decreasing the volume of sand transport at each inlet until comparatively little sand was bypassed to downdrift beaches, starving them of alongshore sediments (Dean 1990).

The literature clearly establishes that tidal inlets and jetties in general generate significant downdrift beach erosion (e.g. Bruun 1995; Bush et al. 2004; Davis and FitzGerald 2004; Dean 1990; Dean and Work 1993; Esteves and Finkl 1998; Galgano 2009; Kraus 2005; Kraus and Galgano 2001; Pilkey et al. 1985). After construction of jetties, it is commonly observed that there is increased deposition updrift of jetties and elevated erosion on adjacent downdrift beaches until the shorelines adjust to new morphodynamic conditions (e.g. Komar 1996). There is a long history of inlet stabilization (e.g. Smith 1988), but this activity was usually accomplished with little knowledge of the consequences for downdrift beaches (e.g. Inman and Nordstrom 1978; Bruun 1986, 1995). It is now widely appreciated that downdrift beaches erode as a consequence of stabilized inlets functioning as littoral drift blockers. Bruun (1995) identifies "short" and "long" distance shoreline recession at littoral barriers (jettied inlets). The beach segment between the downdrift jetty and its attachment bar represents the short distance and has been referred to as an "isolated" beach (Kraus 2005). Longshore sediment-transport input is limited to the isolated beach by the jetty and by the attachment bar, which acts as a groin, and such beaches are a chronic erosion hazard. Further downdrift, the long-term influence of the littoral barrier is manifested as an incrementally smaller rate of shoreline recession with distance from the littoral drift blocker (Carr-Betts et al. 2012).

Although updrift accretion and downdrift erosion was observed, inlet-induced beach erosion was not generally delineated on a systematic basis until two decades ago when Bruun (1995) and Mehta (1996) elucidated the process. Estimates of

Fig. 1.2 Oblique aerial photograph of Hillsboro *Inlet* showing the downdrift shoreline offset. The former shoreline is marked by the shore-parallel line and the relative amount of shoreline recession (erosion) is shown by the *shore-perpendicular line* with *double ended arrows*, marking a distance of about 230 m. When the inlet was first stabilized by jetties, it became a littoral drift blocker and the downdrift beach became starved of bypassing sand. Today, the littoral drift is stabilized by a weir jetty and a floating dredge that bypasses sand from an updrift sand trap to the south side of the inlet (Photograph by C.W. Finkl)

jetty-induced downdrift erosion may vary widely depending on the criteria used, as in the example of Hillsboro Inlet (Fig. 1.2), where there is a considerable range of distances between 4.5 and 48 km (Dean and Work 1993; Douglas and Walther 1994; Walton 1978). Bruun's (1995) global study of jetty-induced downdrift erosion attempted to ascertain the length of shoreline adversely affected by stabilized inlets using shoreline change data. As Bruun (1995, 2005) reports, the erosion hazard moves down coast as two fronts, an initial slow-moving front that migrates down the coast at a slow rate of about 0.3–0.5 km a^{-1} and a secondary, fast-moving front that migrates long distances down the coast at rates of 1–1.5 km a^{-1}. The long-distance erosion front on the Florida southeast coast penetrates from one jettied inlet to the next. That is, the erosion hazard induced by jetties is stopped only when it reaches the next downcoast jetty. As the erosion front moves along the shore, the volume of beach sand decreases and shorelines retreat landward constituting a hazard to coastal infrastructure. The basic mechanics of the inlet-induced beach erosion process are as follows, within the context of the Florida east coast.

With distance southward from the Georgia-Florida state line, coastal sediments are progressively lost from the littoral drift system causing beaches to erode on the downdrift (south) sides of jetties. Although the calculation of littoral sediment

budgets along the southeast coast of Florida is problematical, Dean and O'Brien (1987) estimated the annual flux of sediments along the entire Florida east coast ranges from 500,000 m^3 on the north to only 10,000 m^3 near Miami. This interruption of alongshore drift has been widely appreciated as littoral drift blockers that induce multifaceted morphological changes downcoast (e.g. Dean 1990; Mehta et al. 1991; Finkl 1993). As far as alongshore sediment transport is concerned, the coast is, in effect, compartmentalized by jettied inlets that reproduce the same small-scale morphological responses in the form of updrift fillets on the north side of jetties and downdrift eroded shorelines on the south sides of inlets. Stabilization of tidal inlets in the SFCZ took place at the following times, from north to south: Jupiter (1922), Lake Worth (1918, 1925), South Lake Worth (1927), Boca Raton (1930, 1931), Hillsboro (1952, 1966), Port Everglades (1926–1928), Bakers Haulover (1925, 1975, 1986), and Government Cut (1902, 1907) (see discussions in Finkl 1994a, b).

Dean (1990) estimates that 85–90% of the beach erosion problem is caused by the stabilization of tidal inlets with jetties. This interruption of the natural longshore drift deprives downdrift beaches of sediment that is required to maintain a dynamic balance between erosion and sedimentation. When beaches downcoast from inlets are starved for an adequate sediment supply, they erode and shorelines retreat landward. Loss of beach volume and narrowing of the dry beach thus becomes hazardous along developed beachfronts where coastal infrastructure is threatened by storm surge flooding and wave action.

Loss of recreational beach width due to erosion, formerly a major problem along Florida shores, became particularly troublesome when developed coastal segments were threatened by retreating shorelines. Investment in coastal infrastructure requires protective measures to ensure against land loss and temporary flooding due to super-elevations of sea level by storm surges associated with hurricanes. Studies by Esteves and Finkl (1998) show that about 75% of the Florida shoreline is sandy beaches. Statewide, 61% of beaches front developed shorelines. Overall, with approximately 82% of Florida's sandy beaches in either a state of accretion or in a stable phase, about 6% of the total beach length is viewed as being eroded (Esteves and Finkl 1998) and about 10% has been designated as critically eroded (*cf.* 5% estimate of Bernd-Cohen and M. Gordon 1999). When examining opposite coasts in the State of Florida, the beaches along Gulf of Mexico shores tell a different story when compared to the Atlantic coast. Almost three-fourths of the western Florida coast exhibits a long-term erosional trend, as compared to just over one-fourth of the Florida Atlantic coastal beaches. However, the Florida Atlantic beach erosion has been shown to be highly regionalized. Esteves and Finkl (1998) reported over 90% of the beach erosion measured along the SFCZ occurs directly downdrift from stabilized inlets. As a result, a majority of developed shorelines must impose either hard (e.g., groins, seawalls, breakwaters) or soft (beach nourishment) beach protection strategies, but frequently, these protection measures (especially the hard structures) create more erosional trends along the shoreline.

Fig. 1.3 Rip currents on Dania Beach, south of the entrance to Port Everglades (in Fort Lauderdale), formed during a northeaster. These cross-shore currents are a major hazard to swimmers when strong winds cause wave setup alongshore and underflows, with maximum velocities up to 12 m s^{-1}, return seaward taking hapless swimmers with them. The *arrows* point to rip current locations on this section of beach (Photograph by C.W. Finkl)

More thorough discussion of the erosion hazards that engineering structures pose are summarized, for example, in Cooper and Pilkey (2012), Davis and FitzGerald (2004), Dean et al. (Chap. 13, this volume), and Dean and Dalrymple (2004), Komar (1997).

1.2.2 Rip Currents

Rip currents are strong channels of water flowing in a seaward direction from the shore, typically through the surf line (see also Klein et al., Chap. 16, this volume; Leatherman, Chap. 26, this volume). While shore-normal rip velocities range from 0.5 to 2.5 m s^{-1}, these strong currents can also migrate alongshore, up to tens of meters per day (e.g. Brander 2010). Rip currents result from complex interactions between waves, currents, water levels, and nearshore bathymetry. Forming an integral part of nearshore circulation patterns with alongshore and cross-shore (onshore/offshore) water motion, circulation cells may develop when waves break strongly in some locations and weakly in others (MacMahan et al. 2006). Variable weaker and stronger wave-breaking patterns typically occur on beaches with a bar and channel system in the nearshore (Fig. 1.3). Rips also result from

natural variability of wind waves or when alongshore currents are deflected by groins or jetties that produce a seaward flowing jet. As waves break along the shore or over a sandbar, the increase in water level is referred to as set-up (Sonu 1972). There is usually a difference in set-up between the bar, where waves are breaking strongly, and the channel between bars where little or no wave breaking occurs. Water returns seaward through oceanic underflow or via rip currents that flow through breaks in sandbars (e.g. Brander 2010; Leatherman 2011).

Within the SFCZ, rip currents constitute one of the deadliest natural coastal hazards. The State of Florida, for example, had 364 rip current-related deaths between 1989 and 2008, the most of any state in the United States. Lushine (1991), correlating rip current fatalities in southeast Florida to wind speed, wind direction, and tidal variation, found that onshore winds within 30° of normal and with velocities of 12 m s^{-1} or greater occurred during 90% of rip current rescues and drownings. These meteorological conditions are favorable for rip current formation because they initiate and enhance the set-up process that contributes to development of rip currents. Gensini and Ashley (2010) report that the highest frequency of fatalities due to rip currents occurs in the 100-km section of the SFCZ from Miami Beach to West Palm Beach. This coastal stretch recorded 46 fatalities due to rip currents from 1994 to 2007. On a larger scale, the coastal segment between Jacksonville and Miami over time averages 23 fatalities per 100 km. The rip current fatality capital of the world is thus found in the SFCZ where coastal bathymetry, waves, and high rates of beach visitation converge.

1.2.3 Coastal Storms

The SACZ is affected by several types of meteorological phenomena that constitute coastal hazards of the first degree. Perhaps most well-known are the North Atlantic and Gulf of Mexico hurricanes that threaten the region from June 1st to November 30th. Hurricanes, tropical storms, and tropical depressions all threaten the region with potential wind damage and flooding from high rainfalls. These events can also produce significant shore erosion, depending on the angle of approach from the water as some storms are more or less direct hits passing perpendicularly across the shore, or they approach the shore from a high angle, or remain just offshore as shore-parallel passing storms. Whatever the angle of approach, each storm is unique and the damage that occurs is affected by many factors. In the northern part of the SACZ, for example, the coastal plain is backed by the Appalachian Mountains and there have been examples of copious rainfalls caused by the orographic effect, which does much local damage (Zebrowski and Howard 2007).

Although most deaths from hurricanes are associated with storm surge, high winds may cause more structural damage to homes, businesses, and infrastructure. Two remarkable hurricanes are cited here as examples of storms producing high damaging winds in the SFCZ: Hurricane Andrew (1992) and Hurricane Wilma

Fig. 1.4 Shopping center in Homestead, Florida, situated just south of the Miami metro area, showing complete destruction shops in this mall by Hurricane Andrew. Tornadic winds associated with H. Andrew devastated many built-up areas, attesting to the hazards posed by hurricane-related wind fields (Photograph by C.W. Finkl)

(2005). The SFCZ is especially vulnerable to attack because tropical storms can approach from both Atlantic and Gulf coasts to cross the Florida Peninsula.

Hurricane Andrew was the third Category 5 hurricane to make landfall in the United States, after the Labor Day Hurricane (1935) and Hurricane Camille (1969). Andrew made landfall in the SFCZ just south of Miami causing $41.5 billion (2012 USD) in damage when it struck at Category 5 strength (Rappaport 1993; Stone and Finkl 1995). Its central pressure ranks as the fourth lowest in U.S. landfall records. Andrew was the costliest Atlantic hurricane in U.S. history prior to Hurricane Katrina (2005) and Hurricane Ike (2008). Andrew's peak winds in South Florida were not directly measured because of the destruction or failure of measuring instruments. The Coastal Marine Automated Network (C-MAN) station at Fowey Rocks (Miami), with platform elevation of 43 m recorded an 8-min average wind of 229 km h^{-1} with a peak gust of 272 km h^{-1} before the equipment was destroyed. The highest recorded surface gust, within Andrew's northern eyewall occurred near the shoreline with a gust of 285 km h^{-1}. The anemometer at the Turkey Point Nuclear Generating Station (Miami) recorded sustained winds of 233 km h^{-1} before it failed. A barometric pressure of 922 mb was recorded at the same time (various NOAA, NWS websites). Much of the wind damage associated with Hurricane Andrew was part of tornadic cells that spun off from the eyewall and other bands (Fig. 1.4).

Wilma made landfall on the Gulf coast at Cape Romano, southwest Florida, with winds of 190 km h^{-1}. As Wilma crossed Florida, it weakened to a Category

2 hurricane, but re-intensified to a Category 3 hurricane as its eastern flank reached the Florida Current along the SFCZ. Wilma made several landfalls, with the most destructive effects felt in the Mexican Yucatán Peninsula, Cuba, and Florida. At least 62 deaths were reported and damage was estimated at $32.7 billion and $23.2 billion (in 2012 USD), the latter occurring in Florida. As a result, Wilma is ranked among the top five most costly hurricanes ever recorded in the Atlantic and the fourth most costly storm in United States history (Pasch et al. 2006). Hurricane Wilma caused widespread destruction of critical infrastructure such as electrical power, water supply, and sewer systems. Florida Power and Light, the largest electricity utility in the state, reported more than 3,241,000 customers had lost power, equivalent to approximately 6,000,000 people, with most residents getting power restored in 8–15 days. Running water was restored for most residents within 2 days. Broward and Palm Beach counties were hit particularly hard by tornadoes in the western part of the hurricane.

Even though flooding in the SFCZ generally does not cause as much damage to infrastructure as high winds (because it occurs less frequently), it nevertheless is a major hazard that results in significant disruption of commerce, industry, and home life. In the flat, low-lying SFCZ, flooding is the major concern related to tropical storms of all types. Perusal of isohyetal maps emphasize the flood potential from extreme rainfall events, for example, that high rainfall events focus on the Boca Raton – Ft. Lauderdale area, viz. 1-day rainfalls for 3- (1,651 mm), 5- (2,286 mm), 10- (2,794 mm), 25- (3,810 mm), and 100-year (5,080 mm) return period events and 3-day totals for the 10- (3,302 mm), 25- (4,318 mm), and 100-year (5,588 mm) return period (Trimble 1990). During the months of August and September 1981, an area just south of Miami recorded 12,415 mm of rainfall (SFWMD 1982). At the same time during Tropical Storm Dennis (16–18 August 1981), Biscayne Bay received 6,390 mm of rainfall.

It is not possible to indicate all of the storms that affect the SFCZ, but Hurricanes Andrew and Wilma exemplify the kinds of troubles that beset developed shores when hit by a major storm. Basically, all critical infrastructure is at risk from large tropical storms and the impacts of wind and flood damage can be far ranging. Because of the prevalence of these large meteohydrological events and the wide media coverage and documentation that occurs afterwards, it is not necessary to reiterate here the combined adverse impacts of strong winds, large waves, high rainfalls, coastal and inland flooding, and tornadoes and water spouts that combine to make these events feared by prudent persons. For further information, readers are referred to specialized ancillary summaries such as those prepared by Oey et al. (2006) and Wakimoto and Black (1994), and in Chap. 8, this volume by Coch (2012); and Scheffers et al. (2012).

In addition to tropical storms, the SFCZ is impacted by the passage of intense cold fronts that may bring strong winds, damaging hail, and high rainfalls. These storms are noted for their rain-producing capabilities as cold and warm air masses meet to deliver high rainfalls that produce inland coastal flooding (e.g. Finkl 2000; Finkl and Myers 1996; SFWMD 1982, 1993).

1.2.4 Flooding

Flooding in the SFCZ has proven to be infamous in the past as one of the most deadly types of coastal hazards. Flooding along the ocean shore is transient and related to the passage of storms that produce set-up, as in the case of northeasters, or hurricane storm surge that is much higher and more devastating. As hazardous as coastal flooding is, it is perhaps surprising to note that most problematic to the SFCZ is inland flooding. Even when there are no storms, inland flooding is a constant threat to the urban area due to seepage from water conservation areas. Constant pumping is required to minimize the hazard and maintain safe water levels. The most dramatic problem, however, comes with high-energy events that bring copious rainfall to the region that fills water containment areas and strain the retaining dikes. Good examples of this hazard (i.e. overload of water containment areas) are the 1926 and 1928 hurricanes.

The 1926 Miami Hurricane made landfall as a Category 4 hurricane, causing high storm-surge on Lake Okeechobee which breached a small levee on the west side of the lake, causing the deaths of 386 people. The 1928 Hurricane caused greater damage and fatalities when the storm hit the lake because a small dyke at the south of the lake was breached. The resulting flood affected more than 500 km^2 (e.g. Hebert et al. 1996; Pfost 2003; and various NOAA, NWS websites). The latter part of the storm with opposite winds caused the surge to reverse and the small levee at the northern end of the lake was over topped causing more flooding. It is thought that up to 3,000 people, some half of the population who lived around the lake perished, the vast majority dying as a direct result of flooding from Lake Okeechobee. Only the Galveston Hurricane of 1900 caused more deaths from a natural disaster in the United States.

The adverse impacts of these hurricanes set the stage for the construction of the Herbert Hoover Dike by the U.S. Army Corps of Engineers. The dike is made from earth dredged up from around Lake Okeechobee. Since its construction in the 1970s, the upper limit of lake levels has increased from 4.6 to 5.3 m. The dike is now not deployed as a levee to protect the area from storm surge and flooding, but to contain a permanent water storage area; because the lake is used as a reservoir, the dike functions as a dam. With hydrostatic pressure against the dike nearly all the time, the risk of failure does not come solely from storm surge.

The dike is prone to leaks because it was built from un-compacted peat, gravel, sand and shell. Since its construction, land has been eroding outside the dike, particularly on the south side of the lake. The Herbert Hoover Dike was never intended to be a dam and because flood criteria for dams are more stringent than for dikes, it cannot meet required engineering stipulations (Strowd 2011). Because the dike is now improperly deployed as a dam, it constitutes a coastal flood hazard in itself. It is an accident waiting to happen.

It is instructive to note that a report to Lloyd's Franchise Performance Directorate states that the Herbert Hoover Dike is vulnerable to failure caused by

water seepage and piping at high water levels whether this high water level is produced by long-term changes in rainfall or by hurricane events (Maynard 2011). Consultants to the SFWMD report that *"...The important factor is the seeping going from the lake to the land side. . . .Certain geologic formations that underlie the dyke, and portions of the material that comprise it, bear a striking resemblance to Swiss cheese. Laced with interconnected voids and open channels, not only do these materials conduct large flows of water, they also admit sand and silt-sized soil particles that comprise the bulk of the dyke and its foundation. In a process of unstable feedback called internal erosion or piping, this seepage causes more particles to be removed, which in turn causes more seepage. Eventually, either excessive water pressures cause the dyke slopes to fail, or the dyke simply collapses from the net effect of particle removal one grain at a time. Herbert Hoover Dike has narrowly escaped failure from this process on several occasions and we suspect that its condition may be worsening."* (cited in Maynard 2011).

In addition to the 40,000 residents that live around the lake at risk, there could be far-reaching effects for the SFCZ should the Herbert Hoover Dike fail. The three counties southeast of Lake Okeechobee have a combined population in excess of five million residents and recovery could take years, with potential economic losses running to the tens of billions of dollars (Maynard 2011).

Under dikes and levees, the little-acknowledged coastal hazard of groundwater seepage is most pronounced along the eastern margins of the Florida Everglades. That is, specifically around the eastern edge of Water Conservation Area (WCA) 3A/3B in central/southern Broward County and northern Miami-Dade County (cf. Fig. 1.1b). The transition from Everglades to urban environment is very rapid, often spanning a distance of about 1 km where the levee is separated from homes by the Sawgrass Expressway and a canal in western Broward County, for example. Pumps run continuously to manage the freshwater influx to avoid flooding. In addition to routine maintenance of water levels in the Everglades, is the occurrence of high rainfall events that produce stormwater influxes that threaten the integrity of dikes and levees that must hold back water in Everglades conservation areas from breaching the retaining structures and flooding the urban area.

Perhaps more dangerous is the presence of transvers glades that previously funneled Everglades overflow through the Atlantic Coastal Ridge to the coast. Subsequent to the dike and drain era in the early 1900s (see discussions in Finkl 1995, and Finkl and Restrepo-Coupe 2007), urbanization aided by canalization for drainage and access expanded into transverse glades (Fig. 1.5a, b) (Everglades that trend east–west instead of north–south) and now there are communities situated in these paleo-drainageways. Although these communities are unaware of the flood hazard, they are nevertheless at risk of flooding under extreme rainfalls when freshwater surges will move towards the coast through the east–west glades, as occurred in the past.

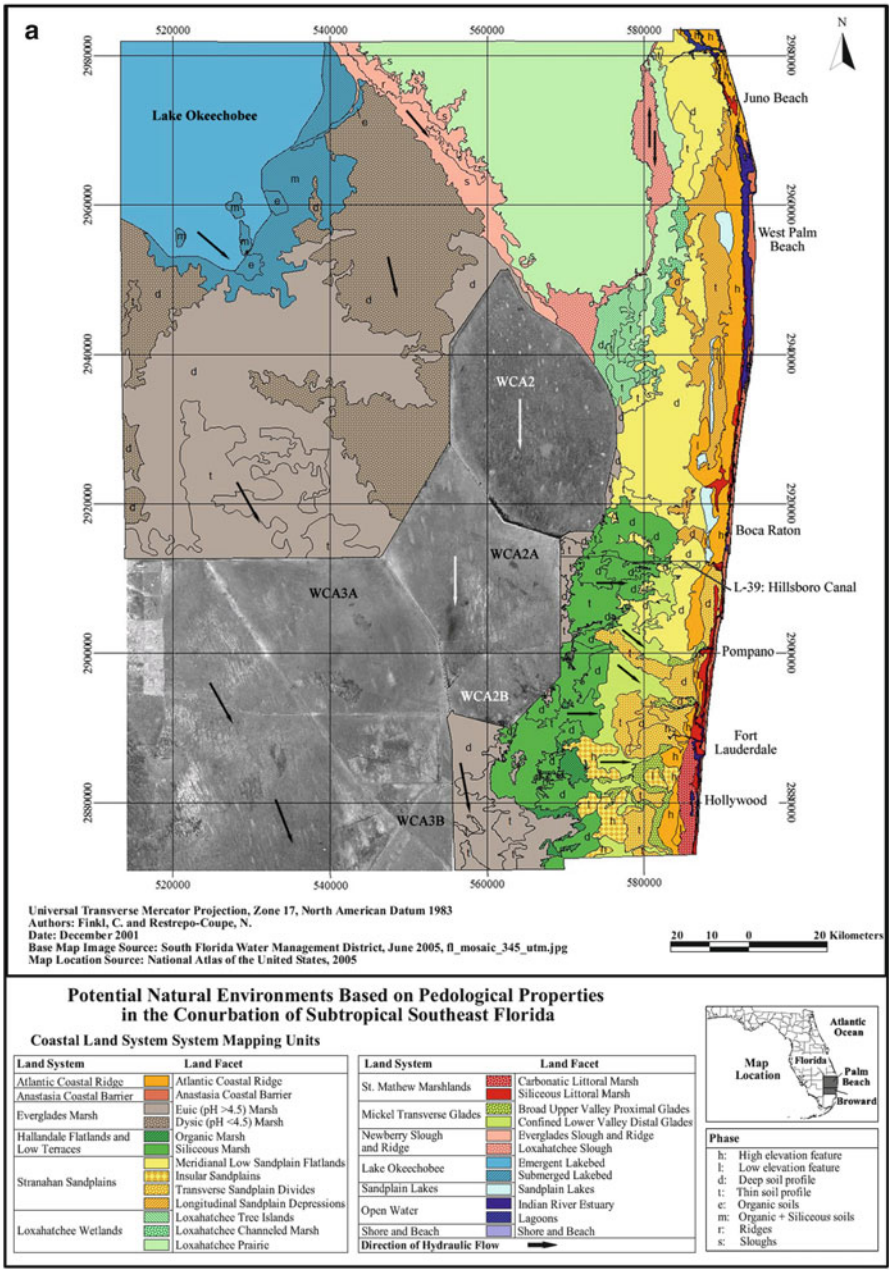

Fig. 1.5 Flooding potential in the northern part of the SFCZ (Broward and Palm Beach counties) based on interpretation of natural environments (land systems and land facets). (**a**) Inland flooding will occur in response to high rainfalls throughout the coastal wetlands (Everglades Marsh, Loxahatchee Wetlands, St. Marthew Marshlands, Newberry Slough) and will ingress into the coastal conurbation through the Mickel Transverse Glades. (**b**) Detail of wetlands and the transverse glades that will re-activate under extreme rainfall events and funnel interior wetland overflows to urban areas. The hazards of these paleodrainages are generally unrecognized and urban sprawl has encroached into these floodways (From Finkl and Restrepo 2007)

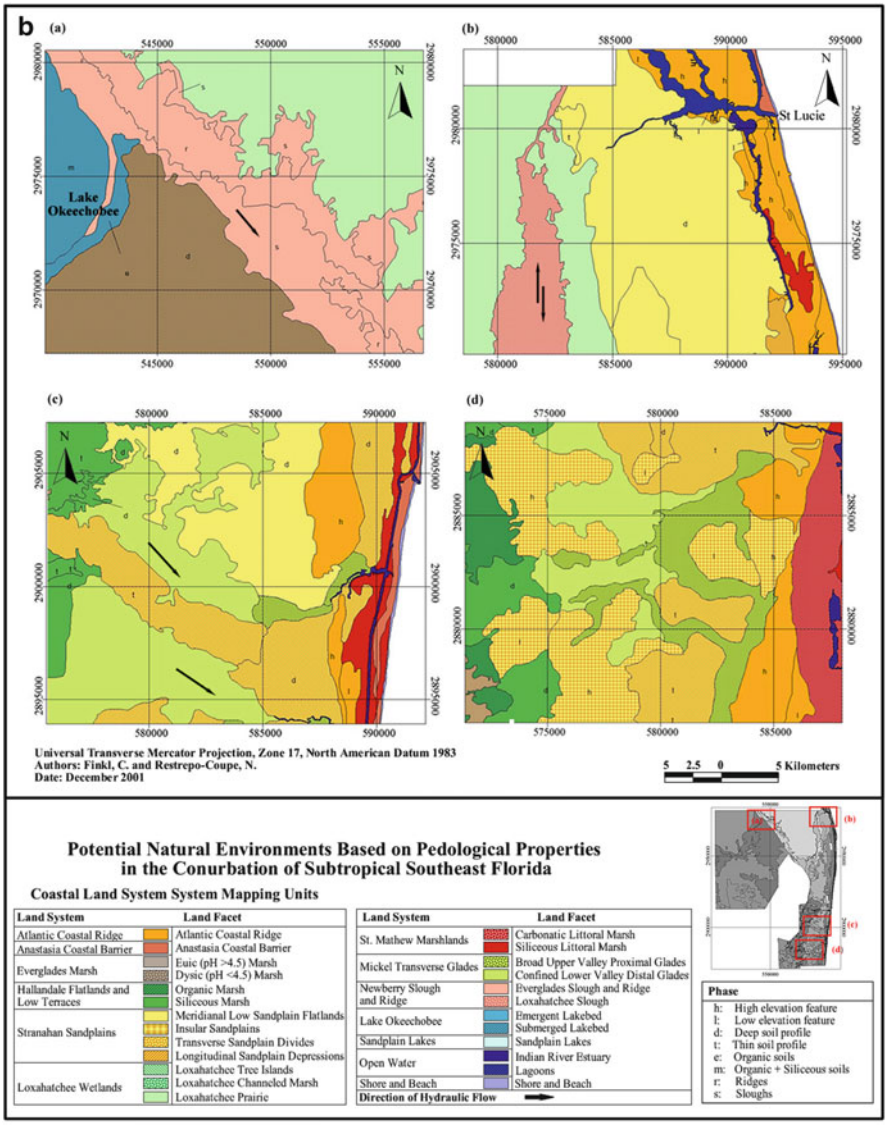

Fig. 1.5 (continued)

1.2.5 Human-Induced Land Degradation

Land degradation, a process that devalues the biophysical environment by human-induced processes acting upon the land, is viewed as any change or disturbance to the land perceived to be deleterious or undesirable; natural hazards are excluded as a cause. In the SFCZ, land degradation primarily relates to a reduction in soil quality and quantity as part of production of agricultural crops as well as off-site effects such as loss of watershed function. With increasing urban sprawl and the need for coastal living space, wetlands were ditched and drained to provide dry sites for building and agriculture. Expansion of building sites increased surface runoff, lowered soil water tables, decreased the soil water storage capacity (Finkl and Myers 1996), and eliminated wetland habitats.

Land degradation takes many forms in this sensitive subtropical environment where there has been extensive ditch and drain activities, land clearing of natural vegetation, leveling of coastal dunes, and agricultural practices that incorporate the addition of soil amendments and stubble burning (Cox et al. 1988; Finkl 1995). The main hazards induced by these activities include contamination of soils and groundwater by added chemicals (e.g. fertilizers and pesticides) and subsidence of organic soils (e.g. Stephens 1984).

Environmental problems in this region are legion and salient among them are drinking and irrigation water supply, urban and agricultural waste disposal, pollution, and coastal hazard mitigation from extreme meteorological events such as northeasters, tropical storms, and hurricanes (e.g. Finkl 1983, 2000; Finkl and Charlier 2003, 2005; Finkl et al. 2005a; LaPointe et al. 1990; SFWMD 1993). The most serious threat emanates from unseen hazards (e.g. Finkl and Krupa 2003) that degrade coastal waters. Causes of the problem and the mechanics of polluted discharge along the coast (Fig. 1.3) are detailed below in terms of land use (and abuse) practices on the coastal plain that directly impact the integrity of coastal ecosystems.

1.2.5.1 Impacts of Soil Amendments

Historically, the Florida Everglades (Fig. 1.6) was composed of sawgrass (*Cladium jamaicense*) marsh with wet prairies, sloughs, and tree islands, covering an area of approximately 1.6 million hectares (16,188 km^2) (Reddy and DeLaune 2008). Its currently diminished size is approximately 0.8 million hectares (3,240 km^2) due to urbanization and agricultural use. The EAA, which encompasses about 27% of the historic Everglades, was originally developed on thick, fertile organic soils that are now substantially degraded due to oxidation and subsidence.

The EAA, lying in thick peat soils south of Lake Okeechobee, occupies 283,280 ha (2,830 km^2) of farmland, created from the drainage of the northern Everglades. Sugar cane is the major crop of the EAA, but winter vegetables are also grown. A typical field in the EAA is 16 ha (0.16 km^2), configured in a rectangle

Fig. 1.6 Low angle oblique aerial photograph taken from a helicopter showing a typical scene of freshwater marsh with tree islands in the Florida Everglades. This is an example of the kind of landscape that was dredged and drained to allow for urban expansion. Today, less than half of the original Everglades remains (Photograph by C.W. Finkl 1997)

about 1 km long by 0.2 km (200 m) wide. The long sides of fields are bordered by ditches connected by adjustable gates through a low dike to 5-m wide canals that border the ends of the fields. The canals connect to the regional system, from which water can be added or removed by pumps. This configuration allows growers to control the groundwater level or flooding in each field.

According to normal cropping practices, sugar cane and truck crops are regularly fertilized and chemicals are added to control insect pests. During the 1950s and 1960s, EAA stormwater contained high phosphorus levels from fertilizer applications, often in excess of 500 ppb. By the 1970s, this excess stormwater was "backpumped" into Lake Okeechobee, causing eutrophication. Because of this problem, EAA chemical-laden stormwater was redirected to Water Conservation Areas (WCAs), including the Loxahatchee Wildlife Refuge and the oligotrophic Everglades National Park (Lodge 2005). This backpumping and redirection of nutrient-rich stormwater adversely impacted wetland habitat communities including macroinvertebrates, macrophytes, and periphyton. Periphyton is a complex assemblage of algae, cyanobacteria, microinvertebrates, their secretions, and detritus attached to submerged surfaces. Most Everglades periphyton are considered calcareous due to the limestone substrate and from surface water inputs containing high concentrations of calcium carbonate. Periphyton is a crucial part of the food web as the primary nutrient source for small consumers, including fish and invertebrates. Because periphyton responds rapidly to changes in the environment, it is an

indicator of changing conditions (Gaiser 2008). Conversion of the Everglades into agricultural and urban land uses contributed to the wide-ranging decline of periphyton communities and their associated fish and macroinvertebrate communities.

Nutrient through-flow to Florida Bay formed the so-called 'Dead or Black Zone' where increased concentrations of nitrogen and phosphorus induced eutrophication. The normally crystal clear water turned dark green and turbid due to blue-green algal blooms that cover a large section of the bay. The thick algal bloom attenuates sunlight in the water column and blocks photosynthesis in sea grasses. Seagrass die-off in turn kills parts of the lower trophic food web, i.e. small larva crabs, larva seahorses, fish larva. These are what the small fish eat and the bigger fish eat up the food chain.

The addition of pesticides, algicides, and fungicides leaches into the groundwater table along with nitrogen and phosphorus contained in fertilizers. This biochemical soup is transported by groundwater flow to tide in about a half century to contaminate coastal marine waters and degrade coral reefs (e.g. Cook et al. 2002; Finkl and Charlier 2003; Finkl et al. 2005a). These nutrient-laden groundwaters flow seaward to locations along the continental shelf where they reach the seafloor through fractures or fissures in the limestone rocks or where they are truncated by the upper continental slope. These groundwaters mingle with coastal marine waters via submarine groundwater discharge (SGD) to constitute a severe hazard to the health and wellbeing of coral reefs and aquatic life (see subsequent discussion). Submarine groundwater discharge (SGD) threatens sustainability of the entire southeast Florida coast because it contaminates coastal waters with high levels of nutrients such as nitrogen and phosphorus. Intensive agriculture and pesticide use, the origin of much of this contamination, constitute an on-going coastal hazard that worsens incrementally with time.

1.2.5.2 Land Subsidence

In the SFCZ, subsidence refers to the lowering of the land surface as a result of draining organic soils. Organic soils (Histosols) contain a minimum of 20–30% organic matter (OM), by weight, depending on the clay content. Most of the soils in the EAA are classified as Histosols, which form when the rate of OM accumulation exceeds the rate of decomposition. These high-organic soils are cumulative because the land is flooded much of the year, resulting in insufficient soil oxygen to maintain an active population of aerobic microorganisms that decompose OM (Tate and Terry 1980). But, when the soils are drained, soil oxygen increases as does the microflora, saprophytic bacteria, nitrifiers, denitrifiers, and cellulose oxidizers (Tate and Terry 1980). When the rate of OM decomposition exceeds the rate of accumulation, the soil disappears and the surface elevation decreases (subsides) (Fig. 1.7). Histosol subsidence also results from a loss of buoyancy following drainage, shrinkage, compaction, soil loss by wind erosion, and by burning of sugar cane.

Subsidence was well known at the time the Everglades were drained in the early 1900s. By 1913, when Everglades drainage began in earnest, surface elevation was reduced by 3.0 m, and by 1992 approximately 4.5 m of subsidence was evident.

Fig. 1.7 Concrete post driven into the organic soil at the University of Florida Everglades Research and Education Center, Belle Glade, in 1924, when the soil surface was even with the top of the post. Photographed in 2003 (Modified from Synder 2004)

In an effort to measure the rate of subsidence in the EAA, a graduated concrete post was driven (in 1924) to bedrock at the University of Florida/IFAS Everglades Research and Education Center (EREC) near Belle Glade. The soil (ground) surface was level with the top of the post, which was 2.7 m in length. Today, just over 1 m of soil remains (Fig. 1.7). The long-term average rate of subsidence is 2.5–3 cm a^{-1} (Stephens 1984; Stephens and Johnson 1951; Stephens et al. 1984).

Based on the study of Histosol profile thickness and subsidence rates, by 2050 nearly half of the EAA will have soils less than 20 cm thick. Sugarcane production will be difficult and costly, but not impossible. The area should be suitable for pasture, but not for most vegetables. Water control will be crucial, requiring a means for rapidly removing excess water and for obtaining irrigation water since soil storage will be minimal. Whether there is extensive agricultural use of lands in the EAA from now until 2050 depends on many factors that are difficult to predict. As the hazard of land subsidence plays out over the next few decades and limestone bedrock is exposed, a once fertile Histosol landscape will have been degraded to a useless rock desert.

1.2.5.3 Ditch and Drain Activities

The Everglades ecosystem includes Lake Okeechobee and its tributary areas, as well as the 80-km wide, 200-km-long wetland mosaic that previously extended from Lake Okeechobee to Florida Bay. Because much of the Everglades was

Fig. 1.8 Oblique aerial photograph showing the juxtaposition of the Everglades Agricultural Area (EAA) and the Florida Everglades, separated by the drainage canal in the foreground. The *dark colored* field in the photo center is sugar cane that has been recently burned. Burning is a double coastal hazard as it pollutes the air with particulate matter and gasses (cf. Fig. 1.9) while consuming the uppermost layers of the organic soil in which it is planted (Photograph by C.W. Finkl)

drained for agriculture (Fig. 1.8) and urban development, only 50% of the original wetlands now remain. Water levels, hydroperiods, and patterns of water flow are largely controlled by an extensive system of levees and canals. The control system was constructed to achieve multiple objectives of flood control, land drainage, and water supply. Figure 1.8 shows the juxtaposition of the EAA (sugar cane farming) and the Florida Everglades, separated by dikes and drainage canals.

In 1903, the Miami Canal was the first canal to cut through an elevated coastal rockland known as the Atlantic Coastal Ridge. Today, Lake Okeechobee is fully enclosed by a dike (see previous discussion of the Herbert Hoover Dike in section 1.2.4) and its overflow waters controlled by a system of seven drainage canals (Cooper and Lane 1987). In the 'ditch and drain' era of the early twentieth century, drainage lowered water tables up to 1.8 m below predevelopment levels (e.g. Finkl 1995). The present network of primary and secondary canals is managed by the South Florida Water Management District and counties. Canal water levels are maintained by operation of pump stations and control structures. During wet periods, water from the canals is either discharged to the ocean or pumped into Everglades National Park in order to reduce potential flooding (SFWMD 1993).

Reclamation efforts in the Everglades began in 1881 with the construction of an 18-km long canal from Lake Okeechobee towards Miami (Blake 1980). Early management policies were practical, referred to as "cut 'n dry" or "ditch and drain." By 1917, four major muck-scalped canals dissected the Everglades from Lake Okeechobee to the Atlantic Ocean (Allison 1950) and later became the backbone of

the system known as the Central and Southern Florida Project for Flood Control and Other Purposes (C & SF Project), which was authorized by Congress in 1948.

The C & SF Project constructed (1952–1954) a series of 2.7–5.5-m high perimeter levees and borrow canals from Lake Okeechobee to the coast. These levees, the eastern boundaries of the WCAs, stopped the sheet flow from the Everglades towards the urbanizing coastal area. Installation of pump stations secured the western and northern boundaries of the WCAs. Levees and canals partitioned 283,290 ha of rich Histosols (named the Everglades Agricultural Area, EAA) from the remainder of the Everglades preserved in the WCAs. Old Everglades Drainage District canals were deepened within the EAA to provide better conveyance into the WCAs. During this time, large water control structures retained water from coastal areas and diverted it towards Everglades National Park (ENP). Completion of the WCAs from 1960 to 1963 using levees and borrow canals segregated vast areas of sawgrass prairie from the remaining Everglades. In the 1970s, there was a need to increase water supply to the ENP and other efforts to direct water during drought to recharge coastal groundwater levels and retard saltwater intrusion into coastal well fields (Blake 1980). During the 1980s, structural modifications were deployed to: (1) reduce nonpoint-source pollution to Lake Okeechobee from the EAAs and (2) further improve water deliveries to ENP (Finkl 1995).

These efforts encouraged farming (e.g. sugar cane, vegetable crops) and urban expansion into the Everglades. Past water management practices and construction of related engineering works resulted in, among other effects: (1) the loss of the transitional glades which provided an early-season feeding habitat for wading birds, (2) modification of flow pattern (attenuated to pulsed) which reduced hydroperiods, (3) unnatural pooling and overdrainage as a result of canals and levees, (4) accelerated reversal from soil formation (mulch building) to degradation (oxidation of peats), (5) abandonment of wading bird nesting areas in ENP due to change in hydroperiod, and (6) unnatural and reduced flow of fresh water to Florida Bay (SFWMD 1993).

The extent of ditch and drain activities and its adverse impacts on the ecology of the region are key indicators of how far out of balance the natural system is driven by human occupance. Water control facilities installed after the 1947 hurricane resulted in improved handling of water in south Florida on a quantity basis; hazardous floods and droughts were successfully mitigated. Because the water control system was not designed initially with water quality issues in mind, modification of water quality and attendant ecological degradations began long before the C & SF Project was constructed. For the past century, the Everglades were beset by a series of hazards as the wetlands were sequentially drained, diked, plowed, and invaded by exotic species.

1.2.5.4 Urbanization

Urbanization of the SFCZ was made possible by the ditch and drain policies of the previous century. Hazardous as those policies were to environmental integrity, impacts associated with increasing population added insult to injury. Urbanization

would not have been possible without ditch and drain and this environmental hazard continues to support urban expansion into new areas. Areas previously developed now undergo vertical compaction of people in high-rise condominiums along the shore.

Overpopulation of the Florida southeast coast invites a myriad of problems that put in jeopardy the delicate sustainability of viable natural systems. The urbanized coastal corridor of southeast Florida contains about 5.7 million people (as of 2011) over about 12,000 km^2 of usable land area (Palm Beach, Broward, Miami-Dade counties), with an expected average increase in the South Florida Metro Area of about 18% by 2035 CE (Abramson 2010). Population densities, based on the area of developed land, range from 221 persons km^{-2} in Palm Beach County and 447 persons km^{-2} in Miami-Dade County to 1,444 persons km^{-2} in Broward County, east of the levee that separates the Florida Everglades from urban land (United States Census 2000). Miami and Hialeah had more than 3,800 persons km^{-2}.

Urbanization in the 1920s originally focused on dry highlands associated with the rocky limestone Atlantic Coastal Ridge. After WW II, the dramatic influx of people to the region quickly populated most high grounds and urbanization spread to lower lying sandplains and wetlands in response to a dredge-and-drain policy (see discussion in Finkl 1995). Much of the land east of the Everglades is built out and there is no room for further urban expansion in Broward County. Limited undeveloped land results in pressures for infill and redevelopment at higher densities in the County. New home construction now requires purchase of an existing home that has to be demolished for rebuilding on the land. Coastal hazards accrue from high population densities in terms of risk from storms (wind damage, shore erosion and flooding) and intense competing uses of coastal marine resources invite confrontation and dangerous mishaps from coming in contact with hazardous marine life.

1.2.5.5 Air Pollution

Air quality is generally good in the SFCZ because winds blowing off the Atlantic Ocean are fresh and clean. When sugar cane field burning takes in the EAA (Fig. 1.9), however, air quality is less than ideal and may become a hazard to coastal inhabitants who suffer from lung diseases such as emphysema and asthma. Considered an air pollutant, emissions from burning sugar cane crops have health ramifications. Studies conducted by Cançado et al. (2006) in Brazil but applicable to the SFCZ, for example, indicated that emissions created by burning sugar cane crops could ignite asthma and other respiratory problems in certain populations, usually the elderly and children. Cane burning in the SFCZ takes place during winter months when winds are light, but sometimes there is a shift in wind direction and emissions (including ash) blow eastward into the urban area creating distress among inhabitants. Incidences of children and elderly admitted into hospitals for asthma and respiratory related illnesses generally increase during harvest burning periods. Studies in Brazil report that the process of harvesting sugar cane releases large amounts of organic and particulate matter into the air. Particle pollution has been

Fig. 1.9 Example of sugar cane burning in the EAA. These controlled burns produce large noxious clouds and pollute the atmosphere above the coastal plain. Soil loss by burning is a major problem because the continued practice will eventually deplete the rich allochthonous organic soils (Histosols) overlying limestone (Photograph by C.W. Finkl)

linked to: irritation of the airways (e.g. coughing or difficulty breathing), decreased lung function, aggravated asthma, development of chronic bronchitis, irregular heartbeat, heart attacks, and premature death in people with heart or lung disease (Uriarte et al. 2009).

The aerosols emitted from sugar cane field burning act as cloud condensation nuclei, enabling the formation but decreasing size of cloud droplets. Associated decrease in formation of larger water droplets and precipitation allows for increase in water and pollutant transport to the upper troposphere. Air pollutants from sugar cane burning include acidic fine particles, such as secondary nitrates and sulfates and carbon compounds. Carbon monoxide and methane react with atmospheric hydroxyl radicals that decrease oxidation efficiency. Burning during the dry season tends to produce increased levels of nitric oxide and hydrocarbons as well as significantly higher concentrations of $HCOO^{-}$, CH_3COO^{-}, ${C_2O_2}^{-4}$, ${SO_2}^{-4}$, NO^{-3}, K^{+}, NH^{+4}, Mg^{2+} and Ca^{2+} (e.g. Darley and Lerman 1975).

1.2.6 Human-Induced Degradation of Coastal Marine Environments

High population densities in the SFCZ require food sources, living space, and methods for waste disposal. Land disposal sites for solid waste are the ‘mountains’ of south Florida but disposal of liquid waste is more problematical because deep

well injection and offshore sewage outfalls pose risk to environmental integrity. Nutrient runoff from the EAA and urban areas as surface flow or in groundwater eventually pollutes coastal marine waters degrading coral reef ecosystems and hardground communities. Ports and harbors, although necessary to maintain life and infrastructure, pose hazards associated with loading and unloading of dangerous cargos as well as groundings by ships.

1.2.6.1 Offshore Sewage Outfalls

Six wastewater treatment facilities (Publicly Owned Treatment Works) in southeast Florida have been discharging treated wastewater to the ocean for decades in outfall pipes 1.6–5 km offshore (EPA 2003). The six plants (Miami Dade Central, Miami Dade North, City of Hollywood, Broward County, Delray Beach and Boca Raton) treat the wastewater to "secondary" levels where treatment plants remove 90% of the pollutants before the wastewater enters coastal waters. There are, however, concerns with nitrogen and phosphorus causing red tides, the effects of pharmaceuticals and endocrine disrupters on wildlife, and human health risks. Even with secondary treatment, wastewater debouching from the ocean outfalls is believed to be the direct cause of death of coral reefs and marine life (Szmant 2002). The primary culprit is nitrogen, in all its forms, that serves as a nutrient for algae. In Palm Beach County alone, some 1.5 billion liters of partially treated sewage is pumped into the Atlantic Ocean each day, while Delray Beach contributes about 200 million liters a day. It is obvious through those observations that sewage outfalls constitute a hazard to the coastal marine environments of the SFCZ. In view of the environmental risk associated with this management practice, it is prudent to determine what is meant by 'secondary treatment' in order to understand the damage that readily occurs.

Secondary treatment removes biodegradable organic matter and suspended solids and includes basic disinfection. Secondary treatment plants are designed to produce effluents that contain no more than 30 mg L^{-1} $CBOD_5$ (carbonaceous biochemical oxygen demand consumed in 5 days) and 30 mg L^{-1} TSS (total suspended solids). State of Florida regulations require that secondary-treated wastewater cannot exceed 20 mg L^{-1} of $CBOD_5$ and 20 mg L^{-1} of TSS or that 90% of $CBOD_5$ and TSS must be removed from the wastewater influent, whichever is more stringent (FAC [Florida Administrative Code] 62–600.420(1)(a)). The effluent pH, after disinfection, must be within the range of 6.0–8.5 (FAC 62–600.420).

Potential ecological stressors that may be present in secondarily treated wastewater include nutrients (nitrogen, phosphorus, iron) that could promote primary productivity and growth of harmful algal blooms, metals, volatile organic compounds, synthetic organic compounds (e.g. organochlorine compounds such as trihalomethanes and chlorinated hydrocarbons), other substances suspected of causing adverse effects on aquatic organisms (e.g. endocrine-disrupting compounds), and substances whose ecological and biological effects are not yet well studied (for example, detergents, surfactants). Potential human health stressors include pathogenic enteric

microorganisms (bacteria, viruses, and protozoans) capable of surviving basic disinfection, heavy metals, organic compounds, endocrine-disrupting compounds, and nutrients such as nitrates and nitrites that can cause human health effects at higher concentrations.

A recent review (NRC 2000) of the causes of eutrophication of coastal waters found that nutrient over-enrichment of coastal marine waters have resulted in the following adverse effects: increased primary productivity, increased oxygen demand and hypoxia, shifts in community structure caused by anoxia and hypoxia, changes in phytoplankton community structure, harmful algal blooms, degradation of seagrass and algal beds and formation of nuisance algal mats, and coral reef destruction.

The primary potential exposure pathways are related to direct exposure of humans to water containing stressors and ingestion of seafood with elevated levels of contaminants. Airborne exposure is also possible if water droplets containing effluent constituents are formed through turbulence or aerosolization. Recreational or fishing activities in or near ocean outfalls could also expose humans to these contaminants. Potential exposure pathways for marine mammals, reptiles, and fish are similar to the above-named pathways. Predation or scavenging of other organisms feeding upon contaminated organisms or algae that contain elevated tissue concentrations of effluent constituents cause bioaccumulation of these constituents. Potential exposure pathways for marine invertebrates include ingestion of particles or dissolved materials containing effluent constituents.

Pathogens are controlled at the treatment plant through chlorination to meet water-quality standards within the required mixing zone. Viruses and most bacteria are expected to be adequately inactivated by chlorine. However, there is no filtration to remove *Cryptosporidium* and *Giardia*. More significantly, lack of treatment to remove pathogenic protozoans probably constitutes the greatest human health risk posed by this wastewater management option (EPA 2003).

1.2.6.2 Nutrient Runoff

Farming in the EAA and maintenance of urban land (yards, gardens, parks, and golf courses) are 'non-point' sources of pollution where surface runoff reaches coastal waters. There are four key non-point land-based drivers of ecological change impacts in the SFCZ: (1) nutrient input from agriculture in urban settings, (2) organic pollutants from pesticides derived from inland agricultural areas, (3) inorganic pollutants from urban runoff, and (4) direct dumping from human populations residing on coastal marine environments (Hu et al. 2004; Lapointe et al. 2005a, b). Escalating nutrient enrichment and eutrophication in SFCZ waters carries severe impacts that include a shift in the acid-based chemistry of seawater, a reduction in subsurface oxygen for coastal waters and open ocean, increased mortality or contamination among fishery stocks, proliferation of harmful algal blooms, coral reef degradation, and a widespread increase in mercury and other pollutants, such as dissolved inorganic nitrogen (DIN) and soluble reactive

phosphorus (SRP) (Lapointe et al. 2005b). A reduction in ocean pH will likely lead to diminished shell and skeleton growth by many marine calcifying species, which include coral colonies and mollusks, and increased runoff from agricultural fertilizers and fossil fuel nitrogen contribute to the severity and sustaining state of coastal hypoxia. One area of major concern in southeast Florida is the Biscayne Bay coastal ridge region, which has become a 'reservoir' for stormwater runoff from urban/residential and agricultural land sources (Caccia and Boyer 2007). It is feared that hypoxic deadzones, like those that have established in Florida Bay and Biscayne Bay, could eventually migrate to the nearshore waters of the Florida Reef Tract, which has been designated the third largest barrier reef system in the world (Precht and Miller 2007).

Less likely comprehended is the association of land use activities on uplands and the subsequent impacts along the SFCZ (e.g. Bierman 2000; Finkl 1995; Finkl and Krupa 2003; Krupa and Gefvert 2005; LaPointe et al. 1990). For example, there is a clear connection between the high-nutrient surface waters and shallow groundwaters from sugarcane farming in the EAA some 30 km inland on the Florida coastal plain and degraded water quality among estuarine and coastal marine environments in the SFCZ (Finkl and Kruempel 2005). The South Florida Water Management District (1993) reported between 1980 and 1989 the total surface water discharge from canal flows to the SFCZ was approximately 1.66×10^9 m^3, with an associated nutrient content of 2,473 t (247 t a^{-1}) for total N and 197 t (1.97 t a^{-1}) for total P.

1.2.6.3 Submarine Groundwater Discharge (SGD)

In addition to surface water nutrient runoff, submarine groundwater discharge (SGD) (Fig. 1.10) threatens sustainability in the SFCZ because it contaminates coastal waters with high levels of nutrients. Serious degradation of the Florida Reef Tract (Dodge et al. 1982) is blatantly obvious as extensive sectors of coral reef die from increased nutrient loading of nearshore waters by elevated nitrogen (N) and phosphorus (P) nutrient levels delivered to the coast by submarine groundwater discharge (SGD) and surface runoff. The main source of N-P input into the Biscayne Aquifer, which has one of the highest carbonate aquifer transmissivities in the world, is from sugar cane farming in the EAA on the SFCZ coastal plain. Groundwater discharges for Palm Beach County are, for example, estimated from a groundwater MODFLOW model at $1{,}659 \times 10^6$ m^3 year^{-1}. Total N in groundwater below the coastal plain adjacent to remnant Everglades averages about 1.25 mg L^{-1}. SGD nutrient fluxes to the coast are 5727 and 414 metric tons per year for P and N, respectively. Surface water contributions for P and N are respectively 197 and 2,471 metric tons per year (Finkl and Krupa, 2003; Finkl et al. 2005b).

Total N in the groundwater (10–50 m below mean sea level) in Palm Beach County, for example, is quite high in areas adjacent to water conservation areas on the coastal plain ($\approx$3 mg l^{-1}) (Krupa and Gefvert 2005). SGD along the southeast

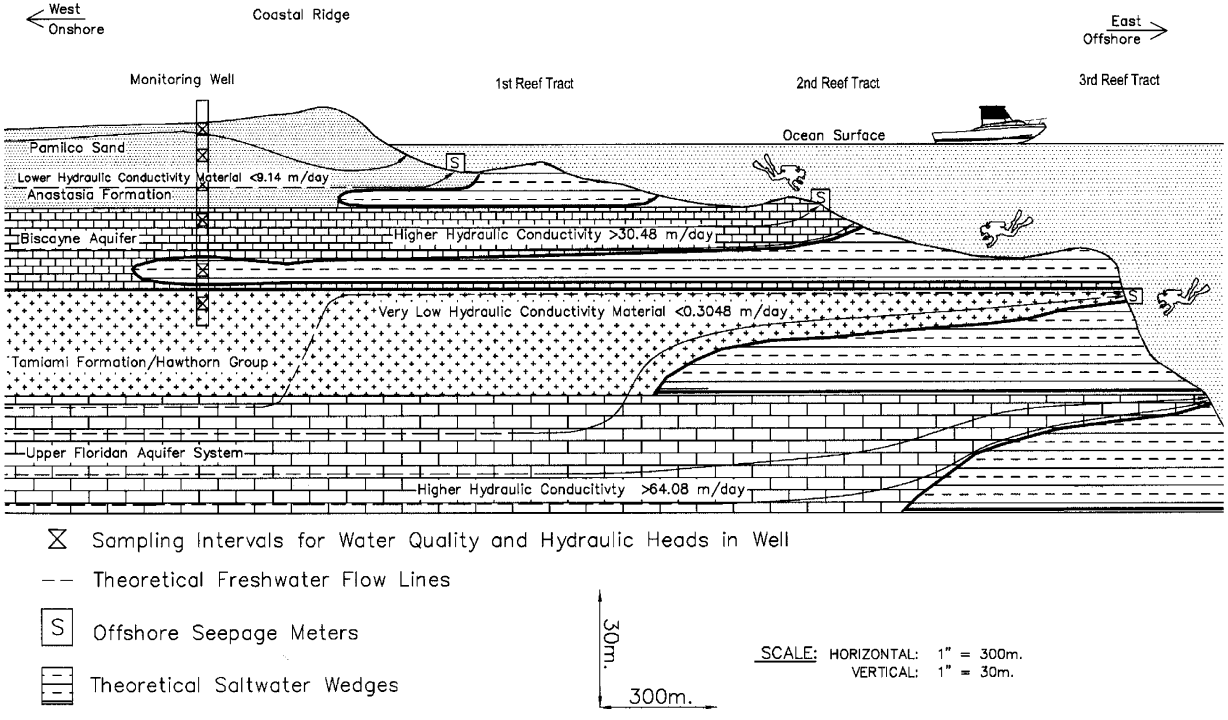

Fig. 1.10 Idealized cross section of the SFCZ, at the latitude of central Palm Beach County, showing two coastal hazards. The truncation of carbonate formations on the continental shelf and upper slope provides a conduit for groundwaters from the EAA to flow to tide in surficial sediments and the Biscayne Aquifer where they contaminate coastal waters with nutrients, mostly nitrogen and phosphorus, and pesticides. Overpumping for drinking water in urban well fields (*vertical shaft*) is an additional hazard that causes saltwater intrusion (stippled wedges pointing landward), as shown in the saltwater wedges extending inland. The approximate scale is 100 m vertically and 4 km horizontally (Figure modified from Krupa and Gefvert 2005)

Florida coast provides notable inputs of freshwater to the ocean reef complex. SGDs are presently estimated to be on the order of 9.99×10^5 m^3 day^{-1} (3.6×10^8 m^3 a^{-1}) (Finkl et al. 2005b). These adverse impacts are the result of incipient agricultural practices 50–60 years ago. The half-century time lag is due to travel (residence) times in the aquifer and effects of contaminated groundwater are expected to cause greater future impacts as estuaries and nearshore environments respond to cumulative effects of continuous nutrient loading (Finkl 1995). Accompanying impacts that reduce aquatic productivity include accelerated accumulation of flocculated detritus, reduced dissolved oxygen concentrations, changes in detritus, microbial, and macro-invertebrate communities, and changing periphyton communities toward reduced diversity and dominance of pollution-tolerant species (SFWMD 1993).

Estimated discharges for Palm Beach County, compiled by Finkl and Krupa (2003), show that annual groundwater discharge (2,211 $m^3 \times 10^6$ a^{-1}) is 133% of surface water discharge (1,661 $m^3 \times 10^6$ a^{-1}). In Palm Beach County sector of the SFCZ, SGD occurs where aquifers are truncated on the inner continental shelf (Fig. 1.10). Low-angle truncation of geologic formations with high hydraulic conductivities up to 30 m day^{-1} provides a large surface area for SGD. As shown in the conceptual diagram (Fig. 1.10), SGD occurs all along the coast but is especially pronounced where the surficial aquifer system (SAS) outcrops on the seabed in association with the Florida Reef Tact. Fresh water discharge takes place in submarine springs and through fissures in the porous limestone, but closer to shore, SGD occurs in materials that have a lower hydraulic conductivity.

Nutrient delivery to beach and nearshore environments is a serious problem that threatens coastal water quality which in turn will impact tourism-related activities such as sunbathing, beach walking, swimming, snorkeling, SCUBA diving, and surf fishing. The full magnitude of the problem has yet to surface because it takes about several decades for groundwater from the EAA to reach nearshore habitats. Pollution of groundwater increases with time, as an insult to injury, due to higher doses of fertilizers on croplands and increased runoff from expanding urban areas.

1.2.6.4 Deep Well Injection

Every day, more than 5.7 billion liters of wastewater leave municipal treatment facilities in Florida bound for reuse or disposal. Relying less on discharges to surface waters, municipalities in the SFCZ depend on reuse, ocean discharge, and deep-well injection. In Miami-Dade County, for every 11 L of wastewater generated, 3.7 L is treated and sent to deep underground saltwater formations. The remaining 7.3 L are piped in ocean falls 6 km offshore to enter coastal waters (EPA 2003). Potential hazards and risks associated with these activities need to be noted.

Deep well injection is a method of liquid (hazardous and non-hazardous) waste disposal. Although fluid wastes injected into near surface or deep bedrock formations are regarded as storage, there are often numerous pathways for injected wastes to migrate vertically and/or horizontally (EPA 2003). Most injection wells

are comprised of concentric pipes that extend nearly 1,000 m from the ground surface to an injection zone in naturally occurring salt waters or brine.

Deep wells in the SFCZ dispose of secondary-treated municipal wastewater. These wells are permitted as Class I municipal wells, which by definition dispose of wastewater beneath the lowermost formations containing, within a minimum of 0.5 km of the well bore, an underground source of drinking water (FDEP 1999). Deep municipal wells inject at depths ranging from approximately 300 m to greater than 800 m below the land surface. Subsurface heterogeneous limestone formations in southeast Florida introduces complexity because unit properties (e.g. hydraulic conductivity, porosity, effective porosity) vary from one unit to the next, within a given unit from one site to another, and even within a given unit at a given site. This heterogeneity presents a significant challenge in evaluating risk. One example of uncertainty regards the presence of fractures, fissures, and solution channels throughout some units. Data obtained from monitoring wells, for example, show that upward migration of injected wastewater has occurred at some sites (EPA 2003). In Miami-Dade County, monitoring wells have recorded elevated concentrations of ammonia at 450 and 550 m depths. Elevated concentrations of dissolved chlorides have also been detected, but these values may also indicate displacement of native formation water in an upward direction. Fecal coliforms have been detected in a number of monitoring wells.

Deep-well injection in the SFCZ is a potential hazard that needs to be carefully evaluated. The risk remains that municipal drinking water well fields can become contaminated by liquid waste disposal underground in the fractured limestones of south Florida.

1.2.6.5 Algal Blooms

When certain species of microscopic and macroscopic marine algae rapidly proliferate, they become a pronounced coastal hazard in the form of a harmful algal bloom (HAB). The impacts of HABs can include the depletion of oxygen from the water column, blocking out the sunlight that other organisms require, and releasing toxins that are dangerous to marine life and humans. The cause and growth of HABs are generally tied to the availability of nitrates and phosphates, which are supplied by surface runoff and SGD, because marine algae grow at different rates depending on the relative abundance of specific substances (e.g., ammonia, urea, nitrate ion). Also important in algal bloom formation are elevated levels of iron, silica, and carbon that are associated with coastal water pollution produced by humans.

Over the past 20 years, the SFCZ has experienced an increase in macroalgal blooms along the coast as a result of increased land-based nutrient runoff input (Lapointe and Hanisak 1997). The Florida Reef Tract is adversely affected by HABs through die-offs of sponges, hard corals, and soft corals from increased hypoxia and anoxia within the nearshore waters (Lapointe 1997; Lapointe et al. 2005b). It has been reported, for example, that invasive harmful marine alga quickly spread from reef to reef along the Florida Reef Tract (Lapointe and Hanisak 1997).

Fringing coral reefs along the SFCZ are seasonally blanketed by a macroalgae that looks like long green seaweed. *Codium isthmocladum* grows on the undershelf of reefs that used to be clear and colorful. Additional problems include blooms of *Caulerpa* algae that cover significant parts of the upper surfaces of many reef tracts. *Caulerp*a normally grows in mangrove habitats but is now found offshore due to nutrient loadings in coastal waters. Blooms of macroalgae occur along the coast and range up to 2 m thick on the downside ledges of the reefs.

1.2.6.6 Poor Water Quality

Poor water quality (those areas that contain irregular water chemistry or pH readings) within the SFCZ is a multi-sourced coastal hazard that stems from large freshwater impulses, the presence of detrimental algal blooms, the deterioration of coral reef environments, wastewater recirculation, *etc*. As a result, poor water quality poses not only an environment impact upon the SFCZ, but also an aesthetic (through degraded water clarity) and economic impact by deterring tourists and beach goers from recreationally using the coast. The most predominant point source of poor water quality within the SFCZ is extreme freshwater pulses flowing from Lake Okeechobee through the St. Lucie Canal down to the St. Lucie Estuary. Water management administrators have dictated that the Lake must be lowered in anticipation of the south Florida rainy season (June-November), and thus, large regulatory pulses of freshwater are sometimes added as runoff to the St. Lucie Estuary and affect the sensitivity of that ecosystem. While Haunert and Startzman (1985) reported that a controlled, 3-week freshwater discharge of 28,316 $L^3\ s^{-1}$ (reported as 1,000 cfs, cubic feet per second) had no significant effect on biota, a controlled, 3-week freshwater discharge of 70,090 $L^3\ s^{-1}$ (reported as 2,500 cfs) did substantially reduce the salinity of the estuary, which led to a composition change in the benthos and a redistribution of fish species. To compound the problem, water from Lake Okeechobee contains elevated concentrations of nutrients from surrounding farming activities of the EAA. These nutrients, in turn, are then introduced into coastal waters through the rapid release of polluted freshwater, and lead to many impacts, *viz*. algal blooms, lesions and disease among fish, invasive species proliferation, *etc*.

Wastewater recirculation is another proponent of poor water quality within the SFCZ. According to McPherson and Halley (1997), Florida's wastewater emissions have shot up 37% since 1985. About 57% of the wastewater ends up in surface water after being treated. About 20% is injected deep below the aquifer to locations where it supposedly cannot recirculate upwards and contaminate the aquifer. The remaining 23% is flushed into septic tanks. There are 1.56 million septic tanks in Florida and each one digests and emits about 510 L of bacteria-rich water each day. With 116,300 septic tanks, Miami-Dade County has more than any other Florida county. In the Florida Keys, these primitive tanks have been lethal to the ecosystem where septic tanks and 10,000 cesspits have poisoned large tracts of coral reef (e.g. LaPointe et al. 1990). Whether stemming from wastewater recirculation or

polluted freshwater pulses, poor water quality leads to the central problem of an negative economic impact for the SFCZ, as associated adverse effects can terminate beach and recreational marine use and limit the main source of beach-generated income for state and local coastal communities.

1.2.6.7 Ship Groundings

The three main ports in the SFCZ (Port of Miami, Port Everglades, and Lake Worth) facilitate large volume tankers and freighters in addition to the ongoing vessel traffic by recreational cruise ships and military craft (e.g., destroyers, cutters, and submarines). High-vessel traffic means that ships can cause coastal impacts by running aground or anchoring on nearshore reef environments (Monty et al. 2006). Mostly due to human navigational errors or inhospitable weather conditions, there were 11 reported groundings and six anchor drag cases from 1993 to 2006 in the SFCZ, which resulted in more than 40,000 m^2 of coral reef injury (Collier et al. 2007; Rubin et al. 2008). One of the most severe cases occurred in 2004 just outside of Port Everglades when two large cargo ships, the MV *Eastwind* and MV *Federal Pescadores*, ran aground on the second reef of the Florida Reef Tract (Rubin et al. 2008). These two combined groundings contributed to the destruction of more than 30,000 m^2 of coral reef habitat (Flesher 2004). Another grounding took place offshore Dania Beach in 1993, when the submarine USS *Memphis* ran aground on the second reef tract in approximately 6–8 m depth of water (Banks et al. 1998). More physical and biological damaged ensued when the crew attempted to free the submarine by blowing ballast tanks and reversing the engines.

Figure 1.11 is an example of a freighter grounding on Fort Lauderdale Beach during a strong northeaster. The ship was anchored offshore waiting to enter Port Everglades when the storm struck. Engine failure and the lack of time to get oceangoing tugs to the rescue left the ship to the whim of wind and waves. Dragging her anchor across coral reefs and biological hardgrounds left scars on the seafloor as evidence of environmental damage. Ship groundings are an ever-present hazard that can strike at almost any moment, regardless of weather conditions. There are incidences, for example, of ship groundings along the SFCZ coast in calm weather due to human error.

Besides the economic impacts incurred from this type of anthropogenic coastal hazard (e.g., damage claims are usually in the multi-million dollar range), the physical and biological ramifications from such damage are immeasurable. Ship groundings on coral reefs not only cause serious damage to the reef builder organisms, but also result in a loss of habitat for other marine life and consequently lead to barren, unproductive areas. These impacts, however, may be further intensified by other stress factors (e.g., disease, pollution, eutrophication, and sedimentation) which decrease coral population size, adversely impact the size of coral breeding stocks, larval supply and recruitment rates, and likely increase post-settlement mortality rates of coral

Fig. 1.11 Coastal freighter driven ashore during a strong northeaster. This ship grounding on Fort Lauderdale Beach is an example of the hazard posed by offshore anchor sites where ships lay over, waiting for berths in Port Everglades. This vessel, dragging its anchor across the Florida Reef Tract and hardbottoms while driven by high winds and waves, caused severe localized environmental damage (Photograph by C.W. Finkl 1995)

colonies (Rubin et al. 2008). Therefore, the impacts of reef grounding coastal hazards are some of the extreme in nature, as they usually result in unlikely recovery of the damaged sites.

1.2.7 Managerial Positionalities That Defeat Sustainable Development

When carrying capacities of natural environments are exceeded, it becomes more difficult to manage resources because of competing demands. It is thus relevant to indicate the plight of coastal dwellers confronted by competing bureaucracies that often are in gridlock. The SFCZ exemplifies the precarious imbalance between human needs for living space and recreational sites and the need to maintain a viable natural environment. Ignorance, arrogance, and disregard for the environment in favor of urbanization and commercialization are poignantly demonstrated by the degradation or destruction of coastal marine resources. The hazardization

that is playing out in this region reflects what is going on in many other coastal zones throughout the world and it is therefore instructive to consider causes and effects.

Sustainability of this subtropical coastal region is a contentious issue because although scientists recognize signs of environmental degradation, political forces encourage continued development for financial gain, authority, and power (e.g. Finkl and Kruempel 2005). In a politically dominated managerial system it is difficult to get the idea across that population cannot exponentially increase in sensitive coastal wetlands. Urban dwellers are often unconcerned about environmental issues (until they are intimately affected). Monoculturalists, those engaged in sugar cane farming, farm only with regard for crop productivity using soil amendments such as fertilizers and pesticides. Impairment of coastal water quality is not part of an awareness paradigm and deterioration along the coast is not seen as a relevant concern. These kinds of practices are not sustainable and can only lead to ruin, a message that apparently is poorly transmitted. Apparently equally incomprehensible to the public is the danger of releasing exotic species into the environment. Some releases were by accident, as in Hurricane Andrew when reptiles escaped from zoos and private collections and invaded suburban neighborhoods and eventually finding sanctuary in the Everglades where there were no predators.

Unfortunately, responsible coastal protection is frequently never accomplished due to bureaucratic overkill, a sociopolitical *modus operandi* that replaces common sense with red tape. The use of RAIs (Request for Additional Information) in the permitting phase of beach renourishments is a managerial positionality that defeats sustainable development. This situation obtains because Florida regulatory agencies require 'additional' information to supplement the original permit application and existing reports before a permit to proceed is granted. While there is a need for a complete and comprehensive checklist of items (such as a method proposal, survey procedures, tasks, engineering plans for excavation of offshore sand deposits, beachfill construction templates, and so on) the regulatory agencies sometimes defeat themselves by asking for ever more information in the form of RAIs. As a result, permit applications that could be reviewed in a matter of days grow to a thousand pages or more and never get read. With permitting agencies perpetually under-staffed and under-funded, projects are in a perpetual state of limbo. The problem is compounded when permit application review timelines keep lengthening and accruing. When an agency sends an RAI back to the potential permitee, regulators receive another 60–90 days to review the new information. If there are three or four RAIs, a project could be delayed over a year! Meanwhile, beach erosion and shoreline retreat continue until the originally proposed fill templates no longer apply. Although the RAI quality assurance-quality control mechanism was established with noble intentions, it has become a coastal hazard in itself through obstruction. It ultimately becomes a power struggle between the permitter and permitee, with the final compromise usually meeting bureaucratic needs instead of truly addressing environmental concerns. Environmental sustainability is not possible under these conditions, because they are founded in obstructional, confrontational, and unintegrous behavior.

1.2.8 Biological Hazards

In addition to human activities and natural events, there are hazards that are largely ignored by the public as not worthy of attention, such as dangerous marine fauna that occur in the coastal zone. These 'biological' coastal hazards are insidious but ever present at certain times of the year. Hazardous marine life can technically be viewed as a misnomer, as the following organisms only pose a risk to humans as either part of their defense mechanisms or innate behaviors. Regardless, because they potentially impact humans along the coast, they should be recognized as significant biological coastal hazards.

1.2.8.1 Jellyfish and Portuguese Man-of-War

In the SFCZ, there is a wide variety of hazardous marine life that constitutes coastal hazards to humans. Jellyfish, which belong to the phylum Cnidaria, are one of the most easily identifiable marine creatures that humans try to avoid. Jellyfish are simple organisms, made of approximately 95% water with less than 5% solid mass. Most species have a hollow body that is shaped like a bell or an umbrella, and are either nearly clear or exhibit a light blue color (Gowell 1993). Some range in size from one inch to over a foot in diameter, while other jellyfish species can grow up to 7 ft long (Sharth 2002).

Jellyfish drift in the water with little control over their movement. They have specialized muscles that allow it to contract its bell, reducing the space under it and forcing water out through the opening. This pulsating rhythm allows for a limited regulation of vertical movement. As water is pushed in one direction, the jellyfish moves in the opposite direction (Weston et al. 2009). Jellyfish move vertically very well in the water column, but their motor skills are no match for strong ocean currents, wind, and waves. At certain times of the year, beaches may become covered with jellyfish that have been washed up by storms or strong winds. Once on shore, they have no way to move back into the sea (Gowell 1993).

Jellyfish are probably most well known for their stinging capability and therefore knowledgeable swimmers try to avoid them. Most humans believe that the jellyfish are attacking them as they are swimming, which is not the case. Jellyfish sting humans when humans swim into their tentacles or simply brush against the tentacles in passing. Like most marine life, jellyfish come equipped with an effective defense and hunting mechanism. Jellyfish contain a specialized venom apparatus, called a cnidoblast, for defense and feeding. A pressurized capsule, referred to as a nematocyst, inside the cnidoblast contains a trigger and the stinging structure (Weston et al. 2009). The nematocyst is responsible for the pain that the snorkelers and swimmers experience when stung.

Contact with a jellyfish tentacle can trigger millions of nematocysts to pierce the skin and inject venom, yet only some species have a sting that will cause an adverse reaction in humans. When a nematocyst is triggered by contact by predator or prey, pressure builds up rapidly inside it up to 136 atm (140 kg cm^{-2}) until it bursts open.

Fig. 1.12 The Portuguese man-of-war (*Physalia physalis*) is the most dangerous jellyfish in southeast Florida. They are phenotypically distinct by their purplish-blue coloring and prominent sail on the gas-filled gut (Photograph acquired from NOAA)

A lance inside the nematocyst pierces the victim's skin, and poison flows through into the victim.

Three common jellyfish in the SFCZ are the Portuguese man-of-war (*Physalia physalis*) (Fig. 1.12), the moon jelly (*Aurelia aurita*) and the upside-down jellyfish (*Cassiopea xamachana*). The Portuguese man-of-war is the most dangerous jelly-like fish and the impact of their sting can be very painful, if not deadly to those humans with an allergic reaction to the toxin. This jelly-like invertebrate has a gas-filled gut, which is used as a modified 'sail' that allows it to ride high atop the ocean waves (Gowell 1993). Although it is thought of as a jellyfish, it belongs to the Hydrozoa subgroup. The moon jelly is the most common jellyfish in Florida and can be found in all the oceans of the world. Their tentacles produce only a mild sting or burning.

The upside-down jellyfish is often found in the warm mangrove islands in the SFCZ. These jellyfish have the unique ability to sit on their dome with their tentacles extended upward towards the sunlight. Within the SFCZ, it is not uncommon to have ocean currents congregate jellyfish into large swarms or "blooms", which could consist of hundreds or thousands of individuals. Bloom formation is a complex process that depends on a wide array of variables, such as ocean currents, nutrients, temperature, predation, and oxygen concentrations. Jellyfish are better conditioned to survive in oxygen-poor waters than their competitors, and thus can thrive on plankton without direct competition or predation. One well-known jelly-fish bloom that recently occurred in southeast Florida was reported in 2011 over

Fig. 1.13 The bull shark (*Carcharhinus leucas*), is the most unpredictable of the shark species within the Southeast Florida Coastal Zone. They are responsible for most of the shark attacks on record (Photograph acquired from NOAA)

Memorial Day weekend. Over 1,600 beach goers within a 16-km stretch were impacted with stings after a steady onshore breeze and east swell brought a large swarm of venomous jellyfish close to shore.

1.2.8.2 Sharks

Sharks are another form of biological coastal hazard that usually strikes fear in the hearts of most people. Sharks are considered fish with a fully cartilaginous skeleton and a highly streamlined body. Their cartilage skeleton is flexible and durable, yet has about half the density of bone. This greatly reduces the skeleton's weight, saving the shark a tremendous amount of energy when swimming. Sharks contain replaceable rows of teeth are used only for capturing their prey and tearing chunks of flesh off. They do not chew their food, but rather gulp it down (Allen 1999).

In southeast Florida, only the bull shark (*Carcharhinus leucas*), tiger shark (*Galeocerdo cuvier*), lemon shark (*Negaprion brevirostris*), and reef shark (*Carcharhinus melanopterus*) pose legitimate potential hazards to humans. The bull shark is considered the most dangerous species in south Florida waters due to its unpredictable behavior (Fig. 1.13). It is unique among other marine sharks as they have a tolerance for fresh water and can travel up rivers, posing a threat to those brackish water systems close to the coast. As a result, they are probably responsible for the majority of attacks on humans in southeast Florida that take place near

the shore, including many attacks mistakenly attributed to other species. The tiger shark, on the other hand, is one of the ocean's largest and most dangerous sharks, with a mature shark averaging between 3.25 and 4.25 m long and weighing between 325 and 425 kg. They are found in many tropical and temperate regions of the world's oceans, but are rarely sighted in the SFCZ. The tiger shark usually hunts alone and at night, and gets its name from the dark stripes down its body, which fade as the shark matures (Budker 1971). Lemon sharks and reef sharks are requiem sharks that are fairly common and known to be only moderately aggressive when provoked.

As such, Florida's Atlantic coast has been designated the most dangerous coast in the world for shark attacks (ISAF 2011). According to the International Shark Attack File (ISAF 2011; http://act.oceana.org), at New Smyrna Beach, Volusia County (approximately 240 km north of the SFCZ), there are more incidents per square kilometer than on any other beach in the world (Luscombe 2008). Swimmers at New Smyrna commonly come within 3 m of a shark (Regenold 2008). These distinctions give New Smyrna Beach the nickname "Shark Attack Capital of the World." Overall, sharks do pose a serious hazard to humans in southeast Florida. According to the International Shark Attack File from 1882 to 2010, 81 shark attacks on humans have occurred within southeast Florida, with two fatalities (ISAF 2011). When a shark attack occurs, it usually is the result of the shark mistakenly perceiving a swimmer or surfer as an injured animal. Since humans are rather awkward in the nearshore water, their movements of splashing around often simulate to the shark a mortally wounded prey item. The shark, carefully selecting a potential meal that will give the least amount of struggle so that no harm comes to it, usually tests to see if the specimen is actually injured. That is why so many shark attack victims live, because the shark becomes disinterested after realizing the prey item is not an injured sea turtle, fish, or marine mammal. The two fatalities occurred not because they were eaten, but rather from a loss of blood (ISAF 2011).

1.2.8.3 Seabather's Dermatitis

There is a major misconception that acute Seabather's pruritic dermatitis, which is identified by severe itching around small red papules 1 mm–1.5 cm in size located on areas of skin that were covered by water-permeable clothing or hair during ocean swimming, are caused by the commonly named pest: sea lice. However, that is a misnomer, as sea lice are tiny marine ectoparasitic (external parasites) copepods (Order Siphonostomatoida, Family Caligidae) that feed exclusively on the mucus, epidermal tissue, and blood of host marine fish (Bravo 2003).

The true cause of Seabather's dermatitis is the hypersensitive skin reaction to the immature nematocysts of larval-stage thimble jellyfish (*Linuche unguiculata*) (Freudenthal and Joseph 1993). These larvae, generally half a millimeter in length, can find their way into bathing suits, even passing through the mesh of some suits, and become trapped against the skin and sting. The larvae are visible to the naked eye, but they become nearly invisible in the water. The best method of identifying when the larvae are about is simply by the appearance of the rash on swimmers or

divers. *L. unguiculata* larvae are most prevalent in the SFCZ from April to August, although they can appear at any time throughout the year. The symptoms will appear very soon (i.e. within 24 h or less) after exposure to the organism and will persist for several days. Some cases have been reported which have a 3- or 4-day delay in onset and a prolonged course lasting several weeks (Tomchik et al. 1993).

In addition to skin irritations, symptoms may include fever, chills, headaches, nausea and vomiting (Freudenthal and Joseph 1993). Severe symptoms occur in children particularly, although adults have also shown similar reactions. Since many of these symptoms are consistent with many other illnesses, diagnosis is sometimes difficult unless the attending physician knows of the diver's exposure to contaminated water. Often the symptoms are very mild, and other causes may be considered or diagnosed incorrectly at first. Many of these cases of sea bather's dermatitis will clear spontaneously, but others may require treatment. Antihistamines and antipruritic (anti-itching) agents may be used, but the results are not good in many cases (Tomchik et al. 1993). Children and individuals with allergies or diseases affecting the immune system may be at risk for severe reactions. Fortunately, the severe reaction is rare, but it can be a danger for some individuals.

1.2.8.4 Sting Rays

Stingrays (Order Myliobatiformes, Suborder Myliobatoidei) are a cosmopolitan group of rays, which are cartilaginous fishes related to sharks, commonly found in coastal tropical and subtropical marine waters throughout the world (Nelson 2006). They usually have a rounded or "diamond-shaped" body and their stings, when present, are located near the middle or lower third of their "tail." Stingrays come in two different general varieties: the "benthic" (i.e. bottom-feeding) stingrays and the "pelagic" (i.e. swimming) stingrays. Within the SFCZ, benthic rays, such as the Atlantic Southern stingray (*Dasyatis americana*), are often found buried in the sand (Fig. 1.14) and feed on worms, clams, shrimp, crabs, snails and occasionally fish. Pelagic rays, like the spotted eagle ray and manta ray, are more active swimmers that have a "bat-like" shape.

The venom apparatus or "stinger" of a stingray is a spine or modified dermal denticle (i.e. the scales covering sharks and stingrays) with two ventral grooves filled with venom-producing tissue (Nelson 2006). The venom apparatus is surrounded by a cell-rich covering or sheath that also may produce lesser amounts of venom (Tricas et al. 1997). The venom itself is a largely protein-based toxin that causes great pain in mammals and may also alter heart rate and respiration. However, since it is proteinaceous, it can be inactivated by exposure to high temperatures (Tricas et al. 1997). Because of this, immersion of the wound in hot water or application of a heat compress are recommended as an immediate treatment for unfortunate victims of a stingray injury or "envenomation" (Meyer 1997). Although this may reduce the initial pain of a stingray injury, victims should still obtain medical assistance so that the wound can be properly examined and cleaned to avoid secondary infections or other complications.

Fig. 1.14 An Atlantic Southern stingray (*Dasyatis americana*) emerging from its sandy burrow along the sea bottom in Palm Beach County, Florida. This species is very common along the coast of the SFCZ and exhibits a docile behavior unless disturbed (Photograph taken by Chris Makowski)

The stinger on most pelagic stingrays is situated near the base of the tail (Tricas et al. 1997). This adaptation may have evolved to discourage predators from biting the animal near its vital organs. In contrast, the stinger of most bottom-dwelling stingrays is located further away from the body, making it a more effective and dangerous "striking" weapon (Flint and Sugrue 1999). However, it should be pointed out that the sting is purely a defensive weapon only and that the "striking" action is an involuntary response rather than a conscious "attack." Stingrays do not aggressively attack humans, though stings do normally occur if a ray is accidentally stepped on. As such, the stingray can easily become a hazard to seagoing bathers. It is recommended to avoid stepping on a stingray by shuffling one's feet while wading in the shallows. All efforts should be taken to avoid stepping on a stingray, as contact with the stinger causes local trauma (from the puncture itself), pain, swelling, muscle cramps from the venom, and later may result in a bacterial infection from the wound (Meyer 1997). The injury is very painful, but seldom life-threatening unless the stinger pierces a vital area on the body. To complicate matter, the stinger barb usually breaks off in the wound and surgery may be required to remove the fragments (Flint and Sugrue 1999).

1.2.8.5 Non-Native, Invasive Species

Due to its tropical and subtropical climate, the SFCZ has been colonized by many non-native, invasive species that can potentially pose a hazard to coastal populations. The term 'invasive species' has become a well-known phenomenon in south Florida, in part mainly because of dangerous invasives like the Burmese Python (*Python molurus*) in the Everglades (Snow et al. 2007). Burmese pythons, or *Python molurus bivittatus*, are very large snakes that kill their prey by asphyxiation, which is achieved through the constriction of their bodies (Mazzotti et al. 2011). To prevent their prey from escaping, the Burmese pythons use specially designed teeth to seize hold of its prey as it is killed. Afterwards, the prey is swallowed whole.

Burmese pythons are native of Southeast Asia but are now established in the Florida Everglades. The invasion comes via the pet trade industry where the snakes are purchased as pets only to be later released when it outgrows its owner (Snow et al. 2007). For example, small Burmese pythons will grow into snakes that have been recorded just shy of 10 m and weighing just over 180 kg (Mazzotti et al. 2011) (Fig. 1.15).

The impact of invasive species on their new environments in south Florida can be severe, as seen in this news article from *ScienceDaily* (USGS 2008):

> Biologists with Everglades National Park confirmed a breeding population of Burmese python in the Florida Everglades in 2003, presumably the result of released pets. Python populations have since been discovered in Big Cypress National Preserve to the north, Miami's water management areas to the northeast, Key Largo to the southeast, and many state parks, municipalities, and public and private lands in the region....
>
> ...Burmese pythons have been found to eat endangered Key Largo woodrats and rare round-tailed muskrats. "This makes it that much more difficult to recover these dwindling populations and restore the Everglades," said park biologist Skip Snow, "and all the more important that pet owners be responsible in their choice of pet and dispose of it properly should they need to. Releasing them into the environment is bad for that pet, bad for native species, and also illegal."

Similarly, the King Cobra (*Ophiophagus hannah*), the longest of the venomous land snakes, growing up 5.5 m in length, have also escaped into the wild in south Florida. The snake's venom is a neurotoxin that affects the central nervous system and the respiratory system and has been known to kill a human being in 15 min (Roy et al. 2010). The large Burmese constrictor and King Cobra are just two examples of many invasive species that have become established in the SFCZ via pet owners who release unwanted pets into non-native habitat.

The poisonous lionfish is another example of a non-native, invasive species in the SFCZ that has decimated fish populations along the Florida Reef Tract (FRT) (Ruiz-Carusa et al. 2006). Lionfish (*Pterois volitans*) (Fig. 1.16) are native to the Indo-Pacific Ocean and the Red Sea, however, in 1992, Hurricane Andrew smashed an aquarium tank in Florida and about a half-dozen spiny, venomous lionfish washed into the Atlantic Ocean, spawning an invasion that could kill off local industry along with the native fish (Courtenay 1995). If the FRT becomes depleted of other fish species because of the lionfish's appetite, the impact could be devastating to the region's economy, which relies heavily on commercial fishing and recreational diving.

Fig. 1.15 A 4.8-m long python with adult deer in its stomach. This snake was discovered by workers from the South Florida Water Management District. After the Burmese python was killed in the Florida Everglades National Park, a whole adult deer was found in its stomach. The reptile, one of the biggest ever found in South Florida, had a girth of 112 cm with the 92 kg deer inside its stomach. The python is an ambush predator that would have staked out a known deer trail, seized the animal in its sharp teeth, crushed it by constriction, and then eaten it (Photograph from Emma Reynolds, *Mail Online*, 29 October 2011)

The lionfish has no known predators and can produce approximately 30,000 eggs in a single spawning event, with a spawning frequency as often as every 4 days (Albins and Hixon 2008).

1.3 Discussion

Within the SACZ, with its subtropical climate and ocean beaches, is an attractive environment that invites tourists and entices newcomers to take up permanent residence. This developed shore region is known for its wide range of public

Fig. 1.16 A lionfish (*Pterois volitans*) swimming over the Florida Reef Tract in Palm Beach County, Florida. Once restricted to the native to the Indo-Pacific Ocean and the Red Sea, the lionfish has invaded the offshore waters of the SFCZ. Note the venomous pectoral spines, which are used to prey upon all native reef fish species (Photograph by Chris Makowski)

amenities and ease of access by air, ship, or car. The increase in population is anticipated to continue and as numbers of people multiply, so does the potential risk of being impacted by any number of the coastal hazards enumerated here. For tourists and residents alike, Atlantic shores provide a source of recreational activities that put people on the beach and/or in the water. Whether in the high hazard beach-coastal ocean zone or just quietly living a few kilometers inland in a house or condominium, some hazards such as storms (e.g. northeasters, tropical storms, hurricanes) are nearly unavoidable. Hazards associated with these high-energy meteohydrological events include coastal and inland flooding, water and wind damage, and shore erosion. Even though not everyone is directly impacted by these or subsequent ancillary events, they are nevertheless inconvenienced by the loss of amenities and provisions, such as electrical power, water supply, short supply of gasoline, closed shops and grocery stores, and so on. Nevertheless, these overarching impacts may be nothing more than slight annoyances compared to some of the other insidious coastal hazards that generally go unnoticed until too

late. In western Broward County, for example, groundwater seepage under the Everglades dikes into urban areas must be controlled by continuous pumping that requires an uninterrupted electrical supply. Many pumps have auxiliary generators that kick in should supply from the grid be interrupted, but fuel is limited by tank size at each pump station.

Even if residents are not directly impacted by a major coastal hazard and are fortunate enough to escape home or property damage by storms, they are inevitably impacted by increased rates on homeowners insurance that apply to everyone in the area. In addition to economic impacts, there are socioeconomic impacts where some homeowners just pack up and leave their homestead as they can't cope with the aftermath of flooding or water-wind damage. Due to the fact that homeowners insurance may not cover the cost of repairs, adequate financial reserves are not present to cover the necessary costs for repair, personal loans are unobtainable, and federal assistance may not be available in a timely manner (if at all), homeowners have no choice but to vacate and leave the neighborhood permanently. The increase of empty, partially destroyed homes in a neighborhood drastically decreases home values for remaining residents and are a blight in the community. These downstream hazards, which are unfortunately disregarded by most people, are very real and can be quite devastating. These situations are usually limited to large storm and flooding events, and fortunately are not frequent.

Hazardous events that occur more frequently are those that are normally not regarded as a coastal hazard at all because they are not on most people's radar or consciousness. These may include slow erosion rates over many years, the submarine nutrient loading of the nearshore waters, or personal encounters with hazardous wildlife that may be either native or invasive. Even though most discussions of coastal hazards focus on storms, shore erosion, flooding, and inundation by sea-level rise, these topics are the subject of hyperbole and have been elucidated for many coastal zones around the world.

What is not so well-known nor discussed within the traditional framework of coastal hazards are dangers that are more or less invisible or unseen. For example, biological coastal hazards are sometimes passed over as 'true' coastal hazards, but due to the possible threat they pose to humans, the designation is warranted.

Another biological hazard arises from the careless or irresponsible dumping of non-native, invasive animals into the urban coastal community or on the fringes of development. The main problem in the SFCZ, and in many similar types of subtropical coastal environments around the world, is that non-native invasive often have no local predators and as a result take over many native niches. The Florida Everglades provides an ideal habitat for many invasive species that are released by pet owners. It is difficult to list all the disastrous consequences within the SFCZ from releases or deliberate introductions of non-native species to control some perceived unwanted condition in the natural environment. Examples of such include the water hyacinth (*Eichornia crassipes*), Brazilian pepper (*Schinus terebinthifolius*), fire ant (*Solenopsis invicta*), and cane toad (*Bufo marinus*) from South America, the spectacled Caiman (*Caiman crocodilius*) from Central America, the broadleaf paperbark tree (*Melaleuca quinquenervia*) and pine tree

(*Casuarina equisetifolia*) from Australia, hydrilla (*Hydrilla verticillata*) from India, and the swamp eel (*Monopterus albus*) from southern Asia. These introductions to the SFCZ have become major pests and control/eradication can prove to be very costly and time consuming. Perhaps more disturbing is the accidental release of very dangerous reptiles, as occurred during Hurricane Andrew within the Miami area in 1992, or their deliberate release when they become too much for the pet owner to handle. It seems clear that it will not be possible to eradicate all of the pythons and cobras that are now free in the Everglades. It is just a matter of time until they become so numerous that they begin to invade the metro coastal area. The consequences of their expanding range are obvious and pose a type of coastal hazard that was needlessly created.

Whether from an anthropogenic, natural, or biological point source, impacts from coastal hazards continue to threaten coastal communities in the SFCZ and hinder the notion that this area of the country is a desirable place to live, work, and visit. Once the seed has been planted in people's minds that a coastal region is inhospitable, then indirect impacts of coastal hazards, such as tourism loss and/or housing market degradation, begin to present themselves. That is why it is in the best interest of the State of Florida, as well as nations throughout the world, to accurately identify and assess all coastal hazards as a cascade of natural, biological, and human-induced hazards that collectively contribute to threaten their coastal communities. By doing so, better coastal hazard mitigation techniques will develop and allow communities that are within close proximity to the coast to initiate an effective disaster resilience and adequately protect themselves against the horrific impacts that could ensue.

1.4 Conclusion

Coastal hazards in the South Atlantic Coastal Zone (SACZ), and more specifically within the SFCZ, have traditionally been studied in terms of coastal erosion and sedimentation, flooding, and the unwanted impacts of remediation efforts as associated with the construction of hard engineering structures, for example. The SACZ is home to all of these hazards and risks, which accrue as coastal populations increase to the point where densities surpass the carrying capacity of the coastal marine environment. The point is not that sustainability is or can be achieved at some future point in time but rather that urban growth has already exceeded the natural limits of what the coastal marine environment can support. What is now seen is the continued gradual degradation of natural resources to the point where it is impossible to even maintain the status quo, which may provide the catalyst for community crash. Further impacts come from the introduction of exotic species that pose threats to native species and to humans when they come into contact. Many ecosystems in southern Florida are oligotrophic (e.g. Everglades, coral reefs) and the introduction of nutrient-laden water rich in nitrogen and phosphorus encourages the growth algae, sea lice, and other organisms that can be hazardous

(or at least very irritating) to the environment and humans. It is thus noted that increasing population densities in sensitive coastal marine environments foster a cascading effect of risks and hazards that pile on top of one another. Residents and tourists alike thus need to be aware of the cadre of risks that they are exposed to by virtue of being present. Increased awareness and a higher level of consciousness are new requirements for those who now venture into the shark-attack and rip-current capital of the world. These newsworthy hazards are often in the medias limelight but it is the unseen and generally unappreciated hazards that can do the most damage or harm to the environment and ultimately to humans themselves over time.

The identification and review of coastal hazards within the southeast Florida coastal zone is a necessary undertaking in the development of a comprehensive strategic coastal disaster plan, as this region is subject to many coastal hazards that are also seen elsewhere throughout the world. By doing so, the goal of educating coastal managers and private citizens on how to strengthen their infrastructure, protect themselves, and improve risk-assessment preparation practices can be achieved. Through the analysis of substantial coastal hazard causes and effects, disaster resilience within southeast Florida will allow for a stronger, safer, and better protected coastal area.

Acknowledgments Heather Vollmer (Coastal Education & Research Foundation, Florida Atlantic University, Boca Raton, Florida) is thanked for preparation of the location diagram. Allan Williams and Mike Phillips (Coastal and Marine Research Group, Swansea Metropolitan University, Swansea, Wales, UK), are thanked for review of the paper and for helpful suggestions for improvement.

References

Abramson A (2010) South Florida rapid growth to return. Palm Beach Post Wednesday, 3 March (Online version)

Albins MA, Hixon MA (2008) Invasive Indo-Pacific lionfish Pterois volitans reduce recruitment of Atlantic coral-reef fishes. Mar Ecol Prog Ser 367:233–238

Allen TB (1999) The shark almanac. Lyons Press, New York, 274 p

Allison RV (1950) The importance of trace elements in Florida agriculture. Soil Sci Soc Fla Proc 11:100–109

Banks KW, Dodge RE, Fisher L, Stout D, Jaap W (1998) Florida coral reef damage from nuclear submarine grounding and proposed restoration. J Coast Res SI(26):64–71

Bernd-Cohen T, Gordon M (1999) State coastal program effectiveness in protecting natural beaches, dunes, bluffs, and rock shores. Coast Manage 27:187–217

Bierman N (2000) Sewage may spoil Miami Beach's holiday. Palm Beach Post, Thursday, 29 June, 1B and 12A (continued)

Blake NM (1980) Land into water – water into land. A history of water management in Florida. University Presses of Florida, Tallahassee

Brander R (2010) Dr. Rip's essential beach book: everything you need to know about surf, sand and rips. University of New South Wales Press, Sydney, 249 p

Bravo S (2003) Sea lice in Chilean salmon farms. Bull Eur Assoc Fish Pathol 23:197–200

Bruun P (1986) Morphological and navigational aspects of tidal inlets on littoral shores. J Coast Res 2(2):123–145

Bruun P (1995) The development of downdrift erosion. J Coast Res 11(4):1242–1257
Bruun P (2005) Bypassing at littoral drift barriers. In: Schwartz ML (ed) Encyclopedia of coastal science. Springer, Dordrecht, pp 210–215
Budker P (1971) The life of sharks. Columbia University Press, New York, 222 p
Bush D, Neal WJ, Longo NJ, Lindeman KC, Pilkey DF, Esteves LS, Congleton JD, Pilkey OH (2004) Living with Florida's Atlantic beaches: coastal hazards from Amelia Island to Key West. Duke University Press, Durham, 338 p
Caccia VG, Boyer JN (2007) A nutrient loading budget for Biscayne Bay, Florida. Mar Pollut Bull 54(7):994–1008
Cançado JED, Saldiva PHN, Pereira LAA, Lara LBLS, Artaxo P, Luiz A, Martinelli LA, Arbex MA, Zanobetti A, Alfesio LF, Braga ALF (2006) The impact of sugar cane–burning emissions on the respiratory system of children and the elderly. Environ Health Perspect 114(5):725–729
Carr-Betts E, Beck TM, Kraus NC (2012) Tidal inlet morphology classification and empirical determination of seaward and down-drift extents of tidal inlets. J Coast Res 28(3):547–556
Coch NK (2012) Anthropogenic Amplification of Storm Surge Damage in the 1935 "Labor Day" Hurricane. In: Finkl, C.W. (ed.), Coastal Hazards. Dordrecht, The Netherlands: Springer
Collier C, Dodge RE, Gilliam D, Gracie K, Gregg L, Jaap W, Mastry M, Poulos N (2007) Rapid response and restoration for coral reef injuries in southeast Florida: guidelines and recommendations. The Southeast Florida Coral Reef Initiative (SEFCRI), Dania, Submitted to Florida Department of Environmental Protection, 61 p
Cook CB, Mueller EM, Ferrier MD, Annis E (2002) The influence of nearshore waters on corals of the Florida Reef Tract. In: Porter JW, Porter KW (eds) The everglades, Florida Bay, and coral reefs of the Florida Keys: an ecosystem source book. CRC Press, Boca Raton, pp 771–788
Cooper RM, Lane J (1987) An atlas of eastern Broward county surface water management basins, Technical Memorandum. South Florida Water Management District, West Palm Beach
Cooper JAG, Pilkey OH (2012) Pitfalls of coastal engineering. Springer, Dordrecht, 333 p
Corcoran W, Johnson E (2005) Climate of North America. In: Oliver JE (ed) Encyclopedia of earth sciences series: encyclopedia of world climatology. Springer, Dordrecht, pp 525–535
Courtenay WR Jr (1995) Marine fish introductions in southeastern Florida. Introduced Fish Sect Newslett 14(1):2–3
Cox S, Lewis D, McCollum S, Bledsol M, Marrotte R (1988) Subsidence study of the everglades agricultural area. U.S. Department of Agriculture, Soil Conservation Service, Greenacres, 25 p
Darley EF, Lerman SL (1975) Air pollutant emissions from burning sugar cane and pineapple residues from Hawaii. EPA Office Air Quality Planning and Standards, Washington, DC, EPA-450/3-75-071
Davis RA Jr, FitzGerald DM (2004) Beaches and coasts. Blackwell, Malden, 419 p
Dean RG (1990) Channel entrances: impacts on coastal erosion. In: Proceedings of the 53rd meeting of the coastal engineering research board, 5–7 June 1990, Fort Lauderdale/Dania, Florida. CERC Final Report, Vicksburg, Mississippi, pp 51–53
Dean RG, Dalrymple RA (2004) Coastal processes with engineering applications. UK Cambridge University Press, Cambridge, 488 p
Dean RG, O'Brien MP (1987) Florida's East Coast inlets – shoreline effects and recommended action. Coastal and Oceanographic Engineering Department, University of Florida, Gainesville, UFL/COEL-87/017, 65 p
Dean RG, Work PA (1993) Interaction of navigation entrances with adjacent shorelines. J Coast Res 18:91–110
Dodge RE, Logan A, Antomus AA (1982) Quantitative reef assessment methods and preliminary results. Bull Mar Sci 32:745–760
Douglas BD, Walther MP (1994) Odd/even analysis modified to account for sediment losses to ebb and flood shoals. In: Proceedings 1994 national beach preservation conference (Florida Shore and Beach Preservation association), pp 354–373
Duever MJ, Meeder JF, Meeder LC, McCollom JM (1994) The climate of south Florida and its role in shaping the Everglades ecosystem. In: Davis SM, Ogden JC (eds) Everglades: the ecosystem and its restoration. St. Lucie Press, Delray Beach, pp 225–248

EPA (Environmental Protection Agency) (2003) Relative risk assessment of management options for treated wastewater in South Florida. EPA, Office of Water (4606 M), Washington, DC, EPA 816-R-03-010, v p. (www.epa.gov/safewater)
Esteves LS, Finkl CW (1998) The problem of critically eroded areas (CEA): an evaluation of Florida beaches. J Coast Res Spec Issue 26:11–18
Fairbridge RW (1989) Crescendo events in sea-level rise. J Coast Res 5(1):ii–vi
FDEP (Florida Department of Environmental Protection) (1999) Miami-Dade Water and Sewer Department, North District wastewater treatment plant application to construct/operate/abandon class I, III, or V Injection Well System, Class I Injection Well Operation Permit for Injection Well No. IW-2 N
Fenneman NM (1938) Physiography of the Eastern United States. McGraw-Hill, New York, 691 p
Finkl CW (1983) Environmental hazards and mitigation in the U.S. middle Atlantic coastal zone. Northeast Environ Sci 2(2):90–101
Finkl CW (1993) Preemptive strategies for enhanced sand bypassing and beach replenishment activities: a geological perspective. In: Mehta A (ed) Conference on beach–inlet interactions, Jacksonville, Florida, 1992. J Coast Res SI(18):59–89
Finkl CW (1994a) Disaster mitigation in the South Atlantic Coastal Zone (SACZ): a prodrome for mapping hazards and coastal land systems using the example of urban subtropical southeastern Florida. J Coast Res SI(12):339–366
Finkl CW (1994b) Tidal inlets in Florida: their morphodynamics and role in coastal sand management. In: Viggósson G (ed) Proceedings of the Hornafjördur international symposium, Höfn, Iceland, pp 67–85
Finkl CW (1995) Water resources management in the Florida Everglades: Are 'lessons from experience' a prognosis for conservation in the future? J Soil Water Conserv 50(6):592–600
Finkl CW (1997) The coastal zone as new battlespace from the purview of an academic graduate program in environmental science. In: Miller MC, Cogan J (eds) conference proceedings coastal zone 97, vol II, pp 584–586
Finkl CW (2000) Identification of unseen flood hazard impacts in southeast Florida through integration of remote sensing and geographic information system techniques. Environ Geosci 7(3):119–136
Finkl CW, Charlier RH (2003) Sustainability of subtropical coastal zones in southeastern Florida: challenges for urbanized coastal environments threatened by development, pollution, water supply, and storm hazards. In: Proceedings of the black sea seminar, Mamaia-Constantza, Romania, 25–28 Sept 2002 (Sponsored by UNESCO, International Commission on the Oceans, International Oceanographic Institute). J Coast Res 19(4):934–943
Finkl CW, Charlier RH (2005) Threatened urbanized coastal environments in southeastern Florida. Proc 2nd Int Congr "Seas Oceans 2005" 2(14):71–81
Finkl CW, Kruempel C (2005) Threats, obstacles and barriers to coastal environmental conservation: societal perceptions and managerial positionalities that defeat sustainable development. In: Gomes FV, Pinto FT, Neves L, Sena A, Ferreira O (eds) Proceedings of the first international conference on coastal conservation and management in the Atlantic and Mediterranean, Algarve, Portugal, 17–20 April 2005, pp 3–28
Finkl CW, Krupa S (2003) Environmental impacts of coastal-plain activities on sandy beach systems: hazards, perception, and mitigation. In: Klein AHF, Finkl CW, Rörig LR, Santana GG, Diehl FL, Calliari LJ (eds) Proceedings of Brazilian Sandy beaches symposium: morphodynamics, ecology, use, hazards and management. J Coast Res SI 35:132–150
Finkl CW, Myers SD (1996) Delineation of potential Inland flooding from extreme rainfal events in Broward County, Florida: a flood study. Coastal Education & Research Foundation, Fort Lauderdale, variable pagination (Submitted to Office of Environmental Services, Broward County Water Management Division)
Finkl CW, Restrepo-Coupe N (2007) Potential natural environments based on pedological properties in the coastal conurbation of subtropical southeast Florida. J Coast Res 23 (2):317–349

Finkl CW, Charlier RH, Krupa SL (2005a) Vulnerability of coastal environments to land use and abuse: the example of southeast Florida. Int J Environ Stud 62(5):535–554
Finkl CW, Krupa S, Giddings JB (2005b) Regional surface flows to tide and submarine groundwater discharges along the inner continental of SE Florida. 1st SEPM congress on sedimentary geology, St. Petersburg, vol 1, p 54
Flesher D (2004) Grounded ship off Fort Lauderdale beach may have damaged reef. Sun Sentinel 12 Oct 2004. Retrieved from http://www.nova.edu/ocean/pescadores.htm
Flint D, Sugrue W (1999) Stingray injuries: a lesson in debridement. N Z Med J 112(1086):137–138
Freudenthal AR, Joseph PR (1993) Seabather's eruption. N Eng J Med 329(8):542–544
Gaiser E (2008) Periphyton as an indicator of restoration in the Everglades. Ecol Indic 9(6 suppl 1): S37–S45
Galgano FA (2009) Beach erosion adjacent to stabilized microtidal inlets. Middle State Geogr 42:18–32
Gensini VA, Ashley WS (2010) An examination of rip current fatalities in the United States. Nat Hazard 54:159–175
Gowell ET (1993) Sea jellies: rainbows in the sea. Franklin Watts, New York, 57 p
Haunert D, Startzman R (1985) Short term effects of a freshwater discharge on the biota of St. Lucie Estuary, Florida. Technical Communication 8772. South Florida Water Management District, West Palm Beach, Florida
Hebert PJ, Jarrell JD, Mayfield M (1996) The deadliest, costliest, and most intense United States hurricanes of this century (and other frequently requested facts). NOAA Technical Memorandum NWS TPC-1. National Hurricane Center, Miami, Florida, 30 p
Houston JR (2002) The economic value of beaches: a 2002 update. Shore Beach 70(1):9–12
Hu C, Muller-Karger FE, Vargo GA, Neely MB, Johns E (2004) Linkages between coastal runoff and the Florida Keys ecosystem: a study of a dark plume event. Geophys Res Lett 31:1–4
Inman DL, Nordstrom CE (1978) On the tectonic and morphologic classification of coasts. J Geol 79:1–21
International Shark Attack File (ISAF) (2011) 1882–2010 map of Florida's confirmed unprovoked shark attacks. Retrieved from http://www.flmnh.ufl.edu/fish/sharks/statistics/gattack/mapfl.htm
Kennish MJ (2002) Environmental threats and environmental future of estuaries. Environ Conserv 29(1):78–107
Klee G (1998) The coastal environment: toward integrated coastal and marine sanctuary management. Prentice Hall, Upper Saddle River, 281 p
Komar PD (1996) Tidal inlet processes and morphology related to the transport of sediments. J Coast Res 23:23–44
Komar PD (1997) Beach processes and sedimentation. Prentice Hall, Upper Saddle River, 544 p
Kraus NC (2005) Coastal inlet function design: anticipating morphologic response. In: Proceedings coastal dynamics 05 (ASCE), pp 1–13
Kraus NC, Galgano FA (2001) Beach erosional hot spots: types, causes, and solutions. ERDC/CHL CHETN-II-44. Vicksburg, Mississippi, 17 p
Krupa SL, Gefvert CJ (2005) Submarine groundwater discharge. In: Schwartz ML (ed) The encyclopedia of coastal science. Kluwer, Dordrecht, pp 915–992
Lapointe BE (1997) Nutrient thresholds for bottom-up control of macroalgal blooms on coral reefs in Jamaica and southeast Florida. Limnol Oceanogr 42(5):1119–1131
Lapointe BE, Hanisak MD (1997) Algal blooms in coastal waters: eutrophication on coral reefs of southeast Florida. Harbor Branch Oceanographic Institute, Fort Pierce, FL, USA. Final Report—Florida Sea Grant Project R/C-E-34
Lapointe BE, O'Connell JE, Garrett GS (1990) Nutrient couplings between on-site sewage disposal systems, groundwaters, and nearshore surface waters of the Florida Keys. Biogeochemistry 10:289–307
Lapointe BE, Barile PJ, Littler MM, Littler DS, Bedford BJ, Gasque C (2005a) Macroalgal blooms on southeast Florida coral reefs I. Nutrient stoichiometry of the invasive green alga codium isthmocladum in the wider Caribbean indicates nutrient enrichment. Harmful Algae 4:1092–1105

Lapointe BE, Barile PJ, Littler MM, Littler DS (2005b) Macroalgal blooms on southeast Florida coral reefs II. Cross-shelf discrimination of nitrogen sources indicates widespread assimilation of sewage nitrogen. Harmful Algae 4:1106–1122

Leatherman S (2011) Rip currents: terminology and pro-active beach safety. In: Leatherman S, Fletemeyer J (eds) Rip currents: beach safety, physical oceanography, and wave modeling. CRC Press, Boca Raton, pp 259–271

Lodge TE (2005) The everglades handbook: understanding the ecosystem. CRC Press, Boca Raton, 422 p

Luscombe R (2008) Surge in fatal shark attacks blamed on global warming. The Observer, 3 May 2008. http://www.guardian.co.uk/environment/2008/may/04/wildlife.climatechange

Lushine JB (1991) A study of rip current drownings and weather related factors. Natl Weather Dig 16:13–19

MacMahan JH, Thornton EB, Reniers AJHM (2006) Rip current review. Coast Eng 53 (2–3):191–208

Maynard T (2011) The Herbert Hoover dike: a discussion of the vulnerability of lake Okeechobee to Levee failure; cause, effect and the future. Lloyd's Emerging Risks Team, Lloyd's Franchise Performance Directorate (FPD), London, 21 p

Mazzotti FJ, Cherkiss MS, Hart KM, Snow RW, Rochford MR, Dorcas ME, Reed RN (2011) Cold-induced mortality of invasive Burmese pythons in south Florida. Biol Invasions 13:143–151

McKnight TL, Hess D (2000) Physical geography: a landscape appreciation. Prentice Hall, Upper Saddle River, pp 200–201

McPherson BF, Halley R (1997) The South Florida environment: a region under stress. U.S. Geological Survey, National Water Quality Assessment Program, Denver, Colorado, USGS Circular 1134, 61 p

Mehta AJ (1996) A perspective on process related research needs for sandy inlets. J Coast Res SI23:3–21

Mehta AJ, Delcharco MJ, Hayter EJ (1991) Tidal inlet management at jupiter inlet: fifth progress report. UFL/COEL-91.012. University of Florida, Coastal and Oceanographic Engineering Department, Gainesville, Florida, 77 p

Meyer P (1997) Stingray injuries. Wilderness Environ Med 8(1):24–28

Monty JA, Gilliam DS, Banks KW, Stout DK, Dodge RE (2006) Coral of opportunity survivorship and the use of coral nurseries in coral reef restoration. In: Proceedings of the 10th international coral reef symposium, Okinawa, Japan, pp 1665–1673

Myers RL, Ewel JJ (eds) (1990) Ecosystems of Florida. University of Central Florida, Orlando, 765p

Nelson JS (2006) Fishes of the world. Wiley, New York, pp 76–82

NOAA (National Oceanic and Atmospheric Administration) (2006) Continental Shelf break: Continental Shelf Boundary for the Southeast U.S. – 1998, NOAA Coastal Services Center. Coastal Zone: Coastal Zone Management Act, Department of commerce (DOC), National Oceanic and Atmospheric Administration (NOAA), National Ocean Service (NOS), Coastal Services Center (CSC), published: 24 May 2006

NRC (National Research Council) (2000) Clean coastal waters: understanding and reducing the effects of nutrient pollution. National Academy Press, Washington, DC,411 p

Oey L-Y, Ezer T, Wang D-P, Fan S-J, Yin X-Q (2006) Loop current warming by hurricane Wilma. Geophys Res Lett 33(L08613), 4 p

OnBoard LLC (2007) http://www.onboardinformatics.com/. Accessed 29 Jan 2012

Pasch RJ, Blake ES, Cobb HD III, Roberts DP (2006) Hurricane Wilma tropical cyclone report. Technical report. National Hurricane Center, Miami, Florida

Pfost R (2003) Reassessing the impact of two historical Florida hurricanes. Bull Am Meteorol Soc Oct, pp 1367–1372

Pilkey OH, Sharma DC, Wanless HP, Doyle LJ, Neal WJ (1985) Living with the east Florida shore. Duke University Press, Durham, 274 p

Precht WF, Miller SL (2007) Ecological shifts along the Florida reef tract. In: Geological approaches to coral reef ecology. Springer, New York, pp 237–312
Rappaport E (1993) Hurricane Andrew preliminary report. National Hurricane Center, Miami
Reddy KR, Delaune R (2008) Biogeochemistry of wetlands: science and applications. CRC Press, Boca Raton
Regenold S (2008) North America's top shark-attack beaches. USA Today 21 Mar 2008. (http://www.usatoday.com/travel/news/2008-04-18-shark-beaches-forbes_N.htm)
Roy A, Zhou X, Chong MZ, D'hoedt D, Foo CS, Rajagopalan N, Nirthanan S, Bertrand D, Sivaraman J, Kini RM (2010) Structural and functional characterization of a novel homodimeric three-finger neurotoxin from the venom of *Ophiophagus hannah* (King Cobra). J Biol Chem 285(11):8302–8315
Rubin ET, Moulding AL, Lopez JV, Gilliam DS, Kosmynin VN, Dodge RE (2008) Scleractinian coral recruitment to reefs physically damaged by ship groundings. In: Proceedings of the 11th international coral reef symposium, Fort Lauderdale, Florida, 7–11 July 2008, pp 326–330
Ruiz-Carusa R, Matheson RE Jr, Roberts DE Jr, Whitfield PE (2006) The western Pacific red lionfish, *Pterois volitans* (Scorpaenidae), in Florida: evidence for reproduction and parasitism in the first exotic marine fish established in state waters. Biol Conserv 128:384–390
Scheffers A, Zhao JX, Yu K (2012) Hurricanes and Tropical Storms. In: Finkl, C.W. (ed.), Coastal Hazards. Dordrecht, The Netherlands: Springer.
SFWMD (South Florida Water Management District) (1982) Report on tropical storm Dennis: 16–18 August 1981. RP 988. South Florida Water Management District, West Palm Beach, 59 p
SFWMD (1993) Draft working document in support of the lower east coast regional water supply plan. South Florida Water Management District, West Palm Beach
Sharth S (2002) Sea jellies: from corals to jellyfish. Franklin Watts, New York
Smith ER (1988) Case histories of corps breakwater and jetty structures, report number 5, U.S. Army Corps of Engineers Waterways Experimental Station, North Atlantic Division. Vicksburg, Mississippi, CERC Technical Report REMR-CO-3, 113 p
Snow RW, Krysko KL, Enge KM, Oberhofer L, Warren-Bradley A, Wilkins L (2007) Introduced populations of Boa constrictor (Boidae) and *Python molurus bivittatus* (Pythonidae) in southern Florida. In: Henderson RW, Powell R (eds) The biology of boas and pythons. Eagle Mountain Publishing, Eagle Mountain, pp 416–438
Sonenshein RS (1995) Delineation of saltwater intrusion in the Biscayne aquifer. Water-Resources Investigations Report 96–4285. U.S. Geological Survey, Eastern Dade County
Sonu CJ (1972) Field observation of nearshore circulation and meandering currents. J Geophys Res 77:3232–3247
Stephens JC (1984) Subsidence of organic soils in the Florida Everglades – a review and update. In: Gleason PJ (ed) Environments of south Florida: present and past II. Miami Geological Society, Coral Gables, pp 375–384
Stephens JC, Allen LH Jr, Chen E (1984) Organic soil subsidence. Geol Soc Am Rev Eng Geol 4:107–122
Stevens JC, Johnson L (1951) Subsidence of organic soils in the upper Everglades region of Florida. Soil Sci Soc Fla Proc 11:191–237
Stone GW, Finkl CW (eds) (1995) The impacts of hurricane Andrew on the coastal zones of Florida and Louisiana: 22–25 August 1992. Coastal Education & Research Foundation, Charlottesville, 364 p
Strowd T (2011) Broward county East Coast Protective Levee technical evaluation. South Florida Water Management District, West Palm Beach, Florida, Project and Lands Committee Meeting (12 Jan 2011), PowerPoint presentation. http://xportal.sfwmd.gov/paa_dad/docs/F7257/PL6%20Broward%20County%20East%20Coast%20Protective%20Levee%20-%20T%20Strowd.pdf. Accessed 20 Oct 2011
Synder GH (2004) Everglades agricultural area soil subsidence and land use projections. University of Florida/Everglades Research and Education Center, Gainesville, 26 p
Szmant AM (2002) Nutrient enrichment on coral reefs: is it a major cause of coral reef decline? Estuaries 25(4b):743–766

Tate RL III, Terry RE (1980) Variation in microbial activity in Histosols and its relationship to soil moisture. Appl Environ Microbiol 40(2):313–317

Tomchik RS, Russell MT, Szmant AM, Black NA (1993) Clinical perspectives on seabather's eruption, also known as 'sea lice'. J Am Med Assoc 269(13):1669–1672

Tricas TC, Deacon K, Last P, McCosker JE, Walker TI, Taylor L (1997) Sharks and rays. Weldon Owen, Sydney, 288 p

Trimble P (1990) Frequency analysis of one and three-day rainfall maxima for central and Southern Florida. Technical Memorandum. South Florida Water Management District, West Palm Beach, 23 p

United States Census (2000) U.S. Gazetteer files: counties. Retrieved 13 Feb 2011 http://www.census.gov/census2000/states/us.html

Uriarte M, Yackulic CB, Cooper T, Flynn D, Cortes M, Crk T, Cullman G, McGinty M, Sircely J (2009) Expansion of sugarcane production in Sao Paulo, Brazil: Implications for fire occurrence and respiratory health. Agric Ecosyst Environ 132(1–2):48–56

USGS (United States Geological Survey) (2008) Python snakes, an invasive species in Florida, could spread to one third of US. ScienceDaily, extracted from the internet on 2 Jan 2012

Wakimoto RM, Black PG (1994) Damage survey of Hurricane Andrew and its relationship to the eyewall. Bull Am Meteorol Soc 75(2):189–202

Walton TL (1978) Coastal erosion – some causes and some consequences. Mar Technol J 12 (4):28–33

Weston J, Colin SP, Costello JH, Abbott E (2009) Changing form and function during development in rowing hydromedusae. Mar Ecol Prog Ser 374: 127–134

White WA (1970) The geomorphology of the Florida Peninsula, Geological bulletin 51. Florida Bureau of Geology, Tallahassee, 164 p

Zebrowski E, Howard JA (2007) Category 5: the story of Camille, lessons unlearned from America's most violent hurricane. University of Michigan Press, Ann Arbor, 276 p

Part II
Remote Sensing of Coastal Hazards (Platforms, Methods, and Procedures)

Chapter 2
Remote Sensing of Coastal Hazards

Victor V. Klemas

Abstract With the coastal population increasing, storms have been inflicting unprecedented losses on coastal communities. Coastal agencies require advance information on the predicted path, intensity and progress of a storm and associated waves and storm surges; near-real-time information during the peak of the storm to monitor flooding and control rescue operations; and post-storm reports to assess the damage and plan the recovery. The same holds true for other disasters, such as oil spills and algal blooms. Coastal communities are also facing a rising sea level, caused mainly by global warming. Airborne and satellite remote sensors, such as multispectral imagers, Lidar and radar, are now able to provide most of the information required for emergency response and coastal management.

2.1 Introduction

More than half of the U.S. population lives in the coastal zone. With events such as the hurricanes of 2004 and 2005, annual losses to coastal communities can total billions of dollars. Environmental impacts from coastal storms include beach erosion, wetland destruction, excessive nutrient loading, algal blooms, hypoxia and anoxia, fish kills, large scale releases of pollutants and debris, and spread of pathogens.

Over the long term, coastal communities are also facing a rising sea level. The sea level is rising because water expands as it is warmed and because water from melting glaciers and ice sheets is added to the oceans. The substantial sea level rise and more frequent storms predicted for the next 50–100 years will affect coastal towns and roads, coastal economic development, beach erosion control strategies,

V.V. Klemas (✉)
School of Marine Science and Policy, University of Delaware, Newark, DE 19716, USA
e-mail: klemas@udel.edu

C.W. Finkl (ed.), *Coastal Hazards*, Coastal Research Library 6,
DOI 10.1007/978-94-007-5234-4_2,

salinity of estuaries and aquifers, coastal drainage and sewage systems, and coastal wetlands and coral reefs (Gesch 2009; IPCC 2007; NOAA 1999).

Because the coastal population continues to increase and road improvements have not kept up with this rapid population growth, more time is needed to carry out an evacuation. As a result, coastal and emergency managers need advance information on the predicted path, intensity and progress of a storm and associated waves and storm surge, near-real-time information during the peak of the storm to monitor flooding and control rescue operations, and post-storm reports to assess the damage, plan urban recovery, restore power lines and roads, and to improve levees and drainage canals (NASA 2005; NASA/GSFC 2010).

Airborne and satellite remote sensors are providing the required information together with observers in aircraft and on the ground. During Hurricane Katrina in 2005, remote sensing played a major role in tracking the storm and the devastation it left behind in urban New Orleans and surrounding wetlands (Hayes 2005; Klemas 2009; Rykhus 2005; Stone and Muller 2005). For instance, airborne Lidar data sets were used to perform a regional storm tide inundation analysis of Hurricane Katrina (Stoker et al. 2009).

Detailed technical descriptions of satellite and airborne remote sensing systems and their capabilities are contained in various other publications (Jensen 2007; Martin 2004; Purkis and Klemas 2011; Robinson 2004). The objective of this article is to review practical applications of remote sensing for monitoring coastal hazards, including storms, algal blooms, oil spills, and mapping their environmental impacts.

2.2 Monitoring Storm Surge and Flooding

One important model used by the National Oceanic and Atmospheric Administration (NOAA) National Hurricane Center to estimate storm surge heights and winds resulting from hurricanes is the SLOSH (Sea, Lake, and Overland Surges from Hurricanes) model. It takes into account the pressure, size, forward speed, track, and winds of a hurricane. SLOSH is used to evaluate the threat from storm surges, and emergency managers use these data to determine which areas must be evacuated. SLOSH model results are combined with road network and traffic flow information, rainfall amounts, river flow, and wind-driven waves to identify at-risk areas (NOAA/CSC 2008).

If the SLOSH model is used to estimate storm surge for an actual, predicted hurricane, forecast data must be put into the model every 6 h over a 72-h period and updated as new data become available (NOAA/NHC 2008). This is achieved to a large extent with the use of remotely sensed data. The remote sensing systems used to provide near–realtime data for the models, include geostationary satellites (GOES), which sit above a fixed point on the equator at an altitude of 36,000 km and can provide estimates of the location, size, and intensity of a storm with their visible and thermal infrared imagers over large areas at a spatial resolution of 4 km

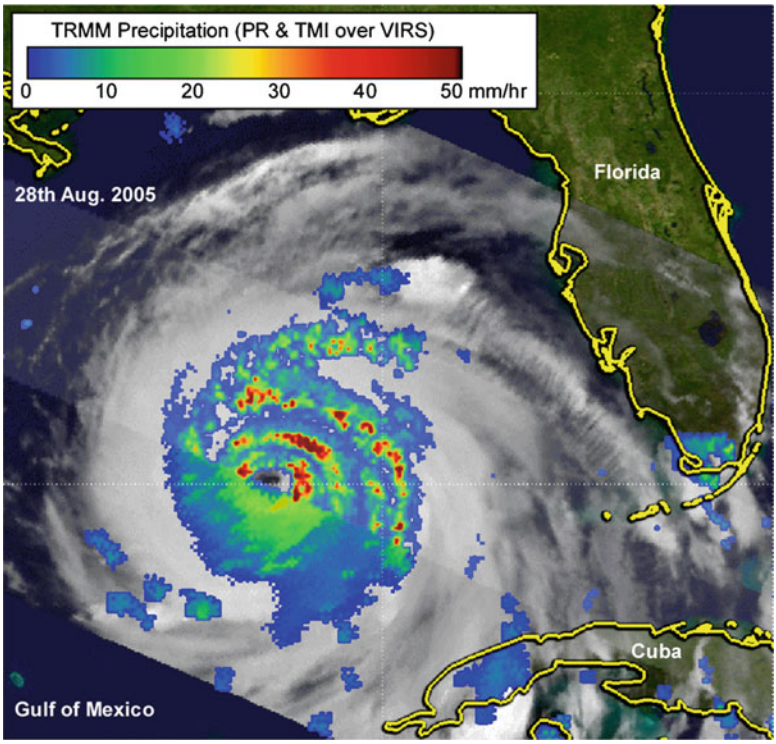

Fig. 2.1 Satellite image of Hurricane Katrina as it passes over the Gulf of Mexico. The image was taken on August 28, 2005, when Katrina had sustained winds of 185 km/h and was becoming a Category 4 hurricane in the central Gulf of Mexico (Credits: NASA 2005)

(NOAA 2006). In the visible region, clouds appear white because they scatter and reflect the sunlight. In thermal infrared images, clouds appear in varying shades of grey, depending on their temperature, which is determined by their height above the Earth. Because geostationary satellites permanently view the same part of the globe, they can provide this information at very frequent intervals (*e.g.,* every 15 min). These images can be supplemented by daily passes of the polar-orbiting NOAA Advanced Very High Resolution Radiometer (AVHRR) sensor, providing a resolution of 1.1 km.

Figure 2.1 shows a satellite image of Hurricane Katrina as it passes over the Gulf of Mexico. The image was enhanced with the use of data from several sensors, including the Tropical Rainfall Measurement Mission (TRMM) satellite and its microwave imager (TMI). By measuring the microwave energy emitted by the Earth and its atmosphere, TMI is able to quantify the water vapor, cloud water, and rainfall intensity in the atmosphere. The image in Fig. 2.1 was taken on August 28, 2005, when Katrina had sustained winds of 185 km/h and was about to become a Category 4 hurricane in the central Gulf of Mexico. The image reveals the horizontal distribution of rain intensity within the hurricane as obtained from TRMM sensors.

Table 2.1 Space-borne ocean sensing techniques

Color scanner	Ocean color (chlorophyll conc., susp. sediment, atten. coeff.)
Infrared radiometer	Sea surface temperature (surface temperature, current patterns)
Synthetic aperture radar	Short surface waves (swell, internal waves, oil slicks, etc.)
Altimeter	Topography and roughness of sea surface (sea level, currents, wave height)
Scatterometer	Amplitude of short surface waves (surface wind velocity, roughness)
Microwave radiometer	Microwave brightness temperature (salinity, surface temp., water vapor, soil moisture)

Rain rates in the central portion of the swath are from the TRMM precipitation radar (PR). The PR is able to provide fine-resolution rainfall data and details on the storm's vertical structure. Rain rates in the outer swath are from the TMI. The rain rates were overlaid on infrared data from the TRMM visible infrared scanner (VIRS). TRMM reveals that Katrina had a closed eye surrounded by concentric rings of heavy rain (red areas) that were associated with outer rain bands. The intense rain near the core of the storm indicates where heat, known as latent heat, is being released into the storm (NASA 2005; Pierce and Lang 2005).

Satellite radar systems can provide additional data on sea surface height, surface currents, surface winds, and wave fields. As shown in Table 2.1, radar satellites can measure wave and sea surface height and currents with altimeters, sea surface winds with scatterometers, and wave fields and other surface features, such as oil slicks, with Synthetic Aperture Radar (SAR) (Ikeda and Dobson 1995; Martin 2004). Satellite microwave radiometers have been used to estimate precipitation amounts and other hydrologic parameters for recent hurricanes like Katrina (Parkinson 2003). Sea surface salinity and soil moisture can also be mapped with microwave radiometers. Table 2.1 includes satellite systems for mapping ocean color (productivity) and sea surface temperature as well.

The International Charter "Space and Major Disasters" (the Charter) has been one of the primary sources of satellite data for the past 11 years to cover events like floods, fires, tsunamis, ocean storms, earthquakes, volcanic eruptions and oil spills. The Charter is a multi-satellite operational system to provide space-borne data on disasters that may have the potential of causing significant loss of life or property (Mahmood 2012). The idea of the Charter as a mechanism to supply satellite data-derived information in situations of crisis was introduced by the European (ESA) and the French (CNES) space agencies in 1999 (Bessis et al. 2003). Once the Canadian Space Agency came on board, the three founding members established the necessary infrastructure to implement the Charter. Since its inception, the Charter membership has grown to 14. The increasing number of satellites and sensors has resulted in a rapid response through shorter revisit frequencies and better recognition of targets with improved spectral and spatial resolutions. The Charter data are delivered to users with fast turn-around times and at no cost. Typically, satellite data are analyzed for change detection by merging the newly acquired, post-disaster imagery with reference imagery retrieved from the archives. The resulting products include maps and geocoded image overlays showing flooded surfaces and

derived water depths, lava flows, impacted roads and bridges, hot spots, burnt areas, and landslide scars. The increasing number of satellites and sensors has resulted in a rapid response through shorter revisit frequencies and better recognition of targets with the improved spectral and spatial resolutions. The Charter data are delivered to users with fast turn-around times and at no cost (Mahmood 2012).

Along the coast, ground-based radars, such as the X-band marine navigation radars, can monitor waves, storm surges, and fronts over a 10-km range with 50-m resolution. Shore-based high-frequency (HF) radars have a range of up to 200 km, but with a resolution of hundreds of meters. HF radars can measure current speeds and wave height and direction. Because shore-based radars are stationary, they can sample frequently and continuously, thus complementing satellite radar data (Cracknell and Hayes 2007; Robinson 2004).

2.3 Assessing Storm Damage to Coastal Ecosystems

Coastal wetlands are a highly productive and critical habitat for a number of plants, fish, shellfish, and other wildlife. Wetlands also provide flood protection, protection from storm and wave damage, water quality improvement through filtering of agricultural and industrial waste, and recharge of aquifers (Morris et al. 2002; Odum 1993). The strong winds, storm surges and heavy rainfall produced by hurricanes in the past have damaged wetland and coral reef ecosystems, especially along the Gulf Coast (Edmiston et al. 2008; Farris 2005).

In southeastern Louisiana, Hurricane Katrina transformed nearly 100 mile^2 (260 km^2) of marsh into open water. Most of the loss east of the Mississippi River was attributed to the effects of Katrina's storm surge. Vegetation was ripped out and sand washed in, scouring and damaging mangrove roots and harming the animals that live there. Large influxes of eroded sediment reduced habitat for coastal birds, mammals, and invertebrate species. Barrier islands were submerged and eroded. Entire seagrass beds, which are critical to fish, sea turtles, and marine mammals, were uprooted and destroyed during the storm. Coral reef beds were scoured, torn, and flattened, causing population reductions in animals such as sea urchins, snails, and fish. Katrina inundated marshes and swamps with saltwater and polluted runoff from urban areas and oil refineries, affecting amphibians and reptiles because of their sensitivity to toxins and other pollutants. Large areas of wetlands were lost, some of them permanently (Barras 2006; Provencher 2007).

The resulting wetland losses caused by Katrina were mapped by NASA, NOAA, and USGS scientists over large areas using medium-resolution satellite imagery and GIS. Time series of Landsat TM, MODIS (Moderate-resolution Imaging Spectroradiometer), and other sensors were used not only to observe the immediate damage to wetlands and forests, but also to monitor their recovery. The satellite images demonstrated how coastal wetlands function to protect inland regions and coastal communities from storm surges unleashed by powerful hurricanes. The wetlands act as a sponge, soaking up water and diminishing the storm surge. If the wetlands

Fig. 2.2 The MODIS Spectroradiometer on NASA's Terra satellite captured this image 13 days after Hurricane Ike came ashore. The *brown* areas in the image are the result of a massive storm surge that Ike pushed far inland over Texas and Louisiana causing a major marsh dieback. Credits: NASA/GSFC

had not been there, the storm surge could have penetrated much farther inland. By contrast, no wetlands existed to buffer New Orleans from Lake Pontchartrain; therefore, the storm forced lake water to burst through the levees that separated it from the city (NASA 2005; NOAA,2008; Stone and Muller 2005).

The value of satellite imagery is illustrated in Fig. 2.2, which shows an image of the Texas coast captured by the MODIS sensor on NASA's Terra satellite 13 days after Hurricane Ike made landfall on September 13, 2008. The storm's surge covered hundreds of kilometers of the Gulf Coast because Ike was a large storm, with tropical-storm-strength winds stretching more than 400 km from the center of the storm. Most of the shoreline in this region is coastal wetland. One can clearly distinguish the brown areas in the image which are the result of the massive storm surge that Ike had pushed far inland over Texas and Louisiana, causing a major marsh dieback. The salty water burned the plants, leaving them wilted and brown. The brown line corresponds with the location and extent of the wetlands. North of the brown line, the vegetation gradually transitions to pale green farmland and dark green natural vegetation untouched by the storm's surge. The powerful tug of water returning to the Gulf also stripped marsh vegetation and soil off the land. Therefore, some of the brown seen in the wetlands may be deposited sediment. Plumes of brown water are visible as sediment-laden water drains from rivers and the coast in general. The muddy water slowly diffuses, turning pale green, green,

and finally blue as it blends with clearer Gulf water. (NASA/GSFC 2010; Ramsey and Rangoonwala 2005).

Traditionally the Landsat Thematic Mapper (TM) and the French SPOT satellite have been reliable sources for land cover and wetland data. Their 30 and 20 m respective spatial resolutions and spectral bands have proven cost-effective for mapping land cover changes in large coastal watersheds (Akumu et al. 2010; Houhoulis and Michener 2000; Jensen 1996; Jensen et al. 1993; Lunetta and Balogh 1999; Porter et al. 2006). However, coastal wetlands and small watersheds frequently require higher resolution data, as provided by aircraft and high-resolution satellite sensors (Adam et al. 2010; Klemas 2011a). As shown in Table 2.2, high resolution imagery (0.6–4 m) can now be obtained from satellites, such as IKONOS and QuickBird. However, cost becomes excessive if the site is larger than a few hundred square kilometers, and in that case, medium resolution sensors, such as Landsat TM (30 m) and SPOT (20 m), become more cost-effective.

A number of advanced new techniques have been developed for mapping wetlands and even identifying wetland types and plant species (Jensen et al. 2007; Klemas 2011a; Schmidt et al. 2004; Yang et al. 2009). For instance, using LiDAR, hyperspectral and radar imagery, and narrow-band vegetation indices, researchers have been able not only discriminate some wetland species, but also make progress on estimating biochemical and biophysical parameters of wetland vegetation, such as water content, biomass and leaf area index (Adam et al. 2010; Gilmore et al. 2010; Ozesmi and Bauer 2002; Schmid et al. 2011; Pengra et al. 2007; Simard et al. 2010; Wang 2010). The integration of hyperspectral imagery and LiDAR-derived elevation data has also significantly improved the accuracy of mapping salt marsh vegetation. The hyperspectral images help distinguish high marsh from other salt marsh communities due to its high reflectance in the near-infrared region of the spectrum, and the LiDAR data help separate invasive *Phragmites* from low marsh plants (Yang and Artigas 2010).

Submerged aquatic plants and their properties are not as easily detectable as terrestrial vegetation. The spectral response of aquatic vegetation resembles that of terrestrial vegetation, yet the submerged or flooded conditions introduce factors that alter its overall spectral characteristics. It is therefore useful to distinguish between submerged and emergent wetland plants, since these factors affect each of them differently. Thus the main challenge for remote sensing of submerged aquatic plants is to isolate the plant signal from the interference of the water column, the bottom and the atmosphere. Furthermore, mapping submerged aquatic vegetation (SAV) and coral reefs requires high-resolution (1–4 m) imagery (Mumby and Edwards 2002; Purkis 2005; Thompson and Schroeder 2010; Trembanis et al. 2008). Coral reef ecosystems usually exist in clear water and their images can be classified to show different forms of coral reef, dead coral, coral rubble, algal cover, sand lagoons and different densities of sea grasses, etc. However, SAV may grow in more turbid waters and thus is more difficult to map. High-resolution (e.g. IKONOS) multispectral imagers have been used to map eelgrass and coral reefs. Hyperspectral imagers improve the results significantly by being able to identify more estuarine and intertidal habitat classes (Garono et al. 2004; Maeder et al. 2002; Mishra et al.

Table 2.2 High-resolution satellite parameters and spectral bands (DigitalGlobe 2003; Orbimage 2003; Parkinson 2003; Space Imaging 2003)

		IKONOS	QuickBird	OrbView-3	WorldView-1	GeoEye-1	WorldView-2
Sponsor		Space imaging	DigitalGlobe	Orbimage	DigitalGlobe	GeoEye	DigitalGlobe
Launched		Sept. 1999	Oct. 2001	June 2003	Sept. 2007	Sept. 2008	Oct. 2009
Spatial resolution (m)	Panchromatic	1.0	0.61	1.0	0.5	0.41	0.5
	Multispectral	4.0	2.44	4.0	n/a	1.65	2
Spectral range (nm)	Panchromatic	525–928	450–900	450–900	400–900	450–800	450–800
	Coastal blue	n/a	n/a	n/a	n/a	n/a	400–450
	Blue	450–520	450–520	450–520	n/a	450–510	450–510
	Green	510–600	520–600	520–600	n/a	510–580	510–580
	Yellow	n/a	n/a	n/a	n/a	n/a	585–625
	Red	630–690	630–690	625–695	n/a	655–690	630–690
	Red edge	n/a	n/a	n/a	n/a	n/a	705–745

2006; Nayegandhi and Brock 2008; Philpot et al. 2004; Wang and Philpot 2007). Airborne LiDARS have also been used with multispectral or hyperspectral imagers to map coral reefs and SAV (Brock and Purkis 2009; Brock et al. 2004, 2006; Palaseanu-Lovejoy et al. 2009; Yang 2009).

The major advantage of airborne remote sensing is that users can define the deployment and characteristics of the remote sensing system. By choosing the appropriate flight altitude and focal length, they can control the spatial resolution and coverage. Furthermore, the user can choose suitable atmospheric (i.e., cloud-free), sun angle and tidal (i.e., low water) conditions (Clark et al. 1997; Myers and Miller 2005). A wide range of multispectral and hyperspectral imagers can be deployed on aircraft. Airborne geo-referenced digital cameras, providing color and color infrared digital imagery are particularly suitable for accurate mapping or interpreting satellite data. Most digital cameras are capable of recording reflected visible to near-infrared light.

2.4 Measuring Beach Profile Changes

Information on beach profiles and coastal bathymetry is important for studies of near-shore geomorphology, hydrology and sedimentary processes. In order to plan sustainable coastal development and implement effective beach erosion control, flood zone delineation and ecosystem protection, coastal managers and scientists need information on long-term and short-term changes taking place along the coast, including changes in beach profiles due to erosion by storms and littoral drift, wetlands changes due to inundation, *etc*. (Finkl 1996; Gesch 2009; Klemas 2011b).

LiDAR techniques, combined with Global Positioning Systems (GPS), make it possible to obtain accurate topographical and bathymetric maps, including shoreline positions (Lillycrop et al. 1997, 2002; West et al. 2001). LiDAR surveys can produce a 10–15 cm vertical accuracy at a spatial resolution greater than one elevation measurement per square meter. This meets the requirements of many coastal research and management applications of LiDAR, including flood zone delineation, monitoring beach nourishment projects, and mapping changes along sandy coasts and shallow benthic environments due to storms or long-term sedimentary processes (Brock and Purkis 2009; Finkl and Andrews 2008; Finkl et al. 2005; Myers and Miller 2005; Pastol 2011). Airborne LiDARs have also been applied with hyperspectral imagers to map wetlands, beaches, coral reefs and SAV (Zawada and Brock 2009).

A LiDAR aircraft mapping configuration usually includes a light aircraft equipped with a LiDAR instrument and GPS, which is operated in tandem with a GPS base station. A typical beach profiling procedure using LiDAR may include cross-shore profiles every 10 m. In coastal applications, the aircraft flies along the coast at heights of about 300–1,000 m, surveying a ground swath directly below the aircraft. The aircraft position throughout the flight is recorded by an onboard

Table 2.3 Typical LiDAR flight parameters

Flying height	300–1,000 m
Vertical accuracy	±15 cm
Horizontal accuracy	DGPS = 3 m; KGPS = 1 m
Maximum depth	50 m (clear water)
Typical *kd* product	4
Coastal *k*	0.2–0.8 (d = 5–20 m)
Estuarine *k*	1.0–4.0 (d = 1–4 m)
Sounding density	3–15 m
Sun angle	18°–25° (to minimize glare)
Scan geometry	Circular (220 m swath)
Sea state	Low (0–1 Beaufort scale)
Water penetration	Green LiDAR (532 nm) used
Aircraft height	Infrared LiDAR (1,064 nm) used

DGPS differential GPS mode, *KGPS* kinematic GPS mode

GPS receiver. The aircraft GPS signals are later combined with signals concurrently collected by a nearby GPS base station. Differential kinematic GPS post-processing determines the aircraft flight trajectory to within about 5 cm (Cracknell and Hayes 2007; Stockdon et al. 2002; Wang 2010).

In LiDAR bathymetry, a laser transmitter/receiver mounted on an aircraft transmits a pulse that travels to the air-water interface, where a portion of this energy reflects back to the receiver. The remaining energy propagates through the water column and reflects off the sea bottom. Since the velocity of the light pulse is known, the water depth can be calculated from the time lapse between the surface return and the bottom return. To maximize water penetration, bathymetric LiDARs employ a blue-green laser with a typical wavelength of 530 nm to range the distance to the seabed.

Laser depth sounding techniques have proven most effective in moderately clear, shallow waters. Typical flight parameters for airborne LiDARs used in bathymetry are shown in Table 2.3. As shown in Table 2.3, the LiDAR system must have a *kd* factor large enough to accommodate the water depth and water turbidity at the study site (k = attenuation coefficient; d = max. water penetration depth). For instance, if a given LiDAR system has a $kd = 4$ and the turbid water has an attenuation coefficient of $k = 1$, the system will be effective only to depths of approximately 4 m. Optical water clarity is the most limiting factor for LiDAR depth detection, so it is important to conduct the LiDAR overflights during tidal and current conditions that minimize the water turbidity due to sediment re-suspension and river inflow (Sinclair 2008). Typically, a LiDAR sensor may collect data down to depths of about three times the Secchi (visible) depth (Estep et al. 1994; Sinclair 1999). Beyond that depth, acoustic (sonar) echo-sounding techniques are used (Brock and Sallenger 2000).

There are various sonar systems available. Echo-sounding profilers, which measure water depth and changes in bottom topography, send out pulses of acoustic energy beneath the boat or other platform. The acoustic "ping" is reflected off the bottom and submerged objects, and recorded by the transceiver. The depth to target

calculation is based on how long it took the reflected pulse to return to the surface and the speed of sound in water under prevailing environmental conditions. The earliest sounders used single beams, but the newer systems use multiple beams, with a large array of beams measuring bottom depths across a wide swath (Bergeron et al. 2007; Cracknell and Hayes 2007). Acoustic backscatter has also been studied in conjunction with Lidar-derived topographic data and habitat classifications in coral reef environments (Foster et al. 2009).

Side-scan imaging sonars emit acoustic pulses in the form of a very wide fan-shaped beam to both sides and at right angles to the track, to produce an image of the seabottom from the backscattered acoustic energy. Sonar echo-sounders and side-scan sonars are frequently housed in a torpedo-shaped "fish", which is towed by cable behind the survey ship at a predetermined height off the bottom (Pittenger, 1989; Thompson and Schroeder 2010). More recently various acoustic sensors have been housed in Remotely Controlled Vehicles (ROVs) or Autonomous Underwater Vehicles (AUV's) (Chadwick 2010).

2.5 Tracking Coastal Currents

Ocean currents influence the global heat transport; weather and climate; larval transport; drift of water pollutants; sediment transport; and marine transportation. Ocean currents are also important to the distribution of the ocean's sea life. Many species of fish rely on currents to move them to breeding grounds, areas with more abundant prey and more suitable water. Knowledge of the current and wave conditions is essential to ships and shipping companies in order to reduce shipping costs, fuel consumption, avoid powerful storms and disasters. Since currents influence so many marine-related activities and processes, meteorologist, oceanographers, ship captains, coastal and fisheries managers, and marine-related agencies need to have up-to-date information on ocean and coastal currents (Briney 2009; Pinet 2009; Purkis and Klemas 2011; Santos 2000).

Satellite remote sensors can determine currents synoptically over extensive ocean and coastal regions. Satellite altimetry is one of the essential remote sensing techniques for monitoring dynamic ocean conditions, including surface currents, local wind speed, and significant wave height. Satellite altimetry measures sea surface heights providing data on geostrophic circulation, including major ocean currents. Ocean currents can also be determined by satellite SAR or tracking the movement of natural thermal and color features in the ocean. The flow patterns of currents like the Gulf Stream are often mapped with satellite thermal infrared scanners (Andersen 1995; Breaker et al. 1994; Canton-Garbin 2008; Clemente-Colon and Pichel 2006; Ducet et al. 2000; Han 2005; Kuo and Yan 1994; Ray and Cartwright 2001; Robinson 2004; Romeiser 2007; Yan and Breaker 1993).

Along the coast and in bays there are local currents generated by tides, winds, storms, and waves. These currents are important for predicting and tracking local disasters, such as coastal flooding, harmful algal blooms, pollutant dispersion, and

sediment transport. Arrays of current meters, ocean drifters and shore-based radar can provide current measurements at local scales. In-situ current sensors can be used to validate remote sensing measurements of currents and to obtain current data at various depths. Coastal engineers distinguish been two basic approaches to coastal and offshore current measurements, the Eulerian and the Lagrangian methods (Morang and Gorman 2005). Eulerian techniques measure the velocity of water flow past a point in the ocean. Lagrangian techniques measure the movement of a parcel of water in the ocean by tracking the position of surface and subsurface drifters or chemical tracers.

The Eulerian method usually involves current meters on buoy moorings which are fixed to the ocean floor and measure currents at various depths, yet only at one specific site. Arrays of such buoy moorings with current meters at various depths are deployed in coastal waters to measure currents at specific sites, such as in tidal inlets or harbor entrance channels. Impeller (propeller) current meters are pointed into the current by a vane, just like moving air orients a wind vane. Current speed is measured by an impeller that is rotated by the force of the current. Thus its rotational velocity is related to the current speed. Acoustic systems, such as Acoustic Doppler Current Profilers (ADCP) and Acoustic Doppler current meters, are more expensive, but can be used in areas where heavy ship traffic or storms might damage impeller current meter moorings (Aanderaa 2004; Davidson-Arnott 2005; InterOcean 2007; Pinet 2009).

Lagrangian ocean drifters are specifically designed to track the movement of water (currents) at various depths. A typical design of such Lagrangian Drifters includes a float or surface buoy connected by a cable to a current drogue. The drogue, set for a specific depth, acts like an underwater sail as it is pushed by the ocean current. The surface float provides buoyancy, contains the electronics and transmits data to satellites. Satellites, ships or coastal tracking stations determine the drifter's position from its transmission signal and relay the data to ground stations, where drift is calculated from the observed positions (Fratantoni 2001; Jenkins 1992; Richardson 1991; Uchida and Imawaki 2003).

Over the past three decades shore-based high frequency (HF) and microwave Doppler radar systems have been deployed to map currents and determine swell-wave parameters along the world's coasts with considerable accuracy. HF radars operate in the 3–30 MHz frequency range and use a ground-wave propagation mode of the electromagnetic waves (Barrick et al. 1977; Bathgate et al. 2006; Essen et al. 2000; Graber et al. 1997; Gurgel et al. 2003; Gurgel and Schlick 2008; Haus et al. 1997; Paduan and Cook 1997; Schofield et al. 2008). The radar surface current measurements use the concept of Bragg scattering from a slightly rough sea surface, modulated by Doppler velocities of the surface currents. When a radar signal hits an ocean wave it usually scatters in many directions. However, when the radar signal scatters off a wave that has a wavelength half of the transmitted signal wavelength, Bragg scattering will return the signal directly to its source, resulting in a very strong received signal. Extraction of swell direction, height, period and current velocity from HF radar data is based on the modulation imposed upon the short

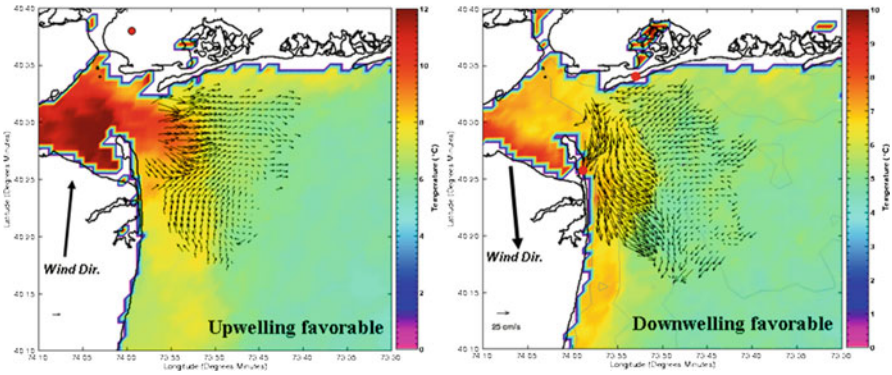

Fig. 2.3 New York Bight surface currents as measured with shore-based HF radar (Courtesy of Coastal Ocean Observation Laboratory, Rutgers University)

Bragg wavelets by the longer faster moving swell (Gurgel et al. 1999; Paduan and Graber 1997; Plant and Keller 1990; Teague et al. 1997).

Surface currents in the New York Bight, as measured with shore-based HF radar for upwelling and downwelling favourable conditions, are shown in Fig. 2.3. This figure also demonstrates how integration of HF data with satellite imagery provides a more complete picture of sea surface dynamics.

Depending on the operating frequency selected, HF radars can attain working ranges of up to 200 km and spatial resolutions between 300 and 1,000 m. Since they can perform continuous measurements, *e.g.* at 10 min intervals, HF radars satisfy the high temporal resolution requirements for tracking tidal and wind-driven currents required for pollution monitoring, ship guidance, rescue operations, and coastal management (Georges et al. 1998; Gurgel et al. 1999; Paduan and Graber 1997; Shearman and Moorhead 1988). Surface current fields have been mapped successfully not only with shore-based, but also with shipborne HF radars (Gurgel 1997; Skop and Peters 1997). Rapid-response HF radar units, such as the SeaSonde, are even being deployed from helicopters to map currents along coastlines in order to improve the modeling and operational prediction of oil slick drift (Kjelaas and Whelan 2011; Paduan and Rosenfeld 1996).

While HF radar provides accurate maps of surface currents and wave information for large coastal areas, their spatial resolution, from hundreds of meters to kilometers, is more suitable for measuring mesoscale features than small-scale currents (Kosro et al. 1997; Romeiser 2007). On the other hand, microwave X-band and S-band radars have resolutions of the order of 10 m, yet have a range of only a few kilometers (Braun et al. 2008; Helzel et al. 2011; Wu et al. 2010). Microwave radars are being used to remotely sense ocean waves and currents close to shore. A new X-band marine radar family (coherent and noncoherent) operating at 10 m scales can measure ocean currents and wave spectra at distances out to a few kilometers (Trizna 2007). Marine radars are also used for tracking coastlines, detecting fixed harbor objects, and other ships, especially in low visibility coastal

fog to avoid collisions. All remote sensing radars, including satellite-borne systems, have the advantage of no instrumentation moored in the open sea, where the instruments may be damaged or lost to storms and ships passing by (Gurgel and Schlick 2008).

2.6 Oil Spill Detection and Tracking

Oil spills can destroy marine life as well as wetland and estuarine animal habitat. To limit the damage by a spill and facilitate containment and cleanup efforts, the shipping operators, oil companies and other responsible agencies must rapidly obtain information on spill location, size and extent of the spill, direction and speed of oil movement, and wind, current and wave information for predicting future oil drift and dispersion. Users of remotely sensed data for oil spill tracking include the Coast Guard, environmental protection agencies, oil companies, shipping/insurance/fishing industries and defense departments (Jha et al. 2008).

Most of the large oil spills in the oceans stem from tanker groundings, break-ups, and collisions resulting in a large fraction of the oil spreading along the surface of the ocean and endangering marine and coastal ecosystems. They are also caused by tankers releasing their ballast water. In most of these cases a wide range of remote sensors have provided the required data for tracking and predicting the future movement of the spilled oil in a timely and reliable manner, helping guide rescue and defensive efforts, including the deployment of skimming vessels and protective booms (DeAngelo 2008; Harris 1997; Klemas 2010).

For oil spill emergencies the main operational data requirements are fast turn-around time and frequent imaging of the site to monitor the dynamics of the spill. Remote sensors on satellites and aircraft meet these requirements by tracking the spilled oil at various resolutions and over wide areas at frequent intervals through multi-temporal imaging. They also provide key inputs to drift prediction models and facilitate targeting of clean-up and control efforts (Brecke and Solberg 2005; Fingas 2010).

There are various models being used to predict the drift and dispersion of oil spilled in the ocean. One such model is the general NOAA Operational Modeling Environment (GNOME) oil spill trajectory model used by the NOAA National Ocean Service's Emergency Response Division (ERD). GNOME is used by ERD in a diagnostic mode to set up custom scenarios quickly. It is also available in a Standard Mode to outside users to predict how wind, currents and other processes might move and spread the spilled oil; learn how predicted oil trajectories are affected by uncertainties in current and wind observations and forecasts; and see how spilled oil is predicted to "weather". After entering information on an oil spill scenario, GNOME displays the trajectory of the oil. (NOAA/ERD 2010).

Most of the remote sensors use electromagnetic waves, even though acoustic sensors on boats and cameras on submerged robot-like vehicles may have to be used to view the subsurface behavior of the oil (Brecke and Solberg 2005; Jha et al. 2008;

Fig. 2.4 Deepwater Horizon oil spill captured on April 29, 2010 by MODIS imager on NASA's Terra satellite. Credits: NASA Goddard Space Flight Center

NOAA/ERD 2010; UCAR 2010). Table 2.4 summarizes the various ways of detecting oil slicks on water using electromagnetic waves. In the ultraviolet region oil fluoresces and thus appears to have a significantly higher reflectivity than water, even for very thin slicks. However, ultraviolet light is strongly scattered by the atmosphere and, in order to avoid such scattering, can be used only on aircraft at low altitudes.

Visible wavelengths are used more commonly due to the availability of relatively inexpensive digital cameras on aircraft and multispectral imagers on satellites. There is also a reasonable atmospheric transmission window for visible wavelengths. In the visible region oil has a slightly higher reflectivity than water. Oil sheen shows up as silvery and reflects light over a wide spectral region. Heavy oil appears brown, peaking in the 600–700 nm region, while mousse looks red-brown and peaks closer to 700 nm. In Fig. 2.4, the MODIS image of the Deepwater Horizon oil spill in the Gulf of Mexico clearly shows the silvery oil slick to the right of the Mississippi Delta. Sunglint and oil sheen help enhance the appearance of the slick.

Improvements in sensor technology have led to the development of hyperspectral sensors, such as the Airborne Visible/Infrared Spectrometer (AVIRIS) and the Airborne Imaging Spectrometer (AISA). A hyperspectral image consists of tens to hundreds of spectral bands and can provide a detailed spectral identification of a

feature, such as differentiating between light and crude oil and detecting small concentrations of oil (Brecke and Solberg 2005; Jensen 2007).

At thermal infrared wavelengths "optically thick" oil layers absorb solar radiation and re-emit it as thermal energy in the 8–14 μm region. Thin oil slicks or sheen cannot be detected by thermal infrared sensors. However, layers thicker than about 150 μm appear hot or bright, while layers less than about 50 μm appear cool and dark. This variability in apparent temperature may help distinguish thick layers of oil from thin layers, yet it also can cause interpreters to have difficulty distinguishing oil from water (Jha et al. 2008).

Radar imagers such as Side-Looking Airborne Radar (SLAR) on aircraft and Synthetic Aperture Radar (SAR) on satellites have the major advantage of not being bothered by cloud cover and other atmospheric effects, which frequently eliminate visible and infrared wavelengths from contention (Table 2.4). Features found frequently in SAR data are regions of low backscatter caused by the presence of oil or other slicks on the sea-surface. SAR imagers view the ocean surface at incidence angles between approximately 20° and 30° from the local vertical. Capillary waves and short gravity waves cause the radar pulse to be scattered, including some backscattering to the radar transmitter. As short surface gravity waves or capillary ripples propagate through a region where an oil film is present, their energy is absorbed as the surface film strains, causing damping of these short waves. The film-covered area backscatters less energy to the radar receiver, since most of the radar pulse is reflected from the flatter surface in the opposite direction. Thus ocean surface areas covered by oil or other slicks show up as dark in radar images. For this to work, low to moderate winds must exist to create the short surface waves. (Brecke and Solberg 2005; Fingas 2010; Harris 1997; Jha et al. 2008; Robinson 2004).

2.7 Mapping Algal Blooms

High concentrations of nutrients from agricultural and urban run-off, or produced by coastal upwelling, are causing algal blooms in many estuaries and coastal waters. Algal blooms induce eutrophic conditions, depleting oxygen levels needed by organic life, limiting aquatic plant growth by reducing water transparency, and producing toxins which can harm fish, benthic animals and humans, and are often referred to as Hazardous Algal Blooms (HAB). The frequency of algal blooms and associated problems, like eutrophication, are increasing in many estuarine and coastal waters because of the effects from increased nutrient loads from urban and agricultural run-off (Boesch et al. 2009; Kennish 2002; Kennish and Townsend 2007; Smith 2006; Yang 2009). The triggers for bloom conditions are not fully understood, but nutrient enrichment of waters, especially by nitrogen and/or phosphates, as well as unusually warm conditions, are recognized as precursors. With such diverse causes, prevention of HABs is difficult. Therefore, a more efficient means of dealing with this threat is through an effective early warning

Table 2.4 Applicability of electromagnetic wave bands for oil detection

EM band	Wavelength	Detection mechanism	Contrast vs. water	Thickness	Night operation	Weather limitations	False targets
Ultraviolet	0.3–0.4 μm	Reflectivity oil > water fluorescence	Bright	No	No	Clear	Low Sun-glint, wind sheen
Visible bands	0.4–0.7 μm	Reflectivity oil > water	Bright	No	No	Clear	High Sun-glint, wind sheen
Reflected infrared	0.7–3 μm	Reflectivity oil > water	Bright	No	No	Clear	High Sun-glint, wind sheen
Thermal infrared	3–14 μm	Emissivity Oil > water (>30 μm)	Dark/bright	Relative	Yes Day-warm, night-cool	Light fog	Medium Thin oil vs. cold water (<100 μm)
Radar	1–30 cm	Damped ripples (Wind 2–12 m/s)	Dark	No (Thick oil vs. sheen)	Yes	Heavy fog and rain	High Other films and slicks
Passive microwave	0.2–0.8 cm	Emissivity Oil > water	Bright	Relative	Yes	Heavy fog and rain	Low Biogenic materials

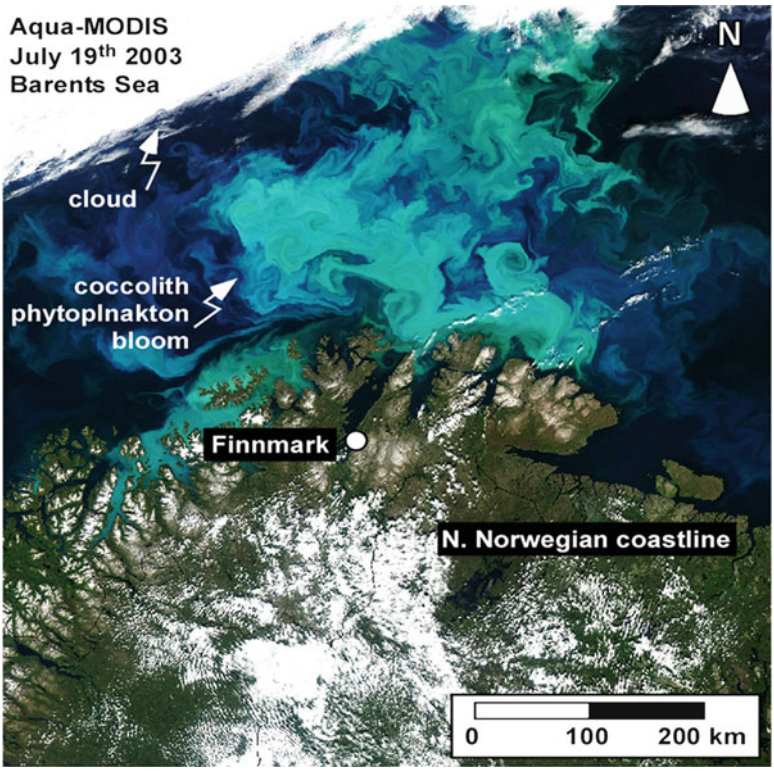

Fig. 2.5 Phytoplankton bloom in the Barents Sea (Arctic Ocean) as seen in Aqua-MODIS imagery on July 19, 2003. The bloom is composed of coccolithophores and covers an area of over 500 km^2 off Finnmark, the most northern and eastern county of Norway. Credit: NASA's Earth Observatory

system based on remotely sensed images of early bloom indicators (Jochens et al. 2010; Stumpf et al. 2009).

Satellite and airborne measurements of spectral reflectance (ocean color) represent an effective way for monitoring phytoplankton by its proxy, chlorophyll-a, the green pigment that is present in all algae. As shown in Fig. 2.5, most algal blooms can be observed with multispectral sensors on satellites because of their distinct color (Klemas 2012; Ruddick 2001; Stumpf and Tomlinson 2005). Furthermore, hyperspectral sensors with spectral bands fine-tuned for specific pigment analysis, allow detection and analysis of algal taxonomy. This can be accomplished because the species-specific algal accessory pigments produce unique spectral signatures. Remote sensing data can complement monitoring networks existing in many parts of the world to obtain data on nutrient loading and algal growth. This gives scientists better insights into overall water quality, distribution of toxin-producing algae and aquatic biogeochemical cycling (Gitelson 1993; Simis 2005).

2.8 Summary and Conclusions

Environmental and economic impacts from coastal storms and other disasters can include beach erosion, wetland destruction, excessive nutrient loading, algal blooms, hypoxia and anoxia, fish kills, large scale releases of pollutants, and spread of pathogens. Over the long term, coastal communities are also facing a rising sea level, caused mainly by global warming. Coastal agencies need advance information on the predicted path, intensity and progress of a storm and associated waves and storm surge; near-real-time information during the peak of the storm to monitor flooding and control rescue operations; and after the storm to assess the damage and plan and implement the recovery. The same holds true for other disasters, such as oil spills and algal blooms. Airborne and satellite remote sensors have helped provide this information, together with observers in aircraft and on the ground.

The Landsat Thematic Mapper (TM) has proven cost-effective for observing land cover changes in large coastal watersheds. Coastal wetlands and small watersheds frequently require higher resolution data, as provided by aircraft. High resolution imagery (0.6–4 m) can now also be obtained from satellites, such as IKONOS and QuickBird. However, cost becomes excessive if the site is larger than a few hundred square kilometers, and in that case, medium resolution sensors, such as Landsat TM (30 m) and SPOT (20 m), become more cost-effective. Wetland species identification is difficult; however, some progress is being made using hyperspectral imagers

In order to plan and implement effective beach erosion control, flood zone delineation and ecosystem protection, coastal managers and scientists need information on long-term and short-term changes taking place along the coast, including changes in beach profiles due to erosion by storms and littoral drift, wetlands changes due to inundation, etc. LiDAR techniques, combined with Global Positioning Systems (GPS), make it possible to obtain accurate topographical and bathymetric maps, including shoreline positions. LiDAR surveys can produce a 10–15 cm vertical accuracy at a spatial resolution greater than one elevation measurement per square meter.

Satellite remote sensors can determine currents synoptically over extensive ocean and coastal regions. Satellite altimetry is one of the essential remote sensing techniques for monitoring dynamic ocean conditions, including surface currents, local wind speed, and significant wave height. Satellite altimetry measures sea surface heights providing data on geostrophic circulation, including major ocean currents. Ocean currents can also be determined by satellite SAR or tracking the movement of natural thermal and color features in the ocean. The flow patterns of currents like the Gulf Stream are often mapped with satellite thermal infrared scanners.

Along the coast and in bays there are local currents generated by tides, winds, storms, and waves. These currents are important for predicting and tracking local disasters, such as coastal flooding, harmful algal blooms, pollutant dispersion, and sediment transport. Over the past three decades shore-based high frequency (HF) and microwave Doppler radar systems have been deployed to map currents and

determine swell-wave parameters along the world's coasts with working ranges of up to 200 km and spatial resolutions between 300 and 1,000 m. Since they can perform continuous measurements, *e.g.* at 10 min intervals, HF radars satisfy the high temporal resolution requirements for tracking tidal and wind-driven currents.

For oil spill emergencies the main operational data requirements are fast turn-around time and frequent imaging of the site to monitor the dynamics of the spill. Remote sensors on satellites and aircraft meet these requirements by tracking the spilled oil at various resolutions and over wide areas at frequent intervals through multi-temporal imaging. They also provide key inputs to drift prediction models and facilitate targeting of clean-up and control efforts.

Algal blooms induce eutrophic conditions, depleting oxygen levels needed by organic life, limiting aquatic plant growth by reducing water transparency, and producing toxins which can harm fish, benthic animals and humans. The frequency of hazardous algal blooms (HABs) and associated eutrophication problems is increasing in many estuarine and coastal waters because of the effects of eutrophication, resulting from increased nutrient loads from urban and agricultural run-off. Satellite and airborne measurements of spectral reflectance (ocean color) represent an effective way for monitoring phytoplankton by its proxy, chlorophyll-a, the green pigment that is present in all algae. Most HABs can be observed with satellite and airborne multispectral sensors because of their distinct color. Furthermore, the spectral bands of hyperspectral sensors can be fine-tuned for specific pigment detection. In sum, it appears that satellite and airborne remote sensors can provide much of the information required for coastal hazard detection and monitoring.

References

Aanderaa (2004) The RCM 9: a recording current meter featuring the Mark II Doppler Current Sensor DCS 3920. Aanderaa Instruments. Data Sheet, D 328, October 2004, pp 1–8

Adam E, Mutanga O, Rugege D (2010) Multispectral and hyperspectral remote sensing for identification and mapping of wetland vegetation: a review. Wetl Ecol Manag 18:281–296

Akumu CE, Pathirana S, Baban S, Bucher D (2010) Monitoring coastal wetland communities in north-eastern NSW using ASTER and Landsat satellite data. Wetl Ecol Manag 18:357–365

Andersen OB (1995) Global ocean tides from ERS-1 and TOPEX/POSEIDON altimetry. J Geophys Res 100:25249–25259

Barras J (2006) Land area change in coastal Louisiana after the 2005 hurricanes – a series of three maps. U.S. geological survey open-file report 06–1274, 12 p

Barrick DE, Evans MW, Weber BL (1977) Ocean surface current mapped by radar. Science 198:138–144

Bathgate J, Heron M, Prytz A (2006) A method of swell parameter extraction from HF ocean surface radar spectra. IEEE J Ocean Eng 31:812–818

Bergeron E, Worley CR, O'Brien T (2007) Progress in the development of shallow water mapping systems. Sea Technol 48:10–16

Bessis JL, Bequignon J, Mahmood A (2003) The international charter "space and major disasters" initiative. Acta Astronaut 54:183–190

Boesch DF, Boynton WR, Crowder LB, Diaz RJ, Howarth RW, Mee LD, Nixon SW, Rabalais NN, Rosenberg R, Sanders JG, Scavia D, Turner RE (2009) Nutrient enrichment drives Gulf of Mexico hypoxia. Am Geophys Union EOS Trans 90:117–118

Braun N, Ziemer F, Bezuglov A, Cysewski M, Schymura G (2008) Sea-surface current features observed by Doppler radar. IEEE Trans Geosci Remote Sens 46:1125–1133

Breaker LC, Krasnopolsky VM, Rao DB, Yan X-H (1994) The feasibility of estimating ocean surface currents on an operational basis using satellite feature tracking methods. Bull Am Meteorol Soc 75:2085–2095

Brecke C, Solberg AHS (2005) Oil spill detection by satellite remote sensing. Remote Sens Environ 95:1–13

Briney A (2009) Ocean currents. About.com. Geography. http://geography.about.com/od/physicalgeography/a/oceancurrents.htm Accessed 29 Nov 2011

Brock JC, Purkis SJ (2009) The emerging role of LiDAR remote sensing in coastal research and resource management. Special Issue 53-Coastal Applications of Airborne LiDAR. J Coast Res 53:1–5

Brock JC, Sallenger A (2000) Airborne topographic mapping for coastal science and resource management. US Geological Survey, Washington, DC, pp 01–46

Brock JC, Wright CW, Clayton TD, Nayegandhi A (2004) LIDAR optical rugosity of coral reefs in Biscayne National Park, Florida. Coral Reef 23:48–59

Brock JC, Wright CW, Hernandez R, Thompson P (2006) Airborne LiDAR sensing of massive stony coral colonies on patch reefs in the northern Florida reef tract. Remote Sens Environ 104:31–42

Canton-Garbin M (2008) Satellite ocean observation in relation to global change. In: Chuvieco E (ed) Earth observation of global change. Springer, Berlin

Chadwick W (2010) Remotely operated vehicles (ROVs) and autonomous underwater vehicles (AUVs). NOAA ocean explorer: submarine ring of fire 2002: background. http://oceanexplorer.noaa.gov/explorations/02fire/background/rovsauvs/rov_auv.html

Clark C, Ripley H, Green E, Edwards A, Mumby P (1997) Mapping and measurement of tropiocal coastal environments with hyperspectral and high spatial resolution data. Int J Remote Sens 18:237–242

Clemente-Colon P, Pichel WG (2006) Remote sensing of marine pollution. In: Gower J (ed) Manual of remote sensing, vol 6, 3rd edn. (A.N.Rencz, Editor-in Chief). American Society of Photogrammetry and Remote Sensing, Washington, DC, ISBN 1-57083-080-0

Cracknell AP, Hayes L (2007) Introduction to remote sensing. CRC Press, New York

Davidson-Arnott R (2005) Beach and near-shore instrumentation. In: Schwartz ML (ed) Encyclopedia of coastal science. Springer, Dordrecht, pp 130–138

DeAngelo L (2008) The sea empress oil spill. http://www.eoearth.org/article/Milford_Haven,_Wales

Digital Globe (2003) Quickbird imagery products and product guide (revision 4). Digital Globe, Inc., Longmont

Ducet N, Le Traon PY, Reverdin G (2000) Global high-resolution mapping of ocean circulation from TOPEX/Poseidon and ERS-1 and -2. J Geophys Res 105:19477–19498

Edmiston HL, Fahrny SA, Lamb MS, Levi LK, Wanat JM, Avant JS, Wren K, Selly NC (2008) Tropical storm and hurricane impacts on a Gulf Coast estuary: Apalachicola Bay, Florida. J Coast Res Spec Issue 55:38–49

Essen HH, Gurgel KW, Schlick T (2000) On the accuracy of current measurements by means of HF radar. IEEE J Ocean Eng 25:472–480

Estep LL, Lillycrop WJ, Parson LE (1994) Estimation of maximumdepth of penetration of a bathymetric lidar system using a Secchi Depth data base. Mar Technol Soc J 28:31–36

Farris GS (2005) USGS reports new Wetland loss from Hurricane Katrina in Southeastern Louisiana. http://www.usgs.gov/newsroom/article. Accessed 13 Mar 2009

Fingas M (2010) Oil spill science and technology. Elsevier, Amsterdam, 1192 pp

Finkl CW (1996) What might happen to America's shorelines if artificial beach replenishment is curtailed: a prognosis for southeastern Florida and other sandy regions along regressive coasts. J Coast Res 12:ii–ix

Finkl CW, Andrews JL (2008) Shelf geomorphology along the Southeast Florida Atlantic continental platform: barrier coral reefs, nearshore bedrock, and morphosedimentary features. J Coast Res 24:823–849

Finkl CW, Benedet L, Andrews JL (2005) Interpretation of seabed geomorphology based on spatial analysis of high-density airborne laser bathymetry (ALB). J Coast Res 21:501–514

Foster G, Walker BK, Riegl BM (2009) Interpretation of single-beam acoustic backscatter using Lidar-derived topographic complexity and benthic habitat classification in a coral reef environment. J Coast Res Spec Issue 53:16–26

Fratantoni DM (2001) North Atlantic surface circulation during the 1990s observed with satellite-tracked drifters. J Geophys Res 106(C10):22067–22094

Garono RJ, Simenstad CA, Robinson R, Ripley H (2004) Using high spatial resolution hyperspectral imagery to map intertidal habitat structure in Hood Canal Washington, USA. Can J Remote Sens 30:54–63

Georges TM, Harlan JA, Lee TN, Leben RR (1998) Observations of the Florida Current with two over-the-horizon radars. Radio Sci 33:1227–1239

Gesch DB (2009) Analysis of Lidar elevation data for improved identification and delineation of lands vulnerable to sea-level rise. J Coast Res Spec Issue, Coast Appl Airborne Lidar 53:49–58

Gilmore MS, Civco DL, Wilson EH, Barrett N, Prisloe S, Hurd JD, Chadwick C (2010) Remote sensing and in situ measurements for delineation and assessment of coastal marshes and their constituent species. In: Wang J (ed) Remote sensing of coastal environment. CRC Press, Boca Raton

Gitelson A (1993) Quantitative remote sensing methods for real-time monitoring of inland water quality. Int J Remote Sens 14:1269–1295

Graber HC, Haus BK, Chapman RD, Shay LK (1997) HF radar comparisons with moored estimates of current speed and direction: expected differences and implications. J Geophys Res 102:18749–18766

Gurgel K-W (1997) Experience with shipborne measurements of surface current fields by radar. Oceanography 10:82–84

Gurgel K-W, Schlick T (2008) Land-based over-the-horizon radar techniques for monitoring the North-East Atlantic Coastal Zone. In: Barale V, Gade M (eds) Remote sensing of the European seas. Springer, Dordrecht, pp 447–458

Gurgel K-W, Essen HH, Kingsley HP (1999) HF radars: physical limitations and recent developments. Coast Eng 37:201–218

Gurgel K-W, Essen HH, Schlick T (2003) The use of HF radar networks within operational forecasting systems of coastal regions. In: Dahlin H, Flemming NC, Nittis K, Petersson SE (eds) Building the European capacity in operational oceanography. Elsevier, Oxford, pp 245–250

Han G (2005) Altimeter surveys, coastal tides and shelf circulation. In: Schwartz ML (ed) Encyclopedia of coastal science. Springer, Dordrecht, pp 27–28

Harris C (1997) The sea empress incident: overview and response at sea. In: Proceedings of the 1997 oil spill conference, Fort Lauderdale, FL, 7–10 April 1997, pp 177–184

Haus BK, Graber HC, Shay LK (1997) Synoptic measurement of dynamic ocean features. Oceanogr: Spec Issue High Freq Radars Coast Oceanogr 10:45–48

Hayes B (2005) Natural and unnatural disasters. Am Sci 93:496–499

Helzel T, Petersen L, Mariette V, Pavec M (2011) Reliability of coastal radar WERA for coastal zone management. J Coast Res Spec Issue 64:1345–1347

Houhoulis PF, Michener WK (2000) Detecting wetland change: a rule-based approach using NWI and SPOT-XS data. Photogramm Eng Remote Sens 66:205–211

Ikeda M, Dobson FW (1995) Oceanographic applications of remote sensing. CRC Press, New York

InterOcean (2007) S4 current meter family. InterOcean Systems, Inc. http://www.interoceansystems.com/s4theory.htm. Accessed 16 March, 2007
IPCC (2007) Intergovernmental panel on climate change. Climate change 2007: the physical science basis. WMO/UNEP, Paris (www.ipcc.ch)
Jenkins WJ (1992) Tracers in oceanography. Oceanus 35:47–55
Jensen JR (1996) Introductory digital image processing: a remote sensing perspective, 2nd edn. Prentice-Hall, Upper Saddle River
Jensen JR (2007) Remote sensing of the environment: an earth resource perspective. Prentice Hall, Upper Saddle River
Jensen JR, Cowen D, Althausen J, Narumalani S, Weatherbee O (1993) An evaluation of the Coast Watch change detection protocol in South Carolina. Photogramm Eng Remote Sens 59:1036–1046
Jensen RR, Mausel P, Dias N, Gonser R, Yang C, Everitt J, Fletcher R (2007) Spectral analysis of coastal vegetation and land cover using AISA + hyperspectral data. Geocarto Int 22:17–28
Jha MN, Levy J, Gao Y (2008) Advances in remote sensing of oil spill disaster management: state-of-the-art sensor technology for oil spill surveillance. Sensors 8:236–255
Jochens TT, Malone TC, Stumpf RP, Hickey BM, Carter M, Morrison R, Dyble J, Jones B, Trainer VL (2010) Integrated ocean observing system in support of forecasting harmful algal blooms. Mar Technol Soc J 44:99–121
Kennish MJ (2002) Environmental threats and environmental future of estuaries. Environ Conserv 29:78–107
Kennish MJ, Townsend AR (2007) Nutrient enrichment and estuarine eutrophication. Ecol Appl 17:S1–S2
Kjelaas AG, Whelan C (2011) Rapidly deployable SeaSonde for modeling oil spill response. Sea Technol 52:10–15
Klemas V (2009) The role of remote sensing in predicting and determining coastal storm impacts. J Coast Res 25:1264–1275
Klemas V (2010) Tracking oil slicks and predicting their trajectories using remote sensors and models: case studies of the Sea Princess and Deepwater Horizon oil spills. J Coast Res 26 (5):789–797
Klemas V (2011a) Remote sensing of wetlands: case studies comparing practical techniques. J Coast Res 27:418–427
Klemas V (2011b) Beach profiling and LIDAR bathymetry: an overview with case studies. J Coast Res 27:1019–1028
Klemas V (2012) Remote sensing of algal blooms: an overview with case studies. J Coast Res 28:34–43
Kosro PM, Barth JA, Strub PT (1997) The coastal jet: observations of surface currents over the Oregon Continental Shelf from HF radar. Oceanogr: Spec Issue High Freq Radars Coast Oceanogr, 10:53–56
Kuo N-J, Yan X-H (1994) Using the shape-matching method to compute sea-surface velocities from AVHRR satellite images. IEEE Trans Geosci Remote Sens 32:724–728
Lillycrop WJ, Irish JL, Parson LE (1997) SHOALS system. Sea Technol 38:17–25
Lillycrop WJ, Pope RW, Wozencraft JM (2002) Airborne lidar hydrography: a vision for tomorrow. Sea Technol 43(6):27–34
Lunetta RS, Balogh ME (1999) Application of multi-temporal Landsat 5 TM imagery for wetland identification. Photogramm Eng Remote Sens 65:1303–1310
Maeder J, Narumalani S, Rundquist D, Perk R, Schalles J, Hutchins K, Keck J (2002) Classifying and mapping general coral-reef structure using Ikonos data. Photogramm Eng Remote Sens 68:1297–1305
Mahmood A (2012) Monitoring disasters with a constellation of satellites – type examples from the International Charter "Space and Major Disasters". Geocarto Int 27:91–102
Martin S (2004) An introduction to remote sensing. Cambridge University Press, Cambridge

Mishra D, Narumalani S, Rundquist D, Lawson M (2006) Benthic habitat mapping in tropical marine environments using QuickBird multispectral data. Photogramm Eng Remote Sens 72:1037–1048
Morang A, Gorman LT (2005) Monitoring coastal geomorphology. In: Schwartz ML (ed) Encyclopedia of coastal science. Springer, Dordrecht, pp 447–458
Morris JT, Sundareshwar PV, Nietch CT, Kjerfve B, Cahoon DR (2002) Responses of coastal wetlands to rising sea level. Ecology 83:2869–2877
Mumby PJ, Edwards AJ (2002) Mapping marine environments with IKONOS imagery: enhanced spatial resolution can deliver greater thematic accuracy. Remote Sens Environ 82:248–257
Myers JS, Miller RL (2005) Optical airborne remote sensing. In: Miller RL, DelCastillo CE, McKee BA (eds) Remote sensing of coastal aquatic environments: technologies, techniques and applications. Springer, Dordrecht, pp 51–68
NASA (2005) EO natural hazards: Hurricane Katrina floods the Southeastern United States. http://earthobservatory.nasa.gov/Natural_ Hazards/natural_hazards_v2. Accessed 2 May 2008
NASA/GSFC (2010) Hurricane Ike: storm surge flooding image of the Gulf Coast. NASA image courtesy Jeff Schmaltz, MODIS Rapid Response Team at NASA GSFC
Nayegandhi A, Brock JC (2008) Assessment of coastal vegetation habitats using LiDAR. In: Yang X (ed) Lecture notes in geoinformation and cartography – remote sensing and geospatial technologies for coastal ecosystem assessment and management. Springer Publications, Heidelberg, pp 365–389
NOAA (National Oceanic and Atmospheric Administration) (1999) Trends in U.S. coastal regions, 1970–1998. In: Addendum to the proceedings: trends, and future challenges for U.S. National Ocean and Coastal Policy, NOAA, Washington, DC, August 1999
NOAA (2006) Hurricanes: unleashing nature's fury. A preparedness guide. U.S. Department of Commerce, NOAA, National Weather Service, Washington, DC, pp 1–24
NOAA (2008) Hurricane Katrina. http://www.katrina.noaa.gov/. Accessed 10 Nov 2008
NOAA/CSC (Coastal Services Center) (2008) Hurricane planning with satellite imagery. http://www.csc.noaa.gov/products/sccoasts/html/hazards/htm. Accessed 19 Nov 2008
NOAA/ERD (2010) General NOAA Operational Modeling Environment (GNOME model). http://response.restoration.noaa.gov
NOAA/NHC (National Hurricane Center) (2008) Hurricane preparedness: SLOSH model. http://www.nhc.noaa.gov/HAW2/surge/slosh.shtml. Accessed 22 Nov 2008
Odum EP (1993) Ecology and our endangered life-support systems, 2nd edn. Sinauer Associates, Inc., Sunderland
Orbimage (2003) OrbView-3 satellite and ground systems specifications. Orbimage Inc., Virginia
Ozesmi SL, Bauer ME (2002) Satellite remote sensing of wetlands. Wetl Ecol Manag 10:381–402
Paduan JD, Cook MS (1997) Mapping surface currents in Monterey Bay with CODAR-type HF radar. Oceanogr: Spec Issue High Freq Radars Coast Oceanogr 10:49–52
Paduan JD, Graber HC (1997) Introduction to high-frequency radar: reality and myth. Oceanogr: Spec Issue High Freq Radars Coast Oceanogr 10:36–39
Paduan JD, Rosenfeld LK (1996) Remotely sensed surface currents in Monterey Bay from shore-based radar (Coastal Ocean Dynamics Application Radar). J Geophys Res 101:20669–20686
Palaseanu-Lovejoy M, Nayegandhi A, Brock J, Woodman R, Wright CW (2009) Evaluation of airborne Lidar data to predict vegetation presence/absence. J Coast Res Spec Issue 53:83–97
Parkinson CL (2003) Aqua: an earth-observing satellite mission to examine water and other climate variables. IEEE Trans Geosci Remote Sens 41:173–183
Pastol Y (2011) Use of airborne LIDAR bathymetry for coastal hydrographic surveying: the French experience. J Coast Res Spec Issue 62:6–18
Pengra BW, Johnston CA, Loveland TR (2007) Mapping an invasive plant, Phragmites australis, in coastal wetlands using the EO-! Hyperion hyperspectral sensor. Remote Sens Environ 108:74–81

Philpot WD, Davis CO, Bissett P, Mobley CD, Kohler DD, Lee Z, Snyder WA, Steward RG, Agrawal Y, Trowbridge J, Gould R, Arnone R (2004) Bottom characterization from hyperspectral image data. Oceanography 17:76–85
Pierce H, Lang S (2005) TRMM – tropical rainfall measurement mission: Katrina intensifies into a powerful hurricane, strikes Northern Gulf Coast. http://trmm.gsfc.nasa.gov/publicationsLdir/katrinaLaug05Lno2.html. Accessed 2 May 2008
Pinet PR (2009) Invitation to oceanography, 5th edn. Jones and Bartlett, Sudbury
Pittenger RF (1989) Exploring and mapping the seafloor. National Geographic 177:61A.
Plant WJ, Keller WC (1990) Evidence of Bragg scattering in microwave Doppler spectra of sea return. J Geophys Res 95:16299–16310
Porter DE, Field DW, Klemas VV, Jensen JR, Malhotra A, Field RT, Walker SP (2006) RESAAP final report: NOAA/NERRS remote sensing applications assessment project. University of South Carolina, Columbia
Provencher J (2007) Stronger storms are bad news for coastal ecosystems. Ocean News 7:2–4
Purkis SJ (2005) A 'reef-up' approach to classifying coral habitats from IKONOS imagery. IEEE Trans Geosci Remote Sens 43:1375–1390
Purkis SJ, Klemas V (2011) Remote sensing and global environmental change. Wiley-Blackwell, Oxford, 384 p
Ramsey E, Rangoonwala A (2005) Leaf optical property changes associated with the occurrence of Spartina alterniflora dieback in coastal Louisiana related to remote sensing mapping. Photogramm Eng Remote Sens 71:299–311
Ray RD, Cartwright DE (2001) Estimates of internal tide energy fluxes from TOPEX/Poseidon altimetry: central North Pacific. Geophys Res Lett 28:1259–1262
Richardson PL (1991) SOFAR floats give a new view off ocean eddies. Oceanus 34:23–31
Robinson IS (2004) Measuring the oceans from space: the principles and methods of satellite oceanography. Springer-Praxis Publishing Ltd., Chichester
Romeiser R (2007) High-resolution imaging of current fields from satellites. Sea Technol September 2007 Spec Issue 53:44–46
Ruddick KG (2001) Optical remote sensing of chlorophyll-a in case 2 waters by use of an adaptive two-band algorithm with optimal error properties. Appl Opt 40:3575–3585
Rykhus RP (2005) Satellite imagery maps Hurricane Katrina induced flooding and oil slicks. Am Geophys Union EOS 86:381–382
Santos AMP (2000) Fisheries oceanography using satellite and airborne remote sensing methods: a review. Fish Res 49:1–20
Schmid KA, Hadley BC, Wijekoon N (2011) Vertical accuracy and use of topographic LIDAR data in coastal marshes. J Coast Res 27:116–132
Schmidt KS, Skidmore AK, Kloosterman EH, Van Oosten H, Kumar L, Janssen JAM (2004) Mapping coastal vegetation using an expert system and hyperspectral imagery. Photogramm Eng Remote Sens 70:703–716
Schofield O, Kohut J, Glenn S (2008) Evolution of coastal observing networks. Sea Technol 49:31–36
Shearman EDR, Moorhead MD (1988) PISCES: a coastal ground-wave HF radar for current, wind, and wave mapping to 200 km ranges. In: Proceedings of IGARSS'88, Tsukuba City, Japan, pp 773–776
Simard M, Fatoyinbo LE, Pinto N (2010) Mangrove canopy 3D structure and ecosystem productivity using active remote sensing. In: Wang J (ed) Remote sensing of coastal environment. CRC Press, Boca Raton
Simis SGH (2005) Remote sensing of the cyanobacterial pigment phycocyanin in turbid inland waters. Limnol Oceanogr 50:237–245
Sinclair M (1999) Laser hydrography – commercial survey operations. In: Proceedings of US hydrographic conference, Mobile, Alabama, USA
Sinclair M (2008) Airborne LiDAR hydrographic survey for homeland security. Sea Technol 49:15–20

Skop RA, Peters NJ (1997) Shipboard deployment of a VHF OSCR system for measuring offshore currents. Oceanography 10:80–81
Smith VH (2006) Responses of estuarine and coastal marine phytoplankton to nitrogen and phosphorus enrichment. Limnol Oceanogr 51:377–384
Space Imaging (2003) IKONOS imagery products and product guide (version 1.3). Space Imaging LLC, Thornton
Stockdon HF, Sallenger AH, List JH, Holman RA (2002) Estimation of shoreline position and change using airborne topographic LiDAR data. J Coast Res 18:502–513
Stoker JM, Tyler DJ, Turnipseed DP, Van Wilson Jr K, Olmoen MJ (2009) Integrating disparate Lidar data sets for regional storm tide inundation analysis of Hurricane Katrina. J Coast Res Spec Issue 53:66–72
Stone GW, Muller RA (2005) Meteorological effects on coasts. In: Encyclopedia of coastal science. Springer, Dordrecht, pp 636–637
Stumpf RP, Tomlinson MC (2005) Remote sensing of harmful algal blooms. In: Miller R, Del Castillo C, McKee B (eds) Remote sensing of coastal aquatic environments: technologies, techniques and applications. Kluwer Academic Publishers, Dordrecht
Stumpf RP, Tomlinson MC, Calkins JA, Kirkpatrick B, Nierenberg K, Currier R, Wynne TT (2009) Skill assessment for an operational algal bloom forecast system (special issue on skill assessment of ecological oceanographic models). J Mar Syst 76:151–161
Teague CC, Vesecky JF, Fernandez DM (1997) HF radar instruments, past to present. Oceanography 10:40–44
Thompson RL, Schroeder AJJr (2010) High-definition 3-D tools for underwater surveying and inspection. Sea Technol 51:43
Trembanis AC, Hiller T, Patterson M (2008) Exploring coral reef sustainability. Hydro Int 12:10–15
Trizna DB (2007) Monitoring coastal processes and ocean wave directional spectra using a marine radar. OCEANS 2006 – Asia Pacific, pp 1–4
UCAR (2010) Ocean currents likely to carry oil along Atlantic coast. http://www2.ucar.edu/news/ocean-currents-likely-to-carry-oil-spill-along-atlantic-coast. Accessed 6 Aug/2010
Uchida H, Imawaki S (2003) Eulerian mean velocity field derived by combining drifter and satellite altimeter data. Geophys Res Lett 30:1229
Wang Y (2010) Remote sensing of coastal environments. CRC Press/Taylor and Francis Group, Boca Raton
Wang C-K, Philpot WD (2007) Using airborne bathymetric LiDAR to detect bottom type variation in shallow waters. Remote Sens Environ 106:123–135
West GR, Lillycrop WJ, Pope RW (2001) Utilization of airborne LiDAR bathymetry for rapid environmental assessment. Sea Technol 42:10–15
Wu L-C, Kao CC, Yang W-H (2010) Sea state monitoring from a mobile X-band radar system. Sea Technol 51:40–42
Yan X-H, Breaker LC (1993) Surface circulation estimation using image processing and computer vision methods applied to sequential satellite imagery. Photogramm Eng Remote Sens 59:407–413
Yang X (2009) Remote sensing and geospatial technologies for coastal ecosystem assessment and management. Springer, Berlin
Yang J, Artigas FJ (2010) Mapping salt marsh vegetation by integrating hyperspectral and LiDAR remote sensing. In: Wang J (ed) Remote sensing of coastal environment. CRC Press, Boca Raton
Yang C, Everitt JH, Fletcher RS, Jensen JR, Mausel PW (2009) Mapping black mangrove along the south Texas gulf coast using AISA + hyperspectral imagery. Photogramm Eng Remote Sens 75:425–436
Zawada DG, Brock JC (2009) A multi-scale analysis of coral reef topographic complexity using Lidar-derived bathymetry. J Coast Res Spec Issue 53:6–15

Chapter 3
Determination of Human Induced Coastal Changes Using RS, GIS and Geostatistics

Elif Sertel and Dursun Zafer Seker

Abstract Black Sea coast of Turkey has been changed significantly as a result of newly constructed interstate road and intense urbanization along the coastline. Several coasts of the world have been facing these kinds of human-induced coastal changes and it is important to monitor and quantify them. This research emphasizes the importance of remote sensing (RS), Geographic Information Systems (GIS) and geostatistics to determine and examine coastal changes. Archive and current images obtained from Lansat 5 TM sensor were used in this research to quantify changes occurred in 25-year period between 1985 and 2012. Transects were generated from these images along the coastline of the study area and they were used for spatial profile and geostatistical analysis to accurately identify coastal changes.

3.1 Introduction

Coasts have been changed physically, ecologically and chemically at local to global scales because of diverse natural processes and human induced coastal degradation. Water level changes, tsunamis, storm surges, coastal erosion are among the natural process causing coastal changes whereas road construction along the coastlines, dredging navigation channels, discharging materials to the water, construction of drainage channels and coastal structures are among the human induced changes.

Several researches have been conducted on the determination of human-induced changes on the coastal environments. Sertel et al 2008, applied integration of

E. Sertel (✉) • D.Z. Seker
Geomatics Engineering Department, Istanbul Technical University,
Maslak, Istanbul 34469, Turkey
e-mail: sertele@itu.edu.tr

C.W. Finkl (ed.), *Coastal Hazards*, Coastal Research Library 6,
DOI 10.1007/978-94-007-5234-4_3,

remote sensing and GIS to Kizilirmak delta, Turkey to find out the impact of construction of drainage channels and change in river bed to the delta and its coast. Kaya et al. 2008, employed spatial and surface profiles created from remotely sensed data to analyze the coastal changes occurred between Kilyos and Karaburun coastline lying along the northern part of Istanbul. They found out that coastline change occurred on the research area due to the disposal of materials extracted from open-pit mining areas to the sea and coastal erosion. Seker et al. 2011, determined the coastal changes occurred in Karasu coastline, Istanbul due to the coastal erosion. They analyzed the coastal changes between 1987 and 2010 using Landsat 5 TM Satellite imageries. Cowell and Zeng (2003), applied a modeling tool to predict coastal hazard using the integration of coastal response model and random simulation in GIS environment. Pattanaik and Prasad (2011), investigated the impact of aquaculture on mangroves, in Mahanadi delta of Orissa, East coast of India. They used Landsat and IRS images to reveal the impacts and suggested the regular monitoring of the mangroves.

The integration of Remote Sensing (RS) and GIS is a powerful and effective tool used by several multi-disciplinary scientists to produce rapid, economic, reliable, and accurate results. Monitoring coastlines to identify coastal changes caused by human activities or natural processes is among the most common application of GIS and RS integration (Musaoglu et al. 2004; Sertel et al. 2008; Seker et al. 2008). In addition to GIS and RS, geostatistical analysis comprises an important technique to analyze the spatial data. Application of geostatistical methods to remotely sensed data could be used to find out spatial changes occurred in a geographical location.

This research uses the integration of RS, Geostatistics and GIS to determine the human induced coastal changes occurred in the Black Sea Coast of Turkey as a result of highway construction and urbanization. 1985 and 2010 Landsat 5 TM images were used to identify coastal changes by means of spatial and semivariogram analysis of the selected transects. Obtained results were visualized in GIS environment to conduct comprehensive analysis.

3.2 Methodology

3.2.1 Geostatistics

Geostatistics comprises statistical techniques in analysis and interpretation of geographically referenced data (Goovaerts 1997; Webster and Oliver 2007). Geostatistics could be used to quantify amount and scale of spatial variability and spatial dependence. Spatial prediction or spatial interpolation is one of the main applications of geostatistics where estimation the value of a variable at an unsampled location conducted based on the values of that variable at neighboring locations. Geostatistical methods overcome the limitations of deterministic interpolation

method and ensure that the prediction of variables at unsampled locations is optimal based on geostatistical assumptions (Burrough and McDonnel 1998).

Semivariograms are the central tool for geostatistics that measure the spatial variation of a regionalized variable, i.e., a random variable whose position in space or time is known and the theory of regionalized variables underpins the analysis that follows (Sertel et al. 2007a). Curran (1988) provides detailed information on the usage of semivariogram in remote sensing.

The experimental semivariogram, which is obtained from real data, can be estimated along the transect where $P(h)$ pairs of observations are separated by the same lag h. Their average semivariance at lag h is given by

$$\hat{\gamma}_s(h) = \frac{1}{2P(h)} \sum_{i=1}^{P(h)} [Z(x) - Z(x+h)]^2$$

The X axis of a semivariogram shows the scale of variation, while the Y axis of a semivariogram shows the amount of variation, and the shape of a semivariogram shows both.

Geostatistical methods could be applied to remote sensing data. Since semivariograms are powerful tools to quantify amount and scale of spatial variation, application of geostatistical methods to satellite images could provide valuable information to quantify spatial variations due to the coastal changes.

3.2.2 Remote Sensing

Integrated usage of remote sensing and space technologies has been utilized for multidisciplinary applications by several scientists. Satellite sensor images provide rapid, economic, update information of earth surface characteristics, and can be used for various researches. Remote sensing accommodates accurate and reliable information to many researchers with high spatial, spectral and temporal resolution, synoptic view and very short data collection time. Land cover which is a fundamental variable impacting and linking many parts of the human and physical environments can be derived using remotely sensed data. Several different applications such as management of environmental and natural resources, sea and coastline studies, land use/cover changes in global and regional scales, weather forecasting and climate modeling can be conducted using the remote sensing technology (Schweiger et al. 2005; Brivio et al. 2002; Ostir et al. 2002).

Utilization of digital image processing techniques to remotely sensed images can produce accurate land use or/and land cover maps of related region for the past and present time which are valuable source of information for coastal, environmental, disaster, planning and climate studies.

3.2.2.1 Radiometric and Atmospheric Correction

The electromagnetic radiation signals collected by satellites are modified by scattering and absorption by gases and aerosols while traveling through the atmosphere from the Earth surface to the sensor. Changes in scene illumination, atmospheric conditions, viewing geometry and instrument response cause radiometric distortions over satellite image. Therefore, satellite sensor images are radiometrically and atmospherically corrected to eliminate system errors and to minimize contamination effects of atmospheric particles through absorption and scattering of the radiation from the Earth surface (Liang 2004; Song et al. 2001). In this research, two images were first converted into radiance values and then dark object subtraction method was applied to radiance images to suppress atmospheric effects.

3.2.2.2 Geometric Correction

Satellite images contain both systematic and non-systematic geometric errors. The systematic errors are primarily functions of scan skew, mirror-scan velocity, panoramic distortion, platform velocity nonlinearities, perspective geometry and Earth rotation which can be corrected using data from platform ephemeris and knowledge of internal sensor distortion. On the other hand, non-systematic errors are mainly caused by variation through time in the position and attitude angles (roll, pitch and yaw) of the satellite platform. Without accurate sensor platform orientation parameters, these errors can only be corrected with the use of Ground Control Points (GCPs) and a suitable precision photogrammetric or empirical model (Sertel et al. 2007b; Toutin 2004).

Accurate geometric correction of satellite images is crucial in order to quantify the amount and spatial distribution of coastal changes accurately and reliably. In this research, both images were geometrically corrected using polynomial equations and GCPs derived from topographic maps.

3.2.3 Geographic Information Systems

A geographic information system (GIS) is a system to create and manage spatial data and related attributes of environmental, meteorological, census data, etc. GIS is a computer based system with the capabilities of integration, storage, editing, analyses, and display of geographically referenced data. Integration of different data sets obtained from different data sources is the main advantage and power of a GIS (Fedra and Feoli 1998; Holsapple and Whinston 1991). Also, spatial analysis and queries could be conducted to produce information from different spatial data.

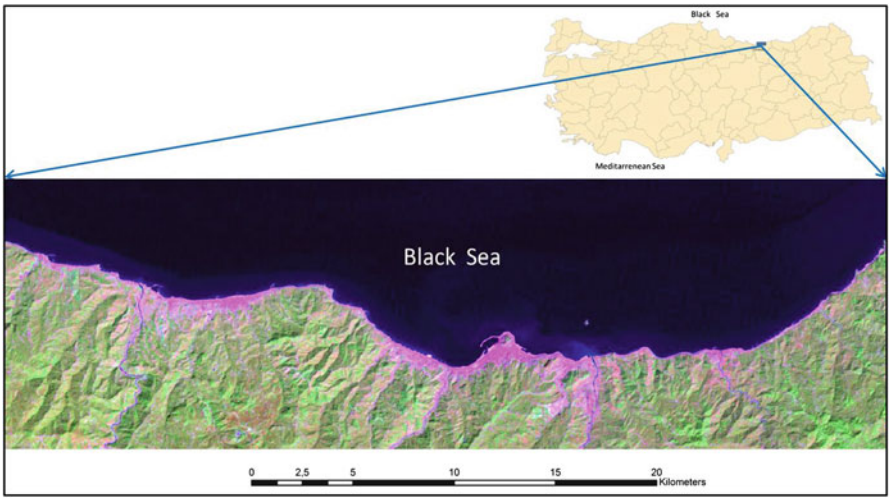

Fig. 3.1 The study area

3.3 Case Study and Results

3.3.1 Study Area

In this study, a section of the Black Sea coast line of Turkey was selected as the study area (Fig. 3.1). The selected section mostly lies on Giresun province, which has been effected more than the other provinces due to D-010 interstate road construction passing through Black Sea Coastline.

Although it is a major west-east state road (1,427 km in length) in northern Turkey connecting most of the coastal towns and cities at middle and eastern Black Sea Region, the construction of this state road has caused serious negative human induced effects on the coastline (URL 1).

3.3.2 Data

In this study, the coastal changes due to the construction of the Black Sea State Road and urbanization were determined by using satellite imageries. Through the spatial profiles obtained from the satellite imageries, the extents of changed areas were determined towards coastline to the sea. Within the context of the study, two different satellite imageries were used as main data source, namely, Landsat 5 Thematic Mapper (TM) 21 June 1985 and Landsat 5 Thematic Mapper (TM) 29 August 2010. Landsat TM data are important data sources to obtain geographical information about the past especially when there is not any field survey available.

Landsat satellite images received in 1985 and 2010 were geometrically corrected and transformed into UTM coordinate system, 35th zone. Layer Stack was used to

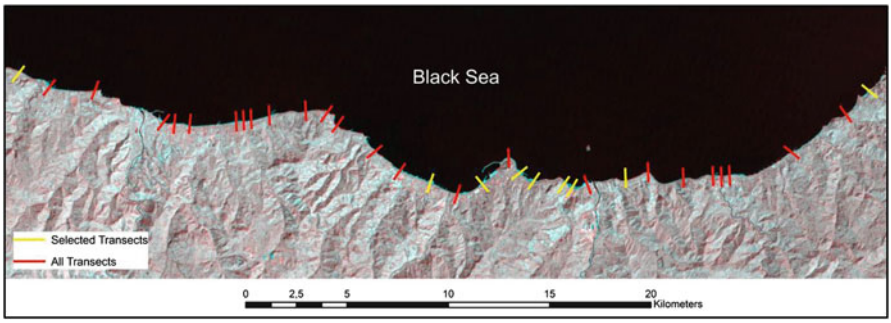

Fig. 3.2 Location of all and selected transects

combine different dated images into one image in order to conduct spatial and GIS analysis readily. The near infrared bands (Band 5) of these imageries were used in layer stack for further analysis, since it is easy to distinguish between land and sea with infrared channels. Spectral profiles of these data were generated to determine the changes occurred on the coastal line within years. Spatial extent of each transect we examined and the location of changing land cover from land to sea was found out to interpret changes occurred in the research area.

At the beginning of the study, 33 transects covering both changed and unchanged areas along the coastline were formed. After examining of all transects, nine of them were selected to be presented in this chapter. Spatial profile analysis were conducted within GIS environment and radiance values of 1985 and 2012 data were extracted for related transects to identify changed and unchanged sections and their locations. Location of the all and selected transects are given in Fig. 3.2.

3.3.3 Semivariogram Analyses

Radiance values of selected transects were extracted from 1985 and 2010 satellite images and these values are used to calculate the semivariograms to quantify spatial variation within the region. Semivariograms of 33 transects were plotted and shape, range, nugget, and sill of these semivariograms were interpreted and eight were used to illustrate this section.

The semivariogram shape was different for 1985 and 2010 transects if the coastline was changed significantly but similar if the coastline was not changed significantly. When the shapes of each transects are analyzed, changes in transects 16, 18, 21, 22 and 23 were clearly identified. Range and sill values of these transects also changed within the related time period. Semivariogram analyses illustrated that range (A_0) values of selected transects changes 21 m or more for the changed transects namely 1, 16, 18, 21, 22 and 25. Whereas, range change was smaller than 201 for the transect 25 and 33 in which there was not any significant change.

The highest range difference (48 m) was observed for transect 22 in which there was 150 m change that was explained in the following section (Figs. 3.3 and 3.4).

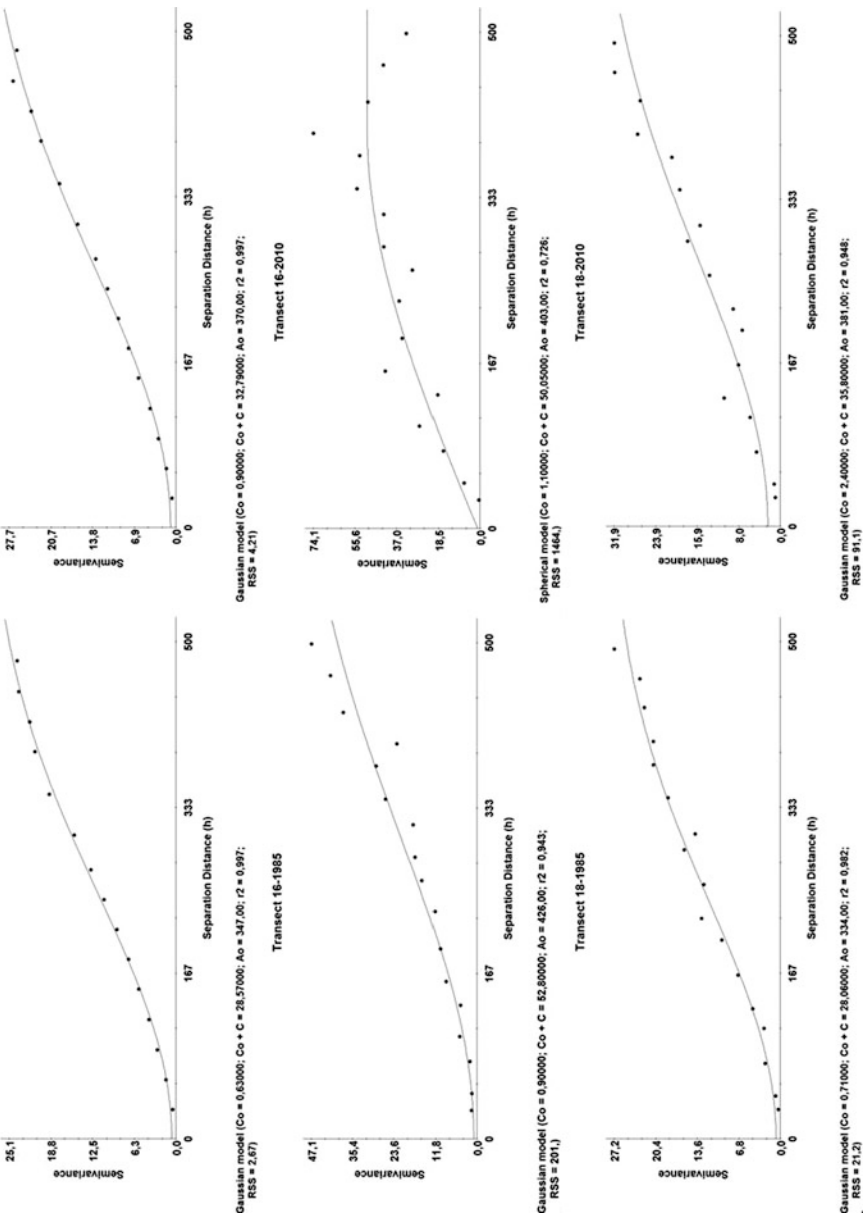

Fig. 3.3 Semivariograms of transects 1, 16 and 18

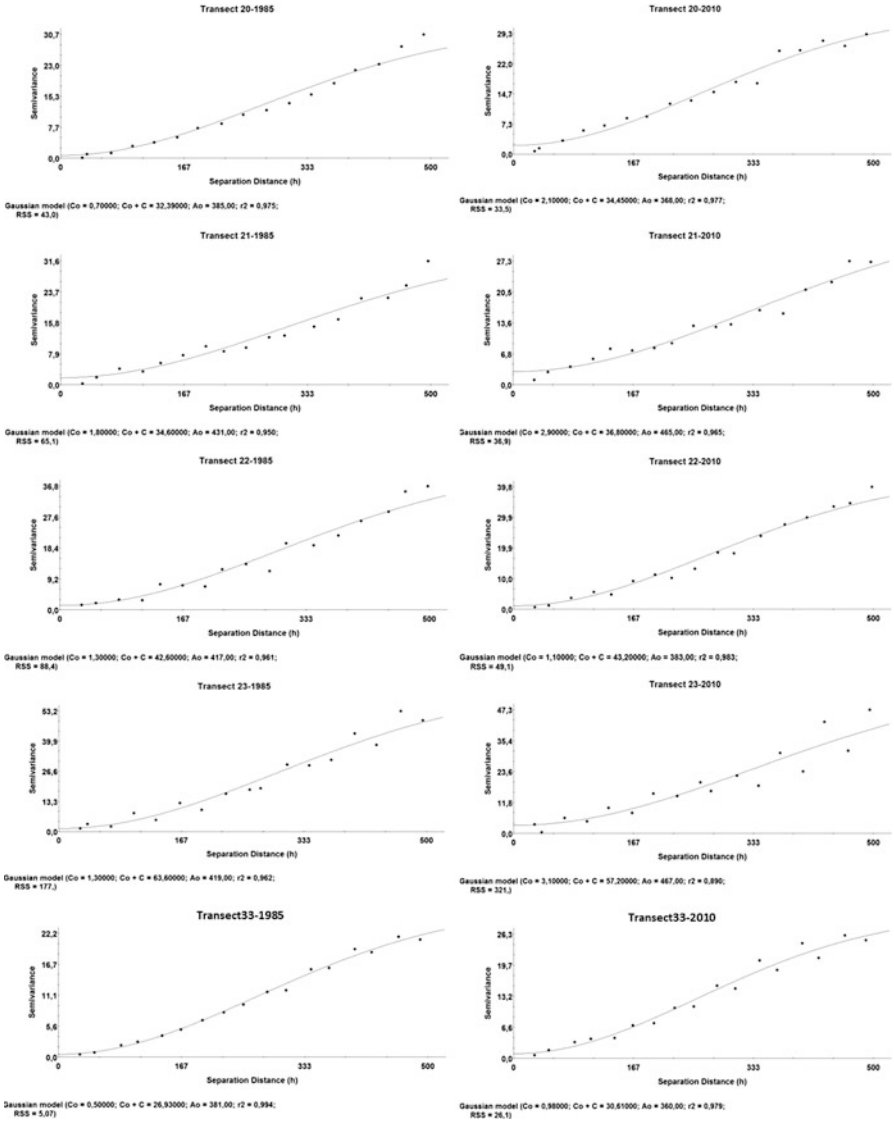

Fig. 3.4 Semivariograms of transects 21, 22, 2, 25 and 33

3.3.4 Transect Analyses

Spatial profile analyses of the selected transects are presented in Figs. 3.5, 3.6 and 3.7. Spectral radiance values along the transects were extracted for 1985 and 2010 to discuss and evaluate the occurred changes in the study area. Radiance values

were obtained from band 5th of each year image considering that this channel can be effectively used to identify land-sea boundaries. Radiance values of transects 1, 16, 18 and 20; transects 21, 22, 23 and 25; and transect 33 are shown in Figs. 3.5 and 3.6, respectively.

Temporal maximum changes occurred on transects 20 and 23. While for the 20th transect, it was calculated that the coastal line was filled as a result of interstate road construction and shifted towards to the sea around 145 m, on the other hand, for transect 23, the costal line moved towards to land side around 150 m as a result of coastal erosion. It was clearly observed that transects 18, 20, 21 and 22 indicate similar properties and have similar temporal changes. On these transects, the sea was filled up from the 35 to 140 m due to the construction of new state road and urbanization. Transect 18, 20 and 21 were close to Giresun city center where the population was 160,995 and 245,381 in 1985 and 2010, respectively. Transect 1 had slight change but similar to the transect 23 since the coastline shifted to land side because of coastal erosion. Transect 25 and 33 are example where there were not any significant temporal changes occurred during the 25 years. Spatial changes along the transects greater than 30 m (1 pixel) were assumed as significant within the scope of this research.

3.4 Conclusions

The purpose of this research was to highlight utility of integrated usage of remote sensing, GIS and geostatistics to determine human induced coastal changes. These technologies could also be used to identify coastal changes as a result of natural processes such as coastal erosion. For further studies, geospatial interpolation methods could be used to model impact of human-induced changes on sea water quality, if geographically distributed field samples of related parameters are available.

The results of this study illustrated that spatial profile and semivariogram analyses of the transects could be used to identify temporal changes occurred on the coastline. The examined profiles indicated that the coastline of the Black Sea changed significantly between 1985 and 2010 because of the construction of an interstate road and urbanization. In addition to human-induced changes, we also found out coastal changes caused by coastal erosion during our analyses.

Landsat satellite images with an archive of almost 35 years provide invaluable information to analyze and visualize past and current positions of coastlines. However, if detailed analyses of coastal changes will be emphasized, higher resolution satellite images should be also preferred.

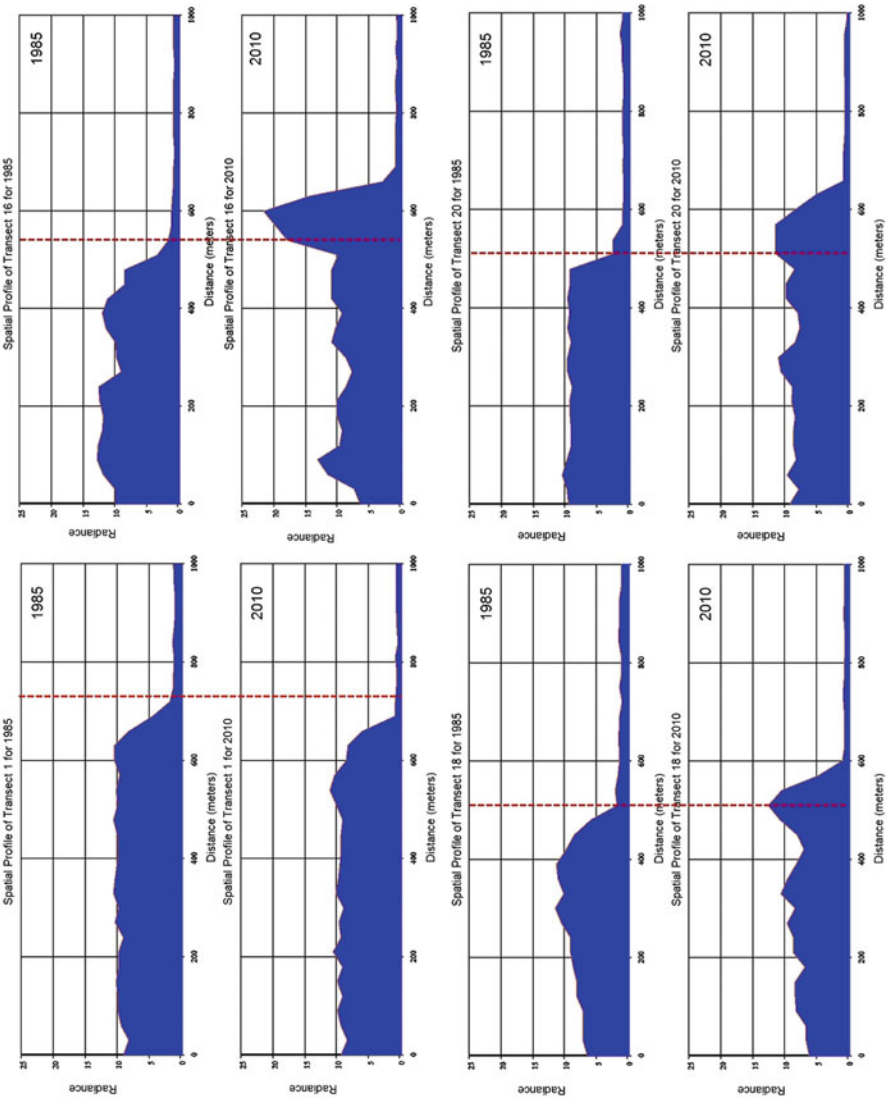

Fig. 3.5 The 1st, 16th, 18th and 20th transects

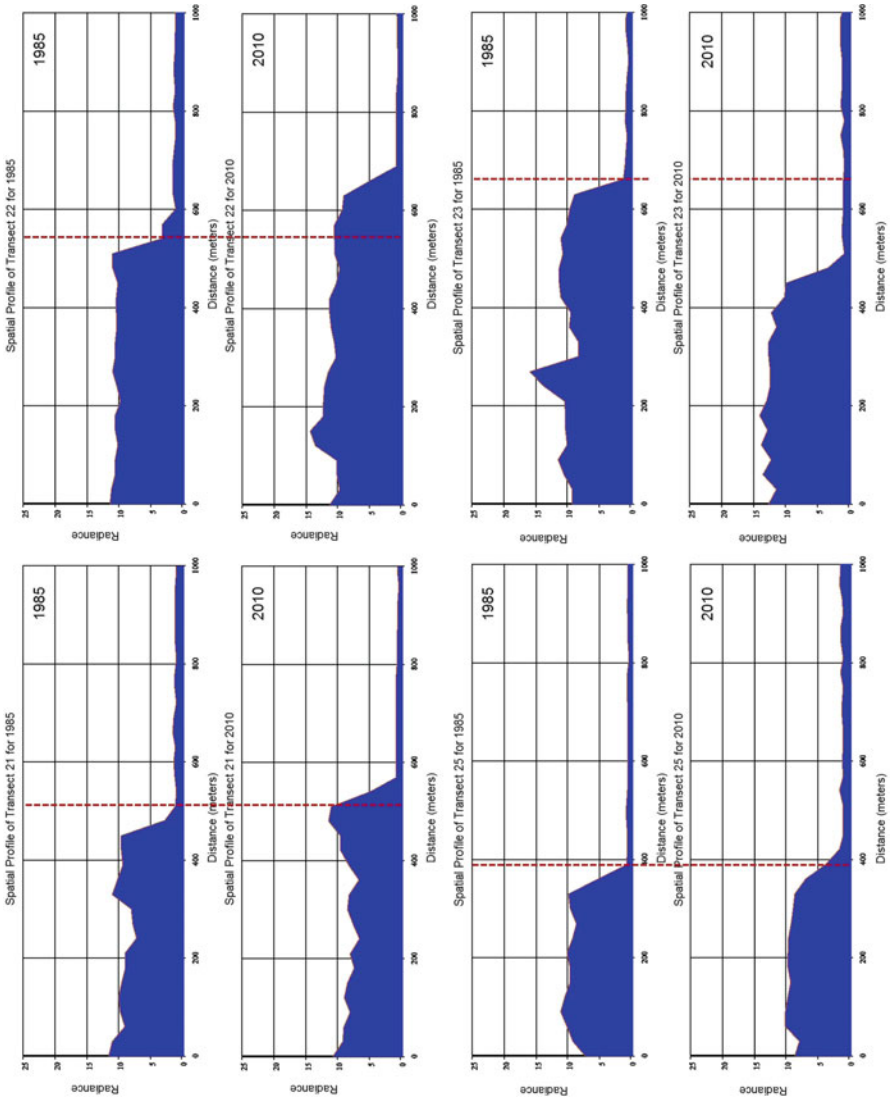

Fig. 3.6 The 21st, 22nd, 23th and 25th transects

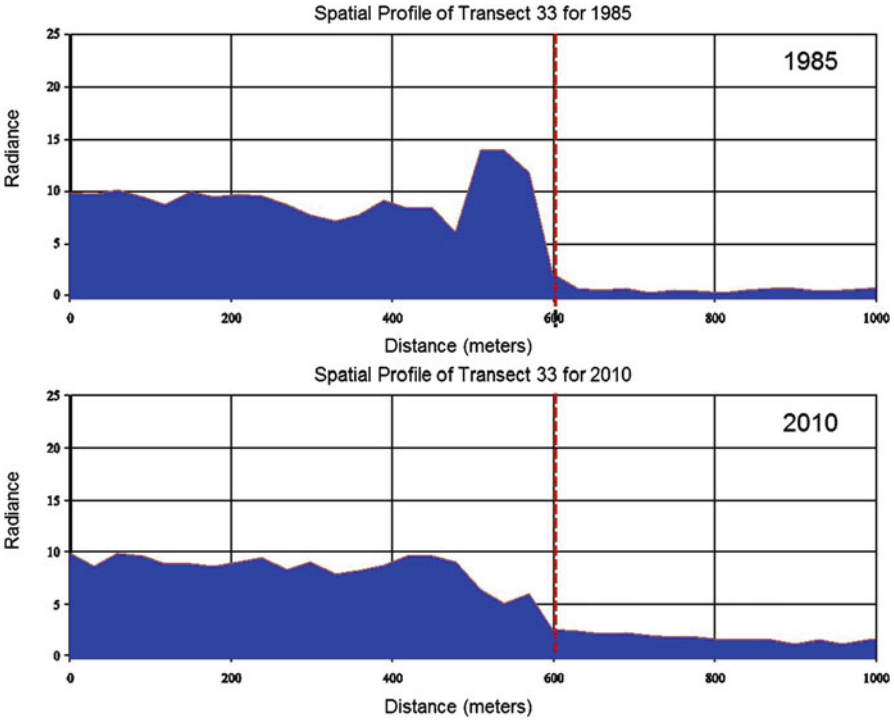

Fig. 3.7 The 33rd transect

References

Brivio PA, Colombo R, Maggi M, Tomasoni R (2002) Integration of remote sensing data and GIS for accurate mapping of flooded areas. Int J Remote Sens 23(3):429–441

Burrough PA, McDonnell RA (1998) Principles of geographical information systems, 2nd edn. Oxford University Press, Oxford

Cowell PJ, Zeng TQ (2003) Integrating uncertainity theories with GIS for modeling coastal hazards of climate change. Mar Geodesy 26:5–18

Curran PJ (1988) The semivariogram in remote sensing: an introduction. Remote Sens Environ 24 (3):493–507

Fedra K, Feoli E (1998) GIS technology and spatial analysis in coastal zone management. EEZ Technol 3:171–179

Goovaerts P (1997) Geostatistics for natural resource evaluation. Oxford University Press, Oxford

Holsapple CW, Whinston AB (eds) (1991) Recent developments in decision support systems, Nato ASI series. Springer-Verlag Berlin Heidelberg New York

Kaya S, Sertel E, Seker DZ, Tanik A (2008) Multi-temporal analysi and mapping of coastal erosion caused by open mining areas. Environ Forensics 9(2):271–276

Liang S (2004) Quantitative remote sensing of land surfaces. Wiley, Hoboken

Musaoglu N, Seker DZ, Kabdasli S, Kaya S, Duran Z (2004) Using remote sensing and GIS for the assessment of visual attributes; case study of the south coastal zone of turkey. Fresenius Environ Bull (FEB) 13(9):854–859

Ostir K, Veljanovski T, Podobnikar T, Stancic Z (2002) Application of satellite remote sensing in natural hazard management: the Mount Mangart landslide case study. Int J Remote Sens 24 (20):3983–4002

Pattanaik C, Prasad SN (2011) Assessment of aquaculture impact on mangroves of Mahanadi delta (Orissa), East coast of India using remote sensing and GIS. Ocean Coast Manag 54 (11):789–795

Schweiger EW, Bolgrien DW, Angradi TR, Kelly JR (2005) Environmental monitoring and assessment of a great river ecosystem: the upper Missouri River pilot. Environ Monit Assess 103:21–40

Seker DZ, Kaya S, Alkan RM, Tanik A, Saroglu E (2008) 3D coastal erosion analysis of Kilyos–Karaburun region using multi-temporal satellite image data. Fresenius Environ Bull 17(11b):1977–1982

Seker DZ, Kutoglu H, Gormus S, Tanik A, Musaoglu N (2011) Investigation the reasons and results of the coastal erosion of Karasu Region (Turkey) using multi-temporal satellite sensor data. In: AGU fall meeting, San Francisco, USA, 5–9 December 2011

Sertel E, Kaya S, Curran PJ (2007a) Use of semivariograms to identify earthquake damage in an urban area. IEEE Trans Geosci Remote Sens 45:1590–1594

Sertel E, Kutoglu SH, Kaya S (2007b) Geometric correction accuracy of different satellite sensor images: application of figure condition. Int J Remote Sens 28(20):4685–4692

Sertel E, Findik N, Kaya S, Seker DZ, Samsunlu A (2008) Assessment of landscape changes in the Kizilirmak Delta, Turkey using remotely sensed data and GIS. Environ Eng Sci 3(25):353–362

Song C, Woodcock CE, Seto KC, Lenney MP, Macomber SA (2001) Classification and change detection using Landsat TM data: when and how to correct atmospheric effects? Remote Sens Environ 75:230–244

Toutin T (2004) Review article: geometric processing of remote sensing images: models, algorithms and methods. Int J Remote Sens 25(10):1893–1924

URL 1: http://en.wikipedia.org/wiki/State_road_D010_(Turkey)

Webster R, Oliver MA (2007) Geostatistics for environmental scientists. Wiley, New York

Part III
Flood Hazards (Storm Surge, Sea-Level Rise, and Populations from Risk of Coastal Flood Hazards)

Chapter 4
Coastal Risk Versus Vulnerability in an Uncertain Sea Level Future

Michael S. Kearney

Abstract Discussions of coastal hazards commonly use terms like risk and vulnerability interchangeably, when in fact they are much different concepts. Vulnerability describes qualities of location, structural condition, past incidence of events, and the like that render an entire coast, individual communities, or even particular coastal structures likely to suffer damage and loss and associated socio-economic impacts. But they are not the events that cause disaster (like coastal storms, exceptionally high tides, or El Niño episodes). Sea level rise and coastal storms are two phenomena especially subject to much confusion about vulnerability and risk. General predictions of future sea level rise and coastal storminess are often treated as risk factors. Apart from uncertainties in the climate and ocean models that form the basis for such predictions, forecasted rates of sea level rise really only set conditions for events like coastal storms comprising the actual hazard. Similarly, overall coastal storm histories, even compendia of actual storm tracks, just indicate the general degree of vulnerability of coasts to future storms, not the likelihood or probability of a storm landfall or even near miss (that could produce damage) in any particular year. However, if high resolution data are available to constrain hazardous, short term increases in sea level in time and space for a reach of coast, then some probabilistic determinations may be made of yearly, seasonal, or monthly risk. Equivalent risk assessments can be prepared for the probability of coastal storm impacts in any one year, assuming the same data requirements – extra-tropical storms, occurring every year are most suited for this kind of analysis. Most coasts in the developed world have data available which are capable of resolving exceptional sea level high stands and coastal storms to hourly levels of temporal resolution and, equally critically, location. It is increasingly evident that the variability in climate and sea level has displayed a sharp upswing since the

M.S. Kearney (✉)
Department of Environmental Science and Technology, University of Maryland, College Park, MD 20742, USA
e-mail: mkearney01@yahoo.com

C.W. Finkl (ed.), *Coastal Hazards*, Coastal Research Library 6,
DOI 10.1007/978-94-007-5234-4_4,

middle 1960s. This recent phase, possibly heralding a major global climate shift, is the period from which risk assessments of hazards from sea level highstands and storms should be based.

4.1 Introduction

With the threat of accelerating global sea level rise, burgeoning coastal populations worldwide, as well as growing pressures on social and social systems, assessing coastal risk has never been more important. Decision makers at all levels, whether public or private, must develop policies that best address present and future coastal development and that strike a balance between protection, funding, and social and political realities. This is a daunting task for countries (e.g., the U.S.) with huge coastlines where costs and benefits must be weighed in light of limited time and physical resources and often fleeting national economic priorities. Commonly, when confronted with a number of choices that entail changes in behavior or lifestyle (not to mention costs), the natural inclination is to consider the most likely outcomes which might occur within a future that can be reasonably planned for (perhaps 20–30 years). Similarly, since it is not unusual that several equally pressing outcomes to emerge, requiring similar levels of resources and effort to address, an allied response is to consider reasons for: (i) addressing one of the outcomes and not the others; (ii) partially addressing some and ignoring the others; or (iii) even delaying making a decision. However, a key factor in breaking any decisional impasse is an elucidation of what *risks* might be incurred over a certain time period if one course of action is followed for a while and not another or the amount of time and effort are required to gather resources to address what must be done. This assessment of outcomes within the framework of probabilities or risk analysis is the subject of this chapter, which discusses what actually constitute physical risks in coastal hazards as opposed to vulnerabilities.

The distinction between vulnerability and risk is one that often is not clearly made in coastal hazard research. Typically, factors such as land elevation, proximity to the shoreline, rates of shore erosion, storm histories, average storm surge levels, etc., are combined (using a GIS) into a map or series of maps (e.g., Gornitz et al. 1994) that purport to show risk. In truth, there is little indication of *when* the confluence of these factors will result in a hazard event because though called risk factors, they are not capable of being considered in probabilistic terms. In other words, they are factors that contribute that to creating the conditions in coastal hazards can occur – i.e., vulnerability – but are not the hazards themselves that might lead to disasters. This is not to say that vulnerability assessments (whether they are purely environmental or include social or economic aspects) are not important because an event (whatever its magnitude), whose uncertainty of occurrence is the subject of risk analysis, only becomes a hazard within a framework of vulnerability. In many coastal vulnerability studies, attempts to incorporate a risk component are usually done by examining the regional or local history of storm events and the amount of erosion or flooding they produced. For example, storm statistics in

Horn and Whitaker (1982) and similar sources (e.g., NOAA) provide information on the average number of extratropical storms that can be expected on average per year, and some idea of the affected area of the coast can be also determined. But such approaches are at best quasi-probabilistic and, therefore, not true risk assessments, even when strengthened by examining sea level trends, past or predicted.

In this chapter, we will examine how amenable the natural hazard components of coastal disasters are to risk analysis since the consequences of an event hinge on whether its likelihood can be delimited. Though the concept of conditional or contingent probability probability[1] certainly comes into play in evaluating the flooding risk for large scale developments – e.g., whether an existing sea wall will be overtopped at some future point by storm waves (as happened at Galveston sea wall during Hurricane Ike) – the focus should be on the phenomena that actually contribute the hazards. However, the differences between vulnerability factors and risk factors are not always clear, particularly when time intervals longer than a few years to a decade are considered. Sea level rise exemplifies this problem as it can be both a long and short term hazard as well as critical factor that contributes substantially to increased vulnerability.

4.2 Coastal Vulnerability Versus Coastal Risk

As noted, most of the studies using the term "coastal risk" are more investigations of *coastal vulnerability* of a physical, social and economic situation where some event – generally a large storm – could exploit and result in a level of damages to these conditions beyond which might occur if they did not exist. There are set assumptions implicit in such studies, viz: that a storm with several general characteristics (e.g., wind speed, track, surge and wave factors) strikes a coast. Other vulnerability characteristics such as demographic changes, economic trends, and the like must rely on predicted growth scenarios. There is no denying that some of these factors associated with framing a coastal vulnerability scenario can contain probabilistic aspects, but the agents, sea level rise and climate, that animate the events (storms) which underpin risk are often dealt with by selecting a known storm (generally recent) for which detailed spatial information on winds, track, tidal heights, etc., are available. A high resolution grid can then be applied in flood models like FEMA's Haz-MH for flood elevations scaled realistically (i.e., considerably less than a kilometer) for developed areas. In essence, though it is argued otherwise, such predictions are of a *sui generis* nature as it cannot be assumed that a similar storm will occur in the future. Alternatives to this, such as using historical records, are subject to similar criticisms.

[1] Conditional probability is the probability of B (in this case, an event) occurring given that we know A has occurred. For example, the likelihood of significant storm surges are contingent on the occurrence of a storm of certain magnitude.

4.3 Sea Level Rise as a Hazard and Contributor to Coastal Vulnerability

4.3.1 General Theoretical Issues

Since the mid-1980s, concerns about the impacts of Anthropogenic Global Warming (AGW) have fostered a rapidly growing literature on the course of future of sea level rise and its effects. Most of these studies have focused on vulnerability aspects (e.g., Titus et al. 2008). Moving beyond vulnerability to risk analyses presents considerable challenges as the calculation of probabilities for future risks must rely on global models, not past trends. Simple linear extrapolation of existing sea level trends, even where tide gauge records are of sufficient length to allow statistical significance, runs counter to what climate scientists agree will be by the mid-twenty-first century a global sea level trend best approximated by a second order function. Hence, there is concern that linear extrapolations could underestimate risks. Beyond this, tide gauge records for many areas simply show no evident trends that may be extrapolated for reasons that are not well understood though oceanographic factors are often suspected (Cazenave and Llovell 2010). In particular cases, human modifications to basin characteristics (like an estuary or harbor) are the likely cause, such as Tokyo Bay where post-WW II harbor construction changed the bay hydrography to an extent that discerning any long term signal from the available tide gauge record is problematical (Fig. 4.1). Other tide gauge records present similar problems, either because they are too short or contain significant gaps, with high inter-annual and inter-decadal variability (Douglas 2001).

A less tractable problem that has come to light in recent years is the degree of inter-decadal variability in long and otherwise "high quality" (i.e., complete and without obvious *in situ* biases) tide gauge records. Statistical analyses of these records show distinct patterns of rapid sea level rises followed by sharp declines (Church and White 2006; Holgate 2007). The amplitude of these departures from high stands to low stands can be up to 8 mm year^{-1} (Fig. 4.2). A puzzling aspect in records long enough to span the whole of the twentieth century is the obvious change in temporal pattern of the high and low stands, which have a greater amplitude and appearance of regularity in the latter half of the century than the first half. Coinciding with this change in phasing was a net reduction in rate post – 1953, with the exception of a very late acceleration in the 1990s (Holgate 2007). Because of the lag in reporting data to repositories such as the Permanent Service for Mean Sea Level (PSMSL), the Holgate and Church and White studies did not incorporate data later than 2003. Recent updates to the records archived in PSMSL show the overall deceleration in rate evident since 1999 continued up to 2010. Though it appears that a new phase of acceleration may have begun in the last several years, it may take until 2020 to determine if this is indeed the case.

The implications of almost decadal long positive and negative departures in the mean sea level trend – especially their possible strengthening since 1960 – have been part of a lively discussion (Houston and Dean 2011; Rahmstorff and Vermeer 2011) about the evidence for acceleration and deceleration in twentieth century sea

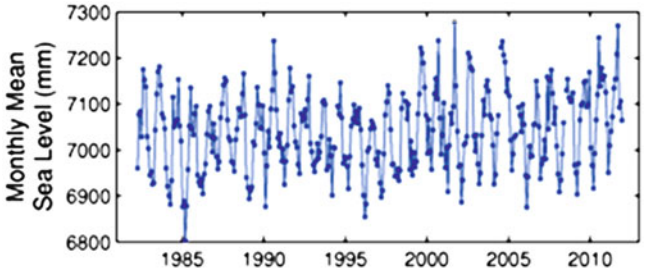

Fig. 4.1 Toyko III monthly tide gauge record (Source: psmsl.org)

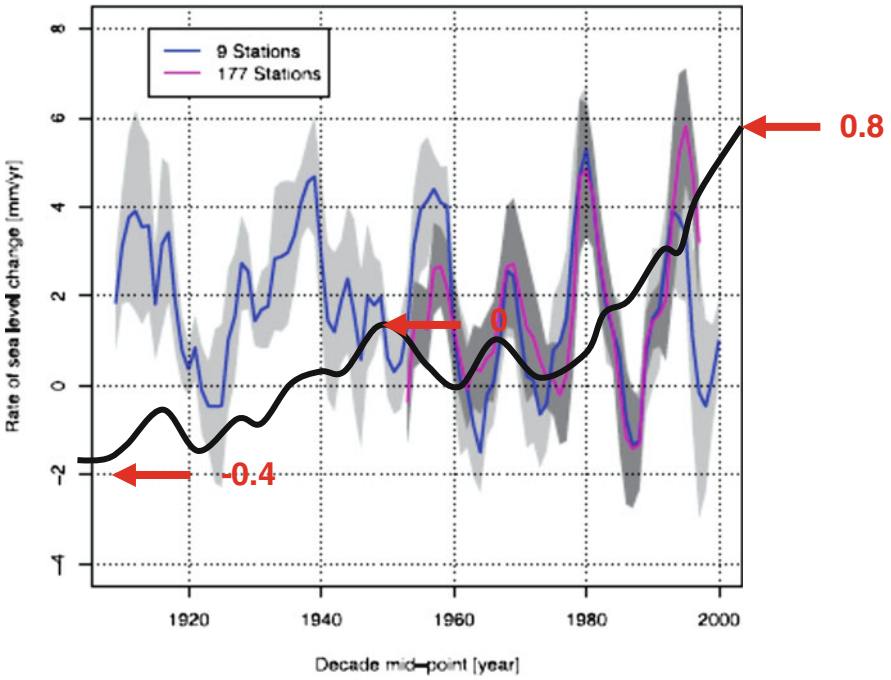

Fig. 4.2 Decadal in twentieth century global sea level rise based on the analysis of 177 tide gauge records, with the trend for global variations since 1880 superimposed on the figure. The *red* numbers are temperature anomalies relative to 1901–2000 mean (see, Fig. 4.4; modified from Holgate (2007))

levels. Of course, the lack of a demonstrable acceleration in sea level rise, if widely confirmed, would be of great significance to vulnerability and risk analysis for coastal studies. Assuming that there has been some acceleration – and Holgate (2007) concludes there was in the last half of the twentieth century (though smaller than the acceleration in the first half) – what do these departures for forecasting changes in vulnerability and, possibly, risk?

Superimposing a theoretical series of positive and negative departures on the estimated sea level trend for this century shows that the decadal departures reconstructed by Holgate (2007), encompassing a change of 8 mm from the 1980s to the late 1990s, introduce a further hurdle for prediction (Fig. 4.2). Terminating the positive departures in several instances are exceptional high stands approaching 20 cm. The processes that drive these phenomena are not fully understood – whether by short term thermosteric expansions or to wind stress field dynamics abetted by ENSO events (Firing et al. 2004) – but the apparent periodicity that characterizes the record since 1960 could be a feature of future conditions that might extend for the next decades.

4.4 Predicting Future Sea Level Rise

Forecasting future sea levels for prediction of coastal risk and vulnerability assessment must account for some of the theoretical problems of inter-decadal and inter-annual variability already discussed, but must also come to grips with the fact that no single model for future sea level trends is definitive. Moreover, whether the models are modest in prediction or more aggressive (i.e., the so-called "high-end" models), the increasing scale of the uncertainties beyond 30–40-years rise so dramatically as to render them essentially impracticable for risk determination. Limiting ourselves essentially to a termination date of ca. 2050–2060 AD for prediction results in a narrower sliding error window, but also avoids the sharp curvilinear phase so characteristic of most models for later decades of this century (see Houghton et al. 2001). This is not to say that the projected mid-twenty-first dramatic rise in sea levels overestimates the atmosphere–ocean response, as the minimal lag displayed by sea surface elevations (Topex-Poseidon) and sea surface temperatures (AVHRR and ERS satellites) indicates little thermal inertia, particularly during ENSO events in the Pacific Ocean (e.g., Andersen et al. 2002), However, focusing on the relative linearity in early phase response that characterizes most sea level rise models until about mid-century (see Rahmstorff 2007) allows for a linear extrapolation for tide gauge records.

4.4.1 Decadal Variability

Selecting a baseline initiation date encapsulates all the concerns noted above. Aside from the problems of record length and continuity, it is clear that for many records that extend back at least to the 1930s, trends for the latter half of the twentieth century differ from those for the first half – in other words, rates based on regressions incorporating the whole record may be biased by antecedent conditions that no longer apply. The tide gauge record for Sydney Harbor (Fig. 4.3) is an example, where the pre-1950 tidal trend obviously differs from the 1950 – present. Reasons for such divergences are often not clear, though in some cases harbor

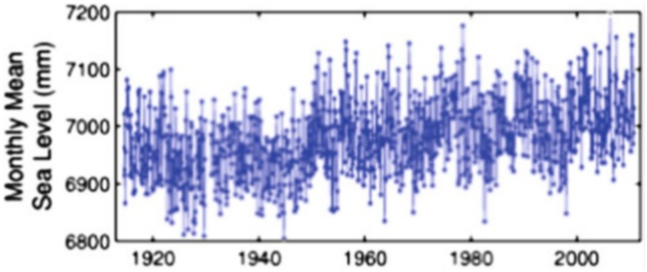

Fig. 4.3 Sydney 2 monthly tide gauge record, 1915–2010 (Source: www.psmsl.org)

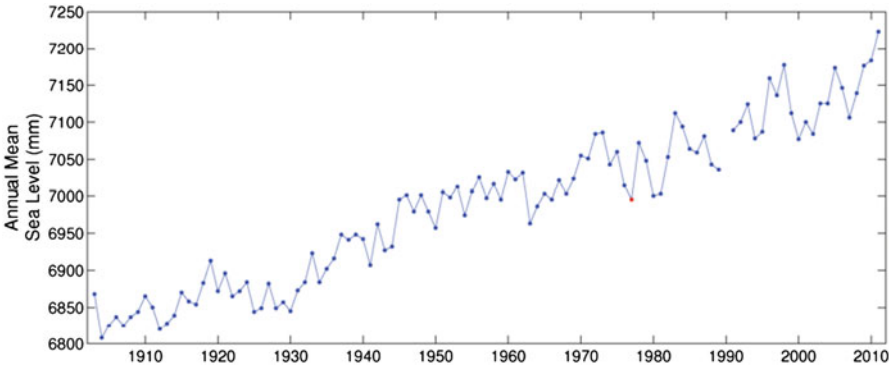

Fig. 4.4 Baltimore annual tide gauge record, 1902–2011 (Source: www.psmsl.org)

construction and its effects on hydrography may be the reason. In any event, conceptually it is hard to argue that using the whole record is proper for obtaining rate of sea level rise for extrapolation.

For the U.S. middle Atlantic Coast, similar differences appear to characterize general trends between the first and last halves of the twentieth century; but particularly noticeable, is the increasing degree of inter-decadal, and, possibly, inter-annual variability after the 1960s. Houston and Dean (2011) for example, derived different rates of sea level rise for 57 long term tide gauge records from across the U.S. depending on whether the beginning was before or after 1930. In the case of the Baltimore tide gauge record, the annual sea level data (Fig. 4.4) suggest two distinct periods: 1910–1960 and 1960–2009. Standard deviations in mean sea levels for each decade since 1910 (the first decade, 1900–1909, not being considered since the 2 years are missing) computed from average yearly sea level data show that since 1960 the overall decadal standard deviations average about 4.5 mm higher than they were from 1910 to 1959 (Table 4.1). The significantly intra-annual variability in between 1960 and 2009 is even more convincing that the factors driving sea level variation in five decades have changed. In fact, the general pattern of sea level changes mimic reliable measurements for surface temperatures, where there appears to be a distinct partition between temperature trends centering around 1960–1965 (Fig. 4.5).

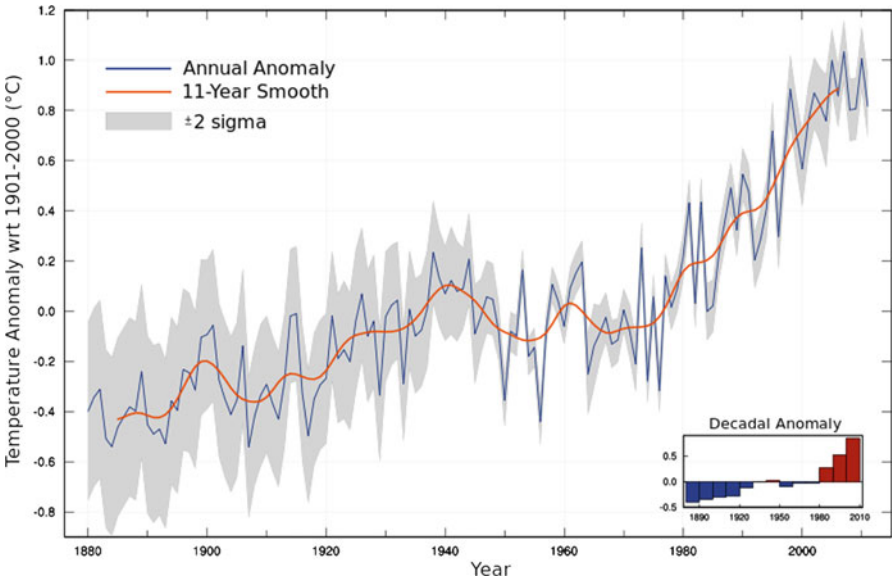

Fig. 4.5 Global land temperature variations 1880–2011 (http://www.ncdc.noaa.gov/oa/climate/research/anomalies/index.html)

4.4.2 Intra-Annual Variability

If the rationale for using the post-1960 (perhaps even the post 1980) tide gauge record as the baseline for extrapolation is clear, late twentieth century to present decadal trends provide a better framework for assessing growing vulnerability rather risk. Essentially, risk is associated with events, like storms that generally transpire within a few days, and decade-level trends provide little insight into such short time scales. An analysis of any long monthly tide gauge record will generally reveal considerable intra-annual variability, especially middle and north Atlantic coasts. There are a variety of factors responsible for this observed variability, but perhaps the most important are broad hemispheric seasonal changes (e.g., Komar and Enfield 1987), ranging on the level of decimeters. Moreover, as is suggested by the monthly standard deviations for sea levels at Baltimore, intra-annual variability seems to be increasing in recent decades (Table 4.1). In the last 30 years, several monthly high stands have equaled or slightly exceeded 20 cm about the mean trend, about half of them terminating almost decade-long sharp accelerations. Realistically, these short high stands in sea level comprise a more *knowable* risk (cf. Hillson 2004) for individual coasts than sea level changes derived from predictions from global models. Moreover, by using simple statistical tools – depending on the availability of high frequency (monthly or shorter) tide gauge records – probabilities can be determined.

Table 4.1 Changes in standard deviations from decadal averages for mean sea level for Baltimore tide gauge record, based on annual and monthly data. Slope of decadal trends based on monthly data are shown for 1960–2009 (Data from Permanent Service for Mean Sea Level (www.psmsl.org))

Decade	$^{\sigma}$X annual (mm)	$^{\sigma}$X monthly (mm)	Slope annual (mm)	Slope monthly (mm)
1910–1919	27.13	109.71	5.78	7.04
1920–1929	17.27	100.99	−2.95	−1.65
1930–1939	34.85	104.91	10.42	11.21
1940–1949	33.75	105.68	8.24	9.55
1950–1959	20.39	112.34	2.4	4.13
1960–1969	22.61	117.99	−0.95	0.13
1970–1979	28.59	120.74	−3.37	−1.86
1980–1989	36.17	126.31	3.36	4.34
1990–1999	34.06	129.28	7.11	7.63
2000–2009	34.17	241.47	8.39	9.89

The Weibull Method, long used in predicting flood recurrence interval in rivers, can readily be applied to assessing high stand recurrence interval and probability. In simplest form, high stands equal to or greater than a specific height are n in the simple equation where m is the magnitude rank order of the high stand:

$$\mathrm{R} = \frac{\mathrm{n}+1}{\mathrm{m}}$$

The probability of the event (i.e., high stand) occurring in any 1 year, of course, is derived by the inverse of R, the recurrence interval. The probability that a certain magnitude high stand will occur over a specific time can be determined by:

$$\mathrm{q} = 1 - \left(1 - \frac{1}{\mathrm{T}}\right)^{\mathrm{n}}$$

where q is the probability of a high stand with a recurrence interval T within a specific time interval n (Costa and Baker 1981).

4.5 Storm Risk

The uncertainties for coastal planning not only concern the course of future sea level rise, but whether the frequency and intensity of major coastal storms will change. There are historical data bases provided by NOAA in the U.S. and various meteorological observatories across Atlantic coast of Europe (Lozanoa et al. 2004). For other parts of the world, especially broad swaths of the Pacific Basin, historical data are far less complete. Fortunately, since the advent of the age of weather satellites, beginning with the TIROS series in 1960s, there are at least data for

every major ocean basin for about almost the last 50 years. However, even where records go well back into the nineteenth century, the records for tracks of the storms becomes less accurate and more inferential, especially before the widespread adoption of ships radio or wireless, where reports of ship encounters with storms in the Atlantic or other oceans could be reported (assuming the ship radio was not damaged).

But there are important differences between using coastal storm records for prediction of future occurrence compared to records of river discharge. For one, though the risk posed by flood level discharges can be gauged by factors of discharge magnitude, site elevation, and proximity to the channel (which are often one in the same for risk assessment purposes), by comparison frequency of previous tracks, storm strength, associated levels of associated storm surge, theoretical angles of attack of largest incident waves, as well as coastal elevations, do not necessarily equate with the storm risks for coasts. A prime example is Hurricane Andrew, a Category 5 hurricane and its effects on Miami in 1992. Despite having at face value ideal conditions for these indicators coupled with the low elevation of Miami, its impact on the city was comparatively minimal because the eye wall made landfall just south of the city and the storm was small and had a rapid forward velocity (http://www.nhc.noaa.gov/1992andrew.html). Had the eye wall made landfall farther north, the storm been larger in size, and the forward velocity slower, the outcome for Miami and adjacent coastal areas would have been much different.

Moreover, along the U.S. middle Atlantic coast, tropical storms need not even make landfall on the coast itself to produce extensive damage and loss of life in coastal areas. Two of the most devastating "coastal" storms of the past 50 years, Hurricanes Camille and Agnes, actually made landfall in the eastern part of the northern Gulf of Mexico. The earlier hurricane, Camille, the second most powerful hurricane to make landfall in the twentieth century on the Northern American mainland, after wreaking untold havoc on the Mississippi coast, traveled up the spine of the Appalachians, and eventually crossed over in the lower part of Chesapeake Bay generating record rainfall amounts that produced extreme floods in Nelson County, Virginia, and down the length of the James River estuary into the coast. Similarly, 3 years later, Tropical Agnes (née Hurricane Agnes), once again making landfall in the eastern part of the northern Gulf of Mexico, tracked up the Appalachians after landfall, causing massive flooding along the western shore of Chesapeake Bay, from Norfolk, Virginia (where the downtown was flooded by water depths of 1 m plus; Stevenson and Kearney 1996) to Baltimore, Maryland. Hurricane Floyd's impact on North Carolina tells a comparable story.

The debate concerning whether hurricanes have become more intense and frequent – or perhaps more long-lived (Emanuel 2005; Webster et al. 2005; Klotzbach 2006) – remains contentious, and is as much an indication of the quality of the data as any other factor. To be sure, predicting future hurricanes (and likely extra-tropical storms) remains *not quite* an unknowable risk if a coast-wide perspective is sought. Elsner et al. (2006), for example, using an extreme-value model combined with best-track HURDAT records from the National Hurricane Center showed that the return of a storm equal to or greater than Katrina in intensity can be

expected to occur somewhere in the northern Gulf of Mexico every 21 years. Of course, recent experience of the Category 4 and 5 hurricanes in the north Gulf demonstrates even catastrophic-level storms that made landfall across such a broad arc of coast from Texas to Alabama can produce effects ranging from high surf and strong gusts to widespread devastation, depending on the proximity of the area to the eye at landfall, coastal configuration, and even the health of coastal marshes and their ability to buffer storm surge (Resio and Westerink 2008). Geomorphic and sedimentological evidence – where there is a high resolution sediment record – can perhaps allow some insights into the impacts on specific coasts, especially with short-lived isotopes like ^{210}Pb and ^{137}Cs for dating. Pre-historic reconstructions ("paleotempestology"), on the other hand, are more problematical, because, as Hurricane Andrew demonstrated, even Category 5 storms may leave little trace on the coast where they made landfall. In addition, considering that sea levels were much lower in past millennia, and combined with significant coastal changes, it is probable the effects of any tropical storm were not only different, but the evidence in the shelf record also could have been removed or altered by subsequent erosion.

Extra-tropical storms, since they characterize middle to higher latitudes of the East Coast of North America most every year, present a more statistically amenable data suite. Even here, storm climatological studies, while suggesting strong, almost bi-decadal trends (Fig. 4.6) lend themselves more to assessments of coastal vulnerability (i.e., expected frequency) rather coastal impact (determined probability). The reasons are much the same as discussed with respect to tropical storms; however, the greater number of these "cold core" storms since the period of improved synoptic (i.e., satellite) observations and reliable damage records hold the promise for some risk assessment. The often idiosyncratic nature exhibited by some of the most notorious nor'easters can be expected to defy reliable prediction for the foreseeable future. The archetypical example is the infamous Ash Wednesday Storm of March 6–8, 1962. This storm, the peculiar confluence of three pressure systems, not only produced 12 m waves, but lingered for five tidal cycles (http://pubs.usgs.gov/of/2003/of03-337/winter.html). This last factor, by promoting greater wave run-up, was as responsible for much of $200 million damage and loss of 40 lives as the storm's intensity. By any standards, the long period of stationary behavior of the Ash Wednesday was highly unusual, and it stands as the "poster child" for what a "bomb" nor'easter can do (Sanders and Gyakum 1980).

For the more typical nor'easter, formed by single area of vorticity, the tracks of the storms as they proceed up the coast ultimately determine whether their coastal impact will be large or small. If the center of a nor'easter tracks overland, depending on how far inland it moves, coastal effects are more likely to be less than if the center of circulation is well offshore (Sanders and Gyakum 1980). Though the prediction of how any individual nor'easter will behave – let alone "bomb" storms – remains challenging, simple statistics should be able to give some idea of risk. As storms comprise a discrete variable, the data bases for occurrence of nor'easters allow for calculation of their average frequency per year, and from this, the ability to determine a Poisson Distribution for the whole coast, or using GIS plot storm hits per cell (Fig. 4.7). From this we could derive the average number of storm

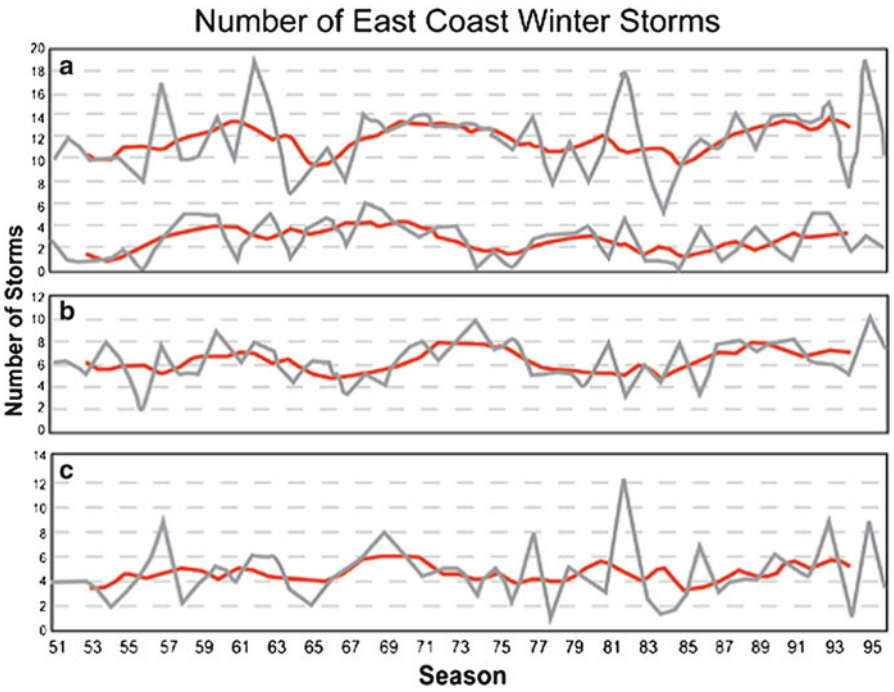

Fig. 4.6 Winter storm occurrence of the East Coast of the United States, 1951–1997. Panel (**a**) compares the occurrence of all winter (extra-tropical) storms in *top* to the strongest storms in the *bottom*. Panel (**b**) shows the occurrence of storms above 35° latitude. Panel (**c**) shows the occurrence of storms that tracked up the length of the East Coast. (Taken from CCSP SAP 3.3 2008)

hits (i.e., those that pass through all cells determined closest to the adjacent coast or city), λ, and assuming the storm history is sufficiently long that distribution is not too skewed, calculate *P(x)*, the probability of a storm hitting any the cells of interest within a certain period (*x*):

$$\mathrm{p(x)} = \frac{e^{-\lambda}\lambda^{\mathrm{x}}}{\mathrm{x!}}$$

4.6 Status of Coastal Risk Research

This chapter has focused on the distinction between vulnerability and risk assessments in analysis of future coastal hazards. The intent has not been to denigrate vulnerability studies, but to examine where actual risk might be determined with respect to environmental factors that are *events* that trigger disasters: sea

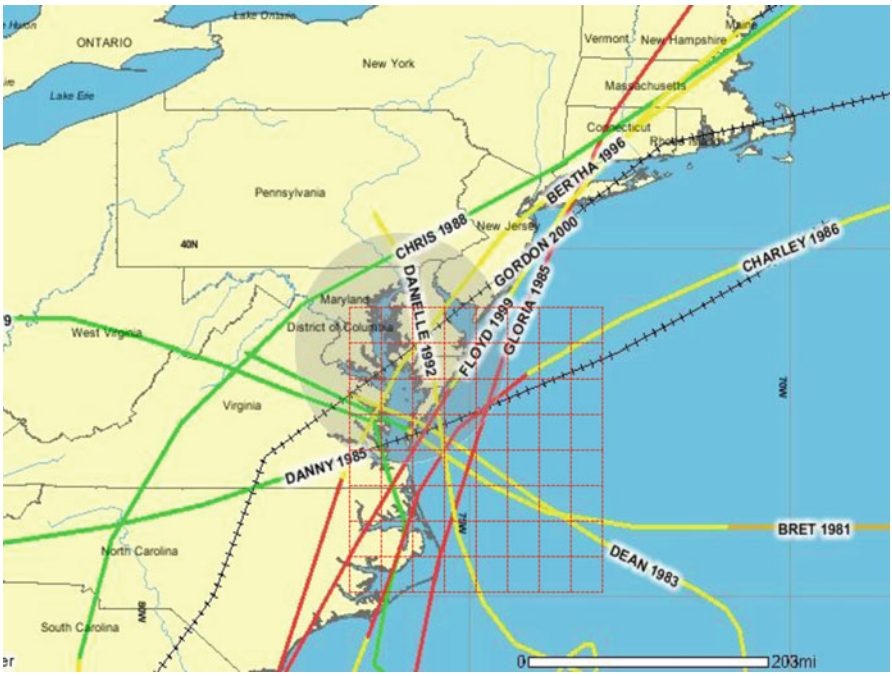

Fig. 4.7 Illustration of a sample grid to sample storm "hits" on different areas of a coast (here the U.S. middle Atlantic Coast). The storms portrayed are hurricanes from 1976 to 2000 that tracked across the middle Atlantic region

level rise and storms. There are, of course, other risk factors that were not discussed that should impinge on any vulnerability/risk analysis – ranging from human perception and bias (Hillson 2004) to engineering determinations where storm exceedance of structural integrity parameters might cause systemic failures – but they are beyond the scope of the chapter.

Sea level rise, as the chapter has tried to make clear, can be viewed from the perspective as either a risk or vulnerability factor. From the standpoint of better forecasting of potential vulnerability alone, more robust estimates of future sea levels derived from existing tide gauge records are likely to be more useful for short range coastal planning than present global models. Similarly, the global forecasts of flood losses based on such models that often extend far into the present century (cf. Hanson et al. 2011) are extremely useful for raising awareness of the global reach of the sea level threat; hopefully, they will help secure a place on the national agendas of the countries identified as potentially vulnerable to ruinous levels of future coastal flooding. But it is precisely because high frequency tidal data for many areas allow for determination of actual flooding risk for short term, *knowable* phenomena that more studies of medium range (several decades) of sea level change/risks are needed. The degree of inter-decadal and inter-annual variability in sea level for the last 30–40 years illustrated here for Baltimore is not

exceptional; a perusal of other tide gauge records for the U.S. Atlantic Coast show comparable short term fluctuations. Given that recent decadal accelerations are often terminated by high stands that will not be matched in predicted global forecasts for several decades, the risk for coastal flooding, especially if they occur at spring tide, is substantial.

By comparison, the problems of deriving storm risk are less amenable to solution. Hurricane risk assessment for much the U.S. Atlantic Coast is hampered by the low number of storms that have tracked close enough to the shore to cause damage; it is not even clear if it possible for the Gulf Coast. Whether this relative immunity to tropical storms may persist in a warming climate is presently unknowable, even if predictions of increased intensity (and possibly) frequency prove accurate. With respect to extra-tropical storms along the U.S. Atlantic Coast, the regular annual occurrence of at least several storms has yielded a sufficiently large data base for probability assessment. Of course, each storm is unique, but with a general idea of probable occurrence for each segment of coast for different time periods combined with the probability of short high sea level high stands, the missing process element can be added to vulnerability.

References

Andersen OB, Knudsen P, Beckley B (2002) Monitoring sea level and sea surface temperature trends from ERS satellites. J Phys Chem Earth 27:1413–1417

Cazenave A, Llovell W (2010) Contemporary sea level rise. Annu Rev Mar Sci 2:145–173

Church JA, White NJ (2006) A 20th century acceleration in global sea level rise. Geophys Res Lett 33:L01602. doi:10.1029/2005GL024826

Costa J, Baker V (1981) Surficial geology building with the Earth. Wiley, New York, 498 p

Douglas BC (2001) Sea level change in the era of the recording tide gauge. In: Douglas BC, Kearney MS, Leatherman SP (eds) Sea level rise: history and consequences, vol 75. Academic Press International Geophysics Series, New York, pp 37–62

Elsner JB, Jagger TH, Tsonis AA (2006) Estimated return periods for Hurricane Katrina. Geophys Res Lett 33:L08704. doi:10.1029/2005GL025452

Emanuel KA (2005) Increasing destructiveness of tropical cyclones over the past 30 years. Nature 326:686–688

Firing YL, Merrifield MA, Schroeder TA, Qiu B (2004) Interdecadal sea level fluctuations at Hawaii. J Phys Oceanogr 34:2514–2524

Gornitz VM, Daniels RC, White TW, Birdwell KR (1994) The development of a coastal risk assessment database: vulnerability to sea-level rise in the U.S. Southeast J Coast Res 12: 327–338

Hanson S, Nicholls R, Ranger N, Hallegatte S, Corfee-Morlot J, Herweijer C, Chateau J (2011) A global ranking of port cities with high exposure to climate extremes. Clim Change 104:89–111. doi:10.1007/s10584-010-9977-4

Hillson DA (2004) Assessing risk probability: alternative approaches. In: 2004 PMI global congress proceedings, Prague, Czech Republic

Holgate SJ (2007) On the decadal rates of sea level change during the twentieth century. Geophys Res Lett 34:L01602. doi:10.1029/2006GL028492, 2007

Horn LH, Whittaker LM (1982) Atlas of northern hemisphere extratropical cyclone activity: 1958–1977. Department of Meteorology, University of Wisconsin, Madison

Houghton JT, Ding Y, Griggs DJ, Nouger M, van der Linden PJ, Dai X, Maskell K, Johnson CA (2001) Climate Change 2001: The Scientific Basis. Third Assessment Report of Work Group I

of Intergovernmental Panel on Climate Change. Cambridge, UK: Cambridge University Press, p 881

Houston JR, Dean RG (2011) Sea-level acceleration based on U.S. Tide gauges and extensions of previous global-gauge analyses. J Coast Res 27:409–417

Klotzbach PJ (2006) Trends in global tropical cyclone activity over the past twenty years (1986–2005). Geophys Res Lett 33:L10805. doi:10.1029/2006GL025881

Komar PD, Enfield DB (1987) Short-term sea-level changes and coastal erosion. In: Nummedal D, Pilkey OH, Howard JD (eds) Sea-level fluctuation and coastal evolution. Society of Economic Paleontologists and Mineralogists, Tulsa, pp 17–28

Lozanoa I, Devoy RJN, May W, Andersen U (2004) Storminess and vulnerability along the Atlantic coastlines of Europe: analysis of storm records and of a greenhouse gases-induced climate scenario. Mar Geol 210:205–225

Rahmstorff S (2007) A semiempirical approach to projecting future sea-level rise. Science 315:368–370

Rahmstorff S, Vermeer M (2011) Discussion of: Houston JR, Dean RG (2011) Sea-level acceleration based on U.S. tide gauges and extensions of previous global-gauge analyses. J Coast Res 27:409–417; J Coast Res 27:784–787

Resio DT, Westerink JJ (2008) Hurricanes and the physics of surges. Phys Today 61:33–38. doi:10.1063/1.2982120

Sanders F, Gyakum JR (1980) Synoptic-dynamic climatology of the "bomb". Mon Weather Rev 108:1589–1606

Stevenson JC, Kearney MS (1996) Shoreline dynamics on the windward and leeward shores of a large temperate estuary. In Nordstrom KF, Roman CT (eds) Estuarine Shores: Hydrological, Geomorphological and Ecological Interactions. New York: John Wiley & Sons, pp. 233–259.

Titus JG, Jones R, Streeter R (2008) Maps depicting site-specific scenarios for wetlands accretion as sea level rises in the Mid-Atlantic region. In: Titus JG, Strange EM (eds) Documents supporting climate change science and sensitivity to sea level rise program synthesis and assessment product 4.1: section 2.2 background: coastal elevations, U.S. Environmental Protection Agency, Washington, DC, pp 176–186

Webster PJ, Holland GJ, Curry JA, Chang H-R (2005) Changes in tropical cyclone number and intensity in a warming environment. Science 309:1844–1846

Chapter 5
Sea-Level Rise Impacts and Responses: A Global Perspective

Sally Brown, Robert J. Nicholls, Colin D. Woodroffe, Susan Hanson, Jochen Hinkel, Abiy S. Kebede, Barbara Neumann, and Athanasios T. Vafeidis

Abstract Coastal hazards have long been present and are evolving due to a variety of different drivers: the long-term threat of climate change, including sea-level rise, adds a new dimension to these problems which is explored here. Globally, sea levels could rise in excess of 1 m this century, but the local rate of relative sea-level rise could be much greater than this because of subsidence or other factors which lower the land surface. This is important as the population of these subsiding areas is significant. Relative sea-level rise will result in inundation, flooding, erosion, wetland loss, saltwater intrusion and impeded drainage. This chapter has investigated the impacts of sea-level rise at a global scale on: (1) Sandy environments; (2) Wetlands and low-lying coasts; (3) Built environments; and (4) Energy and transport systems. Results indicate that without appropriate adaptation, environments could be

S. Brown (✉) • R.J. Nicholls • S. Hanson • A.S. Kebede
Faculty of Engineering and the Environment and the Tyndall Centre for Climate Change Research, University of Southampton, Highfield, Southampton SO17 1BJ, United Kingdom
e-mail: sb20@soton.ac.uk; r.j.nicholls@soton.ac.uk; s.e.hanson@soton.ac.uk; ask2g08@soton.ac.uk

C.D. Woodroffe
School of Earth and Environmental Sciences, University of Wollongong, Wollongong, NSW 2522, Australia
e-mail: colin@uow.edu.au

J. Hinkel
Adaptation and Social Learning, Global Climate Forum e.V. (GCF), Neue Promenade 6, Berlin 10178, Germany

Transdisciplinary Concepts and Methods, Potsdam Institute for Climate Impact Research (PIK), P.O. Box 601203, Potsdam 14412, Germany
e-mail: hinkel@globalclimateforum.org; hinkel@pik-potsdam.de

B. Neumann • A.T. Vafeidis
Coastal Risks and Sea-Level Rise Research Group, Future Ocean Excellence Cluster, Institute of Geography, Christian-Albrechts-University Kiel, Ludewig-Meyn-Str. 14, Kiel 24098, Germany
e-mail: neumann@geographie.uni-kiel.de; vafeidis@geographie.uni-kiel.de

C.W. Finkl (ed.), *Coastal Hazards*, Coastal Research Library 6,
DOI 10.1007/978-94-007-5234-4_5,

significantly impacted, and those remote or financially less well off could become increasingly vulnerable. Further research and action is required into integrated impact assessments (including non-climatic drivers of change) to help those at risk and develop appropriate adaptation polices over short, medium and long timescales.

5.1 Introduction

A range of natural hazards occur on the coast, including storms with high wind speeds, extreme waves and tsunamis, all of which can cause flooding and erosion (Kron 2009). These geophysical events only become a risk when people use or resides in the path of the hazard. According to Munich Re's (2012) risk research which records global natural catastrophes based on insurance claims, in 2011 there were 820 loss events with 74% of these resulting from meteorological or hydrological events. Seventy percent of losses and 85% of fatalities were in Asia. The total overall losses from meteorological and hydrological events was US$144 billion. Seven percent of loss events were a direct consequence of extreme waves from tropical storms, surges or tsunamis (Kron, personal communication from Munich Re 2012 data). However, there are many more coastal events due to landslides, freshwater flooding and other climatological extremes, prompting insurance claims. This emphasises that the coast is a potentially vulnerable place to live. Despite these risks, people are attracted to the coast and it plays an important role in the lives of hundreds of millions of people. Even if a population does not directly live in the coastal zone, they can benefit from it due to the many advantageous natural, cultural and built environments it provides.

Coasts are some of the most densely populated areas in the world, on average containing two or three times greater population density than the same area further inland (McGranahan et al. 2007; Small and Nicholls 2003). More than 205 million people are already vulnerable to coastal flooding through extreme water levels (Mimura 2001; Vafeidis et al. 2011), and this will increase substantially just due to population growth and coastward migration (Nicholls 2004). It is anticipated that virtually all this growth will happen in urban areas (Kamal-Chaoui and Roberts 2009), placing more people and infrastructure (e.g. energy supplies, nodes of transport and industry) in potentially hazardous locations. Coastal ecosystems such as wetlands, estuaries and deltas provide many goods and ecosystem services, such as flood control and natural protection in the event of storms, shoreline stabilisation, habitats for wildlife, pollution filtering, sediment and nutrient retention and cycling, farming, fishing, aquaculture and other wildlife resources, recreation provision and cultural heritage (Barbier 2012; Costanza et al. 1997, 2008; Luisetti et al. 2011). Consequently many countries' economies are focused on the coast, which can be responsible for a larger than average share of its gross national product (Das Gupta and Babel 2005).

However, these coastal environments are under threat from many drivers, such as sea-level rise, natural and human induced subsidence, changes to wind and

storminess, salinisation, rising river levels in their coastal parts (the backwater effect), rising water tables, reduced sediment supply, eutrophication, intertidal destruction and land claim, farming, urbanisation and tourism (Valiela 2006). In flooding, there can be changes to sources, pathways and receptors (Evans et al. 2004), such as follows:

- Sources: e.g. climate variability, eustatic sea level changes, subsidence;
- Pathways: e.g. degradation of natural defences, hard and soft defences, channelling of flood water, decreased surface water drainage due to urbanisation and land claim, changes to water flow due to farming practices through land conversion or changes to crop type;
- Receptors: e.g. the location of people, population density, infrastructure.

Some of these threats are predictable, and therefore adverse impacts can be considered and planned for. An adaptive response can keep risks at an acceptable level. However if there is insufficient time to respond, or threats are unpredictable, risk levels increase, potentially leading to increased flooding and erosion. During the twentieth century, changes in receptors were the major driver that increased flood risk, and will probably remain significant for decades to come. However, changes in the sources, particularly with anticipated climate change, are of increasing importance.

This chapter focuses on the impacts of sea-level rise, with an emphasis on those localities which are vulnerable on a global scale. First, the magnitudes of past and future sea-level rise will be reviewed. Second, impacts on natural and human environments will be described, with a focus on:

1. Sandy environments;
2. Wetlands and low-lying coasts;
3. Built environments;
4. Transport and energy systems.

Finally possible adaptive responses and vulnerability will be explored for places and continents in response to these impacts.

5.2 How Much Will Sea Levels Rise?

Understanding sea-level rise is challenging due to the number of complex and interacting factors which influence the rate of rise and variability over a variety of time and geographic scales. To appreciate how rising sea levels will affect the coastal zone, it is important to consider relative sea-level change – the combination of eustatic sea level change and local vertical movements of the land as this is what produces impacts and requires a response. Where relative sea-level rise increases mean sea levels, lower surge elevations compared with present day levels will produce a sea level rise high enough to cause flooding or erosion (Haigh et al. 2011).

In the twentieth and twenty-first centuries, relative mean sea-level rise comprises:

(a) Eustatic rise of global mean sea levels resulting from a change in ocean volume: thermal expansion, melting ice sheets or changes to fluvial inputs for semi-enclosed seas, such as the Baltic Sea or Black Sea;
(b) Vertical land movement, e.g. due to natural tectonic activity and isostatic uplift, artificial water abstraction and drainage of susceptible soils, sediment compaction and subsidence.
(c) Decadal to seasonal fluctuations, e.g. large scale oceanic processes such as El Niño that can last one year or more, and also short lived storms that can result in extreme waves conditions;

The two main ways humans are believed to have influenced sea-level rise is via temperature-rise induced eustatic changes including: (i) the accelerated melting of land based ice, including the large ice sheets of Greenland and Antarctica, and smaller ice caps and glaciers and (ii) thermal expansion, which increases oceanic volume (Church et al. 2010). It is anticipated that these two ways will be the dominant cause of global relative sea-level rise over the twenty-first century and beyond (Meehl et al. 2007).

There is also concern that human activities are exacerbating existing trends. For example, in highly populated naturally subsiding deltas, over extraction of ground water and drainage can lead to accelerated subsidence. Ericson et al. (2006) investigated 40 deltas (many located in Asia) and their rate of relative sea-level rise, including subsidence from ground water and hydrocarbon extraction. Relative sea-level rise ranged from 0.5 to 12.5 mm/year. Some of the highest rates of subsidence (due to man's actions) occur on deltas which can be a home to cities. Observed subsidence values for cities include Bangkok (2 m from the 1950s), Shanghai (3 m from 1921) and Tokyo (5 m from the 1930s) (see Nicholls 1995). In some parts of these cities, the annual rate of local subsidence is fast, and so agriculture/aquaculture land and infrastructure is inundated (e.g. telegraph polls have been inundated due to relative sea-level rise in the Gulf of Thailand). Where local subsidence occurs in densely populated areas, vulnerability can increase, as investigated in Sect. 5.3. To assess future rise, past changes must be analysed and understood.

5.2.1 Past Changes

Past sea levels over many thousands or millions of years can be interpreted through, for instance, marsh sediment records (e.g. Leorri et al. 2010) or corals (e.g. Chappell and Polach 1991). Over the past 100 years or so, sea level has been recorded through tide gauges. Many of these records are part of the 1,300 tide gauge dataset at the Permanent Service for Mean Sea Level (Woodworth and Player 2003; Woodworth et al. 2011). One of their oldest records (Amsterdam, the Netherlands)

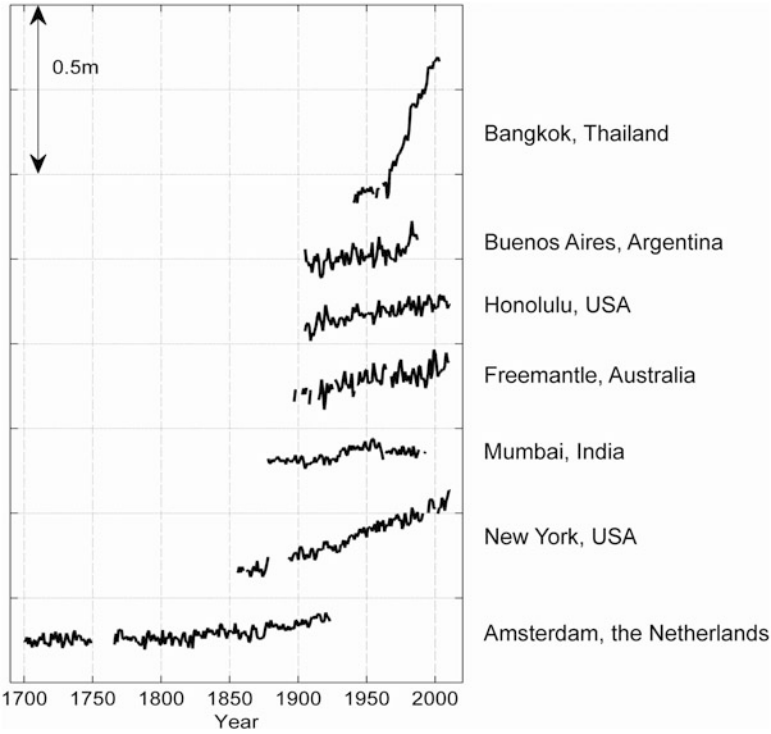

Fig. 5.1 Tide gauge measurements showing relative sea-level rise at selected sites around the world. The sharp rise in Bangkok after 1960 is due to subsidence induced by increased water abstraction. Records are offset for display purposes (Data extracted from Permanent Service for Mean Sea Level (2012))

dates back to 1700. Relative sea-level rise for Amsterdam and six other long term records are shown in Fig 5.1. Each record shows relative sea-level rise, with linear trends of 0.5, 2.8, 0.8, 1.5, 1.4 and 1.6 mm/year for Amsterdam, New York, Mumbai, Freemantle, Honolulu and Buenos Aires respectively. In Bangkok, from around 1960 there was a sharp increase in the rate of relative sea-level rise to around 17 mm/year for the next 50 years. The cause of this is subsidence due to water abstraction, which started in the 1950s at 10,000 m^3/day. Over the following decades, this rapidly increased to over 1 million m^3/day. Although there have been periods of reduced abstraction and restriction of the building of new wells, in 2003 over 1.7 million m^3/day was abstracted from shallow sand aquifers. Controls have meant that subsidence rates in the city centre have declined, but it is still widespread in the suburbs, where rates of up to 35 mm/year have been recorded (Das Gupta and Babel 2005; Nicholls 2010). With restrictions to abstraction, the rate of subsidence in the last 20 years has been reduced (Nicholls 2010).

Church and White (2011) reconstructed global sea levels using long-term tide gauge records and estimated the linear trend of global average sea-level rise

from 1900 to 2009 was 1.7 ± 0.2 mm/year. They also report that there has been considerable variation in rates during the twentieth century. Whilst some of this rise is due to natural variation, part (~75%) is believed to be caused by anthropogenic climate change (Jevrejeva et al. 2009), and it is envisaged that this trend will continue. Satellite altimetry data has supplemented the tide gauge record and provides a quasi-global observational dataset. From 1993 to 2009, satellite measurements indicate a rise of 3.2 ± 0.4 mm/year, whilst the sparse and unequally distributed tide gauge dataset indicate a rise of 2.8 ± 0.8 mm/year for this period. The short timescale of these measurements does not indicate with confidence a long-term significant increase in trend, but illustrates the complex nature of measuring and projecting future sea-level rise.

5.2.2 Future Changes

In 2007, the Intergovernmental Panel on Climate Change (IPCC) produced its Fourth Assessment Report (AR4), and stated that global sea levels could rise 0.18–0.59 m by 2090 to 2099, with respect to 1980 to 1999 (Meehl et al. 2007). The projections varied depending on future emissions, socio-economic scenarios and uncertainties in ice melt processes. In the models run for the IPCC AR4 report, around two thirds of sea-level rise was attributable to thermal expansion. Warming of the oceans takes centuries to reach equilibrium – even if greenhouse gas emissions (and any changes in global mean temperature) stabilise or are reduced today. Thus there is a time lag between an observed temperature rise and oceanic response. This process is known as 'the commitment to sea-level rise'. Given that the global mean surface air temperature has risen 0.76°C from 1850–1899 to 2001–2005 (Solomon et al. 2007), sea-level rise due to thermal expansion is expected to continue through the twenty-first century and beyond.

The remaining third of sea-level rise in the IPCC AR4 projections was attributable to the melting of land-based ice (Meehl et al. (2007) reports that due to a projected increase in precipitation, Antarctica is expected to give a negative contribution to sea-level rise. However, ice melt from Greenland and other land based ice is projected to give a larger positive contribution). However, immediately prior to the publication of the IPCC AR4 report, new rapid changes were observed on the Greenland and Antarctic ice sheets. Subsequently, an additional range of ice melt was added to the IPCC projections (to 0.76 m) in case increased ice sheet discharge was maintained (Solomon et al. 2007). Since then, concerns regarding the rate of ice melt from large ice sheets, glaciers and ice caps have continued (e.g. Rignot et al. 2011; Van de Wal et al. 2008). With improving, but still limited knowledge about ice sheet dynamics, particularly over long time scales, their dynamic behaviour and the rate of ice melt remains subject to debate and challenges scientific knowledge and understanding (Church et al. 2011). Even as new science and understanding emerges, there remains large uncertainties into the historic mass

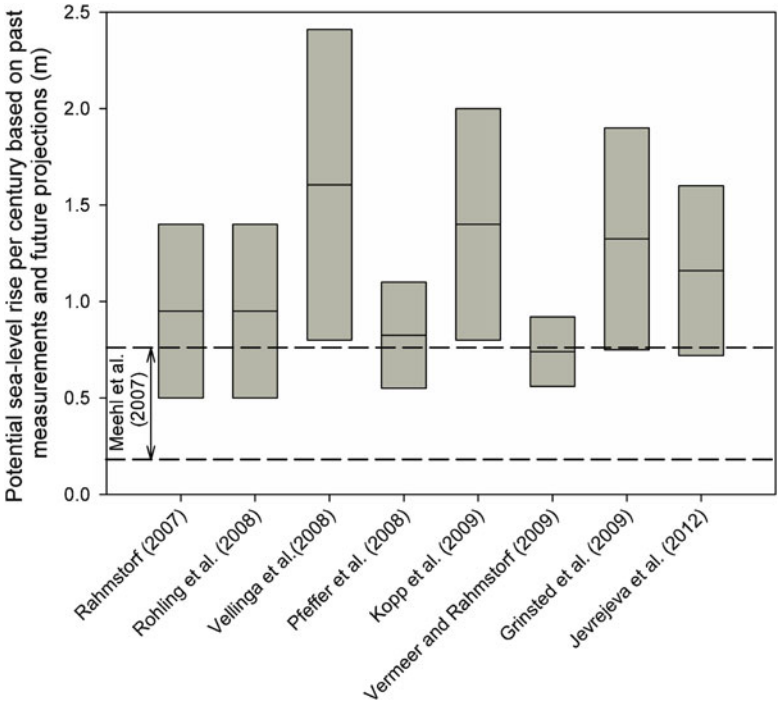

Fig. 5.2 Potential magnitude of global mean sea-level rise per century from post AR4 research (with a range of 0.5–2.4 m) based on past measurements and future projections (Adapted from Nicholls et al. 2011). The AR4 range (Meehl et al. 2007) is shown by the *dashed horizontal lines*

balance of glaciers and ice caps due to the sample size (e.g. Bamber 2012; Jacob et al. 2012). Projecting future changes brings further uncertainties.

Since the AR4 report, further research indicated large uncertainties in the magnitudes of ice melt, and thus sea-level rise. Part of this uncertainty is due to the different ways of measuring sea level response (e.g. semi-empirical methods, paleo-climate analogues and physical constraint analyses). From paleo-studies, scientists have investigated how much sea levels have risen in previous centuries. However it is uncertain that these rates of rise could happen again, but they are not considered impossible (Nicholls et al. 2011). A summary of potential sea-level rise at a century scale based on post-AR4 research is shown in Fig. 5.2, with a range of 0.5–2.4 m of rise per century. It should be noted that high-end projections (greater than 1 m per century), whilst scientifically plausible, are considered unlikely. However, it is prudent to consider the implications of rises greater than 1 m in order to evaluate possible responses and policy options to aid decision making.

The projections in Fig. 5.2 report global mean values, but regional variations will inevitably occur following historical observations. This is seen in evidence through tide gauge records, and more recently satellite altimetry. For instance, in some regions sea levels are rising three times faster than others (Cazenave and Llovel

2010). This is expected to continue and alter as the climate changes. Additionally, some places (e.g. northern Scandinavia) may experience a fall in relative sea levels due to isostatic rebound – where the land uplifts at a greater rate than sea-level rise.

5.3 Impacts

Where climatic and non-climatic factors interact producing a rise in sea levels, it increases the probability of an extreme event, and thus the adverse impacts which can affect natural and human environments. This includes inundation, flooding and storm damage by surges and also by raising rivers in their coastal parts (the backwater effect), saltwater intrusion into surface and ground water, rising water tables, erosion of dunes, beaches and cliffs and wetland loss and change (Nicholls 2010). During extreme events, flooding and erosion are the immediate effects, but over long time scales (many decades) slower subtle changes (e.g. salinisation) can create increased pressures on coastal environments. This can also impact coastal ecosystems and other aspects of the coast such as freshwater resources, agriculture, fisheries, recreation and tourism, biodiversity and infrastructure. Here, the effects on (1) Sandy environments; (2) Wetlands and low-lying areas; (3) Built environments; and (4) Transport and energy systems are investigated, illustrating a contrasting set of natural and human environments.

5.3.1 Sandy Environments

Coastal landscapes and ecosystems will experience the impacts of sea-level rise. Beaches, and the dunes behind them, being composed of unconsolidated sand, will be especially prone to erosion. Beaches can undergo erosion (and subsequent recovery) as a result of a series of factors, including an interruption to longshore drift, or a reduction in sediment supply following damming of a river. Therefore, attributing particular erosional events directly to sea-level rise is difficult. Over a period of time during which the average level of the sea has risen, most sandy shorelines will recede landwards, unless they receive substantial volumes of additional sand. It can be inferred that the coastline has migrated landwards across the inner continental shelves during the rapid sea-level rise that accompanied the melting of the polar ice-caps after the end of the last Ice Age 18,000 years to 6,000 years ago (Roy et al. 1994). However, it remains difficult to use either geological facies models or historical observations to foreshadow the rates at which shorelines will recede in the future.

One of the simplest approaches that has been widely used to project future shoreline position is based on the principle of conservation of mass and assumes that a similar cross-shore profile will be maintained as the shoreline migrates landwards. This method was introduced by Per Bruun (Bruun 1962), and has become

known as the 'Bruun Rule.' It assumes that sand is eroded from the beach as the sea rises and is redistributed across the adjacent shallow-water seafloor as far seaward as waves influence sediment movement (called closure depth). Bruun (1962) inferred that rates of retreat are a function of foreshore gradient, which is typically of the order of 0.01–0.02, producing retreat at 50–100 times the rate of sea-level rise (that is, if the sea level rose by 1 m, the shoreline would be anticipated to retreat between 50 and 100 m).

There has been considerable criticism of this simple 'equilibrium morphology' approach because it only considers one process operating at the shore. Hence, it cannot take into account many factors that can be very significant at particular coastal locations, such as geological constraints or variable rates of longshore sediment transport (Cooper and Pilkey 2004; Ranasinghe et al. 2012). Consequently a more complete model encompassing the entire sediment budget is required (Cowell et al. 2003a, b). Some of the most dynamic sandy coasts are associated with low-lying barrier islands, such as those along the eastern coast of the USA or the northern coast of the Netherlands. Many of these undergo a process of rollover, with sand washed from seaward spilling onto marshy areas behind, in contrast to the seaward movement described above (FitzGerald et al. 2008). Nevertheless, for large area studies, the application of these simple principles is meaningful to attain order-of-magnitude estimates, and in fact, underlies most engineering studies that attempt to forecast where the shoreline will be at successive times in the future. This becomes particularly important along highly developed coasts, where substantial infrastructure or coastal protection occurs behind the active beach (such as promenades, boardwalks, ports, residential and tourist facilities, seawalls and other hard structures). Many beaches will erode, but it will be important to incorporate better estimates of the volumes of sand mobilised during storms of different magnitudes in the context of the entire coastal sediment budget. It is desirable to produce probabilistic estimates that enable coastal managers and policy-makers to consider a wider range of sensitivities and uncertainties in model estimates (Ranasinghe et al. 2012).

The small sandy islands (called cays) that have accumulated on top of coral reefs, and around the rim of atolls, appear particularly threatened by sea-level rise. They are vulnerable to shoreline erosion, inundation of low-lying areas, and saline intrusion into the freshwater lens on which island communities often depend (Woodroffe 2008). Although the carbonate sediments from which these islands are built are still being produced through breakdown of marine organisms, such as corals and shells, human activities have often exacerbated the threats. The Asian region contains some of the most diverse coral reefs and mangrove forests anywhere on earth. These coastal ecosystems provide both direct (timber, shellfish) and indirect (fish nursery) services to many people. The reefs are subject to many stresses, both through pollution and over-exploitation, but also as a consequence of climate change (Hughes et al. 2003).

5.3.2 Wetlands and Low-Lying Coasts

Although it is often perceived that sea-level rise will have particularly far-reaching effects on sandy coasts, the immediate response of unconsolidated sand to wave action means that beaches can undergo rapid adjustments which can, in some cases, increase their resilience. The response of coastal wetlands is slower, and sea-level rise impacts and responses are less obvious but more pervasive (Day 2008). Wetlands flourish on muddy shorelines and support a diversity of organisms. Salt marshes extend across upper intertidal mudflats from polar through to tropical regions, whereas mangrove forests dominate sheltered intertidal coastlines in the tropics. There are often other associated wetland habitats, such as seagrass ecosystems on subtidal flats and freshwater wetlands that occur landward of salt marshes or mangroves.

Intertidal wetland environments have coped with changes of sea level in the past (Woodroffe 1990). The stratigraphy beneath many coastal plains contains sedimentary records of past ecological changes. For example, several metres of muddy sediments, intercalated with peats, underlie coastal plains of northwest Europe and the east coast of North America, exceeding in thickness the intertidal and shallow-marine zones in which the equivalent habitats are presently found. This indicates that they accumulated over a period of gradual sea-level rise (Allen 2000).

As sea level rises, tidal incursion into coastal wetlands is increased and the rate of surface accretion is likely to also increase across the entire wetland surface. The response of the wetland is therefore to continue to accrete vertically provided there is sediment available. Tidal waters will reach further inland, beyond the coastal wetlands, extending into freshwater or upland systems. All too often, further landward incursion of wetland communities will not be possible because their hinterland is occupied by human settlements or defence infrastructure (e.g. sea walls), with the consequence that the intertidal wetlands will contract, a process termed coastal squeeze (Doody 2004).

Many intertidal wetlands have been considerably modified by human activity. Low-lying plains have proved attractive locations for a range of intensive agricultural, industrial and residential developments. They have been subject to both deliberate and unintentional dumping of wastes and land claim. Mangrove shorelines around much of the tropics have been converted into shrimp farms or salt ponds, causing such disruption to the substrate and its chemistry that mangroves can rarely re-colonise. Often these perils can be a greater threat than climate induced sea-level rise, and they have been pervasive over the last few decades (e.g. Coleman et al. 2008; Ericson et al. 2006).

As sea level rises in the future, coastal wetland communities appear increasingly threatened. Scientists now realise that these ecosystems provide a series of goods and services (Costanza et al. 1997), particularly in densely populated parts of the developing world where there is a heavy reliance on seafood produced as part of food chains that rely on mangrove wetlands for their sustainability. Re-establishing such intertidal wetlands is seen as a priority in many parts of the world; for example,

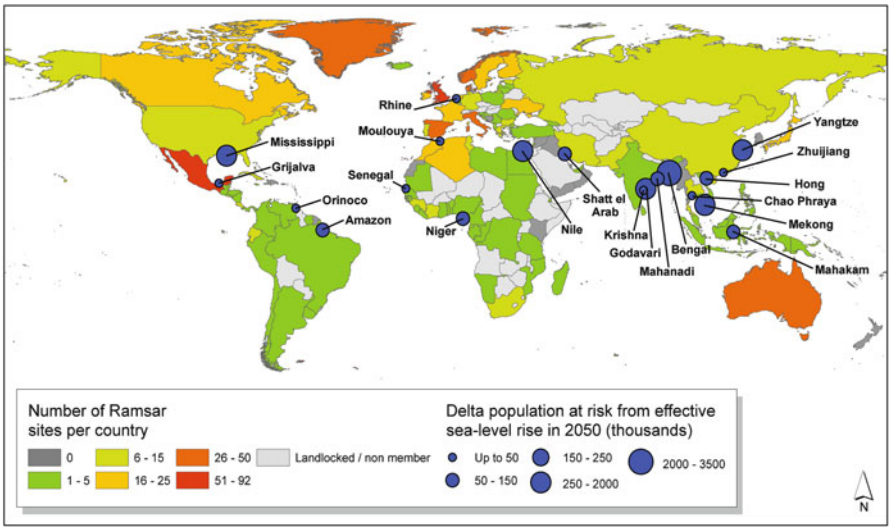

Fig. 5.3 Number of coastal and marine Ramsar sites per country (Ramsar Wetlands International 2007), and the delta population at risk due to effective sea-level rise in 2050 for the top 20 major deltas listed in Ericson et al. (2006). Note that Angola, Eritrea, Guyana, Saudi Araba and Somalia are not part of the Ramsar Convention so do not contain Ramsar sites

a program of managed realignment has been instigated in parts of Europe, where embankments that were built to claim salt-marsh habitat from the intertidal zone are being deliberately breached to promote further marsh establishment as an adaptive measure to sea-level rise and mitigation of coastal habitat destruction (French 2006; Rowlands et al. in review). In tropical regions, buffers of mangroves have been replanted, particularly in parts of south-east Asia, and mangroves are increasingly seen as a valuable form of shoreline protection contributing to better coastal management procedures (Alongi 2002).

Figure 5.3 illustrates coastal and marine Ramsar sites – important designated sites which are subject to international protection and co-operation in their use and resources (Ramsar Wetlands International 2007). The figure illustrates that many of these wetlands are in developed countries where anthropogenic pressures infringe upon the natural environment. Since its initialisation in 1971, numerous developing countries have joined the Ramsar Convention, and many large protected wetlands can be found in these countries. This is encouraging as it demonstrates that people and governments recognise and appreciate the international importance of wetlands and this may influence their future management (Nicholls et al. 2008a).

Not only are coastal wetlands threatened, but the extensive plains that have developed through several millennia of sedimentation, particularly in estuaries or on deltas, are also vulnerable. Deltas are dynamic landforms that have formed extensive low-lying areas as a result of large sediment loads that are carried to the sea by some of the world's biggest rivers. Reduction of sediment delivery as a result of the construction of dams upstream presents a more imminent threat than

sea-level rise for many deltas. Such deltas are already subject to subsidence and sediment compaction, and this has often been exacerbated through human activities such as hydrocarbon and groundwater extraction (Syvitski et al. 2009; Ericson et al. 2006) (also see Sect. 5.2). The rate of relative sea-level rise is accentuated in such situations. Much of New Orleans lies below the level of the Mississippi River and of the highest ocean water level in the Gulf of Mexico. Devastation by Hurricane Katrina in 2005 has forcefully demonstrated the dangers such cities will increasingly face in the future. The defences have since been substantially upgraded at the cost of US$15 billion and the management has moved to a more proactive and risk-based perspective. Time will tell how efficient these defences are and how they perform as New Orleans has a long history of flooding and a similar set of meteorological conditions could occur again (Hanson and Nicholls 2012).

Globally about ten million people on average were estimated to be subject to coastal flooding per year in 1990, based on modelling by Nicholls (2004). The vast majority were in south, south-east and east Asia – often in low-lying delta regions. The proportion of people at risk from these regions is also likely to continue to increase as a result of sea-level rise and also population growth. In addition to Ramsar sites, Fig. 5.3 illustrates the population at risk in 2050 due to sea-level rise based on the analysis of Ericson et al. (2006). For the 20 deltas illustrated it indicates that in excess of two million people could be at risk from flooding in the 2050s, just based on extrapolating present trends. Most of these people are in Asian delta plains that are already subject to extensive flooding and which serve as the 'rice-bowl' of Asia. Bangladesh lies almost entirely on alluvial and deltaic plains deposited where the Ganges and Brahmaputra Rivers converge. The low-lying plains, extending into west Bengal in India, supported a population of about 130 million in 1990 and that is likely to rise to more than 166 million by 2015 (Woodroffe et al. 2006). This area includes the Sundarbans, the largest area of mangroves under conservation in the world, covering approximately one million hectares. Erosion predominates along the Bay of Bengal coastline and these wetlands have decreased in area at an average of about 4 km^2/year over the past several decades (Rahman et al. 2011). More than 11 million people live on the delta plains in each of the Irrawaddy, Chao Phraya, Mekong, Red, Pearl, Changjiang (Yangtse) and Huanghe (Yellow) river deltas (Woodroffe et al. 2006). Each of these experiences shoreline erosion along much of its margin, as well as differential subsidence; as a consequence millions of people are already at risk today and sea-level rise will further exacerbate these problems.

5.3.3 Built Environments

Many of the fastest growing megacities (population greater than eight million) are on or adjacent to deltas (Woodroffe et al. 2006). These and other coastal urban centres are growing faster than the hinterland, driven by rapid economic growth and coastward migration (Alig et al. 2004; Balk et al. 2009; McGranahan et al. 2007;

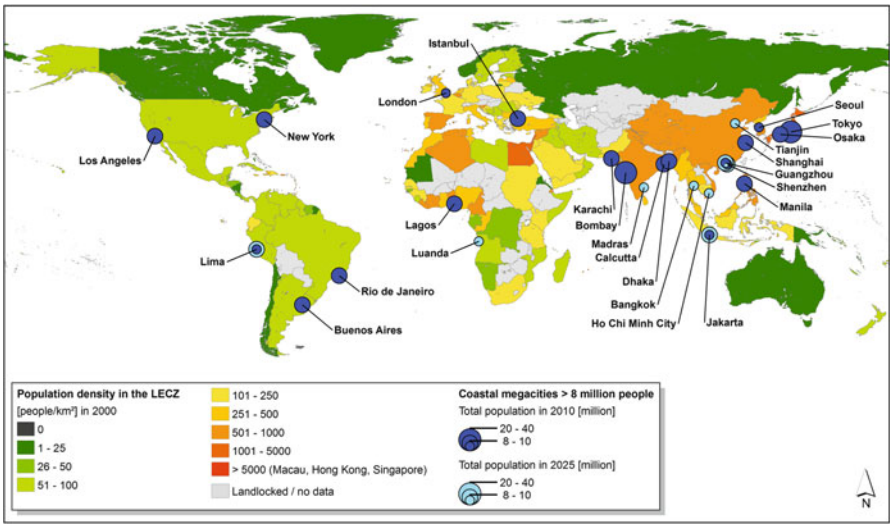

Fig. 5.4 Population density in the LECZ (Vafeidis et al. 2011) and the location of coastal megacities (United Nations 2010)

Smith 2011). These trends, which have strong impacts on the environmental system (Sekovski et al. 2011), are expected to continue and possibly intensify in the future.

When assessing impacts and vulnerabilities of population and assets in coastal built environments, the low-elevation coastal zone (LECZ)[1] is commonly used as a spatial reference (Balk et al. 2009; Lichter et al. 2011; McGranahan et al. 2007). The LECZ occupies approximately 2% of the global land area, but accommodates 10.2% of the global population (year 2000 population estimates) (McGranahan et al. 2007). These types of estimates are commonly employed as a measure of exposure of coastal population to sea-level rise and associated impacts, in particular flooding and submergence. Although they are subject to various limitations (see Lichter et al. 2011) they provide a good first-order indication of the distribution of population and assets in the coastal zone.

Figure 5.4 illustrates the population density in the LECZ (Vafeidis et al. 2011) and the location of coastal megacities with a population greater than eight million. Estimates of current and future populations are from UN population data (United Nations 2010). The highest population densities occur along western Europe and Africa, countries bordering the Mediterranean Sea and south, south-east and east Asia, and particularly in small nation states and islands. These nations are often highly dependent on the coast. In 2010, 20 out of 31 megacities were within the LECZ, with 12 in Asia. The number of megacities in the LECZ is expected to

[1] Defined as the contiguous area below 10 m of elevation that is hydrologically connected to the sea.

Table 5.1 Total area, population and people living in the low-elevation coastal zone (LECZ) in 2000 and projected by 2060, per continent

	Total area and population in 2000		Area and population in LECZ 2000		Total population and population in LECZ in 2060[a]	
Continent	Area (km^2) (000)	Population (000)	Area (km^2) (000)	Population (000)	Total population (000)	Population LECZ (000)
Africa	29,620	811,101	194	54,167	2,955,291	245,245
America:						
Central	2,451	135,555	119	6,768	268,745	8,917
South	17,631	347,433	263	21,909	596,774	37,705
Caribbean	233	38,441	42	3,536	57,523	5,640
America:						
North	18,944	313,289	508	24,617	466,270	45,536
Asia	30,695	3,697,108	860	460,840	6,170,286	983,293
Oceania	8,455	31,130	143	3,333	62,130	6,086
Europe	22,548	726,777	471	50,018	702,346	55,741
World	130,578	6,100,834	2,599	625,188	11,279,364	1,388,162

[a]Scenario assumptions: Population growth towards the highest end of forecasts (rich economies: medium population growth at 50th percentile, coastal growth 1.7 times the inland growth; developing world: high population growth at 90th percentile, coastal growth 1.7 time the inland growth for rural areas and 1.8 times the inland growth for urban areas. See Vafeidis et al. (2011) for details)

increase to 25 by 2025 as shown in Fig. 5.4. More Asian cities emerge, plus one African city – Luanda, Angola.

Vafeidis et al. (2011) indicated that exposure of population in the coastal zone may rise substantially in the future (Table 5.1). According to their study the LECZ population is expected to grow from 625 million (in 2000) to 950 million in 2030, and 1,400 million in 2060 (12% of the global population) for a range of socio-economic scenarios. This is driven by rapid population growth in developing countries and coastward migration. Population growth and urbanisation are expected to be highest in Africa (especially the Sub-Saharan region) for all scenarios, and increase the population exposured to sea-level rise (Hinkel et al. 2012a). By 2060, coastal urban[2] areas could shelter two thirds of Africa's coastal population under highest-end growth assumptions. At the same time, Asia's coastal population, will be growing at only half to two-thirds of the rate of Africa. Nevertheless, the LECZ population in Asia is expected to increase from 460 million (74% of the global population within the LECZ in 2000) to 980 million people (71% of the global population within the LECZ in 2060). North America will experience the highest urbanisation of the coastal zone in the LECZ with an increase of the urban population from 61% in 2000 to up to 78% by 2060 under highest-end growth assumptions. Other countries (e.g. Australia) may have a higher

[2] Defined as places dominated by built environments – see Vafeidis et al. (2011).

percentage of coastal population, but these may not be classed as residents of 'urban' areas, as population is dispersed in less built up zones.

It must be noted however that coastal urbanisation trends can vary significantly between countries and regions. For example, national policies and tight global economic links support the strong coastal urban growth that is observed in China (McGranahan et al. 2007; Pannell 2002, 2003). The opposite, however is true in Bangladesh, where predomiantly the rural population in the LECZ is growing faster than the country's urban average (McGranahan et al. 2007). Thus urban areas and megacities in the LECZ will continue to grow and be at threat from rising sea levels throughout the twenty-first century.

5.3.4 Transport and Energy Systems

Transport and energy networks have important infrastructure located in the coastal zone which, if adversely affected by sea-level rise, could have ramifications over a wide area and indirectly impact much of the world's population. Key within these networks are sea ports and airports, which are often located in low-lying or reclaimed coastal areas, and large-scale energy generation plants which require coastal locations for either transport and/or water supply for cooling. Relocating such infrastructure would be costly, so there is a need for on-going awareness and planning to upgrade facilities appropriately in response to sea-level rise.

Using global data sets, the number of airports, ports, oil refineries and nuclear power plants within 10 km of the coast were estimated to assess the proportion of these key assets located in coastal areas, and their importance within energy and transport networks. A horizontal distance of 10 km around the coastline was chosen to define the coastal zone rather than an elevation limit above mean sea level (e.g. LECZ) due to data quality, as otherwise important areas of the datasets were omitted. Maps showing the number of assets for each country are shown in Fig. 5.5.

Air transport is an important part of the world's transport network with a total of 2.5 billion passengers and approximately 50 million tonnes of freight flown worldwide annually (Oxford Economics 2009). Globally just over 2,000 (approximately 30%) airports are located within 10 km of coast (Fig. 5.5a), of which nearly 200 airports are located on small remote islands in the Atlantic, Indian and Pacific Oceans (data from OpenFlights 2012). For these islands, airports located adjacent to the coast may be susceptible to the effects of sea-level rise (either erosion or flooding) but, due to their land limitations and remoteness, adaptation may be challenging. Therefore small islands are expected to be vulnerable to environmental change and experience some of the worst effects from rising sea levels and other climate change effects (Mimura et al. 2007). Elsewhere, the size of the airport is also important to consider. Large airports on low-lying land may be affordably protected, whereas smaller airports may not. However, these smaller airports (e.g. a landing field) may be easier to move further

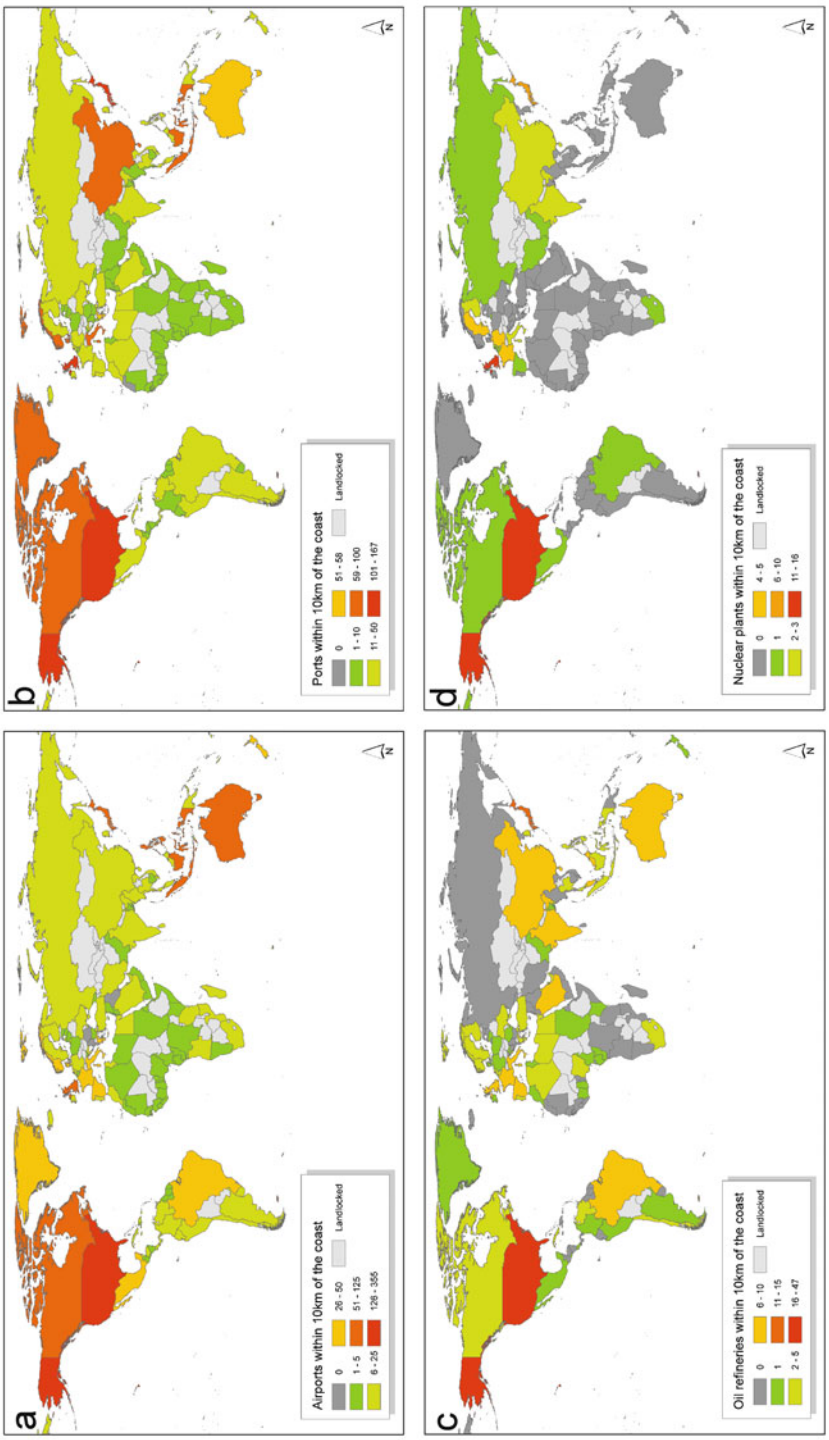

Fig. 5.5 Transport and energy infrastructure within 10 km of the coast. (**a**) Airports (OpenFlights 2012); (**b**) Sea ports (Lloyd's List 2009); (**c**) Oil refineries (GeoCommons 2012); (**d**) Nuclear power plants (GCMD 2010)

inland or even operate under low-tide conditions. This already happens at Barra airport, north-west Scotland where the runway is a beach.

The majority of the world's ports are located on the coast (the remainder being located on major rivers) and are therefore directly affected by changing sea levels. Nicholls et al. (2008b) found that from 136 global port cities (greater than one million people) in 2005, US$3,000 billion assets and 40 million people were at risk from a 1:100 year flood event, and this would increase significantly in the future. Thus protecting and upgrading infrastructure is important to maintain smooth transport links (Hanson and Nicholls 2012; Nicholls and Kebede 2010). Of the over 2,700 ports recorded in Lloyd's List (2009), 2213 are located within 10 km of the coast (Fig. 5.5b). Countries with a large number of coastal ports include the UK, the USA, China, Canada, Japan and Indonesia, the most interconnected in terms of trade routes being China and Germany (UNCTAD 2011). Despite the recent economic downturn, seaborne trade remains vital for the global economy with developing countries accounting for 61% of all cargo loaded and 55% of unloaded cargo, reflecting their growing importance in driving the global economy (UNCTAD 2010, 2011). Forty four of the ports recorded in Lloyd' List (2009) are associated with remote islands, although other important anchorages probably exist. Maintaining boat access to these small ports or harbours or beaches is potentially vital for small islands. These ports are important transport hubs, helping to provide livelihoods by supporting fishery and aquaculture industries and provide trade. If agricultural land is threatened or is subject to salinisation, small islands may become reliant on trade routes for food supplies. Adapting to sea-level rise (including infrastructure) may be costly for small islands particularly due to their large reliance on the coast, but arguably it is vital if they are to survive.

Figure 5.5c illustrates the distribution of the global oil refineries within 10 km of the coast. In 2008 global crude oil imports/exports amounted to 1,970 million tonnes (BP 2009). Globally, about 257 oil refineries (approximately half of the global total) have been identified as being within 10 km of the coast (data extracted from GeoCommons 2012). North-west Europe, the Middle East and the Gulf of Mexico contain a high density of oil refineries. Oil refinery infrastructure is not expected to increase on the coast, and more likely will decline as oil production decreases due to dwindling resources (Nicholls and Kebede 2010). Until recently, defence construction did not take account of long-term trends of extreme events. Therefore older structures are more likely to be at risk from future flooding than more recent constructions (Rayer and MacKenzie 2010). However, if design lifetimes are extended, or infrastructure is used for other purposes (e.g. carbon capture and storage), the exposure to extreme events should be reconsidered.

In 2010, 14% of global electricity generation came from nuclear power (World Nuclear Association 2012a). Nuclear power stations require water as a coolant and are often located on the coast. About 75 (approximately 30%) of the world's nuclear power stations (data extracted from GCMD 2010) are within 10 km of the coast (Fig. 5.5d), with many concentrated around Europe, the USA and east Asia (Nicholls and Kebede 2010). Around two thirds of reactors that are under construction, planned, or proposed are in Asia (many in coastal China – World Nuclear Association

2012b). Due to high safety standards and emergency procedures, risk from extreme water levels from an individual storm may be low, but over time this will increase. To avoid contamination of radioactive waste, sites require high levels of protection (Wilby et al. 2011) over long time scales (greater than 100 years). With high safety standards, defences and their planning require regular review and monitoring, with anticipation of future conditions which could induce flooding or erosion – including sea-level rise, changes to storminess and sediment movement (where it acts as a protective barrier).

Planning to maintain the operability of the coastal infrastructure discussed here will be an important issue over the coming century, requiring the long-term consideration of energy and transport needs, together with existing and new adaptation techniques. Where this cannot be done, alternative methods of transportation or supply nodes need to be considered in advance, and changes phased in to ensure a smooth transition and minimal environmental impact between these nodes. For ports and airports it is also important to remember that, while they are often located in areas of high population and economic activity, they additionally have an important role in allowing and maintaining contacts with isolated locations, such as small islands (e.g. Wright and Hogan 2008). If ports and airports on small islands are threatened, it could locally have knock-on effects due to the connectivity and dependence on these vital transport routes.

5.4 Response to Impacts

With knowledge of potential sea-level rise impacts, climate mitigation and adaptation are two distinct methods to reduce risk. It is important to identify the cause of relative sea-level rise, so to determine which method is appropriate to reduce vulnerability.

Mitigation involves technological change and substitution to reduce inputs and emissions per unit of output. When specifically referenced to climate, this means implementing policies to reduce emissions (and subsequent temperature rise) and enhance sinks for greenhouse gases (IPCC 2007). For non-climatic factors, this involves changing practices to reduce adverse effects, or compensating for them accordingly. Adaptation takes place through actions to reduce vulnerability or improve resilience in response to observed or expected events. This includes planned or unplanned, reactive or anticipatory, private or public, successful or unsuccessful responses (IPCC 2007).

Climate mitigation relies on governments and policy implementations to reduce emissions. Mitigation will not stop sea-level rise, but will reduce the rate of rise. Given the commitment to sea-level rise, the benefits of climate mitigation may take a long time to be felt, but it has multiple advantages to many ecosystems and human environments. These benefits can extend to people and environments who sometimes do not feel that it is appropriate to adapt to rising sea levels or do not have the means to do so. Mitigation of non-climatic factors (e.g. mitigation of subsidence by reducing water abstraction) is more immediate and has long lasting benefits.

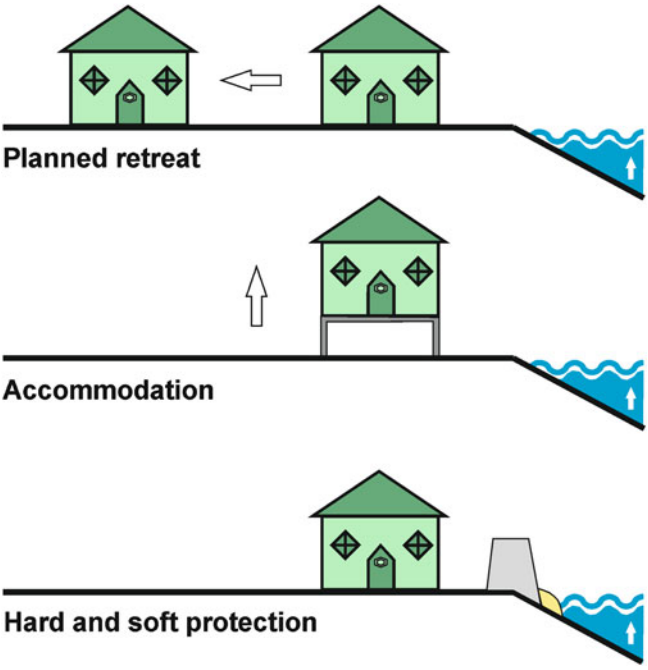

Fig. 5.6 Adaptation response from rising sea levels (After IPCC 1990)

Adaptation is undertaken at local to national levels to reduce vulnerability and/or enhance resilience, including practices, processes and perceptions of risk (Adger et al. 2007). It benefits those in the immediate coastal zone, as well as those further afield who rely on coastal goods and services. Given the commitment to sea-level rise, risk levels can be continually assessed so that adaptation can be strategically planned for, and if necessary, altered as environmental conditions change. Adaptation is frequently seen as the more immediate way to reduce or manage a hazard (Nicholls et al. 2007). However, adaptation can be costly and some schemes require ongoing maintenance and monitoring to ensure that they remain effective. Adaptation schemes may also have unanticipated or adverse effects, or even exacerbate existing problems (e.g. hard defences can lead to increased erosion down-coast, Brown et al. 2011).

For sea-level rise, planned adaptation can be categorised, following IPCC (1990) as shown in Fig. 5.6:

(a) Planned retreat: where a system moves or migrates landward away from the sea;
(b) Accommodation of relative sea-level rise: where environments, including the people who reside there, remain in situ and adjust to the changing environment (either spontaneously, anticipatory or planned) through changes in their behaviour or living conditions;

(c) Protection: by hard (e.g. sea walls, dikes) and soft defences (beach nourishment, planting of vegetation).

Many responses may involve a combination of these measures (Nicholls et al. 2007).

Erosion and flooding may result in landward migration of wetlands, unless it is prevented from doing do so by hard adaptation structures creating coastal squeeze. This could potentially reduce biodiversity and environmental quality. Ecosystems may be able to accommodate sea-level rise, and where crops are grown, if more salt tolerant species are introduced, it may result in a larger or more reliant yield (Foresight 2011). Protection of the natural environment may mean investing in the ecosystem, such as planting mangroves which helps trap sediment and protect the hinterland (see Sect. 5.3). Whilst mangroves take a long time to grow and act as protection, they have dual benefits with their ecosystem goods and services, such as filtering nutrients, reducing pollution and providing a habitat for wildlife (World Bank 2011).

Urban environments and their associated infrastructure require protection from sea-level rise in order to 'hold the line'. This can mean building or extending defences or other adaptive methods, perhaps to a higher standard or supplementing hard defence practices with soft methods. Within Europe, large protection schemes such as the Netherland's Delta Plan or London's Thames Estuary 2100 help to strategically plan for erosion and flood risk across urban areas and the hinterland (Delta Commissie 2008; Environment Agency 2010). There are also innovative ways to accommodate sea-level rise such as raised walkways, floating buildings and multi-functional defences (Stanlenberg 2012). In developing countries, adaptation can mean micro-insurance, changing agriculture patterns, building embankments, raising vital infrastructure (Linham and Nicholls 2010). Cities can try to 'advance the line' by building seaward (i.e. land claim), which has happened in many locations in north-west Europe and east Asia. 'Managed realignment' is possible, but not widely considered in urban areas due to high value of land and logistic complications. However if carefully managed this has the potential to provide additional space for flood water (Sherwin and Nicholls 2007).

Transportation and infrastructure require long term planning, and without adaptation could be subject to significant impacts that extend beyond the coastal zone. This could include relocation, redesign, deployment of temporary barriers, contingency planning for extremes and improved early warning systems for high water levels (Hanson and Nicholls 2012). In a global survey of port administrators, Becker et al. (2011) found that many were 'uninformed' about climate change, including the magnitude of sea-level rise. Given rapid port expansion, greater communication and awareness is required to maintain protection levels. Many coastal oil refineries are located near to ports, so may adapt in a similar way. For nuclear power plants, planned retreat is potentially challenging due to the long-term hazardous nature of the materials involved. Hence regular monitoring and where necessary upgrading of protection is required.

Finally, where coastal environments come under increasing pressure from rising sea levels and other environmental change but are unable to sufficiently adapt, environmental conditions could degrade. For those people who directly rely on or live off the land (often the poorer population), it may be increasingly difficult to reside there. For instance, rising sea levels can result in land salinisation, decreasing agricultural production, resulting in land abandonment, or force people to look for alternative employment. This could result in migration, including forced migration (Black et al. 2011). Whilst many migrants move within their own country, some may wish or need to travel over international borders. This may be particularly important for small islands. International co-operation is required to plan ahead accordingly to assist such migrants.

5.5 Assessing Vulnerability

Section 5.3 illustrated potential localities where impacts due to sea-level rise could occur and highlighted areas that are potentially threatened. However, despite similar geographical conditions, not all of these areas are necessarily highly vulnerable to rising sea levels. Here, vulnerability is defined following the IPCC guidelines as "the degree to which a system is susceptible to, and unable to cope with, adverse effects of climate change, including climate variability and extremes" (IPCC 2007). Vulnerability integrates knowledge on exposure, potential impacts (as discussed in Sect. 5.3) as well as on the adaptation capacity to these impacts (as discussed in Sect. 5.4) and other influencing factors. Using this information, together with research on coastal ecosystem and human systems (e.g. Nicholls et al. 1999), Table 5.2 summarises the potential impacts, adaptation history and potential, and estimates vulnerability at the continent scale.

There is no standard way of assessing vulnerability (Hinkel 2009) and hence approaches differ (Wolf et al. in review). One method is to assess adaptation implicitly and separately from impacts by means of evaluating the adaptive capacity of human systems to respond using socio-economic indicators. The disadvantage of this approach is that the capacity assessed is not specific to the impact considered and it is difficult to combine information on capacity and impacts (Hinkel 2009). Another approach is to assess adaptation explicitly and jointly by means of running impact models that include models of adaptation. The advantage of this approach is that it yields temporally explicit results on cost and benefits of adaptation. The disadvantage of this approach is that usually only a narrow range of adaptation options, in particular defence options, can be considered as only these can be modelled. An example of this approach is the Dynamic Interactive Vulnerability Assessment (DIVA) model which, using projected rates of sea-level rise together with socio-economic projections, calculates potential impacts of sea-level rise (e.g. land loss, people flooded) on a global scale (Vafeidis et al. 2008). Assessments of vulnerability also need to integrate across the wide range of uncertainty about scenarios, impacts and adaptation. For coastal impacts, this means that assessments of vulnerability need to consider the range of plausible socio-economic development in the coastal zone, as well as the range of local sea-level changes expected (Nicholls et al. 2008a).

Table 5.2 Coastal impacts adaptation and vulnerability of relative sea-level rise per continent based on data presented in this report and other research

Continent	Major potential impacts	Adaptation history and potential	Vulnerability
Africa	Deltas/cities/wetlands	Low – little experience, limited resources	High
America: Central, South and Caribbean islands	Deltas/wetlands/cities (hotspots). For small islands, airports/ports	Medium	Medium (small islands have a high risk)
America: North	Wetlands/urban areas/ nuclear/ports/oil	High – mainly land use planning, building regulations (retreat and accommodation), limited protection	Medium, but wetlands highly threatened
Asia	Numerous large densely populated deltas/ wetlands/megacities/ corals	Low to high – depending on wealth (which is increasing), population density and management of coastal resources. Long tradition of defence, especially in east Asia	High, especially in deltaic areas
Oceania	Beaches/corals/oil/ airports/ports	Land use planning, regulations, retreat and accommodation options	Low, but coral reefs highly threatened
Europe	Wetlands/beaches/ nuclear/oil	High, mostly protection especially in north-west Europe	Low, but wetlands highly threatened
Small oceanic islands	Natural environment/ ports/airports/ groundwater	Low – potentially limited resources/capacity	High

5.5.1 A Continental-Level Review

Each continent is considered in turn, together with small islands nations.

Urbanised areas in Africa could experience some of the highest growth rates in coming decades, so there is a need to protect potentially densely populated, only poor urban populations such as the urban strip from Lagos to Abidjan in West Africa. The competing factors of urbanisation and sea-level rise makes the environment and the people who reside there vulnerable. Coastal cities are expected to expand – probably at a greater rate than interior cities. By 2025 expansion is expected to create a new megacity (Luanda, Angola), bringing the African total to two (with Lagos, Nigeria, see Fig. 5.4). Lessons need to be learnt from other

urbanised environments in that the ecosystems and resources required to support them are sustainable and do not adversely affect environmental quality (Black et al. 2011). When environmental quality is compromised, vulnerability increases. Deltas are hotspots of potential impacts, especially the Nile delta which stands out in global terms (Ericson et al. 2006). Other parts of the African coast are less developed, and with a lack of protection structures, the coast has a greater freedom to respond to environmental change. However, if sea levels rise at rates faster than ecosystem response, this could lead to environmental degradation. Some people may depend on the natural environments for their livelihood, so require support to be able to adapt as the environment slowly changes. For instance, sea-level rise could lead to greater salinisation affecting coastal agriculture and therefore food supply (Foresight 2011). Some natural defences are being degraded and there is little experience of human adaptation in Africa. Thus coastal changes could have wide implications for vulnerability. National and local investment in adaptation and maintaining environmental quality is required (Hinkel et al. 2012a).

Central and South America are less coast focused than other continents with many capital cities often being inland (except for the Caribbean). Hence they have mixed impacts and vulnerabilities: Hard, rocky coasts on the western coast, but also cities and deltas on the eastern coast. The Caribbean islands are also vulnerable: Sea-level rise is expected to add significant pressure due to its high exposure of area and population (Anthoff et al. 2006) and its reliance on its coastal resources, habitats and wetlands (Schnack 1993; FAO 2006). Sea-level rise increases risk of disruption to transportation systems, such as ports or airports. Major hotspots include the Guyana, Suriname and the French Guiana coast where the population is concentrated in a narrow coastal lowland. Other areas of South America that are expected to be most affected by sea-level rise and other climate impacts are the low-lying Pampas region including Buenos Aires metropolitan area and cities on the coast of Brazil such as Rio de Janeiro. In Venezuela there are a number of urban centres and the majority of industry is concentrated along the coastal zone, including Lake Maracaibo which is subsiding due to oil extraction. Assessments of exposed land area and population show that this varies considerably between countries. Experience of adaptation is focused on the areas with impacts and required development.

Much of the North American coast is developed and the coast is a major focus for development, with states such as Florida being some of the most populous in the region. The main approach to manage current coastal hazards is land use planning, flood resilience, warning systems and evacuation, and flood insurance allowing rebuilding and repair. Local protection is apparent in a few regions, such as in Louisiana and New Orleans (where subsidence is significant – see Sect. 5.3). Compared to Europe and Japan, higher levels of risk appear to be accepted in North American coastal cities (Nicholls et al. 2008b). East coast barrier beaches are under threat from human influence and rising relative sea levels, and large areas of

wetlands are at risk. Since colonisation in the 1700s, only 47% of wetlands remain in the USA. Wetlands have been lost due to reclamation, with California losing up to 90% of its original wetlands. Recognising the importance of wetlands and the designated laws to protect it, wetland loss has slowed since the 1970s (Watzin and Gosselink 1992).

The south, south-east and east Asian coasts contain a large part of the world's coastal population, often situated in many of the large deltas and recent alluvial plains. In contrast, Russia and the Middle East have a lower coastal population. The continued growth of coastal cities, including megacities, means that their impacts to sea-level rise should be considered. A major threat (which can be greater than climate-induced sea-level rise) in many cities is local subsidence, especially for those located in deltas, where groundwater pumping enhances subsidence (World Bank 2010). Monitoring and mitigating by reducing water extraction helps reduce the problem (see Sect. 5.2). In east Asia in particular, there is a long history of defence, as exemplified by 12,000 km of dike in China (Li et al. 2004), and defence construction and upgrade seems likely in the future. Around poorer parts of Asia, wetlands are under threat (e.g. conversion to farming which is a major issue due to the large and growing population), but these ecosystems offer vital services, soft protection and livelihoods, and so need to be preserved.

Ranging from coral reef and mangrove-fringed shorelines in the tropics to extensive cliffs along the Great Australian Bight, and comprising more than 10,000 beaches, the Oceania coast is very diverse (Short and Woodroffe 2009). Eighty percent of the population lives near the coast. With a growing population and increasing coastward migration, there is pressure for more coastal urban development. However there is increasing awareness and planning, including building setbacks (where development is prohibited within a strip adjacent to the coast) to reduce vulnerability. Parts of the Australian coast have a high tidal range, and so the effects of sea-level rise and changes to salinity can in places extend 100 km inland. Large areas of wetlands, such as mangroves and associated wildlife and adjacent freshwater ecosystems are vulnerable to the effects of sea-level rise. Rising temperatures and reduced river flow could also exacerbate problems. Coral reefs are already showing some of the most dramatic effects of climate change in response to thermal stress and elevated sea surface temperatures. Signs of adverse conditions have already been seen on the Great Barrier Reef. Monitoring programmes need to be enhanced, with all forms of climate change integrated to better assess vulnerability (Harvey and Woodroffe 2008).

In Europe, developed urbanised coastlines are highly threatened by sea-level rise, but where it is economically possible to adapt, this is already being undertaken and planned, thus reducing vulnerability. Dike systems are especially extensive around the southern North Sea in Germany, the Netherlands, Belgium and England. Broadly, Europeans are considering growing vulnerability and are proactive in reducing risk. This includes research and development (e.g. The EU Framework programmes), directives (e.g. the EU Flood Directive), and national planning (e.g. the Delta Commissie in the Netherlands). The natural environment will become increasingly under pressure as sea levels rise, and where natural and built environs coincide,

coastal squeeze could result causing environmental degradation, challenging the EU Habitats Directive. The port and energy sector also needs to plan for sea-level rise, such as raising port infrastructure or regularly assessing or increasing protection around vulnerable areas. Due to awareness of climate change and financial means, vulnerability is low. European Union directives and other international regulations focuses attention on the natural environment.

Small islands, such as the Maldives or Tuvalu, are especially vulnerable places to rising sea levels. The sand cays on the perimeter of coral atolls are some of the most low-lying locations in which people live, few rising more than 3 m above sea level (Woodroffe 2008). They potentially have low adaptive capacity, even if there is large investment in adaptation on an island. Transport by aeroplane or ship may be threatened if there are insufficient resources to protect or raise port infrastructure or if land becomes flooded or eroded. Their natural environment is also threatened (e.g. beaches, salinity) and this could affect the economy (e.g. tourism) or freshwater supplies. This could have further impacts on income, fishing industry and agriculture, threatening livelihoods. With limited resources and capacity to change, small islands, particularly remote islands are some of the most vulnerable places to be affected by sea-level rise (Hinkel et al. 2012b). Small 'high' islands are also at risk due to their remoteness, strong coastal focus in urban areas and associated infrastructure and low adaptive capacity. Subsequently adaptation (e.g. port upgrade) would need to be widespread. Finally some small island states, as well as other coastal states (e.g. Bahamas), may further encounter losses or face disputes over their maritime territory if coastlines retreat and islands become submerged (Houghton et al. 2010).

5.5.2 *Engendering Vulnerability: Awareness, Response and Integration*

From a global perspective it is clear that there are cross cutting issues and challenges to face, and areas where knowledge of vulnerability needs to be improved. This study has illustrated the diversity of problems that occur on each continent. Whilst lessons can be learnt from one country to another, some issues and risks are specific to a global region and need attention in this context.

Environmental change makes people vulnerable and we need to understand, learn, live and ultimately adapt to new conditions. Subtle environmental change (that people may not even be aware of) can potentially result in a slow increase in vulnerability. People assume that the status quo provides sufficient protection and they can ignorant in assessing risks. Large increases in vulnerability can result from rapid changes. People are often more responsive to these large changes of risk because they are more apparent. Mitigation can reduce ongoing risk and vulnerability. In terms of vulnerability over time, the end destination of slow subtle change versus a sudden change may be the same, but the risks en route may not. Subsequently expected human

behaviour due to potential adaptation or mitigation differs as does the decision making processes to reduce risk (or an individuals or organisations perception of that risk). Hence risk and impacts must be periodically reviewed, and adaptation and mitigation options assessed.

Here, only the effects of sea-level rise have been assessed, but this will be accompanied by other climate and marine effects (e.g. storminess, salinity and sea surface temperature) and non-climate-induced environmental problems, compounding the threat of adverse change. As such, there is a need for integrated approaches to assess the complex interdependencies and tradeoffs between management and the natural environment. Knock on effects need to be investigated and their relationship to impacts and vulnerability, such as changes to biodiversity or influences on agriculture or freshwater supplies. Finally, coastal vulnerability driven by non-climatic factors, such as socio-economic development, coastal management, water abstraction or agriculture practices can be profound and yet are often overlooked in impact studies (Nicholls et al. 2008a).

5.6 Conclusion

Relative sea-level rise due to global climate-induced changes, and more local non-climatic changes such as land subsidence, particularly in densely populated areas potentially have serious impacts in the coastal zone affecting the natural environment and human activities. As relative sea levels rise, lower surge elevations are required to bring about a high water level or extreme event. Global mean sea levels may rise more than 1 m during the twenty-first century with the key uncertainties being the contribution of ice melt from Greenland and Antarctica. Due to regional and local factors, local sea-level rise will be variable around this mean with subsidence in some densely populated areas potentially greatly exacerbating the global trends (as observed during the twentieth century). Other places may experience a fall in relative sea levels as land levels rise at a greater rate than sea levels. This chapter has illustrated that there is a large reliance on coastal zone ecosystems and services, including beaches, wetlands, and much of the infrastructure in urban areas, transport and energy systems. These systems are highly interlinked and any adverse consequences of extreme water levels could have major impacts to those on the coast, and those inland who rely on coastal services.

Coastal wetlands are highly vulnerable to sea-level rise, whilst sandy environments are likely to erode as they are more mobile and have greater potential to cope with sea level rise. These environments offer multiple services, such as for habitat creation and also help to protect the coast. What is important is how fast sea levels will rise and how this effects changes to sediment availability. Sediment availability (e.g. in delta regions) is affected by fluvial water availability and erosional processes – both of which could be affected by other climatic and non-climatic drivers. There is a need for further integration between climate and other

environmental drivers of change, in terms of their impacts, potential to adapt, and therefore vulnerability.

Significant growth in the built environment and the transport and energy network is occurring, some of which is planned, others unplanned. Unplanned urban sprawl, growing populations, water abstraction and conversion of wetlands puts increasing pressures on the built environment and its environs making them more vulnerable to rising sea levels and extreme events. Improved regulation, information and monitoring is required to help authorities and stakeholders better understand the risks, and where possible avoid or adapt to them. Examples of proactive planning such as the Delta Commission (Delta Commissie 2008) and the Thames Estuary 2100 (Environment Agency 2010) approaches should be developed into more generic approaches for widespread application.

At the continental scale considered in the paper, there are different impacts and vulnerabilities, and therefore varying needs and challenges to adapt to sea-level rise. Small islands are vulnerable due to their remoteness (particularly those at low elevation), Africa and other parts of the developing world are vulnerable due to a lack of financial capacity to adapt, and south, south-east and east Asia due to high population densities in subsiding deltas. The coastal environment should be carefully monitored and managed: By maintaining or improving the natural environmental quality, benefits can extend to other environs (including human activities), reducing potential problems and economic costs. Climate mitigation aims to reduce the rate of sea-level rise, but this does not stop it instantaneously rising. The benefits of this may take decades to centuries to be apparent, so adaptation is also required. Given that the magnitude of future sea-level rise is uncertain, adaptation measures need to be flexibly planned and integrated taking consideration of other aspects of climate change and relevant non-climatic drivers. By identifying and improving our understanding of local and global drivers of change, different integrated approaches to manage and adapt to hazards in the most effective way possible to reduce risk can be undertaken.

Acknowledgements We thank Dr Ivan Haigh (University of Southampton, UK) for comments on this manuscript. SB, RJN and JH received funding from the European Union Seventh Framework Programme (FP7/2007–2013) under the grant agreement 282746 (IMPACT2C: Quantifying projected impacts under 2°C of warming).

References

Adger WN, Agrawala S, Mirza MMQ et al (2007) Assessment of adaptation practices, options, constraints and capacity. In: Parry ML, Canziani OF, Palutikof JP et al (eds) Climate change 2007: impacts, adaptation and vulnerability, Contribution of working group II to the fourth assessment report of the intergovernmental panel on climate change. Cambridge University Press, Cambridge

Alig RJ, Kline JD, Lichtenstein M (2004) Urbanization on the US landscape: looking ahead in the 21st century. Landsc Urban Plan 69(2–3):219–234. doi:10.1016/j.landurbplan.2003.07.004

Allen JRL (2000) Morphodynamics of Holocene salt marshes: a review sketch from the Atlantic and southern North Sea coasts of Europe. Quat Sci Rev 19:1155–1231

Alongi DM (2002) Present state and future of the world's mangrove forests. Environ Conserv 29:331–349

Anthoff D, Nicholls RJ, Tol RSJ et al (2006) Global and regional exposure to large rises in sea level: a sensitivity analysis. Working paper 96. Tyndall Centre for Climate Change Research, University of East Anglia, Norwich

Balk D, Montgomery MR, McGranahan G et al (2009) Mapping urban settlements and the risks of climate change in Africa, Asia and South America. In: Guzmán JM, Martine G, McGranahan G et al (eds) Population dynamics and climate change. United Nations Population Fund (UNFPA)/International Institute for Environment and Development (IIED), New York/London

Bamber J (2012) Climate change: shrinking glaciers under scrutiny. Nature. doi:10.1038/nature10948

Barbier EB (2012) Progress and challenges in valuing coastal and marine ecosystem services. Rev Environ Econ Policy 6(1):1–19. doi:10.1093/reep/rer017

Becker A, Inouse S, Fischer M et al (2011) Climate change impacts in international seaports: knowledge, perceptions and planning efforts among port administrators. Clim Change. doi:10.1007/s10584-10011-10043-10587

Black R, Bennett SRG, Thomas SM et al (2011) Climate change: migration as adaptation. Nature 478:447–449. doi:410.1038/478477a

BP (2009) BP statistical review of world energy, June 2009. http://www.bp.com/liveassets/bp_internet/globalbp/globalbp_uk_english/reports_and_publications/statistical_energy_review_2008/STAGING/local_assets/2009_downloads/statistical_review_of_world_energy_full_report_2009.pdf. Accessed 19 Mar 2012

Brown S, Barton M, Nicholls R (2011) Coastal retreat and/or advance adjacent to defence in England and Wales. J Coast Conserv 15(4):659–670. doi:10.1007/s11852-011-0159-y

Bruun P (1962) Sea-level rise as a cause of shore erosion. Am Soc Civ Eng Proc J Waterways Harbours Div 88:117–130

Cazenave A, Llovel W (2010) Contemporary sea level rise. Annu Rev Mar Sci 2:145–173

Chappell J, Polach H (1991) Postglacial sea-level rise from a coral record at Huon Peninsula, Papua New Guinea. Nature 349(6305):147–149. doi:10.1038/349147a0

Church JA, White NJ (2011) Sea-level rise from the late 19th to the early 21st century. Surv Geophys 32(4–5):585–602. doi:10.1007/s10712-011-9119-1

Church JA, Roemmich D, Domingues CM et al (2010) Ocean temperature and salinity contributions to global and regional sea-level change. In: Church JA, Woodworth PL, Aarup T et al (eds) Understanding sea-level rise and variability. Wiley-Blackwell, Oxford

Church JA, Gregory JM, White NJ, Platten SM et al (2011) Understanding and projecting sea level change. Ocean 24(2):130–143

Coleman JM, Huh OK, Braud D (2008) Wetland loss in world deltas. J Coast Res 24(1A):1–14. doi:10.2112/05-0607.1

Cooper JAG, Pilkey OH (2004) Sea-level rise and shoreline retreat: time to abandon the Bruun Rule. Glob Planet Change 43:157–171

Costanza R, d'Arge R, de Groot R et al (1997) The value of the world's ecosystem services and natural capital. Nature 387(6630):253–260

Costanza R, Perez-Maqueo O, Martinez ML et al (2008) The value of coastal wetlands for hurricane protection. Ambio 37(4):241–248

Cowell PJ, Stive MJF, Niedoroda AW et al (2003a) The coastal-tract (part 1): a conceptual approach to aggregated modeling of low-order coastal change. J Coast Res 19(4):812–827

Cowell PJ, Stive MJF, Niedoroda AW et al (2003b) The coastal-tract (part 2): applications of aggregated modeling of lower-order coastal change. J Coast Res 19(4):828–848

Das Gupta A, Babel MS (2005) Challenges for sustainable management of groundwater use in Bangkok, Thailand. Int J Water Resour Dev 21(3):453–463

Day J (2008) The need and practice of monitoring, evaluating and adapting marine planning and management – lessons from the Great Barrier Reef. Mar Policy 32:823–831
Delta Commissie (2008) Working together with water. A living land builds for its future. Findings of the Delta Commissie. Delta Commissie, The Netherlands. http://www.deltacommissie.com/doc/deltareport_full.pdf. Accessed 11 Apr 2012
Doody JP (2004) 'Coastal squeeze' – an historical perspective. J Coast Conserv 10:129–138
Environment Agency (2010) Thames Estuary 2100. http://www.environment-agency.gov.uk/homeandleisure/floods/104695.aspx. Accessed 23 Mar 2012
Ericson JP, Vörösmarty CJ, Dingman SL et al (2006) Effective sea-level rise and deltas: causes of change and human dimension implications. Glob Planet Change 50:63–82
Evans E, Ashley R, Hall J et al (2004) Foresight future flooding: scientific summary: volume I – future risks and their drivers. Office of Science and Technology, London
FAO (2006) Third session of the sub-committee on aquaculture: committee on fisheries. Food and Agriculture Organisation of the United Nations, New Delhi
FitzGerald DM, Fenster MS, Argow BA et al (2008) Coastal impacts due to sea-level rise. Annu Rev Earth Planet Sci 36:601–647
Foresight (2011) The future of food and farming. Executive summary. The Government Office for Science, London. http://www.bis.gov.uk/assets/foresight/docs/food-and-farming/11-547-future-of-food-and-farming-summary. Accessed 11 Apr 2012
French PW (2006) Managed realignment – the developing story of a comparatively new approach to soft engineering. Estuar Coast Shelf Sci 67:409–423
GCMD (2010) Nuclear power sites of the world from UNEP/GRID-Geneva and IAEA. Global change master directory, discover earth science data and services. Data sets, entry ID: GNV181. http://gcmd.nasa.gov/records/GCMD_GNV181.html. Accessed 18 May 2010
GeoCommons (2012) Wikipedia, Global oil refineries, world, 2.3.2004. http://geocommons.com/overlays/28. Accessed 26 Mar 2012
Grinsted A, Moore JC, Jevrejeva S (2009) Reconstructing sea level from paleo and projected temperatures 200 to 2100 AD. Clim Dyn 34:461–472. doi:10.1007/s00382-008-0507-2
Haigh ID, Nicholls RJ, Wells NC (2011) Rising sea levels in the English Channel 1900 to 2100. Proc ICE Marit Eng 164(2):81–92
Hanson S, Nicholls RJ (2012) Planning for change in extreme events in port cities throughout the 21st century. In: Aerts J, Botzen W, Bowman MJ et al (eds) Climate adaptation and flood risk in coastal cities. Earthscan, Abingdon
Harvey N, Woodroffe CD (2008) Australian approaches to coastal vulnerability assessment. Sustain Sci 3:67–87
Hinkel J (2009) The PIAM approach to modular integrated assessment modelling. Environ Model Softw 24:739–748
Hinkel J, Brown S, Exner L et al (2012a) Sea-level rise impacts on Africa and the effects of mitigation and adaptation: an application of DIVA. Reg Environ Change 12(1):207–224. doi:10.1007/s10113-011-0249-2
Hinkel J, van Vuuren DP, Nicholls RJ et al (2012b) The effects of mitigation and adaptation on coastal impacts in the 21st century. Clim Change, revised version under review
Houghton K, Vafeidis A, Neumann B et al (2010) Maritime boundaries in a rising sea. Nat Geosci 3:813–816
Hughes TP, Baird AH, Bellwood DR et al (2003) Climate change, human impacts, and the resilience of coral reefs. Science 301:929–933
IPCC (1990) Sea-level rise: a world-wide cost estimate of basic coastal defence measures. Report prepared for Intergovernmental Panel on Climate Change (IPCC) and Rijkswaterstaat. Delft Hydraulics, Delft
IPCC (2007) Climate change 2007. Synthesis report. Contribution of working groups I, II and III to the fourth assessment report of the Intergovernmental Panal on Climate Change. IPCC, Geneva
Jacob T, Wahr J, Pfeffer WT et al (2012) Recent contributions of glaciers and ice caps to sea level rise. Nature. doi:10.1038/nature10847

Jevrejeva S, Grinsted A, Moore JC (2009) Anthropogenic forcing dominates sea level rise since 1850. Geophys Res Lett 36:L20706. doi:20710.21029/22009GL040216
Jevrejeva S, Moore JC, Grinsted A (2012) Sea level projections to AD2500 with a new generation of climate change scenarios. Glob Planet Change 80–81:14–20. doi:10.1016/j.gloplacha.2011.09.006
Kamal-Chaoui L, Robert A (2009) Competitive cities and climate change. OECD regional development working papers, no. 2. OECD, Paris
Kopp R, Simons F, Mitrovica J et al (2009) Probabilistic assessment of sea level during the last interglacial stage. Nature 462:863–867. doi:10.1038/nature08686
Kron W (2009) Coasts – the riskiest places on earth: coastal engineering 2008. World Scientific Publ Co P. Ltd, Singapore
Leorri E, Gehrels WR, Horton BP et al (2010) Distribution of foraminifera in salt marshes along the Atlantic coast of SW Europe: tools to reconstruct past sea-level variations. Quat Int 221 (1–2):104–115
Li C, Fan D, Deng B et al (2004) The coasts of China and issues of sea level rise. J Coast Res SI43:36–49
Lichter M, Vafeidis AT, Nicholls RJ et al (2011) Exploring data-related uncertainties in analyses of land area and population in the "low-elevation coastal zone" (LECZ). J Coast Res 27 (4):757–768. doi:10.2112/jcoastres-d-10-00072.1
Linham MM, Nicholls RJ (2010) Technologies for climate change adaptation – coastal erosion and flooding. UNEP, Roskilde. http://tech-action.org/Guidebooks/TNA_Guidebook_Adaptation-CoastalErosionFlooding.pdf. Accessed 23 Mar 2012
List L's (2009) Ports of the world 2009, volume 1: Albania – Lithuania; volume 2: Madagascar – Yemen. Informa and Maritime, London
Luisetti T, Turner RK, Bateman IJ et al (2011) Coastal and marine ecosystem services valuation for policy and management: managed realignment case studies in England. Ocean Coast Manag 54(3):212–224. doi:10.1016/j.ocecoaman.2010.11.003
McGranahan G, Balk D, Anderson B (2007) The rising tide: assessing the risks of climate change and human settlements in low elevation coastal zones. Environ Urban 19(1):17–37. doi:10.1177/0956247807076960
Meehl GA, Stocker TF, Collins WD et al (2007) Global climate projections. In: Solomon S, Qin D, Manning M et al (eds) Climate change 2007: the physical science basis. Contribution of working group I to the fourth assessment report of the intergovernmental panel on climate change. Cambridge University Press, Cambridge
Mimura N (2001) Distribution of vulnerability and adaptation in the Asia and Pacific Region. Global change and Asia Pacific coasts. In: Proceedings APN/SURVAS/LOICZ joint conference on coastal impacts of climate change and adaptation in the Asia – Pacific region, Kobe, pp 21–25
Mimura N, Nurse L, McLean RF et al (2007) Small islands. In: Parry ML, Canziani OF, Palutikof JP et al (eds) Climate change 2007: impacts, adaptation and vulnerability. Contribution of working group II to the fourth assessment report of the intergovernmental panel on climate change. Cambridge University Press, Cambridge
Munich Re (2012) Natural catastophes 2011. NatCatSERVICE database. Munich Re, München. https://www.munichre.com/touch. Accessed 19 Apr 2012
Nicholls RJ (1995) Coastal megacities and climate change. GeoJournal 37(3):369–379
Nicholls RJ (2004) Coastal flooding and wetland loss in the 21st century: changes under the SRES climate and socio-economic scenarios. Glob Environ Change Hum Policy Dimens 14:69–86
Nicholls RJ (2010) Impacts of and responses to sea-level rise. In: Church JA, Woodoworth PL, Aarup T et al (eds) Understanding sea-level rise and variability. Wiley-Blackwell, Chichester
Nicholls RJ, Kebede AS (2010) The implications on the UK of the impacts of climate change and sea-level rise on critical coastal infrastructure overseas, 2010 to 2100. Government Office for Science, London. http://www.bis.gov.uk/assets/bispartners/foresight/docs/international-dimensions/11-1022-implications-on-uk-climate-change-sea-level-rise. Accessed 12 Mar 2012

Nicholls RJ, Hoozemans FMJ, Marchland M (1999) Increasing flood risk and wetland losses due to global sea-level rise: regional and global analyses. Glob Environ Chang 9(S1):69–88

Nicholls RJ, Wong PP, Burkett VR et al (2007) Coastal systems and low-lying areas. In: Parry ML, Canziani OF, Palutikof JP et al (eds) Climate change 2007: impacts, adaptation and vulnerability. Contribution of working group II to the fourth assessment report of the intergovernmental panel on climate change. Cambridge University Press, Cambridge

Nicholls RJ, Wong PP, Burkett V et al (2008a) Climate change and coastal vulnerability assessment: scenarios for integrated assessment. Sustain Sci 3(1):89–102

Nicholls RJ, Hanson S, Herweijer C et al (2008b) Ranking port cities with high exposure and vulnerability to climate extremes: exposure estimates. Environmental working paper no. 1. Organisation for Economic and Co-operation Development, Paris

Nicholls RJ, Marinova N, Lowe JA et al (2011) Sea-level rise and its possible impacts given a 'beyond 4°C world' in the twenty-first century. Proc R Soc Lond Ser A Math Phys Sci 369 (1934):161–181. doi:10.1098/rsta.2010.0291

OpenFlights (2012) Airport, airline and route data: airport database. http://openflights.org/data.html. Accessed 26 Mar 2012

Oxford Economics (2009) Aviation: the real world wide web. Oxford Economics, Oxford

Pannell CW (2002) China's continuing urban transition. Environ Plan A 34(9):1571–1589. doi:10.1068/a34201

Pannell CW (2003) China's demographic and urban trends for the 21st century. Eurasian Geogr Econ 44(7):479–496

Permanent Service for Mean Sea Level (2012) Data. http://www.psmsl.org/data/. Accessed 2 Mar 2012

Pfeffer W, Harper J, O'Neel S (2008) Kinematic constraints on glacier contributions to 21st-century sea-level rise. Science 321:1340–1343. doi:1310.1126/science.1159099

Rahman AF, Dragoni D, El-Masri B (2011) Response of the Sundarbans coastline to sea level rise and decreased sediment flow: a remote sensing assessment. Remote Sens Environ 115 (12):3121–3128. doi:10.1016/j.rse.2011.06.019

Rahmstorf S (2007) A semi-empirical approach to projecting future sea-level rise. Science 315:368–370. doi:10.1126/science.1135456

Ramsar Wetlands International (2007) About GIS and maps. http://ramsar.wetlands.org/GISMaps/AboutGISMaps/tabid/1001/Default.aspx. Accessed 16 Apr 2012

Ranasinghe R, Callaghan D, Stive MJF (2012) Estimating coastal recession due to sea level rise: beyond the Bruun rule. Clim Change 110(3–4):561–574. doi:10.1007/s10584-011-0107-8

Rayer R, MacKenzie B (2010) A first-order assessment of the impact of long-term trends in extreme sea levels on offshore structures and coastal refineries. In: Church JA, Woodoworth PL, Aarup T et al (eds) Understanding sea-level rise and variability. Wiley-Blackwell, Chichester

Rignot E, Velicogna I, van den Broeke MR et al (2011) Acceleration of the contribution of the Greenland and Antarctic ice sheets to sea level rise. Geophys Res Lett 38:L05503. doi:05510.01029/02011GL046583

Rohling E, Grant K, Hemleben C et al (2008) High rates of sea-level rise during the last interglacial period. Nat Geosci 1:38–42. doi:10.1038/ngeo.2007.28

Rowlands OE, Armstrong SG, Nicholls RJ (in review) Costs of managed realignment: UK experience. Proceedings of ICE – Marit Eng

Roy PS, Cowell PJ, Ferland MA et al (1994) Wave-dominated coasts. In: Carter RWG, Woodroffe CD (eds) Coastal evolution: late quaternary shoreline morphodynamics. Cambridge University Press, Cambridge

Schnack EJ (1993) The vulnerability of the east coast of South America to sea level rise and possible adjustment strategies. In: Warrick RA, Barrow EM, Wigley TML (eds) Climate and sea level change: observations, projections, and implications. Cambridge University Press, Cambridge

Sekovski I, Newton A, Dennison WC (2011) Megacities in the coastal zone: using a driver-pressure-state-impact-response framework to address complex environmental problems. Estuar Coast Shelf Sci 96:48–59. doi:10.1016/j.ecss.2011.07.011

Sherwin CW, Nicholls RJ (2007) Urban managed realignment: application to the Thames Estuary, London. J Coast Res 23(6):1525–1534. doi:1510.2112/1505-0586.1521

Short AD, Woodroffe CD (2009) The coast of Australia. Cambridge University Press, Cambridge

Small C, Nicholls RJ (2003) A global analysis of human settlement in coastal zones. J Coast Res 19(3):584–599

Smith K (2011) We are seven billion. Nat Clim Change 1(7):331–335

Solomon S, Qin D, Manning M et al (eds) (2007) Climate change 2007: the physical science basis. Contribution of working group I to the fourth assessment report of the intergovernmental panel on climate change. Cambridge University Press, Cambridge

Stanlenberg B (2012) Innovative flood defences in highly urbanized water cities. In: Aerts J, Botzen W, Bowman M et al (eds) Climate adaptation and flood risk in coastal cities. Earthscan, Abington

Syvitski JPM, Kettner AJ, Overeem I et al (2009) Sinking deltas due to human activites. Nat Geosci 2:681–686. doi:10.1038/ngeo629

UNCTAD (2010) Review of maritime transport 2010. United Nations conference on trade and development. United Nations, New York and Geneva. http://unctad.org/en/docs/rmt2010_en.pdf. Accessed 11 Apr 2012

UNCTAD (2011) Review of maritime transport 2011. United Nations conference on trade and development. United Nations, New York and Geneva. http://unctad.org/en/docs/rmt2011_en.pdf. Accessed 11 Apr 2012

United Nations (2010) World urbanization prospects: the 2009 revision. File 12: population of urban agglomerations with 750,000 inhabitants or more in 2009, by country, 1950–2025 (thousands). United Nations, Department of Economic and Social Affairs, Population Division, New York. http://esa.un.org/unpd/wup/CD-ROM_2009/. Filename: WUP2009-F12-Cities_Over_750K.xls. Accessed 18 Nov 2011

Vafeidis AT, Nicholls RJ, McFadden L et al (2008) A new global coastal database for impacts and vulnerability analysis to sea-level rise. J Coast Res 24(2):917–924. doi:10.2112/06-0725.1

Vafeidis A, Neumann B, Zimmermann J et al (2011) MR9: analysis of land area and population in the low-elevation coastal zone (LECZ). Review commissioned as part of the UK Government's Foresight project. Migration and global environmental change. Government Office for Science, London

Valiela I (2006) Global coastal change. Blackwell, Oxford

Van de Wal RSW, Boot W, van den Broeke MR et al (2008) Large and rapid melt-induced velocity changes in the ablation zone of the Greenland ice sheet. Science 321:111–113. doi:110.1126/science.1158540

Vellinga P, Katsman C, Sterl A et al (2008) Exploring high-end climate change scenarios for flood protection of the Netherlands. International scientific assessment carried out at request of the Delta Committee. Scientific report WR-2009-05. KNMI/Alterra, The Netherlands. http://www.knmi.nl/bibliotheek/knmipubWR/WR2009-05.pdf. Accessed 30 Apr 2012

Vermeer M, Rahmstorf S (2009) Global sea level linked to global temperature. Proc Natl Acad Sci USA 106(51):21527–21532. doi:10.1073/pnas.0907765106

Watzin MC, Gosselink JG (1992) The fragile fringe: coastal wetlands of the continental United States. Louisiana Sea Grant College Program, Louisiana State University, US Fish and Wildlife Service, National Oceanic and Atmospheric Administration, Baton Rouge, Washington, DC and Rockville. http://permanent.access.gpo.gov/lps70037/fragfringe.pdf. Accessed 11 May 2012

Wilby RL, Nicholls RJ, Warren R et al (2011) Keeping nuclear and other coastal sites safe from climate change. Proc ICE Civ Eng 164:129–136

Wolf S, Hinkel J, Ionescu C et al (in review) Vulnerability definitions and methodologies: a clarification by formalisation

Woodroffe CD (1990) The impact of sea-level rise on mangrove shorelines. Prog Phys Geogr 14:483–520

Woodroffe CD (2008) Reef-island topography and the vulnerability of atolls to sea-level rise. Glob Planet Change 62:77–96

Woodroffe CD, Nicholls RJ, Saito Y et al (2006) Landscape variability and the response of Asian megadeltas to environmental change. In: Harvey N (ed) Global change and integrated coastal management: the Asia-Pacific region. Springer, Dordrecht

Woodworth PL, Player R (2003) The permanent service for mean sea level: an update to the 21st century. J Coast Res 19(2):287–295

Woodworth PL, Gehrels WR, Nerem RS (2011) Nineteenth and twentieth century changes in sea level. Ocean 24(2):80–93

World Bank (2010) Climate risks and adaptation in Asian coastal megacities. A synthesis report. World Bank, Washington. http://siteresources.worldbank.org/EASTASIAPACIFICEXT/Resources/226300-1287600424406/coastal_megacities_fullreport.pdf. Accessed 4 May 2012

World Bank (2011) 37,000 mangroves for Kiribati. http://go.worldbank.org/7SM7HFHK00. Accessed 13 Mar 2012

World Nuclear Association (2012a) World nuclear power reactors and uranium requirements. Mar 2012. http://www.world-nuclear.org/info/reactors.html. Accessed 23 Mar 2012

World Nuclear Association (2012b) Nuclear power in China. Mar 2012. http://www.world-nuclear.org/info/inf63.html. Accessed 23 Mar 2012

Wright KM, Hogan C (2008) The potential impacts of global sea level rise on transportation infrastructure. Part 1: Methodology. US Dot Centre for Climate Change and Environmental Forecasting. http://climate.dot.gov/impacts-adaptations/sea_level_rise.html. Accessed 13 Apr 2012

Chapter 6
Estimating the United States Population at Risk from Coastal Flood-Related Hazards

Mark Crowell, Jonathan Westcott, Susan Phelps, Tucker Mahoney, Kevin Coulton, and Doug Bellomo

Abstract Over the past couple of decades a number of papers have been published that provide estimates of United States population living in coastal areas. These estimates vary widely; ranging from less than 5%, to more than 50% of the U.S. population living in coastal areas. The reason for the wide range in estimates is that there are a variety of criteria that can be combined in a number of permutations to define "coastal areas." For example, coastal areas may be defined based on probability of coastal flooding, inundation caused by future changes in sea levels, or simply by proximity to the coastline itself. In addition, spatial buffers, such as geopolitical units (e.g., counties and census block groups), or prescribed distances (e.g., 50- or 100-mile distance buffers), can also be used to provide a measure of uncertainty associated with economic exposure, or with measurement error. Other types and categories of defining criteria can be used to further characterize coastal areas. In this chapter we focused our attention on estimating U.S. population at risk from the 1% annual chance coastal flood. The 1% annual chance flood (both coastal and riverine) is used by FEMA in the administration of the National Flood Insurance Program (NFIP). The methods used in this analysis followed those of Crowell et al. (J Coast Res 26:201–211, 2010) who used a three-step process to determine coastal population: (1) create a national digital flood hazard database using FEMA

M. Crowell (✉) • J. Westcott • D. Bellomo
Federal Emergency Management Agency, 1800 South Bell Street, Room 942, Arlington, VA 20598, USA
e-mail: mark.crowell@dhs.gov

S. Phelps
AECOM, 4905 Koger Boulevard, Suite 270, Greensboro, NC 27407, USA

T. Mahoney
Federal Emergency Management Agency, Region IV, 3003 Chamblee Tucker Road, Atlanta, GA 30341, USA

K. Coulton
AECOM, 333 SW 5th Avenue, Suite 225, Portland, OR 97204, USA

C.W. Finkl (ed.), *Coastal Hazards*, Coastal Research Library 6,
DOI 10.1007/978-94-007-5234-4_6,

(or FEMA-derived) datasets; (2) use a systematic method to separate coastal from riverine flood hazard areas; and (3) combine 2010 census block group data (assuming uniform population distribution) with the digital coastal flood hazard database using a geographic information system. The results of this analysis indicate that approximately 2.8% of the U.S. population lives in areas directly subject to 1% chance coastal flood. In addition, a total of 395 counties were found to be contiguous with the ocean or Great Lakes coast and/or have at least some coastal flood hazard areas (as based on the 1% annual chance coastal flood) located within their boundaries. About 39% of the U.S. population lives in these "coastal" counties.

6.1 Introduction

Coastal areas are subject to a variety of flood-related hazards, including hurricanes, nor-easters, tsunamis, and erosion. In unpopulated, undeveloped areas, these hazards pose relatively little social and economic risk. However, much of our Nation's coastline is populated and developed; as such, these natural hazards can, in many areas, pose a significant threat to human life and developed infrastructure. The future promises to show an increase in damaging coastal flood events with the merging of two trends: the first is a projected increase in population in coastal regions (Crossett et al. 2004; Wilson and Fischetti 2010); the second is an almost certain amplification of coastal flood hazards caused by rising sea levels and concomitant erosion.

Over the last 100 years or so, eustatic rates of sea level rise have increased by about 0.06–0.08 in. (1.5–2.0 mm) per year (Miller and Douglas 2004; Church and White 2006; IPCC 2007), while in the United States, historical long-term (50–175 years) rates of erosion (a consequence of long-term sea level rise) typically are in the range of one to three or more feet (0.3–0.9 m) per year along the Atlantic and Gulf Coasts (Crowell and Leatherman 1999). These trends will most likely accelerate over the next century as a result of global warming (Zhang et al. 2004; Vermeer and Rahmstorf 2009; Nicholls et al. 2011). In addition, potential changes in the frequency and intensity of coastal storms (Knutson et al. 2010; Bender et al. 2010) may further contribute to an increase in the social and economic risk associated with coastal flood hazards. In order to better understand current and projected risk in coastal hazard areas, one must have a clear understanding of two key factors that define this risk; they are: (1) the probability that a coastal hazard will occur, and (2) the effect of that hazard on human life and property. This chapter addresses the second key factor and focuses on coastal flooding (and associated hazards), and provides estimates of the U.S. population living in areas at risk from the 1% annual chance (sometimes referred to as "100-y") coastal flood hazards.

Over the past few decades a number of efforts have been made to estimate populations living in coastal areas. While seemingly simple at its surface, this is actually a complex undertaking reflecting varying study goals, limited data availability, and nuances in the definition of the word "coastal." The Federal Emergency

Management Agency (FEMA) has a special interest in coastal areas defined by the 1% annual chance flood (defined below), as this is the flood that is integral to the National Flood Insurance Program (NFIP). The NFIP, which is administered by FEMA, is an insurance, land use management, and mapping program. The NFIP covers all categories of flooding, including riverine, lake, and coastal. However, the coastal aspects are some of the more visible parts of the program for many reasons, including the fact that coastal areas are usually more hazardous and land values are generally higher than in the interior.

The following subsections summarize past and current efforts to determine coastal areas and estimate concomitant coastal population. We start out with a brief discussion of papers focusing on global population estimates; then provide a synopsis of coastal population estimates for the U.S. prepared by various entities other than FEMA; and then provide a detailed summary of U.S. coastal population estimates prepared by FEMA, through the NFIP. Finally, we provide details of the most recent coastal population study conducted by FEMA. The FEMA-NFIP population estimates relate to coastal population living in 1% annual chance coastal flood hazard areas, which are based on probabilistic assessments of flooding used by FEMA to administer the NFIP.

6.1.1 Global Population Estimates

A number of estimates of regional to global population living in coastal areas have been published since the early 1990s. Hinrichsen 1990, provided some of the first broadly cited estimates of global coastal population, claiming that "probably 60% of humanity ... live on or near the coast." Hinrichsen's estimates, however, were questioned by Cohen et al. (1997), who found that (in personal communication with Hinrichsen), the author's estimates were determined using questionable "back of the envelope" methods. Hinrichsen's global and U.S., coastal population estimates (Hinrichsen 1990, 1998, 1999) are now generally regarded as flawed (Cohen et al. 1997; Small and Nicholls 2003; Crowell et al. 2007, 2010).

Cohen et al. (1997) and Cohen and Small (1998) used the first publically available worldwide population distribution dataset (Gridded Population of the World (GPW1)) to provide some of the first reasonable estimates of global population living in coastal areas (see Lichter et al. 2011). Cohen et al. (1997) found that 37% of the global population lived within 100 km of a coastline in 1994, and Cohen and Small (1998) determined that 34% of the 1994 global population lived within 100 vertical meters of sea level. Lichter et al. (2011), summarizes these and several more recent papers that provide regional to global-scale estimates of population living in coastal areas. Many of the global estimates use elevation models that typically have a minimum vertical resolution of 1 m, and a minimum horizontal grid spacing of 30 arc-seconds, or approximately 1 km. Lichter et al. (2011) note that global coastal population distribution estimates within 1 m elevation above

mean sea level vary between 108 and 146 million people, and that estimates of population living in land areas with an elevation within 10 m above mean sea level elevation and hydrologically connected to the sea (known as the Low-Elevation Coastal Zone) range from 400 to 634 million people.

6.1.2 *United States Coastal Population Estimates (Exclusive of FEMA Estimates)*

A number of estimates of the U.S. coastal population have been published in a variety of sources over the past several years. These include the following:

- Culliton et al. (1990) estimate that "almost one-half [45%] of our population now lives in coastal areas." The authors identify 451 counties as "coastal counties" (which include counties bordering the Great Lakes); however, it is not clear what criteria were used to make this determination. Further, it appears that the criteria used to determine coastal counties may be inconsistently applied, as the publication states that "for this report, coastal counties are those identified by either the Federal Coastal Zone Management Program. . ., or by individual state coastal management programs."
- Culliton (1998) and Crossett et al. (2004) estimate that there are 673 coastal counties and that 53% of the U.S. population lives in these counties. A "coastal county" is defined in these publications as (1) a county with at least 15% of its total land area located within the Nation's coastal watershed or (2) a county with a portion of its land that accounts for at least 15% of a coastal cataloging unit.[1] Note that Culliton (1998) and Crossett et al. (2004) use the same definition of "coastal county" and list the same counties identified as "coastal." Hereafter, "Culliton (1998)" refers to both Culliton (1998) and Crossett et al. (2004).
- Hinrichsen (1998, 1999) estimates that 55–60% of the U.S. population lives in 772 counties adjacent to the Atlantic and Pacific Oceans, the Gulf of Mexico, and the Great Lakes. It is unclear what criteria were used to identify these 772 counties, and as noted earlier, Hinrichsen's methods have been questioned by other authors.
- The United States Census Bureau (using the 2000 census) noted that 48.9% of the U.S. population lives within 50 miles of the coastline. The Census Bureau clarified these figures by noting that "for this calculation, the coastline was any

[1] According to NOAA (NOAA 2012a), "The coastal watershed is composed of all lands within Estuarine Drainage Areas (EDAs) or Coastal Drainage Areas (CDAs) in NOAA's Coastal Assessment Framework." A coastal cataloging unit is defined by NOAA as "a drainage basin that falls entirely within or straddles an EDA or CDA. Typically, most EDAs or CDAs are composed of several complete cataloging units (drainage basins)".

land that borders the ocean and any of its saltwater tributaries, including bays and tidal rivers, and the Great Lakes" (Crowell et al. 2010).[2]

- Lam et al. (2009) used U.S. Census and LandScan population data, intersected with U.S. Geological Survey (USGS) Digital Elevation Models (DEMs) at a spatial resolution of 1 arc second (approximately 30 m), and determined that about 11.6 million people live "below 3-m elevation" in the conterminous U.S. In addition, the authors intersected LandScan data with NOAA shoreline data buffered to one horizontal kilometer, and estimate that about 19.0 million people reside within 1-km from the shoreline in the conterminous U.S.
- Wilson and Fischetti (2010) focus on "coastline counties," which are defined as any county directly adjacent to water classified as either coastal water or territorial sea. Thus, counties are considered coastal if they border water classified as bay, estuary, gulf, sound, ocean, or sea. The Great Lakes are not included under this definition. The authors note that 254 counties meet these criteria, and that as of 2008, 87 million people (29% of the total US population) live within these counties. These numbers reflect "resident" population, meaning that seasonal (vacation) population is not included.
- Zhang and Leatherman (2011) utilized high resolution satellite imagery from Google Earth™, and 1990 and 2000 census data to estimate population living in coastal barrier islands along the U.S. Atlantic and Gulf Coasts. The authors estimate that about 1.4 million people (permanent residents) live on barrier islands according to the 2000 census.

Two websites of note provide useful coastal-related datasets and interactive tools that facilitate coastal demographic analyses.

- The National Ocean Economics Program (NOEP) maintains a webpage (NOEP 2012) where one can select several different interactive parameters to determine coastal populations. These parameters include the use of areas defined by zip codes, in which the boundaries are located "immediately adjacent to an ocean, Great Lake, or included river or bay," and by coastal zone counties, where such counties are defined using several different criteria (such as watershed based, contiguity with the ocean and/or Great Lakes, and other criteria).
- NOAA maintains a webpage called "Spatial Trends in Coastal Socioeconomics" or STICS (NOAA 2012b). The web site provides access to various national demographic and economic datasets recompiled in a variety of geographic units, including: FEMA 1% annual chance flood hazard areas, and NOAA's coastal watershed areas; and political units, such as counties, states, and state Coastal Zone Management Program boundaries. The datasets facilitate determination of coastal demographic and economic trends.

[2] This information was originally accessed from the U.S. Census Bureau on June 29, 2009, but unfortunately, is no longer available. We include this summary because it appears to be the basis for a number of citations in publications that state that more than 50% of the U.S. population lives within 50 miles of the coast.

6.1.3 FEMA Coastal Population Estimates

FEMA has conducted or funded several studies over the past 25 years in which estimates were made of population and/or infrastructure subject to various coastal hazards, including flood, long-term erosion, and sea level rise. The most recent studies have made use of a variety of digital flood hazard layers of varying ages and quality to capture the areal extent of mapped FEMA coastal floodplains subject to the 1% annual chance flood. At this point it is useful to provide background on how FEMA prepares maps of flood hazard areas, and to discuss available digital flood hazard datasets.

6.1.3.1 FEMA's Flood Insurance Studies and Flood Maps

Key engineering components of the NFIP are Flood Insurance Studies and Flood Insurance Rate Maps (FIRMs). Flood Insurance Studies are prepared in order to determine the elevation and spatial extent of the 1% annual chance flood, which defines the water surface elevations that have a one-percent chance of being equaled or exceeded during any given year. These water surface elevations are termed Base Flood Elevations (BFEs) and are referenced to the National Geodetic Vertical Datum of 1929 (NGVD29), the North American Vertical Datum of 1988 (NAVD88), or a local datum where NGVD29 and NAVD88 are not available (FEMA's current policy is to ensure that all new updated maps are referenced to NAVD88 where it is available). Areas subject to 1% annual chance flooding are termed Special Flood Hazard Areas (SFHAs). Structures located in SFHAs have a mandatory requirement to have flood insurance if the community participates in the NFIP, and if the owner of the structure has a federally backed mortgage. The boundaries and lateral extent of the SFHAs and other flood zones are established when the BFEs are overlain on topographic data. This information is then used to produce FIRMs, which depict the areal extent of SFHAs (and other flood hazard boundaries) and associated BFEs. Over the past several years, as part of a map modernization effort, FEMA has been producing updated FIRMs using digital methods. These geo-referenced, modernized, and generally more accurate FIRMs are published as cartographic map products and as digital geospatial data in the National Flood Hazard Layer (NFHL).

Most riverine SFHAs (meaning the 1% annual chance risk of flooding is from rivers) are categorized as "A Zones" or "AE Zones" and are determined using numerical models designed for riverine flood analyses. These include hydrologic models to estimate flood flows, such as the Hydrologic Engineering Center-Hydrologic Modeling System (HEC-HMS) and the United States Geological Survey (USGS) National Flood Frequency (NFF) program, and hydraulic models to estimate flood areas, such as the Hydrologic Engineering Center-River Analysis System (HEC-RAS) and the Federal Highway Administration (FHWA) Water Surface PROfile (WSPRO). In coastal areas, A or AE Zones are determined using coastal storm surge analyses. These analyses may use tsunami, hurricane, or coastal storm surge models such as the FEMA Standard Storm Surge Model (Surge), the Advanced Circulation (ADCIRC) Model, or the Danish Hydraulic Institute (DHI) Mike 21

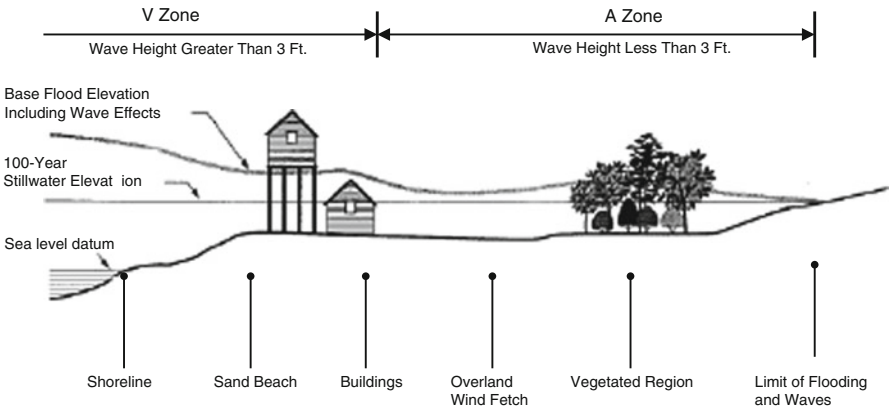

Fig. 6.1 Schematic showing relationship between wave effects, and flood zone delineations and base flood elevations (Modified from FEMA 2003)

hydrodynamic models; or tide gage analyses from long-term NOAA or United States Army Corps of Engineers (USACE) tide gage records. Coastal A Zone BFEs may include additive wave heights less than 3 ft. Current NFIP regulations do not distinguish between coastal and riverine A Zones.

Another type of SFHA, found exclusively in coastal areas, is called the "V Zone" or "VE Zone."[3] V Zones, also termed "coastal high hazard areas," are coastal flood hazard areas that are subject to damaging high velocity wave action. V Zones are determined concurrently with coastal A Zones (using the same coastal storm surge analyses). V Zones may include wave heights equal to or greater than 3 ft, a characteristic that often differentiates V Zones from coastal A Zones. Current practice for mapping the landward extent of the V Zones is to locate and map the most landward of the following (Bellomo et al. 1999; FEMA 2007a):

1. the point where a 3-ft wave height could occur during base flood conditions
2. the location where the eroded ground profile (or non-eroded ground profile, if applicable) is 3 ft below the computed wave runup elevation during base flood conditions
3. the inland limit of the primary frontal dune as defined in NFIP regulations
4. the wave overtopping splash zone (the area landward of the crest of an overtopped barrier where the wave runup elevation exceeds the barrier elevation by at least 3 ft).

V Zones are typically more hazardous than A Zones. Consequently NFIP floodplain management and construction requirements are more stringent, and flood insurance rates are usually much higher in V Zones. Figure 6.1 is a schematic that

[3] AE and VE Zones refer to flood zones in which base flood elevations have been computed (as opposed to A or V Zones in which base flood elevations have not been computed). Hereinafter, for the sake of simplicity, these zones will be referred to as "A" and "V."

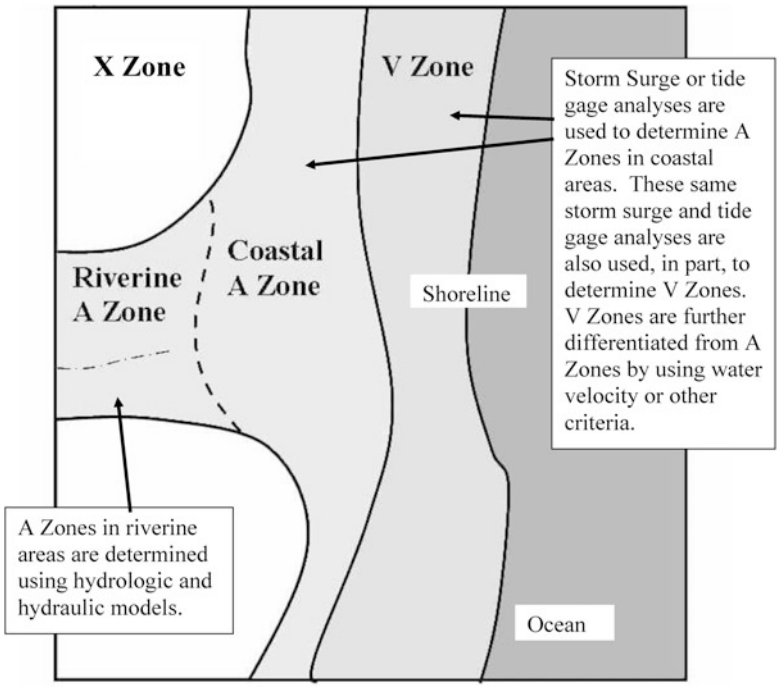

Fig. 6.2 Cartoon showing relationship between A Zones in riverine areas, A Zones in coastal areas, V Zones, and X Zones. A Zones and V Zones are based on the 1% annual chance flood and are known as Special Flood Hazard Areas (SFHAs). A Zones in riverine areas are determined using hydrologic models such as HEC-1 and SWMM; and hydraulic models such as HEC-RAS and WSPRO. A Zones in coastal areas are determined using storm surge analyses. This includes hydrodynamic models such as FEMA Surge, ADCIRC, and Mike 21; or tide gage analyses. V Zones are determined using the same models/analyses as used to determine A Zones in coastal areas, although V Zones are further differentiated from coastal A Zones based on wave, velocity, or primary frontal dune criteria. Shaded X Zones generally represent areas of 500-y floods, whereas unshaded X Zones are areas determined to be outside the 500-y floodplain. X Zones are not considered SFHAs. The *dashed line* separating the coastal A Zone from the riverine A Zone was specifically created for this analysis of coastal population and is not delineated on FIRMS

shows the general relationship between the 3-ft wave, V Zone delineations, and base flood elevations.

Another type of riverine or coastal flood zone, termed "X Zone," is not considered to be an SFHA because it does not represent a 1% annual chance flood hazard area (and therefore mandatory purchase of flood insurance is not required in this zone). There are two types of X Zones: shaded X Zones, which generally represent areas having a 0.2% annual chance flood (sometimes referred to as a 500-y flood); and unshaded X Zones, which are areas generally located outside the 0.2% annual chance floodplain. Figure 6.2 is a cartoon showing the relationship between riverine A Zones, Coastal A Zones, V Zones, and X Zones.

6.1.3.2 Digital Flood Hazard Datasets

The following digital map sources have been used by FEMA to develop estimates of coastal population exposed to flood-related hazards:

- **Q3 Flood Data**: In the 1990s, FEMA developed a digital flood hazard database called Q3 Flood Data (or Q3 for short). This database was compiled by digitally scanning and vectorizing certain features from existing hardcopy FIRMs, such as flood zones and political boundaries. Given that the Q3 database was developed by digitizing existing hard-copy FIRMs of 1970s-1990s vintage that were prepared using older, manual techniques, the Q3 database is considered the least accurate digital representation of flood hazard areas.
- **National Flood Hazard Layer**: The NFHL is a national database currently being compiled by FEMA that comprises all new FIRMs published since 2001.[4] NFHL data are the official definition of the SFHA and represent the best digital spatial data set showing the location and extent of SFHAs and associated floodwater surface elevations. The NFHL incorporates the most recent flood studies, but does not include images or data files scanned from older paper FIRMs. As of 2010, approximately 57% of the 395 coastal counties in the United States (see "Results," below) are represented in the NFHL, either partially or completely, depending on data availability.
- **CoreLogic Dataset**: CoreLogic, a business that provides data and analytic services, has assembled a national flood layer derived from FEMA FIRMs. Prior to 2008, CoreLogic digitized or scanned paper copies of FIRMs to supplement or replace older and less accurate Q3 data. Beginning in 2008, CoreLogic began direct incorporation of FEMA's digital FIRM data into their flood layer.

6.1.3.3 Chronology of FEMA Coastal Population Estimates

Following is a chronological summary of studies in which FEMA developed estimates of coastal population based on proximity to flood-related hazards. Note that the definition of "coastal" varied depending on the specific coastal hazard.

- In 1989, FEMA conducted a study to estimate the cost of mapping long-term erosion hazard areas through the NFIP (FEMA 1989). Because the study

[4] FIRMs may be republished for a variety of reasons, including updated flood hazard analysis, updated topography, changes to vertical datum, or paper to digital map transition. It is important to note that a newly published FIRM does not necessarily indicate that an updated storm surge analysis was performed. Most effective coastal FIRMs are based on storm surge analyses performed in the 1980s, although these FIRMs almost always incorporate revisions that reflect more current wave height analyses and topography. Recently, FEMA committed to updating coastal flood hazard (including storm surge) analysis for most of the nation's populated shoreline. As of the date of publication, these studies are underway.

addressed coastal erosion, it was decided that an area would be determined to be "coastal" if it was located directly on the open ocean or Great Lakes coast (excluded were bays, inlets, deltas, mangrove islands, and the back sides of barrier islands), or if it contained V Zones. Given that FIRMs were generally mapped at a county-wide level, coastal areas were described at the county geographic unit. Thus, any county that bordered the open ocean coast, or that contained V Zones, would be identified as a "coastal county." Since the objective of the study was to determine costs of mapping coastal erosion hazard areas, population data were not compiled. The study, completed in 1989, determined that there were 258 coastal counties, although this tally did not include several boroughs (counties) in Alaska which did not have any FIRMs (FEMA 1989).

- In late 1989, FEMA, in response to a Congressional mandate, initiated a study on the impact of sea level rise on the NFIP. The study was completed and a report was released in 1991 (FEMA 1991). Given that sea level rise was the geophysical process being studied, and FIRMs are generally mapped at a county-wide level, the study identified selected counties that had within their boundaries "nearshore areas inundated by short-term rising water levels associated with oceanic phenomena (hurricane surge, extratropical 'northeaster' storm surge, tsunamis)." Accordingly, Great Lakes counties were not considered in this analysis. It is not known if all of the Alaskan boroughs (counties) were considered. The report tallied 283 coastal counties.
- In 2000 the Heinz Center released a report (Heinz Center 2000) for FEMA titled "Evaluation of Erosion Hazards." The report, conducted in response to a 1994 Congressional mandate, estimated that about 555,000 people lived within 500 ft. of the ocean and Great Lakes shoreline (excluding Alaska). The estimate was based on analysis of 1990 census block group data.[5] The Heinz Center, however, did not include population living in the densest parts of urban areas, such as Miami, New York, Los Angeles, and Chicago, whose shores are heavily protected from erosion.
- Crowell et al. (2007) presented a method to identify coastal counties (and associated population) based on whether a county bordered the open ocean coast (or associated sheltered water bodies) or contained V Zones. This was similar to the method used in the 1989 coastal erosion study; however the boundaries of "the open ocean coast" were more inclusive this time and included bays, inlets, deltas, mangrove islands, and the back sides of barrier islands. Inland limits were truncated where census block groups joined together across open-water areas. Importantly, if a county did not border the open ocean coast, but contained a V Zone, no matter how small, that county was also classified as coastal. The digital boundaries of the coastal counties defined using these criteria were combined with 2000 census data to obtain tallies of coastal counties and estimates of population living therein. The results, as presented in Crowell et al. (2007), show that there are 364 coastal counties containing 37% of the US

[5] Census block groups generally contain 600–3,000 people (U.S. Census, March 8, 2012)

Fig. 6.3 Map showing coastal counties as defined by Culliton (1998) using watershed-based criteria (*light* and *dark gray*); and Crowell et al. (2007) using coastal contiguity or V Zone criteria (*dark gray*)

population (including Great Lakes), or 281 coastal counties containing 30% of the US population when the Great Lakes are excluded. These figures were based on permanent residents and included all of Alaska and Hawaii, but excluded U.S. territories. Crowell et al. (2007) also applied this methodology to smaller census block groups in order to get a more-refined estimate using the "bordering the coast/V Zone criteria." The results indicated that about 3% of the U.S. population lives in coastal census block groups (including the Great Lakes) defined using these criteria. Figure 6.3 displays a map of the United States showing "coastal counties" reflecting the Crowell et al. (2007) criteria (dark gray counties), as well as "coastal counties" based on the Culliton (1998) criteria (light and dark gray counties). This study did not consider coastal A Zones.

- Crowell et al. (2010) followed up on Crowell et al. (2007) and refined their analyses to more directly estimate the U.S. population at risk from the 1% annual chance coastal flood with respect to both V Zones and coastal A Zones. This required developing methods to estimate the boundary line separating coastal A Zones from riverine A Zones at coastal/riverine confluences. As noted earlier, coastal A Zones are areas subject to coastal flooding, but not affected by the significant wave action and high velocity waters associated with V Zones. A challenge to identifying this boundary line is that current NFIP regulations do not distinguish between coastal and riverine A Zones. In order to estimate and

delineate these boundaries, Crowell et al. (2010) relied on a digital coastal flood hazard database predominately comprised of NFHL (2008 or earlier) and Q3 data. Where NFHL and Q3 data were not available, United States Geological Survey (USGS) Digital Elevation Models (DEMs) were combined with estimates of 1% annual chance still-water elevations (SWELs) to complete the database (this procedure is explained in more detail, below). Combining the digital coastal flood hazard database with 2000 census block group data (assuming uniform population distribution), Crowell et al. (2010) concluded that slightly more than 3% of the total U.S. population live in the 1% annual chance coastal flood hazard areas as defined by FEMA when the Great Lakes are included, and slightly less than 3% of the U.S. population when the Great Lakes are not included in the estimate. Inclusion of population from the Atlantic and Pacific territories does not significantly change the percentages. Crowell et al. (2010) also estimated that about 9% of the U.S. population lives in census block groups that border the ocean and Great Lakes coasts or that contain 1% annual chance coastal flood hazard areas as defined by FEMA.

Newly available data and information have allowed an updated estimate of population living in coastal flood zones since the work performed by Crowell et al. (2010). These new data and information include: 2010 census data (rather than 2000 census data), effective and soon-to-be effective FIRMs prepared since 2008 (2008 was the cutoff date for the NFHL data used in Crowell et al. (2010)), and the use of the proprietary CoreLogic dataset (rather than Q3 data) where NFHL data were unavailable.[6] Hereafter, we shall refer to this updated analysis as the "current study." The methods used in the current study (which are almost identical to those used in Crowell et al. (2010)) and the associated results are described below.

6.2 Methods

The first step in estimating population living in coastal flood hazard areas was to create a national coastal map database by compiling the best available coastal-proximate, digital flood hazard data showing the location and extent of coastal and riverine SFHAs. The second step required determination of the landward extent of the V Zone or coastal A Zone. Coastal A Zones at riverine confluences necessitated the development of a systematic method to estimate the boundary separating coastal and riverine A Zones. The third step was to estimate coastal population subject to the 1% annual chance coastal flood. This was done by using a geographic information system (GIS) to combine 2010 census data (for permanent residents) with the national coastal map database created in the first step, and the boundaries for the V Zone and coastal A Zones created in the second step. These steps, discussed below, enabled estimates of the U.S. population subject to the 1% annual chance coastal flood.

[6] The CoreLogic dataset also includes the latest effective digital FIRM datasets.

6.2.1 Step 1: Digital Base Data Compilation

The NFHL and CoreLogic datasets were the primary sources used to compile most of the base coastal data set used for this analysis. Some coastal counties, however, did not have complete representation by NFHL or CoreLogic datasets. These included several sparsely populated coastal counties located in northern Minnesota, Wisconsin, and Michigan, and most Alaskan coastal boroughs. In these areas (as explained below), coastal A Zone boundaries were approximated by associating a 1% annual chance SWEL to a DEM. The best available USGS national terrain datasets were used, which included 1/3 Arc Second (roughly equivalent to 10 m resolution) DEMs for the mainland U.S., and 1–2 Arc Second data (30–60 m resolution) for Alaska and U.S Territories. SWEL is defined as the surface of the water resulting from astronomical tides, storm surge, and freshwater inputs, but excluding wave setup contributions (FEMA 2007a). Figure 6.4 shows NFHL, Core Logic, and SWEL/DEM coverages for the 395 coastal and Great Lakes counties that were identified and used in the current study.

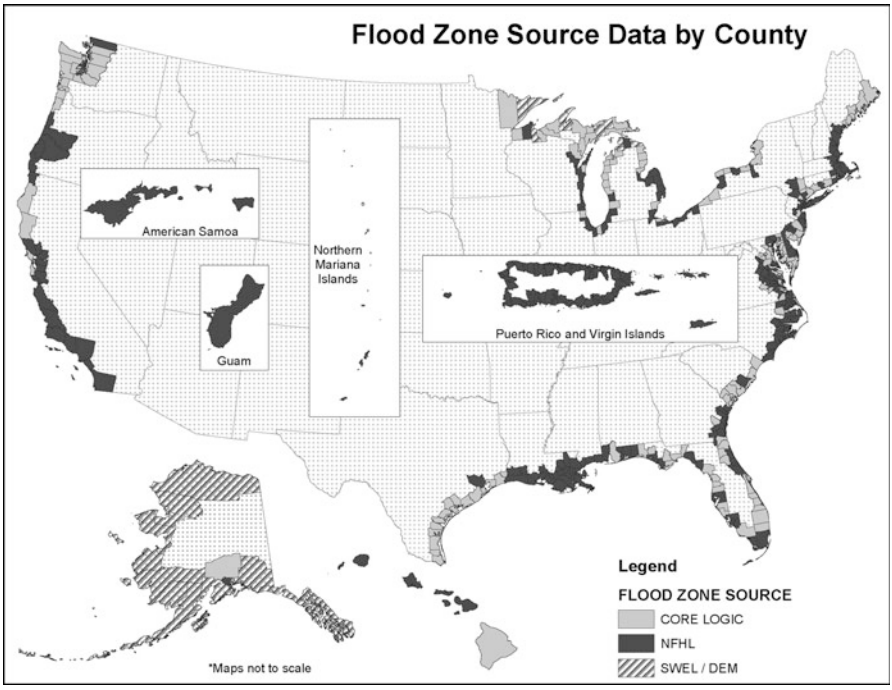

Fig. 6.4 Map of the U.S. showing coastal counties identified, and distribution of digital datasets used, in the current coastal population analysis. In summary, about 57% of the counties had the majority of their A and V zones originating from NFHL datasets; 35% of counties had the majority of their coastal A and V Zones originating from non-NFHL Core Logic datasets; 7% of counties had the majority of their coastal A and V zones originating from SWEL/DEM analyses; and 1% of counties had the majority of their coastal A and V zone datasets originating from a mix of Core Logic and SWEL/DEM datasets

6.2.2 Step 2: Riverine and Coastal A Zone Separation

As shown in Fig. 6.2, the landward extent of a Coastal A Zone may be bounded by (1) X Zones, (2) no flood zones (i.e., areas where there are no other bounding SFHAs or other flood zones present), or (3) riverine A Zones. In the first two cases, determining the landward extent of coastal A Zones (and thus coastal SFHAs) is generally an easy task, as it simply ends at the A Zone-X Zone boundary (or the landward edge of the A Zone if there is no X Zone). However, the third case (at the coastal-riverine confluence) represents a situation where determining the landward extent of coastal A Zone flooding may be more difficult because, as noted earlier, FEMA regulations do not distinguish between coastal and riverine A Zones, and consequently the coastal A/riverine A Zone boundary was not differentiated and delineated on FIRMs.[7] Because of this, methods had to be developed to estimate and delineate the separation line between coastal A and riverine A Zones. This coastal A Zone demarcation line generally represents the landward extent of the one-percent annual chance coastal flood as defined by storm surge.

Two cartographic features common in riverine A Zone mapping that are not present in coastal A Zones proved useful in differentiating between the two zones at their confluence. The first is that riverine BFEs are generally depicted on FIRMs as wavy lines plotted perpendicular to the course of the riverine flooding, with BFEs increasing in an upstream direction. Coastal BFEs, on the other hand, are typically mapped as whole-foot elevations, usually run roughly parallel to the shoreline and coastal terrain features, and are separated by smooth lines (called gutters), with BFEs generally decreasing in an inland direction. As such, from a cartographic perspective for any given A Zone, if the BFEs are depicted as wavy lines, that indicates the riverine flood levels dominate coastal flood levels during a 1% annual chance flood event. If the BFEs are separated by smooth lines, that means coastal flood levels dominate riverine flood levels during a 1% annual chance flood event. In short, where NFHL data and associated BFE locations were available, riverine and coastal A Zones were separated by means of a simple visual inspection of the FIRM panel.

The second cartographic feature used to differentiate riverine A Zones from coastal A Zones at their confluence is the floodway. The floodway is a portion of a river channel and adjacent floodplain that must be reserved in order to discharge the riverine base flood without cumulatively increasing the water surface elevation more than a designated height. Floodways are depicted on FIRMs as crosshatched areas. Floodways are not determined or delineated in coastal flood hazard areas. Less accurate data sources, such as Q3 and the scanned portion of the CoreLogic dataset (i.e., exclusive of their digital FIRM data), do not include BFEs, but usually do include the floodway. For these data sources the riverine and coastal A Zone boundaries were estimated at the downstream limit of floodways. Crowell et al.

[7] New Flood Insurance Studies now include the statistical delineation between riverine and coastal flooding sources.

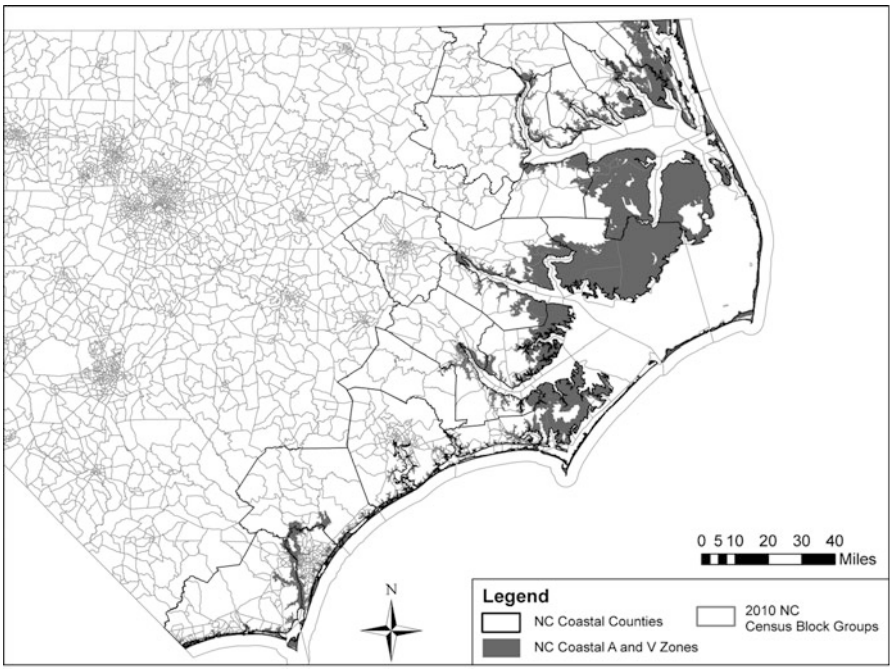

Fig. 6.5 Map of North Carolina showing coastal flood hazard areas (i.e., coastal A Zones and V Zones)

(2010) used FEMA Q3 data for this purpose, whereas the current study substitutes the more recent and more complete CoreLogic data, for Q3 data.

In areas where neither NFHL nor CoreLogic data were available, such as along portions of the Great Lakes and Alaskan coastlines, coastal A Zone boundaries were approximated at confluence and non-confluence areas by associating a 1% annual chance SWEL to a DEM. SWELs were obtained by referencing published FEMA flood insurance study reports and selecting a representative 1% annual chance SWEL for each coastal county without NFHL or CoreLogic data. A polygon coastal A Zone area was then approximated by identifying grid cells from the DEM below the representative SWEL. This process was used for approximately 7% of the total counties analyzed, however, most of these counties are located in sparsely populated areas in Alaska and the northern Great Lakes areas.

6.2.3 Step 3: Estimating Coastal Population

After coastal A Zones were separated from riverine A Zones, the SFHAs seaward of this separation line were classified as coastal flood hazard areas, consisting of coastal A Zones and V Zones (Fig. 6.5 shows coastal flood hazard areas delineated

for North Carolina). Next, GIS unions were performed to spatially combine the coastal flood hazard areas with census block groups. Census block groups that lie partially or entirely within coastal flood hazard areas were identified as "coastal flood hazard census block groups." (Note that census block groups bordering the coast typically extend a significant distance over open sea water, thereby requiring the clipping and removal of "ocean-only" portions of the block groups prior to analysis of the GIS unions.) Tabular data from the GIS unions provided estimates of the portion of each coastal flood hazard census block group located within the coastal flood hazard areas. Importantly, populations were assumed to be uniformly distributed across each block group, and the population within a coastal flood zone was estimated by multiplying the block-group population density (population per square mile) by coastal flood zone area (in square miles).

6.3 Results

Table 6.1 shows a summary of the U.S. population, by state, that lives in areas subject to coastal flooding as defined by the 1% annual chance coastal flood hazard and as mapped by FEMA. As such, the results are strictly associated with FEMA flood hazard zones, and do not rely on geopolitical units, such as counties, to serve as a buffer (see below). Again, the results assume uniform population distribution within census block groups. The data show that for the 50 United States (excluding territories), with a total permanent resident population of 308,745,538 (according to the 2010 U.S. census), approximately 8,622,000 people (2.8% of the total U.S. population) live in areas subject to the 1% annual chance coastal flood hazard. When the Great Lakes coastal flood hazard areas are excluded from the data set, then about 8,484,000 people (2.7% of the total U.S. population) live in coastal flood hazard areas. Importantly, these population estimates are associated with coastal flood hazard areas based predominantly on coastal storm surge and wave action. However, the estimates also include population living in V Zone areas that are not subject to the 1% annual chance coastal flood but are nonetheless mapped as V Zones because of the primary frontal dune. These primary frontal-dune areas, while situated above the 1% annual chance flood elevation, are shore-parallel, narrow reaches and are included in the population estimates because of their coastal-proximate location. According to FEMA estimates, fewer than 70,000 people reside in primary frontal-dune areas (FEMA 2008). Note that these estimates do not include other areas such as bluffs or cliffs that border the ocean or Great Lakes coast, but are not subject to the 1% annual chance coastal flood. Also, these estimates are based on permanent, rather than seasonal (vacation) populations.

A total of 395 counties were found to either be contiguous with the ocean or Great Lakes coast, and/or have at least some coastal flood hazard areas (as based on the 1% annual chance coastal flood) located within their boundaries. About

Table 6.1 Population tallies and area in square miles for locations subject to 1% annual chance coastal flooding

Coast	State	Population	Area (in sq. miles)
Atlantic	Connecticut	112,000	78
	Delaware	49,000	267
	District of Columbia	4,000	5
	Florida	2,969,000	2,317
	Georgia	161,000	1,369
	Maine	28,000	182
	Maryland	149,000	867
	Massachusetts	170,000	221
	New Hampshire	12,000	17
	New Jersey	508,000	664
	New York	584,000	220
	North Carolina	176,000	2,384
	Pennsylvania	16,000	20
	Rhode Island	47,000	51
	South Carolina	311,000	1,589
	Virginia	312,000	853
	Atl. coast total	**5,608,000**	**11,104**
Gulf	Alabama	48,000	296
	Florida	1,100,000	3,887
	Louisiana	1,030,000	10,216
	Mississippi	105,000	338
	Texas	196,000	2,493
	Gulf coast total	**2,479,000**	**17,230**
Pacific	Alaska	27,000	17,595
	California	226,000	454
	Hawaii	70,000	41
	Oregon	16,000	83
	Washington	58,000	211
	Pacific coast total	**397,000**	**18,384**
Great Lakes	Illinois	9,000	5
	Indiana	1,000	1
	Michigan	75,000	281
	Minnesota	3,000	6
	New York	9,000	37
	Ohio	21,000	100
	Pennsylvania	2,000	1
	Wisconsin	18,000	81
	Great Lakes coast total	**138,000**	**512**
United States	**US Coast total**	**8,622,000**	**47,230**

Population tallies are rounded to the nearest thousand

120,475,000 people live in these counties (about 39% of the U.S. population). If the Great Lakes are excluded, then there are 313 coastal counties, containing 101,574,000 people, or 33% of the U.S. population (Fig. 6.4).

6.4 Discussion

6.4.1 Data Accuracy and Uncertainty

When estimating the population at risk from coastal flooding, one needs to consider the uncertainty in the input parameters in order to understand the uncertainty in the final estimates. This includes the uncertainty in estimates of population demographics, and the uncertainty in the calculation and depiction of coastal flood hazards. The discussion below addresses some of these uncertainties.

6.4.1.1 Uncertainty in Population Demographics

A primary source of demographic uncertainty relates to distribution of population. In this and other recent studies conducted by FEMA (see above), population was assumed to be uniformly distributed across each census block group to facilitate GIS analyses with the spatial flood data. However, there is great uncertainty regarding spatial distribution of population living in census block groups (and other census accounting units), especially in suburban and rural areas (Bhaduri et al. 2007). As noted by Small and Nicholls (2003) in their world-wide analysis of human settlements in coastal zones, average population density is lowest directly adjacent to the coast, then increases rapidly to about a 10-km distance from the shoreline, and then gradually decreases inland. Importantly, no attempt was made in the current study to take into account non-uniform population distribution within census block groups. Future enhancements of this study could incorporate finer resolution census block (rather than census block group) datasets; or better still, non-uniform population distribution datasets such as LandScan USA, which contains population data at a sub-census block resolution (Bhaduri et al. 2007).

Another source of demographic uncertainty is that there is not a one-to-one correlation between the shape and number of census block groups between the 2000 and 2010 census datasets. Accordingly, and as discussed in more detail below, this presents potential limitations with respect to temporal trend analyses between Crowell et al. (2010), and the results from the current study.

Finally, only permanent residents were considered in this study. As coastal areas are a very popular vacation destination, had this study considered seasonal residents, then the coastal population estimates would have been greater.

6.4.1.2 Uncertainty in Calculation and Depiction of Coastal Flood Hazards

When attempting to model a complex physical process such as flooding there are many potential sources for introducing uncertainty. Moreover, coastal flood hazard mapping is considerably more complex and uncertain than riverine flood hazard mapping (NRC 2009). It is for this reason that FEMA depicts the results of its

coastal flood hazard analyses to the nearest whole-foot elevation on FIRMs as opposed to developing profiles depicting more precise elevations as is common in riverine areas. Bellomo and Crowell (2010) highlight three analytical components of flood hazard computations that may introduce varying amounts of uncertainty in determining coastal flood boundaries. These include: (1) measurement of the physical environment (i.e., precision and accuracy of the input data); (2) statistical variability in climate and anthropomorphic adaptation (i.e., the variability in the physical process being simulated); and, (3) methods used to make computations (i.e., the skill of models used in computation of the physical parameters). A fourth source of uncertainty, development of derived mapping products (i.e., uncertainty in the methods used to depict results) can be added to this list. Following is a discussion of the analytical and graphical uncertainties.

Uncertainty in Measurements of the Physical Environment

An accurate representation of the physical environment is a key starting point in coastal flood hazard analyses. The physical environment is characterized primarily by the topographic and bathymetric representation of the actual ground surface and seabed, and it is recognized that topographic data are the most important factor in the accuracy of FEMA's flood maps (NRC 2009). Also important, however, is the representation of the climatology (primarily wind and pressure fields) for the physical process being simulated, as well as the data which will be used to validate the results (measured wave and water level data, wave information studies, surveyed high water marks, etc.).

In many areas, FEMA employs large-scale storm surge analyses to determine SWELs, including the contributions of wave setup, for use as starting conditions for the subsequent site-specific wave height analyses. The scale of the storm surge analyses is typically State or FEMA Region-wide (FEMA divides the U.S. into ten regions) in order to capture the scale of the storm surge process itself. It is important to represent the chosen domain using the best available topographic and bathymetric data (for example, Light Detection and Ranging (LiDAR) topography and National Elevation Data on land, and lead-line soundings and dredge reports in waterways), all having widely varying levels of accuracy and precision. These data sets must be carefully compiled and merged into a seamless surface with a consistent datum and resolution in order for the model to be run (USACE-ERDC/CHL TR-11-1, March 2011). In contrast to the large-scale storm surge analyses, the wave height analyses are performed along transects taking into account site-specific topographic and land-use aspects of the flooded terrain. Since these analyses are performed primarily overland and on a communitywide or countywide basis, the data available for these analyses are typically derived from highly accurate LiDAR technologies and do not involve the stitching together of many disparate datasets.

Uncertainty Related to the Variability in Climate and Anthropomorphic Adaptation

Another source of uncertainty relates to the inherent variability in the physical process being evaluated, how mankind will react, and the limited historical data available for making future predictions (Bellomo and Crowell 2010). The statistical components of flood hazard calculations are based largely on observations of historical flood records at tide and river gauges. All statistical computations contain uncertainty, and in the case of estimating flood hazards, no matter the resources or time available, uncertainties are largely bound by the amount of historical data available. While they can be minimized, they will never be eliminated. At its core, the basic premise of flood frequency analyses for the NFIP is to use the past to predict what is possible in the future. This premise is a standard, widely-accepted approach to these analyses but it is not without uncertainty. For example, a long period of record may provide an account of what has happened in the past, but it does not necessarily represent what *could* happen in the future. A structure that has not flooded during the period of record is not necessarily a structure that is safe from flooding in the future.

Past conditions may not be representative of future conditions for a number of reasons. Anthropomorphic factors, such as development and/or construction of flood conveyance, retention, or protection structures will alter flood conditions at a site in response to flooding or over time. Similarly, climatic factors, such as increases in the frequency and severity of coastal storms and sea level rise, will also cause future conditions to be different than past conditions. It is important to note that for statutory and regulatory reasons FEMA does not consider future conditions in flood hazard modeling and mapping. FEMA does, however, regularly reassess the flood maps and updates them to account for changes, both anthropogenic and climatic, that have occurred since the last mapping effort.

While changes in anthropomorphic and climatic factors can cause temporal nonstationarity, thereby limiting predictive power as based on past history, there is another consideration that warrants discussion; that is "luck." Just because an area has not flooded over the past several decades does not mean that it could not flood in the near future. In order to illustrate this concept, consider the hurricane-prone regions of the United States—specifically the mid-Atlantic coast south to Florida and the entire Gulf of Mexico coast. To the casual observer watching the news, hurricanes may seem like large flood events that occur frequently. In reality, most hurricanes are relatively small flood forcing events. The most severe events, which are important for the determination of BFEs, occur infrequently and may only severely impact a small swath of shoreline. The impact of a hurricane is dependent on the physical parameters of the storm, in addition to other factors, which typically have a wide range of variability. For example, consider the variability inherent in the storm track; slight changes in storm track can result in very different flooding locations and impacts. FEMA accounts for the uncertainty in the historical record and for hurricanes by using complex hydrodynamic modeling to simulate not only what has happened in the past, but also what *could* have happened in the past by realistically varying the parameters of the storms being

simulated. In this way, FEMA is able to account for some of the uncertainty in hurricane parameters and develop probabilistic flood elevations that are relatively consistent and not dominated by the historical record alone.

Uncertainty in the Methods Used to Make Computations

FEMA utilizes many models, both physical and empirical, to mimic the complex coastal processes that result in coastal flooding. Each of these models, however, introduces varying amounts of uncertainty into the final result. In the offshore, models are used to generate detailed wind and pressure fields for historic storms, to simulate the effects of these storms on wave and water levels, and to transform waves from deep water. In the nearshore and overland areas, models are used to estimate dune erosion, wave runup, and overtopping, and to estimate the effects of obstructions, such as houses and vegetation, on wave heights as they propagate overland. All models include some level of uncertainty, and care is exercised to minimize that uncertainty.

Model results are validated using the best available data, but in some instances the data available to validate certain portions of the analyses, for example, surveyed high water marks for a given storm, are sparse. All potential validation data are carefully reviewed, and only data with a high level of confidence are used in the validation process. When the model results are not corroborated by the validation data, the model input and models themselves are reviewed and improved until reasonable results are produced. Care is exercised to identify and eliminate any bias in the results. No strict standards exist with respect to the acceptable amounts of uncertainty. Thus, FEMA relies on model validation, engineering judgment, and rigorous review to ensure the results are high-quality and reasonable representations of historical flood conditions.

Uncertainty in the Methods Used to Depict Results

The final step in FEMA's process of identifying coastal flood hazards is to take the results of the flood hazard analyses and depict them on a map. Uncertainty in this step mainly relates to the quality of the topographic data and the methods used to transcribe the modeled flood elevations into a planimetric floodplain product. FEMA flood mapping standards generally require that remotely collected topographic data must be equivalent to or greater than a 2-ft equivalent contour interval for flat terrain, or a 4-ft equivalent contour interval for rolling to hilly terrain, both determined at the 95% confidence interval (FEMA 2003). Fortunately, advances in remote topographic data collection have resulted in topographic data that frequently exceed FEMA standards. Note that these standards only apply to terrestrial data. FEMA has not set standards related to bathymetric data since flood hazard mapping for the NFIP is only performed for on-land areas.

Floodplain boundaries are typically delineated using automated processes, and FEMA has developed the Floodplain Boundary Standard (FEMA 2007b) to ensure that methods used to map the floodplain boundary produce an accurate map product. The standard is a check to verify that the limit of the floodplain is mapped along a topographic contour that is equal to the flood elevation. This standard is applied to all FIRMs produced for the NFIP. The tolerance for how precisely the flood elevation and the ground elevation must match varies based on the type of flood study being performed, the population demographics, and the expected development within the flood hazard area.

One important source of uncertainty that falls under this category and requires further explanation relates to the error in estimating the coastal A Zone/riverine A Zone boundary. Determining the landward extent of coastal A Zones was often straightforward in areas without riverine/coastal confluences and covered by NFHL or CoreLogic data. In these situations, the coastal A Zone ends at the A Zone/X Zone boundary line, or the landward extent of the coastal A Zone where there are no adjoining flood zones. However, as noted in the Methods section, at riverine-coastal confluences, the riverine-coastal boundary had to be estimated using various cartographic techniques; for example, identifying where the BFEs changed from coastal to riverine representations, or identifying the seaward extent of floodways. Areas with neither NFHL nor CoreLogic coverage required associating a county-wide representative SWEL to a correlating DEM in order to determine the landward extent of coastal flood hazard areas for both confluence and non-confluence areas. None of these estimation methods were tested for accuracy, although the SWEL/DEM method is undoubtedly the least accurate given the simplifying assumptions used in estimating the boundary line.

6.4.2 *Comparison of Current Results with Crowell et al. 2010*

Crowell et al. (2010), using 2000 Census Bureau data for the 50 United States, estimated that about 8,508,000[8] people (3.0% of the total U.S. population) live within 1% annual chance coastal flood hazard areas (including the Great Lakes) as defined by FEMA. This compares to the current study, which uses 2010 Census Bureau data for the 50 United States, where we estimate that approximately 8,623,000 people (2.8% of the total U.S. population) live in areas subject to the 1% annual chance coastal flood hazard (including the Great Lakes). As such, the data show an increase in coastal population of 115,000 over the past decade; albeit with a 0.2% decrease in the total U.S. population living in coastal flood hazard areas. Importantly, the changes in population estimates reflect not just demographic shifts that have occurred over the past decade, but changes in the data used in the two analyses. For example:

[8] 8,651,000 people when including territories.

- In the current study about 57% of the coastal counties had the majority of their flood sources based on NFHL data. In Crowell et al. (2010) 35% of the U.S. coastal counties were similarly represented by NFHL data. As noted earlier, the NFHL data are considered to be the most detailed, up to date, and accurate data showing the location and extent of SFHAs.
- In the current study, newer CoreLogic data replaces the older Q3 data used in Crowell et al. (2010).
- In the current study, 7% of counties had the majority of their A and V Zones based on the SWEL/DEM methods (however, as noted earlier, most of these SWEL/DEM counties are located in sparsely populated areas in Alaska and the northern Great Lakes areas). In Crowell et al. (2010) about 9% of the Counties relied on SWEL/DEM methods.
- The current study, and Crowell et al. (2010), both assume uniform population distribution within census block groups, with estimates of coastal population based on the percentage of the coastal area within the given census block groups. In both studies, most census block groups were only partially comprised of coastal flood hazard areas, thereby necessitating proportional estimates of coastal population within these census block groups. However, the census block group boundaries changed between the 2000 and 2010 Census Bureau data, thereby introducing boundary inconsistencies that could affect proportional estimates of coastal population.

In summary, we believe that the decrease in the percent population living in coastal flood hazard areas from Crowell et al. (2010) (using 2000 census data) compared to the current study (using 2010 census data) is most likely the result of an increase in data quality used in the analysis, rather than reflective of a general demographic trend towards a reduction in percentage of the U.S. population living in coastal flood hazard areas.

6.4.3 Definition of "Coastal"

There is no universally recognized definition of "coastal," "coastal zone," "coastal area," "coastal county," etc., thereby creating a great deal of ambiguity in the meaning of these terms (Cohen et al. 1997; Small et al. 2000; Small and Nicholls 2003; Crowell et al. 2007). Crowell et al. (2007, 2010) observe that various combinations of geophysical, geographical, and geopolitical criteria can be used to determine a "coastal area" (and from which to estimate associated "coastal population"), and recommend that the criteria used to determine coastal areas need to be applicable to the specific risk, hazard, or demographic being investigated. Further, Crowell et al. (2007) recommend that papers and reports that reference coastal population statistics need to clearly state how the "coast" is defined. Crowell et al. (2010) recognized four general categories of defining criteria

that can be combined to determine coastal areas. We have refined these categories and they are as follows:

- **Geophysical indicators**: This refers to the geophysical indicator that is of concern to the study. Examples may include: sea level elevations (used to determine inundation areas), coastal watersheds, flood zones such as V Zones, the coastal shoreline,[9] etc. If the geophysical indicator is an area-based indicator, such as the coastal watershed, then anyone living in the coastal watershed would be considered as living in a coastal area. If the geophysical indicator is a "line," such as the shoreline, then a spatial buffer (see below) must be selected in order to establish a defined coastal area and associated population.
- **Inland boundaries or limits**: An inland boundary determines how far inland into bays, inlets, deltas, etc. one can go before an area or shoreline is no longer considered "coastal." Inland boundary limits can be set by area-based geophysical indicators, geopolitical boundaries, or other criteria. The selection or identification of the inland boundary/limit can sometimes be a judgment call where there is ambiguity in the definition and the resulting spatial extent of the geophysical indicator. For example, if an "area-based" geophysical indicator is selected, such as the V zone, then inland boundaries are already set, as V Zones already have mapped spatial boundaries. However, if the geophysical indicator is defined as a line, such as the "coastal shoreline," then one must decide how far inland to go before the shoreline is no longer deemed "coastal."
- **Spatial buffers**: Spatial buffers must be used in conjunction with line-based geophysical indicators, such as the shoreline, in order to establish a coastal area. They may also be useful to provide a measure of uncertainty, or to account for situations where the influence of a hazard associated with a geophysical indicator, such as the V Zone, may extend landward beyond the actual area of inundation. Such hazards may potentially result in job loss, disruption of services, or other disturbances that may affect the tax base of a county, or other administrative unit. Spatial buffers may include geopolitical units such as census block groups, counties, etc., or distance buffers such as 50- or 100-mile buffers. As an example, if a county buffer is used, and the geophysical indicator is the V Zone, then any county that contains V Zone areas, no matter how small, would be considered a coastal county.
- **Geographic regions**: This criterion determines whether or not specific geographic regions are of interest to the study. For example, the Great Lakes coastal areas would not be a geographic region of interest if the study focused on the effects of sea level rise on coastal population.

[9] There is also no universally accepted definition of "shoreline." The spatial and temporal variability of the boundary and its dynamic nature result in a variety of features or "indicators" that are used to represent shoreline location. See Boak and Turner (2005) for a comprehensive discussion.

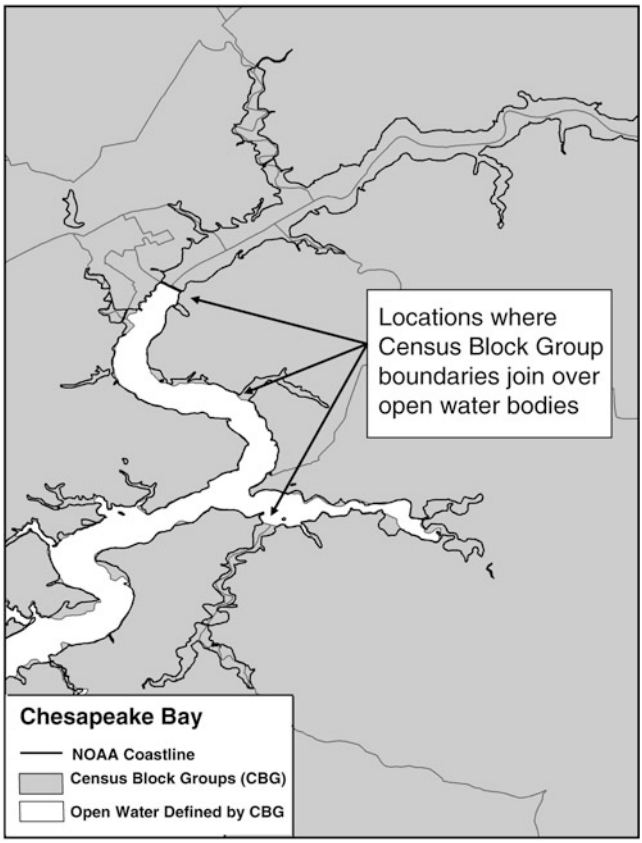

Fig. 6.6 Example showing the selection of the inland limit of the coastal shoreline as used in Crowell et al. (2007 and 2010). At this location (a tributary to the Chesapeake Bay) the inland limits of the coastal shoreline terminates at a point where the block group boundaries join together across water bodies

To illustrate the four criteria using Crowell et al. (2007) as an example, coastal population was estimated based on the following: (1) *Geophysical indicators* were defined by the presence of either the coastal shoreline, or V Zones (which are in turn defined by coastal flooding). (2) *Inland boundaries/limits* were established in two ways. For V Zones, the boundaries were already mapped on FIRMs. For the coastal shoreline, it was decided that the inland limit of the shoreline would terminate at a point where census block group boundaries stop following the physical coastline and join together across open water areas (Fig. 6.6). (3) *Geopolitical buffers* included census block groups in one estimate, and counties in the second estimate. Thus, if any part of the county or census block group, no matter how small, contained either the shoreline or V Zone (or both), then the population in the entire county or census block group was considered to be coastal. (4) Two sets of

Geographic regions were considered in the population estimates, the first included all four major coastal regions (i.e., Atlantic, Pacific, Gulf, and Great Lakes); the second only considered the ocean coasts (i.e., Atlantic, Pacific, and Gulf) and excluded the Great Lakes.

Table 6.2 summarizes and compares the results of the current coastal population study, based on the one-percent annual chance coastal flood hazard areas as defined by FEMA, with results from other studies dating back to 1989 in which estimates of U.S. coastal population or coastal areas have been made. Note how the selection of defining criteria can have a substantial impact on population estimates.

Although flood-related hazards are the focus of this chapter, other non-flood-related geophysical indicators could also be considered in determining coastal areas; hurricane force winds are an example. For comparison, Crowell et al. (2010) used the geographic boundaries of "hurricane prone regions" as defined by the American Society of Civil Engineers (ASCE 2006) and combined these spatial datasets with 2000 census data. The results indicated that 28% of the U.S. population lives in a county in which any part of that county lies within the 90 miles/h wind contour. If the statistics are recalculated using a finer resolution census block group geospatial unit, the results show that about 26% of the population lives in a coastal census block group as defined using the ASCE criteria.

6.4.4 Misuse of Coastal Population Data

Mixing and matching the defining criteria discussed above can result in a wide variety of coastal population estimates that range from less than 5% to greater than 50% of the total U.S. population. This wide disparity in estimates does not necessarily mean that some estimates are correct and others incorrect, rather some methods for determining coastal population may be more applicable to certain coastal processes, hazards, or situations than others. For example, the coastal watershed-based Culliton population statistics are derived from a very inclusive definition of coastal county. The commonly cited (Culliton 1998) statistics "673 coastal counties" and "53 percent of the U.S. population lives in coastal counties" include many counties that might not normally be thought of as coastal. This includes numerous landlocked counties, such as Sussex County, New Jersey, a county located entirely in the highlands and piedmont of New Jersey. In fact, 20 of New Jersey's 21 counties are considered coastal in this definition. Another notable county included in the Culliton definition is San Bernardino County, California, a county of more than 2.0 million people (based on the 2010 census), with a population center located 50 miles from the ocean, and which includes portions of the San Bernardino Mountains and large expanses of the Mojave Desert.

The coastal watershed-based defining criteria and overall inclusiveness of the Culliton definition may make the dataset appropriate to use in certain situations; for example in areas where coastal ecosystems or water quality are a major concern. Problems arise, however, when researchers or authors indiscriminately use coastal

Table 6.2 Selected summary of studies in which estimates of US population have been made

	Geophysical indicator	Inland boundaries	Spatial buffer	Number of coastal counties	Percent of total US population living in defined coastal area, includes Great Lakes
FEMA (1989)	Areas that (1) are adjacent to ocean or Great Lakes coastline, and/or (2) contain V Zones	(1) Inland boundaries terminated at bays, inlet openings, backsides of barrier islands, and other coastal areas where long-term erosion was expected to be minimal; (2) defined by V Zone	Any county that abuts the open ocean or Great Lakes coastline, and/or contains V Zones	Ocean: 177 Great Lakes: 81 Total: 258 (does not include all coastal counties in Alaska)	Not determined
Culliton et al. (1990)	May be partially based on areas containing tidal waters	Unknown, but may be set by inland limits of tidal water boundaries	Any county that contains areas affected by tidal waters?	Ocean: 366 Great Lakes: 85 Total: 451	45% (1990 census projection)
FEMA (1991)	Nearshore areas inundated by short-term rising water levels associated with coastal storm surge and tsunamis (similar to V Zones)	Inland limits of the Geophysical Indicators	Any county that contains areas defined by the geophysical indicators	Ocean: 283 Great Lakes: 0 (may not include all coastal counties in Alaska)	Not determined
Culliton (1998)	Generally, coastal watersheds as defined by NOAA	Inland limits of the Geophysical Indicator (in this case, the coastal watershed)	Any county with at least 15% of its total land area located within the nation's coastal watershed, or coastal cataloging unit	Ocean: 515 Great Lakes: 158 Total: 673	53% (1994 census projection)
Hinrichsen (1998)	Unknown	Unknown	Counties	Ocean: ? Great Lakes: ? Total: 772	55–60% (1990 census)
Crowell et al. (2007)	Areas that (1) are adjacent to ocean or Great Lakes	(1) Inland location where census block-group boundaries stop following	Any county that abuts the open ocean or Great Lakes	Ocean:281 Great Lakes: 83 Total: 364	37% (2000 census)

(continued)

Table 6.2 (continued)

	Geophysical indicator	Inland boundaries	Spatial buffer	Number of coastal counties	Percent of total US population living in defined coastal area, includes Great Lakes
	coastline, and/or (2) contain V Zones	the physical coastline and join together across an open-water area; or (2) defined by V Zones	coastline, and/or contains V Zones		
Crowell et al. (2007)	Areas that (1) are adjacent to ocean or Great Lakes coastline, and/or (2) contain V Zones	(1) Inland location where census block-group boundaries stop following the physical coastline and join together across an open-water area, or (2) defined by V Zones	Any census block group that abuts the open ocean or Great Lakes coastline, and/or contains V Zones	n/applicable	3% (2000 census)
Census Bureau (summarized in Crowell, et al. 2010)	Areas adjacent to ocean or Great Lakes coastline	Ocean and Great Lakes coast including saltwater tributaries, bays, and tidal rivers	50-mile horizontal buffer	n/applicable	49% (2000 census)
Lam et al. (2009)	Areas adjacent to ocean coastline	Unknown	1-km horizontal buffer	n/applicable	6% (2006 LandScan)
Lam, et al. (2009)	Sea level (NAVD88)	Defined by vertical buffer (3-m) projected landward horizontally	3-m vertical buffer	n/applicable	4% (2006 LandScan)
Crowell et al. (2010)	Areas that (1) are adjacent to ocean or Great Lakes coastline, or (2) contain V Zones or coastal A Zones	(1) Inland location where census block-group boundaries stop following the physical coastline and join together across an open-water area, or (2) defined by coastal A or V Zones	None. The Geophysical Indicator served as the boundary line	n/applicable	3% (2000 census)

Crowell et al. (2010)	Areas that (1) are adjacent to ocean or Great Lakes coastline, or (2) contain V Zones or coastal A Zones	(1) Inland location where census block-group boundaries stop following the physical coastline and join together across an open-water area, or (2) defined by coastal A or V Zones	Any census block group that abuts the open ocean or Great Lakes coastline, and/or contains V Zones or coastal A Zones	n/applicable	9% (2000 census)
Wilson and Fischetti (2010)	Areas adjacent to the ocean coast (water classified as "coastal water or territorial sea")	Coastal waters and territorial seas as defined by the U. S. Census Bureau's Topologically Integrated Geocoding and Referencing (Tiger®) system. This includes ocean or sea coasts, including bays, estuaries, gulfs, and sounds. Excludes the Great Lakes	Any county that abuts the ocean coast	254 (excludes the Great Lakes)	29% (2008 census projection)
Zhang and Leatherman (2011)	Barrier islands	Defined by the borders of the barrier islands	None	Not determined	0.5% (2000 census)
Current study	V Zone and coastal A Zone areas	Defined by coastal A or V Zones	None. The Geophysical Indicator served as the boundary line	n/applicable	3% (2010 census)
Current study	V Zone and coastal A Zone areas, or QRRHS that are adjacent to ocean or Great Lakes coastline	Inland location where census-block group boundaries stop following the physical coastline and join tosether across an open-water area, or defined by coastal A or V Zones	Any county that abuts the ocean or Great Lakes coastline, and/or contains V zones or coastal A zones	Ocean: 313 Great Lakes: 82 Total: 395	39% (2010 census)

population data to buttress arguments, exaggerate significance, or otherwise use the data for purposes contrary to sensible use. As an example, Culliton (1998) generally describes the coastal population statistics within the framework of coastal environmental and economic concerns; accordingly, the statistical datasets are introduced within the context of appropriate use. Other researchers or science writers, however, seem to miss this distinction and arbitrarily use the Culliton coastal population datasets without a clear understanding of the statistics' origins and implications. Crowell et al. (2007 and 2010) provide several examples where scientific papers casually and improperly cite the Culliton (1998) and Hinrichsen (1998) data in reference to population impacted by various coastal hazards such as sea level rise, hurricanes, tsunamis, and long-term coastal erosion. The worst offenders cite the Culliton (1998) or Hinrichsen (1998) coastal population estimates in papers within which the societal threats from ocean-related processes, such as sea level rise or extra-tropical storms, are discussed. This is done even though the Culliton (1998) and Hinrichsen (1998) estimates include population counts from areas that would not directly experience the effects of these hazards. Such areas include Great Lakes counties,[10] areas located several kilometers from the coast, and areas located tens or even hundreds of meters above sea level. Other authors have commented on the misuse of *global* coastal population estimates. For example, Small and Nicholls (2003) note that "Unsubstantiated and widely repeated statements such as '50% of the world's population presently live within 60 km of a shoreline' are widely treated as 'facts' without citation to original sources."

6.5 Summary and Conclusions

Estimations of coastal population can vary widely, and are dependent on the various defining criteria used to identify "coastal area." These defining criteria must be selected within the context of the issue being investigated or discussed. A "one-size-fits-all" approach will not work when considering, for example, the effects of sea level rise, as opposed to hurricane flooding, on our Nation's coastal population. Unfortunately, there are numerous examples of scientific papers published in peer reviewed journals over the past decade in which the authors failed to associate the appropriate coastal population statistics with the coastal matter under investigation.

Our analyses of U.S. population distribution yields the following results: a total of 395 counties (including the Great Lakes) were found to either be contiguous with the ocean or Great Lakes coast, and/or have at least some coastal food hazard areas located within their boundaries, as defined by FEMA's 1% annual chance coastal flood. This number reduces to 313 counties if the Great Lakes are excluded. In addition, about 8.6 million permanent residents, or about 2.8% of the U.S.

[10] Culliton (1998) incorporates population counts from 83 Great Lakes counties. In fact, 89% of Michigan's counties and associated population statistics are included in the Culliton dataset.

population, live in areas subject to the 1% annual chance coastal flood. These areas include the Atlantic, Gulf, Pacific, and Great Lakes coasts, but exclude U.S. territories. When the Great Lakes coasts are excluded from the estimates, the population decreases to about 8.5 million, or 2.7% of the U.S. population. These estimates are based on analyses at the census block group level and assume uniform population distribution in each block group.

Importantly, the above figures should not be interpreted as upper bounds on population directly or indirectly exposed to coastal flood hazards. There are numerous examples where the 1% annual chance flood has been exceeded, resulting in damaged homes, businesses, and other infrastructure. This is not unexpected given the size of the U.S. coastal areas, and the wide variety of independent coastal flood hazard drivers (e.g., hurricanes, nor'easters, tsunamis, and others). Moreover, this study only takes into account permanent residents. Consideration of vacationing residents and people working in these areas would certainly increase the number of people whose property and jobs would be impacted by the 1% annual chance flood. Also significant is that the results do not take into account economic exposure. Coastal flood hazards have a direct impact on tourism, shipping, energy, and fishing industries. Further, intra-state commerce are at risk, as much of the U.S. food, energy, and other goods travel along or across our Nation's coastal boundaries. As evidenced by Hurricane Katrina, a major coastal flood event could disrupt people and businesses miles from the shore. Ecosystems could also be disrupted by large coastal storms, particularly when the events result in the release of hazardous materials whose impacts may ripple through the environment and populace, beyond the event footprint. Finally, the results presented here represent a snapshot in time. The population data sets are derived from 2010 census data, and the dates associated with the acquisition of flood hazard information vary considerably. Different results should be expected in the future as populations shift, flood hazards change, and flood hazard studies and maps are updated.

Studies like this and others are valuable but they have limitations and must be used in proper context. They help us better understand our vulnerability. They inform our decisions. They shape the ongoing debate, and move us toward becoming better stewards of the coast.

Acknowledgements The authors would like to thank the following people for their review and comment on this chapter: Darryl Hatheway, Paul Rooney, Erin Walsh, and Theresa Goedeke.

References

American Society of Civil Engineers (2006) Minimum design loads for buildings and other structures, ASCE/SEI 7–05. American Society of Civil Engineers, Reston, VA

Bellomo D, Crowell M (2010) FEMA's coastal population study: comments on data accuracy, current initiatives, and future risk. J Coast Res 26:199–200

Bellomo D, Pajak MJ, Sparks J (1999) Coastal flood hazards and the National Flood Insurance Program. In: Crowell M, Leatherman SP (eds) Coastal erosion mapping and management. Coastal Education and Research Foundation, Royal Palm Beach

Bender MA, Knutson TR, Tuleya RE, Sirutis JJ, Vecchi GA, Barner ST, Held IM (2010) Modeled impact of anthropogenic warning on the frequency of intense Atlantic hurricanes. Science 327:454–458

Bhaduri B, Bright E, Coleman P (2007) LandScan USA: a high-resolution geospatial and temporal modeling approach for population distribution and dynamics. GeoJournal 69:103–117

Boak EH, Turner IL (2005) Shoreline definition and detection: a review. J Coast Res 21:688–703

Church JA, White NJ (2006) A 20th century acceleration in global sea level rise. Geophys Res Lett 33:1–4

Cohen JE, Small C (1998) Hypsographic demography: the global distribution of population with altitude. Proc Natl Acad Sci USA 95:14009–14014

Cohen JE, Small C, Mellinger A, Gallup J, Sachs J (1997) Estimates of coastal populations. Lett Sci 278:1211

Crossett K, Culliton T, Wiley P, Goodspeed T (2004) Population trends along the coastal United States, 1980–2008. NOAA, Silver Spring

Crowell M, Leatherman SP (eds) (1999) Coastal erosion mapping and management. J Coast Res Spec Issue 28:196

Crowell M, Edelman S, Coulton K, McAfee S (2007) How many people live in coastal areas? (editorial). J Coast Res 23:iii–vi

Crowell M, Coulton K, Johnson C, Westcott J, Bellomo D, Edelman S, Hirsch E (2010) An estimate of the U. S. population living in 100-year coastal flood hazard areas. J Coast Res 26:201–211

Culliton T (1998) Population: distribution, density, and growth. NOAA's State of the coast report. NOAA

Culliton TJ, Warren MA, Goodspeed TR, Remer TG, Blackwell CM, McDonough JJ (1990) 50 years of population change along the nation's coast, 1960–2010. National Ocean Service, National Oceanic and Atmospheric Administration, U.S. Department of Commerce, Rockville, Maryland

Federal Emergency Management Agency (1989) Erosion rate data study plan. Unpublished document

Federal Emergency Management Agency (1991) Projected impact of relative sea level rise on the National Flood Insurance Program. http://www.epa.gov/climatechange/effects/downloads/flood_insurance.pdf

Federal Emergency Management Agency (2003) Guidelines and specifications for flood hazard mapping partners. Appendix A: Guidance for aerial mapping and surveying

Federal Emergency Management Agency (2007a) Atlantic ocean and Gulf of Mexico coastal guidelines update. Available at: http://www.fema.gov/library/viewRecord.do?id=2458

Federal Emergency Management Agency (2007b) Revised procedure memorandum No. 38 – implementation of floodplain boundary standards (Section 7 of MHIP v1.0). 9 p, 17 Oct 2007. Available at: http://www.fema.gov/library/viewRecord.do?id=2369

Federal Emergency Management Agency (2008) Coastal AE Zone and VE Zone demographics study and primary Frontal Dune study to support the NFIP, Technical Report. Unpublished, 98 p

Heinz Center (2000) Evaluation of erosion hazard. Report prepared for Federal Emergency Management Agency (FEMA). Heinz Center, Washington, DC. http://www.fema.gov/pdf/library/erosion.pdf

Hinrichsen D (1990) Our common seas: coasts in crisis. Earthscan, London/Nairobi

Hinrichsen D (1998) Coastal waters of the world: trends threats, and strategies. Island Press, Washington, DC

Hinrichsen D (1999) The coastal population explosion. In: Cicin-Sain B, Knecht RW, Foster N (eds) Trends and future challenges for U.S. National Ocean and coastal policy: proceedings of a workshop. NOAA, Washington, DC

IPCC (2007) Climate change: the physical science basis. Contribution of working group I to the fourth assessment report of the intergovernmental panel on climate change. Cambridge University Press, Cambridge, Reston, VA

Knutson TR, McBride JL, Chan J, Emanuel K, Holland G, Landsea C, Held I, Kossin JP, Srivastava AK, Sugi M (2010) Tropical cyclones and climate change. Nat Geosci 3:157–163

Lam NSN, Arenas H, Li Z, Liu KB (2009) An estimate of population impacted by climate change along the U.S. coast. J Coast Res 2(Spec Issue 56):1522–1526

Lichter M, Vafeidis AT, Nicholls RJ, Kaiser G (2011) Exploring data-related uncertainties in analyses of land area and population in the "Low-Elevation Coastal Zone" (LECZ). J Coast Res 27:757–768

Miller L, Douglas BC (2004) Mass and volume contributions to 20th century global sea level rise. Nature 428:406–409

National Research Council of the National Academies (2009) Mapping the zone, improving flood map accuracy. National Academies Press, Washington, DC

Nicholls RJ, Marinova N, Lowe JA, Brown S, Vellinga P, de Gusmão D, Hinkel J, Tol RSJ (2011) Sea-level rise and its possible impacts given a 'beyond 4 °C world' in the twenty-first century. Philos Trans R Soc A 369:161–181

NOAA Webpage (2012a) http://coastalsocioeconomics.noaa.gov/download/metadata/coastal_counties_explanation.pdf. Accessed 25 Mar 2012

NOAA Webpage (2012b) http://coastalsocioeconomics.noaa.gov/about.html. Retrieved 28 Feb 2012

NOEP Webpage (2012) http://www.oceaneconomics.org/. Accessed 28 Feb 2012

Small C, Nicholls RJ (2003) A global analysis of human settlement in coastal zones. J Coast Res 19:584–599

Small C, Gornitz V, Cohen JE (2000) Coastal hazards and the global distribution of human population. Environ Geosci 7:3–12

U.S. Army Corps of Engineers, Engineer Research and Development Center, Coastal Hydraulics Lab (2011) ERDC/CHL TR-11-1. FEMA Region III storm surge study, coastal storm surge analysis system digital elevation model, Report 1: intermediate submission No. 1.1, Vicksburg, MS

U.S. Census Bureau (2012) Cartographic boundary files. http://www.census.gov/geo/www/cob/bg_metadata.html. Accessed 8 Mar 2012

Vermeer M, Rahmstoef S (2009) Global sea level linked to global temperature. Proc Natl Acad Sci USA 106(21):527–532. doi:10.1073/pnas.0907765106

Wilson SG, Fischetti TR (2010) Coastline population trends in the United States: 1960 to 2008. US Dept Commerce, US Census Bureau, Washington. Available at: http://www.census.gov/prod/2010pubs/p25-1139.pdf

Zhang KQ, Douglas BC, Leatherman SP (2004) Global warming and coastal erosion. Clim Chang 64:41–58

Zhang K, Leatherman S (2011) Barrier island population along the U.S. Atlantic and Gulf Coasts. J Coast Res 27(2):356–363

Chapter 7
Public Perception of Hurricane-Related Hazards

Bernhard Lee Lindner and Charles Cockcroft

Abstract A survey was conducted in the South Carolina coastal counties of Berkeley, Charleston and Dorchester with the purpose of assessing current NWS hurricane warning packages and recommending alternatives. Most of the 200 residents that were surveyed stated that they had personal experience with hurricanes. Surprisingly, over half of these residents did not know the definition of a hurricane warning, over half did not realize that the main threat from hurricanes in low-lying coastal areas was from storm surge, half did not realize that more rain was the most significant consequence of a slower moving storm, and the majority were not able to translate a standard National Hurricane Center projection of storm surge depth into a realistic appreciation of the risk posed to their lives, despite their prior experience with hurricanes. These misunderstandings were most prevalent among the poor, among minority groups and among those with no college education. When asked to interpret both a graphic-filled hurricane advisory and the standard NWS text-based advisory, the understanding of the risk from hurricanes was far higher when the graphic-filled advisory was used.

7.1 Introduction

"Just tell me: Am I going to have water in my living room? Quit talking like a bunch of geeky guides" (former National Weather Service (NWS) director David Johnson was quoted by the Charleston Post and Courier newspaper in a speech before the 58th annual Interdepartmental Hurricane Conference, March 2004). On a practical matter, it is actually very difficult to convey the complex science of hurricanes on a simple level while not introducing error or misconceptions. Yet, the effectiveness

B.L. Lindner (✉) • C. Cockcroft
Physics and Astronomy Department, College of Charleston, 66 George St.,
Charleston, SC 29424, USA
e-mail: lindnerb@cofc.edu

C.W. Finkl (ed.), *Coastal Hazards*, Coastal Research Library 6,
DOI 10.1007/978-94-007-5234-4_7,

of NWS hurricane warnings (hereafter simply abbreviated as 'warnings') can have important implications for both the physical and the psychological health of individuals in the path of a hurricane. Thus, warnings must be prepared in a manner in which the general public receives the greatest understanding of the risks, which will allow them to make informed evacuation decisions.

A hurricane is a low probability but high consequence event, and this affects the way hurricane warnings are interpreted (Mileti and Fitzpatrick 1991). The low probability of a hurricane striking any location (Keim et al. 2007) is one reason some people do not respond to the warnings even though the consequences can be high. The low probability of a strike equates with low perceived risk, and low perceived risk leads to non-response to weather service advisories (Mileti and O'Brien 1992). In a study using data from four previous studies, Earl J. Baker (1979) concluded that it was encouraging that those people in most need of evacuation were the most likely to evacuate. This conclusion by Baker speaks to the idea that evacuation is not always the proper response for people in less danger from a hurricane strike, and it also supports the idea that current NWS advisories are in most instances communicating the appropriate information to the public. For example, those who are in a well-constructed house, well inland, isolated from dangerous trees and above any projected storm tide impacts, may perhaps better be served by sheltering in place than by evacuating.

Evacuation decisions should go beyond the immediate threat to health and property. Disaster psychologists have shown that victims of natural disasters can experience a plethora of negative outcomes in response to the event. Individuals often report heightened anxiety, problems with concentration, sleep disturbances as well as other symptoms associated with the experience of trauma (Canino et al. 1990; Freedy et al. 1992; 1994). A portion of the traumatized population may go on to experience posttraumatic stress disorder or other psychiatric illnesses that require professional attention (WHO 2000). It is therefore important to try to minimize as much as possible individuals' exposure to natural disasters such as hurricanes. By educating the public about the risks associated with hurricanes, we can influence greater levels of commitment to evacuate when the population is in danger. Research has shown that how the public reacts to disaster warnings is contingent upon three general characteristics (Mayhorn et al. 2006). These characteristics include the attributes of the hazard, the components of the warning message, and individual differences associated with the receiver of the message. All three of these factors work together to influence whether an individual chooses to take necessary precautions or not. The attributes of the hazard in respect to hurricanes would include features such as the velocity of the wind, the speed of the storm, or the projected path of the storm. Obviously, we would have no control over these factors in real time, but how these factors are communicated to the public through warning messages is an issue that can clearly be addressed. Regarding the last factor, various sociodemographic and personality-related factors might influence how individuals respond. For instance, both socio-economic status and age has been shown to influence storm preparations and the personality trait of locus of control has proven to be predictive as well (Sattler et al. 2000). Evacuation decisions have also

been modeled based on ethnographics (Gladwell et al. 2001). As such, a variety of psychological factors were measured to determine whether they influence warning receptivity.

Warning messages are needed that provide information concerning not only the threat, but also the mitigation measures that are recommended. Warnings written in this manner should enable reasonably vigilant people to decide on an appropriate course of action. This idea, that most people "seek their own counsel," is in accord with previous research that has identified what is now called the warning confirmation process (Drabek 1969; Leik et al. 1981; Riad and Norris 1998; Sorensen 1991; Mileti and Fitzpatrick 1991; Sanders and Westergard 1996). The normal course of the process proceeds as follows: (1) the public receives a hurricane warning, (2) the public attempts to gather more information concerning the threat and recommended mitigation options, and (3) the public evacuates if they confirm the threat is sufficiently grave. The warning confirmation process assumes that everyone responds in a rational manner. They collect information on the possible costs if the hurricane strikes as predicted and the costs and benefits associated with any mitigation measures. Everyone then weighs the costs vs. the potential benefits of any adopted mitigation measures (Clark and Carter 1979; Riad and Norris 1998; Baker 1979; Janis and Mann 1977). Clark and Carter referred to this rational approach as the Maximum Utility Model, but they suggest a less expansive model called the Bounded Rationality Model. The Bounded-Rationality Model differs in that it assumes the subject has complete information concerning the threat upon which to base a decision (Clark and Carter 1979). Complete information must also include discussion of the uncertainty in the forecast position and strength of the tropical system, as this is key to getting the proper response from the public. This assumption of complete information illustrates how important the warning message is in any decision-making process.

Janis and Mann (1977) approach the problem slightly differently. They also consider the decision-making process as a maximization of benefits in a Cost-Benefit sense, but they also consider the psychological stress encountered in emergency decisions. They suggest public response to hurricane warnings differ from everyday decisions that maximize utility because: (1) there is much more at stake, and (2) the amount of time available for decision-making is limited before crucial options are lost. These differences can lead to irrational actions by the public. Furthermore, even if a subject acts rationally, incomplete information may lead him or her to the wrong conclusion.

By combining the concepts of Clark and Carter, and Janis and Mann concerning public response to hurricane warnings we can conceptualize the public undergoing a warning confirmation process. This process is rational in nature but it may produce a maladaptive response by segments of the public due to accompanying psychological stress.

The above considerations lead us to suggestions on how to maximize appropriate self-protective actions. Firstly, the author of the warning must provide complete information, and secondly, the author can minimize psychological stress by increasing time for decision-making (i.e. by providing complete information as early as

possible). The only way the time for decision-making can be increased is by the development of new warning technology and hurricane predictive models that can increase lead times. The prediction of hurricane properties can be based on both active numerical weather prediction models and climatology (e.g., Jelesnianski et al. 1992; Houston et al. 1999; Alsheimer and Lindner 2011). These methods are increasing the accuracy of forecasts and thus increasing lead times. However, it is also critical to clearly convey the degree to which increased lead time yields increased uncertainty in the forecast. Further discussion of means to increase lead times is beyond the scope of this paper, but it is an important factor for improving the response of the public to warning messages. The second suggestion for maximizing self-protective behavior is to provide complete information. The NWS can accomplish this goal by providing credible, consistent, and clear information in local WFO (weather forecast office) warnings such as the Hurricane Local Statement.

Although B.F. McLuckie wrote "Warning—A Call to Action" in 1974, the report is still quite authoritative in its conclusions concerning severe weather warnings. His definition of warning is two-part: (1) It is an alert to danger, and (2) It is a call to action. Other researchers have similar definitions for warnings. The warning should: (1) inform the public of the danger and, (2) provide appropriate mitigation measures (Leik et al. 1981; Mileti and O'Brien 1992; Perry and Nigg 1985). Complete information for both part 1 and part 2 of these definitions is important so each person can make the appropriate decisions. The public needs full information (including uncertainties) on the extent, location and time of expected arrival of the hurricane. It also needs full information on the appropriate mitigation measures and when these measures should be undertaken. By full or complete information, we mean the NWS should communicate up to date forecasts and the reasons behind the forecasts. If the public is completely informed in a timely manner then it will confirm the danger, that is, perceive the risk (Mileti and O'Brien 1992; Riad and Norris 1998). It then will use the information on appropriate mitigation measures to plan their best response to the approaching threat. Communication of a comprehensive and clear warning is the real mission of the NWS, not enforcement of its advisories.

McLuckie (1974) recommended the writers of warning messages should limit the use of terms such as "warning"; that is, they should not assume too much knowledge on the part of the warning recipients, and they should reference the warning to a known landmark. We have investigated these points in the current research. Also, according to McLuckie, the warning message writer should be concerned with the completeness, clarity, consistency, and the balance of the warning. The credibility of the sources for this information is paramount. McLuckie's recommendations reflect his understanding of the interaction between the message senders and the recipients of the messages. He postulated a Stimulus-Actor-Response (S-A-R) model of this interaction, not the simple Stimulus–-response (S–R) model that had been used by many previously. McLuckie's use of the S-A-R model acknowledges the importance of the recipient of the information and is just another expression for the warning confirmation process.

The role of the recipient in the S-A-R model is to confirm the warning, and once this confirmation is completed, the recipient responds accordingly (McLuckie 1974). This model emphasizes that the role of the NWS is the supplier of information. Our suggestions for improvements in WFO hurricane warning messages incorporate many of McLuckie's recommendations. In addition, we are investigating the use of graphics to enhance WFO warning messages.

The NWS has followed advances in the types of research mentioned above and has changed the way warnings are written and packaged as a result (Rappaport et al. 2009). New warning advisory text and graphics have been developed that are very effective and powerful. The NWS is very receptive to suggestions raised to improve the communication and explanation of risks associated with hurricanes, and benefits from lines of research that bridge the areas of research mentioned above with specific recommendations for changes to their warning packages. It is in that spirit that our research was undertaken.

7.2 Experimental Procedure

Using previous research on the effectiveness of warnings as well as consulting with NWS personnel and emergency planning officials, a set of 45 questions formed a basis for an anonymous survey administered to the public. The main ideas included in the survey can be divided into three areas. The first area posed standard socio-demographic questions that allowed the answers to be broken into socio-demographic groups. The second area determined prior experience with hurricanes as well as problems with public education about hurricanes. The third area concerns the use of graphical enhancements to WFO warnings to increase the communicability of these warnings. The entire survey was 31 pages long, was self-completed by the respondents individually, and took approximately an hour to administer.

The socio-demographic section provided multiple-choice answers to questions on gender, age, race, education, income, and marital status. All participants were 18 years and older, and participants were requested to select from six groupings of age. Similarly, income was divided into five brackets with a range of $25,000 each (the top bracket was simply 'over $100,000'). The educational problems category highlighted: (1) the subjects' knowledge of standard NWS terms, (2) the subjects' understanding of the science and probability concepts involved with hurricane forecasting, (3) the subjects' feeling that Internet-based information dissemination would be helpful, and (4) the subjects' feeling concerning the use of an inverted graphic probability map of the strike probability for a hurricane. Within the graphical enhancement category the focus centered on: (1) the efficacy of text-based warnings vs. that of warnings using more graphics, and (2) the use of references to local landmarks, both pictorial and textual, to help in warning communication.

This initial survey was pilot tested on a 30-student Atmospheric-Science class at the College of Charleston. This pilot study identified typographical errors and questions that did not seem to elicit the expected responses (i.e. the subjects may

have misunderstood the intent of the question). These questions were re-phrased to correct the problem.

With the assistance of several undergraduate meteorology majors, 202 subjects from the tri-county metropolitan Charleston, SC area were sampled with this revised survey. The three counties comprised an area of 2,592 miles^2 with a potential pool of 549,033 subjects. A purely random survey would have involved many teams of students covering great distances, including parts of the city that are not considered safe. Instead, convenience/snowball sampling was used. In other words, the students used opportunities as they arose, such as contacting neighbors, acquaintances and service groups such as the local Rotary club and churches. While not as good as a purely random survey in examining every subsection of society (some racial, age and educational subgroups were underrepresented), it nonetheless did provide data on participants from many locations throughout the tri-county area from many socio-demographic groups, as will be detailed in the discussion section.

The survey results were compiled in Microsoft Excel spreadsheets, and basic statistics were computed. The data filter feature of Excel was used to compile results of questions across the demographic factors of gender, age, race, education, and income. A Chi-squared analysis of this data was conducted to examine the statistical significance of the differences in answers observed between comparison groups. The level of significance was set at $p = 0.05$. The formula used to calculate Chi-squared was $\chi^2 = \sum[(O_{ij} - E_{ij})^2/E_{ij}]$, where "$O_{ij}$" is the number of observed events for the cell at row_i, $column_j$. In addition, "E_{ij}" is the expected number of events for the cell at row_i, $column_j$. The expected value, "E_{ij}", was calculated using the formula, $E_{ij} = [(\text{row total})_i(\text{column total})_j]/(\text{overall total})$. If the observed values differ enough from the expected values Chi-squared will be large and the p-value will be small and the differences will be statistically significant (Daniel 1995).

7.3 Data

7.3.1 Public Educational Issues

7.3.1.1 Definition of Hurricane Warning

Subjects were asked whether a hurricane warning means hurricane conditions are expected within 24 h, expected within 36 h, possible within 24 h, or possible within 36 h. Subjects were not reminded of the definitions of hurricane warning and hurricane watch, as the intent of the question is to see how many people are aware of the definition without being reminded. Only 43% of our sample correctly answered that hurricane conditions are expected within 24 h (Table 7.1). In a Chi-squared analysis comparing demographic factors: gender, age, race, education, and income, we did not find a statistically significant difference in the proportion of correct

Table 7.1 Subjects' definition of hurricane warning

	Count	Percent of total
Expected in 24 h	87	43
Expected in 36 h	37	18
Possible in 24 h	18	9
Possible in 36 h	35	17
Don't know	23	11
NA[a]	2	1
Total	202	99[b]

[a]NA is short for no answer
[b]Percent does not add to 100 because of rounding due to significant figures

Table 7.2 Subjects' answers to greatest hurricane danger

	Count	Percent of total
Wind	58	29
Storm surge	95	47
Rain related flooding	13	6
Tornadoes	24	12
NA	11	5
Total	201	99

answers for the definition of hurricane warning across the selected subsets in the sample.

7.3.1.2 Understanding of Scientific Concepts

Storm Surge

A large proportion of our sample exhibited deficiencies in their understanding of many of the basic scientific concepts involved in hurricane forecasts and warnings. When subjects were asked to identify generally the greatest danger from a hurricane from a list consisting of wind, storm surge, rain-related flooding and tornadoes, over 53% could not identify that it was from storm surge (Table 7.2). Note that the topography of this region is very flat and low-lying, and thus most residents will be impacted by a strong surge.

An analysis of demographic factors revealed a statistically significant difference in proportion of correct answers in our sample based on income levels ($\chi^2 = 4.89$, $p = 0.027$) (Table 7.3). Subjects with incomes over $50,000 had a 16% better appreciation of the danger due to storm surge. A similar difference was noted when educational levels were considered (the differences in proportion of correct answers from our sample were statistically significant with $\chi^2 = 4.52$, $p = 0.034$) (Table 7.4). Lastly, there was a statistically significant difference in the proportion of correct answers from our sample when they were compared across racial divisions ($\chi^2 = 5.28$, $p = 0.022$) (Table 7.5). Only Caucasian and African-American subjects

Table 7.3 Income of subject vs. answers to greatest hurricane danger

Income levels	Correct	Incorrect	Total	Percent correct
Low ($0–49,999)	44	66	110	40
High ($50,000 and above)	46	36	82	56
Total	90	102	192	

Table 7.4 Subjects' educational level vs. answers to greatest hurricane danger

Educational level	Correct	Incorrect	Total	Percent correct
Grade to high school	31	52	83	37
Undergraduate and graduate	62	56	118	53
Total	93	108	201	

Table 7.5 Race of the subject vs. answers to greatest hurricane danger

Race	Correct	Incorrect	Total	Percent correct
Caucasian	85	85	170	50
African-American	6	18	24	25
Total	91	103	194	

were considered because the number of people of other racial groups (Asian, Native American and Hispanic) was very small ($n = 6$). There was no statistical difference in the proportion of correct answers for the other demographic factors of gender and age.

To better understand the associations observed in Tables 7.3, 7.4 and 7.5, several analyses of the demographic traits race, income and educational factors were performed. There was a statistically significant difference in the proportion of correct answers when a comparison was made of Caucasians and African-Americans that had achieved either a grade and/or high school education ($\chi^2 = 6.14$, $p = 0.013$). Caucasians and African-Americans who had achieved undergraduate or graduate educations did not exhibit the same statistically significant difference in the proportion of correct answers. African-Americans at different educational levels had a statistically significant difference in the proportion of correct answers ($\chi^2 = 5.71$, $p = 0.017$). On the other hand, educational level was not significantly related to the proportion of correct answers for Caucasians.

NWS Forecast Accuracy at 72 Hours

Approximately 20% of the sample stated, incorrectly, that NWS hurricane forecast accuracy at 72 h before projected landfall was greater than forecast accuracy at 24 h before projected landfall, when given a simple choice between just those two options (Table 7.6). An analysis comparing demographic factors and NWS forecast accuracy found a statistically significant difference between Caucasian and

Table 7.6 NWS forecast accuracy is greater or less at 72 h than 24 h

	Count	Percent of total
Greater	40	20
Less	158	78
NA	4	2
Total	202	100

Table 7.7 Race of the subject vs. answers about NWS forecast accuracy at 72 h

Race	Correct	Incorrect	Total	Percent correct
Caucasian	141	27	168	84
African-American	14	9	23	61
Total	155	36	191	

Table 7.8 Subjects' race/education level vs. answers about NWS forecast accuracy

Demographic factors	Correct	Incorrect	Total	Percent correct
Grade + high school				
Caucasian	50	14	64	78
African-American	10	4	14	71
Total	60	18	78	
Undergraduate + graduate				
Caucasian	91	12	103	88
African-American	4	5	9	44
Total	95	17	112	

African-American subjects of the sample ($\chi^2 = 7.02$, $p = 0.008$) (Table 7.7). No statistically significant difference was found for the other demographic factors.

The differences in proportion of correct answers of Caucasians and African-Americans were compared at the two education levels. There was a statistically significant difference in proportion of correct answers between Caucasian and African-American subjects who had either undergraduate and/or graduate degrees ($\chi^2 = 12.34$, $p = 4.44*10^{-4}$). Grade and/or high school education was not related significantly to the proportion of correct answers (Table 7.8).

Effects of a Decrease in Forward Speed

Subjects were asked the significance of a decrease in the forward speed of an approaching hurricane. When given these four answers: (a) higher wind speeds and enhanced storm surge, (b) less rainfall from a weakening system, (c) more rain from a slower moving storm, or (d) shorter periods under high winds, 53% of our sample was unable to identify that more rain was the most significant consequence

Table 7.9 Most significant effect of a decrease in hurricane's speed

	Count	Percent
Increased wind and storm surge	73	36
Less rain from a weakened storm	16	8
More rain from slower storm	95	47
Less time under high winds	5	3
NA	13	6
Total	202	100

Table 7.10 Subjects' race vs. effects of a decrease in the forward speed of a hurricane

Race	Correct	Incorrect	Total	Percent correct
Caucasian	90	80	170	53
African-American	5	19	24	21
Total	95	99	194	

Table 7.11 Education/race vs. answers concerning the effects of a decrease in the forward speed of a hurricane

Demographic factors	Correct	Incorrect	Total	Percent correct
Grade + High school				
Caucasian	35	30	65	54
African-American	4	12	16	25
Total	39	42	81	
Undergraduate + Graduate				
Caucasian	55	49	104	53
African-American	1	9	10	10
Total	56	58	114	

of a slower moving hurricane (Table 7.9). Not only is an increase in the amount rainfall likely, but the composition of the rain changes as well. Slower moving systems are also likely to have a smaller signature of the ocean in the chemical composition of the rainfall as well (Lindner and Frysinger 2007). We found a statistically significant difference in the proportion of correct answers when comparing Caucasian and African-American subjects ($\chi^2 = 8.67$, $p = 0.003$) (Table 7.10). Other demographic factors had no statistically significant differences.

Examining further the proportion of correct answers by race and educational levels, a statistically significant difference was found in the proportion of correct answers between Caucasians and African-Americans at the grade and/or high school level ($\chi^2 = 4.27$, $p = 0.039$). Furthermore, at the undergraduate and/or graduate level there was also a statistically significant difference in proportion of correct answers for Caucasians and African-Americans ($\chi^2 = 6.71$, $p = 0.010$) (Table 7.11).

Table 7.12 Ranking of the importance of internet information availability

	Don't know	Unimportant	Moderately important	Very important	NA	Total
Raw count	11	21	51	108	12	202
Percent (%)	5	10	25	53	6	99

Table 7.13 Gender vs. ranking of internet information

Gender	Moderate/very important	Unimportant	Total	Percent important
Male	78	22	100	78
Female	77	10	87	89
Total	155	32	187	

7.3.1.3 Internet Information Dissemination

Ten different methods for disseminating information on hurricanes were presented, and participants were asked to rank the importance of each method on a Likert-type scale. When asked about the availability of Internet hurricane information, over 78% of the sample ranked it as either very important or moderately important (Table 7.12), which was the highest rating for any of the ten methods presented. An analysis of the answers revealed a marginally statistically significant difference in the preferences between genders ($\chi^2 = 3.62$, $p = 0.048$) with women more inclined to view Internet information as important (Table 7.13). Other demographic factors had no statistically significant differences.

When further analyzing the proportion of subjects ranking Internet information dissemination as important across gender at educational levels, there was no statistically significant difference in proportion of preferences between males and females at the grade and high school level or at the undergraduate and graduate level.

7.3.1.4 Probability Inversion Format

Whenever a hurricane landfall is potentially imminent, the NWS issues a map that shows the probability of a hurricane striking various coastal cities within a certain amount of time. The intent of this figure is to demonstrate not only the likelihood of a hit but also to show the uncertainty in the forecast as well as to show how broad of an area could potentially be impacted. The NWS has found the public has difficulty interpreting this figure. As an alternative, we inverted the probability so that the map showed the probability of the hurricane missing various cities within a certain amount of time. Participants in our survey were fairly evenly split over which type of figure was preferred, with a slight preference for the current configuration (Table 7.14). This could simply indicate that neither figure was particularly well understood.

When comparing demographic factors to the proportion of yes answers concerning preference for the format change, there were statistically significant

Table 7.14 Subjects' preference for an inverted strike probability

	Count	Percent of total
Yes	75	37
No	85	42
Not sure	38	19
NA	4	1
Total	202	99

Table 7.15 Race vs. preference for an inverted strike probability

Race	Yes	No	Total	Percent yes
Caucasian	55	78	133	41
African-American	18	4	22	81
Total	73	82	155	

differences in the proportion of yes answers when examined across Caucasian and African-American subjects ($\chi^2 = 12.41$, $p = 4.27*10^{-4}$) (Table 7.15). Other demographic factors had no statistically significant differences.

Additionally, when the proportion of yes answers at educational levels across Caucasians and African-Americans in the sample was examined, a statistically significant difference in the proportion of yes answers for Caucasian and African-American subjects at the grade and/or high school level was noted ($\chi^2 = 9.07$, $p = 0.003$). At the undergraduate and/or graduate level the differences in proportion of yes answers were not statistically significant ($\chi^2 = 3.35$, $p = 0.067$).

7.3.2 Graphical Enhancements

7.3.2.1 Graphical Probability vs. Textual Probability

Survey subjects were given a graphic showing the probability of the future location of a hurricane (Fig. 7.1) as well as standard WFO text-based advisory of the same thing (Fig. 7.2). First, participants were asked to use the graphic (Fig. 7.1) to select from six possible answers for the strike probability for Mobile, AL. The correct answer, 20%, was identified by over 62% of the sample. Then, participants were asked to use the text-based advisory (Fig. 7.2) to select from six possible answers for the strike probability for Panama City, FL. Only 10% of the sample was able to determine the correct answer, 24%. The number who didn't know the correct answer was a factor of three higher for the standard text-based advisory than from the graphic (Table 7.16), a strong indication of the value of a graphic-filled advisory.

When the proportion of correct results for the two formats was compared, there was a very statistically significant difference in the proportion of correct answers between the graphical and text-based advisories ($\chi^2 = 58.15$, $p = 2.43*10^{-14}$).

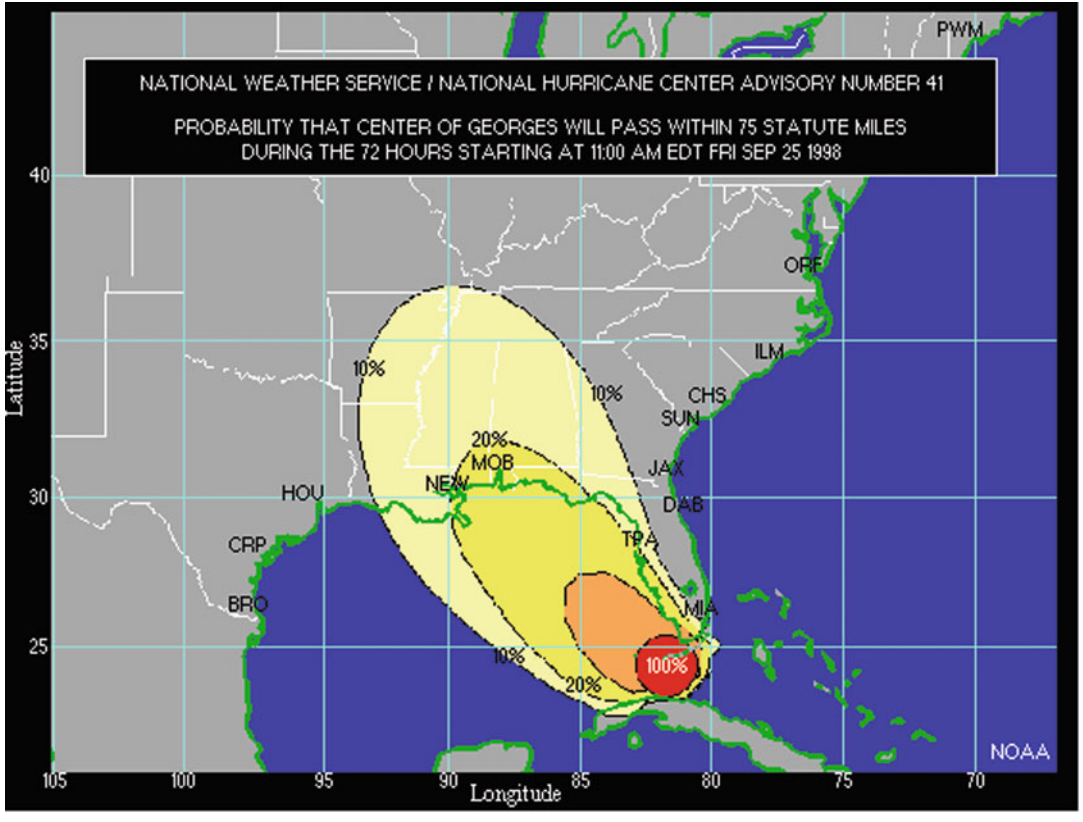

Fig. 7.1 Graphic provided in the survey, showing the probability that the center of hurricane Georges will pass within 75 miles of a particular location within the 72 h after 11 am EDT Sept. 25, 1998

Example of Text-Based Probability Product

The example below is a portion of a strike probability issued for Hurricane Georges in 1998. The rows in the table are the locations, some of which are given in latitude and longitude and others by name. The different columns (labeled "A","B", "C", "D") are probabilities at various forecast times (listed at the bottom of the table in red). The column labeled "E" is the sum of the probabilities in the four periods.

According to this example, Key West FL had the highest probability (99%)of the hurricane center passing within 65 NM (75 mi) during the period between 11 a.m. EDT on Friday, September 25 (the current time) and 8 a.m. on Saturday, September 26. There was a 2% chance that the center would pass within 65 NM of the location
GULF 29N 87W before 8 a.m. Saturday, but a 25% chance between 8 a.m. Saturday and 8 p.m. Saturday . The 2% probability is low for a 24-hour forecast, but the 25% chance at about 36 hours is about as high as is possible.

ZCZC MIASPFAT2 ALL
TTAA00 KNHC DDHHMM
HURRICANE GEORGES PROBABILITIES NUMBER 41
NATIONAL WEATHER SERVICE MIAMI FL
11 AM EDT FRI SEP 25 1998

PROBABILITIES FOR GUIDANCE IN HURRICANE PROTECTION
PLANNING BY GOVERNMENT AND DISASTER OFFICIALS

AT 11 AM EDT...1500Z...THE CENTER OF GEORGES WAS LOCATED NEAR
LATITUDE 24.3 NORTH...LONGITUDE 81.7 WEST

CHANCES OF CENTER OF THE HURRICANE PASSING WITHIN 65 NAUTICAL
MILES OF LISTED LOCATIONS THROUGH 8AM EDT MON SEP 28 1998

LOCATION	A	B	C	D	E	LOCATION	A	B	C	D	E
26.7N 85.3W	54	X	X	X	54	APALACHICOLA FL	8	14	1	1	24
28.1N 86.7W	16	18	X	1	35	PANAMA CITY FL	3	17	3	1	24
29.6N 87.9W	X	15	11	1	27	PENSACOLA FL	X	11	12	2	25
MUHA 230N 824W	16	X	X	X	16	MOBILE AL	X	4	16	3	22
...											
KEY WEST FL	99	X	X	X	99	GALVESTON TX	X	X	X	3	3
MARCO ISLAND FL	56	X	X	X	56	GULF 29N 85W	20	9	1	X	30
FT. MYERS FL	39	X	1	X	40	GULF 29N 87W	2	25	2	1	30

COLUMN DEFINITION PROBABILITIES IN PERCENT
A IS PROBABILITY FROM NOW TO 8AM SAT
FOLLOWING ARE ADDITIONAL PROBABILITIES
B FROM 8AM SAT TO 8PM SAT
C FROM 8PM SAT TO 8AM SUN
D FROM 8AM SUN TO 8AM MON
E IS TOTAL PROBABILITY FROM NOW TO 8AM MON
X MEANS LESS THAN ONE PERCENT

Fig. 7.2 Probability text provided in the survey, showing the probability that the center of hurricane Georges will pass within 75 miles of a particular location within the 72 h after 11 am EDT Sept. 25, 1998

Table 7.16 Survey subjects' estimate of the probability georges hits mobile; graphic advisory was used (top part of table) and survey subjects' estimate of the probability georges hits Panama city; text advisory was used (bottom part of table)

Probability at mobile (using graphic advisory)	Count	Percent of total
100%	26	13
50%	20	10
20%	126	62
10%	3	1
0%	0	0
Don't know	27	13
Total	202	99
Probability at Panama city (using text advisory)		
3%	50	25
17%	34	17
24%	21	10
Don't know	92	46
NA	5	2
Total	202	100

Table 7.17 Ability to interpret strike probability using the graphical advisory for different race, education & income demographics

Demographic factors	Correct	Incorrect	Total	Percent correct
Race				
Caucasian	119	51	170	70
African-American	6	18	24	25
Total	125	69	194	
Education				
Grade + High school	45	38	83	54
Undergraduate + Graduate	81	37	118	69
Total	125	75	201	
Income				
Low ($0 = 49,999)	58	52	110	53
High ($ 50,000 and above)	61	21	82	74
Total	119	73	192	

Furthermore, a statistically significant difference in the proportion of correct answers for the graphic advisory when race ($\chi^2 = 18.60$. $p = 1.61^* 10^{-5}$), education ($\chi^2 = 4.03$, $p = 0.037$), and income ($\chi^2 = 9.26$, $p = 0.002$) were compared (Table 7.17). Age and gender were statistically insignificant. Interestingly, no demographic factors were significant when compared to the proportion of correct answers for the text advisory. Apparently, subjects were equally confused by the text advisory, regardless of their demographic groups.

Examining the proportion of correct answers for the graphical advisory based on both race and educational levels, there is a statistically significant difference in the

Table 7.18 Ability to interpret strike probability using the graphical advisory for combined race and education demographics

Demographic factors	Correct	Incorrect	Total	Percent correct
Grade + high school				
Caucasian	40	25	65	62
African-American	4	10	14	29
Total	44	35	79	
Undergraduate + Graduate				
Caucasian	79	25	104	76
African-American	2	8	10	20
Total	81	33	114	

Table 7.19 Preference for text or graphical advisories for hurricane surge, rain, wind or track uncertainty

	Surge	Rain	Wind	Track uncertainty	Totals	Percent
Text	35	25	31	78	169	25
Graphic	129	137	133	101	500	75

proportion of correct answers for Caucasians and African-Americans at the grade and/or high school level ($\chi^2 = 5.08$, $p = 0.024$) and at the undergraduate and/or graduate level ($\chi^2 = 13.79$, $p = 1.97*10^{-4}$) (Table 7.18).

7.3.2.2 Preference for Graphical Advisories

Four questions compared various text-based WFO advisories with graphically modified versions of the same advisories, and subjects were merely asked which format they preferred. All the questions replaced the standard NWS text message with a combination text and graphic message, but each question focused on a different risk from the hurricane (surge effects, rain effects, wind effects, and track uncertainty). The preference for the graphical version was quite strong and quite consistent across all of the questions, although the preference was not quite as marked for the track uncertainty (perhaps indicating that this was the most challenging concept to convey) (Table 7.19). Please note that all subjects that expressed no opinion or no answer were dropped from the totals.

There was a statistically significant difference in the proportion of format preferences between Caucasians and African-Americans ($\chi^2 = 4.98$, $p = 0.026$). However, both racial groups preferred the graphic format (Table 7.20). Because there was little variability between the four individual questions between racial groups, only the totals for all four questions are shown in Table 7.20.

In addition, there was a borderline statistically significant association between educational level attained and the incidence of format preference ($\chi^2 = 3.83$,

Table 7.20 Race vs. format preference for hurricane advisory

	Text	Graphic	Total	Percent preferring graphic
Caucasian	121	445	566	79
African-American	21	41	62	66
Total	142	486	628	

Table 7.21 Education vs. format preference for hurricane advisory

	Text	Graphic	Total	Percent preferring graphic
Grade to high school	68	151	219	69
Undergraduate to graduate	97	310	407	76
Total	165	461	626	

$p = 0.051$) (Table 7.21). The other demographic factors were not statistically significantly different in the proportions of format preferences. Again, only the totals for all four questions are shown in the table.

When the proportion of format preferences for Caucasians and African-Americans with grade and/or high school educations and undergraduate and/or graduate educations were compared, there was no statistically significant difference in the proportion of Caucasians and African-Americans with a Grade and/or High school education that preferred either format, nor were racial differences exhibited when compared at the undergraduate and/or graduate level.

7.4 Discussion

Because our subjects were not sampled randomly, our demographic percentages differed from the metropolitan area in several significant ways. Our sample contained half as many minorities (16% in our sample vs. 32% for the metropolitan area), four times as many with graduate degrees (28 vs. 6%), one quarter as many who did not complete high school (2 vs. 9%), three times as many households with incomes above $75,000 (22 vs. 7%), and half as many retirees (5 vs. 11%). However, aside from those small subgroups, the bulk of the demographics were reasonably representative (Table 7.1). Nonetheless, these differences limit statistical inferences that can be drawn from this sample to the general population (Daniel 1995). Despite these limitations, the results of this research can be quite useful for indicating directions for further study.

Charleston has experienced tropical storm or hurricane strength winds from a tropical system on average once every 3 years over the past century (Keim et al. 2007), and there were many significant systems that have passed close to Charleston just in the past decade or two (http://www.erh.noaa.gov/chs/tropical/hurrstats_web.shtml). Not surprisingly then, our survey participants considered themselves very hurricane savvy. On yes/no questions, 93% of our survey participants answered that

Table 7.22 Comparison of total metropolitan area demographics (based on 1990 US Census data) and survey sample demographics

	Percent of metropolitan area	Percent of total survey sample	Raw survey count
Sample size	506,875		202
Sex			
Male	50	53	107
Female	50	47	93
Age			
18–25 years	19	23	46
26–45 years	48	41	83
46–55 years	13	24	48
56–65 years	10	6	12
66 years and above	11	6	13
Race			
Caucasian	68	84	170
African-American	30	12	24
Hispanic	2	1	1
Native American	0	2	4
Asian/Pacific Islander	1	1	1
Education			
Grade school	9	2	5
High school	44	39	78
Undergraduate	40	36	73
Graduate	6	28	45
Household income			
Less than $25,000	33	26	50
$25–49,999	43	31	60
$50–74,999	16	20	39
$75–99,999	4	8	16
Above $100,000	3	14	27

Note that very minor differences in age groupings are not accounted for in the table, and that 1% errors in sample numbers may result from those few surveys that omitted demographic questions

they had experienced hurricane effects sometime in their life. While it wasn't asked, that likely means that most had seen NWS advisories or media descriptions of hurricanes. Furthermore, 70% answered that they experienced property damage due to a hurricane or tropical storm. This means that most participants witnessed firsthand the power that a tropical system can have on property. Two-thirds of our subjects answered that they had evacuated after being advised to do so. This indicates again that they had likely received information about an impending hurricane or tropical storm, probably from the NWS or the media.

Considering that the NWS and the media err on the side of caution in issuing warnings, most people who are issued warnings end up with no serious effects from a tropical storm. As a result, most have a lack of trust in the predictions issued by the NWS. When asked whether the NWS overstates the dangers associated with

hurricanes, half felt that they do. Moreover, most admitted that they do not have an evacuation plan in place in case an evacuation is advised. Thus, while most of our subjects had experienced hurricane effects, most were reluctant to believe the NWS or to plan for an evacuation.

7.4.1 Public Educational Issues

7.4.1.1 Definition of Hurricane Warning

The results of this study suggest a large percentage of the residents of Berkeley, Charleston, and Dorchester Counties of South Carolina do not know the meaning of common terms used in WFO advisories. In 1974 McLuckie recommended that severe weather warnings should avoid the use of technical terms, a recommendation that our research supports. Despite their familiarity with hurricanes, 57% of our sample did not know the meaning of the term "Hurricane Warning." An analysis of demographic factors revealed no statistically significant differences in the proportion of correct answers for this question. This analysis indicates that our sample understood the term equally across all sectors, but that understanding was equally poor since a higher level of understanding is desirable. Future studies should explore NWS use of other undefined terms such as storm surge, storm tide, and hurricane watch.

7.4.1.2 Understanding of Scientific Concepts

The results of this study suggest that many Charleston metropolitan residents are deficient in their understanding of some of the scientific concepts involved in hurricane forecasting and warning. Some subsets of this sample, specifically racial and education groups, exhibit less understanding than others. However, the results may indicate a problem with the construction of the survey questions in that the questions may contain cultural biases that are reflected in the significant results observed between racial groups. This possibility is supported by the fact that the differences among the races are significant even when comparable education levels were achieved. If the questions are not the source of the differences observed between the races then these results suggest WFO hurricane advisories and educational efforts may need to be tailored for these groups.

Storm Surge

53% of our sample could not identify storm surge as the greatest danger from hurricanes in low-lying coastal areas. This was answered incorrectly despite the fact that over the past century the majority of deaths and property loss are due to storm

surge. There were statistically significant differences in the proportion of correct answers when measured across income, education, and race. A statistically significant difference occurred in the proportion of correct answers for Caucasians and African-Americans with either a grade and/or high school education. This difference was not exhibited when both groups had undergraduate and/or graduate school educations. There was a statistically significant difference in the proportion of correct answers for African-Americans across the two educational levels. These tests are mutually supportive. It is apparent that African-Americans of lower educational levels within our sample had more difficulty in answering the question correctly. This result may indicate problems with WFO advisories or it may indicate a cultural bias in our sample. A survey using a random sampling scheme would help to confirm the cause of this observation.

NWS Forecast Accuracy at 72 Hours

Almost 20% of our sample answered, incorrectly, that NWS forecast accuracy was greater at 72 h before landfall than at 24 h before landfall, when given a simple choice between which of those was greater. This would appear to indicate an improper understanding of the definition of accuracy or how forecasts are generated. African-Americans answered correctly 61% of the time while Caucasians answered correctly 84% of the time. This difference was found to be statistically significant. Additionally, Caucasians and African-Americans within the sample exhibited a statistically significant difference when both groups had an undergraduate and/or graduate education, but it was not significant when they had a grade and/or high school education. Once again these racial differences within our sample are either indicative of problems with WFO advisories in relation to African-Americans or indicative of a bias within our sample.

Effects of a Decrease in Forward Speed

53% of the sample was unable to identify that more rain was the most significant consequence of a hurricane that slowed its forward speed. A statistically significant difference occurred in the proportion of correct answers for Caucasians and African-Americans within the sample. In addition, the proportion of correct answers for Caucasians and African-Americans across educational levels was analyzed, and statistically significant differences were noted at the grade and/or high school level and also at the undergraduate and/or graduate level. These racial divisions within our sample indicate further research is needed to confirm this disparity in the general population concerning deficiencies in the understanding of scientific concepts. If it is confirmed perhaps the NWS needs to develop educational programs that target African-American citizens. Additionally, over 32% did not understand that errors by the NWS in forecasting the forward speed and direction of hurricanes would affect the time available for evacuation (i.e. increase

or decrease). These results support our hypothesis that the public often does not understand basic scientific principles and this lack of understanding could cause them to ignore, misinterpret or underestimate the threat.

7.4.1.3 Internet Information Dissemination

Our results indicate that Internet dissemination of information about hurricanes was favored across all groups. 83% of our sample ranked Internet information as either very important or moderately important. Gender was found to have a statistically significant difference in the proportion that ranked Internet information as important, although it is borderline significant with $p = 0.048$. An analysis of gender at educational levels revealed no statistically significant difference in the proportions ranking Internet information as important. Perhaps future research could investigate this issue further, but at this point it seems that our sample would like to have the option of the Internet as a source of information. The WFO can provide another source of consistent, credible and complete information by increasing its use of the Internet.

7.4.1.4 Probability Inversion Format

The study sample was fairly evenly split over the use of a message that contained the probability of a hurricane not striking their location (i.e. inverted probability). Over 42% of our sample was not in favor of an inverted hurricane strike probability graph while approximately 37% favored its use. Anecdotally, several of the subjects commented that they were concerned that an inverted format would cause confusion for citizens because the traditional method has conditioned the public toward a presentation of the probability of a hurricane striking a location. This agrees with the Sanders and Westergard (1996) finding that changes in traditional methods may cause confusion in the public response to severe weather warnings. However, it could also be simply that probability is poorly understood, regardless of how it is presented. There was a statistically significant difference in the proportion of Caucasians and African-Americans that preferred a change in format. It is interesting to note that almost 41% of Caucasians preferred changing the format and 81% African-Americans preferred a change. Further analysis found a statistically significant difference in preference for Caucasians and African-Americans at the grade and/or high school level of education. This significance was not seen at the undergraduate and/or graduate level of education. It is interesting to note that at both educational levels there is a marked difference in the proportion preferring the format change with African-Americans consistently preferring it and Caucasians not preferring it. These differences may reflect the cultural preferences of the subjects. Further research may investigate this. Again, perhaps the NWS needs to cater their probability products to the two racial groups.

7.4.2 Graphical Enhancements

The results of our study showed that graphical presentation of probability greatly improved the ability of readers to understand NWS messages when compared to textual presentations. Additionally, a large majority of the sample stated a preference for graphical presentations of NWS messages as opposed to textual presentations.

7.4.2.1 Graphical Probability Advisory vs. Textual Probability Advisory

Our sample was better at answering a question on the probability of landfall of a hurricane based on a graphical presentation. 62% of the sample was correct when answering questions based on a graphical presentation, whereas only 25% were correct with a standard WFO text-based presentation. The difference in proportion of correct answers for the two presentations was statistically significant within our sample. A demographic analysis indicated that race, education and income were statistically significant when measured against the graphic presentation. Further analysis indicated there were significant differences in the proportion of correct answers for Caucasians and African-Americans across both educational levels for the graphic advisory. A demographic analysis of the text advisory did not find any statistically significant differences. These results, from our sample, suggest graphical probability formats are better understood than text probability formats. There is a significant difference between Caucasians and African-Americans in their observed ability to answer the probability question correctly although both groups perform better with the graphic advisory.

7.4.2.2 Preference for Graphical Advisories

Our sample preferred graphically modified versions of standard WFO text-based advisories. 75% of the sample preferred the graphic version to the text version. A demographic analysis found a statistically significant difference in the proportion of Caucasians and African-Americans preferring the graphic version. Also education was borderline statistically significant with $p = 0.051$. Further analysis did not reveal a statistically significant difference in the proportion of Caucasian and African-American subjects at both educational levels who preferred a graphic enhancement of the warning. Most differences found in racial groups, even with similar education, may suggest cultural differences and preferences, although it may be the product of a bias induced by our use of opportunity sampling (convenience/snowball sampling). Overall, our results suggest the effectiveness of WFO advisories could be enhanced with the use of graphics.

FEMA and many other agencies typically depict surge projections by using a map covered by different colors or shades of grey, with each color or shade representing a different depth of water. A large majority of our sample preferred

Fig. 7.3 Simulated inundation for the Sullivans Island Post Office for a Category 4 hurricane making landfall in Charleston at high tide. NHC SLOSH model surge predictions were combined with historical tidal data and USGS elevation data to estimate the depth of inundation

a pictorial approach to information dissemination in contrast to such a map-based approach. Moreover, the use of reference marks, whether text or pictorial, aided in the dissemination of warnings. Combining these approaches and making pictorial references was even more helpful in conveying risk than a simple text-based message of hurricane surge at the landmark. Perhaps most effective might be an interactive map that contained a landmark every couple blocks for which a user could pull up an image upon which was drawn a water depth for a particular hurricane scenario. Figure 7.3 shows a sample of what such a graphic would look like. Our finding that the public had little success interpreting standard inundation maps is similar to the Arlikatti et al. (2006) finding that most people are not even capable of finding their own home on standard hurricane risk area maps. Other researchers have noted a similar advantage of pictorial/text warnings (Sojourner and Wogalter 1998), which suggests that this is a potentially fruitful line of research. Furthermore, Baker (1995) found that presenting the public with standard hurricane probabilities did little to influence evacuation behavior, whereas perhaps a graphical presentation would be more effective.

7.5 Conclusions

Results from a survey of more than 200 residents in Berkeley, Charleston, and Dorchester counties of South Carolina suggest there are problems with WFO hurricane advisories that should be addressed. Our use of opportunity sampling

(convenience/snowball sampling), as opposed to purely random sampling, prevents direct inference to the general population, but it does strongly suggest areas that are ripe for future research. Specifically, we suggest further research, using a random sampling scheme, targeting our results that indicate: (1) The NWS uses too many technical terms in its warnings, (2) The public has deficiencies in their knowledge of scientific concepts involved in hurricane forecasts and warnings, (3) The public supports increased use of Internet-based hurricane educational and warning information by the NWS, (4) The public does not support the change to an inverted strike probability format, although a majority of African-Americans prefer it, (5) A graphic presentation of probabilities is understood by more of the public, (6) The public prefers graphical enhancements to standard WFO text-based advisories, and (7) There are some indications (i.e. the pattern of differences across racial groups, even at similar education levels) that a bias may have been introduced by the construction of the survey questions. Perhaps, future research could use focus groups to identify constructions for questions that avoid cultural biases.

These findings, if confirmed by future research, lead to these simple recommendations: (1) The WFO, locally, can easily alter warning text to include the meaning of any term used to increase public comprehension of the warning. (2) The WFO already has the capability to post information on its website. Use this capability to enhance public education. (3) The WFO needs graphical capability in its local warning products. (4) The NWS and WFO may need to tailor its message to specific subsets of the population. Specifically, our data indicates that various racial, educational and age groups have different levels of understanding and knowledge, and thus the NWS and WFO may need to use different approaches to these different groups. However, our research shows that the NWS has been quite successful in their overall approach to educating and warning the public. After all, they cannot force response to their advisories. Their objective is to inform the public of the threat and all mitigation measures. It is the responsibility of the recipient to act on this information.

Acknowledgements This book chapter was prepared under Subawards # Z10-83390 and S00-22461 with the University Corporation for Atmospheric Research (UCAR) under Cooperative Agreement No. NA06NWS4670013 and NA97W0082 with the National Oceanic and Atmospheric Administration (NOAA), U.S. Department of Commerce (DoC). The statements, findings, conclusions, and recommendations are those of the authors and do not necessarily reflect the views of NOAA, DoC or UCAR.

Rhonda Swickert of the Psychology department at the College of Charleston is thanked for thoughtful comments, corrections and additions to parts of the introduction. Steven Brueske, Science and Operations Officer at the Charleston office of the National Weather Service, Robert Kennedy of the Department of Biometry and Epidemiology at the Medical University of South Carolina, and Laney Mills and Fred Watts of the Physics and Astronomy Department at the College of Charleston provided comments and assistance on the early stages of this research. Additionally, undergraduate students Kristin Bynum, Rhonda Crawley, Kristi Owens, Jay Sonner, Shayna Brisacher and R. Blake Williams assisted with data collection and provided feedback on survey design. The authors also thank the reviewers and editor in chief for thoughtful suggestions that resulted in a better manuscript.

References

Alsheimer F, Lindner BL (2011) Synoptic scale precursors to high impact weather events in the Georgia and South Carolina coastal region. J Coast Res 27:263–275

Arlikatti S, Lindell MK, Prater CS, Zhang Y (2006) Risk area accuracy and hurricane evacuation expectations of coastal residents. Environ Behav 38:226–247

Baker EJ (1979) Predicting response to hurricane warnings: a reanalysis of data from four studies. Mass Emerg 4:9–24

Baker EJ (1995) Public response to hurricane probability forecasts. Prof Geogr 47:137–147

Canino G, Bravo M, Rubio-Stipec M, Woodbury M (1990) The impact of disaster on mental health: prospective and retrospective analyses. Int J Ment Health 19:51–69

Clark JP, Carter TM (1979) Response to hurricane warnings as a process: determinants of household behavior, Natural hazards warning systems report series 79–08. Department of Sociology, University of Minnesota, Minneapolis

Daniel WW (1995) Biostatistics: a foundation for analysis in the health sciences, 6th edn. Wiley, New York

Drabek TE (1969) Social processes in disaster: family evacuation. Soc Probl 16:336–349

Freedy JB, Shaw D, Jarrell MP, Masters C (1992) Towards an understanding of the psychological impact of natural disaster: an application of the conservation resources stress model. J Trauma Stress 5:441–454

Freedy JR, Saladin ME, Kilpatrick DG, Resnick HS, Saunders BE (1994) Understanding acute psychological distress following natural disaster. J Trauma Stress 7:257–273

Gladwell CH, Gladwell H, Peacock WG (2001) Modeling hurricane evacuation decisions with ethnographic methods. Int J Mass Emerg Disaster 19:117–143

Houston S, Shaffer W, Powell MD, Chen J (1999) Comparisons of HRD and SLOSH surface wind fields in hurricanes: implications for storm surge modeling. Weather Forecast 14:671–686

Janis IL, Mann L (1977) Emergency decision making: a theoretical analysis of responses to disaster warnings. J Hum Stress 3:35–47

Jelesnianski CP, Chen J, Shaffer WA (1992) SLOSH: sea, lake, and overland surges from hurricanes, NOAA technical report NWS48. U.S. Dept. of Commerce, National Oceanic and Atmospheric Administration, Rockville

Keim B, Muller RA, Stone GW (2007) Spatiotemporal patterns and return periods of tropical storms and hurricane strikes from Texas to Maine. J Clim 20(14):3498–3509

Leik RK, Carter TM, Clark JP (1981) Community response to natural hazard warnings: summary final report. FEMA Agency Contract No. DCPA01-79-C-0214 Work Unit No. 2234-F, NSF Grant No. PFR77-01452 and NWS Grant No. DOC NA80AAA03283. University of Minnesota, Minneapolis

Lindner BL, Frysinger JR (2007) Bulk atmospheric deposition in the Charleston Harbor watershed. J Coast Res 23:1452–1461

Mayhorn CB, Yim NS, Orrock JA (2006) Warnings and hazard communications for natural and technological disasters. In: Wogalter M (ed) Handbook of warnings. Lawrence Erlbaum Associates, Mahway, NJ, pp 763–769

McLuckie BF (1974) Warning: a call to action. National Weather Service, Washington, DC

Mileti DJ, Fitzpatrick C (1991) The causal sequence of risk communication in the parkfield earthquake prediction experiment. Risk Anal 12(3):393–400

Mileti DJ, O'Brien PW (1992) Warnings during disaster: normalizing communicated risk. Soc Probl 39(1):40–54

Perry RW, Nigg JM (1985) Emergency management strategies for communicating hazard information. Public Adm Rev 45:72–76

Rappaport EN, Franklin JL, Avila LA, Baig SR, Beven JL II, Blake ES, Burr CA, Jiing J-G, Juckins CA, Knabb RD, Landsea CW, Mainelli M, Mayfield M, McAdie CJ, Pasch RJ, Sisko C, Stewart SR, Tribble AN (2009) Advances and challenges at the national hurricane center. Weather Forecast 24:395–419

Riad JK, Norris FH (1998) Hurricane threat and evacuation intentions: an analysis of risk perception, preparedness, social influence, and resources, Preliminary paper #271. Disaster Research Center, University of Delaware, Newark

Sanders RE, Westergard RJ (1996) The public relations/education function of meteorological communication: a study of citizens' understanding and uses of weather information and forecasts and recommendations for improving them. Unpublished Technical Report. Comet Project No. S-9554367, UCAR/COMET, Boulder

Sattler DN, Kaiser CF, Hittner JB (2000) Disaster preparedness: relationships among prior experience, personal characteristics, and distress. J Appl Soc Psychol 30:1396–1420

Sojourner R, Wogalter M (1998) Influence of pictorials on the comprehension and recall of pharma-ceutical safety & warning information. Int J Cogn Ergon 2:93–106

Sorensen JH (1991) When shall we leave? Factors affecting the timing of evacuation departures. Int J Mass Emerg Disaster 9(2):153–165

World Health Organization (2000) World health report 2000. World Health Organization, Geneva

Chapter 8
Anthropogenic Amplification of Storm Surge Damage in the 1935 "Labor Day" Hurricane

Nicholas K. Coch

Abstract On Labor Day, September 2, 1935, the most powerful hurricane in U.S. history (Herbert et al. Greatest storms of this century (and other frequently requested facts) NOAA Technical Memorandum NWS NHC-31, U.S. Department of Commerce, Washington, D.C, 1992) made a landfall in the Middle section of the Florida Keys. At that time, this was a sparsely populated area. However, the 600 World War I veterans engaged in building U.S. 1 had recently increased the population significantly. The hurricane had winds exceeding Category 5 levels 155 miles/h (69.3 m/s) on the Saffir-Simpson Scale (Weatherwise 27:169–186, 1974) and surge levels up to 18 ft (6 m). Superposed wind waves caused damage at much higher levels. Some natives blamed the filling of tidal channels in the building of the Florida East Coast Railway extension in the early 1900s for impounding floodwaters. However, no one has been able to verify their hypothesis or to quantify the degree of tidal prism restriction.

The storm was moving exceptionally slowly at 5 miles/h (2.2 m/s). Normally a slow moving storm draws up all of the warm water above the thermocline and weakens. However, in the Bahamas the slow-moving storm *intensified* to a Category 5+ event, *in 1 day*, as it traveled the 100 miles to Florida. Data cited here allows us to explain the exceptional intensification.

A synthesis of archival material, original Florida Overseas Railroad drawings, survivor interviews, meteorological data, and field studies have been used to explain the surge dynamics and rapid intensification in the 1935 hurricane. Filled railroad embankments totally restricted the return flow, while large (12 f. wide) stone piers restricted tidal flow by 19%. As the hurricane moved onshore, the ocean submerged the Keys and surface structures were obliterated. When the hurricane moved off the Keys, offshore winds started to blow the floodwaters back into the ocean. The bay waters in front of the Keys withdrew relatively quickly across

N.K. Coch (✉)
School of Earth and Environmental Sciences, Queens College of C.U.N.Y.,
Flushing, NY, USA 11367
e-mail: coch@earthlink.net

C.W. Finkl (ed.), *Coastal Hazards*, Coastal Research Library 6,
DOI 10.1007/978-94-007-5234-4_8,

the reef. However, the earthen fills blocked the waters behind the Keys and the flow was restricted as it passed between the stone piers of the railroad viaducts. A significant hydraulic head developed on the ocean side of the Keys. Fluid pressure built up steadily on the Gulf side of the fills, and eventually they were breached.

The slow storm movement actually aided in hurricane intensification in this case, the storm moved over the hot waters of the Bahama Platform and then traversed the Florida Straits, underlain by the 900 ft deep, very warm waters of the Florida Current. The lessons from this hurricane are applied to the rapidly developing coastal areas of Tampa-St. Petersburg and similar U.S. coastal sections.

8.1 Introduction

Intense development is occurring all across the U.S. Atlantic and Gulf shorelines in a time of sea level rise and increasing hurricane frequency. This development frequently includes building of hard structures (groins, jetties, stabilized inlets) to "manage" beach erosion, causeways to cross bays and dredged islands for new bay developments. In addition, many "canal-type" developments have been created so that coastal inhabitants can moor their boats by their homes. This type of development involves dredging canals and using the dredge spoils to raise adjacent land elevations for home sites. The latter type of development leads to stagnation and pollution in the waterways. In addition, it opens up more of the coast to penetration by hurricane waves and storm surge. Most of these bay developments result in a reduction of the tidal prism. This tidal prism reduction greatly increases the flooding as hurricane storm waters are funneled in and out of estuarine areas. At the present, we have not had a direct hit on one of these developed areas in Miami, Norfolk or on Long Island.

What flooding damage can a future hurricane accomplish in a heavily-developed area? One of the best historical clues as to how tidal prism restriction can cause catastrophic flooding can be obtained from a detailed study of the "Labor Day" hurricane of 1935 in the Florida Keys. In that case, anthropogenic changes in the shoreline created catastrophic flooding in the most powerful hurricane that ever hit the United States. To predict what may happen when a major hurricane hits an area where the tidal prism has been greatly reduced we can apply the lessons of the 1935 storm to a heavily developed area, like Tampa-St. Petersburg, Florida. That is the purpose of this paper.

8.2 The Florida Keys

The Florida Keys (Fig. 8.1) is a chain of islands that stretch south from Miami to Key West. They formed during a high stand of Late Pleistocene sea level and are composed of fossil patch reefs and oolite shoals (Hoffmeister and Multer 1968;

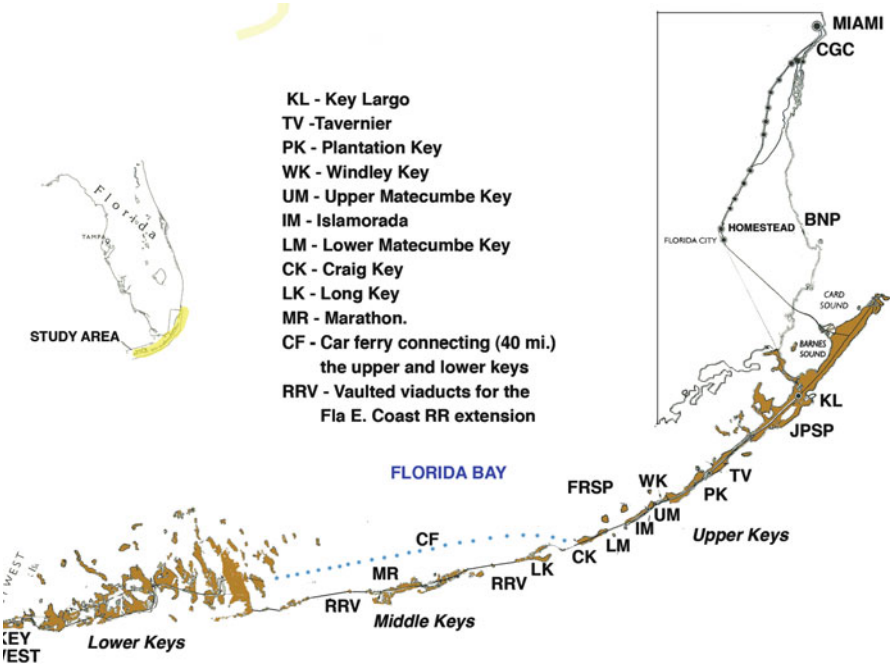

Fig. 8.1 Map of the Florida Keys showing the locations mentioned in the text

Hoffmeister et al. 1967). Prior to the nineteenth century, there was complete tidal exchange between each island (Fig. 8.2). Settlers from the Bahamas first settled the Keys in the mid-1800s. They lived an isolated existence, with each island developing a distinct culture. Travel was largely by boat and agriculture and fishing were the mainstays for the local population. At the southern end of the Keys was Key West, the largest city in Florida in 1900.

In 1905, the oil baron Henry Flagler decided to extend the Florida East Coast Railroad down the Florida Keys to Key West. With the opening of the Panama Canal, Flagler believed that Key West would become a great coaling station for ships. In addition, goods and agricultural items delivered to Key West could then be moved up to Miami by the new railroad and then shipped up the east coast. His engineers faced a daunting task to bridge the islands of the Florida Keys in face of a brutal climate and hurricane threats.

After three hurricanes and the loss of 100 lives, the project finally reached Key West in 1912. The Keys railroad was to change the lives of the local inhabitants for the better. They would now have access to the metropolitan areas of Miami and Key West to sell their crops. However, the changes in the tidal prism brought about by the railroad construction were to set off a disaster for the inhabitants 23 years later.

After the railroad was built, the population in the Keys and the tourist influx increased significantly. During that time, a patchwork of unimproved roads and bridges led up from Key West and down from Miami toward the Middle Keys.

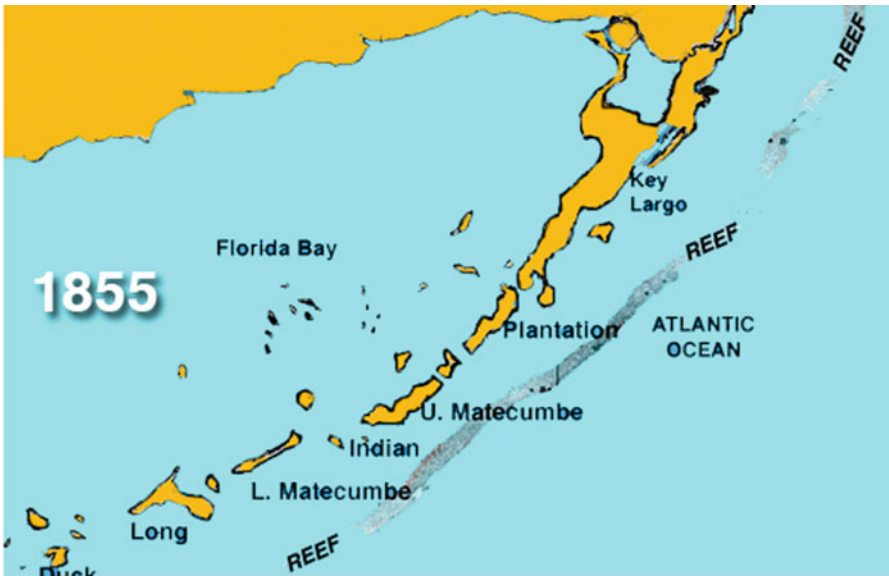

Fig. 8.2 The Florida Keys in 1855. At this time, there was complete tidal exchange between the islands

The 40-mile gap between the ends of the two roads was bridged by a car ferry that took 4 h (Fig. 8.1). The combination of roads and a ferry provided easier access to Key West, and Cuba beyond. Monroe County then decided to build a road that would directly connect the Upper and Lower Keys. Unemployed World War 1 veterans were recruited for the construction. They were housed in tents and frame buildings in several camps on the Keys. Construction of the first few piers for a highway bridge to cross the water traversed by the ferry was started in August 1935, just before the hurricane hit.

8.2.1 The Change in the Tidal Prism Resulting from Railroad Construction

Filling in creeks breached narrower water bodies with sand and coral rock quarried locally (Fig. 8.3b). Concrete arch viaducts bridged the longer stretches over open water (Fig. 8.3a). Shallow creeks were filled in to form long causeways. These raised causeways and viaduct approaches essentially formed a wall between the ocean (left) and the Gulf of Mexico (right). The various elements are shown together in the cross section on Fig. 8.3.

Some local inhabitants suspected that the bridge piers and embankments reduced the tidal flow, leading to catastrophic consequences when the 1935 Hurricane hit. However, no one has attempted to test this idea or estimate the reduction in the tidal

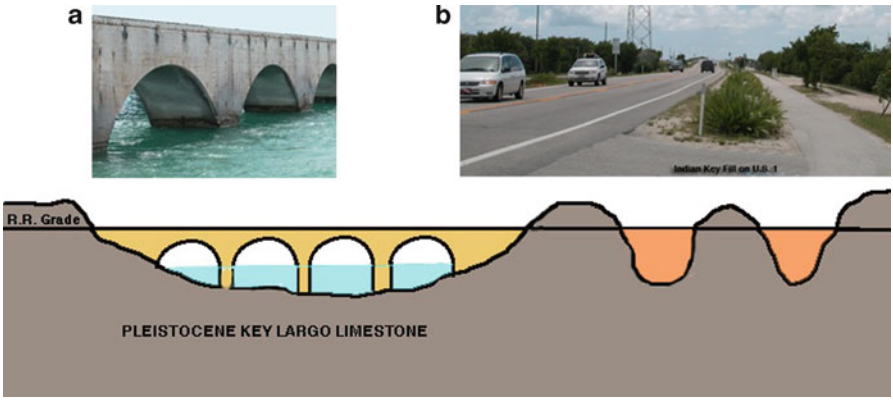

Fig. 8.3 Methods of bridging the Keys. (**a**) Vaulted viaduct that carried the railroad over larger stretches of water. (**b**) Causeways that extend across smaller creeks (**c**) Schematic cross section showing relationships between causeways and viaducts

prism. My synthesis of archival material, original railroad drawings, survivor interviews, meteorological data, and field studies will now be used to explain the tidal flow reduction and rapid intensification in the 1935 hurricane.

I first noticed the tidal retardation at flood tide at the old Long Key viaduct (Fig. 8.4). The original railroad architectural drawings for the vaulted piers are reproduced in Gallagher (2003).

From that diagram (Fig. 8.5), I determined that the piers were 12 ft (3.6 m) wide at the water line. Five of these vaults together measured over 310 ft (93 m), the total widths of each of the piers was 60 ft. This represents a tidal reduction of 19% in the viaduct sections, *from the piers alone*.

Gallagher (2003, figure 139) shows the vaulted bridge connection between Lower Matecumbe Key and Long Key (Fig. 8.6). The straight-line distance between the 2 keys is 4 miles (6.4 km). The final curving course was 6.1 miles According to his figure; the railroad length on vaulted concrete piers was 2.57 miles (4.12 km). From his diagram (Fig. 8.6) the length of fill was 3.49 miles (5.6 km) and the length on vaulted viaduct was 2.57 miles (4.4 km). This fill would have impeded tidal exchange by 100% until it was breached. The length on vaulted viaduct was 2.75 miles (4.4 km). At 19%, the blockage here was .49 miles (.30 km). Thus, the total length of 6.06 miles (9.7 km) was blocked by piers (0.49 miles) and fill (3.45 miles) for a length of 3.94 miles. This calculates out to a *reduction in tidal flow here of 65%*. There are several smaller fills and bridged sections in the hurricane affected area, so this is a *minimum* for the total tidal reduction.

Fig. 8.4 Flood tide retardation at the Long Key Viaduct piers. Ocean is on the *left* and the Gulf is on the *right*

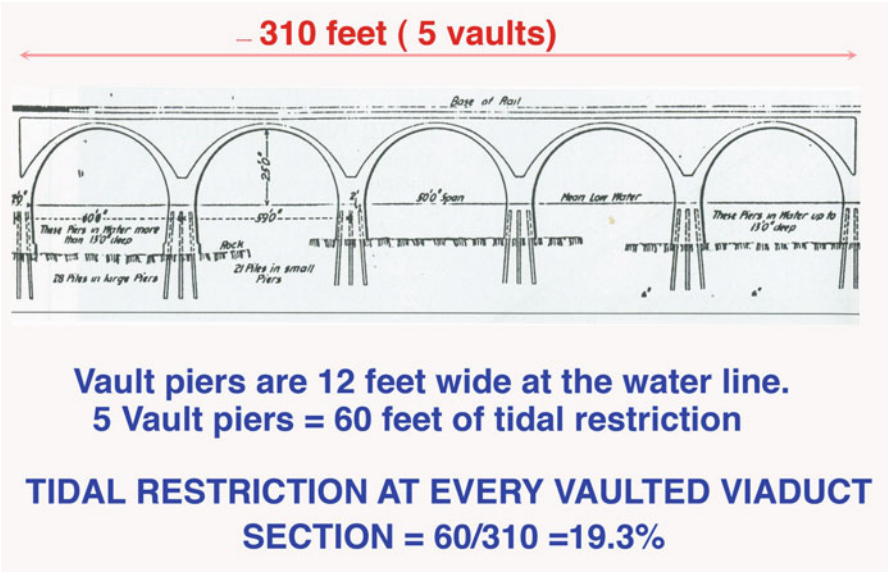

Fig. 8.5 Original railroad architects drawing of a section of the Long Key Viaduct (Modified from original railroad plans reproduced in Gallagher (2003))

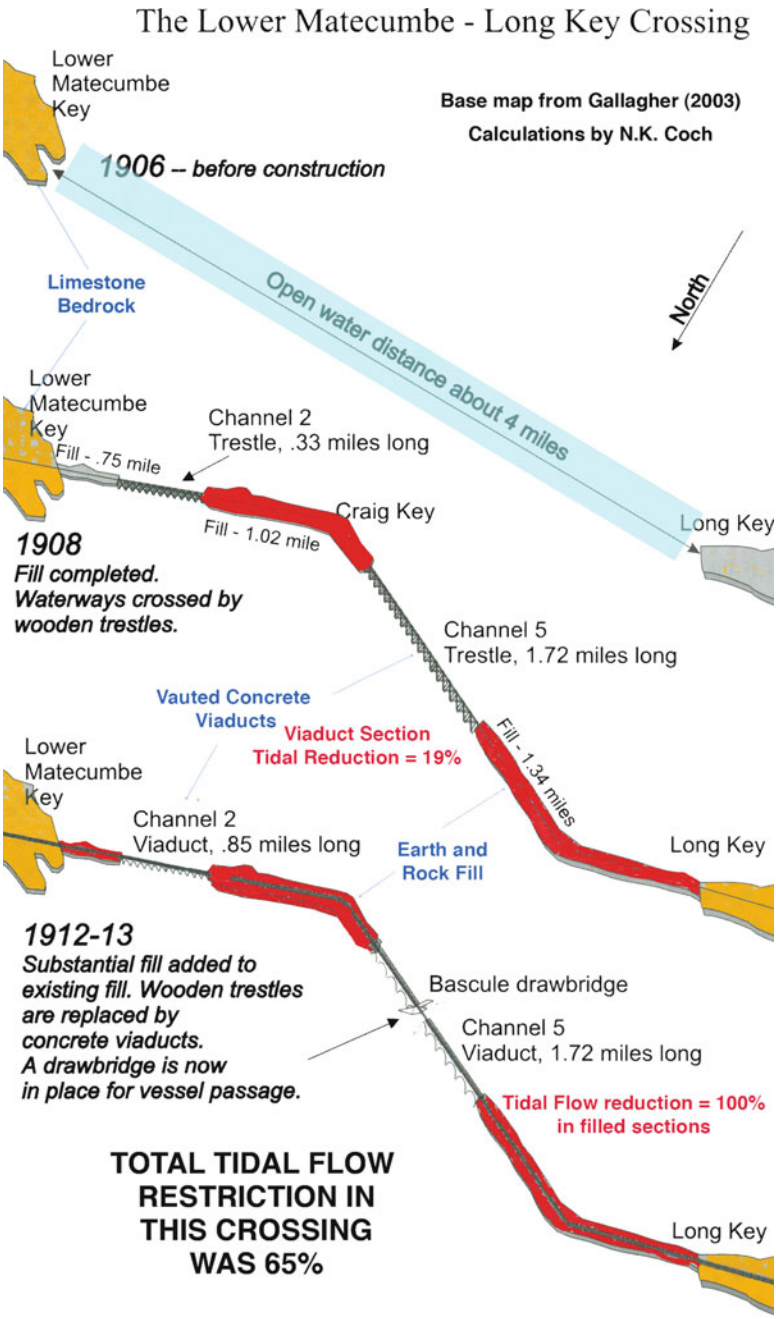

Fig. 8.6 Map of filled and viaduct portions for the Lower Matecumbe Key-Long Key viaduct (Modified from Gallagher (2003))

8.3 The Gathering Storm

On August 30th, the U.S. Weather Bureau noted that a storm was forming in the Bahamas. Their estimate was that the storm would pass between Key West and Cuba. However, the local inhabitants ("conchs") noted that the long period wave fronts from the storm were approaching parallel to the beach (from the east). If the storm were truly passing between Key West and Cuba, the wave fronts should be coming in at an angle (from the southeast). Some of the conchs evacuated at that point, while others watched the barometer. The government authorities counted on the U.S. Weather Service forecasts even though their barometers showed atmospheric pressure was dropping rapidly. By noon on Labor Day, the construction supervisors finally realized the threat from an imminent hurricane strike was real and they requested a train from Miami to evacuate the vets. The train finally reached Islamorada at 8:25 PM, just as the front eye wall of the hurricane made landfall.

8.4 Hurricane Intensification

The 1935 hurricane was a slow-moving Category 1 storm in the Bahamas on the day before it made a landfall on the Keys. In 24 h and 100 miles (62.5 km) it evolved into a very compact Category 5 hurricane. Slow-moving hurricanes in the open ocean typically weaken after they draw up the warm water above the thermocline and tap the cooler ones below. In fact, some are followed by a "cold wake", representing upwelling of the cooler water below the thermocline. However, the 1935 hurricane was wandering slowly across the very warm waters of the Bahamas Platform, heading west toward the waters of the Florida Straits. As it moved slowly over the Florida Straits, the warm and very deep waters of the Florida Current provided abundant heat energy to the slow- moving hurricane, allowing it to intensify rapidly.

Such an intensification scenario was seen recently in Hurricane Rita (2005) in the Gulf of Mexico. The Loop Current in the Gulf of Mexico is a very deep hot water mass that curves through the Gulf (Fig. 8.7). After the Loop Current moves between Cuba and Florida it becomes the Florida Current that underlies the deep waters of the Florida Straits. The Florida Current eventually transitions into the Gulf Stream that crosses the Atlantic. Hurricane Rita increased considerably in intensity and forward speed as it crossed over the Loop Current in the Gulf of Mexico (Fig. 8.7).

The 1935 Hurricane had the lowest central pressure, 26.35, on record and had a compact eye that was only 10 miles (16 km) across. This resulted in very high winds, high surge levels and high wind-driven waves. However, weather records show that the 1935 hurricane was just a category 1 storm in the Bahamas. How could it have intensified in 1 day, and over 100 miles, to the most powerful hurricane in U.S. history? The path and translational velocity of the hurricane

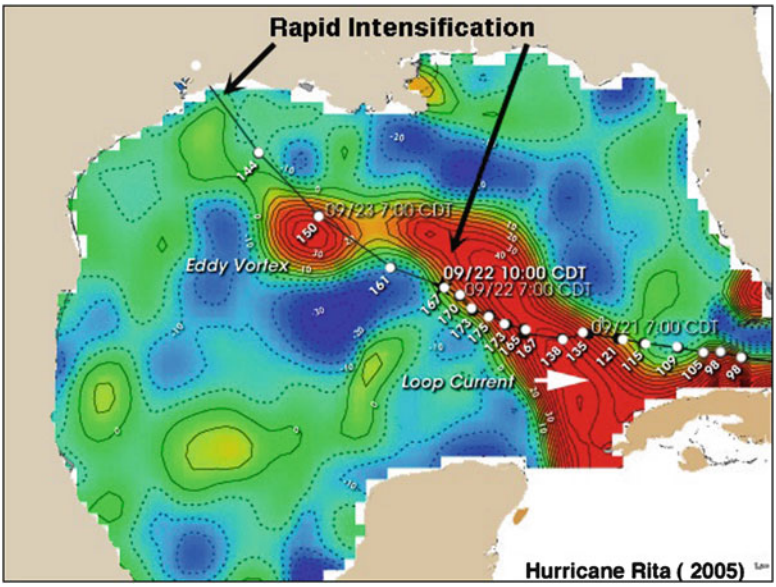

Fig. 8.7 Map of the Gulf of Mexico showing the path of Hurricane Rita (2005), the path of the Loop Current and the warm water eddies shed from the current (*dark tones*). Note the rapid change in the forward speed of the storm after it had passed over the Loop Current. (NOAA)

may provide a clue. It moved slowly over the warm waters of the Bahama Platform before it crossed the deep and warm waters of the Florida Straits. That would have given it time to draw up the warm waters above the thermocline. Boss and Neuman (1995) reported that the very rapid intensification of Hurricane Andrew is suggestive of large-magnitude energy exchanges. They show computer-enhanced radar images (Boss and Neuman, Fig. 8.7) of Andrew as it crossed the Florida Straits. Storm intensification is indicated by the brighter and more continuous radar reflections encircling the eye. Just before landfall in Florida (eye centered at 25°24′ N, 80°00′ W) radar reflections from the eye are very bright and continuous indicative of extreme intensification (Boss and Neuman 1995). Rappaport (1992) noted the extraordinary intensification (declining pressure) in Hurricane Andrew over the very short time interval between leaving Great Bahama Bank and landfall in Florida.

8.5 Winds and Storm Surge

A true and complete record of what happened in the landfall of the 1935 hurricane will never be achieved for a number of reasons. The Keys population was very low, so there were few eyewitnesses. The extreme violence of the storm, the mass confusion of the inhabitants and the reliability of weather instruments at the time

taint most accounts. It is difficult in many cases to distinguish the times of erosion by the flood (onshore) surge and the ebb (seaward) surge from eyewitness accounts Finally, meteorology was a growing science in 1935 and we knew little about the weather conditions higher in the atmosphere at the time. For example, was there shearing at upper levels of the storm? How uniform was the wind field? Were there convective centers generating heavy damage away from the right eye wall (Powell et al. 1991)? Today, our airborne and satellite observations can answer many of these questions. In the following pages, I have utilized all of the available archival data, modern modeling work and my own observations to try and resurrect conditions during the landfall of the 1935 "Labor Day" hurricane.

There is some uncertainty about the actual wind speed during the hurricane. All accounts agree that the storm exceeded Category 5 limits. Drye (2002) states the winds were about 160 miles/h (71 m/s), with gusts to 200 miles/h (89.4). Recent modeling by Houston and Powell (2003) indicate that maximum winds reached 60 m/s (134 miles/h) on the right side of the storm from Windley Key to Tavernier (Fig. 8.1). The wind velocity dropped to 50 m/s (112 miles/h) by Tavernier. However, many survivors swear that the wind far exceeded these levels. How can we account for this discrepancy? First of all, the Keys are low-lying with sparse and low vegetation. This low topography maximizes the wind speed and damage. Secondly, survivors document that there were bursts (gusts) of very high winds during landfall. Two wind speeds are commonly referred to when discussing hurricanes, the mean wind speeds, measured over several minutes, and gust speeds of short duration. Gust speeds are estimated by applying a gust factor to the mean wind of a given averaging period. Krayer and Marshall (1991) derived a gust factor of 1.5, based on a study of a number of major hurricanes. If we apply even a portion of this gust factor to the speeds modeled by Houston and Powell (2003) we can easily account for the gust speeds. For example, a gust factor of 1.25 could raise the maximum-modeled speeds (60 m/s) to 75 m/s or 168 miles/h. A full application of the gust factor would give a gust speed of 90 m/s or 201 miles/h. This approximates the figure given by Drye (2002) and other writers.

A reconstruction of the hurricane wind field when the eye was centered over the Keys is given in Fig. 8.8. These extreme winds created a surge up to 18 ft (U.S. Army Corps of Engineers 1935) as the front eye wall of the hurricane moved onshore. This created massive damage as is shown in the images in (Fig. 8.9). On top of the surge dome were wind-driven waves as high as 30 ft. The heavy (3/8 in.) glass windows of the Alligator Reef Lighthouse, 5 miles (8 km) offshore, were found on a beach in the Keys. The massive wall of water smashed the workers camps into debris piles (Fig. 8.9c) and washed the railroad tracks off their piers (Fig. 8.9d). The flood surge and superposed waves washed the cars of the rescue train off the tracks (Fig. 8.9a), Bernard Russell, whose family settled the Keys in the mid 1800s, took refuge in the heavy locomotive of the rescue train and survived. The next morning, he discovered that the 61 members of the Russell family had been reduced to 11 (oral communication 1992). Drye (2002) describes how a number of construction workers clung to a tank car filled with 10,000 gallons (38,000 liters) of water. The wave hit the tanker and it didn't budge, but all of the

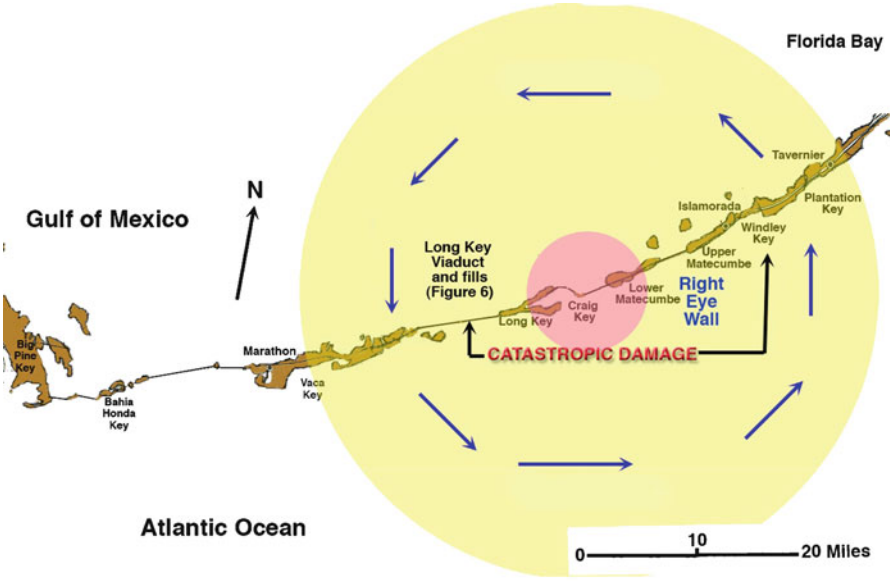

Fig. 8.8 Reconstruction of the 1935 Hurricane wind field as the eye was centered over the Keys. Note the small eye diameter and the difference in the wind directions between the front and rear of the storm

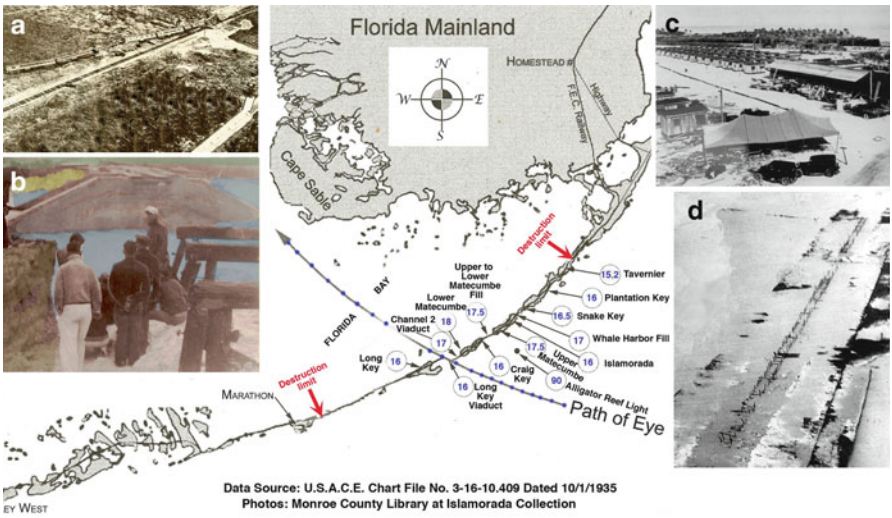

Fig. 8.9 Surge levels and damage in the 1935 Hurricane (Map modified from U.S. Army Corps of Engineers (1935) data presented in Knowles (2009, p. 325)). (**a**) Rescue train washed off the tracks in Islamorada. (**b**) Fill at Snake Creek washed out by the ebb surge. Gulf waters still flowed through a day after the storm. (**c**) The remains of the Upper Matecumbe veteran's camp. (**d**) Washed out track piers and embankment

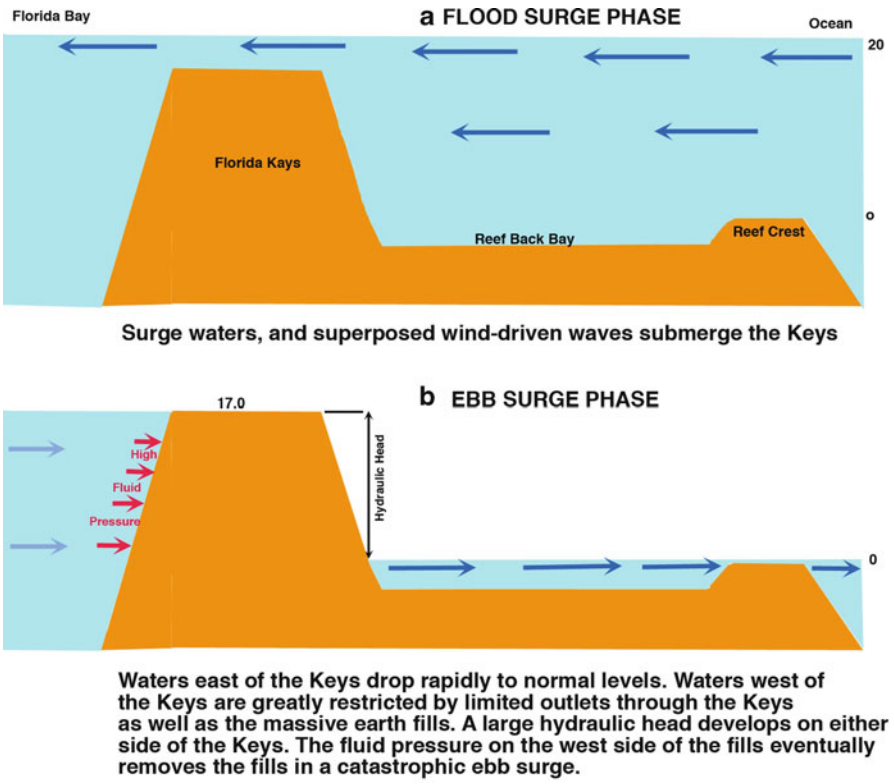

Fig. 8.10 Surge dynamics in the 1935 Hurricane. (**a**) Flood surge sweeps rapidly over the Florida Keys as the hurricane makes landfall. (**b**) Ebb surge starts to move ocean ward as the storm crosses over the Keys. The waters on the ocean ward side of the keys move rapidly into the ocean. However, the waters on the gulf side of the Keys are blocked by the fill embankments and passage through the stone viaducts. A hydraulic head develops between the gulf and ocean sides and the hydraulic pressure eventually causes breaks in the fill embankments

workers were washed away. Bodies were found as far as Cape Sable on the other side of Florida Bay. The U.S. Army Corps of Engineers (1935) estimated that 446,000 cubic yards (338,960 m^3) of fill were eroded from the railroad embankments between Windley Key and Lower Matecumbe Key alone (Fig. 8.1). Many detailed eyewitness accounts of the surge and wind damage are summarized by Knowles (2009).

My interpretation of the surge dynamics is given in Fig. 8.10. As the storm approached the Keys, the onshore winds (Fig. 8.8) pushed ocean waters over most of the Keys (Fig. 8.10a). As the hurricane front moved into the Gulf of Mexico the winds on the back side (Fig. 8.8) blew offshore. The waters in the bay and reef tract were now moving toward the ocean (Fig. 8.10b). However, the waters on the north side could not drop as fast because of the blockage by the earthen fills and the stone piers of the railroad viaducts.

As the bay waters to the south of the Keys began to drop, a hydraulic head developed between the north and south sides of the embankments (Fig. 8.10b). Fluid pressure built up on the gulf side of the fills and eventually they failed quickly and violently. The fill at Snake Creek was washed away and Gulf waters continued to flow seaward for a day after the hurricane landfall (Fig. 8.9b).

Drye (2002) reports several examples of this seaward wind and water flow (ebb surge). Railroad ballast was found on the Alligator Reef Lighthouse catwalk, 5 miles to the south. The railroad track between Grassy Key and Long Key was washed to the south (seaward) of the right of way.

8.6 Aftermath

The 1935 Florida Keys Hurricane is the only natural disaster that launched a congressional investigation (U.S. Congress 1936). The main impetus for the hearings was the loss of so many veterans of World War 1. The volume is rich in details and is recommended reading for those interested in this disaster.

As violent as it was, the 1935 hurricane did not destroy the railroad. Cars were washed away, stations were destroyed and rails removed in some places. However, the bridge structures were almost unscathed. This is a testament to the engineering skills of Flagler's engineers. Railroad business had decreased over the years and the railroad was in receivership. Eventually, The 50 million-dollar railroad was sold for 640,000 dollars to the State of Florida.

The new highway (now U.S 1) was built on the old railroad right of way using the original bridges. The state eventually replaced all the bridges but left the old ones in place as fishing piers. Gallagher (2003) notes, "the state put in new bridges but left all the railroad filled causeways in place, then added much more fill to raise the land levels".

Hurricane wind and water damage removed most of the homes. The Red Cross and the Florida ERA built 28 "hurricane-proof homes". These are the most unique homes in America. The house foundations (Fig. 8.11) were concrete cisterns dug and cemented into the coral limestone – (Fig. 8.11a). The purpose of the cisterns was to raise the homes above minor storm levels and to store precious rainwater that fell on the roof. Steel reinforcing bars were placed in the base and concrete was poured around them. The concrete was one foot thick on the outside and in a reinforcing interior wall and on the roof. Several of these houses are still occupied in Islamorada (Fig. 8.11b). The authorities also built a hurricane resistant structure for a community center. It is now the Islamorada Branch of the Monroe County library. Several years ago, an addition was made to the library for a shelter room. That was also built to Category 5 standards as a "refuge of last resort". The writer heard an interesting story from a local inhabitant. A decade ago, one of the Red Cross houses was to be demolished for a resort development. The wreckers brought a heavy ball to knock down the home. The ball bounced repeatedly off the home. Eventually, it had to be removed by dynamite!

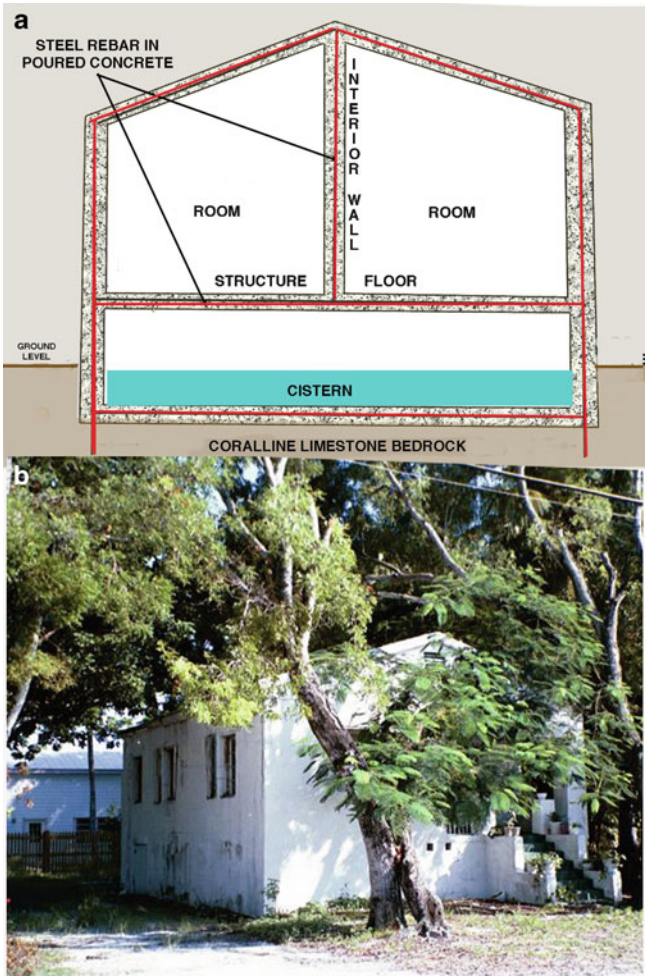

Fig. 8.11 "Hurricane proof" homes built for the survivors by the Red Cross. (**a**). Schematic design of homes built by the Red Cross after the 1935 hurricane. (**b**) One of several surviving houses today. The ocean is visible at the *left* of the home

After the storm, the U.S. Government acquired the railroad right of way and used many parts of the right of way to build U.S. 1. Engineers used the railroad viaducts to mount 2 lane roadways and the fills were re-built (Fig. 8.3b). In subsequent decades, the original bridges were each replaced by modern concrete spans built along the old roadways (Fig. 8.12). The old vaulted viaducts were left as fishing piers, along side of the new bridges (Fig. 8.12a).

At the same time "canal-type" development surged in the Middle and Lower Keys (Fig. 8.12b). In this type of development, channels are cut into the land and the dredged material is placed on the adjacent land to raise its level. This type of

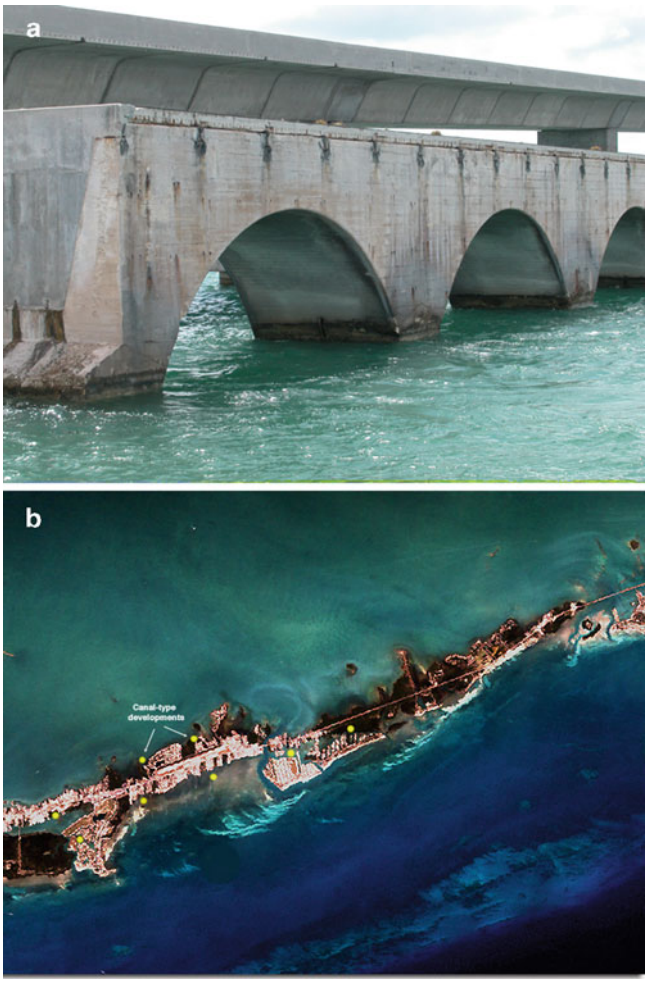

Fig. 8.12 The Florida Keys today. (**a**) Modern bridge (*rear*) next to the original vaulted railroad trestle and former roadbed of U.S. 1. The older structure was retained as a fishing pier. (**b**) Canal-type developments on the Island of Marathon. This type of development is widespread, even though it restricts tidal flow

development allows storm surge to penetrate the coast more deeply, slows tidal flow and cause stagnation in the canals.

In summary, most of the original anthropogenic blockages to tidal flow in the Florida Keys have not been removed and resort development has added many more impediments to water exchange. The barriers that restricted tidal flows before

the hurricane have not been removed. In addition, new canal-type developments have flourished, in summary, the tidal restriction in the Florida Keys is probably *greater* than it was in 1935. The Keys have an evacuation time of 36 h. What will happen in a future Keys hurricane? Have we learned the lessons from the past?

8.7 Lessons for Our Coastal Development

Why concern ourselves with an old hurricane that affected so few people? The answer is simply that it is a harbinger of future damage. Hurricanes hit South Florida with great frequency. Development has soared and canal-type developments and causeways that restrict tidal flow are common here and elsewhere along the U.S. Atlantic and Gulf coasts.

The Tampa- St. Petersburg area, not far from the Florida Keys, is one of the best U.S. examples of how development has reduced natural tidal flow. In 1950, there was little development in Boca Ciega Bay on the east side of St. Petersburg (Fig. 8.13). The picture is far different today. The degree of tidal restriction here was recently described in a hydrologic study by Wang et al (2011). They state (p.50–51):

> "Between the 1940's and 1950's, extensive dredge and fill construction was conducted in Boca Ciega Bay. The engineered islands, as well as the construction of several causeways, resulted in significant reduction of back-bay area and thus a continued decrease in the tidal prism.

Satellite photos (Fig. 8.13) show the degree to which mangrove areas have been converted into canal-type developments and causeways have been placed across Tampa Bay. The causeways are built of fill with only limited passage for tidal waters.

Hurricanes are common in the Gulf of Mexico. They have both passed parallel to and normal to the Tampa-St. Petersburg shoreline. Figure 8.14 shows the wind field for the more common coast-normal track. As the hurricane approaches the coast the southerly flow at the front will push water into Boca Ciega Bay and Tampa Bay. Two bridges and a causeway cross Tampa Bay. Tampa Bay terminates in two funnel-shaped estuary branches (Old Tampa Bay and Hillsboro Bay). The waters in such a funnel-shaped estuary rise as they are confined progressively inland. As a consequence, there will be severe flooding at the north ends of these two waterways.

In far narrower Boca Ciega Bay, the flooding will be much worse both in the flood and ebb surge phases. The degree of flooding here will be severe when canal-type developments retard incoming and outgoing waters.

Canal-type developments and filled causeways are most abundant in New York, New Jersey and Florida. These states have the highest population and population densities (Zhang and Leatherman 2011) in their coastal areas. In a time of rising sea level and increasing hurricane frequency, this poses a problem in the future. We must plan coastal developments to be safe in the changing conditions our coastal areas will experience in the future.

Fig. 8.13 Satellite view of the Tampa Bay-St. Petersburg area showing extensive "canal type" developments along Boca Ciega Bay (NOAA). *Inset* map shows the absence of appreciable development in 1950

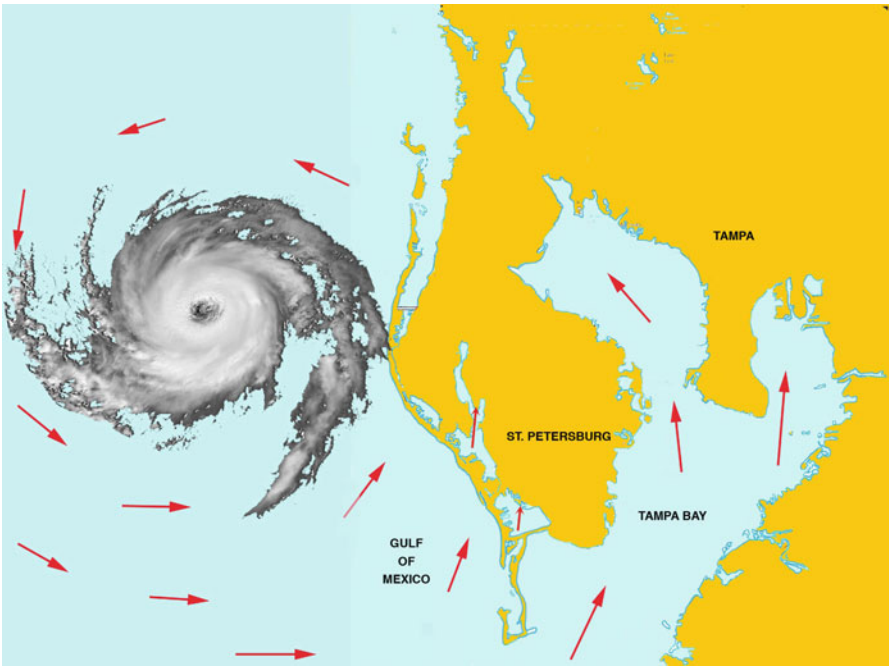

Fig. 8.14 Wind field for a hurricane moving at a right angle across the shoreline into Tampa Bay. The counterclockwise flowing winds will drive estuarine waters into the narrowed cross section of Boca Ciega Bay. Major flooding will develop here and in the *funnel shaped* branches of Tampa Bay. These structures will also impede the return of waters into the Gulf after a future hurricane

8.8 Conclusions

In areas where hurricanes are common, it is essential that we not restrict the tidal prism by development. The 1935 Florida Keys scenario is an extreme case. However, canal - type development and filled causeways are abundant in heavily populated coastal areas of New York, New Jersey and Florida. Canal type developments are environmentally harmful and cut off or retard tidal flow. If passages are required across broad bays, viaducts on piles, rather than filled causeways must be used. This reduces the retardation of tidal flow, and the potential for catastrophic flooding in highly – developed coastal areas such as the Tampa-St. Petersburg region.

Sea level is rising, climate is changing and many tropical meteorologists feel that hurricane frequency will rise in the next decade. We have yet to experience a direct hit on a heavily populated developed coastal area. Such an event is a certainty in the future. We must consider the future threats to the inhabitants of heavily populated coastal areas as we continue to develop them.

References

Boss SK, Neuman AC (1995) Hurricane Andrew on Northern Great Bahama Bank: insights into storm behavior on shallow seas. J Coast Res Special Issue no.21:24–48

Drye W (2002) Storm of the century: national geographic books. National Geographic Society, Washington, DC, 326p

Gallagher D (2003) Florida's great ocean railway-building the Key West extension. Pineapple Press, Sarasota, 198p

Herbert PJ, Jarell JD, Mayfield M (1992) Greatest storms of this century (and other frequently requested facts) NOAA Technical Memorandum NWS NHC-31, U.S. Department of Commerce, Washington, D.C. 40p

Hoffmeister JE, Multer HG (1968) Geology and origin of the Florida Keys. Geol Soc Am Bull 79:1487–1502

Hoffmeister JE, Stockman KW, Multer HG (1967) Miami limestone of Florida and its recent Bahamian counterpart. Geol Soc Am Bull 48:175–190

Houston S, Powell MD (2003) Surface wind fields for Florida Bay Hurricanes. J Coast Res 19 (3):503–513

Knowles TN (2009) Category 5 – the labor day hurricane. University of Florida Press, Gainesville, 349p

Krayer WR, Marshall RD (1991) Gust factors applied to hurricane winds; preprints:eight international conference wind engineering, Association for Wind Engineering, London, Ontario, Canada

Powell MD, Dodge PP, Black ML (1991) The landfall of Hurricane Hugo in the Carolinas-Surface winds distribution. Weather Forecast 6:379–399

Rappaport E (1992) Preliminary report: hurricane Andrew, 16–28 August 1992. National Hurricane Center, Miami, 28p

Saffir H, Simpson R (1974) The hurricane disaster potential scale. Weatherwise 27:169–186

U.S. Army Corps of Engineers (1935) Storm surge washout damage: USACE chart file 3-16-10, 409, dated 21 Oct 1935

U.S. Congress, House of Representatives (1936) Florida hurricane disaster hearings, Report No. 2899, 74th congress, second session, 29 May 1936

Wang P, Beck T, Roberts TM (2011) Modeling regional scale sediment transport and medium-term morphology change at a dual-inlet system examined with the coastal modeling system (CMS): a case study at Johns Pass and Blind Pass. Coastal Education and Research Foundation, West-central

Zhang K, Leatherman S (2011) Barrier island populations along the U.S. Atlantic and Gulf Coasts. J Coast Res 27(2):356–363

Chapter 9
Coastal Flooding Hazard in Low-Tide and High-Tide Coasts: Evidence from the North Aegean Coast

Sotiris A. Lycourghiotis and Stathis C. Stiros

Abstract Based on the analysis of high quality tide gauge data, for the first time available, we have analyzed the relationship between astronomic and meteorological tide in the harbor of Alexandroupolis, in the northern coast of the Aegean; in this area the tide takes the max value for the whole region, but is still small (<10–20 cm). Our analysis was based on a step-by-step geodetic approach, and not an automatic procedure which may miscalculate the periodic components in short-period records. A further comparison of these data with data from other coasts with high tide (several meters) revealed that the amplitude of common surges in the Aegean is high, occasionally of the amplitude of extreme surges recorded in other regions, but the risk of flooding much higher. The ratio of the meteorological versus the astronomic tide in the Aegean is high, of the order of 40 over relatively long periods, about one or two orders of magnitude higher than in high-tide coasts. For this reason intervals with surges leading to flooding are limited to a few hours per day along high-tide coasts (during the high peaks of the astronomical tide), while in low-tide coasts such as the Aegean, in which the total tide is controlled by surges, the risk of flooding is high 24 h/day.

9.1 Introduction

The various costal constructions such as quays, buildings, roads, sinks are built to elevations are adapted to usual periodic and quasi-periodic oscillations of the sea level in each site in the way that they are built in elevations offering functionality and protection from flooding. Harbours for instance are unusual in the parts of the coasts where the tide leaves the sea bottom exposed, fish-tanks since the Roman

S.A. Lycourghiotis (✉) • S.C. Stiros
Geodesy and Geodetic Applications Lab, Department of Civil Engineering,
Patras University, Patras 26500, Greece
e-mail: lykourgiotis@upatras.gr; stiros@upatras.gr

C.W. Finkl (ed.), *Coastal Hazards*, Coastal Research Library 6,
DOI 10.1007/978-94-007-5234-4_9,

time are constructed with their channel to the open sea corresponding to the high water level in order to permit renewing of the water but avoid fish to escape, and houses and other constructions are built above the high water line in order to avoid flooding. Still, the risk of flooding during unusual high waters is always present, and in spite of the numerous studies, efforts and regulations in various countries the impacts of flooding are serious in various regions.

Coastal flooding risk is associated with meteorological effects. In the last years numerous studies were focusing on surges (meteorologically-driven temporal changes of the sea-level) in order to identify the possibility of flooding of low-lying coastal areas (Pirazzoli et al. 2006). Still, the striking majority of these studies were confined to areas with astronomical tides of high amplitude (several meters) and hence the characteristics and the significance of surges in low-tide (average tide $<$0.5 m) areas remain practically unknown (Martin et al. 1991).

In this study we try to shed some light to the problem of surges in the Aegean, a closed sea with low-amplitude ($<$10–20 cm) astronomical tide. In this area the hazards of flooding are poorly known, but definitely high. In our study we used digital signal analysis techniques and analyzed hourly digital recordings covering a 6-month period from the harbor of Alexandroupolis, provided by the Hydrographic Service of the Hellenic Navy. This record is definitely short, but it represents the first high resolution and quality data that have ever been available for a study in this region and are adequate to provide an answer to our problem.

The main output of this study is that even in absence of extreme events the ratio of the meteorological versus the astronomic tide of the component is high, of the order of 40 over relatively long periods and is in high contrast with the corresponding situation in high-tide coasts, in which this parameter is one or two orders of magnitude lower and the surges exceed the astronomical tide only up to a few hours per day. An implication of this result is that the risk of flooding is high in the Aegean 24 h/day, while in areas of high tide this risk is significant only during the short periods corresponding to maximum values of the astronomic tide.

Fluctuations of the sea level recorded by tide gauges reflect the superimposition of two effects, the astronomic and the meteorological tide. The first is actually time-predictable. The latter, usually known as surges, represent rather random meteorological effects tending either to raise (positive surges) or lower the level of the sea defined by astronomic effects (Pugh and Faull 1983; Pirazzoli 2000).

9.2 The Importance of Understanding Surges

The study of surges is important for three reasons. First, meteorological tides (surges), in contrast to the astronomic tide, are not predictable, because these are due to combination of factors such as winds and changes of the barometric pressure. Hence these are poorly known and their understanding is mainly based on stochastic approaches (Pirazzoli et al. 2007a). Second, meteorological tides may be associated with flooding events (De Kraker 2006) or with extreme water lows

(negative surges) causing problems to certain harbors. Third, their effects may be amplified with time, especially in the framework of the climatic change process (Pirazzoli et al. 2006); the case of Venice is a characteristic example (Pirazzoli and Tomassin 2002).

Numerous studies have focused on surges in the last years, mainly in order to identify the possibility of flooding of low-lying coastal areas (Pugh and Faull 1983; McKenzie and Parlee 2003; Pirazzoli et al. 2006, 2007a,b; Marcos et al. 2009; Mercer et al. 2002; Zhu and Li 2008; Wood 2001); still, the striking majority of these studies were mainly confined to areas with high amplitude in the astronomical tide; hence the characteristics and the significance of surges in low-tide areas remain practically unknown.

In this study we try to shed some light to the problem of surges in the Aegean, a closed sea with low-amplitude tide (mean tide between 3 and 18 cm – Hydrographic Military Service 1981). In this area the hazards of flooding are poorly known, but definitely high. For instance, a rather usual surge in 1980 led to the overriding and failure of costal barriers protecting low-lying and reclaimed land in a major delta next to the city of Thessaloniki (N Greece), causing major catastrophes and permanent loss of land (Stiros 2001); a mini Katrina-type disaster.

The main finding of this study is that the characteristics and implications of meteorological tide in this low-tide area are very much different than in other areas, and the associated hazard of flooding of low-elevation coastal areas is much higher, for surges are potentially hazardous 24 h/day.

9.3 Data

In the present study we analyzed hourly recordings from the harbor of Alexandroupolis (40° 50′ N, 25° 52′ E) situated at the NE edge of the Aegean Sea. This record is important because Alexandroupolis is situated at the northern part of the Aegean Sea where mean tide is maximum (±9 cm; see Fig. 9.1c), while the tide in the other Aegean harbors is of the order of ±2–5 cm (Hydrographic Military Service 1981).

The record, available by the Hydrographic Service of the Hellenic Navy, covers the period between 1/1/2001 to 6/30/2001. This record is shorter than records examined by other investigators in the past (up to 7 years; Tsimplis 1992), but it has several advantages which make its suitable for the analysis of surges: (1) it derives from digital data, (2) the frequency of sampling is higher (1-h recordings), (3) time series are continuous, without gaps, and (4) data are free of certain systematic errors affecting older records thanks to a new procedure for tide-gauge operation adopted by the Hellenic Hydrographic Service some years ago.

The available data are plotted as a function of time in Fig. 9.1a. This record is thereafter regarded as the (original) time series #1.

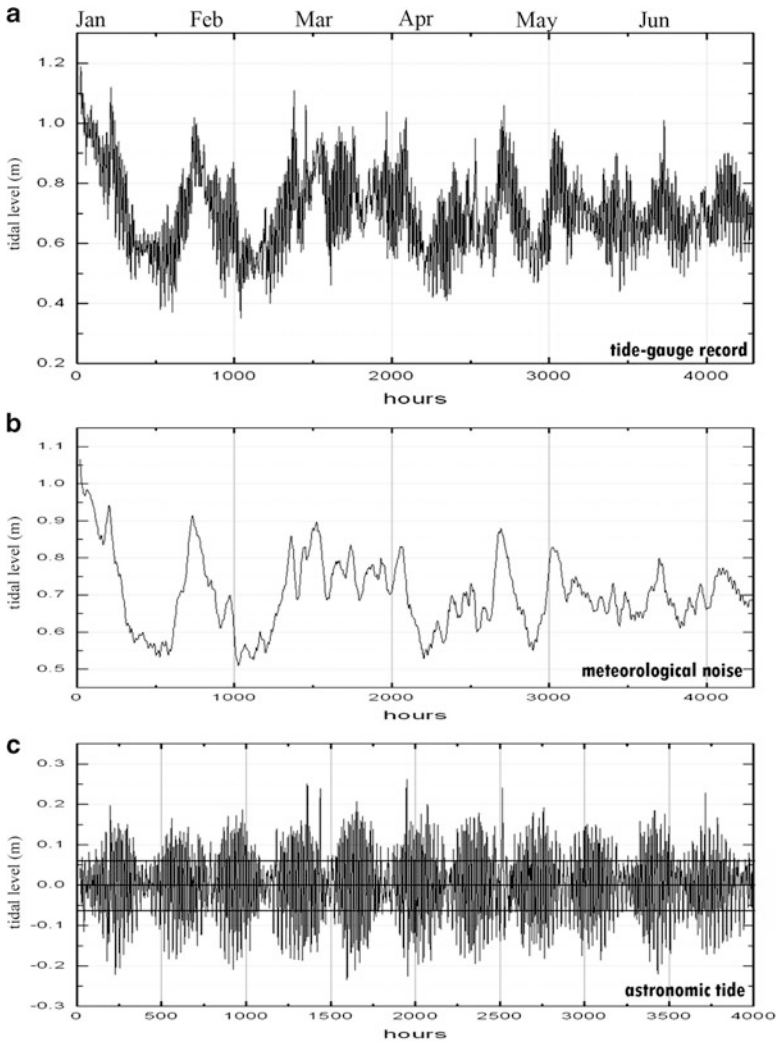

Fig. 9.1 (**a**) Sea-level fluctuations recorded in the Alexandroupolis port during the first semester of 2001 (hourly data). This time series (time series #1) corresponds to the superimposition of the meteorological tide on the astronomical tide (**b**) Long-period signal in the time series in (**a**) obtained using a moving average filter of amplitude 35 h. This time series broadly corresponds to the meteorological tide (time series #2). (**c**) Residual of time series shown in (**a**) minus that shown in (**b**), roughly corresponding to the astronomical tide (time series #3). In (**c**) *parallel lines* indicate the mean sea-level and the mean tide (After Hydrographic Military Service 1981)

9.4 Methodology

Recordings T_j of tide gauges at time j consist of two parts: the astronomical tide, T_{aj}, and a non periodic component, T_{mj}. The first can be represented as the sum of numerous periodic functions *i* of the type

$$T_{aj} = \Sigma \alpha_i (cosw_i t_j + \Phi_i) \tag{9.1}$$

where i stands for each tidal component (constituent) and w_i, a_i and Φ_i indicate the corresponding angular frequency, amplitude and phase, respectively. The second reflects the combined effect of meteorological effects (surges).

Obviously the total tide (tidal recording) is defined by the equation

$$T_j = T\alpha_j + Tm_j \tag{9.2}$$

The values of T_j are available from tide gauges. On the other hand, the astronomic tide T_{aj} can be computed at each time j. Thus, the meteorological tide can be easily estimated from Eq. (9.2). Tidal constituents in the Aegean have been computed by Tsimplis (1992) on the basis of an approximately 7-year long tidal record. However, this record contained gaps and recordings that were recently recognized to be contaminated by certain systematic and random errors (P. Nicolopoulos, Hydrographic Military Service, personal communication); a mater discussed elsewhere in details.

The analysis of tidal data is usually based on standard computation software. Our data set is short and of small amplitude. On the other hand, the meteorological tide exceeds the astronomic tide. Therefore, in order to obtain more objective and testable data, our analysis was based on digital signal analysis techniques from a zero basis. This is mostly based on least-squares and the MATHEMATICA® software in order to avoid pitfalls. In addition, the basic results of our analysis (periods of principal tidal constituents) were tested against the corresponding estimates of other investigators, as it is explained below.

At a *first step* we used a filter to remove short-wavelength effects from the original time series #1, in particular a moving average filter. Tests were performed with filtering of variable width (5, 9, 13, 17, 21, 29, 35, 43 hourly recordings), and finally the 35 point moving average was selected. This is because it leads to the smoothest curve (Fig. 9.2). Moreover, it corresponds to a period approximately 30% longer than the maximum diurnal constituent (approximately 26 h) and hence eliminates both the semidiurnal and diurnal effects. Finally, it represents an approach well adopted in the literature (Keruss and Sennikovs 1999). This smoothed time series, thereafter called them series #2, is regarded as an accurate approximation of the meteorological tide, given that the tidal range is small (Hydrographic Military Service 1981) and the long-period tidal constituents in the Mediterranean are negligible.

At a *second step* we tried to compute the astronomical tide and confirm the significance of our results through a comparison of the computed tidal constituents

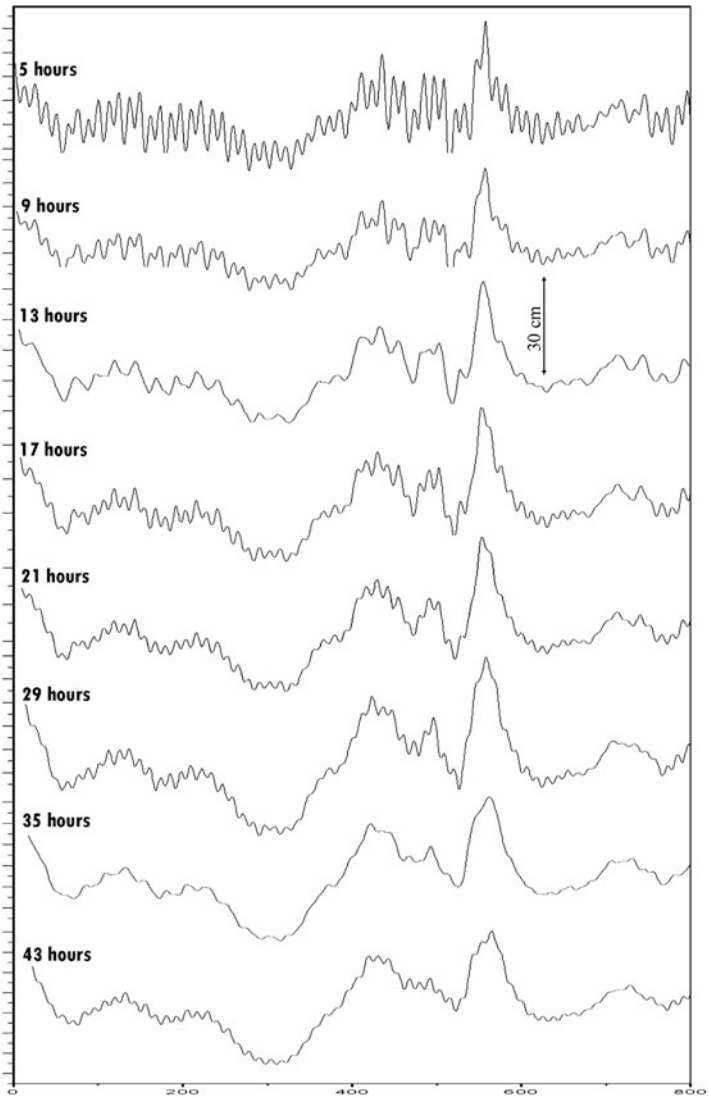

Fig. 9.2 The time series #1 of Alexandroupolis (1/1/2001 to 30/6/2001) tide-gauge record after a moving average filter of variable width. The 13 and 35 h filter leads to the best results for they eliminate both the semidiurnal and diurnal periodic components

with those computed by other investigators. Using Eq. (9.2), the smoothed time series #2 was subtracted from the original time series #1 and the residual corresponds to a new residual time series #3 conspicuously approximating the astronomic tide. If this hypothesis was correct, the spectrum of this last time series would lead to reasonable results. Hence, analysis of the time series #3 approximating the astronomical tide using FFT was used to define the periods (frequencies) of the

dominant tidal constituents. These estimates were then compared with those of other authors (Tsimplis 1992, 1994) and this led to an assessment of our results.

At a *third step* the unknown amplitudes and phases of each constituent and the time series of the astronomical tide were computed using conventional least square techniques and Eq. (9.1).

At a *fourth step* we further analyzed the meteorological noise as a function of the time and of the amplitude of the astronomical tide.

9.5 Data Analysis and Results

The original time series #1, the smoothed time series #2 using a 35-h moving average filter approximating the meteorological noise and the residual time series #3 approximating the astronomic tide, as they explained above, are shown in Fig. 9.1. Figure 9.1a shows the Sea-level fluctuations recorded in the Alexandroupolis port during the first semester of 2001(time series #1). It may be seen a quasi-periodic signal with amplitude of about ±40 cm. A quasi-periodic signal with max amplitude of ±50 cm is illustrated in time series #2 (Fig. 9.1b), while a clear periodic signal with mean amplitude of ±10 cm is illustrated in time series #3 (Fig. 9.1c). It is evident that no extreme surges were observed during the time interval examined. Figure 9.2 shows time series #1 after a moving average filter of variable width.

Using the FFT technique we computed the dominant frequencies of the time series #3 approximating the astronomic tide shown in Fig. 9.1c. Five peaks are clearly visible in the spectrum obtained (Fig. 9.3). These peaks correspond to periods of 6 months and can be easily identified with the O1, K1, N2, M2 and S2 tidal constituents.

Table 9.1 summarizes our results, as well as the values computed by Tsimplis (1994) and the corresponding theoretical values (Tsimplis 1992). All these values are consistent and indicate that the aforementioned approach for computing the meteorological tide is satisfactory.

Subsequently we computed the amplitude and the phase of each of these five main tidal constituents.

Based on Eq. (9.1) we formed a system of equations with five periodic terms corresponding to the computed tidal constituents. The number of equations is equal to the length of the time series, the unknowns were the amplitude and phase of each constituent, ten in total, and the fixed term was the corresponding value of the residual time series #3 (i.e. of the time series approximating the astronomic tide). This system was solved using conventional least squares techniques and the Mathematica® software. The five unknown parameters were computed and are shown in Table 9.2. Subsequently, the time series of the astronomic tide was composed using Eq. (9.1) and the parameters of the previously computed five main constituents. This new computed time series #4 is practically similar to time series #3 shown in Fig. 9.1c, with differences of the order of mm.

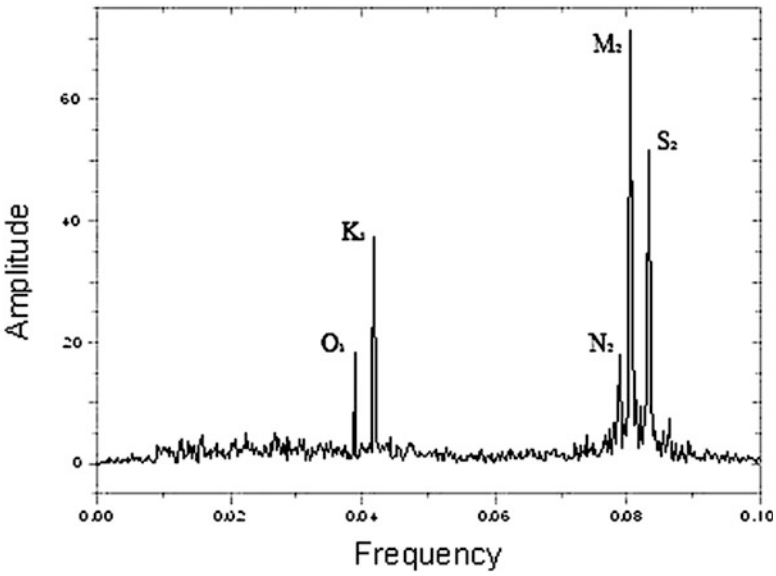

Fig. 9.3 The main frequencies of the tidal record determined by applying FFT to the time series #3 shown in Fig. 9.1c

Table 9.1 Frequencies of the significant tide components for the Alexandroupolis harbour

	Computed in this study	Theoretical values *Tsimplis* 1992	Computed by *Tsimplis* 1994
M2	0.08081112	0.080515297	0.08039732
S2	0.08333138	0.08333332	0.08333333
2N2	0.077965491	0.077459334	0.0774871
K1	0.041766104	0.04178855	0.04178075
O1	0.038746933	0.038729667	0.03873065

Table 9.2 Amplitude of the mean tide components (in cm)

	Amplitude computed in this study (cm)	Computed by *Tsimplis* 1994
M2	7.25	7.14
S2	5.41	4.96
N2	1.76	1.30
K1	3.83	2.60
O1	1.91	1.29

9.6 Tidal Characteristics of the Alexandroupolis Harbour

The tidal characteristics of the Alexandroupolis harbour are shown in Fig. 9.3 as well as in Table 9.2. The results achieved, using 6-month high accuracy data, seems to determine very well the tidal constituents. These data also confirm that the astronomical tide in the Alexandroupolis harbour is of mixed type.

As it can be derived from Fig. 9.1b, the surge oscillation in winter and spring is about 40–45 and 25–30 cm, respectively. This is in good agreement with available sailing information (Hydrographic Military Service 1987), since at the Alexandroupolis port prevail north winds with a force of about 15–20 knots during the winter and 10–15 knots during the spring. The oscillation of the mean sea level expected is about ±40 and ±30 cm during winter and spring, respectively (idem).

9.7 Astronomic versus Meteorological Tide

No extreme events were recorded (Fig. 9.1b) during the study period. However, the available data allows shedding some light on the relationship between the astronomical and the meteorological tide. An efficient way to present this relationship is to compute the ratio between these two variables. The problem in this approach is that due to their periodic character, the amplitude of each of these tides temporarily tends to zero and hence the corresponding ratio has no significance. In order to avoid this problem, we used a band-pass filter excluding from our data (time series #2 and #3) very small values. The amplitude of this filter was selected ±0.02 m, and this led to somewhat shorter time series.

Subsequently, the ratio between the remaining instantaneous values of astronomical and of the meteorological tide was computed and plotted in Fig. 9.4. It is

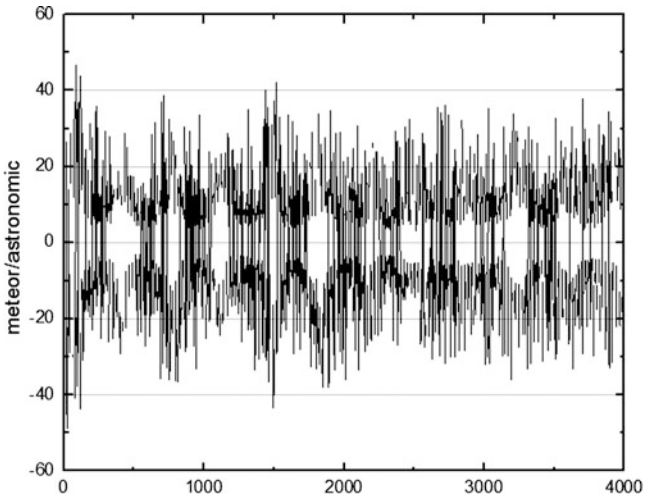

Fig. 9.4 Ratio of the amplitude of the instantaneous values of the meteorological tide (time series #3) versus the astronomic tide (time series #4) as a function of the time for the interval examined. A band-pass filter of amplitude of 2 cm as been used in the astronomic tide to avoid very high ratios. For this reason the number of data in this plot is smaller than in time series #3 and 4

evident from this plot that this ratio is practically in the range 10 to over 40 for most of the period examined.

9.8 Flooding Hazard in the Aegean and in Other Low-Tide Regions

Evidence summarized in Fig. 9.4 is surprising, for it shows that even in absence of extreme meteorological events, the tidal record in the Alexandroupolis harbour is controlled by surges. This is a rather unexpected result, worthy of further analysis because surges represent a threat of flooding for coastal areas.

In order to shed some more light on this effect, we compared tidal data from a representative port in the English Channel with data from Alexandroupolis. Especially to emphasize the differences between these two harbours, we compared a 3-day record from the port of Dover, during a period of an *important* surge (26–28 February 1990, max amplitude 0.7 m; Pirazzoli et al. 2007b) with a record of similar length from Alexandroupolis during a *usual* winter surge (1/1/2001 and 3/1/2001, ~0.9 m amplitude). Data in graph form are shown in Fig. 9.5.

The contrast between the two graphs is striking. In Dover the surge lasted approximately 4 days, but it was felt (i.e. sea level was above the maximum theoretical astronomic tide) during four intervals, each up to a few hours long; during the remaining intervals surge was overshadowed by the astronomic tide because the ratio of the maximum surge to the corresponding amplitude of the astronomic tide was two orders of magnitude long than in the Aegean (0.5–0.7 *m*/6 *m*).

In Alexandroupolis, on the contrary, a surge of the same amplitude can only be considered as a common event, but it affects the coast during the whole of the study period. Since the hazard of flooding depends on both the amplitude and duration of surges, it is evident that this risk is much higher in Alexandroupolis (which can be considered as representative of the wider Aegean) than in Dover, which can be regarded as representative of other harbours in higher-tide environments.

A characteristic example of the flooding hazard in Greece is shown in Fig 9.6. Between 25th December 2009 and 1st January 2010 a *persistent* surge led to flooding of numerous coasts in the Aegean and the Ionian Sea.

9.9 Conclusions

The analysis of a short, though detailed and reliable tide record from the Alexandroupolis harbour allowed to estimate the parameters of the five significant tidal constituents, and to separate the astronomic from the meteorological tide.

Although no unusual or extreme meteorological effect was identified during this period, it was found a striking difference in the relationship between the astronomic and the meteorological tide in Alexandroupolis and other Aegean coasts and in the

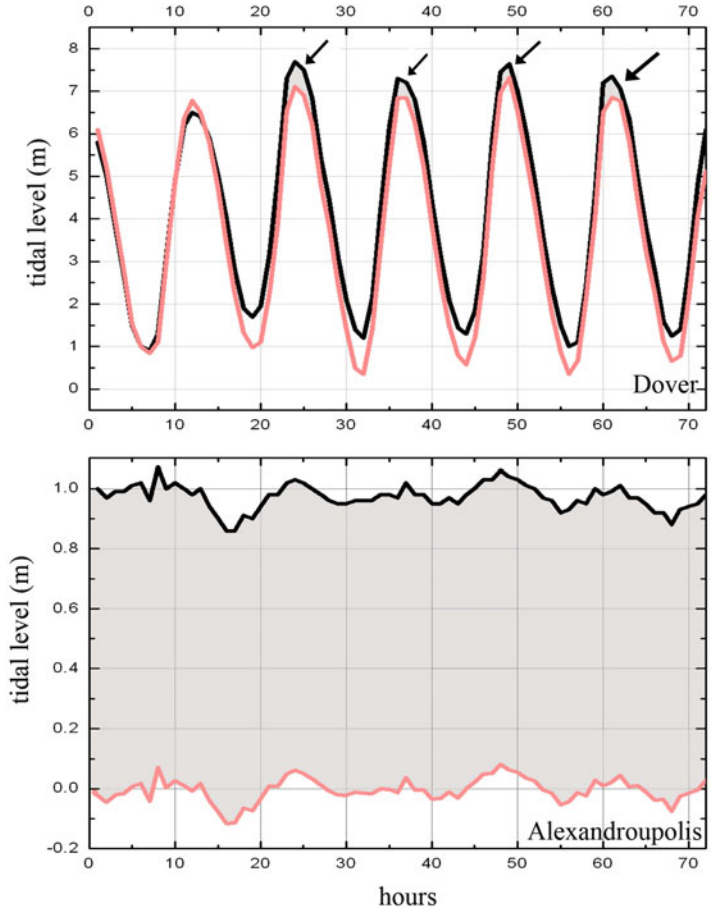

Fig. 9.5 Comparison between total tide (*black*) and astronomic tide (*red*) in the Dover and the Alexandroupolis Port during 3 days-periods (Data from Dover are from Pirazzoli (2007b) and correspond to a significant surge which occurred in 26–28 February 1990, while the data from Alexandroupolis correspond to a usual surge between 1/1/2001 and 3/1/2001). *Shaded areas* indicate the amplitude of the (positive) surge and hence of risk of flooding, which is apparently much higher in the Aegean

English Channel and other high-tide areas. The maximum ratio between meteorological and astronomic tide in the latter is low, of the order of a fraction of a meter, while in the Aegean is high, usually ranging between 5 and 40+. This indicates that various coastal processes in the Aegean are controlled by meteorological events.

An implication of this result is that the threat of flooding events is smaller in the high-tide areas, for this threat exists only during high water periods, i.e. a few hours per day only for meteorological events lasting usually a few days. On the contrary, the threat of flooding is higher in the Aegean because the amplitude of surges

Fig. 9.6 A characteristic photo of a surge lasting for several days in numerous Greek coasts, Mytikas, W. Greece mainland (coordinates $\varphi = 38.66848^{\circ}$, $\lambda = 20.949240^{\circ}$); photo taken at December 25th 2009 by the authors

(common values of the order of 40–50 cm) is relatively higher than other areas, while their effects are continuously felt and are not temporally dissipated due to astronomic sea-level oscillations.

Acknowledgments We thank the Hellenic Hydrographic Service and especially Mr Petros Nicolopoulos for providing tide-gauge data and for fruitful discussions. Comments by an anonymous reviewer were appreciated.

References

De Kraker AMJ (2006) Flood events in the south-western Netherlands and coastal Belgium, 1400–1953. Hydrol Sci J 51(5):913–929

Hydrographic Military Service (1981) Tide data for the Greek harbours (in Greek), 4th edn, Athens, 1981, p 77

Hydrographic Military Service (1987) Pilot: sailing details for the Greek coasts (in Greek), 3rd edn, Athens, p 495

Keruss M, Sennikovs J (1999) Determination of tides in Gulf of Riga and Baltic Sea. In: Proceedings international scientific colloquium "Modelling of Material Processing", Riga, 28–29 May 1999

Marcos M, Tsimplis MN, Shaw GP (2009) Sea level extremes in southern Europe. J Geophys Res 114:C01007

Martin DM, Speed FM, Thurlow CI (1991) Tidal datum computation in low tide range areas Technical Papers – ACSM-ASPRS Annual Convention 1, p 179

McKenzie K, Parlee K (2003) Climate change: a new challenge for coastal development and infrastructure design. Proceedings, annual conference – Canadian society for civil engineering, pp 391–400. http://lw20.com/2012030713182864.html

Mercer D, Sheng J, Greatbatch RJ, Bobanović J (2002) Barotropic waves generated by storms moving rapidly over shallow water. J Geophys Res 107(C10):3152–3168

Pirazzoli PA (2000) Surges, atmospheric pressure and wind change and flooding probability on the Atlantic coast of France. Oceanolog Acta 23(6):643–661

Pirazzoli P, Tomassin A (2002) Recent evolution of surge-related events in the Northern Adriatic Sea. J Coast Res 18(3):537–554

Pirazzoli PA, Costa S, Dornbusch U, Tomasin A (2006) Of coastal flooding risk on the eastern coasts of the English Channel. Ocean Dyn 56:498–512

Pirazzoli PA, Tomasin A, Ullmann A (2007a) Extreme sea levels in two northern Mediterranean areas. Mediterranee 108:59–68

Pirazzoli PA, Costa S, Dornbusch U (2007b) Flood threat anomaly for the low coastal areas of the English Channel based on analysis of recent characteristic flood occurrences. Ocean Dyn 57 (6):501–510

Pugh DT, Faull HE (1983) Tides, surges and mean sea level trends. Proceedings of symposium on shoreline protection, organised by the Institution of Civil Engineers. Thomas Telford, London, pp 59–69

Stiros SC (2001) Subsidence of the Thessaloniki (northern Greece) coastal plain, 1960–1999. Eng Geol 61(4):243–256

Tsimplis MN (1992) Tide harmonic analysis of Greek ports (in Greek), Hydrographic Military Service, pp 73

Tsimplis MN (1994) Tidal oscillations in the Aegean and Ionian Seas. Estuar Coast Shelf Sci 39 (2):201–208

Wood JF (2001) Tidal dynamics. J Coast Res 2(Spec Issue 31):1–389

Zhu Z, Li B (2008) Modelling of couple waves and tidal currents. J Coast Res Spec Issue 52 "surface water modeling" (Fall 2008), pp 223–234

Chapter 10
Sea Level Rise

James Houston

Abstract Sea level rise in the twentieth century was 1.7 mm/year, and there are different accounts as to whether the rise included a very small deceleration or acceleration. From 1993 to 2012, altimeters have measured a greater sea level trend than the twentieth century trend, but it is not known yet whether this is the leading edge of a sustained acceleration or a fluctuation similar to others that occurred in the twentieth century. The Intergovernmental Panel on Climate Change (IPCC) projected a sea level rise of 0.18 to 0.59 m from 1990 to 2100, but did not include scaled-up ice discharges from ice sheets of Greenland and Antarctica in determining its 0.59 m upper limit. There have been a number of projections of sea level rise to 2100 of 1 to 2 m. These are typically maximum possible projections that do not have probabilities associated with them and, thus, are not directly comparable to the 95%-confidence level projection of the IPCC. Assuming highly improbable/impossible events such as the immediate collapse of the West Antarctic ice sheet with the simultaneous quadrupling of carbon dioxide levels in the atmosphere, sea level could rise as much as 1.7 m by 2100. However, this maximum possible sea level rise by 2100 is not useful in planning and design of flood projects, since it is not typically used even for siting nuclear power plants. Instead, planning and design of flood projects require statistics of sea level projections that are at commensurate probability levels with design-floods. Although IPCC did not fully consider the contributions from Greenland and Antarctica, a recent study that did uses IPCC methodology and projects 5, 50, and 95%-confidence-level rises by 2100. Assuming a standard normal distribution, these projections can be used to determine sea level rise probabilities that are consistent with design-flood probabilities. Sea level rise by 2100 will have significant effects on permanent coastal inundation, flooding from episodic events, shoreline erosion and salinity intrusion. The most appropriate response to sea level rise is limiting the long-term rise to a manageable level and

J. Houston (✉)
Director, Emeritus, US Army Engineer Research Center, 3909 Halls Ferry Road, Vicksburg, MS 39180, USA
e-mail: James.R.Houston@usace.army.mil

C.W. Finkl (ed.), *Coastal Hazards*, Coastal Research Library 6,
DOI 10.1007/978-94-007-5234-4_10,

adaptation to the inevitable rise which will occur. The world must work to reach new agreements limiting carbon emissions and thus limit the long-term rise. But since sea level rise has considerable inertia and will produce an inevitable rise, steps must be taken to adapt to the rise.

10.1 Introduction

10.1.1 Historical Context

Sea level has varied over tens of millions of years. During the Paleocene-Eocene Thermal Maximum over 50 Ma, sea level was approximately 75 m higher than today, and the earth was iceless in high latitude areas with alligators living well within the Arctic Circle (Jardine 2011). The remains of deep-ocean- dwelling foraminifera provide a global oxygen-isotope record, which indicates a long-term cooling and sea level fall the past 5 Ma (Lisiecki and Raymo 2005). About 3 Ma ago, the earth began gradually deepening cycles of glacials and interglacials that involved growth and retreat of continental ice sheets in the Northern Hemisphere. Initially cycles lasted about 40,000 years, but a 100,000-year cycle became dominant about a million years ago. These cycles are generally considered to be due to predictable changes in the earth's orbit known as Milankovitch cycles. However, there are a number of unanswered questions about Milankovitch cycles including reasons for the change in the dominant cycle from 40,000 to 100,000 years.

During the Eemian, the last interglacial period about 120,000 years ago, sea level is believed to have been about 4 to 6 m higher than today with temperatures about 2 to 4°C warmer (Jansen et al. 2007). There has been speculation that the Eemian is a good analogue for the response of sea level to future global warming and, therefore, sea level will rise very rapidly in the twenty-first century. However, van de Berg et al. (2011) determined that Northern Hemisphere solar insolation was much greater during the Eemian than today, concluding, "This is why the Eemian melt-temperature relation provides a poor analogue of a future warmer climate. . ." Moreover, Kopp et al. (2009) determined when sea level in the Eemian was close to the current level, the maximum rate of sea level rise was 0.56 to 0.92 m per century. The Intergovernmental Panel for Climate Change (IPCC) projected a 95%-confidence sea level rise for 2100 that falls within this range (Bindoff et al. 2007).

Sea level was about 120 m lower than today during the height of the last ice age about 20,000 years about (Gornitz 2007). The earth began warming and sea level rising as the earth entered the present interglacial period soon after the peak of the last ice age. The rise of sea level was not constant, but over a period of about 15,000 years, it averaged about 0.8 m a century.

About 5,000 to 6,000 years ago glacial melting had essentially ended, but the earth's lithosphere continued changing in a process known as Glacial Isostatic Adjustment (GIA). GIA is the global response of the earth to changes in ice load

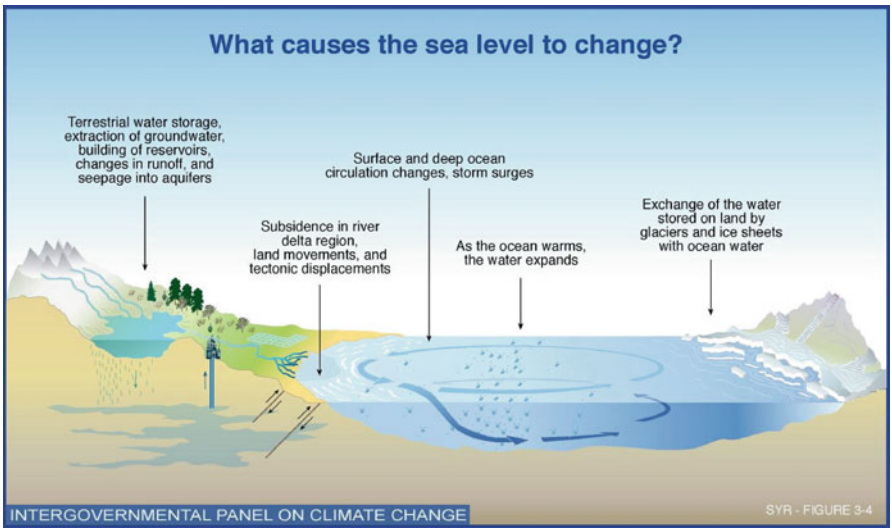

Fig. 10.1 Contributors to relative sea level change (Interagency Panel on Climate Change)

following the last ice age. Fluid mantle material that was forced away from glaciated areas by the weight of massive ice sheets during the last ice age has been returning to formerly loaded areas, and as a result, there have been horizontal and vertical motions over the entire Earth and changes of the sea surface (Peltier 2001). Global sea level was relatively stable, but slowly increasing during this period.

10.1.2 Contributors to Sea Level Rise

Figure 10.1 shows contributors to the sea level rise of about 1.7 mm/year in the twentieth century (Bindoff et al. 2007). Thermal expansion was the primary contributor. Water expands when heated, and in response to global warming, the ocean has been expanding and causing sea level to rise. Melting of glaciers and ice caps also was a major contributor to sea level rise in the twentieth century. There are over 100,000 glaciers and ice caps around the world, many in mountain areas, which are melting and contributing to sea level rise (National Snow and Ice Data Center 2009). The Greenland and Antarctica ice sheets made only small contributions to global sea level rise in the twentieth century, but are expected to make larger contributions in the twenty-first century. Other anthropogenic activities affecting sea level include reservoir impoundment (causing sea level fall) and groundwater extraction (causing sea level to rise, since extracted groundwater eventually finds its way to the ocean through the hydrological cycle). These anthropogenic activities are believed to be almost balanced presently, but

groundwater extraction is expected to make a small contribution to sea level rise in the twenty-first century (Church and White 2011).

Local relative sea level change is caused both by global sea level change and local ground motion and is estimated by subtracting local ground motion (subsidence having a negative sign) from global sea level rise. Local ground motion can be produced by tectonic activity, GIA, subsidence from consolidation of soft sediments, groundwater extraction, and other effects. For example, the ground is rebounding from GIA in high latitude areas of Europe and North America that were weighted down by glaciers during the last ice age, causing a fall in local relative sea level. River delta regions around the world are sinking due to ground subsidence, causing local relative sea level to rise faster than the global average. Relative sea level also is rising faster than the global average at locations such as Chesapeake Bay, United States (US) that bordered ice sheets and were pushed up during the last ice age, but are now subsiding.

10.2 Sea Level in the Twentieth Century

Bindoff et al. (2007) estimated a global average sea-level rise of 1.7 ± 0.5 mm/year during the twentieth century. They cited several sources including estimates by Douglas (2001) and Peltier (2001) of 1.8 mm/year over 70 years and Church and White (2006) of 1.7 ± 0.3 mm/year for the twentieth century. Church and White (2011) determined a trend of 1.7 ± 0.2 mm/year from 1900 to 2009 and Ray and Douglas (2011) a trend of 1.70 ± 0.26 mm/year from 1900 to 2007. Thus a twentieth century sea-level rise of about 1.7 ± 0.5 mm/year has become widely accepted.

Several studies have estimated sea-level acceleration. Jevrejeva et al. (2010) analyzed long-term tide gauge recordings at three locations in Europe and concluded that sea level accelerated an average of approximately 0.01 mm/year^2 over the past 200 years. Douglas (1992) analyzed global tide gauge records and determined a sea-level change of – 0.011 ± 0.012 mm/year^2 from 1905 to 1985 and 0.001 ± 0.008 mm/year^2 from 1850 to 1991. Church and White (2011) used 17 years of satellite altimeter data to estimate empirical orthogonal functions (EOFs), and in conjunction with historical tide gauge data, estimated accelerations of 0.009 ± 0.003 mm/year^2 from 1880 to 2009 and 0.009 ± 0.004 mm/year^2 from 1900 to 2009. Houston and Dean (2011a) analyzed US tide gauges with record lengths of greater than 60 years, extended the global tide-gauge analysis of Douglas (1992) by 25 years, and analyzed revised data of Church and White (2006) from 1930 to 2007. They obtained small sea-level decelerations varying from about –0.001 to 0.013 mm/year^2. Watson (2011) found sea-level decelerations of –0.01 to –0.10 mm/year^2 in four long Australian and New Zealand tide-gauge records.

Sea-level acceleration in the twentieth century has generally been estimated to be between about – 0.01 and 0.01 mm/year^2, which would produce sea level changes of only – 0.05 to 0.05 m in 100 years. The rise during the twentieth century

was essentially linear, with either a small acceleration or deceleration producing a relatively small change in sea level. Ray and Douglas (2011) note "near-linearity" in their analysis of data from 1900 to 2007, saying, "...there is no statistically significant acceleration in global mean sea level over this period." They confirm the conclusion of the seminal paper on acceleration by Douglas (1992) that, "There is no evidence for an apparent acceleration in the past 100+ years that is significant either statistically, or in comparison to values associated with global warming."

10.3 Current Sea Level Rise

Three altimeter satellites, TOPEX (Topography Experiment)/Poseidon, Jason-1, and Jason-1, have measured sea level rise since 1993. TOPEX/Poseidon measured from 1993 to past 2002, Jason-1 from about 2002 to 2009, and Jason-2 since 2008. These satellite altimeters have measured sea-level rise of 3.1 mm/year from 1993 to 2012 (University of Colorado 2012), exceeding the twentieth century trend of about 1.7 mm/year. However, the accuracy these measurements has been questioned. Nerem et al. (2010) noted significant bias of unknown origin between the altimeters, determining a bias of about 100 mm between TOPEX/Poseidon and Jason-1 and about 75 mm between Jason-1 and Jason-2. Watson et al. (2004) used GPS buoys and tide gauges and determined that Jason-1 had an absolute bias of 150 mm. These biases are two to three times the total rise of sea level since 1993. Moreover, Domingues et al. (2008) noted that altimeter and tide gauge measurements agree closely up to 1999 and then began to diverge with altimeters recording a greater trend. They say, "It is unclear why the in situ and satellite estimates diverge, and careful comparison is urgently needed." Disagreement between tide gauge and altimeter measurements is important since tide gauges are used to quantify altimeter bias and drift errors (Nerem et al. 2010).

A few studies have favorably compared tide-gauge and altimeter measurements, but they have shortcomings. Altimeters have recorded remarkable spatial variation in trends over the oceans (Fig. 10.2). Tide gauges are not uniformly distributed across the oceans and therefore miss some of this spatial variation. Therefore, a global trend determined from tide gauges will be biased by an amount dependant on the number of gauges and the degree to which they cover the spatial variation in trend over the oceans. For example, Holgate and Woodworth (2004) compared altimeter measurements with 177 tide gauge records in 13 regions over a 10-year period. However, their tide-gauge records had a significant spatial bias because 7 of the 13 regions were located just in the North Atlantic Ocean (less than 15% of the earth's ocean area). Prandi et al. (2009) compared altimeter measurements with 91 tide-gauge recordings over a 15-year period. However, they weighted the tide gauge recordings equally, producing a spatial bias, since, for example, they had only a single tide gauge recording in the South Atlantic but nine gauge recordings concentrated around the small Sea of Japan. Church and White (2011) addressed spatial bias by using EOFs to reconstruct tide gauge data, but they noted their

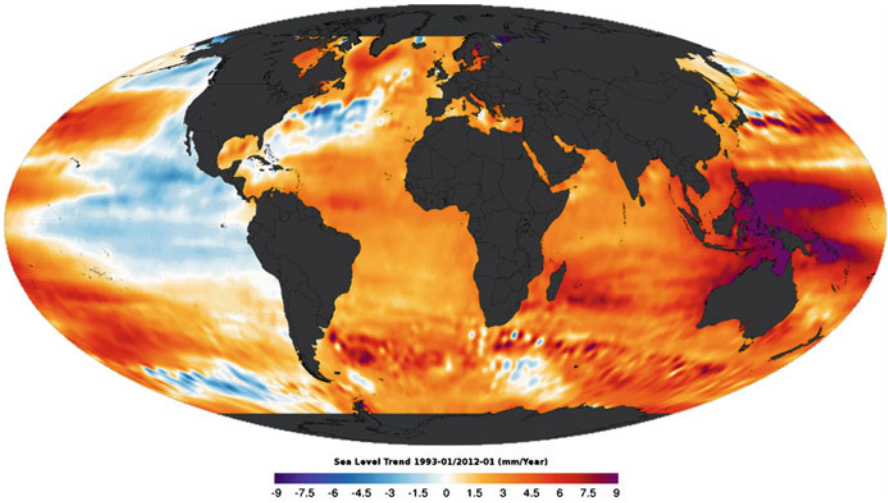

Fig. 10.2 Altimeter measurements of sea level change 1993–2012 (National Oceanic and Atmospheric Administration)

reconstructed data were determined from altimeter measurements and thus not independent of the measurements.

Dean and Houston (2012) determined trends and accelerations recorded by global tide gauges (456 gauges) during the period of altimeter measurements from 1993 to 2011. They reduced spatial bias by having a large number of gauge records with global distribution. They similarly analyzed altimeter data on a 1° by 1° grid covering the oceans. They determined that the tide gauges measured an average trend of 3.0 ± 0.3 mm/year versus a trend of 3.1 ± 0. 4 mm/year measured by the altimeters. Moreover, they developed a method to further reduce the spatial bias due to the tide gauges not being equally distributed and obtained a gauge trend of 3.0 ± 0.3 mm/year. During the 19 years, both the tide gauges and altimeters measured similar decelerations of about –0.04 and –0.08 mm/year^2. Therefore, global trends and accelerations from tide gauge and altimeter measurements agree over the period of altimeter measurements.

The trend of 3.1 mm/year measured by the altimeters though 2011 is higher than the average twentieth-century trend, but not uniquely high. Jevrejeva et al. (2006) analyzed 1,023 gauge records over the twentieth century and showed the global sea-level trend reached a maximum from 1920 to 1945 that was similar to that measured by the satellite altimeters from 1993 to 2011. Holgate (2007) calculated consecutive, overlapping 10-year mean sea-level trends since 1910 for worldwide gauges and found the altimeters have measured only the fourth highest of six peaks in trend since approximately 1910, with the highest trends of 5.31 mm/year centered on 1980 and 4.68 mm/year centered on 1939. Church and White (2011) used 16-year averages from 1880 to 2010 and found the trend measured by the altimeters was not statistically higher than similar peaks during the 1940s and

1970s. Ray and Douglas (2011) used 15-year averages from 1900 to 2007 and found the trend around 1940 was about the same as that measured by altimeters.

Ablain et al. (2009) showed that 3- and 5-year moving averages of the trend measured by the altimeters have continually declined. The 3-year average recently dropped as low as 1 mm/year and the 5-year average approached 2 mm/year. This deceleration may indicate the increased trend measured by altimeters is a fluctuation similar to others in the twentieth century. However, it cannot yet be determined whether the greater trend measured by the altimeters is the leading edge of a sustained rise or a fluctuation similar to others that have occurred in the twentieth century.

10.4 The Threat – Projected Future Sea Level Rise

10.4.1 Introduction

Relative rather than global sea level rise is most important at a location. The present relative sea level change can be determined from tide gauge records at locations around the world and is available online from the Permanent Service for Mean Sea Level (PSMSL) data base at http://www.psmsl.org/data/obtaining/. The data base is described by Woodworth and Player (2003). GPS data of ground motion at locations near tide gauges can be obtained from Étude d'un Système d'Observation du Niveau des Eaux Littorales (SONEL) at http://www.sonel.org/IMG/txt/ULR4_Vertical-Velocities_Table.txt. GIA data are available for each tide gauge location in the PSMSL data base at http://www.psmsl.org/train_and_info/geo_signals/gia/peltier/.

Adding a complication to sea level projections, global sea level rise will not be the same at all locations. Mitrovica et al. (2010) note that ice melting will produce a variable global sea level rise. Presently, the large ice sheets of Greenland and Antarctica produce a gravitational pull that raises local sea level. As the ice sheets melt, the gravitational force they exert lessens, causing local sea level to fall and the water released to flow to the rest of the globe. Similarly, as ice melts, the ground under the ice sheet begins rising pulling mantle material from other locations, causing the ground to subside at these other locations. The earth's rotation introduces a feedback that also affects the spatial distribution of sea level rise. For example, Mitrovica et al. (2001) show that melting ice in Antarctica will raise sea level in the Northern Hemisphere by about 10 to 20% more than the global average. Similarly, melting of Greenland ice will result in average rises lower than the global average in the eastern US and Europe. Melting of mountain glaciers and ice caps will produce lower rises than the global average in Alaska and the west coast of the US, but higher rises in Australia and the South Pacific. Changes in ocean currents also may change the spatial distribution of sea level rise. Hu et al. (2009) show that melting of the Greenland ice sheet could affect the Atlantic overturning current circulation and subsequently raise sea level on the east coast of the US by 0.1 to 0.5 m by 2100. Finally, Katsman et al. (2008) show that even the

effect of thermal expansion will vary regionally from the global average because changes in water temperature and salinity will not be the same everywhere.

Katsman et al. (2011) demonstrate the spatial variability in sea level rise by estimating the effects on the coast of the Netherlands of regional variations of temperature and salinity, melting of glaciers and ice caps, and melting of the Greenland and Antarctic ice sheets. Because the Netherlands is near the Greenland ice sheet and there are glaciers and ice caps melting in Europe, the net effect of these regional differences was to reduce the projected upper limit of a rise by 2100 on the Netherlands' coast by 0.1 m and the lower limit by 0.15 m. At other locations, these same effects could increase sea level rise above the global average.

10.4.2 Projected Maximum Possible Sea Level Rise by 2100

The sea-level-rise section of the 4th IPCC Assessment Report (Bindoff et al. 2007) considered the contribution of ice-sheet melting (called Surface Mass Balance – SMB) in Greenland and Antarctica in its projection of a 95%-confidence level of 0.59 m from 1990 to 2100, but it assumed the flow of ice into the ocean (dynamical ice discharge through marine-terminating glaciers) would continue at rates measured from 1993 to 2003. It estimated sea level could rise an additional –0.01 to 0.17 m above its upper-level projection if the dynamical ice discharge increased linearly with global temperatures. The IPCC typically makes projections from about 1990 to 2100 for comparison purposes, since the first IPCC projections were in 1990.

Projections of sea level rise made by others since the 4th IPCC Assessment Report have typically been higher, generally 1 to 2 m. The difference is usually attributed to greater contributions to sea level rise from the Greenland and Antarctic ice sheets that were projected in these more recent studies. However, a more important factor is that these higher projections are, in general, maximum possible projections with no associated probability, whereas the maximum IPCC projection is at the 95%-confidence level with a 2.5% probability of exceedance. Bindoff et al. (2007) acknowledge that their projection at the 95%-confidence level does not represent the maximum rise that can occur. Projections at the 95%-confidence level and maximum possible projections are not comparable. For most planning and design requirements, projections at the 95%-confidence level or below are appropriate, whereas maximum possible rise projections are rarely appropriate (for example, in the US even siting of nuclear power plants is done at the 99.95%-confidence level and not the maximum possible level).

Nicholls et al. (2011) survey a number of projections of sea level rise by 2100 and from them select what they call a "pragmatic" range of 0.5 to 2.0 m. The 0.5 m is based on a 0.48 m projection by the IPCC at the 95%-confidence level for a mid-level temperature rise scenario of 4.4° C by 2100. However, a level of 0.48 m at the 95% confidence level means that there is only a 2.5% chance that the sea level rise

by 2100 will be greater than 0.48 m, so this is an upper and not lower limit for this scenario.

The upper level of 2.0 m selected by Nicholls et al. (2011) was said to be unlikely to occur and of "unquantifiable probability" and was based on studies projecting rises up to 2.4 m. The upper limit of 2.4 m is from a projection by Rohling et al. (2008) of 1.6 ± 0.8 m that is based on analogy with the rise during the Eemian. Although not covered by Nicholls et al. (2011), Hansen (2007) and later Hansen and Soto (2011) similarly cited the Eemian period and projected sea level rise of 5 m by 2100. However, as mentioned in the Introduction, recent studies show that the Eemian is a poor analogue of sea level response to projected warming by 2100, and the maximum sea level rise in the Eemian when sea level was similar to today was only 0.56 to 0.92 m per century.

Pfeffer et al. (2008) considered glaciological conditions necessary to support projections of multi-meter sea level rise by 2100. They noted the contribution to sea level rise of the Greenland and Antarctic ice sheets consists of SMB and dynamical ice discharge of glaciers into the ocean. They estimated SMB contributes about 30% of the present rise in sea level due to the ice sheets but would only constitute about 4% to a rise of 2 m by 2100. Thus dynamical ice discharge was the major mechanism that could produce large rises in sea level. Their key assumption was that increased temperatures would increase glacier sliding velocities into the ocean. Pfeffer et al. (2008) showed that achieving a rise of 2 m by 2100 would require glacier sliding to accelerate over a decade to velocities an order of magnitude greater than current velocities, and even greater velocities would be required if there were a delay in onset. They noted such velocities far exceed the fastest motion exhibited by any outlet glacier and concluded that increases in sea level greater than 2 m by 2100 were "physically untenable".

The key assumption made by Pfeffer et al. (2008) was that increased temperatures will increase velocities of glacier sliding. This assumption is based on the concept that meltwater during summer months percolates through the glacier and lubricates the ice/rock interface, thereby causing the glaciers to slide more rapidly. A recent study by Sundal et al. (2011) at six Greenland glaciers, however, shows that although this effect causes glaciers to begin sliding during summer months, the warmer the summer, the slower the sliding velocity. They found that during warmer summers the velocity of ice flow was only about 60% of the flow during cooler summers. During warmer summers, there is greater meltwater, but the water begins running off in channels with apparently less water percolating down to the ice/rock interface. With less water lubricating the interface, movement of ice slows during warmer summers compared to cooler summers. Sundal et al. (2011) noted that the same phenomenon was observed by Bingham et al. (2003) and Truffer et al. (2005) for mountain glaciers. Van de Wal et al. (2008) measured a 17-year decrease in the velocity of flow of a Greenland glacier during a period of increased melting due to global warming. Moreover, IPCC (2010) noted that glaciers in southeast Greenland slowed during the recent period of increased temperatures. These observations of actual glacier response to warming invalidate

the key assumption of Pfeffer et al. (2008) and are indicative of the cap in sea level rise by 2100 being less than 2 m.

Nicholls et al. (2011) also considered Rahmstorf (2007) and Vermeer and Rahmstorf (2009) in determining the upper level projection of 2.0 m. Rahmstorf (2007) was the first study that used a "semi-empirical" modeling approach to forecast sea level rise of 0.5 to 1.4 m from 1990 to 2100. His approach attempted to link sea level rise with temperature rise. A subsequent paper by Vermeer and Rahmstorf (2009) increased the rise to 0.75 to 1.9 m. These papers have been criticized in the peer reviewed literature by Holgate et al. (2007), Schmith et al. (2007), Taboada and Anadon (2010), and Houston and Dean (2011b). Since contributions to sea level rise from thermal expansion and glaciers and ice caps are fairly well understood, these relatively large projections hinge on large contributions from the Greenland and Antarctic ice sheets. However, as noted by IPPC (2010), the semi-empirical models were calibrated during past periods of time when contributions from Greenland and Antarctica were almost insignificant. Conditions in the future that are expected to lead eventually to large contributions from Greenland and Antarctica were not acting during the calibration period, leading to questions about how the models could then project into the future.

Rahmstorf (2007) and Vermeer and Rahmstorf (2009) were followed by a series of studies by three authors using semi-empirical models. These studies have received little criticism in the peer-reviewed literature. Jevrejeva et al. (2010), Grinsted et al. (2010), and Jevrejeva et al. (2011) projected rises by 2100 of 0.6 to 1.6, 0.9 to 1.3, and 0.57 to 1.10 m respectively. However, in a recent IPCC workshop (IPCC 2010) attended by over 100 participants who are experts on sea level rise and the Greenland and Antarctic ice sheets, the participants considered semi-empirical models and concluded, "No physically-based information is contained in such models ..." and "The physical basis for the large estimates from these semi-empirical models is therefore currently lacking."

With a portion of the Netherlands below present sea level, the Dutch have a significant interest in projections of sea level rise by 2100 and cannot afford to under predict the rise. Katsman et al. (2011) consider a "severe scenario" of temperature rise that includes the beginning of the collapse of the West Antarctic ice sheet, and they project a global rise by 2100 of up to 1.15 m. Although they consider a "severe" scenario, their maximum projected rise is not the maximum possible rise.

The maximum possible rise can be estimated by determining a cap based on a series of improbable/impossible events. For example, the greatest contribution of Antarctica to sea level rise by 2100 would be a collapse of the West Antarctic ice sheet. The East Antarctic ice sheet is expected to contribute a slight reduction in sea level by 2100, so the worst-case scenario would be collapse of the West Antarctic ice sheet. Bamber et al. (2009) considered sea level rise should the West Antarctic ice sheet collapse and concluded that it could raise sea levels by between 1.9 and 6.4 mm/year. If the collapse were to occur immediately, it would raise sea level from 2012 to 2100 by between 0.17 and 0.56 m. Similarly, Katsman et al. (2011)

consider the rise of sea level should the West Antarctic ice sheet collapse, and they estimate a rise of 0.41 m. So, 0.56 m is likely the maximum possible rise.

Huybrechts et al. (2011) used a global ocean–atmosphere model and determined that sea level would rise only about 0.18 m after quadrupling of carbon dioxide in the atmosphere. Similarly, Ridley et al. (2005) used an ocean–atmosphere model to estimate the contribution that Greenland would make to sea level given a quadrupling of carbon dioxide in the atmosphere. They simulated 3,000 years, and the most rapid contribution to sea level rise during the period was 5 mm/year. The maximum possible rise would be for a contribution from Greenland of 5 mm/year that would begin immediately and produce a rise by 2100 of 0.44 m.

The expected contribution of thermal expansion and glaciers and ice caps outside Greenland and Antarctica to sea level is reasonably well known. Taking the "severe" scenario considered by Katsman et al. (2011), thermal expansion could add 0.49 m and glaciers and ice caps 0.20 m to sea level rise from 1990 to 2100.

Adding all contributions (including the rise of sea level from 1990 to 2012 from Greenland and Antarctica), the maximum possible global rise from 1990 to 2100 would be about 1.7 m. This is a cap on the rise, since it is a sum of highly unlikely/impossible events. This maximum possible rise by 2100 would decline every year that the West Antarctic ice sheet did not collapse and Greenland did not contribute 5 mm/year to a global rise. For example, if neither event occurs in the next 10 years, the projection to 2100 decreases to about 1.6 m. The most recent projections of contributions from Greenland and Antarctica do not point toward rises that would be close to this cap. For example, Graversen et al. (2010) projected a contribution by 2100 from Greenland of 0.0 to 0.17 m and the Arctic Monitoring Assessment Programme (2011) a contribution of 0.10 to 0.19 m. Huybrechts et al. (2011) used an earth-systems numerical model and determined a high-scenario rise for Greenland of about 0.18 m per century over a 500-year period. Greve et al. (2011) used two different global models and projected a total contribution of 0.12 to 0.22 m. Similarly, barring collapse of the West Antarctic ice sheet, Katsman et al. (2011) projected a contribution to sea level rise by 2100 from Antarctica of only −0.01 to 0.07 m.

10.4.3 Projections for Planning and Design Using IPCC Methodology

Maximum possible projections are not useful for project planning and design. For example, in the US, many flood projects are typically designed at the "100-year" flood level (1% chance of being equaled or exceeded in any given year) and even nuclear power siting is designed at the 100,000-year flood level (99.998%-confidence level) and not the maximum possible level.

IPCC methodology provides a range of sea level rise projections with associated probabilities that can be chosen to be consistent with the design-flood probability.

For example, the 100-year flood has a 63% probability of occurring within a 100-year period. The 95%-confidence level projection of IPCC has only a 2.5% chance of exceedance in 100 years and, therefore, is not at a consistent probability level with the 100-year design-flood probability.

Bindoff et al. (2007) did not fully consider contributions of Greenland and Antarctica to sea level rise by 2100, but will undoubtedly do so in its next report due in 2013 to 2014. However, Houston (2012) provides sea level rise projections for 2100 using IPCC methodology and considering the latest trend and acceleration ice-mass losses in Greenland and Antarctica based on satellite measurements. He then adds contributions from thermal expansion and melting of glaciers and ice caps based on information published since Bindoff et al. (2007), obtaining sea level rise projections from 1990 to 2100 of 0.18, 0.48, and 0.82 m at 5, 50, and 95%-confidence levels respectively. Since his projections of individual contributions to sea level rise from Greenland, Antarctica, thermal expansion, and melting of glaciers and ice caps compare favorably with projections in several recent studies, it is likely that the 5th IPCC assessment report will project similar levels from 1990 to 2100

The IPCC methodology can be used to match design-flood levels and sea level rise projections at consistent levels of accuracy by assuming a standard normal distribution. For example, the Dutch plan for the 10,000-year coastal flood level. A 98%-confidence level for sea level rise by 2100 has the same 1% chance of exceedance as the 10,000-year flood has of occurring within 100 years. Using Houston (2012) and assuming a normal distribution, the 98%-confidence sea level rise by 2100 is 1.1 m. Katsman et al. (2011) in a study of sea level rise on the coast of the Netherlands obtained a similar global sea level rise by 2100 of 1.15 m for a "severe scenario" that included collapse of the West Antarctic ice sheet. In the same way, IPCC methodology can be used to match design flood levels and sea level rise with other design-flood levels.

10.5 Coastal Hazards from Future Sea Level Rise

10.5.1 Introduction

Gornitz (1991) notes there are four basic coastal hazards from relative sea level rise – permanent inundation, episodic inundation, increased erosion, and saltwater intrusion of estuaries and aquifers. The vulnerability of coastlines to these threats depends strongly on relative sea level rise. This in turn depends on the average global sea level rise, local variations of sea level rise from the average global rise, and local ground motion. For example, formerly glaciated areas as in parts of Canada or Fennoscandia that are now rebounding with the ground moving up rapidly have a low vulnerability, whereas river delta areas such as the Nile delta

of Egypt, where the ground is sinking rapidly, are highly vulnerable. Impacts depend on factors such as the degree of coastal development and options a local population may have. Sea level rise might not cause great impacts on a coast with little development, whereas an entire low-lying island might be threatened by sea level rise, with the population having no long-term option other than abandonment.

10.5.2 Permanent Inundation

Sea level rise will cause permanent inundation in low-lying areas. Areas most at risk are river deltas, chenier plains, estuaries, lagoons, mudflats, bays, and low-lying islands. River deltas such as those of the Nile, Indus, Irrawaddy, and Ganges-Brahmaputra are heavily populated. In addition to global sea level rise, river deltas are subsiding due to sediment consolidation along with lesser amounts of sediment reaching river deltas due to a variety of causes. Milliman et al. (1989) estimated that within the next 100 years, over 25% of the land of Bangladesh and over 20% of habitable land in the Nile delta could be lost. Populations on low-lying islands cannot retreat from sea level rise by moving inland – the entire island is at about the same height. Coral islands increase in elevation due to coral growth, but Gornitz (1991) notes that maximum calcification growth is about 10 to 12 mm/year, so if sea level rises faster than 1 to 1.2 m/century, coral islands will eventually be inundated.

It is difficult to estimate the impact on populations and economic activity of permanent land inundation from sea level rise by 2100, because there is not a good accounting of the population and economic activity that will be affected. Global data are not available any finer than the 10-m land contour. So, for example, McGranahan et al. (2007) report that 2% of the world's land area and 10% of its population are within 10 m of sea level. Nicholls et al. (2011) estimate that a 0.5 to 2.0 m sea level rise will inundate approximately 0.6 to 1.2% of the world's land area. They note that this could displace 53 to 125 million people in east, southeast, and south Asia alone.

Coastal wetlands will be greatly affected by sea level rise. Salt marshes respond to rising sea level by vertical accretion based on sedimentation. However, with sea level rising, local subsidence, and often reduced levels of sedimentation, coastal wetland loss will increase. Gornitz (1991) estimated that a 1.4 m rise in sea level would lead to 40% of US coastal wetlands lost.

10.5.3 Episodic Inundation

Episodic inundation will have a greater impact on populations and economic activity than simple inundation. In many parts of the world, tropical and extra-tropical storms, backwater flooding of rivers, and tsunamis can affect people up to the 10-m elevation and beyond. Thus the estimate by McGranahan et al. (2007) that

10% of the world's population lives within 10 m of sea level has significance. Meehl et al. (2007) noted that models suggest an increase in intensity of both tropical and extra-tropical storms. Nicholls et al. (2007a) show in a study of the world's 130 largest port cities that flooding due to storm surge exposes 40 million people to the 1-in-100-year coastal flood event. They estimate that this number will increase to 150 million by the 2070s due to the combined effects of sea level rise, increased storminess due to climate change, coastal subsidence, population growth, and increased urbanization. They estimate assets exposed to this threat were 5% of total global Gross Domestic Product in 2005 (about US$3 trillion) and 9% by the 2070s (about US$35 trillion). Miami, US, was projected to have the highest property and infrastructure exposure by the 2070s, with more than US$3.5 trillion of exposed assets, followed by Guangzhou, China, with US$3.3 trillion exposure and New York, US, with US$2.1 trillion.

Although 1-in-100-year flooding events may seem relatively rare, Nicholls et al. (2007a) note that the annual probability of one of the 130 port cities having a 1-in-100 year event is almost 75% and the probability over 5 years is almost 100%. Higher sea levels provide a higher base for storm surges, extending the range of flooding. For example, the US Federal Emergency Management Agency (1991) estimated that rises in sea level of about 0.3 and 0.9 m by 2100 would increase the area flooded in the US by the 100-year flood event from about 31,000 km^2 to 37,000 and 43,000 km^2 respectively. Because of this expanded flood zone and expected growth in the coastal population, the number of flood-prone households was estimated to increase from approximately 2.7 million to 5.7 and 6.8 million by the year 2100 for the 0.3 and 0.9 m scenarios, respectively. It estimated an increase in the expected annual flood damage by the year 2100 for a representative insured property to increase by 36 to 58% for a 0.3 m rise and by 102 to 200% for a 0.9 m rise.

10.5.4 Increased Erosion

Nicholls et al. (2007b) note that many coasts are eroding, but it is unclear as to the extent erosion is due to relative sea level rise versus human activities (e.g., sediment loss from dredging, interruption of littoral drift by coastal structures and navigation channels, sediment supply loss from upland dams). However, the "Bruun rule" (Bruun 1962) is often used to project shoreline erosion from sea level rise. The Bruun rule states that for a shoreline profile in equilibrium, as sea level rises, shore erosion takes place in order to provide sediments to the nearshore so the nearshore bottom can be elevated in direct proportion to the rise in sea level. The Bruun rule became increasingly cited after Dubois (1976) showed it explained shoreline response at a location in Lake Michigan in the United States as lake levels varied. However, relatively rapid changes in lake level may not a good model for the relatively slow rise in sea

level, and the adequacy of the Bruun rule to project shoreline change due to sea level rise has been challenged (Cooper and Pilkey 2004).

A recent study by Absalonsen and Dean (2011) analyzed a remarkable data set that covers almost 140 years of shoreline change over 1,162 km of shoreline along the east and west coasts of Florida, US. Even accounting for sand nourishment of Florida beaches in the modern era, it appears that this coastline has been stable for 140 years despite rising sea level. With relative sea level in Florida increasing at approximately 2 mm/year, the Bruun rule would predict average shoreline loss of about 15 to 30 m during the 140 years. The Bruun rule only considers offshore movement of sediment, but these Florida data are indicative of onshore movement of sediment that compensates for sea level rise. Dean (1991) discusses how onshore sediment transport can modify shoreline response to sea level rise. In addition, the production of calcium carbonate (e.g., shells) by organisms may play a part, since Pilkey et al. (2006) show that the fraction of calcium carbonate in beaches from North Carolina to Florida in the US increases rapidly to the south with one beach in Florida having about 40% of its beach sand consisting of calcium carbonate. The Florida data are indicative of onshore movement of sediment in response to sea level rise and may invalidate simple estimates of shoreline response to sea level using the Bruun rule. In addition, it is possible that there will be regional differences in shoreline response based on the activity of calcium-carbonate-producing organisms.

10.5.5 Salt Water Intrusion

Rising sea level will allow saltwater to penetrate farther inland and upstream, affecting both surface and groundwater supplies. Saltwater intrusion will affect water supplies for urban and agricultural use and harm aquatic plants and animals. The Ghyben-Herzberg principle (Poehls and Smith 2009) says that the distance of the freshwater lens below sea level in a coastal aquifer is 40 times the freshwater's height above local mean sea level. Thus, each increment in sea level rise reduces the thickness of the freshwater lens by a factor of 40.

South Florida, US, is a good example of the challenges that saltwater intrusion caused by sea level rise will pose to ecosystems and human water supplies. Saha et al. (2011) note that the 0.3 m sea level rise measured at Key West, Florida, over the past century (along with human diversions of surface water) has resulted in saltwater intrusion in the Everglades up to 30 km inland. The intrusion is changing the ecosystem from freshwater-dependent species to halophytes, threatening 21 rare coastal species. At the same time, water supplies to urban areas and agriculture in South Florida is threatened. Wiedenman (2010) notes that 90% of the population in highly urban south Florida use groundwater. The saltwater/freshwater interface has been creeping landward and is as far inland as 8 miles in parts of Miami. He lays out alternatives that Miami is considering to address the problem including moving wells inland, treating brackish water from the Florida Aquifer, and desalinating ocean water. The plight of south Florida is not unique. For example, Kashef (1983)

reports that that salt-water intrusion in the Nile Delta extended inland 130 km from the Mediterranean.

10.5.6 Adaptation

Nicholls et al. (2007b) note that sea level rise has a substantial inertia, and the most appropriate response to sea level rise is a combination of adaptation to the inevitable rise and mitigation to limit the long-term rise to a manageable level. They note that adaptation costs for vulnerable coasts are much less than the costs of inaction. However, they also note that adaptation will be more challenging for developing countries than developed countries because of shortfalls in financial resources and capabilities.

Nicholls et al. (2007b) outline coastal adaptation strategies that should be part of an integrated coastal zone management approach. Various retreat alternatives could be part of this approach, including moving of populations and structures out of vulnerable areas, "set back lines" for new construction, and other zoning approaches to reduce vulnerabilities. Retreat options would have to be supported by public education about the threats and adequate information from flood-hazard mapping. There could be an accommodation to sea level rise by flood-proofing or elevating buildings. Coastal assets could be protected by either advancing the coast line by reclaiming land, as has been done for some airports, or closure of estuaries as done by the Dutch in defense of the Netherlands. The present coastline position could be maintained through building dikes or nourishing beaches with sand.

Nicholls and Tol (2006) demonstrate the significant benefits that can be obtained by adaptation. In one case, they consider flood protection against storm surge through dike construction and beach nourishment. They show that with no adaptation, as many as 100 million additional people will experience annual flooding due to sea level rise by the 2080s. If various defense schemes are built, the number drops to about 5 to 15 million people. Nicholls et al. (2011) show there are substantial costs in providing this protection. They estimate annual costs, including maintenance costs, to provide dike and beach nourishment protection at $25 to $270 billion (1995 values) for 0.5 and 2.0 m sea level rises by 2100. They estimate in 2100 the relative mix of nourishment, dike construction, and dike maintenance at 36, 39, and 25% for a 0.5 m rise and 13, 51, and 37% for a 2.0 m rise.

A world-wide adaptation response will be very uneven. Nicholls et al. (2007b) highly recommend an integrated coastal zone management approach. The US is a good example of the difficulties in establishing a coordinated and integrated response to the sea level threat. Each of the 50 states in the US has its own coastal management plan. The federal government is not responsible for construction setback lines or local zoning decisions. It can influence coastal construction through its federally-backed flood insurance program, but the

maximum insurance it provides against flooding is generally much lower than the cost of building on the coast, so coastal construction in the US has not slowed. Building of coastal dikes and beach nourishment in the US are generally shared costs at the national, state, and local level. However, states and local governments and even the private sector can make their own decisions with the only requirement being the need to obtain permits that are generally environmentally related.

In addition to the adaption response likely being uneven in individual countries, Nicholls et al. (2007b) point out the problems with developing countries not having the financial capabilities to adapt to the challenges of sea level rise. There are programs that provide aid to developing countries to address these challenges, but the aid is presently inadequate and is expected to be even more inadequate as problems become more acute. The world community has the opportunity to champion integrated coastal zone management plans when funding adaptation in developing countries. However, it is expected that adaptation will be financed primarily in developed countries and driven by cost versus benefit and available resources. There are tools being developed such as the Dynamic Interactive Vulnerability Assessment (DIVA) model (Hinkel and Klein 2009) that can aid in developing alternatives in an integrated coastal zone management approach.

10.6 Summary and Conclusions

Sea level rise in the twentieth century was 1.7 mm/year, and there are different accounts as to whether the rise included a very small deceleration or acceleration. From 1993 to 2012, altimeters have measured a greater sea level trend than the twentieth century trend, but it is not known yet whether this is the leading edge of a sustained acceleration or a fluctuation similar to others that occurred in the twentieth century. The IPCC (Bindoff et al. 2007) projected a sea level rise of 0.18 to 0.59 m (95%-confidence level) from 1990 to 2100, but did not include scaled-up ice discharges from ice sheets of Greenland and Antarctica in determining its 0.59 m upper limit. There have been a number of projections of sea level rise to 2100 of 1 to 2 m. These are typically maximum possible projections that do not have probabilities associated with them and, thus, are not directly comparable to the 95%-confidence level projection of the IPCC. Assuming highly improbable/impossible events such as the immediate collapse of the West Antarctic ice sheet with the simultaneous quadrupling of carbon dioxide levels in the atmosphere, sea level could rise as much as 1.7 m by 2100. However, this maximum possible sea level rise by 2100 is not useful in planning and design of flood projects, since it is not typically used even for siting nuclear power plants. Instead, planning and design of flood projects require statistics of sea level projections that are at commensurate probability levels with design-floods. Although Bindoff et al. (2007) did not fully consider the contributions from Greenland and Antarctica, a recent study that did

uses IPCC methodology and projects 5, 50, and 95%-confidence-level rises by 2100. Assuming a standard normal distribution, these projections can be used to determine sea level rise probabilities that are consistent with design-flood probabilities. Sea level rise by 2100 will have significant effects on permanent coastal inundation, flooding from episodic events, shoreline erosion and salinity intrusion. The most appropriate response to sea level rise is limiting the long-term rise to a manageable level and adaptation to the inevitable rise which will occur. The world must work to reach new agreements limiting carbon emissions and thus limit the long-term rise. But since sea level rise has considerable inertia and will produce an inevitable rise, steps must be taken to adapt to the rise. These steps should be guided by integrated coastal zone management approaches in each country. However, even with the best of intensions, adaptive responses will likely not be uniform and will be pursued mainly in developed countries where the cost of protection is outweighed by benefits.

References

Ablain M, Cazenave A, Valladeau G, Guinehut S (2009) A new assessment of the error budget of global sea level rate estimated by satellite altimetry over 1993–2008. Ocean Sci 5:193–201

Absalonsen L, Dean RG (2011) Characteristics of the shoreline change along Florida sandy beaches with an example for the Palm Beach County. J Coast Res 27(96A):16–26

Arctic Monitoring and Assessment Programme (2011) Snow, water, ice, and permafrost in the Arctic. http://amap.no/swipa/CombinedDraft.pdf

Bamber JL, Riva REM, Vermeersen BLA, LeBrooq AM (2009) Reassessment of the potential sea-level rise from a collapse of the West Antarctic ice. Science 324:901–903. doi:10.1126/science.1169335

Bindoff NL, Willebrand J, Artale V, Cazenave A, Gregory J, Gulev S, Hanawa K, Le Que're' C, Levitus S, Noijiri Y, Shum CK, Talley LD, Unnikrishnan A (2007) Observations: oceanic climate change and sea level. In: Solomon S et al (eds) Climate change 2007: the physical science basis, Intergovernmental Panel on Climate Change. Cambridge University Press, Cambridge, pp 385–432

Bingham RG, Nienow PW, Sharp MJ (2003) Intra-annual and intra-seasonal flow dynamics of a high Arctic polythermal valley glacier. Ann Glaciol 37:181–188

Bruun P (1962) Sea level rise as a cause if shore erosion. J Waterw Harb Div, Am Soc Civ Eng 1:116–130

Church JA, White NJ (2006) 20th century acceleration in global sea-level rise. Geophys Res Lett 33:L01602. doi:10.1029/2005GL024826

Church JA, White NJ (2011) Sea-level rise from the late 19th century to the early 21st century. Surv Geophys. doi:10.1007/s10712-011-9119-1

Cooper JAG, Pilkey OH (2004) Sea-level rise and shoreline retreat: time to abandon the Bruun Rule. Glob Planet Change 43(3–4):157–171

Dean RG (1991) Equilibrium beach profiles: characteristics and applications. J Coast Res 7(1):53–84

Dean RG, Houston JR (2012) Recent sea level trends and accelerations via an extensive global tide gauge data set. National conference on beach preservation technology, Florida Shore and Beach Association, February 8–10, Hutchinson Island, FL. Available online at: http://www.fsbpa.com/2012TechPresentations/DeanandHouston.pdf

Domingues CM, Church JA, White NJ, Gleckler PJ, Wiffels SE, Barker PM, Dunn JR (2008) Improved estimates of upper-ocean warming and multi-decadal sea-level rise. Nature 453:1090–1094. doi:10, 1038/nature07080
Douglas BC (1992) Global sea level acceleration. J Geophys Res 97(C8):12699–12706
Douglas BC (2001) Sea level change in the era of the recording tide gauge. In: Douglas BC, Kearney MS, Leatherman SP (eds) Sea level rise: history and consequences, vol 3. Academic, San Diego, pp 65–93
Dubois RN (1976) Nearshore evidence in support of the Bruun Rule on shore erosion. J Geol 84(4):485–491
Federal Emergency Management Agency (1991) Projected impact of relative sea level rise on the National Flood Insurance Program. Available online at: http://epa.gov/climatechange/effects/downloads/flood_insurance.pdf
Gornitz V (1991) Global coastal hazards from future sea level rise. Palaeogeogr, Palaeoclimatol, Palaeoecol 89:379–398
Gornitz V (2007) Sea level rise, after the ice melted and today. Available online at: http://www.giss.nasa.gov/research/briefs/gornitz_09/
Graversen RG, Drijghout S, Hazeleger W, van de Wal R, Bintanja R, Helsen M (2010) Greenland's contribution to global sea-level rise by the end of the 21st century. Clim Dyn. doi:10.1007/s00382-010-0918-8
Greve R, Saito F, Abe-ouchi A (2011) Initial results of the SeaRISE numerical experiments with the models SICOPOLIS and IcIES for the Greenland ice sheet. Ann Glaciol 52(58):23–30
Grinsted A, Moore JC, Jevrejeva S (2010) Reconstructing sea level from paleo and projected temperatures 200 to 2100 AD. Clim Dyn 34:461–472. doi:10.1007/s00382-008-0507-2
Hansen JE (2007) Scientific reticence and sea level rise. Environ Res Lett 2:024002. doi:10.1088/1748-9326/2/2/024002
Hansen JE, Sato M (2011) Paleoclimate implications for human-made climate change. Published electronically at arXiv:1105.0968v2 [physics.ao-ph]. http://arxiv.org/ftp/arxiv/papers/1105/1105.0968.pdf
Hinkel J, Klein RJT (2009) Integrating knowledge to assess coastal vulnerability to sea-level rise: the development of the DIVA tool. Glob Environ Change 19:384–395. doi:10.1016/j.gloevcha.2009.03.002
Holgate SJ (2007) On the decadal rates of sea level change during the twentieth century. Geophys Res Lett 34:L01602. doi:1029/2006GL028492
Holgate SJ, Woodworth PL (2004) Evidence for enhanced coastal sea level rise during the 1990s. Geophys Res Lett 31:L07305. doi:10.1029/2004GL019626
Holgate S, Jevrejeva S, Woodworth P, Brewer S (2007) Comment on A semi-empirical approach to projecting future sea level rise. Science 317:1866. www.sciencemag.org/cgi/content/full/317/5846/1866b
Houston JR (2012) Sea level projections to 2100 using methodology of the Intergovernmental Panel on Climate Change. J Waterw, Port, Coast, Ocean Eng, Am Soc Civ Eng (in publication)
Houston JR, Dean RG (2011a) Sea-level acceleration based on U.S. tide gauges and extensions of previous global-gauge analyses. J Coast Res 27(3):409–417
Houston JR, Dean RG (2011b) Discussion of 'Sea-level acceleration based on U.S. tide gauges and extensions of previous global-gauge analyses' by J.R. Houston and R.G. Dean. J Coast Res 27(3):409–417: Response to Discussion by S. Rahmstorf and M. Vermeer (2011)
Hu A, Meehl GA, Han W, Yin J (2009) Transient response of the MOC and climate to potential melting of the Greenland Ice Sheet in the 21st century. Geophys Res Lett 36:L10707. doi:1029/2009GL037998
Huybrechts P, Goelzer H, Janssens I, Driesschaert E, Fichefet T, Goosse H, Loutre M-F (2011) Response of the Greenland and Antarctic ice sheets to multi-millennial greenhouse warming in the earth system model of intermediate complexity LOVECLIM. Surv Geophys 32:397–416. doi:10.1007/s10712-011-9131-5

IPCC (International Panel on Climate Change) (2010) Workshop report of the Intergovernmental Panel on Climate Change workshop on sea level rise and ice sheet instabilities. In: Stocker TF et al (eds) IPCC working group I technical support unit, University of Bern, Bern, Switzerland. Available online at: https://www.ipcc-wg1.unibe.ch/publications/supportingmaterial/supportingmaterial.html

Jansen E, Overpeck J, Briffa KR, Duplessy J-C, Joos F, Masson-Delmotte V, Olago D, Otto-Bliesner B, Peltier WR, Rahmstorf S, Ramesh R, Raynaud D, Rind D, Solomina O, Villalba R, Zhang D (2007) Palaeoclimate. In: Solomon S et al (eds) Climate change 2007: the physical science basis, Intergovernmental Panel on Climate Change. Cambridge University Press, Cambridge, pp 434–485

Jardine P (2011) The Paleocene-Eocene thermal maximum. Palaeontology. Available online at: http://www.palaeontologyonline.com/articles/2011/the-paleocene-eocene-thermal-maximum/

Jevrejeva S, Grinsted A, Moore JC, Holgate S (2006) Nonlinear trends and multiyear cycles in sea level records. J Geophys Res 111:C09012. doi:10.1029/2005JC003229

Jevrejeva S, Moore JC, Grinsted A (2010) How will sea level respond to changes in natural and anthropogenic forcings by 2100? Geophys Res Lett 37:L07703. doi:10.1029/ 2010GL042947

Jevrejeva S, Moore JC, Grinsted A (2011) Sea level projections to AD2500 with a new generation of climate change scenarios. Glob Planet Change. doi:10.1016/j.gloplacha.2011.09.006

Kashef A-A I (1983) Salt-water intrusion in the Nile Delta. Groundwater 21(2):160–167. Available online at: http://info.ngwa.org/gwol/pdf/831023085.PDF

Katsman CA, Hazeleger W, Drijfhout SS, van Oldenborgh GJ, Burgers G (2008) Climate scenarios of sea level rise for the northeast Atlantic Ocean: a study including the effects of ocean dynamics and gravity changes induced by ice melt. Clim Change. doi:10.1007/s10584-008-9442-9

Katsman CA, Sterl A, Beersma JJ, van den Brink HW, Church JA, Hazeleger W, Kopp RE, Kroon D, Kwadijk J, Lammersen R, Lowe J, Oppenheimer M, Plag H-P, Ridley J, von Storch H, Vaughan DG, Vellinga P, Vermeersen LLA, van de Wal Weisse R (2011) Exploring high-end scenarios for local sea level rise to develop flood protection strategies for a low-lying delta – the Netherlands as an example. Climatic Change. doi:10.1007/s10584-011-0037-5. Available online at: http://www.princeton.edu/step/people/faculty/michael-oppenheimer/research/Katsman-et-al- CC-2011.online.pdf

Kopp RE, Simons FJ, Mitrovica JX, Maloof AC, Oppenheimer M (2009) Probabilistic assessment of sea level during the last interglacial stage. Nature 462:863–868. doi:10.1038/nature08686

Lisiecki LE, Raymo ME (2005) Pliocene-Pleistocene stack of 57 globally distributed benthic d18O records. Paleoceanography 20:PA1003. doi:10.1029/2004PA001071

McGranahan G, Balk D, Anderson B (2007) The rising tide; assessing the risks of climate change and human settlements in low elevation coastal zones. Environ Urban 19(1):17–37. doi:10.1177/0956247807076960

Meehl GA, Stocker TF, Collins W, Friedlingstein P, Gaye A, Gregory J, Kitoh A, Knutti R, Co-authors (2007) Global climate projections. In: Solomon S et al (eds) Climate change 2007: the physical science basis. Contribution of working group I to the fourth assessment report of the Intergovernmental Panel on Climate Change, Cambridge University Press, Cambridge, pp 747–846

Milliman JD, Broadus JM, Gable F (1989) Environmental an economic impact of ring sea level and subsiding deltas: the Nile and Bengal. Ambio 18:340–345

Mitrovica JX, Tamisiea ME, Davis JL, Milne GA (2001) Recent mass balance of polar ice sheets inferred from patterns of global sea-level change. Nature 409:1026–1029

Mitrovica JX, Tamisiea ME, Ivins ER, Vermeersen LLL, Milne GA, Lambeck K (2010) Surface mass loading on a dynamic earth; complexity and contamination in the geodetic analysis of global sea-level trends. In: Church JA et al (eds) Understanding sea-level rise and variability, vol 10. Wiley-Blackwell, Chichester, pp 285–313

National Snow and Ice Data Center (2009) World glacier inventory. World Glacier Monitoring Service and National Snow and Ice Data Center/World Data Center for Glaciology, Boulder, CO. http://nsidc.org/data/docs/noaa/g01130_glacier_inventory/

Nerem RS, Chambers DP, Choe C, Mitchum GT (2010) Estimating mean sea level change from the TOPEX and Jason altimeter missions. Mar Geod 33(1):435–446

Nicholls RJ, Tol SJ (2006) Impacts and responses to sea-level rise: a global analysis of the SRES scenarios over the twenty-first century. Philos Trans R Soc 364:1073–1095. doi:10, 1098/rsta.2006.1754

Nicholls RJ, Hanson S, Herwijer C, Patmore N, Hallegatte S, Corfee-Moriot J, ChateauJ, Muir-Wood R (2007a) Ranking of the world's cities most exposed to coastal flooding today and in the future. In a report for: Organization for Economic Co-operation and Development, Available online at: http://www.rms.com/publications/OECD_Cities_Coastal_Flooding.pdf

Nicholls RJ, Wong PP, Burkett VR, Codignotto JO, Hay JE, McLean RF, Ragoonaden S, Woodroffe CD (2007b) Coastal systems and low-lying areas. In: Parry ML et al (eds) Climate change 2007: impacts, adaptation and vulnerability. Contribution of working group II to the fourth assessment report of the Intergovernmental Panel on Climate Change. Cambridge University Press, Cambridge, pp 315–356

Nicholls RJ, Marinova N, Lowe JA, Brown S, Vellinga P, de Gusmao D, Hinkel J, Tol RSJ (2011) Sea-level rise and its possible impacts given a 'beyond 4 °C world' in the twenty-first century. Philos Trans R Soc 369(1934):161–181. doi:10.1098/rsta.2010.0291

Peltier WR (2001) Global glacial isostatic adjustment and modern instrumental records of relative sea level history. In: Douglas BS, Kearney MS, Leatherman SP (eds) Sea level rise: history and consequences, vol 4. Academic, San Diego, pp 65–93

Pfeffer WT, Harper JT, O'Neel S (2008) Kinematic constraints on glacier contributions to 21st-century sea-level rise. Science 321(5894):1340–1343

Pilkey OH, Morton RW, Luternauer J (2006) The carbonate fraction of beach and dune sands. Sedimentology 8(4). Available online at: http://onlinelibrary.wiley.com/doi/10.1111/j.1365-3091.1967.tb01330.x/pdf

Poehls DJ, Smith GJ (2009) Encyclopedic dictionary of hydrogeology, vol 141. Elsevier, Amsterdam, 516 p

Prandi P, Cazenave A, Becker M (2009) Is coastal mean sea level rising faster than the global mean? A comparison between tide gauges and satellite altimetry over 1993–2007. Geophys Res Lett 36:L05602. doi:10.1029/2008GL036564

Rahmstorf S (2007) A semi-empirical approach to projecting future sea-level rise. Science 315:368–370

Ray RD, Douglas BC (2011) Experiments in reconstructing twentieth-century sea levels. Prog Oceanogr 91:496–515

Ridley JK, Huybrechts P, Gregory JM, Lowe JA (2005) Elimination of the Greenland ice sheet in a high CO_2 climate. J Clim 18:3409–3427

Rohling E, Grant K, Hemleben C, Siddall M, Hoogakker B, Bolshaw M, Kucera M (2008) High rates of sea-level rise during the last interglacial period. Nat Geosci 1:38–42. doi:10.1038/ngeo.2007.28

Saha AK, Saha S, Sadle J, Jiang J, Ross MS, Price RM, Sternberg LSLO, Wendelberger KS (2011) Sea level rise and South Florida coastal forests. Clim Change 107:81–108, doi:10.1017/s10584-011-0082-0

Schmith T, Johansen S, Thejll P (2007) Comment on 'A semi-empirical approach to projecting future sea-level rise'. Science 317:1866c. doi:10.1126/science.1143286

Sundal AV, Shepherd A, Nienow P, Hanna E, Palmer S, Huybrechts P (2011) Melt-induced speed-up of Greenland ice sheet offset by efficient subglacial drainage. Nature 469:521–524. doi:10.1038/nature09740

Taboada FG, Anadon R (2010) Critique of the methods used to project global sea-level rise from global temperature. Proc Natl Acad Sci 107(29):E116–E117. doi:10.1073/pnas.0914942107

Truffer M, Harrison WD, March RS (2005) Record negative glacier balances and low velocities during the 2004 heat wave in Alaska, USA: implications for the interpretation of observations by Zwally and others in Greenland. J Glaciol 51:663–664

University of Colorado (2012) Sea level change. Available online at: http://sealevel.colorado.edu/current/sl_ib_ns_global.pdf. Accessed 7 Mar 2012

van de Berg WJ, van den Broeke M, Ettema J, Meijgaard E, Kaspar F (2011) Significant contribution of insolation to Eemian melting of the Greenland ice sheet. Nat Geosci 4:679–683. doi:10.1038/NGEO1245

van de Wal RSW, Boot W, van den Broeke MR, Smeets CJPP, Reijmer CH, Donker JJA, Oerlemanset J (2008) Large and rapid melt-induced velocity changes in the ablation zone of the Greenland Ice Sheet. Science 321:111–113

Vermeer M, Rahmstorf S (2009) Global sea level linked to global temperature. Proc Natl Acad Sci 106(51):21527–21532. doi:_10.1073_pnas.0907765106

Watson PJ (2011) Is there evidence yet of acceleration in mean sea level rise around mainland Australia. J Coast Res 27(2):368–377. doi:10.2112/JCOASTRES-D-10-00141.1

Watson C, White NJ, Coleman R, Church JA (2004) TOPEX/Poseidon and Jason-1: absolute calibration in Bass Strait, Australia. Mar Geod 27:107–131

Wiedenman R (2010) Adaptive response planning for sea-level rise and saltwater intrusion in Miami-Dade County. Ph.D. Dissertation, Florida State University. Available online at: http://www.coss.fsu.edu/durp/sites/coss.fsu.edu.durp/files/DIR_Weidenman_woAppendix.pdf

Woodworth PL, Player R (2003) The permanent service for mean sea level: an update to the 21st century. J Coast Res 19:287–295

Part IV
Hydrologic (Groundwater, Saltwater Intrusion, Brine Disposal) Hazards

Chapter 11
Conceptualizing Seawater Intrusion Processes in Small Tropical Island Via Geochemical Modelling

Ahmad Zaharin Aris and Sarva Mangala Praveena

Abstract Geochemical modelling approach has been applied to demonstrate seawater intrusion phenomena in a coastal aquifer of Manukan Island, Sabah. Geochemical modeling output using PHREEQC showed that the migration of seawater into the fresher parts of the aquifer has resulted to a calcification of the aquifer. The chemical compositions of near coast zone and further landward area have a significant effect on the processes during the intrusion. Moreover, previous numerical modeling output showed upconing process leads to the migration of seawater and the possible route of seawater to influence the groundwater chemistry. Results of geochemical modeling output are the basis for future groundwater management strategies and protection in Manukan Island. SWOT analysis output has highlighted the strengths, weakness, opportunities and threats to facilitate assist in the management of environmental as well as groundwater of Manukan Island. The output of this study has also provided a foundation, which can be used in other small islands of similar hydrogeological condition to illustrate seawater intrusion using geochemical modeling approach.

11.1 Introduction

On the global scale, there are about 30,000 islands in Pacific Ocean, 100,000 islands in Caribbean Sea and 13,500 islands in Indonesia alone. It is impossible to provide a detailed and comprehensive list of all these islands (islands, small islands and very

A.Z. Aris (✉)
Department of Environmental Sciences, Faculty of Environmental Studies, Universiti Putra Malaysia, 43400 UPM, Serdang, Selangor, Malaysia
e-mail: zaharin@env.upm.edu.my

S.M. Praveena
Department of Environmental and Occupational Health, Faculty of Medicine and Health Sciences, Universiti Putra Malaysia, 43400 UPM, Serdang, Selangor, Malaysia
e-mail: smpraveena@gmail.com

C.W. Finkl (ed.), *Coastal Hazards*, Coastal Research Library 6,

DOI 10.1007/978-94-007-5234-4_11,

small islands) owing to the amount of work needed for data collection and its questionable value (Falkland 1991). Tourism in islands is an economic distributor at a local and national scale. International tourism is predicted to increase in future owing to few reasons such as rise in actual per capita income, fall in actual price of air transport and latest technology, the role of world wide web to spread information about famous islands and interesting places all over the world (Praveena and Aris 2009). Coastal and environmental attractions as well as safe groundwater qualities are the major tourists' attractions to islands (Mimura et al. 2007; Gossling 1999). Without proper planning and management, it can be dangerous to island's ecosystems (Belle and Bramwell 2005). Groundwater of islands receives increasing pressures by anthropogenic factors and overexploitation that cause imbalance in the hydrological system and ecosystem. Thus, there is an increasing pressure on islands to overcome the problems for conservation and protection of groundwater, reconceptualize policies as well as management practices to address the emerging issues and challenges in islands. Small islands have limited alternatives to develop their freshwater resources. Praveena and Aris (2010a) mentioned that freshwater in small islands usually depends on recharge, quantity and surface storage. Fresh groundwater is the sole option to meet the water demand, as surface water is absent in small islands. According to Singh and Gupta (1999), groundwater exists as freshwater lenses floating over saline transition zones, grading into seawater in small islands. Groundwater usage for daily supply in the small island which particularly being an attention for tourism activities has drastically increase over the last decade due to the rapid increased in visitors to the island (Isa and Aris 2012). Freshwater lens on small islands may easily be overexploited or polluted due to dense development combined with improper management, vulnerable to climate change and the associated impacts to freshwater resources. Overpumping of freshwater is one of the important factors that distort the natural recharge-discharge equilibrium causes drawdown of the water table a rise or upconing of the saltwater interface (Rejani et al. 2008). This has resulted in an enormous leap on groundwater extraction, leading to a contamination of the wells in the island. With this current practice, incursion of seawater into the island's aquifers especially in the low-lying area of the island, is an expected significance consequence. While it is an unseen phenomenon, the influence of seawater intrusion on the ecology of coastal systems, particularly small islands may be more important than once thought, due to the potential impacts resulting from chemical alterations during the freshwater-seawater mixing (Praveena and Aris 2009). Hence, evaluation and management of seawater intrusion are vital for maintaining supply of a good-quality groundwater resource in these islands (Pereira et al. 2009).

Groundwater contains a variety of dissolved inorganic ions in various concentrations as a result of chemical interactions between groundwater and geological materials through its flow. Availability of various dissolved inorganic ions by reaction mechanisms such as dissolution, precipitation and adsorption, including rates of geochemical process. Analytical techniques namely chromatography and spectrometry offer crucial information on total metal concentration available in water. However, ion in groundwater can form an unlimited number of species due

to complexation and hydrolysis reactions. Geochemical modeling is the widely used methods in seawater intrusion studies. Chemical parameters of groundwater play a significant role in classifying and assessing groundwater quality and types. Geochemical output can be utilized to understand the changes in groundwater quality and types due to rock-water interaction, reaction mechanisms or any type of anthropogenic influences. Chemical parameters of groundwater play a significant role in geochemical model input, classifying for selected minerals and ionic concentration changes in groundwater. Moreover, presentation of geochemical output in a graphical form enhances a simpler and quicker understanding of a complex groundwater system (Praveena et al. 2010). PHREEQC is a computer program designed to perform a wide variety of low-temperature aqueous geochemical calculations. Advantages of using PHREEQC over other geochemical models are that it is capable of handling higher ionic strengths, versatile and suitable to use in density dependent environment (seawater intrusion) which could not be found in other geochemical models. PHREEQC model can be able to provide an understanding of hydrochemical processes that take place in the aquifer during the freshwater–seawater mixing (Parkhurst and Appelo 1999).

The aim of this paper is an attempt to investigate the processes occurring in Manukan Island's aquifer. This paper displays geochemical modelling approach, which has been integrated and successfully used to identify seawater intrusion in a coastal aquifer of Manukan Island. In addition, the paper intends to give an illustration in using geochemical modeling to assess the seawater intrusion phenomena in a coastal aquifer. Lastly, SWOT was used as a useful tool for the planning development and decision- making to be applied to environmental planning and groundwater resource management in Manukan Island.

11.2 Materials and Methods

11.2.1 Study Area

Manukan Island, Sabah, Malaysia in Fig. 11.1 covers an area of 206,000 m^2 surrounded by other magnificent small islands such as Sapi, Mamutik and Sulug. The crystal clear waters and white sandy beach of Manukan island is an ideal location for snorkelling, diving and swimming as well as other water activities. This boomerang shaped tropical island is the second largest of the Tunku Abdul Rahman Marine Park and has good stretches of beaches especially on the southern coastline. The island consists of unconfined sandy aquifer, underlain sedimentary rock (sandstone and shale), is a part of the Crocker range rock formation of the western coast of Sabah (Basir et al. 1991). Small area and low elevations of the island lead to very limited water storage. The topography of the island is relatively hilly land with maximum elevations of approximately 60 m in the western and decreasing elevation towards the eastern coast. The area has a warm and humid climate and receives

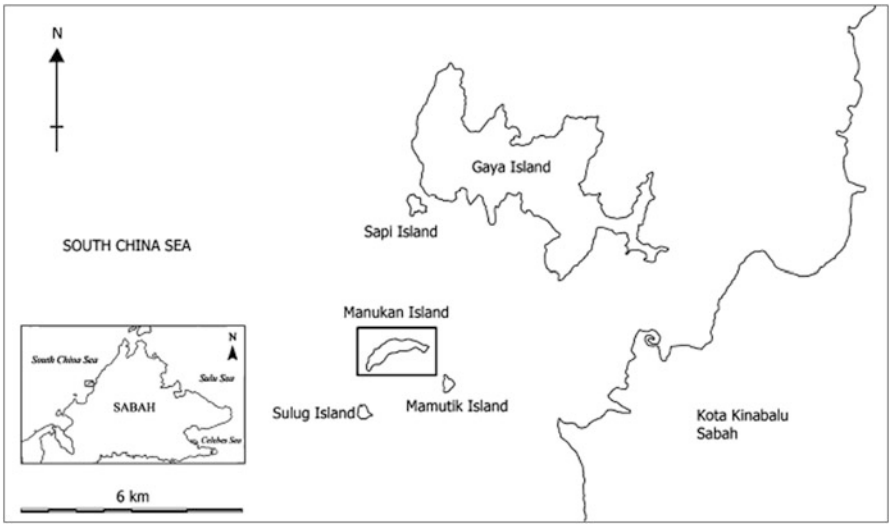

Fig. 11.1 Location of Manukan Island focusing the low lying area (Aris et al. 2009)

annual rainfall between 2,000 and 2,500 mm (Aris et al. 2009). Humidity ranges between 80 and 90% whereas temperature is between 21 and 32°C. Almost 80% of the area is covered by dense vegetation on high relief area (eastern side), while the rest of the area is located on the low lying area of the island (western coastline). The flat low lying area of the island has been developed for tourism activities. The sedimentary rock dips towards the low lying area (east-northeast) with dipping angles of 15–45°, most 80% of the area is covered by dense vegetation on high relief area (eastern part), while the rest of the area is located on the low lying area of the island (western coastline). On the low-lying area of Manukan Island, the small area and low elevations lead to very limited water storage (Praveena and Aris 2010). There are also accommodations available with excellent facilities (i.e., 20 unit chalets, a clubhouse, restaurant, souvenirs, diving centers and recreational facilities such as a swimming pool, football field, squash and tennis courts), and good infrastructure support (i.e. water, electricity, desalination plant, sewerage system, and even a solar powered public telephone).

11.2.2 Water Analysis Procedures

The wells water samples were pumped out for few times (5–10 min) prior to groundwater sampling, to avoid non-representative samples of stagnant or polluted. The water samples were pumped using modified dry vacuum pump technique. The analyses of water samples for geochemical modeling were carried out to assess the major cations and anions, including sodium (Na),

potassium (K), calcium (Ca), magnesium (Mg), bicarbonate (HCO_3), chloride (Cl) and sulphate (SO_4). The water pH and temperature were measured in the field using WTW pH 315i. For major cations, water samples were filtered at the time of collection using 25 mm puradisc syringe filtration unit of 0.45 μm pore size Whatman Milipore®, acidified to pH 2 with concentrated HNO_3 acid and analyzed using flame (air-acetylene burner) atomic absorption spectrometry (FAAS – Zeeman AAS Z-5000, Hitachi, Japan). Cl and HCO_3 were analyzed using argentometric and titration methods APHA (2005), respectively while SO_4 were analysed using HACH (DR/2040 – Loveland, CO, USA) meter.

11.2.3 Laboratory Procedures for Cation Exchange Capacity (CEC)

The content of exchangeable cations (Ca, Mg, Na and K) in sediment samples were determined by ion displacement using separately a 1 M NaCl and a 1 M NH_4Cl solution (Van der Molen 1958; Andersen et al. 2005; Appelo and Postma 2005; Aris et al. 2010). The cation exchange capacity (CEC) was calculated as the sum of these exchangeable cations. About 15 ml was used for the analysis of Ca, Mg, and K from the NaCl supernatant solution and preserved with 1% 7 M HNO_3. The solution from NH_4Cl supernatant was used for determination of Na and also preserved with 1% 7 M HNO_3. Samples analysis for Ca, Mg, Na and K were performed using flame (airacetylene burner) atomic absorption spectrometry (FAAS – Zeeman AAS Z-5000, Hitachi, Japan). The exchangeable cation concentrations are converted from meq/100 g to equivalent fractions ($\boldsymbol{\beta}$T) as suggested by Appelo and Postma (2005).

11.2.4 Numerical Model Design

Low-lying area was selected for this study (Fig. 11.1) as it has been developed for tourism activities. Moreover, all the wells for groundwater extraction are located on the low-lying area of the island (eight wells have been shut down, and only one well is currently operating). Boreholes (installed by hand auger manually) were constructed across the study area (Fig. 11.2) to provide a good horizontal and vertical spatial distribution of hydrologic data. This installation is based on flow measurements conducted by Abdullah (2001). The details of the boreholes installations can be found in Praveena et al. (2010).

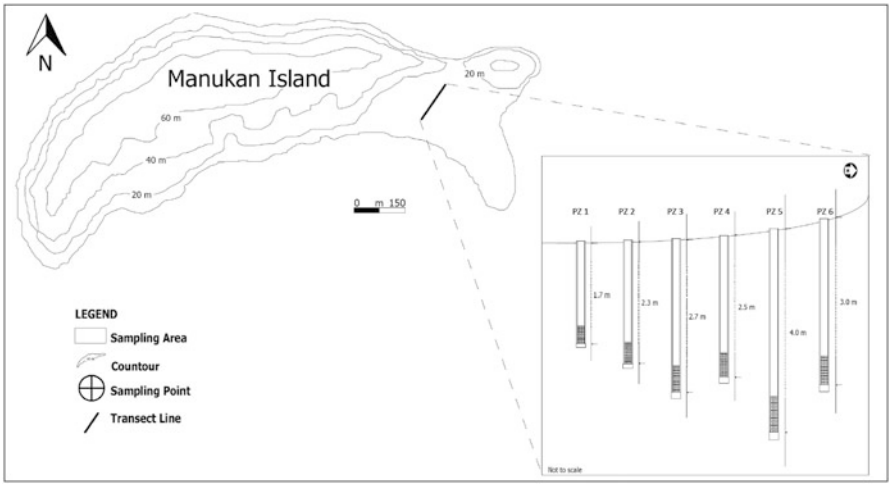

Fig. 11.2 Installation of multilevel nested boreholes at different depth in Manukan Island

11.2.5 Geochemical Model Design

A transect (from the coastline to landward area of the Manukan island) is represents by a 100 m horizontal column sectioned into 50 cells of 2 m in length. The incursion of seawater into the sandy aquifer of Manukan island can be justified by the predominantly horizontal intrusion front as suggested by Aris et al. (2010). The model setup only describes the processes in the mixing zone of the aquifer and not in the saline wedge. In the model, the initial groundwater is a mixture of freshwater and seawater end members as a result of incursion of seawater into the aquifer. Details of the model setup are given in Table 11.1. The seawater chemistry data, which was set as the intrusion seawater is the average surface seawater chemistry presented in Table 11.2. The transect data was measured just prior to the samples collection and seawater-groundwater chemistry data is used as the initial chemical condition. The variable's data were then simulated with PHREEQC Parkhurst and Appelo (1999) for the reaction transport modeling in the aquifer.

11.3 Results and Discussion

11.3.1 Groundwater Quality by Geochemical Approach

The obtained data for the studied parameters (pH, Eh, Temp, EC, TDS, Na, K, Ca, Mg, HCO_3, Cl and SO_4) were compared with previous work done by Abdullah et al.

Table 11.1 Parameters for the PHREEQC 1-D reactive transport model

Model setup parameters	Value	Comments
Physical parameters		
Model domain	100 m	Divided into 50 cells of 2 m
Boundary conditions flow	Flux	Steady state flow
Dispersivity	0.4 m	Fitted
Simulation time	0.7 year	Fitted
Chemical parameters		
Initial pore water composition	0.80 m; 15% seawater	Proposed result of seawater intrusion (Aris et al. 2009)
	80–100 m: freshwater	Data from Abdullah et al. (1996)
Boundary conditions chem	Associated flux	Composition is fixed near the recharge area
CEC	0.50 m: 5.7 meq/100 g 50–100 m: 6.9 meq/100 g 6.3 meq/100 g	Average measured values (this study)
SI calcite	Seawater: SI ~ 0.81	Values along flowing were calculated with PHREEQC Dissolution is when SI <0

(1996) in Manukan Island. The comparison between current and previous study showed there were significant changes in groundwater composition. In overall, it was found that for the 10 years period of 1996 to 2006–2007 there was about 99–999% increase of Ca, Na, Cl and SO_4 content in groundwater of the study area. The increase of such major elements in seawater (i.e. Na, Cl and SO_4) showed that overpumping of groundwater had significantly attributed to the mitigation of seawater into the fresh groundwater aquifer of the island. In general, the comparison data between the study conducted in 1996 and 2006–2007 are shown in the following Table 11.2.

The classification of groundwater types in Manukan Island using geochemical approach is illustrated in Fig. 11.3. Two types of groundwater groups were found from this study: (1) Na-Cl (2) Ca-Cl. The water types were largely dominated by Na-Cl water type while only 9% of Ca-Cl water type was encountered in this present study. Previous study by Abdullah et al. (1996) indicated three water types were found in the study area: (1) Ca-HCO_3, (2) Ca-Cl and (3) Na-Cl. Largely dominated Na-Cl water types indicate a strong seawater influence to the aquifer in the past of 10 years. The seawater intrusion has been probably favoured by preferential path such as overpumping. The overpumping has resulted in Ca-rich to Na-rich water type shift, which could be explained by cation exchange processes. This shift is clearly evidence in the cation triangle and from the evolution of Na-Cl water type to Ca-Cl water type and from Ca-Cl water type to Na-Cl water type.

Table 11.2 Mean value of hydrochemical parameters for water samples from Manukan Island

	pH	Ca (mg/l)	Mg (mg/l)	Na (mg/l)	K (mg/l)	Cl (mg/l)	SO_4 (mg/l)	HCO_3 (mg/l)
Fresh groundwater[a]	6.96	60.95 (1.52)	12.03 (0.50)	0.92 (0.04)	4.69 (0.12)	170.90 (4.82)	39.87 (0.42)	355.70 (5.83)
Mixing zone groundwater[b]	7.05	932.48 (23.27)	85.26 (3.51)	1352.27 (58.86)	38.21 (0.98)	2003.55 (56.51)	271.44 (2.83)	477.80 (7.83)
Seawater	8.10	414.00 (10.33)	42.51 (17.49)	11120.20 (483.70)	416.00 (10.64)	19750.20 (557.10)	2,600 (27.07)	125.12 (2.05)

( ) bracket indicates mmol/l value

[a]From Abdullah et al. (1996)

[b]Mean value of hydrochemical parameters for groundwater samples collected at the depth of 1.27–2.93 m from g.s.l

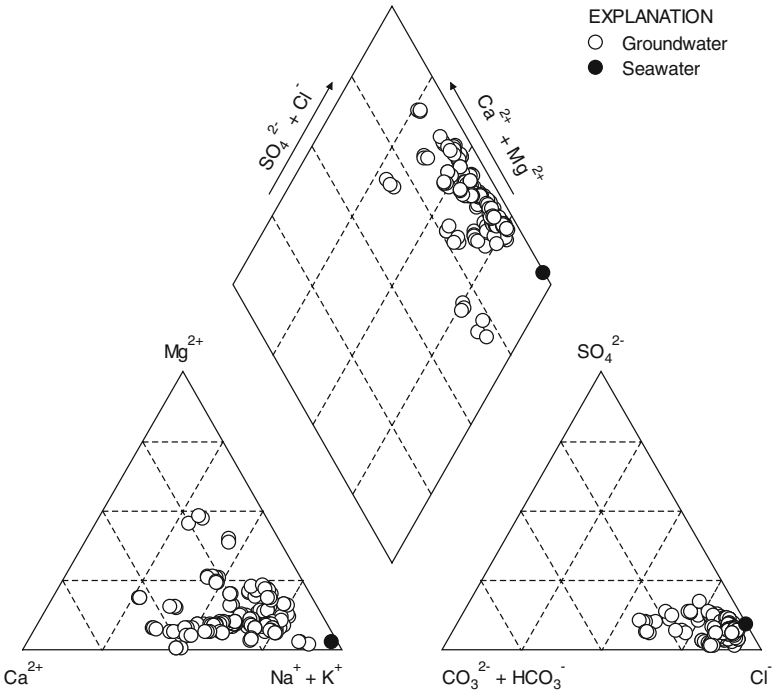

Fig. 11.3 Piper plot for studied groundwater of Manukan Island

11.3.2 Geochemical Modeling Output Using PHREEQC

The model results are shown in Fig. 11.3. The Manukan aquifer displays a Na-Cl type of water at its up-flow end (PZ 1), changing to groundwater enriched in Ca-Cl further down the flow path. The HCO_3 increases along the flow path (i.e. from Na-Cl; PZ 1 to Ca-Cl; PZ 2). The pattern is typically observed for freshening of an aquifer that originally has been filled with saline water. Representative hydrochemical facies in the aquifer show a marked difference between the headwaters (freshwater from recharge area), where the dominant type is Ca-HCO3, and the coastal strip, where a Na-Cl facies dominates, and this progression clearly indicates freshwater and seawater mixing. In addition to seawater flushing from the aquifer, the Ca in the freshwater will replace Na in the cation exchange on the sediment grains by ion exchange process. Since the amounts of adsorbed Na are much larger than the Ca concentration in the flushing solutions, the ion exchange fronts will move much slower through the aquifer than the chloride front (Appelo and Postma 2005). In addition, the ion exchange fronts may be coupled to mineral dissolution since binding of Ca ions can cause calcite dissolution, raising the pH and the bicarbonate concentration as seen in PZ 2 monitoring wells. The salt water had been flushed from the

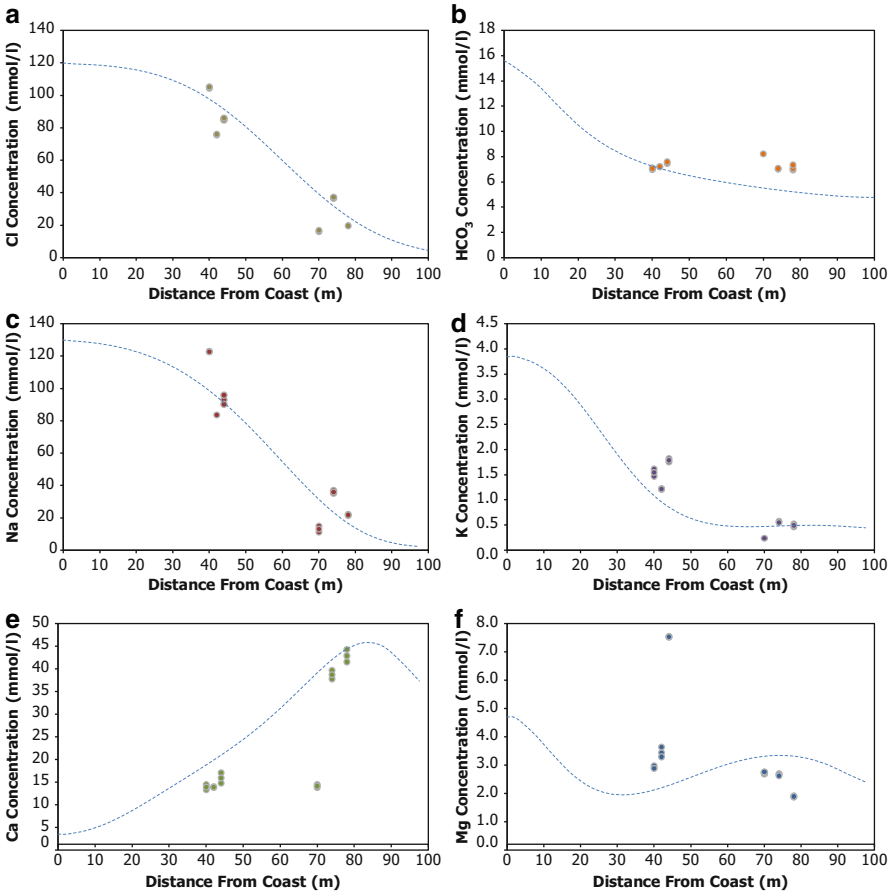

Fig. 11.4 Observed distributions (*solid symbols*) along flow path from coast of: (**a**) Cl, (**b**) HCO_3, (**c**) Na, (**d**) K, (**e**) Ca and (**f**) Mg (all in mmol/l). *Dashed lines* are modeled distributions using PHREEQC with 15% of diluted seawater mix with fresh groundwater

aquifer, where the current Cl concentrations at PZ 2 are less than the previous recorded concentrations from the other wells in Manukan island (16–37 mmol/l). The modeled Cl concentration (Fig. 11.3a) describes the obtained Cl data quite well with a steep decrease in the seawater influence at 40–100 m. Even though the aquifer has been displaced by recharge water, the sediment ion exchanger still contains the saline cations Na, K and Mg and these are at present being displaced by Ca from the recharging water. The concentrations of Na, K and Mg decreased at around 40 m from the coastline following the decreased in Cl (Figs. 11.4 and 11.5) which indicates that major parts of the cation distribution are due to advective transport. From about 70–100 m, Ca gradually displaces the seawater derived cations Mg, Na and K from the exchanger, resulting in Ca concentrations enrichment (Figs. 11.4 and 11.5). The water shifted from Na-Cl to Ca-Cl in all monitoring wells at this distance from the

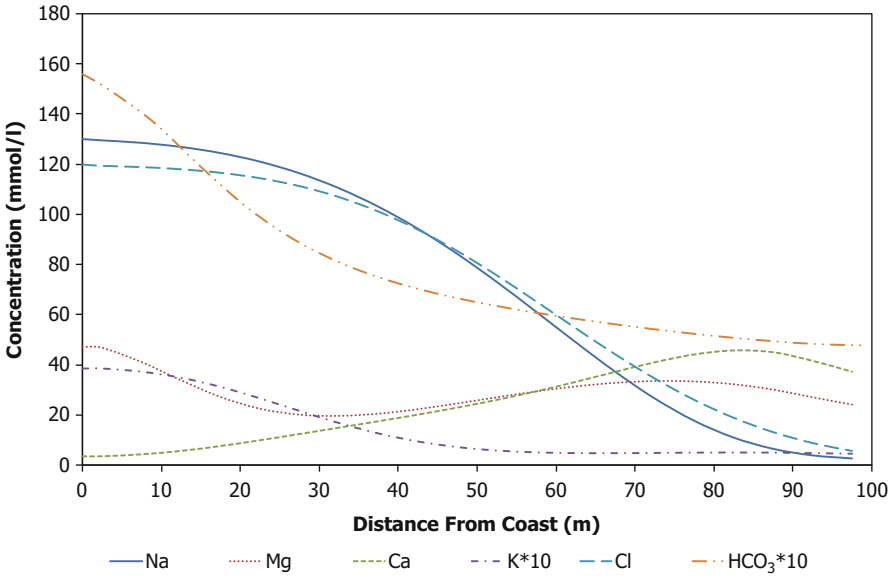

Fig. 11.5 Overall modeled distributions using PHREEQC

coastline. The shifts clearly indicate the effect of the ion exchange by the decrease in Na and increase in Ca concentrations.

Seawater intrusion process was found to be one of the factors that control the saturation states of the carbonate minerals. The mixing of freshwater–seawater creates a diversity of geochemical processes that has altered the theoretical composition of the fresh-water and seawater mixture in the Manukan island's aquifer. The processes involved were complex and varies, spatially and temporally. Praveena et al. (2009) showed the possible process attributed to the mixing mechanisms of saline water and fresh groundwater and current status of seawater intrusion in a coastal aquifer of Manukan Island, Sabah. Intensive and unregulated exploitation of groundwater from unconfined layer of Manukan Island by pumping wells contributed to the upconing process leads the advancement of the seawater at the bottom of the aquifer result from the density difference between seawater and freshwater. The upconing process showed in Fig. 11.6 by the numerical model output is the possible process attributed to the mixing mechanisms of saline water and fresh groundwater in low lying area of Manukan Island. The upconing process is taking place at the beneath of the pumping well. This finding supports the PHREEQC output which indicated the migration of seawater into the fresher parts of the aquifer apparently leads to a calcification of the aquifer despite the seawater being supersaturated for calcite; an indication of seawater chemistry influence to the fresh groundwater aquifer. Thus, the numerical modeling output using SEAWAT-2000 has explained the upconing process is the possible route of seawater to influence the fresh groundwater aquifer chemistry. When a well is

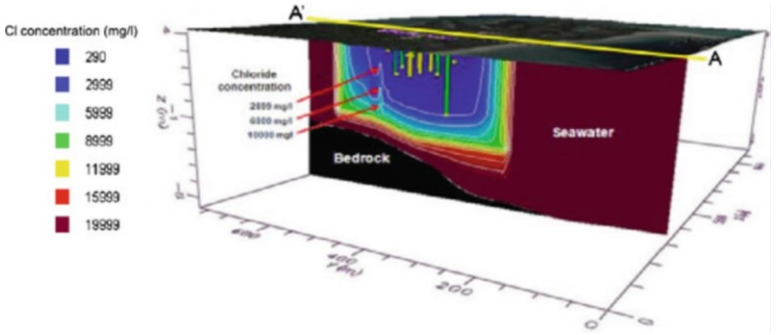

Fig. 11.6 Upconing process in Manukan Island attributed to seawater intrusion by Praveena et al. (2009)

pumped in an unconfined aquifer, it can induce a vertical flow component from the underlying saltwater regions, causing the saltwater to migrate upwards and become intercepted by the pumping.

11.4 Groundwater Management: SWOT Approach

SWOT analysis is a useful tool for the planning development and decision- making and has widely been applied to environmental planning and water resource management (Baser 2001). A detailed examination of existing conditions of groundwater resource in Manukan Island has been used in SWOT analysis (Fig. 11.7). Strengths and weaknesses that influence the aquifer system were identified. Moreover, opportunities and threats were also analyzed in order to facilitate the sustainable management of the groundwater.

The strengths of Manukan Island are the limited industrial activities, pristine environment, NGO aid to the island and existence of recent hydrogeological studies. As this island more focused in providing and promoting tourism related services, the groundwater quality data, which low in heavy metal pollution, gives strength to groundwater as the prime source of freshwater supply. NGO aid to the islands plays an important role in strength of groundwater resource in this island. The Indigenous Women's Biodiversity Network Meeting on Manukan Island in 2004 was an example of managing ecosystem services on an international level with NGO participation. Existences of recent hydrogeological studies are important because utilization of groundwater resources needs an accurate assessment of hydrogeological data to be included in groundwater modelling studies. Groundwater modelling will provide new information and contribute to the planning of better strategies in order to achieve water sustainability.

Strengths	Weaknesses
Limited industrial activities, pristine environment	Lack of adequate monitoring data (groundwater levels, quality data)
NGO aid to the island	Inadequate practices of an efficient water use
Existence of recent hydrogeological studies	
Opportunities	**Threats**
Financial opportunities for groundwater resources management, research and activities	Human pressure (overpumping)
Adaptations of experiences in integrated management of coastal aquifer systems from other similar islands	Seawater intrusion due to natural pressures
Environmental education and training	Island ecological balance disturbed due to over extraction of its groundwater
	Climate change

Fig. 11.7 SWOT analysis for groundwater resources in Manukan Island

Weaknesses in Manukan Island are lack of adequate monitoring data (groundwater levels, quality data) and inadequate practices of an efficient water use. Adequate monitoring data provides the information for rational management decisions on groundwater resources sustainability. It also detects trends in groundwater levels and quality as well as identifying actual and emerging problems. Inadequate practices of an efficient water use can indicated via the changes of groundwater composition in study area (i.e. Ca-rich to Na-rich water type shift).

On the other hand, opportunities available in Manukan Island are financial opportunities for groundwater resources management, research and activities, adaptations of experiences in integrated management of coastal aquifer systems from other similar islands and environmental education. Financial opportunities such as from Government of Malaysia have played a vital role in groundwater resources research and activities in Manukan Island. It has helped to understand the island's condition and contributed in the implementation of the wide range of management initiatives in Manukan Island. Adaptations of experiences in

integrated management of coastal aquifer systems from other similar islands are important in terms of groundwater management in Manukan Island. For an example, integrated watershed and coastal zone management in Caribbean Island practices using community-based management. This has shown improved an understanding of the groundwater management, island ecosystem coupled with greater capacity building (Breton et al. 2006). As such example can be implemented in the groundwater management of Manukan Island. Environmental education programs have been conducted in many islands as ways to educate local and island managers and to share the responsibility to manage the groundwater in islands. Threats are situations that might cause problems in Manukan Island. Human pressure (overpumping) is one of the major threats as such found in the Manukan Island. This has resulted in seawater intrusion and also disturbed the island's ecological balance as showed in previous study conducted (Aris et al. 2007, 2009). Natural pressures such as tsunami, drought and climate change (global warming, sea level rise) will also give effects to the groundwater quantity and quality in Manukan Island.

Based on SWOT analysis results, the following recommendations are proposed in order to restore, protect and manage the groundwater of Manukan Island sustainably. Lastly, continuous and systematic monitoring of both groundwater quality and quantity are crucial and requires appreciation. A good sustainability groundwater management puts effective planning, management and control in a good relationship between islands and tourism.

- Reduction of groundwater abstraction should be applied in the areas that are affected by seawater intrusion
- Water-saving techniques should be applied in order to decrease the groundwater quantities used for tourism and domestic use
- Complete water balance component report for Manukan Island
- Training courses should be organized in order to educate people in using methods to optimize water use
- Environmental education for the local people
- Collaborations between higher institutional and Sabah Parks for a better strategy for groundwater resource management in Manukan Islands
- Enhance the resilience of whole island socio-ecological systems, rather than concentrating on the groundwater resources

11.5 Conclusion

This study has successfully demonstrated seawater intrusion in a coastal aquifer of Manukan Island using geochemical modeling approach. The low topography of the study area of Manukan island makes this aquifer prone to frequent inundations of seawater aggravated by continuous groundwater abstraction from its sandy aquifer. These inundations are causing density driven seawater to migrate further into the

fresh region of the aquifer (up to 100 m from the coast) and thereby constitute an important additional mechanism for the transport of seawater into the aquifer. The main chemical process responsible for an increase of the calcite saturation state is ion exchange process related to the mixing of seawater and fresh groundwater in the carbonate system. Groundwater quality of Manukan Island is affected by seawater intrusion attributed to over extraction of freshwater from the aquifer supported by previous numerical model study done in study area. The upconing process is taking place at the beneath of the pumping well and attributed to the seawater intrusion occurring in low lying area of Manukan Island. The seawater intrusion has been probably favoured by preferential path such as overpumping and lead in Ca-rich to Na-rich water type shift. Combination of geochemical analysis and modelling and numerical modelling as well as SWOT analysis has proved to list all the strengths, weakness, opportunities and threats. SWOT output enables to assist the stakeholders, government bodies and publics to improving the sustainability of the groundwater resources of Manukan Island. The results of this study are foundation in order to work out comprehensive strategies for mitigation of possible future saline groundwater contamination through management and planning.

References

Abdullah MH (2001) Phreatic water extraction from shallow aquifer of a small island. Ph.D. Thesis, Universiti Teknologi Malaysia, Malaysia

Abdullah MH, Musta B, Ramli MZ (1996) Groundwater quality as freshwater resource in Manukan island – A preliminary finding. In: Proceedings of the geology and environmental seminar, Universiti Kebangsaan Malaysia, Bangi, pp 33–37

Andersen MS, Jakobsen VNR, Postma D (2005) Geochemical processes and solute transport at the seawater/freshwater interface of a sandy aquifer. Geochimica et Cosmichimica Acta 69: 3979–94

APHA (2005) Standard methods for the examination of water and wastewater, 21st edn. APHA/AWWA/WPCF, Washington, D.C

Appelo CAJ, Postma D (2005) Geochemistry, Groundwater and Pollution. 2nd edition. Rotterdam, Balkema, p 649

Aris AZ, Abdullah MH, Kim KW, Praveena SM (2009) Hydrochemical changes in a small tropical island's aquifer: Manukan Island, Sabah, Malaysia. Environ Geol 56:1721–1732

Aris AZ, Abdullah MH, Praveena SM, Yusoff MK, Juahir H (2010) Extenuation of saline solutes in shallow aquifer of a small tropical island: a case study of Manukan Island, North Borneo. EnvironmentAsia 3:84–92

Aris, AZ, Abdullah, MH, Ahmed A, Woong KK (2007) Controlling factors of groundwater hydrochemistry in a small island's aquifer. Int J Environ Sci Technol 4:441 – 450

Baser O (2001) SWOT analysis: a practical guide for young managers. http://www.baserler.com.tr/onur/isletme/management% 20skills-swot.htm

Basir J, Sanudin T, Tating FF (1991) Late Eocene planktonic foraminifera from the Crocker Formation, Pun Batu, Sabah. Warta Geologi 14:1–15

Belle N, Bramwell, B (2005) Climate change and small island tourism: Policy maker and industry perspectives in Barbados. J Travel Res 44:32–41

Breton E, Rousseau V, Parent J-Y, Ozer J, Lancelot C (2006) Hydroclimatic modulation of the diatom/Phaeocystis blooms in the nutrient-enriched Belgian coastal waters (North Sea). Limnol Oceanogr 51:1–14

Falkland A (1991) Hydrology and water resources of small islands: a practical guide, vol 49, Studies and Reports on Hydrology No. 49. UNESCO, Paris

Gossling S (1999) Ecotourism: a means to safeguard biodiversity and ecosystem functions? Ecol Econ 29:303–320

Isa NM, Aris AZ (2012) Preliminary assessment on the hydrogeochemistry of Kapas Island, Terengganu. Sains Malays 41:206–220

Mimura N, Nurse L, Mclean RF, Agard J, Briguglio L, Lefale P, Payet R, Sem G (2007) Small islands. In: Parry ML, Canziani OF, Palutikof JP, Van Der Linden P, Hanson CE (eds) Climate change 2007: impacts, adaptation and vulnerability. Contribution of working group II to the fourth assessment report of the Intergovernmental Panel on Climate Change. Cambridge University Press, Cambridge, UK

Parkhurst DL, Appelo CAJ (1999) User's guide to PHREEQC (Version 2) -A computer program for speciation, batch-reaction, one-dimensional transport, and inverse geochemical calculations. U.S. Geological Survey Water Resources Investigation Report

Pereira LS, Cordery I, Iacovides I (2009) Water conservation and saving: concepts and performance. Springer, Dordrecht, p 382

Praveena SM, Aris AZ (2009) A review of groundwater in islands using SWOT analysis. World Rev Sci, Technol Sustain Dev 6:186–203 (SCOPUS)

Praveena SM, Aris AZ (2010) Groundwater resources assessment using numerical model: a case study in low-lying coastal area. Int J Environ Sci Technol 7(1):135–146

Praveena SM, Aris AZ, Abdullah MH (2009) Modeling of seawater intrusion for a small tropical island aquifer in East Malaysia. International conference on Chemical, Biological and Environmental Engineering (CBEE 2009), Singapore, 9–11 October 2009, pp 202–205

Praveena SM, Abdullah MH, Aris AZ (2010) Groundwater solution techniques: environmental applications. J Water Resour Prot 2:8–13

Rejani R, Jha MK, Panda SN, Mull R (2008) Simulation modeling for efficient groundwater management in Balasore coastal basin, India. Water Resour Manage 22:23–50

Singh VS, Gupta CP (1999) Feasibility of groundwater withdrawal in a coral island. Hydrol Sci J 44:173–182

Van der Molen WH (1958) The Exchangeable Cations in Soils Flooded with Sea Water. The Hague, Staatsdrukkerijl, p 167

Chapter 12
Reducing the Risk Associated to Desalination Brine Disposal on the Coastal Areas of Red Sea

Adrian Ciocanea, Viorel Badescu, Richard B. Cathcart, and Charles W. Finkl

Abstract By the end of 2005 the global installed capacity for desalination of seawater was about 24.5·106 m^3/day. The geographical distribution of the desalination plants was as follows: 77 % in the Middle East and North Africa, 10 % in Europe, 7 % in the Americas and 6 % in the Asia-Pacific region. The volume of brine discharged in the Red Sea increased from 6.4 million m^3/day (in 1996) to 6.8 million m^3/day (in 2008) and is still increasing due to the observed tendency to improve the average recovery ratio from 30 to 50 %. This will make the environmental concerns much more important in the future. There are two main sources of problems, i.e. the concentrate and chemical discharges and the cooling water effluent discharges. The salinity is expected to increase in the long term if larger and larger amounts of desalinated water are removed from the water bodies. A proper solution for the desalination waste brine disposal process requires a good balance between technical constraints (i.e. placing a pipe on the sea-bottom), environmental conditions (i.e., finding an optimum distance from the seashore

A. Ciocanea (✉)
Department of Hydraulics, Polytechnic University of Bucharest, Spl. Independentei 313, Bucharest 060042, Romania
e-mail: adrian.ciocanea@yahoo.com

V. Badescu
Candida Oancea Institute, Polytechnic University of Bucharest, Spl. Independentei 313, Bucharest 060042, Romania

Romanian Academy, Calea Victoriei 125, Bucharest 010071, Romania
e-mail: badescu@theta.termo.pub.ro

R.B. Cathcart
Geographos, 1300 West Olive Avenue, Suite M, Burbank, CA 91506, USA
e-mail: rbcathcart@gmail.com

C.W. Finkl
Charles E. Schmidt College of Science, Department of Geosciences, Florida Atlantic University, Boca Raton, FL 33431, USA
e-mail: cfinkl@fau.edu

C.W. Finkl (ed.), *Coastal Hazards*, Coastal Research Library 6,
DOI 10.1007/978-94-007-5234-4_12,

where high salinity brine should be discharged without significant environmental impact; also, the availability for long run of brine disposal placement should be considered) and as low as possible overall economic costs.

Since the potential cumulative impacts of desalination activity on the marine environment is expected to be more significant in case of regional seas, in this chapter we focus on the desalination plants in Red Sea. The objective is to discuss a modeling framework for the environmental-hydraulic design of the outfall system for desalination plants. The chapter presents an interdisciplinary combination of environmental issues with physical processes and discharge modeling. We assess the technical viability of disposal the brine effluent produced by desalination plants into Red Sea coastal regions via submarine pipes.

There are several approaches to mitigate the environmental effects of the brine discharges. By tradition, the brine is discharged back to the sea in open channels. Impacts from high salinity may be avoided by pre-dilution of the desalination plant rejected stream with other waste streams, such as power plant cooling water. Impacts from high temperature may be avoided by ensuring heat dissipation from the waste stream to the atmosphere before entering the water body. However, simulations models for the brine plume dispersion from desalination power plants reveal the inadequacy of using surface discharging outfalls in order to brine discharging. Large capacity plants require submerged discharges which ensure a high dilution, reducing the harmful impacts on the marine environment. Mixing and dispersal of the discharge plume can be enhanced by installing a diffuser system, and by locating the discharge in a favorable oceanographic site which dissipates the heat and salinity load quickly.

The central concept of the brine disposal by submerged pipes is the available head at the discharge point. Higher values of the available head ensure larger jet dispersion lengths and better conditions for ejected brine dilution. We have shown that the quality of the dilution process is well quantified by the Froude number of the brine discharge jet, whose optimum values range between 20 and 25. Using the Froude number allowed us to find the optimum pipe length and the optimum depth of the discharge point.

About half of the Red Sea desalination plants are based on reverse osmosis. The percentage of RO plants is expected to increase, taking into account the lower production costs and the favorable technological evolution. The most representative RO desalination plants around the Red Sea coast are considered both by country and by capacity points of view. In order to provide relevant conclusions for the study reduced capacity desalination plants were selected due to their large number. For not available/existing desalination plants some hypothetic “case studies” were considered.

Optimum brine dispersion may be obtained by using underwater pipes for any sort of high capacity and low capacity RO desalination plants operating on the Red Sea coasts. In case of large capacities, a pipe length around $lX = 1{,}000$ m allows optimum operation. A pipe length about $lX = 500$ m is needed for low capacity RO desalination plants.

12.1 Introduction

Countries with water resources of less than 1,000 m^3/capita/year are usually listed among those with problems from both social and demographic aspects (Al-Gobaisi 1997). In this context, desalination is an important source of fresh water for the states which have seas or oceans as natural borders. In 1998 the total daily capacity of installed desalination plants worldwide was $22.7 \cdot 10^3$ m^3. This is an increase of 70% from that previously reported in 1990 (Buros 1998; IDA 2006–2007). The cost of the desalination plants depends on their location and on the local unit costs and operations. Averagely speaking, these costs decreased from \$1.5/m^3 in 1990 to \$0.50/m^3 in 2003 (Pankratz 2004).

Seawater desalination may provide a constant supply of good quality drinking water, offering many human health and socio-economic benefits. Also, seawater desalination does not affect natural freshwater ecosystems. However, concerns are raised due to some potential negative impacts on coastal water quality and marine life. There are two main sources of problems, i.e. the concentrate and chemical discharges and the cooling water effluent discharges. The energy consumption and the land use are other aspects of concern in relation with seawater desalination plants operation (Tobias et al. 2009).

A good presentation about the waste products carried by the desalination plants into the coastal environment is made by Lattemann and Höpner (2003). The amount of intake water that can be desalted depends of the desalting process. It is about 10% for the thermal processes, such as multi-stage flash distillation (MSF) and up to 50% in case of reverse osmosis (RO). The rest of the seawater is usually discharged back to the sea. The reject streams from distillation plants consist in most cases in concentrated salt brine with increased temperature, residual chlorine levels, antiscalant and anti-foaming additives. Antiscalants and coagulants may be present in RO reject streams, if the backwash water from coagulation and media filtration is combined with the process wastewater before discharge. Low concentrations of metals from corrosion are usually found. Copper contamination may be a concern in the reject streams of those desalination plants with heat exchangers made of copper-nickel alloys. The reject streams of RO plants may contain harmful cleaning solutions if these are mixed with the concentrate and discharged into the sea.

By the end of 2005 the installed capacity for desalination of seawater was about $24.5 \cdot 10^6$ m^3/day. The geographical distribution of the desalination plants was as follows: 77% in the Middle East and North Africa, 10% in Europe, 7% in the Americas and 6% in the Asia-Pacific region. Two thirds of this capacity was based on thermal processes, mainly in the Middle East. Membrane desalination was the dominating process on the rest of the globe.

The observed tendency of the installed desalination capacity is to follow the future increase in regions population. Another observed tendency is to improve the average recovery ratio from 30 to 50%. Both tendencies will have as a result the increase of the brine salt concentration. This will make the environmental concerns much more important in the future.

Most of the Middle East desalination plants are located on the borders of the Arabian Gulf (AG) and Red Sea (RS). These semi-enclosed seawater bodies are characterized by very low annual precipitations, from 90 to 150 mm and very high evaporation rates, from 1.2 to 2 m annually. Therefore, the AG and RS waters have a higher salt content than the planetary ocean (Anton et al. 2005). The salinity is expected to increase in the long term if larger and larger amounts of desalinated water are removed from the water bodies.

Since the potential cumulative impacts of desalination activity on the marine environment is expected to be more significant in case of regional seas, in this chapter we focus on the desalination plants in Red Sea. The countries bordering the Red Sea are: Egypt, Israel, Jordan, Sudan, Eritrea, Saudi Arabia, Yemen and Djibouti. The objective is to discuss a modeling framework for the environmental-hydraulic design of the outfall system for desalination plants. The chapter presents an interdisciplinary combination of environmental issues with physical processes and discharge modeling.

12.2 Desalination Plants on Red Sea Coasts

The Red Sea surface area is about 450,000 km^2. Other characteristics are as follows: a gross length of about 2,000 km, a mean width of about 225 km, a mean depth of around 500 m and a maximum depth of 3,040 m (Anton et al. 2005).

No river enters the Red Sea. Therefore, there is virtually no surface water runoff. The Red Sea exchanges water with the Gulf of Aden at the strait of Bab el Mandab (Shahin 1989; Morcos 1970). The water exchange rate is about $0.5 \cdot 10^6$ m^3/s during November to May while during June to October this quantity is about $0.16 \cdot 10^6$ m^3/s (Thompson 1939; Murray and Johns 1997). The annual mean Red Sea outflow transport is estimated to about $0.37 \cdot 10^6$ m^3/s (Murray and Johns 1997). This agrees with Siedler's (1969) estimated amount of $0.33 \cdot 10^6$ m^3/s. The rainfall over the Red Sea and its coasts is about 60–100 mm/y with an average volume of about 233,000 km^3. The renewal of water in the Red Sea is estimated to take 20 years (Red Sea 2008).

In 1996 about $6.4 \cdot 10^6$ m^3/day brine water was discharged into the Red Sea. In 2008, this figure has increased to $6.8 \cdot 10^6$ m^3/day. The estimate for 2050 is $26.6 \cdot 10^6$ m^3/day. Table 12.1 shows the desalination capacity for several countries located on the border of the Red Sea.

Figure 12.1 shows that the desalination technologies used in Red Sea area are Reverse Osmosis, Multi-stage Flash Distillation and Multi-effect Distillation (MED) (Lattemann and Höpner 2008; IDA 2006). Saudi Arabia owns large desalination plants. On the other hand, the desalination plants in Egypt are larger in number but of smaller capacity. Therefore, the capacity values shown in Fig. 12.1 for Egypt are cumulated values for small desalination plants located in the same area.

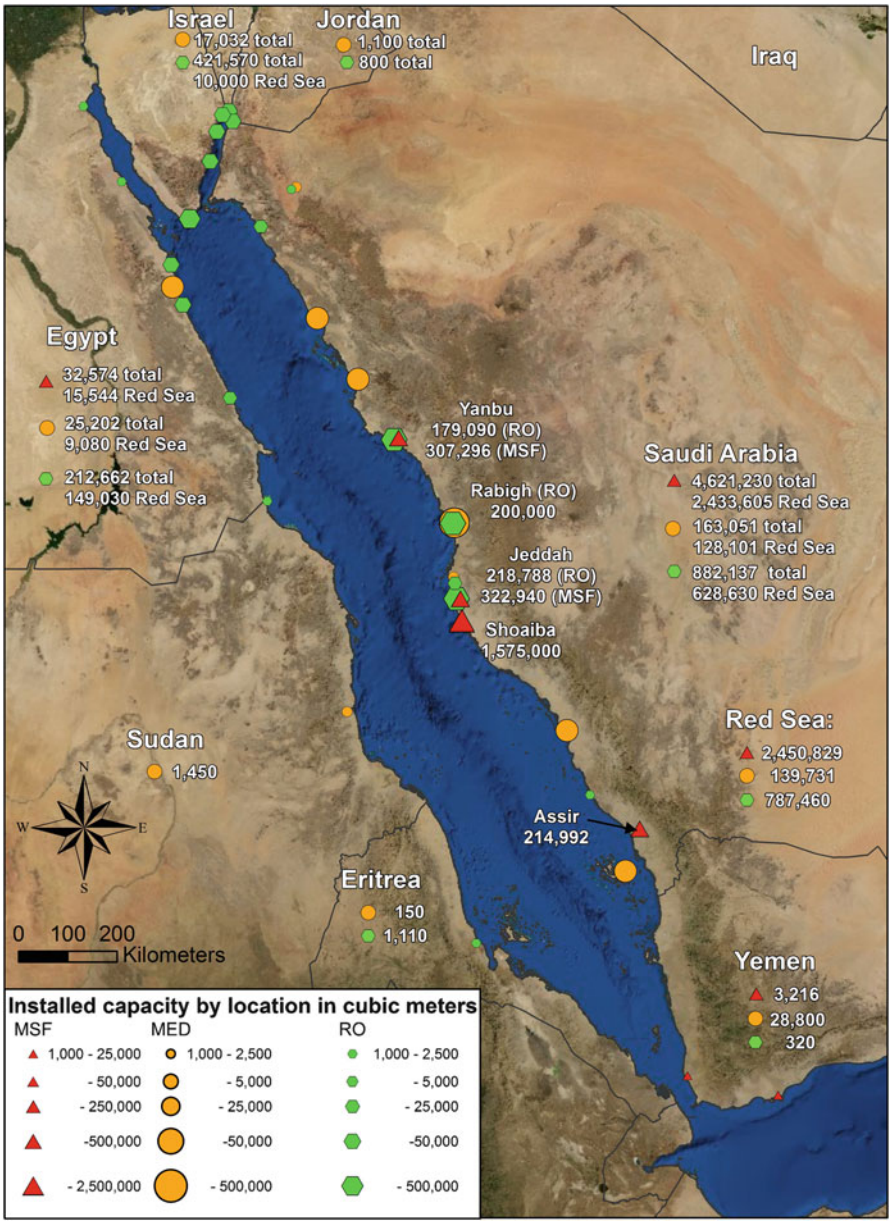

Fig. 12.1 Seawater desalination capacity in the Red Sea (m^3/day). Desalination technologies are: *RO* Reverse Osmosis, *MSF* Multi-stage Flash Distillation,*MED* Multi-effect Distillation (Adapted from Lattemann and Höpner (2008)) (Source of background: Esri, i-cubed, USDA, USGS, AEX, GeoEye, Getmapping, Aerogrid, IGN, IGP, and the GIS User Community)

Table 12.1 Desalination capacity and amount in cubic meters per capita per year at the end of 1996, 2008 and 2050, for countries on the Red Sea shore

	Desalination capacity (1,000 m^3 /day)						Desalination capacity (m^3/capita/year)		
	1996		2008		2050		1996	2008	2050
	QF	QB	QF	QB	QF	QB	QF	QF	QF
Egypt (including MS)	102.1	238	491.1	737	1,479.6	1,480	0.51	2.14	2.68
Israel (including MS)	90.4	211	630.1	945	1,703.6	1,704	5.27	31.54	36.4
Jordan	7.0	16	173.0	260	382.1	382	0.48	9.94	7.51
KSA (including AG)	5,006	11,681	7750.8	11,626	39,669	39,669	74.4	98.0	184.7
Sudan (including MS)	1.0	2	23.0	35	51.1	51	0.01	0.20	0.13
Yemen	37.0	86	47.0	71	272.5	272	0.66	0.73	0.88

In some cases the capacities include those located on the borders of the Arabian Gulf (AG) and Mediterranean Sea (MS) (Magazine 2005; IDA 2006, 2006–07, 2007–08, 2008–09; Lattemann and Höpner 2008; ; Worldwater 2009; ; Ghabayen et al. 2004)
QF Freshwater production from desalination, *QB* Brine Discharge

12.2.1 Perspectives for Desalination Technologies in Red Sea Area

Table 12.2 shows that the reverse osmosis technology is dominating the world market (Wittholz et al. 2008). Most of the desalination capacities installed in the last 25 years were based on this technology.

However, in the Middle East and North Africa (MENA) region, most of the installed desalination capacities are using the MSF technology although the installed capacity for reverse osmosis has increased in the last years (Table 12.3). The lower percentage of the RO technology in MENA region is mainly due to the fact that this technology is used for small capacities.

Since 2000 the recovery ratio of the RO technology has significantly increased at 44% (for a seawater intake salinity value of 41.7 ppt and brine outlet of 74 ppt – Raed et al. 2007). The production cost of the reverse osmosis seawater desalination decreased from 2.5 to less than 0.5 $/m^3$, mainly in those locations which are favourable in terms of water intake access point and cost operation. Table 12.4 shows that RO technology is in most cases more competitive than the MSF and MED technologies. An Australian case study shows that because of its lower cost and improved membranes RO became competitive for large size desalination plants (Table 12.5) (Karagiannis and Soldatos 2008; Wittholz et al. 2008).

The desalination technologies will face various technical and economical issues as well as environmental issues due to the increase of the amount and the salinity of the discharged waters, associated to the increase of the fresh water demand. The volume of brine discharged in the Red Sea increased from 6.4 million m^3/day

Table 12.2 World's installed desalination capacity by technology (IDA 2002)

Technology	Percent of world's capacity (%)
Reverse osmosis (RO)	44
Multi-stage flash distillation (MSF)	40
Electrodialysis/Electrodeionization (ED)	6
Vapor Compression (VC)	5
Multi-effect distillation (MED)	3
Other	2

Table 12.3 Cumulative contracted capacity by technology since 1944 in the Middle East and North Africa (MENA) region (Source GWI 2010)

Technology	Percent of total installed capacity (%)
Multi-stage flash distillation (MSF)	53
Reverse osmosis (RO)	35
Multi-effect distillation (MED)	11

Table 12.4 Relative operating costs of desalination process ($/m^3) (Bushnak 2010; GWI 2010)

Technology	RO	MSF	MED
Parts	0.03	0.01	0.01
Chemicals	0.07	0.05	0.08
Labour	0.10	0.08	0.08
Membranes	0.03	0.00	0.00
Thermal energy	0.00	0.27	0.27
Electrical energy	0.23	0.19	0.06
Total	0.46	0.60	0.50

(in 1996) to 6.8 million m^3/day (in 2008) – (Bashitialshaaer et al. 2011) and is still increasing. The larger amount of brine will increase locally the salinity of the seawater used as intake by the desalination plants. As a result, the recovery ratio is expected to decrease and this will raise the cost of desalinated water – this can already be observed in some areas of the Arabian Gulf.

Some aspects related to the brine discharge in Red Sea by RO desalination plants will be considered next.

12.3 Hazards for Brine Disposal

The total dissolved solids in the Red Sea is 41 g/L, which is higher than 34.5 g/L for typical seawater (Magazine 2005). The desalination processes produce a concentrate which contains residues of pretreatment and cleaning chemicals, their reaction (by-) products, and heavy metals due to corrosion. Depending on the desalination technology, the concentrate may be increased in temperature. Most

Table 12.5 A summary of costs for different technologies for four different capacities (Wittholz et al. 2008 – case study Adelaide Australia)

	10,000			50,000			275,000			500,000		
Capacity (m^3/day)	RO	MSF	MED	RO	MSF	MED	RO	MSF	MED	RO	MSF	MED
Capital cost ($\$\times 10^6$)	20.1	48.0	28.5	74.0	149.5	108.4	293.0	498.1	446.7	476.7	759.6	734.0
UPC ($)	0.95	1.97	1.17	0.7	1.23	0.89	0.5	0.74	0.67	0.45	0.62	0.60

RO Reverse Osmosis, *MSF* Multi-Stage Flash Distillation, *MED* Multiple-Effect Distillation, *UPC* Unit Product Cost

desalination plants are using chemical pretreatment and cleaning. In thermal plants these include the treatment against biofouling, scaling, foaming and corrosion while the membrane plants are using treatments against biofouling, suspended solids and scale deposits. The chemical residues and by-products are usually discharged into the sea along with the concentrate. The effluent is a mix of these pollutants, which may have effects on marine life.

The amount of natural evaporation in Red Sea is much larger than the total amount of water extracted for desalination. However, evaporation takes place all over the surface area but the amount extracted for desalination is local and may have a greater effect than evaporation. The salt concentrations of the brines are usually found to be close to double that of natural seawater (Vanhems 2001). The salinity may increase by 70% after the brine of RO desalination plants is discharged into the sea (Ruiz-Mateo et al. 2007). Constructions close to the coastline give opportunities for one or more outfalls to the sea. This may reduce the local environmental impact of brine discharge (Raed et al. 2007). At the level of the whole Red Sea the increase in brine discharge raises significantly the salt concentration. The salinity of Red Sea in late 1996 and 2008 and predictions for 2050 is (in g/L) 0.22, 0.49 and 1.16, respectively. As seawater salinity increases, the recovery ratio decreases, which raises the cost of desalinated water.

Some of the environmental impacts of desalination plants, such as the land use, are similar to other development projects. Specific effects are the impingement and entrainment of organisms due to the intake of large quantities of seawater. The construction of the intake structure and pinping causes an initial disturbance of the seabed. This results in the re-suspension of sediments, nutrients or pollutants into the water column. After installation, the structures can affect water exchange and sediment transport, act as artificial reefs for organisms, or may interfere with shipping routes or other maritime uses.

The concentrate and chemical discharges to the marine environment are the key concerns of desalination plants. They may have adverse effects on water and sediment quality, impair marine life and the functioning of coastal ecosystems. The most negative effects occur when high waste water discharges coincide with sensitive ecosystems. The impacts on the marine environment depend on both, the properties of the reject streams and the biological features of the receiving environment. More sensitive to desalination plant discharges are the shallow sites with abundant marine life. Less sensitive are the open-sea locations, which are more capable to dilute and disperse the discharges.

The distribution of marine species is mainly controlled by salinity and temperature. Most organisms can adapt to minor deviations from optimal salinity and temperature conditions. Extreme situations may be tolerated temporarily. A continuous exposure to unfavourable conditions has however bad consequences on the survival rate. Thus, a constant brine discharge of high salinity and temperature may be fatal for marine life. This may change the composition and abundance of species in the discharge site. The more adapted species to the new situation will eventually prevail in the discharge site.

The discharge brines of RO and thermal plants have different effects on the seawater. The brine of RO plants has higher density than seawater. It will spread

over the sea floor in shallow coastal waters unless it is dissipated by a diffuser system. The most affected by the high salinity and chemical residues will be the benthic communities, such as seagrass beds. The brine of the thermal plants are typically positively or neutrally buoyant, especially when combined with power plant cooling waters. They will affect mainly the open water organisms.

The regulations usually refer to the limiting pollutant levels in the reject streams at the point of discharge (ES – effluent standards) and in the receiving environment (AS – ambient standards). For instance, the ratio ES/AS for copper is about 100 while for chlorine is 27. For most chemical and physical parameters (such temperature) the ratio ES/AS ranges between 5 and 1,000. This ratio describes appropriately the impact of the pollutants on the eco-system. Indeed, the ES may be considered to protect against acute (lethal) effects on organisms, while the AS is supposed to prevent long-time chronic influences. The necessary dilution that must be attained through physical mixing or by biological decay and chemical transformation processes may be equally well described by the ratio ES/AS.

A "combined approach" has been proposed in case of distillation brine discharge (Tobias et al. 2009). In analogy to wastewater discharges, it requires a regulatory mixing zone regulation. The mixing zone is defined as follows (Tobias et al. 2009):

> "The ambient standards apply in the case of point sources outside and at the edge of the mixing zone. The mixing zone is a spatially restricted region around the point source whose dimensions shall be specified either according to water body type and use or on an ad-hoc basis."

A similar approach is already used in the United States, the Sultanate of Oman and other countries (Tobias et al. 2009).

12.4 Brine Disposal by Submerged Pipe

There are several approaches to mitigate the environmental effects of the brine discharges. By tradition, the brine is discharged back to the sea in open channels. In the case of membrane technologies, dense RO effluent flow behave as negatively buoyant plume and spread on the sea floor. In the case of thermal technologies the effluent from thermal desalination plants could behave both neutral to positive buoyant flux causing the brine to rise and spread on the sea surface. Therefore effluent properties (i.e. flow, temperature, density, salinity etc.) have to be calculated at the discharge point. Impacts from high salinity may be avoided by pre-dilution of the desalination plant rejected stream with other waste streams, such as power plant cooling water. Impacts from high temperature may be avoided by ensuring heat dissipation from the waste stream to the atmosphere before entering the water body. Cooling towers may be used for this purpose. In the case of submerged disposal using long pipes the effluent temperature is decreasing while flowing towards the output section. However, simulations models for the brine plume dispersion from desalination power plants reveal the inadequacy of using surface discharging outfalls in order to brine discharging (Alameddine and El-Fadel 2007).

Large capacity plants require submerged discharges which ensure a high dilution, reducing the harmful impacts on the marine environment. Mixing and dispersal of the discharge plume can be enhanced by installing a diffuser system, and by locating the discharge in a favorable oceanographic site which dissipates the heat and salinity load quickly.

12.5 Technical and Environmental Evaluation

In this section we assess the technical viability of disposal the brine effluent produced by desalination plants into Red Sea coastal regions via submarine pipes. The largest operating capacities of desalination plants along Red Sea coast are located in Saudi Arabia, Egypt, Israel and Jordan. Thus, we shall consider a number of such facilities in order to assess technical and environmental solution for an optimum brine disposal. For other countries such as Yemen, Eritrea and Sudan similar case studies may be elaborated in the future.

Figure 12.2 shows the largest RO desalination plants operation on the Red Sea border. Most of these plants are located in Saudi Arabia. Smaller RO desalination plants are spread over the Egyptian coast. The Red Sea area belonging to Saudi Arabia has the following geographical characteristics: sea-surface area = 215,978 km^2, seabed area = 216,274 km^2, mean seabed slope = 1.42°, maximum seabed slope = 31.32° and the maximum depth offshore is −2,284 m (Costello et al. 2010). These values may be considered as representative for all calculations in this chapter.

Details about the technical and economical evaluation are presented in Sect. 12.5 for the particular case of the Rabigh desalination plant. This plant is using an Independent Water Steam Power Production unit (IWSPP) to generate electrical power with a 5 × 115 MW Steam Turbine Power Plant for supplying 16 trains RO units. The total installed capacity is about 192,000 m^3/day. Results for all representative stations in Fig. 12.2 are presented and discussed in Sect. 12.6.

The top of the hypothetical submarine pipe is located at a particular place on the Saudi Arabia coast. The pipe is couched on the bottom of the sea following a straight-line direction through Red Sea axis as shown in Fig. 12.3a.

Preliminary results obtained by the authors in case of a desalination plant located at Jeddah are reported in Badescu et al. (2012). The maximum length of the submarine pipe in that study was 10,000 m. This value has been obtained under the constraint of a maximum dispersion for the brine plume. The same maximum pipe length of 10,000 m is adopted in the present work since the geographical characteristics of Jeddah and Rabigh are quite similar. It corresponds to region A in Fig. 12.3a. In this chapter pipes of different length are considered in region A, which has been split in five sections. The sea-bottom in these regions is delimitated by the points described in Table 12.6. Points A1 to A5 in Fig. 12.3b are associated to the sea water free surface while points A1' to A5' in Table 12.6 represent potential discharge points of the underwater duct.

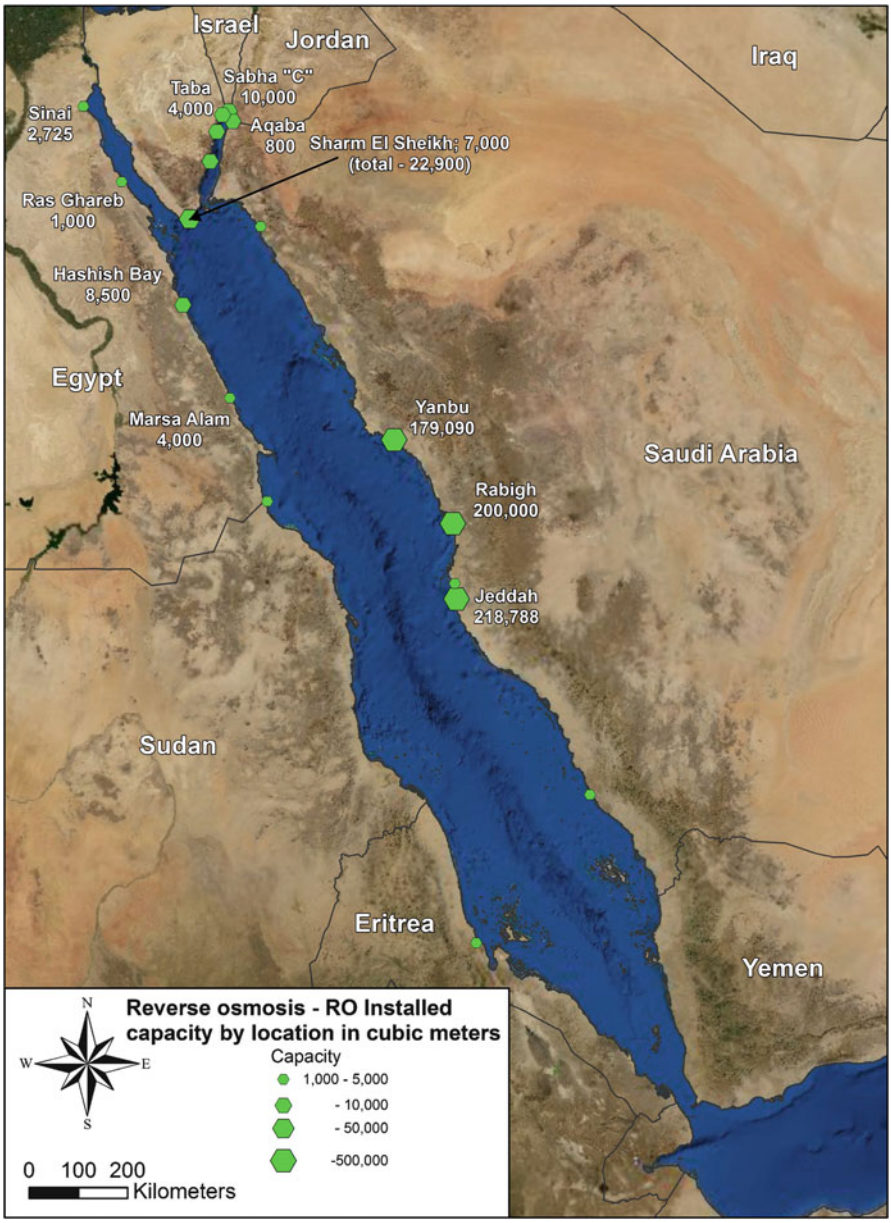

Fig. 12.2 Several RO desalination plants on Red Sea coast (El-Sadek 2010; Lattemann and Höpner 2008; Mohsen 2007; Khalil 2004; Semiat 2001) (Source of background: Esri, i-cubed, USDA, USGS, AEX, GeoEye, Getmapping, Aerogrid, IGN, IGP, and the GIS User Community)

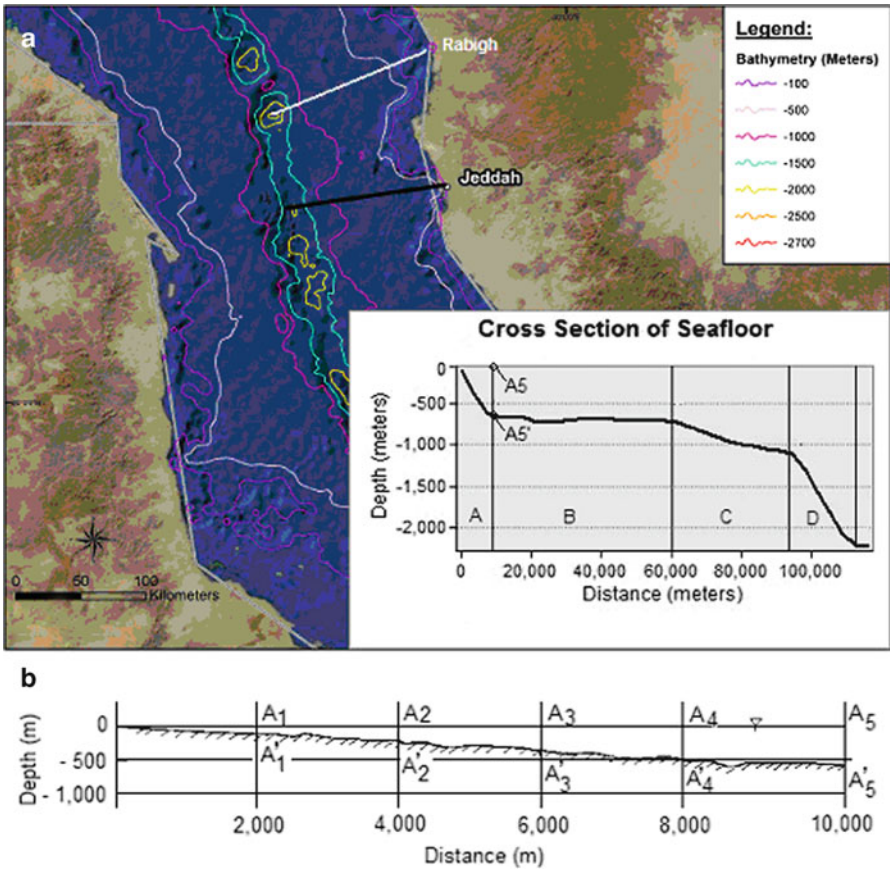

Fig. 12.3 (**a**) Course of the desalination concentrate pipe hugging the sea-bottom from Jeddah; (**b**) Cross section through region A

Table 12.6 Several parameters for pipes with discharge points A1' to A5' inside region A in Fig. 12.3b

Discharge point	Pipe discharge length l_X (m)	Pipe discharge depth $H_{n'}$ (m)
A1'	2,000	−110
A2'	4,000	−225
A3'	6,000	−335
A4'	8,000	−450
A5'	10,340	−580

12.5.1 Optimization of Brine Pipe Diameter

A simple hydraulic model is developed here. It involves computation of the optimum brine pipe diameter. A detailed presentation of the model is made in

Badescu et al. (2012) and a brief presentation is included here. The input data for this model consists of temperature values as well as salinity values for both the seawater and the brine inside the duct, at various depths. The influence of natural sea currents as well as seasonal climate variations is neglected.

These assumptions allow using data for seawater temperature and salinity provided by Tomczak and Godfrey (2003). Relationships from Millero et al. (1980) were used to calculate brine and seawater density as function of salinity, pressure and temperature. For convenience the brine salinity inside the pipe is a constant in time and space ($S_B = 74$ ppt), according to Raed et al. (2011), and the seawater salinity at the intake of the desalination plant in $S_I = 41.7$ ppt. Therefore, the brine density at the discharging end of the pipe is function just of pressure and temperature. Data for relevant discharge points A1' to A5' (see Fig. 12.3b) are presented in Table 12.7.

Figure 12.4 shows the brine basin of the desalination plant and the pipe. This figure is used to derive the equations for the optimization of the discharge pipe diameter. The brine level in respect to the seashore basin is denoted h. The basic scenario assumes $h = 0$ m, i.e. the surface of the brine in the basin is at the level of the sea surface. The discharging end of the pipe may be placed at the deeper extremity of one of the discharge points A1' to A5' in Fig. 12.3a, b.

For convenience, here we denote by X (=A1,A2,A3,A4,A4) any of the five sub-regions of region A. Similarly, n'(=1',2',3',4',5') denotes any of the five points on Fig. 12.3a, b and Table 12.6 . These points are placed at depth $H_{n'}$.

The length of the pipe whose discharging end is placed at the deepest point n' (=1',2',3',4',5') of region X(=A1,A2,A3,A4,A5) in Fig. 12.3b is denoted l_X. That pipe has a constant diameter denoted d_X. One denotes by $\rho_{B,0}$ and t_0, respectively, the mass density and the temperature of the brine in the basin of the desalination plant. Also, $\rho_{B,X}$ denotes the average mass density of the brine in the pipe, for a certain region X. This quantity is calculated as the arithmetical mean between the density of the brine in the basin ($\rho_{B,0}$) and the brine density $\rho_{B,n'}$ at the appropriate discharge point n'(=1',2',3',4',5') of the pipe, respectively:

$$\rho_{B,X} = \frac{\rho_{B,0}(t_0, p_{atm}, S_B) + \rho_{B,n'}\left(t_{sw,n'}, p_{n'} S_B\right)}{2} \tag{12.1}$$

Equation 12.1 shows that the brine density in the basin, $\rho_{B,0}$, depends on the atmospheric pressure p_{atm} and on the brine salinity S_B. The brine density in point n' depends on the brine temperature ($t_{n'}$) and pressure ($p_{n'}$) as well as on the brine salinity S_B, which is a constant along the pipe. The seawater density in points n (=1,2,3,4,5) at sea surface level and in points n'(=1',2',3',4',5) is denoted $\rho_{sw,n}$ and $\rho_{sw,n'}$, respectively. The average density of the seawater column of height $H_{n'}$ is denoted $\rho_{sw,X}$. It is computed as an arithmetical mean between the seawater density at surface ($\rho_{sw,n}$) and at the depth $H_{n'}$ ($\rho_{sw,n'}$) of the appropriate discharge point n'(=1',2',3',4',5'):

Table 12.7 Data for pipes with discharge points A1' to A5' in Fig. 12.3b

Discharge point	Pipe discharge length l_X (m)	Pipe discharge depth $H_{n'}$ (m)	Average brine density $\rho_{B,X}$ (kg/m^3)	Average seawater density $\rho_{sw,X}$ (kg/m^3)
A1'	2,000	−110	1,054.84	1,030.47
A2'	4,000	−225	1,055.06	1,030.69
A3'	6,000	−335	1,055.26	1,030.91
A4'	8,000	−450	1,055.49	1,031.14
A5'	10,340	−580	1,055.75	1,031.40

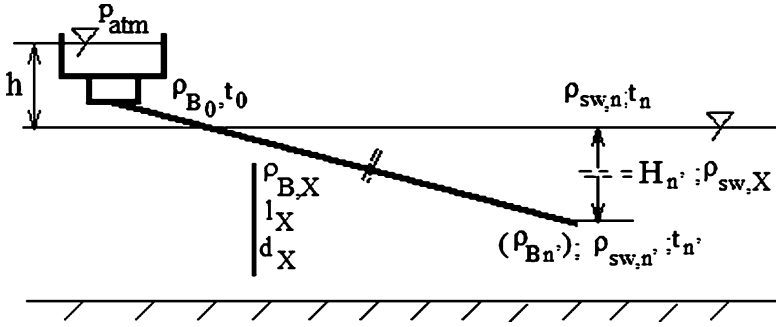

Fig. 12.4 Brine pipe layout for the hydraulic model considered

$$\rho_{sw,X} = \frac{\rho_{sw,n}(t_{sw,n}, p_{atm}, S_{sw,n}) + \rho_{sw,n'}(t_{sw,n'}, p_{n'}, S_{sw,n'})}{2} \tag{12.2}$$

Equation 12.2 shows that the seawater density in points n (=1,2,3,4,5') at sea surface level depends on the seawater temperature and salinity in that point, $t_{sw,n}$ and $S_{sw,n}$, respectively. Similarly, the seawater density in points n'(=1',2',3',4',5') depends on the seawater temperature, pressure and salinity in that point, $t_{sw,n'}$, $p_{sw,n'}$ and $S_{sw,n'}$, respectively.

One denotes by $V_{n'}$ the brine discharge velocity in point n' (=1',2',3',4',5'). The energy balance for the steady-state brine flow is:

$$\rho_{B,X} g(h + H_{n'}) = \frac{\rho_{B,X} V_{n'}^2}{2} + \rho_{sw,X} g H_{n'} + \Delta p_{lin,X} + \Delta p_{loc,X} \tag{12.3}$$

The l.h.s. of Eq. 12.3 represents the pressure due to the brine' weight at the discharge point n' (=1',2',3',4',5') of the pipe. The first and second terms in the r.h.s. of Eq. 12.3 are, respectively, the kinetic pressure of the brine at the discharge point and the seawater static pressure at the same point. Finally, $\Delta p_{lin,X}$ and $\Delta p_{loc,X}$ in Eq. 12.3 are de linear and local pressure losses inside the pipe, respectively. These last two quantities may be computed by (Florea and Panaitescu 1979):

$$\Delta p_{lin,X} + \Delta p_{loc,X} = \frac{\rho_{B,X}}{2}\left(\frac{4Q_B}{\pi d_X^2}\right)^2\left(\lambda_{lin,X}\frac{l_X}{d_X} + \zeta_{loc,X}\right) \tag{12.4}$$

where $\zeta_{loc,X}$ and $\lambda_{lin,X}$ are the coefficients of local and linear pressure losses, respectively. Local pressure losses may be neglected in case of very long pipes, as we shall do here. The coefficient $\lambda_{lin,X}$ has been computed by:

$$\lambda = \frac{8g}{C^2}, \tag{12.5}$$

where the Chézy coefficient C could be calculated, in this stage, by using Bazin's formula (Florea and Panaitescu 1979):

$$C = \frac{87}{1 + \frac{\gamma}{\sqrt{R}}}, \tag{12.6}$$

For an average pipe roughness (fabric pipe tape, for instance), R = d/4 and $\gamma = 0.6$ in Eq. 12.6. Usage of Eqs. 12.3, 12.4, 12.5, and 12.6 yield another form of the energy balance equation:

$$\rho_{B,X} g(h + H_{n'}) = \rho_{sw,X} g H_{n'} + \frac{\rho_{B,X}}{2}\left(\frac{4Q_B}{\pi d_X^2}\right)^2\left(0.01036\frac{\left(\sqrt{d_X} + 0.32\right)^2}{d_X^2} l_X + 1\right) \tag{12.7}$$

The available head in the discharge section of the brine pipe is given by:

$$H_a = H_t - h_d, \tag{12.8}$$

where H_t is the total head and h_d is the friction losses in the pipe, associated to the waste brine discharge point n' in section X. These quantities are given by:

$$H_t = \frac{H(\rho_{B,X} - \rho_{sw,X})}{\rho_{sw,X}};\ h_d = \frac{\Delta p_{linX}}{\rho_{B,X} g} \tag{12.9a,b}$$

where H is seawater depth. Equation 12.7 may be used to obtain the optimum diameter of the underwater pipe which maximizes the available head H_a. Results are shown in Table 12.8 for the sub-regions A1 to A5 of region A in Fig. 12.3a, b.

A few explanatory comments follow. The optimum pipe diameter d_X is about 1.4 m, for all input values for the pipe length l_X. The available head H_a increases by increasing the pipe discharge depth $H_{n'}$. However, the linear losses increase by increasing $H_{n'}$, since this means a longer pipe length l_X. Therefore, using pipes longer than about 2,000 m is not justified from a hydraulic point of view. Indeed,

Table 12.8 Results for the optimum pipe diameter in sub-regions A1' to A5' of region A in Fig. 12.3a, b

Discharge point	Pipe discharge length l_X (m)	Pipe discharge depth $H_{n'}$ (m)	Average brine density $\rho_{B,X}$ (kg/m^3)	Average seawater density $\rho_{sw,X}$ (kg/m^3)	Linear loses coefficient λ (−)	Linear head losses h_d (m)	Total head H_t (m)	Brine velocity $V_{n'}$ (m/s)	Available head $H_a = H_t - h_d$ (m)	Pipe diameter d_X (m)
A1'	2,000	110	1,054.84	1,030.47	0.0167	2.44	2.60	1.42	0.16	1.410
A2'	4,000	225	1,055.06	1,030.69	0.0167	5.09	5.31	1.43	0.22	1.400
A3'	6,000	335	1,055.26	1,030.91	0.0167	7.62	7.91	1.44	0.28	1.399
A4'	8,000	450	1,055.49	1,031.14	0.0167	10.27	10.62	1.45	0.35	1.397
A5'	10,340	580	1,055.75	1,031.40	0.0167	13.26	13.69	1.45	0.42	1.396

Volumic brine flow rate is $Q_B = 2.222$ m^3/s, which corresponds to Rabigh desalination plant

using longer pipes is not associated to a decrease of the pipe diameter, which would result in a relative decrease of pipe cost.

However, the optimization of the pipe diameter should take into account the brine dispersion process at the outlet section of the pipe. Discharging the desalination brine on the seabed of the Red Sea increases locally the salt concentration of the seawater. This may disrupt the ecosystem in the dilution zone, leading to dehydration, decrease of turgor pressure, and death of benthic marine organisms. The distance the plume travels before it contacts the ocean bottom is defined as the mixing zone (Kimes 1995). The mixing zone is a function of both pipe diameter d_X and available head H_a.

12.5.2 Optimization of Pipe Length and Brine Jet Dispersion Length

The environmental issues considered in the Sect. 12.5.1 require calculation of the maximum brine flow velocity at discharge, the optimum pipe length related to emitted jet length and the extent of the maximum dilution zone. The most efficient method for brine discharging into the seawater is a subject of intense R&D. A common solution to ensure better dilution is to use inclined under-sea jets, (30–45° above horizontal) obtained by throttling the cross-section of the pipe end. This requires knowledge of the hydraulic energy available at the outlet pipe cross-section. Results in Sect. 12.5.1 show that the discharge point A1' (i.e. $l_X = 2{,}000$ m, $H_{n'} = 110$ m, $h = 0$ m) is the best solution from the hydraulic point of view. However, a more precise value of the available head H_a is needed in order to evaluate more accurately the available brine jet length. Several parameters have been computed for the discharge points A1' to A5' (see Table 12.7). For all these points, the notation and computational procedure of Sect. 12.5.1 have been used. Jet velocities emissions produced by a nozzle placed at each discharge points A1' to A5' have been computed by using a relationship similar to Eq. 12.4:

$$\rho_{B,X} g H_{n'} = \rho_{sw,X} g H_{n'} + \frac{\rho_{sw,X} V^2_{nozzlen'}}{2}(1 + \zeta_{nozzle}) + \frac{\rho_{B,X} V^2_{n'}}{2} \lambda_X \frac{l_X}{d_X} \tag{12.10}$$

Here the notation of Fig. 12.4 has been used while $V_{n'}$ and $V_{nozzle\ n'}$ is the velocity of the brine along the pipe and at nozzle discharge point, respectively. In Eq. 12.10, ζ_{nozzle} is the coefficient of local head losses related to the d_{nozzle}/d_X ratio (Florea and Panaitescu 1979). Note that V_{nozzle} enters the flow equation:

$$\left(\frac{d_{nozzlen'}}{d_X}\right)^2 = \frac{V_{n'}}{V_{nozzlen'}} \tag{12.11}$$

Three values of the ratio d_{nozzle}/d_X have been considered as input.

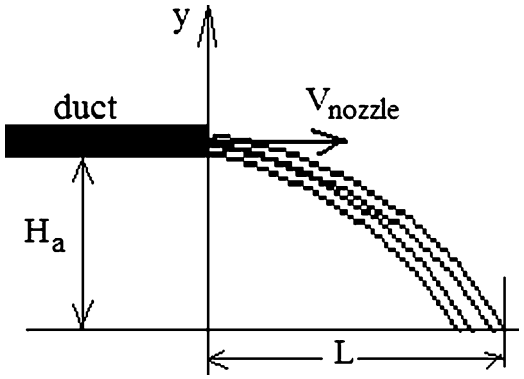

Fig. 12.5 Geometrical configuration of the brine jet

Figure 12.5 shows the geometrical configuration of the brine jet. A point (x, y) on brine jet trajectory obeys the following standard kinematic relationships:

$$x = V_{nozzle}t; y = H_a - \frac{g'_0 t^2}{2} \tag{12.12}$$

where:

$$g'_0 = g\frac{\rho_{B,X} - \rho_{sw,X}}{\rho_{sw,X}} \tag{12.13}$$

is the reduced gravity. Using Eqs. 12.12 and 12.13 yields:

$$y = H_a - \frac{g(\rho_{B,X} - \rho_{sw,X})}{2\rho_{sw,X}V^2_{nozzle}}x^2 \tag{12.14}$$

Equation 12.14 allows deriving the jet horizontal length L, taking into account that $y = 0$ is associated to $x = L$:

$$L = V_{nozzle}\sqrt{\frac{2H_a}{g\frac{\rho_{B,X}-\rho_{sw,X}}{\rho_{sw,X}}}} \tag{12.15}$$

Equation 12.15 and Table 12.8 are used now to compute the jet horizontal length L for the five discharge points A1' to A5' defined in Table 12.7. Results are given in Table 12.9. The dependence of the jet length L on the sea water depth H in shown in Fig. 12.6.

Table 12.9 shows that the values of $V_{nozzlen'}$ range between 3.53 and 6.41 m/s for d_{nozzle} values ranging between 0.47 and 0.28 m. This is in reasonable agreement with results of similar calculations (Tobias et al. 2009). Generally, larger ejection nozzle velocities increase the horizontal length of the brine jet. Also, the jet length increases by increasing the depth of the discharge point. However, knowing the length L of the brine jet is not enough to evaluate the efficiency of the brine dispersion process. It remains to be assessed whether the surface area covered with brine on the sea-bottom is large enough to obey the ecological constraints.

Table 12.9 Horizontal length *L* of the brine jet for given discharge point and values of the ratio d_{nozzle}/d_X

Discharge point	Pipe discharge length l (m)	Pipe discharge depth H_n, (m)	Pipe diameter d_X (m)	Brine velocity V_n, (m/s)	Diameter ratio $\frac{d_{nozzle}}{d_X}$ (−)	Nozzle Losses coefficient ζ (−)	Nozzle diameter d_{nozzle} (m)	Nozzle velocity $V_{nozzle\ n}$, (m/s)	Jet horizontal length L (m)	Densimetric Froude number $(F_o)_{max}$ (−)	Raynolds number (Re x $10^6)_{max}$ (−)
A1'	2,000	110	1.41	1.42	0.33	0.4	0.47	3.53	4.16	10.68	1.27
					0.25	0.42	0.35	4.17	4.91	14.57	1.13
					0.2	0.45	0,28	4,59	5.41	17.9	0.99
A2'	4,000	225	1.40	1.43	0.33	0.4	0.46	3.9	5.46	11.87	1.4
					0.25	0.42	0.349	4.82	6.75	16.94	1.29
					0.2	0.45	**0.28**	**5.53**	**7.74**	**21.71**	**1.91**
A3'	6,000	335	1.399	1.45	0.33	0.4	0.466	4.02	6.33	12.23	1.44
					0.25	0.42	0.35	5.08	8.00	17.84	1.36
					0.2	0.45	**0.28**	**9.94**	**9.36**	**23.35**	**1.28**
A4'	8,000	450	1.397	1.45	0.33	0.4	0.465	4.116	7.18	12.53	1.47
					0.25	0.42	0.349	5.254	9.17	18.47	1.41
					0.2	0.45	**0.279**	**6.22**	**10.87**	**24.47**	**1.33**
A5'	10,340	580	1.396	1.45	0.33	0.4	0.465	4.164	7.96	12.68	1.49
					0.25	0.42	0.349	5.361	10.24	18.84	1.44
					0.2	0.45	**0.279**	**6.41**	**12.26**	**25.22**	**1.37**

The associated *Re* and F_o numbers are also shown. *Bold values* denote the best design solutions

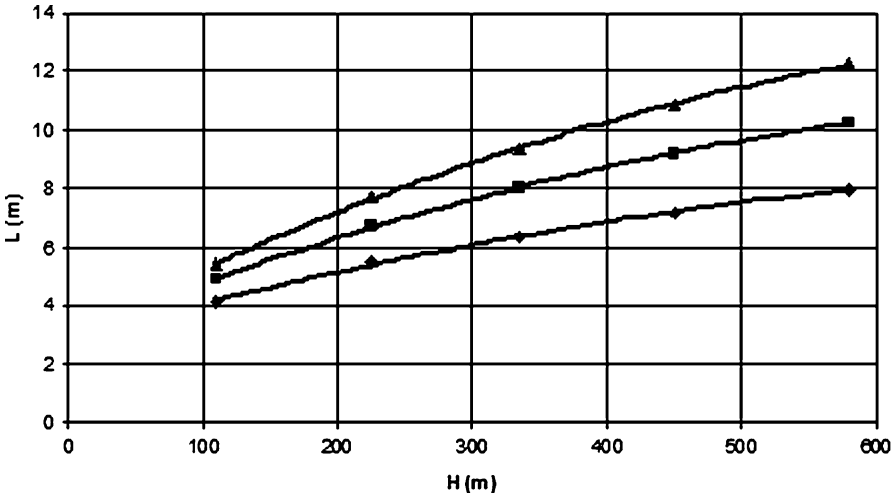

Fig. 12.6 The horizontal brine jet length L as a function of seawater depth H for three values of nozzle diameter ratio, d_{nozzle}/d_X (▲-0.2; ■-0.25; ♦- 0.33)

The space distribution of brine concentration depends on the sitting of the outfall and the amount of mixing and transport capacities of the prevailing marine current. High mixing efficiencies occur at high-flow velocities at offshore discharge location (Bleninger and Jirka 2008). A few models were developed previously to predict dispersion and mixing of brine discharges (see CORMIX (Cornell Mixing Zone Expert) by Doneker and Jirka 2001). However, they have limited relevance since data concerning pollutant concentration along the brine plume are not readily available. Indeed, obtaining consistent data sets requires monitoring to be carried out every 6 months for a period of 4 years on a radius of 200 m around the submarine outfall point . From this point of view evaluation of sediment chlorite levels enables the desalination effects to be quantified (Alharbi et al. 2012). Since elevated chlorite levels are directly linked to the desalination technology and site specific feature it is suggested that such studies be undertaken at desalination plants on regular basis. In practice, the appropriate value of the brine dilution is obtained by choosing a value of the densimetric Froude number F_o within the (empirically derived) recommended range of variation. Next, this value is used to compute the surface area of the pipe discharge section. However, our method computes the optimum brine flow geometrical data associated to the maximum available head H_a. Therefore, a reversed approach is adopted here to assess the quality of the dilution process. It uses the Froude (F_o) and Reynolds (Re) numbers of the brine discharge jet, defined as follows (Bleninger et al. 2009)

$$F_0 = \frac{V_{nozzlen'}}{\sqrt{|g_0'|d_{nozzle}}};\ \mathrm{Re} = \frac{V_{nozzlen'}\, d_{nozzle}}{v_{brine}}; \tag{12.16}$$

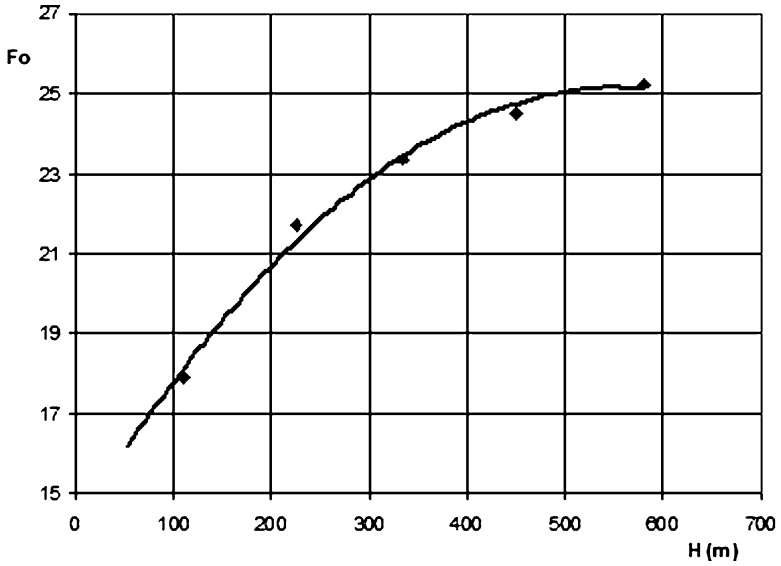

Fig. 12.7 Dependence of Froude number at maximum nozzle velocity $V_{nozzle\ n'}$ on seawater depth H

Here ν_{brine} (= 1,3 10^{-6} m^2/s) is the brine kinematic viscosity. Good mixing conditions are fulfilled if $F_o > 10$ (with an optimum ranging between 20 and 25) and Re >4,000 (Tobias et al. 2009). Results are shown in Table 12.9. A pipe length l_X = 2,000 m (associated to the discharge point A1', which has been found in Sect. 12.5.1 to be the optimum hydraulic solution) corresponds to a Froude number F_o = 18, which is not in the optimum range 20–25. Thus, the hydraulic optimum of the pipe length does not coincide with the optimum pipe length from the point of view of brine jet dissipation.

Figure 12.7 shows the dependence of the Froude number F_o on the sea depth H for several values of the maximum speed $V_{nozzlen}$'. Using Fig. 12.7 and Table 12.9 one sees that an optimum dissipation of the brine jet is obtained for pipes of lengths ranging between 3,000 and 4,000 m. This is not acceptable from a technical and economical viewpoint.

Therefore, other design solutions should be found in order to ensure a good dissipation of the brine discharge. A few comments follow concerning the methods of increasing the brine jet dilution effectiveness. Higher values of the available head H_a are needed in order to obtain higher values of the jet length L (see Eq. 12.15). Higher values for H_a may be obtained by using longer pipes. However, this solution is not always acceptable from an economic point of view (see Sect. 12.5.3). A second solution is to use a seashore basin for brine storage placed at a certain level h above the sea level (see Fig. 12.4). This second solution is considered and analyzed in some details next. A brine storage basin placed at h = 5 m above current sea level is considered. Also, the pipe discharge end is placed in point A1'

(i.e. $H_{n'} = 110$ m; $l = 2{,}000$ m; see Table 12.8). Equations 12.7, 12.8, 12.9, 12.10, 12.11, 12.12, 12.13, 12.14, and 12.15 are used. Results are shown in Table 12.10.

The best results are obtained for $F_o = 26$. Indeed, higher Froude numbers are associated to higher pressure losses (Bleninger et al. 2009).

A proper solution for the desalination waste brine disposal process requires a good balance between technical constraints (i.e. placing a pipe on the sea-bottom), environmental conditions (i.e., finding an optimum distance from the seashore where high salinity brine should be discharged without significant environmental impact; also, the availability for long run of brine disposal placement should be considered) and as low as possible overall economic costs. First, the technical constraints required to properly design, place and operate a submerged pipe. This means, for the bottom-line, calculation of the optimum brine pipe diameter d_X and pipe length l_X for which the maximum available head H_a is obtained. The basic scenario for region *A1* (see Table 12.9) may be used as a reference. Second, the environmental issue requires us to obtain the maximum horizontal discharge jet length L. This ensures a high dilution near the pipe end. The basic scenario for region A1 (see Table 12.10) may be used again as a reference. Third, cost estimates are briefly outlined in Sect. 12.5.3. A short discussion on these lines of thought follows. Common practice of extant desalination plants shows that 200 m from shore is the geographical limit to intake seawater while the ordinary limit to brine discharge is at least 500 m. Thus, we shall consider a pipe of length $l = 1{,}000$ m discharging in point A1" at seawater depth $H = 56$ m. These assumptions agree with the seabed slope of Fig. 12.3a, b. A brine basin placed at height $h = 5$ m above sea level is assumed. Results are presented in Table 12.11.

As expected, the values of the Froude number in Table 12.11 for discharge point A1" are higher than those of Table 12.10 for discharge point A1'. The values in Table 12.11 correspond to very good dilution. The best solution is found for $F_o = 21.6$. Further decreasing of the pipe length may increase the water salinity near the Red Sea border.

A competing solution, with similar effects, is to use free-surface channels for brine disposal. This solution is cheaper but has two major weaknesses. First, gravitational brine falling towards the seabed may be perturbed uncontrollably by natural and unnatural marine currents. Second, increasing the desalination process efficiency will increase the brine salinity, which, in turn, will increase the negative environmental impacts.

12.5.3 Cost Estimates

Only building costs are considered here. Maintenance costs and other costs such as costs associated to damage repairs are not considered. Details can be found in Badescu et al. (2012). To compute the cost of the brine discharge pipe first its capacity is estimated, as a function of the length l_X and diameter d_X. Results are shown in 2010 US dollars in Fig. 12.8.

Table 12.10 Pipe diameter d_X and horizontal length L of the brine jet related to F_o numbers for discharge point A1'

Discharge point	Pipe discharge length l (m)	Pipe discharge depth $H_{n'}$ (m)	Pipe diameter d_X (m)	Brine velocity $V_{n'}$ (m/s)	Diameter ratio $\frac{d_{nozzle}}{d_X}$ (−)	Nozzle Losses coefficient ζ (−)	Nozzle diameter d_{nozzle} (m)	Nozzle velocity $V_{nozzle\ n'}$ (m/s)	Jet horizontal length L (m)	Densimetric Froude number $(F_o)_{max}$ (−)
A.1'	2,000	110	1.44	2.163	0.33	0.4	0.381	5.57	8.94	18.73
					0.25	**0.42**	**0.285**	**6.69**	**10.75**	**25.99**
					0.2	**0.45**	**0,228**	**7,48**	**12.01**	**32.49**

Bold entries correspond to optimum Froude values

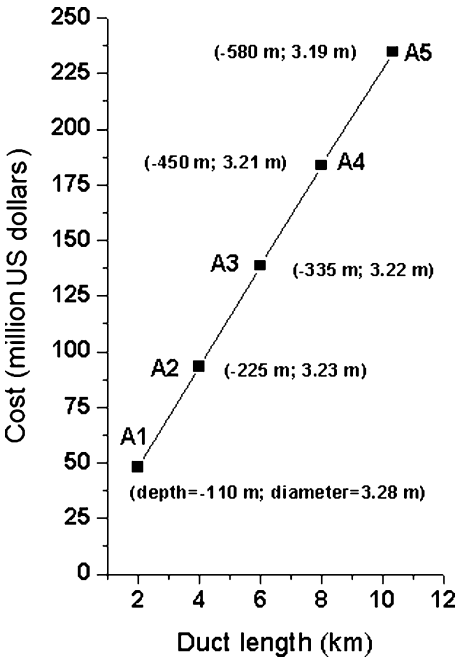

Fig. 12.8 Cost of pipes of various lengths, depending on the depth of discharge point and pipe diameter. Discharge point at the end of regions A1 to A5 in Table 12.7. The presumed pipe material is steel

The costs range from $48 \cdot 10^6$ $ for discharge point A1 to $237 \cdot 10^6$ $ for discharge point A5. Costs are significantly reduced when plastic or fabric is used (see Badescu et al. 2012 for details). In case of plastic pipes the cost ranges from $39 \cdot 10^6$ $ for discharge point A1 to $190 \cdot 10^6$ $ for discharge point A5. When fabric pipes are considered, the cost ranges from $44 \cdot 10^6$ $ for discharge point A1 to $163 \cdot 10^6$ $ for discharge point A5.

12.6 Data for Some Desalination Plants Located on the Red Sea Coasts

Figures 12.1 and 12.2 show that about half of the Red Sea desalination plants are based on reverse osmosis. The percentage of RO plants is expected to increase, taking into account the lower production costs and the favorable technological evolution. The most representative RO desalination plants around the Red Sea coast are considered next both by country and by capacity points of view. In order to provide relevant conclusions for the study reduced capacity desalination plants were selected due to their large number. For not available/existing desalination plants some hypothetic "case studies" were considered. Also, the same bathymetric conditions were selected. The method described in Sects. 12.5.1 and 12.5.2 is used

Table 12.11 Pipe diameter d_X and horizontal length L of the brine jet related to F_o numbers for discharge point A1" ($l_x = 1{,}000$ m, $H_{n'} = 56$ m)

Discharge point	Pipe discharge length l (m)	Pipe discharge depth $H_{n'}$(m)	Pipe diameter d_X (m)	Brine velocity $V_{n'}$ (m/s)	Diameter ratio $\frac{d_{nozzle}}{d_X}$ (−)	Nozzle Losses coefficient ζ (−)	Nozzle diameter d_{nozzle} (m)	Nozzle velocity $V_{nozzle\ n'}$ (m/s)	Jet horizontal length L (m)	Densimetric Froude number $(F_o)_{max}$ (−)
A.1"	**1,000**	**56**	**1.042**	**2.607**	**0.33**	**0.4**	**0.347**	**6,14**	**8.94**	**21.63**
					0.25	0.42	0.260	7.08	12.76	28.81
					0.2	0.45	0.208	7.66	13.8	34.84

Bold entries correspond to optimum Froude values

to estimate the optimum design solution of the underwater discharge pipes associated to all these plants.

The best brine dispersion on the sea bottom is associated to values of the Froude number ranging from 21 to 23. Table 12.12 shows that these Froude number values may be obtained by changing the free-surface level h of the brine in the desalination plant's basin. A few comments about the results obtained for a ratio $d_{nozzle}/d_x = 0.33$ follow.

Large and very large desalination plants (exceeding 25,000–50,000 m^3/day) are first considered. In Sect. 12.5.1 it has been shown that the optimum pipe length is about $l_X = 1{,}000$ m. Optimum Froude number values associated to this optimum pipe length, are obtained for a brine free-surface level $h = 5$ m.

In case of smaller desalination plants, ranging between 4,000 and 10,000 m^3/day, the same brine free-surface level $h = 5$ m yields optimum values of the Froude number for pipe length around $l_X = 1{,}000$ m. Shorter pipes should be also considered, since such smaller plants are subjected to more restrictive economical constraints. For example, in case of shorter pipes around $l_X = 500$ m a smaller brine free-surface level (around $h = 3$ m) is needed to obtain optimum Foude number values.

For very small desalination plants, ranging between 500 and 3,500 m^3/day, the brine free-surface level should be increased to about $h = 8$ m in order to obtain optimum Froude numbers for pipe length around $l_X = 1{,}000$ m. In case of shorter pipes ($l_X = 500$ m) the brine free-surface level should be decreased to about $h = 3$ m.

Table 12.12 shows that the optimum brine dispersion may be obtained by using underwater pipes for any sort of high capacity and low capacity RO desalination plants operating on the Red Sea coasts. In case of large capacities, a pipe length around $l_X = 1{,}000$ m allows optimum operation. A pipe length about $l_X = 500$ m is needed for low capacity RO desalination plants. Desalination capacities exceeding 15,000 m^3/day need longer underwater pipes and brine basins located on the sea shore. Optimum dispersion is associated to Froude numbers ranging between 20 and 23 and corresponds to a brine free-surface level in the basin around $h = 5$ m.

The model developed in this chapter covers a large range of brine flow rates. The linear pressure losses increase by decreasing the underwater pipe diameters. Thus, the range of optimum Froude number values should be extended towards larger values. However, using the recommended optimum Froude number values (Tobias et al. 2009) is a conservative attitude.

12.7 Conclusion

Increasing the efficiency of the seawater desalination process increases the salt concentration in the waste brine. This may raise ecological problems if the brine disposal is made by free-surface channels into the nearby Red Sea. A solution to avoid these problems is to use submerged pipes for brine disposal. The geometry

Table 12.12 Optimum brine dispersion – for similar F_o numbers – using underwater pipes for any sort of high capacity and low capacity RO desalination plants operating on the Red Sea coasts

Country	Desalination plant	Capacity C (m^3/day)	Pipe discharge length l_X (m)	Pipe discharge depth $H_{n'}$ (m)	Available head $H_a = H_t - h_d$ (m)	Pipe diameter d_X (m)	Brine velocity $V_{n'}$ (m/s)	Diameter ratio $\frac{d_{nozzle}}{d_X}$ (−)	Nozzle losses coefficient ζ (−)	Nozzle diameter d_{nozzle} (m)	Nozzle velocity $V_{nozzle\ n'}$ (m/s)	Jet Horiz. length L (m)	Densimetric Froude number $(F_0)_{max}$ (−)
Saudi Arabia	Jeddah	218,788 (Lattemann and Höpner 2008)	1,000	56	0.398	**1.096**	2.685	0.33	0.40	**0.365**	**6.251**	**11.58**	**21.47**
								0.25	0.42	0.274	7.180	13.30	28.47
								0.2	0.45	0.219	7.73	14.33	34.31
	Rabingh	192,000 (Lattemann and Höpner 2008)	1,000	56	0.376	**1.042**	2.607	0.33	0.40	**0.347**	**6,14**	**11.06**	**21.63**
								0.25	0.42	0.260	7.08	12.76	28.81
								0.2	0.45	0.208	7.66	13.80	34.84
	Yanbu	179,090 (Lattemann and Höpner 2008)	1,000	56	0.366	**1.014**	2.566	0.33	0.40	**0.338**	**6.08**	**10.78**	**21.71**
								0.25	0.42	0.253	7.03	12.47	28.99
								0.2	0.45	0.202	7.62	13.51	35.12
Egypt[a]	Hashish Bay	8,500 (Khalil 2004)	1,000	56	0.108	**0.318**	1.235	0.33	0.40	**0.106**	**3.47**	**3.35**	**22.11**
								2.25	0.42	0.079	4.39	4.24	32.36
								0.2	0.45	0.063	5.17	4.99	42.55
			500	30	0.137	0.285	1.535	0.33	0.40	0.095	4.13	4.49	27.80
					0.102[c]	**0.309[c]**	1.305[c]			**0.103[c]**	**3.48[c]**	**3.27[c]**	**22.49[c]**
								0.25	0.42	0.071	5.1	5.55	39.65
										0.077	4.26	4.00	31.82
								0.2	0.45	0.057	5.84	6.36	50.75
										0.061	4.85	4.56	40.47
	Sharm El Sheikh (Southern Water Co.)	7,000 (El-Sadek 2010)	1,000	56	0.100	**0.296**	1.176	0.33	0.40	**0.098**	**3.32**	**3.1**	**21.96**
								0.25	0.42	0.074	4.22	3.94	32.26
								0.2	0.45	0.059	4.99	4.66	42.61
			500	30	0.126	0.265	1.462	0.33	0.40	0.088	3.97	4.14	27.74
										0.096[c]	**3.34[c]**	**3.03[c]**	**22.43[c]**
					0.095	**0.288[c]**	1.243[c]	0.25	0.42	0.066	4.93	5.14	39.73
										0.072	4.12	3.72	31.93
								0.2	0.45	0.053	5.67	5.91	51.12
										0.057	4.72	4.26	40.83
								0.33	0.40	**0.08**	**2.92**	**2.49**	**21.43**

Israel	Shabba "C"	10,000 (Semiat 2001)	1,000	56	0.114	**0.338**	1.28	0.33	0.40	**0.112**	**3.59**	**3.56**	**22.23**
								0.25	0.42	0.084	4,54	4,50	32.41
								0.2	0.45	0.067	5.32	5.27	42.46
			500	30	0.146	0.303	1.59	0.33	0.40	0.101	4.27	4.81	27.90
										0.109[c]	**3.39**[c]	**3.5**[c]	**22.51**[c]
								0.25	0.42	0.076	5.25	5.90	39.55
					0.110	**0.329**[c]	1.35[c]			0.082	4.38	4.27	31.70
								0.2	0.45	0.060	5.98	6.73	50.38
										0.065	4.96	4.84	40.13
Jordan	Aqaba[b]	800 (Mohsen 2007)	1,000	56	0.056	0.144	0.709	0.33	0.40	0.048	2.08	1.45	19.71
										0.044[d]	**2.40**[d]	**1.79**[d]	**23.61**[d]
								0.25	0.42	0.036	2.72	1.89	29.78
					0.064[d]	**0.134**[d]	0.818[d]			0.033	3.15	2.35	35.74
								0.2	0.45	0.028	3.32	2.31	40.62
										0.026	3.85	2.87	48.86
			500	30	0.056	0.123	0.88	0.33	0.40	0.043	2.54	1.78	25.42
										0.046[c]	**2.15**[c]	**1.34**[c]	**20.76**[c]
								0.25	0.42	0.032	3.28	2.30	37.96
													30.89
					0.045[c]	**0.140**[c]	0.75[c]			0.035	2.78	1.73	
								0.2	0.45	0.025	3.95	2.76	51.05
										0.028	3.33	2.07	41.38
Case study 1	N.A.	25,000	1,000	56	0.163	**0.478**	1.61	0.33	0.40	**0.159**	**4.34**	**5.16**	**22.62**
								0.25	0.42	0.119	5.36	6.36	32.22
								0.2	0.45	0.095	6.14	7.28	41.24
Case study 2	N.A.	50,000	1,000	56	0.216	**0.621**	1.90	0.33	0.40	**0.207**	**4.95**	**6.76**	**22.59**
								0.25	0.42	0.155	5.98	8.16	31.51
								0.2	0.45	0.124	6.71	9.17	39.56

[a]In Egypt there are several desalination plants with the same capacity – 4,000 m^3/day

[b]In Jordan there are also desalination plants with higher capacities (e.g. Akman: 3,028 m^3/day – Mohsen 2007) but here location was selected for exemplification purposes

[c]$h = 3$ m

[d]$h = 8$ m

Bold entries correspond to optimum Froude values

of these pipes should be optimized in order to allow larger brine dispersion lengths. A case study is presented in this paper, focusing on brine disposal for the desalination plant Rabigh in Saudi Arabia, on its Red Sea shoreline.

The central concept of the brine disposal by submerged pipes is the available head at the discharge point. This quantity should be as high as possible. Higher values of the available head ensure larger jet dispersion lengths and better conditions for ejected brine dilution. We have shown that the quality of the dilution process is well quantified by the Froude number of the brine discharge jet, whose optimum values range between 20 and 25. Using the Froude number allowed us to find the optimum pipe length and the optimum depth of the discharge point.

Higher values for the available head may be obtained either by extending the desalination brine waste pipe length or by using an onshore basin for brine storage placed at a certain level h above the existing local sea-level. The first solution may be economically prohibitive. The case treated in this paper shows that an onshore brine storage basin placed about 5 m above sea-level allows a good brine jet dispersion even for relatively short discharge pipes.

A proper decision about the brine disposal method must take into account technical, environmental, as well as economic constraints. The cost depends on pipe length and pipe material, as expected. Costs are significantly reduced when plastic or fabric pipes are used instead of traditional steel-made pipes.

About half of the Red Sea desalination plants are based on reverse osmosis. The percentage of RO plants is expected to increase, taking into account the lower production costs and the favorable technological evolution. Using underwater pipes for avoids some of the hazards of brine disposal. Optimum brine dispersion may be obtained by using underwater pipes for any sort of high capacity and low capacity RO desalination plants operating on the Red Sea coasts. In case of large capacities, a pipe length around $l_X = 1{,}000$ m allows optimum operation. A pipe length about $l_X = 500$ m is needed for low capacity RO desalination plants.

References

Alameddine I, El-Fadel M (2007) Brine discharge from desalination plants: a modeling approach to an optimized outfall design. Desalination 214:241–260

Al-Gobaisi DMA (1997) Sustainable augmentation of fresh water resources through appropriate energy and desalination technology. IDA World Congress on Desalination and Water Reuse, Madrid

Alharbi OA, Phillips MR, Williams AT, Gheith AM, Bantan RA, Rasul NM (2012) Desalination impacts on the coastal environment: Ash Shuqayq, Saudi Arabia. Sci Total Environ 421–422:163–172

Anton P, Al-Barwani HH, Smith R (2005) Calculating the environmental cost of seawater desalination in the Arabian marginal seas. Desalination 185:79–86

Badescu V, Ciocanea A, Cathcart RB, Finkl CW et al (2012) Desalination brine disposal by submerged pipes in Red Sea. J Coast Res DOI:10.2112/JCOASTRES-D-12-00060.1

Bashitialshaaer RAI, Persson KM, Aljaradin M (2011) Estimated future salinity in the Arabian Gulf, the Mediterranean Sea and the Red Sea consequences of brine discharge from desalination. Int J Acad Res 3(1 Part I):133–140

Bleninger T, Jirka GH (2008) Modelling and environmentally sound management of brine discharges from desalination plants. Desalination 221:585–597

Buros OK (1998) The ABCs of desalting, 2nd edn. International Desalination Association Topsfield, Topsfield

Bushnak AA (2010) Water: sustainable management of a scarce resource. In: Mohamed El_Ashry, Najib Saab, Bashar Zeitoon (ed) Chapter 8: Desalination. Pub. Arab Forum for Environmental and Development (AFED). Beirut, Lebanon

Costello MJ, Cheung A, De Hauwere N (2010) Surface area and the seabed area, volume, depth, slope, and topographic variation for the world's seas, oceans, and countries. Environ Sci Technol 44:8821–8828

Doneker RL, Jirka GH (2001) CORMIX-GI systems for mixing zone analysis of brine wastewater disposal. Desalination 139:263–274

El-Sadek A (2010) Water desalination: an imperative measure for water security in Egypt. Desalination 250:876–884

Florea J, Panaitescu V (1979) Mecanica fluidelor. Ed. Tehnică, Bucharest, p 359

Ghabayen S, McKee M, Kemblowski M (2004) Characterization of uncertainties in the operation and economics of the proposed seawater desalination plant in the Gaza Strip. Desalination 161:191–201

GWI (2010) Water market Middle East 2010. Global Water Intelligence, Oxford

IDA (2002) Worldwide inventory of desalination plants. Report 17, Topsfield, MA

IDA (2006) IDA worldwide desalting plant inventory, No. 19 in MS Excel format, Media Analytics Ltd., Oxford

IDA (2006–2007) International Desalination Association Yearbook

IDA (2007–2008) International Desalination Association Yearbook

IDA (2008–2009) International Desalination Association Yearbook

Karagiannis IC, Soldatos PG (2008) Water desalination cost literature: review and assessment. Desalination 223:448–456

Khalil EE (2004) Water strategies and technological development in Egyptian coastal areas. Desalination 165:23–30

Kimes JK (1995) The regulation of concentrate disposal in Florida. Desalination 102:87–92

Lattemann S, Höpner T (2003) Deawater desalination– Impact of brine and chemical discharges on the marine environment, desalination publications, L'Aquila, Italy, 142

Lattemann S, Höpner T (2008) Environmental impact and impact assessment of seawater desalination. Desalination 220:1–15

Magazine – Water Condition & purification, January 2005

Millero F, Chen C, Bradshaw A, Schleicher K (1980) A new high pressure equation of state for seawater. Deep Sea Res, Pt A 27:255–264

Mohsen SM (2007) Water strategies and potential of desalination in Jordan. Desalination 203:27–46

Morcos SA (1970) Physical and chemical oceanography of the Red Sea. Oceanogr Mar Biol Annu Rev 8:73–202

Murray SP, Johns W (1997) Direct observations of seasonal exchange through the Bab El Mandab Strait. Geophys Res Lett 24:2557–2560

Pankratz T (2004) An overview of seawater intake facilities for seawater desalination, the future of desalination in Texas Vol 2: Biennial report on water desalination, Texas Water Development Board

Raed AI, Bashitialshaaer, K, Persson M, Aljaradin, M (2011) Estimated future salinity in the Arabian Gulf, the Mediterranean Sea and the Red Sea consequences of brine discharge from desalination. International Journal of Academic Research, Baku Azerbaijan, Part I, 3(1), 133–140

Raed AIB, Kenneth MP, Magnus L, Mustafa E (2007) Impact of brine disposal from EMU desalination plant on seawater composition, IDA World Congress-Maspalomas, Gran Canaria –Spain, October 21–26

Red Sea (2008) In Encyclopædia Britannica. Retrieved June 11, 2008, from Encyclopædia Britannica; Online: http://www.britannica.com/EBchecked/topic/494479/Red-Sea

Ruiz-Mateo, Antequera M, Gonzalez J (2007) Discharges to the sea from desalination plants. MEDCOAST-07, Alexandria, Egypt, 13–17 Nov 2007

Semiat R (2001) Desalination education capacity in Israel. Desalination 141:191–198

Shahin M (1989) Review and assessment of water resources in the Arab region. Water Int 14:206–219

Siedler G (1969) General circulation of water masses in the Red Sea. In: Degens ET, Ross DA (eds) Hot brines and recent heavy metals deposits in the Red Sea. Springer, New York, pp 131–137

Tobias B, Lattemann S, Purnama A, Al-Barwani HH, Doneker RL, Jirka GH (2009) BrineDis - environmental planning, prediction, and management of BRINE DIScharges from seawater desalination plants. Arab Water World (aWW) XXXIII(4):6–10

Thompson EF (1939) Chemical and physical investigations. The exchange of water between the Red Sea and Gulf of Aden over the "sill". John Murray Expedition 1933–34 scientific report, vol 2(3), pp 83–103

Tomczak M, Godfrey JS (2003) Regional oceanography: an introduction. Daya Publishing House, Delhi, pp 215–219. ISBN 8170353068

Vanhems C (2001) Critical review of desalination concentrate disposal to surface water, USA, 1992, (After: UNEP, 2001)

Wittholz MK, O'Neel BK, Colby CB, Lewis D (2008) Estimating the cost of desalination plants using a cost database. Desalination 229:10–20

Worldwater (2009) http://www.worldwater.org/data.html (latest information January 2009)

Part V
Coastal Erosion and Sedimentation (Detection and Measurement of Shoreline Retreat)

Chapter 13
Beach Erosion: Causes and Stabilization

R.G. Dean, T.L. Walton, J.D. Rosati, and L. Absalonsen

Abstract Natural and human-related causes of beach erosion are discussed and illustrated by examples. Sea level rise, trapping of sand by natural inlets and migration of natural inlets are the most pervasive natural causes. Construction of navigation works, followed by reduction in sediment delivery to the coast and subsidence induced by ground fluid extraction are the most prevalent human-related causes. Application of the Bruun Rule to sea level rise is discussed including its limitations and extensions to include beach nourishment and barrier islands. Prediction of shoreline changes caused by natural phenomena on decadal scales can only be accurately calculated with historical data. However, predictions of shoreline and volume changes due to human-induced effects such as construction of a littoral barrier or a beach nourishment project can reasonably be calculated with analytical and numerical models. Societal responses to beach erosion are expensive and limited to: retreat, stabilization with structures, nourishment and combinations of the last two. Each beach is unique thus placing a need to understand the cause of the erosion, develop a prognosis for "without response" conditions and prescribe the best approach for the future. Fortunately, long-term shoreline changes are available in some areas as are the effectiveness of some stabilization projects to guide this process. It is concluded that it will be possible to maintain some highly developed areas for one or two centuries with available technology and resources. Some areas will undoubtedly require abandonment within this period.

R.G. Dean (✉) • L. Absalonsen
Department of Civil and Coastal Engineering, University of Florida, Gainesville, FL 32611, USA
e-mail: dean@coastal.ufl.edu

T.L. Walton
Beaches and Shores Resource Center, Florida State University, Tallahassee, FL 32310, USA

J.D. Rosati
Engineer Research and Development Center, U. S. Army Corps of Engineers, Vicksburg, MS 39180, USA

C.W. Finkl (ed.), *Coastal Hazards*, Coastal Research Library 6,
DOI 10.1007/978-94-007-5234-4_13,

13.1 Introduction

Beach erosion can occur as a slow pervasive process or rapidly during major storm events and can be a result of natural or human related causes. Regardless of the rate or cause, continued beach erosion poses a significant threat to coastal infrastructure including coastal highways, homes, businesses and industry.

The investment along the world's shoreline is immense. Along the U. S. east and Gulf of Mexico coastlines alone, the National Research Council (1999) estimated that "about $3 trillion in infrastructure adjacent to the shoreline is vulnerable to erosion and other natural hazards." Beach erosion is fairly ubiquitous: the Heinz Center (H. John Heinz Center for Science and Environment 2000) reported "Over the next 60 years, erosion may claim one out of four houses within 500 feet of the U. S. shoreline." Many coastal highways are threatened by erosion, which may jeopardize their function as evacuation routes during major storm events. The societal responses to future beach erosion are limited and expensive. Thus, it is imperative that better understanding of the merits of the various response options be developed so that the most advantageous can be identified and implemented when and where appropriate. We are indeed fortunate that at present, there are numerous reasonably long-term surveys and data quantifying shoreline behavior (more than a century in places) and project performance (more than 80 years) that provide guidance for the future.

This chapter comprises nine sections commencing with the balance of forces in the nearshore, progressing through measurement of beach erosion, a number of case studies, natural and human-related causes of beach erosion, the range of societal responses available, shoreline stabilization and a summary of future options and needs.

13.2 Long-Term Sea Level Rise and Responses

13.2.1 Equilibrium Beach Profiles

A brief discussion of the forces acting in the nearshore will be useful to later examination of beach profile response to changes in sea level. Although our quantitative understanding of the forces and responses in this complex zone is immature, it is generally recognized that there are constructive (shoreward acting) and destructive (seaward acting) forces acting on sediment particles, see Fig. 13.1. Gravity is the most obvious destructive force which, in conjunction with wave generated turbulence, facilitates seaward directed sediment transport. The constructive forces are less obvious but clearly exist, otherwise beaches with their profiles sloping upwards toward shore would not exist. Constructive forces include a near-bottom current (called a "streaming" current) and intermittent sediment suspension such that sediment suspended during wave breaking at the crest phase is displaced shoreward during its suspension and is less prone to seaward displacement when the wave induced currents are directed seaward under the trough phase.

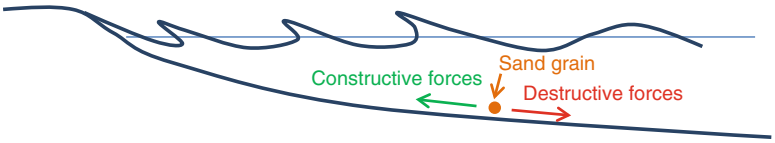

Fig. 13.1 Constructive and destructive forces acting on a sand particle

The key concept from this discussion is that a state of equilibrium under constant wave and water levels exists and that any perturbation such as sea level rise or increased or decreased storminess or other unstated changes will disturb this equilibrium and result in changes in the nearshore profile. A secondary useful concept is that if an excess of sand (relative to equilibrium) exists in the profile, landward transport will occur to reestablish an equilibrium profile. Contrariwise, if a deficit of sand occurs in the profile, seaward transport will occur.

13.2.2 Long-Term Sea Level Changes and Associated Morphological Responses

There are many depictions of global sea level rise over the past 20,000 years. One of these is presented in Fig. 13.2. It is seen that global sea level rose rapidly from about 20,000 years ago to 7,000 years ago and has risen at a much smaller rate since. Currently there is considerably uncertainty as to what the rate of global sea level rise will be over the next century with estimates ranging from approximately 0.5 m (Bindoff et al. 2007) to 5 m (Hansen 2007 and Hansen and Sato 2011).

The nearshore response to past sea level rise is relevant to present shoreline and nearshore volume changes. During lower stands of sea level, rivers discharged sediment to the offshore. During the period of rapid sea level rise, there may not have been sufficient time for the constructive forces to achieve equilibrium and thus much of this sand delivered by the rivers was left in place. With the slower sea level rise rate during the past 7,000 years, and with more sand delivered to the continental shelves over this more stable period, much of this sand that was deposited during the lower stands was displaced landward and either widened the beaches (evident in aerial photographs through beach ridges) or formed barrier islands. The latter is the classical theory of de Beaumont (1845) for the formation of barrier islands. Other theories of barrier island formation include those of Gilbert (1890) which considers barrier islands as the result of spit generation and those of Hoyt (1967) who, in examining the barrier islands of the state of Georgia, concluded that some were the result of drowned sand dunes. Figure 13.3 presents a Google image of an area on the eastern shoreline of Florida where a relict (previous) shoreline is evident by its linearity. This shoreline may have formed during a previous higher-than-present sea level stand or developed prior to the present seaward barrier island.

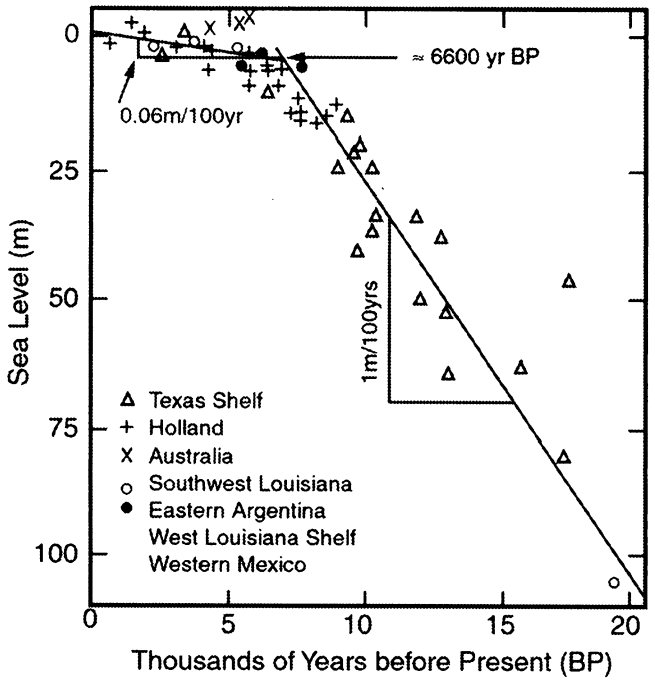

Fig. 13.2 Global sea level rise over the last 20,000 years (From Shepard 1963)

Fig. 13.3 Google photograph showing relict shoreline along Florida's east coast

13.3 Societal Responses to Beach Erosion

As noted, societal responses to sea level rise are limited and expensive. Prior to fixed infrastructure and other structures and facilities, more mobile societies simply moved inland which still remains as one of the limited options for living with rising seas. These options are: (1) Relocate, (2) Fix the shoreline through armoring or other structures, (3) Nourishment, and combinations of the latter two. There will be interest in relocation and, over a century or more, that may be an appropriate option in some locations. However, if that decision is made too soon or too late or in the wrong location, the incremental cost may be substantial, placing greater need on understanding related physical responses and societal impacts of such actions.

13.4 Definitions and Measurement Methods

Although some formal definitions of beach erosion refer to a loss of volume, beach erosion is commonly associated with shoreline recession and the two descriptions here will be considered as synonymous. These two definitions of erosion and recession provide a segue into the best approach to measuring beach conditions.

Usually in establishing the rate of beach erosion, one will be confronted with a decision to rely primarily on beach profiles or the position of a reference elevation on the beach such as Mean Sea Level (MSL), Mean High Water (MHW) or Mean Higher High Water (MHHW). Thus, it is relevant to review the methods used to measure these quantities. The earliest beach surveys in the 1800s typically measured the debris or wrack line which is most closely aligned with the beach berm crest and MHW or MHHW (Shalowitz 1964); these oldest surveys are often combined with modern measurements to document long-term shoreline evolution.

13.4.1 Measurement of Mean Sea Level or Mean High Water Locations

Of interest is that the shoreline can recede without loss of sand volume. This is the case hypothesized in the Bruun Rule (discussed later) in which in response to sea level rise, sand is removed from the upper portions of the profile and deposited on the lower portions with the sand volume conserved in the profile. Yet, according to this Rule, the upper contours of the profile have receded permanently suggesting that for some purposes, changes in the upper profile contours may be more relevant than changes in the profile volume. Clearly, these upper contour locations are much easier to measure. Ideally, in order to understand the system and the cause of erosion, one would have available both quality beach profiles and upper contour values.

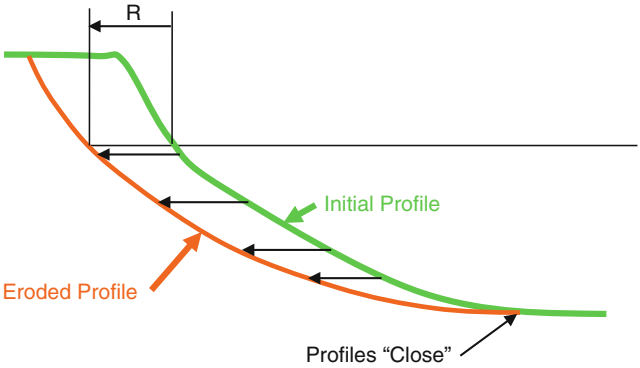

Fig. 13.4 Definition sketch of profiles that "close" thereby providing a good basis for volume change quantification

Oldest surveys of the MHW position were made with plane table survey or other early survey methodology. Today, the MHW position can be extracted from aerial photographs with sufficient color delineation to define the wrack line. If this method is used, it is recommended that the same person extract the data for consistency. More accurate estimates of the MSL and MHW positions are obtained from more detailed profile or topographic/bathymetric measurements, discussed next.

13.4.2 Beach Profiles

Beach profiles represent a cross-section of the beach. Ideally, two successive profiles at the same location will "close" at their seaward ends as illustrated in Fig. 13.4. Otherwise the analyst is confronted with the concern that at least one of the profiles is inaccurate or the profiles did not extend sufficiently far offshore to capture all of the volume changes. Of course, once a beach profile has been established, it is easy to extract a MHW, MHHW or MSL shoreline position.

Figure 13.4 presents an idealized case in which volumetric erosion is associated with a shoreline recession, R, and in which profile closure occurs. Eleven profiles conducted at a location over a period of 11 years are shown in Fig. 13.5. It is seen that these profiles do not close at their seaward ends and it would be difficult to determine volumetric changes with confidence. For more discussion of this issue, the Reader is referred to Nicholls et al. (1996).

Many different methods have been employed to measure beach profiles. The sections below describe the most-often used methods in some detail followed by brief descriptions of the less used approaches.

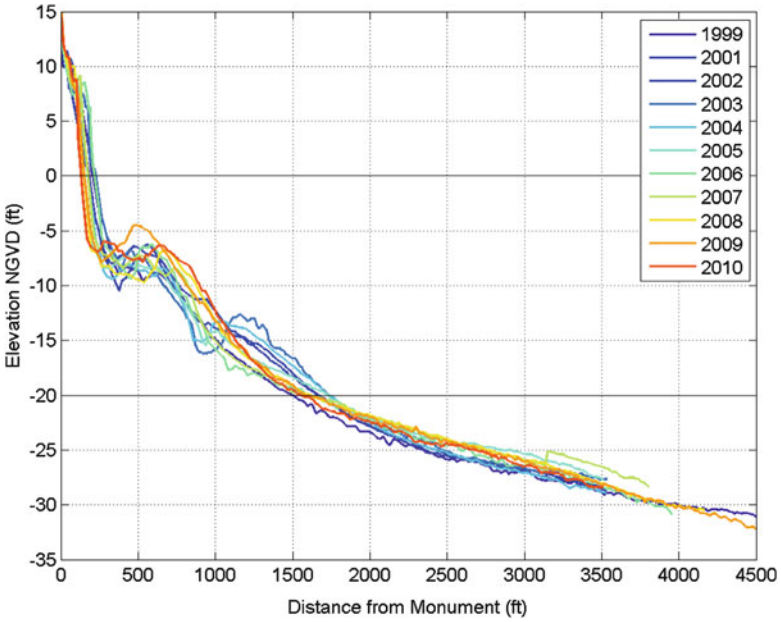

Fig. 13.5 Eleven successive profiles at a location along Florida's east coast (Note non-closure at seaward ends of profiles)

13.4.2.1 Pre-GPS Profile Measurements

Beach profiles measured prior to the advent of Global Positioning System (GPS) technology are of interest as these provide an historical basis for determining volume changes. Early methods comprised the use of a combination of so-called wading profiles in which a person with a leveling rod would walk out into the nearshore zone and stop periodically allowing a person with a shore-based level to measure the height on the leveling rod. This method provided quite an accurate representation of the nearshore profile. In some cases, the person with the level rod would swim out to depths on the order of 5 m, thus extending the more accurate nearshore portion of the profile. The seaward portion of the profile was conducted with a boat-mounted fathometer and, under ideal conditions would overlap with and be conducted on the same day as the nearshore portion of the profile. Because the fathometer measurements were related to a floating platform, an accurate estimate of the tide at the time of measurement was required. If a permanent tide gage was not available nearby, a temporary tide gage was usually installed in the area being surveyed. The aforementioned "overlap" in the wading and boat portions of the profiles provided good assurance that the tide adjustments were appropriate. The wader and boat were generally kept on line by either the person on the level through radio contact, visually by lining up markers on the beach or through early electronic means.

13.4.2.2 Post-GPS Methods of Profile Measurement

GPS with Boat and Fathometer

These methods basically allow replacement of the tide gage and horizontal position control with GPS and computer packages to advise the boat operator whether the survey line is being maintained. The method usually has two nearby GPS stations on known reference points allowing the roving GPS to function in the Kinematic GPS (KGPS) mode. The upland and nearshore portion of the profile are measured by a person with a back pack mounted GPS. Thus, GPS technology has both simplified and increased the accuracy of measured profiles.

GPS with Personal Water Craft

A GPS mounted on a Personal Water Craft (PWC) along with the two base stations allow one person to conduct the water portion of a profile survey in the kinematic mode. See MacMahan et al. (2002) for further discussion.

Water Penetrating LIDAR

Light Detection and Ranging (LIDAR) is a methodology that utilizes an airborne GPS and a laser capable of penetrating relatively clear water to measure beach profiles including their upland portions. The method is generally limited to water depths corresponding to two to three "Secchi disk depths" which may range up to 50 m. A Secchi disk ranges from 20 to 30 cm in diameter and can be either plain white or have a black and white pattern. A "Secchi disk depth" is the depth at which the disk is just visible when lowered into the water. The water penetrating laser beam usually pulses at approximately 1,000 Hz and with the aid of an oscillating or rotating mirror or prism sweeps out a swath with a sea surface width proportional to the airplane's altitude. Under favorable conditions, horizontal and vertical accuracies are estimated as 2.5 m and 15 cm, respectively. Figure 13.6 illustrates the concept.

13.4.3 Other Less Applied Methods for Measuring Beach Profiles

A number of other methods have been applied over the years to improve accuracy of profile surveys. One is discussed below.

Sea sleds consist of a platform with a mast that is either skidded or rolled along the bottom through towing with a cable from shore. The mast can be graduated for measurements by level or can contain a GPS or prism for electronic measurement.

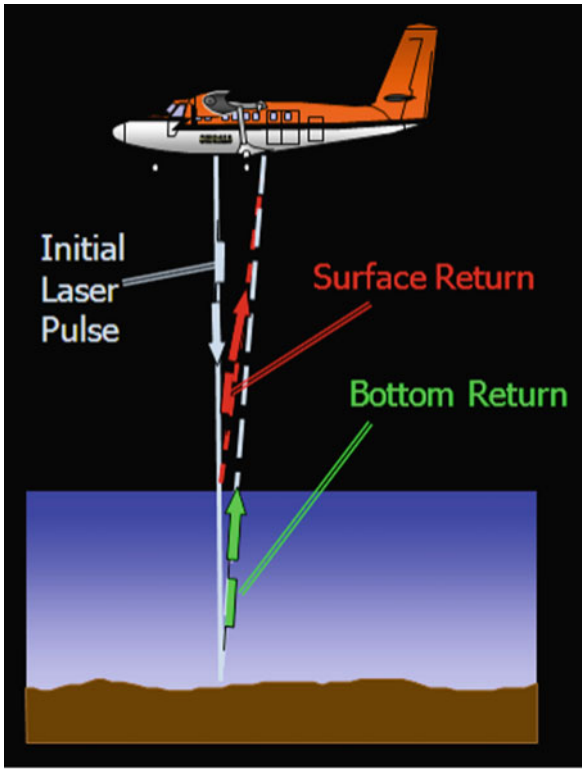

Fig. 13.6 Airborne LIDAR for measuring bathymetry

One advantage of this methodology is that the entire profile is measured in one continuous process. Upon completion of a profile, the sea sled is relocated offshore on the next profile ready for the next towing and measurement phase to commence. Advantages of sea sleds include accuracy and use of the same methodology for the water and land portions of the profile. Disadvantages are the comparatively long time to complete a profile and difficulties in areas with offshore reefs which may interfere with the sled operation.

13.5 Predictability of Decadal Scale Beach Erosion (and Accretion)

Beach erosion and accretion on decadal time scales can only be predicted reliably if the nearshore system is significantly out of balance or if a long-term trend is known. In their natural conditions, beaches fluctuate on a wide range of temporal and spatial scales due to a variety of causes including inlet evolution, sea level rise, storms and other causes resulting in shoreline changes which are not predictable except in a statistical sense. Shorelines can be considered “noisy”. Even if beaches

are stable in the long-term (several decades), they may exhibit reasonably large fluctuations over annual and single decadal periods. In addition to seasonal and episodic storms, the causes of these large annual to decadal fluctuations may include inlet migration and shoal welding processes and sand waves that move along the shoreline (discussed later) causing alternating shoreline recession and advancement.

Other than sea level rise, usually an imbalance over several decades is due to human related causes but could be natural such as natural inlet migration, inlet breaching and shoal welding as discussed previously, or a landslide or river flood providing a large amount of sediment to the nearshore system. Two other examples of natural imbalances are consolidation of subsurface sediments at river deltas and beaches and a sudden tectonic lowering or raising of the nearshore.

13.5.1 Sea Level Rise and the Bruun Rule

Two definitions are provided for the following discussion. Eustatic or global sea level change refers to the worldwide change in sea level as was shown in Fig. 13.2. Local or relative sea level change is a term applied to site-specific sea level change, and can be greater or less than the eustatic change, even showing a relative sea level decline when the eustatic sea level is rising.

Relative Sea Level Rise (RSLR) contributes to beach recession as the relatively lowered profile allows larger waves to propagate closer to shore. It is evident that global shorelines have retreated during the 100 m or so of global sea level rise over the approximately past 200 centuries (Fig. 13.2). Bruun (1962) developed a relationship between the rise in sea level, S, and the shoreline recession, R as

$$R = S\frac{W_*}{h_* + B}$$

in which W_* and h_* are the width and depth of the active profile, respectively and B is the berm height, see Fig. 13.7.

The Bruun Rule can be described in three steps (Fig. 13.7). In the first step, the profile is displaced landward a distance R, yielding a positive sediment volume, $\Delta V_+ = R(h_* + B)$. In the second step, a sea level rise S is considered which results in a sediment void of $V_- = SW_*$. The third and final step consists of equating V_+ and V_-which results in the Bruun Rule.

For most beaches, the ratio $\frac{W_*}{h_*+B}$ falls in the range of 50–100. Thus for the twentieth Century rate of global sea level rise of 1.7 mm/year, the recession would amount to 8.5–17 cm/year, a reasonably small amount that can be controlled by beach nourishment. The Bruun Rule can be easily extended to include the volume of sand per unit length of beach added by beach nourishment, v to offset RSLR

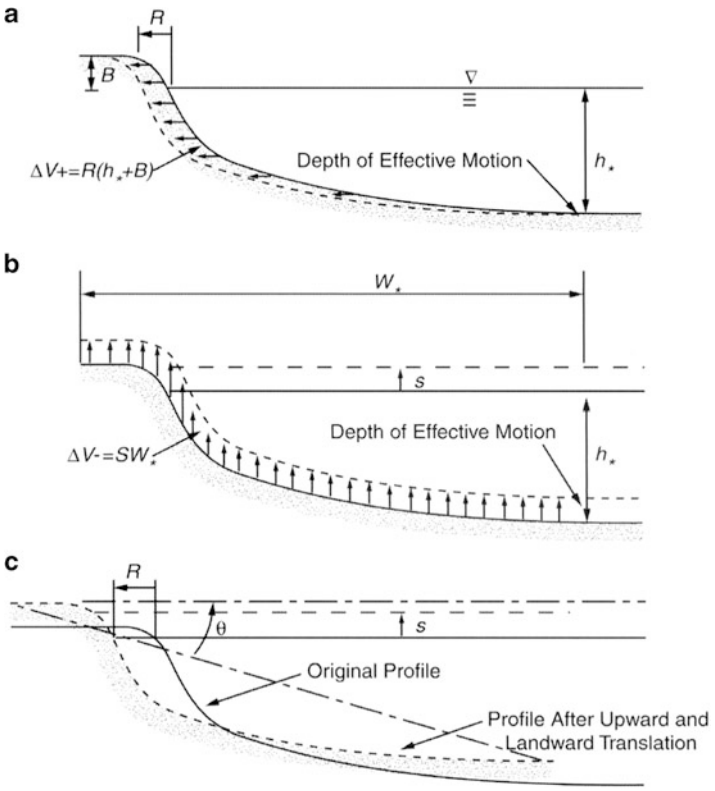

Fig. 13.7 The basis for the Bruun Rule

$$\Delta y_T = \Delta y_{RSLR} + \Delta y_{NOUR} = \frac{1}{h_* + B}(-SW_* + v)$$

in which Δy_T is the total shoreline change, Δy_{RSLR} is the shoreline change due to RSLR, and Δy_{NOUR} is the shoreline change due to beach nourishment. As an example, the sand volume per unit length of beach to maintain the shoreline stable over a century for the parameters discussed earlier is

$$v = SW_*$$

in which it is seen that the volume per unit length in the above equation is that required to raise the sea floor over the active profile exactly by the amount of the RSLR. A reasonable estimate of W_* for moderate wave climates and typical beach sand sizes is 500 m. Thus, the sand volume per unit length of beach required over a Century is approximately 85 m^3/m. When compared to a reasonably robust beach nourishment project of 250 m^3/m, this volume required is a manageable quantity.

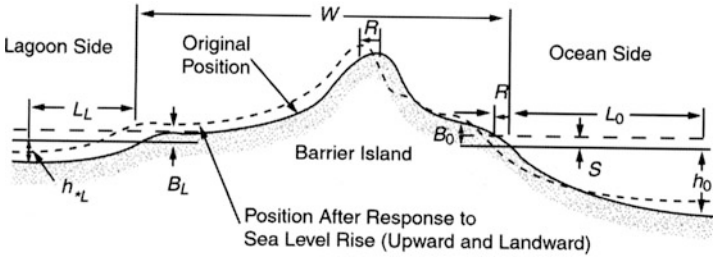

Fig. 13.8 The basis for the Bruun Rule extended to a barrier island (Dean and Maurmeyer 1983)

As noted, it is of interest that although the Bruun Rule predicts shoreline recession due to an increase in water level, the volume within the profile is unchanged. Sand is simply displaced from the upper contours to the lower contours of the profile. Thus, if we were to base our estimates of worldwide profile erosion on the Bruun Rule, the volume changes would be zero!

Consistent with the objectives of this chapter, it is relevant to question how well the Bruun Rule has been verified with laboratory and/or field data. In summary of these efforts, it is reasonable to say that application of the Rule over a large number of profiles may yield reasonable average results; however attempts to apply it to one or a few profiles will generally fail, in part, due to the high degree of local variability as will be demonstrated later. Moreover, the Bruun Rule is useful in developing estimates of shoreline recession due to future sea level rise scenarios as it is the only method that is available for this purpose. Dean and Maurmeyer (1983) extended the Bruun Rule to the case of barrier islands in which sediment volume is not conserved on the seaward side of the barrier island but rather is overwashed or transported by aeolian processes onto the lagoon side to maintain the equilibrium profile there, see Fig. 13.8. The relationship for this case is:

$$R = S\frac{L_o + W + L_L}{h_{*o} - h_{*L}}$$

with the terms as defined in Fig. 13.8. It is seen that the smaller denominator and the larger numerator results in a substantially increased recession for a given sea level rise.

13.5.2 Sand Waves

Sand waves, defined as sinuous or rhythmic features that may be stationary or translating along the shoreline, have attracted a great deal of interest in the coastal science and engineering communities. Relevant to this chapter, sand waves are of interest as they can add "noise" to the shoreline changes that is not representative of

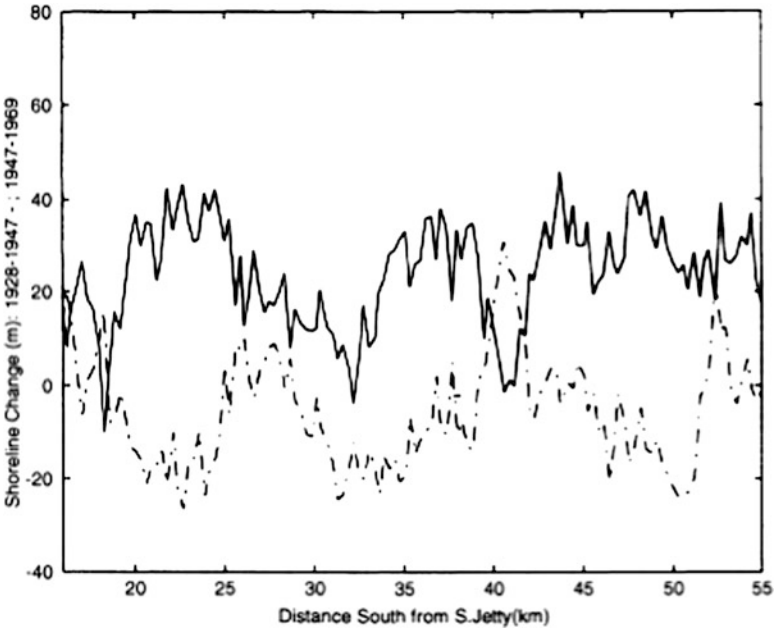

Fig. 13.9 Pre- and post-entrance sand waves along the Brevard County shoreline (From Walton 1999). Distance is south from south jetty at Port Canaveral. *Solid line*: 1928–1947 and *dashed line*: 1947–1969. Beach nourishment is not a factor in these data

the long term trend. Two examples of sand wave studies will be reviewed briefly. The Reader is referred to the references associated with the articles describing these examples for additional discussion.

13.5.2.1 Sand Waves Along Brevard County, FL

Walton (1999) provided an extensive review of sand waves of various scales and has examined sand wave features along the Brevard County, FL shoreline. He analyzed data which included pre- and post-human influence and found similar sand wave features in both data sets, see Fig. 13.9. The wavelengths of the features were found to be similar for the two time periods considered at approximately 12 km. The sand wave amplitudes of approximately 40 m are large and sufficient to result in positive or negative shoreline changes depending on where and when the observations are conducted. Although the later wave forms appear to be displaced downdrift (south) relative to those earlier, it is not clear that this can be interpreted as movement of these features.

13.5.2.2 Sand Waves Along the South Shore of Long Island, New York

Thevenot and Kraus (1995) report on a 16-month observation of 11 damped sand waves along the coastline of Southampton on Long Island, New York. The sand waves were interpreted as the result of a periodic breakthrough of an ephemeral inlet to Mecox Bay, and the subsequent welding of the resulting ebb tidal shoal to the shoreline and migration westward (downdrift). The average wavelength of these features was 0.75 km, much shorter than those investigated by Walton; however the amplitudes were approximately the same (40 m). The Southampton waves were found to migrate faster (1.09 km/year) under the more energetic winter waves and slower (0.35 km/year) in the summer. Numerical modeling of the sand waves was conducted with generally good agreement although the modeling results showed more rapid decrease in amplitude than the observations. Wave refraction over the wave bathymetric contours was found to improve correlation between the model and observational results.

13.5.3 Detailed Examination of Shoreline Changes in Florida

13.5.3.1 General Data Base, Procedures and Results

The Bureau of Beaches and Coastal Systems of the state of Florida maintains an extremely valuable data base of historical MHW shorelines (from the mid 1800s to 2010 or so) and beach profiles (since the 1970s). These data are available at: http://www.dep.state.fl.us/beaches/programs/mon-res.htm.

In order to illustrate the non-predictable character of MHW shoreline changes in natural systems, an overall review of the study will be presented followed by a more detailed review of shoreline changes in two counties. The data are available at a spacing of approximately 300 m at 3,865 locations along the 24 counties included in the state statutes as sandy beach shorelines as shown in Fig. 13.10. Absalonsen and Dean (2010) updated an earlier analysis of the extensive Florida MHW data by Dean et al. (1998). The more recent analysis included 57,342 MHW locations and an average of 140 years of available data. The data analysis was organized over three time periods: (1) The "early" period from the beginning of the available data to the mid-1970s selected to pre-date beach nourishment effects on the shoreline changes, (2) the "recent" period which included the data from the 1970s to the most recent data in 2010 or so, and (3) the entire data set. Results from the more recent Absalonsen and Dean (2010) analysis are reviewed below.

At each of the 3,865 monuments (locations along the shoreline), an average of approximately 15 shoreline positions were available for analysis. For each of these monuments, least squares fits were established for the early, recent and total time spans, thereby establishing the trend for each time span and monument. Additionally, the standard deviations of the data about the trend line were quantified. These

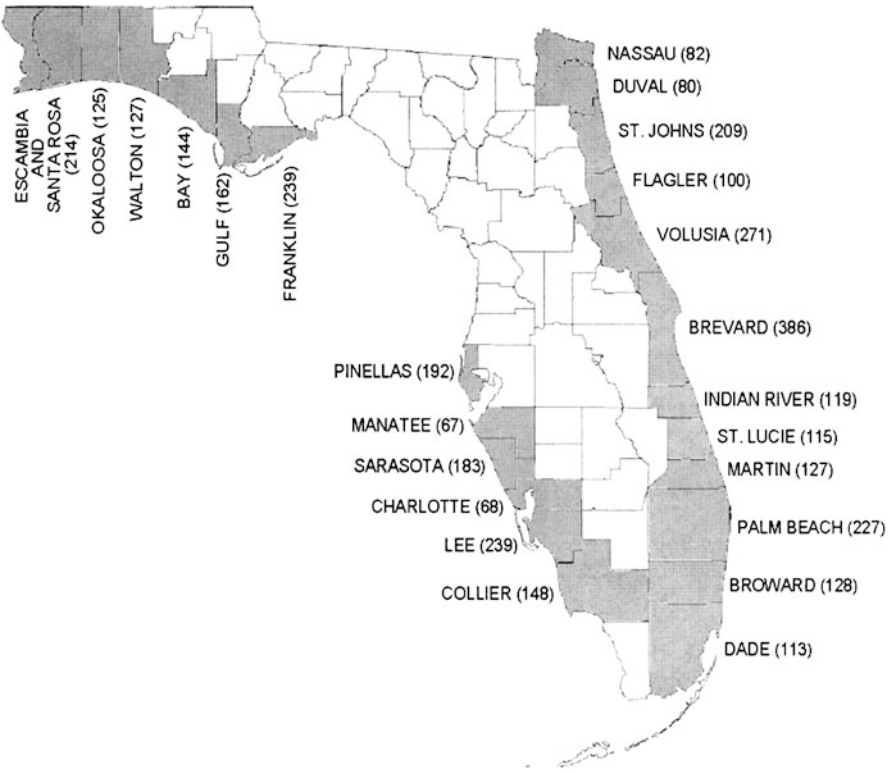

Fig. 13.10 Numbers of monuments in each of the 24 coastal counties in the Florida data base (Note Escambia and Santa Rosa Counties are considered as a single county in the data base)

standard deviations are a reflection of the combination of seasonal and storm induced changes and other unknown contributions including survey inaccuracies which were probably greater in the earlier surveys.

Figure 13.11 presents an example for Monument R-024 in Nassau County, which is the northern county on the east coast of Florida. This monument has 15 data points available for the total period with six available in the early period and ten available in the recent period (the 1974 data point was included in the analysis of both periods). The trend lines for all periods are shown and the deviation from the trend line for one data point is also shown. The results are presented in graphical and tabular form for each of the monuments and periods. Figure 13.12 presents the graphical representation for the early period in Nassau County in which Monument R-024, the subject of Fig. 13.11, is identified. The standard deviations about the trend lines for each monument are shown as the lines perpendicular to the trend lines and their scales are shown at the base of the figure. These early shoreline changes in this county display interesting features. The shoreline is advancing over the northern 6 km of the county, then eroding over the 2 km to the south and advancing or stable over the 9 km immediately south and finally eroding over the southern 5 km of the county shoreline. The advancement in the northerly portion of

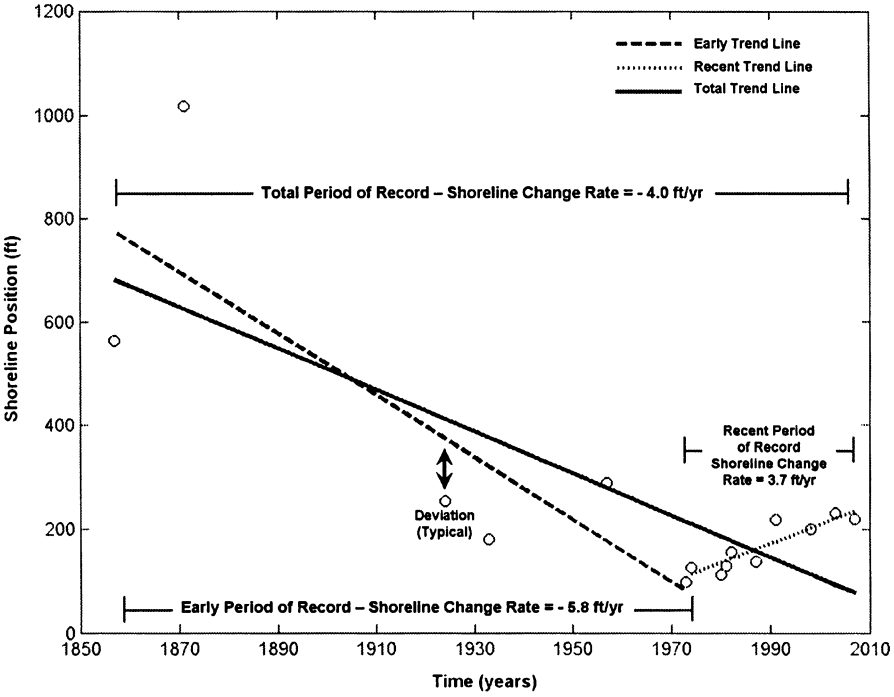

Fig. 13.11 MHW shoreline changes at Monument R-024 in Nassau County

the county has been investigated by Olsen (1977) who determined this to be a result of the ebb tidal shoal collapsing and moving shoreward after the 1881–1904 construction of the jetties at St. Marys River which forms the county northern boundary. The erosion at the south end of the county is probably cyclical at the entrance to Nassau Sound, an unstructured entrance during the period of this figure. The tabulation for the portion of the county including Monument R-024 is presented as Fig. 13.13 in which the characteristics of the monument are highlighted.

The overall results from this study for all 24 counties are summarized as follows (Absalonsen and Dean 2011, b). The average shoreline change on the east coast of Florida during the early and recent periods were + 18 and + 23 cm/year, respectively. On the west coast, these values are – 2 and + 55 cm/year, respectively. Note that the recent period of analysis includes the influence of beach nourishment which is estimated to be 101 and 70 million m^3 for the east and west coasts, respectively (Program for the Study of Developed Shorelines 2012). The average standard deviations, reflecting the shoreline fluctuations about the trend lines were approximately 16 m. It was found that, on average, this variability increased to approximately 41 m near inlets and decreased to the open coast value over a distance of approximately 4.5 km. What is fascinating about this analysis is that beaches in these 24 counties have

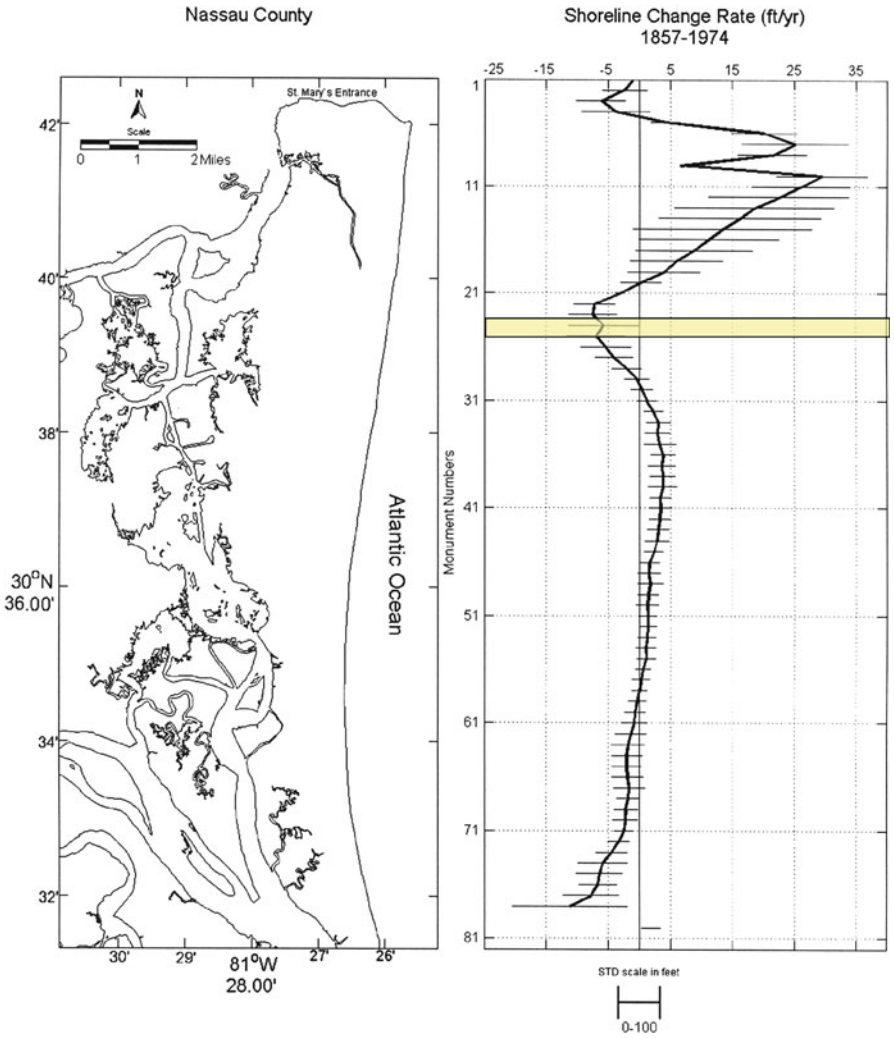

Fig. 13.12 Early MHW shoreline changes for Nassau County for the 1857–1974 time period (117 years). Monument R-024 is *highlighted*. Note, the first ten monuments are located along the inner banks inside St. Marys Entrance. This period includes negligible beach nourishment

been overall accretional prior to effects of beach nourishment with a relative sea level rise along these shorelines exceeding the global rate of 1.7 mm/year.

The following sections examine MHW shoreline changes for two additional counties for the recent period to illustrate the complexity of natural shoreline changes.

Nassau County

Monument Number	Early (1857-1974) Shoreline Change Rate (ft/yr)	Standard Deviation (ft)	Number of Data Points	Recent (1974-2007) Shoreline Change Rate (ft/yr)	Standard Deviation (ft)	Number of Data Points	Total (1857-2007) Shoreline Change Rate (ft/yr)	Standard Deviation (ft)	Number of Data Points
R-001	-0.9	31.7	6	-0.5	26.0	12	-1.2	30.9	17
R-002	-2.4	108.3	6	-1.1	36.9	8	-1.8	80.9	13
R-003	-6.1	119.0	6	-1.8	22.6	11	-4.5	93.1	16
R-004	-3.8	166.1	6	2.3	52.7	8	-2.0	140.4	13
R-005	4.3	70.8	6	2.4	16.9	8	3.7	54.6	13
R-006	20.1	160.8	6	-2.1	48.5	11	14.1	236.7	16
R-007	25.1	263.1	6	-1.0	64.3	7	18.3	349.6	12
R-008	21.4	168.0	6	4.0	67.5	8	16.3	237.1	13
R-009	6.5	2.6	3	-1.2	49.2	10	0.9	53.6	12
R-010	29.5	223.0	6	6.9	48.0	10	23.7	265.0	15
St. Marys Entrance									
R-011	26.1	236.2	6	3.6	42.0	9	19.5	293.8	14
R-012	22.4	340.9	6	3.6	49.5	11	14.9	327.8	16
R-013	18.5	385.3	6	2.8	46.1	9	12.2	344.0	14
R-014	16.2	395.2	6	4.0	39.3	10	10.2	325.0	15
R-015	13.4	432.6	6	5.1	41.4	12	8.1	309.8	17
R-016	11.2	339.4	6	3.8	21.7	10	7.2	255.0	15
R-017	8.8	282.9	6	3.7	34.5	10	5.9	206.6	15
R-018	5.9	225.2	6	4.2	40.3	12	4.2	149.2	17
R-019	4.0	175.6	6	4.5	43.9	11	3.0	118.9	16
R-020	0.3	97.1	6	4.1	41.7	10	0.4	75.7	15
R-021	-3.2	19.3	6	3.6	47.1	12	-1.7	71.7	17
R-022	-7.2	101.3	7	3.2	28.2	9	-4.7	131.9	15
R-023	-7.5	117.0	7	4.5	32.2	9	-5.0	138.6	15
R-024	-5.8	169.0	7	3.7	20.0	9	-4.0	144.4	15
R-025	-7.0	141.2	6	3.3	29.9	8	-4.1	143.3	13
R-026	-5.4	121.6	6	2.8	27.3	8	-3.1	118.1	13
R-027	-4.1	90.9	6	2.6	19.6	9	-2.4	87.0	14
R-028	-2.1	70.9	6	1.2	13.3	8	-1.0	60.3	13
R-029	-0.4	58.0	6	0.8	25.8	8	-0.1	45.5	13
R-030	0.4	53.0	6	1.1	24.4	9	0.5	40.2	14

Fig. 13.13 Tabular output for that portion of Nassau County with Monument R-024 (*highlighted*)

13.5.3.2 Detailed Case Study of MHW Shoreline Changes St. Joseph Spit and Cape San Blas in Gulf County, Florida

St. Joseph Spit and Cape San Blas are located in Gulf County on the west coast of Florida and provides an example of rapid shoreline changes that are not predictable except on the basis of historical data. Figure 13.14 presents a Google image of St. Joseph Spit and Cape San Blas which is the only feature of this type in the State of Florida.

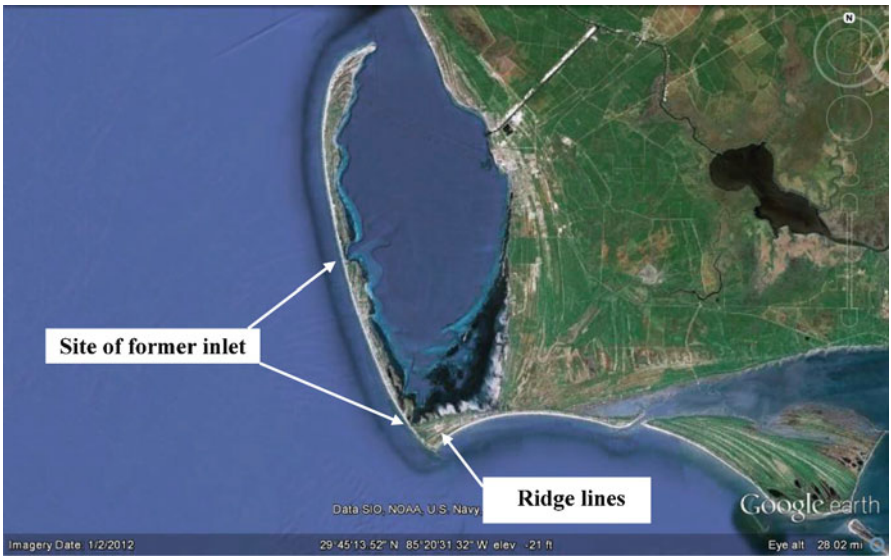

Fig. 13.14 Google image of St. Joseph Spit and Cape San Blas. The locations of two former inlets are shown

Figure 13.15 presents the long-term shoreline change pattern for the "early" period of 1857–1973, a period of 116 years. It is seen that the long term erosion rates at location A are more than 26 ft/year (8 m/year). At location B, the shoreline is advancing at rates of 3 ft/year (0.9 m/year). This advancement is evident by the ridge lines in Fig. 13.14. Five lighthouses have been located near location A and four of them have been lost to erosion. The advancement of 25 ft/year (7.6 m/year) at the north end of St. Joseph Spit is due to the spit growth into St. Joseph Bay. During this period, all shoreline changes were natural. It is clear that this area has changed over past millennia. The locations of two former inlets are evident where indicated in Fig. 13.14.

13.5.3.3 Detailed Case Study of MHW Shoreline Changes in Indian River County, Florida

Indian River County is located on the east coast of Florida and the long-term shoreline changes, shown in Fig. 13.16, present two features of interest. Sebastian Inlet serves as the boundary between Indian River County to the south and Brevard County to the north. The net longshore sediment transport in this area is estimated at 270,000 m^3/year southward. Examination of the shoreline changes establishes that Sebastian Inlet has caused erosion over a distance of at least 5 miles (8 km). Analysis of more recent data extends that distance to 16 km (Dean 2005).

The second feature of interest is the indentation in the shoreline near the south end of the county and the associated long-term shoreline advancement up to

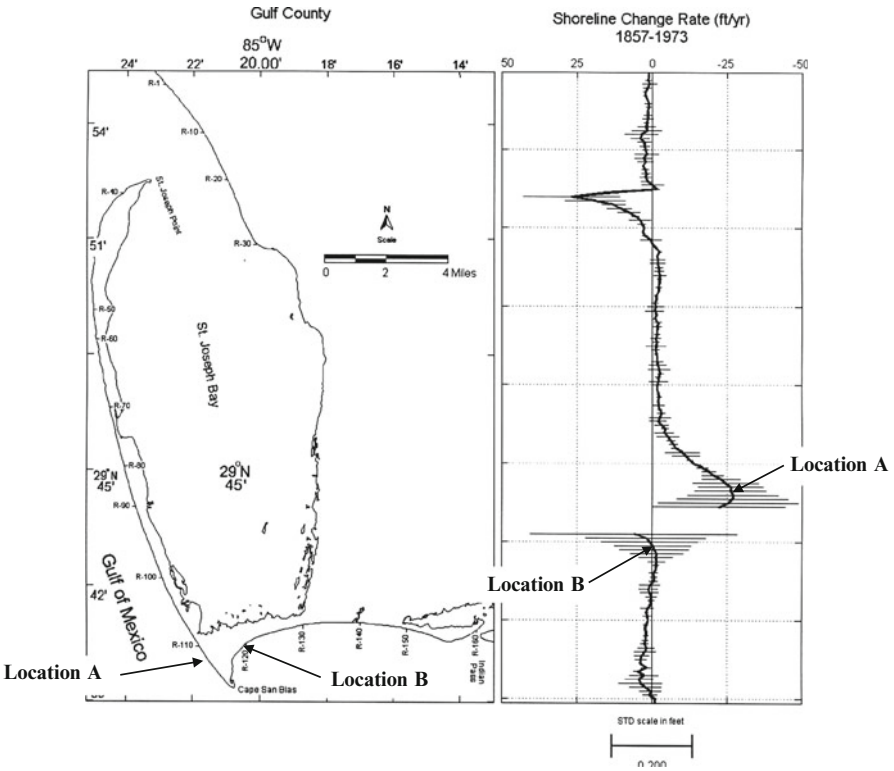

Fig. 13.15 Long-term (1857–1973, 116 years) shoreline change rates for Gulf County on the west coast of Florida. The *vertical lines* are the standard deviations of the shoreline positions around the shoreline change trend line with scale at *bottom* of *right hand panel*. Note the large changes in the vicinity of Cape San Blas. Also note that the plot in the *right hand panel* is shifted relative to the *left hand panel*

approximately 5 ft/year (1.5 m/year) and extending more than 7 miles (12 km). The cause of this indentation is not known. If it were the remnant of an inlet, one would expect to find relict flood tidal shoals inside the location of the former inlet, yet none are evident. One hypothesis is related to a submerged reef at the north end of the inlet that trends offshore to the south. With sea level rise and abrasion of this reef, it has become less effective in preventing sand from being transported southward and now more sand is passing over the reef and is filling the indentation. The rate at which sand is deposited in the indentation is estimated at 75,000 m^3/year.

In summary of this examination of the early period, MHW shoreline changes over periods ranging from 116 to 120 years for the three Florida counties, it is shown that segments of shoreline advancement and recession occur. This early period was selected to not include major beach nourishment projects although many of the navigational improvements were conducted prior to the 1970s, the end of the

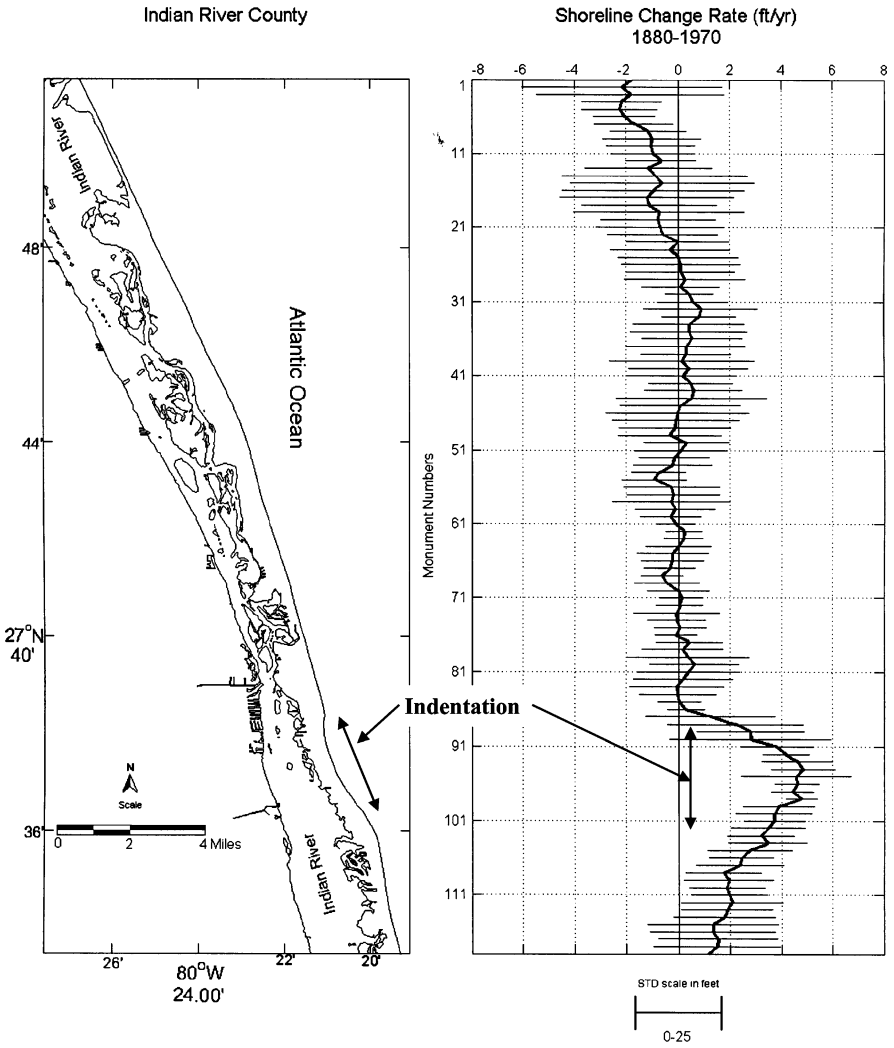

Fig. 13.16 Long-term (1850–1970, 120 years) shoreline change rates for Indian River County on the west coast of Florida. The *vertical lines* are the standard deviations of the shoreline positions around the shoreline change trend line with scale at *bottom* of *right hand panel*. This data period precedes any nourishment but includes the effects of Sebastian Inlet which is located at the north limit of this figure

early period. It is concluded from this investigation that it is difficult to calculate natural shoreline changes for beaches with complicated coastal processes and morphologies. Although the Bruun Rule predicts shoreline recession due to RSLR which was certainly occurring over this early period, its application on Florida's east coast predicts recession whereas average shoreline advancement

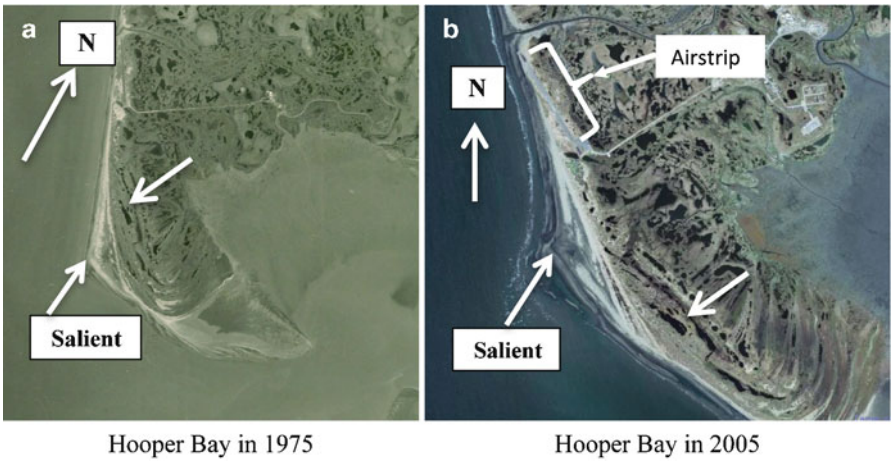

Fig. 13.17 Two photographs of a salient along the Hooper Bay, Alaska, shoreline. The *dashed arrows* point to common features in the two photographs (Note, photographs are of different scale). The salient in (**b**) has translated approximately 2 km to the north from its position in (**a**) over the period 1975–2005 at an average rate approximating 70 m/year. Examination of photographs at intermediate dates supports this interpretation

occurred. Although the reason for this difference is not known, it may be due to one or a combination of: a negative net transport gradient from north to south along the east coast, biogenous production of carbonate sediments or onshore transport of sand.

13.5.4 Hooper Bay, Alaska

Figure 13.17a, b present two photographs of the shoreline of Hooper Bay, a small Alaskan community of Native Americans. The earliest photograph in 1975 shows a salient that formed at the southwest corner of Hooper Bay. Although uncertain, this salient may have been the result of an ebb tidal shoal moving shoreward under the action of waves and eventually welding onto the shore. Figure 13.17b in 2005 shows the shoreline some 30 years later when it is evident that the salient has translated some 2 km to the north resulting in an average migration rate of approximately 70 m/year. This conclusion of salient translation is supported by examination of a number of intermediate photographs. The movement of the salient was an issue in this case because as it translated, it sequestered sand from both the north and south beaches and endangered the airstrip which is the only link to the outside from Hooper Bay. The ability to predict this translation is simply non-existent and highlights the uniqueness of individual settings.

13.5.5 *Shoreline Changes in the United States: Results from the Heinz and Other Studies*

In 2000, the Heinz Center released the results of a study conducted for the Federal Emergency Management Agency (FEMA) to determine the risk of coastal erosion (available at http://www.fema.gov/pdf/library/erosion.pdf). The study considered the number of coastal structures within 500 ft. of the shoreline and included the U. S. mainland, the Great Lakes and Hawaii. The report Summary reads, in part "Over the next 60 years, erosion may claim one out of four houses within 500 feet of the U. S. shoreline. To the homeowners living within this narrow strip, the risk posed by erosion is comparable to the risk from flooding, especially in beach areas.". As part of the study, a fairly detailed analysis was conducted for a number individual counties in coastal states. Some of these results are summarized in Fig. 13.18 and Table 13.1. The shoreline recession rates are shown in Fig. 13.18 where, if the rate was less than 1.0 ft/year (or positive), it was listed as "<1 ft/year".

Leatherman et al. (2003) state that: "Rates of beach erosion along the U.S. east coast average slightly less than a meter per year, putting expensive beach-front development at risk to storm impact."

13.6 Anthropogenic (Human) Causes of Beach Erosion

A number of human-related causes of beach erosion have occurred with the dominant site-specific cause varying with the area depending on the natural physiography and type of human activities. Listed in approximate order of dominance, the causes are: (1) interruption of natural longshore sediment transport patterns, (2) interruption of river-borne sediment supply to the coast, and (3) subsidence due to ground fluid withdrawal. Each of these is discussed below with examples.

13.6.1 *Interruption of Natural Longshore Sediment Transport*

Interruption usually occurs through construction of a longshore barrier such as a jetty or a groin or through channel deepening and placement of the deposited material in deep water. Additionally, sand transported into inlets represents a loss to the outer beach system and will be manifested as beach erosion, e.g. Kana 1995, 2011. In the first case of a simple impoundment of sand on the updrift side of a littoral barrier and erosion downdrift with no sediment lost to the outer shoreline system, the shoreline recession may be balanced by shoreline advancement on the updrift side.

Fig. 13.18 Average erosion rates at some of the counties examined in detail in the Heinz study

Table 13.1 Average shoreline changes from "Coastal erosion mapping and management", (Leatherman and Crowell 1999)

State	Average shoreline change rate (ft/year) (Heinz study)	State	Average shoreline change rate (ft/year) (Heinz study)
MA	− 0.89	AL	− 3.5
NY	− 1.5	TX	− 2.6
DE	− 3.67	CA	− 0.33
NJ	− 0.53	OR	+ 1.0
VA	− 1.39	WA	+ 1.15
East FL	+ 1.35	HI	+ 0.04
West FL	− 0.21		

13.6.1.1 Overall Effect of Littoral Barriers on Florida's East Coast

In studies of the Florida MHW data base discussed earlier, Dean, in Dean et al. (1988) has found that 80–85% of the beach erosion along the east coast of Florida is due to navigational entrances. This is due, in part, to the net southerly net longshore sediment transport as shown in Fig. 13.19. In the early days of east coast harbor construction, Florida disposed of 55 million cubic yards of sand in deep water. This loss amounts to an average of approximately 9 m recession along the 650 km length of Florida's east coast sandy shoreline.

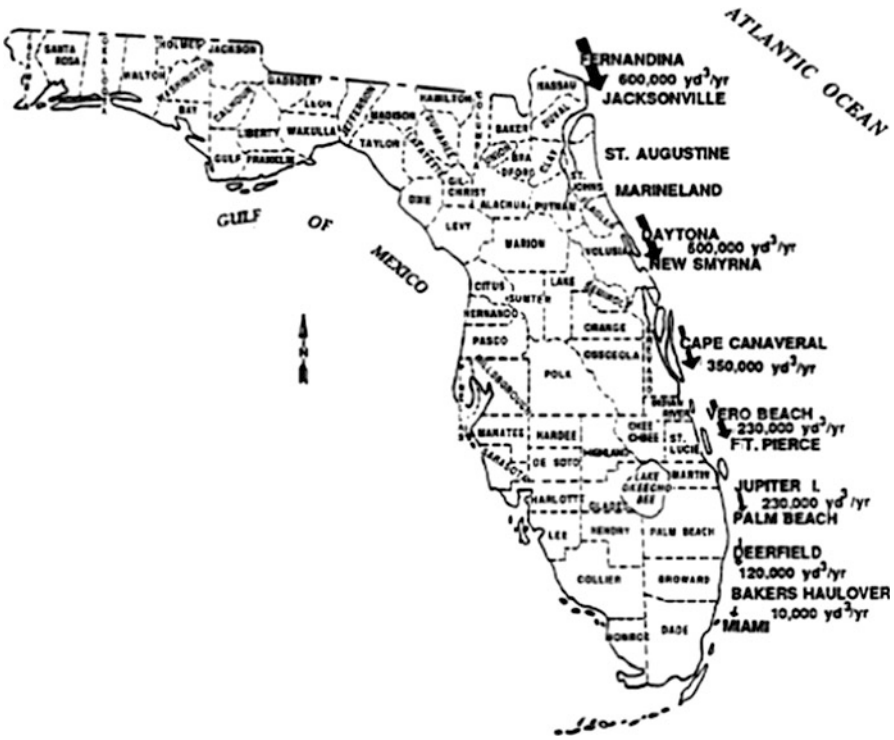

Fig. 13.19 Estimated net longshore sediment transport along Florida's east coast. Transport quantities in cubic yards per year

13.6.1.2 Case Study of Jupiter Island, Florida

In 1892, St. Lucie Inlet was cut across a barrier island in southeast Florida, separating the present Hutchinson Island to the north and Jupiter Island to the south. The net longshore sediment transport in this area is approximately 180,000 m^3/year to the south. In 1918, a north jetty was constructed at St. Lucie Inlet and a short south jetty was constructed in 1981. During the 89 years prior to construction of the south jetty, sand was lost from Jupiter Island due to the interruption of the net southward longshore sediment transport and the northward sand transport from the north end of Jupiter Island into St. Lucie Inlet, primarily on the flood tidal currents. The erosion on Jupiter Island during this period amounted to some 26 million m^3 and resulted in the north end of this island being literally uninhabitable. Figure 13.20 presents the shoreline changes from 1883 to 1970 along the northern 13 miles (21 km) of the island. The dots are based on surveys and the solid line is based on the Pelnard Considère theory (1956) which agrees quite well with the data.

The Town of Jupiter Island with its northern boundary some 9 km south of St. Lucie Inlet has conducted an aggressive beach nourishment project over the last

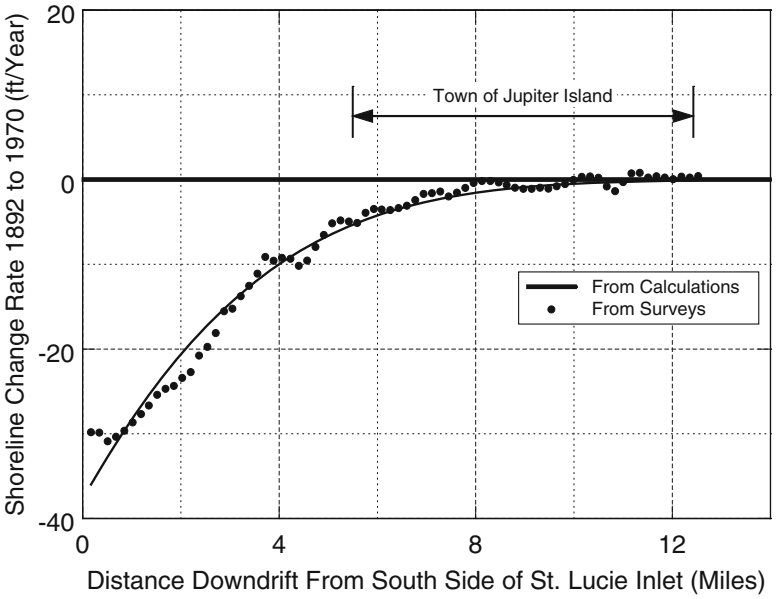

Fig. 13.20 Shoreline change rate downdrift (south) of St. Lucie Inlet. The *dots* are based on surveys and the *solid line* is a best fit with the Pelnard Considére theory. This fit allows quantification of the effective wave height and direction

40 years and, with the addition of more than 12 million m^3 of sand placement, has managed to maintain the Town's shoreline at approximately the position that it was in the earliest (1883) survey.

13.6.1.3 Impoundments Reducing Sand Delivery to the Coast

Areas with steep inland morphology and high episodic precipitation are usually characterized by large sediment supplies to the shoreline. With the construction of reservoirs for water supply, flood protection and recreation, this sediment is impounded and supply to the coast is greatly reduced. Prior to human intervention, if the supply was large, deltas formed which acted to feed sand to the adjacent shorelines. With the reduction in sediment supply, these deltas are retreating at rapid rates. Eventually, this erosional effect will be manifested on the adjacent shorelines that were previously advancing.

13.6.1.4 Rosetta Outlet of the Nile River, Egypt

The Rosetta Outlet of the Nile River in Egypt is a classic case of the effect of reduction in sediment supply through the construction of upstream impoundments. The Nile River has two main outlets, the Rosetta Outlet to the west and the

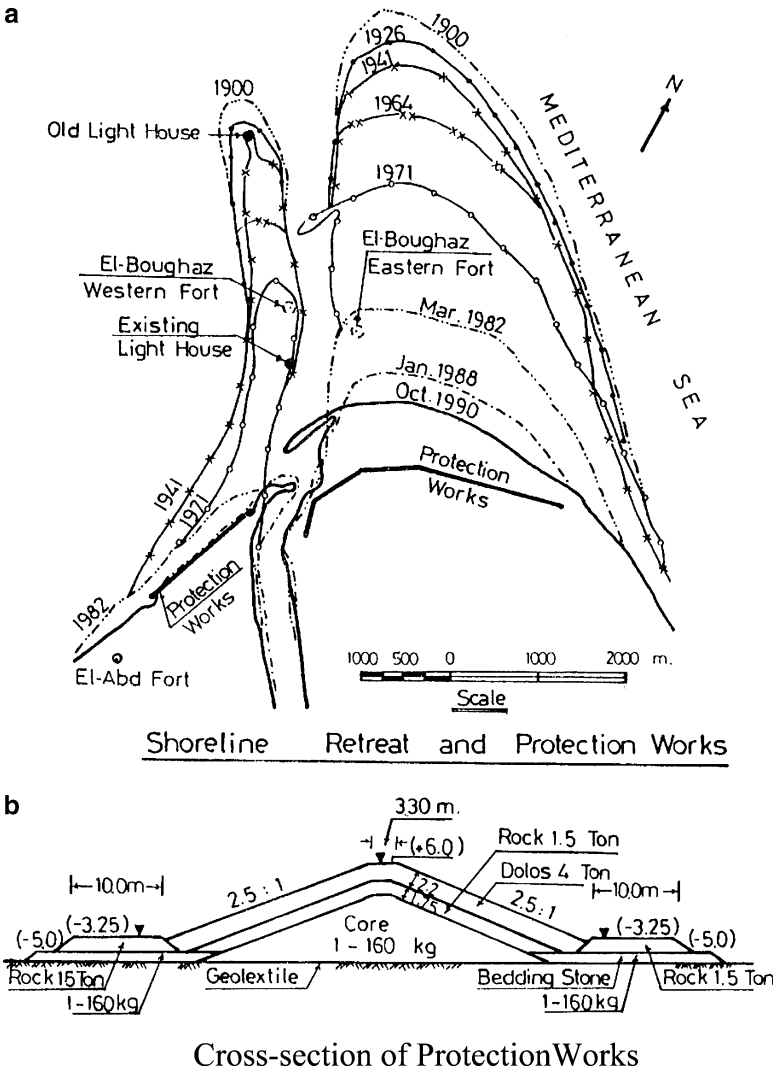

Fig. 13.21 The Rosetta outlet of the Nile River. *Upper panel*, shoreline positions, 1900–1990, *Lower panel*, cross-section of protective works (From Fanos et al. 1995)

Damietta Outlet to the east. Construction of the Low Aswan Dam commenced in 1902 and, at present, there are nine impoundment structures on the Nile River with the latest, the Aswan High Dam completed in 1964. Prior to these impoundments, the Nile River delivered an estimated 70 million m^3 of sediment annually through the two outlets, an amount that has been presently reduced to near zero (Fanos et al. 1995). Based on old maps, the Rosetta promontory was advancing at a rate of approximately 36 m/year and the sediment supply through this outlet was some 13 million m^3/year (Inman and Jenkins 1984). This promontory commenced retreating soon after construction of the Aswan Low Dam in 1902. Figure 13.21

Table 13.2 Retreat rates of the western and eastern lobes of the Rosetta outlet (Fanos et al. 1995)

	Promontory retreat rates (m/year)	
Period (years)	Western lobe	Eastern lobe
1900–1941	18	16
1941–1964	33	26
1964–1971	93	115
1971–1982	230	130
1982–1989	40	100

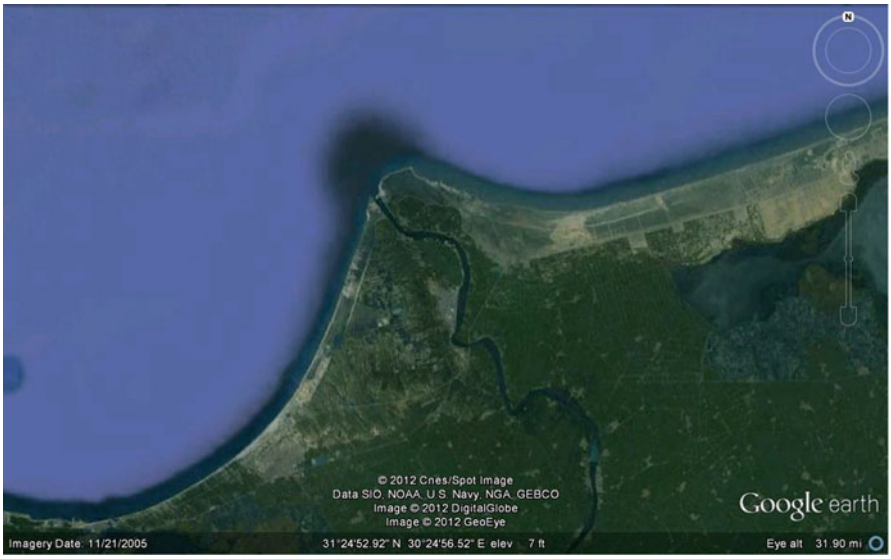

Fig. 13.22 Google photograph of the Rosetta Outlet of the Nile River

presents the shorelines from 1900 to 1990 and also indicates the location of substantial protective works (dolos armor units) that were constructed on the two lobes of the Rosetta promontory in 1989–1991. The average retreat rates of the eastern and western lobes of the Rosetta promontory are presented in Table 13.2. Figure 13.22 presents a 2005 Google image in which it is seen that the erosion has progressed to the protective works and that large groins have been constructed on the two flanks of the promontory. The erosion of the eastern Damietta Outlet has been discussed by Fanos et al. 1992.

13.6.1.5 Mississippi River Outlets

A few definitions are given to assist in the following discussion. *Suspended load* is the portion of sediment being transported that remains buoyed by the energy of the flow conditions, and *bedload* is the sediment that is transported by the flow near the bed by rolling, sliding, or hopping (saltating) near the bed. The Mississippi River drains 41% of the conterminous U.S. land area and the reduction in its sediment

supply has had a long-term detrimental effect on its delta. Prior to upstream impoundments, it is estimated that the suspended sediment load delivered annually to the coastal zone was approximately 236 million m^3 (Meade and Moody 2010). By 2007, this discharge had decreased by approximately two-thirds to 86 million m^3. The relatively small bedload sediment transport component is estimated at a few percent of the suspended load. Causes of sediment transport reduction include sediment impoundment by reservoirs, reduction in peak water flows, improved farming practices and channel management practices. The reduction of sediment for delta growth and maintenance is further exacerbated by the construction of levees along the Mississippi with the objective of reducing flooding of adjacent regions and reducing dredging for channel maintenance. Unfortunately, the result has been that the Mississippi River Delta and levee system have extended Gulfward, and now delivers sediments off the continental shelf into deep water. Finally, general subsidence in the area ranging up to more than 1 cm per year at the southern limits of the delta has contributed to the overall loss of the delta wetlands currently estimated at approximately 40 km^2 per year.

13.6.2 Subsidence

Nearshore subsidence has the same effect on beach recession as sea level rise and, of course, is a component of RSLR. Anthropogenic induced subsidence is generally due to extraction of ground fluids including hydrocarbons (petroleum and gas), water and possibly due to loading through placement of fill materials. Somewhat ironically, because many tide gages are located in ports which have been expanded through fill placement and in the vicinity of water extraction, these gages can reflect these recent construction projects.

13.6.2.1 Subsidence in Manila, Philippines

Figure 13.23 presents an example for the Manila, Philippines tide gage. These average annual tide levels show an increase in RSLR beginning in the 1960s which coincides with harbor expansion and increased usage of ground water, principally for domestic usage. Rodolfo and Siringan (2006) have compared the rate of ground water extraction in the Manila area with sea level based on the Manila Harbor tide gage as shown in Fig. 13.24.

13.6.2.2 Subsidence at Terminal Island, California

In 1940, ground water extraction commenced at the Terminal Island Naval Shipyards, California. By 1951, subsidence had increased to 2 ft per year

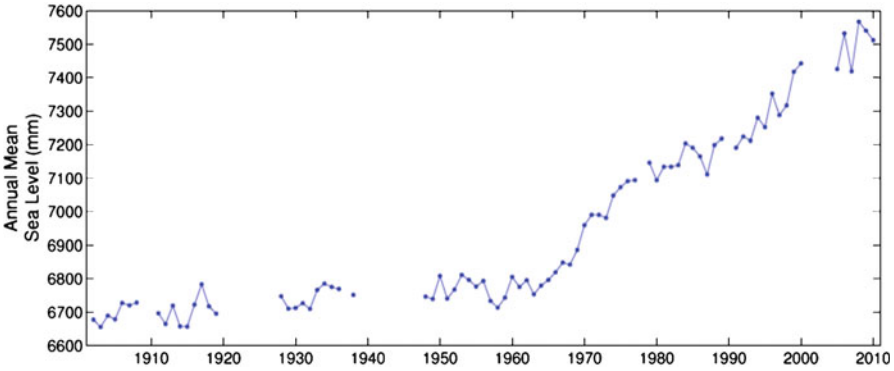

Fig. 13.23 Manila, Philippines record of annually averaged tide levels, Permanent Service for Mean Sea Level (PSMSL)

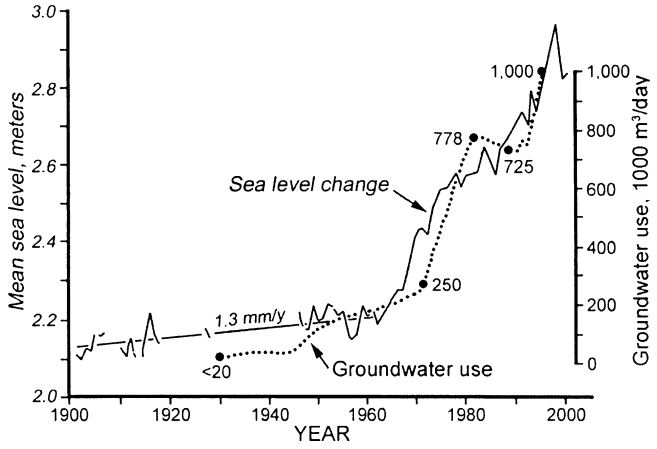

Fig. 13.24 Comparison of rate of ground water usage in the Manila area and mean sea level based on Manila Harbor tide gage (From Rodolfo and Siringan (2006))

and by 1958 the subsidence extended over a 20 square mile area with a maximum value of 29 ft. causing flooding of wharves and severe damage to pipelines and bridges. Figure 13.25 shows the areal extent of this damage. It was realized that hydrocarbon extraction was primarily responsible for the subsidence and in 1958, the state passed the California Subsidence Act which limited further hydrocarbon extraction. Prior to this Act, experiments had commenced with water injection into the hydrocarbon bearing aquifer and had demonstrated its efficiency in secondary hydrocarbon recovery and also, through pressurizing the aquifer, stopping subsidence. Further injection resulted in a rebound of up to 2 ft.

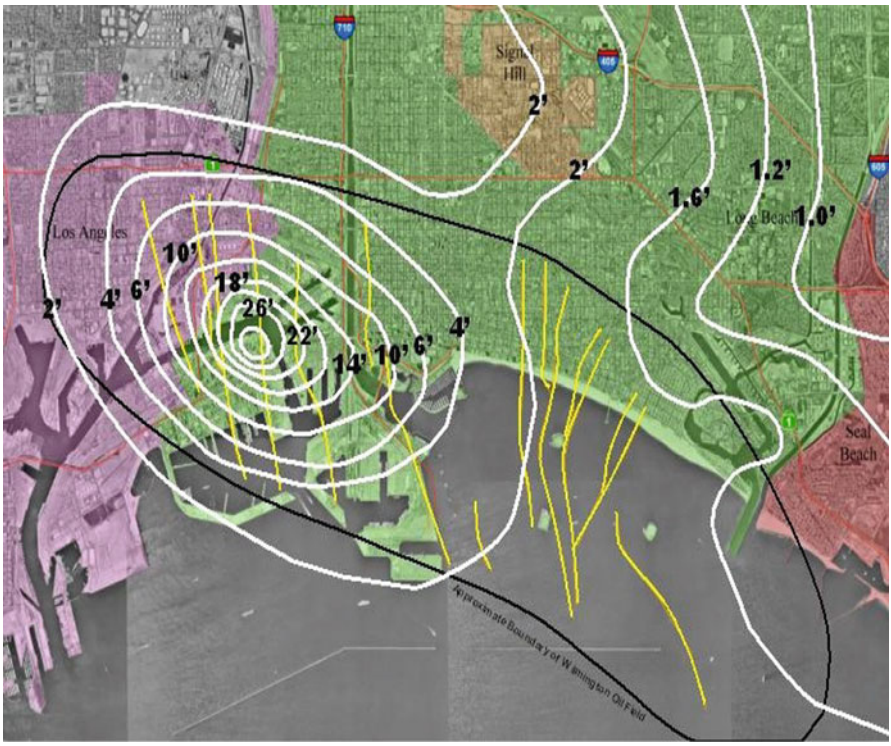

Fig. 13.25 Isolines of subsidence centered at Terminal Island, CA (From City of Long Beach website http://www.longbeach.gov/oil/subsidence/story.asp)

13.6.2.3 Subsidence at Niigata, Japan

Subsidence in the Niigata coastal plane has been caused by extraction of water bearing natural gas for industrial and domestic use. Up to 10,000 wells extracted approximately 60,000 m^3 of water per day. First order leveling documented up to nearly 2 m of subsidence as shown in Fig. 13.26.

13.6.2.4 Subsidence in Other Areas

Many other coastal areas, too numerous to mention here, have been impacted by ground fluid extraction. Directional drilling capabilities have allowed offshore hydrocarbon reservoirs to be accessed from wells located on land, thereby contributing to nearshore subsidence. Subsidence has been especially prevalent along portions of the Southern California coast including Huntington Beach,

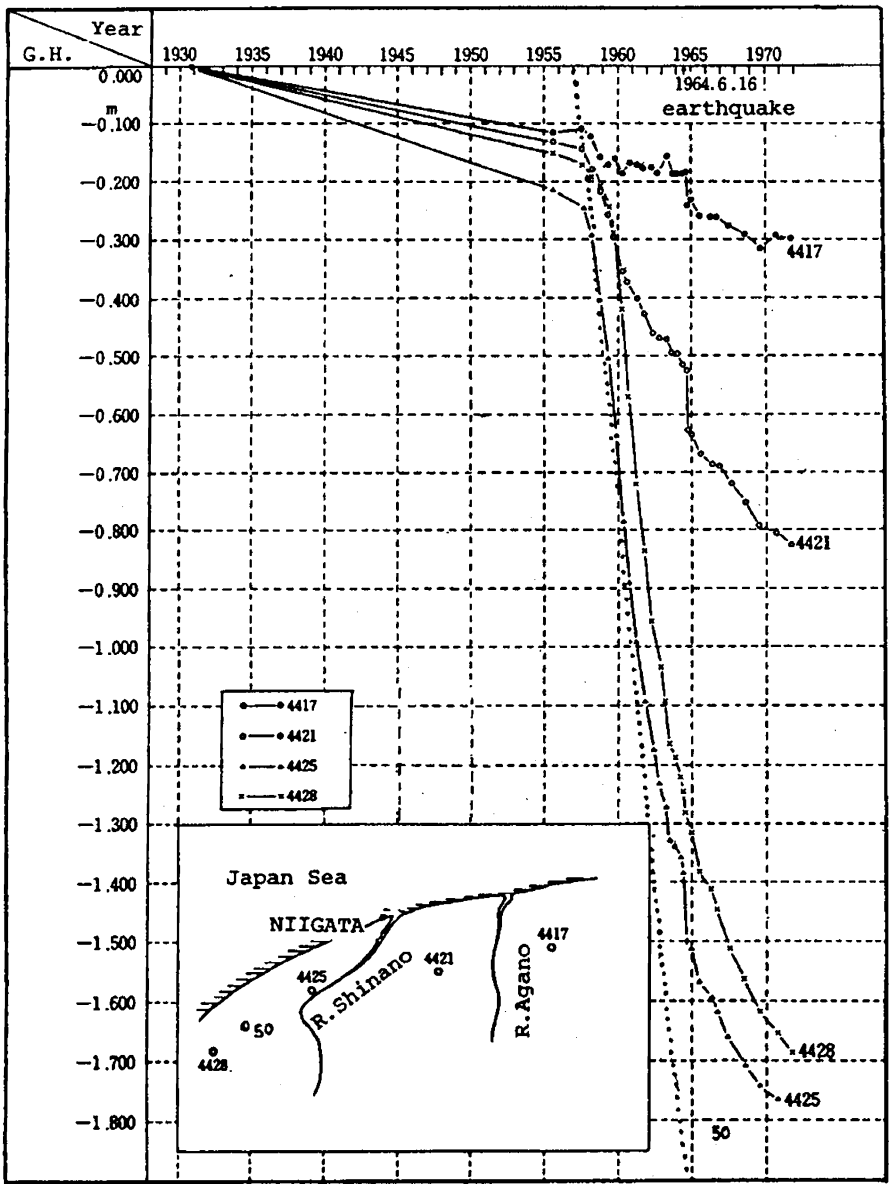

Fig. 13.26 Subsidence in the Niigata coastal plane, Japan (From http://wwwrcamnl.wr.usgs.gov/rgws/Unesco/PDF-Chapters/Chapter9-7.pdf)

portions of Santa Monica Bay and Santa Barbara. Additionally, offshore wells in the Gulf of Mexico have certainly contributed to subsidence along the adjacent coast. Morton et al. (2005) have provided a careful documentation of the subsidence associated with onshore hydrocarbon fields in the Mississippi River delta region.

13.7 Stabilization Measures

13.7.1 General

Approaches to beach stabilization generally fall within "soft structure" and "hard structure" classifications and combinations of the two. Soft structure measures are synonymous with beach nourishment and nearshore placement; hard structures include shore parallel structures (seawalls, revetments and detached breakwaters) and shore perpendicular structures (primarily groins). It is of interest to examine the approaches of various countries (and states) to shoreline stabilization. It seems that to some degree, the earlier-constructed approaches somewhat "set the pattern" for later stabilization. Japan has clearly opted for hard structures. Spain has constructed many pocket beaches which are a combination of hard and soft structure types. The Netherlands has generally adopted soft structures for flood control although many groins are present. In the United States, the approach varies significantly from state to state; however, hard structures were initially adopted and lately beach nourishment has become much more popular.

In considering beach stabilization at a particular location, it is important to recognize that each location is unique in terms of the wave, tide and current forces and offshore conditions. Thus, many of the statements to follow in this section should be considered as generalizations and may not apply to a particular area.

It is necessary to recognize that we are dealing with a "sand-sharing" system and that, with few exceptions, sand sequestered in one area will be associated with erosion in another area, especially in areas with substantial net longshore sediment transport. With the exception of beach nourishment, other stabilization measures have as their objective the stabilization or rearrangement of the existing sand in the system. Thus, unless the sand stabilized by structures would be lost to the system, or sand is placed within the structures, they will induce erosion at a different location.

13.7.2 Beach Nourishment Including Examples

Beach nourishment comprises the placement of large quantities of good quality sediment in the nearshore to advance the shoreline seaward. Good quality sediment is defined here as sand of a similar or larger size than exists on the native beach. The objective of beach nourishment is usually to reestablish the shoreline on an eroding beach to some previous location. Beach nourishment is a fairly young technology with the earliest large scale designed projects occurring in the 1970s. Experience obtained in maintenance of these beaches has provided a basis for design with greater confidence. Of the stabilization measures, beach nourishment is the only method that can restore the recreational, ecological and storm protection functions to their earlier conditions.

Although beach nourishment usually does not remedy the cause of the erosion, in many situations it can provide a relatively stable beach for many decades with

modest renourishment requirements. In other cases, more frequent nourishment may be required. The difference is usually related to whether there was a substantial pre-existing erosion rate or not. Two examples are presented below.

13.7.2.1 Miami Beach, Florida

The 17 km long Miami Beach project was constructed over the period 1976–1981 with 10.6 million m^3 of sand obtained from offshore borrow areas at a cost of $ 51 million. At the time of construction, permitting and environmental constraints were relatively minimal and, of interest, it is very doubtful that this project could be constructed under today's regulatory climate.

This project is located in an area of small net longshore sediment transport (estimated at between 6,000 and 12,000 m^3/year southward) and is "compartmented" by jetties at the north and south ends. Although some leakage of sand out of this compartment could occur at the south end, very little net erosion has occurred. Two erosional hot spots (local areas that erode more than desirable) have occurred and have required attention including relatively minor renourishments. Wiegel (1992) provides an excellent account of the physical aspects of the project including its response to Hurricane Andrew in 1992 which occurred as he was completing his manuscript. The economy of Miami Beach project has been revitalized by the acquisition of its new beach. Houston (1996, 2002) has examined the impact of the project on the local economy and has noted that Miami Beach has more visitors annually than the three most heavily frequented U. S. national parks combined. Of interest is that most visitors to this beach are unaware that it is an "artificial" beach.

13.7.2.2 Santa Monica Bay and Other California Beaches

Most of the material here is based on Leidersdorf et al. (1993) who present an excellent account of this project. The 35 km central and southern segments of Santa Monica Bay, California, were nourished with more than 20 million m^3 of sand from 1938 to 1964 with "sediments of opportunity" that is, sediment derived from other projects such as harbor construction or, in one case, excavation of a foundation. Although the sand from the different projects was of variable size, it has generally performed well. One groin has been constructed to reduce deep water losses into a submarine canyon and by 1991, the last date when data are available in Leidersdorf et al. a relatively small amount (<3 million m^3) of post-1964 nourishments had been carried out and the average beach width was found to be approximately 100 m advanced relative to its 1938 position.

A number of other southern California beaches have benefitted similarly through sediments of opportunity. Herron (1980) presents an account of several of these beaches. Between 1919 and 1978 a total of 108 million m^3 were deposited on southern California beaches. Herron lists 28 million m^3 placed in the Santa Monica

Bay cell leaving 80 million m^3 placed on beaches other than those in Santa Monica Bay. Based on personal observation, many of these beaches, like those at Santa Monica Bay, remain today and have performed well.

Of interest is that most of these southern California beach nourishments were performed prior to the extensive design procedures required today and the lengthy environmental review. Yet the performance of these beaches is a testament to their effectiveness and, to the best of our knowledge, no environmental damage has been reported. In fact is likely that the near natural beaches have resulted in a positive change to the beach ecology rather than the seawalls that were present along some of those beaches prior to nourishment activities.

13.7.3 Groins and Other Structures

Groins are shore-perpendicular structures that can be constructed with various configurations, such as simple linear structures or as T-head structures. The objective of a single groin or a field of groins is to stabilize sand within a sand sharing system. Unless the groins can somehow allow the pre-installation transport processes to continue unaffected, they will result in erosion to the adjacent beach system. Pre-filling the groin(s) with compatible sand can reduce their impact; however, in the presence of net longshore sediment transport, groins can be expected to cause downdrift erosion. Groins may cause the formation of rip currents leading to hazardous swimming conditions.

13.7.3.1 Case Study at Willoughby Spit, North Carolina

Figure 13.27 is a Google photograph of a field of groins and detached breakwaters at Willoughby Spit, North Carolina. Net sediment transport is from east to west (right to left) toward the end of the spit. The structures have clearly been effective and if not present, it appears that the transported sand would be either lost to the present system or the spit would continue to grow toward the west. Because the structures extend to the end of the present spit system, they are not depriving the existing spit of sediment supply.

13.7.3.2 Coastal Structures in Japan

The effects of installation of coastal structures and other anthropogenic influences along the Japan coastline have been very nicely documented by Uda (2010). The associated erosion commencing in the 1970s is a result of the construction of almost 3,000 fishing ports, 1,000 commercial ports and construction of 2,532 large dams which have reduced severely the supply of sand to the coast. Uda states *"Thus, almost all of the causes of beach erosion in Japan are due to anthropogenic effects"*. Two examples of the responses to erosion along the Japanese coast are provided below.

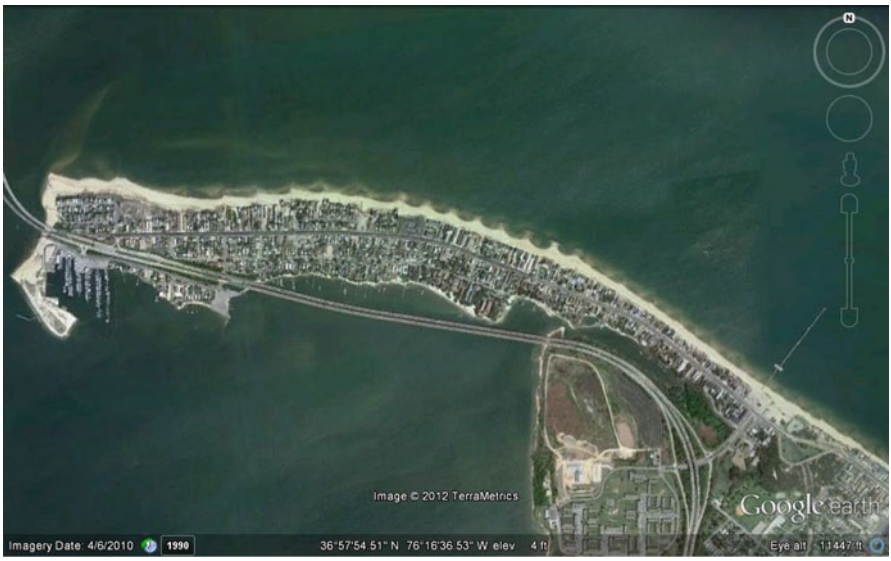

Fig. 13.27 Google image of Willoughby Spit, Virginia, in which a series of detached breakwaters and groins have been constructed near the terminal end of the spit to the west. The net transport is from east toward west. There are eight detached breakwaters near the center of the photograph and numerous groins on either side. Clearly the structures are effective in maintaining the shoreline

Figure 13.28 presents an aerial photograph in the Ibaraki Prefecture in Japan which has been stabilized by T-head groins with lengths of approximately 200 m. The groins in this photograph appear to be of limited effectiveness.

Figure 13.29 presents detached breakwaters that have been constructed along the coastline of Honshu in Japan. These breakwaters are approximately 125 m in length and 120 m or so from the shoreline resulting in a mild salient.

13.7.4 Detached Breakwaters: Emergent and Submerged

Detached breakwaters include those that are generally emergent or those with submerged crests. Constructed in a sand-sharing environment, detached breakwaters can sequester sand and stabilize the local shoreline and can reduce longshore sediment transport resulting in downdrift beach erosion.

Emergent breakwaters have been constructed extensively in Japan, see Fig. 13.29. The deposits landward of emergent breakwaters may be rather small or may attach to the breakwater forming a tombolo. Usually the construction of a detached breakwater in an area of longshore transport will lead to the need to construct another downdrift structure to address erosion there. Detached breakwaters may be an appropriate application depending on the objective and location.

Fig. 13.28 Google image of T-head groins constructed along the Ibaraki Prefecture

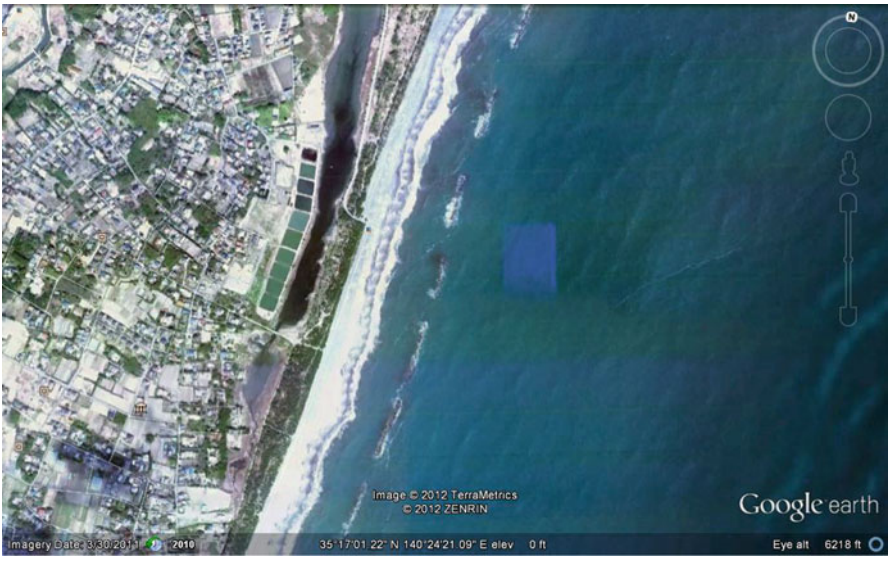

Fig. 13.29 Google image of detached breakwaters in Honshu, Japan

One advantage of submerged breakwaters is that they are less visually obtrusive. Significant disadvantages include navigational and beach hazards to swimmers and boaters, and elevated water levels that usually accompany major storms reduce significantly their effectiveness. A requirement of submerged breakwaters in order

that they be effective is that they cause significant dissipation of wave energy. To significantly reduce wave dissipation requires a fairy wide breakwater crest. The crest widths for some applications in Japan are 40 m resulting in an expensive structure.

Dean et al. (1997) report on a full-scale test of a submerged pre-fabricated unit breakwater located off Palm Beach, FL. The breakwater was constructed of pre-fabricated units termed PEP units (Prefabricated Erosion Prevention). The breakwater consisted of 330 units, each of 1.8 m in height and 3.7 m long. The crest width of the units was approximately 30 cm. The project was monitored from July 1992 through June 1995 and consisted of 11 surveys encompassing 1,260 m of breakwater length and 630 m north and south of the breakwater to serve as "control" areas. Two wave gages were installed inboard and outboard of the breakwater. Overall it was found that the units tended to settle due to an inadequate foundation and that the area landward of the breakwater system lost sand amounting to 81,700 m^3 compared to the combined losses in the two control areas landward of the breakwater alignment which lost 14,500 m^3. This loss landward of the breakwater was hypothesized to be the result of water pumped over the breakwater crest by the waves and that the presence of the breakwater prevented direct return flow of this water which was diverted a longshore. Attempts to measure these currents in the field were not successful but this hypothesis was demonstrated in small wave basin studies. The wave transmission coefficient, defined as the ratio of wave height shoreward as compared to the height seaward of the structure, was found to be quite large ranging from 0.76 to approximately unity.

13.7.5 Headland Bay Beaches

Headland bay beaches are inspired by natural pocket beaches such as those shown in Fig. 13.30. These types of beaches are defined as those that contain sediment within a defined region, whether through constructed structures or natural headlands. Most constructed headland bay beach systems include both structures and beach nourishment. Several examples will be presented.

13.7.5.1 Fisher Key, Florida

Bodge and Olsen (1992) and Bodge (1998) have described headland bay beaches constructed on Fisher Key, Florida, and in the Caribbean. A Google photograph of the Fisher Key project is presented in Fig. 13.31. Of additional interest is that the sediment placed in this project was Aragonite sand transported from the Bahamas.

Fig. 13.30 Google photograph of two natural pocket beaches on the north island on New Zealand. The northern beach is approximately 1 km in length

Fig. 13.31 Google photograph of Fisher Key, Florida

Fig. 13.32 Yorktown during a storm in 1978 prior to headland beach installation (Photograph courtesy of Scott Hardaway)

13.7.5.2 Chesapeake Bay, USA

Hardaway and Gunn (1999 and 2010) reported on the design and installation of more than 60 headland bay beach systems in Chesapeake Bay. Some of these have been installed since the mid-1980s and all seem to have performed quite well. The Yorktown installation is located on the south side of the Yorktown River, near its mouth. This system was installed in phases commencing in 1994 and was completed in 2005. Prior to its installation, the shoreline was badly eroded. Figure 13.32 presents a photograph during a 1978 storm showing various debris placed in an attempt to curtail the erosion. Figure 13.33 presents a photograph of the completed project. This project was not damaged by Hurricane Isabel in 2003.

13.7.5.3 Headland Bay Beaches in Spain

Many headland bay beaches have been constructed in Spain primarily for recreational purposes. Figure 13.34 is a Google photograph of an installation near Malaga on the southern coast of Spain.

Fig. 13.33 Photograph of the headland beach system constructed on the south side of Yorktown River. Portions of this installation had been in place for 18 years as of 2012 and were undamaged by Hurricane Isabel in 2003 (Photograph courtesy of Scott Hardaway)

In summary of this presentation of headland bay beaches, they can be quite effective in maintaining recreational and storm protective beaches and, if constructed in areas where the net longshore sediment transport is minimal and placed with sufficient beach nourishment, appear to not cause adverse effects to the adjacent shorelines.

13.7.6 Terminal Structures

Terminal structures are those that are installed near the end of a littoral system which commonly occurs at the ends of a barrier island or beach and is adjacent to an inlet. When natural channels through barrier islands are deepened for navigation, erosion tends to occur on the ends of the barrier islands. This erosion is due to the steepening of the local slope resulting in increased sand transport into the channel. To maintain a navigable depth, sand is dredged from the channel and placed offshore, in the nearshore or on the adjacent beaches. If placed offshore, the cycle continues to contribute to erosion on the ends of the adjacent barrier islands. Terminal structures can restrict the sand flow into the deepened channel, thereby reducing the dredging requirement as well erosion on the adjacent beaches.

An interesting case history is Boca Grande Pass on the southwest coast of Florida (Dean 1993). This area was the site of a phosphate loading terminal constructed in the 1920s on the west side of Gasparilla Island. Dredging from a

Fig. 13.34 Google photograph of a headland beach installation near Malaga on the southern coast of Spain

natural channel depth of 4–6 m inside the bay was required to provide the draft required by the vessels used to transport the phosphate. With dredging of this loading terminal, sand transported from the Gulf of Mexico and south side of Gasparilla Island was sequestered in the channel, resulting in erosion rates of 11 m/year, among the highest in the State. In the 1970s, a deepened fuel loading pier located in Fig. 13.35b at (b) was constructed thereby exacerbating the erosion problem. A seawall was constructed on the Gulf side to protect the eroding end of a railroad line used in the loading process. This ever protruding seawall acted as a groin and further limited sand transport from the Gulf side to the deepened loading area, thus placing more erosional pressure on the south end of Gasparilla Island. An historic lighthouse near the southern tip of Gasparilla Island was in danger of being undermined by the erosion. Two terminal structures were constructed in the 1980s and both reduced the dredging needs at the loading terminals and also advanced the shoreline by some 60 m. Thus this is a case in which the terminal structures both reduced shoaling of the loading areas and reduced beach erosion. Dean (1993) presents other examples.

13.7.7 Legal Approaches: Sand Rights and Others

Sand Rights is a legal concept parallel to Water Rights and attests that the rights of sand flowing to and along the coast should be held in common ownership such that any interference should be subject to restrictions associated with these legal doctrines. See Stone (1999) for further discussion regarding sand rights. In 1999,

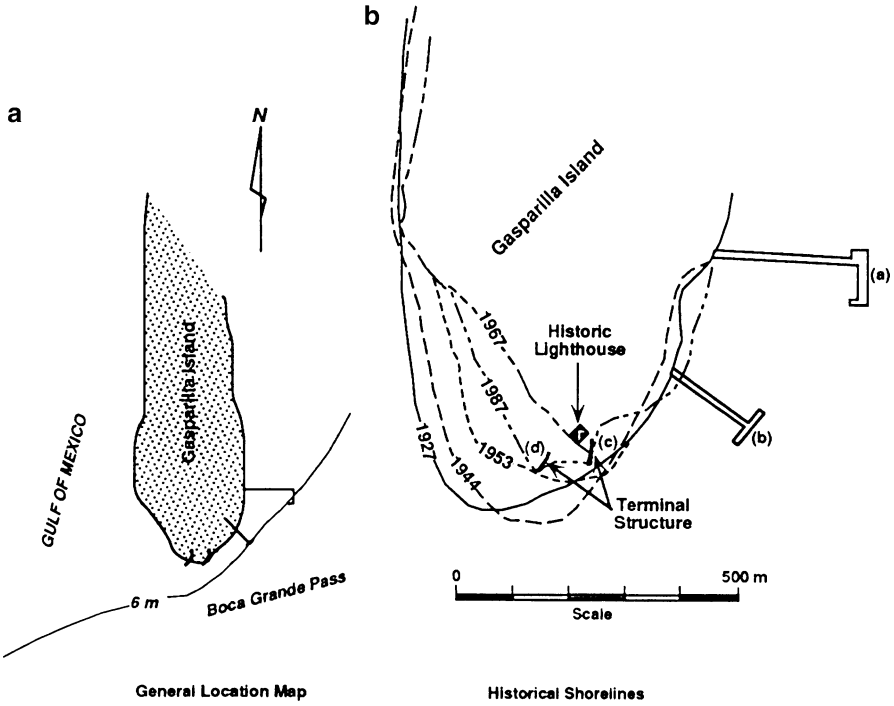

Fig. 13.35 Shoreline positions on the southern extremity of Gasparilla Island, showing the endangered lighthouse and the beneficial effects of the two terminal structures (From Dean 1993)

a conference was held in California with a focus on Sand Rights http://www.csbpa.org/sandrights/info.html .

Beaches are quite valuable to the state of Florida and other states; in recognition of the impact of navigational entrances, Florida legislation has been passed with the intent to reinstate net longshore sand transport around the inlets along the state's shoreline (there are 56 inlets). This program has been moderately effective, especially where so-called "inlet districts" have been formed, thereby providing organizational and financial resources (the districts have taxing authority) for the required sand bypassing.

13.7.8 Innovative Erosion Control Structures

Due to the cost of beach stabilization, an understandable desire to find less expensive measures exists. Many have been proposed ranging from the use of heavy sand to beach drains to artificial seaweed to nets placed perpendicular to the beach. Some of these ideas have been patented and some have been tested in laboratory and field settings.

An overall assessment of innovative approaches must be a judgment call, but our position is as follows starting with a reiteration that we are dealing with a sand-sharing system (i.e. a zero sum game from the standpoint of sand). If the stabilization systems are effective in accumulating sand at one location or in stabilizing a previously eroding beach, they will transfer that erosion elsewhere except in those special cases where the stabilized sand would otherwise be lost as in the Gasparilla Island case.

The real proof of whether innovative projects are effective is whether they are in use many years after their introduction and, so far, this has not been the case. Artificial seaweed was first field tested in the 1970s and is not in use today. Beach drains were introduced in the 1980s and have not been widely accepted nor proved beneficial. If an effective low-cost method were proven to work, it would be readily accepted and applied by coastal engineers and coastal communities; however, it must be recognized that erosion forces are pervasive and persistent and there are constraints (the sand-sharing system) which Nature will not let us forget. The state of Florida has adopted the requirement that for innovative methods to be judged effective, they must introduce new sand from offshore. Woodruff and Dean (2000) provide several examples from the state of Florida.

As noted previously, shoreline change signals are noisy, and may undergo erosion and accretion cycles on periods of various time scales. Thus, in considering the evaluation of an innovative approach, it is worthwhile to carefully establish criteria and required results to be met for the methodology to be judged effective or ineffective. To reduce the possibility of misinterpretation of data, adjacent control sites should be established and monitored and evaluation programs should be carried out and evaluated by third-party entities. “Triggers” should be established which would require removal of the project if its continued presence would be disadvantageous to the physical, ecological or recreational functions of the beach. It may be advantageous in many cases to require an “escrowed account” to provide funding if project removal becomes necessary.

Overall, in fairness and in order to avoid claims that coastal engineers and the dredging industry are concerned that less expensive methods will be found to address beach erosion, it is probably desirable to continue testing these methods but to establish test programs and effectiveness criteria to ensure to the degree possible that results obtained will be conclusive.

13.8 The Future for Shoreline Erosion and Stabilization

Realistically, it will not be possible in all cases to reinstate natural sediment supplies to the coast that were reduced or eliminated by the anthropogenic effects of jetties, navigational channels, impoundments and land subsidence. While it is useful to seek solutions and implement remedial measures where possible, some of these impacts commenced more than a century ago, would be very expensive and are considered impractical to remedy (for example, the levee and dam

impoundments on the Mississippi River). Perhaps pessimistically, it is more productive that the major part of our effort be directed toward recognizing the areas for which retreat is the best option; as well as causes and magnitudes of the anthropogenic induced erosion in other areas and to identify and implement the most effective approaches to management of these areas.

13.9 Summary

Beach erosion at a specific location can be the result of natural or human-induced causes and can be described as a loss of sediment volume or a shoreline recession. Most natural erosion cases can only be predicted statistically and through evaluation of historical data at the site. Ability to predict shoreline changes is much better for nearshore systems that are significantly out of balance such as result through the construction of littoral barriers or beach nourishment projects. It appears that much, if not most of the erosion in developed countries is due to anthropogenic factors including construction of littoral barriers, reduction of sediment supply through dam construction, and ground fluid extraction-induced subsidence.

The societal responses to beach erosion are limited to retreat, shoreline hardening, beach nourishment and combinations of the last two. Intelligent selection of the appropriate option at the appropriate time requires a much better understanding of the nearshore processes and responses than are presently available. Consideration of time scales is important in evaluating responses to beach erosion. Although global sea rise is ubiquitous and pervasive, according to the best available model (Bruun Rule), the erosional pressure that global sea level rise places on the shoreline over a century is reasonably modest considering twentieth century rise rates. We now have long-term shoreline change data and project performance data that support the likelihood that it is practical to stabilize many highly developed shorelines for one or two centuries with beach nourishment and structures. During that same period it will likely be appropriate to abandon some highly vulnerable and less developed shorelines as in the case for sites with greater relative sea level rise rates. The knowledge base to intelligently guide this process is presently deficient as is the conditioning of the Stakeholders to the conditions and timing which would make such actions appropriate.

References

Absalonsen L, Dean RG (2010) Shoreline change characteristics along the sandy beaches of the State of Florida: an atlas, Department of Civil and Coastal Engineering, University of Florida. Available: http://nsgl.gso.uri.edu/flsgp/flsgpm10001.pdf. Accessed 5–18 2012

Absalonsen L, Dean RG (2011) Characteristics of the shoreline change along Florida sandy beaches with an example for Palm Beach County. J Coast Res 27(6A):16–26

Bindoff NL, Willebrand J, Artale V, Cazenave A, Gregory J, Gulev S, Hanawa K, Le Quéré C, Levitus S, Noijiri Y, Shum CK, Talley LD, Unnikrishnan A (2007) Observations: oceanic

climate change and sea level. In: Solomon S et al (eds) Climate change 2007: the physical science basis, Intergovernmental Panel on Climate Change. Cambridge University Press, Cambridge, pp 385–432
Bodge KR (1998) Beach fill stabilization with tuned structures: experience in the Southeastern USA and Carribbean. In: Allsop NHW (ed) Coastlines, structures and breakwaters. Thomas Telford, London, pp 82–93
Bodge KR, Olsen EJ (1992) Aragonite beachfill at Fisher Island, Florida. Shore Beach 60(1):3–8
Bruun P (1962) Sea level rise as a cause of shore erosion. J Waterw Harb Coast Eng Div, ASCE 88 (1):117–130
Crowell M, Leatherman SP (eds) (1999) Coastal erosion mapping and management, J Coast Res, Special issue no. 28. Coastal and Environmental Research Foundation, Royal Palm Beach, Florida, p 196
De Beaumont LE (1845) Leçons de GeologiePratique, 7me Lećon-Levees de Sables etGalets, Paris
Dean RG (1993) Terminal structures at ends of littoral systems. J Coast Res 18:195–210
Dean RG (2005) Analysis of the effect of Sebastian inlet on adjacent beach systems using DEP surveys and coastal engineering principles, Department of Civil and Coastal Engineering Report UFL/COEL-2005/003. University of Florida, Gainesville
Dean RG, Maurmeyer EM (1983) Models for beach profile response. In: Komar PD (ed) Handbook of coastal processes and erosion. CRC Press, Boca Raton, pp 151–166
Dean RG, Pilkey OH, Houston JR (1988) Eroding shorelines impose costly choices. Geotimes 33 (5):9–14
Dean RG, Chen R, Browder AE (1997) Full scale monitoring study of a submerged breakwater, Palm Beach, Florida, USA. Coast Eng 29:291–315
Dean RG, Cheng J, Malakar SB (1998) Characteristics of the shoreline change along the sandy beaches of the State of Florida: an atlas, UFL/COEL-98/015. Department of Coastal and Oceanographic Engineering, University of Florida, Gainesville
Fanos AM, Khafagy AA, Komar PD (1992) Erosion of the Damietta promontory, The Nile Delta. In: Proceedings, twenty-third international conference on coastal engineering. American Society of Civil Engineers, Venice, pp 3246–3259
Fanos AM, Khafagy AA, Dean RG (1995) Protective works on the Nile Delta coast. J Coast Res 11 (2):516–528
Gilbert GK (1890) Lake Bonneville. U. S. Geological Survey, Washington, D.C
H. John Heinz Center for Science, Economics and the Environment (2000) Evaluation of erosion hazards, Washington, D. D. Available online at: http://www.fema.gov/pdf/library/erosion.pdf. Accessed on 21 May 2012
Hansen JE (2007) Scientific reticence and sea level rise. Environ Res Lett 2:024002
Hansen JE, Sato M (2011) Paleoclimate implications for human-made climate change, published electronically at arXiv:1105.0968v2 [physics.ao-ph]. http://arxiv.org/ftp/arxiv/papers/1105/1105.0968.pdf
Hardaway CS, Gunn JR (1999) Chesapeake Bay: design and early performance of three headland breakwater systems, Proceedings, coastal sediments '99, ASCE, pp 826–843
Hardaway CS, Gunn JR (2010) Design and performance of headland bays in Chesapeake Bay, USA. Coast Eng 57(2):203–212
Herron WJ (1980) Artificial beaches in Southern California. Shore Beach 48(1):3–12
Houston JR (1996) International tourism & U.S. beaches. Shore Beach, J Am Shore Beach Preserv Assoc 64(2):3–4
Houston JR (2002) The economic value of beaches – 2002 update. Shore Beach, J Am Shore Beach Preserv Assoc 70(1):9–12
Hoyt JH (1967) Barrier island formation. Bull Geol Soc Am 78:1125–1136
Inman DL, Jenkins SA (1984) The Nile littoral cell and man's impact on the coastal zone of the Southeastern Mediterranean, SIO reference series 84–31. Scripps Institute of Oceanography, La Jolla, 43 p

Kana TW (1995) Signatures of coastal change at mesoscales. In: Coastal dynamics '95, proceedings of international conference on coastal research in terms of large scale experiments. ASCE, New York, pp 987–997

Kana TW (2011) Coastal erosion and solutions – a primer, 2nd edn. Coastal Science & Engineering, Columbia, 40 p

Leatherman SP, Douglas BC, LaBrecque JL (2003) Sea level and coastal erosion require large-scale monitoring, Eos Trans. AGU 84(2):13. doi:10.1029/2003EO020001

Leidersdorf CJ, Hollar RC, Woodell G (1993) Beach enhancement through nourishment and compartmentalization: the recent history of Santa MonicaBay. In: Stauble DK, Kraus NC (eds) Beach nourishment engineering and management considerations. American Society of Civil Engineers, New York, pp 71–85

MacMahan J, Thieke RJ, Miller G, Engle J, Stanton T, Reiner A, Ruggerio P, Gulfenbaum G, Dean RG (2002) Feasibility of measuring currents from a personal water craft, Proceedings, ASCE conference on ocean wave measurement and analysis, pp 66–75

Meade RH, Moody JA (2010) Causes for the decline of suspended sediment discharge in the Mississippi River system. Hydrol Process 24(1):35–49

Morton RA, Bernier JC, Barras JA, Ferina NC (2005) Rapid subsidence and historical wetland loss in the Mississippi Delta plain: likely causes and future implications, USGS open file report 2005–2016, 116 pages

National Research Council Committee on Coastal Engineering and Education Needs (1999) Meeting research and educational needs in coastal engineering. Marine Board, Commission on Engineering and Technical Systems, National Research Council, National Academy Press, Washington, D. C

Nicholls RJ, Birkemeier WA, Hallermeier RJ (1996) Application of the depth of closure concept. In: Proceedings, of the twenty-fifth international conference on coastal engineering, Orlando, Florida, pp 3874–3887

Olsen EJ (1977) A study of the effects of inlet stabilization at St. Mary's Entrance, Florida, Coastal sediments '77. American Society of Civil Engineers, New York

Pelnard Considère R (1956) Essai de Théorie de l'Evolution des Formes de Rivage en Plages de Sable et de Galets, 4th Journees de l'Hydraulique, Les Energies de la Mer, Question III, Rapport No. 1

PSDS (Program for the Study of Developed Shorelines) (2012) http://www.wcu.edu/1038.asp. Accessed 29 May 2012

PSMSL (Permanent Service for Mean Sea Level) http://www.pol.ac.uk/pmsl/. Accessed 29 May 2012

Rodolfo KS, Siringan FP (2006) Global sea-level rise is recognized, but flooding from anthropogenic land subsidence is ignored around Northern Manila Bay, Philippines. Disasters 30 (2):118–139

Shalowitz AL (1964) Shoreline and sea boundaries, vol 2. U.S. Coast and Geodetic Survey, U.S. Department of Commerce Publication 10–1, Washington, D.C, 420p

Shepard FP (1963) Submarine geology, 2nd edn. Harper and Row, New York, 557 Pages

Stone KE (1999) Sand rights: a legal system to protect the 'shores of the sea'. In: Ewing L, Magoon OT, Robertson S (eds) Proceedings of the sand rights '99 bringing back the beaches, pp 4–17

Thevenot MM, Kraus NC (1995) Longshore sand waves at Southampton Beach, New York: observation and numerical simulation of their movement. Mar Geol 126:249–269

Uda T (2010) Japan's beach erosion: reality and future measures, vol 31, Advanced series in ocean engineering. World Scientific, Hackensack, 428 Pages

Walton TL Jr (1999) Shoreline rhythmic pattern analysis. J Coast Res 15(2):379–387

Wiegel RL (1992) Dade County, Florida beach nourishment and hurricane surge protection project. J Am Shore Beach Preserv Assoc 60(4):2–28

Woodruff PE, Dean RG (2000) Innovative erosion control technology in Florida. In: Proceedings, of the 27th international conference on coastal engineering, Sydney, Australia, Summer, pp 3853–3860

Chapter 14
Innovative Technique of Predicting Shoreline Change in Developing Countries: Case of Accra Erosion and Causal Factors

Kwasi Appeaning-Addo and Emmanuel Lamptey

Abstract The world over, coastal zones are known to support a wide range of critical habitats, unique biodiversity, host 50% of human populations and site development projects. These make coastal zones quite complex, dynamic and fragile and therefore challenging to manage. Shoreline status assessment is an invaluable tool for coastal resource management given the escalating impacts of emerging global geophysical changes, such as rising sea levels, and rapid coastal development. In this contribution, shoreline change detection of Accra, Ghana was modeled with an innovative technique that combined dated historic maps, aerial photography, satellite imagery, conventional or global position system (GPS) ground surveys and laser altimetry data. Such a technique shows the relative response of coastal geomorphic features and geology to coastal processes. The results of the assessment revealed that the Accra shoreline has receded at an average rate of 1.13 m/year, which is attributable to several factors. This rate of change poses a looming threat to coastal lands and infrastructure in the zone. Essentially, this study demonstrate that reliable historic erosion rates can be estimated using the proposed technique for developing nations where geospatial data is scarce. These findings have important implications for formulating reliable and sustainable coastal management strategies in developing countries.

14.1 Introduction

The coastal zone, the world over, constitutes one of the highly invested and populated areas. Coastal zones harbour many major cities and as such support about 25% of global productivity (Al-Tahir and Ali 2004) and home to about 50%

K. Appeaning-Addo (✉) • E. Lamptey
Department of Marine and Fisheries Sciences, University of Ghana,
P. O. Box LG 99, Legon, Ghana
e-mail: kappeaning-addo@ug.edu.gh; elamptey@ug.edu.gh

C.W. Finkl (ed.), *Coastal Hazards*, Coastal Research Library 6,
DOI 10.1007/978-94-007-5234-4_14,

of global total population (Woodroffe 2003). Increasing levels of industrialization and fast growing economy in most coastal areas poses looming threats to the ecology and economy of the zone. Threats to the coastal environment have reached an alarming proportion where it is estimated that about 38% of Africa's coastal ecosystem is highly threatened (FAO 1998). This has called for urgent need to sustainably manage the resources of the coastal zone. Among the many benefits derived from coastal resources include provision of habitats for valuable biodiversity (e.g., wildlife); dunes create excellent natural flood barriers and natural filter for drinking water; salt marshes absorb wave energy during storm surges and minimises erosion; and beaches are an essential asset for generating revenue from the tourism industry.

Ostensibly, sustainable management of coastal resources has become increasingly challenging to coastal managers due to the recent issues of global climate change and its associated sea level rise. Although current model predictions indicate significant inconsistency in future sea level rise at both the regional and local levels, the impacts are going to be severe (IPCC 2007). Higher sea levels will affect the coastal zone in several ways. It will result in wave action moving closer to the beach and thus enabling storm surge to move onto the beach. This situation will facilitate the breaking of waves closer to the beach affecting sediment's equilibrium state. This in turn will develop rapid shoreline retreat, increasing coastal erosion and causing waterfront property destruction. It will also result in salt water intrusion into underground water systems, flooding of low lying areas as well as collapsing of vulnerable coastal industries.

The problem of shoreline recession/erosion are as a result of escalating impacts of emerging global geophysical changes, such as rising sea levels, and coastal development (Rakocinski et al. 1996). Thus, although coastal erosion is a natural phenomenon, it has been exacerbated significantly by changes in the coastal climate regimes. This and other factors including human activities along the coast have resulted in erosion of about 70% of sandy beaches globally (Bird 1985). Over 20% of the European coastline is affected by erosion and this problem could increase in view of the effects of climate change (EUROSION 2004). Sea level rise is considered a major cause of coastal erosion in the low lying coastal zones (Feagin et al. 2005). In Western Africa, human activities such as damming of major rivers have altered the sediment budget locally (World Bank 1996). In Ghana for instance, construction of the Akosombo dam in 1965 accelerated coastal erosion east of Accra (Keta) to about 4 m per year (Ly 1980), as against the overall rate of about 2 m/year (Boateng 2011). The historic rate is expected to increase as the sea level continues to rise at a rate of about 2 mm/year (Appeaning Addo 2009). However, the degree of coastal erosion that may result from sea-level rise is very uncertain (Cooper and Pilkey 2004). Models of coastal sediment flux under climate warming scenarios show some 'soft' coasts retreating by more than 40 m per century whilst others show accretion of about 10 m per century (Walkden and Hall 2005; Dickson et al. 2007).

Analysis of shoreline changing trend, under the influence of both climatic and anthropogenic forcing, is hampered by the availability of archival time series data,

especially in developing nations where there is scarcity of data. However, the novelty/innovation is the coupling of these archival data with remotely sensed data in data starved nations, especially developing nations, to obtain reliable information for developing shoreline management strategies. Studies by Moore and Griggs (2002) used two shoreline positions obtained from aerial photographs for 1994 and 1953 to estimate long term cliff retreat along the central shores of the Monterey Bay, while Gibeaut et al. (2003) used four shoreline positions to determine long term rates of change along the bay shorelines of the West Bay system of Galveston Bay in Texas. Morton et al. (2004) calculated average shoreline rates of change along the US Gulf of Mexico by comparing three historical shorelines (1980s, 1930s, 1970s) with an operational mean high water shoreline derived from LIDAR surveys (post 1998). Studies by Hapke et al. (2006) analyzed rates of change by incorporating shoreline positions from four time periods of mid to late 1800s, 1920s–1930s, 1950s–1970s and post 1997, while Dickson et al. (2007) assessed recession in North Norfolk (UK) from four datasets spanning 1885–2002. Crowell et al. (2005) report that historic shoreline change maps often contain four to eight or more plotted shorelines that span a significantly long time.

14.1.1 Methods/Techniques of Measuring Shoreline Recession

Various methods have been adopted to accurately map the highly uncertain shoreline position that is represented by proxies such as the high water line (HWL). The HWL, the most commonly used proxy (Robertson et al. 2004), models the appearance of a shoreline that is detectable on the ground at all times. These techniques have evolved from manual to semi-automated over the years and have reduced uncertainty in shoreline mapping. According to Moore (2000), the frequent change in technology has prevented the emergence of a standard method of shoreline mapping since none of the methods address the entire range of cartographic and photogrammetric techniques required for accurate coastal mapping (Thieler and Danforth 1994a). Mapping the shoreline is significant since they are recognized by the International Geographic Data Committee (IGDC) as one of the 27 most important features to be mapped and monitored (Li et al. 2002).

The mapping methods adopt techniques that extract the shoreline positions from different data sources. The conventional data sources consist of archival (historic) maps, aerial photographs and repeated field measurement, while the current sources are obtained from remote sensing technologies using airborne, spaceborne and land based techniques. The methods used for mapping the shoreline position from the conventional data sources include photogrammetric approach (analogue, analytical and digital) for the aerial photographs; digitising (manual or scanning) for the historic maps; and physical survey (planetable, total station, kinematic GPS) for the *in situ* approach. Remote sensing advancement, which has enabled the provision of a continuous monitoring of the shoreline globally, has improved shoreline mapping and data storage. Again, increasing resolution of satellite imagery and

improved performance of GIS as well as the development of LIDAR for coastal zone mapping and relative elevation determination has introduced new developments in shoreline mapping.

14.1.1.1 Selecting Appropriate Methods for Shoreline Measurement

Selecting a particular method for shoreline mapping is influenced largely by several factors. These include the level of accuracy required, type of output desired, method of ground control point collection, availability of funding and/or equipment, and the method to be adopted to analyse historic rate of change of the shoreline. Data from archival sources present information on where the shoreline was in the past, while data from current sources indicate the present position of the shoreline. Combining shoreline data from the two sources present a unique opportunity to trace how the shoreline has evolved over the period to its present position. This provides the baseline information to analyse the cyclic behaviour of the shoreline in the short and long term and how other factors influence the lateral morphological change as well as estimate the shoreline's historic rates of change that enables the prediction of the future position of the shoreline using various modelling techniques (Bray and Hooke 1997; Walkden and Hall 2005; Appeaning Addo et al. 2008; Hapke et al. 2010).

Analysing shoreline change in developing countries presents huge challenges to coastal scientists and managers due to several factors that affect their reliability. Data scarcity prevents studies into the past behaviour of the shoreline position and how it has metamorphosed into the present trend. Where data exist, the inconsistencies in the period of data capture influences systematic change analysis that fails to account for important events. Methods adopted for mapping the shoreline introduce uncertainties in the results that affect their reliability. The relatively huge cost involved in employing recent techniques in mapping the shoreline positions and lack of funds for continuous monitoring of the shoreline position affects the effectiveness of management strategies adopted to manage coastal resources. They also affect trend analysis of change using modelling techniques. Selecting a particular method for any shoreline change project should therefore depend on the objective and the temporal variables of the project, since the results should be in reasonable agreement with the actual physical situation (Dolan et al. 1991). Also temporal-spacing of data, accuracy and consistency influence the method selected.

14.1.2 Modelling Shoreline Rate of Change

Modelling shoreline change and evolution trend is significant since it provides understanding into the complex and dynamic large scale system. Understanding the system behaviour facilitates developing sustainable and pragmatic policies to manage the coastal environment. Various models estimate shoreline rates of change

based on the number of shoreline data available that span several years. These techniques have evolved through time with advances in computer technology (Zuzek et al. 2003). The models which are basically statistical assume that the change is linear through time (Genz et al. 2007). Consequently, rates of change are expressed in terms of distance of change per year and the result is expressed as either positive for accreting shoreline or negative for eroding shoreline. Statistical methods for computing shoreline rates of change include end point rates, average of rates, linear regression, jack-knife and weighted linear regression methods (Morton et al. 2004). Each of the methods has their sources of uncertainty that influence the reliability of the calculated rates.

Numerous studies have identified the differences and similarities between the various methods of modelling shoreline rates of change. Dolan et al. (1991) compared long term and short term erosion rates using four different statistical methods. By plotting the rates from one method vs. the rates of another method, it merged that average of rates is most variable, while linear regression and jack-knife share a high degree of similarity. Studies by Theiler et al. (1995) on beach erosion at Rincon, Puerto Rico, calculated erosion rates using end point rate, linear regression, jack-knife and average of rates in the Digital Shoreline Analysis System (DSAS). They divided their study site into four separate areas and calculated an average shoreline change rate at each section for each of the four methods. All four methods resulted in significant similar rates, but they identified average of rates as the most appropriate shoreline change rate method at Rincon.

Studies by Crowell et al. (1997) using temporally complete sea level records as surrogate data sets to evaluate various shoreline rate of change methods, such as linear regression, end point rates and a technique based on minimum description length criterion. They compared predictions from subsets of sea level data sampled temporally to mimic shoreline data sets to actual sea level values. They identified that in the clear majority of cases, linear regression method gave superior results. Again, studies by Dean and Malakar (1999) used three shoreline change rate methods that included linear regression, end point rates and average of rates in mapping Florida's hazard zones. They compared the three methods by calculating correlation coefficients and identified that all three methods compared favourably with each other. However, end point rate and linear regression methods correlated better with each other than they both did with average of rates. They selected linear regression as their preferred method based on the reliability of the results it provided. Correlation between linear regression and end point rates methods was confirmed by Zuzek et al. (2003) who investigated issues specific to fresh water shorelines in the Great Lakes by comparing linear regression and end point rates methods. They also identified that end point rates and linear regression methods gave similar results.

The issue of the most appropriate method of calculating rates from shoreline position data has been subjected to considerable interest. This is because despite the studies that have sought to describe past and predict future shoreline change, little consensus has emerged on the best methodology for calculating rate of change (Honeycutt et al. 2001). This is as a result of the extreme variations in coastal

morphology and oceanographic climatology. Genz et al. (2007) identify that previous studies have not comprehensively tested shoreline rate of change methods while Honeycutt and Krantz (2002) report that errors associated with each method have not been evaluated in great detail.

14.1.3 Study Objectives

The main objective of the study is to develop an innovative technique that combines archival data that may exist in developing nations with modern data to achieve optimum results in shoreline rates of change, while accounting for uncertainties.

14.2 Approach/Methodology

14.2.1 Study Setting

The study was conducted in Ghana, West Africa, located in the western Gulf of Guinea sub-region, about 750 km north off the equator between latitudes 4° and 12° N and longitudes 3° W and 1° E. Ghana has a coastline of 550 km and relatively narrow continental shelf to a depth of around 75–120 m. The coastline of Ghana has been geomorphologically and geologically zoned into three: the west, central and east coastlines (Fig. 14.1). The west coast covers 95 km of stable shoreline and

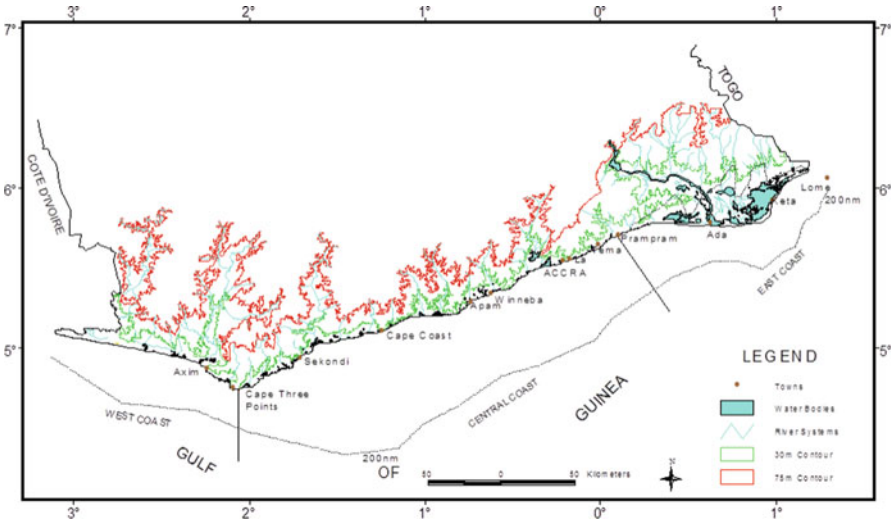

Fig. 14.1 Map of coastline of Ghana

extends from Ghana's border with Côte d'Ivoire to the estuary of the Ankobra River. According to Ly (1981), it has a depositional and low-energy beach. The gentle beaches have fine sand and backed by coastal lagoons. The littoral transport on this coast is from west to east. This transport is significantly reduced on the immediate west of Cape Three Points where much of the sediment is deposited. Deposition of sediment occurs not only on the beach causing a slight progradation of the shoreline but also in estuaries as tidal deltas. Vegetation in this coastal zone is rain and semi deciduous forest.

The central zone is 321 km shoreline long (actual study area) and extends from the estuary of Ankobra river near Axim to Prampram (east of Accra). It represents an embayed coast of rocky headlands, rocky shores and littoral sand barriers enclosing a number of coastal lagoons. Igneous, sedimentary and metamorphic rocks of Precambrian, Paleozoic, and Mesozoic age as well as unconsolidated Quaternary sediments are exposed along the shoreline under wave attack. Except for a few outcrops of friable sandstones and shales, the rocks are usually resistant to wave attack and are thus not a significant source of sand to the beach sediment budget. Beaches in the central coast result from the sand filling between the rock headlands and older sandcliffs. Two units of Quaternary sediments are exposed in seacliffs along the Accra – Tema shoreline. The lower unit is composed of a basal gravel and coarse to medium sand. From archaeological evidence this lower unit is believed to have been deposited about 12,000 years ago (Talbot 1976). The lower unit is overlain by a sheet of coastal dune sand which was formed approximately 5,000 years ago (Talbot 1976). At the present time this coastal dune represents a narrow band (50–200 m wide) of sand deposit parallel to the shoreline. In the seacliffs these two units are separated by a red soil, rich in iron oxide (2–3 m thick), developed on top of the lower unit. The Quaternary sediments locally overlie the igneous, sedimentary and metamorphic rocks which dip gently beneath the beach and are exposed on the sea floor in the depth ranging from 0 to 4 m below sea level.

The central coast represents a medium-energy environment with wave heights usually not exceeding 1.5 m in the surf zone. The coast is characterized by a southwesterly prevailing wind causing an oblique wave approach to the coastline. This wave approach causes a net littoral transport from west to east, which is evidenced by deposition and erosion of sand around the rock headlands or breakwaters. The central coast is characterized by several streams among which only one, the Pra river, is perennial. This river drains the terrains of metamorphosed lavas, pyroclastic rocks, phyUites, schists and granites. The other streams are small and may carry sediments only during short periods of the wet season. The predominant vegetation in this zone includes semi deciduous forest and scrub and grassland.

The east zone, which is made up of 139 km of shoreline, extends from Prampram eastwards to Aflao, at the border with Republic of Togo. It is characterized by a continuous, sandy shoreline with the deltaic estuary of the Volta river situated halfway in-between. The Volta River is the largest in Ghana with a regulated flow of about 900 cumecs. The east coast has a large proportion of its land covered by the Keta Lagoon, the Volta Estuary and the Songor Lagoon as well as impacted by the eroding delta. Evidence of coastal erosion occurs on many parts of this coast.

The coast represents a medium- to high-energy beach with wave heights often exceeding 1 m in the surf zone. With a smooth and sandy shoreline trending east to northeast and a southwesterly prevailing wind, the coast is characterized by an active littoral transport, generally from west to east (Ly 1980). A major part of the Quaternary sediments on the eastern coast derived from the main Volta River of the area. This river drains various terrains of sandstones, shales, mudstones, granites, basalts, andesites, quartzites, schists emd gneisses. However, its sediment discharge has been significantly reduced since the construction of the Akosombo dam on the river in 1961. The continental shelf west of Cape Three Points is a very flat and featureless surface, 40 km wide. In the central and eastern coasts this shelf represents a strip of variable width. It is narrow, 22 km wide, at the eastern side near the mouth of the Volta River, and broadens up to 100 km just east of Cape Three Points where irregularities in bathymetry are represented by several peaks of rock outcrops observed from seismic surveys.

14.2.2 Data Source

Adequate and reliable long-term data enable accurate detection of shoreline position. The data used for the shoreline position detection were obtained from various sources. These include the 1904 bathymetric map (hard copy format) from the Ghana ports and harbours authority (GPHA), the 1974 and 1986 digital topographic maps from the survey and mapping division of the Ghana lands commission, as well as 2002 digital map and scans of every second photograph from the archive of near-vertical film aerial photography that was used in the production of the 2002 map from CTK Aviation. Although obtaining data in developing nations are problematic, sparse data may exist that are not captured following a regular time series pattern. The wide gaps in the available data prevent consistency in time series analysis. However, combining the available archival data with modern data facilitate analysis of the changing trend in the shoreline position. The archival data is relatively affordable and the modern data can be obtained from various sources at comparative rates.

14.2.2.1 Mapping Techniques/Data Analysis

Data Accuracy

The 1904 paper map was digitised manually using a Calcomp 3400 digitiser with a resolution of 0.005 in (0.127) mm. Assuming a similar level of precision, at a map scale of 1:50,000 this implies a digitising uncertainty of 6.3 m on the ground. The digitiser has up to 12,700 lines per inch (500 lines per mm) real resolution and a baud rate of 300–38,400. The point operating mode method enabled the manual digitising and thus reduced coordinate resolution uncertainty. The root mean square error (RMSE) for the map registration as calculated by the transformation

process was 0.5 μm. The RMSE obtained is acceptable and it signifies that the digitising process was accurate and thus maintained highly accurate geographic data (McGowan 1998). Affine transformation was used since it acts as a reliable model to correct map errors that may represent the effect of rotations, translations and scale changes (D'Alge and Alves 1992).

The aerial photograph was georectified to the 2002 map using conjugate points of detail within ArcGIS in order to allow subsequent analysis and to aid subsequent visualisation of the predicted change. Confidence in using these maps for analysis was informed by the similarities in their geometric parameters that made them compatible for change analysis and modelling. The maps had a common scale of 1:50,000 and the shoreline proxy used was the high water line (HWL). All the maps also share a common datum (Clarke 1880_RGS spheroid) and projection (Transverse Mercator), and the spring high water line (HWL) proxy was used to define all the shoreline positions. The 1974 and 1996 data are used as the major source of information for land related issues in Accra, and the 1904 map is used as the base map by the Ghana Ports and Harbours Authority for some of their operations.

Various mapping methods were used to establish the instantaneous shoreline positions on the maps. The 1904 shoreline was originally mapped using the planetable survey method (onshore) and echo sounding (offshore, last revision in 1992), while the remaining three shoreline positions were mapped from aerial photographs. The 1974 shoreline was extracted using analogue photogrammetric methods; the 1996 shoreline was mapped by analytical photogrammetric methods, and the 2002 shoreline was mapped using digital photogrammetric methods. The variation in approach and the differences in their accuracy levels introduced uncertainty in the mapped shoreline position. However, the span of the data set for a period of 98 years will reduce any uncertainty and increases the reliability. This is because it will prevent the erosion/recovery cycle associated with severe storm events that obscure the underlying trend of erosion for decades (Crowell et al. 2005). Using limited shoreline position data sets that span long period for historic shoreline change analysis and modelling is not new in coastal erosion studies (Appeaning Addo et al. 2008).

Positional accuracy of the shoreline positions as recorded on the different date maps was also analysed. The 2002 shoreline, assumed to be the most accurate because it was mapped using digital photogrammetric methods, was selected as the reference with which to test the accuracy of the remaining data. Preliminary investigations to identify problematic shoreline data before determining their positional accuracy was done. This involved comparing the shoreline positions with an extracted shoreline position in the rocky areas on the 2002 aerial photographs. This approach, which was based on the assumption that the shoreline position within the rocky areas will experience relatively minimal change, enabled unreliable data to be identified and corrected. A Global Position System (GPS) survey, using a mapping grade receiver with accuracy within 1 m and run in 2005 was used to validate the 2002 shoreline position. Ten control points were established at roughly equal intervals along the 40 km shoreline (Fig. 14.2) and used to consecutively survey the HWL proxy of the instantaneous shoreline position.

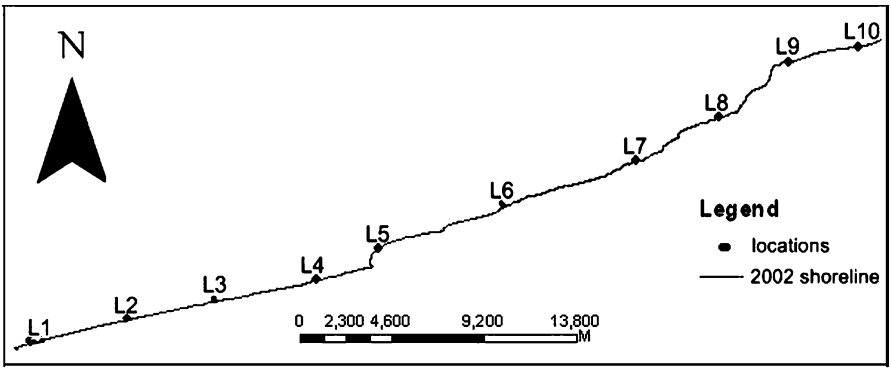

Fig. 14.2 Selected ten locations alongshore to detail the HWL proxy shoreline

Table 14.1 Observed coordinates and difference between HWL 2002 and 2005 shoreline

Ref. point	Eastings (2002)	Northings (2002)	Eastings (2005)	Northings (2005)	Displacement (m)
1	347,981.47	92,447.57	347,981.15	92,448.53	±1.0
2	–	–	–	–	–
3	–	–	–	–	–
4	359,656.03	94,970.61	359,655.55	94,971.92	±1.5
5	362,245.41	96,233.39	362,244.62	96,234.18	±1.1
6	–	–	–	–	–
7	372,788.47	99,831.15	37,278,648	99,833.57	±3.1
8	376,152.45	101,587.46	376,152.37	101,590.35	±2.9
9	379,026.45	103,846.22	379,026.29	103,848.45	±2.2
10	381,861.33	104,449	381,860.72	104,451.95	±3.0

The surveyed coordinates of the 2005 HWL positions was plotted against the 2002 shoreline positions to enable the displacements in the two different date positions to be determined. Results of the GPS survey are presented in Table 14.1, which shows that some locations experienced significant migration. Three control points (2, 3 and 6) were vandalised and could therefore not be coordinated. The observed difference between the surveyed 2005 HWL points and the 2002 shoreline positions is as a result of the likely impact of wave and tide actions on the cliffs that resulted in landward migration of the shoreline. The difference at all the locations was small and therefore acceptable.

The shoreline positional accuracy on the remaining maps was assessed by identifying 20 conjugate features on them and determining their root mean squares error (RMSE) relative to their 2002 position. The conjugate features include buildings, rail lines and road intersections. The square error was determined for each coordinate using the equation below,

$$r^2_{error} = (x_{2002} - x_{test})^2 + (y_{2002} - y_{test})^2 \tag{14.1}$$

The horizontal RMSE was calculated by adding up the square error, estimate the mean and taking the square root. The 95% confidence level (CL) was calculated by multiplying the RMSE by 1.7308 (Givens 1999). The results of the positional accuracy test for the 1996, 1974 and 1904 maps are shown in Tables 14.2, 14.3, and 14.4. The RMSE for 1996 digital map is 0.102 m and the horizontal accuracy is 0.17 m at the 95% confidence interval. The 1974 map has a RMSE of 0.108 m and the horizontal accuracy is 0.18 m at the 95% confidence interval.

Only 11 conjugate features could be identified on the 1904 map. Their RMSE was found to be 5.72 m and the horizontal accuracy is 9.93 m at 95% confidence interval. The 1904 map displays relatively low accuracy, probably due to the planetable method of survey which may have uncertainty of about 10 m (Moore 2000) and the digitising method which has an error of about 6.3 m.

14.2.2.2 Creating Database in GIS Environment and Historic Rates of Change Estimation

The Ghana Metre Grid coordinate system was used to compile the 1974, 1996 and 2002 digital maps in ArcGIS. The shoreline positions on the maps were extracted along specific sections in ArcMap and saved separately as shape files. The process was repeated to reduce uncertainty in the digitising process. Each of the four shoreline data sets was coded with six attribute fields that included ObjectID, shape, shape length, ID, date (original survey year) and accuracy in readiness for the recession rates calculation. A baseline, which was used as reference for the rates computation, was established onshore following closely the orientation of the coast. Historic rate of change in the shoreline position was computed using the Digital Shoreline Analysis System (DSAS) Version 3.0. A relatively small transect interval of 100 m was selected for this study. This was informed by studies by Doukakis (2004) which identified that transect spacing below 100 m does not result in improved estimates of shoreline change rate. The DSAS software calculates the rate of change statistics at the points of shoreline and the orthogonal transect intersection. It also allows the reliability of the estimated rates of change results to be established.

The linear regression method was selected for this study since it is considered the most statistically robust quantitative method when limited numbers of shorelines are available (Crowell et al. 1997) and it enables all data to be used regardless of changes in trend or accuracy. The method is also widely accepted by coastal researchers for computing long term rates of shoreline change since it consistently gives better long term forecasting results than other techniques (Dean and Dalrymple 2002). It is also purely a computational method based on accepted statistical concepts, which facilitates the use of related available statistical techniques to test and measure the quality of the straight-line fit as well as estimates the variance of the data. Although linear regression assumes linear behaviour, which technically is incorrect, it is however adequate for a first approximation according to Barton et al. (2003). Because linear regression fails to recognize the

Table 14.2 Positional accuracy for 1996 digital map using 2002 digital map as reference data

X_{2002} (m)	X_{1996} (m)	Δx	Δx^2	Y_{2002} (m)	Y_{1996} (m)	Δy	Δy^2	$\sqrt{(\Delta x^2 + \Delta y^{2)}}$
353,507.300	353,507.300	0.040	0.002	94,076.700	94,076.600	0.040	0.002	0.003
358,899.000	358,899.100	−0.130	0.017	95,640.000	95,640.000	0.060	0.004	0.021
360,518.900	360,518.900	0.040	0.002	95,997.900	95,997.800	0.020	0.000	0.002
361,891.100	361,891.100	0.060	0.004	95,532.100	95,532.200	−0.040	0.002	0.005
363,703.000	363,703.100	−0.030	0.001	97,299.300	97,299.100	0.250	0.063	0.063
364,856.600	364,856.600	0.040	0.002	97,034.400	97,034.400	0.070	0.005	0.007
369,195.300	369,195.200	0.020	0.000	98,912.600	98,912.500	0.030	0.001	0.001
367,305.900	367,305.900	−0.020	0.000	98,355.800	98,355.900	−0.100	0.010	0.010
370,029.100	370,029.300	−0.140	0.020	99,105.000	99,105.000	−0.020	0.000	0.020
372,581.300	372,581.300	−0.010	0.000	100,065.800	100,065.800	0.050	0.003	0.003
377,956.500	377,956.500	0.020	0.000	103,796.900	103,796.900	0.030	0.001	0.001
381,875.400	381,875.400	0.020	0.000	104,479.600	104,479.700	−0.020	0.000	0.001
361,676.700	361,676.700	0.020	0.000	95,626.600	95,626.600	−0.020	0.000	0.001
362,876.800	362,876.800	0.030	0.001	97,093.500	97,093.400	0.120	0.014	0.015
362,574.300	362,574.300	−0.020	0.000	96,954.100	96,954.000	0.070	0.005	0.005
363,998.200	363,998.200	−0.020	0.000	97,739.700	97,739.600	0.090	0.008	0.009
363,765.300	363,765.200	0.150	0.023	97,967.200	97,967.100	0.020	0.000	0.023
358,743.000	358,743.100	−0.10	0.010	95,597.500	95,597.500	−0.020	0.000	0.010
362,493.500	362,493.600	−0.040	0.002	97,309.500	97,309.400	0.030	0.001	0.003
371,281.100	371,281.100	0.060	0.004	99,479.200	99,479.200	0.020	0.000	0.004
							SUM	0.207
							MEAN	0.010
							RMSE	0.102
							95% CL	0.176 m

Table 14.3 Positional accuracy for 1974 digital map using 2002 digital map as reference data

X_{2002} (m)	X_{1974} (m)	Δx	Δx^2	Y_{2002} (m)	Y_{1974} (m)	Δy	Δy^2	$\sqrt{(\Delta x^2 + \Delta y^{2)}}$
353,507.3	353,507.2	0.14	0.02	94,076.7	94,076.7	−0.06	0.004	0.023
358,899	358,899	−0.02	0	95,640	95,640.1	−0.06	0.004	0.004
360,518.9	360,518.9	0.02	0	95,997.9	95,997.8	0.05	0.003	0.003
361,891.1	361,891.1	0.06	0.004	95,532.1	95,532.2	−0.07	0.005	0.009
363,703.1	363,703	0.03	0.001	97,299.3	97,299.4	−0.06	0.004	0.005
364,856.6	364,856.6	0.01	0	97,034.4	97,034.3	0.17	0.029	0.029
369,195.3	369,195.2	0.09	0.008	98,912.6	98,912.5	0.06	0.004	0.012
367,305.9	367,305.9	0.05	0.003	98,355.8	98,355.9	−0.06	0.004	0.006
370,029.1	370,029.2	−0.05	0.003	99,105	99,105.1	−0.12	0.014	0.017
372,581.3	372,581.3	0.03	0.001	100,065.8	100,065.8	0.08	0.006	0.007
377,956.5	377,956.5	0.06	0.005	103,796.9	103,797	−0.04	0.002	0.006
381,875.4	381,875.4	0.02	0	104,479.6	104,479.7	−0.06	0.004	0.004
361,676.7	361,676.7	−0.01	0	95,626.6	95,626.5	0.06	0.004	0.004
362,876.8	362,876.8	0.03	0.001	97,093.5	97,093.4	0.13	0.017	0.018
362,574.3	362,574.3	0.02	0	96,954.1	96,954.2	−0.13	0.017	0.017
363,998.2	363,998.1	0.03	0.001	97,739.7	97,739.7	−0.09	0.008	0.009
363,765.3	363,765.3	0.06	0.004	97,967.2	97,967.3	−0.18	0.032	0.036
358,743	358,743.1	−0.04	0.002	95,597.5	95,597.5	0.01	0	0.002
362,493.5	362,493.5	0.06	0.004	97,309.5	97,309.4	0.09	0.008	0.012
371,281.1	371,281.2	−0.07	0.005	99,479.2	99,479.3	−0.08	0.006	0.011
							SUM	0.233
							MEAN	0.012
							RMSE	0.108
							95% CL	0.187 m

potential for temporal differences in trend (trend reversals) and accelerations or decelerations, average trends and rates of shoreline change in this study were calculated for short term (most recent) time scales in addition to the long term. The long term rates of change were determined at each transect by taking the slope of the regression line applied to all four shoreline positions. Rates were also computed between the periods 1974–1996 and 1996–2002 to allow analysis of the temporal variations in trend.

14.2.2.3 Reliability of Calculated Rates of Change

Uncertainty was quantified to reduce its effect and thereby increase confidence in the rates calculated. The results of the calculated rate of change are associated with uncertainty inherent from various sources. This includes human impacts, natural patterns of shoreline change and methodology adopted for estimating the rates of change. Shoreline data capture accuracy, using field survey or photogrammetric methods depends on the surveyor or operator's skill in identifying the HWL. This and cartographer's pen size for drawing the shoreline can affect the shoreline positional accuracy. Shoreline data manipulations in ArcMap such as digitising of the shoreline position, overlay of multiple layers and inconsistency in non-linear information (metadata) are other sources of uncertainty. The use of linear regression to compile the shoreline position also introduced uncertainty in the results since it assumes linear behaviour and fails to recognise trend reversal. Uncertainties associated with cartographer's pen size and variability of actual behaviour of the shoreline were rejected. This is because the majority of the shoreline data were in digital format and the Accra shoreline does not experience storms and has a small tidal range of approximately 1 m. The HWL proxy was used to represent the shoreline positions on all the data and a common datum (Clarke 1880 ellipsoid) as well as projection (Transverse Mercator) were used for the entire shoreline mapping that reduced uncertainty as a result of data manipulation in ArcMap.

However, uncertainties were quantified for shoreline data capture (using planetable and photogrammetric methods) and digitising. This is because they will have significant effect on the positional accuracy of the shoreline extracted.

Various studies (Crowell et al. 1991; Thieler and Danforth 1994b; Moore 2000; Morton et al. 2004) provide estimates of typical measurement errors associated with mapping methods and shoreline digitising, and these were considered in this study. The largest errors were found to be positioning errors of $\pm$ 10 m (Moore 2000), which were attributed to scales and inaccuracies in the original 1904 survey using the planetable method. Shoreline position error due to photogrammetric method of mapping is $\pm$ 6.1 m (Crowell et al. 1991). The significantly large errors are due to the sources of uncertainty associated with the planetable method of surveying used to map the 1904 shoreline position such as interpretation of the HWL at the rodded points, error due to sketching between rodded points and location of the planetable, while source of uncertainty associated with the photogrammetric method include delineating the HWL position on the aerial photograph

by the operator. However, according to Morton et al. (2004), the influence of large shoreline position errors on long term rates of change can be reduced if the period under analysis is so long, which is 98 years for this study. Morton and Miller (2005) estimate that shoreline data from other sources conform to similar standards identified by previous studies.

Estimates for the maximum errors for this study are provided in Table 14.5 that show how each error contributes to uncertainty in the shoreline position and in the rate of change. A total shoreline positional error for each epoch (E_n), Eq. 14.2, incorporates all the measurement errors by taking the square root of the sum of squares of planetable survey error (E_s), digitising error (E_d) and photogrammetric error (E_p) as they apply to specific shoreline data. The root mean square error (RMSE) was calculated as a realistic assessment of combined potential error because these individual errors are considered to represent standard deviations. The maximum planetable error incorporates all of the errors associated with the mapping process including distance to rodded points, planetable position and identification of HWL (Morton et al. 2004). This is applied only to the 1904 map as the more recent shorelines were derived from aerial photographs. Digitising error was applied to the 1904 and 1974 maps originally produced in hard copy format. Photogrammetric mapping error, which represents the error involved in locating relative positions of shorelines taken from aerial photographs (Crowell et al. 1991), was applied to the 1974, 1996 and 2002 maps since they were all mapped using photogrammetric methods. The total shoreline position error is thus expressed as:

$$E_n = \sqrt{\left(E_s^2 + E_d^2 + E_p^2\right)} \tag{14.2}$$

where n = shoreline number (1–4).

A separate total error (E_n) was calculated for each shoreline and the results are provided in Table 14.5. The positional error for each period was then incorporated into an error for each transect. That value was annualised (Ea) to provide error estimation for the shoreline change rate at any given transect and expressed as:

$$E_a = \frac{\sqrt{\left(E_1^2 + E_2^2 + E_3^2 + E_4^2\right)}}{T} \tag{14.3}$$

where E_1, E_2, E_3, and E_4 are the total shoreline position error for the various years and T is the 98 years period of analysis.

The maximum annualised error using best estimates for the study area is 0.17 m/year (Table 14.5). Annualised errors were also calculated for the period between 1904 and 1974; 1974 and 1996; 1996 and 2002 as shown in Table 14.6.

Further statistical analysis was performed on the results using supplemental statistics provided by the DSAS software. Standard error of the estimates (SLE), which reflects the degree to which the points diverge from the best-fit regression line, was estimated as 0.09 m. The R-squared statistic was also computed for each of the

Table 14.4 Positional accuracy for 1904 map using 2002 digital map as reference data

X_{2002}	X_{1904}	Δx	Δx^2	Y_{2002}	Y_{1904}	Δy	Δy^2	$\sqrt{(\Delta x^2 + \Delta y^{2)}}$
361,911.000	361,916.500	−5.510	30.360	95,521.500	95,522.300	−0.800	0.640	31.000
361,845.000	361,840.500	4.520	20.430	95,779.000	95,780.000	−1.070	1.145	21.575
364,856.600	364,860.400	−3.750	14.060	97,034.400	97,032.800	1.630	2.657	16.719
361,676.700	361,676.100	0.550	0.300	95,626.600	95,620.500	6.100	37.210	37.513
361,822.500	361,830.600	−8.080	65.280	95,548.900	95,545.300	3.580	12.816	78.103
363,983.700	363,980.300	3.450	11.900	97,346.400	97,348.000	−1.610	2.592	14.495
360,511.700	360,507.500	4.290	18.400	95,986.800	95,990.300	−3.430	11.765	30.169
366,621.400	366,624.400	−2.980	8.880	98,116.800	98,120.500	−3.640	13.250	22.130
362,569.800	362,573.500	−3.690	13.610	96,942.300	96,940.000	2.300	5.290	18.906
361,732.100	361,727.900	4.270	18.230	97,061.500	97,065.200	−3.660	13.396	31.629
362,985.600	362,979.300	6.300	39.690	97,708.200	97,712.500	−4.260	18.148	57.838
							SUM	360.076
							MEAN	32.734
							RMSE	5.721
							95% CL	9.903 m

Table 14.5 Estimated measurement errors for the study area

Measurement errors (m)	1904	1974	1996	2002
Planetable survey error (E_s)	10.00	–	–	–
Digitising error (E_d)	6.30	6.30	–	–
Photogrammetric mapping error (E_p)	–	6.10	6.10	6.10
Total shoreline position error (E_n) (m)	11.82	8.76	6.10	6.10
Annualised transect error (E_a) (m/year)	± 0.17			

Table 14.6 Potential root mean square error for the various periods

Period	Uncertainty (m/year)
1904–1974	± 0.21
1974–1996	± 0.49
1996–2002	± 1.08

transect lines. It ranges from 1.0 to 0.0 and measures how successfully the best-fit line accounts for variations in the data. The smaller the variability of the residual values around the regression line relative to the overall variability, the better the prediction.

14.3 Results

Historic rates of shoreline change reflect a summary of the processes that altered the shoreline cumulatively for the periods analysed. They are expressed as long term or short term. Short term rates of change data often prove problematic because of the excessive influence of inconsistent shoreline locations as a result of climatic conditions that can be considered as noise. Such noise can obscure the underlying trend of erosion for decades due to inadequate recovering period. However, they are relevant in providing significant information for short term planning and monitoring of the coastal environment. The use of long term rates of change data is beneficial because such data helps to stress on the change rather than the noise and they enable future trend to be predicted. Long term data sets are reliable because the erosion and recovering cycle associated with extreme events such as storm and surge that can influence the erosion trend are minimal.

For this study, long term and short term rates of change were determined. The long term is defined as the period beyond 50 years and the short term for periods below 50 years (Gibeaut et al. 2001). A threshold of 50 years was selected for this study because below 50 years, the shoreline is considered to be recovering from events that resulted in recession while beyond 50 years the shoreline is considered to have reached a form of equilibrium and thus represent approximately its true landward or shoreward movement. The shoreline positions of 1904, 1974, 1996 and 2002 which span a 98 year period, and the 70 year period between 1904 and 1974 were therefore considered as long term for this study. Rates computed from the combined four shoreline positions were used for long term analysis, while the 1904–1974 period

Table 14.7 Estimated long-term rates of change

Period	Mean erosion rate (m/year)	Percentage (%)	
		Erosion	Accretion
1904–2002	−1.13 ± 0.17	82	18
1904–1974	−1.29 ± 0.21	86	14

Table 14.8 Estimated long-term rates of change in the three geomorphic regions

Period	Mean erosion rate (m/year)		
	Western zone	Central zone	Eastern zone
1904–2002	−1.30 ± 0.17	−0.40 ± 0.17	−1.50 ± 0.17
1904–1974	−1.70 ± 0.21	−0.20 ±0.21	−1.90 ± 0.21

was used to validate the observed trend. This is because the four combined different date shoreline positions accounted for variability in the shoreline positions that reduced uncertainty in the estimated results. They also facilitated statistical analysis of the computed rates of change results using the linear regression method and hence the results are reliable for further applications. The R-squared values for the linear regression analysis are closer to 1 than 0, which implies the best-fit line explains most of the variation in the dependent variable. Field observations suggest that the trends and relative rates of change presented in this study are accurate.

14.3.1 Long-Term Rates of Change

Long term rates of change computed for the study area enabled the erosion trend to be analysed along the Accra shore while the estimated rates of change in the three regions facilitated the identification of erosion hot spots and vulnerable areas. Estimated historic rates of change in the Accra shoreline for both the 98 and 70 year long-term periods are presented in Table 14.7, while Table 14.8 shows the rates of change results in the three geomorphic zones. The three geomorphic regions were further subdivided into six sub-regions based on geological conditions, geomorphic behaviour, bathymetry and the degree of human intervention. Table 14.9 presents the long term rates of change in the sub-regions for the 98 year period. Uncertainty rates quantified for each period are reported in units of m/year, which represents 95% confidence interval for the slope of the regression line i.e. with 95% statistical confidence that the true rate of shoreline change falls within the range defined by the reported value plus or minus the error value.

Recession trends differ significantly in each of the three geomorphic zones. This is because the recession process is not always continuous and steady due to the prevailing geomorphic and geological features as well as the level of human intervention. The recession trend and pattern for the 70 year period is presented in Fig. 14.3, while Fig. 14.4 shows the uncertainty range of the upper and lower limits.

Table 14.9 Estimated long term rates of change in the sub-regions

Period	Erosion rate in sub-regions (m/year)					
1904–2002	A	B	C	D	E	F
	-1.86 ± 0.17	-1.11 ± 0.17	-0.05 ± 0.17	-0.41 ± 0.17	-0.71 ± 0.17	-1.15 ± 0.17

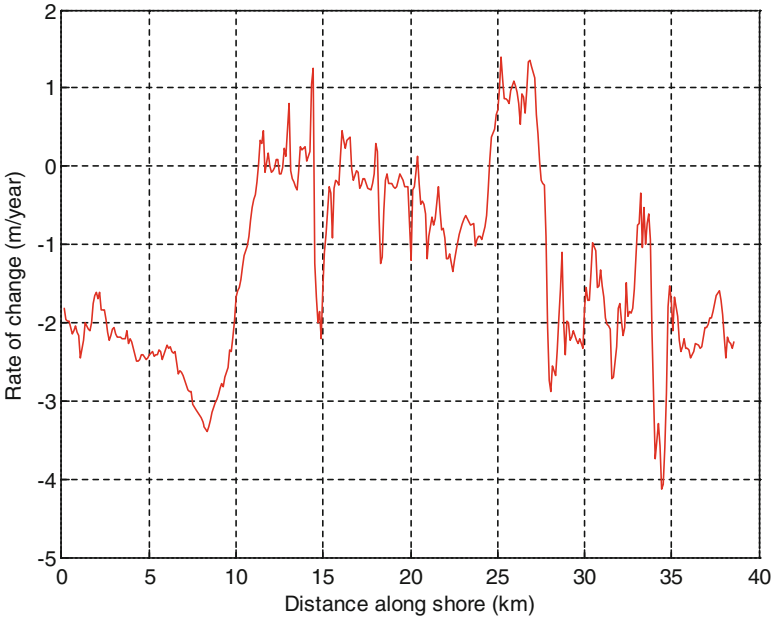

Fig. 14.3 Long term rates of change trend using 1904 and 1974 shoreline positions calculated by linear regression

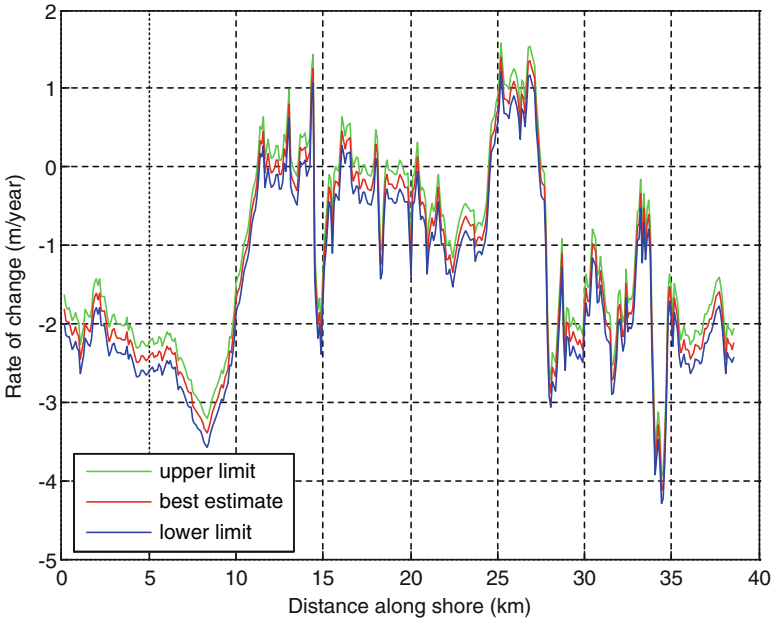

Fig. 14.4 Long term rates of change trend with uncertainty bound

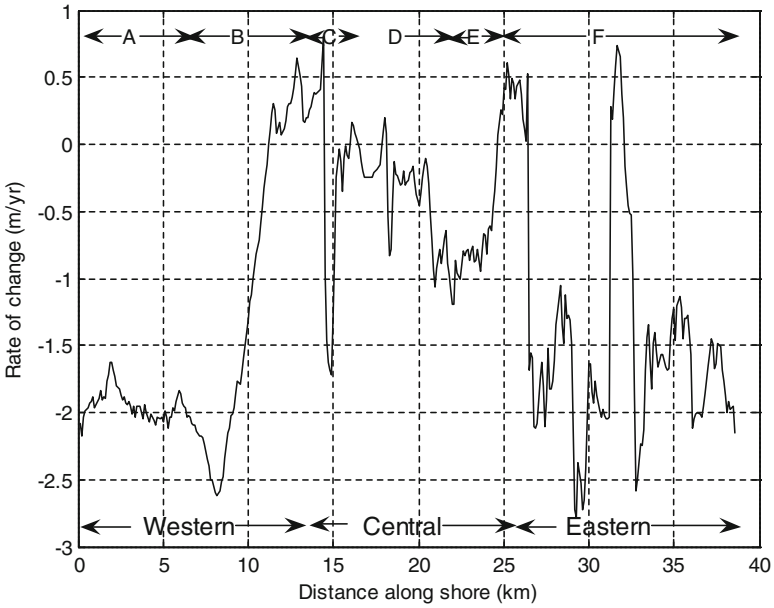

Fig. 14.5 Long term rates of change trend using 1904, 1974, 1996 and 2002 shoreline positions calculated by linear regression

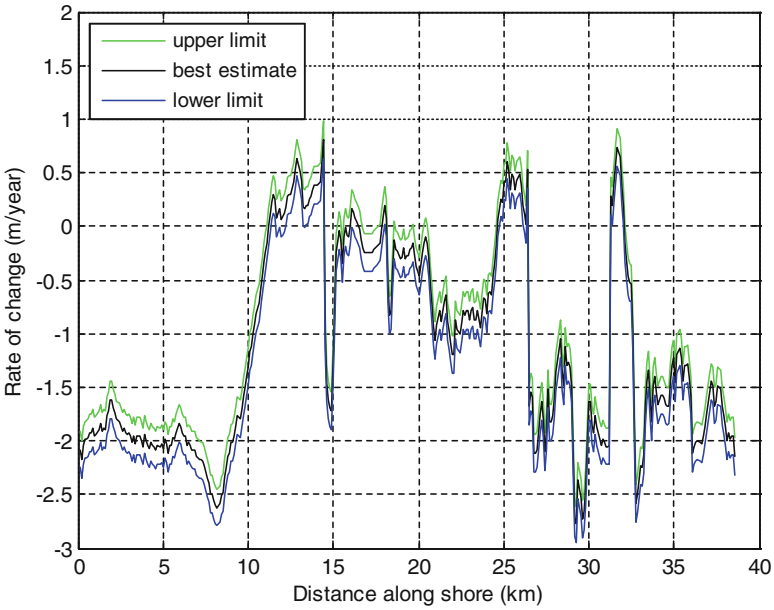

Fig. 14.6 Long term rate of change trend with uncertainty range

Table 14.10 Estimated short-term rates of change

Period	Mean erosion rate (m/year)	Percentage (%)	
		Erosion	Accretion
1974–1996	−0.91 ± 0.49	79	21
1996–2002	+0.65 ± 1.08	36	64

Table 14.11 Estimated short-term rates of change in the three geomorphic regions

Period	Mean erosion rate (m/year)		
	Western region	Central region	Eastern region
1974–1996	−0.35 ± 0.49	−0.82 ± 0.49	−1.74 ± 0.49
1996–2002	−0.51 ± 1.08	+0.19 ± 1.08	+2.70 ± 1.08

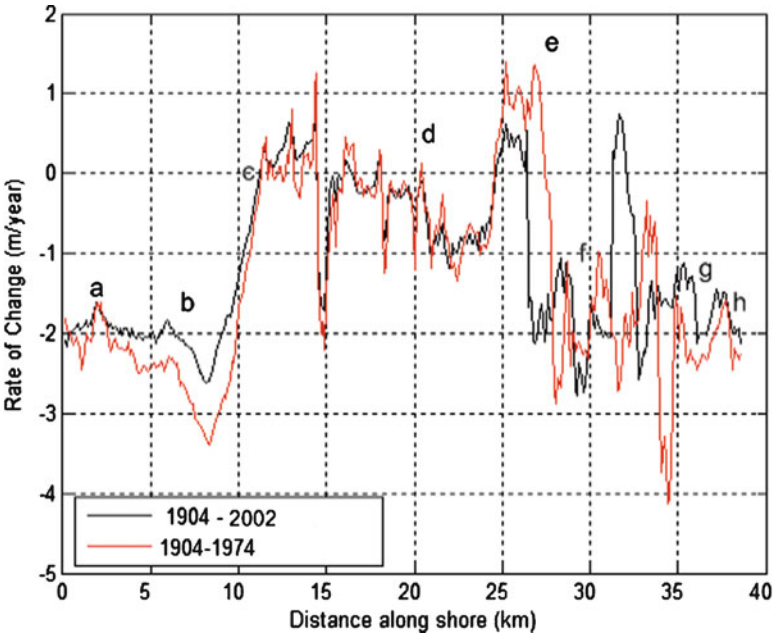

Fig. 14.7 Overlay of the two long-terms rates of change trend

The long term recession trend and pattern for the 98 years period is presented in Fig. 14.5, while Fig. 14.6 shows the positions of the upper and lower uncertainty limits relative to the best estimates.

The two long-term rates of change were overlaid as shown in Fig. 14.7, which enabled the trend and patterns of change to be compared in each of the three geomorphic regions. Similar trends occurred at locations a, c, d, f, and h while locations b, e and g displayed similar change patterns. The results reveal that the long-term trend in the 98 year period is similar to the trend in the 70 year period. The observed trend in the 98 year period is thus reliable and can be used to represent the long term changing pattern in the Accra shoreline.

Confidence in the analytical results exists because the historic rates of change estimated at the transect points are relatively high which indicate that erosion is occurring and they have persisted for decades as revealed by the 98 year span period and confirmed by the 70 years long term span period. The erosion trend has been consistent for long stretches of the coast that indicate that rates along the transect points are reliable. In addition, familiarity of the study area and the GPS survey run in 2005 (to validate the 2002 shoreline position) adds to this confidence.

14.3.2 Short-Term Rates of Change

Short term rates of change were determined for the periods from 1974 to 1996 and 1996–2002. The rates were estimated for the entire study area and each of the three geomorphic zones. The periods are considered short term because they fall below the 50 years threshold adopted as short term for this study. The short term rates of change for the study area are presented in Table 14.10 in units of m/year that show the rates of change for the 22 and 6 years periods of span while Table 14.11 shows the rate of change in the three zones. Quantified uncertainties at 95% confidence interval are also reported in units of m/year.

Although short term erosion pattern and trend are driven by conditions similar to the long term, significant disturbance in the coastal region influence the trend. The rates of change are therefore unreliable for developing effective coastal management strategies and predicting future trends (Gibeaut et al. 2003). However, they are relevant in providing significant information for short term monitoring and recognising trend reversal.

The results of this study enabled erosion 'hot spots' in the Accra shoreline to be identified. This includes locations with historic rates of change greater than 1.50 m/year. The threshold value of 1.50 m/year was adopted since locations with rates lower than the threshold rate are assumed to be eroding in conformity to the average long term erosion rate estimated for the entire length of Accra's shoreline. Figure 14.8 shows that the erosion 'hot spots' (the shaded portions) located in the western and eastern zones.

14.4 Discussion

14.4.1 State of the Accra Coast

Accra's shoreline is eroding in the long-term. The results indicate that the shoreline position has changed progressively since 1904 to its position in 2002. The observed trend is predicted to continue as a result of increasing sea level rise due to global climate change. Different geological conditions prevail in each of the three geomorphic zones and have influenced the slope of the offshore profiles. Analysis of the

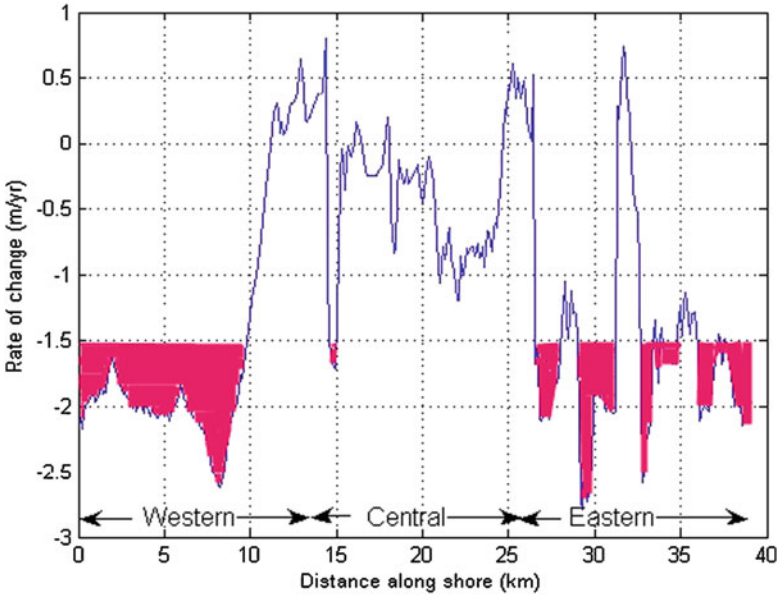

Fig. 14.8 Erosion hot spots along Accra's shore

bathymetric data indicate that the western and central zones have relatively gentle but significantly steep slopes, while the eastern zone has a considerably steeper slope (Appeaning Addo et al. 2008). These conditions have significantly influenced the trend of shoreline recession in each of the three geomorphic zones and thus confirm observations made by Anokwa et al. (2005) that erosion intensity varies along the Accra coast. The offshore profile slopes and the shoreline orientation regulate wave energy that reaches the foreshore. The Accra shoreline's direction estimated by Appeaning Addo et al. (2008) is approximately 253 , which is south-west. The orientation enables waves (swell type) to approach the shores obliquely, break and generate longshore currents that move parallel to the shoreline direction.

Field observations indicate that beach volume along the Accra coast is relatively small and is assumed to range between 1 and 5 m^3 per metre of length. Significantly, some locations in the eastern and central areas of the coast are without beach. Studies have revealed that recession rates for beach volume below approximately 10 m^3 per metre length were independent of beach volume change (Walkden and Dickson 2006). The relationship between sea eroding forces and the resistance of beach materials can also explain the observed scenario. Since the low volume beach sand offers less resistance to the eroding forces, its impact from erosion is minimal. Thus the prevailing beach volume along the Accra coast has not influenced the detected migration of the shoreline and will not control future rates of change. This obviously disagrees with observations by Armah (1991) that the beach has influenced erosion trends along the coast.

14.4.2 Historic Recession Trend in the Accra Shoreline

Measurement of detected changes in the Accra shoreline positions over the period of 98 years, for which data is available, has revealed that the shoreline is eroding in the long term at a rate of 1.13 m/year. Evidence of long term erosion along the Accra shoreline has been reported by various studies (Armah 1991; AESC 1988; Campbell 2006) that corroborate the erosion trend identified herein this study. The presence of exposed rock substratum along portions of the central and eastern areas of the Accra coast were cited by AESC (1988) and Armah (1991) as significant evidence of coastal erosion, while Campbell (2006) attributed the collapse of about 17 coastal buildings within a period of 26 years to erosion. Norley (2006) also reported the destruction of natural fish landing sites (used for fishing boats) as significant proof of increased inland migration of the shoreline in recent times. Erosion in the eastern zone threatened the Accra-Tema beach road (AESC 1988), which is an economic important road that links Accra to the Tema harbour. The shoreline erosion advanced so far inland that protection of this road became necessary. Consequently, the Accra-Tema beach road sea defence project was initiated in the early 1980s that provided groynes and revetment along the most threatened coastal stretch.

Estimated long-term rates of change, using the four different date shoreline positions, indicate that about 82% of the shoreline is eroding, while the remaining 18% is either accreting or stabilised (see Table 14.7). The results also revealed that accretion or stabilised shoreline generally occurs at the engineered portions of the shoreline in the three geomorphic zones. The trend and pattern of the long-term change from 1904 to 2002 was confirmed by validating with the previous results of the period from 1904 to 1974. The analysis established that the entire length of the Accra shore is under considerable threat of erosion. The estimated rates of change along the orthogonal transect lines are significantly high and the trend has been consistent for long stretches of the coast, which suggests good reliability of the results. The observed erosion trend in the Accra shoreline corroborates the observations by other authors (AESC 1988; Luc and Boon 1999; Ghana National Report 2002) that coastal erosion problem is indeed critical in Accra coast.

Although the entire length of the Accra shoreline is eroding in the long term, the trend however differs in each of the three geomorphic zones. This is because the prevailing geomorphic, geological and hydrodynamic condition, as well as the extent of human influence modifies the erosion pattern and trend in a particular region. The coastal geology along the Accra coast varies in each of the three geomorphic zones and hence exhibits different levels of rock resistance to erosion forces. Different lithology and the presence of lithological stratification as well as varying bathymetry have contributed to the shape of the Accra shoreline and the beaches in each of the geomorphic zones.

14.4.3 Recession Trend in the Three Geomorphic Zones

The western zone of Accra is eroding in the long term at a rate of 1.30 ± 1.7 m/year. The long-term recession trend was confirmed by comparing the rates of change obtained from the four different shoreline position dates and that of the period between 1904 and 1974 (Fig. 14.7), which reveals a similar pattern of change. This was expected since the 1904–1974 period dominated the shoreline data and confirms observations by Crowell et al. (1993) that data sets spanning long periods of time are important for forecasting shoreline change. Rates of change estimated for the short term periods (Table 14.11) also revealed that the zone is experiencing a recession trend similar to the long term, which further confirms that the western zone is susceptible to erosion and as a result unstable. The trend identified corroborates observations by Anokwa et al. (2005) that the region is 'highly sensitive' to erosion.

The central zone is eroding in the long term at a relatively low rate of about 0.40 ± 0.17 m/year. The recession pattern reveals an alternating trend of erosion and accretion (Fig. 14.7), which indicates that the region is relatively stable in the long-term. The eastern geomorphic zone is eroding in the long-term at a rate of about 1.50 ± 0.17 m/year (Table 14.8). The pattern of change (Fig. 14.7) indicates that the eastern region is unstable in the long term, which agrees with observations by Anokwa et al. (2005) that the region is susceptible to erosion in the long term.

14.4.4 Causes of Observed Recession Trend in the Accra Shoreline

Various factors account for the recession trend identified in the Accra shoreline that includes natural and human induced factors (AESC 1980; Armah 1991). The long-term erosion trend is a result of relative sea level rise, a deficit sediment budget for littoral transport, orientation of the shoreline and anthropogenic influences. The observed accretion or stability (refer to Fig. 14.8) is due to engineering structures constructed to control the spread of erosion and protection from exposed rock substratum as a result of persistent erosion (Armah 1991). Similar factors account for the observed short-term trend in the Accra shoreline.

14.4.4.1 Relative Sea Level Rise Causing Erosion in Accra Shoreline

Available geo-chronological data indicates that sea level rise has facilitated shoreline erosion along the Accra coast since the Holocene. Analysis of tide gauge measured data in Takoradi-Ghana (Fig. 14.9), obtained from PSMSL of POL, indicate that the sea level is rising at an estimated historic rate of about 2 mm/year (Ibe and Quelennec 1989). This conforms to the global trend estimated by IPCC (Armah et al. 2005; IPCC 2007). Evidence of sea level rise along the Accra coast

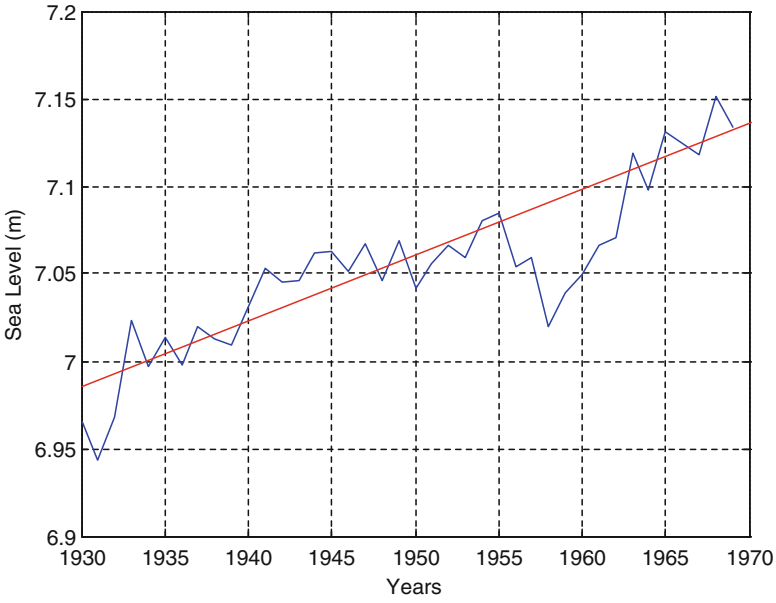

Fig. 14.9 Annual mean values of sea level data measured in Takoradi, Ghana (Data source: PSMSL 2002)

has been reported by various studies (Muff and Efa 2006; Geoconsultants 2005; Armah 1991). The rise in sea level has resulted in a continuous adjustment of the coastal morphological system.

Relative sea level rise induces beach erosion because of the geometry of the coastal profile, which is concave upward. According to CETS (1987), this results in the wave energy being dissipated in smaller water volume than without sea level rise, and thus the turbulence generated within the surf zone is greater. The profile responds by conforming to a gentler nearshore slope, which requires additional sediment to be eroded from the beach. This in-part explains the long-term erosion trend observed in the western zone from 1904 to 2002 and between 1904 and 1974 as well as the prevailing relatively gentle slope profile in the zone. Relative sea level rise, which occasionally results in a significantly higher tidal climate, and aided by the relatively gentle slope in the offshore profiles in the western zone facilitates shoreline to move further onshore during high tide. Spring high tide, estimated around 1.26 m along the Accra coast (Wellens-Mensah et al. 2002) consequently attacks the cliff face by up-rush that results in sediment removal and transport. This in-part accounts for both the long- and short-term erosion trends observed in the western geomorphic zone.

The presence of a relatively steep profile slope in the eastern geomorphic zone, presence of relatively small or no beach and the prevailing significantly steep offshore profiles have resulted in a deep water volume due to sea level rise, which enables eroding wave forces to directly attack the shore. Since the steep

Fig. 14.10 Open coast with a south-west direction shoreline (Source: Google Earth)

profile prevents the eroded sediment from building up the beach, the significantly strong longshore current transports the eroded sediment that results in erosion. This in-part explains the relatively high erosion trend observed in the eastern geomorphic zone between 1904 and 2002.

14.4.4.2 Shoreline Orientation Causing Erosion in Study Regions

Orientation of Accra's shoreline contributes largely to the observed recession trend along the coast (Armah 1991). The shoreline is almost a straight line and runs in the south-west direction (Fig. 14.10).

The relatively open Accra coast facilitates considerably strong unimpeded swell waves to reach the coast at an angle. The south-westerly prevailing wind generates swells with a significant wave height of about 1.4 m for 50% of the time and period of between 10 and 15 s. The waves break obliquely and generate longshore currents that induce an eastwards beach drift (Ly 1980; AESC 1980). The breaker type is plunging and the longshore current it generates ranges between 0.5 and 2 m/s (AESC 1980), which is significantly high and thus responsible for the relatively high rate of sediment transport in the littoral zone and the subsequently observed erosion trend. The shoreline orientation in the western and eastern geomorphic zones has contributed significantly to the high rate of erosion relative to the central geomorphic zone. The presence of a bay and headland in the central zone reduces the impact of the energy of the breaking waves and this in part explains the alternating trend of erosion and accretion that has resulted in a relatively long term stability in the shoreline in the central geomorphic zone.

14.4.4.3 Sediment Imbalance Causing Erosion in Study Regions

Fluvial sediment is the dominant sediment in the littoral drift (Boateng 2006) and dotted along the shores are lagoons connected by rivulets that supply sediment to the littoral zone, especially during the rainy season (i.e. the peak periods). Climate change (from wetter to drier) has decreased the volume of sediment carried by the rivulets as changes in the rainfall pattern have resulted in prolonged drought and depletion of fresh water resources (Poku-Adussei 2006). Some of the lagoons, such as the Korle lagoon, are polluted (Churcher 2006) and trap fluvial discharge, which further reduces the volume of sediment reaching the shore for littoral transport.

Sediment transport for the Accra shoreline intensity increases from the western towards the eastern zone (Wellens-Mensah et al. 2002), which is along the direction of the littoral drift. The net sediment supply is approximately 2×10^5 m^3/year (Wellens-Mensah et al. 2002). Sediment supply to the littoral zone is much less than the littoral transport capacity of the waves (AESC 1980) and this explains the observed erosion trend along the entire length of the Accra shoreline.

The imbalance in the sediment budget has occurred as a result of reduction in fluvial sediment supply and the diminutive sediment supplies from the sea floor (Armah 1991). According to Ly (1980), sediment supplies from the eroding cliffs, dunes and sandbars are also insufficient to balance the deficit in the sediment budget. The erosion forces, as a result, dislodge significant volume of sediment from the foreshore to make up for the shortfall in the sediment budget, which results in the observed erosion trend. This in part explains the relatively high rate of erosion in the western geomorphic zone, where the significant reduction in fluvial sediment and volume of water that are discharged into the sea. This is due to a dam constructed over the river, which has reduced considerably the neutralisation process of the relatively high wave energy, thus enabling the waves to erode the barrier ridge.

The salt industry (located in the Densu wetland site) method for harvesting, using the saltpan, has also affected the coastal process through a large scale destruction of wetland vegetation that covers about 1,130 ha (Oteng-Yeboah 1999). The vegetation previously trapped sediment, which contributed significant volumes of sediment to the littoral zone. This partly explains the erosion trend observed between 1974 and 2002 in the western region. Relatively high rates of erosion observed around La, behind the Independence Square and the Nautical College, in the long term can be attributed to the sediment deficit trend observed along the Accra shoreline.

14.4.4.4 Dam Construction

River Densu in the western geomorphic zone used to be the main source of fluvial sediment supply to the littoral zone until it was dammed. The river's once fast currents resulted in a process of hydraulic groyne action that developed and maintained the barrier ridge, which protects the wetland from the sea. The dam

was constructed in the 1920s and the size was increased to cover a catchment area of approximately 2,460 km^2 in the 1960s (Hollis et al. 1988; GWCL 2004). The dam has reduced the volume of water that reaches the sea and hence the process of fluvial sediment transport into the littoral zone since sediment from upstream is trapped in the lake. The reduction in the volume of fresh water and sediment downstream has also affected the performance of the water inlet significantly in terms of facilitating fresh water flow with sediment into the sea.

Formerly the balance was such that the inlet could be maintained throughout the year (AESC 1988). The reduced inlet hydrodynamics has resulted in a more permanent closure of the coastal barrier and led to increased attack by erosion forces. This partly explains the relatively high rate of erosion in the western geomorphic zone observed between 1904 and 2002. Natural breaching by excess river discharge is reached only at higher lagoon water levels, a situation that threatens the salt industry by flooding the saltpans. Periodically, a bulldozer is used to open the inlet to allow fresh river water to enter the sea. This produces a negative feedback since it impacts other parts of the coastal system and consequently disturbs the equilibrium established in the shoreline profile, which results in further attack of the barrier ridge by erosion forces, and has thus partly resulted in the long term erosion trend observed between 1904 and 2002 in the western geomorphic zone.

14.4.4.5 Coastal Defence Structures

Structures constructed along the shores of Accra to check the spread of erosion and guide harbour entrance channels have exacerbated the erosion situation along the adjoining shores. Jetties constructed in 1906 (Dickson 1965) to protect the navigation entrance channels to the defunct Accra harbour in the central zone have influenced changes in the shoreline position since they trap sediment in the up drift side. This accounted for the observed trend of relative stability in the shoreline around Jamestown in the central zone. The jetties starve the down drift side of sediment, which has resulted in a significant increase in erosion in the long term around the Independence Square shoreline. The deposited sediment on the up drift side attracted sand mining activities, which initiated 'severe' coastal erosion by sea waves and current action around the National Fire Service Training School that destroyed significant coastal infrastructure (AESC 1988). This resulted in the construction of coastal defence structures comprising of groynes and revetments.

The short-term erosion trend between 1974 and 1996 in the western zone, which indicates a reduction in erosion rate can be explained by the engineering interventions embarked upon in the early 1980s to check the spread of erosion and the Korle lagoon restoration project in the 1990s. The coastal defence project reclaimed coastal land in front of the Fire Service Training School, which created stability and accretion in the shoreline.

The groynes constructed to check the spread of erosion trap sediment in the littoral drift that builds the up drift side of the structure and thus starve the down

drift side, while the revetments prevent the shore from contributing sediment to the littoral drift. The beach that was built has since attracted sand mining activities that have extended to the littoral zone and subsequently resulted in increased erosion problems. This explains the observed increased erosion trend for the 6 year period between 1996 and 2002 (Table 5.5) and reveals the effect of non-enforcement of the ban on beach sand mining activities.

14.4.4.6 Sand Mining

Sand mining along Accra's shoreline is not adequately controlled and the activity is a major cause of erosion in the coast of Accra. According to Amatekpor (1994), sand from the beach system along the Accra coast has been used for landfill and civil engineering purposes for a long time and its contribution to the construction sector increased from 17 in 1986 to 21% in 1993 (Mensah 1997). Although the practice is presently illegal, it is still a significant source of sand supply for the construction of houses (Armah and Amlalo 1998). Sand mining activities partly give credence to the observed long-term erosion trend along the beaches at Rivera in Osu in the central geomorphic zone and around Bortianor in the western geomorphic zone of the study area, where the practice is active.

Evidence that excessive sand mining activities have resulted in persistent erosion along significant portions in the central and eastern zones is apparent due to the presence of exposed rock substratum (Armah 1991), as identified around the La beach covering a distance of about 400 m (Muff and Efa 2006). Relatively large scale sand mining from the La beach for construction works have contributed to the erosion trend observed along this portion of the shoreline between 1904 and 2002, while the accretion observed between 1996 and 2002 can be ascribed in part to the protection the exposed rock stratum provides. The breaking wave intensity reduces the energy of the erosion forces and serves as a sink by trapping sediment, which builds the beach and thus operates like offshore breakers.

The lack of beach material in the eastern geomorphic zone is as a result of significantly high sand mining activities in the region (AESC 1988), which in part explains the erosion trend observed in the region between 1904 and 2002. This is as a result of the increasing rate of the eastward littoral drift arriving in this region that would have been expected to result in accumulating beaches due to the complete blockage of sediment transport by the Tema harbour (further east of the region).

Beach sand from this zone was used to construct the entire Tema township in the early 1950s (EPA 2003). This observation explains the observed long-term erosion trend between 1904 and 2002 in this region. Sand mining in the coastal area to the west of the Tema harbour is still on-going because the harbour authorities fear of shoaling problems at the harbour entrance. This explains the short-term erosion trend observed between 1974 and 1996 since the mining activity results in a slow recovery process in the region despite the positive feedback from the Tema harbour structures. This is a clear indication of the lack of integrated coastal zone management (city planning, infrastructure, tourism development, port activities,

fisheries etc.) and the resulting need for the establishment of a stronger relationship between the various governmental authorities (such as GPHA, Ministry of Works and Housing, and the Accra Metropolitan Assembly) dealing with the coastal zone.

14.4.4.7 Coastal Population Increase

Population increase along the Accra coast has resulted in an urbanisation rate of 52% per year (Churcher 2006) that has also initiated and exacerbated erosion in the shoreline. Opportunity for employment has caused migration of people from inland to the coast and the population density of 3,388 persons per km ^{2} (Churcher 2006) implies that significant portions of the coastal zone are habited. This has imposed more pressure on the coastal lands as natural habitats have been altered to accommodate the increased population.

Coastal resources such as wetlands have been drained for settlement in the western region and vegetation (e.g. mangrove) has been destroyed through over cutting (Alvarado 2003). The practice has destroyed the natural windbreak and coastal erosion protection system, and this in part explains the short term erosion trend between 1974 and 1996 as well as between 1996 and 2002 in the western region. The encroachment on the coastal land has also resulted in a 'coastal squeeze' situation, whereby less space is now available for the coastal zone to accommodate eroding forces or adjust to changes such as sea-level rise. This explains the increasing problems associated with coastal erosion in the western geomorphic zone, such as the destruction of about 17 coastal houses, as the shoreline moves to more populated areas in the coastal region.

Coastal population increase has also created irrational coastal land use development and unwise management practices by both the local population and the authorities. Inappropriate location of coastal infrastructures has been identified by the World Bank (1998) as a significant cause of increased erosion in Accra since it was undertaken with little regard to the environment (Luc and Bonn 1999). The situation has resulted in unsustainable use of coastal resources and this partly explains the long term erosion trend revealed between 1904 and 2002 in the eastern region, especially around Teshie and Nungua. The absence of reliable quantitative data on historic recession trends in the Accra shoreline is a major cause of the haphazard development along the Accra coast. This is because effective planning has the potential to avoid the occurrence of relatively high impact coastal erosion by diverting development away from hazardous zones. The risk of coastal infrastructure damage as the shoreline continues to migrate inland is thus significantly high since coastal development did not leave much space for natural beach dynamics to take place. This further emphasises the significance of the results of this study as it provides the information that is relevant for developing sustainable management strategies for the Accra coastal zone.

14.5 Conclusion

This study has shown that the generic technique involving linear regression to estimate historic rates of change and model the erosion trend in the Accra shoreline has proved to be appropriate and cost-effective. This therefore holds promise for other developing countries that lack the resources for consistent shoreline monitoring and thus data paucity. In this study, the rates were estimated along 100 m interval perpendicular transects alongshore that cover the entire length of Accra's shoreline. The estimated rate of change is therefore representative of the Accra shoreline and hence credible. The linear regression method, which is considered the most statistically robust quantitative method when limited numbers of shorelines are available (Crowell et al. 1997), as pertains in developing countries such as Ghana, was used to compute the change detection rates. Linear regression reduces the effect of spurious data points on the calculated rates of change and enables the use of related available statistical techniques to test and measure the quality of the straight-line fit as well as estimate the variance of the data (Crowell et al. 2005). Since linear regression consistently gives better long-term forecasting results (Crowell et al. 2005) due to its robustness, it can be inferred that the average recession rate of change estimated in the Accra shoreline is reliable. The generic technique developed for this study can therefore be applied to other data-sparse coastal regions in developing countries.

The study revealed that the Accra shoreline has receded at an average rate of 1.13 m/year. This will result in destruction of coastal land and infrastructure if left unattended to. The western and eastern geomorphic zones are eroding more relative to the central geomorphic zone and are also the location of the erosion 'hot spots'. Coastal infrastructure, ecology, industries and the local population in the study area are therefore under varying levels of erosion threat. The results have therefore provided insight into the evolutionary trend in the Accra shoreline and the factors responsible for this morphological change. It has also greatly improve understanding into the dynamics of coastal processing along the Accra coast that aid in developing sustainable management strategies for the Accra coastal resources.

References

AESC (1980) Coastal erosion and proposed protection works at Keta. Accra

AESC (1988) Fact-finding mission report-Ghana coastal environment. Accra

Al-Tahir R, Ali A (2004) Assessing land cover changes in the coastal zone using aerial photography. Surv Land Inf Sci 64:107–112

Alvarado F (2003) The story of the Tsokomey Nature Centre. Environmental Studies Department, University of California, California, p 99

Anokwa Y, Martin N, Muff R (2005) Coastal stability map of greater Accra metropolitan area. Environmental and Engineering Geology Map of Greater Accra Metropolitan Area, Accra

Amatekpor JK (1994) Environmental baseline studies: soils, land use, and land degradation of the densu delta ramsar site. In: Ghana Coastal Wetlands Development Project. Accra, Ghana

Appeaning Addo K (2009) Detection of coastal erosion hotspots in Accra, Ghana, J Sustain Dev Afr 11(4), Clarion University of Pennsylvania, Clarion

Appeaning-Addo K, Walkden M, Mills JP (2008) Detection, measurement and prediction of shoreline recession in Accra, Ghana. J Photogramm Remote Sens 63:543–558

Armah AK (1991) Coastal erosion in Ghana: causes, patterns, research needs and possible solutions. In: Coastal zone '91 conf. ASCE (American Society of Civil Engineers), New York, pp 2463–2473

Armah AK, Amlalo DS (1998) Coastal zone profile of Ghana, vol Vii. Gulf of Guinea Large Marine Ecosystem Project. Ministry of Environment, Science and Technology, Accra, p 111

Armah AK, Wiafe G, Kpelle DG (2005) Sea-level rise and coastal biodiversity in West Africa: a case study from Ghana. In: Low PS (ed) Climate change and Africa. University pres, Cambridge, UK, pp 204–217

Barton CC, Dismukes JS, Morton RA (2003) Complexity analysis of the change in shoreline position at Duck, NC. In: Proceedings coastal sediments '03. ASCE (American Society of Civil Engineers), Texas, p 7

Bird ECF (1985) Coastline changes. Wiley, Chichester

Boateng I (2006) Shoreline management planning: can it benefit Ghana? A case study of UK SMPs and their potential relevance in Ghana. https://www.fig.net/pub/accra/papers/ts16/ts16_04_boateng.pdf. Accessed 20 Nov 2006

Boateng I (2011) An assessment of the physical impacts of sea-level rise and coastal adaptation: a case study of the eastern coast of Ghana. Clim Change. doi:10.1007/s10584-011-0394-0

Bray MJ, Hooke JM (1997) Prediction of soft-cliff retreat with accelerating sea-level rise. J Coast Res 13(2):453–467

Campbell MO (2006) The sustainability of coconut palm Cocos Nucifera Linnaeus 1753 in coastal Ghana. J Coast Res 22(5):1118–1124

CETS (1987) Responding to changes in sea level: engineering implications. http://books.nap.edu/openbook.php?record_id=1006&page=40. Accessed 28 Nov 2007

Churcher C (2006) Linking national and regional efforts in ocean and coastal management: African perspectives. http://www.globaloceans.org/globalconferences/2006/pdf/AlbertOwusu-Sarpong.pdf. Accessed 10 Dec 2011

Cooper JAG, Pilkey OH (2004) Longshore drift: trapped in an expected universe. J Sediment Res 74(5):599–606

Crowell M, Letherman SP, Buckley MK (1991) Historical shoreline change: error analysis and mapping accuracy. J Coast Res 7(3):839–852

Crowell M, Leatherman, SP, Buckley MK (1993) Erosion rate analysis: long term versus short term. Shore and Beach 61(2):13–20

Crowell M, Douglas BC, Leatherman SP (1997) On forecasting future US shoreline positions: a test of algorithms. J Coast Res 13(4):1245–1255

Crowell M, Leatherman SP, Douglas B (2005) Erosion: historical analysis and forecasting, in encyclopedia of coastal science. In: Schwartz ML (ed) Encyclopedia of Earth Sciences Series. Springer, Netherlands, pp 428–432

D'Alge JCL, AlvesDS (1992) Input procedures for TM-landsat photographic products into a GIS environment. ISPRS Congress, Washington, DC. http://www.dpi.inpe.br/~julio/arquivos/Isprs92-3.pdf. Accessed 14 Oct 2011

Dean R, Dalrymple RA (2002) Coastal processes with engineering applications. University Press, Cambridge, UK, pp 35–69

Dean RG, Malakar SB (1999) Projected flood hazard zones in Florida. J Coast Res 28:85–94

Dickson KB (1965) Evolution of seaports in Ghana: 1800–1928. Ann Assoc Am Geogr 55 (1):98–109

Dickson ME, Walkden MJ, Hall JW (2007) Systemic impacts of climate change on an eroding coastal region over the twenty-first century. Clim Change 84(2):141–166

Dolan R, Fenster MS, Holme SJ (1991) Temporal analysis of shoreline recession and accretion. J Coast Res 7(3):723–744

Doukakis E (2004) Transect spacing and coastal evolution, 3rd international energy, energy and environmental symposium. http://www.ntua.gr. Accessed 20 Nov 2011
EPA (2003) Information for Africa Climate Technology Transfer (IACTT). http://www.epa.gov.gh/iACTT/Ghana_VA%20Coastal%20Zone%20.pdf. Accessed 10 Dec 2011
EUROSION (2004) Living with coastal erosion in Europe: sediment and space for sustainability part I – Major findings and policy recommendations of the EUROSION project. http://www.eurosion.org/reports-online/part1.pdf. Accessed 01 Dec 2011
FAO (1998) Coastal environments under threat. FAO factfile. Food and Agriculture Organisation. http:/www.fao.org/NEWS/FACTFILE/FF9804-E.htm[Geo-2-239]
Feagin RA, Sherman DJ, Grant WE (2005) Coastal erosion, global sea-level rise, and the loss of sand dune plant habitats. Front Ecol Environ 3:359–364
Genz AS, Fletcher CH, Dunn RA, Frazer LN, Rooney JJ (2007) The predictive accuracy of shoreline change rate methods and alongshore beach variation on Maui, Hawaii. J Coast Res 23(1):87–105
Geoconsultants (2005) Proposed bridge over River Densu on the Mallam-Kasoa road. Result of test borings-(1), Accra
Ghana National Report (2002) Ghana's initial national communication under the United Nations framework of climatic change. Environmental Protection Agency (EPA), Accra
Gibeaut JC, Hepner T, Waldinger R, Andrews J, Gutierrez R, Tremblay TA, Smyth R, XuL (2001) Changes in Gulf shoreline position, Mustang, and North Padre Islands, Texas. http://www.beg.utexas.edu/coastal/presentations_reports/Mustangfinalrpt.pdf. Accessed 30 Nov 2011
Gibeaut JC, Waldinger R, Hepner T, Tremblay TA, White WA, Xu L, (2003) Changes in bay shoreline position, West Bay System, Texas. http://www.beg.utexas.edu/coastal/presentations_reports/WestBayfinalreport.pdf. Accessed 14 Nov 2011
Givens JM (1999) Positional accuracy handbook: using the national standard for spatial data accuracy to measure and report geographic data quality. http://server.admin.state.mn.us/pdf/1999/lmic/nssda_o.pdf. Accessed 17 Jan 2012
GWCL (2004) Ghana Water Sector Restructuring Project, dam safety assessment. http://wwwwds.worldbank.org/servlet/WDSContentServer/WDSP/IB/2004/05/25/000160016_20040525173550/Rendered/PDF/E9510vol01.pdf. Accessed 17 Nov 2011
Hapke CJ, Reid D, Richmond BM, Ruggiero P, List J (2006) National assessment of shoreline change: part 3: historical shoreline changes and associated coastal land loss along the sandy shorelines of the California coast: U.S. geological survey open-file report 2006–1219
Hapke C, Lentz EE, Bradley M, Williams J, Schwab B, Gayes P (2010) Sediment budgets, shoreline change and nearshore sediment sources. Fire Island, New York
Hollis GE, Holland MM, Maltby E, Larson JS (1988) Wise use of wetlands. Nat Res (UNESCO) XXIV(1):2–12
Honeycutt MG, Crowell M, Douglas BC (2001) Shoreline-position forecasting: impact of storms, rate-calculation methodologies, and temporal scales. J Coast Res 17(3):721–730
Honeycutt MG, Krantz D (2002) Shoreline change along Delaware's Atlantic coast: analyses of spatial variability and erosion-forecast uncertainty. Shoreline change conference proceedings NOAA coastal services centre session IV. http://www.csc.noaa.gov/shoreconf/shoreline_-change_conf_proceedings.pdf. Accessed 08 Dec 2011
Ibe AC, Quelennac RE (1989) Methodology for assessment and control of coastal erosion in West Africa and Central Africa. UNEP regional sea reports and studies no. 107, United Nations Environment Programme, New York, USA
IPCC (2007) Climate change 2007: the physical science basis (summary for policymakers). Contribution of working group I to the fourth assessment report of the Intergovernmental Panel on Climate Change. http://www.ipcc.ch/SPM2feb07.pdf. Accessed 20 Feb 2012
Li R, Ma R, Di K (2002) Digital tide-coordinated shoreline. Mar Geod 25(1):27–36
Luc H, Boon EK (1999) Institutional, legal and economic institution in Ghana Environmental Policy. Environ Manage 24(3):337–351
Ly CK (1980) The role of the Akosombo Dam on the Volta River in causing erosion in Central and Eastern Ghana (West Africa). Mar Geol 37:323–332

Ly CK (1981) Sources of beach sand from the central and eastern coasts of Ghana (West Africa). Mar Geol 44:229–240
McGowan E (1998) Planning a digitising project. The NCGIA GIS Core Curriculum for Technical Programs. Unit 12. http://www.ncgia.ucsb.edu/cctp. Accessed 13 Apr 2006
Mensah JV (1997) Causes and effects of coastal sand mining in Ghana. Singap J Trop Geogr 18 (1):69–88
Moore LJ (2000) Shoreline mapping techniques. J Coast Res 16(1):111–124
Moore LJ, Griggs GB (2002) Long term cliff retreat and erosion hotspots along the central shores of the Monterey Bay National Marine Sanctuary. Mar Geol 181(1):265–283
Morton RA, Miller TL (2005) National assessment of shoreline change: part 2 historical shoreline changes and associated coastal land loss along the U.S. Southeast Atlantic coast (open-file report 2005–1401). http://pubs.usgs.gov/of/2005/1401/. Accessed 15 Dec 2011
Morton RA, Miller TL, Moore LJ (2004) National assessment of shoreline change: part 1: Historical shoreline changes and associated coastal land loss along the U.S. Gulf of Mexico, U.S. geological survey open-file report. http://pubs.usgs.gov/of/2004/1043/. Accessed 20 Dec 2011
Muff R, Efa E (2006) Ghana-Germany technical cooperation project: environmental and engineering geology for urban planning in the Accra-Tema area. Explanatory notes for the geological map for urban planning 1:50 000 of Greater Accra metropolitan area. Accra
Norley N (2006) Agambila alarmed at sea erosion. Ghanaian Chronicle, Accra
Oteng-Yeboah AA (1999) Development of a management plan for the Densu Delta Ramsar Site. Accra
Poku-Adusei (2006) African climatologists meet in Accra. Daily Graphic, Accra
PSMSL (2002) Obtaining sea level data. http://www.pol.ac.uk/psmsl/datainfo/. Accessed 18 Oct 2006
Rakocinski CF, Heard RW, LeCroy SE, McLelland JA, Simons T (1996) Responses by macrobenthic assemblages to extensive beach restoration at Perdido Key, Florida, U.S.A. J Coast Res 12(1):326–353
Robertson W, Whitman D, Zhang K, Leatherman S (2004) Mapping shoreline position using airborne laser altimetry. J Coast Res 20(3):884–892
Talbot MR (1976) Quaternary palaeoenvironments in the Accra-Tema area of the Southern Ghana. Annu Rep Res Inst Geol Univ Leeds 20:66–67
Thieler ER, Danforth WW (1994a) Historical shoreline mapping.1. Improving techniques and reducing positioning errors. J Coast Res 10(3):549–563
Thieler ER, Danforth WW (1994b) Historical shoreline mapping (II): application of the digital shoreline mapping and analysis systems (DSMS/DSAS) to shoreline change mapping in Puerto Rico. J Coast Res 10(3):600–620
Thieler ER, Rodriguez RW, Carlo M (1995) Beach erosion and coastal development at Rincon, Puerto Rico. Shore Beach 63(4):18–28
Walkden M, Dickson M (2006) The response of soft rock shoreprofiles to increased sea-level rise, Tyndall centre working paper no. 105
Walkden MJA, Hall JW (2005) A predictive mesoscale model of the erosion and profile development of soft rock shores. Coast Eng 52(6):535–563
Wellens-Mensah J, Armah AK, Amlalo DS, Tetteh K (2002) Ghana national report phase 1: integrated problem analysis. GEF MSP sub-Saharan Africa project (GF/6010-0016): development and protection of the coastal and marine environment in Sub-Saharan Africa, Accra
Woodroffe CD (2003) Coasts: form, process and evolution. University press, Cambridge
World Bank (1996) Development in practice: toward environmental sustainable development in Sub-Saharan Africa, a World Bank Agenda
World Bank (1998) Findings, African region 113. http://www.worldbank.org/afr/findings/english/find113.htm. Accessed 27 Feb 2012
Zuzek PJ, Nairn R, Thieme SJ (2003) Spatial and temporal considerations for calculating shoreline change rates in the Great Lakes Basin. J Coast Res 38:125–146

Chapter 15
Detection of Coastal Change by Geo-Informatics Means

Jay Gao

Abstract The coastal zone is a special geographic area prone to change induced by a variety of processes and factors. Timely monitoring of coastal evolution is critical to enactment of policies for effective planning and minimization of coastal hazards. This paper comprehensively and critically evaluates the methods that have found applications in monitoring coastal change: photogrammetry, GPS and laser scanning. Coastal changes that have been successfully monitored using these methods range from shoreline determination and change detection, to monitoring of cliff retreat and dune erosion. Although the photogrammetric method is able to supply accurate information, it is subjective and tedious to delimit shoreline on photographs. By comparison, the GPS method is very fast and inexpensive, but constrained by site accessibility. The scanning method is also fast but expensive. It can determine shoreline accurately over large areas. In detecting cliff retreat no method is perfect. The GPS method is inapplicable due to the difficulty in accessing this precarious site. Neither vertical photography nor airborne laser scanning is able to sense cliff face. The difficulty in sensing cliff faces is overcome with terrestrial implementation. Terrestrial laser scanning yields more accurate results than the rigorous close-range photogrammetric method. All three methods are capable of detecting dune erosion. The GPS method is rather slow as many widely dispersed data points must be logged. Laser scanning is very fast but can be expensive. It yields more accurate dune heights than photogrammetry that requires complex post-processing. Given their complementary nature, the combination of these technologies will enable the coastal environment to be monitored at unprecedented accuracy and frequency with ever greatest ease.

J. Gao (✉)
School of Environment, University of Auckland, Auckland, New Zealand
e-mail: jg.gao@auckland.ac.nz

C.W. Finkl (ed.), *Coastal Hazards*, Coastal Research Library 6,

DOI 10.1007/978-94-007-5234-4_15,

15.1 Introduction

A huge population around the world lives within a close proximity to the coast owing to its attractive scenery. However, the coastal zone also happens to be the most vulnerable to change. Hurricanes, waves and tsunamis can all cause dramatic changes to it even within a short period of time. In particular, sandy coasts can be severely eroded easily in a storm. Accurate information on the coastal environment and its change over time is needed for planners in devising strategies for laying the infrastructure and in mitigating coastal hazards.

Several methods are available for monitoring the coastal zone. With advances in technology, the classic method of ground survey using a theodolite has been gradually augmented with modern methods based on remote sensing. They range from the conventional photographic method to more advanced laser scanning. These methods are comprehensively evaluated in this paper for their ability to detect coastal change, including the strengths and limitations in different fields of application. Also identified in this paper are the factors important to the accuracy of the obtained results. Under the broad topic of change detection in the coastal zone, these fields of application range from 2D mapping of shoreline position and its change, landward retreat of seacliffs, to 3D detection of dune erosion.

15.2 Shoreline Change

Shoreline position is defined as the boundary between wet and dry sand on the beach. In the field or on aerial photographs, this position is taken as the high water line or the interface of land with seawater at high tide (Hicks et al. 2000). Temporally, this position is not fixed as it is subject to the influence of tidal height. Shoreline, especially sandy shoreline, tends to change rather quickly due to the influence of storms and waves that can either deposit sand on the beach or erode it away. Thus, up-to-date knowledge on shoreline requires timely and periodic monitoring via aerial photography, global positioning system (GPS) and laser scanning.

15.2.1 Photography

Aerial photographs have been used to document shoreline position and change with the longest history (Anders and Byrnes 1991). Monitoring of shoreline position is ideally achieved from vertical photographs (Fig. 15.1) whose bird's eye view clearly illustrates the transition from wet beach to dry sand over the entire beach. Delineation of shoreline position on the photographs relies usually on

Fig. 15.1 Vertical aerial photographs faithfully record the position of shoreline that can be demarcated based on photo tone and texture. The same shore line can also be logged using a GPS unit on the ground (Source: Gao 2003)

tonal variation that signifies the transition (Gibeaut 2003). On black-and-white photographs, wet beach has a dark tone, in contrast to light tone indicative of dry sand. However, it is unreliable to demarcate the high water line based on tone alone because tonal variation can also be caused by other features (e.g., debris lines), and the high water line may be occasionally smeared by instant swash lines (Robertson et al. 2004). This ambiguity surrounding shoreline can cause an error as large as 6.1 m in its delineated position (Crowell et al. 1991). Other factors that can potentially degrade the delineation accuracy are photo scale, camera parameters, flight elevation, and accuracy of ground control (Hapke and Richmond 2000). Photo scale affects the delineation as it is related to photo resolution that dictates the amount of details discernable on the ground. Fine resolution images are especially pivotal in detecting shoreline change in the range of centimeters. A fine resolution in the range of 0.5–3.0 m horizontal accuracy is desirable to detect small changes.

The uncertainty in delimiting shoreline position from aerial photographs is significantly minimized if the foredune position is used as the proxy. The transitional boundary between the backshore and foredune or beach-dune junction is much more distinctive and conspicuous on aerial photographs than the high water

line, especially if viewed stereoscopically. Located at a higher elevation, the foredune is drier and may be distributed with coastal vegetation occasionally. It is hence lighter in tone and easier to separate from the beach face (Gao 2003). The beach face with a higher moisture content tends to have a darker tone. The absence of vegetation makes its texture rather smooth. This proxy is considered superior and more reliable as it is not subject to wave run-up at high tides. No matter how the shoreline is defined, manual delimitation of shoreline from photographs is always tedious, labor intensive, and hence very slow for large areas (Stockdon et al. 2002). Besides, caution must be exercised in interpreting the results as aerial photographs are virtually snapshots that record the tidal height at a particular time. The delineated shoreline position is correct only at that moment and may change over time.

About a decade ago a new generation of very high resolution satellite images emerged, offering a spatial resolution comparable to that of aerial photographs. They opened an avenue by which shoreline may be mapped from space. The first very high resolution imagery is IKONOS, available in both panchromatic (1 m resolution) and multispectral (4 m resolution) modes. Shoreline position derived from 1 m simulated IKONOS imagery has the most optimistically estimated error of around 2–4 m (Zhou and Li 2000). The accuracy from 4 m IKONOS images is much lower at 8.5 m (Li et al. 2004). Apart from imagery resolution itself, the accuracy is also subject to ground control in geo-referencing the imagery. Geo-referencing is essential for those earlier images that do not have a ground coordinate system associated with them. The accuracy, as measured using the root-mean-square error, of IKONOS-derived shoreline deteriorates to 12.27 m from the reference shoreline derived from orthophotos after the geo-referencing inaccuracy is taken into account. Apart from the lower accuracy, tidal height is uncertain at the time of imaging. So the derived shoreline should be treated with caution if subsequently used for shoreline change detection.

Shoreline change is detected by overlaying all the positions derived from time series aerial photographs or satellite images (Shao et al. 1998). Change in shoreline position is easily detected from large-scale aerial photographs or mosaics of orthophotos. A very important consideration in the change detection is the digital transformation of all these materials to a common coordinate system at a similar accuracy level. Any discrepancy in the planimetric accuracy of the source shoreline position will eventually propagate into the final results, causing inaccurate or even false detection outcomes. In the change detection, it is rather easy to find recent photographs, but not historical data. If no appropriate archived aerial photographs are available, topographic maps (T-sheets) that document past shoreline positions may have to be relied on to stretch the span of detection (Fletcher et al. 2003). It is also possible to augment the database with satellite images such as IKONOS imagery in case of no appropriate photographs.

Care must be taken in using T-sheets that are virtually the second generation of information. Dissimilar to aerial photographs that show the original shoreline graphically, the shoreline on T-sheets has been drawn already, most likely at an unknown accuracy level. Shoreline on T-sheets is estimated to have a standard

deviation of 2.5–20 m from that of aerial photographs, depending on the scale (Li et al. 2004). It is absolutely imperative that shoreline position be identically defined and geo-referenced to the same coordinate system before the diverse sources of data can be compared to each other spatially. For instance, these data must be recorded at the same tidal height if shoreline is defined as the high water line (e.g., either mean high water level or the contour height of water level at high tides) in order to generate genuine information on shoreline movement. This task is almost impossible with historical photographs. So an alternative proxy has to be used.

Apart from airborne vertical photographs and space-borne satellite images, shoreline can also be determined from ground-based video images, such as those obtained by the ARGUS optical video system (Harley et al. 2010). This ground sensing method enables long-term monitoring of coastal morphodynamics at a fine resolution. Time series shoreline location is derived by averaging alongshore values at a fixed interval (e.g., hourly or daily). Each of the located shoreline may be quality checked to remove noises caused by shadow and lines of wave breaking (Harley et al. 2010). The advantage of this method is its ability to study minute change over any period of time from a huge amount of frame images. Since the entire process of beach erosion/accretion is captured continuously, it is also possible to link such temporal variation of beach change to waves to investigate environmental forcing and response. The disadvantage of this method is the huge amount of data to be processed. Objective extraction of shoreline from this vast quantity of video images can be expedited via computerized methods of processing (Alexander and Holman 2004). Although a semi-automatic object-oriented algorithm is available for efficiently classifying intertidal beach video images (Quartel et al. 2006), such shore-based monitoring has a limited field of view in sensing the shoreline. Thus, it is difficult to judge whether the identified change at the observation vantage point is representative of the change experienced by the entire coastline. To answer this question, more observation points are needed.

The detection of shoreline change, or the horizontal differences between high water lines derived from various data and contour, is easily implemented in the geographic information system (GIS) environment. GIS is capable of integrating diverse sources of data (field surveys with total station, air photographs and topographic maps) and digitally analyzing them to quantify shoreline change (Ojeda Zújar et al. 2002). Data stored in a GIS may be visualized to show the current state of shoreline and its rate of change, in addition to answering spatial queries of shoreline change, and compiling regional statistics of shoreline change and trends of change (Schupp et al. 2004). Customized ArcGIS tools are preferred in calculating rates of shoreline change along a huge number of transects (Zuzek et al. 2003). Although the powerful and versatile functionality of a GIS enables the detection task to be readily achievable, it cannot resolve any spatial discrepancy between the datasets in use. Besides, technological superiority cannot resolve the influence of sampling strategy and water level. For this reason, caution must be exercised in selecting historical sources of positional data with an appropriate transect spacing in order to minimize sampling errors.

15.2.2 GPS Method

Apart from historical maps, aerial photographs, and satellite images, coastal evolution can be easily tracked with GPS. This positioning technology works by receiving signals from a number of satellites overboard simultaneously. Simultaneous tracking of signals from four satellites is able to determine the distance from the GPS receiver to the satellites whose position in space is known. The four distances will fix the position of the GIS receiver on the ground unequivocally. If a GPS unit is mounted on a vehicle moving along the shoreline, then logging of points at a constant interval is able to yield its position. With proper post-processing, GPS results can be displayed on top of properly geo-referenced photographs and satellite images (Fig. 15.1). The overlay and comparison of the logged linear position with historical aerial photographs or satellite images enables the change in shoreline position to be quantified rather quickly and accurately. This method is able to generate objective results as it does not involve subjective judgment as where the wet beach ends and where the dry sand starts, as with photointerpretation.

Apart from its objectivity, the GPS method is also preferred for its cost effecttiveness, speed, and accuracy. Shoreline position can be logged rather inexpensively. GPS-based survey of shoreline position can be completed within hours. This duration is shortened further if the GPS unit is mounted on the top of a vehicle. Vehicle-based GPS survey is reported to have a horizontal inaccuracy of 2.5–5.0 m in position on a beach with a 1:50 slope (Ruggiero et al. 1999). Accuracy is further improved via differential correction. For instance, real-time kinematic (RTK) GPS is able to achieve more accurate loggings than ordinary receivers owing to its ability to track carrier phases of the GPS signals using multiple units, one of which serves as the base station. With RTK GPS it is possible to acquire centimeter accuracy in locating shoreline.

However, the GPS method is constrained in two aspects. First, GPS logging is restricted by site accessibility. It is practical only along moderately long segments of coast and only where the shoreline is accessible to vehicles (Gibeaut 2003). Second, GPS can only log the current shoreline position. Thus, it is impossible to detect the change in shoreline variation over time unless historical GPS surveys have been undertaken or a similar survey will be carried out in the future. In this case the logging route must be kept identical. This requirement, however, may be difficult to fulfill due to the varying tidal heights. Thus, it is important to log the same route that is accessible at all times (e.g., not subject to the tidal height).

15.2.3 Laser Scanning

The extremely rapid development in sensing technology over the last two decades has witnessed the advent of laser scanning, a new form of remote sensing able to provide sub-meter height accuracy (Brock et al. 2002). Variously known as LAser

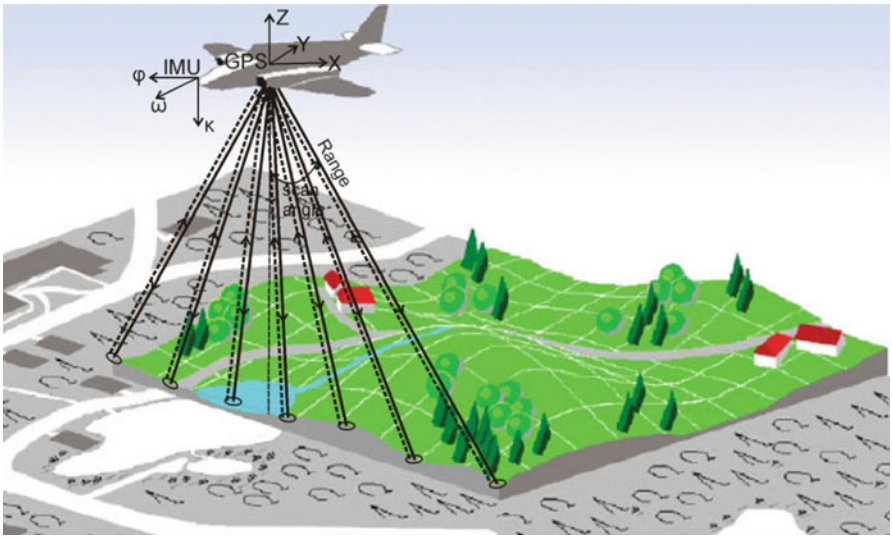

Fig. 15.2 Principle of airborne laser scanning (Source: modified from TopoSys GmbH 2004)

Detection And Ranging (LADAR) or Light Detection And Ranging (LiDAR), this scanning method is very similar to aerial photography in that a sensor is mounted on an aircraft to obtain information on the target (e.g., the coast). Unlike aerial photography, scanning results in dense point data rather than graphic images. Airborne laser scanning works by transmitting laser signals to the target at short durations (e.g., up to 25,000 times per second) and then receiving the signal bounced back from the target. Through timing the duration of laser signal transmission, it is possible to calculate the distance between the sensor and the target. In addition, both positional and orientational information of the scanner is also collected during scanning, together with laser ranges and associated scan angle information (Wehr and Lohr 1999). Orientational information such as roll, pitch and yaw available from an Inertial Measurement Unit (IMU) is needed for converting the slant distance between the sensor and the target into increments in the 3D space (Fig. 15.2). The absolute aircraft positions (trajectory) derived from a differential, geodetic GPS network serves to transform the coordinates of the sensor to those of the target. As LiDAR surveys are facilitated with an onboard GPS-enabled IMU, the acquired data are automatically geo-referenced to a known ground coordinate system.

Operational since the mid-1990s, airborne topographic LiDAR is capable of rapidly acquiring continuous 3D point cloud data along extensive shorelines. This strength makes it likely to supersede other technologies in monitoring shoreline position and change (Gibeaut 2003). Nevertheless, LiDAR data themselves are merely data points of 3D coordinates (easting, northing and height). As such, airborne laser scanning is perfectly suited to produce digital elevation models (DEMs) and surface models automatically (Ackermann 1999). On the other hand, the high water line is just an intangible mark on the beach that does not have any

distinctive topographic features associated with it. Hence, LiDAR-derived DEM does not bear any relationship with shoreline. There are two methods by which shoreline may be derived from LiDAR data. The first is to find the height of shoreline on the ground. A contour line corresponding to this height is then generated from the LiDAR-derived DEM. This method is the only option if the generated shoreline is to be compared with historical shoreline position in detecting its change (Gibeaut 2003). The second method is to locate an abrupt transition in elevation in the DEM if the shoreline is defined as the toe of the foredune. In this case, the inaccuracy in determining shoreline position may be drastically reduced via fitting a function to cross-shore profiles of laser altimetry data located in a vertical range around the datum (Stockdon et al. 2002). This method is advantageous in places where low-relief tidal flats and marshes exist along bay shorelines. Their presence makes it extremely difficult to identify shoreline features reliably on aerial photographs. Such foredune-based shoreline position is also more stable than high water line measurements as it avoids short-term fluctuations in wave energy and water levels (Robertson et al. 2004). No matter which method is used to transform LiDAR data to shoreline, laser scanning is suitable for studying impacts of large-scale storms on beaches and quantifying the response of coastline to storms, which may lead to a more in-depth and comprehensive understanding of large-scale coastal processes (Stockdon et al. 2002).

Dense LiDAR data are able to provide accurate information about shoreline changes at several scales, ranging from small to large. The accuracy of LiDAR-derived shoreline is affected by many factors, such as the flying height, scan range, point data density, and the method of shoreline determination. Shoreline can be accurate to $<\pm 0.05$ m at a scan range up to 300 m (Rosser et al. 2005). LiDAR-based shoreline position differs from its vehicle-based GPS survey counterpart by a root mean square error of 2.9 m (Stockdon et al. 2002). LiDAR data-derived shoreline position via projecting contour levels is more accurate than that traced from the high water line on aerial photographs. How LiDAR-derived shoreline measures up in relation to other methods in terms of time and cost remains unknown, even though it is generally accepted that LiDAR is very fast but expensive.

15.3 Cliff Retreat

Seacliff is a special coastal feature that involves an abrupt and huge change in elevation over a short horizontal distance. As such, it is difficult to determine its precise position. On the other hand, it is vital to determine their position in order to assess the long-term trend of coastal erosion and retreat as sea cliffs usually afford a scenic view of the sea and are prized for residential development. Due to the risk of coastal erosion and potential collapse, near-vertical cliffs pose an insurmountable logistic barrier in determining their position accurately. It is challenging to log the position of precarious cliffs using terrestrial GPS due to its site accessibility

requirement. However, their base can still be logged using a GPS, albeit at a lower accuracy as a result of signal obstruction by the adjacent upright wall. Instead, determination of cliff position relies more on remote sensing methods. This section introduces two of them, photogrammetry and laser scanning. Both can be airborne or terrestrial.

15.3.1 Photogrammetry

On vertical aerial photographs it is the cliff crest edge that is detected (Zviely and Klein 2004). Detection of cliff edge is based on tonal contrast, relief and shadow on photographs. In the event of cliff retreat resulting from active landslides, the back scar is commonly assumed to be the indicator of cliff edge as there is a sharp discontinuity in tone (color), slope and vegetation here (Rosser et al. 2005). The interpreted position involves more uncertainty if the cliff edge is blun. In addition, the accuracy of detection is lowered by several factors, the most important being the lack of ground control. Since the beach below is mostly featureless, ground control, if available, is leaned heavily towards the landward side, causing an imbalance in the spatial distribution of ground control points (GCPs). A balanced distribution of quality GCPs is essential to generate reliable photogrammetric measurements. Lack of accurate ground control in this coastal environment can potentially introduce a high margin of error to the photographs-derived cliff position.

Even if accurate geometric control is established on the ground, it is still difficult to ensure a high demarcation accuracy due to obscurity and relief displacement. The precise position of the cliff can be obscured by coastal vegetation. Trees growing near the cliff edge or tree branches protruding over a cliff may disguise the exact cliff position on photographs, together with their shadow. Both tree and cliff shadow can mask the exact cliff top and hence increase the ambiguity and difficulty in precisely locating its position. Even if the cliff top is clear of vegetation obstruction, cliff top is displaced outward from the photo isocenter as a consequence of the large vertical relief at the interface of the beach and the land. This horizontal displacement is much larger on large-scale photographs and for taller cliffs. Depending on the position from which the photographs are taken, this displacement occurs in different directions and at varying magnitudes. Unless all the multi-temporal photographs used in detecting cliff retreat are taken at the same height and from the same position in air, the position of the cliff top on the photographs will be shifted in varying directions and magnitudes. This discrepancy is then translated into artificial change in the cliff position and subsequently cliff retreat rates, leading to inaccurate or even false results. This limitation can be successfully remedied with the use of orthophotographs on which relief displacement is completely eliminated after its magnitude is estimated from the spot height in a DEM. Nevertheless, the shadow problem still persists with orthophotos.

Another drawback of using orthophotos is its inability to study cliff face. Despite being the most rigorous methodologically, photogrammetry at most is able to detect cliff top while changes in the cliff base, where the steeply sloping cliff face intersects the beach, cannot be studied. Neither can it detect processes of undercutting and small scale iterative failures of localized sections on the cliff face (Rosser et al. 2005). On the other hand, it is basal erosion that reflects changes in beach sand level and basal talus deposits, and thus should receive adequate attention. This deficiency of vertical aerial photographs in studying cliff face stems from the oblique viewing angles. Cliff face hardly registers on vertical photographs as a result of heavy image compression. The tiny footprint of a long cliff face on vertical photographs does not allow minor but critical features such as overhangs to be studied.

The alternative is to make use of close-range photogrammetry that operates in the same principle as aerial photogrammetry. The cliff face is sensed by taking stereoscopic photographs using a camera mounted on a tripod from two positions on the beach. The precise location of these positions and the camera orientation are established using the classic survey method with a total station. The acquired stereoscopic photographs are then scanned and properly oriented with the assistance of GCPs established by drilling bolts in the cliff walls (Wangensteen et al. 2007). The generated 3D stereo model may be used to produce a relief map of the cliff face (Pan 2004), or construct a detailed digital terrain model (DTM). Owing to the horizontal view angle, this method is unable to determine the precise position of the cliff top. Nevertheless, the cliff retreat rates can still be calculated by differencing the detailed DTMs produced in multiple surveys. This volume-based method of yielding cliff retreat rates is more scientific than that based on the cliff top position. It is accurate to 10 mm if the distance between camera and cliff walls is sufficiently short (e.g., $<$15 m). Compared to its aerial counterpart, close-range photogrammetry enables the study of cliff face changes that include failures and deposits anywhere on the cliff profile (Young et al. 2009). Dissimilar to its airborne counterpart, close-range photogrammetry can quantify cliff erosion rates over relatively small areas. So the survey may be replicated a number of times over an extensive cliff.

15.3.2 Scanning Method

The use of laser scanning in studying cliffs is underpinned by the same principle as its application in determining shoreline position, the only difference being the way in which the target is detected. Unlike shoreline position that is impossible to detect from laser scan data directly, cliffs can be easily detected by setting a relief threshold. Any relief above the defined threshold is considered an indicator of cliff. The vegetation problem associated with the photographic method does not apply to LiDAR owing to its stronger capability of penetration. The problem of shadow cast by the cliff and coastal forest is non-existent with LiDAR, either.

However, the inability of sensing cliff faces still persists with airborne scanning. This difficulty is overcome by mounting the scanner on a tripod in the ground, a technology commonly known as terrestrial laser scanning. During scanning, non-topographic elements such as bushes or tree branches on a cliff are sensed, in addition to the cliff face itself (Suchocki 2009). The distance between the instrument and the cliff walls should be within the specified range. If the scanner can acquire data at a very high speed (e.g., 50,000 points per second), the point cloud data can have a sub-millimeter resolution, detailed enough to study cliff face features likely to be missed from air-borne LiDAR or even large-scale aerial photographs.

Apart from being excellent in directly monitoring changes on cliff faces, terrestrial laser scanning can also determine the height and position of the cliff, even though the accuracy may be lower than with bare beaches or dunes. With this method cliff failures can be quantified to an unprecedented accuracy (e.g., sub-centimetre) level (Gulyaev and Buckeridge 2004). The scale of these failures ranges from the detachment of blocks of a few centimetres in dimension to large rock, debris or soil, falls, slides and flows over 1,000 m^3 (Rosser et al. 2005). Another advantage of laser scanning is the calculation of the bulk recession rate based on volumetric changes of the entire cliff face (Young et al. 2009). This can then be used to derive average annual cliff face retreat rates. This new approach to recording the volumetric changes in complex coastal cliffs avoids the uncertainty of whether the cliff top or cliff base is used in calculating cliff retreat rate that has been variously characterized in the literature. Such information will form a significant input in zoning coastal hazards (Young and Ashford 2006). This method of data collection is fast and hence cost effective for large areas, painting a detailed picture about the nature of seacliff erosion. However, as with any detection, one-time off laser scanning, either airborne or terrestrial, does not yield any information on cliff retreat. The method will supply data sufficient to project short to medium term volumetric changes over time.

The relative accuracy of photogrammetry and laser scanning in determining cliff position has not been comparatively studied. It is speculated that the photogrammetric method should yield better planimetric accuracy if the photographs used have a fine spatial resolution (e.g., 0.15 m) that is an order of magnitude higher than the spatial resolution of LiDAR footprint (e.g., 2 m) (Adams and Chandler 2002). Both are accurate enough for short-term soft cliff monitoring. Given that both methods have their respective advantages in monitoring cliffs, it is logic to combine them to generate high-quality data to study the processes of cliff evolution (Lim et al. 2005). In this combination high resolution photographs are resampled with the fixed accuracies of the terrestrial laser survey. The complex surfaces are accurately depicted by dense scanning point clouds, free from the optical variations that degrade photographic data. With the combined use of satellite geodesy and digital photogrammetry, highly accurate rates of cliff retreat can be generated consecutively over a long period. This combined approach has the potential to improve our understanding of the activity patterns of sea cliffs. However, it is important that no systematic errors are residing in each of the dataset prior to the integration.

Besides, caution must be exercised in interpreting the detected change from photographs and LiDAR data separated by a short temporal span as change is not necessarily attributable to geomorphologic processes alone. Growth and removal of coastal vegetation on the cliff can cause significant morphological differences, as well (Adams and Chandler 2002).

15.4 Dune Erosion

Accurate knowledge on surface relief or roughness is important in a number of coastal applications, such as assessment of the effectiveness of beach nourishment. This knowledge enlightens us on how a dune system responds to severe weather events such as hurricanes. This understanding of dune system response is critical to mitigation of coastal erosion hazards. Dune erosion is much harder to detect than shoreline change and cliff retreat as it involves 3D. Unlike shoreline change, dune erosion can take place both horizontally and vertically. Horizontal retreat of dunes is very similar to shoreline change, even though its precise detection is very challenging because of the complex and changing morphology of the dune field (Mitasova et al. 2005). In addition, the dune system can also be subject to erosion in its surface caused by sand depletion. Through such 3D monitoring it is possible to identify dune movement and to quantify areas of sand loss and rapid horizontal migration. Three methods can be used to detect dune change, photogrammetry, GPS and LiDAR, each having its own unique strengths and limitations.

15.4.1 Photogrammetry

This method is very similar to close-range photogrammetry in studying cliff face except that the pair of stereoscopic photographs is taken from air. A 3D view of the dune field is established from two consecutive, overlapping photographs taken in the same flight line. With the assistance of GCPs or tie points the two photographs can be oriented properly (e.g., restoration of their relative position in the air). Simultaneous viewing of the two photographs of nearly the same scale taken in slightly different perspectives enables the establishment of a 3D impression of all ground features from the differing relief displacements. This optical impression is then used to trace contours or used to produce a DEM of the dune field via soft photogrammetry (Ojeda Zújar et al. 2002). Vertical accuracy of the DEM ranges from 1.03 to 3.75 m, with a mean of 2.77 m (Chang et al. 2004). This accuracy level is significantly improved to 0.43 m for a relatively flat terrain of 20 m relief covered by grass (Adam and Chandler 2002). This accuracy is affected by the distribution and reliability of GCPS, the spatial resolution of the photographs, surface cover and relief of the dune field. In the coastal environment there is a lack of distinctive points that can serve as reliable GCPs. If distinctive points can be identified on the

ground and on the photographs, the deployment of GPS receivers is able to generate highly accurate ground control. The scale of the photographs also exerts an influence on the accuracy of the DEM constructed. Finally, dune height may be influenced by the presence of vegetation, and the slope of the dune surface. Coastal shrubs mask the genuine dune height, and their impact has to be eliminated.

Detection of dune erosion or accretion is implemented as a comparison of the topographic surface in the form of DEMs of an equal grid size constructed either from tracing contours on topographic maps followed by spatial interpolation, or the 3D model directly in a GIS. This comparison yields not only the rate at which the backshore and foredune are eroded but also the volume of sand lost or gained. Naturally, the accuracy of detected dune change is affected by the DEM cell size.

This photogrammetric method has the advantage of producing highly accurate results from large-scale aerial photographs for the entire area of survey if reliable ground control is available. The produced DEM can be fine detailed from stereoscopic aerial photographs of a fine spatial resolution. The disadvantage of this method is long time needed to plan the flight to take photographs and the high cost. Besides, post-processing is very complex and demands special skills in operating a suite of sophisticated photogrammetric packages.

15.4.2 GPS Method

GPS quantification of dune erosion shares the same principle as GPS determination of shoreline position except the focus being the third coordinate, Z, or height rather than horizontal coordinates. GPS determination of dune erosion requires data logging at discrete points dispersed throughout the dune field. Such point-based data are then used to construct a DEM of the dune field via spatial interpolation, just like with LiDAR data. The accuracy of spatial interpolation depends on the regularity of the surface relief and its complexity. Low accuracy is expected in highly irregular and complex dunes (e.g., a huge vertical relief over a short horizontal distance). Besides, a sufficient number of data points widely dispersed throughout the area to be surveyed is indispensable in producing acceptable and reliable dune topography everywhere. The quantity of point data required varies with the complexity of the dune surface. Few points are needed if there is little vertical variation. More points are needed for dune fields whose surface relief is large and unpredictable.

The accuracy of the GPS-constructed topographic surface is reported to be around ± 10 cm (Schmidt and Persson 2003), or higher (e.g., ± 5.3 cm at the 95% confidence level) in open fields (Featherstone and Stewart 2001). This accuracy is subject to the influence of a number of factors, such as the capability of the GPS receiver (e.g., how many channels it has to receive the signal from satellites simultaneously in locating the position), the ambient environment (e.g., whether the logging site is surrounded by tall cliffs or obscured by trees), data processing (e.g., whether the logged data are differentially corrected following

the data logging session), and the baseline length in case of RTK GPS. At a baseline of <500 m, the RMS error is as low as ±2.26 cm (Satalich and Ricketson 1998). The accuracy, speed, and efficiency of all-terrain vehicle-mounted RTK GPS prove that it is suitable for 3D survey of beaches, including dune fields (Harley et al. 2010).

In spite of its high accuracy and low cost, the GPS method is disadvantaged by its requirement of site access. Site restriction to sensitive dunes may limit logging to transects or at critical points of dune crests, ridges and peaks (Mitasova et al. 2005). The logging of data distributed throughout a dune field is a daunting task that may prove impossible occasionally. Logging of a huge amount of data certainly slows down data acquisition. Thus, it can be a very lengthy process to study a large dune field. The interpolated DEM may contain few details if sparse data points are contained in the input or when the surface is so irregular and hard to predict spatially. This problem, however, is easily overcome in airborne laser altimetry.

15.4.3 Laser Altimetry

Since their advent in the 1990s, airborne LiDAR technologies have advanced to such a level that they are able to map beach erosion, dune scarping, and overwash deposition with amazing detail. Such data are an excellent source for mapping dune erosion on the regional scale in a timely fashion. LiDAR data can be used to survey coastal topography and study short-term storm-induced changes to the dune system. Their ease of acquisition has enabled LiDAR data to quantify beach changes caused by extreme events such as hurricanes (Zhang et al. 2005). The swath of LiDAR data along the shoreline can also provide measurements of dune height and volume, which are important parameters in sediment budget calculations and in determining the susceptibility of the coast to storm damage (Gibeaut 2003).

In order to detect dune surface change, LiDAR point cloud data need to be interpolated into a regularly spaced grid or DEM in a manner reminiscent of GPS data. The DEM may suffer from spurious details in case of excessive data points in the input. During interpolation, the spatial resolution of the DEM must be specified the same as that of all other data layers used in the volumetric change detection. Moreover, these data layers must be geo-referenced to the same coordinate system. Any residuals in transforming the original datasets to the common system will propagate into the final detection results. More importantly, all data layers must use the same datum for surface height. Different datum levels need to be unified through data transfer. As with any change detection, systematic errors in each of the input layers must be checked and eliminated prior to change detection. Dune volume is calculated by differencing cell height multiplied by cell size.

In detecting dune surface and sand volume, the vertical accuracy of LiDAR data is more important than their positional accuracy. A vertical accuracy of 0.15 m is

possible if the laser scanner has a height of <1 km (Mitasova et al. 2005). The same mean accuracy level of 0.15 m (maximum: 0.3 m) is also reported over an inland test site (Chang et al. 2004). The LiDAR accuracy reported by Adams and Chandler (2002) is lower at 0.26 m. This discrepancy in the vertical accuracy of LiDAR data is due to several factors, one of the important ones being surface cover. If the dune field is covered by vegetation, it is imperative to discount its effect by recording multiple returns. The subtraction of the second return from the first return can effectively reveal vegetation height that should be deducted from the LiDAR spot heights in generating the dune surface model and in calculating sand loss.

Apart from airborne, LiDAR can be implemented as ground-based. Due to the short range, high resolution ground-based LiDAR achieved a positional accuracy of 6 mm at a spatial resolution of 10 cm, sufficient to study the morphology of sand dunes (Nagihara et al. 2004). Unlike its air-borne counterpart, terrestrial LiDAR survey is performed on transects. These transect data are converted to a continuous surface model of the dune field via spatial interpolation in a manner highly reminiscent of GPS. Although the surface model is able to depict the dune morphology, inaccuracy may result in detecting the vertical variation of the dune surface.

15.4.4 A Comparison

Each of the three methods has its own strengths and limitations in studying coastal change (Table 15.1). The GPS method, especially RTK GPS, is the most accurate, but can be very slow over a large area. This method requires logging of data distributed throughout the dune field. So it is the most restrictive in its deployment. Accuracy is ostensibly lower in remote and inaccessible spots where data logging is not feasible. Of the two remote methods, both LiDAR and digital photogrammetry tend to generate heights slightly lower than the terrain surface (Adams and Chandler 2002). Laser scanning is a quick and efficient method of obtaining 3D point data at a high density, much faster than GPS while photogrammetry is the slowest. However, the entire area of study can be viewed stereoscopically using this method. Laser scanning has a nominal vertical accuracy of 0.1 m. In reality, the actual accuracy achievable is lower due to the influence of terrain and surface cover. In fact, the quality of LiDAR data is heavily influenced by the conditions of scanning site (Lim et al. 2005). LiDAR is more accurate than photogrammetry consistently in monitoring soft cliffs. Its vertical RMS error of 0.26 m is much lower than 0.43 for photogrammetrically derived elevations that are more subject to the influence of slope. Elevation is overestimated in steeper slopes, and vice versa. The higher accuracy of LiDAR may be attributed probably to the lower (1,000 m) height of the scanner than aerial photography (2,375 m). This accuracy level is also affected by surface roughness. The low accuracy of the photogrammetric method (2.77 m) has also been reported by Chang et al. (2004). The varying levels of accuracy of the photogrammetric method are attributed to the accuracy of ground

Table 15.1 Comparison of the strengths and limitations of different methods in studying coastal evolution

Coastal feature	Photogrammetry	GPS	Laser scanning
Shoreline	Fast from existing photos; accuracy subject to the definition of shoreline	Fast, vehicle access essential for long beaches	Fast elevations, shoreline hard to determine based on height
Cliff	Rigorous but hard to identify cliff top due to shadow or trees; ground control not easy to establish	Inapplicable due to inaccessibility	Terrestrial scanning able to identify cliff face in addition to top; positive not accurate
Dune	Detailed and very reliable surface model if quality ground control exists; post processing complex, and slow	Dense points need to be logged throughout an area; inexpensive; time-consuming	Excellent for dune evolution as points are dense; fast but expensive

control, the scale and spatial resolution of the aerial photographs used. Irrespective of these factors, the photogrammetric method is the lengthiest and the least accurate as it takes a long time to plan the flight.

Since each of them has its unique strengths, in practice more than one method is utilized to gain a better understanding of rapid changes in coastal topography (Mitasova et al. 2004). This combination brings out more advantages. For instance, the integration of photogrammetry with airborne laser scanning can result in more accurate and complete products that will open new areas of application (Baltsavias 1999). The combined use of GPS and soft-copy photogrammetry seems to be the best in monitoring coastal changes (Ojeda Zújar et al. 2002). The combination of RTK GPS and LiDAR, assisted with improved spatial interpolation techniques, produces detailed topographic surfaces. LiDAR-derived elevation data combined with RTK GPS measurements enable the determination of the dynamics of beach topography, its geometric properties, and estimation of eroded and deposited sand volumes.

15.5 Summary and Conclusions

The coastal zone is a special geographic area that tends to change rather quickly over a short span as a consequence of both natural (e.g., waves and storms) and human (e.g., coastal settlement) processes. Such changes need timely monitoring and detection in order to mitigate coastal hazards and to safeguard infrastructure and properties in this visually appealing and environmentally sensitive zone. These changes can be monitored and detected using a number of geo-informatics technologies that include photogrammetry, GPS, and laser scanning. The photogrammetric method requires expertise in separating dry and wet beaches in interpreting shoreline position. By comparison, the GPS method is much faster,

especially if the receiver is mounted on a vehicle. Ground tracking avoids the ambiguity of shoreline position on photographs. The scanning method is quick in determining beach surface height, but does not yield shoreline position directly. If the shoreline height is projected to the LiDAR-derived DEM, then accuracy can be very high if a cross-shore fitting is applied. Both the photogrammetric and laser scanning methods are able to detect cliff tops from the air, even though the former is heavily disadvantaged by the presence of overhang trees and shadow. For this reason laser scanning yields more accurate results. Nevertheless, neither is able to detect cliff face that may contain minor but vital features indicative of landward retreat and cliff instability. This limitation can be overcome with terrestrial scanning or close-range photogrammetry. Terrestrial laser scanning is considered superior as such features as debris and tree branches on cliff faces can all be sensed. In detecting dune erosion, the photogrammetric method is able to yield accurate information over the entire study area but requires lengthy planning in acquiring stereoscopic aerial photographs. Similarly, airborne LiDAR is able to assess dune erosion quickly, and is more accurate than photogrammetry. Its accuracy is affected by scanning range, point cloud data density and topographic relief. The GPS method can be very accurate if RTK is used. Logging of data throughout the area of study makes this method very slow or even impractical in remote or inaccessible sites. Therefore, the combined use of such methods (e.g., use of RTK GPS for accurate ground control for photogrammetry) is preferred as it enables the changing coastal environment to be monitoring at an unprecedented frequency and accuracy with ever greater ease.

References

Ackermann F (1999) Airborne laser scanning – Present status and future expectations. ISPRS J Photogramm Remote Sens 54(2/3):64–67

Adams J, Chandler J (2002) Evaluation of lidar and medium scale photogrammetry for detecting soft-cliff coastal change. Photogramm Rec 17(99):405–418

Alexander PS, Holman RA (2004) Quantification of nearshore morphology based on video imaging. Mar Geol 208(1):101–111

Anders FJ, Byrnes MR (1991) Accuracy of shoreline change rates as determined from maps and aerial photographs. Shore Beach 59(1):17–26

Baltsavias EP (1999) A comparison between photogrammetry and laser scanning. ISPRS J Photogramm Remote Sens 54(2/3):83–94

Brock JC, Wright CW, Sallenger AH, Krabill WB, Swift RN (2002) Basis and methods of NASA Airborne Topographic Mapper lidar surveys for coastal studies. J Coast Res 18(1):1–13

Chang H-C, Ge L, Rizos C, Milne T (2004) Validation of DEMs derived from radar interferometry, airborne laser scanning and photogrammetry by using GPS-RTK. In: Proceedings of the IEEE international geoscience and remote sensing symposium (IGRASS), Anchorage, Alaska, 20–24 Sept 2004

Crowell M, Leatherman SP, Buckley MK (1991) Historical shoreline change: error analysis and mapping accuracy. J Coast Res 7(3):839–852

Featherstone WE, Stewart MP (2001) GPS equipment and its users for height determination. J Surv Eng 127:31–51

Fletcher C, Rooney J, Barbee M, Lim SC, Richmond B (2003) Mapping shoreline change using digital orthophotogrammetry on Maui, Hawaii. J Coast Res 38:106–124
Gao J (2003) Utility of IKONOS satellite data in studying the coastal environment. In: Proceedings of the New Zealand Geographical Society 22nd conference, Auckland, 6–11 July 2003, pp 58–62
Gibeaut JC (2003) LIDAR: mapping a shoreline by laser light. Geotimes 48(11):22–27
Gulyaev SA, Buckeridge JS (2004) Terrestrial methods for monitoring cliff erosion in an urban environment. J Coast Res 20(3):871–878
Hapke C, Richmond B (2000) Monitoring beach morphology changes using small-format aerial photography and digital soft-copy photogrammetry. Environ Geosci 7(1):32–37
Harley MD, Turner IL, Short AD, Ranasinghe R (2010) Assessment and integration of conventional, RTK-GPS and image-derived beach survey methods for daily to decadal coastal monitoring. Coast Eng. doi:10.1016/j.coastaleng.2010.09.006
Hicks SD, Sillcox RL, Nichols CR, Via B, McCray EC (2000) Tide and current glossary. NOAA National Ocean Service, Center for Operational Oceanographic Products and Services, Silver Spring, 29 p
Li R, Di K, Ma R (2004) A comparative study of shoreline mapping techniques. In: Bartlett D, Smith J (eds) GIS for coastal zone management. CRC Press, Boca Raton, pp 27–34
Lim M, Petley DN, Rosser NJ, Allison RJ, Long AJ, Pybus D (2005) Combined digital photogrammetry and time-of-flight laser scanning for monitoring cliff evolution. Photogramm Rec 20(110):109–129
Mitasova H, Drake TG, Bernstein D, Harmon RS (2004) Quantifying rapid changes in coastal topography using modern mapping techniques and geographic information system. Environ Eng Geosci 10(1):1–11
Mitasova H, Overton M, Harmon RS (2005) Geospatial analysis of a coastal sand dune field evolution: Jockey's Ridge, North Carolina. Geomorphology 72:204–221
Nagihara S, Mulligan KR, Xiong W (2004) Use of a three-dimensional laser scanner to digitally capture the topography of sand dunes in high spatial resolution. Earth Surf Process Landf 29:391–398
Ojeda Zújar J, Borgniet L, Pérez Romero AM, Loder JF (2002) Monitoring morphological changes along the coast of Huelva (SW Spain) using soft-copy photogrammetry and GIS. J Coast Conserv 8(1):69–76
Pan PSY (2004) Monitoring coastal environments using remote sensing and GIS. In: Bartlett D, Smith J (eds) GIS for coastal zone management. CRC Press, Boca Raton, pp 35–49
Quartel S, Addink EA, Ruessink BG (2006) Object-oriented extraction of beach morphology from video images. Int J Appl Earth Observ Geoinf 8(4):256–269
Robertson WV, Whitmantt D, Zhang K, Leathermant PL (2004) Mapping shoreline position using airborne laser altimetry. J Coast Res 20(3):884–892
Rosser NJ, Petley DN, Lim M, Dunning SA, Allison RJ (2005) Terrestrial laser scanning for monitoring the process of hard rock coastal cliff erosion. Q J Eng Geol Hydrogeol 38 (4):363–375
Ruggier OP, Cote J, Kaminsky G, Gelfenbaum G (1999) Scales of variability along the Columbia River littoral cell. Coastal sediments '99. ASCE, Long Island, pp 1692–1707
Satalich J, Ricketson R (1998) Field test of Trimble 4000 real-time kinematical GPS survey system. J Surv Eng ASCE 124:40–48
Schmidt F, Persson A (2003) Comparison of DEM data capture and topographic wetness indices. Precis Agric 4:179–192
Schupp CA, Thieler ER, O'Connell JF (2004) Mapping and analyzing historical shoreline changes using GIS. In: Bartlett D, Smith J (eds) GIS for coastal zone management. CRC Press, Boca Raton, pp 219–227
Shao G, Young DR, Porter JH, Hayden BP (1998) An integration of remote sensing and GIS to examine the responses of shrub thicket distributions to shoreline changes on Virginia Barrier Islands. J Coast Res 14(1):299–307

Stockdon HF, Sallenger AH Jr, List JH, Holman RA (2002) Estimation of shoreline position and change using airborne topographic lidar data. J Coast Res 18(3):502–513

Suchocki C (2009) Application of terrestrial laser scanner in cliff shores monitoring. Rocznik Ochrona Srodowiska 11(1):715–725

TopoSys GmbH (2004) Falcon LiDAR sensor system: airborne acquisition of digital elevation models and ortho images. Hamburg, Germany. www.toposys.com

Wangensteen B, Eiken T, Ødegård RS, Sollid JL (2007) Measuring coastal cliff retreat in the Kongsfjorden area, Svalbard, using terrestrial photogrammetry. Polar Res 26(1):14–21

Wehr A, Lohr U (1999) Airborne laser scanning—An introduction and overview. ISPRS J Photogramm Remote Sens 54:68–82

Young AP, Ashford SA (2006) Application of airborne LIDAR for seacliff volumetric change and beach-sediment budget contributions. J Coast Res 22(2):307–318

Young AP, Flick RE, Gutierrez R, Guza RT (2009) Comparison of short-term seacliff retreat measurement methods in Del Mar, California. Geomorphology 112(3–4):318–323

Zhang K, Whitman D, Leatherman S, Robertson W (2005) Quantification of beach changes caused by Hurricane Floyd along Florida's Atlantic coast using airborne laser surveys. J Coast Res 21 (1):123–134

Zhou G, Li R (2000) Accuracy evaluation of ground points from IKONOS high-resolution satellite imagery. Photogramm Eng Remote Sens 66(9):1103–1112

Zuzek PJ, Nairn RB, Thieme SJ (2003) Spatial and temporal considerations for calculating shoreline change rates in the Great Lakes Basin. J Coast Res 38:125–146

Zviely D, Klein M (2004) Coastal cliff retreat rates at Beit-Yannay, Israel, in the 20th century. Earth Surf Process Landf 29(2):175–184

Chapter 16
Spatial and Numerical Methodologies on Coastal Erosion and Flooding Risk Assessment

Jarbas Bonetti, Antonio Henrique da Fontoura Klein, Mariela Muler, Clarissa Brelinger De Luca, Guilherme Vieira da Silva, Elírio E. Toldo Jr., and Mauricio González

Abstract In the last decades the combination of an increasing human occupation along the coast combined with an anticipated intensification in the frequency of meteorological extreme events stimulated the development of different methodological alternatives to assess and predict coastal risk. Conceptually, a global risk analysis may involve susceptibility and vulnerability, in both temporal and spatial scales, with the goal of identifying critical hazard areas. In this work, two different analytical approaches are presented within the perspective of their future integration: spatial analysis based on Geographic Information Systems and numerical modeling. In the first approach, individual information layers associated with various themes (*e.g.* backshore landforms, backshore altitude, shoreline displacement, shoreline exposure to wave incidence and man-made structures at risk) were integrated and allowed the development of a numerical index of coastal vulnerability. In order to define inundation levels, a wave run-up study integrated numerical modeling and *in situ* measurements, allowing the recognition of sensible variations

J. Bonetti (✉) • A.H. da Fontoura Klein • M. Muler
Coastal Oceanography Laboratory, Department of Geosciences, Federal University of Santa Catarina, Florianópolis, SC CEP 88040-900, Brazil
e-mail: jarbas.bonetti@ufsc.br; antonio.klein@ufsc.br; muler.mariela@gmail.com

C.B. De Luca
Coastal & Port Engineering Master Program, University of Cantabria, 39005 Santander, Cantabria, Spain
e-mail: clarissabdeluca@gmail.com

G.V. da Silva • E.E. Toldo Jr.
Centro de Estudos de Geologia Costeira e Oceânica – CECO, Instituto de Geociências – IG, Universidade Federal do Rio Grande do Sul – UFRGS, Porto Alegre, RS CEP 91509 900, Brazil
e-mail: oc.guilhermevs@gmail.com; toldo@ufrgs.br

M. González
Instituto de Hidráulica Ambiental "IH Cantabria", Universidad de Cantabria, C/Isabel Torres No. 15, Parque Científico y Tecnológico de Cantabria, 39011 Santander, Spain
e-mail: gonzalere@unican.es

C.W. Finkl (ed.), *Coastal Hazards*, Coastal Research Library 6,
DOI 10.1007/978-94-007-5234-4_16,

along an embayed beach. Finally, an erosional hot spot area was investigated by calculating longshore sediment transport rates. For this, a numerical model of wave propagation defined the coastal wave climate and the average sediment budget was determined in the surf zone. The three case studies of beaches with historical sensibility to erosion and storm surge flooding presented a very good correlation with reality.

16.1 Introduction

During the last few decades there has been an increase in the frequency and intensity of natural disasters (Freeman et al. 2003). Events such as floods and storms seem to have intensified in the last century, especially after the 1950s (EM-DAT 2011; Freeman et al. 2003). In southern Brazil, for example, significant wave height is expected to increase by 2.5 cm/year and sea levels are estimated to rise by 1–3 mm/year (CEPAL-ONU 2011a). Global warming can make these events worse (Pezza and Simmonds 2005), impacting those living close to the coast. Inundations levels, i.e., the topographic level achieved by a certain event, that cause coastal flooding and coastal erosion are closely related to climate changes. Destruction of man-made structures located close to the shoreline as a result of the erosion process depends on the elevation achieved by the water relative to the height of the adjacent beach (Ruggiero et al. 2001).

Coastal erosion is the encroachment of land by the sea and is measured using the average over a period of time that is sufficiently long enough to eliminate the impacts of weather, storm events and local sediment dynamics. Coastal erosion is usually the result of a combination of factors, both natural and human-induced, that operate on different scales. As expressed under the framework of the EUROSION European project (EUROSION 2004), the most important natural factors are as follows: (1) winds, (2) storms, (3) near shore currents (wave-induced and/or tidal currents), (4) relative sea level rise and (5) slope processes (collapse, slippage, or toppling of coastal cliff blocks). On the other hand, human-induced factors of coastal erosion include the following: (1) river basin regulation works, (2) coastal structures in urban, tourist or industrial coastal zones, (3) land claiming, (4) dredging, (5) vegetation clearing (dune areas and on the top of cliffs) and (6) gas mining and water extraction. The resulting coastal erosion can be related to three different types of impacts: (1) loss of land with economic value, (2) destruction of natural sea defenses (usually a dune system) as a result of a single storm event, which causes the backshore to flood more easily and (3) undermining of artificial sea defenses, potentially leading to an increased flood risk.

Coastal flooding is a random phenomenon arising from the combination of various marine processes. In a simplified form, this phenomenon can be represented as shown in Fig. 16.1. At a given time, a point on the coast is characterized by a certain reference sea level comprising the astronomical and the meteorological

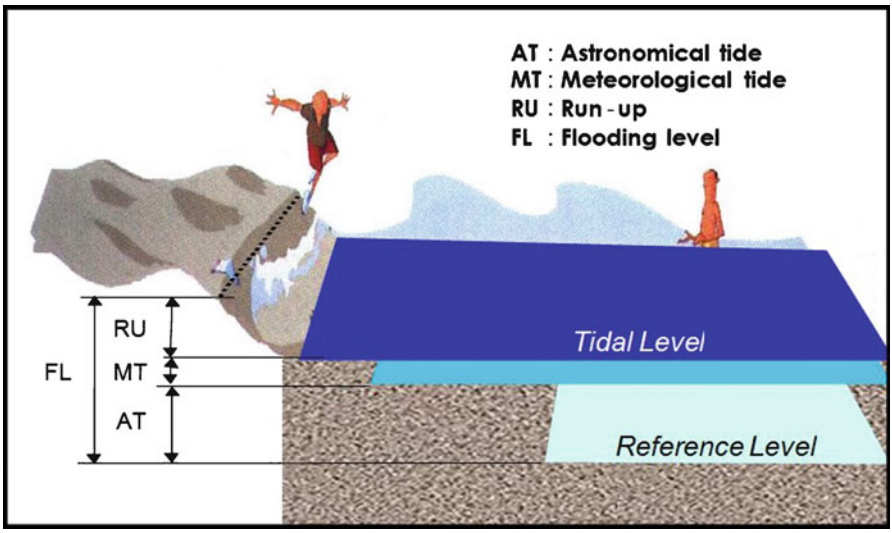

Fig. 16.1 Schematic diagram of the factors affecting the flood level at a certain point on the coast

tides (AT + MT) and the bathymetry. The MT may include super-elevations caused by hurricanes and the effects of el Niño and la Niña (ENSO). In addition to this level are the swell waves which, depending on their characteristics and the bathymetry close to the beach, are propagated toward the coast. When reaching the coast, the swell breaks (on the beach, levee or rockfill breakwater, waterfront, etc.) producing an upward movement of the water mass along the coastal profile, called run-up (RU). All of these factors are inter-related. In addition to the interaction between the elements (tidal level, bathymetry, swell and run-up), the phenomenon of flooding offers the added complication that some factors (waves and winds) cannot be easily predicted in advance due to their random behavior; therefore, their effects are related to a given probability of occurrence.

To evaluate coastal impacts associated with flooding and long-term erosion processes, one possible conceptual framework is based on the definition of risk as the probability of harmful consequences or expected losses resulting from a given hazard to a given element in danger of peril over a specified time period (Schneiderbauer and Ehrlich 2004). Therefore, risk depends on the specific impact analyzed (e.g., loss of human lives), the probability that the threat will occur (e.g., flooding frequency), the exposure of the studied elements (e.g., presence of urban areas) and their adaptive capacity (e.g., sensitive groups and their resilience).

The hazard assessment is based on the numerical modeling of the dynamics under study (waves, sea level, erosion, etc.) to understand the probability, frequency, intensity, and duration of a hypothetical event, as well as the potentially affected area. Once the hazards have been identified and analyzed, vulnerability assessments are carried out for each identified hazard and for each location. The comparison between hazard and vulnerability assessment results will provide

information about the real risk a certain coastal sector is subjected to. The vulnerability assessment of the exposed elements, given the complexity of coastal areas, is based on an integrated approach, which is essential to consider the interrelationships between the various coastal dimensions and spatial variations. This assessment is usually based on the development of a set of themes and descriptors supported by a Geographic Information System that allows for the graphical and spatial representations of physical, environmental, social, economic and infrastructure characteristics of the coast. Different spatial and temporal scales should also be considered because both factors change the amount and type of the exposed elements (susceptibility) and their vulnerability. A final global risk analysis (hazard, susceptibility and vulnerability analyses for every dimension using both temporal and spatial scales) identifies critical areas and the coping capacity weaknesses, allowing the formulation of a set of risk reduction measures.

Coastal vulnerability and hazard assessments are based on the spatial analysis of the exposed elements and the numerical modeling of the dynamics. Some methodological approaches and numerical tools to evaluate these elements are discussed in the following sections and will be illustrated with some case studies applied to southern Brazil.

16.2 Spatial Analysis

The analysis of the exposed spatial elements and their vulnerability is an initial step to evaluate the consequences of coastal impacts and associated risks because it provides, by itself, a comprehensive diagnosis for coastal hazards (flooding, erosion, climate change, etc.). Once existing elements of the coastal landscape that indicate real exposure have been accounted for, hot spots along the coast can be identified with a degree of accuracy.

Although the term vulnerability may be found in the literature associated with different concepts, it is generally related to human interaction with the environment (Cutter 1996; White et al. 2001; Alcántara-Ayala 2002; Wu et al. 2002; Dolan and Walker 2003; ISDR 2004; UNDP 2004). Vulnerability may be considered as a function of a pre-existing condition of hazard exposure (susceptibility) and the capacity for community adaptation, i.e., the combination of natural hazards and the human exposure to them.

Many proposals for vulnerability analysis have been explored internationally due to the apparent increase of natural disasters. In Brazil, serious disasters have been reported concerning river floods and landslides, which in many cases were associated with casualties. Therefore, vulnerability assessments gained importance, becoming highly relevant for the protection of the population. Those assessments identify and characterize risk areas and vulnerable settlements, helping decision makers to effectively determine prevention and mitigation strategies.

There are different alternatives to assess vulnerability. A popular European methodology was presented in the project DINAS-COAST – “Dynamic and

Interactive Assessment of National, Regional and Global Vulnerability of Coastal Zones to Climate Change and Sea-level Rise", that applied a tool called the Dynamic and Interactive Vulnerability Assessment (DIVA). This tool encompasses a global database, an integrated model and a graphical user interface that enable users to produce quantitative information about a range of coastal vulnerability indicators to select climatic and socio-economic scenarios and adaptation strategies (Hinkel and Klein 2009). DIVA is efficient for small-scale analysis but may not be useful for coastal planning, which usually requires more detail than what is visible in national or regional maps.

The vulnerability assessment and methodology for the regional study on the effects of Climate Change along the coast of Latin America and the Caribbean (CEPAL-ONU 2011a, b, c) focus on the physical, socioeconomic and ecologic conditions of the region's coastal areas. Overall, 15,000 units of study representing 5 km in area and variables such as land surface, land uses, croplands, ecosystems, population, infrastructures or coastal typologies were characterized and studied to define a quantitative assessment of the coastal vulnerability and exposure to marine hazards. The methodology for this robust diagnosis was also developed on small to regional scales, which must be taken into account for the practical application of its results.

Another methodology for the vulnerability assessment was designed by the National Oceanic and Atmospheric Administration's Coastal Services Center and is called "The Community Vulnerability Assessment Tool (CVAT)" (Flax et al. 2002). Its goal is to assist emergency managers and planners in their efforts to reduce hazard vulnerabilities by creating hazard maps, overlaying those maps (representing different hazards) and finally using a scoring system, which gives the greatest values to the most vulnerable areas. This approach deals specifically with socioeconomic factors.

The State of Hawaii has an atlas of natural hazard assessments comprised of a technical map series displaying the ranked nominal intensity of each hazard (Fletcher et al. 2002). Those rankings are applied as a relative scale based on a logical interpretation of environmental variables, such as geology and coastal zone slope. Additionally, this publication compiles and constructs a hazards' history in the Hawaiian Islands. With continued monitoring, the aim is to predict the chronology and intensity of hazards, which is extremely important for coastal management.

The "Geomorphic Stability Mapping – GSM", an Australian approach proposed by Sharples (2006), is an indicative and descriptive mapping of geomorphic vulnerability to coastal hazards. It considers the basic coastal geological and geomorphic characteristics that may be related to vulnerability, such as intertidal landforms, backshore landforms, backshore profiles, shoreline exposure and rock types. For this method, the shoreline is segmented, bringing multiple pieces of information attached to the vector lines representing the coast. Because descriptive maps are not always easy to compare or interpret by decision makers, this approach is an important first step to investigative the effort necessary to recognize an area of interest.

Another important methodology is the Coastal Vulnerability Index (CVI) proposed by Gornitz (1991) and the United States Geological Survey (USGS). This approach is a relative ranking based on scaled indexes wherein each factor receives a value for vulnerability classification. Those factors are relief, rock types, landform, relative sea-level change, shoreline displacement, tidal range and maximum wave height and are integrated in a mathematical relation (weighted sum) to obtain to the final vulnerability indication.

It is important to underline that, although the CVI (Gornitz 1991) and the GSM (Sharples 2006) work well in applied studies, they consider vulnerability exclusively related to physical factors. In practical terms, it is essential to include human factors, taking into account that damage occurs due to human presence/influence in the environment. In other words, an effective vulnerability assessment has to consider human losses; otherwise, it may be considered a susceptibility measurement.

These approaches all try to recognize relationships and integrate descriptors to generate new information and spatial analysis using Geographic Information Systems (GIS) is the tool usually adopted for this type of research.

Vulnerability assessments require a structured database that integrates environmental, social, economic and political factors to be used as proxies for the evaluation of the degree of vulnerability.

In Brazil, specifically, the lack of reference data has been a strong limitation to a comprehensive understanding of coastal environments on a more complex or extensive analysis. Although an improvement is expected in the next years, at the moment the available data are accessible from different sources that are not always interoperable and sometimes lack metadata because they are not obtainable from centralized spatial data infrastructures (SDI).

Once obtained, the data can be inserted and represented in a GIS using two basic models: raster and vector. The choice of the data model will depend on how they will be individually categorized into classes of vulnerability and crossed, aiming for a final integrated assessment. Most of the time, different scales and legends have to be harmonized, causing technical difficulties in model construction and forcing researchers to spend a considerable amount of time on structuring the database. To improve the flux of activities, geodatabase models are important in the edifice of the correct structure that will be used to establish the relations and interactions between the data. Currently, it is essential to adequately choose the spatial data model that best fits the selected data. For instance, the GSM presents its results as vectors while the CVI has both vector and raster representations (Gornitz 1991; Thieler and Hammar-Klose 2000).

16.2.1 Case Study

In this example, spatial analysis was used to assess coastal vulnerability to storm surges. The adopted geoprocessing technique was the weighted sum of data layers applied to the creation of an index that could represent the vulnerability in a

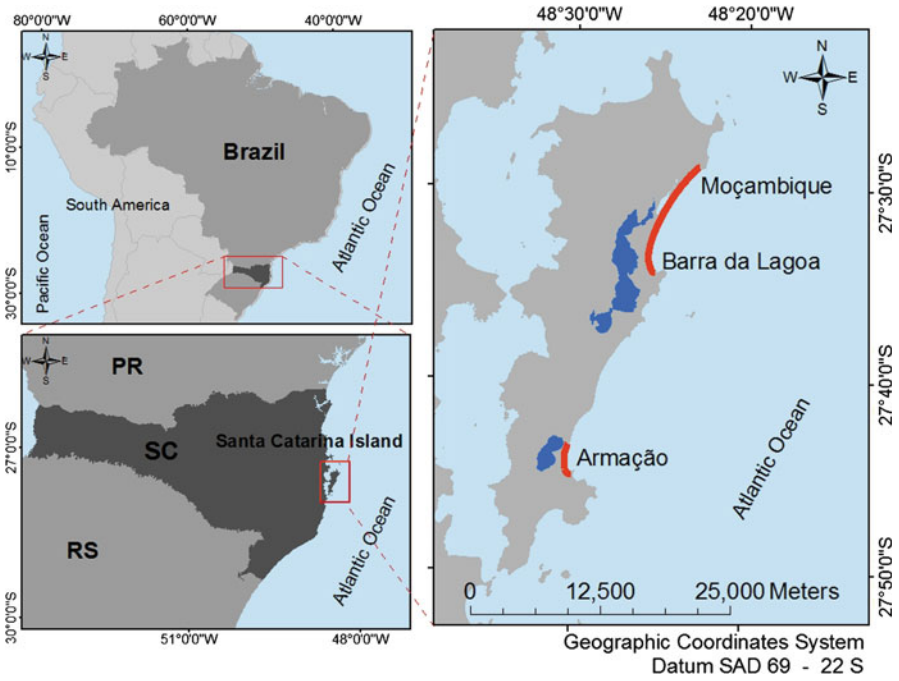

Fig. 16.2 Location of the interest areas in southern Brazil with details of Santa Catarina Island and the studied beaches (*red lines*)

practical and efficient way. This index was based on the CVI (Gornitz 1991); however, the variables considered were different because they were adapted to a local scale taking into account the availability of data for study area. Thus, this research aimed to identify the best descriptors for the vulnerability analysis in the local context.

Extreme events affect the coast disproportionately and damage will depend on the environmental, social and economic characteristics of the coastal sector. Therefore, it is efficient to segment the coastline in homogeneous parts and to classify them individually. Vector representation was chosen, thus relevant information related to vulnerability was attached to the shoreline feature.

The study sites were two beaches located on Santa Catarina Island (Florianópolis – SC, Brazil) that have suffered damages due to storm surges in the last few years: (1) the beach arc between Barra da Lagoa and Moçambique, which is located on the central-east coast and (2) Armação beach, which is located on the southern coast (Fig. 16.2).

Among Santa Catarina's coastal municipalities, Florianópolis is the most threatened by storm surges, experiencing damage most often (Rudorff et al. 2006), which causes severe consequences to coastal communities, such as the destruction of facilities and tourism devaluation.

The proposed index includes five descriptors for the vulnerability assessment. The first refers to backshore landforms and considers the main characteristics related to land use, vegetation, dune features, etc. of the areas adjoining the sandy beaches. The results were obtained by visually classifying high resolution satellite images. The second variable was the backshore altitude, considering that flat areas are more susceptible to inundation. Heights were obtained from detailed planialtimetric charts with a scale of 1:2.000.

The third input variable was shoreline displacement to obtain a better understanding of the dynamics of this feature over the last few decades. The five decades time series of shorelines was extracted from aerial photographs processed by the ArcGIS extension (DSAS – Digital Shoreline Analysis System; Thieler et al. 2009 by USGS) that calculates the shoreline displacement rate (meters per year) for the period covered by the photos.

A fourth descriptor was shoreline exposure to wave incidence. The mean shoreline orientation was associated with wave incidence direction and with the frequency of extreme events registered for each direction. Another ArcGIS extension from the USGS, the Wind Fetch Model (Finlayson 2005), was used to estimate the wind fetch. For the statistical analysis of extreme events, a wave database covering the period from 1948 to 2008 was used.

The fifth implemented variable in the vulnerability assessment was related to population and buildings at risk. Structures facing the sea were quantified from 2009 Quickbird images and then the constructed area was delimited as a polygon feature. The inland extent of the vulnerable area was determined by considering its predicted position in the next 50 years from the trend identified in a 52-year series of aerial photos. Using census data (IBGE 2010), it was possible to estimate the number of residents in the risk area.

The final index calculation followed the formula: $CVI = \frac{\left(\sqrt{a \times b \times c \times d \times e}\right)}{n}$, where a, b, c, d, e are the variables described above after categorization (attribution of vulnerability intervals, from 1 to 5) and n is the number of considered parameters. The final vulnerability classification (from very low = 1 to very high = 5) was based on percentiles obtained from the CVI results. This estimate can be easily performed using ArcGIS by combining the shoreline segments containing information on the five parameters.

The results showed areas of very low and low vulnerability in the north sector of Armação beach and in the central and north sections of Barra da Lagoa/Moçambique arc (Fig. 16.3), all of which have very low populations. In the central part of Armação beach, the vulnerability reaches moderate values and to the south, where effective erosion problems are concentrated, vulnerability presents high and very high values. This sector of very high vulnerability coincided with the area where houses were destroyed by waves in a storm surge event in the year 2010. The same thing happened at Barra da Lagoa/Moçambique (Fig. 16.4), where its southern sector had more vulnerable index values (moderate and high).

This proposed index is relatively simple to apply, but it should not be considered a fast preliminary approach because it requires specific data from different nature and a diversity of sources. Because the required data are not always available in

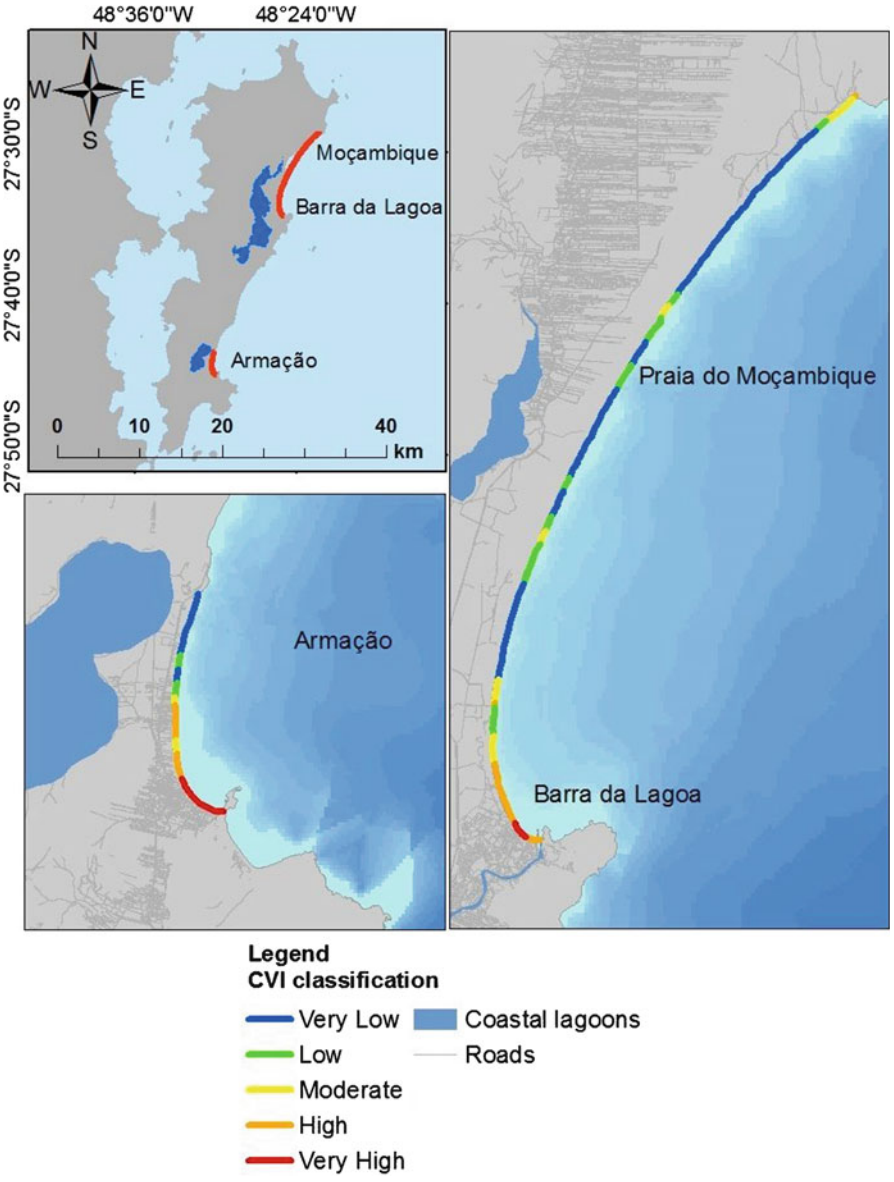

Fig. 16.3 Resulting vulnerability index map obtained for Moçambique, Barra da Lagoa and Armação beaches

an appropriate GIS format, the assembly and treatment of the reference data can be very time consuming.

Although the index still generates only an indicative coastal vulnerability assessment, such as the GSM or the CVI methodologies, there are two important differences that will be explored in more detail in future studies. First, this new

Fig. 16.4 Morphological impacts of an extreme storm event (April 2010) along the beaches of Barra da Lagoa and Moçambique (Photos by J. Bonetti)

index is suitable for local scale assessment, which allows it to more efficiently support applied development planning. Second, the effects of population and man-made structures were incorporated, allowing the quantification of the losses that may result from erosional processes induced by extreme storm surges.

16.3 Numerical Modeling

The practice of numerical modeling has grown during the last few years due to the improvement in both the knowledge of coastal dynamics and computer processing capability. Numerical modeling uses data from the past (e.g., a hindcast of waves, wind, currents, tides, and total levels) to understand the ocean processes according to a given spatial scale and tries to predict coastal behavior (forecasting). Considering the wide range of numerical models available, it is important to choose the one that best fits the aim and the spatial/temporal scale of the project. That choice will depend on: (a) the model operability, (b) the type of dynamic to be analyzed and (c) the spatial scale to be considered.

Ease of model operation combined with a poor understanding of the modeled dynamics can lead to incorrect results, which may induce misinterpretation. Misinterpretation can be avoided by having a good theoretical background and by critically analyzing the results.

Despite the increase in computer processing capabilities, it's still not possible to calculate/account for the transformation that happens on macro scales (kilometers/centuries) by integrating mega or micro scale processes (centimeters/minutes) (Cowell and Thom 1997). Processes that occur on different scales must be analyzed using a wide range of models and formulations. Because of this, it is very important to define the scales (both spatial and temporal) that processes should be modeled to apply the best model.

The database characteristic used as an input in the modeling process is an important point to be considered. Data with high spatial and temporal resolutions are necessary in coastal hazards studies, such as inundation levels and beach erosion because they guarantee a detailed study about the environment and fortify the decision making process.

After defining a problem, the processes that govern it, the spatial and temporal scales, and the data available, a model should be chosen and applied to the study area. As examples, two model applications will be shown in this section to assess coastal hazards: (a) inundation levels and recurrence intervals and (b) beach erosion.

16.3.1 Case Studies

16.3.1.1 Common Aspects of the Methodology

To assess both recurrence times of inundation levels and beach erosion it is important to have a wave climate established near the study area. To do that, a 60-year dataset was used. The astronomical tide data (1948–2008) was generated by a TPXO (TOPEX/Poseidon Global Inverse Solution) model (Egbert et al. 1994; Egbert and Erofeeva 2002) using eight tidal harmonic constants (M2, S2, N2, K2, K1, O1, P1 and Q1). Meteorological data were obtained using a numerical model (ROMS – Regional Ocean Modeling System) developed by the Rutgers Ocean Modeling Group; its formulations were described by Shchepetkin and McWilliams (2003). The 60-year wave hindcast dataset was transferred from deep water to shallower water by using a SWAN model (Booij et al. 1999), and its parameters were obtained at the study area. The wave hindcast data were calibrated using satellite data (TOPEX), Reguero et al. (2012). This was performed by propagating 200 wave cases using a case selector (MaxDiss) and re-constructing the complete series using an interpolation method (RBF), as proposed by Camus et al. (2011a, b).

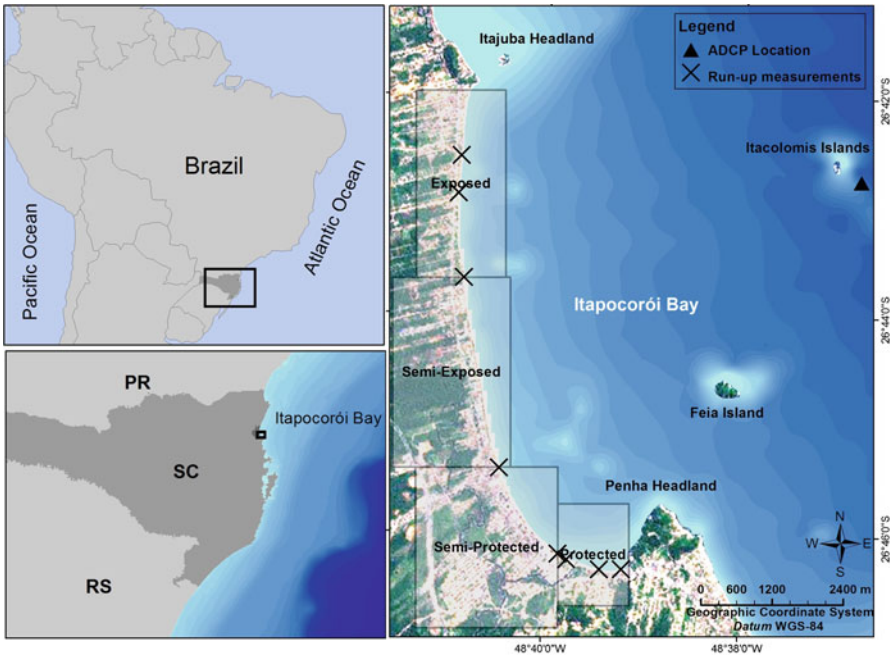

Fig. 16.5 The wave run-up measurement points on the beach face (X) and the ADCP (*triangle*) moored at Itapocorói Bay in the northeastern state of Santa Catarina (Background satellite image source: Google Earth)

16.3.1.2 Inundation Levels

The case study area is a 9 km long embayed beach located in southern Brazil (Fig. 16.5). Its southern part (Itapocorói beach) is protected from wave action by the presence of a headland. Araujo et al. (2010) classified it as a dissipative beach, being its southernmost part composed by fine sands and a narrow beach profile (about 50 m wide). Toward the north, the energy increases and the beach (Piçarras) becomes reflective, characterized by medium sand and a wider (up to 200 m), sub-aerial beach profile.

To assess the wave run-up behavior along the embayed beach, a numerical model was used in conjunction with a methodology to evaluate the headland influence over the wave run-up. Field work was carried out to calibrate the wave run-up formulations. Wave and tidal data were obtained for a period of 1 month (by mooring an ADCP-AWAC) and, on separate occasions, wave run-up data were determined over 30 min at each of the seven points along the shoreline (Fig. 16.5) using a dynamic positioning system (GPS-RTK). The beach profile has been measured using a trigonometric method (with a total station) to calculate the

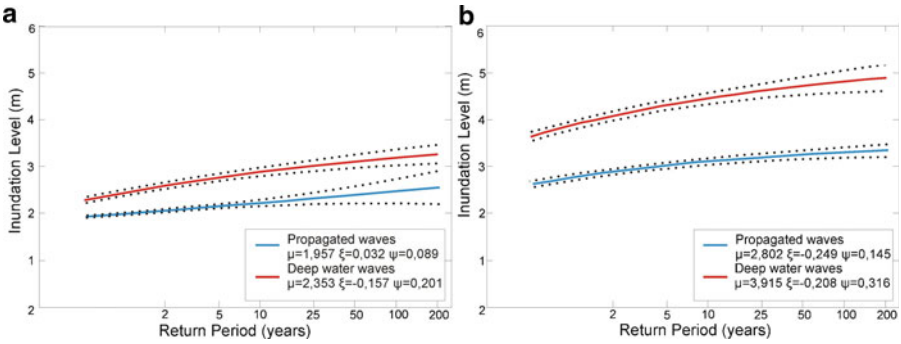

Fig. 16.6 Return period calculated for protected (**a**) and exposed beaches (**b**)

beach face slope. As expected, the available wave run-up formulation worked for the exposed area but did not present a good performance for the protected sector. Formulation developed by Nielsen and Hanslow (1991) was then calibrated for four distinct beach sectors: protected, semi-protected, semi-exposed and exposed, according to a best-fit linear regression.

The calibrated equations for each sector are as follows:

Protected: $R_{2\%protected} = 0.269 \times R_{2\%Nielsen\ and\ Hanslow\ (1991)} + 0.360$
Semi-protected: $R_{2\%semi-protected} = 0.195 \times R_{2\%Nielsen\ and\ Hanslow\ (1991)} + 0.59$
Semi-exposed: $R_{2\%semi-exposed} = 0.529 \times R_{2\%Nielsen\ and\ Hanslow\ (1991)} + 0.421$
Exposed: $R_{2\%exposed} = 0.601 \times R_{2\%Nielsen\ and\ Hanslow\ (1991)} + 0.603$

Having the wave climate near the study area (same position as the ACDP-AWAC was moored, at 15 m depth) and the hourly astronomical tides, meteorological tides and wave run-up data, the inundation levels were calculated by summing these data for each hour of the series, resulting in an hourly inundation level from 1948 to 2008. A return period was also calculated for each beach sector. To do that, a maximum annual significant wave height was identified and then a Generalized Extreme Value (GEV) function was applied over the series. To compare the efficiency of the wave propagation method used to assess coastal flooding, the inundation levels were calculated for both propagated and offshore wave data. The results are shown in Fig. 16.6.

By analyzing Fig. 16.6, the importance of using a wave model to transfer wave data to the study area and the importance of calibrating the wave run-up equations becomes clear. Wave models can reproduce most of the processes that a wave undergoes as it propagates to shallower water, and the propagated waves are more realistic to assess coastal hazards because they represent the real sea state of the study area. Additionally, wave run-up calibration has an important role in assessing coastal flooding on embayed beaches. The available formulations were developed for exposed areas, and if they were applied without a calibration the results would be overestimated (over 2 m), especially in the protected sectors of the beach.

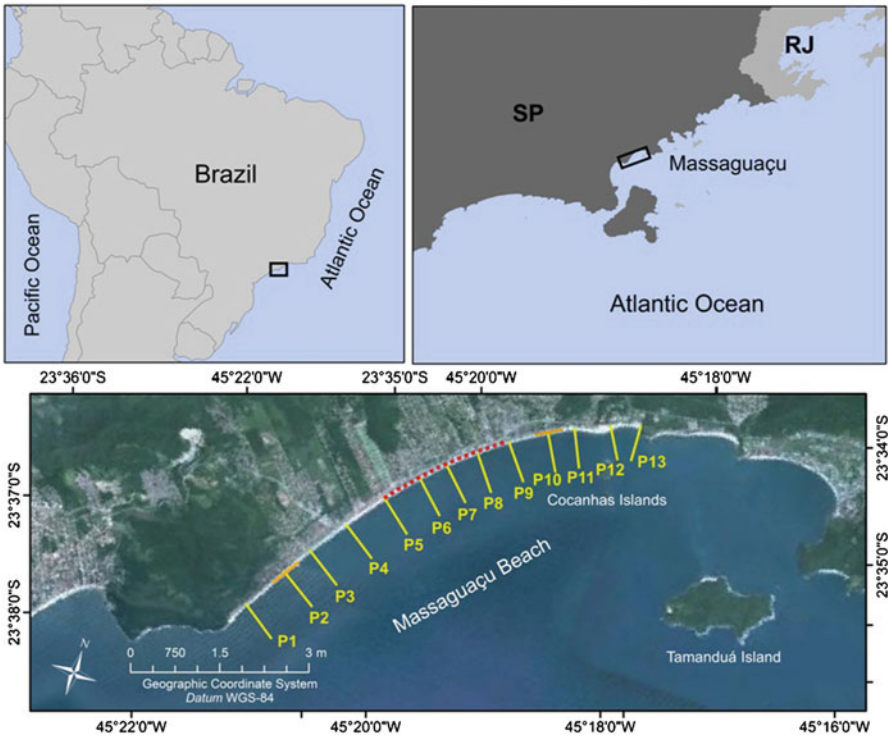

Fig. 16.7 Location of beach profiles at Massaguaçu beach, state of São Paulo. The littoral drift was calculated for the surf zone (*yellow lines*), the shoreline position of each profile appears in *orange* and the erosional hot spots identified by Nuber (2008) are the *red points* (Background satellite image source: Google Earth)

16.3.1.3 Beach Erosion

The chosen area for this study is an embayed beach located in Southeastern Brazil that is approximately 7.5 km in length called Massaguaçu (Fig. 16.7). Over the past few decades, this beach has been experiencing erosion, with high retreat rates in some segments, commonly termed as Erosional Hot Spots (EHSs; singular EHS). Nuber (2008) identified these areas along the central part of Massaguaçu during the period from 2006 to 2008 (Fig. 16.7). According to Kraus and Gangano (2001), depending on the cause of the erosional hot spot, the redistribution of the eroded material may create or preserve one or more accumulation areas along the beach (Erosional Cold Spot, ECS).

Waves, currents and the sediment supply are the primary controls of the longshore sediment transport process, and the evaluation of the causes and consequences of erosion requires an understanding of the processes involved in sediment transport and the local sediment budget. In this example, erosion is

represented on a local scale by the sediment transport generated by wind waves in the surf zone.

To calculate the longshore sediment transport in the surf zone, the wave climate had to be transferred to coastal areas (Camus et al. 2011a, b), and a numerical model of wave propagation had to be run (OLUCA-SP; González et al. 2007, 2010; Raabe et al. 2010). The purpose was to obtain the wave climate at specific points in the surf zone, where it was considered relevant to calculate sediment transport. The CERC (1984) formula (Shore Protection Manual, modified by Del Valle et al. 1993) was used to predict the total rate of the longshore sediment transport.

The following results represent the annual average of net longshore sediment transport rates during the period from 1948 to 2008 (Table 16.1 and Fig. 16.8). The estimate was carried out using values corresponding to D50 (mean grain size) in the studied profiles and the shoreline position, assuming that each profile represents the mean transport condition for the area in which it is located.

Waves and currents can transport considerable amounts of sediment along the coast and the longshore sediment transport will often be the dominant factor in the sediment budget. This is particularly important on an embayed coast, where the presence of large physical barriers (headlands) trap alongshore-moving sediment, resulting in net erosion/accretion at the updrift/downdrift ends of the beach (Harley et al. 2011). In this study, this process is represented by italic (erosion) and bold (accretion) numbers, respectively, in Table 16.1.

The values of net sediment transport in Table 16.1/Fig. 16.8 show an irregular transport in both directions between profiles 1 and 4 (Fig. 16.9) due to the presence of a rocky ledge that causes irregular currents in the SW part of the beach. As a result, consecutive erosion and accretion zones can be observed there.

Between profiles 5 and 6, it is possible to identify an erosional process that extends to profile 10 due to divergent directions of sediment transport and the occurrence of oblique waves resulting from local shoreline instability. The results obtained by Nuber (2008), using sedimentological and morphological data, show that Massaguaçu beach, in this zone, can be characterized as an erosional hot spot.

Furthermore, it is important to emphasize that the sediment accumulation in profiles 11, 12, and 13 are the result of a decrease in the sediment transport rates (possible cold spot areas). Nuber (2008) observed a shoreline progradation of up to 15 m in this section during the period from 2006 to 2008.

An appropriate transport dynamic representation was obtained from Massaguaçu beach by numerical modeling, which corroborates the real environment situation. After analyzing the sediment transport at Massaguaçu beach and the beach plan and profile forms using long-term models, it can be concluded that the existing erosion process in the central part of this beach is due to a non-equilibrium in plan-form from profile 5 to profile 11. This the lack of equilibrium generates a current system that is highly dependent on incident waves, which transport fine sediments from SW to NE. This system favors an accelerated erosion process in the central portion of the beach (erosional hot spot area) and sediment accumulation on its NE side (a possible cold spot area).

Table 16.1 Sediment transport rates at Massaguaçu beach (105 m^3/year)

Profiles	1	2	3	4	5	6	7	8	9	10	11	12	13
Positive (+)	0.32	0.45	0.61	0.61	2.45	0.16	0.095	0.0001	0	0	0.005	0.61	4.28
Negative (−)	0.45	0.44	0.92	0.58	0.12	1.02	1.40	2.0	3.5	4.16	1.15	1.76	0
Liquid	*−0.13*	**0.01**	*−0.31*	**0.03**	*2.33*	*−0.86*	*−1.31*	*−2.0*	*−3.5*	*−4.16*	**−1.15**	**−1.15**	**4.2**

Positive values represent the net sediment transport in the NE-SW direction and the negative values represent the opposite transport direction (SW-NE). Liquid transport values in *bold represent accretion* and *italic values represent erosion processes*

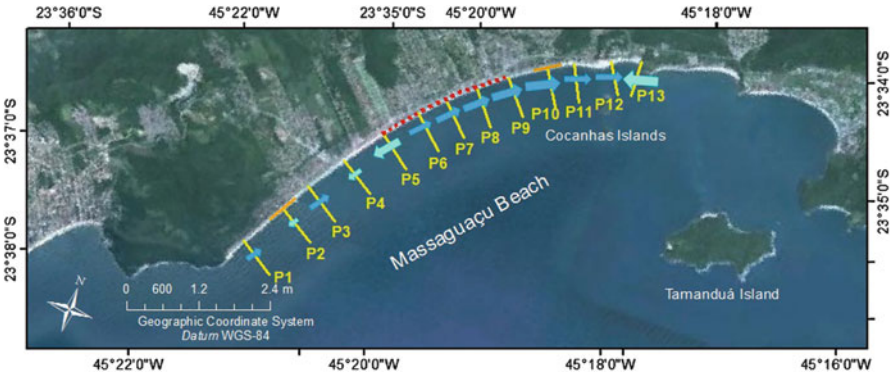

Fig. 16.8 A conceptual model of net sediment transport variability at Massaguaçu beach. *Cyan arrows indicate* the net sediment transport to the NE and the *blue arrows* represent the opposite transport direction. *Red points* are the erosional hot spots (Nuber 2008) (Background satellite image source: Google Earth)

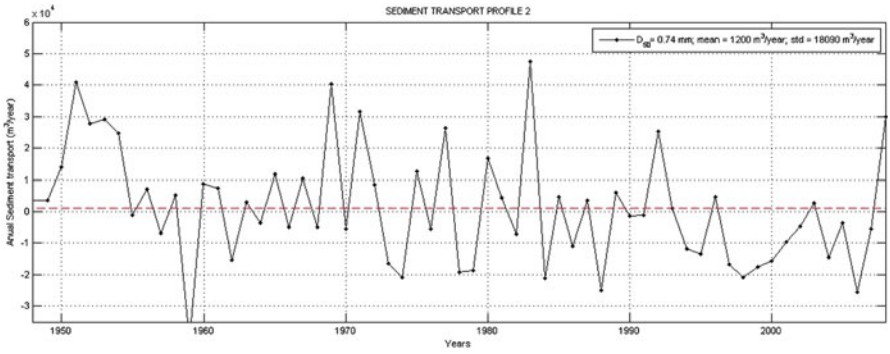

Fig. 16.9 Annual average of net long shore sediment transport in profile 2

16.4 Concluding Remarks

16.4.1 Spatial Analysis

The organization of spatial data in open and integrated infrastructure services is a relatively new task and, due to the lack of structured information in many countries, vulnerability maps tend to be subjective and based on the perception of the exposure to coastal hazards. However, in the last decade, many quantitative approaches for susceptibility mapping have been proposed, most of which were developed at regional or national levels, using small-scale data and not directly quantifying human exposure in the assessment (vulnerability).

The dichotomy of spatial model selection (raster vs. vector) seems to have been overcome, being the main actual challenge the adequate selection of the representative variables and their categorization in significant intervals.

In this chapter, an alternative that incorporates previous approaches related to the coastal vulnerability index calculation is proposed. The inclusion of a shoreline change forecast associated with sea level rise rates allowed for the quantification of the zone at risk under the worst case scenario. Additionally, the statistical analysis of the wave climate and the weighted integration of the most important wave directions with the areas of urban settlements allowed for a more precise definition of the areas sensitive to coastal flooding by storm surges and other extreme events.

16.4.2 Numerical Modeling

A robust method to quantify the level achieved by an instantaneous event (inundation level) and its return period was also presented here. The errors caused by imprecise data, especially by estimating wave run-up on bay beaches, have been minimized by calibrating equations and by transferring wave data close to the study point. In this study, the observed overestimation (not considering wave propagation) could reach over 1 m. In terms of affected surface, it can be even more important. Considering that, this work may be very valuable for coastal managers because it indicates the area that may be affected by coastal flooding without overestimating the levels achieved by an event within a certain recurrence period.

The beach erosion model was able to quantify the sediment transport rate through simulations, and the results corroborated field data. Thus, numerical modeling of sediment longitudinal transport at embayment beaches can be used as a valid tool to determinate the final form of a beach after a period of time, indicating the sectors that are more sensitive to erosion in an intermediate spatial scale between run-up and assessment estimations.

Although spatial analysis and numerical modeling have been applied separately in the presented examples, the authors expect that both approaches will be used in an integrated methodology to assess/define exposure to coastal hazards. Further studies are needed to define how spatial assessment results obtained in different spatial scales could feed numerical forecast models.

Acknowledgements The authors are thankful to the IH Cantabria and to the Oceanographic Institute of the University of São Paulo who provided the necessary data used in the study of the erosion at Massaguaçu beach and the wave/tides hindcast for Itapocorói Bay. We also thank the UNIVALI for the field support in the run-up experiment and Shawn Brazil in the wave attenuation experiment. This research was partially supported by a CNPq fellowship and by the CNPq Project 575008/2008 – CTTrans.

References

Alcántara-Ayala I (2002) Geomorphology, natural hazards, vulnerability and prevention of natural disasters in developing countries. Geomorphology 47:107–124

Araujo RS, Sprovieri FC, Freitas D, Klein AHF (2010) Variation in beach morphology and identification of an erosional hot spot at Itapocorói Bay. SC Braz J Aquat Sci Technol 14:29–38

Booij N et al (1999) A third-generation wave model for coastal regions, part I, model description and validation. J Geophys Res 104:7649–7666
Camus P, Mendez FJ, Medina R (2011a) A hybrid efficient method to downscale wave climate to coastal areas. Coast Eng 58:851–862
Camus P et al (2011b) Analysis of clustering and selection algorithms for the study of multivariate wave climate. Coast Eng 58:453–462
CEPAL-ONU (2011a) Dinámicas, tendencias y variabilidad climático. Docu-mento 1 del estudio de "Efectos del cambio climático en la costa de América Latina y el Caribe"
CEPAL-ONU (2011b) Vulnerabilidad y exposición de las costas de ALyC frente al Cambio Climático. Documento 2 del estudio de "Efectos del cambio climático en la costa de América Latina y el Caribe"
CEPAL-ONU (2011c) Impactos del Cambio Climático en las costas de ALyC. Documento 3 del estudio de "Efectos del cambio climático en la costa de América Latina y el Caribe"
CERC (1984) Shore protection manual. Coastal Engineering Research Center. U.S. Army Corps of Engineers, Washington, DC
Cowell PJ, Thom BG (1997) Morphodynamics of coastal evolution. In: Carter RWG, Woodroffe CD (eds) Coastal evolution, late quaternary shoreline morphodynamics. Cambridge University Press, Cambridge
Cutter SL (1996) Vulnerability to environmental hazards. Hum Geogr 20(4):529–539
Del Valle R, Medina R, Losada MA (1993) Dependence of coefficient K on grain size. J Waterw, Port, Coast, Ocean Eng 119:568–574
Dolan AH, Walker IJ (2003) Understanding vulnerability of coastal communi-ties to climate change related risks. J Coast Res SI 39. In: Proceedings of the 8th international coastal symposium, Itajaí, SC, Brazil
Egbert GD, Erofeeva SY (2002) Efficient inverse modeling of barotropic ocean tides. J Atmos Ocean Technol 19:183–204
Egbert GD, Bennett AF, Foreman MGG (1994) TOPEX/POSEIDON tides estimated using a global inverse model. J Geophys Res 99:24821–24852
EM-DAT (2011) The OFDA/CRED international disaster database. http://www.em-dat.net/. Accessed 5 Oct 2011
EUROSION (2004) Living with coastal erosion in Europe: sediment and space for sustainability, part I-major findings and policy recommendations of the EUROSION project. Report in the framework of EUROSION project, Directorate General Environment, European Commission, EU
Finlayson D (2005) Puget sound fetch. University of Washington, School of Oceanography. http://www.umesc.usgs.gov/management/dss/wind_fetch_wave_models.html. Accessed 13 Nov 2011
Flax LK, Jackson RW, Stein DN (2002) Community vulnerability assessment tool methodology. Nat Hazards Rev 34(163):1527–6988. doi:10.1061/(ASCE)
Fletcher CHIII, Grossman EE, Richmond BM, Gibbs AE (2002) Atlas of natu-ral hazards in the Hawaiian coastal zone. U.S. Department of the Interior. U.S. Geological Survey. http://pubs.usgs.gov/imap/i2761/. Accessed 10 Dec 2011
Freeman PK, Keen M, Mani M (2003) Dealing with increased risk of natural disaster: challenges and options. IMF working paper. International Monetary Fund
González M, García E, González-Ondina J, Méndez FJ, Medina R, Osorio A (2007) An integrated coastal modeling system for analyzing beach processes and beach restoration projects, SMC. Comput Geosci 33(7):916–931. doi:10.1016/j.cageo.2006.12.005
González M, Medina R, Losada M (2010) On the design of beach nourishment projects using static and dynamic equilibrium concepts: application to the Spanish coast. Coast Eng 57:227–240. doi:10.1016/j.coastaleng.2009.10.009
Gornitz V (1991) Global coastal hazards from future sea level rise. Palaeogeogr, Palaeoclimatol, Palaeoecol (Glob Planet Change Sect) 89:379–398
Harley MD, Turner IL, Short AD, Ranasinghe R (2011) A reevaluation of coastal embayment rotation: the dominance of cross-shore versus alongshore sediment transport processes, Collaroy-Narrabeen Beach, southeast Australia. J Geophys Res. doi:10.1029/2011JF001989

Hinkel J, Klein RJT (2009) Integrating knowledge to assess coastal vulnerability to sea-level rise: the development of the DIVA tool. Glob Environ Change 19:384–395

IBGE – Instituto Brasileiro de Geografia e Estatística (2010) Ministério do Pla-nejamento, Orçamento e Gestão. Agregados por setores censitários, 2nd edn. http://www.ibge.gov.br/home/estatistica/populacao/defaulttab_agregado.shtm. Accessed 5 May 2010

ISDR-International Strategy for Disaster Reduction (2004) Living with risk: a global review of disaster reduction initiatives. World Meteorological Organization and the Asian Disaster Reduction Center, Geneva. http://www.unisdr.org/eng/about_isdr/bd-lwr-2004-eng.htm. Accessed 13 Dec 2010

Kraus NC, Galgano FA (2001) Beach erosional hot spots: types, causes, and solutions. US Army Corps of Engineers. http://chl.erdc.usace.army.mil/library/publications/chetn/pdf/chetn-ii-44.pdf. Accessed 20 May 2012

Nielsen P, Hanslow DJ (1991) Wave runup distributions on natural beaches. J Coast Res 4:1139–1152

Nuber E (2008) Evolução morfológica e sedimentológica do Arco Praial de Massaguaçu, Litoral Norte de São Paulo. Thesis. São Paulo University

Pezza AB, Simmonds I (2005) The first South Atlantic hurricane: unprecedented blocking, low shear and climate change. Geophys Res Lett. doi:10.1029/2005GL023390

Raabe ALA, Klein AHF, González M, Medina R (2010) MEPBAY & SMC: software tools to support different operational levels of headland bay beach coastal engineering projects. Coast Eng 57:213–226. doi:10.1016/j.coastaleng.2009.10.008

Reguero BG, Menéndez M, Méndez FJ, Mínguez R, Losada IJ (2012) A Global Ocean Wave (GOW) calibrated reanalysis from 1948 onwards. Coast Eng 65:38–55. doi:10.1016/j.coastaleng.2012.03.003

Rudorff F de M, Bonetti J, Moreno D (2006) Maré de Tempestade. In: Herrmann ML de P (ed) Atlas de Desastres Naturais do Estado de Santa Catarina, Florianópolis, Santa Catarina, Governo do Estado de Santa Catarina/Secretaria de Estado de Segurança Pública e Defesa do Cidadão, pp 117–120

Ruggiero P, Komar P, McDouglas W, Marra JJ, Beach RA (2001) Wave runup, extreme water levels and the erosion of properties backing beaches. J Coast Res 17:407–419

Schneiderbauer S, Ehrlich D, (2004) Risk, hazard and people's vulnerability to natural hazards. A review of definitions, concepts and data. European Commission. Joint Research Centre

Sharples C (2006) Indicative mapping of Tasmanian coastal geomorphic vulnerability to sea-level rise using GIS line map of coastal geomorphic attributes. Explanatory report (first edition). Consultant Report to Department of Primary Industries & Water, Tasmania

Shchepetkin AF, McWilliams JC (2003) A method for computing horizontal pressure-gradient force in an oceanic model with a nonaligned vertical coordinate. J Geophys Res. doi:10.1029/2001JC001047

Thieler ER, Hammar-Klose ES (2000) National assessment of coastal vulnerability to sea-level rise: preliminary results for the U.S. Pacific Coast. http://woodshole.er.usgs.gov/project-pages/cvi/. Accessed 20 Apr 2012

Thieler ER et al (2009) Digital Shoreline Analysis System (DSAS) version 4.0—An ArcGIS extension for calculating shoreline change: U.S. Geological Survey Open-File Report. http://pubs.usgs.gov/of/2008/1278/. Accessed 10 Oct 2011

UNDP – United Nations Development Programme (2004) Reducing disaster risk: a challenge for development. http://www.undp.org/bcpr. Accessed15 Jan 2011

White GF, Kates RK, Burton I (2001) Knowing better and losing even more: the use of knowledge in hazards management. Environ Hazards 3:81–92

Wu SY, Yarnal B, Fisher A (2002) Vulnerability of coastal communities to sea-level rise: a case study of Cape May County, New Jersey, USA. Clim Res 22(4):255–270

Chapter 17
Coastal Erosion and Protection Policies in Europe: From EU Programme (Eurosion and Interreg Projects) to Local Management

Giovanni Randazzo, Jordi Serra Raventos, and Lanza Stefania

Abstract The European Union, a political entity established in 1952, has undergone continuous expansion of its borders. However, aggregating territories has very different implications from the geographical, the political, or the ethical standpoint. Of the current 27 Member States, 22 open directly onto five different seas. Thus, over the last few decades, there has been an increasing trend of people living along coastal areas. This has caused significant changes to the coastal environment, placing increasing demands on coastal resources and increasing exposure to coastal hazards, such erosion and flooding, these together being considered as among the most serious problems.

Currently, the total coastal area lost in Europe due to marine erosion is estimated to be about 15 km^2 per year and the International Commission on Climate Change (IPCC) of the United Nations has estimated that the related cost will average 5.4 billion Euros annually in the period between 1990 and 2020. In this light, the European Commission's DG Environment with the programme EUROSION sought to analyse the problem as a whole, to identify the causes related to different geographic areas and to outline possible solutions. With the subsequent cross-border programmes (INTERREG and ENPI), the European Union has undertaken the general dissemination of information acquired locally, focusing attention on and expanding knowledge of different situations, including those of social perspectives. EUROSION has tried to transform the conceptual positions related to the problem of coastal erosion, examining the actual effects of the different seas, defining the

G. Randazzo (✉) • L. Stefania
Dipartimento di Scienze della Terra, Università degli Studi di Messina,
Via F. Stagno D'Alcontres, 31, 98166 Messina, Italy
e-mail: grandazzo@unime.it; lanzas@unime.it

J.S. Raventos
Department d'Estratigrafia, Paleontologia i Geociències Marines, Universitat de Barcelona,
Martí i Franquès s/n, 08028 Barcelona, Spain
e-mail: jordi.serra@ub.edu

C.W. Finkl (ed.), *Coastal Hazards*, Coastal Research Library 6,
DOI 10.1007/978-94-007-5234-4_17,

main causes of erosion, distinguishing between natural and human causes, and referring them to a temporal-spatial scale.

For each coastal system, more than one policy option was specified, but the ramifications have not always been completely clear. In some case studies, coastal-defence policies at a national level have not yet been adopted, leaving management of erosion problems often to local and/or regional authorities (e.g. many Islands and autonomous regions use a regional approach). Generally, however, a dual approach is taken: a proactive approach refers to a policy of anticipating erosion processes whereas a reactive approach refers to the implementing of coastal-defence measures in order to reduce the effects of existing erosion processes.

Within the various geographical areas, levels of attention and response to the problem have differed sharply due to conceptual and cultural differences coupled with variable socioeconomic circumstances. Generally, countries seek to "hold the line" and to avoid realignment; however, in some local circumstances realignment has been possible and in these cases has been supported by adequate rational policy frameworks. Cross-border programs have revealed that implementation at national level has varied and has been discontinuous due both to the local legislative context, but also to a poor ability to transpose the European guidelines.

It can be shown that, even in relation to countering the problems of coastal erosion, at a strategic European level, a truly common policy that clearly states the line to follow is lacking. Consequently, the development of knowledge tools that could solve the problem and provide consistency of approach between countries is difficult to guide and finance. There is a need to adopt a true Coastal Zone Management Plan approach and to provide for costs and benefits at local and regional levels. Beyond the contents of a simple intervention, it is therefore important to aim at an overall development that takes into account the realistic potential and the different potential of various geographical and socio-economic contexts.

17.1 Introduction

This chapter examines the state of the art concerning coastal erosion and outlines the policies to be adopted by various states to meet this problem:

To do what is necessary to address two complex problems. First of all is the extreme geomorphological variability of coasts, which border on five different seas, with different hydraulic and oceanographic characteristics. Second, the coasts are used differently in different areas, both because of climate and of historical and cultural characteristics as well as the degree of development of the different states. Furthermore, the EU membership constitutes a further problem because the number of EU Member States is increasing and the information and statistics relating to each of them are highly variable and differ chronologically. In fact, this is like trying to repair the body, electrical system, and motor of a car while it is moving.

For these reasons, to look for a point common to most states, to reach the lowest common denominator, this chapter is based mainly on two sources to which the authors have given their decisive contribution: EUROSION and Messina.

EUROSION is the most important study on coastal erosion directly funded by DG Environment and updated to 2004. The study evaluated the state of the coasts of European Union Member States, based on an analysis of 60 cases studies divided according to geographic ranges, but especially according to characteristics of the coastlines and their use.

The study led to the prescription of some good practices that should have been enacted by Member States, but after 8 years, and in the middle of an economic crisis that leads legislators to overlook even the environment to safeguard the Euro itself, only some of these Members, which were already in good condition, have maintained or implemented the actions previously taken, while the other Members, where possible, have also reduced their actions and in every way are trying to attract private capital to boost economic return and to lower management expenses. The example of the Spanish Law for the Coasts from 1988, progressive at that time, is to be changed in this context.

The MESSINA (Managing European Shoreline and Sharing Information on Near shore Areas) Project, an Interreg IIIc program, intends to: (1) break "knowledge isolation" of some local authorities and institutions in Europe, (2) raise their managerial and technical capabilities through a mutualization of the experience accumulated by each of them, (3) and upgrade existing shoreline-management guidelines through the integration of the latest techniques and methods available in Europe. The overall objective of MESSINA has lately been to maximize the profits of future investments in coastline management and raise the public awareness about the need to manage the coastline in a sound and sustainable way. With this project, which had obviously more limited expectations, the monitoring and management of coastal areas have been undertaken in several geographically limited areas (provinces or municipalities), but this has been important as an example and for educational value. Somehow this action, triggered locally, fomented the growth of a plant that has influenced the sensitivity and attention of the intermediate political level (region) that has begun, albeit amid considerable economic difficulties, useful activities for the creation of a new Coastal Management Plan, based on monitoring and direct knowledge.

The European Union is a rather complex political entity and is still evolving; as of 1 January 2007 (the entry date of the last two states), the EU has 27 member states. The original six nations that formed the EU (in 1952 with the founding of the CECA): Belgium, France, Italy, Luxembourg, Netherlands, West Germany, were gradually followed by other states: Denmark, United Kingdom and Ireland (since 1973), Greece (since 1981), Austria, Finland and Sweden (since 1995), Cyprus, Czech Republic, Estonia, Hungary, Latvia, Lithuania, Malta, Poland, Slovakia, Slovenia (since 2004), Romania and Bulgaria became part of 'EU in 2007.

At present, there are numerous on-going negotiations to allow the entrance to Croatia, Turkey and Macedonia. Other states that in the future may enter the European Union include Albania, Bosnia, Herzegovina, Serbia, and Montenegro.

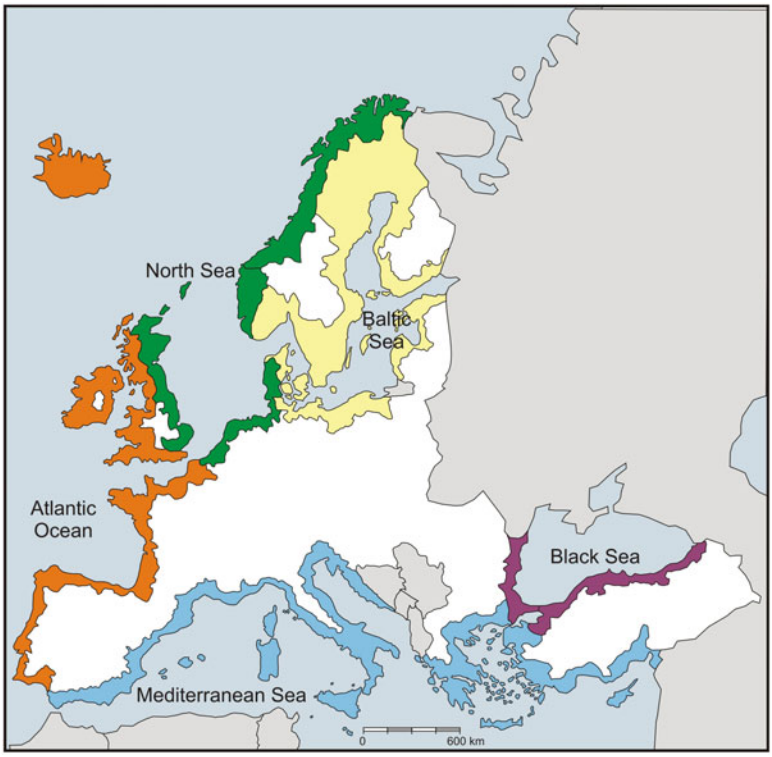

Fig. 17.1 European Union coastal State Members (present, future and possible)

Of these 27 Member States, 22 border on five different seas which have very different geographical and oceanographic features: Baltic Sea, North Sea, Atlantic Ocean, Mediterranean Sea and Black Sea (Fig. 17.1).

Current demographic trends show rapid growth in the coastal population and density throughout Europe. The present resources attract millions of people to the coastal areas, increasing the population densities to almost three times the global mean (Small and Nicholls 2003). In fact, over the last few decades the population living in coastal areas has grown exponentially, reaching, around 205 million people in 2008, i.e. 41% of the EU population, mostly on the Mediterranean Sea (36%) and north-eastern Atlantic Ocean (29,4%, EUROSTAT 2009). This is causing significant changes to the coastal environment, placing increasing demands on coastal resources and increasing exposure to coastal hazard such erosion and flooding, these considered among of the most serious problems.

Coastal erosion is a process that threatens several EU member states but it is of growing concern around the world (Bartlett and Smith 2005). It is caused by natural forces such as currents, waves, storm surges, and winds, as well as anthropogenic developments (Heo et al. 2009; Paskoff 1998). It is a global problem and has economic implications for coastal tourism and sustainable development. Coastal

changes are considered to be environmental indicators, all the more important, given that they have direct impact on coastal economic development and land management (Stokkom et al. 1993; Chaaban et al. 2012).

The overall picture of the erosion process on a continental scale, for 21 coastal countries is provided by EUROSION (2004), which estimated that about 20,000 km of coastline, 20% of the total, were affected by varying degrees of coastal erosion. Areas of about 15 km^2 are abandoned each year because of coastal erosion; particularly during the period between 1999 and 2002 in Europe, about 250–300 houses have been abandoned because of the risk of imminent coastal erosion and another 3,000 houses have was devalued by about 10% of their value. In 2004, 934 km of coastline was affected by new coastal defence structures, of which the majority (63%) were located within a radius of 30 km from previous coastal defence works. The most critical erosion hot-spots are coastlines of the Mediterranean Sea (30% erosion loss), the North Sea (20%) and the Black Sea (13%).

Furthermore, observations over the last few decades with respect to the evolution of shorelines, associated with growing scientific literature on climate change, suggest that there will likely be an increase in the intensity of certain coastal hazards in the short and medium term (GIEC 2007). The most recent IPCC (2007) report underlines that climate-related changes over the twenty first century will include an acceleration in Sea Level Rise, further rise in sea-surface temperature, more extreme weather events and storm surges, altered precipitation, and ocean acidification.

Clearly the cost of protection interventions is growing and in fact, in 2001, public spending diverted to the coastal defence against the risk of erosion and flooding was about 3,200 million Euros, with an increase of 30% compared to 1986 (2,500 million spent in 1986). Certainly, these expenses reflect primarily the need to protect property and people from the imminent risk of coastal erosion but do not indicate the damage due to the growing human pressure over the long term. Although differences exist at national level, studies conducted for the International Commission on Climate Change (IPCC) of the United Nations estimates that the cost of coastal erosion will average 5,400 million euros annually in the period between 1990 and 2020. Close to 85% of the total coastal protection expenditure (1998–2015) to protect Europe's coasts against flooding and erosion is borne by five countries (the Netherlands, UK, Germany, Spain, and Italy).

The management of these common goods has led the EU to make important decisions on Integrated Coastal Zone Management (ICZM). On the other hand, several states have not found a single management system, and therefore some laws have anticipated expectations and others did not provide adequate answers to the growing problems. This unevenness in management corresponds to a different technical approach, almost always influenced by local customs. Precisely for this reason the European Union has funded a study on coastal erosion in Europe (EUROSION) directly by DG Environment, in which they followed a series of cooperation programs aimed at providing the best scientific knowledge in the various premises of administrations that ultimately must provide for the defence and maintenance of the coasts.

Individual programs such as Beachmed I and II, MESSINA, CLAIMS, SANDPIT (and many others) and a new cluster of programs called Constance have greatly facilitated the dissemination of information locally, but despite this, a large knowledge gap persists between different areas and not always with a purely geographical connotation, since it is linked to the sensibilities of local administrators.

This chapter, starting from the numerous studies undertaken on behalf of the European Union, aims to provide a framework for the coastal characteristics of the different member states as a function of the seas, primarily considering the characteristics and the main coastal erosion problems. For these aspects, the EUROSION (2004) and MESSINA (2006) data base has been implemented and adapted to the new EU borders.

17.2 The Shape of the Problem at the European Level

Coastal erosion concerns different environments in ways that often differ sharply from the way in which Member States have responded by proposing action targeted at territorial use. The processes of coastal erosion and accretion have always existed and have contributed throughout history to shape European coastal landscapes, creating a wide variety of coastal types. Erosion of inland soils induced by rainfall and movement along riverbeds in some areas provides considerable amounts of sediments to the coast. These sediments together with those derived from coastal features (such as eroding cliffs and marine sand banks) provide essential material for the development of sandy beaches, sand dunes, and transitional marshes. In turn, these coastal habitats provide a wide range of outstanding benefits, including locations for economic and recreational activities, protection from flooding in low-lying areas, absorption of wave energy during storm surges, reduction of eutrophication of coastal waters.

Coastal erosion is usually the result of a combination of factors – both natural and human induced – that operate on different scales. Natural causes include: winds and storms, near-shore currents, relative sea-level rise (a combination of vertical land movement and sea-level rise) and slope processes. Human-induced factors of coastal erosion include: sand mining from riverbeds, coastal engineering, land reclamation, river-basin regulatory works (especially construction of dams), vegetation clearing, gas mining, and water extraction.

In the EUROSION Project, an initial conceptual differentiation was proposed, indicating two different types of erosion in relation to their characteristics:

- Structural erosion is a continuing process of erosion due to adaptation of the coastal system to changing conditions. A common natural cause is (accelerated)

sea-level rise. Human influence often triggers or exacerbates structural erosion. A sediment deficit may arise as a result of land subsidence due to the extraction of gas/water or as a result of the reduction in sediment supply to the coast due to activities in the river catchments (canals, dams, irrigation works, etc.). Furthermore, structural erosion is induced locally by an interruption of the net longshore transport due to construction works (groins, harbour moles, etc.).

- Acute erosion is caused mainly by storm events. During a storm, erosion rates can be very high. However, during calm periods, following the stormy period, the sediment is often redistributed and the beach will (at least partly) be rebuilt. In many cases, acute erosion due to storm events is therefore only a problem for sedimentary beaches when infrastructure, buildings or other structures are threatened or destroyed. Acute erosion is a more serious problem along coastal cliffs, since the cliffs cannot be rebuilt under calmer conditions.

In particular, however, when the causes of erosion are considered, the dominant time and spatial scale of the underlying processes need to be taken into account. It is meaningless to discuss erosion without pointing out the scale considered. In the management of erosion problems, the coastal system to be dealt with is normally larger than the area in which erosion takes place. A coastal system should be considered under a consistent and adequate time and spatial scale. The problem of coastal erosion and more generally of coastal management is therefore becoming increasingly urgent both in general or on a national scale in terms of soil loss, particularly in situations where special interests, whether private (hotels, houses, and beaches) or public (waterfront roads, ports, and other destination areas) have been threatened or destroyed by the sea.

In Europe, an attempt was made to analyse the two aspects involved in the question and research programmes were carried out considering global situations and large-scale local case studies, included in different environments. In addition to this type of direct analysis, involving several studies, the historical path suffered coastal erosion protection works has been highlighted. The results were often compared with the studies undertaken in the United States of America.

The synthesis of the research has led to a series of procedures known by the acronym ICZM (Integrated Coastal Zone Management) which itself contains a summary of what would be useful and necessary to defend the coastline. The key point is to keep tight control of all the processes that directly or indirectly influence the evolution of the sea. Lately, a series of initiatives, not always connected to each other, have been followed, sometimes for the coastal defence that gave quite varied reactions. For example, Bernatchez and Fraser (2011) stated that the effects of defence structures on the time course of beach sediment budgets depend on the type of coast, and should take into account, in some way, the technical choices made upstream.

Construction of coastal defences date to remote times; in fact, attempts seem to have been made as soon settlements appeared along the coasts (Charlie et al. 2005). However, the coastal protection against an advancing sea became an increasing concern for governments only during the last century and a half. In the nineteenth

and twentieth centuries, coastal protection against an advancing sea centred on a variety of hard structures (groins, breakwaters, seawall, tetrapods, etc.) and artificial nourishment. Environmental concerns have played a steadily more important role. Some 40 types of alternative schemes have been proposed over the last few decades, with a large number of them faulted for negative environmental impacts (Charlier et al. 2005). Any of these coastal-protection works would need to be thoroughly evaluated before being implemented, as all of them represent a particular interference with the coastal environment and, hence, lead to multiple, divergent and location-specific impacts (Roebeling et al. 2011).

A significant part of the European coastline is artificial. About 3.4% of the coastline is covered by harbours and other protective structures covering 1.8% of the entire area. Therefore, more than 5% of the European coastline is protected against erosion by 'hard' structures. The main areas with an artificial coastline are located on the North Sea. This is explained by the fact that extensive areas of these countries have been retrieved from the sea and by the high importance and large dimensions of ports.

Over the past few decades, there has been a gradual change from hard to soft coastal-defence techniques in Europe. Traditionally, adaptation to coastal hazards has been concentrated on protecting land using hard structures but, in the last few decades, there has been growing interest in soft protection such as beach nourishment and dune rehabilitation. In addition, accommodation and realignment are being increasingly applied by adapting spatial-planning regulations that include new building codes or land-use restrictions as well as establishing set-back zones (Klein et al. 2001; Nicholls 2007). Since then, soft methods have encompassed beach nourishment, bypassing, back-passing, dumping and stockpiling, and occasional and continuous nourishment; but there is also de-watering, profile nourishment, and berm feeding, a more sophisticated offshore dumping method.

In fact, in some European countries, since the latter part of the twentieth century planners responsible for coastal protection have keep their distance, whenever possible, from the option of hard structures. Several new approaches have been developed, both to protect the coasts and to rebuild beaches ravaged by erosion. The alternative, soft approach of artificial nourishment is not so new. The method has been used in the United States since just after World War I, when sand was deposited on some California beaches (Charlier et al. 2005). In these years, the effectiveness of soft and hard remedial measures for sandy beaches were assessed based on laboratory, field, and modelling experiences. Studies have shown that the impact of coastal defences vary widely according to the techniques used, their specific design, and the characteristics of the local environment.

The impacts of hard engineering are usually more severe than soft engineering. Hard engineering generally results in long-term changes in coastal morphology, particularly erosion, alongside protected areas. It also often leads to a reduction in the width of the shoreline as low-lying backshore areas are reclaimed behind defences. This leads to a reduction in the size of shore habitats, a phenomenon termed coastal squeeze. By contrast, soft engineering is generally a more environmentally friendly approach which works towards providing a dynamic equilibrium

on the coast whereby erosion and flooding are kept to a minimum. This also generally requires more space to be used, thereby alleviating coastal squeeze.

Hard defence techniques (groins and breakwaters), which reduce upper shore and cliff erosion also disrupt longshore sediment transport, which often leads to the accelerated erosion of adjacent shorelines (Figs. 17.2 and 17.3).

However, nourishment techniques, if not carefully designed, and/or if improper fill material is used, can increase the turbidity of coastal waters, and the continued wash-out of fine material can have long-term negative effects on adjacent benthic and inter-tidal ecosystems. Changes in beach-grain distribution can lead to the incursion of coarse-grained material over supra-tidal ecosystems, such as lower cliff or dune communities (Fig. 17.4).

Sea walls and other upper-shore structures, if placed too close to the waterline, reduce the active width of the beach and dune during storms. This significantly disrupts the sediment balance and causes erosion especially along downdrift stretches of coastline. They also result in wave reflection leading to a lowering of the foreshore and sometimes to the undermining of the toe of the seawall, which may ultimately cause it to collapse. Sea walls prevent sediment transport between the beach and dune, resulting in the deterioration of these environments (Fig. 17.5).

For each coastal system, it should be noted that more than one policy option may be valid in the same case study. In addition, the distinction between the policy options is not always completely clear. Policy options vary from the European level down to the local level. In some case studies, coastal-defence policies at a national level have not yet been adopted, leaving management of erosion problems often to local and/or regional authorities (e.g. many Islands and autonomous regions use a regional approach). A proactive approach refers to a policy of anticipating erosion processes. Technical measures or plans (management plans, flood warning systems etc.) are adopted to prevent erosion or minimize the expected effects of erosion. On the contrary, a reactive approach refers to the policy of performing coastal-defence measures to reduce the effects of existing erosion processes. Another part of the strategy is to decide whether to use hard or soft measures to deal with erosion.

Following this general overview, the scheme adopted by EUROSION is noteworthy, as it derives from DEFRA (Department for Environment, Food and Rural Affairs), for which it is useful to examine the action within the framework of the different seas (Fig. 17.6)

Do nothing. This means there is no investment in coastal-defence assets or operations, i.e. no shoreline management activity. Hold the line. The existing defence line is held by maintaining or changing the standard of protection. This policy covers situations where works are undertaken in front of the existing defences to improve or maintain the standard of protection provided by the existing defence line. Policies that involve operations to the rear of existing defences should be included under this policy where they form an integral part of maintaining the current coastal defence systems. Move seaward. This means to advance the existing defence line by constructing new defences seaward of the original defences. Such policies are limited to management units where significant land reclamation is considered. Managed realignment. A new line of defence is identified and, where

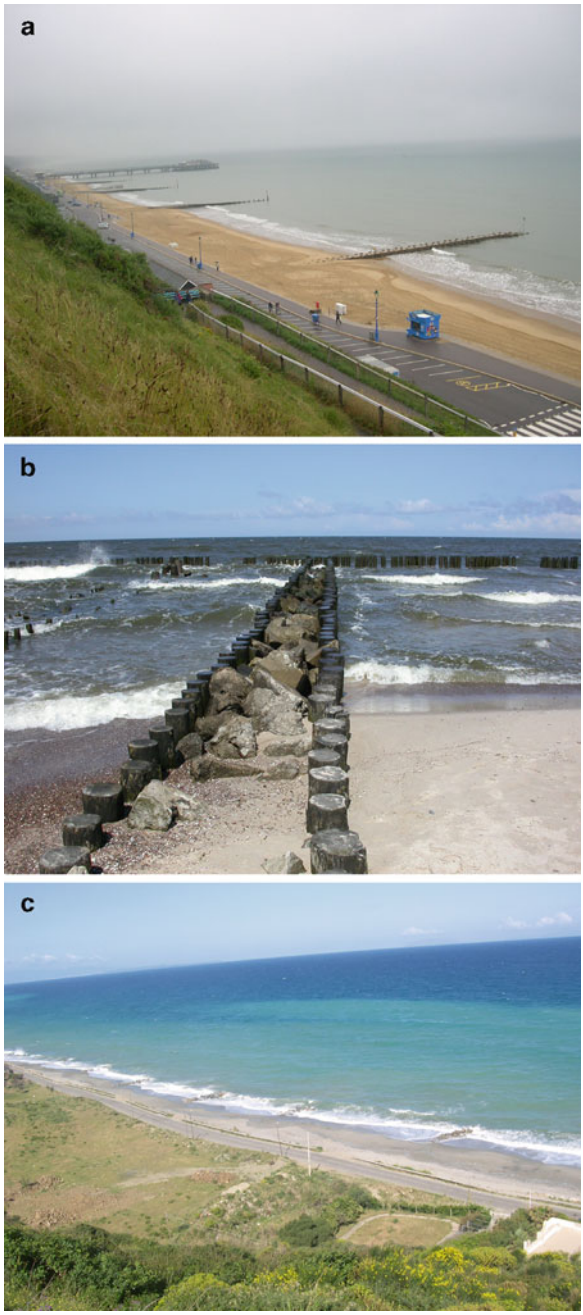

17.2 Some examples of groins: (**a**) in concrete (UK), (**b**) in wooden (Poland) and (**c**) in natural rocks (Italy)

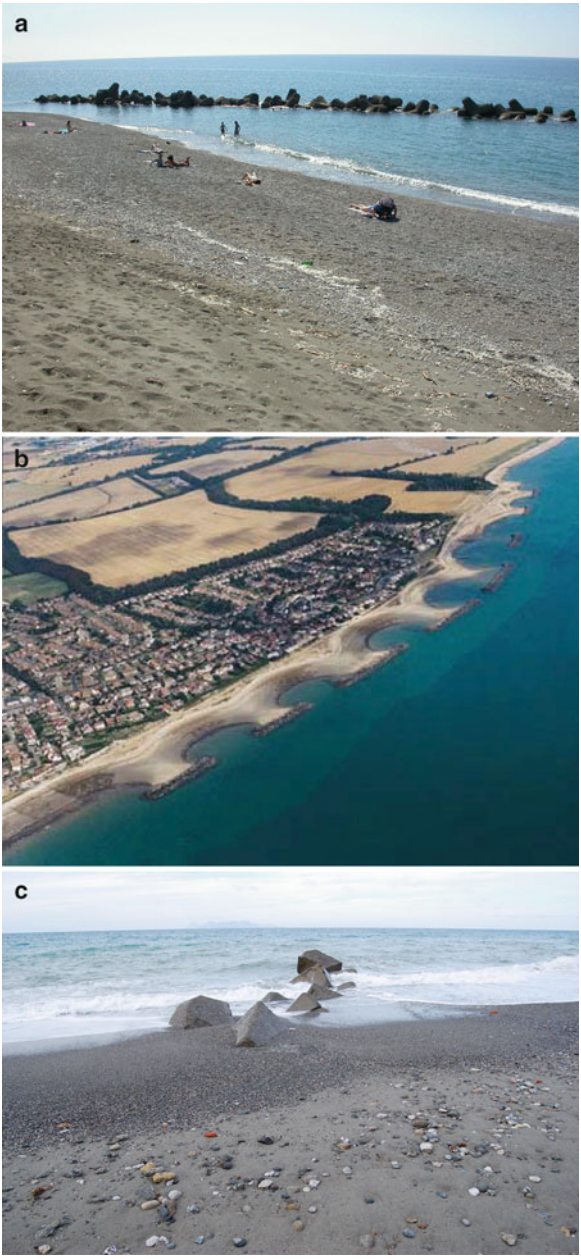

Fig. 17.3 Some examples of breakwaters: (**a**) in tetrapods (Italy), (**b**) in natural rocks (UK) and (**c**) in concrete blocks

appropriate, new defences are constructed landward of the original defences. Limited intervention. This involves working with natural processes to reduce risks while allowing natural coastal change. This may range from measures that attempt to slow down rather than stop coastal erosion and cliff recession

Fig. 17.4 Example of soft engineering protection: Nourished beach (Giardini Naxos – Sicily – Italy)

(e.g. nourishment), to measures that address public-safety issues (e.g. flood-warning systems, dune and forest maintenance, building restrictions on the coastal strip).

To prepare the framework for the different technical solutions adopted by different Member States or at least to compile a preliminary list is necessary to refer these to the different geomorphological conditions, which are strongly tied with the geographical setting of the coastline.

17.3 Geographical Setting

It is evident that the pressure on the different coastal areas, as well as being determined by the policies and traditions of different Member States, is also strongly associated with geographical and geomorphological characteristics of the seas that they border. For this reason, to follow the model proposed by EUROSION and then by other projects proposed by the DG Environment, it is vital for Member States to provide a comprehensive overview of the basic features of the seas of the European Union, defining the various physical aspects.

The length of the coastline for the 22 EU Member States bordering the sea is estimated to be (136,106 km) (five states are not bordered by the sea). The European coastal regions account for 43% of the total. These data are extremely difficult to confirm because of varying purposes of the study; for this reason we can group the different countries in three subgroups in relation to the national coastal length.

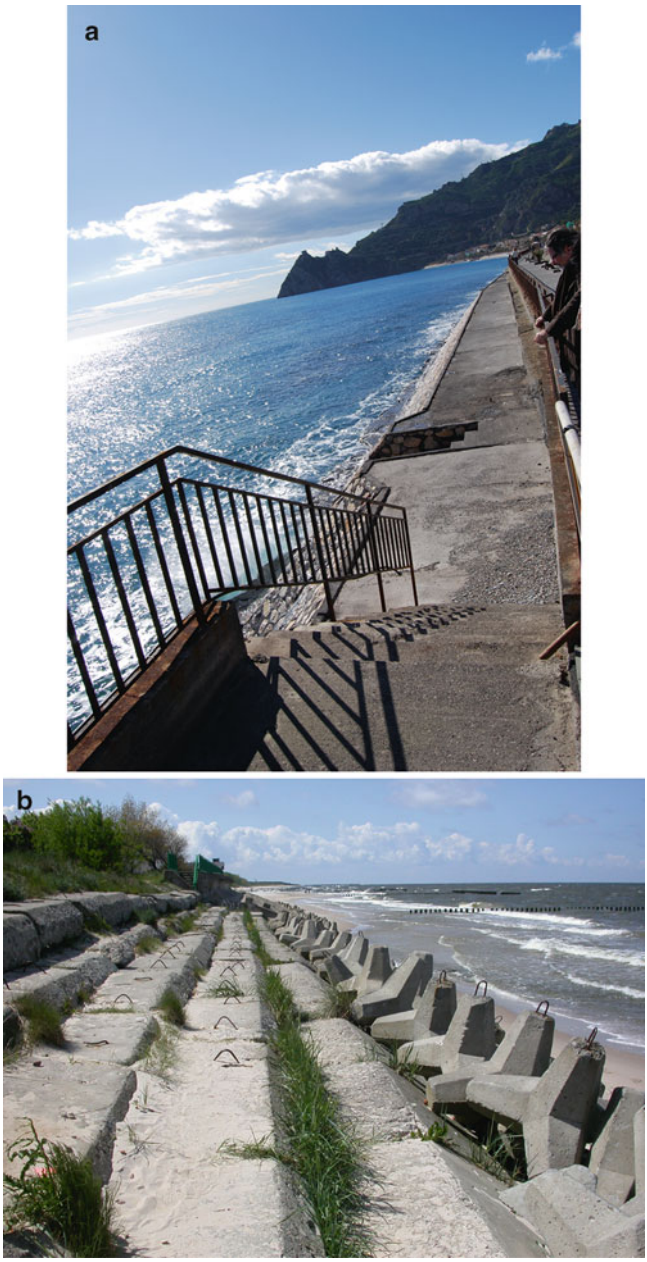

Fig. 17.5 Some examples of sea walls: (**a**) double sea wall in concrete and volcanic rocks, (**b**) in squared tetrapods

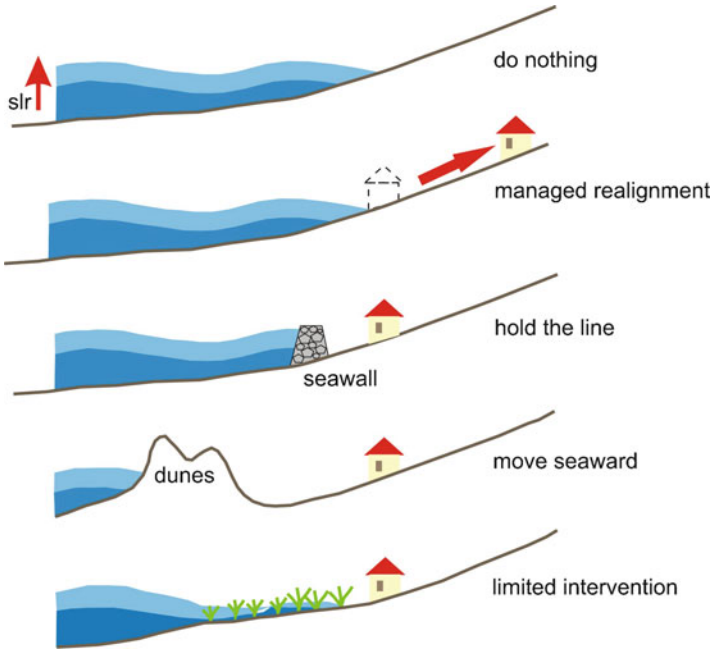

Fig. 17.6 Protection options, following EUROSION

One country has more than 16,000 km of coastline, three countries have between 14,000 and 8,000 km, seven countries have between 8,000 and 2,000, and the other ten have less than 2,000 km. Six EU countries (Sweden, France, Finland, Italy, Spain and Greece) have coastal regions representing more than 100,000 km^2 and together occupy 75% of the EU coastal area. It is evident that this sub-division conflicts with the social and the economic importance of the coast also in small countries or islands that completely depend on their coasts (Fig. 17.7).

Among the six main sea basins which border the EU territory, the Baltic and Mediterranean zones occupy by far the largest area (67%) compared to the four other sea basins, of which three (Black Sea, Outermost Regions and North Sea) represent less than 10% of the total coastal areas.

17.3.1 Baltic Sea

The Baltic Sea is a semi-enclosed intracontinental shallow sea characterized by brackish water and shallow coastal areas derived from glacial and post-glacial

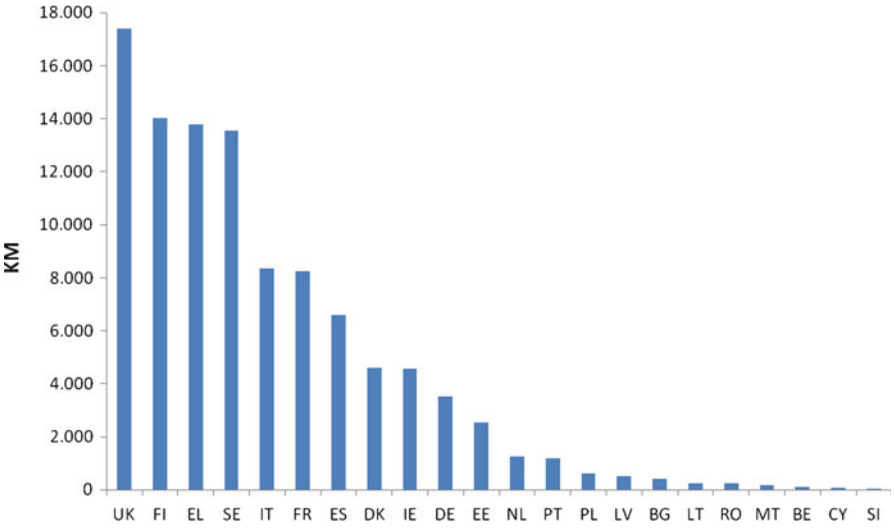

Fig. 17.7 Coastal length of the European Union State Members

deposits. It is bordered by eight EU countries: Sweden, Finland, Estonia, Latvia, Lithuania, Germany and Denmark.

The sea covers 415,266 km^2 with an average depth of around 50 m. The deepest waters are in the Landsort Deep in the Baltic Proper, where depths of 459 m have been recorded. This basin is characterized by extremely complex geometry, highly varying wind fields, extremely rough wave conditions at times, extensive archipelago areas with specific wave propagation properties, and ice cover during a large part of each year. The combination of its relatively small size and the vulnerability of its ecosystems make this region particularly susceptible to climate changes (Dailidiene et al. 2012).

The Baltic Sea originally was a lake , until the rising sea level pushed salt water upstream to the Danish channels due to sea-level rise after the last Ice Age. This sea has been influenced in its development by the variations in strengths of two competing geological phenomena, both being direct consequences of the melting of the glaciers: land uplift and sea-level rise. The sea-level rise of the Littorina transgression has led to major changes in coastlines along the southern Baltic Sea coast. Here, the initial phase of the transgression with an annual sea-level rise of 2 cm has forced a "drowning" of the coast (Kliewe and Janke 1982; Meyer and Harff 2005). Later, together with a slower sea-level rise, erosion, transport, and accumulation of sediments controlled by wind and currents have played a major role (Lemke 1998; Meyer and Harff 2005). By contrast, the northern part of the area of the Baltic Sea has had a totally different history of coastline displacement, shown by comparison of relative sea-level curves. The northern part is dominated by regression, caused by the isostatic uplift of Scandinavia (Meyer and Harff 2005).

Since the end of the latest Ice Age, several marine transgressions caused active erosion of Quaternary glacial drift deposits and consequently affected the alongshore sediment distribution along the Baltic coast. The common feature of this geographical zone therefore lies in the abundance of sediment supply, much of it derived from the soft glacial material deposited during the various ice ages, especially at the end of the last glaciation. Furthermore, along hard rocky coasts, indentations and small islands formed during the transgressions. As a result, the common coastal and sediment types in the Baltic Sea are soft moraine cliffs, hard rocky cliffs, sand dunes, and beaches. The sediment characteristics vary over a wide range within the Baltic Sea region.

17.3.1.1 Physical Processes

The morphology of the Baltic coast is influenced by the ice cover for a variable period, depending on the zone, from 2 to 6 months. This favours a double genesis of sediment supply characterized by pebbles and boulders where the presence of ice has more influence. In general, the coastal transport is fed from the rate of erosion of soft cliffs and only in the main rivers (Oder in Poland, in the Gulf of Riga Daugava and Nemunas River in Lithuania) from the solid river load.

There is a clear relationship of action and reaction in particular between the soft cliffs and beaches, where the beaches of downstream eroding beaches are well fed while the downstream coastline artificially protected from erosion is itself affected by deep erosion.

The climate has a significant impact on the coastal system, in some ways not so controversial. The prevailing winds in intensity and persistence come from North America and alternate to the southwest, causing (especially the former) storm waves that affect the Baltic States as well as eastern Germany and Poland to south; during storm surges, the wind can raise or lower the water level by at least 1 m. In this way, the water level can attain considerable heights.

Despite this, some observations (in the last case for decades), indicate an increase in storm frequency and intensity, especially in the south-western area, in Estonia, Latvia, and Lithuania. This could be related to climate change. Another important issue connected with the climate change concerns relative sea-level rise (RSLR). Global predictions are rather mixed, and against an alleged rise in local sea about 1–2 mm/year, with peaks such as the Gulf of Riga (Latvia) about 4 mm, the forecast for the next 100 years is about 4–5 mm/year (Warrick et al. 1996), these values will have different influences on the coastal strip, as the impact will be very serious on the coasts of Denmark, Germany, and Poland, involved in a discrete subsidence, while on the northern shores of the sea-level rise will be completely offset by the land uplift rates. The total global average sea-level rise during the twentieth century is estimated to be 0.17 m (0.12–0.22 m), and the global average sea level rose at an average rate of 1.8 mm/year (1.3–2.3 mm/year) from 1961 to 2003 (IPCC 2007). The rate was faster from 1993 to 2003, about 3.1 mm/year (2.4–3.8 mm/year) (IPCC 2007). The mean Baltic sea-level change has been analysed in relation to the eustatic and the isostatic land-uplift processes.

17.3.1.2 Erosion

Coastal erosion is complex, being caused by disparate processes, such as sea-level rise, variation in sediment supply, waves, storm surges, longshore sediment removal and transport, and sorting of sediment on the beach under wave action.

Anthropogenic activities make it even more difficult to predict the coast recession on a long-term scale (Zhang et al. 2011). However, from the structural standpoint, the Baltic Sea probably has two characteristic aspects. One is linked to the fact that the solid transport along the coast is quite low. On the other hand, the relative sea-level rise, which, as mentioned above, occurs mainly in the southern part of the Baltic Sea (Poland, Germany, Denmark and southern Sweden) is assumed to be one of the main causes for structural erosion in recent decades.

The sea level determines the level of coastal *wetlands*. A rise in sea level will result mostly in the loss of marshes. When the landward boundary of the marshes is restrained in a further landward shift, the process of coastal squeeze will occur. Here the tidal range is a key factor: in general, the narrower the tidal range, the greater the susceptibility to a given sea-level rise. Since tidal influence is negligible in the Baltic, the marshes there are highly susceptible to sea-level rise. Furthermore, acute erosion has also increased, especially in the open Baltic Sea, where several intense storms have been noticed in the last few decades. Structural erosion rates of sedimentary beaches range from 0.5 to 1.5 m/year; however, during storm events, dozens of meters can be eroded at once (acute erosion). Besides the natural causes, human interference can exacerbate erosion significantly, particularly in ports, port extensions, and piers, which in the last century greatly disturbed longshore transport and thus the existing equilibrium.

Other examples of human interference are local coastal-protection measures, executed by plot owners that have counter-effective results also when causing problems further downstream. Local dams and regular sea-bottom dredging and coastal mining has corrupted the northbound longshore sediment-drift dredging, essentially reducing the coastal sediment budget. These interventions have caused a deficit of sediment output feeding the foreshore and beaches of the sedimentary coast. This deficit has in turn hastened the coastline retreat in the adjacent areas.

Acute erosion processes occur essentially on the morainic, craggy, and rocky coasts in both high and low relief areas, where the underlying geological structures are relatively resistant to the erosive forces of sea, rain, and wind. Therefore, against hard rock cliffs, the erosion in general has low rate and is caused mainly by wave attack.

17.3.2 North Sea

The North Sea is situated between Norway, Denmark, Germany, the Netherlands, Belgium, and the United Kingdom. It is directly linked to the Atlantic Ocean in the north, via a wide stretch of open water between Scotland and Norway, while in the

south-west, via the English Channel. To the east it connects with the Baltic Sea, and the Kattegat is considered an interchange zone between the North Sea and the Baltic Sea.

Including estuaries and fjords, the total surface area of the North Sea is approximately 750,000 km^2 and the average depth is about 95 m, although along the Dutch and Belgian continental shelf, the North Sea is relatively shallow (average depth of about 20 m). The depth of the sea increases towards the Atlantic Ocean to about 200 m. The deepest locations of the North Sea are located near Norway (up to 700 m).

Also in the North Sea the glaciers made profound alterations in the topography of the glaciated regions, levelling hilly sections to low, rolling plains, both by erosion and by deposition of drifts, eroding hollows that later became lakes, and forcing rivers to cut new channels by filling their former beds. Because this evolution occurred around 11,000 BP, the coasts vary from coastlines intersected by fjords, via cliffs with pebble beaches to low cliffs with valleys to sandy beaches with dunes and estuaries with mudflats and saltmarshes. Along most of the North Sea coastline the remnants of the glacial deposits from the Pleistocene overlie much older deposits from the Tertiary and Mesozoic. Offshore, the seabed is covered with sand deposits, sand and mud, or smaller pockets of gravel. Much of these deposits have been transported and reformed to morphological dynamical bank systems along the coastline during the Holocene marine transgressions and occasional regressions of the sea. In the last 1,000 years the marine transgression has decreased considerably and a large-scale erosion process is affecting the present coastline; on the other hand, the effects of rivers, current climate changes and human intervention are starting to become more enhanced, especially on a local scale.

The North Sea coastline is characterized by sandy beaches and dunes, shingle beaches, saltmarshes and estuaries. Along the estuaries and along several coastlines, especially in The Netherlands, dikes and revetments were built, resulting in artificial coastlines.

17.3.2.1 Physical Processes

From the physical standpoint, the North Sea has an extremely variable tidal regime as well as wave climate. The tidal range varies from a micro-tidal condition with about 0.5 m near Denmark to micro-, meso-, or macro – tidal with about 6 m in the Channel. On the two sides of the coast of the UK the tidal currents move in opposite directions: to south on flood and to north on ebb on the west side and to north on flood and to south on ebb on the east side. Tidal-current velocities range from 1 to 2 m/s.

The dominant wind and wave direction affects the North Sea coastline in a different way, related to the coast itself; therefore, in the eastern part of the North Sea the winds from the north-west or from the south-west are dominant, with mean annual offshore wave heights of about 1–2 m and extreme wave heights of up to

10 m. Storm surges can also occur during northerly winds because of the connection with the Atlantic Ocean, where northerly wind directions cause the largest surges, up to 3 m. Along the eastern coast of the United Kingdom, a north-easterly wind and wave direction is dominant. The orientation of the south-eastern part of the coast of the United Kingdom tend to protect this part of the English Channel from strong winds, so that an average wave height of about 0.5 m is recorded, although this coast can be severely affected by easterly storms.

A sea-level rise in the North Sea of about 2 mm/year was recorded in the last 40 years, while predictions are extremely vague for the next century, varying from 0.5 and 9 mm/year, including the effects of soil subsidence. Also, the sediment transport depends on various factors, such as the orientation of coast and the direction and height of the waves.

17.3.2.2 Erosion

Along the North Sea coasts, structural or acute types of erosion are evident because of a large variety of coastal types constituted by soft cliffs, beaches, and estuaries. Sometimes because of the presence along the same stretch of coast of different types of erosion can be observed. The main causes of erosion along the North Sea coasts are: storm surges along coastal cliffs and dunes, gradients in longshore sediment transport for sedimentary coasts, sea-level rise for estuaries.

Soft-rock coasts along the North Sea are present in Holderness and Essex, but they are locally scattered, often associated with sedimentary coast (sandy or shingle beaches or estuarine coasts). These coasts are affected by a series of landslips which occur after a severe storm. Erosion rates up to 20 m have been reported within a single storm. Following the classic evolution of the cliffs, after the loss of several meters, no cliff erosion occurs over a long period. The eroded material protects the foot of the soft cliff itself, but it also serves as a sediment source for the beaches directly in front of the cliffs and for the coastal system as a whole. Therefore, structural erosion of the beaches in front of the cliffs indirectly threatens the stability of the cliffs over the long term.

The micro-tidal sedimentary coasts, in the south-eastern part of the North Sea, are represented by sandy beaches and dunes, sometimes with lagoons behind them.

Erosion occurs when dunes are effaced as a result of severe wave attack. Since the area is exposed to rather high waves during storms, severe erosion rates can occur. Beach erosion is the result of diverging longshore sediment transport along sandy coasts. During storms, the longshore sediment transport rates are greater, augmenting not only the sediment transport but also the erosion rates. The macro-tidal sedimentary coasts can be subdivided into two different types: sandy beaches with dunes, and estuaries with saltmarshes. Along coasts where sandy beaches and dunes are present the erosion is usually a combination of longshore and cross-shore transport processes.

Sea-level rise is considered to be the main natural cause of erosion in the estuaries and salt marshes along the British and Dutch coast. Estuaries respond by accretion and erosion in different parts so that they rise and move landwards, but the estuary's ability to adapt to the quickening rate of sea-level rise is uncertain.

In many cases, erosion is limited by natural features, such as the local geology, or by the presence of defences. In North Sea, human interference plays a major role in the erosion of coastal zones, significantly altering the natural processes of sediment transport and the subsequent erosion and sedimentation.

The main actions and measures taken are: hard constructions for coastal protection, construction of ports and jetties and sand mining and dredging. As observed in other European regions in the past, mainly hard constructions were applied for protecting the coastline from erosion processes. The main disadvantage of these measures is that they are irreversible and inflexible and generally protect the coastlines behind them, producing erosion downdrift. In the North Sea, while these constructions provide short-term protection to the properties directly involved, in the long run, such protection will fail. This could pose safety problems and therefore danger to users of beaches, which could also be easily undermined during periods of beach "drawdown".

Because of the characteristics of the North Sea, for ensuring safe navigation into the port and preventing the silting of navigation channels, new ports were constructed and long jetties were constructed for better protection of the existing structures. This activity has resulted in increased erosion rates at various locations because of the block the longshore sediment transport.

If, on one hand, beach nourishment may have a positive effect on coastal erosion, sediment mining can locally give rise to erosion of the foreshore of the coast and perhaps lead to the erosion of the beach and dune system over the longer term. Wave patterns could be altered by the deepening of the seafloor, particularly when mining activity is conducted in coastal areas at a few meters of bottom depth. This can increase the tidal-current velocities and the tidal volume of an estuary, resulting in local erosion.

Regarding future erosion, EUROSION (2004) showed different scenarios defined above all for sea-level rise. Each of these scenarios shows that sea-level rise will remain one of the most important issues in coastal-zone management. Not only are sea-level rises expected, but, as a result of global warming along the North Sea coastline, an increase in frequency and duration of storms can be expected, provoking more frequent and higher floods. Therefore, erosion as a result of sea-level rise is expected to continue and on-going adaptation would be required. However, the estimation of the quantity of the erosion is uncertain. Foreshore erosion is a long-term threat to sea defence and increases the expenditure needed to keep them in an acceptable condition. Ultimately, maintaining the sea defences could become so difficult that it would be necessary to set them back to a new line or carry out other works elsewhere which would achieve the same effect.

17.3.3 Atlantic Ocean

The six western EU countries – the United Kingdom, Ireland, France, Spain, and Portugal – are bordered by the Atlantic Ocean, which in the north is connected with the North Sea, and in the south is connected to the Mediterranean Sea via the Strait of Gibraltar.

In this study, we do not consider the Atlantic Ocean as whole. The Atlantic Ocean is also important for the coastlines of remote overseas regions such as the Azores (Portugal), Canary islands (Spain), and French Guiana (France). The nine islands of the Azores are located on the Micro-plate of Azores, which lies at the intersection of three tectonic plates; the African, the North-American and the Euro-Asian plates. The group extends some 480 km in a northwest-southeast direction. The Azores islands have a population of 238,000. The Canary Islands lie along the north-west coastline of Africa, directly west of Morocco. The archipelago consists of seven large islands and five smaller ones and have a population of around 950,000. French Guiana is located in northern South America, bordering the Atlantic Ocean, between Suriname and Brazil. The country has an area of 91,000 km^2 with a coastline of 378 km. Population of French Guiana is c. 172,600. Because of its size, it is difficult to summarize the evolution of the whole area, while it is evident that the southern coastline is the result of tectonic movements such as deformation or isostatic changes which have drowned a landscape where cliffs and beaches alternately occur.

In the North, the topography of Ireland and the United Kingdom is largely influenced by the more recent glacial age. In the recent past, the high energy level of the waves and tides sculpt the current irregular coastline of hard and soft rock cliffs interspersed with sedimentary coasts (sandy beaches, estuaries, dunes etc.). The coasts of Ireland, southern United Kingdom, northern Spanish, and Portuguese consist of many cliffs, while the more protected French and southern Spanish coasts are more often interspersed with softer coastal types such as bays, dunes, and sandy beaches. Among the outermost islands, such as the Azores and the Canary Islands, where the volcanic material, composed mostly by basalts, is dominant, the beaches consequently consist of volcanic sediments.

17.3.3.1 Physical Processes

The European side of the Atlantic Ocean is affected by a micro- to macro-tidal regime, with a medium range of 2 m neap tide and 4 m spring tide. Mont-Saint Michel, in Lower Normandy (France) is the locality where the highest tidal range (up to 15 m) is registered during spring tide. Connected to this tidal energy along the whole oceanic coast, the current ranges between 1 and 2 m/s, involving large spatial variability of the physical parameters.

The dominant wave direction is NW (~50%), which, along the directly exposed coast, creates a wave climate characterized by a long-distance swell with a medium

significant wave height ranging from 2 to 3 m, while along Upper Normandy (French coast) the mean annual significant wave height is higher: 3.5–4.5 m, due to the channel effect.

Storms with significant wave heights (exceeding 8 m) affect the north Atlantic coast between October and March. The high-energy waves create a strong southerly or easterly longshore drift, transporting large amounts of sediment. During calmer periods, sediments are transported with the tidal currents. Because of coast orientation, the resulting current (net difference between ebb-and-flow tides) is north to south along the Irish and Portuguese coasts and east to west along the northern French and Spanish coasts. In the estuaries, inlets, and channels the main role is played by tidal transport. Above all in France, sediment transport by the wind contributes to the deposition of high dunes.

The sea-level rise up to now has shown minor effects, perhaps because it was offset by post glaciations land uplift. In the southern part of the United Kingdom the tide gauge measurements have provided estimations for a relative sea-level rise of 2.0 mm/year to 4.0–5.0 mm/year (EUROSION 2004).

17.3.3.2 Erosion

The high-energy waves combined with the macro-tidal regime give rise to strong erosive forces along the Atlantic coastline. Strong longshore tide-and/or wave-driven currents and cross-shore wave-driven currents erode beaches and undermine cliffs. Different coastal types show different behaviour. High and low relief hard-rock cliffs erode at a slow rate (the Azores), often depending on their lithological composition. Macro-tidal regimes ensure that the waves can undermine the cliffs more effectively. By contrast, for soft-rock cliffs the erosion rate is faster, also if the process is moderated by the presence of shingle beaches at the foot of the cliffs. If these are removed, cliff erosion is accelerated.

For macro-tidal sedimentary coasts, storm events in combination with high tides reaching the beaches and dunes cause heavy erosion. During relatively calm periods, the beaches and dunes are replenished with sediment. In many cases, human interference prevents the natural replenishment of the beaches because of the presence of defence constructions, ports and other activities which interrupt the sediment supply such as damming of rivers and sand extraction.

Along areas affected by expanding urbanization, local coastal defence often accelerates natural erosion rates in surrounding areas by interfering with the delicate dynamic balance between the sea and the land. Groins and harbour piers impede natural sediment movement patterns, causing the erosion of sedimentary coasts downstream. Seawalls and cliff-stabilization works directly reflecting the waves, block natural replenishment. Torrential river flooding often transports large amounts of sediment and are important for the local sediment budget, but they are blocked by the building of dams.

17.3.4 Mediterranean Sea

The Mediterranean Sea, representing only 1% of the world oceanic surface (Er-Raioui et al. 2009), is the main sea in Europe and has several basins with sea names: Tyrrhenian, the Adriatic, Ionian, Aegean. This situation is the result of the an interplate system involving Europe, Africa, and Asia with compressional and extensional events occurring close together, producing an area of about 2,500,000 km^2 with an average depth of 1,500 m, where the deepest point is over 5,000 m in the Ionian sea, between Greece and Sicily. A semi-enclosed sea, it has a limited tidal range (often less than 30 cm) and a fragile and vulnerable ecosystem with deep basins and large-scale layered circulations (Er-Raioui et al. 2009). The geology of the Mediterranean is extremely complex and subject of continuous scientific debate.

The coastline extends 46,000 km, involving 22 countries on three continents. About 54% of the coast is rocky and 46% sedimentary: the latter areas are most vulnerable to climate change (Nicholls and Hoozemanbs 1996). The Mediterranean Sea is connected to the Atlantic Ocean by the Strait of Gibraltar on the west and to the Sea of Marmara (an inland sea between Mediterranean and Black Sea) by the Dardanelles on the east, while the Suez Canal in the southeast artificially connects the Mediterranean with the Red Sea. Many islands rich of history and archaeological heritage are present: Cyprus, Crete, and Rhodes in the east, Sardinia, Corsica, Sicily, and Malta in the centre and the Balearic Islands to the west. Today, 82 million people live in coastal cities; by 2025 there will be an estimated 150–170 million. Today the southern countries account for 32% of the region's population; by 2025 that is expected to have reached 60%. Seasonal population pressures are also expected. Over 100 million tourists flock to Mediterranean beaches every year and this number is expected to double by 2025.

17.3.4.1 Physical Processes

The circulation pattern of the Mediterranean is complex, with a limited exchange with the Atlantic Ocean through the Strait of Gibraltar. Fresh water supply comes from a few large river systems, including the Nile, the Rhone, the Ebro and the Po, with numerous smaller rivers and streams. The basin is relatively salty, because of the excess of evaporation over fresh water influx. Because the Mediterranean is more or less land locked, the climate is dominated by land masses rather than marine influence. The main circulation in the Mediterranean is an anti-clockwise movement of the water. The water coming in through the Strait of Gibraltar flows eastward along the north coast of Africa, and then branches off. In the western Mediterranean the current continues along the north coast of Sicily, and then moves to the north, west, and south, along the coasts of Italy, France and Spain, back to Gibraltar. The outflow to the Atlantic Ocean is a subsurface current below the inward current. The current flows with a speed of one to two knots (one knot is one nautical mile or 1,852 m/h). It is more powerful in summer than in winter, because

there is more evaporation during the summer. There are a few secondary currents moving in the same direction: one to the north of Algiers, and another to the west of the Tiber. These special currents are strong and dangerous in narrow channels, such as the Strait of Messina.

The Mediterranean is micro-tidal, with small variations alongshore due to basin shape. Seas that are almost completely closed have, like lakes, only a very small tidal range, i.e. a small difference in sea level between high and low water. In the Mediterranean the tides are significant only in the Gulf of Gabes (to the south-east of Tunisia) and the northern Adriatic. The general Mediterranean astronomical tidal range is about 20 cm. In the Adriatic it can reach about 90 cm. The latter sea can be regarded almost as a channel, between the straight Italian coast, and the coast of the Balkan peninsula, with many small islands, most of which run parallel to the coast. In the Adriatic Sea the tidal range is different, as the surface currents are created primarily by the wind and can reach a speed of three and a half knots.

Water-level variations result from climatic influence in the form of atmospheric-pressure changes and winds. The complex basin geometry, and the variations in weather hinder the description of one wind- and wave-climate. A number of special winds occurs. Some of these are: Levanter, Gibleh, Sirocco, Mistral (or Maestrale), Libeccio, Tramontana, and Bora.

Sediment sources can be fluvial, cliff erosion, biogenic production, and alongshore redistribution. On insular and certain parts of the Mediterranean the contribution of biogenic carbonates (shells of various organisms) plays an important role in the sediment budget. The production of biogenic carbonates can be coupled to specific habitats on shoreface and slope, dominated by *Posidonia Oceanica* or Mediterranean seagrass now in a process of serious degradation.

The eastern Mediterranean has been subject to a high sea-level rise during the past decade at a rate up to 20 mm/year in the Levantine basin. A sea-level rise of 5–10 mm/year is also observed in the Algerian-Provencal basin as well as in the Tyrrhenian and Adriatic seas. The northern Ionian sea, on the other hand, shows an opposite trend, i.e. a sea level drop of ~−5 mm/year.

The relative sea-level rise can have important implications for the future of the deltas of the Mediterranean Sea. However, here the pattern of change is much more complex, with tectonic movements caused by a variety of influences (e.g. volcanic activity and earthquakes). When this is coupled with human influences which exacerbate the sea-level rise, significant problems of erosion, salt-water intrusion and flooding can occur. These effects are especially important in the major deltas where a decrease in sediment availability due to the dam effect and subsidence due to water pumping or the sheer weight of infrastructure may be some of the factors which give rise to substantial problems of erosion and flooding as is experienced in several of the major Mediterranean deltas.

17.3.4.2 Erosion

The Mediterranean is a good example of a coastal region where human pressure is already significant and increasing (Jeftic et al. 1992). Around the Mediterranean

Basin, the total estimated population in coastal areas by 2015 will grow by 31 million inhabitants compared to 2000 (Plan Bleu 2006).

Driving forces of erosion processes along the Mediterranean coast are quite similar amongst them, but a high diversity results from geomorphologial features of each different area (Geodiversity). As a natural process of hundreds of years, erosion is due mainly to winter storms, when most of the material is removed from beaches and transported elsewhere down the coast line, a fraction of it being lost permanently under the bathymetric of −10 m/¯15 m and, naturally replaced by new material from continent-shelf erosion transported by rivers.

All these forces reach to a natural equilibrium where as much material is eroded as it is sedimented. However, the rising of sea level upsets that equilibrium with different forces coming into action. Lately, since most of the new material remains trapped in dams and reservoirs along Mediterranean river basins, at least one of the forces cannot act and thus the equilibrium does not occur naturally. Moreover, a large number of anthropic factors act throughout the Mediterranean Sea: obstacles to longshore drift (e.g. ports, marinas, dykes), and a weakening of the coastal material resilience due to urban development and infrastructures. Consequently, many erosive problems along the coastline are the evident manifestations of disturbances of the coastal dynamics.

In the Mediterranean, while sea-level fluctuations in historical times seem to be determined largely by local tectonic effects, climate change may have represented an additional factor particularly affecting the most important natural wetlands and coastal lowlands in different littoral areas. Human-induced effects maximize the problems linked to sea-level rise, via the following damaging activities: a reduction of river sediment supply; the destruction of natural shoreline defences, such as sand dunes, coastal ridges and posydonia meadows; and anthropic works for coastal urban development related to commercial or tourist activities. On the other hand, the excessive pumping of groundwater may increase subsidence due to the lowering of piezometric surfaces of confined aquifers, as well as to compaction phenomena. Dams prevent natural sedimentation processes by restraining the flow of riverine fresh water, thereby reducing the sediment supply to the coastal system and deltas and associated coastal sedimentary cells.

Of the over 6,000 large dams in Europe, Spain has the most (1,200), followed by Turkey, France, Italy and United Kingdom, each of which have more than 500 large dams. Mediterranean regions are very clear examples of problems related to damming. In fact, most rivers have a torrential regime and so the effects of dams are stronger: in this case, dams have a short life span and detain voluminous sediments that otherwise would reach the beaches. The example of the Ebro delta is highly representative: less than a 5% of the sediment carried before damming is reaching the delta (Serra 1997; Montoya and Galofré 1997).

In streams, gravel mining, together with dams, is the main cause of sediment deficit in many rivers. Stream mining directly alters the channel geometry and bed elevation while disrupting the continuum of sediment downstream.

One of the most dramatic examples of wild gravel mining in the Catalan Coastal Ranges can be followed in the unregulated Tordera River (970 km^2). There, around

5,106 tonnes of sand and gravel were extracted during the 1960s and 1970s until 1982, when mining was prohibited. This means ten times more the annual sediment yield of the Tordera River, including both suspended and bedload (Rovira et al. 2002). Strong erosion is now affecting the 60 km of coast in the Maresme region (northern Barcelona), where beach nourishment was first applied in Spain from 1989. Fluvial sediments were converted to aggregates for construction in the Costa Brava area during the rapid growth of tourism during those decades.

Also roads, buildings, and other types of infrastructure can limit or affect the natural response of coastal ecosystems to sea-level rises. As populations in coastal areas have grown and economic activity has intensified, so a range of often inter-related and conflicting pressures have emerged in these areas, focused around agricultural use, industrial and port use, residential use, tourism, coastal water quality, and fisheries. These in turn have exerted pressure on coastal development and land reclamation around estuaries and lagoons.

In France, for example, natural coastal areas are being lost at a rate of 1% a year; 15% have disappeared since 1976, and 90% of the French Riviera is now developed (EUROSION 2004).

17.3.5 Black Sea

The Black Sea is the largest semi-closed sea bordered by Europe to the North, West and East and by Asia to the South. It is connected by the strait of Kerch to the shallow Azov Sea and with the Marmara Sea (the Mediterranean Sea, respectively) by the strait of Bosphorus (Stanchev et al. 2011a). Romania, Bulgaria, and the European portion of Turkey borders it on the west. The Northern and Eastern shores are bordered by Ukraine, Russia, and Georgia; the entire southern shore is Turkish territory. The Crimean Peninsula projects into the Black Sea from the north, forming the shallow Sea of Azov on the east and the Karkinitskiy Gulf on the west. The Black Sea has a surface (excluding its northern arm, the Sea of Azov) of about 436.400 km^2 with a maximum depth of about 2.245 m. The Black Sea basin is divided into two parts, the Western and Eastern basins, separated by the mid-Black Sea ridge.

The salinity of the Black reaches around 33‰, and is influenced by the supply of fresh water and the supply of Mediterranean salt water. The basin is strongly stratified, with the upper 200 m being well mixed and oxygenated, and the water below being oxygen depleted. A lack of dissolved oxygen below 100 m, together with high concentrations of hydrogen sulphide prohibits the growth of anything except for specially adapted bacteria. This also gives the water a dark 'gloomy' appearance beyond the shallow shelf areas

The origin of the Black Sea has long been discussed, and it has been proposed that the entire Black Sea was rifted starting during Aptian-Albian period (Gorur et al. 1993), but the age of the rifting for the Eastern Black Sea is less well known (Spadini et al. 1996). Following the closure of the Neotethys, the Black Sea began

to close during the Eocene-Oligocene age, and the Eastern Black Sea continued to close from the Miocene to the present. (Keskin et al. 2011) The whole region is at present tectonically active.

During the Quaternary, the Black Sea level shifted many times, in accordance with drastic climatic changes (glaciations and inter-glaciations). The Bosphorus strait, with its sill at about −34 m, determined a specific regional behaviour of the Black Sea: when the water level was lower than the sill depth, the connection with the Mediterranean Sea was interrupted and the Black Sea water level varied under the local hydrological and climatic conditions (Panin 1999, 2009). These Quaternary changes of the water level had also significantly influenced the alterations and evolution of its coastline and area, respectively (Stanchev et al. 2011a, b).

17.3.5.1 Physical Processes

The Black Sea is nearly tideless, because it is not coupled to any oceans, and it is too small to generate tides of its own. Wind and waves are therefore the main forces that act on the shores. Winds and associated pressure systems can lead to temporary changes in the sea-level of up to 40 cm. The dominant wind direction is from the North, both in intensity (wind speed) and in duration. Storms occur mainly in winter periods. The wave directions follow the wind directions. Waves with a height of up to 6–7 m reach the shores, from all directions but west. Given the orientation of the western Black Sea coastline (roughly north–south), and the dominant wave direction the resulting residual current is directed from north to south. Sediment-transport is also directed from north to south (EUROSION 2004). The sea level over the Black Sea's history has been rather complex and controversial; there is still little consensus on the Black Sea variations in level, and different scenarios have been proposed to explain the evolution of this body of water since the Last Glacial Maximum (Keskin et al. 2011)

The maximum rise in the Black Sea (3–5 m above current level) took place 3.5–4 ka ago during the Subboreal period. At this time, the so-called Old Black Sea terrace was formed (Panin and Popescu 2007). A rapid lowering of the water level by 25–28 m followed, coeval with the first Greek colonization of the Black Sea coast. A new, short-lived ingression of the sea to a stand of +1 to +3 m then occurred. By about the tenth century AD, the level of the Black Sea dropped 1–2 m, then slowly rose, a trend that continues today (Panin and Popescu 2007). The mean values of average sea-level rise for the western part of the Black Sea vary between 1.5 and 3 mm/year (Pashova and Jovev 2007). Although such rates are not dramatic for the Bulgarian coast, there would be a case of sudden sea-level surge under certain meteorological events (Stanchev 2009).

17.3.5.2 Erosion

Only the western bank of Black Sea actually pertains to the EU with two new entry countries: Romania and Bulgaria. In the near future, Turkey (2015?) should join the EU, while the Ukraine, Russia and Georgia are not on list for membership.

The coastline length ranges between 4,020 and over 4,400 km. Values for the Black Sea area also vary in large diapason: between 413,500 and 436,000 km^2 (Stanchev et al. 2011a, b). The area, in the north sector, is geographically dominated by the Danube delta, and it is striking that erosion is one of the main problems along the coast of Romania. At present, the shoreline is strongly affected by anthropic structures (hydrotechnical offshore works placed on Midia Head and Singol Head). Protection systems (hard and soft) have been built along the coastline of Romania since 65 years ago.

In Bulgaria an average erosion rate of about 0.1 m/year, is affecting nearly the entire coastline. The rate of coastal erosion is highest in the north coastal zone (up to 1.5–2.0 m/year.) and in the southern part (up to 2.0–2.5 m/year.). A scour of the accreted sand coasts has further been recorded (Dachev 2000).

Natural and anthropogenic factors have been pointed out as the main causes for the sea-level rise. In any case, it is untenable to consider this variety of causes for coastal erosion without taking into account the Danube delta and the remainder of the coast. Hydrotechnical works built both on the Danube and tributaries have seriously impeded the Danube's sediment load, with negative consequences on the littoral sediment balance. Since 1858 until 1988 the flow volume increased from 178 to 203 km^3/year but the sediment load decreased from 65 to 38 million tonnes/year. The Danube Delta coastline has erosive problems on 57% of the shores, while 36% are accreting and 7% remain stable.

The human modifications and actions accelerate the local problems of coastal erosion. Jetties, groins, and breakwaters, for example, are designed to trap littoral sediments. Removal of sediment from the coastal sediment budget by human actions is also a concern. These include commercial extraction of sediments from coastal rivers, dredging, disposal of sediment in confined or upland areas, and improper beach-cleaning and management techniques. Also, stream-gravel mining is, together with dams, the main cause of sediment deficit in many rivers. Stream mining directly alters the channel geometry and bed elevation while disrupting the continuum of sediment downstream. Removal of sediment from the coastal sediment budget by human actions is a common activity. These include commercial extraction of sediments from coastal rivers, both in Romania and Bulgaria.

The Romanian coast suffers a dramatic disequilibrium from the damming and the diversion of the Danube. This has drastically reduced the coastal sedimentary budget given the greater erosion along the entire coastline. Also in Bulgaria, numerous dams (more than 2,000?) have been built. Since the beginning of the twentieth century until the present, the control of coastal erosion and landslide processes along the Bulgarian coast has been implemented using hard-defence options, such as seawalls, solid groins, and dykes (Stancheva 2005; Stancheva and Marinski 2007).

In addition, large ports (harbours) and small ports (marinas and piers) are among the main causes of coastal erosion, especially in wave-dominated coasts with important sediment transport drift. Roads, buildings, and other infrastructures can limit or affect the natural response of coastal ecosystems to sea-level rise. As populations in coastal areas have grown and economic activity has intensified, so

a range of often interrelated and conflicting pressures have emerged in the coastal zones focused on agricultural, industrial, and port use, residential use, tourism, coastal-water quality and fisheries. These in turn have caused pressure for coastal development and land reclamation around estuaries and lagoons. Therefore, as in all countries, the acceleration of the coastal erosion in Romania and Bulgaria is driven by the development of the coast. The permanent extension of commercial activities has led to the necessity of building tourism infrastructures and resort complexes near the beaches even if in many cases they are not secure.

17.4 Policy Options

As shown previously, all coastal Member States of European Union suffer coastal erosion. About 20,000 km (20% of the overall coastal development) have undergone serious impact. Most of the affected areas are under the negative influence of protection structures built before. To solve this problem, all of these member states have implemented coastal-protection measures (mainly to protect against flooding and erosion) to some extent in the past. Countries with historical experience of flooding and extreme weather events along their coasts seem to embed such measures in dedicated coastal plans and programs. Consequently, North Sea and some Atlantic Ocean countries currently have the most complete coastal-protection or development plans. Mediterranean countries are focusing their policies mainly to protect beaches for touristic purposes.

Above all, to ensure sustainable co-existence between human activity and natural resources of this great variety and complexity, the European Union is seeking to implement a policy of Integrated Coastal Zone Management (ICZM). This policy has received a very different response at the local level. The EU Member States facing this problem have taken on a diverse set of initiatives. This diversity has different reasons and often rooted in historical processes and cultural legacies that would lead us away from the objective of this text. Almost all Member States have adopted a restrictive policy of the chafing that forbids the building of new facilities, although this type of legislation may present several exceptions in order to maintain existing buildings and act in its defence at all costs. Only a few states, mainly in northern Europe and in France, have introduced measures for retreating absorption. France, with the action of the Conservatoire du Littoral and the Barrier Act has regulated the purchase of erosion-hazard areas and the abandonment of the coastline for the evolutionary purpose.

In the Baltic Sea, most countries implement accommodation and retreat measures by means of spatial-planning regulation. Most Baltic countries give the land back to the sea in case of flooding or erosion in uninhabited areas. The pressure and anthropogenic uses of the coastal strip, over the past decades, can be traced to historical and cultural reasons. It is therefore possible, starting from a common base of knowledge, really to try to narrow the policies adopted in relation to erosion

processes that are most active. The Baltic Sea is bordered by nine countries: Sweden, Finland, Russia, Estonia, Latvia, Lithuania, Poland, Germany and Denmark. The main driving forces for erosion in the Baltic Sea region are wind and wave action while in the future, accelerated sea-level rise will become increasing important. Tidal influence in the Baltic is negligible. Therefore, the sediment supply in the Baltic originates mainly from wave-induced sediment transport, erosion of soft moraine and alluvial cliffs, and river-sediment discharge.

The impact of erosion in the coastal zone depends on different parameters. First, the population density is high in the big cities all around the Baltic (>500 persons/km^2). Furthermore, other functions can be threatened such as tourism, nature, and economic value. The economic value at risk is usually high in low-lying areas where flooding can occur, such as Germany, Poland, parts of Denmark, and southern Sweden. On cliffs and elevated land, only the property threatened directly by erosion is at risk. Coastal protection is applied mainly to protect human lives and economic value in the Baltic area. In some cases, tourism or natural values have been actively protected (Fig. 17.8); the awareness of the importance of these other functions has been growing in recent years.

Strict laws and regulations are applied to define set-back zones and building restrictions for their coastal zone. Coastal protective measures against flooding, erosion, and extreme weather events are undertaken only when there is a specific need for it. In these cases, public or private property owners need to gain permission at the national level, and beach nourishment or soft defences are preferred.

At present the responsibility for planning coastal-protection schemes is usually taken at a national level. The most frequently applied policy options in the coastal zone of the Baltic area are to hold the line and limited intervention. Limited intervention is applied in areas where the threat to economic values is small; the advantages of dynamic coasts for nature conservation have also been acknowledged in the Baltic. The option “hold the line” is still applied when high economic values are threatened by erosion, while historically it was executed mainly with hard measures like seawalls, revetments, slope protection, groins, and more sparsely detached breakwaters.

However, since the 1970s, a shift towards the use of soft measures and nourishment started in Germany and Denmark. During the last decade, this shift has taken place in all Baltic countries and the use of nourishments has increased significantly in the entire area. Hard measures turned out to be failing after some time by storm damage or increased foreshore erosion, and furthermore have caused increased erosion downstream. Nourishment, although only temporarily effective, have proved to be successful in mitigating the effects of interruption of long-shore transport and not causing a disturbance of the natural equilibrium in the Baltic area. Repetition of nourishment is needed for effectiveness over the long term.

In the past, private landowners or local groups have often tried to protect their property individually in the Baltic Sea area. This individual approach often resulted

Fig. 17.8 Pomarian Coast (Poland): Ruins of Gothic church from fourteenth/fifteenth century on Morrenic sediments easely eroded by waves (view from east (**a**) and from west (**b**))

in unprofessional designs and a lack of maintenance, causing quick deterioration of the structures, and a lack of common approach, causing the problem to be moved but not solved. Through the failures of these coastal protections, the importance of a common approach, a design by professionals and good maintenance was acknowledged in the Baltic area. However, maintenance is still relatively poor and underestimated in some parts of the Baltic. In addition, or even instead, measures to stop or slow down erosion, measures like foredune and forest

maintenance are applied to mitigate the effects of storm surges in the Baltic. This strategy has been shown to be cost effective mainly in countries with low labour costs, such as the Baltic States. This is likely to change with entry to the EU, when labour costs are likely to increase.

The ICZM is in a very early stage in the Baltic Sea area, though some ICZM programmes have started in the past few years (HELCOM – Helsinki Commission Baltic Marine Environment Protection Commission, VASAB 2100 – Vision and Strategies around the Baltic Sea 2010, Baltic21 and Procoast). In some projects, steps towards integral approach for the planning and financing has been seen (mainly in Denmark and Germany); furthermore the importance of other functions besides safety, like tourism and nature, has clearly been acknowledged, but this has generally not yet been implemented in legislation or organization in the Baltic area.

The North Sea is bordered by eight countries: Norway, Sweden, Denmark, Germany, the Netherlands, Belgium, France and United Kingdom. Various natural causes of erosion can be identified along the North Sea. Summarized, these include sea-level rise (2 mm/year on average), gradients in long-shore sediment transport for sedimentary coasts and storms (cross-shore sediment transport) for cliff and dune coasts. To some extent, as observed in the Baltic Sea, the northern coasts are generally less susceptible to erosion and flooding because of rising land levels and more resilient rock. Erosion is also caused by human interference, affecting the natural processes of sediment transport. Examples are the construction of coastal-protection structures, construction of ports and jetties, or sand mining and dredging.

Historically, the most frequently used policy option was to hold the line when safety of human lives and of economic investments were at stake. This was executed mainly with hard measures, but the last few decades the emphasis is shifting in the direction of soft measures (nourishment). The do-nothing policy has historically been applied when no investments or human lives were threatened. Later, the option to do nothing was also suggested when a coastal-protection measure would have effects that were too negative along the adjoining coastal stretches or when this option enhanced the natural behaviour of coastlines and estuaries.

North Sea countries use primarily hard and soft protective measures (beach nourishments, heightening of dykes) (Richards and Nicholls 2009). Along the North Sea, protective measures have been used for decades. Whereas all countries traditionally focused on hard defences such as dykes and breakwaters, “soft where possible and hard where needed” is currently the preferred policy. At present, beach nourishment constitutes a major part of the coastal-protection expenditure in the Netherlands and Belgium, whereas only in Germany does the majority of coastal expenditure still go to hard infrastructures. In the UK, Individual Schemes, developed according to the guidelines of the Shoreline Management Plans, detail the exact measures to be implemented, these differing for each coastal segment.

Most of the North Sea countries have been protecting their coasts for decades (Fig. 17.9). Compared to 1998, especially the Netherlands and the UK have intensified coastal protection expenditure to cope with the effects of climate change and extreme storm-wind surges, especially after the disaster of 1953 and recent storms where the alarm level has been reached in the Netherlands (Fig. 17.10).

Fig. 17.9 Holland coast: dykes and channels

Fig. 17.10 Ministry of Coasts (RIKZ) Sea-level control alarm station (Eurosion 2004, J. Serra picture)

Their expenditure is expected to rise further, but changing progressively to realignment policies.

As a result of the economic situation and the rather high population, authorities are willing to invest in the preservation of areas that are ecologically valuable, such as salt marshes, mud flats, and islands where bird colonies breed. Because of rehabilitation of the natural sea-land environment, new technical potentialities, and political accents made since the 1970s, preference is now given to soft measures, i.e. beach nourishment, respecting the natural dynamics of the shoreline (coast or estuary). A further advantage is the sufficient availability of sediment in the relatively shallow North Sea. On the other hand, the long-term consequences of structural deepening of the foreshore due to sand extraction is not well known.

A less accepted policy option is Managed realignment. Large flooding in the past with loss of life and property left a legacy in the present-day attitude towards coastal-zone management in low-lying countries in the North Sea region. The general perception of the necessary defence against the sea hinders the acceptance of the managed-realignment option. Despite this, at least in south-eastern England a major policy shift has been made in the direction of managed realignment, which recognizes the implications of coastal squeeze with its loss of intertidal land and the value of recreating habitat both of nature conservation and as a contribution to a more sustainable sea defence.

In the North Sea area, most countries have a long tradition of coastal management and of integrated strategies. Compared to other countries in Europe, these countries have therefore made the most progress in implementing ICZM, although national legislation concerning ICZM is not present yet in any of the North Sea countries. It is clear that there are moves to develop ICZM –either on a statutory or non-statutory basis– in all the North Sea countries. At the moment, however, the picture is by no means uniform.

The Atlantic Ocean borders Western Europe along the following EU-countries: the United Kingdom, Ireland, France, Spain and Portugal. Erosion of the Atlantic coastline is a consequence of natural and human-induced factors. The high-energy, storm-generated waves from the Northern Atlantic and the macro-tidal regime (medium range 2–4 m, maximum up to 15 m in Bay of Mont Saint-Michel, France), are dominant for high volumes of longitudinal transport and at the same time strong erosive forces along the continental European Atlantic coastline. Together, they create extreme circumstances with strong alongshore tide and/or wave-driven currents and cross-shore wave-driven currents that can easily erode beaches and undermine cliffs. In the future, climate change is expected to induce accelerated sea-level rise (at present 2–4 mm/year) as well as a potential increase in storminess. Both will enhance erosion along the Atlantic coast. Human interference, such as the construction of seawalls or groins, damming of rivers or managing estuaries and sand mining, has enhanced the erosion locally.

The policy option “hold the line” is often applied when seaside resorts or other recreational facilities are at risk. Especially in the southern countries of France, Spain, and Portugal (and the Azores), but also often, in the southern part of the United Kingdom and Ireland, tourism plays a leading role at the protected sites.

Fig. 17.11 Sea wall protection in north Portugal

Furthermore, high population densities and economic investments are protected by applying the hold-the-line policy option, as in the United Kingdom, Ireland, and Portugal (Fig. 17.11).

The policy options "do nothing" and "managed realignment" are possible at some of the seaside resorts and recreational facilities if the capital at risk is relatively low and the recreation facility or houses can be moved landward without excessive problems. The policy to do nothing is usually applied along cliff coasts where no flooding risks are present and therefore the capital at risk is relatively low (example: picture of Wight Island, UK). In a flood area, a new defence line is usually defined (e.g. managed realignment).

Atlantic Ocean countries implement both protective and accommodation measures. France, Portugal, Ireland, and part of Spain seem to use a combination of soft and hard protective measures but also accommodating options can be identified. Furthermore in France, for example, counties are encouraged to establish risk-prevention plans (Fig. 17.12).

In addition, the French government created the public agency Conservatoire du Littoral to acquire and restore threatened natural areas on the coast, lake shores, and stretches of water throughout the country. Also in Portugal, there seems to be a hierarchy of spatial planning instruments for regulating the organization and use of the national territory.

Fig. 17.12 Dune system protection in Aquitaine (France)

Beach nourishment is executed on a much smaller scale (in terms of m^3) than in the North Sea and the Baltic Sea regions. In the North Sea regions, soft measures are often undertaken to combat erosion, whereas along the Atlantic Ocean coasts the soft solutions are often combined with hard measures. Due to the high-energy conditions of the coast and the steep foreshore, nourished sediment is quickly transported in an offshore direction.

Integrated Coastal Zone Management is still in an orienting phase in the Atlantic region. About half of the regions have developed some kind of progress in ICZM. Although national ICZM-policies are not yet present in any of the continental and peripheral Atlantic Sea countries, on a local scale, it is implemented by means of, for instance, interregional cooperation (e.g. Normandy and Picardy, France). The ICZM-projects (OSPAR) concern mainly environmental issues and they are executed mainly on a local scale. Some of the TERRA and LIFE projects focus on coastal erosion issues.

The Mediterranean Sea borders 22 states but only 5 are EU Member States.

Driving forces of erosion processes along the Mediterranean coast are quite similar, but high diversity results from geo-morphological features and local climate of each area. Erosion is due mainly to winter storms, when material from beaches is transported elsewhere, partly into deeper water. Natural sediment input from torrential rivers previously balanced the loss. The large rivers feed only their own Holocene build-up deltas, without contributing sediment to neighbouring

coastal areas (the most evident example is given by the Nile Delta (Randazzo et al. 1998). Relative sea-level rises shifted the equilibrium. The sea-level rise is high in the eastern parts of the Mediterranean (up to 20 mm/year in the Levantine basin), as well as in the Tyrrhenian and Adriatic Seas (5–10 mm/year.) influenced by the tectonic activity. A fall in sea level can be found in the north Ionian Sea (5 mm/year). Part of the observed sea-level change in the Mediterranean is related to the water temperature. Besides, sediment is trapped in rivers by dams and reservoirs, the effect of which is ongoing. Moreover, a considerable number of anthropic factors are present: obstacles to alongshore drift (ports dykes e.a.) and a weakening of the coastal-material resilience due to development and urbanization processes.

Over 100 million tourists flock to Mediterranean beaches every year and this number is expected to double by 2025. This exerts a high pressure on the environment. In general, beach erosion affects tourism, threatens valuable property, and increases the risk of flooding. Part of the erosion problem is not the erosion itself, but the growing investments in the coastal zone. The comfortable climate boosts the many tourist towns and resorts along the Mediterranean Area. Residential housing of local inhabitants is expanding as well.

In most Mediterranean and Black Sea countries, specialised technical standards and guidelines for the design of coastal-defence structures seem to be lacking. As a result, the investments in protective measures along these marine basins, if any, are provided mainly for *ad hoc* hard defences such as breakwaters and groins, often resulting in mal-adaptation causing further impact (i.e. rate of erosion) on other parts of the coastline. Examples all along Mediterranean coasts are quite similar: Tuscany (Italy) with its defences (sea walls and groins) made with Carrara marble (Marina di Massa (Cipriani and Pranzini 2009)), Giardini – Naxos (Sicily, Italy (Lanza and Randazzo 2012)) where groins and breakwaters have not been allowed the advancement of the coastline (subsequently beach nourishment has brought some better results; Fig. 17.13), Sitges beach (NE Spain (Serra Raventos 2004)) with a long history of CZM policies and poor results and the Cyprus coast with large coastal erosion is reaching agricultural properties (Fig. 17.14).

Coastal management since about 1960 has resulted in some heavily engineered coastlines in the Mediterranean Sea at places where human interests had to be protected. Hard constructions were built in an effort to stop erosion. Although in many cases the works did not have the desired result, many seawalls and groins continued to be constructed and shifted the problems to the future or neighbouring areas. As the pressure on the coastal zone due to human-induced activities and relative sea-level rise keeps expanding, the need for sustainable solutions that do justice to the environmental values is growing.

Over the last few decades a trend has developed towards more flexible solutions. Soft measures (nourishment) are being applied more often. A disadvantage of nourishment is a necessary repetition and possible (irreversible) damage to sea grass protected communities (*Posidonia oceanica*), which have a very important role on sand-bottom stabilisation, apart from ecological value. Integrated Coastal Zone Management principles are not commonly used in the Mediterranean, but nevertheless there are some local willing experiences (Randazzo and Lanza 2011).

Fig. 17.13 Examples of Italian intervention: (**a**) Massa Carrara and (**b**) Giardini Naxos

The Black Sea is an inland sea lying between south-eastern Europe and Asia Minor. The total length of the Black Sea coastline is over 4,400 km and belongs to 6 states, which are not currently Member States. The northern and eastern shores are bordered by Ukraine, Russia, and Georgia; the entire southern shore is Turkish

Fig. 17.14 Other intervention in Mediterranean Sea: (**a**) Stiges (Spain) and (**b**) Cyprus

territory. The large variety of geomorphologic types of these coasts corresponds to different geological environments surrounding the Black Sea.

Given the length and variation of the western Black Sea coast, there are various causes for coastal erosion. First of all, the ongoing sea-level rise results from the eustatic world-wide change, and a related local subsidence or uplift . The local part introduces variations in relative sea-level rise along the Western Black Sea between 2 and 4 mm/year. The relative sea-level rise is larger in the Danube delta area (local subsidence) than along the remainder of the shores. The natural factors involved

Fig. 17.15 Coastal defences on the southern Danube delta coast (Romania)

include changing river discharge into the Black Sea, rainfall-evaporation balance and water exchange through the straits linking the Black Sea to the Mediterranean. Human causes vary from large-scale impact by the reduction of the fluvial contribution in sediments, due to damming, mining, and interruptions in the alongshore sediment transport by jetties, to the local impact of various hard measures.

Erosion in the Danube delta exerts impact on the ecologically important wetlands of the delta and locally on coastal communities. Erosion on the remainder of the western Black Sea coasts affects coastal communities and has impact on major economic activities. In this respect, tourism is the most important factor for most sites on the Black Sea.

The applied policies to deal with coastal erosion vary, from limited interventions, i.e. "hold the line", to "do nothing". In the Danube delta, only a small percentage of the beaches are kept in place (hold the line; Fig. 17.15) and the remainder is allowed to prograde and retreat (do nothing). This follows the role of the Danube delta as an ecologically, rather than in economically important area. The hold-the-line option is applied in Bulgaria and Romania, where economic factors are at risk.

Technical measures on the Black Sea shores are mainly hard, where experience with nourishment is limited and not very positive. The not-so-positive experience is related to the technical details of the particular nourishment, and not the with technique in general. Hard measures vary from dykes and sea walls to detached breakwaters. The effectiveness of the hard measures varies strongly depending on their design in relation to the erosion problem.

Future developments follow the trends observed today. Pressure on the shorelines will undoubtedly increase, when population and tourism increase as the economy in Bulgaria and Romania grows. An accelerated sea-level rise may add to the already existing problems.

Integrated Coastal Zone Management is starting in Bulgaria and in Romania. Coastal zone management plans are being developed, with strategies to deal with erosion and environmental rehabilitation.

17.5 The Next Step

It is evident that the coastal-erosion problem and the same coastal management is becoming of primary importance both at the global and local scale, in terms of soil lost, above all where specific interests exist, both private (hotel and other receptive structures) and public (seaside way, ports, and infrastructures) which are threatened or destroyed by sea action.

The measures currently undertaken per marine basin to protect against coastal flooding and erosion can be summarized as:

- Baltic Sea: Coastal risk-reduction measures related mainly to spatial planning;
- North Sea: Mostly a mixture of hard and soft protective measures;
- Atlantic Ocean: Some countries implement protective measures, other countries combine "protect" and "accommodate";
- Mediterranean Sea: Rely mostly on *ad hoc* hard defences;
- Black Sea: Rely mostly on *ad hoc* hard defences.

In Europe, to analyse the two aspects involved in the question, many research programmes have been funded considering the subject at the global level or at the local one and study cases refer to different environments.

With this type of direct analysis, during several studies, it has been possible to highlight the historical development of the coastal protection from the erosion, making the comparison with the actions made in the United States of America, where the equilibrium of the coast must undergo frequent and strong hurricanes which, in a wide area of the country, introduce another major erosion factor.

The synthesis of the different research has highlighted a series of procedures which take the acronym ICZM (Integrated Coastal Zone Management), which has the objective of summarizing the tools necessary for the defence of the coastal area for the sustainable growth of the whole coastal belt, which should include at least a 1-km strip from the sea and to consider all the factors which influence it. A focal point is to maintain strong control of the processes that both directly and indirectly have influenced the coastal evolution.

It is clear that it is hardly possible to prescribe a single system for all EU Member States, especially because the coastal landscape markedly differs not only in physical and morphological features, but also in the use and management of public goods.

Coastal-erosion management should move away from piecemeal solutions to a planned approach based upon accountability principles, by optimising investment costs against values at risk, increasing social perception and acceptability of actions, and keeping options open for the future. This move should be driven by

the need to restore the coastal resilience and the favourable sediment status and be supported by Coastal Management Plans (CMP).

In strategic terms (MESSINA), it is important to highlight:

- the costs which include:
  - costs of preliminary studies including technical feasibility, environmental-impact assessment, cost-benefit analysis, and social-perception studies.
  - costs necessary to implement the shoreline-management scenario. These costs include the collection and production of baseline data and indicators, consulting fees for shoreline modelling, and technical design, expenses related to input materials and field operations, and the costs of project management and administration.
  - operating and maintenance costs, which are the costs to be spent annually to maintain the effectiveness of the shoreline-management solution over its life expectancy.
  - operating cost of environmental-monitoring procedures, which is to say the costs of measures and procedures to monitor and mitigate the adverse effects of the shoreline-management scenario, as defined by the environmental-impact-assessment study.
  - external costs and benefits, respectively, reflect a decrease or increase in values induced by the different scenarios.
- The human value derived from goods (including lands) which can be extracted from, or built on near-shore areas, as a direct result of mitigated coastal erosion, such as new infrastructure built in areas less prone to coastal flooding, new hotel resorts built along waterfronts and to a lesser extent small-scale mining activities of sea products.
- The economic value of products, services and/or rights derived from a land parcel or from assets built on this parcel (such as infrastructure). The economic value may be expressed in a variety of ways in terms of capital invested, land market value, replacement costs, turnover, or jobs. It may concern a wide range of economic sectors: tourism, mining, agriculture, aquaculture, fisheries, services, etc.
- The ecological value may be expressed in terms of replacement costs or willingness of the public to pay for protection and represent the value derived from functions fulfilled naturally (i.e. without human intervention) by a coastal land parcel. This includes, for example, re-establishing resilience, dunes protecting freshwater lagoons and filtering waters; wetlands and local marine habitats providing suitable conditions for fisheries and aquaculture, marshes and flats absorbing nutrients and contaminants drained by rivers.
- The heritage (or existence or information), which represent the value derived from the benefits which do not involve using the site in any way, the value that people derive from the knowledge that the site exists, even if they may never actually visit it. The heritage value may be estimated for designated buildings and monuments (e.g. churches), designated natural parks (national, regional

parks, site of scientific interest), archaeological sites, historic gardens, parks, or battlefields, and sites of special interest.

The next step for determining the coastal area from the erosion hazard is that to reach a management system, continuous care should be taken of the real urban necessity of the area, and a framework established for them in a vision of sustainable policy which do not anticipate a future intervention of the defence of the present coastal works.

It is necessary to guarantee the resilience of the system for a medium to long period in the coastal area so that the beach and more in general the coastal area could react in a natural way to the retreat of the coastal area.

It is necessary to activate all the policies needed to internalize the costs of the intervention so as to stop the continuous request for funds at high levels, which should be allocated only for sustainable proposals.

References

Bartlett D, Smith J (2005) GIS for coastal zone management. CRC Press, Boca Raton

Bernatchez C, Fraser P (2011) Evolution of coastal defence structures and consequences for beach width trends, Québec, Canada. J Coast Res. doi:10.2112/jcoastres-d-10-00189.1

Chaaban F, Darwishe H, Battiau-Queney Y, Louche B, Masson E, El Khattabi J, Carlier E (2012) Using ArcGISH modelbuilder and aerial photographs to measure coastline retreat and advance: North of France. J Coast Res. doi:10.2112/jcoastres-d-11-00054.1

Charlier RH, Chaineux MCP, Morcos S (2005) Panorama of the history of coastal protection. J Coast Res 21(1):79–111

Cipriani LE, Pranzini E (2009) Minimising Conflicts among Stakeholders within a Littoral Cell. In E. Ozhan (Editor) MEDCOAST: 525–536, 10-14 November 2009, Sochi, Russia

Dachev V (2000) Implications of accelerated sea-level rise (ASLR) for Bulgaria. In: Proceedings of the SURVAS expert workshop on European vulnerability and adaptation to impacts of accelerated Sea-Level Rise (ASLR), Hamburg, Germany, pp 25–28

Dailidiene I, Davuliene L, Kelpsaite L, Razinkovas A (2012) Analysis of the climate change in Lithuanian coastal areas of the Baltic Sea. J Coast Res 28(3):557–569

Er-Raioui H, Bouzid S, Marhraoui M, Saliot A (2009) Hydrocarbon pollution of the Mediterranean coastline of Morocco. Ocean Coast Manage 52:124–129

EUROSION (2004) Living with coastal erosion in Europe; sediment and space for sustainability. Office for Official Publications of the European Communities, Luxembourg

EUROSTAT (2009) Nearly half of the population of EU countries with a sea border is located in coastal regions. Agriculture and fisheries – statistics in focus 47/2009. Author: Unit E1, Farms, Agro-environment and rural development. European Communities 2009

GIEC (2007) Climate Change 2007: The physical science basis. Contribution of Working Group I to the Fourth Assessment Report of the Intergovernmental Panel on Climate Change. Cambridge University Press, Cambridge

Gorur N, Tuysuz ZO, Aykol A, Sakinc M, Yigitbac E, Akkok R (1993) Cretaceous red pelagic carbonates of northern Turkey: their place in the opening history of the Black Sea. Eclogae Geologicae Helvetica 86:819–838

Heo J, Kim JH, Kim JW (2009) A new methodology for measuring coastline recession using buffering and non-linear least squares estimation. Int J Geogr Inform Sci 23(9):1165–1177

IPCC (2007) Climate change 2007: the physical science basis. Summary for policymakers. Contribution of working group I to the fourth assessment report of the intergovernmental panel on climate change. Cambridge University Press, Cambridge

Jeftic L, Milliman JD, Sestini G (1992) Climate change and the Mediterranean. Edward Arnold, London

Keskin S, Pedoja K, Bektas O (2011) Coastal uplift along the Eastern Black Sea coast: new marine terrace data from Eastern Pontides, Trabzon (Turkey). J Coast Res 27(6A):63–73

Klein RJT, Nicholls RJ, Ragoonaden S, Capobianco M, Aston J, Buckley EN (2001) Technological options for adaptation to climate change in coastal zones. J Coast Res 17 (3):531–543

Kliewe H, Janke W (1982) Der holoza¨ne Wasserspiegelanstieg der Ostsee im nordo¨stlichen Ku¨ stengebiet der DDR. Petermann Geogra Mitt 2:65–74

Lanza S, Randazzo G (2012) Tourist-beach protection in north-eastern Sicily (Italy). Journal of Coastal Conservation. Springer Science+Business Media. DOI 10.1007/s11852-012-0217-0

Lemke W (1998) Sedimentation und paläogeographische Entwicklung im westlichen Ostseeraum (Mecklenburger Bucht bis Arkonabecken) vom Ende der Weichselvereisung bis zur Litorina transgression. Mar Sci Rep 31:1–156

MESSINA (2006) Managing European Shorelines and Sharing Information on Nearshore Areas. Four Volumes: (1) Practical Guide Monitoring and Modelling the Shoreline, (2) Practical Guide Valuing the Shoreline, (3) Practical Guide Engineering the shoreline. Introducing environmentally friendly engineering techniques throughout the World, (4) Practical Guide Integrating the Shoreline into spatial policies. DG Environment, Brussels

Meyer M, Harff J (2005) Modelling Palaeo coastline changes of the Baltic Sea. J Coast Res 21 (3):598–609

Montoya F, Galofré J (1997) El Ebro en el Delta. Revista de Obras Publicas 3368:33–46

Nicholls RJ (2007) Adaptation options for coastal areas and infrastructure: an analysis for 2030. Rep Unite Conv Clim Change 14:1–33

Nicholls RJ, Hoozemanbs FMJ (1996) The Mediterranean: vulnerability to coastal implications of climate change. Ocean Coast Mange 31(2–3):105–132

Panin N (1999) Global changes, sea level rising and the Danube Delta: risks and responses. GeoEcoMarina 4:19–30

Panin N (2009) Contributions to the study of the sediment sink processes within the Danube – Black Sea system. GeoEcoMarina 15:29–35

Panin N, Popescu I (2007) The northwestern Black Sea: climatic and sea-level changes in the late Quaternary. In: Yanko-Hombach Y, Gilbert AS, Panin N, Dolukhanov P (eds) The Black Sea flood question: changes in coastline, climate, and human settlement. Springer, Dordrecht, pp 387–404

Pashova L, Jovev I (2007) Geoid modeling for the Black Sea and future prospects. In: Guedes Soares C, Kolev P (eds) Maritime industry, ocean engineering and coastal resources. Taylor & Francis Group, London, pp 761–768

Paskoff R (1998) Les littoraux. Impact des aménagements sur leur évolution, 3rd edn. Armand Colin, Paris

Plan Bleu (2006) A sustainable future for the Mediterranean: the blue plan's environment and development outlook – executive summary. Plan Bleu, Regional Activity Centre. Reports related to Coastal Areas

Randazzo G, Stanley DJ, Di Geronimo SI Amore C (1998) Human-Induced Sedimentological Changes in Manzala Lagoon, Nile Delta, Egypt. Environmental Geology 36(3-4):235–258

Randazzo G, Lanza S (2011) Improvements to a Coastal Management Plan in Sicily (Italy): new approaches to borrow sediment management. J Coast Res Spec (64):1357–1361

Roebeling PC, Coelho CD, Reis EM (2011) Coastal erosion and coastal defense interventions: a cost-benefit analysis. J Coast Res SI 64:1415–1419

Rovira A. Batalla R, Sala M (2003) Sediment budget of the Mediterranean Lower Tordera River (NE Iberian Peninsula). In IAHS Pub 278:341–345

Richards JA, Nicholls RJ (2009) Impacts of climate change in coastal systems in Europe. PESETA-Coastal Systems study. JRC European Commission

Serra Raventos J (1997) El sistema sedimentario del Delta del Ebro. Revista de Obras Públicas 3368:15–22

Serra Raventos J (2004) Stiges, EUROSION Case Study. Office for Official Publications of the European Communities, Luxembourg

Small C, Nicholls RJ (2003) A global analysis of human settlement in coastal zones. J Coast Res 19(3):584–599

Spadini G, Robinson A, Cloetingh S (1996) Western versus Eastern Black Sea tectonic evolution: pre-rift lithospheric controls on basin formation. Tectonophys Dyn Ext Basins Invers Tecton 266(1–4):139–154

Stanchev H (2009) Studying coastline length through GIS techniques approach: a case of the Bulgarian Black Sea coast. CR Acad Bulg Sci 62(4):507–514

Stanchev H, Palazov A, Stancheva M, Aposto Lov A (2011a) Determination of the Black Sea area and coastline length using GIS methods and Landsat 7 satellite images. Geo-EcoMarina 17:27–31

Stanchev H, Palazov A, Stancheva M (2011b) 3D GIS model for flood risk assessment of Varna Bay due to extreme sea level rise. J Coast Res SI56:1597–1601

Stancheva M (2005) Technogenous impact on the Bulgarian Black Sea coast – State and problems. Proc Inst Oceanol 5:215–229

Stancheva M, Marinski J (2007) Coastal defense activities along the Bulgarian Black Sea coast – Methods for protection or degradation? Coastal structures 2007. In: Proceedings of the 5th international conference, Venice, Italy, pp 480–489

Stokkom H, Stokman G, Hovenier J (1993) Quantitative use of passive optical remote sensing over coastal and inland water bodies. Int J Remote Sens 14:541–563

Warrick RA, Le Provost C, Meier MF, Oerlemans J, Woodworth PL (1996) Changes in sea level. In: Houghton JT, Meira Filho LG, Callander BA, Harris N, Kattenburg A, Maskell K (eds) Climate change 1995, the science of climatic change. Cambridge University Press, Cambridge, pp 359–405

Zhang WY, Harff J, Schneider R, Wu CY (2011) A multi-scale centennial morphodynamic model for the southern Baltic coast. J Coast Res 27(5):890–917

Part VI
Coastal Dune Hazards (Erosion and Management)

Chapter 18
Coastal Dune Hazards

Sara Muñoz Vallés and Jesús Cambrollé

Abstract Coastal dunes constitute plastic systems with a recognized ecological, geomorphological, geological, historical, archaeological, scenic, cultural, and socio-economic value. Furthermore, coastal dunes play a relevant protective barrier role, preventing groundwater salinization due to intrusion of sea water and preserving other natural areas and human settlements from the effects of storm waves, tides and wind. Nevertheless, the current decline of coastal dunes has become in many cases a serious ecologic and economic problem. Dune stabilization, expansion of invasive plant species, anthropogenic impacts mainly associated to urban development and tourism, and effects of climate change are identified as the main current threats to these ecosystems. After examining the main hazards to coastal dunes, the current paradigm of coastal dunes management and conservation focuses on maintaining healthy, equilibrated and dynamic dunes, recovering their natural functioning, what needs for a major scientific-based knowledge of the entire dune systems functioning, the commitment of administrations, managers and urban and landscape planners, and the implementation of integrated coastal zone management programs, as well as a change of mentality toward new and more sustainable designs of development, respecting the coastal dune frame.

18.1 Coastal Dunes: Meaning, Functions and Status

Coastal dunes are aeolian sedimentary landforms originated from the combined action of waves and wind, that mainly develop in association with dissipative coasts dominated by the marine winds, and with an ample supply of loose, sand-sized sediment (Carter 1988; Martínez et al. 2004b; Van der Maarel 1993a). They are distributed worldwide, from polar to tropical latitudes, comprising very diverse

S. Muñoz Vallés (✉) • J. Cambrollé
Departamento de Biología Vegetal y Ecología, Universidad de Sevilla,
Avda. Reina Mercedes, S/N, Seville 41012, Spain
e-mail: saramval@us.es; cambrolle@us.es

C.W. Finkl (ed.), *Coastal Hazards*, Coastal Research Library 6,
DOI 10.1007/978-94-007-5234-4_18,

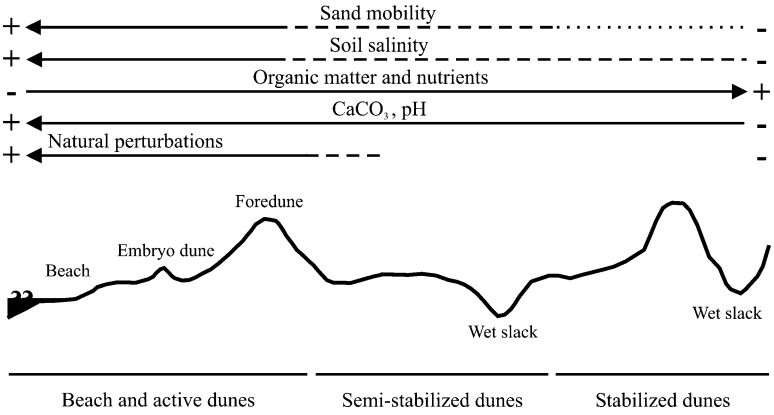

Fig. 18.1 Generalized environmental gradients on coastal dunes (based on Brown and McLachlan 1990; Carter 1988; Ley Vega de Seoane et al. 2011; and Muñoz Vallés, non published data)

climates and biomes, and occurring on ocean, lake and estuary shorelines, leading to a large variety of forms and dimensions related with spatial and temporal variations in sediment supply and wind regime (Hesp 2000, 2004; Nordstrom et al. 1990), but comprising a really limited global area. Located on the transition between two of the great systems of the biosphere, continents and oceans, they constitute very dynamic and plastic systems, linked to the constant sediment exchange between the sea, the beach and the more stable landwards dunes (Carter 1988; Ranwell 1972), and they suffer both natural and anthropogenic perturbations (Carter 1988; Hesp and Martínez 2007; Nordstrom 2008; Panario and Piñeiro 1997; Psuty 2004).

Coastal dunes support particular, complex ecosystems, where species of fauna and flora coexist with a harsh environment, characterized by the scarcity of water and nutrients, substrate mobility and sand burial, incidence of salt spray and sand blasting, high air and soil temperatures and light intensities in low and medium latitudes, and saltwater flooding in the strandline (Carter 1988; Chapman 1976; Heslenfeld et al. 2004; Martínez et al. 1993; Martínez et al. 2004b; Maun 1998, 2009; Ranwell 1972; Van der Maarel 1993b). Most of these factors are ordered in gradients from the shoreline and landwards, associated to the sea and marine winds influence (Fig. 18.1). A characteristic vegetation including unique species with specific adaptations to the environmental conditions establish on them, closely related with sediment dynamics and geomorphological processes of the dune, and continuously interacting with them (Carter 1988; Martínez et al. 1993; Ranwell 1972). All this results in dynamic systems with singular functioning, subjected to delicate equilibriums that originates, in addition, a particular type of landscape (Brown and Mclachlan 1990; Carter 1988; Ranwell 1972).

Apart from the ecological traits, coastal dune systems have a recognized geomorphological, geological, historical, archaeological, scenic, cultural, and socio-economic interest (Heslenfeld et al. 2004; Martínez et al. 2004b; Nordstrom et al. 2000; Van der

Meulen et al. 2004). In addition, coastal dunes play a relevant protective barrier role on the coast, dissipating energy and buffering the effects of storm waves, tides and wind, preventing groundwater salinization due to intrusion of sea water, and acting as sand reservoirs that preserve other natural areas (e.g. coastal wetlands) and human settlements (Carter 1988; Gómez-pina et al. 2002; Kidd 2001), which means an additional significant functional value.

Rates of alteration and degradation of natural ecosystems have notably increased since the last third of the last century (Carter 1988; Martínez et al. 2004a; Nilsson and Grelsson 1995), and this has led to the need to develop techniques and policies aiming the protection, conservation and management of ecosystems. Among the different coastal ecosystems, coastal dunes have suffered the highest degree of human pressure (Carter 1988; Holdgate 1993). Many coastal dune systems worldwide are being seriously degraded at present, some of them irreversibly altered, due to an excessive exploitation of the natural resources and services they offer (e.g. coastal defense, recreation, water and substrate extraction, agriculture, livestock grazing, etc.), as well as to the human demographic expansion and urban and industrial development (Baeyens and Martínez 2004; Carter 1988; Heslenfeld et al. 2004; Martínez et al. 2004a; Van der Meulen and Salman 1996; Williams et al. 1997; Williams et al. 2001). In this regard, most of the existing literature on coastal dune ecology focuses any chapter on the identification of present and potential threats and dune conservation approaches (e.g. Brown and McLachlan 1990; Carter 1988; García Novo et al. 1997; Martínez and Psuty 2004; Maun 2009; Packham and Willis 1997; Ranwell 1972). Different authors identify as the main current threats to these ecosystems both the anthropogenic habitat degradation and destruction (mainly associated to urban development and tourism), dune stabilization and eutrophication, and invasion by alochthonous species (Isermann et al. 2007; Jørgensen and Kollmann 2009; Kutiel et al. 2004). According to Nordstrom (2008), changes associated with the development of coastal areas for human use involves, among others, the loss of natural habitats and biodiversity (Beatly 1991), landscape fragmentation (Berlanga Robles and Ruiz Luna 2002), risks to endangered species (Melvin et al. 1991), reduction of seed sources and decrease on resilience of plant communities after storms in undeveloped areas adjacent to developed ones (Cunniff 1985) or loss of the original aesthetic and recreational value (Da Cruz 1996; Demirayak and Ulas 1996), and loss of natural heritage and image of the coast, among others. The human action is compounded by the effects of global warming and progressive sea level rise (Carter 1988; Panario and Piñeiro 1997; Tsoar 2005).

The following is an attempt to examine the main current hazards to coastal dunes and current approaches for conservation and management.

18.2 Dune Stabilization

Dune fixation and stabilization are terms that have been indistinctly used to refer the process involving the progressive reduction of sand movement. This reduction is closely related to an increase on the vegetation coverage, following a positive

feedback mechanism (Yizhaq et al. 2007), and it entails significant changes in the dune functioning, as well as in the type of communities growing on them (Kutiel et al. 2004; Levin and Ben-Dor 2004; Moreno-Casasola 1986; Muñoz Vallés et al. 2011b). The *stabilization* term has traditionally received a sense of natural process (e.g. Lichter 1998; Martínez et al. 2001; Olson 1958) and, subsequently, it has also been used to designate certain human actions aimed at controlling the excessive advance of sand dunes. On the other hand, *fixation* has been used more frequently in relation with those human actions.

Dune stabilization is a natural process of development in coastal dune succession, from embryo to mature dunes (see Fig. 18.1 in the Introduction section). Nevertheless, the recent increase of sands stability in coastal dunes in different parts of the world is becoming an important environmental problem, resulting in negative consequences to richness and diversity of plant and animal species (Alvarez and Cushman 2002; Avis 1995; Conser and Connor 2009; Isermann 2008b; Isermann et al. 2007; Kutiel et al. 2004; Marchante et al. 2008; Wiedemann and Pickart 1996). The stabilization process encompasses, not only the loss of sands mobility due to an increase on vegetation coverage, but also an increment of organic matter in the incipient soil, which increases the availability of both soil moisture and nitrogen (Connell and Slatyer 1977; Muñoz Vallés et al. 2011a, b; Olson 1958). It promotes changes in the richness and diversity of the plant community species, shifts in dominant species, and species replacement based on burial tolerance (Dech and Maun 2005), resulting in a decrease in the abundance of sand-living flora and fauna species that are specifically adapted to the habitat of shifting sands. At the long term, it may lead to a significant change on the landscape and dune morphology, and the loss of this singular kind of habitat (Kutiel et al. 2004; Levin and Ben-Dor 2004). Furthermore, according to Lubke (1985) and Panario and Piñeiro (1997), the immobilization of a significant portion of dune system can lead to the loss of the protective function of coastal dunes, resulting in coastal recession in the medium and long term by preventing natural sand transfer from dunes to the coast.

Several factors have been identified as causes of the observed increase in sand stabilization rates. On one hand, the reduction or disruption of agricultural and/or livestock land-uses acting as disturbance to sand dune vegetation has, in some cases, allowed this vegetation to spread more efficiently on the dunes where they grow, thus stabilizing them (Isermann et al. 2007; Levin and Ben-Dor 2004). In the Mediterranean coastal dunes of Israel, e.g., Tsoar and Blumberg (2002) found a decreasing average rate of advance of 15 dunes from 3.4 to 1.9 m/year during the period between 1944 and 1995, following the interruption of intense agricultural and pastoral activity, while the vegetation cover increased from 4.3 to 17%. On the other hand, the decrease in herbivory either by domestic livestock or wild grazers such as wild rabbit in some dunes (i.e. due to diseases such as myxomatosis) has led to a rapid evolution of dune vegetation from open grasslands to scrubland and woodland (Levin and Ben-Dor 2004; Ranwell 1960; Thomas 1960). Global or local climatic changes can also lead to an increase on sand stability, mainly induced by changes in wind pattern and power that enables the establishment and densification of dune vegetation (Panario and Piñeiro 1997; Tsoar 2005; Tsoar et al. 2009).

Nevertheless, the main and more immediate cause of dune stabilization in different parts of the world has been essentially anthropogenic. The high mobility of some coastal dunes has seriously threatened human interests such as houses, crops and infrastructure. In attempts to prevent dune erosion, to stabilize blowing transgressive sand sheets, and to preserve the function of dunes as a natural defense of the coast, together with a widespread interest in expanding the beach for recreational needs (Nordstrom and Lotstein 1989), considerable efforts have been invested in stabilizing such systems around the world. Since the end of the eighteenth century, different countries have implemented dune stabilization techniques that included the planting of rapid-grow herbaceous and/or woody species, tolerant to the dune environmental stressful conditions (Avis 1989; Buell et al. 1995; Kith-y-Tassara 1946; Kutiel et al. 2004; Li et al. 2009; Pye 1983; Van der Meulen and Salman 1996). In some cases, the plantation of species without any regard to their exotic or native character has led to their excessive spread beyond the plantation areas over time, sometimes displaying invasive behaviors, and causing the further stabilization of surrounding dune systems followed by serious problems for the ecosystem conservation (Avis 1995; Conser and Connor 2009; Isermann 2008a; Kutiel et al. 2004; Marchante et al. 2008; Wiedemann and Pickart 1996).

The loss of functional, natural and ecological value due to coastal dune stabilization is not an easy problem to solve. According to Tsoar et al. (2009), the fact is that, once the dunes were stabilized by vegetation they could not be naturally activated even by increased wind power (Levin and Ben-Dor 2004; Tsoar 2005; Tsoar et al. 2009). Levin and Ben-Dor (2004) observed that military maneuvers, and pedestrians and off-road vehicles traffic increased the dune fragmentation but did not lead to the reactivation of the sands. In this regard, manual thinning of plant cover may seem a suitable management strategy (Kutiel et al. 2000); in any case, the response of fauna and flora to artificial thinning and reactivation of dune mobility must be taken into account.

18.3 Expansion of Invasive Plant Species

Biological invasions are a worldwide problem that affects almost all ecosystems as well as human interests, and has considerable impact on either ecological functioning or human well-being (Perrings et al. 2010). In the last decades, introduction on allochthonous species has increased considerably (Hulme 2009). Coastal ecosystems, and particularly dunes, are among the most threatened and affected by invasion of allochthonous plants. This is mainly due to the significant pressure from human activities to which they are exposed, which favors the introduction and expansion of some of these species (Campos et al. 2004). Furthermore, nearly 50% of the 34 plant species identified by IUCN among the 100 of the world's worst invasive alien species are recognized to occur in coastlands (Lowe et al. 2000).

The expansion of allochthonous species in new habitats depends on the characteristics of both the species themselves (e.g. adaptation to the environmental

conditions, production and dispersal of propagules) and those of the source and the sink habitat, such as ecosystem structure (e.g. diversity, plant covering) and disturbances (Alpert et al. 2000; Davis et al. 2000; Orians 1986; Peters et al. 2006; Perrings et al. 2010). Coastal dunes are susceptible to plant invasions due to a usual low number of species, the existence of micro-sites open to their establishment and to low levels of plant-plant competition (Jørgensen and Kollmann 2009), as well as recurrent natural and anthropogenic perturbation. Some of the invasive species in coastal sand dunes are dune-specific and occupy similar habitats in their native countries; but some others are ruderal species, not exclusive to the littoral strip, also abundant in other types of disturbed habitats (Campos et al. 2004; Isermann 2008a; Muñoz Vallés et al. 2011a, b). In fact, native species can also display invasive behaviors (Alpert et al. 2000), negatively affecting other species and/or significantly altering the ecosystem functioning (e.g. *Retama monosperma* in SW Spain coastal dunes, Muñoz Vallés et al. 2011a, b; *Hippophae rhamnoides* in coastal grey dunes of North Sea island Spiekeroog, Isermann 2008b; *Larrea tridenta* in Chihuahuan Desert of North America; Peters et al. 2006).

Due to a good adaptation to the dune environment and to a rapid and convenient grow form, the introduction of allochthonous species to stabilize sand dunes has been a common practice in the past and still at present (e.g. *Ammophila arenaria, Hippophae rhamnoides, Rosa rugosa*, several species from the genus *Carpobrotus, Acacia, Eucalyptus, Pinus* and *Retama*, among others – Avis 1989; Buell et al. 1995; Isermann 2008b; Kith-y-Tassara 1946; Kutiel et al. 2004; Wiedemann and Pickart 1996; among others). In addition, the widespread recreational use of coastal areas and urban development has been involved with the introduction of such species also in relation with aesthetic, and the associated disturbances from human activities on surrounded dunes have facilitated their arrival and establishment (Gallego-Fernández et al. 2006; Van der Meulen and Salman 1996).

Impacts of allochthonous invasive species in coastal dunes lead to a decrease in the abundance of sand-living flora and fauna species and cause serious problems for the ecosystem conservation (Avis 1995; Conser and Connor 2009; Isermann 2008b; Kutiel et al. 2004; Marchante et al. 2008; Wiedemann and Pickart 1996; among others). Their expansion facilitates, in many cases, the further establishment of other neophytes and alien species (Isermann 2008a; Muñoz Vallés et al. 2011a, b). In addition, the rapid expansion and increase in coverage of some species (particularly shrubs, but also ground cover species such as *Carpobrotus* or *Oenothera*, or with relative dense growth form as *Ammophila*) significantly contributes to the dune stabilization process, promoting a significant change on the dune landscape, causing the lack of sand supply to beaches from the dune, and altering the functioning of the whole ecosystem. (Isermann 2008a; Isermann et al. 2007; Kutiel et al. 2004; Lubke 1985; Wiedemann and Pickart 2004). In the Western coast of North America, for instance, *Ammophila arenaria* has displaced and/or replaced the native dune-forming species in most places, modifying the open and high diversity foredunes, and it has also invaded many back dune ridges and stabilized some formerly active dunes (Wiedemann and Pickart 2004). Nevertheless, it has had a slighter impact on the dunes ecosystem in Southern Cape Coast (Africa; Lubke

2004). Coastal dunes in south Israel have experienced a significant stabilization process and an increase in dune vegetation cover, by 82%, between the years 1965 and 1999, due to the expansion of introduced species (Kutiel et al. 2004). On the other hand, in the case of coastal dunes, degradation subjected to human pressure and/or management for recreation or stabilization leads to a common presence of allochthonous species in these habitats. Aria (1999) found that 52% of total dune vegetation, or 82% of non-forested vegetation, was dominated by introduced species at the Humboldt Bay dunes, California. In six coastal dune systems in the Gulf of Cadiz, SW Spain, Gallego-Fernández, Muñoz Vallés and Dellafiore (2006) recorded an abundance of allochthonous plant species ranging from 4.3 to 25.3% of the total species. Castillo and Moreno-Casasola (1996) found that 89.8% out of 644 species inventoried throughout the coastal dunes located along the Gulf of Mexico were ruderal or secondary species from other nearby communities.

The full extent of the impacts of plant invasions on dune systems is still unknown, and further studies, including measures for control and eradication on invasive species, as well as approaches aiming the restoration of dune species composition, diversity and natural processes, are required.

18.4 Urban Development and Tourism

Humans have used coastal dunes since the ancient times for different purposes, traditionally related to agriculture, livestock grazing and the establishment of settlements (Baeyens and Martínez 2004; Carter 1988; Heslenfeld et al. 2004). Nevertheless, it has not been until recently that dunes have suffered a major degradation and loss rates. At present, it is estimated that 60% of a growing world population of seven billion people live in the coastal region (Holdgate 1993; U.S. Census Bureau International Data Base). Worldwide, coastal dunes are at present seriously threatened by human activities such as urban, engineering and industry development (Fig. 18.2). These activities cause, among others, net loss of habitat, fragmentation of living areas, soil and aquifers alterations, and water and air pollution, what leads to significant changes or complete loss of flora, fauna, landscape quality and functionality of dunes over short periods of time (Carter 1988; Heslenfeld et al. 2004; Martínez et al. 2004a; Williams et al. 1997; Williams et al. 2001). In addition, the establishment of ports and yacht marinas, and hard coastal defense, has altered the natural sedimentary dynamics, causing serious problems of erosion on some coastal stretches. Only in Europe and since 1900, a net loss of coastal dune surface of 25% has been recorded and about 55% of the remaining surface has lost its natural character. It is estimated that approximately 85% of the currently existing dunes in Europe is endangered (Heslenfeld et al. 2004). Coastal dunes are considered, in addition, among the most demanded habitats for recreational use (Kutiel et al. 1999; Martínez et al. 2004a; Williams et al. 1997). In particular, tourism has become the major source of income for the coast but, at present, tourism and its associated impacts cause significant

Fig. 18.2 Dune narrowing and degradation caused by the establishment of infrastructure associated with urban development, and poor management of parking and access to reach the beach (Rota beach, Cádiz, SW Spain)

degradation and direct loss of dunes, and it has led as well to an increase in urban and demographic pressures (Kutiel et al. 2004; Kutiel et al. 1999; Martínez et al. 2004a; Nordstrom 2008; Nordstrom et al. 2000).

Derived impacts from urban development, building of facilities and activities associated to tourism (e.g., gulf courses, recreational use of beaches) range from the obvious direct loss of dune surface (which can easily comprise the total dune surface in some cases) and serious alteration in the coastal sedimentary dynamics and erosion (e.g. due to hard coastal defence works such as groins and breakwaters), to the direct and indirect environmental degradation by pressure of use on the surrounding natural areas (Gallego-Fernández et al. 2003; García Mora et al. 1998; Jackson and Nordstrom 2011; Martínez et al. 2004a; Milne et al. 2012; Nordstrom et al. 2000). Although this second aspect is not so obvious, it can lead alone to the loss of the protected dune plant communities and associated fauna, as well as the natural dynamic of the dune. For instance, intensive and uncontrolled traffic of tourists implies serious environmental modifications such as soil compression, reduction of litter and soil organic matter in the upper layer of the soil, erosion and changes in microclimate, and it also promotes the reduction in plant cover, species richness and diversity, and alterations for fauna species (Andersen 1995a, b; Brown and McLachlan 1990; Heslenfeld et al. 2004; Kutiel et al. 1999; Nordstrom et al. 2000; Williams et al. 1997).

Furthermore, human impact acts as an important destabilizing factor of dune systems, altering the natural stabilization–destabilization balance, and being

Fig. 18.3 Coastal dune disaggregation caused by uncontrolled tourists traffic and inadequate design of access in Zahara de los Atunes beach, Cádiz (SW Spain)

directly related to the coastal dune instability and disorganization and to the loss of coastal dunes' protecting role (Barrère 1992; Brown and McLachlan 1990; Nordstrom et al. 2000; Panario and Piñeiro 1997; Psuty 2004) (Fig. 18.3). Continuous and intensive trampling may induce changes in plant composition, from species specifically adapted to the dune geomorphological processes to other functional groups of species with lower skills to stabilize sands (García Mora et al. 2000; Santoro et al. 2012). This, together with the loss of vegetation cover and wind erosion, causes the formation and growth in wide and depth of bare deflation corridors that contribute to dune fragmentation and negatively affect to the geomorphologic integrity of the dune (Fig. 18.4) (Gallego-Fernández et al. 2003; Muñoz Vallés et al. 2005). Therefore, the system becomes more fragile to natural disturbances. In SW Spain, Muñoz Vallés et al. (2011a, b) compared the status of two dune systems under different tourism pressure and accessibility level. They concluded that ineffectiveness of access structures in avoiding human impact on the dune system makes that coastal segment lacking of adequately designed accesses reach similar levels of dune segmentation and alteration that coastal segment where visitors can come and go uncontrollably.

On the other hand, actions such as mechanical beach cleaning, container establishment or aid positions damage or eliminate beach vegetation and incipient dunes, seed sources for pioneer dune colonizers, food for fauna, and habitat for nesting birds. Besides, the variability in microenvironments necessary for biodiversity gets reduced (Campos et al. 2004; García Mora et al. 1998; Nordstrom et al. 2000). The intensive development of industry and urban settlements and facilities in the coast

Fig. 18.4 The coalescence of antropogenic bare deflation corridors leads to the dune fragmentation and intrusion of sea water in the dune system

flat has also resulted, in many cases, in coastal stretches with high urban development and some isolated dune systems among them (Gallego-Fernández et al. 2011; García Mora et al. 1998; Heslenfeld et al. 2004; Jackson and Nordstrom 2011). This can lead to a disruption to the natural dynamics of dispersion and colonization of plant species, a fact that would also affect the species equilibrium at a regional scale.

18.5 Climate Change Implications

Increases in global average air and ocean temperatures, greater at higher northern latitudes, widespread melting of snow and ice, and related rising global average sea level of 1.8 mm/year over 1961 to 2003 (of about 3.1 mm/year from 1993 to 2003) are among the main changes observed in climate in recent decades (IPCC 2007). Present and predicted climate change effects have the potential to considerably exacerbate hazard risk to coastal dunes, and associated dangerous trends for coastal dunes conservation are mainly related to changes in wind power, rainfall, sea level rise by itself and groundwater salinization (Carter 1991; IPCC 2007; Panario and Piñeiro 1997; Ross et al. 1994; Tsoar 2005; Vestergaard 1997).

Low rainfall and high wind power are driving forces related to climate that negatively affect vegetation growth and cover in coastal dunes, and are in fact closely related with a higher mobility of sand dunes. Changes in rainfall and wind

power can therefore determine the trend of dunes from vegetated, stabilized or semi-stabilized dune systems to bare, mobile dunes of shifting sands or vice versa (Ashkenazy et al. 2011; Panario and Piñeiro 1997; Tsoar 2005). Extremes in both senses would result in loss of ecological value of dunes (Heslenfeld et al. 2004). Trends on this aspect also depend on other factors such as climatic zones, dune dimensions, vegetation cover quality and human impacts (Heslenfeld et al. 2004; García Mora et al. 2000), so generalized predictions for climate change impacts are difficult to reach in this line. For instance, based on empirical data and sand transport model, Panario and Piñeiro (1997) predicted coastal recession in the medium and long term at Cabo Polonio (Uruguay), due to a decrease in coastal dunefield activity induced by changes in wind pattern. But they observed that coastline recession was also related to the antropogenic forestation process that caused the immobilization of a significant portion of the dune system, preventing natural sand transfer to the coast. These changing conditions are added to the projected increase in sea level, heights and incidence of waves, and frequency of flooding by extreme tides, storm surge and wave effects, which causes relevant redistribution of sediments by influencing the coastal erosion/accretion processes. This can cause accumulation of eroded material and rapid foredune creation and development in some areas along the coast, and insufficient sediment supply and erosion in other areas (Carter 1991; Milne et al. 2012; Vestergaard 1997).

Associated reorganization of sands in the dune habitat can also imply ecosystem changes such as sand deposition on wet slacks and semi-stabilized and stabilized dunes, and consequent changes in vegetation composition in accordance with burial tolerance of species (Dech and Maun 2005; Vestergaard 1997). In this regard, generalized sea level rise constitutes a serious problem for conservation of coastal dune communities due to their impossibility of migrating toward inner or upper areas where their habitat is inexistent. Changes in precipitation and wind power can lead to serious threat for rare, drought-sensitive coastal plant species (Fischer et al. 2009). In addition, the progressive sea level rise together with the global redistribution of precipitation caused by climate change leads to an increase of aquifers salinity, and it is predicted that coastal ecosystems will be likely affected by decreased fresh water availability due to saltwater intrusion, negatively affecting specific dune flora (Christensen et al. 2007; Greaver and Sternberg 2006; IPCC 2007; Ross et al. 1994; Sternberg and Swart 1987). One of the most recent research lines on ecology of dunes (and other types of terrestrial habitat) consists of the study of the sources of water (e.g. ocean, ground, and rain) taken up by vegetation, using isotopic analysis of stem water (Andrews et al. 2012; Ehleringer and Dawson 1992; Greaver and Stenberg 2007, 2010). Contrary to the traditionally conceived idea that freshwater from dune aquifer and rain are the only water sources for plants in coastal dunes, recent studies have found that some dune species are able to use ocean water uptake during pronounced drought periods and periodic ocean water influx (Gallego-Fernández et al. 2010; Greaver and Stenberg 2007). Nevertheless, further studies on quantifying species tolerances in this regard are necessary to determine thresholds of community sustainability, in order to assess the coming effects of sea-level rise scenarios and to design suitable management approaches.

18.6 Management and Conservation Paradigm

Diverse risk factors operating at different levels and scales are currently threatening coastal dunes, including other local hazards not described above. Unfortunately, some of these factors were identified at least four decades ago (i.e. coastal impacts of human activities such as urban development or introduction of allocthonous species; Brown and McLachlan 1990; Carter 1991; García Novo et al. 1997; Ranwell 1972), but it appears that associated conservation problems still remain unsolved, somehow. For instance, the introduction of allochthonous plant species for gardening and stabilization of slopes in coastal housings are still common. Administrations and managers invest considerable effort in the eradication of the most problematic species. Nevertheless, the expansion of invasive species is still a problem that leads to the stabilization of the dune, or favors changes in the plant community composition, sometimes towards species with lower skills to stabilize sands (García Mora et al. 2000; Santoro et al. 2012). In these situations, the uncontrolled traffic of tourists through the dune system accentuates these community changes but it does not remobilize the dune (Levin and Ben-Dor 2004) (Fig. 18.5). In both cases, the dune becomes more vulnerable to face wind, sea and waves battering. This vulnerability is significantly higher when the dune barrier has been narrowed or removed due to industrial and urban development, or due to changes on sedimentary dynamics promoted by the establishment of coastal defense structures. Among all, present and future effects of climatic change is likely the most dramatic hazard to coastal dunes, specifically the progressive sea level rise and accentuation of climatic extremes, since they can be predicted but they can hardly be managed in the short term.

In contrast, management approaches have evolved toward preferable "soft" measures and impact removal or minimization, aiming to maintain natural dynamics, functions and values of dunes, and helping natural processes to recover by themselves (Gómez-Pina et al. 2002; Heslenfeld et al. 2004; Ley Vega de Seoane et al. 2011; Pethick and Crooks 2000). Such measures include the morphological dune reconstruction, revegetation with appropriate native species, elimination of allochthonous invasive plant species, beach nourishment, either on the beach or on the shore face, use of passive sand-trapping fences and protection systems, efficient designs of accesses in limiting and routing uncontrolled tourist traffic, allowing the dune mobility and vegetation development, avoidance of buildings and parking areas in the dune system, monitoring of any restoration or conservation work and maintenance. In addition, environmental information appears to be an efficient tool against dune degradation (Carter 1991; Gómez-Pina et al. 2002; Heslenfeld et al. 2004; Ley Vega de Seoane et al. 2011; Muñoz Vallés et al. 2011a, b). These does not necessarily exclude the requirement of implementing some "hard" engineering interventions (such as submerged breakwaters) in certain extreme situations, taking into account the associated consequences on the natural dynamics of dunes and the whole coastal frame in any case (Antunes do Carmo et al. 2010; Heslenfeld et al. 2004).

Fig. 18.5 Foredune totally covered and stabilized by *Carpobrtus edulis* (Cádiz, SW Spain)

Taking into account what has previously been stated, the assessment of coastal dune vulnerability seems an interesting approach that integrates the main factors affecting dune resilience. Dune vulnerability is understood here as "the capacity that a particular ecosystem has to absorb disturbance without undergoing permanent alterations", being an antonym of the concept of "elasticity" (Orians 1975) or "resilience" (Pimm 1991). Different vulnerability indexes have been used in the lasts decades, and methods used to this aim have diversely considered natural and human-induced disturbances (Cooper and McLaughlin 1998; García Mora et al. 2001; Panario and Piñeiro 1997; Pethick and Crooks 2000; Williams et al. 2001). Nevertheless, the use of a holistic evaluation integrating morphosedimentological, ecological and antropogenic features by the application of specific checklists is desirable, and some of these indexes have recently included the vegetation quality as additional variable to monitor for a more complete assessment (García Mora et al. 2001; Martínez et al. 2006; Muñoz Vallés et al. 2011a, b). This is a relevant goal for conservation of dune ecosystems and functions, since vegetation gives structure to ecosystems, it is one of the main supports for wild fauna, and natural diversity of native species provides the characteristic dynamic equilibrium of dunes (Margalef 1977; Van der Putten and Petters 1995). The application of these indices allows the identification of homogeneous units in the coastal frame, determines the main factors affecting them (geomorphological, related with wind or sea impacts, antropogenic or based on vegetation status), and predicts the system response to environmental variations, facilitating the design and implementation of concrete management actions from local to regional scale. Such indexes have been useful in

dune vulnerability assessment in different countries around the world, such as France (Bodére et al. 1991), United Kingdom (Williams et al. 1993), Portugal (Alveirinho Dias et al. 1994; Matias et al. 1998), Spain (García Mora et al. 2001; Muñoz Vallés et al. 2011a, b), Turkey (Marlow and Morris 2003), or Mexico (Martínez et al. 2006).

Coastal dunes are dynamic systems that quickly respond to factors affecting them (García Mora et al. 2001; Heslenfeld et al. 2004; Williams et al. 1993), maintaining a naturally occurring mosaic of dynamics that includes active fronts, semi-stabilized and stabilized dune areas (Martínez et al. 2004b). This equilibrium and plasticity of dunes makes them unique habitats that act as centre of speciation and global biodiversity, and implies one of the major environmental services that dunes offer to human interests as coastal protective barrier in the present natural hazards scenario associated to climate change. Nevertheless, other main environmental benefits that coastal dune offers are likely related nowadays with sustainable tourism, landscape quality or natural carbon sink, in addition to the traditional uses for agriculture or livestock grazing.

We are still relatively far from a wide understanding of the combined effects of hazards on coastal dunes, and from implementing a suitable integrated management of these complex systems. Nevertheless, we are in position to state that, at present, management should be focused to maintain healthy, equilibrated and dynamic dunes that can accomplish their protective role on coastal areas, remaining less vulnerable to erosion, being cheaper to maintain, preserving higher natural values and maintaining the global biodiversity that these habitats support. These goals needs for a major scientific-based knowledge of the entire dune systems functioning, as well as the commitment of administrations, managers and urban and landscape planners, and the implementation of integrated coastal zone management programs, in order to solve this ecologic and economic problem of the current decline of coastal dunes. It is also required a change of mentality toward new and more sustainable designs of development, respecting the coastal dune frame, under the consciousness of the rising sea levels and the protective value of coastal dune barrier.

References

Alpert P, Bone E, Holzapfel C (2000) Invasiveness, invisibility and the role of environmental stress in the spread of non-native plants. Perspect Plant Ecol Evol Syst 3:52–66

Alvarez ME, Cushman JH (2002) Community level consequences of a biological invasion: effects of a non-native vine on three plant communities. Ecol Appl 12:1434–1444

Alveirinho Dias JM, Curr R, Davies P, Pereira A, Williams AT (1994) Dune management vulnerability assessment: Portugal and northwest Europe. In: Association EUROCOAST (ed) Proceedings of Littoral'94 (Lisbon, Portugal), pp 837–848

Andersen UV (1995a) Resistance of Danish coastal vegetation types to human trampling. Biol Conserv 71:223–230

Andersen UV (1995b) The influence of human trampling on the vegetation on artificial coastal grassland in Denmark. In: Salman AHPM, Berends H, Bonazountas M (eds) Coastal management and habitat conservation, vol I, PC96. EUCC, Leiden, pp 427–438

Andrews SF, Flanagan LB, Sharp EJ, Cai T (2012) Variation in water potential, hydraulic characteristics and water source use in montane Douglas-fir and lodgepole pine trees in southwestern Alberta and consequences for seasonal changes in photosynthetic capacity. Tree Physiol 32(2):146–160

Antunes do Carmo J, Schreck Reis C, Freitas H (2010) Working with nature by protecting sand dunes: lessons learned. J Coast Res 26(6):1068–1078

Aria KT (1999) Using aerial photographs rectified with a geographic information system to map coastal dune vegetation and land use in Humboldt County, California. M.S. thesis, Humboldt State University, Arcata, 62 p

Ashkenazy Y, Yizhaq H, Tsoar H (2011) Sand dune mobility under climate change in the Kalahari and Australian deserts. Clim Change. doi:10.1007/s10584-011-0264-9

Avis AM (1989) A review of coastal dune stabilization in the Cape Province of Sotuh Africa. Lands Urban Plann 18:55–68

Avis AM (1995) An evaluation of the vegetation developer alter artificially stabilizing South African coastal dunes with indigenous species. J Coast Conserv 1:41–50

Baeyens G, Martínez ML (2004) Animal life in sand dunes: from exploitation and prosecution to protection and monitoring. In: Martínez ML, Psuty NP (eds) Coastal dunes, ecology and conservation, vol 171, Ecological studies. Springer, Berlin, pp 279–296

Barrère P (1992) Dynamics and management of the coastal dunes of the Landes, Gascony, France. In: Carter RWG, Curtis TGF, Sheehy-Skeffington MJ (eds) Coastal dunes. Balkema, Rotterdam, pp 25–32

Beatly T (1991) Protecting biodiversity in coastal environments: introduction and overview. Coast Manage 19:1–19

Berlanga Robles CA, Ruiz Luna A (2002) Land use mapping and change detection in the coastal zone of northwest Mexico using remote sensing techniques. J Coast Res 18:514–522

Bodére JC, Cribb R, Curr RHF, Davies P, Hallégouet B, Meur C, Pirou N, Williams AT, Yoni C (1991) La gestion des milieux dunaires littoraux. Evaluation der leur vulnérabilité à partir d'une liste de contrôle. Etude de cas dans le sud du Pays de Galles et en Bretagne occidental. Norois 38:279–298

Brown AC, McLachlan A (1990) Ecology of Sandy Shores. Elsevier, Amsterdam, 328 p

Buell AC, Pickart AJ, Stuart JD (1995) Introduction history and invasion patterns of *Ammophila arenaria* on the north coast of California. Conserv Biol 9:1587–1593

Campos JA, Herrera M, Biurrun I, Loidi J (2004) The role of alien plants in the natural coastal vegetation in central-northern Spain. Biodiv Conserv 13:2275–2293

Carter RWG (1988) Coastal environment. An introduction to the physical, ecological and cultural environment. Academic, London, 617 p

Carter RWG (1991) Near-future sea-level impacts on coastal dune landscapes. Lands Ecol 6:29–39

Castillo SA, Moreno-Casasola P (1996) Coastal sand dune vegetation: an extreme case of species invasion. J Coast Conserv 2:13–22

Chapman VJ (1976) Coastal vegetation. Pergamon Press, Oxford, 292 p

Christensen JH, Hewitson B, Busuioc A, Chen A, Gao X, Held I, Jones R, Kolli RK, Kwon W-T, Laprise R, Magaña Rueda V, Mearns L, Menéndez CG, Räisänen J, Rinke A, Sarr A, Whetton P (2007) Regional climate projections. In: Solomon S, Qin D, Manning M, Chen Z, Marquis M, Averyt KB, Tignor M, Miller HL (eds) Climate change 2007: the physical science basis. Contribution of working group I to the fourth assessment report of the Intergovernmental Panel on Climate Change. Cambridge University Press, Cambridge/New York, pp 849–940

Connell JH, Slatyer RO (1977) Mechanisms of succession in natural communities and their role in community stability and organization. Am Nat 111:1119–1144

Conser C, Connor EF (2009) Assessing the residual effects of *Carpobrotus edulis* invasión, implications for restoration. Biol Invas 11:349–358

Cooper JAG, McLaughlin S (1998) Contemporary multidisciplinary approaches to coastal classification and environmental risk analysis. J Coast Res 14:512–524

Cunniff SE (1985) Impacts of severe storms on beach vegetation. In: Magoon OT, Converse H, Miner D, Clark D, Tobin LT (eds) Coastal Zone'85, Proceedings of the Fourth Symposium on Coastal and Ocean Management. American Society of Civil Engineers, New York, pp 1022–1037

Da Cruz H (1996) Tourism and environment in the Mediterranean. In: Salman L, Salman AHPM, Langeveld MJ, Bonazountas M (eds) Coastal management and habitat conservation, vol II. European Union for Coastal Conservation, Leiden, pp 113–116

Davis MA, Grime JP, Thompson K (2000) Fluctuating resources in plant communities: a general theory of invisibility. J Ecol 88:528–534

Dech JP, Maun MA (2005) Zonation of vegetation along a burial gradient on the leeward slopes of Lake Huron sand dunes. Can J Bot 83:227–236

Demirayak F, Ulas E (1996) Mass tourism in Turkey and its impact on the Mediterranean coast. In: Salman AHPM, Langeveld MJ, Bonazountas M (eds) Coastal management and habitat conservation, vol II. European Union for Coastal Conservation, Leiden, pp 117–123

Ehleringer JR, Dawson TE (1992) Water uptake by plants: perspectives from stable isotope composition. Plant Cell Environ 15:1073–1082

Fischer DT, Still CJ, Williams AP (2009) Significance of summer fog and overcast for drought stress and ecological functioning of coastal California endemic plant species. J Biogeogr 36 (4):783–799

Gallego-Fernández JB, García Mora MR, Ley Vega de Seoane C (2003) Restauración de ecosistemas dunares costeros. In: Rey Benayas JM, Espigares Pinilla T, Nicolas Ibarra JM (eds) Restauración de Ecosistemas Mediterráneos. Asociación Española de Ecología Terrestre, Alcalá de Henares, pp 157–171

Gallego-Fernández JB, Muñoz Vallés S, Dellafiore CM (2006) Introduction of exotic plants caused by beach and dune management. In: Michallef A, Vasallo A, Cassar M (eds) Proceedings of the second international conference on the management of coastal recreational resources – Beaches, yatchting and coastal ecotourism, Gozo, Malta, pp 355–363, 464 p

Gallego-Fernández JB, Muñoz Vallés S, Dellafiore CM (2010) Expansión de un arbusto nativo-invasivo en dunas costeras: causas y consecuencias ecológicas. Revista Chagual 8:41–48

Gallego-Fernández JB, Sánchez IA, Ley C (2011) Restoration of isolated and small coastal sand dunes on the rocky coast of northern Spain. Ecol Eng 37:1822–1832

García Mora MR, Gallego-Fernández JB, Williams AT (1998) The coastal area of SW Spain: between conservation and tourist development. In: Monsó de Prat JL (ed) Sustainable waterfront and coastal developments in Europe: socioeconomics, technical and environmental aspects, Barcelona, pp 177–185

García Mora MR, Gallego-Fernández JB, García Novo F (2000) Plant diversity as a suitable tool for coastal dune vulnerability assessment. J Coast Res 16(4):990–995

García Mora MR, Gallego-Fernández JB, Williams AT, García Novo F (2001) A coastal dune vulnerability classification: a case study of the SW Iberian Peninsula. J Coast Res 17 (4):802–811

García Novo F, Crawford RM, Díaz Barradas MC (eds) (1997) The ecology and conservation of European dunes. Secretariado de publicaciones de la Universidad de Sevilla, Seville, 375 p

Gómez-pina G, Muñoz-Pérez JJ, Ramírez JL, Ley C (2002) Sand dune management problems and techniques, Spain. J Coast Res 36:325–332

Greaver TL, Sternberg LLS (2006) Linking marine resources to ecotonal shifts of water uptake by terrestrial dune vegetation. Ecology 87:2389–2396

Greaver TL, Sternberg LLS (2007) Fluctuating deposition of ocean water drives plant function on coastal sand dunes. Glob Change Biol 13:216–223

Greaver TL, Sternberg LLS (2010) Decreased precipitation exacerbates the effects of sea level on coastal dune ecosystems in open ocean islands. Glob Change Biol 16:1860–1869
Heslenfeld P, Jungerius PD, Klijn JA (2004) European coastal dunes: ecological values, threats, opportunities and policy development. In: Martínez ML, Psuty NP (eds) Coastal dunes, ecology and conservation, vol 171, Ecological studies. Springer, Berlin, pp 335–351
Hesp PA (2000) Coastal sand dunes: form and function. Massey University/Rotorua Printers, New Zealand, p 24
Hesp PA (2004) Coastal dunes in the Tropics and temperate regions: locations, formation, morphology and vegetation processes. In: Martínez ML, Psuty NP (eds) Coastal dunes, ecology and conservation, vol 171, Ecological studies. Springer, Berlin, pp 29–49
Hesp PA, Martínez ML (2007) Disturbance processes and dynamics in coastal dunes. In: Johnson EA, Miyanishi K (eds) Plant disturbance ecology. Academic Press, Burlington, Massachusetts, pp 215–248
Holdgate MW (1993) The sustainable use of tourism: a key conservation issue. Ambio 22:481–482
Hulme PE (2009) Trade, transport and trouble: managing invasive species pathways in an era of globalization. J Appl Ecol 46:10–18
Intergovernmental Panel on Climatic Change (IPCC) (2007) Climate change 2007: the scientific basis. Cambridge University Press, Cambridge
Isermann M (2008a) Classification and habitat characteristics of plant communities invaded by the non-native Rosa rugosa Thunb. in NW Europe. Phytocoenologia 38(1–2):133–150
Isermann M (2008b) Expansion of Rosa rugosa and Hippophaë rhamnoides in coastal grey dunes: effects at different spatial scales. Flora 203:273–280
Isermann M, Diekmann M, Heemann S (2007) Effects of the expansion by *Hippophaë rhamnoides* on plant species richness in coastal dunes. Appl Veg Sci 10:33–42
Jackson NL, Nordstrom LF (2011) Aeolian sediment transport and landforms in managed coastal systems: a review. Aeolian Res 3:181–196
Jørgensen RH, Kollmann J (2009) Invasion of coastal dunes by the alien shrub *Rosa rugosa* is associated with roads, tracks and houses. Flora 209(4):289–297
Kidd R (2001) Coastal dune management: a manual of coastal dune management and rehabilitation techniques. NSW Department of Land and Water Conservation Coastal Unit, DLWC, Newcastle, 96 p
Kith-y-Tassara M (1946) El problema de las dunas del SO de España. Revista de Montes 11:414–419
Kutiel P, Zhevelev H, Harrison R (1999) Te effect of recreational impacts on soil and vegetation of stabilised coastal dunes in the Sharon Park, Israel. Ocean Coast Manage 42:1041–1060
Kutiel P, Peled Y, Geffen E (2000) The effect of removing shrub cover on annual plants and small mammals in a coastal sand dune ecosystem. Biol Conserv 94:235–242
Kutiel P, Cohen O, Shoshany M, Shub M (2004) Vegetation establishment on the southern Israeli coastal sand dunes between the years 1965 and 1999. Lands Urban Plann 67:141–156
Levin N, Ben-Dor E (2004) Monitoring sand dune stabilization along the coastal dunes of Ashdod-Nizanim, Israel, 1945–1999. J Arid Environ 58:335–355
Ley C, Gallego-Fernández JB, Vidal C (2011) Coastal dunes restoration manual. Ministerio de Medio Ambiente, Rural y Marino, 251 p
Li Y, Cui J, Zhang T, Okuro T, Drake S (2009) Effectiveness of sand-fixing measures on desert land restoration in Kerqin Sandy Land, northern China. Ecol Eng 35:118–127
Lichter J (1998) Primary succession and forest development on coastal Lake Michigan sand dunes. Ecol Monogr 68(4):487–510
Lowe S, Browne M, Boudjelas S, De Poorter M (2000) 100 of the world's worst invasive alien species A selection from the global invasive species database. Published by the Invasive Species Specialist Group (ISSG) a specialist group of the Species Survival Commission (SSC) of the World Conservation Union (IUCN), 12 p. Updated and reprinted version: November 2004
Lubke RA (1985) Erosion of the beach at St. Francis Bay, Eastern Cape. Biol Conserv 32:99–127

Lubke RA (2004) Vegetation dynamics and succession on sand dunes of the eastern coasts of Africa. In: Martínez ML, Psuty NP (eds) Coastal dunes, ecology and conservation, vol 171, Ecological studies. Springer, Berlin, pp 67–84

Marchante E, Kjøller A, Struwe S, Freitas H (2008) Short- and long-term impacts of *Acacia longiflora* invasion on the belowground processes of a Mediterranean coastal dune ecosystem. Appl Soil Ecol 40:210–217

Margalef R (1977) Ecología, 2nd edn. Omega, Barcelona, 951 p

Marlow R, Morris A (2003) The vulnerability and management of three sand dune sites in southwestern Turkey. In: Özhan E (ed) Proceedings of the sixth international conference on the Mediterranean coastal environment, MEDCOAST 2003, Ravenna, Italy, vol 2, pp 1381–1391

Martínez ML, Psuty NP (eds) (2004) Coastal dunes, ecology and conservation, vol 171, Ecological studies. Springer, Berlin, 380 p

Martínez ML, Moreno-Casasola P, Castillo S (1993) Biodiversidad Costera: Playas y Dunas. In: Salazar Vallejo SI, González NE (eds) Biodiversidad Marina y Costera de México. Centro de Investigaciones de Quintana Roo y CONABIO, Chetumal, pp 160–181

Martínez ML, Vázquez G, Sánchez Colón S (2001) Spatial and temporal variability during primary succession on tropical coastal sand dunes. J Veg Sci 12(3):361–372

Martínez ML, Maun MA, Psuty NP (2004a) The fragility and conservation of the world's coastal dunes: geomorphological, ecological, and socioeconomic perspectives. In: Martínez ML, Psuty NP (eds) Coastal dunes, ecology and conservation, vol 171, Ecological studies. Springer, Berlin, pp 355–369

Martínez ML, Psuty NP, Lubke RA (2004b) A perspective on coastal dunes. In: Martínez ML, Psuty NP (eds) Coastal dunes, ecology and conservation, vol 171, Ecological studies. Springer, Berlin, pp 3–10

Martínez ML, Gallego-Fernández JB, García Franco JG, Moctezuma C, Jiménez CD (2006) Coastal dune vulnerability along the Gulf of México. Environ Conserv 33:109–117

Matias A, Dias JA, Ferreira O, Williams AT (1998) Applicability of a dune vulnerability checklist to the Ria Formosa system. In: de Carvalho S, Gomes V, Pinto T (eds) Seminario Dunas da Zona Costeira de Portugal. Instituto de hidráulica e Recursos Hidricos, Leiria, pp 213–224

Maun MA (1998) Adaptations of plants to burial in coastal sand dunes. Can J Bot 76:713–738

Maun MA (2009) The biology of coastal sand dunes. Oxford University Press, Oxford, 265 p

Melvin SM, Griffin CR, MacIvor LH (1991) Recovery strategies for piping plovers in manager coastal landscapes. Coast Manage 19:21–34

Milne FD, Dong P, Davidson M (2012) Natural variability and anthropogenic effects on the morphodynamics of a beach–dune system at Montrose Bay, Scotland. J Coast Res 28 (2):375–388

Moreno-Casasola P (1986) Sand movement as a factor in the distribution of plant communities in coastal dune system. Vegetatio 65:67–76

Muñoz Vallés S, Gallego-Fernández JB, Dellafiore C (2005) Foredune fragmentation and tourist pressure in two natural places in the coast of Huelva, SW Spain. In: Sena A, Ferreira O, Noronha P, Veloso F, Taveira F, Correira F, das Neves L (eds) Book of abstracts of the international conference on coastal conservation and management in the Atlantic and Mediterranean. ICCCM'05, Tavira, Portugal, pp 375–378

Muñoz Vallés S, Gallego-Fernández JB, Dellafiore CM (2011a) Dune vulnerability in relation to tourism pressure in Central Gulf of Cádiz (SW Spain), a case study. J Coast Res 27(2):243–251

Muñoz Vallés S, Gallego-Fernández JB, Dellafiore CM, Cambrollé J (2011b) Effects on soil, microclimate and vegetation of the native-invasive *Retama monosperma* (L.) in coastal dunes. Plant Ecol 212:169–179

Nilsson C, Grelsson G (1995) The fragility of ecosystem: a review. J Appl Ecol 32:677–692

Nordstrom KF (2008) Beach and dune restoration. Cambridge University Press, Cambridge, 185 p

Nordstrom KF, Lotstein EL (1989) Perspectives on resource use of dynamic coastal dunes. Geogr Rev 79(1):37–53

Nordstrom KF, Psuty N, Carter B (1990) Coastal dunes: form and process. Wiley, Chichester, 410 p
Nordstrom KF, Lampe R, Vandemark LM (2000) Reestablishing naturally functioning dunes on developed coasts. Environ Manage 25(1):37–51
Olson JO (1958) Rates of succession and soil changes on southern Lake Michigan sand dunes. Bot Gaz 119(3):125–170
Orians GH (1975) Diversity, stability and maturity in natural ecosystems. In: Van Dobben WH, Lowe-McConnell RH (eds) Unifying concepts in ecology. W. Junk B.V. Publishers, The Hague, pp 139–150
Orians SH (1986) Site characteristics favoring invasions. In: Mooney HA, Drake JA (eds) Ecology of biological invasion in North America and Hawaii. Springer, New York, pp 133–148
Packham JR, Willis AJ (1997) Ecology of dunes, salt marsh and shingle. Chapman and Hall, London, 335 p
Panario D, Piñeiro G (1997) Vulnerability of oceanic dune systems under wind pattern change scenarios in Uruguay. Clim Res 9:67–72
Perrings C, Mooney H, Williamson M (2010) The problem of biological invasions. In: Perrings C, Mooney H, Williamson M (eds) Bioinvasions and globalization. Oxford University Press, Oxford, pp 1–16
Peters DPC, Yao J, Gosz JR (2006) Woody plant invasion at a semi-arid/arid transition zone: importance of ecosystem type to colonization and patch expansion. J Veg Sci 17:389–396
Pethick JS, Crooks S (2000) Development of a coastal vulnerability index: a geomorphological perspective. Environ Conserv 27:359–367
Pimm SL (1991) The Balance of Nature: Ecological Issues in the Conservation of Species and Communities. The University of Chicago Press, Chicago, 434 p
Psuty NP (2004) The coastal foredune: a morphological basis for recreational coastal dune development. In: Martínez ML, Psuty NP (eds) Coastal dunes, ecology and conservation, vol 171, Ecological studies. Springer, Berlin, pp 11–27
Pye K (1983) Coastal dunes. Prog Phys Geogr 7:531–557
Ranwell DS (1960) Newborough Warren, Anglesey: III. Changes in the vegetation on parts of the dune system after the loss of rabbits by mixomatosis. J Ecol 2:385–395
Ranwell DS (1972) Ecology of salt marshes and sand dunes. Chapman and Hall, London, 258 p
Ross MS, O'Brien JJ, Stenberg LSL (1994) Sea-level rise and the reduction in pine forests in the Florida Keys. Ecol Appl 4(1):144–156
Santoro R, Jucker T, Prisco I, Carboni M, Battisti C, Acosta ATR (2012) Effects of Trampling Limitation on Coastal Dune Plant Communities. Environ Manage 49(3):534–542
Sternberg LSL, Swart PK (1987) Utilization of freshwater and ocean water by coastal plants of Southern Florida. Ecology 68:1898–1905
Thomas AS (1960) Changes in vegetation since the advent of mixomatosis. J Ecol 48(2):287–306
Tsoar H (2005) Sand dunes mobility and stability in relation to climate. Phys A: Stat Mech Its Appl 357(1):50–56
Tsoar H, Blumberg DG (2002) Formation of parabolic dunes from barchans and transverse dunes along Israel's Mediterranean coast. Earth Surf Process Landf 27:1147–1161
Tsoar H, Levin N, Porat N, Maia LP, Herrmann HJ, Tatumi SH, Claudino-Sales V (2009) The effect of climate change on the mobility and stability of coastal sand dunes in Ceará State (NE Brazil). Q Res 71(2):217–226
Van der Maarel E (ed) (1993a) Dry coastal ecosystems: ecosystem of the world, vol 2A. Elsevier Scientific Publishing, Amsterdam, 600 p
Van der Maarel E (1993b) Dry coastal ecosystems: scope and historical significance. In: der Maarel V (ed) Dry coastal ecosystems: ecosystem of the world, vol 2A. Elsevier Scientific Publishing, Amsterdam, pp 1–6
Van der Meulen F, Salman AHPM (1996) Management of Mediterranean coastal dunes. Ocean Coast Manage 30(2–3):177–195

Van der Meulen F, Bakker TWM, Houston JA (2004) The costs of our coasts: examples of dynamic dune management from Western Europe. In: Martínez ML, Psuty NP (eds) Coastal dunes, ecology and conservation, vol 171, Ecological studies. Springer, Berlin, pp 259–277

Van der Putten WH, Peters BAM (1995) Possibilities for managenet of coastal foredunes with deteriorated stands of *Ammophila arenaria* (marram grass). J Coast Conserv 1:29–39

Vestergaard P (1997) Possible impact of sea-level rise on some habitat types at the Baltic coast of Denmark. J Coast Conserv 3:103–112

Wiedemann AM, Pickart AJ (1996) The *Ammophila* problem on the Northwest Coast of North America. Lands Urban Plann 34:287–299

Wiedemann AM, Pickart AJ (2004) Temperate zone coastal dunes. In: Martínez ML, Psuty NP (eds) Coastal dunes, ecology and conservation, vol 171, Ecological studies. Springer, Berlin, pp 53–65

Williams AT, Davies P, Curr RHF, Koh A, Bodéré J-C, Hallégouët B, Meur C, Yoni C (1993) A checklist assessment of dune vulnerability and protection in Devon and Cornwall, UK. In: Magoon O (ed) Proceedings of coastal zone '93. American Society of Civil Engineering, New York, pp 3395–3408

Williams AT, Randerson P, Sothern E (1997) Trampling and vegetation response on sand dunes in South Wales, UK. In: García Novo F, Crawford RMM, Díaz Barradas MC (eds) The ecology and conservation of European dunes. Universidad de Sevilla, Sevilla, pp 287–300

Williams AT, Alveirinho Días J, Garcia Novo F, García Mora MR, Curr R, Pereira A (2001) Integrated coastal dune management: checklists. Cont Shelf Res 21:1937–1960

Yizhaq H, Ashkenazy Y, Tsoar H (2007) Why do active and stabilized dunes coexist under the same climatic conditions? Phys Rev Lett 98(18):188001–1–188001–4

Chapter 19
Erosion and Management in Coastal Dunes

Silvia Cristina Marcomini and Ruben Alvaro López

Abstract This chapter summarizes the concepts of geomorphology and ecology in coastal dunes and analyzes the environmental variables that regulate its functioning, development and evolution. It also discusses the responses to global and local climate change at different scales of time (from years to centuries) and their response in the geomorphological and ecological conditions.

Then we synthesized the action of man in modifying coastal dunes and the causes and consequences that lead to alterations in the coastal dynamics, enhancing the erosion phenomenon.

Finally, we show and discuss appropriate management strategies for coastal dunes and raised suitable methodologies for coastal protection, beach remediation and reconstruction of the foredune.

19.1 Introduction

Coastal sand dunes are unique and complex systems. They are widely distributed environments in the world and occur in almost every latitude – from tropical to polar. Dune systems are of great value to society because they act as natural sea defenses, wildlife refuges and recreational areas.

On the Atlantic coast of South America dune systems are very common and much of the population has settled on them without knowledge of the aeolian aerodynamic and its relation to coastal hydrodynamics. In southern Brazil, Uruguay and northeastern Argentina coastal dune fields are associated with Holocene barriers composed of unconsolidated sand, and are therefore highly vulnerable to erosion (Tomazelli and Villwock 2000; Tomazelli et al. 1999; Toldo et al. 1999;

S.C. Marcomini (✉) • R.A. López
Facultad de Ciencias Exactas y Naturales, Departamento de Geología, Universidad de Buenos Aires, Buenos Aires, Argentina
e-mail: scm@gl.fcen.uba.ar; rlopez@gl.fcen.uba.ar

C.W. Finkl (ed.), *Coastal Hazards*, Coastal Research Library 6,
DOI 10.1007/978-94-007-5234-4_19,

Gruber et al. 2003; Dillenburg et al. 2000, 2005). Transgressive dune fields are also frequently hanging on cliffs whose dynamics are controlled by aeolian ramps.

Dune coasts are very sensitive to climate changes especially in relation to wind regime, rainfall, water-table and sea level variations that condition dune activity by changes in the sand supply to the littoral system. Natural ecosystems that settle on such environments should develop adaptive strategies to survive under environmental stress. Man initially considered dunes to be unproductive environments, but was then required to find adaptive strategies to settle on them, including the stabilization of dune fields by afforestation for further urban development.

Human intervention has altered the rates of aeolian and marine sediment supply to coastal zones, intensifying foredune erosion and degradation.

Dune coasts are highly vulnerable to erosion due to lack of compaction of aeolian deposits and often, once the process starts, it is irreversible.

This chapter describes the most frequent aeolian landform in coastal dune fields, the ecology of associated systems and their response to climate change. We will then analyze the most common factors that cause the erosion process, dune management and optimal strategies for remediation along coastal dunes.

19.2 Coastal Dunes Geomorphology

Coastal beaches and dunes begin with the accumulation of marine sand that is transported to the coast by waves and currents. In the case of dunes, sand is subsequently reworked by strong winds (greater than 5 m/s) and then deposited behind the beach.

Coastal dune landforms of various size and morphology are formed depending on variables such as: availability of the sediment supply, dominant wind velocity and direction, soil moisture, vegetation, and beach morphodynamics. Sand deposition, accretion, and erosion within the coastal environment result in the development of a variety of dune morphologies (Fig. 19.1).

19.3 Landforms in Coastal Dunes

19.3.1 Foredune

Foredunes are defined as shore-parallel dune ridges formed on the top of the backshore by aeolian sand deposition within vegetation (Hesp 2002) (Figs. 19.2 and 19.3a).

A general classification into primary and secondary dunes is made based on relationship to foredune sand exchange, morphology, and sequence in development (Davis 1980; Psuty 1988; Psuty et al. 1988; Masselink and Hughes 2003). Primary

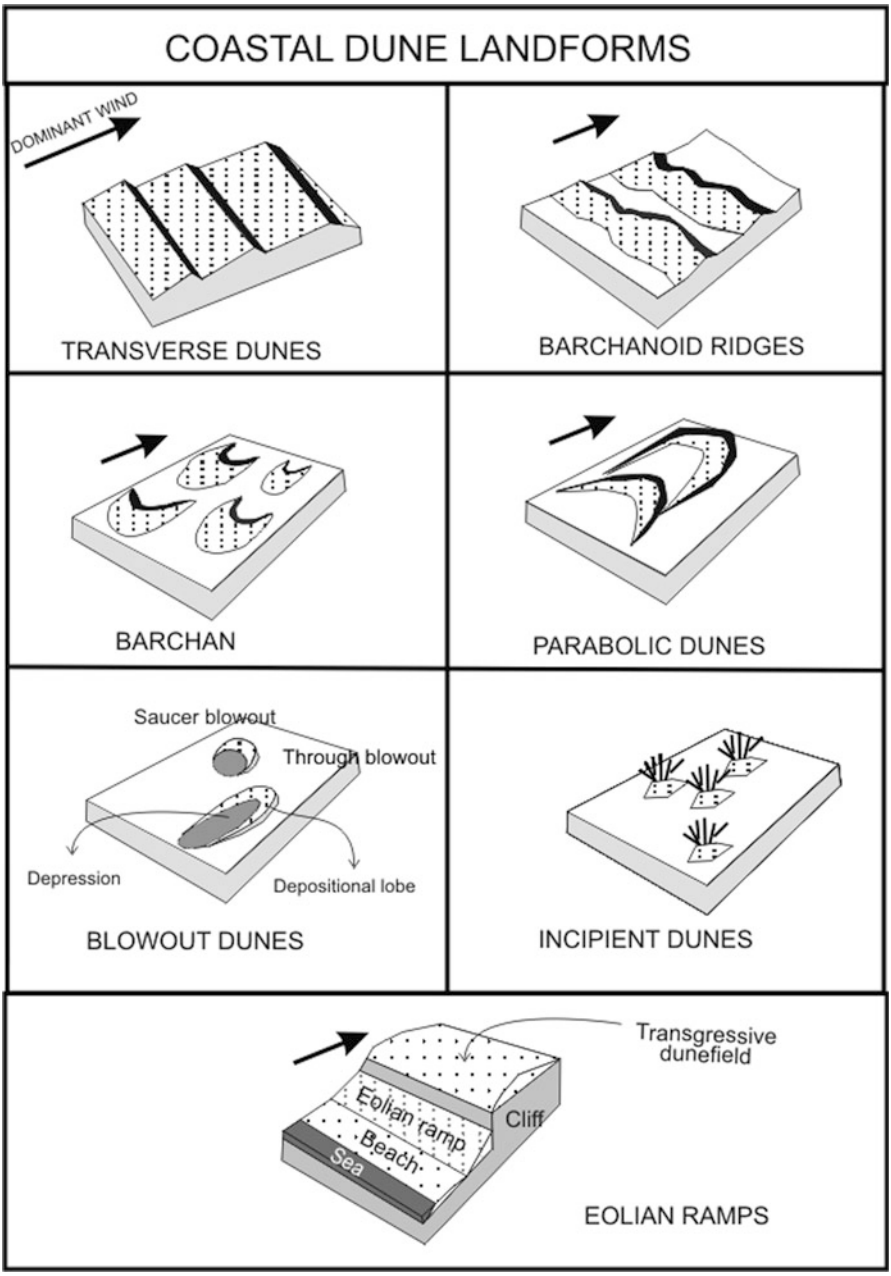

Fig. 19.1 Most common landforms in dune coast

Fig. 19.2 Incipient and established foredune in the coast of Río Negro, El Observatorio, near San Antonio Oeste

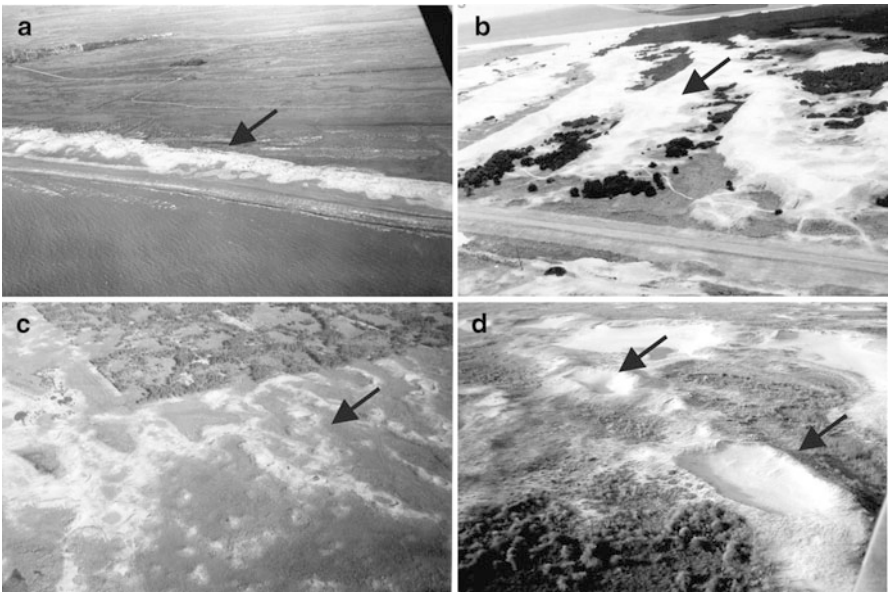

Fig. 19.3 Examples of aeolian landforms in coastal zones. (**a**) Foredune, (**b**) Transverse ridges. (**c**) Parabolic with blowouts sobreimposed. (**d**) Blowouts

dunes are composed of sand blown directly from the beach face (active beach), whereas secondary dunes develop following the subsequent modification of primary dunes.

Foredune development is controlled by three main factors. They are: beach width, sediment supply, and wind velocity (Davidson-Arnott and Law 1996). The first two ones are intimately tied to surfzone-beach type (Hesp 1988; Short and Hesp 1982), and influenced the foredune height and volume. Larger foredunes occur on dissipative beaches (widest beaches and maximum potential sediment supply) and the smaller ones occur on reflective beaches (narrowest beaches and minimum potential sediment supply) (Hesp 1988; Ruz et al. 1992; Sherman and Bauer 1993; Ruz and Allard 1994; Sherman and Lyons 1994).

The morphology of foredunes is varied and they can be classified into three main types: incipient foredunes, established foredunes, and relict foredunes (Short and Hesp 1982; Hesp 1984a; b; 2002).

19.3.1.1 Incipient Foredune

Incipient foredunes are sometimes ephemeral features, tending to be eroded or completely removed by severe storm events at irregular intervals varying from a few months to several years, but they may survive and grow to become a larger established foredune, or become relict and stable as a new incipient foredune develops to seaward (Hesp 1999, 2002) (Fig. 19.2).

Incipient foredunes, also called embryo dunes, may be seasonal where formed around annual plants and require invasion by perennial plants in order to survive. The morphology of dune is dependient on the plant species, architecture, density, height, sediment texture, sand velocity and the rate of sand transport (Hesp 1988, 1989). Secondary factors such as the rate of occurrence of swash inundation, storm wave erosion, overwash incidence, and wind direction can also be important in determining subsequent dune evolution (Cowles 1898; Ranwell 1972; Davies 1980).

Incipient foredunes may also form on the backshore by relatively laterally continuous alongshore growth of pioneer plant seedlings in the wrack line or spring high tide region, and/or by rhizome growth onto the backshore region.

19.3.1.2 Stablished Foredune

Established foredunes also originate at the landward edge of the beach, parallel to the shoreline. They develop from an incipient foredune and have a greater height, width, age, and/or morphological complexity (Hesp 2002). They are commonly distinguished by the growth of intermediate, often woody plant species, and by their greater morphological complexity, height, width, age, and geographical position.

As an incipient foredune builds up, and out, sand inundation and salt spray levels decrease, while nutrient levels and vegetation cover increase, resulting in more

stable dunes. The lee slope (landward slope) is gradually often colonised by shrub plant species that prefer more stable conditions (Hesp 1999, 2002).

Coastal progradation by aeolian ridges is distinguished in the coast of Rio Negro near San Antonio Oeste. An incipient foredune is seen in the seafront occupied by herbaceous plants with low diversity. Landward an established foredune is observed colonised by shrub plant species (Fig. 19.2).

19.3.2 Transgressive Dunefields

Transgressive sand sheets and dunefields (Fig. 19.1) are relatively large-scale aeolian sand deposits formed by the downwind and/or alongshore movement of sand over land; (Hesp and Thom 1990). Transgressive sheets are relatively flat to undulating, largely dune-less sheets (bed sheets), whereas transgressive dunefields comprise various types of dunes on the surface. Transgressive dunefields have also been termed mobile dunes, sand drifts, and migratory dunes. Such dunefields may range from quite small (hundreds of metres) to very large (many kilometres). They may be largely unvegetated, partially vegetated, or completely vegetated (relict). They may be featureless sandsheets, or comprise a variety of dune types ranging from simple barchans, transverse, barchanoidal transverse, to parabolic dunes.

19.3.3 Blowout

A blowout is a saucer, cup or trough-shaped depression formed by wind erosion on a preexisting sand deposit (Figs. 19.1 and 19.3d). The adjoining accumulation of sand, the depositional lobe, derived from the depression, and possibly other sources, is normally considered part of the blowout (Glenn 1979; Carter et al. 1990; Hesp 1996).

Blowouts are common in coastal dune environments, particularly where beaches and foredunes are occasionally eroded and/or receding, but also occur in stable and accretionary environments where wind and wave energy is high. The blowouts may be initiated in a variety of ways including: (1) wave erosion along the seaward face of the dune; (2) topographic acceleration of airflow over the dune crest; (3) climate change; (4) vegetation variation in space or change through time; (5) water erosion; (6) high velocity wind erosion, sand inundation and burial; and (7) human activities (Hesp 2002).

19.3.4 Parabolic Dunes

This dune type consists of an actively advancing nose and depositional lobe with two trailing arms that enclose a deflation basin (Fig. 19.3c). They present a characteristic U-shape or V-shaped dune (Hesp 1999). As they develop over a

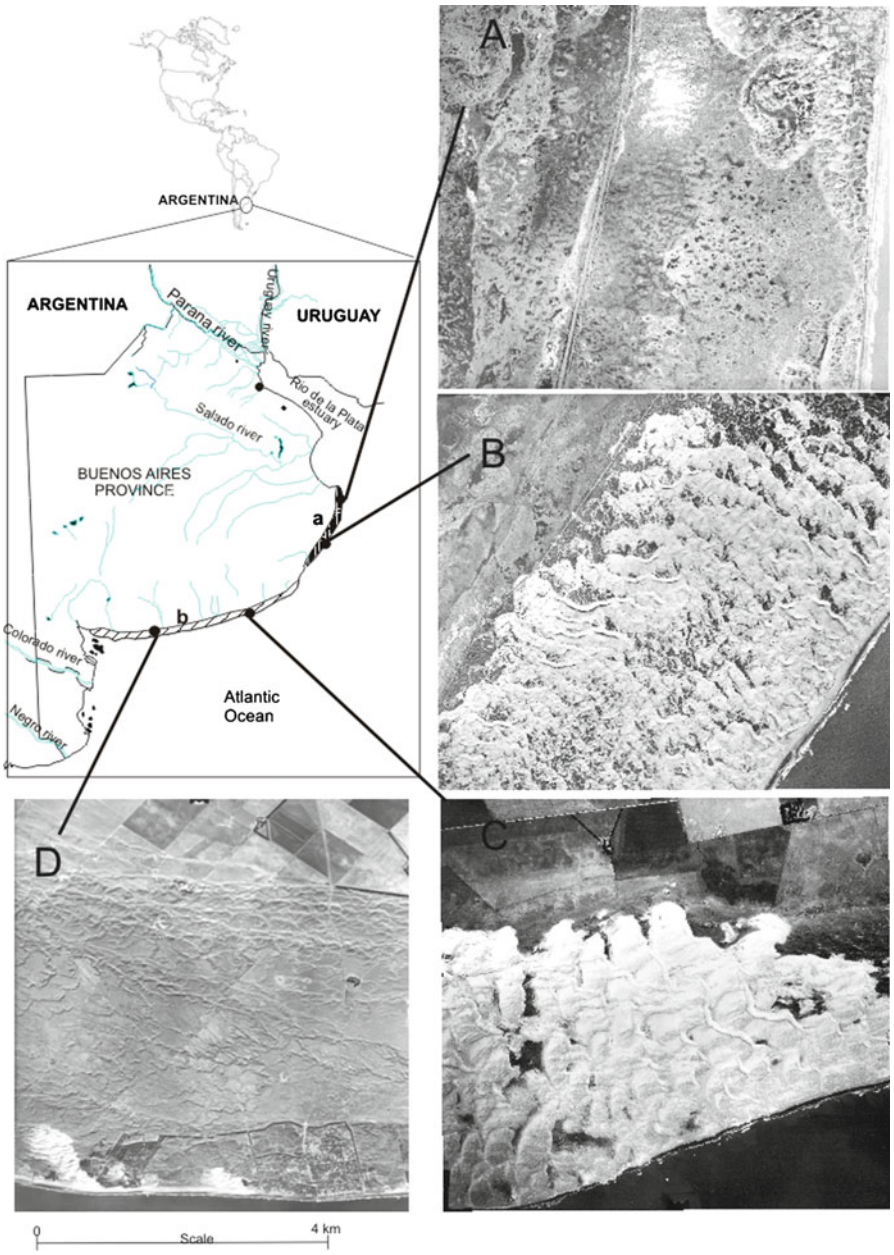

Fig. 19.4 Location of the dune barriers along the coast of Buenos Aires. (**a**) Municipio de La Costa, (**b**) Villa Gesell, (**c**) Cabo Blanco, (**d**) Pehuen-có. Partial reproduction of air photographs of Dirección de Geodesia, Ministerio de Infraestructura of Buenos Aires province and Servicio de Hidrografía Naval

period of time their long axis orientation is closely aligned with that of the dominant wind direction (Bird 2000). Shorter and wider parabolic dunes form where there is a wider range of wind directions (Davis 1980; Bird 2000).

There are two principal sub-types of parabolic dunes: long walled and elliptical types (Hesp 1999). The first one display long trailing ridges and extensive deflation basins. The trailing ridges may range from hundreds of metres to several kilometres in length. The second display a shorter form, often with more semi-circular or elliptical deflation basins.

19.3.5 Brachan

Cooke et al. (1993) define a barchan as a crescentic dune isolated on a firm coherent basement such as sabkha, pediment or desert pavement. The dunes are typically crescentic in shape, terminating downwind with horns or wings. A slipface is usually formed around the downwind edge of the dune. Barchans have been observed to develop in virtually all latitudes and in most coastal and desert regions (Bagnold 1941).

19.3.6 Transverse Dunes and Barchanoid Ridges

They occur within dunefields and result from winds having a single dominant direction with their crest at right angles to them. Brachanoid ridges forms parallel rows of coalesced barchans while transverse ridges are essentially parallel straight ridges (McKee 1979) (Fig. 19.3b). They occur commonly occur in a define sequence as a function of the amount of available sand. Transverse dunes develop where sand is abundant and they attain a maximum height where there is a balance between strength of wind and sand supply.

19.3.7 Dune Ramps

The dune ramps are typically ephemeral features that can form in a few weeks to months and they are often eroded or removed completely during storms with large surges. They play a significant role in the dynamic processes associated with beach/dune interaction and with the ongoing landward coastal retreat. The dominant forcing processes are the local beach sediment budget (beach width), the frequency and magnitude of large storm surges, and the pattern of wind speed and direction as it controls aeolian sediment transport (Christiansen and Davidson-Arnott 2004).

19.4 Coastal Dune Systems in Buenos Aires

There are two dunefields in the province of Buenos Aires, one situated to the north, which spans from the Mar Chiquita lagoon to Punta Rasa, and the other situated to the south, from Miramar to Pehuen-Có (Fig. 19.4). They have been defined as eastern and southern dune barriers, respectively (Isla 1989, 1997) and have evolved due to the fluctuation in the sea level from the mid-Holocene.

The eastern barrier is composed of a transgressive dunefield, with a maximum length of 4 km in Punta Médanos. It develops over two barriers spit systems formed during the Holocene (Fig. 19.5). There are three different geomorphologic units to be identified, depending on dune activity. Active, semi-active and stabilized dune fields.

Active dune fields consist of barchanoid ridges, barchans, and foredunes (Fig. 19.4b). Barchanoid ridges have greater aeolian activity; vegetation grows only in the interdune sectors and there is usually *Spartina coarctata*, *Cakile maritima* and *Panicum racemosum*. These ridges have an easterly-westerly orientation and heights reaching 25 m (Figs. 19.3b and 19.4b).

The foredune runs like a continuous stretch parallel to the coast and reaches heights of up to 5 m. Semi-active dune fields have degraded dunes and blowouts. The first are ancient barchanoid ridges that have been transformed by the overlapping of blowout dunes. The blowout dunes are mostly round in shape (saucer blowout) and can have up to 36% of their accumulation lobes totally covered by vegetation.

Stabilized dune fields contain parabolic dunes that make up a surface with a trellis design (Marcomini 2002; Marcomini and López 2007) (Figs. 19.3c and 19.4a).

The southern barrier (Fig. 19.4) is a transgressive dunefield that advanced over ancient Plio − Pleistocene cliffs generating *hanging dunes*, whose sediment input is regulated by the presence of aeolian ramps (Fig. 19.6). In their evolution, Isla and Bujalesky (1995), recognized a first stage of abundant sediments during the maximum transgressive period. After the regression, the dune ramps deactivate due to lack of sediment, ancient cliffs and wave-cut platforms are exhumed.

The southern dune barrier has a maximum length of (6.5 km) and its greatest natural stabilization is towards the south. An example is the Pehuen-Có district (Fig. 19.4d), which features parabolic dunes whose horns point towards the west, which have been classified into two subunits, one with a dune height of 8 m northward and the other seaward with heights between 2 and 6 m (Marcomini et al. 2005; Marcomini et al. 2009a).

Active dunefields are scarce and form patches on the stabilized field (Fig. 19.4d). Morphologically, the barchanoid ridges and barchans with a SW-NE direction dominate the scene, indicating prevailing W-NW wind directions. The foredune is partially stabilized with natural and introduced vegetation, and makes up a belt that runs parallel to the coastline, between 40 and 80 m wide, with an overlapping of plate blowouts.

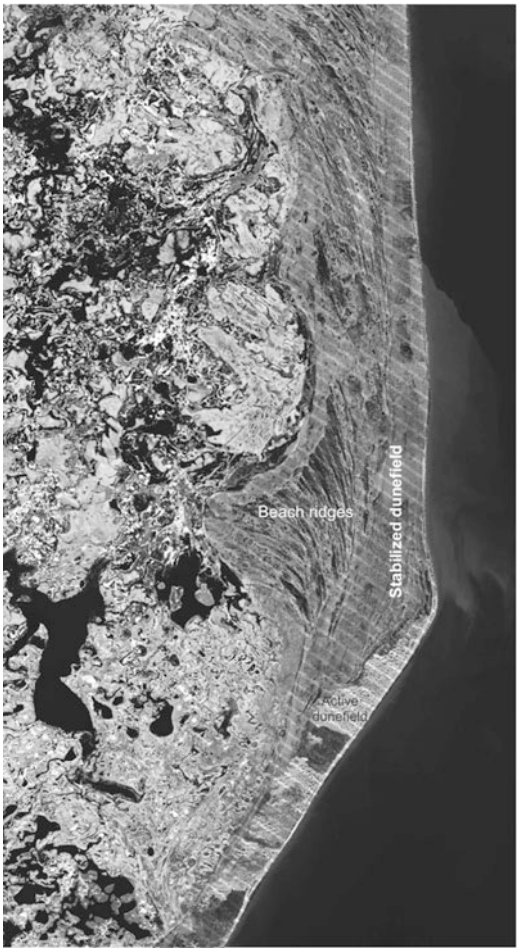

Fig. 19.5 Images showing the northern holocene barrier spit system composed by a beach ridge plain of about 2.5 m height. Over this marine landform the eastern transgressive dunefield is observed. Partial reproduction of Image Landsat of Cabo San Antonio taken in November 26, 2002. Extracted from USGS EROS Digital Image Gallery. http://earthobservatory.nasa.gov/IOTD/view.php?id=4200

Towards the northeast of the southern barrier, the field activity increases, with the greatest areal development in the district known as Cabo Blanco, south of Necochea (Fig. 19.4c). This district boasts the highest dunes of the entire dune barrier. The dominant morphologies are reversive barchanoid ridges with a NW-SE orientation, which reach a height of 70 m and wave lengths of between 220 and 400 m (Spinoglio 2010).

The dynamics of this southern barrier are related to the beach's aeolian activity. The migration of sand from the beach to the dune field takes place through aeolian ramps that climb the cliffs in a manner similar to the climbing dunes (Fig. 19.6).

The action of sand ramps at present is very important in regulating the hydro and aerodynamic balance of the coast. The sand supply from aeolian ramps depends on the beach hydrodynamics but also on the activity of the hanging dunes.

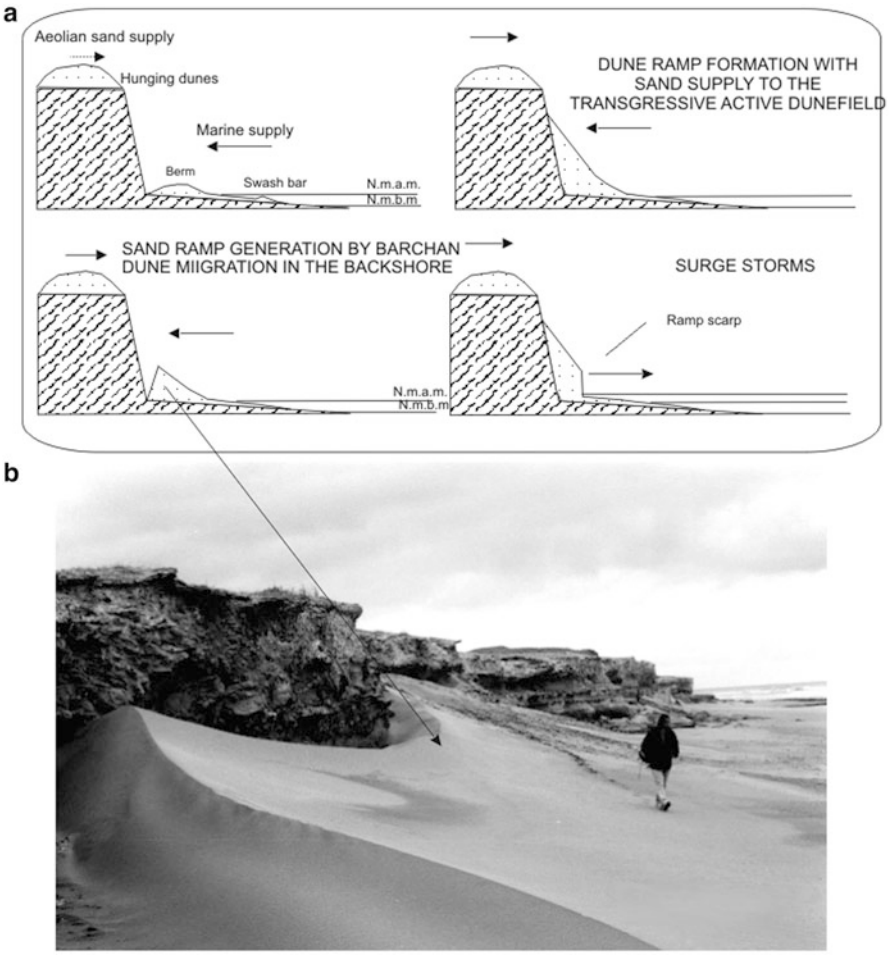

Fig. 19.6 (**a**) Behavior model of sand ramps. In hunging dunefields of Argentina, (Modified from Marcomini et al. (2007)). (**b**) Sand ramps in Cabo Blanco, near Necochea, Buenos Aires, Argentina

Marcomini et al. (2007) have proposed a model defining the degree of vulnerability to erosion according to the configuration and morphology of the coast. The vulnerability to erosion increases from coasts with active dunes, to stabilized coastal dunes, cliffs with ramps, cliffs with mixed ramps, inactive cliffs and active cliffs. Passing from one state to another depends essentially on the activity of the coastal dune and the development of the beach.

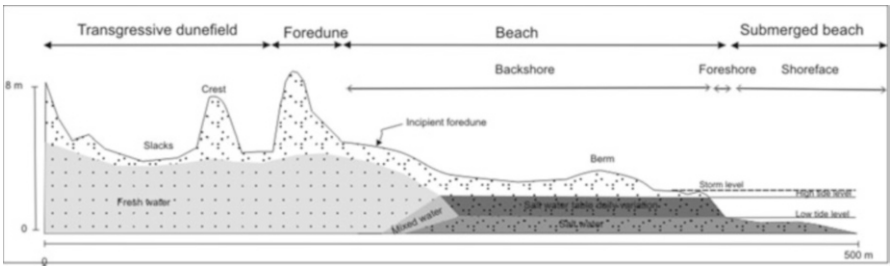

Fig. 19.7 Coastal dune transverse profile in Faro Querandi natural reserve

19.5 Coastal Dune Ecosystems

19.5.1 Plant Communities

Plant communities in dune systems are the result of the interaction between tolerance of plant species and sandy substrate, high wind velocities, salt spray, salt accretion and environmental heterogeneity. Propagules of many plant species are dispersed by water or wind and deposited on the water line. Most of the species find ideal conditions for germination but seedling establishment, growth and reproduction is restricted to species with ecological amplitude sufficient to withstand the physical stress associated with the sand movement.

Figure 19.7 shows the typical environments in coastal dunes of Buenos Aires. The beach can be divided into three sub-environments, backshore, foreshore and shoreface. Landward, the foredune forms a parallel string to the coast and then a transgressive dunefield is extended to the continental side. Physical variables for each environment influence the development of plant communities.

Then we will analyze the environmental conditions for each landform that regulate plant facilities.

19.5.1.1 Foreshore

This zone stretches from the water's edge to the driftline and is consequently subject to frequent erosion and renewal of the sand by wind and wave action. The foreshore is within the normal tide range and is always wet because it is continually being washed by waves. The sand contains the higher amount of salt because it is regularly submerged by tides, wave action and storms. Surface sand may contain algae, bacteria, roifers, copepods and tardigrades.

19.5.1.2 Backshore

This zone covers the area between the mean high tide and the base of the foredune. This habitat is most favorable to plant growth. However sand is blown inland by wind burying plants or forming embryo dunes. The habitat is inundated by waves

only periodically, and the area is highly variable depending on the intensity of the seasonal surge storms and the beach hydrodynamic. The sand left by waves is lacking in nutrients. The only source of nutrients is sea spray and dead organisms. Usually dead organisms are washed into the backsohe forming strandings of diverse origins. The presence of these accumulations of post-storm organisms has shown that they are generators of incipient dunes on the coast of Buenos Aires. This is due to the increase in nutrient content and because they favor the accumulation of sand in their surroundings.

On the coast of Buenos Aires, different associations of these embankments are registered (Fig. 19.8), related to: (1) flood periods of the Paraná basin, (2) surges storms referred to as "sudestadas", (3) algae blooming periods, (4) strong rains and (5) reproductive cycles (Fig. 19.8 b1 and b2).

Extreme floods in the Paraná basin, introduce freshwater plants into marine environments transporting them by currents for more than 300 km. An example of this event is the introduction of water hyacinth *Ponteredia rotundifolia* in 1997 (Fig. 19.8c).

Surgestorrms usually cause mollusk strandings (Fig. 19.8d). They remove sand from submerged beach to foreshore forming embakments of species such as subtidal bivalves (*Amiantis purpurata* and *Tivela isabelleana*), gastropods (*Adelomelon brasiliana)* with anemones associated (*Antholoba, achates with Zidona Buccinanops dufresnei*) (López et al. 2008).

Phytoplankton blooms also increase the nutrient content in the backshore. These episodes are more frequent with a predominance of *Asterionellopsis glacialis* sp. (Fig. 19.8 a1 and a2)

This is essentially a dynamic, diverse and ephemeral environment that is inhospitable to the survival of most perennial species. Under such condition the annual growth habit is favored, however in spite of the unfavorable conditions some annual and incidental perennial species are able to survive.

Usually, few species are able to establish and complete their life cycles.

On the backshore vegetation is spread out in isolated mats, forming low herbaceous steppes with a low specific richness. The pioneer and dominant plant of this environment in northern Buenos Aires is *Spartina coarctata*. Later in the succession appears *Panicum racemosum* and *Cakile maritima*

(Marcomini et al. 2009b, 2010, 2011) and *Sporobolus rigens*, *Calycera crassifolia* y *Salsola kali* in the southern dune barrier (Monserrat and Celsi 2009; Celsi and Monserrat 2006).

The survival mechanisms' common adaptative traits are a short life cycle, the ability to survive under harsh conditions, high fecundity, good dispersal ability, high phenotypic plasticity, seed dormancy and large seed mass (Maun 2009).

19.5.1.3 Foredune

This is a highly unstable environment where species are continuously subjected to tunneling and erosion caused by the wind. Available water is generally fresh water,

Fig. 19.8 Increase of nutrients in the shore during extreme events, such as: (**a1** and **a2**) Phytoplankton blooms of *Asterionellopsis glacialis* sp. (**b1** and **b2**) Stranding of *Adelomelon* free giant egg capsules, Poststorm and some days after storm. (**c**) *Ponteredia rotundifolia* in 1997 Strandings of mollusks (*Adelomelon brasiliana, Zidona dufresnei, Buccinanops gradatum,* and *Amiantis purpurata*)

due to the high degree of permeability of sediments which help retain the water from rain and regulate the phreatic aquifer. This is an area that is subjected to salt spray, with a steeper gradient facing the sea. The action of the waves may create erosion scarps on the foredune after a storm but this subsequently recovers. In general, there is vegetation zoning between the seaface and the continental face.

A large number of plant species belonging to the Poaceae, Convolvulaceae, Asteraceae, Cyperaceae, Caryopphyllaceae, Fabaceae and Aizoaceae occupy this zone in temperate, subtropical and tropical regions (Maun 2009).

Foredune species have properties that are fundamental to their survival. They (a) are geophytes, (b) spread either as rhizomes or stolons, (c) disperse to new locations or establish new populations by fragmentation of rhizomes and stolons, (d) are characterized by the ability to occupy bare areas rapidly (within a year) (Maun 1998); (e) establish seedlings stochastically in most cases, which is related more to the amount and regular distribution of rainfall.

19.5.1.4 Dune Ridges

Dunes ridges are characterized by sand burial, wind erosion and low soil moisture.

The conditioning factors that generally favor the establishment of vegetation are the dune activity, its orientation as regards the prevailing winds, their relationship with isolation and distance from the sea (salt spray) (Maun et al. 1996).

The dune activity is related to the contribution of sediment, and in general, as the sand comes from the beach, the closest field dunes are more highly active.

Depending on the orientation to the sun at different latitudes, the soil temperature is usually higher and soil moisture lower on the windward side of the dune ridge. Since this habitat receives direct insolation from the sun the soil temperature is usually about 2–4°C higher and the surface soil dries up faster than other aspects (Baldwin and Maun 1983).

When dunes start losing mobility, they become stable and the environmental conditions become more favorable for vegetation. Therefore, in general, active dunes lack vegetation.

19.5.1.5 Slacks

Dune slacks are depressions between dune ridges, where the freshwater table is at or just below the sand surface. The environmental conditions favors the establishment of plants because of the proximity to the water table, the frequently soil moisture and the presence of nutrients.

In active dunes, vegetation is established only in interdune areas (Fig. 19.9a). Dominant species *C. maritima* in lows and *Spartina coarctata, C. maritima and P. racemosum* on incipient dunes along the humid slacks.

The slacks between stabilized dunes present highest plant covert value with overlapping vegetation strata (Fig. 19.9b). In the deepest lows *Typha* sp. domain, accompanying by *Mikania parodii*, *Eleocharis* aff. *viridans* and *H. bonariensis*. In the most shallow lows, dominated *Melilotus aff indicus*, *Eleocharis aff viridians*, *Melilotus albus*, *C. selloana and H. Bonariensis (10%)*. On the margins of the lows an association of *C. selloana and A. tenuifolia* domain.

Table 19.1 shows the most abundant plant species of the dune coast of northern province of Buenos Aires. More abundant plants are listed for sub-ambient from the beach to the transgressive dunefield from (Marcomini et al. 2009b, 2010 and 2011).

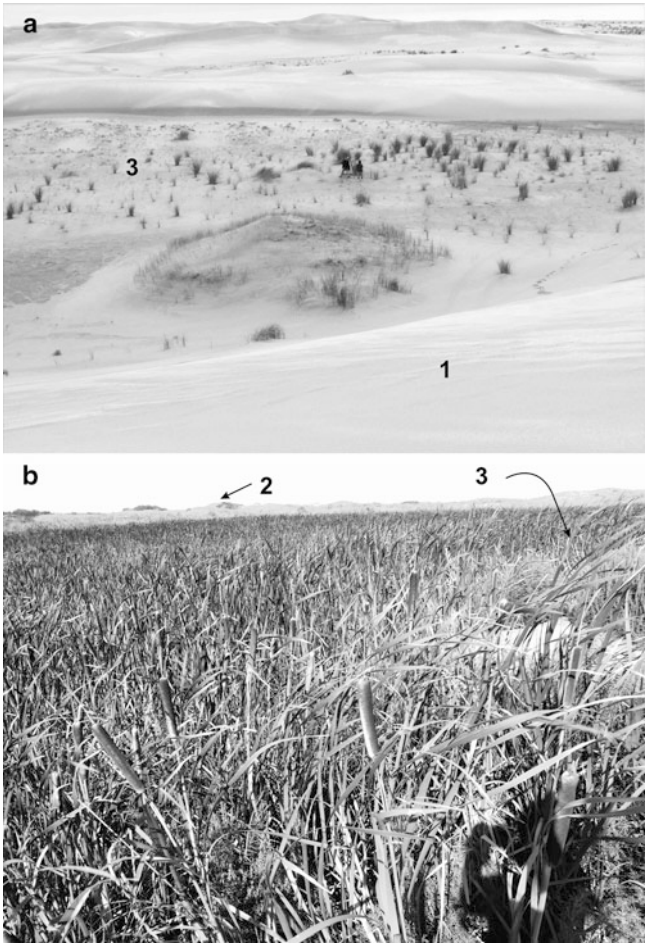

Fig. 19.9 Plant communities in dune slacks of active (**a**) and inactive (**b**) coastal dunefields, Faro Querandí, Buenos Aires Argentina. *1* Barchanoid ridges without vegetation, *2* Parabolic dunes, *3* Slack in the inactive dune occupied mainly *Typha* sp. with overlapping plant layers

The profile shown in Fig. 19.7 represent the different environments recognized in Faro Querandí, Buenos Aires.

19.5.2 Environmental Variables

Dunes are very vulnerable systems and, consequently, the organisms that live on them, including man, need to adapt to a series of environmental variables that affect the adaption of organisms.

Table 19.1 Dominant plant species in the dune communities of Buenos Aires, Argentina

Environment			Characteristic	Plant type
Foreshore			Zone between the sea water edge and the mean high tide line	No plant
Backshore			Zone between the mean high tide line and the dune base	*Spartina coarctata*
Foredune			First frontal dune	*Panicum racemosum* *Calycera crassifolia* *Cakile marítima* *Baccharis genistifolia* *Tessaria abstinthioides* *Androtrichum trigynum*
Transgressive dunefields	Stabilized	Ridge	Parabolic dunes and blowouts	*Achirocline satureoides* *Panicum racemosum* *Ambrosia tenuifolia* *Adesmia incana var. grisea* *Schoenoplectus punges*
		Slacks	Lows with lagoons with transitory regime	*Typha* sp. *Cortaderia selloana* *Mikania parodi* *Eleocharis aff viridens* *Hydrocotyle bonariensis* *Ambrosia tenuifolia* *Melilotus albus* *Tessaria absinthioides*
	Active	Ridge	Transverse dunes barchanoid ridges and barchans	No vegetation
		Slacks	Lows with embryo dunes	*Spartina coarctata* *Cakile maritime* *Panicum racemosum*

Modified from Marcomini et al. (2009b, 2011)

Usually dune ecosystems are characterized by halophyte plants due to their high level of tolerance to salt and psammophyllous species due to the high mobility of the substrate. In general, they are very low in specific richness. These environments are under stressful conditions such as high temperatures, sandy and well-drained soils, winds and sea sprays, low disposal of organic matter and direct exposure to sunlight, conditions that are seemingly responsible for the low species diversity in the area.

Most species have succulent leaves, nanophyll (small leaf area), amphistomatic leaves that are thick (>600 μm), with water-storage tissue, and dorsiventral mesophyll with few intercellular spaces. Some leaf characteristics are peculiar to some of the species such as the presence of Kranz anatomy and microphyllous cells (Maun 2004, 2009). The microphyllous leaves of *H. bonariensis*, *C. rosae* and *I. pescaprae* are more vertically oriented in relation to the soil's surface than the leaves of the remaining species. The morphological characteristics mentioned above are, apparently, strategies of the leaves to reduce water loss, and the effects of the high light intensity and temperatures during some hours of the day, mainly during the hottest months of the year, thus allowing greater efficiency in the physiological processes (Boeger and Wisniewski 2003).

19.6 Response to Minor Climate Change

The effects of past and future changes in climate, sea level changes and human activities on coastal dunes and associated beach systems have been of international interest (Carter 1991; Pye 1990; Neal 1993; Pye and Neal 1994; Arens and Wiersma 1994; Seeliger et al. 2000).

Aeolian processes and landforms are very sensitive to climate change and surface conditions because they result from the interaction between winds and land surfaces and they are very sensitive to changes in atmospheric parameters and surface conditions. Thus, wind action is influenced by changes in wind strength and direction that may be the direct result of global or regional climate changes; it is also influenced by changes in vegetation cover, wet soil and sediment availability that are indirect effects of climate change. Changes in annual precipitation also play a primordial role on aeolian dynamics.

Lancaster (1997) defined minor climate change as short-term variations from decades to centuries. The changes involved are minor compared to those associated with glacial–interglacial cycles but are very significant in regional terms.

Among these climate changes, we need to consider the natural El Niño phenomenon, which regulates these climate changes. The ocean and atmospheric conditions in the Pacific tend to fluctuate between El Niño (warming) and a drop in temperature in the tropical Pacific, known as La Niña. The fluctuations are fairly irregular, but have a tendency to appear between every 3–6 years. The extremes of the Southern Oscillation are partly responsible for large portions of climate variability at interannual scales in Latin America. Therefore, some of the variations in the

foregoing elements could be associated with manifestations of climate variability, such as the El Niño phenomenon, which represents the low phase of the Southern Oscillation; the positive phase is referred to as La Niña. Atmospheric circulation patterns are more perturbed during El Niño than during La Niña years (Salles and Compagnucci 1995, 1997).

As active dunes respond directly to actual rainfall and wind regimes, ENSO (El Niño/Southern Oscillation) effects will be transferred to all the dynamic processes controlled in a direct or indirect manner by the regional climate.

Maia et al. (2005) related the coastal dune migration in northeastern Brazil to El Niño events. They recognized the highest migration rates (33.2 m/year) during the El Nino 1982–1983 event and the lowest rates (9.5 m/year) during the La Niña 1985–1986 event.

Morphological changes have been recorded in dune fields along Argentina's northern coast, associated with climatic trends on scales of 100 years and during periods of extreme drought or floods. These recent changes in dunes have arisen mostly as a result of the rainfall variations, more than due to changes in wind regime.

In the last 100 years, Buenos Aires's dune barriers have experienced climate changes with a tendency towards conditions with greater humidity and minor cycles related to extreme droughts and floods. This fact favors dune stabilization due to the increase in wet soil and a decrease in the sediment supply by sub-saturation in the littoral drift.

Since 1960, a climatic trend towards humid conditions and soil moisture caused an increase in coastal dunefield stabilization areas, and thus diminished the sediment supply. This major climate variation induced the degradation of the active dunefield with a dune landform transition between transverse ridges to degraded, complex and compound parabolic and blowout dunes. The increase in humid conditions, as well as forestation, enlarged the vegetation cover by about 70%.

Extreme floods, like the one that occurred in July 2001 in Buenos Aires also modified dune field morphology. During this climate event, monthly precipitation amounted to between 90 and 140 mm to 200 and 337 mm. Accumulated annual precipitation for 2000 was 913 mm and for 2001 it was 1,181 mm, when the average for the area is 800 mm. The increase in rains together with the floods in the Humid Pampa region has led to a significant increase in the phreatic level of the free aquifer. The interdune areas were flooded, forming permanent lakes that began to generate new ecosystems.

Circular and elongated lakes were formed with depths of up to 1.5 m, which covered the interdune spaces of active dune fields (Fig. 19.10a). The smallest lakes were circular or elongated and covered the basins of blowout dunes. They had a low degree of compactation in the margins and on the bottom. The large amount of sand contributing to this system, as it forms part of an active dunefield, came in through the surface of these lakes, slowly decanting to the bottom, creating sandy swamps. The drop in the phreatic level was very slow and took over 3 years to return to the initial level.

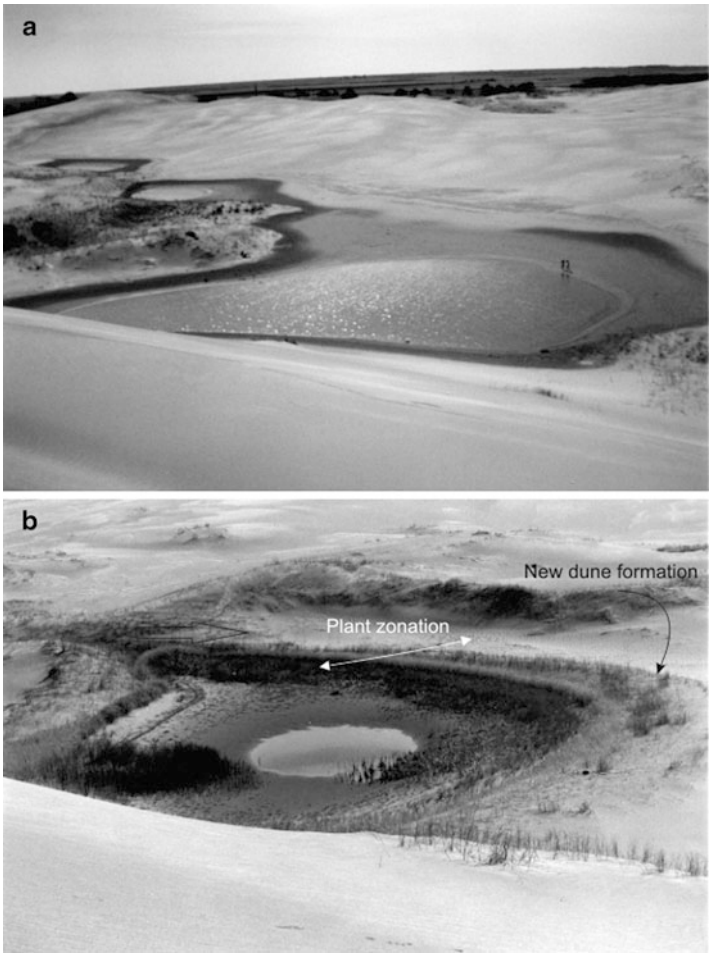

Fig. 19.10 Response of aeolian landforms to large regional flooding in Buenos Aires province. (**a**) View of dune slacks in the active dunefield after the large flood occurred in Buenos Aires during 2001 (Photograph taken in January 2002). Severals lagoons of about 1 m depths covered the interdune areas between barchanoid ridges. (**b**) Photograph taken in August of 2004. A plant zonation is registered which started the development of circular incipient dunes around the lagoons

After the flood, lakes began to be colonized by algae and fungi probably transported by winds. Diatoms (*Rhopalodia*, *Nitzschia, Navicula*, *Cymbella* and *Neidium* spp.); chlorophytes (*Chlamydomonas, Cosmarium, Bulbochaete, Oedogonium and Chaetopheridium* spp.); euglenophytes (*Euglena* spp.). Cyanobacteria (*Nostoc* spp.) and unidentified filamentous fungi grew between submerged macrophytes (Marcomini and Maidana 2006). Diatoms (*Cymbella, Rhopalodia, Surirella, Amphora and Nitzschia* spp.), dinoflagellates and ostracods appeared on the bottom of the lakes.

An important bioturbation was also detected on the margins, caused by toads (*Bufo arenarum*) and worms that produced holes and tubes with complex trellis patterns, respectively. Toads also used those lakes for breeding during summer. By the end of January a large number of toads aged around 1–3 months were found in the lakes. Numerous spiders (*Licosidae trochosa*) were sub-superficially buried on the subaqueous margin of the lakes. Actively reproducing diatoms, cyanobacteria (cocoid and filamentous forms), chorophytes and dinoflagellates were predominant in the lakes during rainy months.

These lakes suffered salinity variations due to the alternation between rainy periods (August – November and March) and dry periods (December – January and February) where evaporation was very intense. During the dry spell there was mucilage as a result of the adaptation to the desiccation and a predominance of dead diatoms over live ones at the bottoms of the lakes. In contrast, during the rainy periods there were predominantly fertile species of diatoms, cyanobacteria and filamentous, flagellate and dinoflagellate cyanophytes (Marcomini and Maidana 2006). They increased the nutrient content in the lake margins, driving growth of the first vascular plants.

The flooding of these lakes coincided with a reproductive cycle of species (spring), which is why it acted as an ideal scenario for the reproduction of animal species (insects, vertebrates) and plant species which rapidly colonized the new ecosystem (Marcomini 2002 and Marcomini.)

The first plant species that began to germinate from seeds on the margins of the lake were *Spartina cilata* and *Panicum racemosun*. Subsequently, the bottoms were covered by lines of *Cortadeira celloana*. After more than 2 years, the lakes dried up, causing a plant zonation aligned with the lagoons margin direction (Fig. 19.10b). After the large flood started also a plant succession in the margins of the lake to accommodate the new sudden changes in environmental conditions. This vegetation gave rise to the formation of incipient dunes that surrounded the lake forming circular crests that have quickly increased in height over the past few years (Marcomini and López 2008).

Currently, these dune fields are experiencing one of the most extreme droughts. These lakes have not only disappeared, but the phreatic level is at a depth of over 1.5 m. However, the traces of these humid cycles have left behind their mark in a generation of new dunes with sub-circular designs in the inderdunes and by an increase in the plant cover which resulted in the stabilization of the interdune areas.

In considering their urban planning, coastal settlements should take into consideration the current climate change and its impact on the ecosystem.

19.6.1 Afforestation and Urbanization

Buenos Aires's dune fields have been altered by urbanization since the early twentieth century, with a maximum urban growth in 1970, which produced changes in the natural aeolian landforms and on the associated vegetation cover.

Plant communities in natural coastal dunes are composed of herbaceous plants integrated by 20 dominant species. The dune plant communities are characterized by *Cakile maritima, Spartina coarctata, Senecio crassiflorus, Baccharis genistifolia, Androtrychium trigynum, Panicum racemosum* and *Calycera crassifolia* (Marcomini et al. 2009b, 2010 and 2011).

Of these 20 species, 17 are native, 2 adventitious, and 1 is cosmopolitan. The adventitious plants are *C. marítima y Melilotus albus*. The first are of european origin and the second are native to Europe and Asia. At present, none have acquired the characteristics of invasive species. *Juncus acutus* is the only cosmopolitan plant recognized as a dominant species, and occurs in interdune lows when the dunefield is stabilized.

Afforestation activities resulted in the replacement of native herbaceous species by trees, transforming the active and semi-active dunefields into stabilized in most parts of the aeolian barriers.

The first afforestation works on coastal dunes began in 1918 in the locality of Cariló. Later tasks spread to other locations such as Villa Gesell in 1933, Pinamar in 1941, and Valeria del Mar in 1947 along the northern aeolian barrier.

The methods used for dune stabilization involved the plantation of a local species called Esparto (*Spartium* sp.) by shrub fragmentation. Fish bone detritus and guano were used to increase nitrogen contents for soil fertilization. This method could not stop the intense sand burial. Therefore, by 1933 various species were introduced to stabilize the dune field, obtaining the best result with a forage species *M. albus*, used to promote nitrogen fixation in the soil, allowing subsequent growth of other species. The best results were obtained after 1939 with the introduction of *Acacia trinervis*, planted to act as wind barriers to protect the pines winward.

A more systematic methodology began to be implemented after 1940, and consisted of planting pieces of ground with *M. albus*, rye and alfalfa, simultaneously with the introduction of forest species grown in nursery gardens.

The tree species initially employed were maritime pine (*Pinus pinaster*), insignis pine (*Pinus radiata*), poplar (*Populus alba* and *Populus nigra*), acacia (*A. trinervis* and *A. saligna*), cypress (*Cupressus lambertiana*), eucalyptus (*Eucaliptus* sp.), willow (*Salix humboldtiana*), tamarisc (*Tamarix gallica*) and casuarina (*Casuarina* sp.).

The introduced tree species are mostly exotic, with the exception of the willow (*S. humboldtiana*) native to North America. *P. pinaster, T. gallica, P. alba* and *P. nigra* are from Europe; *A. trinervis, A. saligna, Eucaliptos* sp. *and Casuarina* sp. are from Australia; and *P. radiata* and *C. lambertiana* from the United States.

Afforestation has altered the natural landscape features (Fig. 19.11a, b), increasing the stabilization of the dune fields and changing wind transport rates within the dune field and toward the beach (Fig. 19.11b). This is reflected in an increase on beach erosion as a result of the decrease in sediment supply to the littoral drift currents.

The native herbaceous vascular species typical of these communities that allowed the accumulation of sand favoring the growth and migration of the dunes have been replaced by woody plants, consequently altering the plant communities.

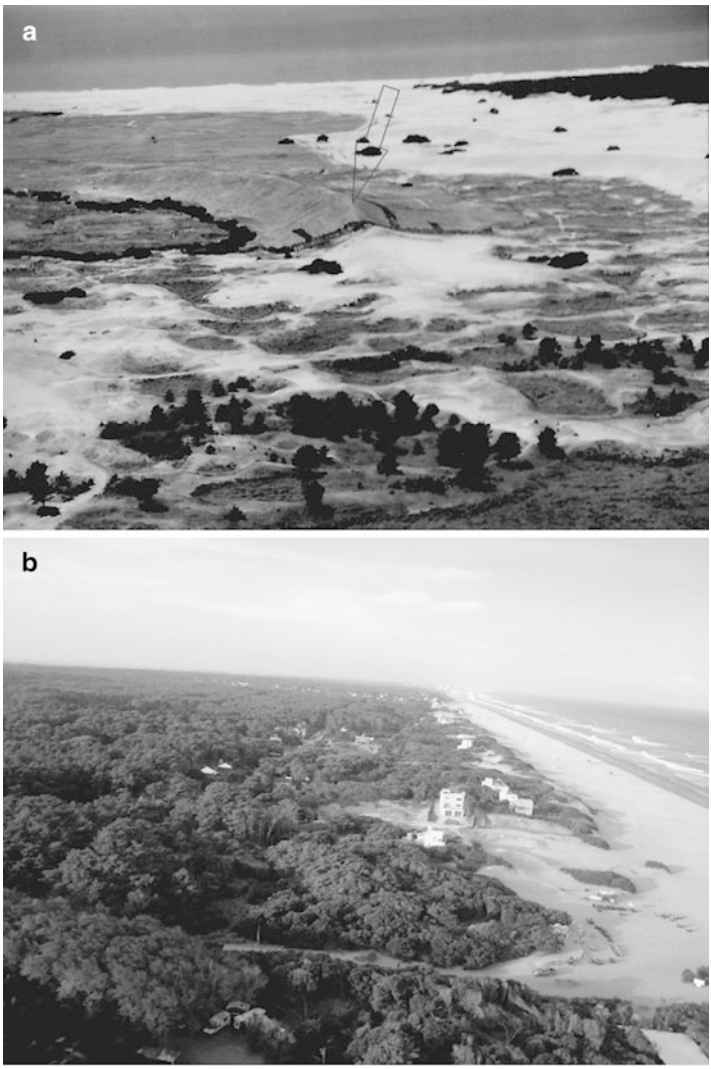

Fig. 19.11 Dune stabilization for afforestation and urbanization along the eastern aeolian barrier. (**a**) Montecarlo. (**b**) Mar Azul Villa Gesell

In the future coastal management, it will be necessary to regulate the future growth of forested areas on the dune-barrier, as well as to preserve the dune fields that have not been altered until now as *nature reserves*.

If this policy is not implemented, the erosive process suffered by the beaches of these resort towns will increase due to a deficit in sediment.

19.6.2 Coastal Erosion

Erosion and coastal degradation in dunes coasts is a very serious environmental. Natural causes, such as climate change and variations in sea level, have been enhanced by the actions of man, with the increasing population in coastal areas.

Coastal erosion may be fast, moderate or slow. Fast erosion is caused after surge-storms (Fig. 19.12), leading to loss of sand beach, and migration of sandbars to the shoreface. Later, when weather conditions improve, the swell transports the sand back to the foreshore and naturally the profile is recomposed. On the coast of Buenos Aires these records correspond to storms called "sudestadas" which raise the sea level up to 2 m above the expected tide (Fig. 19.12).

In dune coasts with gently sloping beaches surge-storms produce the foreshore erosion with the development of a scarp in the foredune

Several surge-storms of significant magnitude were recorded in February and June 1993, July 1996, April 1997, January 1999, July and December 2003. These have resulted in loss of properties in some areas and the formation of dune scarps (Fig. 19.13a, b, c).

Moderate erosion is usually caused by anthropogenic action on the coastal system and its effect is seen several years after the disturbance.

The slow erosion responds to a global event such as an increase in sea level or climate change and is also called chronic erosion. The sea level rise in Buenos Aires is estimated at 1.6 mm for the last 100 years (Lanfredi et al. 1988). Although this rise is low, it may produce general chronic erosion. However, the main factor of erosion is variations in sediment budget along the littoral area. Climate change recorded in Buenos Aires is mainly associated with an increase in average rainfall and changes in the directions of prevailing winds (Marcomini 2002). This fact has significantly influenced the stabilization of active sand dunes, changing sediment budget, increasing rates in coastal erosion and beach loss.

Always, before starting to analyze coastal erosion, it is essential to characterize the regional area, studying the coastal dynamics, areas and types of sediment input, coastal currents, and small-scale climate variations.

For example, in the province of Buenos Aires there is a net littoral drift from south to north that feeds on the sand available in the coastal area. This model recognizes three main coastal sand supply sources: from cliff erosion, from active dunefields and from river input. The first two being of great importance in littoral sedimentary balance.

Human activity has disturbed coastal dune environments directly or indirectly. Initially, this was due to a total lack of knowledge of the environmental variables and of their associated ecosystems. Today, these impacts are often irreversible.

Sediment supply to the beach varies with dune activity. The supply is determined by the quantity of sand carried onshore and longshore by waves and wind, the amount and kind of sediment discharged by rivers, cliff and dunes and the degree of human interference with natural sand transport (for example, the interruption of longshore currents by jetties and groins).

Fig. 19.12 Surge storm in dune coasts, Mar del Tuyu, Buenos Aires, Argentina. Photograph taken in January 2007

Human intervention on the coastal system is a major cause of sediment imbalance and human action throughout the years has modified aeolian transport rates to the beach and the saturation in sediments of the littoral currents. As a consequence, increased urban growth phenomena intensified chronic erosion.

The erosion caused by man is direct when there is some degradation in the natural landform, and indirect when man's actions alter any environmental factor that will accelerate erosion in the near future.

Among the factors of direct human erosion (Fig. 19.14) are: sand exploitation from the beach and foredunes (Marcomini and López 1999a) (Fig. 19.14b), predation and degradation of foredunes, streets perpendicular to the coast, artificial fluvial discharge to the sea (Fig. 19.14d), modifications in surface runoff, car and pedestrian traffic on the beach and dunes.

Indirect causes of human erosion are: the interruption of longshore drift by jetties, piers, docks (Fig. 19.14a), ports and groins; afforestation of transgressive active dune fields (Fig. 19.11a, b), introduction of exotic plants in the foredunes (Fig. 19.11b) (Tamarisk and acacia), generation of wind barriers, building on the beach front, subdivisions incompatible with preexisting dune topography, construction of seawalls on the backshore and building of resorts on the beach (Fig. 19.14d). The human actions previously described have affected the physical environment intensifying coastal erosion and loss of sand beaches.

In Buenos Aires's coastal dunes, the highest coastal retreat was around 5 m/year in Mar Chiquita (Isla 1997). Other areas show critical accelerations in coastal

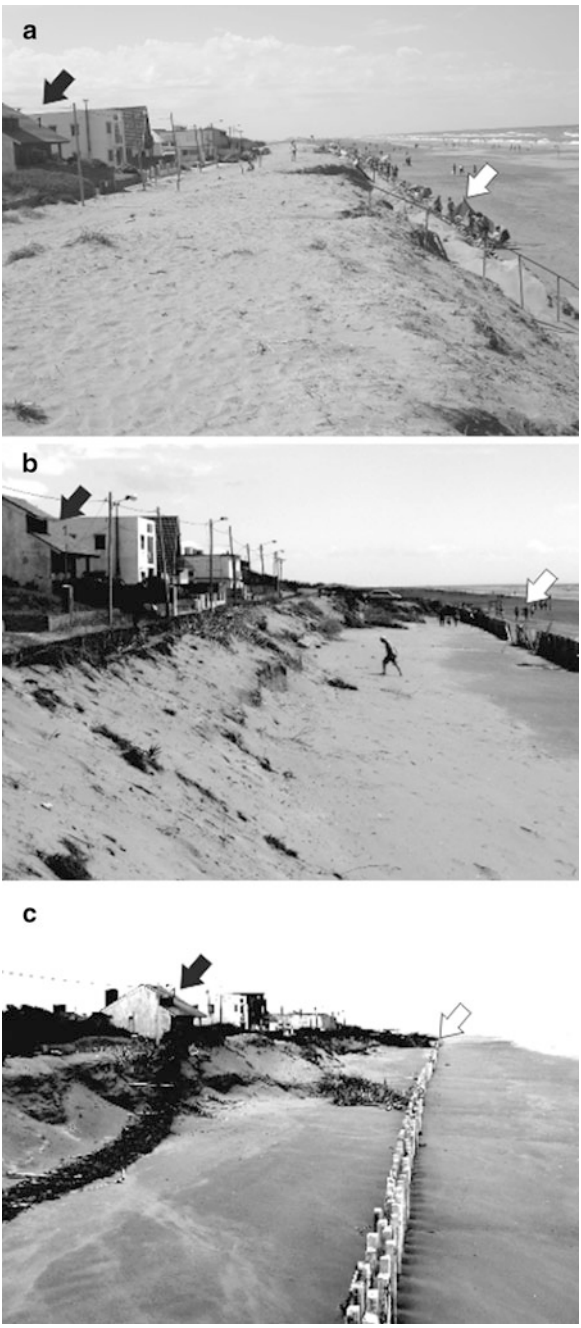

Fig. 19.13 Erosion of a rebuild foredune in Las Toninas, Buenos Aires Argentina, located on the eastern dune barrier. Photograph taken in: (**a**) Janeiro 2008 (**b**) Janeiro 2009 (**c**) July 2009

Fig. 19.14 Human direct and induced causes of erosion. (**a**) Effect of piers in the interruption of littoral drift, Mar del Tuyu. (**b**) Exploitation sand from the beach, Las Toninas, 2012. (**c**) Artificial fluvial discharge to the sea. (**d**) Seawall in the front of beach resorts, Pinamar

recession associated with urban centers such as Villa Gesell, Pinamar, Mar del Tuyú and Las Toninas, reaching rates of 2.45 m/year (Marcomini and Lopez 1997) (Fig. 19.15).

Coastal progradation has also been recognized in undeveloped areas along the eastern aeolian barrier (Fig. 19.15) associated with inflections in the configuration of the coastline (López and Marcomini 2010).

A beach is undergoing erosion when the volume of sand decreases in any sub-environment in the long-term, beyond the annual beach cycles. By decreasing the amount of sand, beach profiles also change and, consequently, their sub-environments do. The central beaches of Villa Gesell Pinamar, Mar de Ajó, Mar del Tuyú and Las Toninas evidence marked human-induced erosion (Fig. 19.15)

19.7 Coastal Management

The management of coastal areas is subject to the social and economic conditions of each municipality, as well as to the possibilities of accessing qualified technical advisory services to carry out comprehensive plans involving the natural resources.

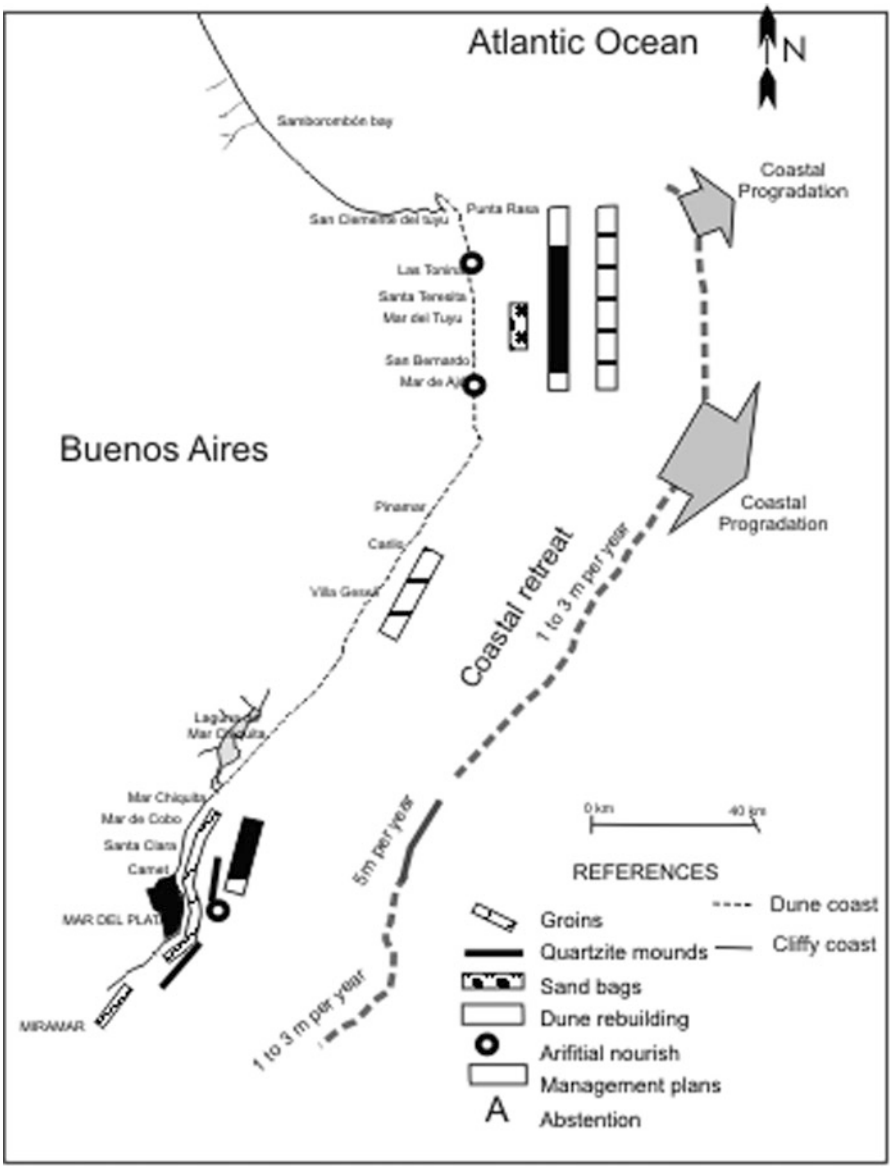

Fig. 19.15 Erosion/progradation rates for the dune coast of Buenos Aires, coastal protection types applied and management carried out

In most cases, works to defend the coast have been carried out without contemplating the environmental consequences. Many times, there is also a lack of awareness of the natural physical processes and, consequently, an urban project may not be adequate for the hydrodynamic conditions of the natural environment.

There have been several discussions from a number of authors on a range of coastal management options when dealing with eroding coasts (Bird 1996; French 1997, 2001; Pope 1997; Komar 1998). Marcomini and López (1993); López and Marcomini (2002, 2005, 2010) proposed different coastal management options to minimize coastal and/or beach erosion in Buenos Aires. They define five functional classes which are summarized in Fig. 19.16. They are: *armoring, moderation, restoration, abstention and adaptation*, based on Pope (1997).

19.7.1 Armoring

Armoring establishes a physical limit of the coast, using defense structures such as seawalls, revetments, levees and dykes. There are two subgroups: stable elements, constructed using hard structures (concrete or rocks) (Fig. 19.17b) and removable elements, using geotextile tubes (Fig. 19.17c) and sand bags (Fig. 19.17a). Armoring is recommended when there is storm erosion, instead of chronic erosion. An artificial coast line is drawn which is used to determine the territory to be protected, without considering its effect on the beach. These defense works have been applied both on cohesive cliff coasts and on dunes. The most significant impact on the physical environment is the erosion caused on the adjacent beach.

The most frequent alterations caused are: (1) decrease in sand supply from the protected area (cliff or dune) to the littoral drift (2) increase in wave height, (3) wave reflection along the edges of the structures during storms, undermining the structure, (4) changes of the coastline configuration on straight coasts.

This work type is being carried out to minimize the coastal recession and is not taking into account the conservation of the beach. If these kinds of works extends longshore, it will cause the sub-saturation of the littoral currents with the consequent erosion of the adjacent beaches.

The general impacts of sea walls and other erosion management techniques have been well documented recently and can include a general reduction of available sediment in the coastal cell, down-drift erosion (e.g. flanking erosion), basal scout and beach down-draw (French 2001, 1997; Hansom and McGlashan 2000; Bird 1996; Kraus and MacDougal 1996; Tait and Griggs 1990; Kraus and Pilkey 1988).

19.7.2 Moderation

The main purpose of moderation is to decrease beach erosion without protecting the coast. Stable structures such as groins and mounds are used and applied in areas suffering from chronic erosion. Although it is used to recover the beach, many times, indirectly, it protects the coast. Other factors to consider in choosing this alternative are the proximity to the outcrops of rocks for block production (quartzite

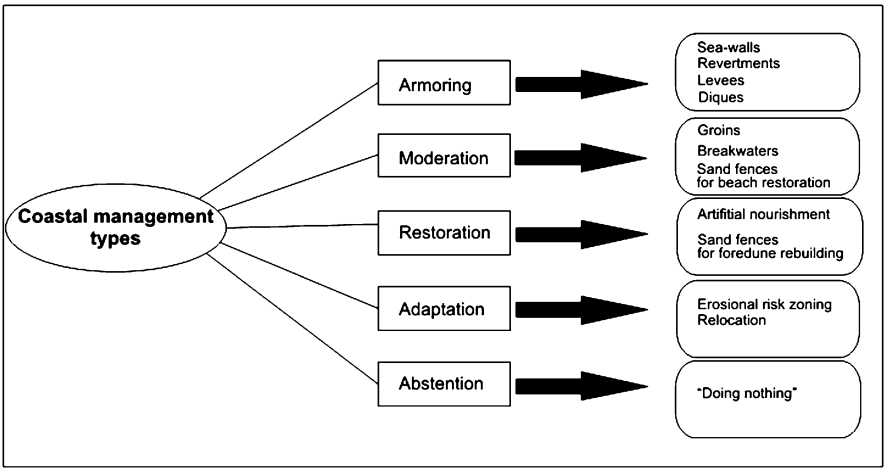

Fig. 19.16 Diagram showing different types of management for the province of Buenos Aires (Modified from Pope (1997))

or other resistant rock) and the presence of a rocky substrate (wavecut platform) which provides it with support. Although sand is recovered locally, they produce an adverse effect on nearby downdrift areas due to the loss in saturation of the littoral drift.

When used in dune coasts they bring about environmental problems, such as: (1) subsidence of structures due to lack of support (quartzite over sand beaches), (2) sub-saturation of sand in the littoral currents downdrift (3) settlement of aloctone biological ecosystems (introduction of hard substratum species in sandy beaches).

Hard structures such as groins and mounds have been frequently applied in Buenos Aires along cliffy coasts with pocket beaches (Mar Chiquita to Miramar) associated to populated areas with social and economic resources.

The removable structures include sand bags to reconstruct the beach berms and sand fences for foredune dunes and beach rebuilding (Fig. 19.17d, e, f). When they are set up on the beach they are temporary and should be removed at the beginning of the summer season. The dynamic techniques to reconstruct beach and foredune with fences or mobile structures will be addressed in the following item.

19.7.3 Restoration

The restoration involves planning engineering works of higher costs to add sand on the beach and generate a deposit that will protect it from storm erosion. These works may involve projects or episodes of artificial nourish depending on the volume of sand required. The most representative example of a proyect of artificial nourishment is Mar del Plata, on the beaches of Varese, Grande and Bristol, where

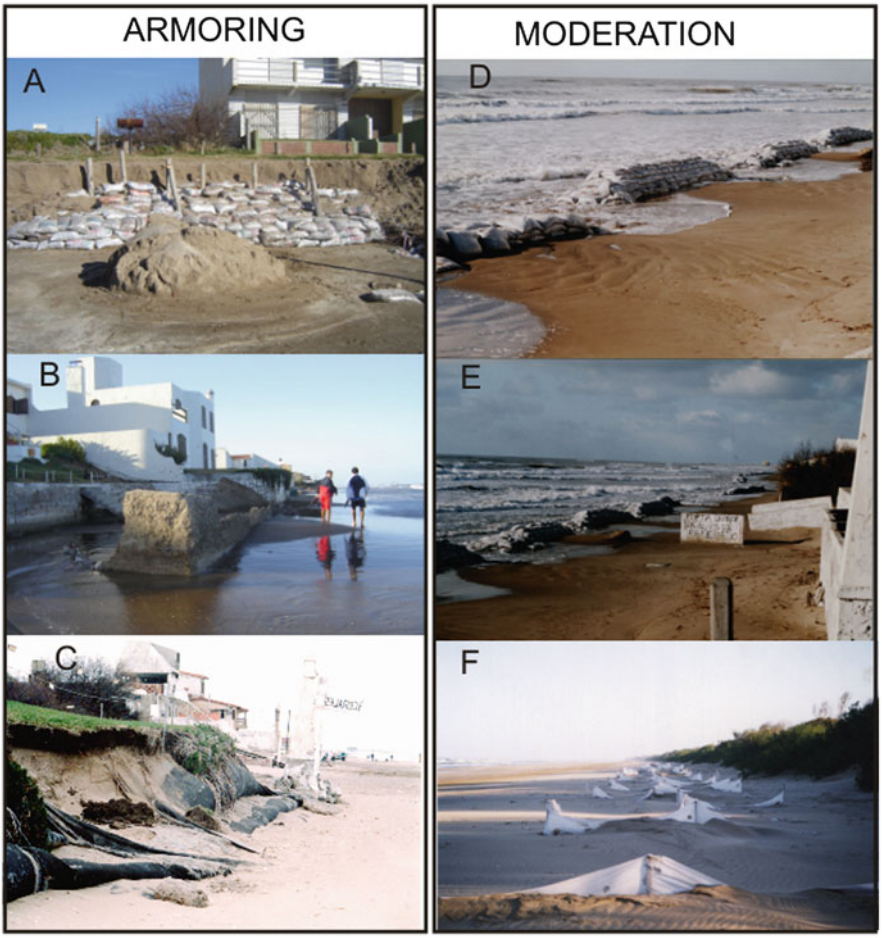

Fig. 19.17 Application of armoring and moderation classes for the dune coast of Buenos Aires. (**a**) Sand bags in Mar Del Tuyu for coastal protection. (**b**) Concrete seawalls. These rigid structure do not stop coastal retreat and collapse by undermining. (**c**) Geotubes. They also collapsed by wave undercutting and are very degradable with sand radiation. (**d, e**) Sand bags for foreshore restoration. (**f**) Membrane fences for backshore reconstruction

about 2,000,000 m^3 of sand was dumped to broaden the abovementioned beaches by more than 100 m. Without going into details, the environmental impacts that this proyect caused (Marcomini and López 1999b, 2006), represents an important change in the provincial policy in addressing coastal erosion issues, considering the tourist potential of the recreation areas. Episodes of nourishments, involving smaller volumes of sediments, have also developed on dune coasts, with the purpose of restoring the original beach conditions (Las Toninas, Mar del Tuyú and Mar de Ajó). The sand used to fill the beach came from inland dunes and beach ridges and is transported by truck. Figure 19.18 shows an episode of artificial

Fig. 19.18 Episodes of artificial nourishment in the beach of Mar de Ajo, Municipio de la Costa, Buenos Aires

nourishment conducted in the dune coast of Mar de Ajó in November 1999. The sand which is used to nourish is placed on the backshore, where stabilization is greater and the benefits are immediate. To carry out such projects requires knowledge of the sand source, its quality and quantity. Recharge projects require large volumes of sand that are usually extracted from offshore by dredging.

19.7.4 Adaptation

The application of adaptation as a functional class arises from a detailed knowledge of all variables that play a part (social, cultural, economic, physical, biotic, etc.) in the coastal environment. Restrictive policies are implemented to direct man in adapting to the possibilities and limitations of the natural coastal system. The population is taught about how to adapt to the natural erosion-accretion cycle. The adaptation includes the delimitation of the risk zone of the different sectors of the coast, where human use of the territory must accept the consequences of its development on the beach, to avoid increasing the deterioration caused.

One of the alternatives to adaptation is managed relocation. The definition of managed relocation is the intact relocation of a building inland that may have been in a vulnerable position on a dynamic coast (Mcglashan 2003). Managed relocation can be an effective option especially where investment in structures is low; there is

relatively inexpensive land is available in the surroundings and low-density development with a limited number of threatened buildings. Building relocation could allow for natural processes to continue without the need for protection measures for vulnerable buildings or the need to stabilize or sterilize naturally mobile features. The relocation option should result in a one-off expense as opposed to the construction of hard and soft structures that will require maintenance and potentially rebuilding over time.

19.7.5 Abstention

In the abstention phase, no works are carried out. Non-intervention: there is no human interference and natural processes are allowed to continue. The municipality decides, after assessing the financial and social possibilities and the limitations of the physical environment, to apply the political decision of "doing nothing". Generally, there is no feasible economic solution to resolve the issue.

19.7.6 Management in Dune Coasts

The evaluation of different types of coastal defenses and management policies applied to the dune coast of Buenos Aires have shown, first of all, the need to establish basic objectives considering the local and regional variables. Furthermore, the protection or remediation projects that will be applied in the future should implement legal systems that will ensure economic sustainability to continue with the projection of the work in the short-, medium- and long-term.

On dune coasts, it is advisable to implement adaptation or abstention policies in those municipalities without sufficient economic resources. Works such as regeneration and restoration of the coastal dune have obtained very good results on coasts subjected to a moderate degree of erosion. By implementing these tasks the project employed local people and used local materials to restore the beach and indirectly stabilize the coastline (López and Marcomini 2005, 2006, 2010).

The high mobility of the foot of the dune and the lack of consolidation makes it inappropriate to implement hard structures, both to stabilize the coast (seawalls) and to reconstruct the beach (groins, jetties and breakwaters). Additionally, these structures frequently deteriorate considerably after storms as they do not have a resistant substrate to which to hold onto and increase the reflective phenomena with the consequent decline in the beach level.

Soft protection strategies are recommended for dune coasts such as beach recharge (Komar 1998; Valverde et al. 1999; Peterson et al. 2000), vegetation-linked structures (e.g. structures made of wood with vegetation and soil placed

Table 19.2 More efficient methods of coastal protection and beach-dune remediation for dune coasts

Management types	Results in dune coasts
Armoring	This functional class is not recommended because coastline is flexible and mobile and composed of unconsolidated sand. Hard structures sink into the sand because they lack of a hard substrate to sustain and increase the beach erosion around them
Moderation	Sand fences are useful to restore the backshore
	No hard structure is recommended
Restoration	Episodes of beach and dune nourish are recommended. The source of sand should not come from the beach or foredune
	Permanent sand fences gave very good results to rebuild the foredune
Adaptation	Zonification of coastal vulnerability to erosion
	Relocation of properties at risk
Abstention	Implementation of strategies to minimize the human induced erosion

Experiences of coastal management in Buenos Aires, Argentina

within the structure during construction: Schiechtl and Stern 1997), geotextile and vegetation planting or vegetative planting and bank regrading (e.g. planting or regrading without the need for structures) (Hansom and McGlashan 2000) (Table 19.2).

19.8 Dune Remediation

Several methods are used to repair damaged dunes where a low sand supply has inhibited dune formation or where dunes have been destroyed.

Sand fences are frequently used to enhance sand accumulation (Smolen et al. 1988; Hotta et al. 1991; Mendelssohn et al. 1991) but recommendations for the most effective sand fence configurations vary among sites. Several kinds of fences have been used worldwide. Synthetic fabrics of appropriate porosity (around 50%) are as good as wooden slat fences in accumulating sand. Biodegradable materials are preferred for sand fences as non-biodegradable materials may pose a hazard for burrowing animals. Geojut fabric is a biodegradable product with appropriate porosity that is frequently used in erosion, but is expensive.

Vegetation implantation for trapping sediments is essential for anchoring accumulated sand (Dahl and Woodard 1977). Because plant recolonization may be slow, recommendations for dune restoration usually include planting of native grasses, with deep fibrous roots that efficiently trap and stabilize sands. In addition, these plants are adapted to harsh beach conditions (salt spray, low soil nutrients, low soil moisture and sand abrasion).

Aeolian fences are classified considering three main factors: durability, plan view and spatial disposition (López and Marcomini 2006).

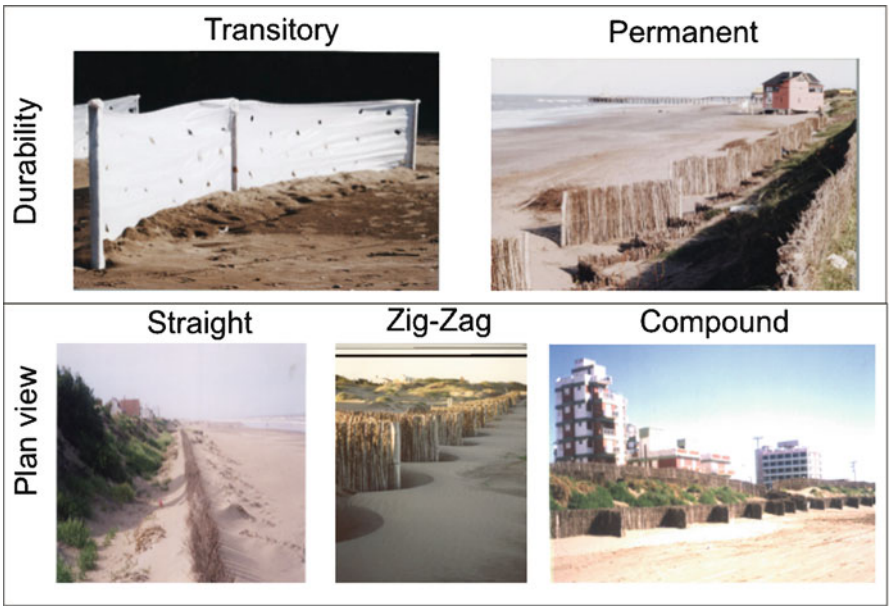

Fig. 19.19 Classification of sand fences (Modified from López and Marcomini (2006))

According to their durability they are divided as permanent or transitory (Fig. 19.19).

Permanent fences are fixed fences composed of branches and stakes made of poplar. These fences do not degrade until buried and have usually been used to rebuild the foredune. They are made with wooden stakes that are 5 cm wide and 1.5 m high, spaced at 5 m, stuck in the sand at a depth of 1 m (Fig. 19.20). Branches are placed between each stake, held together by steel wire. These barriers have a height of 1.5–1.8 m to improve accumulation efficiency and durability.

Transitory fences involve plastic trellis or geotextiles (Fig. 19.19). They are used to nourish the backshore and are frequently exposed to erosion during surge-storms.

The aeolian fences are grouped, according to their alignment, into straight, compound or zigzag groups. According to their spatial distribution, they are classified as Type A: parallel to the coast along foredune crest, Type B: parallel to coastline along seaward base of the dune, Type C: transverse to foredune, and Type D: at an angle to the foredune (Fig. 19.20).

Several parameters are defined for sand accumulation by fences in the foredune (Fig. 19.21). Some of them are related to the structure design, such as He: Barrier height, Pe: Barrier burial depth, and others related to sand accumulation induced by the fence. They are: Hd: barrier height accumulation, Hi: effective height Hdc: height of the sand deposit in the continental face, Hds: height of the sand deposit in the sea face, Ad: Deposition width. Considering these parameters we can calculate the vertical buried velocity (vd) and volumetric deposit velocity (Vv), where: Vd: dHd/dt, Vv: dVs/dt.

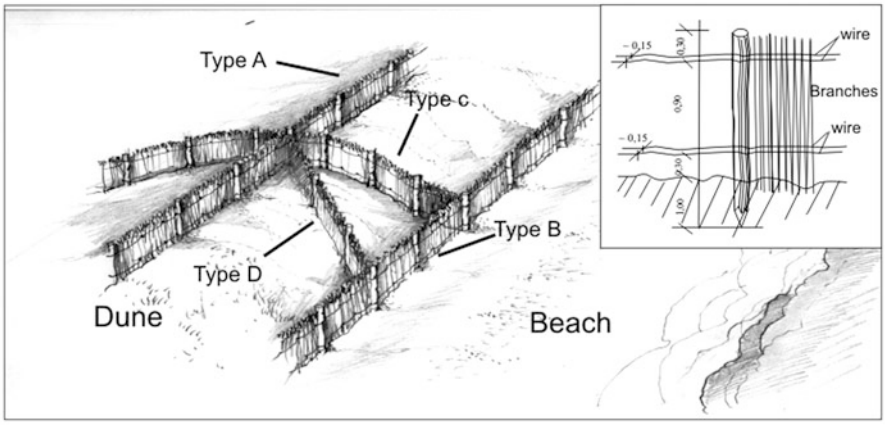

Fig. 19.20 Distribution and design of permanent fences

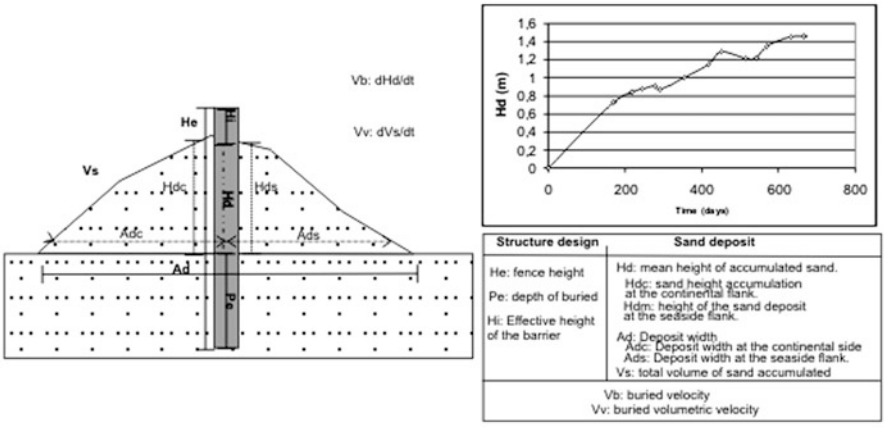

Fig. 19.21 Parameters for monitoring evolution of permanent sand fences

Dune height change (Hd) is measured by monitoring the relative height variation against a benchmark along transverse dune profiles. Volumetric sand accumulation is calculated with the surface profile variation for each surveyed profile multiplied by the length of the deposit.

López and Marcomini 2006 surveyed transverse profiles to quantify the accumulation rates and disposition of sand deposited by fences along the coast of Buenos Aires. Vertical height and volumes of sand were measured to calculate the accumulation rates. After monitoring several permanent fences on the foredune for about 2 years (September – March) obtained a model of effectiveness for the dune recovered. Curves (Fig. 19.21) showed a point of maximum efficiency 150–250 days after the structure emplacement where it reached the highest volume accumulation rate (Vv: 0.12 m^3/m/day) and vertical accretion velocities

(Vb: 0.4 cm/day). After this point the accumulation velocities (Vv) diminished to 0.08 m^3/m/day and the vertical accretion velocities (Vb) to 0.1 cm/day. This change took place when the fence reduced the effective height (Hi) to about 50% because of sand colmatation.

The higher velocities of vertical accretion obtained varied between 0.4 and 0.5 cm/day with a mean speed of 0.25 cm/day. Erosion cycles were also detected with rates of −0.11 to 0.33 cm/day showing vertical erosion. These erosive episodes came about as a result of the increase in the speed of the wind between simple parallel barriers, which caused local accelerations in the wind speed, increasing the erosive effect. That is why it is important, in designing the fences, not to set up the barriers running parallel to the direction of the prevailing winds, or other wise use compound barriers.

Similar values of Vv were obtained by Miller et al. 2001, in Florida, following the overwash of Hurricane Opal. They recognized accumulation rates (Vv) of 0.016 m/day and vertical accretion (Vb) varying between 0.06 and 0.1 cm during the first year. Foredune reached higher heights and less width in Buenos Aires in comparison to Florida.

Figure 19.22 shows the development of a new foredune in San Clemente del Tuyu between October 1997 and April 1999, employing permanent fences. An important recovery of the foredune height and width was detected after structure emplacement, as well as an increase of the beach level with a seaward displacement of the beach sub-environments. The development of the backshore using transitory fences increased the beach height and diminished the vulnerability to erosion during storms. The fences were emplaced on the beach in May 1998. After 4 months the barriers reached their maximum accumulation capacity (Hd).

The natural parameters that regulate the accumulation rates are: (1) wind speed (2) wind frequency by direction (3) sand supply and (4) fetch sand area. The orientation, height and gap of the barrier control the distribution and morphology of artificial deposits.

The sediments trapped by barriers usually show moderate differences in the textural statistical parameters of fences on the seaside in comparison with the natural foredune. Between pre and post structure emplacement the mean grain size became coarser, more poorly sorted and the skewness changed to negative.

The regenerated foredune must be stabilized after reconstruction with fences. Suitable plants should be chosen for environmental dynamic adaptation to these systems, which may, in turn, favor the growth of the foredune.

S. coarctata has proved to be the best species for dune stabilization on the Buenos Aires coast (Fig. 19.22c). This pioneer grass beach plant has a higher salt tolerance than many other coastal species and is a hardy grower. It is a rhizomatous and native to Argentina and Uruguay. It measures about 0.15–0.50 m in height. Transplants from the vicinity of the project are more likely to survive than imported ones. If suitable stands cannot be found on the property where the vegetation project will be undertaken, it may be possible to obtain plants from a neighboring property by agreement with property owners. Mean percentage of survival ranged from 60 to 70% during the first year and reached 50% in 3 years. Planting took place from July

Fig. 19.22 Dune reconstruction in san Clemente del Tuyú between 1997 and 2004, Buenos Aires. (**a**) Barrier fences instslation; (**b**) Sand deposition after 2 years; (**c**) S. coarctata plantation; (**d**) Current view

to September (winter). Immediate watering of transplants is not imperative, but success is increased if transplanting is done after a rain or if the dune is watered before transplanting. No supplement water was necessary after planting.

Our experiment shows the usefulness of sand fences for rapid sand accumulation along the northern coastal dune of Buenos Aires. About 800,000 m^3 of sand along the foredune has been recovered along 15 km of coastline during 1 year. The plan implementation has also been positive in creating jobs in the Municipality, because it applied about 2,800 occupations between 1997 and 1999 with a cost-benefit relation of the project estimated at 1–6.

The materials employed for the fence construction are native to the area since they were built with branches of Populus which is considered a plague tree in the area and needs to be pruned several times in a year.

Permanent fences reached their maximum efficiency 150–250 days after the structure was put in place. The transitory fences lasted about 120 days leaving the beach less vulnerable to subsequent storms.

Winds blowing parallel to the fence produced sand excavation instead of the sand accumulation, so we recommended compound or zigzag configurations for fences parallel to the coast.

Acknowledgments This work was funded by grants received from the University of Buenos Aires, X129, X709 and W371.

References

Arens SM, Wiersma J (1994) The Dutch foredunes: inventory and classification. J Coast Res 10:189–202

Bagnold RA (1941) The physics of blown sand and desert dunes. Chapman and Hall, London, p 265

Baldwin KA, Maun MA (1983) Microenvironment of Lake Huron sand dunes. Can J Bot 61:241–255

Bird ECF (1996) Beach management John Wiley, Chichester City of New York Parks and recreation 1998. http://nycparks.completeinet/sub_yo. . .cal_signs/hs_historical_sign.php?id = 204. Accessed 9 Jan 2002

Bird ECF (2000) Coastal geomorphology: an introduction. Wiley, Brisbane

Boeger MRT, Wisniewski C (2003) Comparação da morfologia foliar de espécies arbóreas de três estádios sucessionais distintos de floresta ombrófila densa (Floresta Atlântica) no Sul do Brasil. Rev Bras Bot 26:61–72

Carter RWG (1991) Near future sea level impacts on coastal dune landscapes. Landsc Ecol 6:29–39

Carter RWG, Hesp PA, Nordstrom KF (1990) Erosional landforms in coastal dunes. In: Nordstrom KF, Psuty NP, Carter RWG (eds) Coastal dunes: form and process. Wiley, London, pp 217–249

Celsi C, Monserrat AL (2006) Valor y funcionalidad ecológicos de las dunas costeras de Coronel Dorrego, Buenos Aires. Bosque 27(2):201–202

Christiansen M, Davidson-Arnott R (2004) Rates of landward sand transport over the foredune at Skallingen, Denmark and the role of dune ramps. Dan J Geogr 104(1):37–43

Cooke R, Warren A, Goudie A (1993) Desert geomorphology. UCL Press, London, p 526

Cowles HC (1898) The ecological relations of the vegetation on the sand dunes of Lake Michigan. Bot Gaz 27:97–117

Dahl BE, Woodard DW (1977) Construction of Texas coastal foredune with sea oats (*Unicula Paniculata*) and bitter panicum (*Panicum amarum*). Int J Biometeorol 21(3):267–275

Davidson-Arnott RGD, Law MN (1996) Measurement and prediction of long-term sediment supply to coastal foredunes. J Coast Res 12:654–663

Davis JL (1980) Geographical variation in coastal development. Longman, London, p 204

Dillenburg SR, Roy PS, Cowell PJ, Tomazelli LJ (2000) Influence of antecedent topography on coastal evolution as tested by the shoreface translation-barrier model. J Coast Res 16(1):71–81

Dillenburg SR, Tomazelli LJ, Martins L, Barboza EG (2005) Modificações de longo período da linha de costa das barreiras costeiras do Rio Grande do Sul. Gravel 3:9–14

French PW (1997) Coastal and estuarine management. Routledge, London

French PW (2001) Coastal defences. Routledge, London

Glenn M (1979) Glossary. In: McKee ED (ed) A study of global sand seas. United States Geological Survey professional paper, 1052. US Govt. Printing Office, Washington, DC, pp 399–407

Gruber NLS, Barboza EG, Nicolodi JL (2003) Geografia dos Sistemas Costeiros e oceanográficos: subsídios para Gestão Integrada da Zna Costeira. In: Martins LR, Barboza EG (eds) Gravel, vol 1. CECO/IG/UFRGS, Porto Alegre, pp 71–84

Hansom JD, McGlashan DJ (2000) Managing lakeshore erosion: Impacts of bank protection on Loch Lomond, Scotland. The Scottish Geographical Magazine, 116(3):213–229

Hesp PA (1984a) The formation of sand 'beach ridges' and foredunes. Search 15:289–291

Hesp PA (1984b) Foredune formation in Southeast Australia. In: Thom BG (ed) Coastal geomorphology in Australia. Academic, Sydney, pp 69–97

Hesp PA (1988). Morphology, dynamics and internal stratification of some established foredunes in southeast Australia. In: Hesp PA, Fryberger S (eds) Eolian sediments. J Sediment Geol 55:17–41

Hesp PA (1989) A review of biological and geomorphological processes involved in the initiation and development of incipient foredunes. In: Gimmingham CH, Ritchie W, Willetts BB, Willis AJ (eds) Coastal sand dunes, vol 96B, Proceedings of the Royal Society of Edinburgh. Roy. Soc. Edinb, Edinburgh, pp 181–202

Hesp PA (1996) Flow dynamics in a trough blowout. J Bound-Layer Meteorol 77:305–330

Hesp PA (1999) The beach backshore and beyond. In: Short AD (ed) Handbook of beach and shoreface morphodynamics. Wiley, Chichester, pp 145–170

Hesp PA (2002) Foredunes and blowouts: initiation, geomorphology and dynamics. Geomorphology 48:245–268

Hesp PA, Thom BG (1990) Geomorphology and evolution of active transgressive dunefields. In: Nordstrom KF, Psuty N, Carter B (eds) Coastal dunes: form and process. Wiley, Brisbane, pp 253–288

Hotta S, Kraus NC, Horikawa K (1991) Functioning of multi-row sand fences in forming foredunes, Coastal sediments´91. ASCE, New York, pp 261–275

Isla FI (1989) The Southern Hemisphere sea level fluctuation. Quat Sci Rev 8:359–368

Isla FI (1997) Procesos de canibalización de la barrera medanosa entre Faro Querandí y Mar Chiquita, Buenos Aires. Revista de la Asociación Geológica Argentina 52(4):539–548

Isla FI, Bujalesky G (1995) Tendencias de disponibilidad de arena. Revista de la Asociación Argentina de Sedimentología 1(2):75–89

Komar PD (1998) Beach processes and sedimentation. Prentice Hall, Englewood Cliffs

Kraus NC, MacDougal WG (1996) The effects of sea walls on the beach: part 1 an updated literature review. J Coast Res 12:691–701

Kraus NC, Pilkey OH (1988) The effects of sea walls on the beach. J Coast Res 4:146

Lancaster N (1997) Response of eolian geomorphic systems to minor climate change: examples from the southern California deserts. Geomorphology 19:333–347

Lanfredi NW, Pousa JL, Donofrio ED (1988) Sea level rise and related potential hazards on the Argentine coast. J Coast Res 14(1):47–60

López RA, Marcomini SC (2002) Pautas para el manejo costero en costas de dunas y acantilados. Provincia de Buenos Aires Revista de Geología Aplicada a la Ingeniería y al Ambiente 18:59–68

López RA, Marcomini SC (2005) Eficiencia de las obras de defensa en costas de dunas, Municipio de la Costa. Revista de Geología Aplicada a la Ingeniería y al Ambiente 21:157–165, ISSN 0326–1921

López RA, Marcomini SC (2006) Monitoring the foredune restoration by fences at Buenos Aires Coast. J Coast Res SI 39:955–958, ISSN 0749–0208

López RA, Marcomini SC (2010) Plan de manejo costero para mitigar la erosión en el Partido de la Costa, Provincia de Buenos Aires. Revista de Geología Aplicada a la Ingeniería 25:1–8

López R, Penchaszadeh P, Marcomini SC (2008) Storm-related strandings of molluscs in the northeast coast of Buenos Aires, Argentina. J Coast Res 24:925–935

Maia LP, Freire GSS, Lacerda LD (2005) Accelerated dune migration and aeolian transport during El Nino events along the NE Brazilian coast. J Coast Res 21(6):1121–1126

Marcomini SC (2002) Morfodinámica, Sedimentología, Geomorfología Ambiental y Sus Alteraciones Antropogénicas en costas de dunas del Noreste de la provincia de Buenos Aires. Ph.D. thesis, Universidad de Buenos Aires, 312 p

Marcomini SC, Lopez RA (1993) Coastal protection effects at Buenos Aires, Argentina. Luisiana. In: Magoon OT, Wilson WS, Converse H, Tobin LT (eds) Proceedings Coastal Zone '93 3:2724–2738

Marcomini SC, Lopez RA (1997) Influencia de la urbanización en la dinámica costera, Villa Gesell, provincia de Buenos Aires, República Argentina. Asociación Argentina de Sedimentología Revista 4:79–96

Marcomini SC, López R (1999a) Alteración de la dinámica costera por efecto de la explotación de arena de playa, partidos de General Alvarado y Lobería, Provincia de Buenos Aires. Revista de la Asociación Argentina de Sedimentología 6(1–2):1–18

Marcomini SC, López RA (1999b) Recarga artificial de las playas. Revista Gerencia Ambiental 6 (56):408–414
Marcomini SC, López RA (2006) Evolution of a beach nourishment project in Mar del Plata. J Coast Res SI39:835–838, ISSN 0749–0208
Marcomini SC, Lopez RA (2007). Erosión y manejo costero de Villa Gesell. Unión por Gesell. CD-ROM, Buenos Aires
Marcomini S, López R (2008). Incidencias de las variaciones climáticas en la geomorfología eólica de la costa de la provincia de Buenos Aires. In: Actas del XVII Congreso Geológico Argentino, Jujuy, Argentina, pp 994–995
Marcomini SC, Maidana N (2006) Response of aeolian ecosystems to minor climatic changes. J Coast Res SI39:204–208, ISSN 0749–0208
Marcomini SC, Uehara F, López RA (2005). Morfodinámica costera y su aptitud para las explotaciones de áridos para construcción en Pehuen-có. XVI Congreso Geológico Argentino, La Plata, III:559–566
Marcomini SC, López RA, Spinoglio A (2007) Uso de la morfología costera como geoindicador de susceptibilidad a la erosión en costas cohesivas. Revista de la Asociación Geológica Argentina 62(3):396–404
Marcomini SC, Quesada A, Lopez AR (2008) Modelo evolutivo de costas erosivas con progradación eólica, Orense, provincia de Buenos Aires. XII Reunión Argentina de Sedimentología, 106 p
Marcomini SC, López RA, Uheara F (2009a) Manejo Costero en la costa de dunas de Pehuen-có, Buenos Aires. Revista de Geología Aplicada a la Ingeniería y al Ambiente 23:75–83, ISSN 0326–1921
Marcomini SC, Lopez RA, Madanes N, Picca P, Bertolin L (2009). Geoformas y vegetación en la Reserva del Faro Querandí, Provincia De Buenos Aires. V Congreso Argentino de Cuaternario y Geomorfología, XII Congresso da Associação Brasileira de Estudos do Quaternário y II Reunión sobre el Cuaternario de América del Sur, pp 139–148
Marcomini SC, Lopez RA, Picca P, Madanes N, Bertolin L (2010). Alteración en la morfodinámica del campo de dunas litoral por introducción de vegetación exótica, Provincia de Buenos Aires, Argentina. ANTROPICOSTA IBEROAMERICA 2010. São Paulo, Iguape e Cananéia, Brasil Abs, 3 p
Marcomini SC, Lopez RA, Picca P, Madanes N, Bertolin L (2011) Cambios en la vegetación n costas de dunas y su influencia en el balance sedimentario. In: Lopez RA, Marcomini SC (eds) Problemática de los Ambientes Costeros, Sur de Brasil, Uruguay y Argentina. Croquis, Buenos Aires, pp 193–205
Masselink G, Hughes MG (2003) Introduction to coastal processes and geomorphology. Oxford University Press, New York
Maun MA (1998) Adaptations of plants to burial in coastal sands dunes. Can J Bot 76:713–738
Maun MA (2004) Burial of plants as a selective force in sand dunes. In: Martinez ML, Psuty NP (eds) Coastal dunes ecology and conservation. Springer, Berlín, pp 119–135
Maun MA (2009) The biology of coastal sand dunes. Oxford University press, New York, p 265
Maun MA, Elberling H, D'Ulisse A (1996) The effects of burial by sand on survival and growth of Pitcher's thistle (*Cirsium pitcheri*) along Lake Huron. J Coast Conserv 2:3–12
McKee E (1979) Introduction to a study of global sand seas. In: McKee E (eds) A study of global sand seas. Geological Survey professional paper 1052, Washington DC, pp 10–11
Mcglashan DJ (2003). Funding in integrated coastal zone management partnerships. Marine Pollution Bulletin 46:393–396
Mendelssohn IA, Hester MW, Montefemente FJ, Talbot F (1991) Experimental dune building and vegetative stabilization in a sand deficient barrier island setting on the Lousiana Coast, USA. J Coast Res 7:137–149

Miller DL, Thetford M, Yager L (2001) Evaluation of sand fences and vegetation for dune building following overwash by hurricane opal on Santa Rosa Island, Florida. J Coast Res 17 (4):936–948

Monserrat AL, Celsi CE (2009) Análisis regional de la costa pampeana austral en el marco del sistema de áreas protegidas y caracterización de un área clave como reserva, en el Partido de Coronel Dorrego. BioScriba 2(1):1–23

Neal A (1993). Sedimentology and morphodynamics of a Holocene coastal dune barrier complex, Northwest England. Ph.D. thesis, Unive Reading (Unpublished)

Peterson CH, Hickerson DHM, Johnson GG (2000) Short-term consequences of nourishment and bulldozing on the dominant large invertebrates of a sandy beach. J Coast Res 16:368–378

Pope J (1997) Responding to coastal erosion and flood damages. J Coast Res 13:704–710

Psuty NP (1988) Sediment budget and dune/beach interaction. J Coast Res SI3:1–4

Psuty NP, Allen JR, Starcher R (1988) Spatial analysis of dune crest mobility, Fire Island National Seashore, New York. Dune/beach interaction. J Coast Res 3:115–120

Pye K (1990) Physical and human influences on coastal dune development between the Ribble and Mercy estuaries, Northwest England. In: Nordstrom KF, Psuty NP, Carter RWS (eds) Coastal dunes form and processes. Wiley, London, pp 339–359

Pye K, Neal A (1994) Coastal dune erosion at Formby Point, north Merseyside, England: causes and mechanisms. Mar Geol 119:39–56

Ranwell DS (1972) Ecology of salt marshes and sand dunes. Chapman and Hall, London, p 258

Ruz MH, Allard M (1994) Coastal dune development in cold climate environments. Phys Geogr 15:372–380

Ruz MH, Hequette A, Hill PR (1992) A model of coastal evolution in a transgressed thermokarst topography, Canadian Beaufort Sea. Mar Geol 106:251–278

Salles MA, Compagnucci RH (1995) Características de la circulación de superficie durante 1976–1977 y su relación con las anomalías en el sur de Sudamérica. Meteorológica 20:7–16

Salles MA, Compagnucci RH (1997) Características de la circulación de superficie durante el período diciembre de 1971 – febrero de 1974 y sus relaciones con las anomalías ENOS en el sur de Sudamérica. Meteorológica 1(22):35–48

Schiechtl HM, Stern R (1997) Water bioengineering techniques: for watercourse bank and shoreline protection. Blackwell Science, London

Seeliger U, Cordazzo CV, Oliveira CPL, Seeliger M (2000) Long-term changes of coastal foredunes in the Southwest Atlantic. J Coast Res 16(4):1068–1072

Sherman DJ, Bauer BO (1993) Dynamics of beach-dune systems. Prog Phys Geogr 17:413–447

Sherman DJ, Lyons W (1994) Beach-state controls on Aeolian sand delivery to coastal dunes. Phys Geogr 15:381–395

Short AD, Hesp PA (1982) Wave, beach and dune interactions in southeastern Australia. Mar Geol 48:259–284

Smolen MD, Miller DW Wyatt LC, Lichthardt J, Lanier AL (1988) Erosion and sediment control planning and design manual. North Carolina Sedimentation Control Commission; North Carolina Department of Environment, Health, and Natural Resources; and Division of Land Resources Land Quality Section, Raleigh

Spinoglio A (2010) Geomorfología costera e impacto ambiental del sector comprendido entre Quequén y el balneario Los Angeles. Thesis, Universidad de Buenos Aires

Tait JF, Griggs GB (1990) Beach response to the presence of a sea wall: a comparison of field observations. Shore Beach 58:11–28

Toldo EE Jr, Almeida LESB, Barros C, Martins LR (1999) Retreat of the Rio Grande do Sul coastal zone, Brazil. In: Martins LR, Santana CI (eds) Non living resources of the Southern Brazilian coastal zone and continental margin. Editora CECO-IG-UFRGS, Porto Alegre, pp 62–68

Tomazelli LJ, Villwock JA (2000) O Cenozóico do Rio Grande do Sul: geologia da planície costeira. In: Holz M, DeRos LF (eds) Geologia do Rio Grande do Sul. Edições CIGO/UFRGS, Porto Alegre, pp 375–406

Tomazelli LJ, Villwock JA, Barboza EG, Buchmann FSC, Santos LAO (1999) A Erosão Costeira no Rio Grande do Sul: Uma Avaliação das Causas e Conseqüências. Porto Seguro, Brasil. In: Congresso Da Associação Brasileira De Estudos Do Quaternário, 7. 1999. Anais ... Porto Seguro: ABEQUA, CD-ROM

Valverde HR, Trembanis AC, Pilkey OH (1999) Summary of beach nourishment episodes on the US east coast barrier islands. J Coast Res 15:1100–1118

Part VII
Coastal Storms (Tropical Cyclones and Extra-Tropical Winter Storms)

Chapter 20
Coastal Hazards from Tropical Cyclones and Extratropical Winter Storms Based on Holocene Storm Chronologies

S.M. May, M. Engel, D. Brill, P. Squire, A. Scheffers, and D. Kelletat

Abstract Aware of past and future climate changes, the question arose whether modern instrumental data adequately reflect the chronology of tropical cyclones and extratropical winter storms for the period of the present eustatic sea level highstand (approx. the past 6,000 years). For pre-instrumental times, geological and sedimentological methods have been applied at geo- and bioarchives such as coastal marshes, lagoons, washover features or beach ridges, showing a frequency of strong cyclones roughly every 100–300 years, which is in contrast to the high number of major cyclones recorded recently. Many of these palaeotempestological records are discontinuous or contain hiatuses and it may be difficult to evaluate whether these sections of the record represent quiet phases without major cyclones or simply erosion or fluctuations in the ability of an archive to record the signature of cyclones. Manifold questions are still unanswered: as the potential number of former cyclones may be stored in landforms and sediments, how can the intensity of these cyclones be identified? Is the crest height of beach ridges a good indicator for storm surge heights, air pressure, and cyclone categories? This paper reviews important achievements in palaeotempestology and discusses open questions of cyclone distribution, frequency and energy (i.e., hazard potential) in the last few decades and reconstructions of these parameters back into Mid-Holocene times.

S.M. May (✉) • M. Engel • D. Brill • D. Kelletat
Institute of Geography, University of Cologne, Albertus-Magnus-Platz, 50923 Cologne, Germany
e-mail: matthias.may@uni-koeln.de

P. Squire • A. Scheffers
Southern Cross GeoScience, Southern Cross University, PO Box 157 Lismore, NSW 2480, Australia
e-mail: anja.scheffers@scu.edu.au

C.W. Finkl (ed.), *Coastal Hazards*, Coastal Research Library 6,

DOI 10.1007/978-94-007-5234-4_20,

20.1 Introduction

During the last decade the world has witnessed the massive economic, social, and ecological impacts of tropical cyclones in different ocean basins and countries. Our understanding of their occurrence patterns influences planning activities and risk analyses from calculating insurance premiums to developing conservation strategies. The ongoing intense debate on climate change seeks answers to questions whether the number of tropical cyclones has increased in the last 150 years (e.g., Knutson et al. 2010; Mumby et al. 2011) and if existing instrumental records capture the full natural variability of cyclone frequency and magnitude (Webster et al. 2005; Nott et al. 2007). The impact of cyclone activity in different ocean basins on growing populations and (often expensive) infrastructure demands for more accurate and extensive records. However, trend detection is impeded by substantial limitations in the availability and quality of prehistorical and historical data. High-resolution and precise records of cyclone dynamics or frequency in the pre-satellite era are required to provide an appropriate context for twenty-first century projections and to validate geophysical and climate models (Jansen et al. 2007).

The depositional coastlines of the world potentially store the history of extreme wave events over the time span of the Mid- to Late Holocene eustatic sea level highstand. Extreme wave events create a particular spectrum of landforms, deposits (such as beach ridges, washover fans, barriers), or erosional features. Based on studies of modern events, for which climatological parameters are instrumentally recorded and documentation of geomorphological and sedimentological effects is available, they can be reconstructed using coastal geoarchives. This interdisciplinary research branch, summarized under the term "palaeotempestology", has the potential to (i) significantly improve our knowledge of past natural coastal disasters, storm frequencies and magnitudes, and (ii) support realistic hazard assessment (Donnelly and Woodruff 2007; Frappier et al. 2007; Yu et al. 2009; Scheffers et al. 2012a).

This paper first reviews occurrence patterns of atmospherically induced extreme wave events of the instrumental era and those reconstructed from historical sources. The term "storm" is used here for both high latitude "winter storms" and "tropical cyclones" (referred to as "hurricanes" in the W Atlantic and "typhoons" in the NW Pacific Ocean) of categories 1–5 according to the Saffir-Simpson Hurricane scale (SSH). A discussion of methods and key results in palaeotempestology follows. Sedimentary evidence from lagoons, coastal lakes or swales is compared with the one from landforms like beach ridge sequences. These data (from tropical and extratropical regions) represent the basis of a discussion on the state of the art and open questions in palaeotempestology.

20.1.1 Tropical Cyclones and Extratropical Winter Storms

The term tropical cyclone generally describes warm-core and front-independent low-pressure systems, mainly occurring over tropical or subtropical oceans. Their formation relies on pre-existing atmospheric disturbances and instability, sea surface temperatures (SST) warmer than 26°C, associated high evaporation and

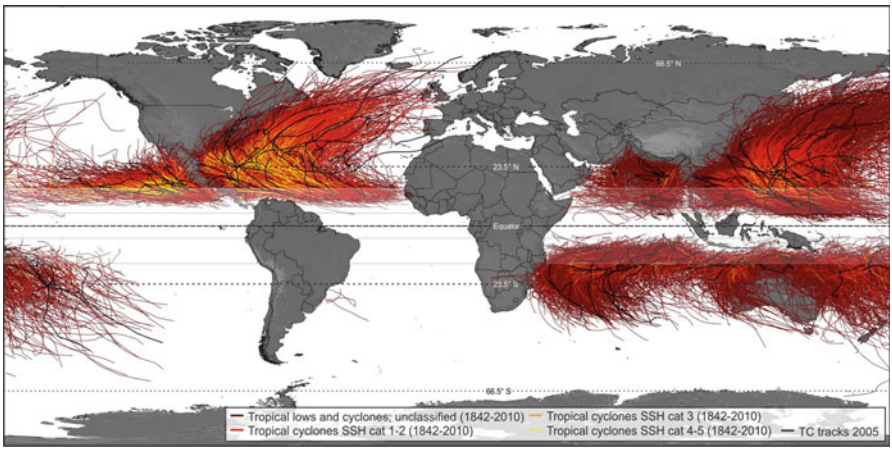

Fig. 20.1 Worldwide distribution of tropical cyclones from 1842 to 2010 (Based on tropical cyclone best track data [IBTrACS]; NOAA, Knapp et al. (2010)). Typical areas of cyclone genesis are located around the Cape Verde Islands, off E Australia and the China Sea. Cyclone genesis generally occurs between ~5–15°N and S (*marked corridors*). Classification of cyclone track intensity is based on maximum sustained winds. Differences in the number of strong tropical cyclones between ocean basins are mainly due to unclassified data in the Indian and Pacific Ocean

convective energy as well as sufficient momentum of the Coriolis force. The latter two characteristics are the prerequisite for their typical circular form and the rotation around the central eye (Hobgood 2005). In fact, best preconditions for their formation exist between around 5–10° N; this has a significant effect on cyclone distribution (Dando 2005). Consequently, tropical cyclones show a clear latitudinal or zonal orientation and distribution (Fig. 20.1); a narrow belt around the equator is void of cyclones, because the Coriolis force is negligible in these very low latitudes.

Mostly from about 15° N and 15° S, the cyclones approach the coastlines on a parabolic track from E to W, deflected to the right on the Northern Hemisphere and to the left on the Southern Hemisphere (Fig. 20.1). Thus, they potentially affect very long coastal stretches, for example along the E and S coasts of the USA or SE Asia.

Depending on a number of factors such as SST, the equatorial extent of the westerlies and the land-sea ratio, the latter considerably differing between the Northern and Southern Hemisphere, the poleward extent and the characteristics of tropical cyclone tracks vary between the ocean basins (Fig. 20.1). The continents of South America and Africa (except for a small central east coast section) are nearly unaffected by tropical cyclone impacts. Cold ocean currents influence SSTs in the eastern N Pacific and in the Southern Hemisphere oceans, even reaching the equator west of South America, and generally resulting in cyclone dissipation at lower latitudes compared to the N Pacific and N Atlantic. Here, the North Polar Sea is more sheltered from the Atlantic Ocean, and only narrow corridors exist for southward reaching polar currents, such as the Labrador Current off the coast of North America, the East Greenland Current or the Oyashio Current off Kamchatka. A third reason for the irregular geographical distribution of cyclones is attributed

to the currents of warm tropical waters drifting north-eastward (Gulf Stream in the N Atlantic Ocean, Kuro-Shio in the N Pacific), sustaining the warm core characteristics of cyclones into comparably high latitudes.

In contrast to tropical cyclones, extratropical cyclones (or extratropical winter storms) are cold-core, high latitude cyclones generally deriving their energy from the baroclinic temperature gradients in the atmosphere (Hobgood 2005). Generally associated with cold fronts, warm fronts or occluded fronts, the majority of the strongest extratropical storms occur during winter, due to maximum atmospheric temperature differences (Barredo 2010; Wehrli et al. 2010). Betts et al. (2004) define an extratropical storm by a pressure below 990 hPa; the lowest pressure ever measured was 916 hPa between Iceland and Greenland in December 1986 (Gadd et al. 1990). In contrast, tropical cyclones are often below 950 hPa and the lowest pressure measured was below 880 hPa (Hoarau 2000). In the Southern Hemisphere, where no landmass interrupts the westerly winds and the horizontal temperature differences between the Antarctic ice and warmer latitudes are more significant, they may develop high wind speeds and are known as the Roaring 40s, the Brave West Winds or the Furious 50s.

20.1.2 Frequency, Intensity and Spatial Distribution from Historical/Modern Datasets

According to Hobgood (2005), an annual average of c. 90 tropical cyclones is recorded worldwide. While this annual number is relatively consistent on a global scale, a remarkable variability is observed in terms of spatial distribution. Figure 20.2 visualises the spatial distribution of strong tropical cyclones (categories 4 and 5 according to SSH) for four large ocean basins and adjacent coastlines during the last decades of instrumental data.

In the Indian Ocean and the SW Pacific, a mean of 3.2 strong tropical cyclones occur annually, in the NE Pacific, the annual mean is 6.4, in the NE Pacific 2.6, and in the Atlantic Ocean only 1.4. According to Webster et al. (2005), the percentage of categories 4 and 5 tropical cyclones (SSH) varies significantly. The authors report 20% in 1970 and 35% at the turn of the millennium. Based on these average frequencies, for Holocene time scales, c. 40,000 high-category cyclones must be assumed to have occurred during the last 3,000 years, and more than 100,000 during the last 8,000 years, illustrating the difficulties to reconstruct the palaeostorm history of the tropical latitudes alone.

Fluctuations in strong tropical cyclone frequency have been recorded in all ocean basins: in the NW Pacific and Atlantic oceans, activity was above average before 1960/1965 and after 1995, whereas between these dates decreased activity was recorded (Webster et al. 2005; Trenberth and Shea 2006). This pattern is connected to climatic cycles such as the El Niño-Southern Oscillation (ENSO) or the North Atlantic Oscillation (NAO) (see also Camargo and Sobel 2005; Saunders

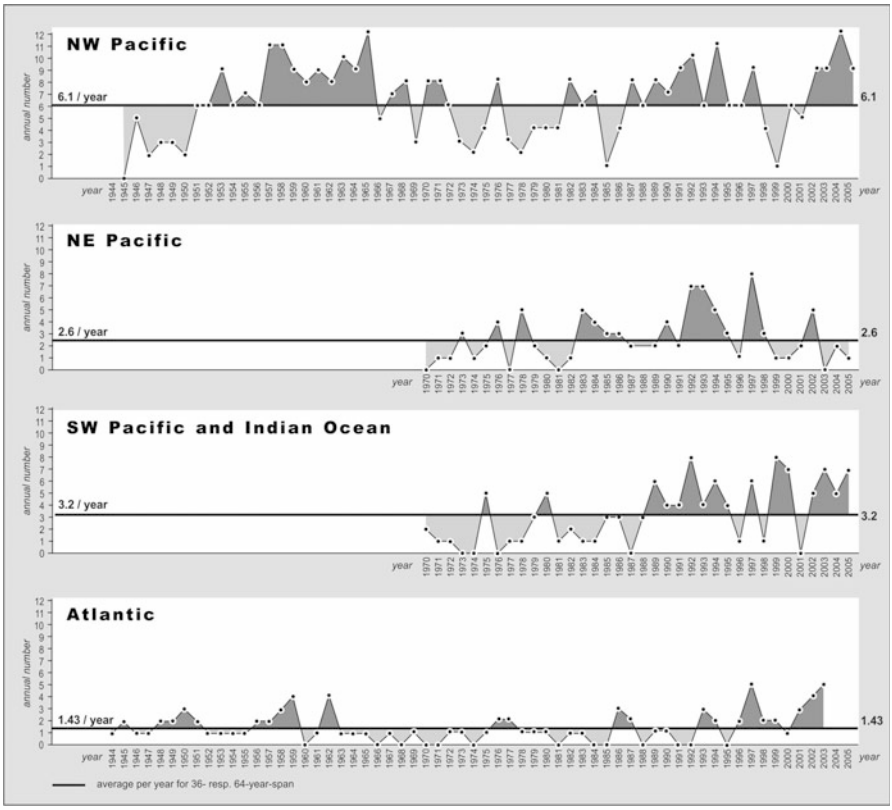

Fig. 20.2 Number of category 4 and 5 tropical cyclones occurring in the four large ocean basins (Based on data from Webster et al. 2005)

and Lea 2008), likely combined with other more regular intervals, and does not necessarily point to a constantly rising SST (Klotzbach 2006; Landsea et al. 2006).

The time span of continuous and instrumental observations on tropical storms around the world is rather short (Fig. 20.2; Webster et al. 2005), but it has been extended by catalogues of historical events from different sources (Chenoweth 2007; Garcia-Herrera et al. 2007; Elsner et al. 2008). Modern catalogues mostly comprise less than 150 years, though still reflecting extreme spatial and temporal discrepancies. Queensland (NE Australia) registered 175 cyclones in 141 years (1.2 per year), while Western Australia had only 44 cyclones in 135 years (one in 3 years). However, in both regions of Australia, some years had several strong cyclone landfalls, with a maximum of three per year in Western Australia (1975, 1995, 1996), and a maximum of five per year in Queensland (e.g. 1940, 1950). Ten cyclones made landfall along the coast of Japan in 2004, five affected the Cook Islands in a 5-week period in 2005 (Power and Pearce 2007), and an extremely

active cyclone season was registered in the N Atlantic in 2004 and 2005 (Beven et al. 2008). As Trewin (2007) found, the total number of cyclones has probably been underestimated prior to 1950 and then overestimated between 1950 and 1970, whereas the number of high-category cyclones is underestimated before 1985, and especially before 1970. The reason is that details from the older events have not been registered in remote areas or over the oceans.

The extraordinary tropical cyclone season of 2005 (2005–2006 in the Southern Hemisphere) and its relation to high levels of recorded SST (0.9 C above 1901–1970 average (Trenberth and Shea 2006)) triggered an increase in discussions on occurrence patterns and the impact of rising SST on cyclone number and intensity. 56 cyclones occurred in this season worldwide, from which 23 were classified as categories 4 and 5 (see also Fig. 20.1). The most intense was the N Atlantic hurricane season with 15 hurricanes, from which seven were major ones (categories 4 and 5) and four category 5 (Beven et al. 2008). Although this record-breaking hurricane season is in line with increased frequencies since 1995 (Webster et al. 2005), the 2005 hurricane impact in this part of the world – nearly 1,700 fatalities and more than 100 billion $ damage in the US alone – was outstanding (Trenberth and Shea 2006). According to Cechet and Arthur (2007), the worldwide average annual death toll due to landfalling hurricanes is 20,000 people and the damage 10 billion $ US.

In the aftermath of the cyclone season 2005–2006, research focused on testing hypotheses whether and to what extent tropical cyclones changed their frequency and intensity due to rising SST during the instrumental era. Multiple methods have been applied, but the results in some parts are still controversial. This concerns the number of cyclones, the percentage of strong ones (categories 4 and 5), their duration, the length of the cyclone season, destructive forces, and the influence of rising temperatures, dust particles in the atmosphere, wind shear, ENSO-effects, and other climate-controlled parameters (Table 20.1).

While Lambert (1996) illustrated a relationship between the number of intense extratropical storms and ENSO years for the Pacific Ocean in the Northern Hemisphere, extratropical storm frequency is linked to the NAO (North Atlantic Oscillation) index (Ulbrich and Christoph 1999; Andrade et al. 2008; Donat et al. 2009; Trouet et al. 2012) in the N Atlantic and in W Europe, which is reflecting the position and extent of the Iceland low atmosphere pressure cell (Fig. 20.3). The NAO is responsible for “see-saw” like patterns of climate dynamics and severe windstorm-induced economic losses varying on seasonal to decadal scales (Dawson et al. 2004; Lockwood 2005; Barredo 2010). For instance, by analysing N Atlantic storminess, Dawson et al. (2004) found a correlation between cold winters in Greenland and warmer ones with higher storminess in W Europe, which, however, is subject to significant interannual and spatial differences. For example, in Northern Ireland, more than 105 days with gales have been registered in 1905, whereas in 1920 and 1925 there were only less than 10 days.

The NOAA National Climatic Data Center of the USA has compiled a list of extratropical storms with air pressure below 970 hPa (storms with wind force Bft. 10, 89–102 km/h and more), i.e. an intense event according to Lambert (1996), for

Table 20.1 Selection of studies concerning the relation of climate change and (in most cases Atlantic) tropical cyclone activities during the last decades by different authors

Oc Bs	Authors	Time period (years)	Main conclusions
All	Hoyos et al. (2006)		Increased intensities by rising SST
All	Landsea et al. (2006)	35	Older data are not reliable enough to accurately discuss a trend in hurricane intensity
All	Slott et al. (2006)		Small increases in storm wind speed are likely to have large impacts on coastal morphodynamics
All	Sriver and Huber (2006)	40	All around the world intensities have increased
All	Webster et al. (2005)	35 and 63	Total number of storms/year has not changed, but category 4 and 5 hurricanes increased from 20 to 35% of all storms
SP, IO	Callaghan et al. (2007)	50	Four percent increase of wind speed for every 1°C warming, i.e. up to 30% increase in destructiveness based on cubic wind speeds and more intense storms lasting longer
NA	Chang and Guo (2007)		Before WW I on average 2.1 storms per year are missed in the registration, since the 1920s about 1 per year
NA	Donnelly and Woodruff (2007)	5,000	Higher SST are not a prerequisite for increased intensity
NA	Elsner (2006)	135	SST plays a direct role for rising hurricane intensity, but with a time lag of 1–9 years
NA, NP	Emanuel (2005)	55	Intensities and damage potential (wind speed and duration) has doubled because of increasing SST
NA	Evan et al. (2006)	22	Dust from Africa suppresses Atlantic hurricane activity
NA	Kafatos et al. (2006)		Peak intensities (Katrina in 2005) when difference of SST to air temperature is greatest
NA	Keim and Robbins (2006)	155	Severity and length of the storm period influenced by rising SST
NA	Klotzbach (2006)	20	Ten percent rise from the first to the second decade of cat. Four and five hurricanes, but no change in total number
NA	Knutson et al. (2008)		Models indicate fewer but stronger hurricanes worldwide by rising SST
NA	Landsea (2007)	106	Not frequency but intensity changed
NA	Mann and Emanuel (2006)	130	Cooling effect of aerosol pollution
NA	Mann et al. (2007)		Number of landfalling cyclones remained constant
NA	Michaels et al. (2006)	24	Rising SST increase percentage of cat. 3+ hurricanes but not intensities
NA	Nyberg et al. (2007)	270	Wind shear is regionally important for hurricane intensity
A, P	Santer et al. (2006)	100	22 models tested to find out what is causing the sea to warm and storms to intensify: 84% chance that 67% of recent ocean warming is due to rising levels of greenhouse gases

(continued)

Table 20.1 (continued)

Oc Bs	Authors	Time period (years)	Main conclusions
NA	Saunders and Lea (2008)		Forty percent increase in hurricane intensity by each 0.5°C of sea surface warming
NA	Trenberth and Shea (2006)	130	SST counts for 25% of increase on intensities, plus ENSO
NA	Wang and Lee (2008)	>150	Weak decrease in the number of landfalling storms globally

Main conclusions are depicted
Oc Bs Ocean Basin, *A* Atlantic, *NA* North Atlantic, *P* Pacific, *NP* North Pacific, *SP* South Pacific, *IO* Indian Ocean

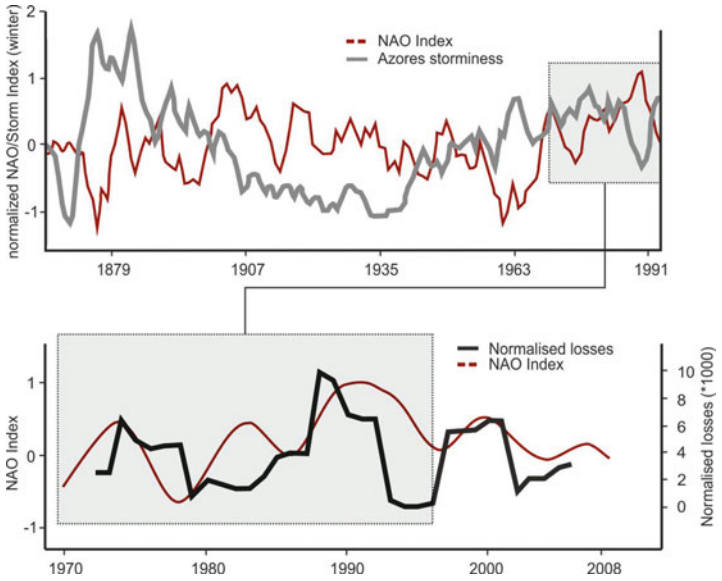

Fig. 20.3 Complex relation of NAO index winter variability, normalised Azores winter storminess (*top*; Andrade et al. 2008, p.752, 5-year moving) and 5-year moving average of annual windstorm losses in Europe (*bottom*; Barredo 2010, p.101; major storm disasters normalized to 2008 values). NAO index is data based on Osborn (2011)

the years 1899–1991. The average number for all high latitude ocean sections is around 30 per winter, with a minimum of around 10 and a maximum of >50 (Lambert 1996). Comparably, Weisse et al. (2005) analysed storms in the NE Atlantic and the North Sea of Europe from 1958 to 2001. They found the total number of storms to be 11–33 per year, taking Bft. 8 as the lower limit of intensity.

Table 20.2 General characteristics of tropical cyclones and extratropical storms

	Air pressure (hPa)	Wind speed (km/h)	Duration	Forecast	Storm surge (m)	Inundation	Rain risk	Frequency (per year)
Tropical cyclones	<900	>250	Several days	Reliable	>7	Potentially wide		High
0–12								
Extratropical winter storms	>950	150	Several days	Reliable	3–4	Wide		
(without dikes)	Small	2–6						

In fact, 15 years between 1958 and 2001 have been without any severe storm (Bft. 10), and the maximum of severe storms in this region was 4 per year. Around the Azores in the Atlantic Ocean, Andrade et al. (2008) found that since 1836 an average storm lasts 2.3 days and the annual frequency of storms is only 3.1.

However, the reconstruction and comparison of extratropical winter storm activity patterns may be hindered by several parallel measuring scales, especially in historical times (Dawson et al. 2004). Extratropical winter storms are often registered only as the number of days with gales, implying a wind speed of more than 17.2 m/s (Bft. 8) for at least 10 min (Betts et al. 2004). This is much less than the lowest category of a tropical cyclone – according to the SSH, category 1 has more than 119 km/h sustained winds (i.e., winds for at least 1 min). Dawson et al. (2004), for instance, document annual winter gale day frequencies from historical records for Scotland, Iceland and Ireland, illustrating prevalent frequencies of c. 60, but also years of >120 gale days (Iceland, Ireland) as well as a high inter- and intraregional variability during the last two centuries. To a certain extent, these scale-dependent differences are the reason why the numbers of extratropical storms appear to be much higher than those of tropical cyclones. In the Southern Hemisphere, where the fetch is nearly unlimited, extratropical storms are stronger and more frequent than in the N Atlantic or N Pacific. The differences in the character and parameters of tropical cyclones and extratropical winter storms are summarized in (Table 20.2).

As an example of extratropical storm activities and impacts on coastlines, some facts from the southern North Sea have been summarized by Lamb (1991). Within 1169 years from 838 to 2007 AD, 33 extreme storm floods hit the coastlines of the Netherlands and Germany (six of them also hit Belgium and two Denmark). Death toll in this period was around 450,000–600,000, which is at least 13,000 per major flood on average with a maximum of more than 100,000 fatalities during one event. Prior to the construction of high dikes (until 1953 in the Netherlands, and until 1962 in Germany), inundation reached more than 20 km inland (along rivers such as the Elbe more than 120 km!). Islands completely disappeared, elongated barrier islands were breached, most of them overwashed. More than 100–200 km^2 of marshland got lost in huge bays, some of which are still open after 700 years. Regionally, the retreat of the marsh coastline of NW Germany was more than 40 km and several remnants of the marsh still exist as small exposed islands in the Wadden Sea.

20.2 Approaches and Methods to Decipher the History of Ancient Storms

Palaeotempestology is a relatively young research discipline, though it has never been of more importance (Hippensteel 2010). Instrumental data span too short a time to be able to establish the real risks of winter storm surges or severe tropical cyclones during the Late Holocene; as a consequence, future predictions of occurrence patterns with assumed higher SST also contain considerable uncertainties. This also implies that periods of higher cyclone magnitude or frequency may have existed during the past, as suggested by recent studies (Nott and Hayne 2001; Liu 2004).

Clearly, historical human experience does not entirely comprehend what the climate system is capable of in terms of epic storms. To capture the maximum possible magnitude of storms, reliable reconstructions by proxy data that extend far back before the instrumental record are needed. This is an essential issue because, in addition to their hazard potential for human life and economy, tropical and extratropical cyclones play a significant role in perturbation of reefs and other littoral ecosystems by influencing morphology and community composition (Tanner 1995; Hughes and Connell 1999; Hughes et al. 2003).

Proxy records collected from marginal marine environments offer the potential to extend the palaeo-storm record back several thousand years, potentially providing better statistical constraints on storm prediction and a better understanding of the influence of global warming on catastrophic storm development (Fig. 20.4). In many regions, Holocene sea level reached its present position c. 6,500 years ago (Pirazzoli 1991; Peltier 2002) involving the evolution of coastal lakes, lagoons, swamps, tidal inlets but also cliff coasts. In these geo-bioarchives, as well as in fields of coastal boulders or blocks, coarse-clast ridges or ramparts, in long-living corals, speleothems and even tree-rings the frequency and magnitude of cyclones can be recorded (Nott and Hayne 2001; Miller et al. 2006; Donnelly and Woodruff 2007; Frappier et al. 2007; Hetzinger et al. 2008; Yu et al. 2009), though the signals within the archives have to be separated from other processes (Fig. 20.4). The preservation potential of storm events in these archives is very site-specific. Moreover, it must be stated that different proxies reflect different aspects of a cyclone's impact and have different sensitivity thresholds to cyclone impact magnitudes (Liu et al. 2009).

20.2.1 Fine Grained Washover Records

Over the past decade a growing list of palaeotempestological studies and post-storm observations have confirmed that washover sand layers stored in coastal lakes, lagoons and marshes have the potential to represent a reliable proxy for hurricanes or winter storms (see also Fig. 20.5). Most authors conclude that only severe

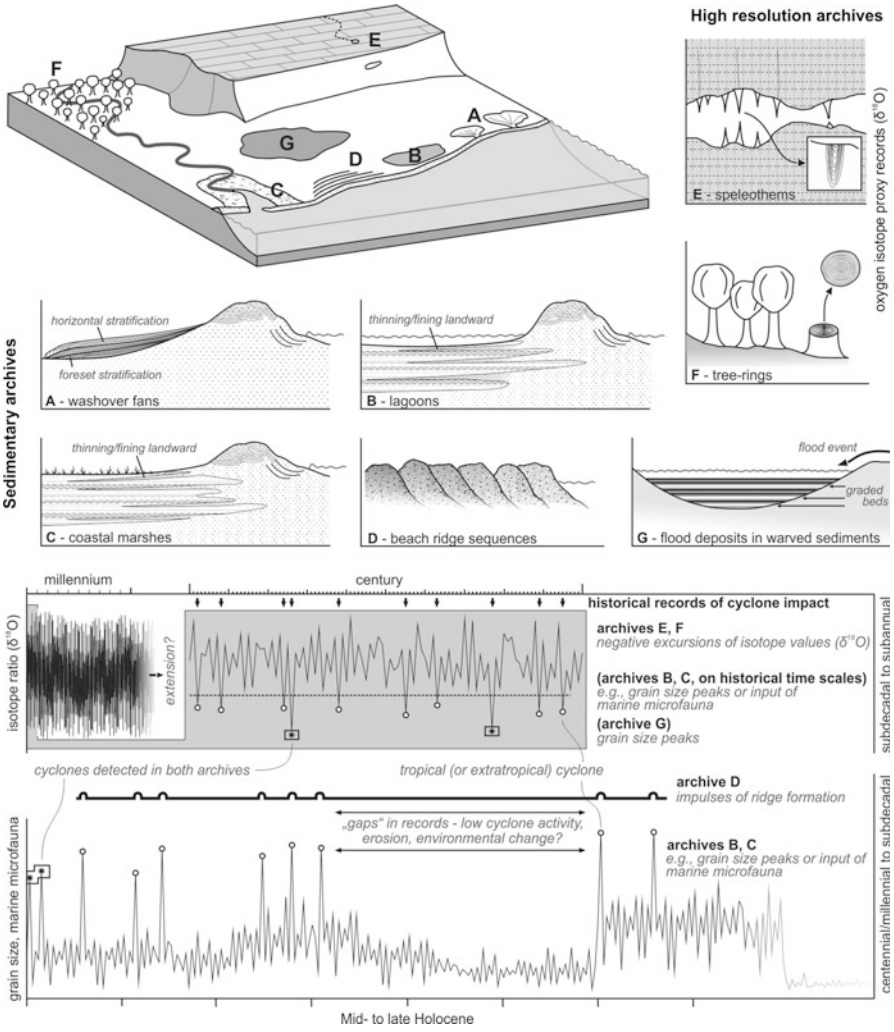

Fig. 20.4 Different geological archives (schematic, idealised), their geographical setting and their potential resolution in palaeotempestological research. Plots of cyclone proxies (*bottom*) represent hypothetical values and are not based on measurements

cyclones or extreme winter storms may leave those deposits (Hippensteel 2008; McCloskey and Keller 2009; Otvos 2011).

Sedimentary and geochemical criteria as well as offshore-indicative foraminifers were used to detect washover storm deposits in coastal lakes and back-barrier marshes of the Gulf of Mexico, Alabama (Lake Shelby) and NW Florida (Liu and Fearn 1993, 2000; Lambert et al. 2008). According to these authors, increased tropical cyclone activity is reflected in the investigated sedimentary record between 3400 and 1000 BP, framed by periods of lower cyclone

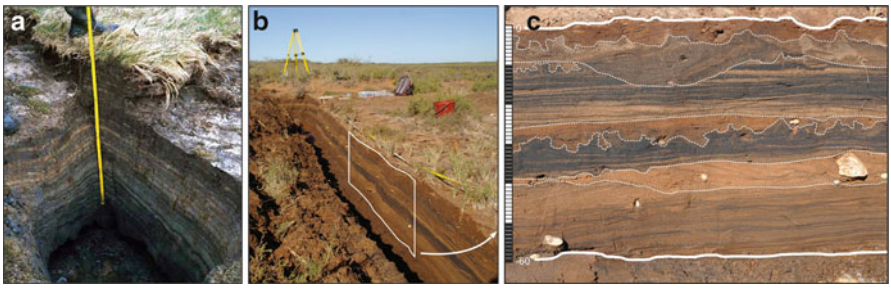

Fig. 20.5 (**a**) Alternating sand deposited by storm surges (*light colour*) and soil (*dark colour*) in a marsh of northern Germany. The 70 cm deep section shows evidence of at least 25 floodings and sedimentation within less than 100 years. (**b**, **c**) Well-stratified washover deposits of historical cyclones (sand with heavy mineral layers) 500 m from the sea in arid NW Australia, showing different generations of overwash events, channel structures and intercalating bioturbation horizons (Photos by D. Kelletat, S.M. May)

activity. By comparing estimated minimum return levels and periods of strong hurricane impact from the Lake Shelby geological record (indicating an average return period of 318 years) with storm catalogue-based modelled site-specific return levels, Elsner et al. (2008) confirmed the consistency of the results. In contrast, Scott et al. (2003) infer inverted higher cyclone intensity along the coasts of South Carolina over the last 1,000 years, suggesting variability in jet stream occurrence and the position of the Bermuda High pressure system (see also Hippensteel and Martin 1999).

At the central coast of Belize, McCloskey and Keller (2009) took 21 sediment cores and found up to 16 events as sand or clay layers in peat deposits. For the last 500 years, they analyzed and dated 5–6 strong cyclones; the observations in modern times show about one per decade (i.e., ten times this number). McCloskey and Knowles (2008) suggested a migration of the storm belt by movements of the Inner-Tropical Convergence Zone (ITCZ) and the Bermuda High of up to 10 latitudinal degrees within the younger Holocene in order to explain cyclone variability. For the W Atlantic, the US East Coast and the US Gulf Coast, it has been found that the zone of maximum shift for tropical cyclone landfalls was to the N from 8000–4000 BP to 1100–600 BP (the last is the Medieval warm period) and to the S from 4000 to 2400 BP (Sub-Boreal to Sub-Atlanticum II, cooler and moister), as well as 400–200 BP (Little Ice Age) (McCloskey and Knowles 2008). The same authors assume that only deposits of cyclones of category 3 or higher are distinguishable from other sediments in coastal stratigraphical sequences from central Belize.

Kiage et al. (2011), based on field research in Georgia, detected nine deposits within the last 1,900 years indicating an increased storm activity 2000–1100 BP and in the last 100 years and a period of reduced storm impact between 1100 and 250 BP. They found that the relative thickness of sand layers in the sedimentary record is not necessarily indicative of hurricane magnitude.

Donnelly and Woodruff (2007) and Woodruff et al. (2008) reconstructed the hurricane climatology at Puerto Rico and concluded that periods of no apparent overwash activity between 3600 and 2500 BP and since 1000 BP are exceptionally long and unlikely (above 99% confidence) under the current climate conditions, and that the western N Atlantic has experienced significant changes in hurricane climatology over the last 5,500 years.

Likewise, extratropical storms are capable to produce sediment sheets in coastal geological archives such as marshlands, and may even play an important role in sediment supply, long-term shoreline stability and long-term coastal sand drift activity (Goodbred and Hine 1995; Stone et al. 2004; Deicke et al. 2007; Clarke and Rendell 2009).

As shown in these and further studies, washover deposits from sedimentary environments can provide important evidence for fluctuations in storm activity on millennial scales. However, it is very difficult to evaluate a statistical average return period from these data. Furthermore, return periods of decades to centuries are in striking contrast to the much higher landfall numbers in modern times (compare also Table 20.3). As summarized by Liu (2004), long-term coastal changes, such as barrier progradation, aggradation or erosion, as well as relative sea level changes result in a dynamic susceptibility of a coastal lake or marsh to accumulate and preserve washover sediments of storm surges. The elevation of storm surge significantly differs on each side of a counter-clockwise rotating cyclone. A high-category landfalling cyclone may only cause minor flooding and not create an washover deposit if its track is to the right of the sediment archive (Liu 2004).

Direct evidence of barrier overwash or breaching is brought by washover or scour fans, i.e. lobate sedimentary structures extending from barriers into back-beach coastal lagoons or coastal lowlands (Carter and Orford 1984; Kraus 2003; Andrade et al. 2004; Donnelly et al. 2004; Matias et al. 2008). These landforms represent an important feature of coastal geomorphology worldwide; induced by high-energy wave events, they represent both geomorphological and sedimentary evidence of either tropical cyclones, extra-tropical winter storm surges, or tsunamis (e.g. Dawson 1996; Sedgwick and Davis 2003; Donnelly et al. 2004; Tuttle et al. 2004; Matias et al. 2008; Switzer and Jones 2008; Goff et al. 2009; May et al. in press).

While numerous washover structures are reported to have formed during one single event (e.g. Schwartz 1982; Sedgwick and Davis 2003; Williams 2011), detailed reports on multiphase structures are rare and mostly include a succession of few subrecent or recent events (Wang and Horwitz 2007; Switzer and Jones 2008). To date, the potential of these landforms for palaeotempestological research needs to be verified. However, detailed geomorphological, sedimentological and geochronological investigations on barrier systems, where washover structures of different age are present – either located along one single barrier or along a succession of barriers –, may provide insight into the applicability of these landforms for palaeotempestological purposes.

Table 20.3 Frequency of strong storm and cyclone impacts based on palaeotempestological studies from the USA and Australia (hiatuses of >400 years as well as data inversions are excluded)

Location	Period	No of events	Frequency	Reference
Data from cores in lagoons or washover fans				
Alabama, USA	3500-0 BP	11	318 years (28–888 years)	Elsner et al. (2007)
Alabama, USA	4200-0 BP	5		Huang (2009)
Laguna Madre, Texas, USA	5300-800 BP		200–250 years	Wallace and Anderson (2010)
New England, USA	1200-2000 AD		134 years (16–200 years)	Cheung et al. (2007)
Georgia, USA	2000-1100 BP	9	(100 years)	Kiage et al. (2011)
Data from beach ridge systems				
Shark Bay, W Australia	6000 years	16	154 years (10–290 years)	Nott (2011)
Shark Bay, W Australia	6000 years	13	181 years (10–335 years)	Nott (2011)
Shark Bay, W Australia	6000 years	6	147 years (5–335 years)	Nott (2011)
Curacoa Is., E Australia	6000 years	17	222 years (35–390 years)	Nott and Hayne (2001)
Pormpuraaw, NE Australia	3000 years		100 years	Nott (2009)
Cowley Beach, NE Australia	5500 years		260 years	Nott (2009)
Abrolhos Is., W Australia	5500 years	9	133 years (65–355 years)	Scheffers et al. (2012b)
Abrolhos Is., W Australia	5500 years	10	155 years (5–305 years)	Scheffers et al. (2012b)
Abrolhos Is., W Australia	2600 years	16	146 years (5–320 years)	Scheffers et al. (2012b)
Abrolhos Is., W Australia	5000 years	4	279 years (210–340 years)	Scheffers et al. (2012b)
Abrolhos Is., W Australia	5700 years	9	197 years (10–385 years)	Scheffers et al. (2012b)

20.2.2 *Beach Ridges as Palaeo-Storm Archives and Recorders of Wave Regimes*

As indicated above, numerous palaeotempestological studies have been relying on the stratigraphy and dating of vertical sequences of washover deposits preserved in coastal lagoons, lakes or marshes. Another natural test for the frequency (and possible energy) of former storms are beach ridge sequences along sedimentary coasts (Fig. 20.6).

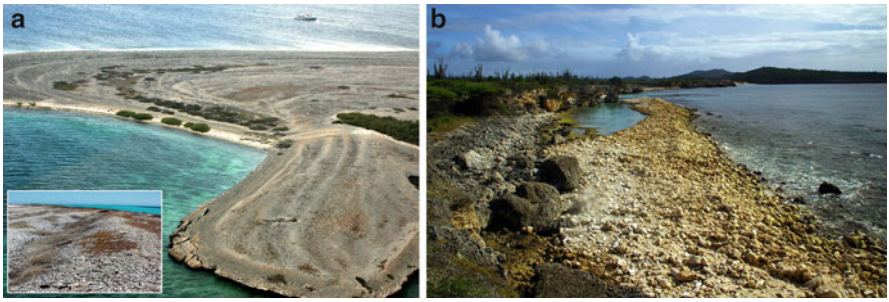

Fig. 20.6 Storm-generated coral rubble ridges on the Abrolhos Islands (**a**; Western Australia) and Bonaire (**b**; Leeward Antilles, Caribbean) (Photos by A. Scheffers, S.M. May)

Worldwide, the majority of ridges consist of sand, but Anthony (2008, p. 289) also noted that "gravel beaches are an extremely important component of the world's coastlines, especially in temperate to high latitude zones". Here, ridges may consist of pebbles, cobbles, and boulders (in formerly glaciated areas, the so-called "paraglacial" coastlines), as well as coral rubble, where coral reefs represent the sediment source in lower latitudes (Brückner and Schellmann 2003; Scheffers 2005; Scheffers et al. 2009a, 2012a). Coarse material may also dominate coastlines in arid landscapes or tectonically active areas. Hayes et al. (2010) recently summarized the status of current knowledge on the dynamics and processes of gravel and boulder beaches.

In most cases, investigations on beach ridge systems have been undertaken to decipher coastal evolution, focussing on changes in a number of processes such as sediment supply, longshore drift, river discharge, wave climate, sea level history and variations or neotectonics (Carter and Orford 1984; Kelletat 1985; Brückner and Schellmann 2003; Harvey 2006). The internal stratigraphy of beach ridges may be highly complicated, therefore indicating varying growth stages for each ridge (Stapor and Tanner 1977). Missimer (1973) provided time spans of 12–16 years for beach ridges on Sanibel Island (N Gulf Coast of Florida) and discarded suggestions that such ridges could be formed during one or two storm events.

Nevertheless, ridge systems were in some cases investigated with respect to event histories (cyclones and tsunamis) as well. Examples for the tropical latitudes are, among others, Hayne and Chappell (2001), Nott and Hayne (2001), Kunte and Wagle (2005), Nott (2011) or Scheffers et al. (2009b, 2012b) and for extratropical zones Clemmensen et al. (2001), Rink and Forrest (2005), Nielsen et al. (2006), Sanjaume and Tolgensbakk (2009) or Schellmann and Radtke (2010). These studies suggest that it is highly likely that beach ridge systems record significant wave impulses or storm events.

On Bonaire (Leeward Antilles, S Caribbean), Hurricane Lenny in 1999 formed fresh ridges with a crest of 2.5 m above mean sea level in a micro-tidal environment with less than 1 m of storm surge and waves of 5–6 m (Fig. 20.6b). Coral rubble ridges were formed in the lower part of the waves where orbital velocity was

dampened by friction (Scheffers 2005). Similarly, numerical dating of coral rubble ridges on the Abrolhos Islands off Western Australia points to Holocene overwash processes, with mixing of material behind the active beach ridge (Fig. 20.6a). Strong overwash events may affect significant parts of beach ridge systems, partly filling in swales with coral rubble different in size and type compared to that of the ridge crests (Scheffers et al. 2009b, 2012b). It is concluded that beach ridge systems record only a minimum number of events and dating of a system leads to periodicities that span maximum time intervals between major events. Recent erosion affects almost all of the Abrolhos ridge systems, where those closest to the shoreline have ages between several hundred and more than 1,500 years (Scheffers et al. 2012b).

Generally, coarse-clast coral ridges and transported coral blocks as two types of geoarchives are direct evidence for past extreme events and they are ideal for high-precision U-series dating (Yu et al. 2004, 2006; Zhao et al. 2009; Scheffers et al. 2012b). Yu et al. (2009) demonstrated that large transported coral blocks on reef flats and elevated sedimentation rates in atoll lagoons of the South China Sea are excellent proxies for past strong storms. They found three periods of high storm activity around 800 BP, 2400 BP and 3200 BP, respectively.

20.2.3 High Resolution Proxies

Nott (2011) assumed that long-term sedimentary records of tropical cyclones in the form of coral shingle, shell and sand ridges and sheets register only the most extreme events at multi-century to millennial scales. The resolution of these records might be too coarse to determine the natural variability of events (Nott et al. 2007). Higher (annual) resolution can be obtained from isotope variations in speleothems, which may reflect occurrence patterns of tropical cyclones (Lawrence and Gedzelman 1996; Malmquist 1997; Frappier et al. 2007).

Nott et al. (2007) presented an 800-year long (1200–2004) speleothem record from the Cairns region of N Queensland. It stores the isotopic signature of tropical cyclone rainwater within an annually layered limestone cave stalagmite. Comparison of the first 100 years of the record against Australia's Bureau of Meteorology's best track cyclone database showed that every major cyclone and more than 75% of all cyclones to track within 300 km of the site (130 km inland of Cairns) were registered in the stalagmite. The centuries from 1600 to 1800 AD and 1400 to 1500 AD were very active, whereas the period 1200–1400 AD was exceptionally quiet. Since 1800 AD, activity has been moderately quiet and especially so since the European settlement of the region in the late nineteenth century.

Frappier et al. (2007) correlate low $\delta^{18}O$ values of a stalagmite from central Belize with certain cyclone-induced rainfall events between 1977 and 2000. The authors point out the potential of similar studies for palaeotempestological research at different time scales and also conclude that high-resolution cyclone proxies

gained by advanced sediment core analysis can provide decadal to seasonal records (see also Elsner et al. 2008; Li et al. 2011).

However, high-resolution records may also be obtained from sedimentary archives. Besonen et al. (2008), for instance, detected a series of anomalous graded beds in varved sediment records from Boston, Massachusetts and interpreted these sediments to correlate with strong flooding events corresponding to hurricane strikes. According to the authors, the dataset shows strong centennial-scale variations in flood (and hurricane) frequency which are consistent with other palaeoclimate indicators.

Moreover, oxygen isotope variations from long leaf pine tree-rings have been used to trace back tropical cyclone influence in the SE USA. Anomalously low $\delta^{18}O$ isotope values have shown to correspond with cyclone-related rainfall events (Miller et al. 2006).

20.3 Discussion – Benefits and Remaining Challenges

20.3.1 Storm Frequencies and Intensities from Sedimentary Records

By comparing the variability of intense cyclones and mid-latitude storms with other palaeoclimate records, it may be possible to detect modulations of this variability by atmospheric and oceanic dynamics such as ENSO. However, the presented and other follow-up studies from different regions worldwide led to a series of debates as to the validity of their approach. Several regional studies (Table 20.3) show the benefits but also some of the remaining problems in palaeotempestology.

Otvos (2011) published a general criticism of the reconstruction of quiet and hyperactive phases of palaeo-storms based on sedimentary evidence since a very high number of parameters influence the kind of deposition and preservation (see also Liu 2004). Changes in sea level, shoreline positions, or the impact of transgression and regression processes on estuaries and their deposits play important roles in setting the stage for overwash processes, and bioturbation distorts the storm record as well. Significant lateral variations in the number and thickness of intercalated sand layers at closely adjacent sites suggest the importance of local differences in sources, transport and preservation processes. Variations in the number, thickness and ages of sand laminae may not directly be related to the number of storms and their intensities.

Apparently, washover deposits in coastal lakes may be the product of severe reworking of ancient offshore, beach and dune sediments, including shells or foraminifers. Dating of these fossils rather yield the age of the fossil and not necessarily the time of storm deposition. In addition to the problems related to the interpretation and dating of these records, it is difficult to distinguish marine washover deposits caused by storm from those caused by tsunami flooding where

both processes coexist. Catalogues of sedimentary signatures from storms and tsunamis document differences based on individual case studies (Morton et al. 2007), though most of these signatures are potentially generated by both processes (Kortekaas and Dawson 2007; Engel and Brückner 2011). However, a large number of signatures more likely to occur in either of both processes and information on the source area of the sediment, reflected by the microfossil assemblage (e.g. Uchida et al. 2010) or heavy mineral content (e.g. Switzer et al. 2005), which might be out of reach for storm waves, support the interpretation. These ambiguities have again been emphasized by Shanmugan (2011, p. 17) stating that "at the present level of knowledge, sedimentological features alone are unreliable for distinguishing paleotsunami deposits from paleocyclone deposits, without historical information".

There are, however, surface deposits created by waves or water power much stronger than a category 5 cyclone. These are blocks of exceptional mass (100–2,000 tons) found in extraordinary elevation along the coast (up to +50 m), often in cliff-top position and even further inland than fine washover sediments (Frohlich et al. 2009; Benner et al. 2010; Scheffers et al. 2010; Costa et al. 2011; Engel and May 2012).

At first glimpse it seems simple to analyse storm frequency from a beach ridge sequence: each ridge represents an event and should simply be dated. In fact, the problems are manifold, starting with appropriate and consistent sampling procedures, being the prerequisite for comprehensible interpretation of ridge composition and formation. Similar to the fine-grained sedimentary record, one difficulty involved in all of these studies is proper numerical dating. Dating of beach ridges is indeed more challenging than initial impressions may suggest regarding the rather simple morphological aspect of such systems. Old, reworked and young, fresh particles (for example, shell, coral and foraminifera) are often mixed in one ridge and existing ridges in a system do not remain protected from younger events, as demonstrated by observations of recent hurricane or tsunami inundations. Furthermore, gaps in deposition are clearly developed in various beach ridge subsystems that have been truncated by younger systems developed along erosional contacts. The relative chronological pattern of these subsystems is rather easy to discern, as is the relative age in a strictly parallel ridge system, but – in the absence of numerical data – the time of deposition remains uncertain. To date, the results of investigations indicate that reversals as well as a high variability of time spacing may have occurred, even in similarly-spaced systems (Scheffers et al. 2012b).

For ridge systems, particularly the relationship between coral rubble ages and timing of ridge formation is a critical point. To date, due to the fact that extensive dating approaches require extensive funding resources, most studies established chronologies based on a very limited number of dates per ridge (see Scheffers et al. 2012a). However, a multiple dating approach was recently undertaken by Zhao et al. (pers. comm. J-X Zhao, University of Queensland, Australia 2012). They studied a coral rubble ridge accumulated by Cyclone Hamish in Queensland, Australia (2009), by applying high-precision U/Th dating of 32 samples of coral fragments. Ages ranged between 20 and 174 years BP, clearly demonstrating the necessity to use multiple U/Th dates of coral rubble to define the maximum age

of the cyclone event responsible for the ridge formation in future studies. However, in a wide beach ridge sequence this would require many hundreds of data points to establish the event history (personal communication J-X Zhao 2012). Similarly, four samples of well-preserved coral rubble brought onshore by Hurricane Ivan (2004) on Bonaire (S Caribbean) revealed modern U/Th ages offset by 20–60 years (1984, 1969, 1957, 1945) from the hurricane event (personal communication, C Giry and T Felis, University of Bremen, Germany 2012). These results suggest that well-preserved corals transported onshore by storm events may be stored in the foreshore environment for several decades, but are reliable age indicators of the wave event on centennial to millennial timescales.

Promising results were obtained by several authors using luminescence techniques for age determination of storm deposits as well. Nott et al. (2009) used optically stimulated luminescence (OSL) on a beach ridge sequence in Queensland, Australia, the formation of which is most likely driven by the strongest local storm surges of the past 6,000 years. Madsen et al. (2009) demonstrated the potential of OSL by dating hurricane washover sediments in a coastal marsh of Massachusetts, USA. In the Gulf of Maine, Buynevich et al. (2007) OSL-dated relict scarps in barrier systems indicating severe beach erosion and retreat due to major erosional storm events. OSL allows for directly dating the process of ridge formation or overwash and, thus, does not imply uncertainties of a delay between the death of an organism used for ^{14}C or U-series dating and its incorporation into the geological record.

As Taylor and Stone (1996) have discussed, many authors conclude that beach ridges are constructed more often during moderate wave conditions and that storm wave conditions may initiate erosion or modify existing ridges. This may apply to sandy ridges in many cases, but in the case of those built up by rubble (from coral reefs) or gravel and boulders strong waves are needed to move a significant amount of material in order to build up ridges above the high tide level. Thus, concerning the connection of beach ridge development with strong or extreme wave events, a distinction has to be made between sandy and coarser ridge material. Even in coral rubble ridges it is found that high-category cyclones are more constructive (Scheffers and Scheffers 2006; Scheffers et al. 2009a), compared to medium and low category storms that are more destructive.

Another open point of debate is the estimation of the required intensity of a storm to form a beach ridge. Usually, the relative intensity of a devastating storm at one spot can be reconstructed. This has been calculated by modelling in a line of steps (e.g., Nott and Haynes 2001; Nott et al. 2009): each of the ridges relates to one severe cyclone and the crest height of a beach ridge is assumed to indicate minimum heights of the related storm inundation. The lowest air pressure in the storm centre can be calculated from the estimated storm surge elevation and is used as a direct indicator for the storm category (SSH 1–5). Further input parameters incorporated in the model comprise coastal bathymetry and configuration as well as the relationship between surge height and radius of maximum winds, angle of cyclone approach, distance of cyclone landfall from the study site, the cyclone‘s

translational velocity, and estimations of the tide level. However, modelling of former cyclone intensities remains problematic, since (i) the preservation of the original crest height is never guaranteed and (ii) the relation of storm surge elevation and ridge crest height has not universally been confirmed by field documentation. Observations on Funafuti (Baines et al. 1974), as well as on Bonaire (Leeward Antilles) (Scheffers and Scheffers 2006) definitely exhibited, at least for coarse debris ridges, crests of up to 5 m below onset waves. Coarse ridges, according to these observations, may also be formed at the base of breaking surf waves. Generally, storm surges from the same cyclone have different surge elevations along a closed long mainland shoreline and small islands off the mainland. Therefore, the same cyclone will leave different ridge crest heights, even in close proximity to each other, which also depends on the availability of source material and whether the cyclone makes landfall.

A problem remains with respect to the interpretation of storm periodicity and palaeotempestology from ridge system dating: do we really see signatures of climatic conditions, or are these hidden by small sea level variations or (natural or human-induced) variations in sediment supply? There are more problems involved in establishing event histories and in particular in comparing event histories of different sites. In order to harmonise the data on the Abrolhos, Scheffers et al. (2012b) excluded all data inversions and interpreted hiatuses of 400 years or more as the effect of erosion/abrasion of existing ridges and not a period without storms. Nevertheless, the frequencies elaborated are nearly of the same order (Table 20.3).

However, similar to sea level studies, only local inferences can be made from local evidence. A reliable picture of past global cyclone occurrence will require extensive local evidence in order to distinguish between local, regional and global factors and to detect any shifts in the areas of cyclone occurrence.

20.3.2 The Problem of Event Numbers – Discrepancies Between Instrumental Data and Palaeotempestological Evidence

If cyclone activity has not changed significantly in frequency and intensity during the last several thousand years (with variations of ±20%), many hundreds or even up to thousands of cyclone landfalls in certain regions since the Mid-Holocene can be expected. Such a large number of events has never been found in any geological record, even when combining different locations and archives in one region. The highest number of past storms detected by grain size analyses in sediments of a coral reef lagoon (Yongshu Reef, South China Sea) is supposedly 77 within c. 3700 years (Yu et al. 2009).

Holocene beach ridge sequences, such as along the coast of Hudson Bay, Canada (several hundreds of beach ridges), Dungeness Foreland, S England (up to 500 ridges, preserved in parts), Store Molvik Bay, W coast of Varanger Peninsula, N Norway (more than 200 ridges), appear to be more promising, if we assume that beach ridge formation is linked with major storm events. Along tropical coasts with

sufficient sediment supply more than 130 beach ridges may have developed locally (Scheffers et al. 2012a). However, even these sequences obviously underestimate real numbers of major storms of Mid- to Late Holocene times.

A remarkable similarity of storm periodicities seems to exist at similar latitudes (Table 20.3), with longer spacing in latitudes with tropical cyclone activity (about 150–300 years) than in extratropical and high-latitude regions with winter storms, where recurrence intervals seem to have shorter spans (many decades, up to just over a hundred years [Scheffers et al. 2012a]).

The number of events stored in a geological archive depends on numerous factors. Local geographical setting, storm surge and swell as well as storm track directions and characteristics, tidal conditions during cyclone landfall and the archive's preservation potential (e.g., Liu 2004; Otvos 2011) determine time scale and quality of the record. Even though the same coastal section is affected by recurring cyclone landfall, the characteristics of each event and its geomorphological and sedimentological impact vary from storm to storm; their geomorphological and sedimentological fingerprint is thus irreproducible. Even in the best case, every single geological archive apparently only records a fraction of events which should be expected to have impacted the coastal section. Based on this assumption, it is debatable whether the past super storm hypothesis (e.g., Nott and Hayne 2001), indicating stronger and more frequent storms in the past than at present, is valid. However, we should count on events in the Late Holocene (and the future), which had intensities never observed by modern registrations.

Apart from the aforementioned pitfalls and challenges, palaeotempestological research still promises to give valuable insights into past climatic processes and changes. Where possible, the comparison and combination of sedimentary records – such as sequences of washover sediments or coarse-clast ridges – with high resolution proxies like speleothem, tree-ring and potentially coral records is needed for evaluation and mutual crosscheck. Although the use of corals in palaeotempestological research is limited to date (e.g., Hetzinger et al. 2008), its potential as a high resolution archive is underlined by recent studies, e.g. concerning past SST variability (Giry et al. 2012). Preferably, these studies should combine different datasets from one location or from one narrow region. However, such comparisons are restricted to areas, where different types of archives are available, and a large number of study areas do not offer these preconditions. Finally, deciphering regional storm impact relies on a large number of study locations, implying years of thorough and detailed work and sufficient funding.

To a certain extent, the success of these investigations relies on the appropriate dating of the geological archive: the application of OSL datings, combined with other dating methods for crosscheck, would avoid negative effects through reworking of wave transported material, though implying other, different uncertainties (Nott et al. 2009; Madsen et al. 2009). As shown by the promising preliminary study of Zhao (Zhao et al. 2009; personal communication, J-X Zhao 2012), the use of U-dating series, due to its comparatively small error range, may be preferred to less precise ^{14}C or ESR datings when investigating ridges of coral or other carbonate materials (see also Schellmann et al. 2011). Perspectively, further

development and improvement (e.g. of dating accuracy and resolution) of different dating approaches, such as the application of in situ-produced cosmogenic nuclides for storm-laid coarse clast ridges, may promise further possibilities for alternative dating of sedimentary records in palaeotempestology.

Evidence from one single location may not be representative for temporal changes in cyclone activities of a broader region since the spatial variability of cyclone landfall is remarkably high. Thus, in a next step, a number of local evidences may comprise regional palaeotempestological datasets, which could be further combined with those from other regions. The combination of these regional datasets may contribute to consistent conclusions about past global trends of storm frequencies and intensities as well as interrelations between different oceanic basins (cf. Frappier et al. 2007). Ultimately, these datasets can be linked to different climate proxy datasets and may thereby contribute to the successful reconstruction of the influence of climatic variables, e.g. ENSO and NAO cycles, jet stream variability and changes in SST, on past and future storm activity. In this context, however, the "ideal paleostorm record" does not necessarily have to be reproducible, i.e. two records from the same depositional setting must be identical (cf. Hippensteel 2010); as a consequence of the natural variability of geological archives – including the variability of sedimentological, geomorphological, environmental as well as topographic and bathymetric settings –, the pattern of geological records may differ significantly even on a very local scale. It is thus emphasized that, regarding the high variability of both storm impact and geological archives, no ideal proxy exists. It is rather suggested to better understand and carefully correlate existing ones.

20.4 Conclusions

Throughout the last decades, registered strong storms (tropical cyclones and extratropical winter storms) show a rather high frequency (up to several events per year in the same region), although there is good agreement among scientists that the number of strong storms during the last decades did not significantly increase (despite local shifts of up to ±200% around the average). However, the debate regarding storm intensities is still ongoing. Up to a doubling of the destruction potential of tropical cyclones within the last 55 years, or even an increase in the intensity of 40% per 0.5°C rising of SST, has been concluded (Table 20.1, Saunders and Lea 2008). The latter means a 320% increase in cyclone intensity if SST rises by 2°C, the possibility of which is under debate for the year 2100 (Jansen et al. 2007). The rather new discipline of palaeotempestology combining investigations on coastal sediment traps, like washover deposits, lagoons and swales, has contributed significantly to understand storm processes along the coastlines of the world, but its main focus is on former tropical cyclone activities. For N and W Europe this is partly compensated by long and rather accurate historical records regarding inundations and coastal changes by storm floods from Early Medieval times onwards. Within the last 10 years, beach ridge sequences are more often used to establish long storm chronologies, but discussions exist on the identification of

former storm intensities and the problem of hiatuses in the chronologies: Do they represent times without storms or just signatures of net erosion, caused by a lack of sediment supply or relative sea level fluctuations?

A general problem is the strong discrepancy between the analysed number of palaeo-events (with frequencies of 100–300 years for major storms) and the high frequency of registered strong cyclones in modern times. To solve this and other questions, more detailed case studies involving numerical dating are necessary along beach ridge systems and in other geo-bioarchives with a high potential of preservation at all latitudes, in particular at latitudes where a small climate-induced shift of storm conditions (for example, the cyclone belt, the ITCZ or the winter storm fringe) may have influenced the frequency of beach ridge formation or washover deposition. The use of high resolution archives such as speleothems may promise evaluation of these sedimentary archives as well as more detailed insights into past cyclone occurrence. With respect to the higher latitudes, we may be able to place the glacio-isostatic emergence of beach ridges back in time to the Late Pleistocene period, which includes the important climatic disturbances of late glacial times when strong and significant climatic oscillations occurred, such as the Younger Dryas.

References

Andrade C, Freitas MC, Moreno J, Craveiro SC (2004) Stratigraphical evidence of Late Holocene barrier breaching and extreme storms in lagoonal sediments of Ria Formosa, Algarve, Portugal. Mar Geol 210:339–362

Andrade C, Tigo RN, Freitas MC, Gallego MC, Borges P, Ramos AM (2008) Comparing historic records of storm frequency and the North Atlantic Oscillation (NAO) chronology for the Azores region. Holocene 18:745–754

Anthony EJ (2008) Shore processes and their palaeoenvironmental applications. Developments in Marine Geology 4:1–519

Baines G, Beveridge P, Maragos J (1974) Storms and island building at Funafuti Atoll, Ellice Islands. Proc 2nd Int Coral Reef Symp 2:485–496

Barredo JI (2010) No upward trend in normalised windstorm losses in Europe: 1970–2008. Nat Hazards Earth Syst Sci 10:97–104

Benner R, Browne T, Brückner H, Kelletat D, Scheffers A (2010) Boulder transport by waves: progress in physical modelling. Z Geomorphol 53(SI 3):127–146

Besonen MR, Bradley RS, Mudelsee M, Abbott MB, Francus P (2008) A 1,000-year, annually-resolved record of hurricane activity from Boston, Massachusetts. Geophys Res Lett 35: L14705

Betts NL, Orford JD, White D, Graham CJ (2004) Storminess and surges in the South-Western Approaches of the eastern North Atlantic: the synoptic climatology of recent extreme coastal storms. Mar Geol 210:227–246

Beven JL, Avila LA, Blake ES, Brown DP, Franklin JL, Knabb RD, Pasch RJ, Rhome JR, Stewart SR (2008) Atlantic hurricane season of 2005. Mon Weather Rev 136:1109–1173

Brückner H, Schellmann G (2003) Late Pleistocene and Holocene shorelines of Andréeland, Spitsbergen (Svalbard): geomorphological evidence and palaeo-oceanographic significance. J Coast Res 19:971–982

Buynevich IV, FitzGerald DM, Goble RJ (2007) A 1500 yr record of North Atlantic storm activity based on optically dated relict beach scarps. Geology 35:543–546

Callaghan J, Shepherd I, Burton A (2007) Priorities for climate change research linked to tropical cyclones: regional perspectives. In: Power S, Pearce K (eds) Tropical cyclones in a changing climate: research priorities for Australia. Abstracts and recommendations from a workshop held on 8 December 2006 at the Bureau of Meteorology in Melbourne. BMRC research report 131:33–37

Camargo SJ, Sobel AH (2005) Western North Pacific tropical cyclone intensity and ENSO. J Clim 18:2996–3006

Carter RWG, Orford JD (1984) Coarse clastic barrier beaches: a discussion of the distinctive dynamic and morphosedimentary characteristics. Mar Geol 60:377–389

Cechet B, Arthur C (2007) Impact of tropical cyclones on Australia. In: Power S, Pearce K (eds) Tropical cyclones in a changing climate: research priorities for Australia. Abstracts and recommendations from a workshop held on 8 December 2006 at the Bureau of Meteorology in Melbourne. BMRC research report 131:17–20

Chang EKM, Guo Y (2007) Is the number of North Atlantic tropical cyclones significantly underestimated prior to the availability of satellite observations? Geophys Res Lett 34:L14801

Chenoweth M (2007) Objective classification of historical tropical cyclone intensity. J Geophys Res-Atmos 112:D05101

Cheung KF, Tang L, Donnelly JP, Scileppi EM, Liu K-B, Mao X-Z, Houston SH, Murname RJ (2007) Numerical modelling and field evidence of coastal overwash in southern New England from hurricane Bob and implications for palaeotempestology. J Geophys Res-Earth 112: F03024

Clarke ML, Rendell HM (2009) The impact of North Atlantic storminess on western European coasts: a review. Quat Int 195:31–41

Clemmensen L, Richardt N, Andersen C (2001) Holocene sea-level variation and spit development: data from Skagen Odde, Denmark. Holocene 11:323–331

Costa PJM, Andrade C, Freitas MC, Oliveira MA, da Silva CM, Omira R, Taborda R, Baptista MA, Dawson AG (2011) Boulder deposition during major tsunami events. Earth Surf Proc Land 36:2054–2068

Dando WA (2005) Asia, climates of Siberia, Central and East Asia. In: Oliver JE (ed) Encyclopedia of world climatology. Springer, Dordrecht

Dawson A (1996) The geological significance of tsunamis. Z Geomorphol NF Suppl 102:199–210

Dawson A, Elliott L, Noone S, Hickey K, Holt T, Wadhams P, Foster I (2004) Historical storminess and climate 'see-saws' in the North Atlantic region. Mar Geol 210:247–259

Deicke M, Karius V, Jahnke W, Kallweit W, Rebens M, Reyer D (2007) Charakterisierung von Sturmflutablagerungen auf Hallig Hooge – Quantifizierung des Sedimentwachstums seit 1914. In: Gönnert G, Pflüger B, Bremer J-A (eds) Von der Geoarchäologie über die Küstendynamik zum Küstenzonenmanagement. Proceedings of the 25th Annual Meeting of the German Working Group on Geography of Oceans and Coasts, 26–28 April 2007, Hamburg. Coastline Reports 9:93–102

Donat MG, Leckebusch GC, Pinto JG, Ulbrich U (2009) Examination of wind storms over Central Europe with respect to circulation weather types and NAO phases. Int J Climatol 30:1289–1300

Donnelly JP, Woodruff JD (2007) Intense hurricane activity over the past 5000 years controlled by El Nino and the West African monsoon. Nature 447:465–468

Donnelly JP, Butler J, Roll S, Wengren M, Webb T III (2004) A backbarrier overwash record of intense storms from Brigantine, New Jersey. Mar Geol 210:107–121

Elsner JB (2006) Evidence in support of the climate change-Atlantic hurricane hypothesis. Geophys Res Lett 33:L16705

Elsner JB, Jagger TH, Liu K-B (2008) Comparison of hurricane return levels using historical and geological records. J Appl Meteorol Clim 47:368–374

Emanuel K (2005) Increasing destructiveness of tropical cyclones over the past 30 years. Nature 436:686–688

Engel M, Brückner H (2011) The identification of palaeo-tsunami deposits – a major challenge in coastal sedimentary research. In: Karius V, Hadler H, Deicke M, von Eynatten H, Brückner H, Vött A (eds) Dynamische Küsten – Grundlagen, Zusammenhänge und Auswirkungen im Spiegel angewandter Küstenforschung. Proceedings of the 28th Annual Meeting of the German

Working Group on Geography of Oceans and Coasts, 22–25 April 2010, Hallig Hooge. Coastline Reports 17:65–80
Engel M, May SM (2012) Bonaire's boulder fields revisited: evidence for Holocene tsunami impact on the Leeward Antilles. Quat Sci Rev. doi:10.1016/j.quascirev.2011.12.011
Evan AT, Dunion J, Foley JA, Heidinger AK, Velden CS (2006) New evidence for a relationship between Atlantic tropical cyclone activity and African dust outbreaks. Geophys Res Lett 33: L19813
Frappier AB, Sahagian D, Gonzalez LA, Frappier BR (2007) Stalagmite stable isotope record of recent tropical cyclone events. Geology 35:111–114
Frohlich C, Hornbach MJ, Taylor FW, Shen C-C, Moala 'A, Morton AE, Kruger J (2009) Huge erratic boulders in Tonga deposited by a prehistoric tsunami. Geology 37:131–134
Gadd AJ, Hall CD, Kruze RE (1990) Operational numerical prediction of rapid cyclogenesis over the North Atlantic. Tellus 42A:116–121
Garcia-Herrera R, Gimeno L, Ribera P, Hernandez E, Gonzalez E, Fernandez G (2007) Identification of Caribbean hurricanes from Spanish documentary sources. Clim Change 83:55–85
Giry C, Felis T, Koelling M, Scholz D, Wei W, Lohmann G, Scheffers S (2012) Mid- to late Holocene changes in tropical Atlantic temperature seasonality and interannual to multidecadal variability documented in southern Caribbean corals. Earth Planet Sci Lett 331–332:187–200
Goff JR, Lane E, Arnold J (2009) The tsunami geomorphology of coastal dunes. Nat Hazards Earth Syst Sci 9:847–854
Goodbred SL, Hine AC (1995) Coastal storm deposition: salt-marsh response to a severe extratropical storm, March 1993, West-Central Florida. Geology 23:679–682
Harvey N (2006) Holocene coastal evolution: barriers, beach ridges, and tidal flats of South Australia. J Coast Res 22:90–99
Hayes MO, Michel J, Betenbaugh DV (2010) The intermittently exposed, coarse-grained gravel beaches of Prince William Sound, Alaska: comparison with open-ocean gravel beaches. J Coast Res 26:4–30
Hayne M, Chappell J (2001) Cyclone frequency during the last 5000 years on Curacoa Island, north Queensland, Australia. Palaeogeogr Palaeocl 168:207–219
Hetzinger S, Pfeiffer M, Dullo W-C, Keenlyside N, Latif M, Zinke J (2008) Caribbean coral tracks Atlantic Multidecadal Oscillation and past hurricane activity. Geology 36:11–14
Hippensteel SP (2008) Preservation potential of storm deposits in back-barrier marshes. J Coast Res 24:594–601
Hippensteel SP (2010) Paleotempestology and the pursuit of the perfect paleostorm proxy. GSA Today 20:52–53
Hippensteel SP, Martin RE (1999) Foraminifera as an indicator of overwash deposits, barrier island sediment supply, and barrier island evolution, Folly Island, South Carolina. Palaeogeogr Palaeocl 149:115–125
Hoarau K (2000) Supertyphoon forrest (September 1983): The overlooked record holder of intensification in 24, 36, and 48 h. Weather Forecast 15:357–360
Hobgood J (2005) Tropical cyclones. In: Oliver JE (ed) Encyclopedia of world climatology. Springer, Dordrecht
Hoyos CD, Agudelo PA, Webster PJ, Curry JA (2006) Deconvolution of the factors contributing to the increase in global hurricane intensity. Science 312:94–97
Huang Y (2009) Sediment record of modern and prehistoric hurricane strikes in Weeks Bay, Alabama. MS thesis, Louisiana State University, Baton Rouge
Hughes TP, Connell JH (1999) Multiple stressors on coral reefs: a long term perspective. Limnol Oceanogr 44:932–940
Hughes TP, Baird AH, Bellwood DR, Card M, Connolly SR, Folke C, Grosberg R, Hoegh-Guldberg O, Jackson JBC, Kleypas J, Lough JM, Marshall P, Nyström M, Palumbi SR, Pandolfi JM, Rosen B, Roughgarden J (2003) Climate change, human impacts, and the resilience of coral reefs. Science 301:929–933
Jansen E, Overpeck J, Briffa KR, Duplessy J-C, Joos F, Masson-Delmotte V, Olago D, Otto-Bliesner B, Peltier WR, Rahmstorf S, Ramesh R, Raynaud D, Rind D, Solomina O, Villalba R, Zhang D (2007) Palaeoclimate. In: Solomon S, Qin D, Manning M, Chen Z, Marquis M,

Averyt KB, Tignor M, Miller HL (eds) Climate change 2007: the physical science basis. Cambridge University Press, Cambridge
Kafatos M, Sun D, Gautam R, Boybeyi Z, Yang R, Cervone G (2006) Role of anomalous warm gulf waters in the intensification of Hurricane Katrina. Geophys Res Lett 33:L17802
Keim BD, Robbins KD (2006) Occurrence dates of North Atlantic tropical storms and hurricanes: 2005 in perspective. Geophys Res Lett 33:L21706
Kelletat D (1985) Studien zur spät- und postglazialen Küstenentwicklung der Varanger-Halbinsel, Nord-Norwegen. Essener Geographische Arbeiten 10:1–111
Kiage LM, Deocampo D, McCloskey TA, Bianchette TA, Hursey M (2011) A 1900-year paleohurricane record from Wassaw Island, Georgia, USA. J Quat Sci 26:714–722
Klotzbach PJ (2006) Trends in global tropical cyclone activity over the past twenty years (1986–2005). Geophys Res Lett 33:L10805
Knapp KR, Kruk MC, Levinson DH, Diamond HJ, Neumann CJ (2010) The International Best Track Archive for Climate Stewardship (IBTrACS): unifying tropical cyclone best track data. Bull Am Meteorol Soc 91:363–376
Knutson TR, Sirutis JJ, Garner ST, Vecchi GA, Held IM (2008) Simulated reduction in Atlantic hurricane frequency under twenty-first-century warming conditions. Nat Geosci 1:359–364
Knutson TR, McBride JL, Chan J, Emanuel K, Holland G, Landsea C, Kossin JP, Srivastava AK, Sugi M (2010) Tropical cyclones and climate change. Nat Geosci 3:157–163
Kortekaas S, Dawson AG (2007) Distinguishing tsunami and storm deposits: an example from Martinhal, SW Portugal. Sediment Geol 200:208–221
Kraus NC (2003) Analytical model of incipient breaching of coastal barriers. Coast Eng J 45:511–531
Kunte P, Wagle B (2005) The beach ridges of India: a review. J Coast Res 42:174–183
Lamb HH (1991) Historic storms of the north sea, British Isles and Northwest Europe. Cambridge University Press, Cambridge
Lambert SJ (1996) Intense extratropical northern hemisphere winter cyclone events: 1899–1991. J Geophys Res 101:21319–21325
Lambert WJ, Aharon P, Rodriguez AB (2008) Catastrophic hurricane history revealed by organic geochemical proxies in coastal lake sediments: a case study of Lake Shelby, Alabama (USA). J Paleolimnol 39:117–131
Landsea CW (2007) Counting Atlantic tropical cyclones back to 1900. Eos 88:197–202
Landsea CW, Harper BA, Hoarau K, Knaff JA (2006) Can we detect trends in extreme tropical cyclones? Science 313:452–454
Lawrence JR, Gedzelman SD (1996) Low stable isotope ratios of tropical cyclone rains. Geophys Res Lett 23:527–530
Li F, Roncevich L, Bicknell C, Lowry R, Ilich K (2011) Interannual variability and trends of storminess, Perth, 1994–2008. J Coast Res 27:738–745
Liu K-B (2004) Palaeotempestology: principles, methods, and examples from Gulf Coast Lake sediments. In: Murname RJ, Liu K-B (eds) Hurricanes and typhoons: past, present and future. Columbia University Press, New York
Liu K-B, Fearn ML (1993) Lake-sediment record of late Holocene hurricane activities from coastal Alabama. Geology 21:793–796
Liu K-B, Fearn ML (2000) Reconstruction of prehistoric landfall frequencies of catastrophic hurricanes in northwestern Florida from lake sediment records. Quat Res 54:238–245
Liu K, Lu H, Shen C (2009) Some fundamental misconceptions about paleotempestology. Quat Res 71:253–254
Lockwood JG (2005) Atmospheric circulation, global. In: Oliver JE (ed) Encyclopedia of world climatology. Springer, Dordrecht
Madsen AT, Duller GAT, Donnelly JP, Roberts HM, Wintle AG (2009) A chronology of hurricane landfalls at Little Sippewissett Marsh, Massachusetts, USA, using optical dating. Geomorphology 109:36–45
Malmquist DL (1997) Oxygen isotopes in cave stalagmites as a proxy record of past tropical cyclone activity. In: Preprints of the 22nd conference on hurricanes and tropical meteorology. American Meteorological Society, Boston

Mann ME, Emanuel KA (2006) Atlantic hurricane trends linked to climate change. Eos 87:233–244
Mann ME, EmanuelKA HGJ, Webster PJ (2007) Atlantic tropical cyclones revisited. Eos 88:349–350
Matias A, Ferreira Ó, Vila-Concejo A, Garcia T, Alveirinho Dias J (2008) Classification of washover dynamics in barrier islands. Geomorphology 97:655–674
May SM, Vött A, Brückner H, Smedile A (in press) The Gyra washover fan in the Lefkada Lagoon, NW Greece – possible evidence of the 365 AD Crete earthquake and tsunami. Earth Planets Space
McCloskey TA, Keller G (2009) 5000 year sedimentary record of hurricane strikes on the central coast of Belize. Quat Int 195:53–68
McCloskey TA, Knowles JT (2008) Migration of the tropical cyclone zone throughout the Holocene. In: Elsner JB, Jagger TH (eds) Hurricanes and climate change. Springer, New York
Michaels PJ, Knappenberger PC, Davis RE (2006) Sea-surface temperatures and tropical cyclones in the Atlantic basin. Geophys Res Lett 33:L09708
Miller D, Moro CI, Grissino-Mayer HD, Mock CJ, Uhle ME, Sharp Z (2006) Tree-ring isotope records of tropical cyclone activity. Proc Natl Acad Sci USA 103:14294–14297
Missimer T (1973) Growth rates of beach ridges on Sanibel Island, Florida. Gulf Coast Assoc Geol Soc Trans 23:383–388
Morton RA, Gelfenbaum G, Jaffe BE (2007) Physical criteria for distinguishing sandy tsunami and storm deposits using modern examples. Sediment Geol 200:184–207
Mumby PJ, Vitolo R, Stephenson DB (2011) Temporal clustering of tropical cyclones and its ecosystem impacts. Proc Natl Acad Sci USA 108:17626–17630
Nielsen A, Murray A, Pejrup M, Elberling B (2006) Optically stimulated luminescence dating of a Holocene beach ridge plain in Northern Jutland, Denmark. Quat Geochronol 1:305–312
Nott J (2009) Long-term natural variability of tropical cyclones in Australia. In: Elsner JB and Jagger TH (eds) Hurricanes and Climate Change. Springer, Dordrecht
Nott J (2011) A 6000 year tropical cyclone record from Western Australia. Quat Sci Rev 30:713–722
Nott J, Hayne M (2001) High frequency of 'super-cyclones' along the Great Barrier Reef over the past 5,000 years. Nature 413:508–512
Nott J, Haig J, Neil H, Gillieson D (2007) Greater frequency variability of landfalling tropical cyclones at centennial compared to seasonal and decadal scales. Earth Planet Sci Lett 255:367–372
Nott J, Smithers S, Walsh K, Rhodes E (2009) Sand beach ridges record 6000 year history of extreme tropical cyclone activity in northeastern Australia. Quat Sci Rev 28:1511–1520
Nyberg J, Malmgren BA, Winter A, Jury MR, Kilbourne KH, Quinn TM (2007) Low Atlantic hurricane activity in the 1970s and 1980s compared to the past 270 years. Nature 447:698–702
Osborn TJ (2011) Winter 2009/2010 temperatures and a record-breaking North Atlantic Oscillation index. Weather 66:19–21
Otvos EG (2011) Hurricane signatures and landforms – toward improved interpretations and global storm climate chronology. Sediment Geol 239:10–22
Peltier WR (2002) On eustatic sea level history: last glacial maximum to Holocene. Quat Sci Rev 21:377–396
Pirazzoli PA (1991) World atlas of Holocene sea-level changes. Elsevier Oceanogr Ser 58:1–300
Power S, Pearce K (eds) (2007) Tropical cyclones in a changing climate: research priorities for Australia. Abstracts and recommendations from a workshop held on 8 December 2006 at the Bureau of Meteorology in Melbourne. BMRC Research Report 131
Rink WJ, Forrest B (2005) Dating evidence for the accretion history of beach ridges on Cape Canaveral and Merritt Island, Florida, USA. J Coast Res 21:1000–1008
Sanjaume E, Tolgensbakk J (2009) Beach ridges from the Varanger Peninsula (Arctic Norwegian coast): characteristics and significance. Geomorphology 104:82–92

Santer BD, Wigley TML, Gleckler PJ, Bonfils C, Wehner MF, Achuta Rao K, Barnett TP, Boyle JS, Brüggemann W, Fiorino M, Gillett N, Hansen JE, Jones PD, Klein SA, Meehl GA, Raper SCB, Reynolds RW, Taylor KE, Washington WM (2006) Forced and unforced ocean temperature changes in Atlantic and Pacific tropical cyclogenesis regions. Proc Natl Acad Sci USA 103:13905–13910

Saunders MA, Lea AS (2008) Large contribution of sea surface warming to recent increase in Atlantic hurricane activity. Nature 451:557–561

Scheffers A (2005) Coastal response to extreme wave events: hurricanes and tsunami on Bonaire. Essener Geographische Arbeiten 37:1–96

Scheffers A, Scheffers S (2006) Documentation of the impact of Hurricane Ivan on the coastline of Bonaire (Netherlands Antilles). J Coast Res 22:1437–1450

Scheffers SR, Haviser J, Browne T, Scheffers A (2009a) Tsunamis, hurricanes, the demise of coral reefs and shifts in prehistoric human population in the Caribbean. Quat Int 195:69–87

Scheffers SR, Scheffers A, Kelletat D (2009b) Severe storms drive Holocene island evolution and coral reef biodiversity of the Houtman Abrolhos Archipelago. WA IOP C Ser Earth Environ 6:072056

Scheffers A, Scheffers SR, Kelletat D, Haslett S (2010) Coastal boulder deposits at Galway Bay and the Aran Islands, Western Ireland. Z Geomorphol 54(SI 3):247–279

Scheffers A, Engel M, Squire P, Kelletat D, Scheffers S (2012a) Beach ridge systems – archives for Holocene coastal events? Prog Phys Geogr 36:5–37

Scheffers A, Scheffers SR, Kelletat D, Squire P, Collins L, Feng Y, Zhao J, Joannes-Boyau R, Schellmann G, Freeman H, May SM (2012b) Coarse clast beach ridge sequences as suitable archives for past storm events? Case Study on the Houtman Abrolhos, Western Australia. J Quat Sci doi:10.1002/jqs.2558

Schellmann G, Radtke U (2010) Timing and magnitude of Holocene sea-level changes along the middle and south Patagonian Atlantic coast derived from beach ridge systems, littoral terraces and valley-mouth terraces. Earth Sci Rev 103:1–30

Schellmann G, Radtke U, Brückner H (2011) Electron Spin Resonance Dating (ESR). In: Hopley D (ed) Encyclopedia of modern coral reefs: structure, form and process; Part 5. Springer, New York

Schwartz RK (1982) Bedform and stratification characteristics of some modern small-scale washover sand bodies. Sedimentology 29:835–849

Scott DB, Collins ES, Gayes PT, Wright E (2003) Records of prehistoric hurricanes on the South Carolina coast based on micropaleontological and sedimentological evidence, with comparison to other Atlantic Coast records. Bull Geol Soc Am 115:1027–1039

Sedgwick PE, Davis RA (2003) Stratigraphy of washover deposits in Florida: implications for recognition in the stratigraphic record. Mar Geol 200:31–48

Shanmugan G (2011) Process-sedimentological challenges in distinguishing paleo-tsunami deposits. Nat Hazards. doi:10.1007/s11069-011-9766-z

Slott JM, Murray AB, Ashton AD, Crowley TJ (2006) Coastline responses to changing storm patterns. Geophys Res Lett 33:L18404

Sriver R, Huber M (2006) Low frequency variability in globally integrated tropical cyclone power dissipation. Geophys Res Lett 33:L11705

Stapor FW, Tanner WF (1977) Late Holocene mean sea-level data from St. Vincent Island, and the shape of the late Holocene sea-level curve. In: Tanner WF (ed) Coastal Sedimentology. Proceedings of the 3rd Symposium on Coastal Sedimentology, Tallahassee, Florida State University

Stone GW, Liu B, Pepper DA, Wang P (2004) The importance of extratropical and tropical cyclones on the short-term evolution of barrier islands along the northern Gulf of Mexico, USA. Mar Geol 210:63–78

Switzer AD, Jones BG (2008) Setup, deposition, and sedimentary characteristics of two storm overwash deposits, Abrahams Bosom Beach, Southeastern Australia. J Coast Res 24 (1A):189–200

Switzer AD, Pucillo K, Haredy RA, Jones BG, Bryant EA (2005) Sea level, storm or tsunami: enigmatic sand sheet deposits in a sheltered coastal embayment from southeastern New South Wales, Australia. J Coast Res 21:655–663

Tanner W (1995) Origin of beach ridges and swales. Mar Geol 129:149–161
Taylor M, Stone GW (1996) Beach-ridges: a review. J Coast Res 12:612–621
Trenberth KE, Shea DJ (2006) Atlantic hurricanes and natural variability in 2005. Geophys Res Lett 33:L12704
Trewin B (2007) Tropical cyclone re-analysis. In: Power S, Pearce K (eds) Tropical cyclones in a changing climate: research priorities for Australia. Abstracts and recommendations from a workshop held on 8 December 2006 at the Bureau of Meteorology in Melbourne. BMRC research report 131:23–24
Trouet V, Scourse JD, Raible CC (2012) North Atlantic storminess and Atlantic meridional overturning circulation during the last millennium: reconciling contradictory proxy records of NAO variability. Global Planet Change 84–85:48–55
Tuttle MP, Ruffman A, Anderson T, Jeter H (2004) Distinguishing tsunami from storm deposits in Eastern North America: the 1929 Grand Banks tsunami versus the 1991 Halloween storm. Seismol Res Lett 75:117–131
Uchida J-I, Fujiwara O, Hasegawa S, Kamataki T (2010) Sources and depositional processes of tsunami deposits: analysis using foraminiferal tests and hydrodynamic verification. Isl Arc 19:427–442
Ulbrich U, Christoph M (1999) A shift of the NAO and increasing storm track activity over Europe due to anthropogenic greenhouse gas forcing. Clim Dyn 15:551–559
Wallace DJ, Anderson JB (2010) Evidence of similar probability of intense hurricane strikes for the Gulf of Mexico over the late Holocene. Geology 38:511–514
Wang P, Horwitz MH (2007) Erosional and depositional characteristics of regional overwash deposits caused by multiple hurricanes. Sedimentology 54:545–564
Wang C, Lee S-K (2008) Global warming and United States landfalling hurricanes. Geophys Res Lett 35:L02708
Webster PJ, Holland GJ, Curry JA, Chang H-R (2005) Changes in tropical cyclone number, duration, and intensity in a warming environment. Science 309:1844–1846
Wehrli A, Sauri D, Herkendell J (2010) Storms. In: European Environment Agency (ed) Mapping the impacts of natural hazards and technological accidents in Europe. EEA Technical report 13/2010:33–40
Weisse R, von Storch H, Feser F (2005) Northeast Atlantic and North Sea storminess as simulated by a regional climate model during 1958–2001 and comparison with observations. J Clim 18:465–479
Williams HFL (2011) Stratigraphic record of hurricanes Audrey, Rita and Ike in the Chenier plain of southwest Louisiana. J Coast Res SI 64:1921–1926
Woodruff JD, Donnelly JP, Mohrig D, Geyer WR (2008) Reconstructing relative flooding intensities responsible for hurricane-induced deposits from Laguna Playa Grande, Vieques, Puerto Rico. Geology 36:391–394
Yu KF, Zhao JX, Collerson KD, Shi Q, Chen TG, Wang PX, Liu TS (2004) Storm cycles in the last millennium recorded in Yongshu Reef, southern South China Sea. Palaeogeogr Palaeocl 210:89–100
Yu KF, Wang PX, Shi Q, Meng QS, Collerson KD, Liu TS (2006) High-precision TIMS U-series and AMS ^{14}C dating of a coral reef lagoon sediment core from southern China Sea. Quat Sci Rev 25:2420–2430
Yu KF, Zhao J, Shi Q, Meng Q (2009) Reconstruction of storm/tsunami records over the last 4000 years using transported coral blocks and lagoon sediments in the southern South China Sea. Quat Int 195:128–137
Zhao JX, Neil DT, Feng YX, Yu KF, Pandolfi JM (2009) High-precision U-series dating of very young cyclone-transported coral reef blocks from Heron and Wistari reefs, southern Great Barrier Reef, Australia. Quat Int 195:122–127

Chapter 21
U.S. Pacific Northwest Coastal Hazards: Tectonic and Climate Controls

Paul D. Komar, Jonathan C. Allan, and Peter Ruggiero

Abstract The coast of the U.S. Pacific Northwest (PNW), the ocean shores of Washington, Oregon and Northern California, experience property impacts ranging from the erosion and flooding that occur during the hours to days of an extreme winter storm, on a decadal time scale with the erosion processes enhanced by strong El Niños, and with the expectation of future increased hazards associated with the global rise in sea level and the possibility that storm intensities and their generated waves will continue in the future. The PNW is noted for its extreme waves, with measured significant wave heights during winter storms having reached 15 m, combining with tides elevated by a surge to erode both foredunes and sea cliffs. The beach morphology plays an important role, particularly rip current embayments that act to localize the sites of maximum property impacts. Of concern, wave buoy measurements have documented that the storm-generated wave heights have been increasing since at least the 1980s, and research underway has found climate controls on the levels of storm surges. The impacts of rising sea levels are variable along this shore, in that while the entire PNW coast is tectonically rising, the local rate of rise in the land varies in comparison with the eustatic rise in sea level, with some stretches of shore being submergent while others are emergent. Projections of accelerated rates of global sea-level rise indicate that by the end of this century the entire PNW coast will be submergent, experiencing significantly increased hazards from erosion and flooding. In recent decades the most extreme erosion impacts have occurred during strong El Niños, specifically those in 1982–1983 and 1997–1998 when measured tides were elevated by 25–50 cm throughout the winter, caused by warmer water

P.D. Komar (✉) • P. Ruggiero
College of Earth, Oceanic and Atmospheric Sciences, Oregon State University,
Corvallis, OR 97331, USA
e-mail: pdkomar@gmail.com; ruggierp@geo.oregonstate.edu

J.C. Allan
Coastal Field Office, Oregon Department of Geology and Mineral Industries,
P.O. Box 1033, Newport, OR 97365, USA
e-mail: jonathan.allan@dogami.state.or.us

C.W. Finkl (ed.), *Coastal Hazards*, Coastal Research Library 6,

DOI 10.1007/978-94-007-5234-4_21,

temperatures and ocean currents. During those El Niños there was also a diversion of the storm tracks with waves arriving more from the southwest, producing northward displacements of sand on the beaches, resulting in extreme "hot-spot" erosion north of headlands and tidal inlets. With these multiple climate controls on the processes, it is certain that during this century there will be far more erosion and flooding problems along the U.S. PNW than in the past. The ultimate hazard, however, are the predictions by seismologists that there will be another major subduction earthquake like that which occurred on 26 January 1700, with the land along this coast abruptly dropping by 1–2 m, followed minutes later by the arrival of immense tsunami waves, producing devastating impacts comparable to those recently experienced in Sumatra and Japan.

21.1 Introduction

Geographically the Pacific Northwest (PNW) of the United States is generally viewed as consisting of the states of Washington and Oregon, the coastal region mapped in Fig. 21.1. However, as considered in our investigations of this region's coastal hazards, the extent of the PNW is more logically defined in terms its tectonics, a factor of fundamental importance to multiple aspects of the hazards. As diagramed in Fig. 21.2, the ocean shores of Washington, Oregon and Northern California south to Cape Mendocino are encompassed by three of Earth's tectonic plates, the Gorda and Juan de Fuca plates offshore and the large continental North American plate that contains the land mass of the PNW. The ocean plates are moving eastward relative to the land, where they collide with and are being subducted beneath the continental crust, the PNW representing a segment in the "Ring of Fire" that approximately follows the circumference of the Pacific Ocean. In this tectonic setting, destructive earthquakes and tsunami have occurred on the PNW coast in the distant past, most recently on 26 January 1700, with the prospects of a repeat occurrence representing this coast's most extreme potential hazard.

The active tectonics of plate subduction also have significant consequences to progressive changes in the PNW's land elevations, with some stretches of shore tectonically rising faster than the present rate of rise in the global sea-level, producing emergent shores, while along other stretches of this coast the rise in the land is slower than the increase in sea level, the coast being submergent. These contrasting combinations of changing land elevations and global (eustatic) sea levels, determining the local trends and rates in relative sea levels, exert a primary control on whether or not coastal properties are experiencing significant erosion and/or flooding impacts.

The hazards faced by developments along the PNW coast are also governed by various climate controls. Particularly important in recent decades have been occurrences of major El Niños such as those in 1982–1983 and 1997–1998, when the tides and monthly-mean sea levels were elevated by tens of centimeters throughout the winter, permitting the more frequent attack of shore-front properties

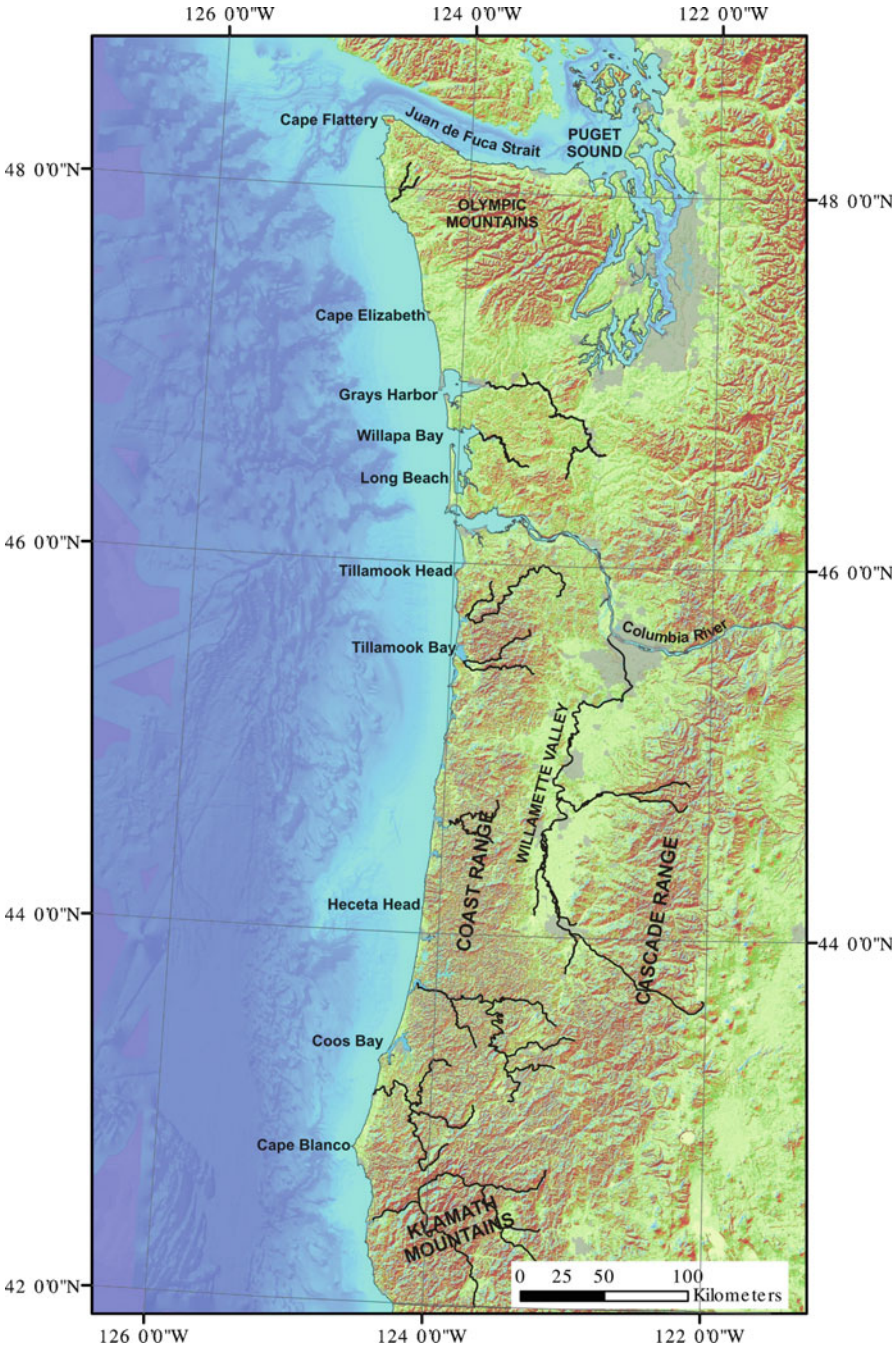

Fig. 21.1 Geography of the PNW coast, the ocean shores of Washington and Oregon

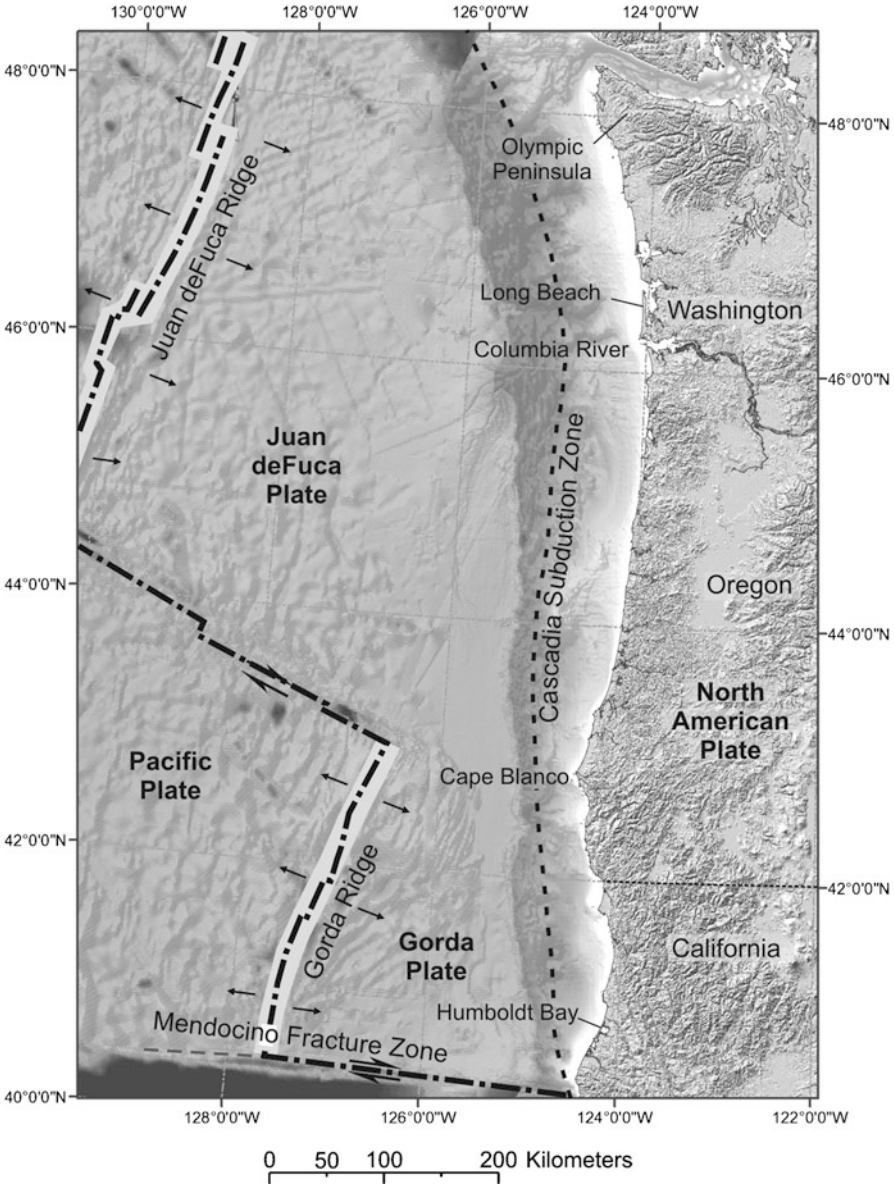

Fig. 21.2 The tectonics of the PNW, the oceanic plates moving eastward where they collide with and are subducted beneath the continent

by the superimposed storm waves. In addition, the tracks of storms and the heights of their generated waves were altered during those El Niños, it being the combined effects of these processes that produced extensive erosion and property damage. There are of course major concerns regarding the prospects of global warming, with

the expectation of there being accelerated rates of rising sea levels during this century. A prospect for the future is that stretches of the PNW coast that are now emergent will revert to being submergent, with significant erosion occurring where it has been minimal in the past, and with far greater impacts occurring along the shores that are already submergent. Furthermore, this coast has experienced multi-decadal increases in storm intensities and the heights of their generated waves, which clearly have been an important climate-induced factor in the enhanced erosion of this coast.

With the expectation of there being accelerated rates of rising sea levels, that storm intensities and wave energies will likely continue to increase, and the certainty that there will be repeat episodes of strong El Niños, the prospect is that the PNW will experience still greater impacts in the future than occurred during the twentieth century. There is also the prospect of another major subduction earthquake and tsunami during the next 100 years, a repeat of the event that last struck this coast 300 years ago, an occurrence that would be comparable to the March 2011 earthquake and tsunami that devastated the Pacific shores of Japan. The objective of this chapter is to examine this range of potential hazards faced by communities along the PNW coast of the United States.

21.2 Geology, Coastal Morphology, and Beach Sediments

As a result of its active tectonic setting, the geology of the PNW coast contains both resistant volcanic rocks (basalts) and more easily eroded sedimentary deposits (Tertiary marine siltstones, and Pleistocene sandstones that are uplifted beach and dune sands). The result is a highly variable topography, including alternating stretches of rocky shores containing large headlands, contrasting with stretches of sand beaches backed by sea cliffs eroded into the less resistant sedimentary rocks, or backed by extensive fields of dunes where land elevations are low (Komar 1997). These characteristics are illustrated in Fig. 21.3 for the Oregon coast, showing Siletz Spit covered with dunes and developed with expensive homes, and the sea cliffs that otherwise dominate this stretch of shore. A number of large bays and estuaries of rivers that originate in the low mountains of the Coast Range are found along this coast, bodies of water that generally are separated from the ocean by sand spits; Siletz Bay in Fig. 21.3 is a typical example. The Columbia River forms the boarder between Washington and Oregon, the largest river on the U.S. west coast in terms of its drainage area and flow discharges. The Long Beach Peninsula extends to the north of the river's mouth, Fig. 21.4, a sand spit of barrier-island scale that constitutes nearly half of the ocean shore of Washington, separating the large expanse of Willapa Bay from the ocean. At the north end of Washington's ocean shore is the glacially carved Strait of Juan de Fuca, which extends inland to Puget Sound (not considered in this chapter).

With the PNW having alternating stretches of resistant rocky shores versus those backed by more easily eroded sedimentary formations, the coast consists of a series

Fig. 21.3 Siletz Spit and Bay within the Lincoln City Littoral Cell on the northern Oregon coast, while to its north and south the beach is backed by high cliffs composed of coarse-grained Pleistocene marine-terrace sands (Photo P.D. Komar)

of *littoral cells*, stretches of beach within embayments that are confined by bounding rocky headlands. The example in Fig. 21.3 is the central portion of the Lincoln City Littoral Cell on the mid-Oregon coast, containing Siletz Spit but with the beach otherwise backed by sea cliffs cut into Pleistocene uplifted marine-terrace sandstones, the erosion of which is the principal source of sand to the beach. Along the Oregon coast each stretch of shore within a littoral cell is in effect a pocket beach, with its sand generally unable to pass around the headlands that extend well offshore into deep water (Komar 1997). The cells range widely in their along-coast lengths, from a few kilometers to tens of kilometers, governed by the distances between the bounding headlands; the longest is the Coos Littoral Cell that contains the massive Oregon Dunes, the largest field of coastal dunes in the United States. The major headlands and the names of the littoral cells along the Oregon and Washington coasts are identified respectively in Figs. 21.5 and 21.6. In contrast to the isolated pocket-beach character of Oregon's littoral cells, the Washington coast is dominated by the large Columbia River Littoral Cell (CRLC), including the Long Beach Peninsula where there is a net transport of beach sand toward the north, with Point Grenville being the terminating northern boundary of this cell (Gelfenbaum and Kaminsky 2010). Further to the north, beyond the CRLC, the Washington coast is predominantly rocky, containing only relatively small pocket beaches of sand and gravel; this shore is less developed, containing Native American settlements and the coastal portion of the Olympic National Park.

Fig. 21.4 The mouth and north jetty of the Columbia River, and the Long Beach Peninsula on the southwest coast of Washington, part of the Columbia River Littoral Cell

The mineralogies of the beach sands found within the littoral cells along the Oregon coast demonstrate that they have had multiple sources, and that much of this sand is "relict" in having reached the cells, now isolated by headlands, thousands of years ago (Clemens and Komar 1988). This history is most evident for the littoral cells and small pocket beaches that may contain significant quantities of sand but lack any obvious modern-day source for that sand; and equally significant, the mineralogy of the beach sand has an identifiable distant source. Those potential sources of beach sand were identified in our investigation of the beach-sand mineralogies along the entire Oregon coast, as well as the heavy minerals found in rivers that might have been sources of the sand. Geologically three regional source terrains were identified, summarized in Fig. 21.7 in terms of their inland

Fig. 21.5 The major headlands defining the principal littoral cells along the Oregon coast

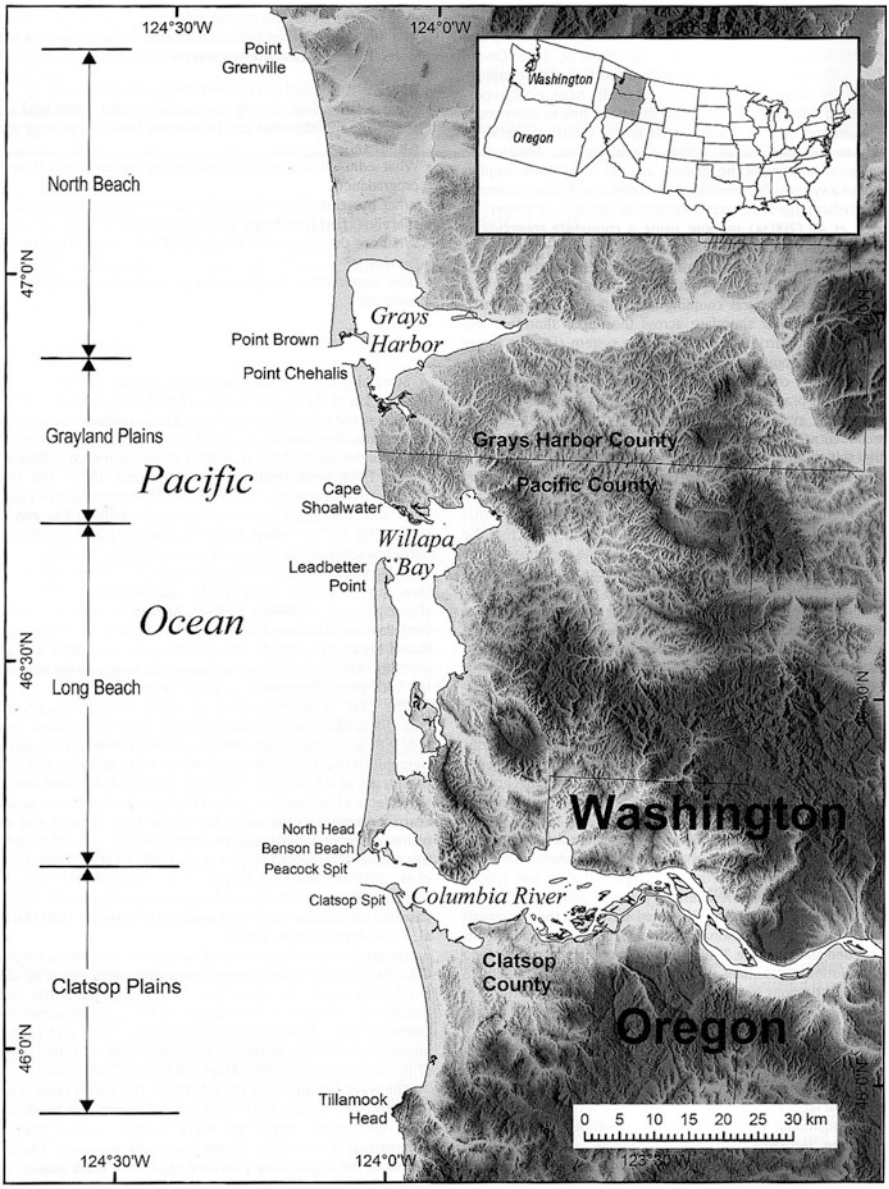

Fig. 21.6 The Columbia River Littoral Cell and its series of sub-cells on the southwest coast of Washington (From Kaminsky et al. (2010b))

rocks and the resulting suites of heavy minerals contained in the beach sands. Most distinctive are the heavy minerals derived from the Klamath Mountains in southern Oregon and northern California, where the rocks are predominantly metamorphic;

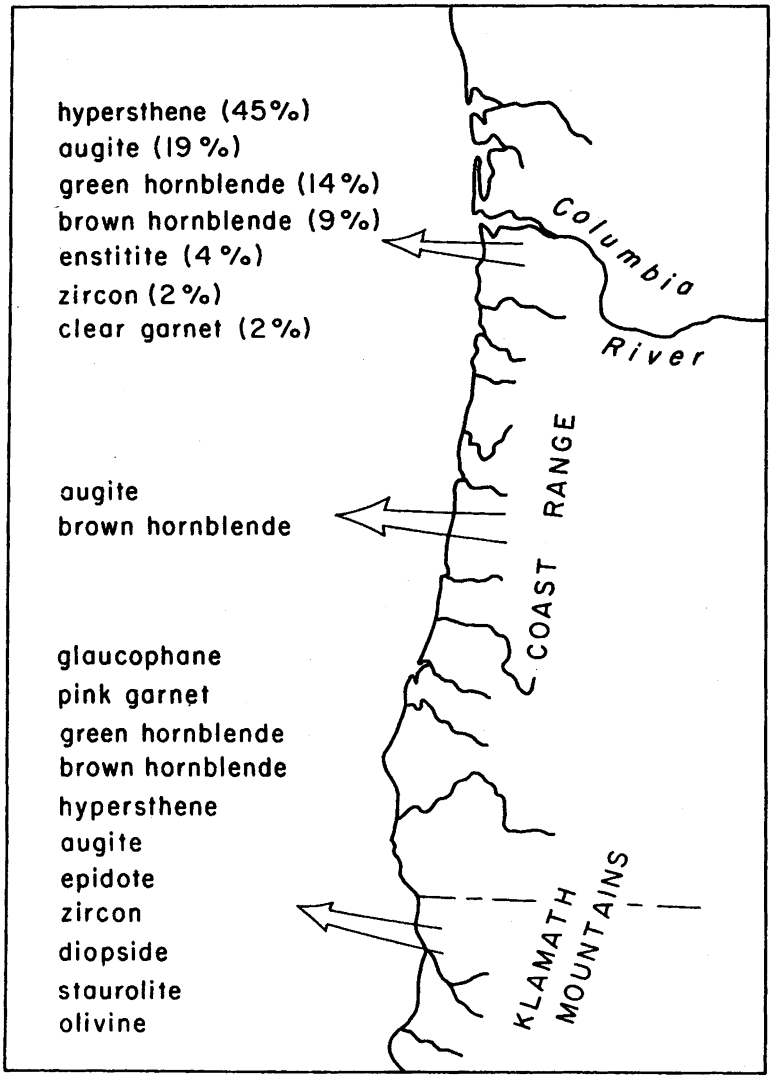

Fig. 21.7 Source-rock terrains that have supplied sand to Oregon's beaches, and the heavy minerals identify those sources (From Clemens and Komar (1988))

the rivers and beaches in that region contain a distinctive pink garnet, glaucophane, staurolite, epidote, zircon, hornblende, hypersthene, and other minerals that have metamorphic-rock origins. In contrast, the rivers that drain the Coast Range mountains to the north generally contribute sand that contains only two heavy minerals, dark-green augite and a small amount of brown hornblende, derived from the volcanic rocks that originated offshore and were later accreted to the Coast Range during subduction of the ocean plates. The Columbia River is the third

potential source of sand (Fig. 21.7); that river drains a vast area containing many types of rocks, reflected in the diversity of its heavy minerals. As expected, its mineralogy completely dominates the beaches of the CRLC to the north of the river's mouth along the Washington coast, and also to the south on the Oregon coast but only as far as the community of Seaside, with Tillamook Head preventing further movement of the modern-day riverine sand along the Oregon coast.

The heavy-mineral contents of a large number of beach-sand samples collected along the length of the Oregon coast were determined microscopically, and their percentage variations were subjected to the factor-analysis statistical technique to determine the "end-member" suites of minerals that when mixed could account for the spatial variations found along this coast (Clemens and Komar 1988). That analysis was successful in that the compositions of the three principal components correspond closely to the mineralogies of the three source terrains identified in Fig. 21.7, such that their proportions within an individual beach-sand sample provided a measure of the contributions from those respective sources. Of interest, it was found that the Klamath Mountain minerals comprise significant proportions of the beach sands far to the north of that mountain source, the pink garnet in particular being prominent visually in the black-sand deposits that form on those beaches when the heavy minerals are concentrated during winter storms (Komar and Wang 1984). With the large number of prominent headlands along the Oregon coast now preventing the existence of a net northward longshore transport of the beach sands, it was concluded that the presence of these minerals far to the north of their Klamath source could only be accounted for by the existence of a net longshore transport during low stands of sea levels, thousands of years ago when that movement was not hindered by headlands (Clemens and Komar 1988). The heavy-mineral contents of the continental shelf sands confirmed the occurrence of a northward net transport during the Pleistocene lower stands of sea levels. With the rise in sea level beginning about 20,000 years ago, sand on the shelf would have been carried shoreward by the waves, until about 7,000 years ago it reached the bounding headlands, having become trapped on the beaches within Oregon's littoral cells.

Analyses of the beach-sand mineralogies demonstrated that as the Klamath-derived sand was transported to the north during low stands of sea levels, it was diluted by sand eroded from the Coast Range mountains such that its heavy minerals became dominant, as found both in the shelf sands and in the present-day beaches along most of the length of the Oregon coast, even though Klamath-derived minerals still constitute a significant portion of the beach sands. There may have been some addition of river-derived Coast Range sand during the past few thousand years since the beaches became isolated within the series of littoral cells, although there is evidence that flooding of the estuaries occurred as the sea rose to its present level, acting to trap the riverine sand so it no longer reaches the ocean shores. It is observed that the smaller littoral cells, lacking any modern-day river source, tend to be richest in Klamath Mountain minerals, but have only small buffering beaches and hence experience more problems with property erosion (e.g., the Beverly Beach Littoral Cell north of Newport on the mid-Oregon coast).

The Columbia River heavy minerals make their appearance in small percentages in the beach sands along the northern Oregon coast south of Tillamook Head, but jump to 100% in the beach sand to the north of that headland were it has continued to be supplied by that river, being the southern portion of the CRLC. Of interest, microscopic analyses of the roundness of the mineral grains documented a marked difference north and south of Tillamook Head, with the grains to the north being highly angular with sharp edges, evidence for its recent contribution by the Columbia River, whereas in the beaches to the south of that headland the mineral grains are well rounded, having resided in the beaches for thousands of years since they arrived during lower stands of sea levels (Clemens and Komar 1988).

A expected, the shores of the Long Beach Peninsula to the north of the river and along the remainder of the CRLC shoreline (Fig. 21.6) also consist of essentially 100% Columbia River derived minerals, that river always having been the dominant source. The proportions of the minerals vary, however, as they are selectively sorted according to their differences in densities and grain sizes as they are transported by the waves to the north, being components of the net northward longshore sand transport (Li and Komar 1992). The concentration of heavy minerals in the eroding beach to the immediate north of the river and its jetties has given rise to extensive black-sand deposits (both beach and dunes), with progressive decreases further to the north along the length of the Peninsula. While the Columbia River has clearly been a major volumetric source of sand to the CRLC throughout the Holocene and up to about a century ago, the construction of some 200 dams in the river's watershed, including small dams on its many tributaries and the series of major dams on the river's main channel, have essentially cut off that sand supply to the ocean beaches. Instead, recent investigations have demonstrated that the source of sand now supporting the net longshore transport to the north is supplied by shoals in shallow to mid-water depths on the continental shelf in proximity to the river's mouth. There have been extensive investigations of all aspects of the CRLC, with an overview summary provided by Gelfenbaum and Kaminsky (2010), and with the other papers in that issue of *Marine Geology* presenting details in the results of those comprehensive investigations.

21.3 Littoral-Cell Sand Volumes and Sediment Budgets

Depending on the availability of beach-sand sources and the overall balance in the sediment budget, there are significant differences in the quantities of sand contained within Oregon's series of littoral cells, the amount of sand per unit shoreline length. Those quantities are directly reflected in the width of the beach, which determines its capacity to act as a buffer between storm waves and the dunes or sea cliffs backing the beach. It is this degree of protection offered by the fronting beach together with the local rate of tectonic uplift of the land relative to the eustatic rise in sea level that together represent the primary controls on the degrees to which

backshore properties have been eroding, and will determine their future susceptibilities to hazards with the projected accelerated rates of rising sea levels.

For the most part the sediment budgets of Oregon's pocket-beach littoral cells are relatively simple, but have not been well quantified in terms of their annual-average gains of sand from the sources (rivers and sea-cliff erosion), or their losses when sand is blown inland to form dunes or carried offshore and through inlets into the bays and estuaries. It appears that these gains and losses to Oregon's cells are not particularly large volumetrically, and as a result the net balances in their sediment budgets cell-wide have tended to be close to zero and difficult to assess. The rivers that drain the Coast Range do not transport particularly large quantities of sand to the coast, and furthermore it appears that very little of that sand passes through the estuaries to reach the ocean beaches. Instead, where investigations have been undertaken of the mineralogies of the sand deposited within estuaries (Kulm and Byrne 1966; Peterson et al. 1982; Komar et al. 2004), the evidence is that they are "sinks" of beach sand carried in by the tides, representing a debit in the sediment budget. The only clearly identifiable credit in the sediment budgets for many of Oregon's littoral cells is the sand derived from sea-cliff erosion, where the waves are cutting into uplifted Pleistocene terrace deposits, former beach and dune sands. Sea-cliff erosion as a source of beach sand is particularly significant in the Lincoln City Littoral Cell (Fig. 21.3), the cliffs there being composed mainly of Pleistocene coarse-grained sand, and locally have been eroding at higher rates than found elsewhere on the Oregon coast (Shih and Komar 1994). However, even with that supply of sand to the beach, it was estimated that the volumes are only sufficient to maintain the continued existence of a beach under the present local rate of rise in the relative sea level, considering that some of the sand supplied by cliff erosion is likely carried into Siletz Bay, a debit in that cell's sediment budget.

In addition to beach sand losses into bays and estuaries, another debit of potential significance in PNW sediment budgets has been the progressive growth of foredunes, which has been substantial since about the 1930s due to the importation of European dune grass, initially planted locally to control the dunes but with its subsequent rapid spread along the entire coast. The foredunes have sequestered large volumes of sand, and now reach substantially higher elevations that act to protect the backshore properties, showing cycles of cut back during major storms and reformation during the subsequent months to years between extreme storm events, that is if left for Nature to take its course. Unfortunately, many of these foredunes have been developed along the Oregon and Washington coasts, particularly being prime real estate on the sand spits. As will be discussed later, owners of homes within foredunes have had to protect their properties by the construction of massive structures, only to have them later buried with the return of the sand, the problem then being the overabundance of sand that tends to bury their homes.

Where assessments of beach-sand budgets have been attempted for Oregon's littoral cells, the annual-average quantities for their credits and debits have tended to be small with high uncertainties (Komar 1997); the corresponding uncertainties in the assessed net balances in the budgets have therefore been large, such that for many cells we cannot even be certain whether the balance is in the "red"

(net erosion) or "black" (accretion). However, with our increasing ability to obtained detailed surveys of the beaches, including periodic Lidar surveys that cover most of the coast, we are beginning to resolve these uncertainties in the sediment budgets for the primary littoral cells of management interest. But assessments of sediment budgets for an entire littoral cell are further complicated by there in recent years having been significant longshore redistributions of the sand within individual cells, or carried offshore by unusually extreme storms, to depths where the sand might not return to the beach for years, decades, or ever. As will be reviewed later, during recent strong El Niños such as those in 1982–1983 and 1997–1998, the beach sand within Oregon's littoral cells has generally shifted alongshore from the south to the north in response to the altered ocean waves (Komar 1986, 1998a; Revell et al. 2002; Allan et al. 2003). While the cell-wide sediment budget might still have a balance that is close to zero, or too small to be assessed with confidence, with this redistribution the budget locally for a portion of the shore can either be significantly in the red or black, with the pattern generally being one of net erosion at the south ends of the cells (north of headlands), evident in the extensive erosion of shore-front properties, while accretion has occurred at the north ends of the cell's shorelines. Furthermore, the effects of the alongshore sand redistributions during the 1997–1998 El Niño were compounded by a series of major storms, particularly in the following winter of 1998–1999, the most extreme having generated 14- to 15-m significant wave heights, the highest in recent decades (Allan and Komar 2002). The result has been net losses of sand on the beaches within the Neskowin and Rockaway Littoral Cells on the northern Oregon coast, the volumes amounting to one to three million cubic meters, with the sand presumed to have moved offshore (Allan et al. 2003, 2009). The question is whether that loss from the beach is permanent, or with time (decades) the sand will progressively be carried back onshore by moderate waves, such decadal cycles having been found on other coasts following particularly extreme storms [e.g., Thom and Hall (1991)].

The sediment budget for the CRLC on the Washington coast is similarly localized by there being a net longshore sand transport to the north, or more precisely due to there being a longshore variation (a gradient) in the local rate of transport, erosion occurring where that gradient is positive (increasing transport to the north), while accretion occurs along stretches of shore where the gradient is negative, the reduction in the volume of sand being transported to the north "leaving behind" a volume that results in shoreline accretion (Ruggiero et al. 2010a).

21.4 Morphodynamics of PNW Beaches

The beaches of the PNW are composed predominantly of medium-grained, quartz and feldspar sand, although locally pocket beaches of gravel and cobbles can be found within the rocky stretches of coast. Along many of its shores the beaches are

"mixed", in that they contain both sand and a coarse-grained fraction ranging from pebbles to cobbles [*Composite Beaches* in the classification by Jennings and Schulmeister (2002)]. This variation in sediment grain sizes from one beach to another has significant effects on their morphologies and dynamics under the changing waves and tides, and ultimately on their relative stabilities and the resulting hazards to short-front properties from erosion and flooding.

The common PNW medium-grained sand beaches are *Dissipative* in the morphodynamics classification of Wright and Short (1983), wherein the categories range from *Reflective* to *Intermediate* to *Dissipative* as the beach slope decreases for smaller sediment grain sizes, depending also on the wave steepness. The high energy and long-period waves typical of the PNW combine to reduce the slopes of the sand beaches, especially during the winter such that they generally have slopes that range from about 1-in-25 to 1-in-50 (0.04–0.02). The morphologies and dynamics of the sand beaches correspond closely to those described by Wright and Short (1983) in their development of this classification based on beaches in Australia, the profiles of the PNW Dissipative beaches consisting of series of alternating sand bars and troughs, oriented roughly parallel to the shore, with there being local gaps in the bars cut by seaward-flowing rip currents. In general, such Dissipative beaches differ from the Intermediate category where the morphology becomes more three-dimensional in its patterns of offshore bars and troughs, and with the shoreline being rhythmic in its development of embayments cut into the beach by stronger rip currents. During the summer months of reduced waves, the shoreward portions of PNW beaches experience accretion and the growth of a dry berm, being typical of a normal seasonal cycle found on most beaches (Komar 1998b), with their slopes becoming steeper in the summer at which time they may become Intermediate in the morphodynamics classification, only being fully Dissipative during the winter.

While the strong rips, their eroded embayments and deeper channels in the offshore represent hazards to recreational beach users during the summer, at that time of year those features are not a significant factor in the erosion of backshore properties since the profiles have accreted with wide protective berms. However, there are a few coarse-sand beaches along this coast that remain Intermediate throughout the entire year, such that as the berm becomes narrow when winter storm waves transport the sand to offshore bars, the deepened rip embayments may cut entirely through the remnant berm to become localized "hot spot" sites of erosion, resulting in the maximum extent of foredune or sea-cliff erosion, commonly with accompanying property losses. An interesting example is found in the Lincoln City Littoral Cell on the north-central Oregon coast, the area in Fig. 21.3 showing Siletz Spit and the sea cliffs to the south in the community of Gleneden Beach. The erosion of these cliffs is the source of the coarse sand on this beach, the reason for its having steeper beach slopes and being Intermediate in the morphodynamics classification. As a result, over the years this area has experienced frequent and damaging erosion of properties within the foredunes on Siletz Spit and atop the Gleneden Beach sea cliffs (Komar and Rea 1976; Komar and McKinney 1977; Shih and Komar 1994; Komar 1997).

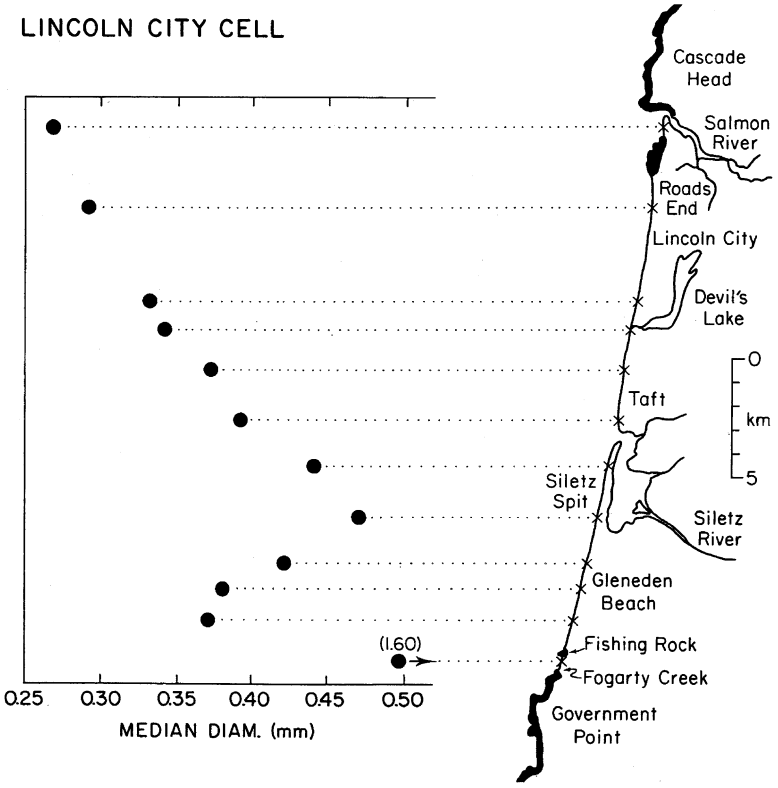

Fig. 21.8 The Lincoln City Littoral Cell on the central Oregon coast, having a marked longshore variation in the medium-grain sizes of the beach sands due to the introduction of a coarse-sand mode by sea cliff erosion in Gleneden Beach and its advection/diffusion along the coast, mixing with the medium-grained sand. Furthest to the south, Fogarty Creek, is a separate coarse-grained pocket beach partially sheltered by offshore rocks, being a steep Reflective beach (From Shih and Komar (1994))

The input of coarse-grained sand into the beach as a result of this sea-cliff erosion is largely limited to the Gleneden Beach shoreline, but as that coarse sand is transported alongshore by the waves both to the north and south from this local source area, it mixes with the more common medium-grained sand that otherwise dominates the beaches within this littoral cell. The resulting longshore variations in the median grain sizes are graphed in Fig. 21.8, while summer and winter profiles are shown in Fig. 21.9 for 11 survey sites along this shore (Shih and Komar 1994). It is evident from these graphs that the slopes of the beaches and envelopes of seasonal profile changes are greatest along the shores of Gleneden Beach and Siletz Spit, where Intermediate-category beaches are found. In contrast, further to the north and south along the shore of the Lincoln City Littoral Cell the beaches have lower slopes and smaller seasonal profile envelopes. As a result, those beaches are Dissipative throughout the year, being far more stable and having experienced

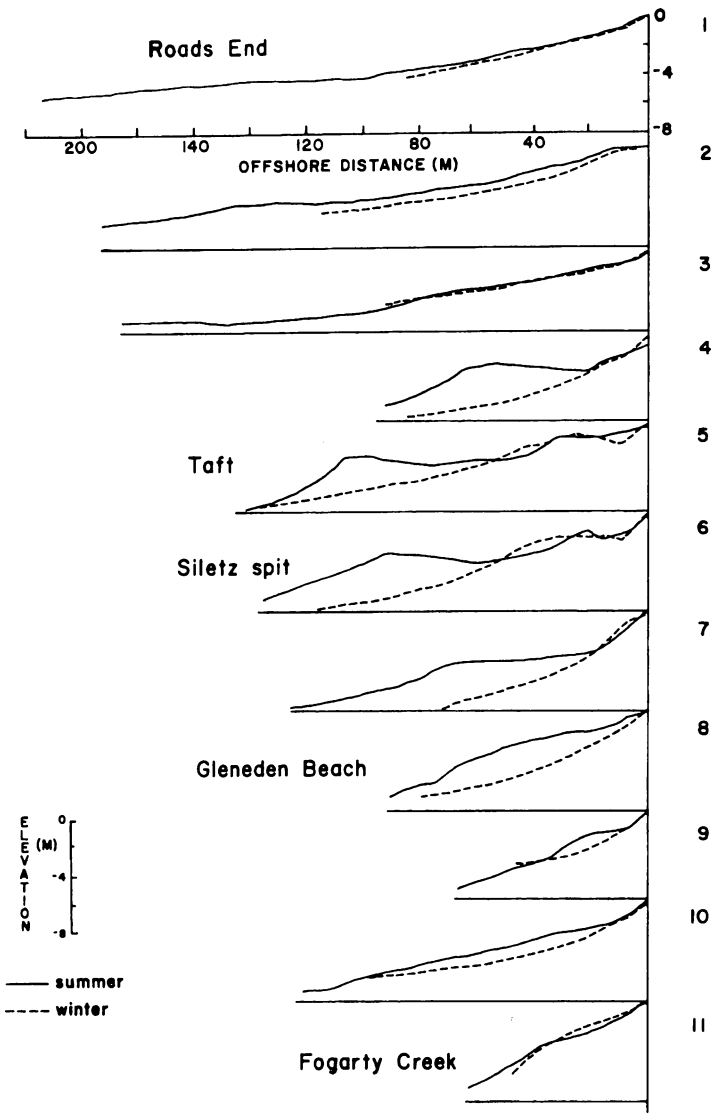

Fig. 21.9 Summer and winter beach profiles at survey sites along the Lincoln City Littoral Cell, showing the differences is slopes and seasonal envelops of profile changes (From Shih and Komar (1994))

fewer problems with property erosion, providing a contrast with the dynamic, coarse-grained Intermediate beaches found along Gleneden Beach and Siletz Spit (Shih and Komar 1994).

Sea cliff erosion and landslides along the rocky stretches of the PNW coast yield resistant basaltic gravel and cobbles that locally accumulate in pocket beaches, the

steep slopes of those beaches being Reflective in the morphodynamics classification of Wright and Short (1983). The dynamics of a Reflective beach are characterized by plunging breakers and intense swash up the steep beach face, there not being a surf zone of wave bores that act to dissipate the wave energy as found on Dissipative and Intermediate beaches. Instead, the initial reduction in wave energy on these cobble beaches is by reflection, the seaward return of a significant portion of the arriving wave energy. As a result of this energy reduction and by virtue of the tendency for the cobbles to resistant movement by the waves, Wright and Short (1983) concluded that Reflective beaches are generally more stable than Intermediate-category beaches that can experience significant morphologic changes and erosion impacts during storms. At the other end in the range of morphodynamic categories, Dissipative beaches are again stable because their wide surf zones result in the decay of the wave bores, and during a storm with extreme waves the surf zone widens in proportion and thereby results in a greater reduction in the wave energy by the time the waves reach the shore. Such morphodynamic controls on the PNW beaches have played a significant role in determining which shores have experienced impacts during past extreme storm events (e.g., the Intermediate-category beaches of Siletz Spit and Gleneden Beach), while the coast's Dissipative and Reflective beaches have acted to protect ocean-front properties from the arriving storm waves.

Gravel and cobbles derived from the erosion of the rocky headlands that form the boundaries between Oregon's littoral cells are also carried alongshore by the waves into those embayed sandy shores, where they form "mixed beaches" containing significant portions of both sand and a coarse-grained component. Such beaches have been classified by Jennings and Schulmeister (2002) based on their common occurrences along the coasts of New Zealand, the classification categories depending on the patterns and degrees of sorting and separation of those contrasting grain-size fractions; the categories are respectively *Mixed Sand-and-Gravel Beaches* where the fractions are mixed together, and *Composite Beaches* where the gravel and cobbles have accumulated in a ridge at the back of the sand beach. While both types of "mixed" beaches are found along the PNW coast, most common are the Composite Beaches, an example shown in Fig. 21.10. Of significance is that a Composite Beach combines a Dissipative sand beach with a Reflective cobble beach, the two end members in the morphodynamics classification that have the highest levels of stability. Together they can provide a substantial measure of protection to backshore properties, the example in Fig. 21.10 showing the presence of a heavily vegetated sea cliff that has been protected from the impacts of storm waves over the decades. Generally, the fronting sand beach is sufficiently wide during the summer that waves cannot reach the landward gravel/cobble ridge, whereas during winter storms the sand beach is cut back to the extent that the waves can reach and transport the coarse-grained sediments (Allan and Komar 2004). Important during winter storms, there continues to be some dissipation of the waves by the wide surf zone provided by the remnant sand-beach profile, with significant additional protection offered by the cobble ridge, both by reflecting

Fig. 21.10 The Composite Beach at Oceanside on the northern Oregon coast, offering protection to the vegetated sea cliff along that community (Photo J.C. Allan)

the wave energy and by absorbing the swash runup that percolates into the coarse-grained beach face.

The protection offered to properties by coarse-grained Reflective beaches had been noted at many sites along the Oregon coast, so that when erosion was experienced in a park on the Oregon coast it was decided to construct an artificial "cobble berm" at the back of the sand beach, duplicating the effectiveness of a natural Composite Beach (Allan and Komar 2004). This management strategy as a substitute for the construction of a hard engineered structure, a rock revetment (riprap) or a seawall, has also been successfully used in Yaquina Bay to protect its eroding shores and infrastructure of the Oregon State University Marine Science Center.

21.5 PNW Erosion—A Brief History

21.5.1 Jetty Construction and Shoreline Changes

The earliest well-documented cases of erosion along the PNW coast were associated with the construction of jetties on the inlets to bays and estuaries, having occurred during the late nineteenth to early twentieth centuries. Most dramatic was the destruction of a resort community on Bayocean Spit, at Tillamook Bay on the

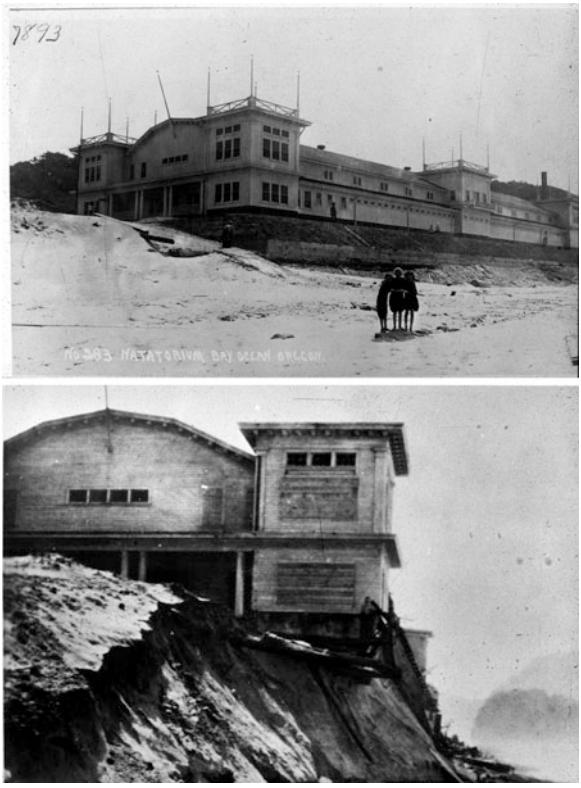

Fig. 21.11 Progressive loss of the Natatorium (containing an indoor swimming pool) on Bayocean Spit: (*Top*) from 1910 and (*Bottom*) in 1932 after a jetty had been constructed on the inlet to Tillamook Bay (Courtesy of the Pioneer Museum, Tillamook, Oregon)

northern Oregon coast, leading to breaching of the spit in 1952 (Terich and Komar 1974; Komar et al. 1976; Komar 1997). Documentations of the large-scale redistributions of beach sand and accompanying shoreline changes that occurred in response to jetty construction were based largely on surveys undertaken by the U.S. Army Corps of Engineers as the construction was underway, and in the case of the losses at Bayocean Spit by the numerous photographs taken as the resort was eroded (Fig. 21.11). Investigations of the shoreline changes demonstrated different patterns from those that generally occur when jetty construction blocks a net longshore transport of the beach sand, this difference being illustrated schematically in Fig. 21.12. In the cases of jetty construction on the Oregon coast, a roughly symmetrical pattern of shoreline change occurred, with beach-sand deposition having taken place to both the immediate north and south of the jetties, while erosion and net shoreline retreat occurred at greater distances from the jetties to supply the sand to those zones of deposition (Komar et al. 1976). Individual examples of this pattern depended on such factors as the degree of obliqueness of the jetties to the overall shoreline trend, and with the extent of beach erosional retreat depending on the length of shore to the headlands that bound the littoral cell, the shorter that distance the greater the erosion per unit of shoreline length. The catastrophic losses that occurred on Bayocean Spit were due to the fact

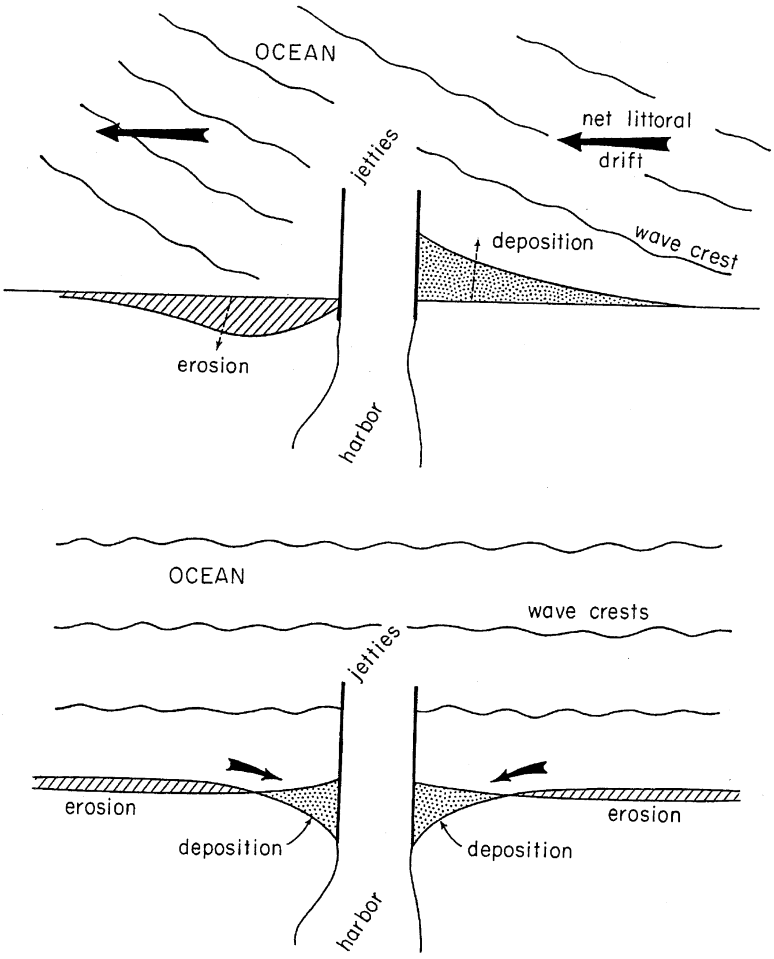

Fig. 21.12 Patterns of sand deposition and erosion in response to jetty construction: (*Top*) the jetties blocking a net longshore sand transport; (*Bottom*) the shoreline change where the net transport is effectively zero, as occurred on the Oregon coast

that only a single jetty was initially constructed, resulting in beach sand being continuously carried into the Bay over the years. When a second jetty was added in the 1970s, the modified pattern of shoreline geometry then corresponded to that depicted in Fig. 21.12 (*bottom*).

This symmetrical pattern of beach deposition versus erosion on the Oregon coast due to jetty construction, Fig. 21.12 (*bottom*), can be attributed to that coast consisting of a series of littoral cells, within which there is a seasonal reversal of longshore sand movement but with the long-term net transport being effectively zero (Komar et al. 1976). The result was that while the shoreline changes caused by jetty construction were in some instances significant, for the most part they were

largely completed within a decade or two, so that other than the unusual case of the erosion of Bayocean Spit with its single jetty, the presence of jetties on the Oregon coast have not generally represented a continuing problem as found on coasts where they do block a net longshore transport of the beach sand. However, as will be discussed later, jetties on the coast of the PNW can still act as mini-headlands, affecting the seasonal redistributions of sand within the littoral cells and leading to localized "hot-spot" erosion during major El Niños.

The effects of jetty construction on the ocean shore of Washington differ somewhat from Oregon in that within the Columbia River Littoral Cell (CRLC) they do block a net northward longshore transport of sand. However, the resulting pattern of beach accretion versus erosion, and changing shorelines, differed from the usual response when jetties block a net transport in having been a combination of those depicted schematically in Fig. 21.12. Most extreme were the altered shorelines by the construction of jetties on the mouth of the Columbia River between 1885 and 1917. Detailed analyses of those changes were undertaken by Kaminsky et al. (2010), with the historic shoreline positions and rates of change having been derived from a series of NOS T-Sheets for the period from 1868 to 1957, and from aerial photographs since the 1950s. The results of their analyses are shown in Fig. 21.13, with the pre-jetty shorelines represented by those in 1868 and 1892, superimposed on the 1870 chart from that period. The 1910, 1926, 1955 and 1999 shorelines demonstrate the extreme extent to which the shoreline positions were altered, with their initially having been significant accumulations of sand both to the north and south of the jetties, with most of that accumulation having been completed by the 1920s.

The accumulation to the south, Fig. 21.13, took the form of a spit that grew northward until it reached the south jetty. Problems were experienced with the sand leaking through the porous, rubble-rock jetty, entering the navigable channel, but the jetty was sealed later by the Corps (Komar and Li 1991). As evident in the 1926 and subsequent shorelines, following jetty construction this beach (Clatsop Beach) to the south along the Oregon shore became straight with the south jetty essentially acting as an artificial headland. For a time this shore rotated clockwise, with some erosion along the 4-km northern end adjacent to the jetty while there was considerable sand accumulation in the south, along the community of Seaside north of Tillamook Head, where previously the shore had been dominated by cobbles. To a degree the south jetty on the Columbia acts as a headland for the Clatsop Beach shoreline, representing a sub-cell within the CRLC, the evidence being that sand is no longer reaching it from the Columbia River, but instead is "leaking" to the north past the jetties and supplying sand for the beaches to the north on the Long Beach Peninsula (Kaminsky et al. 2010).

Following jetty construction on the Columbia, it is seen in Fig. 21.13 from Kaminsky et al. (2010) that sand also accumulated to the north of the jetties, along what previously had been the rocky shore of Cape Disappointment. For a time the seaward migration of the beach was so rapid it had kept up with the extension of the jetty as it was being constructed. This documentation of the changing shoreline positions, forming Benson Beach, shows it having reached its

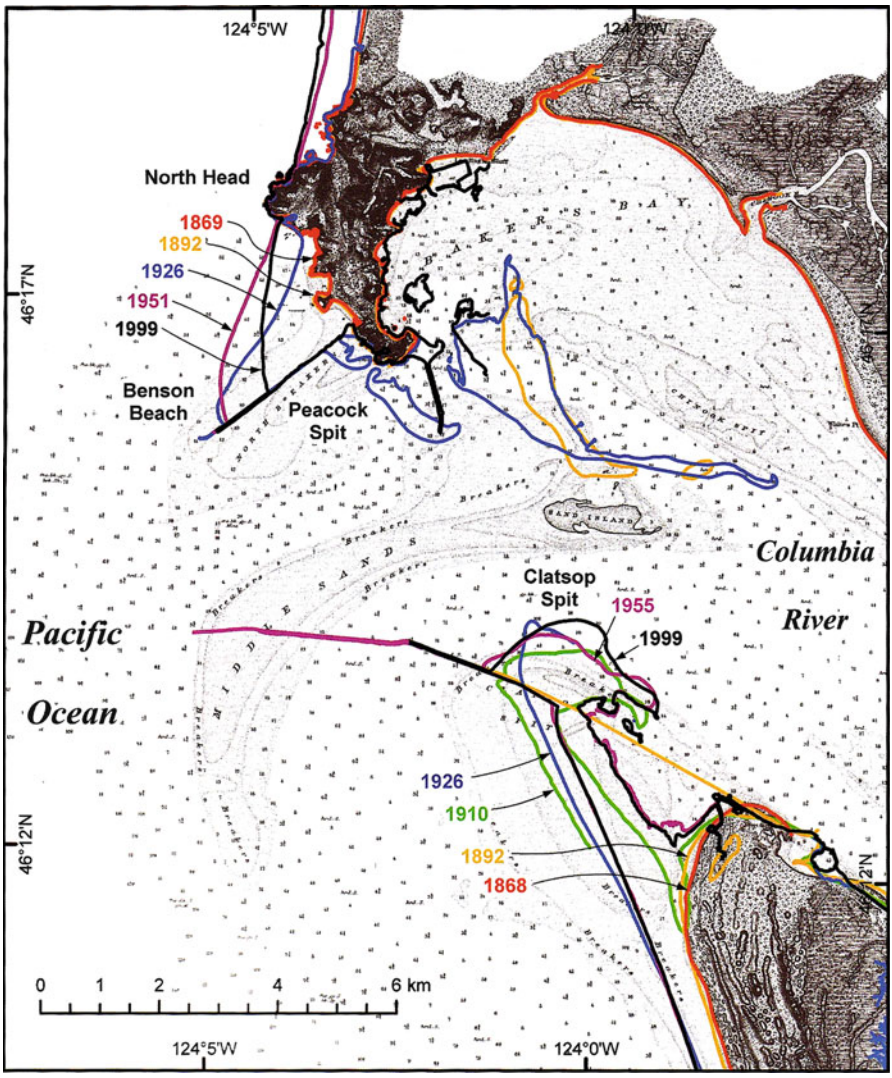

Fig. 21.13 Historic changes in the shorelines at the mouth of the Columbia River due to the construction of the jetties, shown superimposed on the pre-jetty 1870 U.S. Coast and Geodetic Survey chart (From Kaminsky et al. (2010))

most seaward position in about 1955, after which it began to erode, continuing to do so up to the present. Serving as a feeder beach for a portion of the net northward longshore sand transport on the Long Beach Peninsula, this progressive erosion has led to the formation of a massive black-sand placer deposit on Benson Beach, including both the beach and foredunes (Komar and Li 1991; Li and Komar 1992).

In its natural state prior to the construction of the jetties (1885–1917), the quasi-equilibrium of the CRLC shorelines would have been such that depending on the balance between the sand delivered by the river and its distribution along the shore by the waves, it is expected that there would have been a net northward sand transport along the Long Beach Peninsula on the Washington coast, and with a smaller transport southward along Clatsop Beach on the Oregon coast (Komar 1973). At the time of jetty construction there would already have been some alteration of this natural condition in that analyses of the CRLC sediment budgets show that the sediment supply from the Columbia has substantially declined during historic decades, including prior to jetty construction, largely due to dam construction within the river's extensive watershed (Gelfenbaum et al. 1999). Significant is that over 200 small dams were constructed within its upper watershed, prior to the major dams having been built on the river during the 1930s (Bonneville, etc.); blockage of sand delivered to the coast can therefore be expected to have been gradual. With the presence of those small dams in the upper watershed, and particularly the major dams on the Columbia used for hydroelectric power generation, the result has been a significant change in the seasonality of the regulated river discharges, decreases in the maximum discharges that would have flushed sand within the estuary to the ocean shores. Finally, also significant has been dredging of the river's estuary and disposal of the sand well offshore, in 40-m water depth (Gelfenbaum et al. 1999), well beyond where it would be expected to be carried by waves to the CRLC beaches. With these multiple human modified changes to the Columbia River, the exchange of sand between the river's estuary and the coast is now uncertain, and it is possible that at present the Columbia River no longer supplies sand to the CRLC beaches (Kaminsky et al. 2010).

The general pattern of shoreline changes associated with jetty construction at the entrance to the Columbia River, with accretion both to the north and south, is similar to that found within the littoral cells along the Oregon coast, depicted in Fig. 21.12 (*bottom*). On the other hand, subsequent to those changes during jetty construction, there is clear evidence for there being a net northward transport along the Long Beach Peninsula, particularly the persistent erosion of Benson Beach since the 1950s (Fig. 21.13). Kaminsky et al. (2010) accounted for these changes in the shorelines through a review of the responses of the offshore bathymetry to jetty construction. Cell wide the bathymetric data and other evidence show a consistent pattern of erosion of the mid- to lower shoreface, at water depths of approximately 10–25 m, with accumulation on the upper shoreface and in the nearshore. The bathymetric changes in the more immediate proximity to the jetties (Kaminsky et al. 2010) reveal additional effects, of interest being those during the 1868–1925 time period when the jetties would have had their greatest impacts. During those 50 years there was some 10–20-m of sand accumulation in the arc-shaped offshore bar that extends around the river's mouth and jetties, this bar extending to the north shore such that the formation of Benson Beach was clearly part of that otherwise submerged accumulation. In contrast, erosion prevailed to the south of the jetties, increasing water depths in the offshore by some 10–12 m, even though there had been accretion in the nearshore in the form of spit growth

(Fig. 21.13). These offshore bathymetry changes have continued subsequent to jetty construction, although in modified form, the arc of bar accumulation having shifted further offshore, reverting to erosion in closer proximity to the inlet and jetties, with that offshore erosion extending to Benson Beach, explaining its erosional retreat in recent decades.

The conclusion has been that with there being a net northward longshore transport, the ebb-tidal shoals and shoreface to the south of the jetties have been the source of the sand volumes for that transport, sufficient to maintain the beach sediment volumes in spite of the loss of sand derived directly from the Columbia River (Kaminsky et al. 2010). The decline of river-supplied sand in recent decades therefore has had a relatively small impact to the CRLC beaches in that the ebb-tide shoals and shoreface have provided significant volumes since jetty construction. However, those contributions can be expected to decrease with time, so the future stabilities of the Long Beach Peninsula and of the beaches further to the north within the CRLC are uncertain.

Jetties were also constructed (1898–1916) at Grays Harbor to the north within the CRLC. Kaminsky et al. (2010) have undertaken similar analyses of the resulting changes in the shoreline positions, and also of the offshore bathymetry. Although differing in details, the overall patterns are similar to those found for the Columbia River jetties.

The greatest extent of shoreline erosion on the coast of the PNW (and anywhere along the U.S. West Coast) is that which has been occurring for more than a century on the shores of the inlet to Willapa Bay, which is not controlled by jetties. The south shore of the inlet (Leadbetter Point) is the northern tip of the Long Beach Peninsula, the north shore having been Cape Shoalwater, which by the 1960s had been cut away by the erosion (Terich and Levenseller 1986; Kaminsky et al. 2010). The general pattern of change from the 1800s to the present has been the northward migration of the channel accompanied by its overall increase in width. Thanks to the relatively light development of this area, the impacts fortunately have been relatively modest, mainly having been to move the coastal highway inland away from the north of the inlet, and moving an historic Pioneer Cemetery before it was lost.

21.5.2 Major Storms and Erosion Impacts

There has also been a history of major storms along the PNW coast, although there had been little documentation of their erosion and flooding impacts until the 1960s, beyond the photographs of Bayocean Spit showing the damage of individual storms. While newspapers reported on occurrences of strong PNW storms throughout the early twentieth century (Stembridge 1975), those accounts focused largely on the strong winds and their damage, not the destructive impacts on shore-front developments; in part this was because prior to about the 1950s there was relatively little development of those properties. Of the historic accounts, most significant was the extreme storm on 3 January 1939, for which we have photographs of Newport

and Cannon Beach on the northern Oregon coast showing the shorefront of the former being immersed by the combined waves and tides, to levels that have not been experienced in recent decades. Photos of the Cannon Beach downtown show it immersed by flood water, also representing an unusual extreme occurrence. As such, that 1939 storm has been assessed by FEMA to be the 75-year event in terms of the generated significant wave heights, though it may be closer to having been the 100-year event in terms of the total water levels of elevated tides and superimposed swash runup of its waves, it being this combination that is significant to erosion and flooding hazards. Following the storm, the Corps of Engineers obtained aerial-photo coverage of nearly the entire Oregon coast, providing the earliest coast-wide documentation of its beaches and backshore properties, showing the extensive impacts of that extreme storm event.

With the expansion of rapid development along the PNW coast beginning in the 1960s and 1970s, the erosion of ocean-front properties became more common, with increased management concerns. Much of this development was within foredunes on sand spits where the homes were particularly vulnerable to erosion during storms. The first major sand-spit erosion, when both the processes and impacts were document, occurred on Siletz Spit during the winter of 1972–1973 (Komar and Rea 1976; Komar and McKinney 1977; Komar 1983). There was already a number of recently-built homes, and a reconnaissance visit the previous year had raised concerns since the line of homes followed the crest of a distinct morphologic ridge within the dunes, following the length of the spit, interpreted to have been a dune-erosion escarpment but with the dunes over a number of years having built back out to their former extent. In view of this observation, the erosion that occurred during the following winter of 1972–1973 was not unexpected.

An aerial view of Siletz Spit is shown in Fig. 21.3, the homes being evident. The susceptibility of this spit to erosion was discussed earlier, it having a coarse sand, steeply-slopping beach, being an Intermediate Beach in the morphodynamics classification of Wright and Short (1983). Having its dynamic responses, the berm on Siletz Spit was progressively cut back by a series of winter storms, but ultimately of greatest consequence to the property impacts was the development of strong rip currents and their eroded embayments, also characteristic of Intermediate Beaches. As seen in the oblique aerial photograph of Fig. 21.14, taken in December 1972, there was one particularly prominent rip embayment that had cut entirely through the berm and was in the process of attacking the foredunes. As seen in Fig. 21.15, one home under construction was lost to the erosion, while a group of three homes were hastily protected by the installation of a riprap revetment, initially along their seaward sides but since the adjacent empty lots were left unprotected, the dune retreat continued so that riprap also had to be placed along the sides of the homes, leaving each on a promontory of rocks extending out onto the beach face. When the continued erosion of the empty lots threatened the loss of the access road and utility lines, these gaps in the riprap were filled by the developer. In subsequent summers sand was bulldozed from the beach back into the eroded lots to restore them, so they could be resold; this was possible in the 1970s, due to the near absence of firm management controls.

Fig. 21.14 Rip current embayments along Siletz Spit during the winter of 1972–1973, leading to the property erosion shown in Fig. 21.15 (From Komar (1997))

Fig. 21.15 A house under construction lost to the 1972–1973 erosion of Siletz Spit, and a house protected by a riprap revetment (From Komar (1997))

Further investigations of the spit's morphology revealed evidence for previously eroded rip embayments, which had formed prior to development in the 1960s. It was evident that under natural conditions, the numerous drift logs as found on PNW beaches were washed into each eroded embayment, and that the matrix of these logs helped trap the wind-blown sand to reform the dunes. Old rotting logs had been observed in the freshly eroded dune scarp during the 1972–1973 erosion episode, even when that scarp had reached its most landward position beneath the homes, providing evidence for the extremes in these erosion processes, extending well beyond the newly constructed homes. Analyses of old aerial photographs and coastal charts led to the conclusion that over at least a century there had been cycles of episodic dune erosion, each of which was followed by decades of dune reformation, it being such cycles that dominate the hazards to this shore; the occurrence of any long-term net trend of shoreline erosion or accretion was not evident, at least at this PNW location.

In hindsight, it is evident from the pre- and post-development occurrences of erosion on Siletz Spit that the establishment of a hazard zone (setback lines) had

been needed, one that would have avoided this extent of episodic foredune retreat, expected during the most extreme storms. Lacking such guidelines, there was a number of erosion episodes over the subsequent decades, similar to that during the winter of 1972–1973, but typically having impacted different properties as the positions of the largest rip embayments from one winter to another changed; for a specific property, a repeat of the erosion impacts might not occur for decades, depending on the return of a rip embayment to that location. As such, with the moving sites of dune erosion episodes, the result has been that the entire length of Siletz Spit is now protected by a continuous line of riprap, separating the expensive homes of this prime ocean-front development from their beach and its recreational use.

The erosion experienced on Siletz Spit is fairly typical of that experienced along the PNW coast on shores backed by foredunes. For example, large storm waves combined with high spring tides during February 1978 causing extensive erosion in many areas of the PNW coast (Komar 1978). Significant was the high perigean spring tide plus a storm surge that raised water levels by another 25 cm, producing measured tides that were substantially higher than those during the December 1972 erosion of Siletz Spit. Most critical was the erosion that occurred along Nestucca Spit on the northern Oregon coast, which threatened a new housing development and breached an uninhabited area of the spit. The focus of these erosion impacts was again determined by the locations of prominent rip current embayments. The beach at Nestucca Spit is finer grained so the embayments were broader than at Siletz Spit, so that the dune erosion extended over a greater length of shoreline. Drift logs were again exposed within the eroding dunes, more rotten than those found within Siletz Spit suggesting that erosion episodes on Nestucca Spit are rare.

The most unusual aspect of the February 1978 erosion was the breaching of Nestucca Spit, a comparable large-scale breach having occurred only at Bayocean Spit in 1917, caused by jetty construction. It took the unusual circumstances of the 1978 storm to produce the breach—high perigean spring tides, exceptional storm waves plus a surge, and the development of a rip-current embayment that by chance focused the erosion along the thinnest section of the spit (Komar 1978). Fortunately this breach occurred toward the south end of the spit, well away from any homes. When the storm struck the coast, several houses were still under construction within the foredunes, while others had only recently been occupied. As seen in Fig. 21.16 (*upper*), the homes were protected by the rapid placement of large quantities of riprap, one of the largest revetments that have been constructed along the PNW coast. Nestucca Spit began to mend during the following summer, and after a few years so much sand had returned to the beach the revetment was completely buried, and as seen in Fig. 21.16 (*lower*) the over abundance of sand threatened to bury the houses. Here and at other PNW sites facing this problem, dune management programs must be first developed and approved before the sand can be removed.

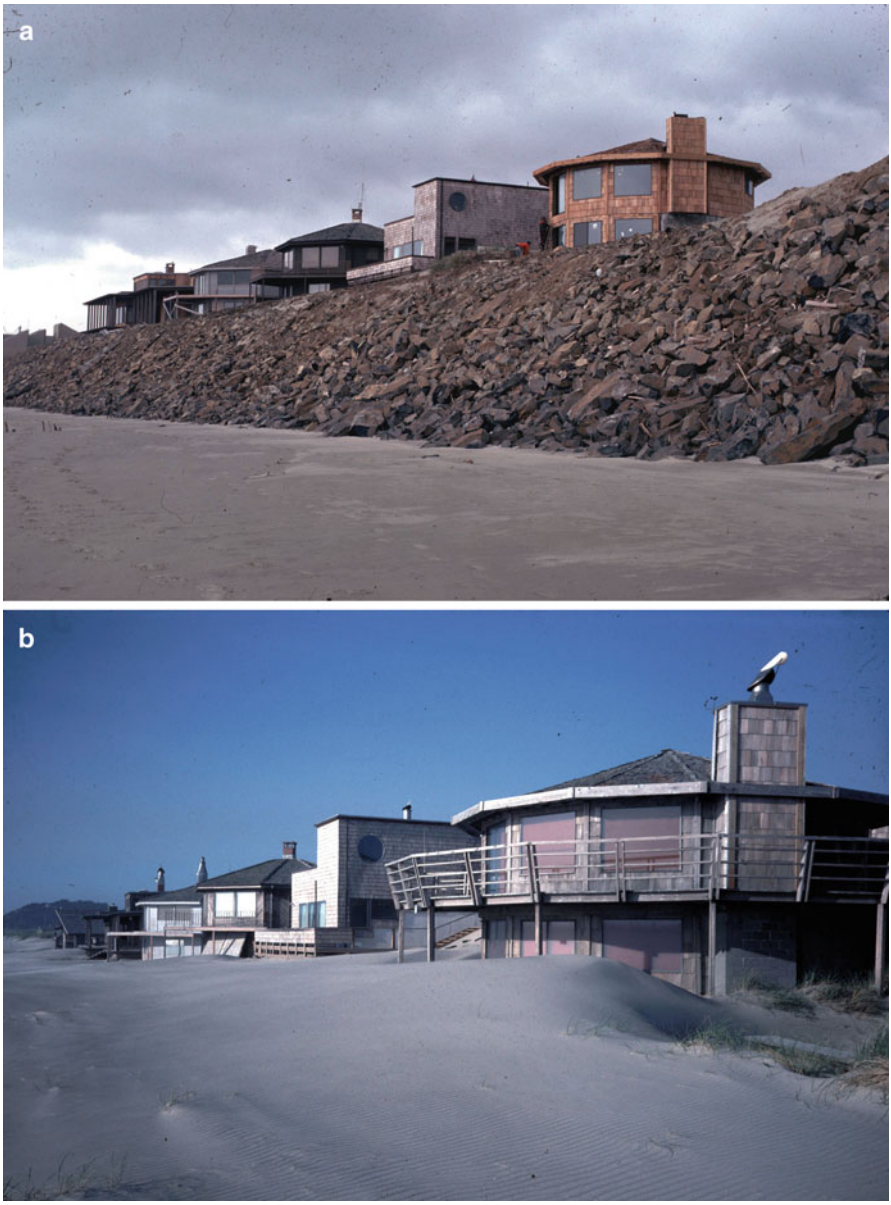

Fig. 21.16 The erosion on Nestucca Spit in 1978 with the construction of a riprap revetment, and a later photo when the revetment had been covered with sand blown in from the beach, accumulating to the extent that the sand threatens to cover the homes (From Komar (1978))

21.5.3 El Niños and Hot-Spot Erosion

Until about 1980 our analyses of episodes of PNW erosion, whether they were in foredunes or properties atop sea cliffs, focused simply on individual storms or the cumulative effects of multiple winter storms—their extreme waves, tides elevated by a surge, and the localized effects of rip current embayments. That simple view changed during the winter of 1982–1983, with an unusually large number of significant property erosion occurrences at sites all along the PNW coast, as well as along the shores of California. It was concluded that in the PNW there was a regularity to the locations of this erosion, having been greatest to the north of headlands, and to the north of tidal inlets to bays and estuaries that were free to migrate in response to the storm waves arriving from the southwest. Those locations came to be referred to as "hot-spot" sites of erosion, recognized to be the response to the occurrence of a major El Niño in 1982–1983, with the maximum enhancement of its erosion processes (waves and tide levels) having taken place during the winter months (Komar 1986, 1998a; Komar et al. 1988). With the occurrence of another strong El Niño in 1997–1998 and with a near repeat of hot-spot erosion occurrences at the same PNW sites (Komar 1998a; Kaminsky et al. 1998), we came to appreciate the importance of the full range of El Niño/La Niña climate events as representing a major control on its weather and ocean processes. Here we briefly review a few case studies of these erosion impacts, while later in the chapter the enhancement of the causative processes will be examined.

Particularly important to the State of Oregon was the massive erosion in Cape Lookout State Park (CLSP), which occurred during both the 1982–1983 and 1997–1998 El Niños, in each case with damage to the park having continued for some 2–3 years following the actual climate event since the beach was slow to recover (Komar 1986, 1998a). CLSP is located within one of the smallest pocket-beach littoral cells on the Oregon coast, with Netarts Spit forming most of its shore between the large Cape Lookout headland to the south and Cape Meares to the north. With the park located toward the south end of this littoral cell, north of Cape Lookout, it represented a typical example of El Niño related hot-spot erosion.

There had been minimal erosion impacts of CLSP during historic times, due largely to its relatively wide, dissipative sand beach. Backing the beach along the park were high protective dunes covered by large trees, further evidence for its past stability. In the late 1960s a seawall had been constructed of large logs at the back of the beach, but there is no record of the reason for its construction and it may have been to prevent people from walking across the fragile dunes. The sudden and dramatic erosion during the 1982–1983 El Niño therefore came as a surprise. Being one of the smallest of the littoral cells on this coast, the pocket beach within the Netarts cell underwent a marked reorientation due to the approach of the storm waves from the southwest. This depleted the beach of sand to the immediate north of Cape Lookout, leading to hot-spot erosion of the low-lying sea cliffs north of that headland, but then extended further to the north impacting the dune-backed park. The southern half of the log seawall was quickly destroyed by the waves,

Fig. 21.17 El Niño hot spot erosion in Cape Lookout State Park on the northern Oregon coast, with the loss of its log seawall seen in the distance, leaving only the vertical supporting I-beams. Also seen is the remnant of tree-covered dunes that formerly had extended alongshore protecting the bathrooms, now being threatened by the erosion (From Komar (1986))

combining with the measured tides that were raised by some 25–50 cm above their predicted levels, an important enhancement of the ocean processes during strong El Niños (to be discussed later). Erosion of the large dunes followed, and as seen in Fig. 21.17 the park's campground previously sheltered by those dunes came under attack by the storms and hot-spot erosion. Although the erosion halted short of the public bathrooms during the 1982–1983 El Niño and they were protected by the local placement of a rock revetment, wave overtopping of the park grounds led to the abandonment of those bathrooms and the campground had to be closed for the winter.

The CLSP beach slowly recovered during the several years following this major El Niño event, but the winter of 1997–1998 saw the return of another strong El Niño, with its hot-spot erosion having picked up where the 1982–1983 impacts had ended. The remaining northern half of the old log seawall was lost, as were the tree-covered dunes, exposing the full length of the campground and recreational area to direct attack by winter storms. In something of a "one-two punch", the following 1998–1999 winter experienced multiple strong storm events, with the last storm on 2–3 March 1999 having been the most extreme, generating deep-water significant wave heights of 14–15 m (Allan and Komar 2002), which combined with the high tides to inundate the park's campground. State Parks considered abandoning the campground entirely, one of the most important on the Oregon coast, but then

examined the possibility of constructing a large-scale rock revetment along its entire length, an option that would have been both expensive and undesirable in not wanting a massive engineered structure in a state park (while at the same time, Start Parks being the agency that reviews permit applications to build structures to protect private properties, often having to deny them). Instead, it was recommended to State Parks that they construct a cobble berm (dynamic revetment) backed by an artificial foredune having sand-filled geotextile bags within its core to increase their stability (Allan and Komar 2004). As discussed earlier, the construction of this cobble berm at CLSP represented an attempt to duplicate the protection offered by the natural Composite Beaches found along the Oregon coast, a dissipative sand beach backed by a reflective cobble beach, with the addition of the "reinforced" restored foredunes to prevent wave overtopping. In spite of the structure not having been built to the design elevations required to prevent overtopping during major storms, which occurs almost every winter, and not having undertaken periodic maintenance needed for such semi-mobile structures, the cobble berm in CLSP can be viewed as having been a success in providing sufficient protection for the campground to keep it open, even during the winter storm season.

Also within the Netarts Littoral Cell, particularly dramatic and newsworthy was the erosion during the 1997–1998 El Niño at the Capes, Fig. 21.18 (*upper*), a recent development of expensive condominiums built on the high bluff to the immediate north of the inlet to Netarts Bay (Komar 1998a). Being north of an inlet free to migrate due to the arrival of the storm waves from the southwest, this site represented another hot-spot zone of enhanced El Niño erosion. With the reduced buffer protection of the generally wide dissipative sand beach, the elevated tides and storm-wave runup combined to attack the high bluff below The Capes; with the condos having been constructed with only a 3-m setback from the bluff edge, the threat was immediate. Significantly exacerbating the hazard, the condos had been located atop an "inactive" massive landslide, its upper portion consisting of dune sand, the lower-most portion of the eroding bluff consisting of mud that appeared to be squeezed out like toothpaste by the weight of the overlying old dune sands. Reactivation of the landslide produced a slip face in the loose dune sand that came a meter from the condos (Fig. 21.18, *lower*). While several of The Capes' bluff-edge condominiums had to be evacuated during the 1997–1998 El Niño and 1998–1999 winter of major storms, they survived and are once again occupied. But they face the expectation of there being another major El Niño with its characteristic hot-spot erosion, permitting the waves to renew their attack on this ill-conceived and highly susceptible development.

The area that suffered the greatest erosion during the 1982–1983 El Niño was Alsea Spit on the central Oregon coast, another hot-spot site to the north of the inlet to Alsea Bay (Komar 1986). With the northward migration of the inlet, the tip of the southward-directed spit was quickly cut away threatening several homes, but then erosion developed along nearly the entire length of the spit as the inlet channel was deflected to the north in the offshore, deepening the water. This significantly enhanced the wave attack, threatening a number of homes that had been constructed in the foredunes. The extent of the hazard is evident in the oblique-aerial photo of

Fig. 21.18 The Capes development of condominiums north of the inlet to Netarts Bay located on an old landslide: (*Upper*) Toe erosion during the 1997–1998 El Niño, having reactivated movement of the slide; (*Lower*) The first line of condos being threatened by the slip-face of landslide movement (From Komar (1998a))

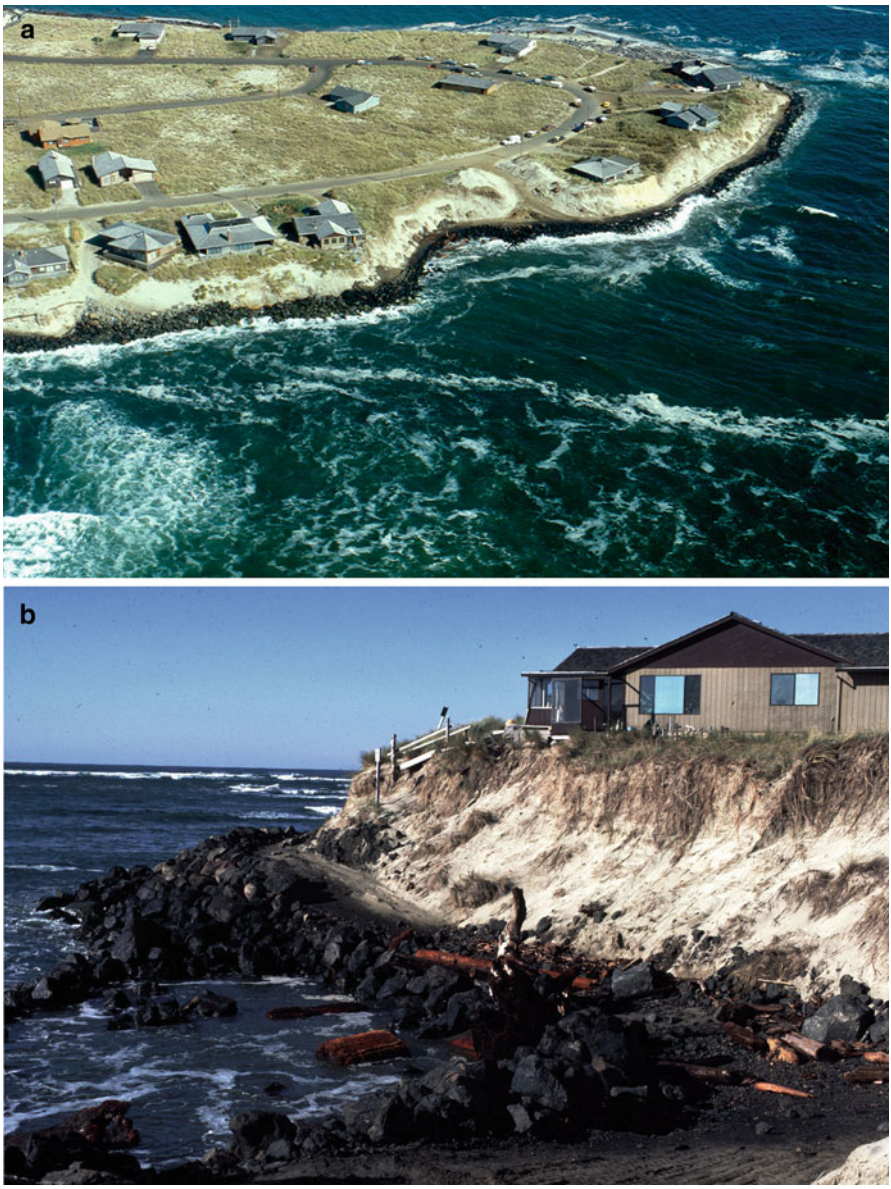

Fig. 21.19 The erosion of Alsea Spit beginning during the 1997–1998 El Niño. (*Upper*) The complete loss of the beach along the Spit, with a riprap revetment having been constructed to protect the homes. (*Lower*) The home located next to the "embayment" in the line of riprap evident in the upper photo, where the erosion of an empty initially had been allowed to continue (From Komar (1998a))

Fig. 21.19 (*upper*), showing the complete loss of the fronting beach but with a riprap revetment having been hastily dumped to protect the homes—only one had been lost.

Although the erosion at Alsea Spit originated during the 1982–1983 El Niño, the impacts continued for 3–4 years due to the disruption from its normal conditions. The beach fronting the Spit finally began to expand during the summer of 1986, restoring some stability for the development. However, much as occurred on Nestucca Spit following the construction of a large riprap revetment in the 1970s, seen in Fig. 21.16, during the next several years more sand returned to Alsea Spit, entirely covering the length of its revetment and threatening to bury several homes. At the same time additional houses were constructed along the Spit, but the developer had forgotten exactly where the now buried revetment was, the result unfortunately having been that a few of the homes were located seaward or atop that hidden structure. With the return of erosion during the 1997–1998 El Niño and extreme 1998–1999 winter storms, those homes were quickly threatened necessitating the construction of another line of riprap at their locations (Komar 1998a).

Erosion also occurred in the communities of Neskowin and Rockaway on the northern Oregon coast during the winters of 1997–1998 and 1998–1999. In previous decades both communities had wide beaches and substantial volumes of sand in their foredunes, at times too much with homes having lost their ocean views and with the threat of being buried. That abundance changed significantly during those two winters, and 15 years later these areas are still the principal stretches of the PNW coast where homes are in danger of being lost to the impacts of major storms (Allan et al. 2009).

Neskowin is located at the south end of its littoral cell, immediately north of Cascade Head, an expected hot-spot erosion site so that the loss of its beach and foredunes beginning during the 1997–1998 El Niño could have been anticipated. However, prior to that El Niño there is no record of this site having experienced hot-spot erosion, not even during the strong 1982–1983 El Niño. The beach is steep, composed of coarse-grained sand, an Intermediate Beach in the morphodynamics classification, this being another factor contributing to its susceptibility in that the presence of a large rip current embayment was important to wave attack of the properties during both the 1997–1998 and 1998–1999 winters. The extreme waves of both winters appear to have been particularly significant in transporting sand eroded from the beach and dunes into the offshore, such that about one million cubic meters of sand still cannot be accounted for, based on repeated surveys along the 15-km length of this littoral cell (Allan et al. 2009). The present condition and threat to Neskowin is evident in Fig. 21.20, where the homes and condominiums are defended by a riprap revetment, but the high water levels of waves and tides are still able to overtop the structure and wash against the dwellings.

Rockaway is one of several communities along the central portion of its 25-km long littoral cell, with Bayocean and Nehalem Spits respectively forming the southern and northern-most portions of this cell's shoreline. Although the jetties on the inlet to Tillamook Bay acted as a mini-headland during the 1997–1998 El Niño, having blocked the winter northward displacement of the beach sand and to a degree causing hot-spot erosion to their north (Allan et al. 2003), the inception of the erosion at Rockaway further to the north was most likely again caused by the

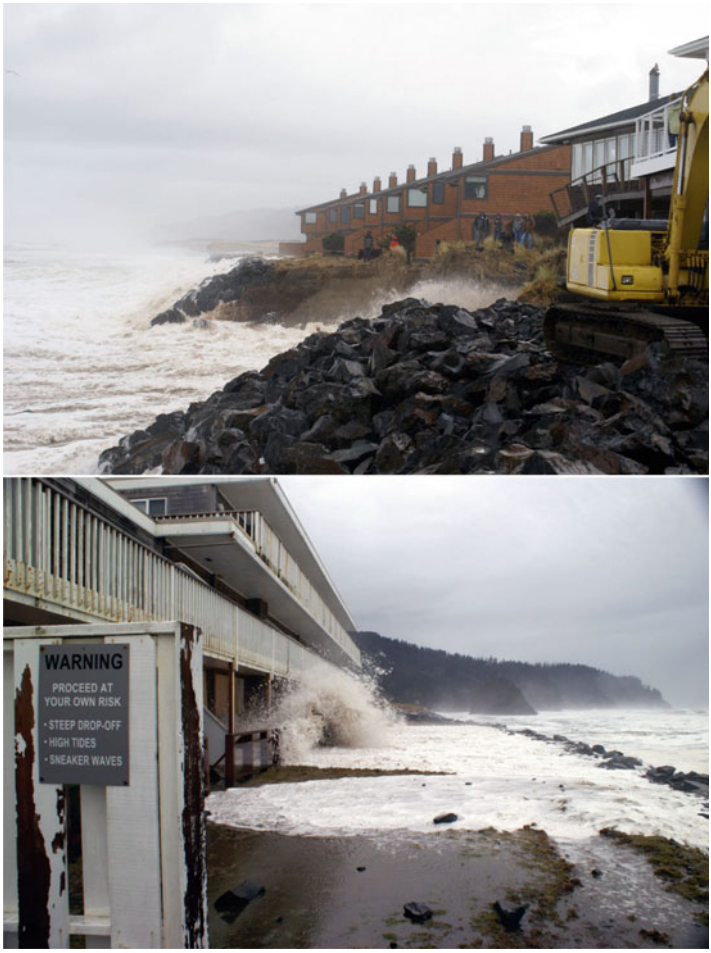

Fig. 21.20 Homes in the community of Neskowin, protected by a riprap revetment after erosion cut away its foredunes beginning during the 1997–1998 El Niño and 1998–1999 extreme storms. Overwash of the revetment during a storm (Photos courtesy of Armant Thibault)

major storms during the "one-two punch" winters of 1997–1998 and 1998–1999. Surveys determined that some 2.5 to 3 million cubic meters of sand had moved offshore from the beaches and dunes of this littoral cell, still not having returned to this shore a decade later (Allan et al. 2009). It is known from other coasts that following particularly extreme storms that carry sand offshore to deeper water than usual, it may take several years to more than a decade for the sand to return to the beach [e.g., the study by Thom and Hall (1991) on the coast of New South Wales, Australia]. It therefore is possible that this "missing" sand will eventually be transported by the waves back onshore to the Rockaway beach, perhaps even

eventually burying the large riprap revetment just as occurred on Nestucca Spit during the 1970s (Fig. 21.16).

21.6 PNW Erosion Processes—Storms, Waves and Sea Level

While the volumes of sediments contained within the PNW beaches, together with their grain sizes and compositions, determine the stabilities and degrees to which they protect shore-front properties from the forces of the ocean, the storm-generated waves plus the levels of the tides combine to attack those shores. The trends and variations in Earth's climate contribute by raising the level of the sea, increasing storm intensities, and through the range of El Niño/La Niña climate events that enhance multiple ocean processes. These processes are reviewed here.

21.6.1 Storms and Extreme Waves

The coast of the PNW is noted for the severity of its storms and extremes in the heights of the waves they generate. Annually, deep-water significant wave heights (SWH) during winter storms commonly range from 5 to 10 m, with the most severe in recent decades (3–4 March 1999) having generated 14- to 15-m SWHs (Allan and Komar 2002, 2006). As reviewed above, most episodes of ocean-front property erosion have occurred during such storms, particularly if they corresponded in their timing with unusually high tides, possibly elevated by a storm surge. There is strong evidence that the intensities of storms and the heights of their generated waves have increased over the decades. Of concern to the management of the PNW coast is that this increase will continue through the twenty-first century, acting together with the projected rise in sea level to produce even more devastating occurrences of erosion and flooding.

With its latitudes ranging from 40°N to 48°N, the coast of the PNW lies in the path of extratropical storms that cross the North Pacific, formed by cold air masses moving down from subpolar regions, colliding with warm air. The strongest storms develop during the winter, with the winds at times achieving hurricane intensities. The cyclonic pattern of the winds and pressures of an individual storm can span such a large area that it impacts nearly the entire length of the PNW shore. The extent of those impacts can also be increased in that many storms follow northeasterly tracks, roughly paralleling the coast, and are known to intensify as they cross the continental shelf, the result being continued wave generation right up to the shore. For example, the March 1999 storm that generated the 15-m SWHs developed into a meteorological "bomb" when it was in close proximity to the coast, with extremes in its winds and waves having been achieved as it crossed the shore of northern Oregon and Washington. That event and other unusually severe storms

during the winters of 1997–1998 (a strong El Niño) and 1998–1999 (a mild La Niña) were analyzed in detail by Allan and Komar (2002).

Analyses by climatologists of North Pacific extratropical cyclones have concluded that their intensities (wind velocities and low atmospheric pressures) have progressively increased over the decades, beginning as early as the 1940s (Graham and Diaz 2001; Fravre and Gershunov 2006). This increase has been attributed by some climatologists to global warming, specifically the accompanied increase in sea-surface temperatures, while another hypothesis suggested that "black carbon" aerosols derived from industries in India and China could have been a contributing factor. While several investigations of mid-latitude extratropical storms in the Eastern Pacific have confirmed this trend of increasing intensities, they have also found changes in the frequencies of occurrences of storms, and that over the decades their tracks have shifted to higher latitudes. For example, McCabe et al. (2001) found a statistically significant decrease in the annual storm frequencies over the years 1959–1997, whereas Geng and Sugi (2003) determined that this decrease typically occurred in the weak to medium range of storm intensities, while the strong storms have shown an increase in frequency. It was found that the tracks of the storms have systematically shifted poleward during the latter half of the twentieth century. Both the frequencies of storms and their paths are thought to have been altered by changes in the high-latitude temperature distributions related to greenhouse warming; the poles are warming faster than the lower latitudes, and this north-south gradient (the baroclinicity) has had an important role in affecting these multiple aspects of storm generation.

Although more research is required to determine the climate controls on the North Pacific extratropical storms, most important to the PNW erosion and flooding impacts is that the storms have clearly intensified over the decades. One therefore would expect that the heights and energies of the storm-generated waves would also have increased, and this has been documented by analyses of buoy measurements along the U.S. West Coast, with the highest waves and greatest rate of increase having occurred on the PNW coast (Allan and Komar 2000, 2006; Méndez et al. 2006; Ruggiero et al. 2010a). Recent confirmation for this increase in wave heights throughout the Northeast Pacific has been provided in the analyses by Young et al. (2011) of measurements since the 1980s derived from satellites.

Fundamental to assessments of existing coastal erosion hazards and their projections into the future are developments of wave climates that document the ranges of significant wave heights (SWHs), periods, and approach directions to the coast (Komar et al. 2010). Also needed are investigations of the possible climate controls on past trends and variations, supporting assessments of the degrees to which the waves might change in the future. The required wave data have been derived mainly from buoys, from hindcast analyses based on the storm parameters (wind speeds, fetch and storm duration), and the century-long records of visual estimates of wave heights and periods. Recently, the satellite altimetry measurements have become important in obtaining a global perspective of the

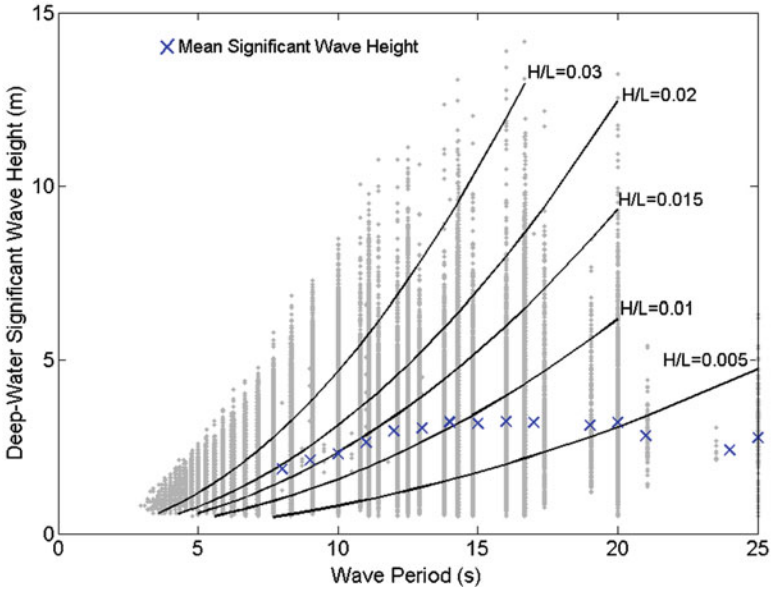

Fig. 21.21 Scatter diagram of hourly deep-water SWHs versus wave periods measured by NDBC buoys #46005 and #46089 (1975–2010) off the PNW coast (Analyses by Erica Harris 2011)

decadal trends in wave heights, and of the wind speeds important to their generation, as reported in the study by Young et al. (2011).

A number of buoys have been deployed along the PNW coast, by the National Data Buoy Center (NDBC) of NOAA and the Coastal Data Information Program (CDIP) at the Scripps Institution of Oceanography. The earliest were deployed during the mid-1970s, ranging from deep-water to mid-shelf water depths. As part of our PNW hazards research, considerable effort has been directed toward documenting the deep-water wave climate based on this buoy data, including its multidecadal climate-controlled trends (Tillotson and Komar 1997; Allan and Komar 2000, 2006; Ruggiero et al. 2010b). An updated graph of the SWHs versus periods is presented in Fig. 21.21 as a "scatter diagram", based on 35 years of buoy measurements (1975–2010). The graph includes a series of curves for the wave steepness, H_s/L_∞ where H_s is the SWH and L_∞ is the deep-water wavelength that depends on the wave period; the X symbols in the graph are the average SWHs for each band of measured wave periods. The overall scatter in the data demonstrates that the highest SWHs are on the order of 12 to nearly 15 m, having periods centered on about 15–17 s, representing swell waves generated by strong storms. Low-wave conditions with SWHs of only 1–2 m range widely in periods from 3 to 25 s, the lowest periods representing locally generated waves while the longest periods are likely low-steepness forerunners generated by distant storms, with the 12- to 15-m highest recorded waves likely having been the later arriving waves from those distant storms.

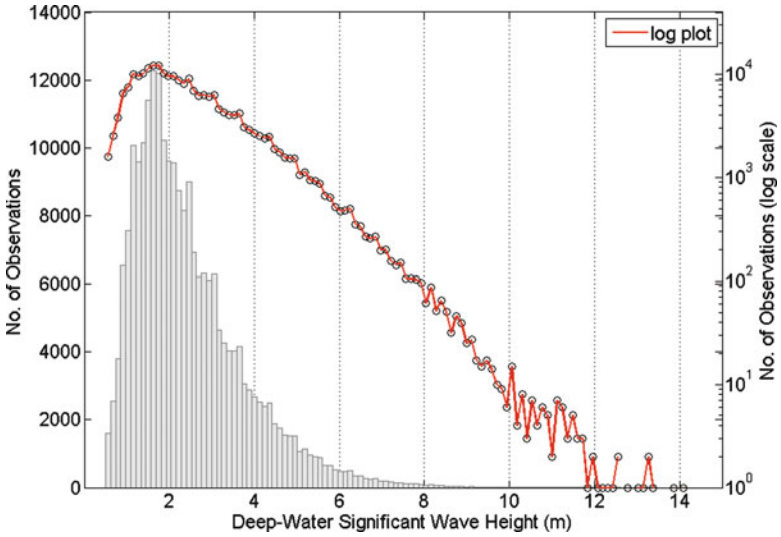

Fig. 21.22 Histograms of the hourly deep-water SWHs measured by the NDBC buoys, the numbers of observations being plotted with linear and log scales (*red*) (Analyses by Erica Harris 2011)

The PNW wave climate is characterized by a marked seasonal variation in the deep-water SWHs, with the summer months having average heights that range from about 1.5 to 2.0 m, increasing on average during the winter from 2.5 to 4.0 m (Tillotson and Komar 1997; Komar 1997; Allan and Komar 2006). Potentially damaging major storms are generally limited to the months of October through March, with erosion and flooding occurrences mainly developing late in that season, after the beaches had been cut back in their normal seasonal profile cycles, and with rip-current embayments having reached their maximum development. It has also been demonstrated that the heights of waves along the PNW coast depend on the El Niño/La Niña range of climate events, being higher during an El Niño winter, lower during an average year or in a La Niña, demonstrated through a correlation with the Multivariate ENSO Index (MEI) that provides a measure of this range of climate variations (Allan and Komar 2006).

The overall histogram of measured deep-water SWHs is graphed in Fig. 21.22 in terms of the numbers of observations during the 35-years of data collection by the NDBC buoys. The numbers of observations are graphed using both linear and log scales, the latter providing a clearer documentation of the most extreme SWHs, with 10^0 representing 1 observation in the decades of measurements (Komar and Allan 2007). Of particular interest to hazard assessments are the storm events when the SHWs exceeded about 10 m, in total being roughly 100 h during those 35 years of buoy measurements, representing on the order of 35 major storm events. Based on this accumulated data and assuming that the measurements represent a "static" data set, unaffected by Earth's changing climate, the projected 50- to 100-year

extremes of interest in future hazard assessments and in engineering design would be on the order of 16–17 m.

While the histograms in Fig. 21.22 of SWHs measured during the past 35 years represent a reasonable present-day wave climate for the PNW, this analysis has omitted a critical aspect of the climate, that on average the measured wave heights and periods have been increasing since the buoys became operational, the wave climate in fact not having been "static" (Allan and Komar 2000, 2006; Komar et al. 2010; Ruggiero et al. 2010b). This time-variation in the PNW wave climate requires methodologies that differ from the traditional extreme-value analyses, in order to obtain improved projections of future extreme wave heights that account for Earth's changing climate.

We first became convinced that the heights of storm waves have been increasing on the PNW coast when five major storms during the winters of 1997–1998 and 1998–1999 generated SWHs that exceeded what previously had been projected to be the 100-year event. This increase is evident in Fig. 21.23, an updated analysis of that originally undertaken by Allan and Komar (2000, 2006), presenting a series of graphs for averages of the hourly-measured SWHs. The top-most graph is for the annual averages, the second the averages for only the "winter" months (October through March) that are important to coastal impacts, and followed by assessments of the more extreme storm wave measurements each year, averages of the five highest measured SWHs and the maximum measured SWH of each winter. It is evident in this series of graphs that there is a systematic pattern with the more extreme wave assessments having increased at greater rates than the averages which included measurements of the more moderate SWHs. The linear regression for the top-most graph of the annual averages for the entire year yields a rate of increase of 0.018 m/year, of interest in that it is comparable magnitude to that found in analyses of wave data from the Northeast Atlantic measured off the coast of England (Carter and Draper 1988; Bacon and Carter 1991, 1993), suggesting that extratropical storms in both oceans might be responding to similar climate controls. The second plot in Fig. 21.23 for the averages during the "winter" (October through March) is of more immediate relevance to the PNW hazards, its regression yielding a higher rate of increase, 0.032 m/year, an increase of 0.8 m in 25 years.

Of significance to hazard assessments are those in Fig. 21.23 for the annual averages of the five strongest storms of the winters, its rate of increase having jumped to 0.095 m/year, and the highest SWH measured each winter that yields a rate of increase of 0.108 m/year (2.7 m in 25 years). However, those rates are presently under review in light of an examination by Gemmrich et al. (2011) of this data from NDBC buoy #46005, having suggested that modifications by NDBC of the hardware and analysis procedures may have resulted in "steps" in the annual-average magnitudes. Most convincing is the "step" from 1980 to 1981, prior to which the heights of the individual measured waves was limited to 11 m, with the highest reported SWHs by this buoy having been 9 m. From the analysis presented in Fig. 21.23, a "step" at that time is evident in the bottom-most graph for the annual maximum SWHs, and possibly also in the graph for the five largest storms; in that the annual averages and winter averages are determined mainly by the vast number

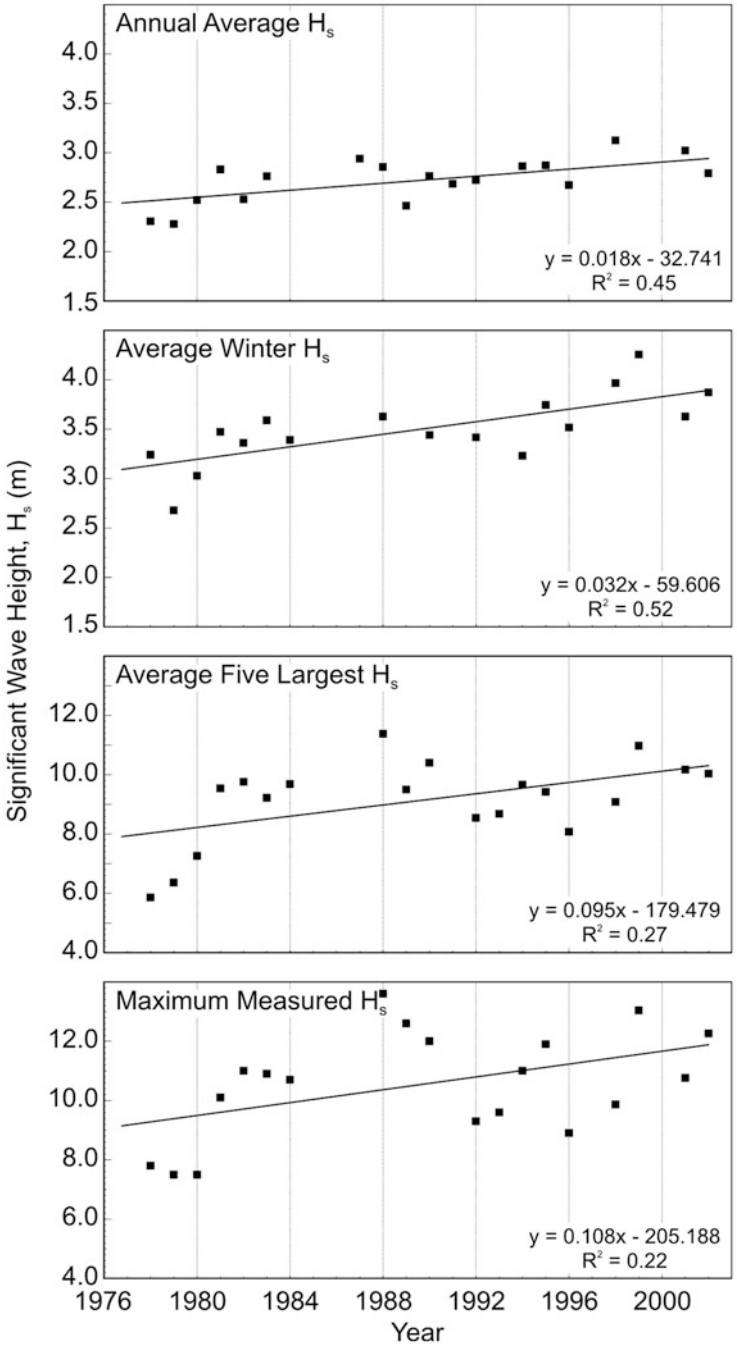

Fig. 21.23 Regressions of increasing waves off the coast of the U.S. Pacific Northwest, the series representing progressively more extreme events (Updated from Allan and Komar (2006))

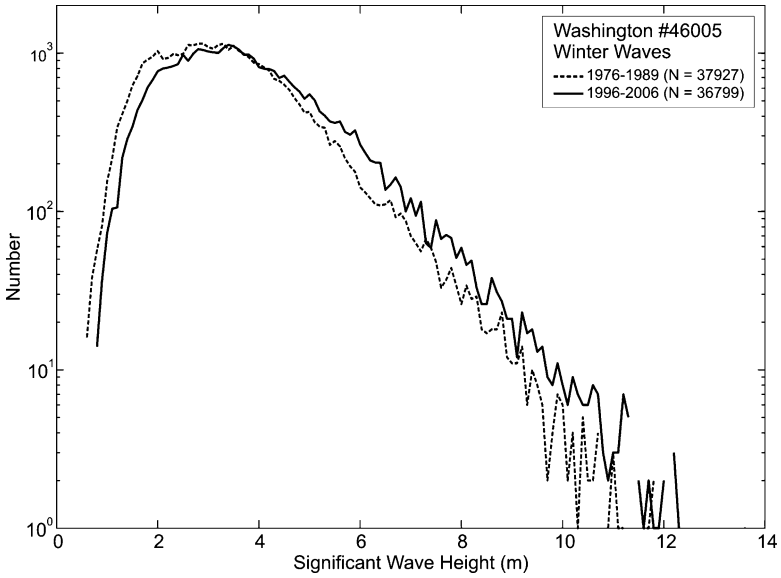

Fig. 21.24 A pair of histograms of the ranges of measured significant wave heights by a buoy off the coast of the PNW, documenting the shift to higher values in recent decades (From Komar et al. (2010))

of measured moderate SWHs, they are unlikely to change from those graphed in Fig. 21.23.

It is noteworthy that analyses of the wave periods measured hourly by the NDBC buoys over the decades also show trends of progressive increases since the 1980s, when NDBC first began to report their hourly values (Allan and Komar 2000, 2006). Such a joint increase in both wave periods and SWHs would be expected to result from the greater storm intensities in the North Pacific that have been documented by climatologists.

The increases in buoy-measured wave heights over the decades have also been documented with pairs of histograms of the SWHs, Fig. 21.24, providing comparisons for the full range of measured values, a more complete documentation of the changing PNW wave climate (Komar and Allan 2007; Komar et al. 2010; Ruggiero et al. 2010b). The years compared by the respective histograms are 1976–1990 and the recent decade 1998–2007—nearly the same numbers of observations are included in each of the histograms. It is seen that there has been a systematic shift to higher values in the entire range of hourly measured SWHs, with the most dramatic increase having been the highest wave events, reflected in the right limbs of the histograms. Of interest, the histograms also indicate that the low waves of the summer, the left limbs of the histograms, have also increased over the decades. Although this is not important to coastal erosion occurrences, there have been increased hazards to fishing and recreational boating along the PNW coast.

The shift in the histograms over the decades has resulted in an increase in the skewness, Fig. 21.24, which is also directly reflected in the series of graphs in Fig. 21.23 where the rate of increase from the regressions progressively increases, being greatest for the highest measured SWHs. As demonstrated by Ruggiero et al. (2010b) in a comparison between these empirical histograms based on the data and theoretical lognormal distributions (e.g., the Weibull Distribution), a modest increase in the annual-average SWHs has a significant impact on the increased magnitudes of the most extreme events, just as seen in the pair of histograms graphed in Fig. 21.24. This result for the PNW SWHs represents a clear example of the phenomenon noted in general terms by Wigley (1988), that a gradual change in the mean climate of an environmental variable (e.g., temperatures, river discharges, etc.) can result in significant increases in the frequencies or magnitudes of the more extreme events and their hazards.

With the multidecadal increase in measured waves off the PNW coast, evident in both Figs. 21.23 and 21.24, it follows that projections of the extreme values will also have increased with time, the SWHs expected during 50- to 100-year storm events. This analysis requires statistical procedures that account for time-varying changes in data populations, extending the methodology commonly used to analyze a static population. Such statistical procedures for non-stationary data populations represent a significant advance over classical extreme-value theory, and have been applied to a variety of environmental processes (temperatures, rainfall, floods, etc.) expected to be affected by global warming.

Figure 21.25 shows the results of an analysis by Ruggiero et al. (2010b) of the PNW buoy data, having applied the generalized extreme value (GEV) distribution that can treat either static or time-varying data sets. Here the data analyzed have been the five highest SWHs measured each year, the occurrences associated with individual storms, not their averages as analyzed in Fig. 21.23 to determine the trends in annual averages. The three lines included in Fig. 21.25 are for the 25-, 50- and 100-year projections, each increasing at a rate of approximately 0.09 m/year as determined by the non-stationary GEV analysis. An analysis based on only the single highest measured SWH each year yielded essentially the same result, the rate of increase being slightly greater, 0.1 m/year. Having modeled the extreme values the rates of increase found in the GEV analysis have a much higher level of statistical significance than did the simple least squares regressions graphed in Fig. 21.23 (Ruggiero et al. 2010b).

In summary, although much remains to be documented about the climate controls on the North Pacific extratropical storms and the waves they generate, it is certain that both the storm intensities and their generated waves have increased during the twentieth century. This increase in SWHs and periods along the PNW coast has been documented with buoy data, the results being consistent with the North Pacific increases measured by satellites since the 1980s (Young et al. 2011). The focus in this section has been the PNW wave climate in deep water, based on measurements derived from buoys that are well offshore in water depths greater than 200 m, prior to the shoaling transformations of the waves as they cross the shallower depths of the continental shelf. Of more immediate relevance to erosion

Fig. 21.25 Statistical analyses of the increasing extreme-value projections of buoy data for PNW wave data, applying the GEV model applicable to time-varying data sets (After Ruggiero et al. (2010b))

and flooding hazards along this coast are processes within the nearshore, on the PNW beaches, including the ranges of wave breaker heights and the levels to which the waves swash up the sloping beaches, potentially impacting the backshore properties. Those are the topics of the following section.

21.6.2 The Nearshore Processes Climate—Wave Breaking and Swash Runup Levels

Having defined the PNW deep-water wave climate based on the buoy data, the next stage in our analyses of potential coastal hazards involve what constitutes the "nearshore processes climate", including those processes that depend directly on the wave conditions, but also on the morphology of the beach (Komar and Allan 2002). Of greatest relevance to the potential impacts to shore-front properties, whether they are located atop cliffs or within foredunes, are the wave-breaker heights that represent a measure of the overall energy at that shoreline location, and the swash runup elevations reached by the waves, foremost being those that occur during storms and high tides. This nearshore climate differs from site to site

due to the local beach morphology, specifically the beach slope that is a factor in calculations of the wave runup.

Several studies have developed semi-empirical formulae that correlate the heights of measured breaking waves on beaches to their corresponding deep-water wave heights and periods [see review in Komar (1998b, pp. 214–217)]. The measurements to establish these formulae have come from controlled laboratory wave-tank experiments and field studies on a number of beaches that represent a variety of morphologies and wave-energy levels. The most successful correlation for the breaker height, H_b, is the formula

$$H_b = 0.39 g^{1/5} \left(T H_\infty^2\right)^{2/5} \tag{21.1}$$

where T is the wave period and H_∞ is the deep-water wave height. Perhaps unexpected, according to this formula and those developed by others there is not a dependence on the beach slope, a conclusion based on data collected over a large range of slopes. Uncertain is the degree to which this formula accounts for energy losses due to bottom friction, although it is presumed to on average empirically include some effects of bottom drag and wave energy losses, especially in the field data used to derive this formula. It needs to be recognized that the resulting nearshore climate of calculated wave breaker heights for the PNW is only approximate, providing a general representation of the wave-energy levels, with the results not actually being used quantitatively in deriving assessments for the coastal erosion and flooding hazards.

Each combination of buoy-measured SWHs and periods used to define the deep-water wave climate (Fig. 21.21) was used in calculating the corresponding breaker heights with equation (1), yielding the histograms in Fig. 21.26. As expected, these histograms for the breaker heights are closely similar in form to those for the deep-water SWHs, Fig. 21.22, the breakers systematically being somewhat higher with their extremes having reached 16 m. There is no direct verification of these magnitudes, only the indirect indication that during storms the extent of the surf-zone width governed by the initial wave breaking expands to water depths that would correspond to the breaker-height magnitudes in the histogram of Fig. 21.26. The SWHs of these extreme waves during storms do provide a general indication of the severity of the hazards faced by properties along the PNW coast.

While the calculated breaker heights are not actually used in the hazard assessments, of significance are the storm-wave runup levels that combine with the elevations of the measured tides to determine the total water elevations (Ruggiero et al. 2001). The wave swash runup level and its horizontal distance of flow across the beach width depend on both the deep-water SWH and period, and also on the slope of the beach, the greater the slope the higher the runup. Therefore, important to erosion events are the major storms that generate combinations of extreme SWHs and long periods, the highest waves in the 15- to 20-s period range in the "scatter diagram" of Fig. 21.21. It also follows that with there having been a decadal increase in the deep-water SWHs and periods along the PNW coast, there

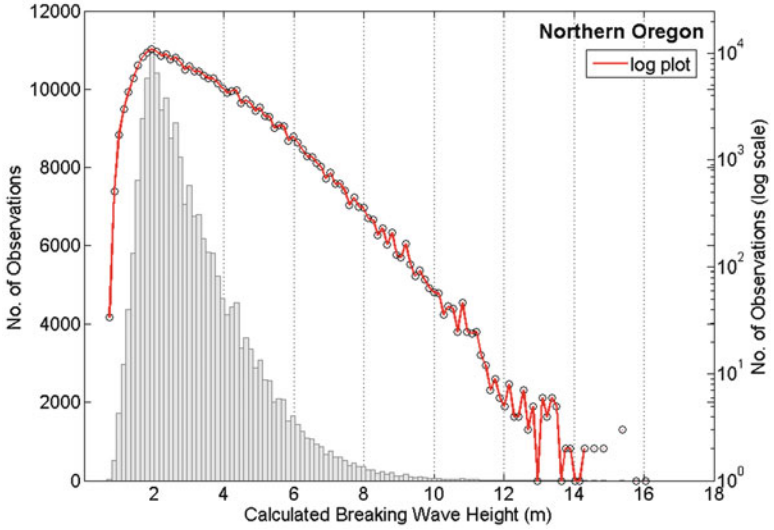

Fig. 21.26 Wave-breaker heights calculated with Eq. (21.1) from the deep-water wave climate (Analyses by Erica Harris 2011)

would have been a corresponding increase in the levels of the swash runup on the beaches, combining with the net rise in sea level to result in progressively greater erosion and flooding impacts. Of concern is how this combination of sea-level rise and storm-wave runup will increase in the future, leading to still greater impacts during the next 100 years.

A number of research investigations over the years have focused on analyses of wave runup on beaches (reviewed by Komar (1998b)), in part due to its obvious importance to occurrences of property erosion, where the elevation achieved by the runup as a function of the offshore wave heights and periods is of principal interest. In our analyses of runup on the PNW beaches, we have employed the formula derived by Stockdon et al. (2006), who analyzed time series of water-level measurements derived from ten field investigations, representing diverse beaches in the morphodynamics classification of Wright and Short (1983). Of significance is that included in the derivation of their formulae were runup measurements collected on the Oregon coast, which had been used to calibrate an earlier form of their relationship (Ruggiero et al. 2001, 2004). The semi-empirical analyses by Stockdon et al. (2006) separately considered the mean wave setup at the shore and the additive wave swash, with analyses of the latter to consider both the incident and infragravity energies within the motions and maximum levels of the swash. Their general expression for all beaches based on the multiple sets of data and including these multiple causative processes is

$$R_{2\%} = 1.1\left\{0.35S(H_\infty L_\infty)^{1/2} + \frac{1}{2}\left[H_\infty L_\infty\left(0.563S^2 + 0.004\right)\right]^{1/2}\right\} \qquad (21.2)$$

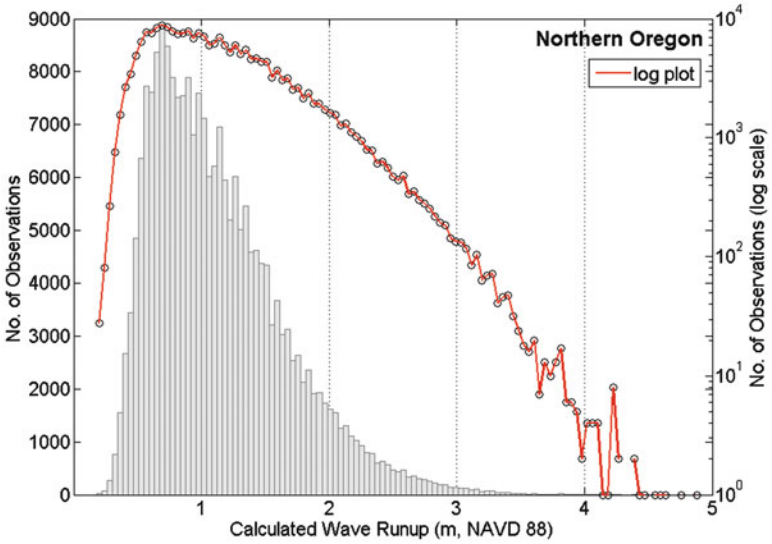

Fig. 21.27 Linear and log graphs of the wave swash runup levels (the vertical component), calculated with Eq. (21.2) from the deep-water wave climate and for a representative S = 0.04 beach slope (Analyses by Erica Harris 2011)

with the runup level, $R_{2\%}$, representing the 2% exceedance value in the distribution of individual measured swash maxima, an extreme in the distribution but a level that occurs sufficiently often within an hour that it represents a meaningful factor for the impacts to backshore properties. This equation shows the dependence on the beach slope, S, as well as on the deep-water wave parameters; with the wavelength being given by $L_\infty = (g/2\pi)T^2$, the calculated runup depends on the combination, $TH_\infty^{1/2}$, a stronger dependence on the wave period than on the deep-water SWH, contrasting with the dependence in equation (21.1) for the wave-breaker heights where the SWH is dominant.

Each combination of deep-water SWH and period is again used, now to calculate the swash runup levels for a beach slope $S = 0.04$ (1-in-25), representative of the PNW dissipative sand beaches (Allan et al. 2003), the results being graphed in Fig. 21.27 as histograms. The histogram is again similar to that for the deep-water SWHs (Fig. 21.22), even though the magnitudes of the runup are more strongly dependent on the periods. It is evident that storms having periods on the order of 15–20 s within the scatter diagram of Fig. 21.21 must be those responsible for the most extreme $R_{2\%}$ runup magnitudes. These extremes achieve a runup level of about 5 m, which on a 1-in-25 beach slope involves 125 m of horizontal motion by the swash on the dissipative beaches, a reasonable result in that this calculation represents the 2%-exceedence swash level during the most extreme deep-water waves that had been measured in 35 years. Far more common are runup levels of 1–2 m, resulting in 25- to 50-m distances in crossing the beach, again reasonable on these low-sloping beaches.

The above analyses of the wave breaker heights and swash runup levels on a PNW beach represent the present-day nearshore processes climate, just as did the histogram of deep-water SWHs (Fig. 21.22) for the wave climate. However, since the deep-water SWHs and periods have progressively increased over the decades, it would be expected that the wave breaker heights and runup levels have increased in tandem. The increases in these PNW beach processes have been analyzed in a series of publications, initially as an example application in the development of nearshore processes climates (Allan and Komar 2002), then in analyses of the climate controls on both the deep-water waves and nearshore processes important to U.S. West Coast erosion (Allan and Komar 2006), and most recently in a comparison between the trends of increasing runup levels determined by the deep-water SWHs versus the trends in PNW rising sea levels (Ruggiero in press).

Figure 21.28 graphs the trends in the wave breaker heights and runup levels based on data from NDBC buoy #46005, the same buoy used above to document the deep-water wave climate, except that the analyses here are limited to the post-1980 years since data for the wave periods are required as well as the SWHs. The analyses are based on the winter averages, October through March (Allan and Komar 2006). The regression for the annual average wave-breaker SWHs is 0.027 m/year, an increase of 0.68 m in 25 years, corresponding closely to the rate of increase in the deep-water SWHs for the winter averages (Fig. 21.23). The regression for the winter averages of the swash runup levels for the PNW is 0.008 m/year, a 0.2-m vertical increase that corresponds to a 5-m horizontal transgression of the water across a 1-in-25 PNW dissipative sand beach. This reduced rate of increase compared to the breaker heights can be attributed to the dependence of equation (21.2) for the runup on the SWH-period combination $TH_{\infty}^{1/2}$, the net trend thereby depending mainly on the wave period and with annual variations in SWHs mainly contributing scatter to the annual runup magnitudes. Although this 0.008 m/year rate of increase is small, it is significant in that it is equivalent to an 8 mm/year rise in the winter mean swash runup levels, affecting the average shoreline position and in effect having caused a transgression of the winter water levels that is of the same order of magnitude as the rise in mean sea levels (Allan and Komar 2002, 2006).

The significance of this trend in the multidecadal rise in the wave-swash runup levels versus magnitudes of change in relative sea levels along the PNW coast has been analyzed in detail by Ruggiero (in press), of interest being their relative importance to coastal erosion and flooding, at present and in the future as both the wave runup elevations and sea levels continue to increase. The analysis is complicated by the fact that, as will be reviewed later, the PNW coast is experiencing tectonic uplift such that the present trends of relative sea-level change are both up and down, different stretches of shore being either emergent or submergent. According to the analyses by Ruggiero (in press), under a range of future climate change scenarios the increasing storm-wave heights and runup at the shore may continue to increase the probability of property impacts to a greater degree than the projected rise in sea level. Of concern, their combined effects increasing the total water levels could cause as much as a factor of five increase in the frequencies of erosion and flooding over the coming decades.

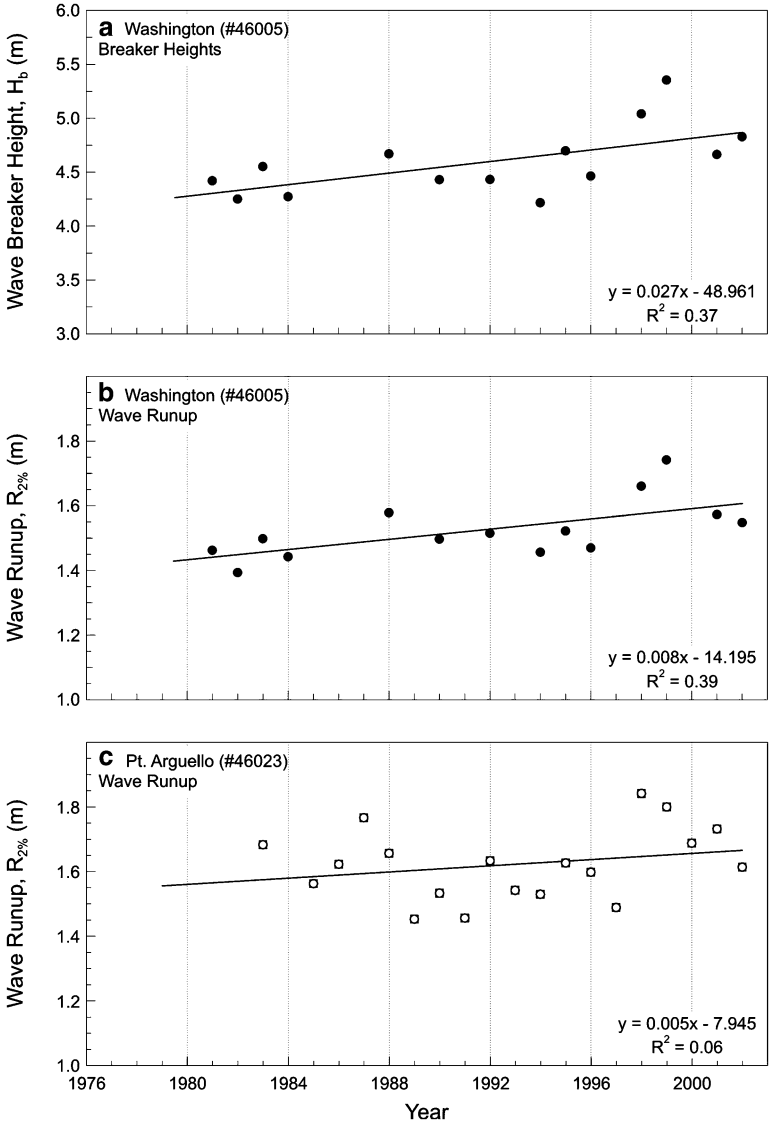

Fig. 21.28 Calculated wave breaker heights and wave runup levels on a representative PNW beach with a slope S = 0.04, showing trends of increase due to the multidecadal increases in deep-water SWHs and periods, compared with an analysis for Pt. Arguello in southern California. (After Allan and Komar (2006))

21.6.3 PNW Tides—Predicted and Measured

The predicted astronomical tides along the PNW coast have a mean range of about 2 m, 3 m during Spring tides, and a maximum range of about 4 m. There are two highs and two lows each day, with successive highs (or lows) usually having markedly different elevations (classified as Mixed Tides). Having these ranges, on a typical sand beach with a 1-in-25 slope the horizontal migration of the still-water shoreline can amount to 50–100 m, representing a significant control on the hour-to-hour water levels and positions of the shore. The tidal cycles therefore largely determine occurrences when the superimposed swash runup of storm waves can reach and impact backshore properties.

While the elevations of the predicted tides in themselves are important to PNW erosion and flooding hazards, significant are the enhanced levels that are actually measured by the tide gauges, which can be on the order or 1–2 m higher than predicted, representing an additional 25- to 50-m landward shift in the position of the still-water shoreline. There are a number of processes responsible for these elevated measured tides on the PNW coast, each having its climate controls: (1) a seasonal variation with the greatest increase in the measured versus predicted tides occurring during the winter months; (2) a considerable magnification of that seasonal cycle due to the El Niño/La Niña range of climate events, with the highest winter water levels occurring during strong El Niños; and (3) the hours to days increase caused by storm surges, being on the order of 1.5 m. These processes, their magnitudes, and roles in PNW erosion and flooding have been an important focus of our research, with the results reviewed here.

There are seasonal variations in mean water levels along all ocean shores, generally due to month-to-month variations in water temperatures and to a small degree their salinities, it being the resulting changes in water density that alternately depress or raise the monthly mean water levels, by tens of centimeters on some coasts. Usually water temperatures are warmest during the summer, in the Northern Hemisphere generally achieving their maximum in August, producing a thermal expansion of the water and a rise in the summer water levels. In contrast, the cold water of the winter is denser, depressing the sea level, the result being a well-defined seasonal cycle between summer and winter in the coastal monthly-mean sea levels. Such variations have been analyzed from tide-gauge records by simply averaging the hourly values of the measured tide minus the predicted astronomical tide to determine the monthly mean nontidal factors that affect the measured tides. Although in most tide-gauge records this cycle is found to be caused simply by seasonal variations in water temperatures, with the maximum increase occurring during the summer when the water is warmest, changes in water levels can also be affected by coastal currents and their seasonal variations, and by surges generated during storms. All of these processes are important to the cycles and magnitudes of the monthly-mean water levels along the PNW coast, with the results however being significantly different than found on most other coasts in that the maximum elevated water levels occur during the winter, thereby being a significant factor in

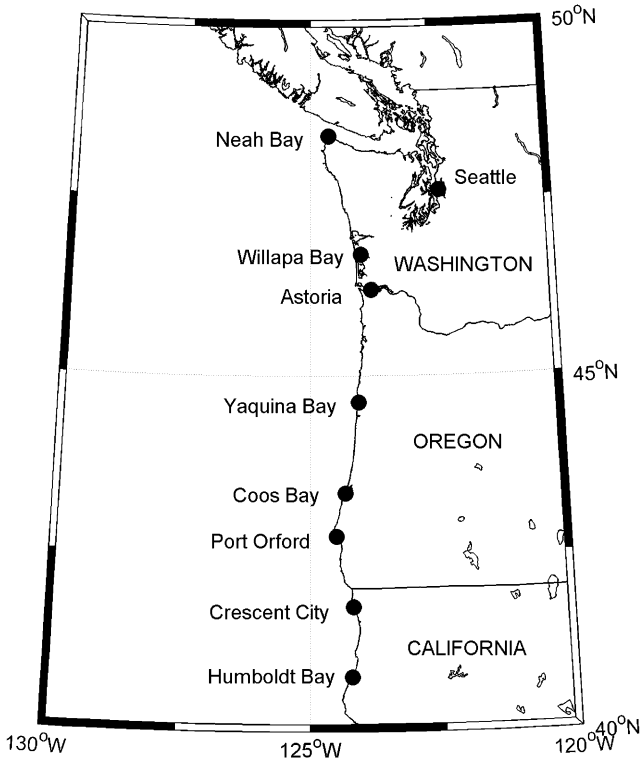

Fig. 21.29 NOAA tide gauges along the PNW coast

this coast's erosion and flooding since the elevated water levels occur in concert with the highest storm-wave heights and swash runup levels.

There are 16 tide gauges along the PNW coast, Fig. 21.29, operated by the National Ocean Service (NOS) of NOAA, with the longest records being from Crescent City (77 years) near the Oregon-California border, Astoria (85) on the Columbia River, and Neah Bay (75) at the north end of Washington's ocean shore. The Seattle gauge in Puget Sound (110 years) is sometimes included in our analyses, especially of the trends in sea levels since it is located inland in a more tectonically stable area than the gauges along the coast (Komar et al. 2011a). The records from the other coastal tide gauges, Fig. 21.29, range in lengths from 30 to 40 years. In addition to providing hourly measurement of the tides, records from these gauges have been used to analyze the seasonal variations in monthly-mean water levels, the magnitudes of storm surges, the trends and rates of change in relative sea levels, and the heights of tsunami waves.

Figure 21.30 graphs the cycle of the monthly-mean water levels based on records from the Yaquina Bay (Newport) tide gauge on the mid-Oregon coast, being averages of the hourly water-level departures from the predicted tides (Komar et al. 2011a, b). The solid curve is for the long-term averages based on the complete

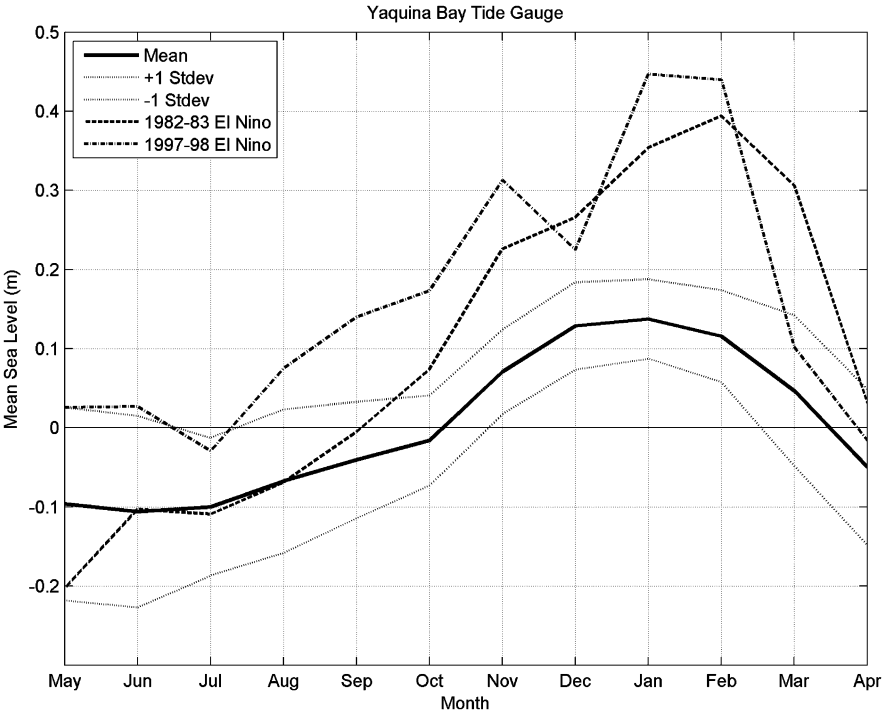

Fig. 21.30 Monthly-mean water levels on the mid-Oregon coast, the seasonal cycle of the long-term average and during the 1982–1983 and 1997–1998 major El Niños (From Komar et al. (2011a, b))

41-years record of measurements, showing that the lowest water levels occur during the summer, reaching a low in June, on average about 0.1-m lower than the predicted tides. The highest water levels occur during the winter, the months of December through February, elevated by about 0.1 m above the predicted levels. There are multiple processes that account for this seasonal variation and the fact that the maximum water elevations occur during the winter, rather than in the summer as found on most other coasts. Most important in bringing about this inverse on the PNW coast is the occurrence of upwelling during the summer, introducing cold deep-ocean water onto the shallow continental shelf, the water being denser than during the winter when the monthly-mean water levels are therefore higher relative to those in the summer. The seasonal changes in upwelling are initiated by the altered directions and magnitudes of the shelf currents that flow parallel to the coast, being directed toward the south during the summer, north in the winter. With the southward currents of the summer, there is an offshore-directed component to the flow as it tends to turn toward the right due to the effects of the Coriolis force (the Earth's rotation); the water moving offshore is replaced by the cold upwelling water arriving from the ocean's depths. In contrast, during

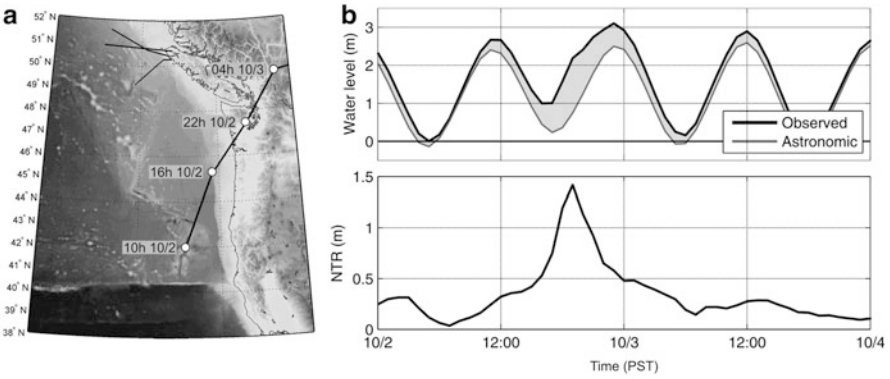

Fig. 21.31 Analysis of a storm surge on October 2–3, 1967, measured by the Yaquina Bay tide gauge on the mid-Oregon coast (From Allan et al. (2011))

the winter the shelf current is mainly toward the north in response to the prevailing winds of that season. Although this current is essentially parallel to the coast, it is again deflected to the right, now toward the coast where it raises water levels along the PNW shore, measured by its tide gauges. The stronger the northward-directed current, the greater the Coriolis force deflection and the higher the measured tides.

Also graphed in Fig. 21.30 are the seasonal variations in monthly-mean water levels for the 1981–1982 and 1997–1998 twelve-month periods, centered on the summer and following winter, those years being of interest due to occurrences of major El Niño climate events. It is evident in the diagram that the monthly-mean water cycles experienced during those strong El Niños departed significantly from the long-term average cycle. Most important to coastal erosion and flooding, the water levels during the winter were far higher than normal, having been approximately 40–50 cm higher in the winter than during the preceding summer, some 25–30 cm higher than during an average winter. With those enhanced water elevations, the average winter shoreline would have shifted landward by another 6–7.5 m beyond that normally experienced during a winter, accounting for the observation that during those two strong El Niño winters the beach profiles were essentially flooded out, even at times of low tides, permitting the wave swash to reach much higher elevations on the beach and to impact shore-front properties on nearly a daily basis. The result was property erosion at numerous sites along the PNW coast (Komar 1986, 1998a, b; Komar et al. 2000; Kaminsky et al. 1998), reviewed earlier.

On shorter time spans of hours to a few days, significantly higher measured than predicted tides can occur during the winter months due to surges generated by strong storms. An example is shown in Fig. 21.31, measured by the Yaquina Bay tide gauge on the Oregon coast, the track of the storm shown on the left being typical of the oblique approach to the PNW shore, in this example having crossed the shore of Washington (Allan et al. 2011). The analysis in the diagram compares the measured versus predicted astronomical tides, the difference

being a surge that reached a maximum level of 1.4 m, with levels above 1 m having lasted about 4 h. In terms of surge magnitudes along the PNW coast, this occurrence represents a fairy major surge event. In our analyses of the unusual series of storms during the 1997–1998 and 1998–1999 winters, we identified surges on the order of 0.5 m on the Oregon coast, and as much as 1.6 m on the central Washington coast, generated by the extreme storm on March 2–3, 1999 (Allan and Komar 2002). Although not nearly as high as surges along the U.S. East Coast due to hurricanes and Nor'easters, a 1- to 2-m surge on the low-sloping PNW beaches could result in some 35–50 m landward shift in the mean shoreline position, important to property impacts with the expectation that the surge would be accompanied by the runup of the large waves also generated by the storm.

There has been comparatively little research in the past directed toward investigations of PNW storm surges, it therefore having become the focus of our continuing investigations to determine their significance in episodes of property erosion and flooding. Of interest in this research is a documentation of the ranges in magnitudes and extremes in the surge levels, and how they relate to the meteorology and tracks of the storms, much as undertaken in our previous publication limited to the 1997–1998 and 1998–1999 winters (Allan and Komar 2002). In addition, we are now also emphasizing the longer-term climate controls, including the possibility that the surge magnitudes have increased over the decades, considering that the storm intensities and the heights of their waves have increased.

Our published results thus far presented analysis results based on the 44-year record of measured tides by the Yaquina Bay tide gauge (Allan et al. 2011), the results expected to be reasonably representative of the PNW in terms of the numbers and magnitudes of surge events, and how they may have changed over the decades. A storm-surge water level is generally defined as the difference between the measured tide and predicted astronomical tide, this difference commonly being referred to as the non-tidal residual (NTR), the excess water levels generated by a severe storm (Pugh 2004). While this simple procedure would generally be satisfactory in investigations of the U.S. East Coast surge events where their levels can reach magnitudes on the order of 5–10 m, that methodology is insufficient on the coast of the PNW where the surge levels are smaller and there are additional ocean processes that significantly affect the daily and monthly-mean water levels, particularly during major El Niños as reviewed above. A PNW storm surge will therefore commonly be superimposed on an already elevated measured tide, tens of centimeters above the predicted tide. Accordingly, we have had to develop analysis procedures that first account for those non-surge portions of the NTRs, essentially representing the measured tides in the days prior to and following the storm and its surge, the non-surge portion being deducted from the measured water levels to leave only the portion that can be attributed to the surge (Allan et al. 2011). With this isolation of the surge contribution, our analyses then focus on the ranges of surge magnitudes and frequencies of occurrence over the decades, the existence of any trends and variations that might have climate controls,

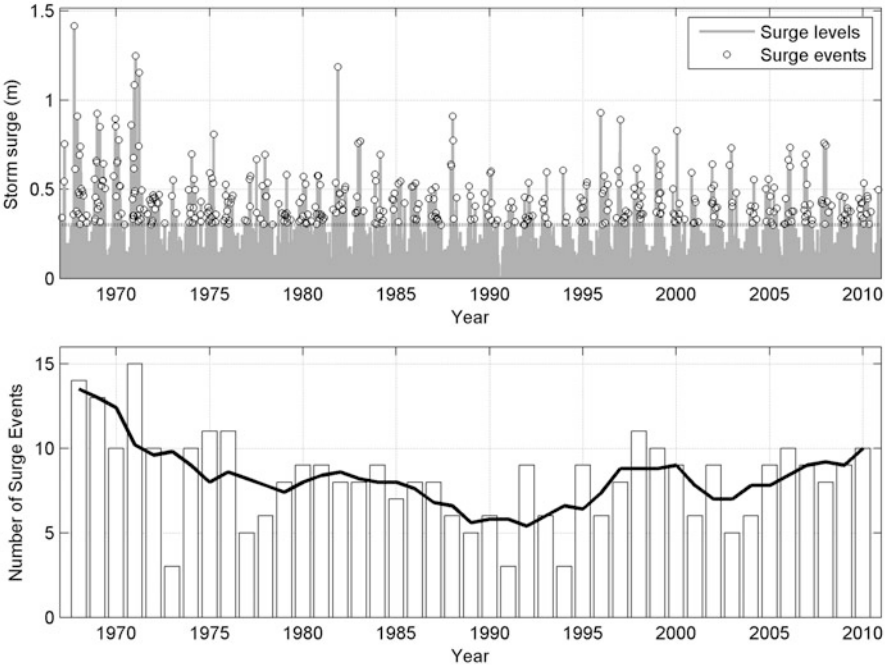

Fig. 21.32 (*Upper*) Temporal pattern in the magnitudes of storm surges measured by the Yaquina Bay tide gauge. (*Lower*) Numbers of annual surge events and a curve based on the 5-year running average (From Allan et al. (2011))

and the hourly variations of individual extreme surge events and their dependence on the storm meteorology.

The results of our analyses based on the Yaquina Bay tide gauge are graphed in Fig. 21.32, the upper panel being the storm-surge magnitudes, having removed the effects of other processes (e.g., El Niños). Collectively the levels of the surge magnitudes approximate a normal distribution (Allan et al. 2011), and on that basis we defined the "significant" surge events of interest to coastal hazards to be those that exceeded two standard deviations above the mean value, based only the winter data when extreme surges and coastal impacts occur (Zhang et al. 2001). In this case for the Yaquina Bay tide gauge, the critical value for the occurrence of significant storm surges was determined to be 0.30 m, a level that is noted by the horizontal dashed line in Fig. 21.32. Additional filtering was then undertaken using a 2-day duration window to constrain the individual storm events, avoiding the potential for secondary peaks that might be associated with the same storm.

The resulting significant surge events and their maximum levels are highlighted in the upper plot of Fig. 21.32 by the open circles. Evident are groupings of years during which there were higher magnitude surges, separated by decades of low surge magnitudes, with only an occasional high-magnitude event. Noteworthy is the concentration of high surges from the beginning of the record in 1965 through

the winter of 1971–1972, followed by a relatively quiet period that continued until the winter of 1996–1997, when high surges again occurred during the decade up to 2008, the coast at present appearing to again be in a quiet phase.

The lower panel of Fig. 21.32 graphs the annual numbers of winter storm-surge events above the 0.30-m threshold level. The maximum number, 15, occurred in the winter of 1971–1972, when water levels also reached magnitudes of 1.1 to 1.3 m. Overall, the annual numbers of surge events show a similar trend to their magnitudes, having decreased since the late 1960s, reaching a low in the late 1970s, and having increased slightly in the early 1980s. The numbers of surge events decreased throughout the late 1980s and early 1990s, before increasing to another peak in the late 1990s. Since 2005 surge frequencies have remained relatively high (8–10 events/year). Thus, the frequency of surges point to there possibly having been cycles of occurrences within the overall multidecadal variations (Allan et al. 2011).

With it having been well documented from analyses of PNW buoy data that the SWHs and wave periods have progressively increased since at least 1980 (Allan and Komar 2000, 2006; Ruggiero et al. 2010b), the expectation was that there would have been a parallel increase in the magnitudes and frequencies of storm surges. However, it is evident in Fig. 21.32 that this has not been the case, at least for surges measured by the Yaquina Bay tide gauge. There is even a suggestion that the surge levels and frequencies have decreased somewhat over the decades. However, that apparent decrease is governed in large part by the cluster of significant surge magnitudes and numbers during the late 1960s and early 1970s, after which there may have been sporadic occurrences of high surges but generally having achieved levels that were less than 1 m, below what would be considered to be an extreme event (Allan et al. 2011).

Our investigations of PNW storm surges are continuing, including the other tide gauges along this coast so we will have surge measurements from the open coast (the Crescent City, Port Orford and Neah Bay breakwaters), as well as from additional bays and estuaries. With this expanded coverage we should have a much improved documentation of the climates of surge magnitudes and numbers of annual occurrences, including the important assessment of their potential extremes. Of special interest will be the presence of multidecadal trends and cycles having climate controls.

In summary, there are important variations in multiple ocean process and their climate controls the affect the mean water levels along the PNW coast, producing elevated measured tides that are well above predicted elevations. There is the expected seasonal variation in monthly-mean water levels in response to changes in water temperatures, but important to coastal hazards is that the PNW cycle is unusual in that the maximum mean water levels and enhanced measured tides occur during the winter months, concurrent with extremes of winter storms and waves. Significantly higher winter water levels occur during major El Niños, such as those in 1982–1983 and 1997–1998, having been a significant factor in erosion and flooding along the entire PNW coast. Also important are storm surges, with as many as 15 significant occurrences during a winter, and with the surge magnitudes

having reached 1.5 m, the expectation being that extreme surge events could reach 2.0 m.

These processes elevate the measured tides on an hourly to monthly basis, or in the case of a strong El Niño through the entire winter. Important is that these mean water levels establish the elevations and shoreline positions beyond which the runup of the wave swash occurs, it being this combination that results in episodes of PNW erosion and flooding. With a future rise in sea levels, the elevations of these processes will correspondingly increase, continuing to be an important part of the coastal hazards.

21.6.4 PNW Sea Levels—Measured Trends and Future Projections

Of the climate-controlled coastal hazards, the primary concern globally is the prospect of there being an accelerated rate of rise in sea levels during this century, a consequence of global warming. While mean ocean levels during the twentieth century increased by some 0.15–0.20 m, based on assessments from long-term tide gauge records, projections into the future by various investigators have generally ranged from about 0.5–1.0 m by the end of this century, the more extreme projections being as great as 1.5 m. Although these magnitudes remain uncertain in that they depend on society's future emissions of greenhouse gases as well as on the physical processes of the climate responses, any increase in the rate of sea-level rise would result in greater erosion and flooding impacts than had occurred during the past century. For this reason, in the development of management strategies, the primary focus has been on future sea levels and the resulting enhanced coastal hazards.

The present-day and future increases in sea levels along the PNW coast have been an important aspect of our hazard investigations (Komar et al. 2011a), but with the analyses and implications for future impacts being more complex than on most other coasts. This is a result of the tectonic setting of the PNW coast, with plate subduction producing a progressive rise in land elevations along its shores, with some areas rising faster than others, affecting the relative rates of sea-level rise such that at present some stretches of shore are submergent while others are emergent. An important question is how these present-day alongcoast patterns and magnitudes of trends in relative sea levels will change in the future with accelerated rates of rising global sea levels.

There are 16 NOS/NOAA tide gauges along the PNW ocean shores, Fig. 21.29, providing excellent alongcoast coverage to document the trends in relative sea levels (RSL), determined by the combination of the eustatic rise in global sea level and the rate of change in the land elevation at the site of the gauge. Particularly important in our analyses have been the long-term records from Crescent City, California (77 years), Astoria (85) on the Columbia River, and Neah Bay (75) at the

north end of Washington's ocean shore, and the Seattle gauge in Puget Sound (110 years) which provides a more stable location inland from the affects of plate subduction that are causing the changes in coastal land elevations (Komar et al. 2011a). The records from the other coastal tide gauges range in lengths from 30 to 40 years, somewhat short for confident determinations of the rates of change in RSLs from regression analyses, especially in that the annual sea levels are affected by the El Niño/La Niña range of climate events, adding significant scatter to the annual averages.

In our analyses of the PNW coastal erosion and flooding hazards, for each tide gauge we have documented the multidecadal trend in the RSL, and also the annual extremes that occur during major El Niños, which can produce a sea-level rise of tens of centimeters within a couple of months, lasting through the winter and therefore important to the coastal impacts (Komar et al. 2011a). This duel interest led to our development of a methodology in which we separately analyze the summer and winter records for their respective mean-water levels, "winter" being defined as the 3-month period around the peak of that season's maximum, typically the months of December through February, the "summer" representing 3 months of its minimum levels. Three example results are shown in Fig. 21.33, representing the length of the PNW ocean shore, analyses of the tide-gauges at Neah Bay, Yaquina Bay and Humboldt Bay in California on the southern-most shore of our study area. In each record the winter data and its regression line are seen to be displaced above those for the summer by 0.2–0.3 m, this difference reflecting the seasonal cycles as graphed in Fig. 21.30 for the Yaquina Bay gauge, the winter water levels consistently being higher than during the summer. Neah Bay is seen in Fig. 21.33 to be on an emergent stretch of coast, having a downward trend of lowered RSLs, whereas Yaquina Bay and Humboldt Bay have positive trends, being submergent shores where the eustatic rate of sea-level rise exceeds the rate of coastal tectonic uplift.

The results in Fig. 21.33 demonstrate that our analysis methodology based on the seasons has had its intended effect, providing a documentation of the magnitudes of the elevated water levels that occur during El Niño winters, while at the same time the graphs based on the summer months reduced the data scatter and yield improved assessments for the multidecadal trends in RSLs. Based on the statistics of the regressions, it was found that with one exception (Crescent City), the analyses limited to the summer tide-gauge records provide improved assessments of the trends compared with those based on the annual averages or monthly averages (Komar et al. 2011a). This smoothing of the summer records is due to their not having been affected by storm-surge events, nor the extreme water levels during major El Niños that are instead emphasized by the winter records. Therefore, in our hazard assessments the multidecadal trends in RSLs have been based on analyses of the "summer" records, illustrated in Fig. 21.34 including the result for Crescent City that is also on an emergent shore. This diagram demonstrates the extent of variations in the trends and rates of change in RSLs along the PNW coast, with alternating stretches of shore being submergent and emergent, depending on the alongcoast changes in the rates of tectonic uplift of the land compared with the eustatic rise in sea level.

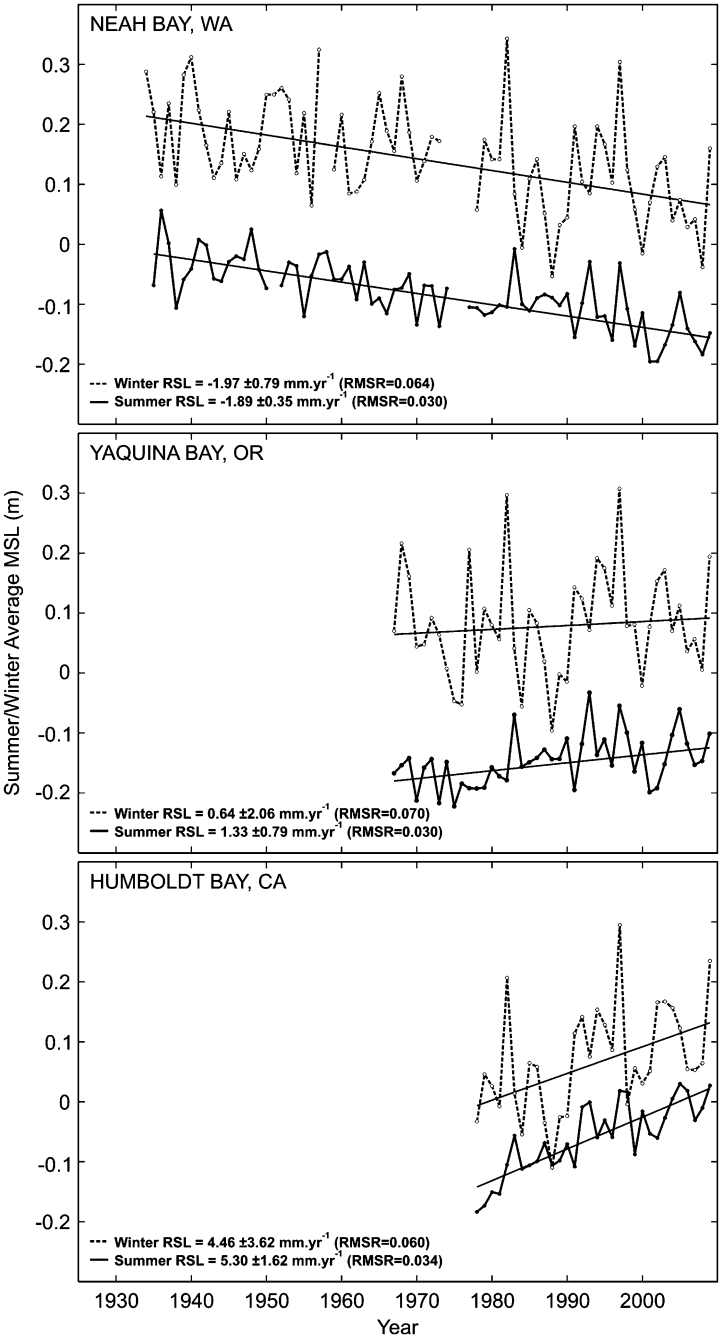

Fig. 21.33 Trends and variations in the winter (*dashed lines*) versus the summer (*solid lines*) relative sea levels for the Neah Bay, Yaquina Bay, and Humboldt Bay tide-gauge records (From Komar et al. (2011a))

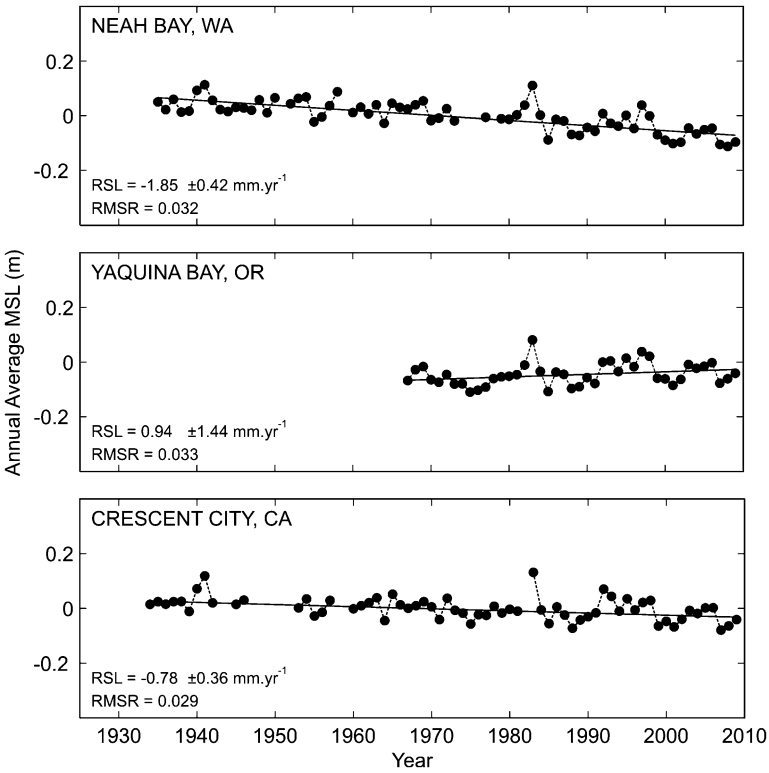

Fig. 21.34 Tide-gauge analyses based on the summer records to determine their multidecadal trends, documenting stretches of emergent and submergent shores (From Komar et al. (2011b))

A more detailed documentation of these variations is possible along the coast of Oregon, where Burgette et al. (2009) analyzed the land-elevation changes based on periodic surveys of benchmarks. In order to compare the tide-gauge RSL trends derived in our analyses with the rates of change in land elevations derived from the benchmark surveys, it was necessary to add the regional eustatic rate of sea level rise to the benchmark rates. As demonstrated by the geophysical analyses of Clark et al. (1978), the rates of sea-level rise at specific coastal sites can differ significantly from a globally-averaged rate such as the 1.74-mm/year value found by Holgate (2007) based on tide gauges throughout the world. Burgette et al. (2009) derived an average rate of 2.28 $\pm$ 0.20 mm/year for the PNW regional eustatic component of the sea-level rise, based on the Seattle tide-gauge record with an assumption that it is stable. The resulting comparison derived from our analyses of the tide-gauge records and those by Burgette et al. (2009) from the benchmark surveys is shown in Fig. 21.35, where the results are in reasonably good agreement as to the magnitudes of the trends in RSLs and the alongcoast variations, with alternating stretches of submergent and emergent shores. Exact agreement is not expected between the tide gauge and benchmark sea-level rates, in that as shown by

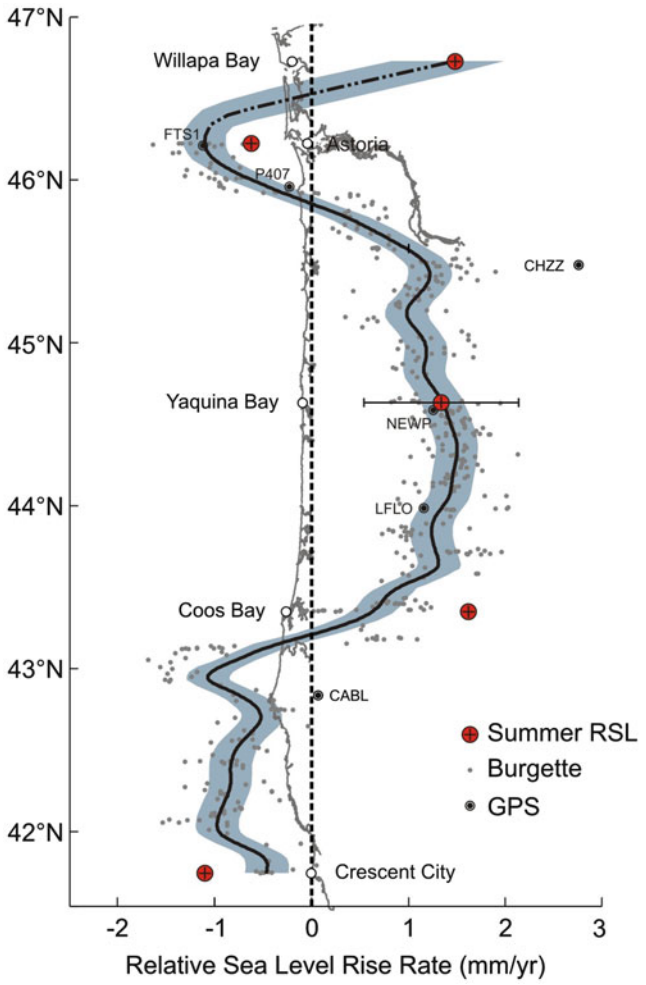

Fig. 21.35 Comparison between the multidecadal trends in relative sea levels derived from tide gauges and land-elevation changes based on GPS data and benchmark surveys analyzed by Burgette et al. (2009) (Modified from Komar et al. (2011a))

Burgette et al. (2009) the rate of uplift of the land decreases with distance inland from the coast, being dependent on the position of the benchmark relative to the descending plate that is being subducted; the rate of RSL change measured by a tide gauge is similarly affected. The high rate of increase in RSL measured by the Humboldt Bay tide gauge, 5.30 mm/year (Fig. 21.35), is due to its close proximity to the subduction zone where the crust is being dragged down, this being the only area along the PNW coast where the land is tectonically subsiding.

This alongcoast variation in the rates and directions of changing RSLs represents a primary factor in governing which stretches of shore are experiencing erosion

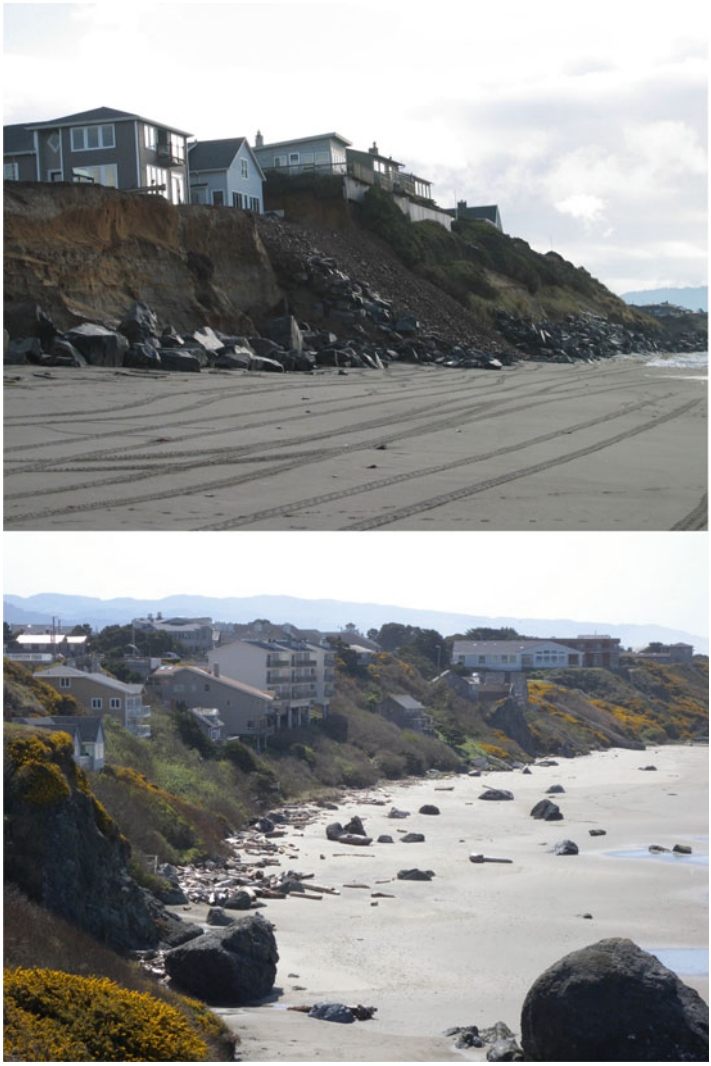

Fig. 21.36 Alongcoast differences in erosion impacts: (*Upper*) The eroding sea cliff on the submergent shore of Gleneden Beach on the north-central Oregon coast; (*Lower*) The emergent stable shore at Bandon on the southern Oregon coast (Photos by J.C. Allan)

versus those being stable or accreting (Komar and Shih 1993). The variable impacts are illustrated in Fig. 21.36, contrasting the submergent coast north of Yaquina Bay where sea-cliff erosion is endangering homes, compared with the emergent shore of Bandon on the southern Oregon coast. A long-term history of former erosion is evident at Bandon, where the presence of large numbers of sea stacks offshore attest to there having been severe erosion in the past, but with little if any having occurred during the twentieth century, the sea cliff now being well vegetated.

Our interpretation based on this geomorphic evidence is that massive erosion occurred following the subduction earthquake in 1700, when the Bandon shore dropped down by on-the-order of 1 m, whereas since that time it has been tectonically rising faster than the global rise in sea level, with the toe of its sea cliff now being beyond the reach of the waves except perhaps during the most extreme storms and tides (Komar et al. 1991).

Although Bandon has not experienced sea-cliff erosion in over 100 years, demonstrated by old photographs, its future is uncertain due to the prospects that there will be an accelerated rate of rise in sea levels during this century due to global warming. The concern along the PNW coast is that areas such as Bandon, which have been emergent, will become submergent resulting in erosion and flooding where it has not occurred for more than a century. And stretches of shore such as that in Fig. 21.36 (*upper*) on the northern Oregon coast, which are already submergent and eroding, will experience far greater erosion and flooding in the future, resulting in extensive property losses. To provide assessments of these potential future hazards, important in our investigations have been projections of the possible changes in RSLs along the PNW through the twenty-first century, based on recent analyses by others that have projected the potential increases in global sea levels, together with our analysis results that have documented the present-day PNW trends in RSLs governed by the local tectonic uplift of the land.

The primary uncertainty in making these projections is the wide range of assessments that have been derived for the global rise in mean sea level by the end of the twenty-first century, the cause of this range being the need for an improved understanding of the underlying physical processes, and because the results are dependent on the assumptions and models applied in arriving at the projections. The most recent IPCC Assessment Report suggested that global sea levels could rise by 0.18–0.59 m above the 1990 level by the year 2100 (Meehl et al. 2007), projections that were derived using physics-based climate models. While the IPCC report did not include analyses of the dynamic responses of the melting ice sheets, it was suggested that it could account for an additional 0.1–0.2 m rise by the end of this century. Pfeffer et al. (2008) has attempted to constrain the estimates that include ice-flow dynamics, concluding that projections of 0.8–2.0 m sea-level rise by 2100 are possible.

Rather than modeling the complex details of the climate and glacial processes, a semi-empirical approach was developed by Rahmstorf (2007, 2010), one that statistically relates the rate of sea-level rise to the changes in global mean surface temperatures. Unlike the physical-based models, these semi-empirical models have been able to reproduce the historic trends in sea levels from the tide-gauge records (Rahmstorf 2007, 2010). Applied to project the future elevated sea levels, these statistical models have resulted in estimates of 0.5–1.4 m (Rahmstorf 2007), 0.5–1.0 m (Horton et al. 2008), 0.9–1.3 m (Grinsted et al. 2009), 0.75–1.90 m (Vermeer and Rahmstorf 2009), and 0.6–1.6 m (Jevrejeva et al. 2010), the rise in sea level by 2100 for the full range of climate scenarios developed by IPCC.

Faced with this wide range of projections for the future global sea levels, we developed a "consensus" projection that is based on the curves published by

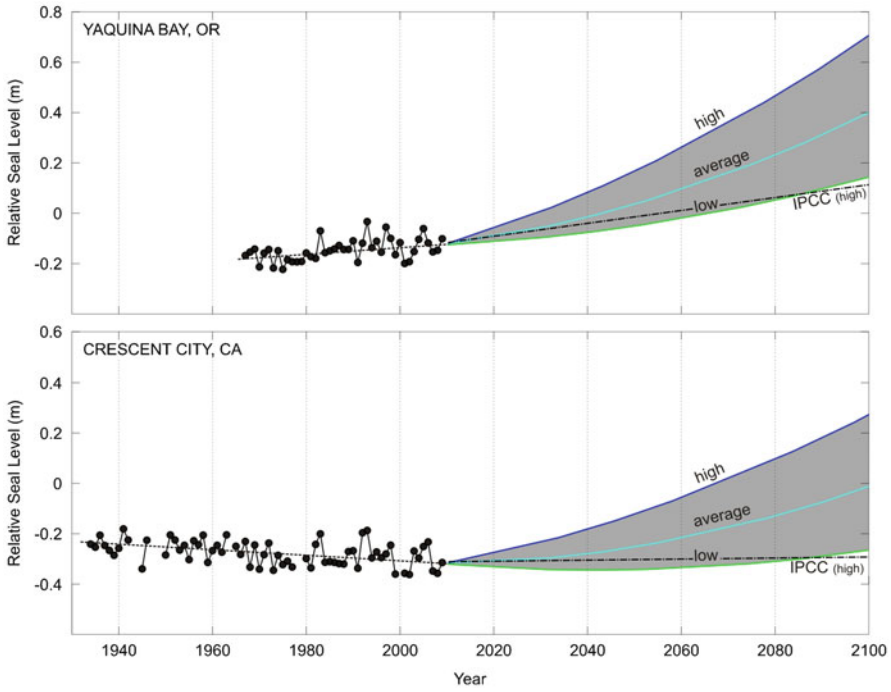

Fig. 21.37 Projected MSLs extending into the future beyond those measured by the Yaquina Bay and Crescent City tide gauges, illustrating the effects of an accelerated rate of sea-level rise respectively on submergent and emergent PNW shores

Horton et al. (2008), Vermeer and Rahmstorf (2009), Grinsted et al. (2009), and Jevrejeva et al. (2010). To obtain projections to be used in our PNW hazard assessments, those sea-level rise estimates were used to extract levels for the decadal intervals 2030, 2040, 2050, 2070, 2080, and 2100 (Baron 2011; Harris 2011). A quadratic curve was fitted through the averages of all the middle or "best guess" curves published by those authors to create our "Average" projection, with similar curves derived to represent the ranges, the "High" and "Low" estimates.

These projections of the global-average sea levels are applied in our assessments of future RSLs along the PNW coast, generally the water levels in 2030, 2050 and 2100, time-frames of interest in management applications, the results depending on the location and its rate of change in land elevations. The forms of the projected curves are illustrated in Fig. 21.37 for the Yaquina Bay tide gauge representing a submergent shore, contrasting with the present-day emergent coast of the Crescent City record. In each case the "Average" curves for the projected accelerated rates of sea-level rise are attached as a tangent to the regression line for the past tide-gauge records, providing a natural transition that in effect accounts for the land-elevation changes. As expected, the results for Yaquina Bay demonstrate the potential future enhanced sea levels, with our 2100 projection being about 0.30-m higher than the

IPCC 2007 projection. The "Average" curve for Crescent City shows it initially continuing downward, reaching a minimum in about 2030, and then rapidly turning upward to convert this location into a submergent coast, with the expectation of there being greater problems with erosion and flooding. In contrast, the IPCC projection for Crescent City indicates that the RSL would continue to drop, remaining an emergent coast until 2100. Although there is not a tide gauge located in Bandon on the southern Oregon coast, the benchmark data in Fig. 21.35 suggests that the changes in its sea-level trends would be similar to those for Crescent City, that its present-day stable sea cliff seen in Fig. 21.36 will begin to erode before the middle of the twenty-first century.

While analyses of the twentieth-century and present-day rates of change in RSLs, documented from tide-gauge records and recent satellite altimeter measurements, are of fundamental importance to assessments of coastal erosion and flooding hazards, of equal importance along the PNW coast are considerations of the annual winter extreme mean water levels that occur during El Niño climate events. This was evident in Fig. 21.30 that included graphs of the monthly-mean water level cycles during the 1982–1983 and 1997–1998 major El Niños, demonstrating that their winter levels are tens of centimeters higher than occur during "normal" years. A documentation of this dependence of the winter water-level extremes on the full range of El Niño/La Niña climate variations was the primary motivation for undertaking separate analyses in Fig. 21.33 of the "winter" and "summer" water-level trends and variations. Particularly evident in that diagram are the highest water-level peaks during the 1982–1983 and 1997–1998 El Niños, with the actual water levels reached during those winters having been the summation of the regression trend for the progressive change in the RSL and the enhanced water levels during those El Niño winters, the levels of the peaks above the regression lines.

The goal of our analyses based on Fig. 21.33 was therefore to measure the residual mean sea levels (MSL), the annual winter levels above or below the regression line for each tide gauge, and then to relate those levels to the El Niño versus La Niña occurrences. The analysis directed toward accomplishing this is illustrated in Fig. 21.38, based on the Yaquina Bay gauge record. The top-most panel is a graph of the winter MSLs, the same as included in Fig. 21.33, the second panel having been detrended since we are interested in the residual MSLs, the observed annual variations above and below the regression trend. The third panel is a graph of the Multivariate ENSO Index (MEI) that provides a robust measure of the varying climate from La Niñas (MEI < -0.4) to El Niños (MEI > 0.5), with "normal" conditions between (Wolter and Timlin 1993). The correspondence between the variations in the measured residual MSLs and the MEI is evident in a comparison between these upper panels, while the fourth panel provides a direct correlation between MEI and the detrended residual MSLs for the winter months, its regression demonstrating that El Niños raise the winter water levels, whereas La Niña tend to depress the MSLs, presumably due to the development of cold, denser water along the coast.

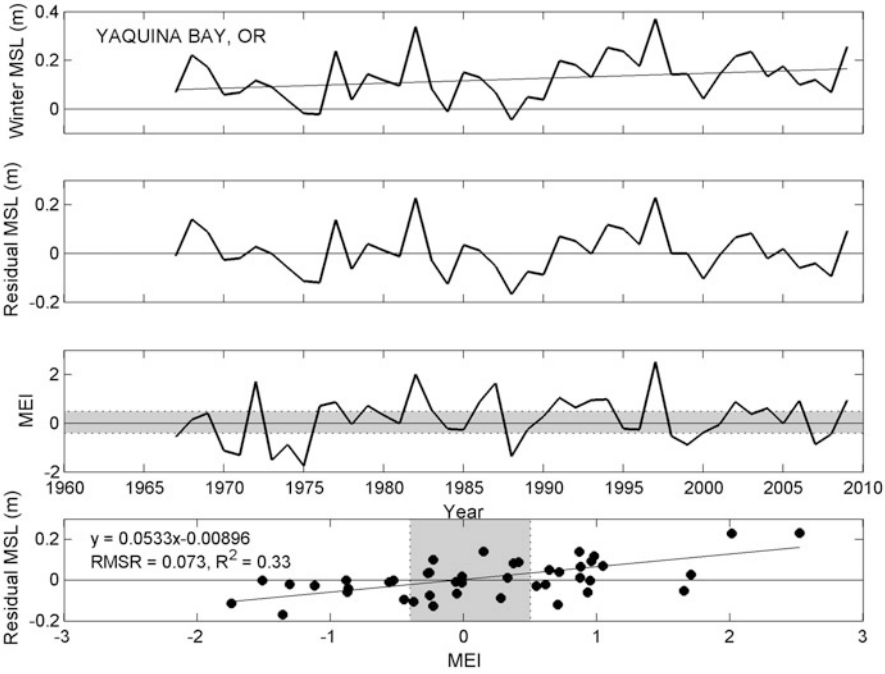

Fig. 21.38 Detrended residual mean sea levels for the Yaquina Bay tide-gauge record and their correlation with the MEI, showing that the strongest El Niños elevate water levels the most, while the cold, dense water of a La Niña depresses the water levels (After Komar et al. (2011a))

A comparison in Fig. 21.33 between the annual variations in the winter-average water levels for Neah Bay, Yaquina Bay and Humbolt Bay demonstrates that they are almost exactly the same, the patterns of the data being nearly congruent except for the differences caused by their contrasting net regression trends in RSLs. It is evident that the response of the winter water levels to the El Niño/La Niña range of climate events is nearly uniform along the entire length PNW coast. Not surprising, therefore, the correlations between the detrended residual MSLs and the MEI, as illustrated in Fig. 21.38 for the Yaquina Bay tide-gauge record, are also essentially the same for all of the ocean shore PNW tide-gauge records (Komar et al. 2011a).

21.6.5 El Niños—Littoral Cell Sand Redistributions and Hot-Spot Erosion

As reviewed earlier, occurrences of major El Niños during the winters of 1981–1982 and 1997–1998 resulted in the greatest erosion impacts experienced along the PNW coast in recent decades, and can be expected to similarly represent a significant hazard in the future. The variations between El Niño and La Niña

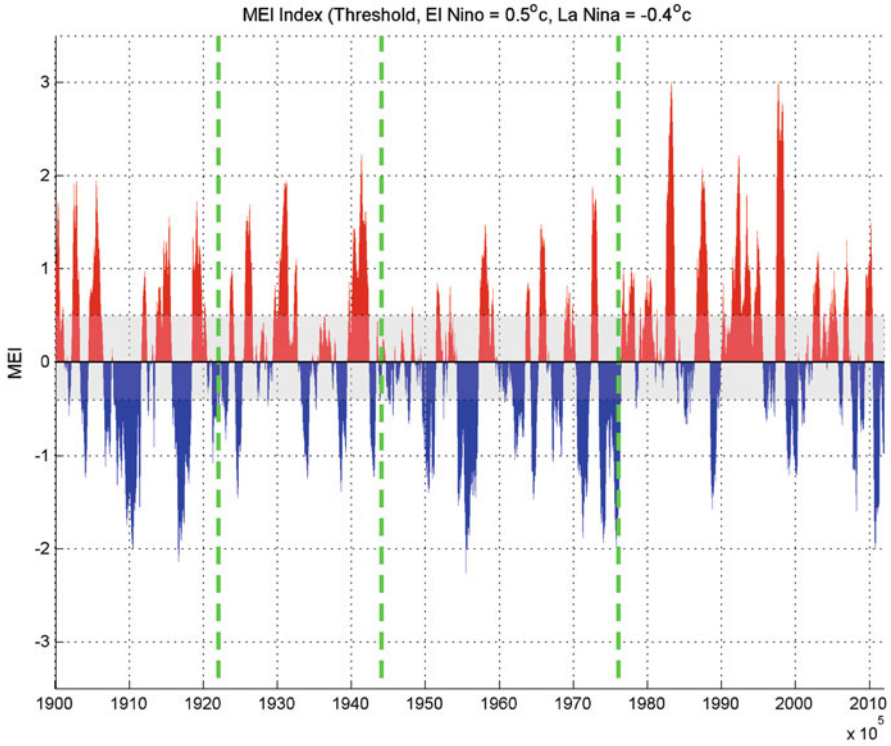

Fig. 21.39 Variations in the MEI from 1900 to the present, showing occurrences of El Niños (*red*) and La Niñas (*blue*), with the limits of the PDO cycles given by the green vertical *dashed lines*

occurrences since 1900 are given in Fig. 21.39, a graph of the Multivariate ENSO Index (MEI) that provides a measure the event's intensity. It is evident that occurrences of significant El Niños (in red) dominated the period from 1976 to about 1998, with more La Niñas (in blue) having occurred from 1945 to 1970. This multidecadal shift in dominance of those respective climate events is known as the Pacific Decadal Oscillation (PDO), recognized in the variations of a number of environmental physical conditions (e.g., Pacific Ocean water temperatures, particularly along the equator), and also in biological responses such as populations of salmon. Within that 1976–1998 period of El Niño dominance there was a total of seven El Niños, the 1982–1983 and 1997–1998 events with the highest MEI values clearly having been the strongest. The period between 1990 and 1998 was unusual in being characterized by persistent El Niño conditions, the longest sustained within this record since 1900. It appears from the patterns in Fig. 21.39 that following the major El Niño in 1997–1998, the phase has shifted to being dominated by La Niñas, with a strong occurrence of that climate event during the winter of 2011–2012.

Aspects of the enhanced ocean processes during El Niños have already been reviewed in the above sections, particularly significant having been winter water levels that during the strong 1982–1983 and 1997–1998 events were some 25–30 cm higher than during a "normal" winter, having raised measured tides by about 40 cm above their predicted astronomical elevations throughout those winters. At the same time it was found that the heights of the storm waves were greater than normal, it having been this combination of elevated tides and the swash runup of storm waves that contributed to beach and property erosion.

In addition to the effects of El Niños on the winter water levels and wave heights, those major events produced significant redistributions of beach sand volumes within the littoral cells, leading to occurrences of "hot-spot" erosion, examples having been reviewed earlier. In that those stretches of shore experienced the greatest erosion and flooding, this aspect of a major El Niño represents its most significant hazard to ocean-front properties. It became evident that this redistribution of the sand and its resulting areas of hot-spot erosion followed a consistent pattern in the littoral cells, illustrated schematically in Fig. 21.40 where the effects of an El Niño on the sediment movement and erosion within a littoral cell is contrasted with its relative stability during "normal" years (Komar 1986, 1998a). Within the pocket-beach cells on the Oregon coast bounded by headlands, as diagramed to the left in this diagram during normal years there is a quasi-equilibrium with the winter storm waves predominantly arriving from the southwest transporting sand alongshore to the north, while the summer waves from the northwest return the sand to the south; in the long term there is on average a net-zero longshore sediment transport. In contrast, during a major El Niño the pattern of change involves occurrences of massive hot-spot erosion north of headlands and also north of inlets due to their migration, or where inlets are controlled by jetties the hot-spot erosion can occur because they act much like mini headlands. At the same time, beach sand accumulated south of the headlands. It is clear from this pattern that these changes had been produced by an unusual degree of northward transport and displacement of the beach sand within the littoral cells during the El Niño winters, far greater than in normal years, produced by exceptional storm waves that arrived from the southwest (Komar 1986, 1998a).

This interpretation based on a northward displacement of sand within the PNW littoral cells is supported by analyses of the El Niño storms (Seymour 1996, 1998), showing that their centers had shifted to the south compared with normal years such that their tracks mainly crossed the coast of central California rather than approaching the shores of the PNW. As a result, when their generated waves did reach the Oregon coast from a more southwesterly quadrant, they created an abnormally large northward transport of the beach sand within the littoral cells, accounting for the hot-spot erosion impacts along the shores of central to northern California, and particularly along the PNW coast.

The El Niño impact patterns depicted in Fig. 21.40 were first recognized during the 1981–1982 extreme episode when extensive erosion occurred at a number of sites along the Oregon coast (Komar 1986). However, with limited resources and the primitive equipment available at that time, there was little opportunity to

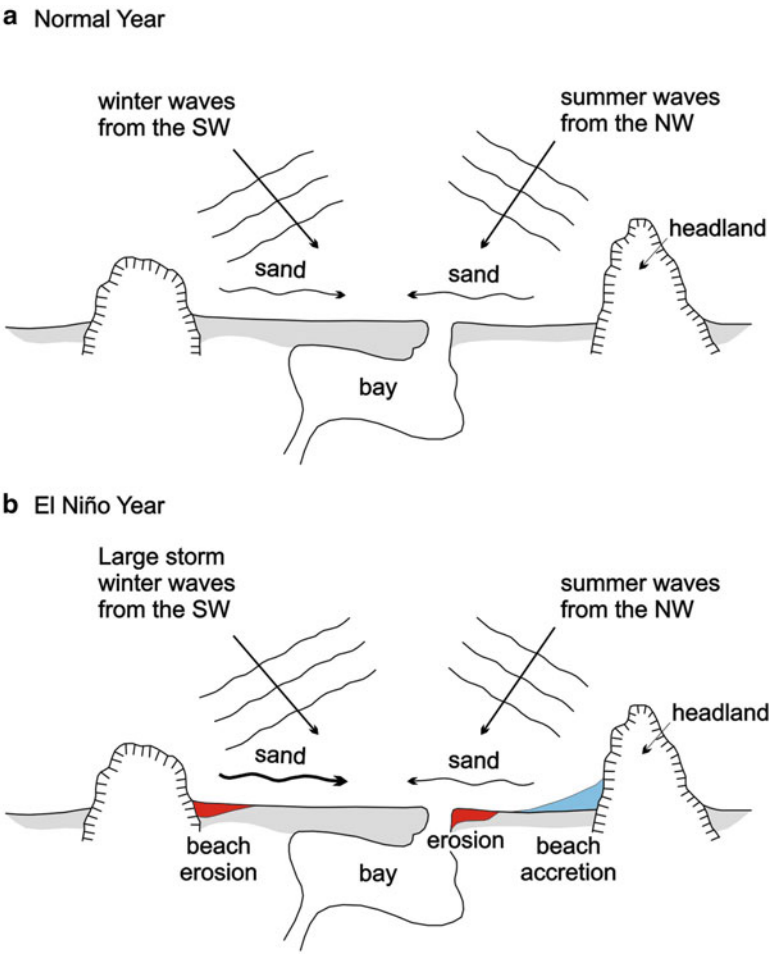

Fig. 21.40 The alongshore seasonal movement of beach sand on the Oregon coast: (**a**) during a normal year; and (**b**) during an El Niño with "hot-spot" erosion (in red) having occurred north of headlands and inlets (After Komar (1998a))

document with beach profiles the northward displacements of the beach sand volumes within the littoral cells. That opportunity came during the next major El Niño in 1997–1998, a near-repeat event in its processes and impacts (Revell et al. 2002). In anticipation of that event, aerial Lidar surveys were undertaken of most of the U.S. West Coast shores, first in October 1997 and repeated in April 1998 to document the changes in the beach elevations that had occurred, this having been a cooperative effort between NASA, NOAA and the USGS. Our initial application of the acquired surveys was to the Netarts Littoral Cell on the northern Oregon coast, a comparatively small littoral cell that is well confined between large rocky headlands, the stretch of sand beach consisting of Netarts Spit plus that fronting

the community of Oceanside at the north end of the cell. The erosion within this cell during the El Niños was discussed earlier, and that in Cape Lookout State Parks and at The Capes developed shown respectively in Figs. 21.17 and 21.18.

The detailed Lidar surveys permitted a documentation of the average elevations of the dry beach at 100-m alongshore intervals, representing 40 by 100 m rectangular segments of the dry portion of the upper beach (Revell et al. 2002). Comparisons between their surveyed elevations in October 1997 and April 1998 yielded calculated volumes of either the erosion or accretion that had occurred over the span of the El Niño winter. The changes in volumes of the upper portion of the beach would reflect both the normal shift in the seasonal profiles, where its summer berm is eroded by winter storms with the sand transported to offshore bars, and the sand volume changes that could be attributed to the El Niño, a northward longshore displacement within the littoral cell as depicted in Fig. 21.40.

The result of our analysis is presented in Fig. 21.41a, the sand volume change from October to the following April, except that the mean value of the erosion has been removed, assumed to represent the sand that had been transported to the offshore bars, which occurs during normal years. The remaining volume magnitudes in the graph are expected to be those that reflect the impacts of this major El Niño, and it is seen that in general there has been erosion along the southern-most 3 km of the Netarts Spit shore, with sand deposition having occurred to the north along the 8 km remaining length of the cell's shoreline (that shore having actually eroded, when the loss of sand to the offshore bars is included). It is seen in Fig. 21.41a that there were large cycles in the changes in sand volumes within that stretch of shore; these cycles were due to the northward migrations of rip current embayments, their positions in October having been filled with sand to produce the peaks in the graph, while the troughs in the volume changes corresponded to the locations of the rip embayments when surveyed the following April (Revell et al. 2002).

The graph in Fig. 21.41b is a north-to-south summation of the volumes that were eroded or accreted in the 40 by 100-m segments of beach, the values graphed in Fig. 21.41a, this summation having started with 0 at the south end of the cell, at the location of the bounding headland. The northward volume of displaced sand is seen to have rapidly increased to a maximum of 6,700 m^3 at about the 3-km longshore distance, that distance representing the zone of hot-spot erosion north of the headland, evident in Fig. 21.41a. The depositional stretch of shore further to the north is seen to have been a gradually reduced volume of sand transported by the waves, as progressively more and more sand is left behind on the upper beach. The local loss of sand between October and the next April in the northern-most 0.5 km of shore, just south of that headland, is due to the development of a large rip current embayment, its size increased by the northward-flowing longshore currents generated by the waves arriving from the southwest, this being a common feature that forms during the winter on PNW littoral cells, although larger in their development during El Niños.

Although there may not be another major El Niño event in the next 25 years like those in 1982–1983 and 1997–1998 that impacted PNW coast, if the PDO cycle (Fig. 21.39) holds with the dominance of La Niñas, it is inevitable that

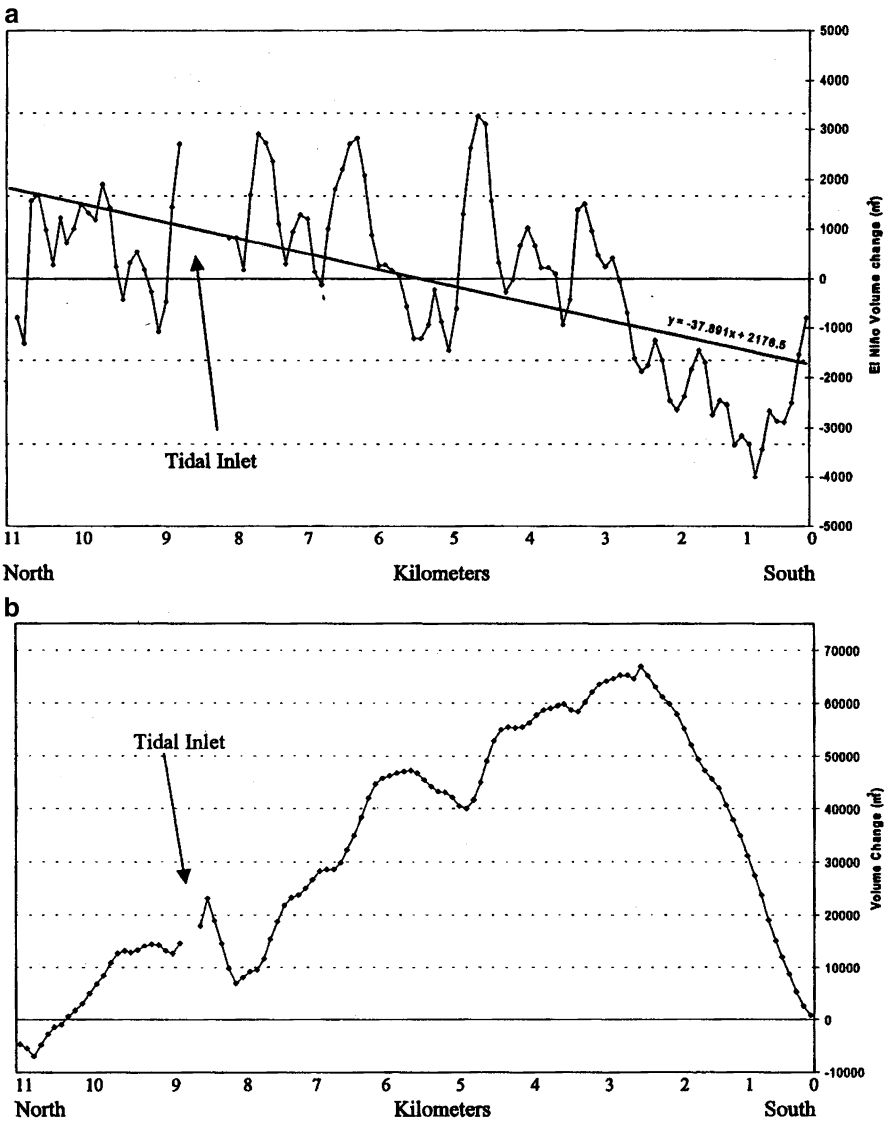

Fig. 21.41 (**a**) Longshore variations in beach-sand volume changes between the October 1997 and April 1998 Lidar surveys, reflecting the patterns of erosion and sand accumulation during that major El Niño. (**b**) South-to-north summation of the beach sand volumes eroded or accreted as they were displaced to the north by El Niño storm waves arriving from the southwest (From Revell et al. (2002))

they will occur within the span of the twenty-first century, with a repeat of hot-spot erosion and flooding along this coast. But its impacts will be complemented by the extent of global sea-level rise and the possibility that storm intensities and the

heights of their generated waves will also have increased. The development of management strategies to protect the PNW ocean-front homes and infrastructure from this range of coastal processes and hazards are clearly needed.

21.7 Hazard Assessments—Models and Applications

As reviewed in the preceding section, multiple ocean processes are important to episodic occurrences of PNW erosion and flooding, and in the longer term due to climate-induced increases in sea levels and storm-wave heights, with the occasional development of a major El Niño. Analysis procedures are required that combine these processes in a meaningful way to account for their impacts during a storm that may last for a day or two, applied to project the most extreme storm erosion that might occur during the next 25–100 years, and analyses that include the global rise in sea level and potential changes in storm intensities and wave heights. The resulting extent of the erosion depends on the condition of the backshore, whether it consists of dunes or resistant sea cliffs, so different analysis procedures have had to be developed in order to deal with those contrasting environments and their management strategies.

In the analysis methodologies we have developed for application along the PNW coast (applicable on other coasts as well), the first stage is to combine the ocean processes that determine the total water levels (TWL) at the shore (Ruggiero et al. 1996, 2001). The essence of this model is diagramed in Fig. 21.42 (*Upper*), which shows the elevation of the measured tides that can be raised above predicted levels by a storm-surge or during an El Niño, above which the swash runup calculated from the deep-water wave climate is superimposed to determine the TWL reached by the water. As depicted, the property impacts are determined through comparisons of the extremes in TWLs with the elevations of the backshore properties, in the example illustrated this being the beach/dune junction elevation E_J, the toe of the foredunes (conversely, that of a sea cliff). In the long term the projected rise in the relative sea level is also added, as are assessments of the potential increases in swash runup levels produced by the deep-water wave heights and periods, the objective being to determine the possible erosion and flooding hazards decades into the future.

Having evaluated the extremes in the TWLs with the Ruggiero et al. (2001) model, the follow-up analyses in our hazards determinations are to evaluate the actual extent to which the property erosion might progress. This of course depends on the resistance of the backshore, specifically whether the development is within foredunes or atop a sea cliff. Illustrated in Fig. 21.42 (*Lower*) is the model we have developed to be applied in assessments of the potential erosion or overtopping/flooding of foredunes, with the elevations of the toe and crest of the dunes respectively being important (Komar et al. 1999). This model is "geometric" in that the dunes are cut back following the slope of the fronting beach, up to the maximum reached by the TWL during an extreme storm. An additional foredune

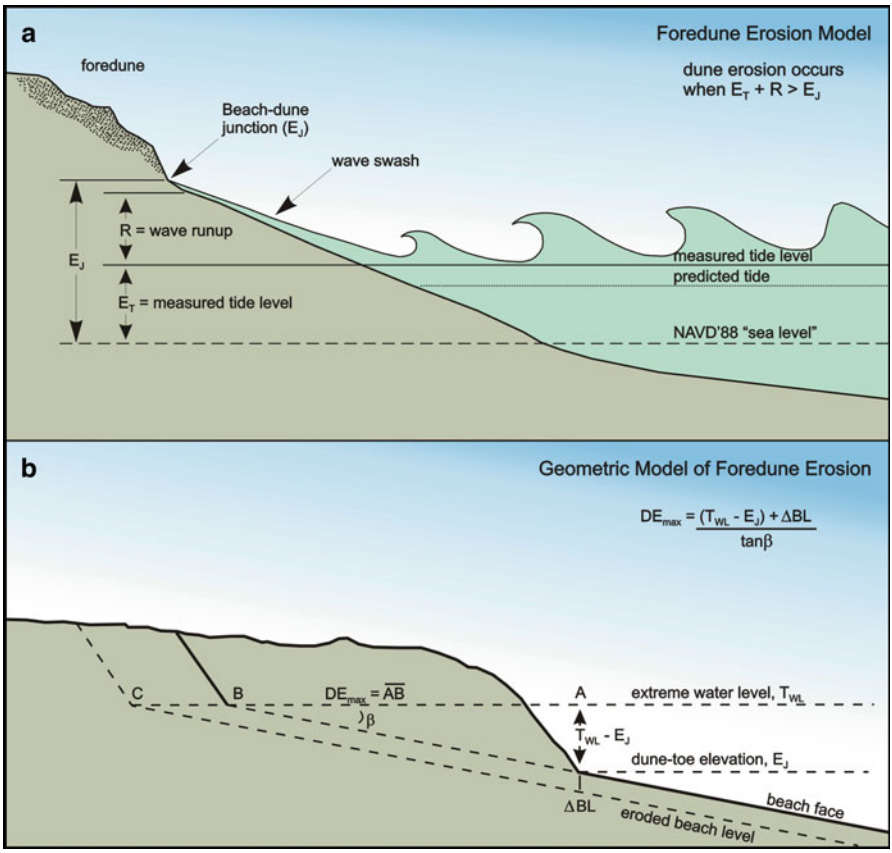

Fig. 21.42 (*Upper*) The model applied to assess the TWLs at the shore resulting from the summation of the measured tide and the contribution of the wave-swash runup on the beach face, the TWL being compared with the elevation of the toe of a foredune (Ruggiero et al. 2001). (*Bottom*) The geometric dune erosion model used to estimate the expected extent of dune loss during storms, dependent on the model-evaluated TWLs (Komar et al. 2002)

retreat produced by the presence of a rip current can be included by lowering the elevation of the fronting beach profile to reflect the presence of the rip embayment. The result of this analysis is an assessment of the potential maximum extent of dune erosion, inherently providing a margin of safety, important in the establishment of hazard zones (setback distances).

Conceptually the model of Ruggiero et al. (2001) to evaluate the TWLS from the combined processes, Fig. 21.42 (*Upper*), is relatively simple but its applications require detailed analyses of the measured waves and tides, as reviewed earlier. Various approaches are then possible in deriving model assessments of the TWLs. In our applications to the PNW coast we initially followed an approach of developing "Scenarios" (Komar et al. 1999, 2002), TWLs that could reasonably be expected from combinations of storm wave heights and periods and their resulting

runup levels on the beaches, added to the measured high tides ranging from those expected on a monthly basis during the winter, levels enhanced by a surge during a major storm, to the most extreme levels that occur during major El Niños. The probabilities of the joint occurrences of these processes can be approximately estimated from extreme-value analyses of the individual processes and considering their degrees of independence, yielding combinations that are considered to be "possible" in representing the 50- to 100-year extreme hazards to the PNW, therefore serving as a useful guide in management applications. However, the analysis methodologies developed by Ruggiero et al. (2001) are more realistic in being based on the hourly simultaneous measurements of the PNW tides and buoy data for the deep-water SWHs and periods, combining them on an hour to hour basis. As reviewed earlier, both wave and tide data sets are sufficiently long that a large number of significant extratropical storm events are represented by their ranges of extremes in the measured SWHs and surge levels, with the 15-year joint records analyzed by Ruggiero et al. (2001) also included the 1982–1983 major El Niño that raised measured winter tides well above their predicted levels. Analyses in that study of the hourly TWLs based on the simultaneously measured tides plus the swash runup thereby yielded assessments of the distributions and extremes in the TWL magnitudes, representing the present-day climate but also serving as the basis for deriving projections into the future that reflect Earth' changing climate.

Particular effective in deriving assessments of the hazards experienced at a specific coastal site and shore-front properties, the TWL model analysis in Fig. 21.42 (*Upper*) can yield evaluations of the return periods and numbers of hours per year that the combined tides and wave runup were sufficient to reach and impact the toe of the foredune or sea cliff, depending on its junction elevation E_J with the fronting beach. Such a product is illustrated in Fig. 21.43 based on the analyses by Ruggiero et al. (2001) for a representative beach slope 0.03 (1 in 33) and for the 15-year record of combined waves and tides. The results show a marked sensitivity of both the return periods and numbers of impact hours per year to a range of E_J *elevations*. Figure 21.44 shows the analysis results for a 20-km length of shore south of Newport, within the Newport Littoral Cell, part of which is backed by dunes, about two-thirds being backed by sea cliffs composed of moderately cemented Pleistocene marine terrace sandstones, typical of the Oregon coast. It is seen that even within this 20-km stretch of shore there is significant range of junction elevations E_J for both the dunes and sea cliffs, with those variations being reflected in the calculated numbers of impact hours per year. Aerial photo analyses of the rates of sea-cliff erosion for the southern portion of the cliff (11–20 km alongshore distance) are graphed in Fig. 21.45, showing strong correlations with both E_J and the wave impact hours per year.

Having been based on 15 years of hourly measurements of PNW waves and tides, the calculated hourly TWL magnitudes and their impacts per year along this portion of the Oregon coast, analyzed by Ruggiero et al. (2001), constitutes a present-day "property impacts climate". With the inclusion of projected increasing sea levels and storm-generated waves, projections are possible for the future TWLs

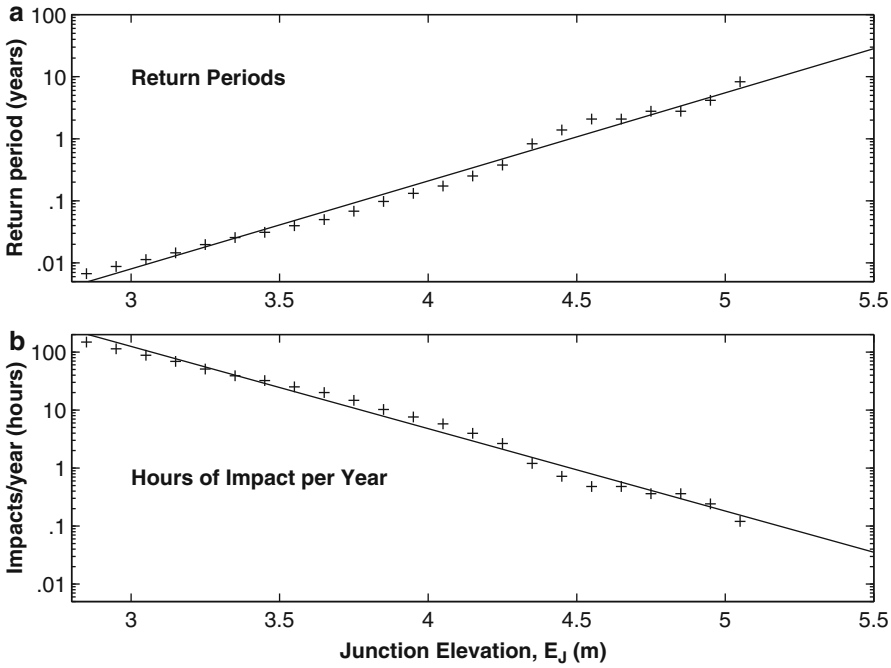

Fig. 21.43 Return periods and wave impact hours per year derived from the 15-year combined measured tides and calculated runup levels from buoy data, yielding hourly assessments of the total water levels (From Ruggiero et al. (2001))

and their enhanced impacts on the shore-front properties. The results thereby provide an assessment of the susceptibility of a property to erosion in terms of the impact hours per year. The follow-up analyses in our hazard determinations are to evaluate the actual extent to which the property erosion might progress in response to the changing climate. This of course depends on the resistance of the backshore, whether the development is within foredunes or atop a sea cliff.

Most difficult are projections of future rates of sea-cliff recession, which are highly sensitive to the rock resistance, being dependent on its composition but also on structure components such as joints and faults, and layering in sedimentary units. The development of models to predict the extent of sea-cliff erosion during a storm or over the decades with rising sea levels are challenging in that in addition to the evaluated TWLs and impact hours per year derived from the Ruggiero et al. (2001) model, it is necessary to quantitatively assess the cliff resistance based on those several factors. For example, investigations such as that by Benumoff and Griggs (1999) on the southern California coast have quantified the cliff resistance through "hardness" measurements of the rocks, having also included considerations of the presence of layering, joints and faults in the cliff face that provide natural zones of weakness. Recent investigations have developed models that combine considerations of the wave impact elevations and forces versus the resistance of

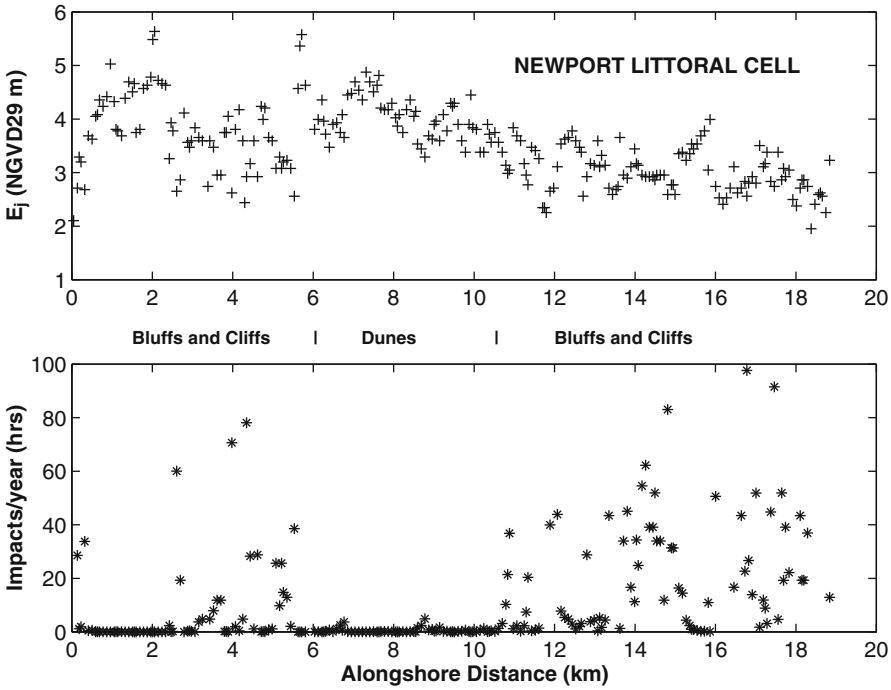

Fig. 21.44 Beach/backshore junction elevations (E_J) and model-derived analyses of the impact hours per year, along the 20-km stretch of the sea cliffs and dunes south of Newport on the mid-Oregon coast (From Ruggiero et al. (2001))

the sea cliff (Hall et al. 2002; Collins and Sitar 2008), models that have the potential for management applications on the PNW coast, although additional research is needed on this complex problem prior to their being used in our hazard assessments. In the mean time, in our applications to derive hazard zones (setback distances) for properties on sea cliffs, the assessments have been based mainly on direct documentations (aerial photos, etc.) of long-term cliff recession rates, together with the inclusion of safety factors to account for the potential future enhanced rates.

Critical for the PNW coast has been the development of hazard zones (setbacks) in foredunes, considering their histories of episodic erosion and property losses during storms, and the possibility each winter of there being a repeat occurrence. In these applications we have based the analyses mainly on the geometric dune-erosion model illustrated in Fig. 21.42 (*Lower*), requiring measurements of beach slopes and determinations of the dune toe and crest elevations, respectively being important to the potential erosion or overtopping of the properties. Generally we are interested in analyzing the extent of dune cutback during extreme storm events, which depend mainly on its highest TWLs but with the presence of a rip embayment increasing the susceptibility of the property to the attack by the waves. The result of

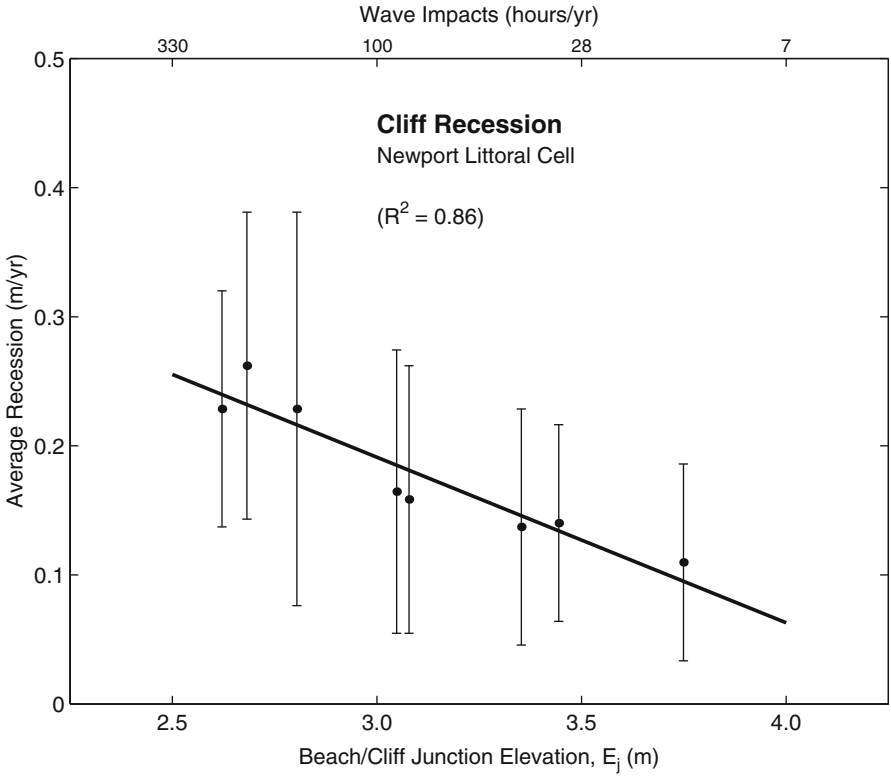

Fig. 21.45 (**a**) Sea-cliff recession rates derived analyses of aerial photos versus the E_J elevations of the cliff toe, and (**b**) model-calculated wave impact hours per year (From Ruggiero et al. (2001))

this analysis is expected to be an assessment of the potential maximum dune erosion during that TWL, a maximum in that being geometric the model does not account for any delay in the progress of the erosion. This is acceptable in management applications to determine conservative hazard zones, inherently providing a worst-case margin of safety for homes constructed in these vulnerable foredunes. There has been some field verification of the magnitudes of dune erosion derived from this model, through comparisons with episodes experienced on Siletz Spit and elsewhere along the PNW coast. This model also has the advantage that it can be applied on a coast-wide basis to yield hazard assessments, in our applications mainly using available Lidar surveys, and with this simple model being easily understood by the general public. If more detailed analyses are required for specific properties, dune-erosion models are available that include considerations of the time involved to transport the eroded dune sand into the offshore, accounting for the lag in the dune retreat relative to the erosion processes. This has been accomplished in recent hazard analyses, having first applied the geometric dune-erosion model to determine the maximum probable extent of dune recession during extreme storms,

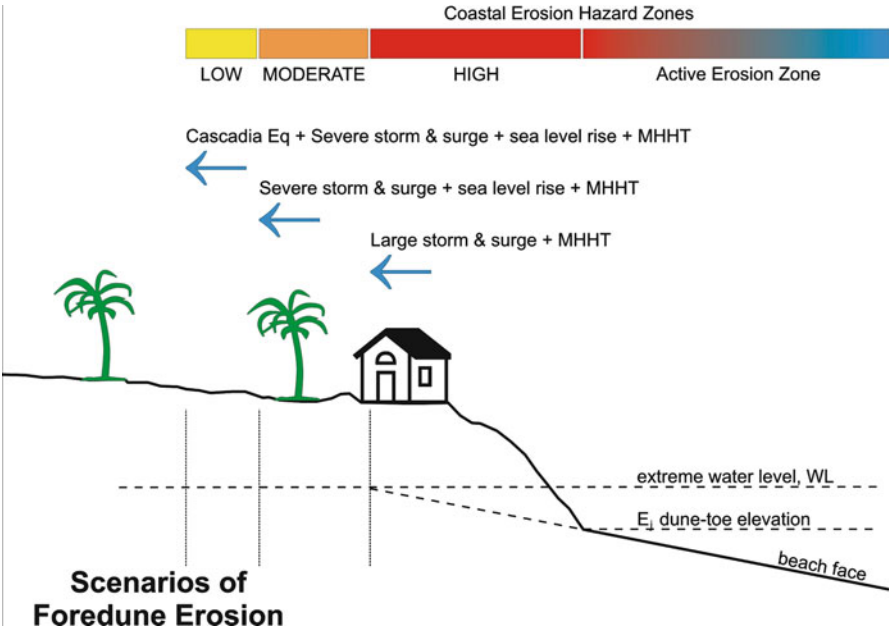

Fig. 21.46 Conceptual model developed by DOGAMI for defining coastal erosion hazard zones in foredune areas along the Oregon coast (After Allan and Priest (2001))

and then empirically adjusting that result by applying a model to approximately account for the reduced erosion due to its time dependence.

Erosion and flooding hazards have been determined for several littoral cells along the Oregon coast, the analysis having been undertaken by the Department of Geology and Mineral Industries (DOGAMI). The range of erosion hazards are defined conceptually in Fig. 21.46, most important being the HIGH category of most immediate danger during episodic storms. Three example sites of application are shown in Fig. 21.47, sites that were included in our earlier review of past and present erosion impacts: Neskowin in part being in a zone of hot-spot erosion, that has continued since the 1997–1998 El Niño; Pacific City within the Nestucca Littoral Cell, having suffered its principal impacts in 1978; and Rockaway that was particularly impacted during the extreme 1998–1999 winter storms. The recent retreat of the foredunes in those areas are shown by the 1998, 2002 and 2009 surveys of the dune toe (~6 m elevations), with the high-risk hazard zones shown in red originally having been based on the 1998 survey. As reviewed earlier, particularly in the context of the episodic erosion that had occurred on Siletz Spit, an episode of dune retreat is commonly followed by years to decades during which the dunes rebuild to essentially their former extents. Dominated by this cycle, nearly all of the homes on that spit are located within the high-risk hazard zone, and this is

Fig. 21.47 Examples of high-risk erosion hazard zones in foredunes along the Oregon coast. *Lines* included in the figure indicate the positions of the dune toe (~6 m elevation) in various years, while the red areas represent the high-risk hazard zones (After Allan and Priest (2001))

also seen to be the case for the three sites included in Fig. 21.47 where an additional factor has been the progressive retreat of the dunes.

The entire length of Siletz Spit is now covered with riprap, as are much of the lengths of the communities in Fig. 21.47. Although now to a degree protected, the integrity of these structures are somewhat uncertain in that some were placed on an emergency basis with the rock dumped in place, and the costs to maintain these structures are expected to be considerable as greater wave energies are coupled with increasing sea levels in the future, and especially if the beaches remain in a degraded state with the loss of much of their sand.

Recent research advances in developing our methodologies to evaluate PNW hazard zones have included a probabilistic approach, one that takes into account the uncertainties in the climate controls on future rates of sea-level rise, future changes in storm intensities and generated SWHs, and possible occurrences of strong El Niños (Baron 2011; Ruggiero et al. 2011). These uncertainties, in particularly that associated with projecting the expected accelerated rates of sea-level rise, have been reviewed in earlier sections of this chapter. The recent analyses, applied to the Neskowin Littoral Cell on the northern Oregon coast, examined 20 scenarios representing combinations of the erosion factors, including the ranges in sea-level projections, future wave-height changes that range from continuing at their present rates based on the buoy measurements to actually decreasing in the future, and projections of frequencies of future El Niño occurrences. Exposure analyses are also included by having added socio-economic data such as locations of homes and

infrastructure such as roads. By having included analyses based on both the models of the physical processes and the community that would be threatened by future erosion and flooding, detailed results were obtained for the numbers of homes and businesses, and the lengths of road that would be exposed to those hazards, from the present to the end of this century (Ruggiero et al. 2011).

21.8 Summary and Discussion

The goal of this chapter has been to review the multiple factors and ocean processes important to erosion and flooding hazards along the Pacific Northwest (PNW) coast of the United States. With the research directed toward the hazards to shore-front homes and infrastructure, its objective has been to develop management strategies and guidelines for safer development. The directions of investigations have included measurements of the range of ocean processes that have been responsible for property losses over the years (waves, tides, mean sea levels, etc.), the responses of the PNW beaches to those processes, their combinations that have led to episodes of erosion during winter storms, the extremes in the processes and impacts during strong El Niños, and analyses directed toward projections into the future in response to Earth's changing climate. Based on that research and cumulative experience in dealing with PNW coastal erosion problems, models have been developed that combine these factors and processes, models that can be applied to the establishment of meaningful hazard zones to protect coastal properties.

In summary, the more significant factors that have governed erosion and flooding occurrences along the PNW coast include the following:

- There are limited modern-day sources of sand to Oregon's beaches, with much of it being "relict" in having arrived thousands of years ago at a time of lowered sea levels when headlands did not prevent the alongcoast movement of the beach sediments, the result being that many beaches today are deficient in sand volumes and therefore do not provide sufficient buffer protection to backshore properties during winter storms;
- While the Columbia River in the past had been the direct source of sand to Southwest Washington's beaches (to the Columbia River Littoral Cell), the construction of dams in its watershed and other human environmental modifications have essentially eliminated that source, the sand reaching the beaches now being attributed to offshore sources that can be expected to decline in the future;
- Affected by tectonic-plate collision and subduction, during the past 300 years since the last subduction earthquake this coast has experienced uplift, at variable rates along its shore such that when compared with the twentieth century eustatic rise in sea level some shores are submergent while others are

emergent, this representing a significant control on the present-day rates of erosion and property losses;
- With projections of accelerated rates of rising sea levels due to global warming, it is predicted that the entire PNW coast will be submergent by the end of this century, with erosion occurring where it has not been experienced before, and with increased erosion and flooding impacts along the shores that are already submergent;
- The PNW is characterized by high wave energies, with measured significant wave heights during winter storms having reached 14–15 m, the concern being that storm intensities have increased during the latter half of the twentieth century with buoy and satellite measurements of the waves having documented their increase, in part accounting for growing problems with beach erosion and property losses;
- In addition to the importance of the trends and rates of change in relative sea levels and increasing wave heights to occurrences of PNW coastal erosion, also significant have been the enhanced ocean processes during strong El Niños (1982–1983 and 1997–1998), which elevate monthly-mean sea levels and tides by tens of centimeters throughout the winter, and produce a shift in the storm tracks that results in along-coast redistributions in sand volumes on the beaches, leading to extreme "hot-spot" beach erosion and property losses north of headlands and tidal inlets to bays and estuaries.

It is evident from this summary that there are both significant tectonic and climate controls on the processes important to the PNW coastal hazards, the later requiring that global warming with its effects on sea levels and storm intensities, and the periodic occurrences of strong El Niños, all be accounted for in future hazard assessments. Reviewed in this chapter are the models we have developed for application on the PNW coast to evaluate the property hazards and recommended setbacks, which with some modification could be applied to other coasts. The first model focuses on evaluations of the total water levels (TWLs), particularly the extremes in its elevations at the shore that are a result of elevated measured tides due to storm surges or El Niños, plus the runup levels of the storm waves calculated from their buoy-measured significant wave heights and periods. In order to project the hazard assessments into the future, trends of increasing sea levels and the potential increase in runup levels that could occur if storm intensities continue to increase are also added to determine TWLs through this century. Occurrences and the extent of the resulting property erosion depend on the elevations of these extreme TWLs, compared with the elevations of the backshore, and whether the properties are within foredunes or atop sea cliffs. These models have been widely applied along the shores of the PNW to derive rational assessments of hazard zones, setback distances that should maintain homes safer from these potential hazards.

Ultimately, the most-extreme hazards faced along the U.S. Pacific Northwest would be the occurrence of another subduction earthquake and tsunami, a repeat of that which occurred on 26 January 1700, at 9 pm, the exact time of the event having been based on the arrival of the tsunami on the coast of Japan (Satake et al. 1996).

The initial evidence for that major prehistoric earthquake, estimated to have been about magnitude 9, came from investigations of estuarine marsh sediments buried by sand layers, deposits which suggest that portions of the coast had abruptly subsided by 1–2 m, followed by an extreme tsunami that swept inland to deposit the sand carried from the beaches (Atwater 1987). Based on the numbers of such layers found in bays and estuaries along the PNW coast, and with the same sequence of turbidites found in deep-sea sediments, it is clear that catastrophic earthquakes have repeatedly occurred along the PNW coast, at intervals roughly ranging from 300 to 600 years (Goldfinger et al. 2010). Given this frequency of past occurrence, there is a strong probability that another major subduction earthquake and tsunami will occur during the next 25–100 years. A recent reminder of the extent of the potential destruction faced by the PNW in a local subduction earthquake was provided by the 11 March 2011 magnitude 9 earthquake off the coast of Japan, which generated a tsunami that crossed the Pacific Ocean and impacted the shores of the PNW, the maximum tsunami wave height having been 4.24 m in Crescent City, with the surge of the waves having inundated its harbor and in places washed inland to damage private properties (Allan et al. 2012). This recent tectonic event can be viewed as having been an inverse of that which occurred 300 years ago on the PNW coast, with the expectation that a repeat occurrence sometime in the future would be comparable in the extent of its destruction.

The shores of the PNW over the years to centuries have experienced an enormous range of hazards, from the erosion and flooding of winter storms, to the decadal enhancement of those hazards during strong El Niños, while at the same time facing near total destruction with the repeat of another subduction earthquake and tsunami. The focus of this chapter has been on the former, "lesser" hazards of more immediate concern to the safety of homes and infrastructure on this coast, it being uncertain when the next "ultimate" event will occur, this year or a century in the future.

Acknowledgements Much of the review presented in this chapter is the product of collaborative research undertaken with graduate students at Oregon State University—it is important to recognize their participation and contributions. Specific for this paper, thanks to Erica Harris for having undertaken extra-credit analyses of the Pacific Northwest wave climates. The senior author (PDK) gratefully acknowledges the support over the years by the Sea Grant Program, having funded our research and supported these students. Our recent investigations of the climate controls and developments of management application strategies were funded by NOAA's Climate Program Office Sectoral Applications Research Program (SARP)—many thanks for their support.

References

Allan JC, Komar PD (2000) Are ocean wave heights increasing in the eastern North Pacific? EOS Trans Am Geophys Union 81(47):561–567

Allan JC, Komar PD (2002) Extreme storms on the Pacific Northwest Coast during the 1997–98 El Niño and 1998–99 La Niña. J Coast Res 18:175–193

Allan JC, Komar PD (2004) Environmentally compatible cobble berm and artificial dune for shore protection. Shore Beach 72(1):9–18

Allan JC, Komar PD (2006) Climate controls on US West Coast erosion processes. J Coast Res 22(3):511–529

Allan JC, Priest GR (2001) Evaluation of coastal erosion hazard zones along dune and bluff backed shorelines in Tillamook County, Oregon: cascade head to Cape Falcon. Oregon Department of Geology and Mineral Industries, Portland, p 126

Allan JC, Komar PD, Priest GR (2003) Shoreline variability on the high-energy Oregon coast and its usefulness in erosion-hazard assessments: shoreline mapping and change analysis. J Coast Res, Spec Issue #38, Byrnes MR, Crowell M, Fowler C (eds), pp 83–105

Allan JC, Witter RC et al (2009) Coastal geomorphology, hazards, and management issues along the Pacific Northwest Coast of Oregon and Washington. Volcanoes to Vineyards: geologic field trips through the dynamic landscape of the Pacific Northwest: Geological Society of America Field Guide 15. O'Connor JE, Dorsey RJ, Madin IP, The Geological Society of America, pp 495–519

Allan JC, Komar PD, Ruggiero P (2011) Storm surge magnitudes and frequency on the central Oregon coast: Solutions to Coastal Disasters. Am Soc Civil Eng, pp 53–64

Allan JC, Komar PD, Ruggiero P, Witter R (2012) The March 2011 Tohoku tsunami and its impacts along the U.S. West Coast. J Coast Res 28(5):1142–1153

Atwater BF (1987) Evidence for great Holocene earthquakes along the outer coast of Washington State: Science 236:942–944

Bacon S, Carter DJT (1991) Wave climate changes in the North Atlantic and North Sea. Int J Climatol 11:545–558

Bacon S, Carter DJT (1993) A connection between mean wave height and atmospheric pressure gradient in the North Atlantic. Int J Climatol 11:545–558

Baron HM (2011) Coastal Hazards and Community Exposure in a Changing Climate: The Development of Probabilistic Coastal Change Hazard Zones: Master of Science thesis, Oregon State University, Corvallis, Oregon, p 82

Benumoff BT, Griggs GB (1999) The dependence of seacliff erosion rates on cliff material properties and physical processes, San Diego County, California. Shore Beach 67(4):29–41

Burgette RJ, Weldon RJ, Schmidt DA (2009) Interseismic uplift rates for western Oregon and along-strike variation in locking on the Cascadia subduction zone. J Geophys Res 114:B01408. doi:10.1029/2008JB005679

Carter DJT, Draper L (1988) Has the northeast Atlantic become rougher? Nature 332:494

Clark JA, Farrell WE, Peltier WR (1978) Global change in post-glacial sea level: a numerical calculation. Quaternary Res 9:265–287

Clemens KE, Komar PD (1988) Oregon beach-sand compositions produced by the mixing of sediments from multiple sources under a transgressing sea. J Sediment Petrol 56:15–22

Collins B, Sitar N (2008) Processes of coastal bluff erosion in weakly lithified sands, Pacifica, California, USA. Geomorphology 97:483–501

Fravre A, Gershunov A (2006) Extra-tropical cyclone/anticyclonic activity in North-Eastern Pacific and air temperature extremes in Western North America. Clim Dyn 26:617–629

Gelfenbaum G, Kaminsky GM (2010) Large-scale coastal change in the Columbia River Littoral Cell: an overview. Mar Geol Spec273(1–4):1–10 (Special issue)

Gelfenbaum G, Sherwood CR, Peterson CD, Kaminsky GM, Buijsman MC, Twitchell DC, Ruggiero P, Gibbs AE, Reed C (1999) The Columbia River littoral cell: a sediment budget overview. Proc Coast Sediments 99:1660–1675

Gemmrich J, Thomas B, Bouchard R (2011) Observational changes and trends in northeast Pacific wave records. Geophys Res Lett 38:L22601. doi:10.1029/2011GL049518

Geng Q, Sugi M (2003) Possible change of extratropical cyclone activity due to enhanced greenhouse gases and sulfate aerosols—study with high-resolution AGCM. J Clim 16:2262–2274

Goldfinger C, Nelson CH, Morey A, Johnson JE, Guterrez-Pastor J, Eriksson AT et al. (2010) Turbidite event history: methods and implications for holocene paleoseismicity of the Cascadia Subductgion Zone. U. S. Geological Survey Professional Paper 1661-F, Reston, VA

Graham NE, Diaz HF (2001) Evidence for intensification of North Pacific winter cyclones since 1948. Bull Am Meteorol Soc 82:1869–1893
Grinsted A, Moore JC, Jevrejeva S (2009) Reconstructing sea level from paleo and projected temperatures 200 to 2100 AD. Clim Dyn 34(4):461–472
Hall JW, Meadowcroft IC, Lee EM, van Gelder PHAJM (2002) Stochastic simulation of episodic soft coastal cliff recession. Coast Eng 46(3):159–174
Harris EL (2011) Assessing physical vulnerability of the coast in light of a changing climate: an integrated, multi-hazard, multi-timescale approach. Masters of Science thesis, Oregon State University, 91 p
Holgate S (2007) On the decadal rates of sea level change during the twentieth century. Geophys Res Lett 34:1–4
Horton R, Herweijer C, Rosenzweig C, Liu J, Gornitz V, Ruane AC (2008) Sea level rise projections for current generation CGCMs based on the semi-empirical method. Geophys Res Lett 35(L02715):5
Jennings R, Schulmeister J (2002) A field based classification scheme for gravel beaches. Mar Geol 186:211–228
Jevrejeva S, Moore JC, Grinsted A (2010) How will sea level respond to changes in natural and anthropogenic forcings by 2100? Geophys Res Lett 37(L07703):5
Kaminsky GM, Ruggiero P, Gelfenbaum G (1998) Monitoring coastal change in southwest Washington and northwest Oregon during the 1997/98 El Niño. Shore Beach 66(3):42–51
Kaminsky GM, Ruggiero P, Buijsman MC, McCandless D, Gelfenbaum G (2010) Historical evolution of the Columbia River Littoral Cell. Mari Geol 273(1–4):96–126
Komar PD (1973) Computer models of delta growth due to sediment input from rivers and longshore transport. Geol Soc Am Bull 84:2217–2226
Komar PD (1978) Wave conditions on the Oregon coast during the winter of 1977–78 and the resulting erosion of Nestucca Spit. Shore Beach 46:3–8
Komar PD (1983) The erosion of Siletz Spit, Oregon. In: Komar PD (ed) Handbook of coastal processes and erosion. CRC Press, Boca Raton, pp 65–76
Komar PD (1986) The 1982–83 El Niño and erosion on the coast of Oregon. Shore Beach 54:3–12
Komar PD (1997) The Pacific Northwest coast: living with the shores of Oregon and Washington. Duke University Press, Durham
Komar PD (1998a) The 1997–98 El Niño and erosion of the Oregon coast. Shore Beach 66:33–41
Komar PD (1998b) Beach processes and sedimentation, 2nd edn. Prentice-Hall, Inc., Upper Saddle River, 544 p
Komar PD, Allan J, Dias-Mendez GM, Marra JJ, Ruggiero P (2000) El Niño and La Niña: Erosion processes and impacts. Proc 27th Int Coastal Eng Conf, pp 2414–2427
Komar PD, Allan JC (2002) Nearshore-process climates related to their potential for causing beach and property erosion. Shore & Beach 70(3):31–40
Komar PD, Allan JC (2007) A note on the depiction and analysis of wave-height histograms. Shore Beach 75(3):1–5
Komar PD, Good JW, Shih S-M (1988) Erosion of Netarts Spit, Oregon: continued impact of the 1982–83 El Niño. Shore Beach 57:11–19
Komar PD, Li MZ (1991) Black-sand placers at the mouth of the Columbia River, Oregon and Washington. Mar Min 10:171–187
Komar PD, Lizarraga-Arciniega JR, Terich TA (1976) Oregon coast shoreline changes due to jetties. J Waterways Harbors Coast Eng, ASCE 102(WW1):13–30
Komar PD, McKinney BA (1977) The Spring 1976 erosion of Siletz Spit, Oregon, with an analysis of the causative storm conditions. Shore Beach 45:23–30
Komar PD, McDougal WG, Marra JJ, Ruggiero P (1999) The rational analysis of setback distances: applications to the Oregon coast. Shore Beach 67(1):41–49
Komar PD, Rea CC (1976) Erosion of Siletz Spit, Oregon. Shore Beach 44:9–15
Komar PD, Shih S-M (1993) Cliff erosion along the Oregon coast: a tectonic – sea level imprint plus local controls by beach processes. J Coast Res 9:747–765

Komar PD, Wang C (1984) Processes of selective grain transport and the formation of placers on beaches. J Geol 92:637–655
Komar PD, Torstenson RW, Shih S-M (1991) Bandon, Oregon: coastal development and the potential for extreme ocean hazards. Shore Beach 59:14–22
Komar PD, Marra JJ, Allan JC (2002) Coastal-erosion processes and assessments of setback distances. Proceedings, Solutions to Coastal Disasters Conference. Am Soc Civil Eng, pp 808–822
Komar PD, McManus J, Styllas M (2004) Sediment accumulation in Tillamook Bay, Oregon: natural processes versus human impacts. J Geol 112:455–469
Komar PD, Allan JC, Ruggiero P (2010) Ocean wave climates: trends and variations due to Earth's changing climate. In: Kim YC (ed) Handbook of Coastal and Ocean Engineering. World Scientific Publishing Co., Hackensack, pp 971–975
Komar PD, Allan JC, Ruggiero P (2011a) Sea level variations along the U.S. Pacific Northwest Coast: tectonic and climate controls. J Coast Res 27(5):808–823
Komar PD, Allan JC, Ruggiero P (2011b) Earth's changing climate and enhanced erosion on the U.S. Pacific Northwest coast. Proceedings, Solutions to Coastal Disasters. Am Soc Civil Eng, pp 209–220
Kulm LD, Byrne JV (1966) Sedimentary response to hydrography in an Oregon estuary. Mar Geol 4:85–118
Li MZ, Komar PD (1992) Longshore grain sorting and beach placer formation adjacent to the Columbia River. J Sediment Petrol 62:429–441
McCabe GJ, Clark MP, Serreze MC (2001) Trends in Northern Hemisphere surface cyclone frequency and intensity. J Clim 14:2763–2768
Meehl GA, Stocker TF, Collins WD, Friedlingstein P, Gaye AT, Gregory JM, Kitoh A, Knutti R, Murphy JM, Noda A, Raper SCB, Watterson IG, Weaver AJ, Zhao Z-C (2007) Global climate projections. In: Solomon S, Qin D, Manning M, Chen Z, Marquis M, Averyt KB, Tignor M, Miller HL (eds) Climate change 2007: the physical science basis. Contribution of working group i to the fourth assessment report of the intergovernmental panel on climate change. Cambridge University Press, Cambridge, UK/New York
Méndez FJ, Menéndez M, Luceño A, Losada IJ (2006) Estimation of the long-term variability of extreme significant wave height using a time-dependent peak over threshold (POT) model. J Geophys Res 111(C07024):13
Peterson C, Scheidegger K, Komar PD (1982) Sand dispersal patterns in an active-margin estuary of the northwestern United States as indicated by sand composition, texture and bedforms. Mar Geol 50:77–96
Pfeffer WT, Harper JT, O'Neel S (2008) Kinematic constraints on glacier contributions to 21st-century sea-level rise. Science 321:1340–1343
Pugh D (2004) Changing sea levels. Cambridge University Press, Cambridge, UK
Rahmstorf S (2007) A semi-empirical approach to projecting future sea-level rise. Science 315:368–370
Rahmstorf S (2010) A new view on sea level rise. Nature 4:44–45
Revell DL, Komar PD, Sallenger AH (2002) An application of LIDAR to analyses of El Niño erosion in the Netarts Littoral Cell, Oregon. J Coast Res 18(4):792–801
Ruggiero P (in press) Is the intensifying wave climate of the U.S. Pacific Northwest increasing flooding and erosion risk faster than sea level rise?. J Waterways Ports Coastal Ocean Eng
Ruggiero P, Komar PD, McDougal WG, Beach RA (1996) Extreme water levels, wave runup and coastal erosion: Proceedings 25th International Coastal Engineering Conference. Am Soc Civil Eng, pp 2793–2805
Ruggiero P, Komar PD, McDougal WG, Marra JJ, Beach RA (2001) Wave runup, extreme water levels and the erosion of properties backing beaches. J Coast Res 17(2):407–419
Ruggiero P, Holman RA, Beach RA (2004) Wave runup on a high-energy dissipative beach. J Geophys Res 109:C06025. doi:10.1029/2003JC002160

Ruggiero P, Buijsman M, Kaminsky GM, Gelfenbaum G (2010a) Modeling the effects of wave climate and sediment supply variability on large-scale shoreline change. Mar Geol 273 (1–4):127–140 (Special issue)

Ruggiero P, Komar PD, Allan JC (2010b) Increasing wave heights and extreme-value projections: the wave climate of the U.S. Pacific Northwest. Coast Eng 57:539–552

Ruggiero P, Baron H, Harris E, Allan J, Komar P, Corcoran P (2011) Incorporating uncertainty associated with climate change into coastal vulnerability assessments: Solutions to Coastal Disasters, Am Society Civil Eng, pp 602–613

Satake K, Shimazaki K, Tsuji Y, Ueda K (1996) Time and size of a giant earthquake in Cascadia inferred from Japanese tsunami records of January 1700. Nature 379:246–249

Seymour RJ (1996) Wave climate variability in southern California. J Waterway Port Coast Ocean Eng Am Assoc Civil Eng 122:182–186

Seymour RJ (1998) Effects of El Niño on the West Coast Wave Climate. Shore Beach 66:3–6

Shih S-M, Komar PD (1994) Sediments, beach morphology and sea cliff erosion within an Oregon coast littoral cell. J Coast Res 10:144–157

Stembridge JE (1975) Shoreline changes and physiographic hazards on the Oregon coast. PhD dissertation, University of Oregon, Eugene

Stockdon HF, Holman RA, Howd PA, Sallenger AH (2006) Empirical parameterization of setup, swash, and runup. Coast Eng 53:573–588

Terich TA, Komar PD (1974) Bayocean Spit: coastal and ocean engineering. Shore Beach 42:3–10

Terich TA, Levenseller T (1986) The severe erosion of Cape Shoalwater, Washington. J Coast Res 2:465–477

Thom BG, Hall W (1991) Behavour of beach profiles during accretion and erosion dominated periods. Earth Surf Process Landf 16:113–127

Tillotson K, Komar PD (1997) The wave climate of the Pacific Northwest (Oregon & Washington): a comparison of data sources. J Coast Res 13:440–452

Vermeer M, Rahmstorf S (2009) Global sea level linked to global temperature. Proc Natl Acad Sci 106(51):21527–21532

Wigley TML (1988) The effect of changing climate on the frequency of absolute extreme events. Clim Monit 17:44–55

Wolter K, Timlin MS (1993) Monitoring ENSO in COADS with a seasonally adjusted principal component index. In: 17th climate diagnostics workshop, Climatology Survey CIMMS and the School of Meteorology, University of Oklahoma, Oklahoma, pp 52–57

Wright LD, Short AD (1983) Morphodynamics of beaches and surf zones in Australia. In: Komar PD (ed) Handbook of coastal processes and erosion. CRC Press, Boca Raton, pp 35–64

Young IR, Zeigler S, Babanin AV (2011) Global trends in wind speed and wave height. Science 332:451–455

Zhang K, Douglas BC, Leatherman S (2001) Beach erosion potential for severe noreasters. J Coast Res 17(2):309–321

Part VIII
Wave Hazards (Extreme Coastal Waves, Storm Surge, and Runup)

Chapter 22
Extreme Coastal Waves, Ocean Surges and Wave Runup

Zai-Jin You and Peter Nielsen

Abstract Extreme coastal waves together with elevated water levels due to storm surges and wave runup often cause damage to coastal property and infrastructure, erode sandy beaches and dunes, inundate coastal and estuarine lands, and gradually degrade coastal ecosystems. Knowledge of extreme waves and elevated water levels is essential for coastal and offshore structure designs, coastal development planning, shore protection measures, and coastal port operations. Estimates of extreme coastal waves and elevated water levels are also required by almost all coastal engineering studies. The purpose of this book chapter is to provide coastal engineers/scientists with basic theories and practical methodologies for estimation of extreme coastal waves, storm surges and wave runup. For the completeness of this chapter, short-term wave analysis is also presented to determine coastal wave statistics. A zero-crossing wave power spectrum is developed to explain the discrepancy between significant wave heights calculated from the zero-crossing method and from the zero-*th* moment of the wave spectrum. Long-term wave analysis is then presented to extrapolate historical wave records to extreme wave heights, and the uncertainty in estimates of extreme wave heights is also discussed in detail. Oceanic surges driven by both wind field and low atmospheric pressure system are estimated, and an analytical solution is also presented to describe the growth of a wind-driven surge. Finally, semi-empirical formulas are proposed to calculate regular wave runup, irregular wave runup, and extreme wave runup on coastal sandy beaches.

Z.-J. You (✉)
Coastal and Marine Science Unit, Science Division, Office of Environment and Heritage, Locked Bag 1002, Dangar, NSW 2309, Australia
e-mail: bob.you@environment.nsw.gov.au

P. Nielsen
School of Civil Engineering, University of Queensland, St Lucia, QLD 4072, Australia
e-mail: P.Nielsen@uq.edu.au

C.W. Finkl (ed.), *Coastal Hazards*, Coastal Research Library 6,
DOI 10.1007/978-94-007-5234-4_22,

Preface

Coastal hazards such as beach erosion and inundation generally result from coastal storms of low-pressure systems that generate extreme waves and storm surges and also from local effects of winds and coastal waves that elevate the mean water surface between the break point and wave runup limit as schematically illustrated in Fig. 22.1. High storm tides can inundate low-lying coastal areas especially when they are combined with the wave setup and runup. Extreme storm waves can also cause severe damage to coastal infrastructure and beachfront properties, erode sandy beaches and dunes, and degrade coastal ecosystems. Therefore, accurate estimation of extreme waves, storm surge, and wave runup is of practical engineering importance and also of enormous economic and environmental implications.

This book chapter is written based on the authors' research work undertaken over the last many years and especially on the most recent work on *extreme waves and elevated water levels along NSW coast*. This chapter consists of four sections. In Sect. 22.1, short-term wave analysis is presented to determine characteristic wave heights in deep waters. A modified zero-crossing method is also derived to explain the discrepancy between significant wave heights calculated in the time and frequency domains. In Sect. 22.2, long-term wave analysis is provided to estimate extreme wave heights from a historical time-series wave record, and the uncertainty in estimates of extreme wave heights is also discussed. In Sect. 22.3, oceanic surges, which are driven by wind field and low atmospheric pressure system, are described, and an analytical linear solution is derived to describe the growth of storm surge. The last section is about swash hydrodynamics, wave runup and extreme wave runup.

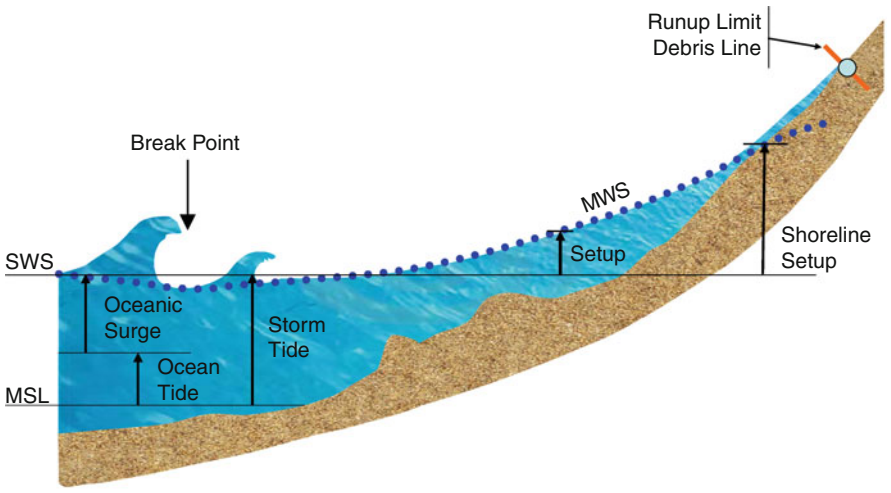

Fig. 22.1 Storm surge terminology: the ocean surge (= offshore MWS – astronomical tide) and hence the still water surface (*SWS*) is uniform over the surf zone, and the mean water surface (*MWS*) variation in the surf zone is generated by wave radiation stress and local wind stress

22.1 Coastal Wave Statistics

22.1.1 Introduction

As ocean waves propagate from deep water to intermediate and shallow waters, they are able to penetrate to the seabed to induce wave orbital velocity and dynamic wave pressure in the vicinity of the seabed and also transmit amounts of wave energy into the seabed through wave-induced bottom shear stress and dynamic wave pressure. You (2009a) presented an explicit criterion to define deep, intermediate and shallow waves as $k_0h \geqslant \pi$, $0.1 < k_0h < \pi$ and $k_0h \leqslant 0.1$ respectively based on linear wave dispersion equation $k_0h = kh\tanh(kh)$, where k is the wave number in water depth h and k_o is the wave number in deep water. The nearbed wave orbital velocity or wave-induced bottom shear stress interacts with the seabed, resulting in frictional dissipation of wave energy, mobilization of seabed sediment, formation of different bed forms, and modification of bottom shear stress (You 1994, 1998, 2005). The dynamic wave pressure is another important wave parameter for calculation of wave forces on coastal structures and ocean platforms, determination of the stability of seabed oil and gas pipelines, and design of coastal and ocean structures. The wave period is also an important design parameter for marine floating systems. The resonant motion of marine floating structures will occur when individual wave periods are close to the natural motion period of the marine floating structures.

22.1.2 Short-Term Wave Analysis

Ocean waves are studied with two basic approaches: the wave spectral method in the frequency domain and the zero-crossing method in the time domain. The wave spectral method is developed based on the Fourier transformation of the sea surface. A discretely measured time series of the sea surface η(t) is approximated by a linear summation of an infinite number of sinusoidal waves with different amplitudes and frequencies

$$\eta(t) = \sum_{i=1}^{\infty} a_i \cos(2\pi f_i t + \phi_i), \tag{22.1}$$

where a_i, f_i and ϕ_i are the amplitude, frequency and phase of the ith harmonic, respectively. The zero-th moment of the wave spectrum $m_0 = \sum \frac{1}{2}a_i^2$ is equal to the variance σ_η^2 of the sea surface elevation η(t). The wave spectral method is used to determine the distribution of wave energy density with frequency. The Fast Fourier Transform (FFT) method is most commonly used in the wave spectral analysis.

The wave-by-wave or the zero-crossing method is used to define individual irregular wave height and period (H, T) in the time domain. An irregular wave is

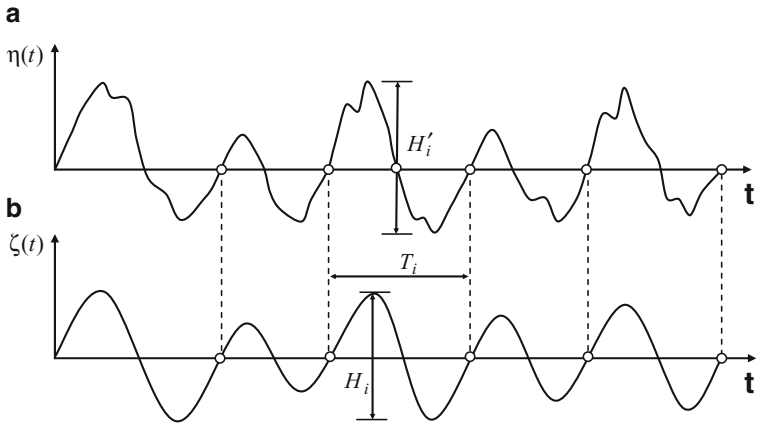

Fig. 22.2 Irregular waves with zero up-crossing periods T_i are uniquely transformed into individual regular waves with (H_i, T_i) based on wave energy balance between individual irregular wave and transformed regular wave

defined when the sea surface elevation profile crosses the mean water level or the zero-line upward and continues until the next crossing point as illustrated in Fig. 22.2a. The wave height H is the difference in the levels of the highest crest and the lowest trough between two successive zero-up crossings, and the wave period T is the difference in the times of two successive zero-up crossings. Note the zero-down crossing method is also used for analysis of irregular wave height and period (H, T). The wave data (H, T) are then used to calculate the distribution of H or T and the joint distribution of H and T.

The significant wave height $H_{1/3}$, which is averaged from the largest one-third of all wave heights analysed with the zero-crossing method, is found to be different from the significant wave height H_{mo} calculated with the wave spectral method. For example, $H_{1/3} = 0.925H_{mo} = 0.925 \times (4\,\sigma_\eta)$ was suggested by Longuet-Higgins (1980), where m_{o} is the zero-*th* moment of the wave spectrum and $\sigma_\eta = m_0$. Similar empirical relationships are $H_{1/3} = 0.942H_{mo}$ proposed by Forristall (1978) and $H_{1/3} = 0.927H_{mo}$ by Holthuijsen (2007). A modified zero-crossing method (MZC), which is derived as follows, enables us to explain this discrepancy and also combines the zero-crossing and the spectral methods to one unified method for short-term wave analysis.

Let η(t) be the measured sea surface elevation of n consecutive irregular waves and the n irregular waves are assumed to be stationary over the time period of D [see Fig. 22.2a]. An irregular wave with zero-crossing period T_i of the n irregular waves can be uniquely transformed as a regular wave with the same period T_i

$$\zeta_i(t) = \tfrac{1}{2}H_i \sin\,[\omega_i(t - \varepsilon_i)], \tag{22.2}$$

where $\zeta_i(t)$ is the transformed sea surface of the ith regular wave, ω_i is the angular frequency ($= 2\pi/T_i$), $\varepsilon_i = \sum_{k=1}^{i-1} T_k$ and H_i is the wave height. Equation (22.2) is then used to derive the identity as

$$\frac{1}{T_i}\int_{\varepsilon_i}^{T_i+\varepsilon_i} {\zeta_i}^2(t)\,dt = \frac{1}{T_i}\int_0^{T_i} {\zeta_i}^2(t')\,dt' = \frac{1}{8}H_i^2, \tag{22.3}$$

where $t' = t - \varepsilon_i$ is a new time variable. The wave energy of the ith wave is shown not to be dependent on the initial time ε_i. Based on Eqs. (22.2) and (22.3), the mean wave energy of the n sinusoidal waves, σ_ζ^2, can be derived as

$$\begin{aligned}\sigma_\zeta^2 &= \frac{1}{D}\int_0^D \zeta^2(t)dt = \frac{1}{D}\left[\int_0^{T_1}\zeta^2(t)dt + \int_{T_1}^{T_2+T_1}\zeta_2^2(t)dt + \cdots \int_{\varepsilon_1}^{T_1+\varepsilon_1}\zeta_i^2(t)dt + \cdots \int_{\varepsilon_n}^{T_n+\varepsilon_n}\zeta_n^2(t)dt\right] \\ &= \frac{1}{n}\left[\frac{H_1^2}{8}\left(\frac{T_1}{\bar{T}}\right) + \frac{H_2^2}{8}\left(\frac{T_2}{\bar{T}}\right) + \cdots + \frac{H_i^2}{8}\left(\frac{T_i}{\bar{T}}\right) + \cdots + \frac{H_n^2}{8}\left(\frac{T_n}{\bar{T}}\right)\right],\end{aligned} \tag{22.4}$$

where $\bar{T}$ is the mean wave period and $\bar{T} = \frac{1}{n}\sum_{i=1}^n T_i = \frac{1}{n}D$. On the other hand, the variance of the measured sea surface elevation $\eta(t)$ of the n irregular waves can be also determined as

$$\begin{aligned}\sigma_\eta^2 &= \frac{1}{N}\sum_{j=1}^N \eta_j^2 = \frac{1}{N}\left[\sum^{m_1}\eta_1^2 + \sum^{m_2}\eta_2^2 + \cdots + \sum^{m_i}\eta_i^2 + \cdots + \sum^{m_n}\eta_n^2\right] \\ &= \frac{1}{N}\left[\frac{T_1}{m_1\Delta t}\sum^{m^1}\eta_1^2 + \frac{T_2}{m_2\Delta t}\sum^{m^2}\eta_2^2 + \cdots + \frac{T_i}{m_i\Delta t}\sum^{m^i}\eta_i^2 + \cdots \frac{T_n}{m_n\Delta t}\sum^{m_n}\eta_n^2\right] \\ &= \frac{1}{n}\left[\sigma_{\eta_1}^2\left(\frac{T_1}{\bar{T}}\right) + \sigma_{\eta_2}^2\left(\frac{T_2}{\bar{T}}\right) + \cdots + \sigma_{\eta_i}^2\left(\frac{Ti}{\bar{T}}\right) + \cdots + \sigma_{\eta_n}^2\left(\frac{T_n}{\bar{T}}\right)\right],\end{aligned} \tag{22.5}$$

where $T_i = m_i \times \Delta t$, $N\Delta t = n\bar{T}$, N is the total number of discrete data points from the measured sea surface $\eta(t)$ of the n irregular waves, m_i is the number of discrete data points for the surface sea elevation $\eta_i(t)$ of the ith irregular wave, Δt is the constant time step, and σ_i^2 is the variance of $\eta_i(t)$.

If the wave energy of an irregular wave is equal to that of the transformed regular wave, H_i can then be uniquely determined by equalling Eq. (22.4) to (22.5)

$$H_i = 2\sqrt{2}\sigma_{\eta_i}, \tag{22.6}$$

where $\sigma_{\eta_i}^2$ is the variance of the sea surface elevation $\eta_i(t)$ of the ith irregular wave. After individual waves (σ_i, f_i) are analysed from Eq. (22.5) of the MZC method, the

wave frequencies ($f_i = 1/T_i$) together with their standard deviations or wave heights can be divided into a number of frequency bins and then uniquely assigned into the defined frequency bins to obtain the zero-crossing wave spectrum

$$\sigma_\eta^2 = \sum_{k=1}^{M} S(f) \times \Delta f = \sum_{k=1}^{M} \left[\left(\frac{1}{n} \frac{\bar{f}}{f_k} \right) \sum_{f_k}^{f_k+\Delta f} \sigma_{\eta_j}^2 \right]_k . \tag{22.7}$$

The zero-crossing wave spectrum S(f) is more easily and accurately computed by Eq. (22.7) of the MZC method than by Eq. (22.1) of the Fourier Transformation method (FT). The MZC method computes $S(f)$ directly from the measured sea surface η(t) without making any approximations or assumptions, while the FT method estimates $S(f)$ by using a linear summation of a large numbers of *sinusoidal* waves to approximate the measured sea surface η(t). Furthermore, the harmonic amplitudes and frequencies, which are calculated with the FT method, don't necessarily represent real wave heights and periods observed in the field and the wave energy density from long waves may be generally overestimated (You 2010). The wave spectra, which are calculated by both the FT and MCZ methods, are expected to be quite similar.

Now, Eq. (22.4) is used to explain the discrepancy between $H_{1/3}$ and H_{mo}. If ocean waves in deep water are assumed to be simple sinusoidal waves with different periods, the root-mean-square wave heights H_{rms} calculated by both the zero-crossing and wave spectral methods are shown to be identical only under the assumption of a narrow-banded sea or $T_i = \bar{T}$ according to Eqs. (22.4) and (22.5)

$$\sigma_\eta^2 = \sigma_\varsigma^2 = \frac{1}{8n} \sum_{i=1}^{n} H_i^2 = \frac{1}{8} H_{rms}^2 . \tag{22.8}$$

For a finite-banded random sea or $T_i \neq \bar{T}$, however, we have $H_{rms} < \sqrt{8}\sigma_\eta$ (Longuet-Higgins 1980; Forristall 1978; Holthuijsen 2007). The use of $H_{rms} \approx \sqrt{8}\ \sigma_\eta$ will generally overestimate the wave height H_{rms} for the finite-banded random sea. A new wave parameter $H' = H\sqrt{T/\bar{T}}$, which is derived from Eq. (22.4) and physically represents the wave energy of individual wave, may be used to describe characteristics of individual ocean waves.

22.1.3 Distribution of Wave Height

The distribution of coastal wave height can be directly determined when the sea surface elevation η(t) of n consecutive irregular waves is measured for a short period of 15–30 min in a stationary sea state. The sampling rate of wave measuring devices such as waverider buoys is often set to be 2 ~ 5 Hz for ocean swell and

about 10 Hz for short wind waves in order to collect enough data points for individual waves. The zero-crossing method can be then applied to extract the n irregular waves (H, T) from the measured sea surface η(t), see Fig. 22.2a. The histogram of wave height H is computed by assigning the n wave heights into different wave height classes

$$p(H) = \frac{1}{\Delta H}\frac{k}{n} \quad \text{and} \quad Q(H) = 1 - \sum p(H)\,\Delta H = \frac{m}{n} \tag{22.9}$$

where k is the number of waves falling into a wave height class, ΔH is the wave bin width and n is the total number of waves, Q(H) is the probability of exceeding and m is the number of wave heights being equal to or larger than a given wave height H. The cumulative probability P is then calculated as $P = (1 - Q)$.

The distribution of wave height may be also computed from multiple wave segments that were collected under different sea states provided each of the segments is stationary. The probability of dimensionless wave heights can be determined by (i) calculating the root-mean-square wave height H_{rms} for each wave segment, (ii) scaling individual wave heights in each wave segment by its H_{rms}, (iii) assigning individual dimensionless wave heights H/H_{rms} from all wave segments into different dimensionless wave classes, and (iv) calculating the histogram and probability of dimensionless wave height $\hat{H}$ as

$$p(\hat{H}) = \frac{1}{\Delta \hat{H}}\frac{k}{n} \quad \text{and} \quad Q(\hat{H}) = 1 - \sum p(\hat{H})\Delta\hat{H} = \frac{m}{n}, \tag{22.10}$$

where $\hat{H} = H/H_{rms}$, k is the number of dimensionless wave heights $\hat{H}$ falling into a dimensionless wave height bin and n is the total number of waves from multiple wave segments. The *rms* wave height $\hat{H}_{rms}$ of dimensionless wave heights $\hat{H}$, which is calculated from N consecutive wave segments ($N = 1, 2, 3, \ldots$..), should be equal to 1 and also independent of N. Thus, the dimensionless wave height data, which are constructed from N consecutive wave segments with the same sampling length, are also expected to be stationary provided individual wave segment is stationary. Figure 22.3 shows an example of the histogram and the exceedance probability of dimensionless wave pressure amplitudes, which are calculated from Mac4001 of You and Hanslow (2001) via Eq. (22.10).

The distribution of wave height has been extensively studied theoretically by a larger number of researchers (e.g. Longuet-Higgins 1952, 1975; 1963; 1983; Tayfun 1980, 1981; Vinje 1989; Dean and Dalrymple 1991; Mei 1991; Sultan and Hughes 1993; Ochi 1998; Massel and Sobey 2000; Song and Wu 2000; Hou and Guo 2006; You 2009a, b). Rudnick (1951) first found the Gaussian distribution of the sea surface elevation by analysing his field wave data. Longuet-Higgins (1952) first applied the Rayleigh distribution to study the distribution of wave height in deep water under the assumption of a narrow-banded Gaussian sea

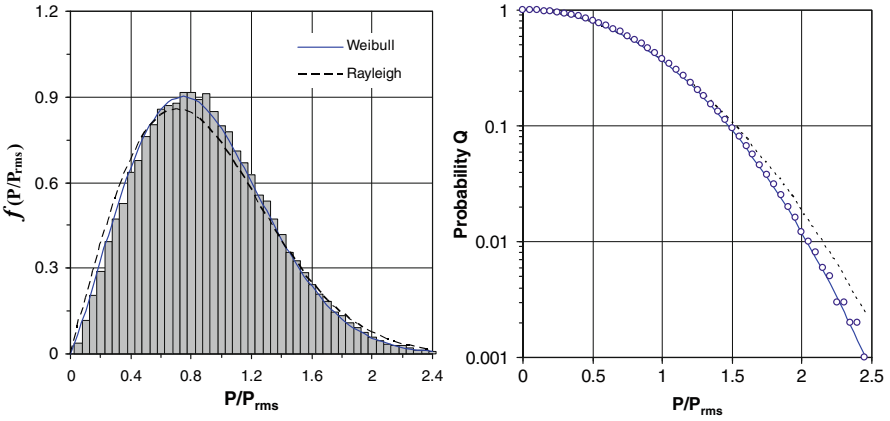

Fig. 22.3 The histogram and the exceedance distribution of dimensionless wave pressure amplitude P/P_{rms} are calculated from wave pressure data Mac4001 of You and Hanslow (2001) via Eq. (22.10) and also compared with the distributions of the Rayleigh (*dashed line*) and the Weibull (*solid curve*)

$$Q = \exp\left[-\left(\frac{H}{H_{rms}}\right)^2\right]. \tag{22.11}$$

Under a finite-banded Gaussian sea, Longuet-Higgins (1980) modified Eq. (22.11) by introducing a scale parameter $C = 0.925$ to account for finite wave spectral bandwidth

$$Q = \exp\left[-\left(\frac{H}{C\,H_{rms}}\right)^2\right] = \exp\left[-\left(\frac{H}{H_r}\right)^2\right], \tag{22.12}$$

where H_{r} is the reference wave height less than H_{rms}, but larger than the mean wave height H_1. Note that the modified Rayleigh distribution with one degree of freedom should give a better fit to the wave data than the Rayleigh distribution with no degree of freedom. A new value of $C = 0.96$ is recently proposed by You (2009a, b) based on the field wave pressure and orbital velocity data of You and Hanslow (2001).

With introducing a shape parameter α rather than the scale parameter C, the Rayleigh distribution is modified as a Weibull distribution

$$Q = \exp\left[-\left(\frac{H}{H_{rms}}\right)^{\alpha}\right], \tag{22.13}$$

which also has one degree of freedom. The Rayleigh distribution in Eq. (22.11) may be considered as a special case of the Weibull distribution in Eq. (22.13) with

$\alpha = 2$. Forristall (1978) proposed the Weibull distribution with $\alpha = 2.13$ to study the distribution of wave heights in the Gulf of Mexico. A similar value of $\alpha = 2.15$ is recently proposed by You (2009a, b).

It is shown in Fig. 22.3 that the Rayleigh and Weibull distributions are compared with the histogram and the distribution of dimensionless wave pressure amplitudes measured in Mac4001 of You and Hanslow (2001). The modified Rayleigh distribution, Eq. (22.12), is found to be quite close to the Weibull and thus not included for the comparison in Fig. 22.3. The wave pressure data were collected at 1 m above the seabed at a 2 Hz sampling rate for 17.07 min every hour over a period of about 2 year in a coastal water depth of 23 m in the Tasman Sea, Australia. The Rayleigh distribution Q(H) is shown to generally overestimate the probability of large waves, while the Weibull distribution with $\alpha = 2.15$ agrees well with the field data. Note the Weibull distribution with one degree of freedom is more flexible and should give a better fit to the data than the Rayleigh distribution with no degree of freedom.

The distribution of the Rayleigh, the modified Rayleigh or the Weibull can be now applied to calculate the average height H_Q of m largest waves in a wave record of n irregular waves. For example, $H_{1/3}$ is the average height of the highest one-third of all waves and also called the significant wave height, H_1 the average height of all waves and $H_{1/10}$ the average height of the largest one-tenth of all waves. The significant wave height $H_{1/3}$ is the most commonly-used wave height to describe a sea state. The average wave height H_Q is defined as

$$H_Q = \frac{1}{m}\sum_{i=1}^{m} H_i = \frac{n}{m}\sum_{j=1}\left[\left(\frac{1}{\Delta H}\frac{k}{n}\right)H\right]_j \Delta H \approx \frac{1}{Q}\int_{\hat{H}_Q}^{\infty} H f(H)\, dH\,, \tag{22.14}$$

where m is the number of the largest waves to be averaged from a wave record of n irregular waves, i is the subscript for the largest ith wave, j for the jth wave height class, k is the number of wave heights falling into the jth wave height class, ΔH is the wave class width, f(H) is the probability density function and $f(H) = -dQ/dH \approx k/(n\Delta H)$ when ΔH is sufficiently small, $Q = n/m$ and $\hat{H}_Q$ is the wave height with the probability Q. In substituting the Rayleigh distribution into Eq. (22.14), H_Q is then calculated as

$$\frac{H_Q}{H_{rms}} = \sqrt{-\ln Q} + \frac{\sqrt{\pi}}{2Q}\, erfc\left(\sqrt{-\ln Q}\right), \tag{22.15}$$

where $erfc(x)$ is the error function. The relationship $\hat{H}_Q/H_{rms} = \sqrt{-\ln Q}$ derived from the Rayleigh distribution is also used in the derivation. For engineering applications, You (2009b) approximated the $erfc(x)$ function to simplify Eq. (22.15) as

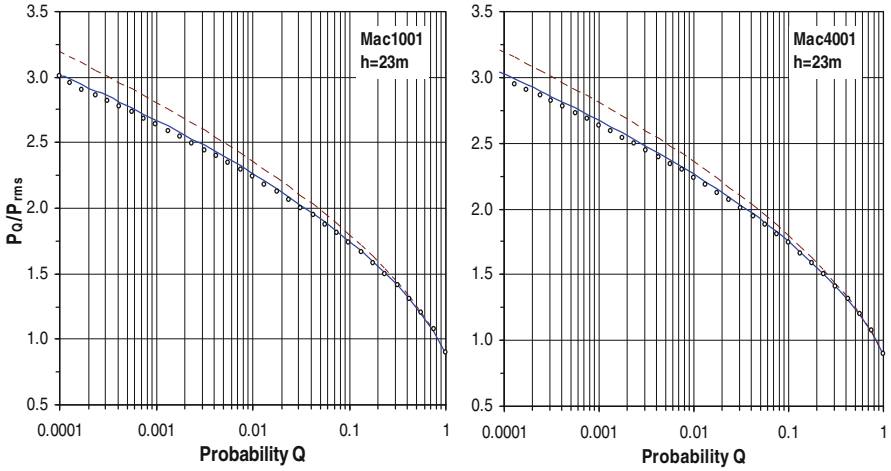

Fig. 22.4 The average wave pressure amplitudes P_Q measured in Mac1001 and Mac4001 of You and Hanslow (2001) are compared with those calculated from the Rayleigh (*dashed*) and the Weibull (*solid*)

$$\frac{H_Q}{H_{rms}} \approx \sqrt{-\ln Q} + \frac{1}{\sqrt{-\ln Q} + \sqrt{-\ln Q + \pi/4}}, \tag{22.16}$$

which has the maximum error about 3% at $Q = 0.9$ and the exact solution at $Q = 1$. Similarly, H_Q can be also derived from the modified Rayleigh distribution as

$$\frac{H_Q}{H_{rms}} = C \times \left[\sqrt{-\ln Q} + \frac{\sqrt{\pi}}{2Q}\, erfc\left(\sqrt{-\ln Q}\right)\right], \tag{22.17}$$

and from the Weibull distribution as

$$\frac{H_Q}{H_{rms}} = (-\ln Q)^{1/\alpha} + \frac{1}{\alpha Q}\,\Gamma(1/\alpha, -\ln Q), \tag{22.18}$$

where $\Gamma(a, x)$ is the upper incomplete gamma function. Note that Eq. (22.18) with $\alpha = 2$ and Eq. (22.17) with $C = 1$ will all reduce to Eq. (22.15) of the Rayleigh distribution.

The comparison of the computed wave pressure amplitudes P_Q from the Rayleigh and Weibull distributions with those measured in Mac1001 and Mac4001 is shown in Fig. 22.4. The wave pressure amplitude is assumed to be of the same distribution as the wave height according to linear wave theory. The Rayleigh distribution is seen to overestimate large wave pressure amplitudes and is less accurate in predicting P_Q than the Weibull distribution. When $Q = 1$, the mean wave height H_1 calculated from the Rayleigh distribution is equal to $H_1 = 0.886$ H_{rms} and almost identical to that from the Weibull, but slightly larger than from the modified Rayleigh distribution, $H_1 = C \times 0.886$ H_{rms}, where $C < 1$. This indicates

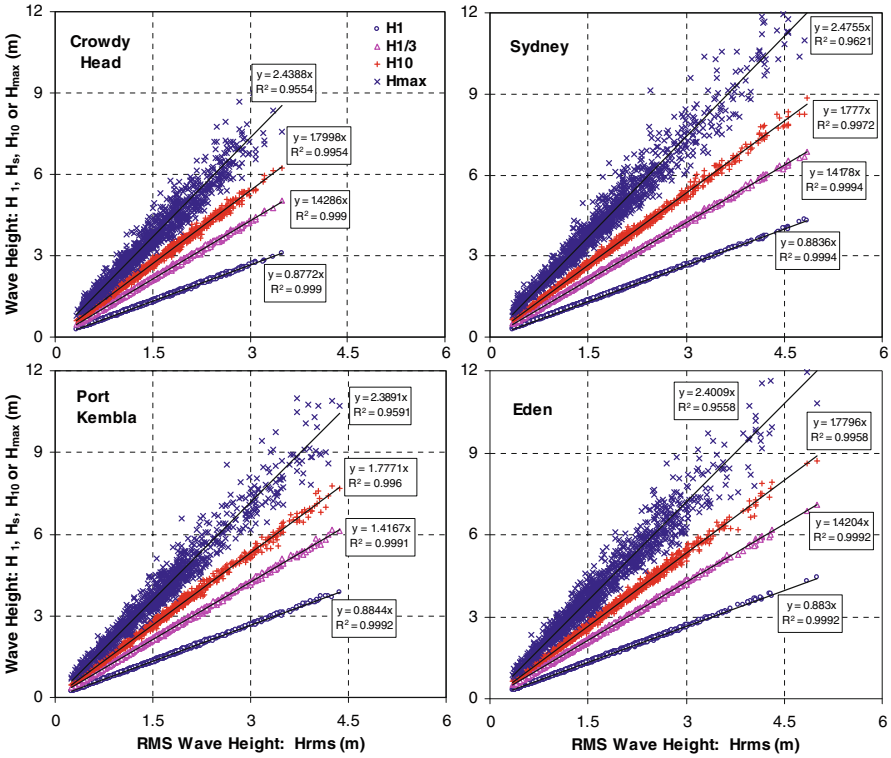

Fig. 22.5 The wave height ratios, H_1/H_{rms}, $H_{1/3}/H_{rms}$, $H_{1/10}/H_{rms}$ and H_{max}/H_{rms}, measured in deep waters off the NSW coast of Crowdy Head, Sydney, Port Kembla and Eden in the Tasman Sea, Australia, where the slope of the line regression lines is equal to the mean wave height ratio

that the mean wave height H_1 may not be accurately estimated from the modified Rayleigh distribution. Figure 22.4 also shows that the Rayleigh distribution gives a good estimation of P_Q when $Q \geq 0.1$. Thus, characteristic wave heights (e.g. $H_{1/10}$, $H_{1/3}$, H_1) can be accurately and conveniently computed from Eq. (22.15) or (22.16) of the Rayleigh distribution.

Figure 22.5 also shows the wave height ratios H_Q/H_{rms}, which are directly estimated from the waverider buoy data collected from 1st June to 30th July 2007 in deep waters off the NSW coastline of Crowdy Head, Sydney, Port Kembla and Eden in the Tasman Sea, Australia. The waverider buoy data on the sea surface elevation were recorded at a sampling rate of 5 Hz for 34 min and sampled every 1 h. The five wave heights, H_{rms}, H_1, $H_{1/3}$, $H_{1/10}$ and H_{max}, were determined from each of 1,330 wave segments with the zero-crossing method. The linear plot of H_Q versus H_{rms} in Fig. 22.5 gives the mean ratio of H_Q to H_{rms} or the slope of linear regression line, which is estimated from the 1,330 data points on (H_{rms}, H_Q). The mean wave height ratios, which are averaged from the four sites, are $H_1/H_{rms} = 0.881$, $H_{1/3}/H_{rms} = 1.421$, and $H_{1/10}/H_{rms} = 1.782$ respectively, and agree well with the predicted values of 0.886, 1.461 and 1.801 from the Rayleigh distribution.

22.1.4 Distribution of Maximum Wave Height

An important engineering application for study of the distribution of wave height is to estimate the expected value of maximum wave height $H_{\max}$ in a short-term wave record of finite size n. Individual maximum wave heights in different wave records with the same size n are expected to be different, but may follow a certain statistical distribution. The cumulative probability that all n wave heights in a wave record of finite size n shall be less than $H_{\max}$ may be estimated from the nth order statistics as

$$P = (1 - \Psi)^n = \left\{ 1 - \exp\left[-\left(\frac{H_{\max}}{H_{rms}} \right)^2 \right] \right\}^n, \tag{22.19}$$

where ψ is the probability for any one of the n wave heights being less than or equal to $H_{\max}$. When the Rayleigh distribution is used for Ψ, the probability density function (pdf) of $H_{\max}$ derived from Eq. (22.19) is asymmetric and becomes narrowly distributed with increasing n (You 2009b). When n is quite large (e.g. $n > 20$), Eq. (22.19) may be approximated as

$$\begin{aligned} P(x) &= \exp\left[-\exp\left(x_0^2 - x^2 \right) \right] \quad \text{or} \\ f(x) &= 2x \exp\left[\left(x_0^2 - x^2 \right) - \exp\left(x_0^2 - x^2 \right) \right], \end{aligned} \tag{22.20}$$

where $x = H_{\max}/H_{\text{rms}}$ and $x_0 = \sqrt{\ln n}$. When $n \to \infty$, the identity, $(1 + x/n)^n = \exp(x)$, is also used in the derivation of Eq. (22.20). The expected wave height of $H_{\max}$, denoted by $\mathrm{E}(H_{\max})$, can be estimated from Eq. (22.20)

$$\frac{E(H_{\max})}{H_{rms}} = \int_0^\infty x f(x)\, dx \approx \sqrt{\ln n} + \frac{\gamma}{2\sqrt{\ln n}} - \frac{(\gamma^2 + \pi^2/6)}{8(\ln n)^{1.5}}, \tag{22.21}$$

where γ is Euler's constant (= 0.5772). Eq. (22.21) was derived by You (2009b) differently from that of Longuet-Higgins (1952). Similarly, in replacing ψ with the modified Rayleigh distribution in Eq. (22.19), $E(\mathrm{H}_{\max})$ can be estimated as

$$\frac{E(H_{\max})}{H_{rms}} = C \left[\sqrt{\ln n} + \frac{\gamma}{2\sqrt{\ln n}} - \frac{(\gamma^2 + \pi^2/6)}{8(\ln n)^{1.5}} \right], \tag{22.22}$$

and with the Weibull distribution

$$\frac{E(H_{\max})}{H_{rms}} = x_0 + \frac{\gamma}{\theta\, x_0^{\theta-1}} - \frac{(\gamma^2 + \pi^2/6)(\theta - 1)}{2\theta^2\, x_0^{2\theta-1}}, \tag{22.23}$$

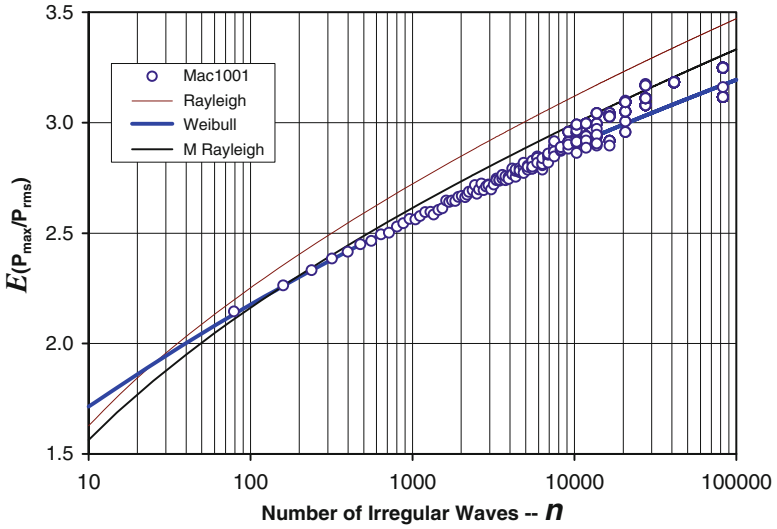

Fig. 22.6 The expected values of P_{max}/P_{rms} computed from the Rayleigh, modified Rayleigh and Weibull are compared with those measured from the wave pressure data Mac1001 of You and Hanslow (2001)

where $x_0 = (\ln n)^{1/\alpha}$. When $C = 1$ and $\theta = 2$, both Eqs. (22.22) and (22.23) will reduce to Eq. (22.21) of the Rayleigh distribution. Note that Eq. (22.21), (22.22) or (22.23), is generally dominated by the first term. For example, when $n \geq 100$, the second and third terms in Eqs. (22.21)–(22.23) are generally less than 6 and 1% of the first term.

Figure 22.6 shows the comparison of the expected values of P_{max}/P_{rms} calculated from Eqs. (22.21) to (22.23) with those measured from the wave pressure data Mac1001, where P_{max} the maximum pressure amplitude and P_{rms} is the *rms* wave pressure amplitude. The wave pressure data were sampled at a 2 Hz rate for 17.07 min every hour in a water depth of 23 m in the Tasman Sea, Australia. There are 1,038 wave pressure segments collected in Mac1001 ($N = 1{,}038$). The N segments are then evenly divided into k segments of $k \times 17$ min, where $k = 1, 2, \ldots, N$. Each of the k segments gives only one value of P_{max}/P_{rms}. The mean of P_{max}/P_{rms} is then estimated from k maxima from the k segments with the number of waves ranging from 80 to 100,000 in Fig. 22.5. Note the segments of $k \times 17$ min are stationary as the *rms* value of the dimensionless wave pressures P/P_{rms} in each of the segments is always equal to 1. The expected values of P_{max}/P_{rms} calculated from the Rayleigh are shown to be slightly larger than those measured in Mac1001 and those computed from the modified Rayleigh and the Weibull.

22.1.5 Distribution of Wave Period

The distribution of wave period has not been studied as extensively as the distribution of wave height. Under the assumption of a narrow-banded random sea, different waves are assumed to have the same period. However, statistical properties of wave periods are of engineering importance for estimating a possible critical resonant condition of floating coastal structures. When the natural motion period of a floating coastal structure is nearly equal to water wave periods, for example, the resonant motion of the floating structure may occur and subsequently result in damage to the floating structure. Bretschneider (1959) determined the distribution of wave period under the assumption that the wavelength L follows the Rayleigh distribution. Since L is proportional to T^2 according to linear wave theory, the distribution of T^2 should also follow the Rayleigh distribution. The distribution of wave period, which was proposed by Bretschneider (1959), is expressed as

$$f(T) = \frac{\pi}{1.2}\frac{x^3}{\bar{T}}\exp\left[-\frac{\pi}{4.8}x^4\right] \quad \text{or} \quad Q = \int_T^\infty f(T)dT = \exp\left[-\frac{\pi}{4.8}x^4\right], \tag{22.24}$$

where $\bar{T}$ is the mean wave period and $x = T/\bar{T}$. Longuet-Higgins (1962) also derived a different distribution for wave period

$$\begin{aligned} f(x) &= 0.5\,v^2\left[v^2 + (x-1)^2\right]^{-1.5} \quad \text{or} \\ Q &= \int_T^\infty f(T)dT = 0.5\left[1 - \frac{x-1}{\sqrt{v^2 + (x-1)^2}}\right], \end{aligned} \tag{22.25}$$

where ν is the spectral width parameter. Equation (22.25) does not satisfy the boundary condition of $f = 0$ at $T = 0$ when $\nu \neq 0$. You (2009a) also proposed a normal distribution function for the wave period based on his extensive field data

$$\begin{aligned} f(T) &= \frac{1}{C_0\,T_{rms}\sqrt{\pi}}\exp\left[-\left(\frac{x - C_1}{C_0}\right)^2\right] \quad \text{or} \\ Q &= \int_T^\infty f(T)dT = 1 - \Phi\left(\frac{\sqrt{2}(x - C_1)}{C_0}\right), \end{aligned} \tag{22.26}$$

where $C_0 = 0.95$, T_{rms} is the root-mean-square wave period, $\bar{T}$ is the mean zero-crossing period, Φ is the norm distribution, and C_1 is constant for a given water depth. The density distribution of T/T_{rms}, Eq. (22.26), was compared with the field data of You and Hanslow (2001) in Fig. 22.7. The measured density distribution is shown to be nearly symmetry about the mean wave period and it is lower and

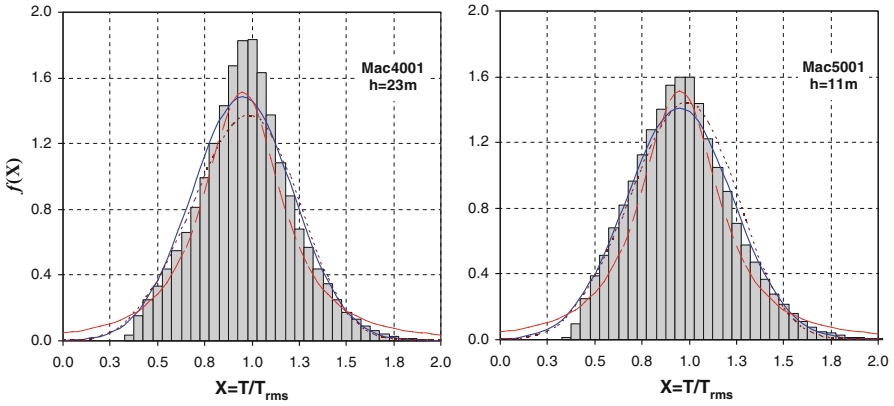

Fig. 22.7 Probability density distributions of zero-crossing wave period T computed from Mac4001 and Mac5001 of You and Hanslow (2001) are compared with Eq. (22.24) of Bretschneider (1959) (*dashed*), Eq. (22.25) of Longuet-Higgins (1980) (*long dashed*) and Eq. (22.26) of You (2009a) (*solid curve*)

spreads out farther in the 11 m water depth than that in the 23 m water, where $C = 0.36$ is determined for the 11 m water depth and $C = 0.33$ for the 23 m water. The probability distribution of wave period in Eq. (22.26) is shown to be much narrower than that of wave height and it lies mainly in the range of $T = (0.5 - 1.5)\ \bar{T}$. This is termed as the narrow-banded condition in which all wave periods are in a narrow period band about $\bar{T}$.

A simple empirical relationship between different wave periods was also derived by You and Hanslow (2001) as

$$T_{\max} \approx T_{1/10} \approx T_{1/3} = 1.05 T_{rms} = 1.09 \bar{T}, \tag{22.27}$$

where $T_{\max}$ is the maximum wave period, $T_{1/3}$ is the mean of wave periods corresponding to the largest one-third of all wave heights and similarly $T_{1/10}$ is the mean of wave periods from the largest one-tenth of all waves heights.

22.1.6 Joint Distribution

The probability distributions of wave height and period have been separately described above. If wave heights are uncorrelated to wave periods, the joint distribution of wave height and period, Q(H, T), can be easily computed as Q(H, T) = Q(H) × Q(T), where Q(H) and Q(T) are the distributions of wave height and period, respectively. In real sea states, wave heights and periods are generally correlated. The joint probability distribution of wave height and period was first developed by Longuet-Higgins (1975) for an arrow-banded random sea and was later modified by Longuet-Higgins (1983) for a finite-banded random sea.

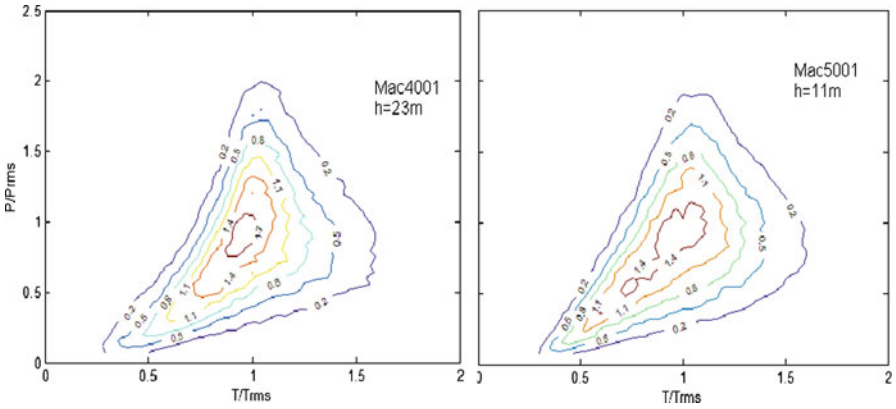

Fig. 22.8 The joint probability density distribution of P/P_{rms} and T/T_{rms} computed from the wave pressure data Mac4001 and Mac5001 of You and Hanslow (2001) via Eq. (22.28).

Figure 22.8 also shows the joint density distribution of dimensionless wave pressure amplitude $\hat{P}$ and wave period $\hat{T}$, which is calculated form the field wave data Mac4001 and Mac5001 of You and Hanslow (2001)

$$p(\hat{P},\hat{T}) = \frac{k}{n}\frac{1}{\Delta\hat{P}\,\Delta\hat{T}} \tag{22.28}$$

where n is the total number of waves and k is the number of waves $(\hat{P},\hat{T})$ falling into the ith wave class $(\hat{P}_i, \hat{T}_i)$ and $\Delta\hat{P}$ and $\Delta\hat{T}$ are the bin widths. The joint distributions measured in the shallow and deep waters are shown to be generally similar.

In Fig. 22.9a, it is also shown how the distribution of wave period is affected by different values of P/P_{rms}. The distribution of wave period is shown to follow a Weibull distribution when $P/P_{\mathrm{rms}} < 1$, but it is moving towards the right and obeys the normal distribution when $P/P_{\mathrm{rms}} \geq 1$. It is also shown in Fig. 22.9b that the mean wave period of small waves with $P < P_{\mathrm{rms}}$ increases nonlinearly with P, while the mean wave period of large waves with $P > P_{rms}$ becomes nearly constant. Based on this finding, it may be concluded that the assumption of a narrow-banded random sea is more justified for large sea waves than small ones.

22.2 Extreme Coastal Waves

22.2.1 Introduction

Extreme coastal storm waves together with strong winds and possible heavy rainfalls can cause severe damage to coastal infrastructure and beachfront property,

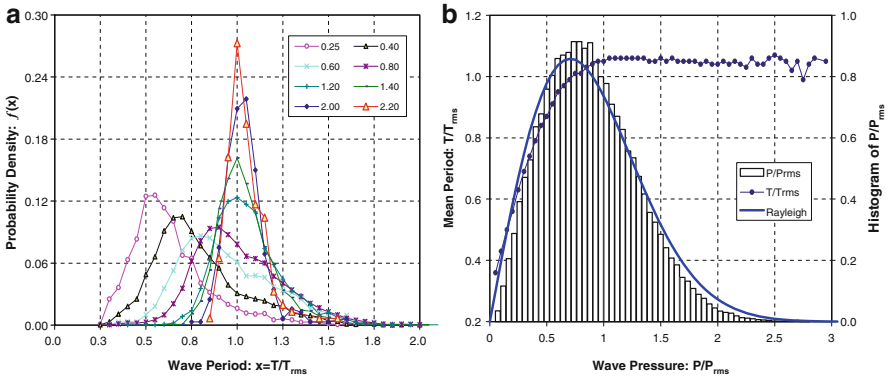

Fig. 22.9 (**a**) Distribution of wave period with different values of P/P_{rms} ranging from 0.25 to 2.2 from the wave pressure data Mac4001 of You and Hanslow (2001), and (**b**) Histogram of P/P_{rms} and the variation of T/T_{rms} with P/P_{rms}

erode sandy beaches and dunes, inundate coastal land, and degrade coastal ecosystems. A recent severe coastal storm, for example, which was formed on the central coast of New South Wales, Australia on 8 June 2007 (Mills et al. 2010), produced huge seas with maximum wave heights of up to 14 m, beached a large coal ship, Pasha Bulker of 76,741 tones and 225 m long, on Nobbys Beach in Newcastle (see Fig. 22.10). This coastal storm also eroded coastal beaches, damaged coastal properties and dumped flooding rains on the NSW coastal areas, resulting in the total damage of about US$1.35 billion (McAneney et al. 2007). Extreme wave conditions are also required for coastal and offshore structure designs, coastal inundation studies, beach nourishment programs, coastal construction planning, coastal port operations and navigations (You and Lord 2008). Thus, accurate estimation of extreme coastal waves is of practical engineering importance and also of enormous economic implications.

22.2.2 Methodology

There are a large number of studies undertaken for estimation of extreme wave heights by many researchers, e.g. Issacson and Mackenzie (1981), Muir and El-Shaarawi (1986), Goda (1988), Ochi (1998), Kamphuis (2000), You and Jayewardene (2003), Cao et al. (2006), You and Yin (2007), Goda (2011) and You (2012). The commonly-used approach is to extrapolate statistically independent storm wave data to extreme wave heights based on the extreme-value theory, which was initially developed by Fréchet (1927) and Fisher and Tippett (1928) and summarised by Gumbel (1958). The general procedure may be divided into four steps: (i) Generating a set of statistically independent storm wave data from a historical time-series wave record with the Annual Maximum (AM), the Peaks-

Fig. 22.10 A large coal carrier, Pasha Bulker of 225 m long and 76,741 tones, ran aground on Nobbys Beach of the NSW coast, Australia during a major coastal storm with maximum wave heights of up to 14 m on 8 June 2007. The coastal storm eroded coastal beaches, damaged coastal infrastructure and properties, and dumped flooding rains on the NSW coastal areas resulting in the total damage of about US$1.35 billion (Photo by Vincent)

Over-Threshold (POT) or the Annual *n*-Largest method (ANL); (ii) Estimating the empirical distribution from the set of storm wave data with suitable plotting position formula; (iii) Fitting candidate distribution functions to the empirical distribution or return wave height data for estimation of the distribution parameters with the method of moments (MM), the least-squares method (LS) or the maximum likelihood method (ML), and selecting the best-fit distribution of candidate distributions; and (iv) Extrapolating the best-fit distribution to extreme wave heights with required confidence. The calculation procedure is summarised in Fig. 22.11. Different approaches have been developed, revised and refined to minimise the uncertainty in generation of statistically independent storm wave data, computation of the empirical distribution, selection of candidate distribution functions, estimation of distribution parameters, and development of selection criteria on the best-fit distribution.

22.2.3 Extreme-Value Analysis

Historical time-series wave data, which were measured or numerically hindcasted, may not be directly extrapolated to extreme wave heights. The time-series wave data may not be statistically independent especially during coastal storms, resulting in a direct conflicting with the assumption of the extreme-value theory. Another main reason is that we are interested only in large wave heights for extreme wave

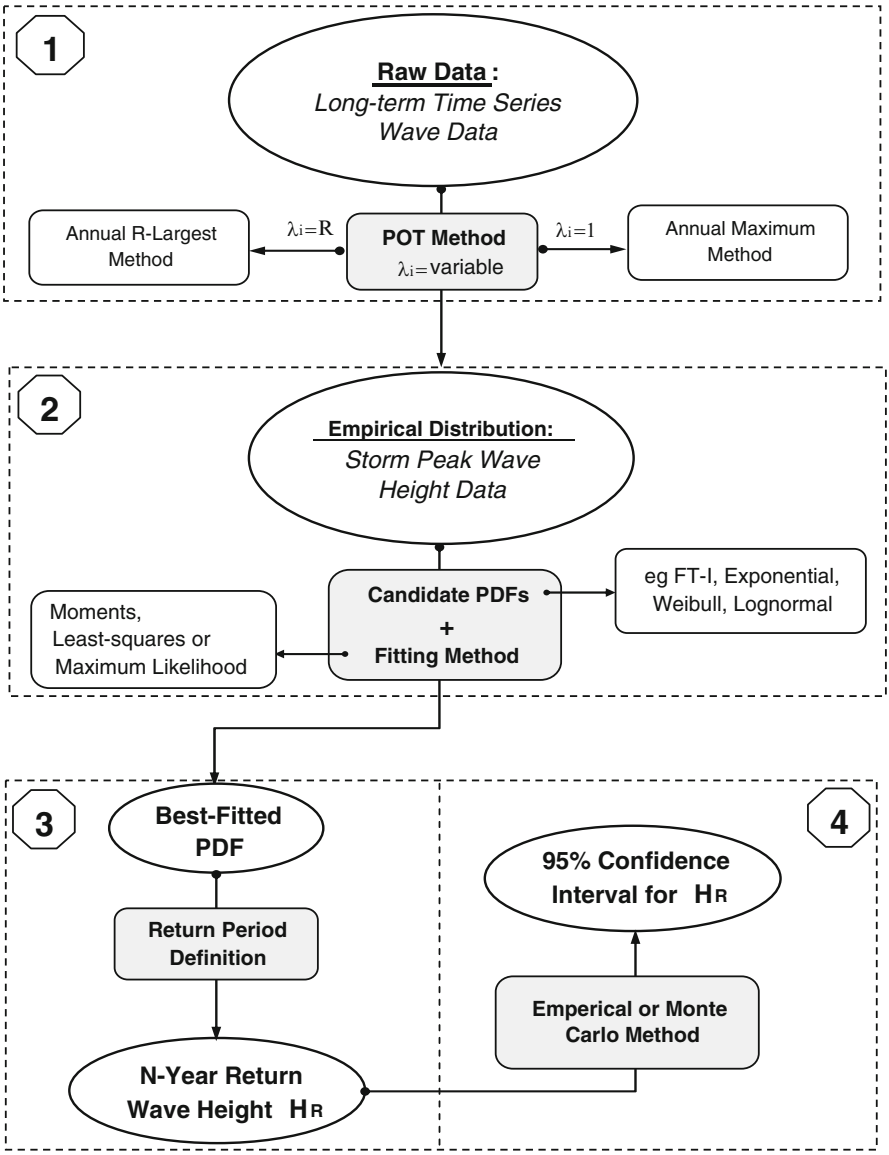

Fig. 22.11 Flowchart of extrapolating a historical time-series wave record to extreme wave heights, where λ_i is the number of storm events per year

analysis rather than small non-storm waves. The inclusion of all wave heights will take enormous amount of computing time especially when the maximum likelihood method is used to estimate the parameters of three-parameter distribution functions such as the Weibull and Pearson-III. For example, the peak storm wave height data

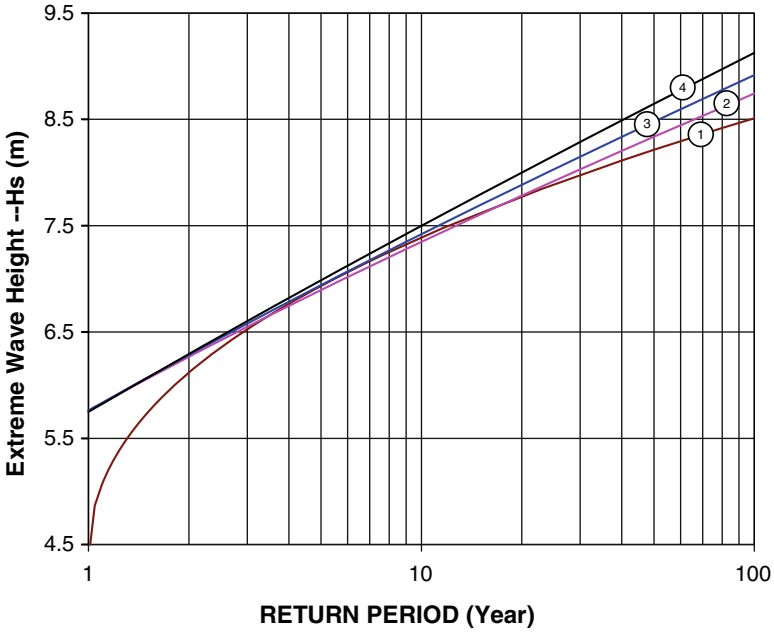

Fig. 22.12 Extreme wave heights are extrapolated with the Weibull distribution from four different sets of storm wave data that are generated from the same 23-year wave record measured off the coast of Sydney in the Tasman Sea with: ① the AM method; ② the ANL method with $n = 10$; ③ the ANLwith $n = 15$; and ④ the POT method

collected off the coast of Sydney in the Tasman Sea, Australia is less than 0.3% of the total wave data collected over a period of 23 years.

Three methods excluding the total sample method described above are commonly used to generate statistically independent extreme wave data from historical time-series wave records, i.e. the annual maximum (AM), the peaks-over-threshold (POT) and the annual n-largest (ANL) method. In the POT method, the number of storm events per year varies from year to year, but the same threshold height is used. In contrast, in the ANL method, the number of peak storm wave heights per year is constant, but different threshold heights are used to obtain n annual largest wave heights per year. The AM method is a special case of the ANL method with $n = 1$.

Estimates of extreme wave heights calculated with the three methods are compared in Fig. 22.12. The 23-year wave record, which was collected off the coast of Sydney in the Tasman Sea, Australia, was analysed to obtain statistically independent storm wave data with the AM, ANL and POT methods, respectively. The three-parameter Weibull distribution is used to extrapolate four sets of storm wave data to extreme wave heights in Fig. 22.12, where the curve ① is made with the AM method ($n = 1$), ② and ③ with the ANL ($n = 10$, $n = 15$), and ④ with the POT. It can bee seen from Fig. 22.12 that the AM method always underestimates

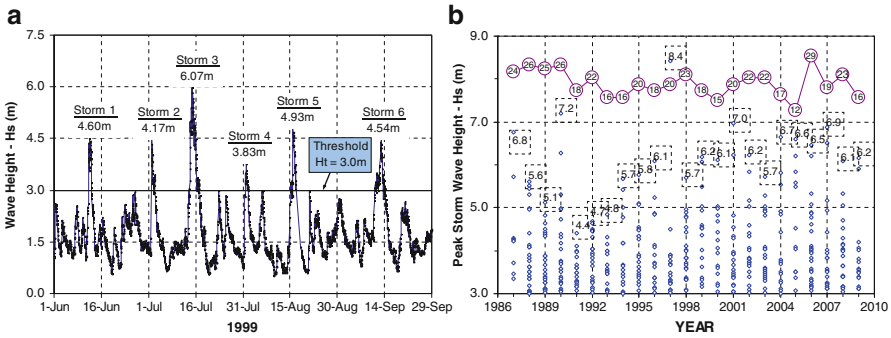

Fig. 22.13 (a) Extraction of individual peak storm wave heights from a time-series wave record, and (b) a set of peak storm wave data is generated from the 23-year time-series wave record collected off Sydney in the Tasman Sea from 1987 to 2009, where the numbers inside the *dashed squares* are the annual peak storm wave heights and the numbers inside the *circles* are the number of storm events per year

extreme wave heights especially when the return period is less than 3 years. The ANL method is also shown to underestimate large storm wave heights when $T_R > 10$ years, but this uncertainty becomes less significant with increasing n. The underestimation is caused by the fact that the lowest wave heights selected in years of higher wave energy are even higher than those in years of lower wave energy. The POT gives the highest estimate of extreme wave heights. Figure 22.12 also implies that the estimates of extreme wave heights are affected by the number of largest storm wave heights per year used in the ANL. Thus, the POT method is preferred to the AM and ANL methods for generation of statistically independent storm wave data from the historical time-series wave record.

Statistically independent extreme wave heights of individual storm events can be extracted from a historical time-series wave record with the POT method when all storm wave heights are larger than a given threshold height and the storm duration is longer than a few hours. The storm duration is the length of time during which the storm wave heights persist above the assigned threshold height H_T. The peak storm wave heights are then obtained from these defined storm events. Each storm event has only one peak storm wave height. Figure 22.13a shows an example of how individual storm events are defined with the POT method, where the threshold wave height is $H_T = 3$ m. The number of storm events per year should decrease with increasing H_T. Physically, the threshold height H_T should be slightly larger than the peak storm wave height of annual smallest storm events that are just about to cause beach erosion, rather than just an arbitrarily assigned value (You 2012).

Figure 22.13b shows a set of peak storm wave height data that are extracted from the 23-year time-series significant wave record collected off the coast of Sydney in the Tasman Sea, Australia from 1987 to 2009 with waverider buoy. The total number of 451 storm events is identified from the 23-year wave record with a threshold of $H_T = 3$ m. The number of storm events per year varies from 12 to 29, and the average number of storm events per year is $\lambda = 20.3$. λ is an important

parameter for estimation of the total number of storm events, i.e. $N = \lambda \times T_R$, which may occur over a given return period of T_R years. It can be also seen from Fig. 22.13b that the annual maximum storm wave height H_a generally varies from year to year, e.g., $H_a = 7.2$ m in 1990, but only $H_a = 4.4$ m in 1991. The annual maximum H_a in 1991 is shown to be much smaller than the five largest wave heights in 1990 and thus the AM method always intends to underestimate extreme wave heights (CEM 2002).

22.2.4 Empirical Distribution

The empirical distribution is required to be known before the least-squares method can be used to determine the distribution parameters. Even though the method of moments and the maximum likelihood method can estimate the distribution parameters directly from the peak storm wave height data, the empirical distribution is still required to show how well the observed storm wave heights are fitted by candidate distribution functions before the best-fit distribution function can be selected for the extrapolation of extreme wave heights. In other words, the determination of the empirical distribution is always required before or after the distribution parameters are estimated. The empirical distribution of ranked peak storm wave heights may be estimated from the general plotting position formulae (Gringorten 1963; Cunnane 1978).

$$Q(\hat{H} \geqslant H) = \frac{n - a}{m + b}, \tag{22.29}$$

where n is the nth peak storm wave height ranked in descending order, m is the total number of peak storm wave heights observed, and a and b are constants. The values of a and b in Eq. (22.29) have been chosen so that the median of the ordered extreme values is assigned a percentile rank of 50%. Many of the plotting positions commonly used are members of a family $b = 1 - 2a$, where a ranges from 0 to 0.5. The value of Q for large peak storm wave heights is expected to vary greatly with a when $n < 10$. For example, Q estimated with $a = 0$ for the largest peak storm wave height is almost twice larger than with $a = 0.5$. The use of different plotting position formulas will cause the uncertainty in estimation of Q for large storm wave heights. More recently, Makkonen (2006, 2008) concluded that only the plotting position, $P = n/(m + 1)$ derived for the Weibull distribution, should be used to estimate the empirical distribution for all distribution functions, but his conclusion was subsequently rejected by Cook (2011a, b). Most recently, You (2011, 2012) proposed that only the plotting position formula

$$Q(\hat{H} \geqslant H) = \frac{n}{m} \tag{22.30}$$

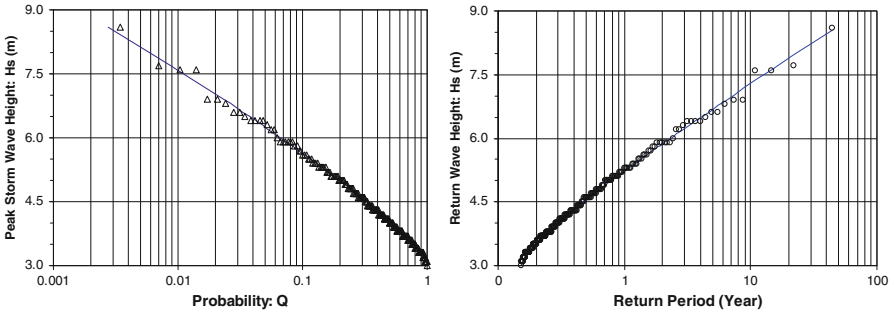

Fig. 22.14 The empirical distribution (Q, H) derived from the storm wave data of Mazas and Hamm (2011) via Eq. (22.30) is shown to be equivalent to the distribution of observed return wave heights (T_R, H) via Eq. (22.31), where the solid curve is the Weibull distribution

should be used to calculate the empirical distribution and valid for all distributions. Equation (22.30) is consistent with the definition of the return period T_R

$$T_R = \frac{1}{Q\lambda} = \frac{m}{n} = \frac{T}{m} = \frac{T}{n}, \tag{22.31}$$

where $Q = n/m$, $\lambda = m/T$, and T is the total wave record length, and n is the number of peak storm wave heights being equal to or larger than a given wave height H. Note that when $Q = 1$ or $n = m$ in Eq. (22.30), most of extreme-value distribution functions will become invalid and thus the smallest storm wave height in the storm wave dataset will be excluded for estimation of extreme wave heights. This limit will not affect the accuracy of extreme wave heights estimated. The empirical distribution Q(H) in Eq. (22.30) is inverse to the return period T_R(H) in Eq. (22.31) as the parameters m and T are constant and thus $T_R \propto Q^{-1}$. Figure 22.14 shows the comparison of the empirical distribution and the return wave height distribution, which are derived from the storm wave data of Mazas and Hamm (2011) via Eqs. (22.30) and (22.31), respectively. The observed empirical distribution is shown to be equivalent to the measured return wave height distribution in Fig. 22.14.

22.2.5 Candidate Distributions

There are a number of extreme-value distribution functions that have been used for extreme wave analysis, e.g. FT-I, II and III, GP-I, II and III, Lognormal, Pearson-III and Weibull (You 2011a, b). The Generalised Extreme Value (GEV) asymptotic distribution is expressed as

$$P(x) = \exp\left[-\left(1 + \frac{1}{\alpha}\left(\frac{x-\gamma}{\beta}\right)\right)^{-\alpha}\right] = \exp\left[-\left(\frac{x-\gamma'}{\beta'}\right)^{-\alpha}\right], \tag{22.32}$$

where γ, β and α are called the location, scale and shape parameters and $\beta' = \alpha\beta$ and $\gamma' = (\alpha\beta - \gamma)$. The type of the GEV is determined solely by the shape parameter α. The GEV with $\alpha = \pm\infty$, $\alpha > 0$ and $\alpha < 0$ is called the FT-I, II and III, respectively. Both the FT-II and FT-III will reduce to the FT-I or called the Gumbel distribution when $\alpha = \pm\infty$

$$P(x) = \exp\left[-\left(-\frac{x-\gamma}{\beta}\right)\right] \tag{22.33}$$

The FT-III may not be a suitable distribution for extreme wave analysis as it converges quite slowly as α increases and eventually reduces to the FT-I at $\alpha \rightarrow -\infty$ before the best fit to a set of storm wave data may be achieved (You 2012). Thus, only the FT-II including the FT-I of the GEV is suitable for extreme wave analysis.

Similar to the GEV distribution, another generalized asymptotic distribution is the Generalized Pareto distribution (GP) and also used to compute extreme values above a specified threshold

$$P(x) = 1 - \left(1 + \frac{1}{\alpha}\frac{x-\gamma}{\beta}\right)^{-\alpha} = 1 - \left(\frac{x-\gamma'}{\beta'}\right)^{-\alpha}, \tag{22.34}$$

where $\beta' = \alpha\beta$ and $\gamma' = (\alpha\beta - \gamma)$. The shape of the GP is also determined solely by the shape parameter α. The GP with $\alpha = \pm\infty$, $\alpha > 0$ and $\alpha < 0$ is called the GP-I, II and III, respectively. The GP-I is in fact the exponential distribution function, and the GP-II and III will reduce to the exponential distribution when $\alpha = \pm\infty$

$$P(x) = 1 - \exp\left(-\frac{x-\gamma}{\beta}\right). \tag{22.35}$$

The identity, $(1 + x/\alpha)^{\alpha} = \exp(x)$ at $\alpha = \pm\infty$ is used to derive Eq. (22.35) from Eq. (22.34). The GP-I and GP-II may not be the suitable distributions of the GP for extreme wave analysis. The GP-I is found to generally overestimate extreme wave heights (You 2007), while the GP-II converges quite slowly as α increases and eventually reduces to the GP-I at $\alpha = \infty$ before the best fit to the storm wave data can be achieved. Thus, only the GP-III of the GP is suitable for extreme wave analysis.

In addition to the two generalised asymptotical distributions, the Weibull and the Lognormal distributions are also used for extreme wave analysis. The Lognormal distribution is one of the distributions that were first used for extreme-value analysis

$$P(x) = \Phi\left(\frac{\ln x - \gamma}{\beta}\right) \quad \text{or} \quad X = \Phi^{-1}(P) = \frac{\ln x - \gamma}{\beta}, \tag{22.36}$$

where Φ is the normal distribution and Φ^{-1} is the inverse normal distribution. As discussed by You (2007, 2011b), estimates of extreme wave heights are often

under-predicted by the Lognormal. As a result, the lognormal distribution may not be suitable for extreme wave analysis.

The Weibull distribution function is the most commonly-used distribution for extreme wave analysis and expressed as

$$P(x) = 1 - \exp\left[-\left(\frac{x-\gamma}{\beta}\right)^{\alpha}\right], \tag{22.37}$$

where $\alpha > 0$. The Weibull automatically reduces to the Exponential at $\alpha = 1$, the Rayleigh at $\alpha = 2$, and approximately the Gaussian or normal distribution at $2.6 < \alpha < 3.7$, respectively. The Weibull is skewed to the right at $\alpha \leq 2.6$ and to the left at $\alpha \geq 3.7$ and has zero skewness at $2.6 < \alpha < 3.7$. The Weibull with only the shape parameter of $1 < \alpha < 2$ is suitable for extreme wave analysis. The FT-III is sometimes mistakenly called the Weibull distribution even though the simplified form of the FT-III in Eq. (22.32) is apparently different from the Weibull of Eq. (22.37). The Weibull in Eq. (22.37) is well approximated by the GP-III or its simplified form in Eq. (22.34) (You 2012).

Another three-parameter distribution, the Pearson-III or also called the three-parameter Gamma distribution, which is often used for estimation of extreme flood levels in hydrology, has been also used for extreme wave analysis

$$\begin{aligned} P(x) &= \frac{1}{\Gamma(\alpha)} G(\alpha, \frac{x-\gamma}{\beta}) \quad \text{or} \\ f(x) &= \frac{1}{\beta\Gamma(\alpha)} \left(\frac{x-\gamma}{\beta}\right)^{\alpha-1} \exp\left[-\frac{x-\gamma}{\beta}\right], \end{aligned} \tag{22.38}$$

where G is the three-parameter gamma distribution. Even though the Pearson-III is not available in a closed form, the distribution parameters can be estimated with the least-squares method

$$X = \frac{x-\gamma}{\beta} = \frac{G^{-1}(\alpha, P)}{\Gamma(\alpha)}, \tag{22.39}$$

where G^{-1} is the inverse Gamma function and only the function of P and α. The true value of α can be determined when the linearly transformed equation, Eq. (22.39), is found to give the best fit to the storm wave data.

The probability density functions of the FT-I, II and III, GP-I, II and III, Lognormal, Weibull and Pearson-III are compared in Fig. 22.15. For simplicity, the location and scale parameters of $\gamma = 0$ and $\beta = 1$ are used for all distributions, the shape parameter of $\alpha = 1.5$ for the FT-II, GP-II, Weibull and Pearson-III, and $\alpha = -2.5$ for the FT-III and GP-III in Fig. 22.15. The common properties of the nine distributions are asymptotic and unbounded at the upper end. Note that the long upper tails of the FT-III and GP-III can be obtained in Fig. 22.15 if a large value of $|\alpha|$ was taken. As discussed above, both the FT-III and GP-II are

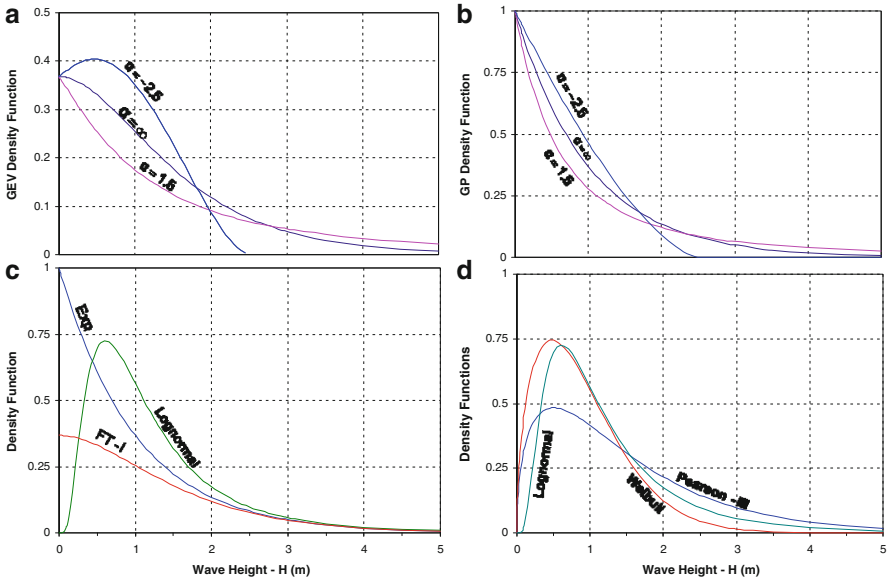

Fig. 22.15 Nine extreme-value distribution functions: (**a**) the FT-I, II and III ($\alpha = 1.5, -2.5, \pm\infty$), (**b**) the GP-I, II and III ($\alpha = 1.5, -2.5, \pm\infty$), (**c**) two-parameter functions, the Lognormal, FT-I and Exponential, and (d) the bell-shaped functions, the Lognormal, Weibull ($\alpha = 1.5$) and Pearson-III ($\alpha = 1.5$), where $\beta = 1$ and $\gamma = 0$ are used

found to converge slowly with increasing $|\alpha|$ and eventually they reduce to the FT-I and GP-I respectively when $|\alpha|$ becomes infinite (e.g. $|\alpha| \geq 500$). Estimates of extreme wave heights are often found to be under-predicted by the Lognormal, but over-predicted by the GP-I or Exponential distribution. Thus, only the FT-II including the FT-I, GP-III, Weibull and Pearson-III of the nine distributions are preferably used for extreme wave analysis.

22.2.6 Distribution-Parameter Estimators

Three estimators, the method of moments (MM), the maximum likelihood method (ML) and the least-squares method (LS), are most commonly applied to determine the parameters of extreme-value distribution functions even though other parameter estimators such as the weighted probability moments (Greenwood et al. 1978), the L-moments method (Hosking 1990; Hosking and Wallis 1995; Goda 2011), and the maximum product of spacing (Cheng and Amin 1983) are also used.

The MM method estimates the distribution parameters by equaling the first two or three moments (i.e., mean, variance and skew) calculated from a set of storm wave data to those computed from an extreme-value distribution function. This method is applicable to those simple distribution functions, of which the first, second

and third moments can be derived analytically and explicitly. This method is more applicable to two-parameter distributions than three-parameter distributions.

The LS method estimates the distribution parameters by transforming a non-linear distribution function into linear equation and then fitting linear regression line to the observed empirical distribution to obtain the distribution parameters. Therefore, the LS method is applicable only to those distribution functions that can be transformed into linear equation. The parameters of all nine distribution functions in Fig. 22.15 discussed above can be estimated with the LS method.

The ML method evaluates the distribution parameters by making it maximum the multiplication of the probability density function for individual observations with respect to each distribution parameter. Theoretically, the ML should be applicable to any distribution function, but in reality the ML has its difficulties in estimating the parameters of three-parameter distributions such as the Weibull and Pearson-III (Mazas and Hamm 2011). It was also shown by You (2012) that the LS method is a special case of the ML method under the assumption that the difference between measured storm wave heights and those computed from linear regression line follows the Gaussian distribution.

Carter and Challenor (1983) compared the MM, LS and ML methods and found no one obviously better in estimating the parameters of the FT-I distribution. In a most recent study of Mazas and Hamm (2011), the ML was found to be less accurate than the LS in estimating the parameters of the three-parameter Weibull and Pearson-III distributions. The LS method may be preferred to the MM and ML methods (Goda 1998; Kamphuis 2000; You and Yin 2006). This is because the goodness of fit can be directly visualised from a linear plot and abnormal data (not outliers) can be easily identified and subsequently removed from extreme wave analysis. More importantly, the LS method can manipulate storm wave data to enable candidate distribution functions to give a better fit to large storm wave data or the upper portion of the empirical distribution. The requirement of the empirical distribution by the LS method may be a drawback, but the MM and ML methods also require the empirical distribution or the return wave height distribution in Fig. 22.14 to compare with those estimated. Thus, all parameter estimators require the empirical distribution before or after the distribution parameters are estimated.

The LS method was extended by You (2007, 2011b) for estimation of three-parameter distributions. In order to fit linear regression line to the empirical distribution, candidate distribution functions need to be rewritten in the simple linear form

$$Y = \beta X + \gamma, \tag{22.40}$$

where X is called the reduced variable. The variables (X, Y) derived from the nine distributions are given in Table 22.1, where $Y = H$ except for the Lognormal distribution. Note that Q is calculated first from the storm wave data ranked in descending order via Eq. (22.30) and then $P = (1 - Q)$.

Table 22.1 Extreme-value distribution functions transformed as the linear form $\mathbf{Y} = \beta x + \gamma$, where the location and scale parameter of the GEV and GP are determined from the simplified distributions in Eqs.(22.32) and (22.34)

Distribution Type	Parameters	Y	X
Lognormal	(γ, β)	$\ln H_s$	$\Phi^{-1}(P)$
FT-I	(γ, β)	H_s	$-\ln[-\ln(P)]$
FT-II, III	(γ, β, α)	H_s	$[-\ln(P)]^{-1/\alpha}$
GP-I	(γ, β)	H_s	$-\ln Q$
GP-II, III	(γ, β, α)	H_s	$Q^{-1/\alpha}$
Weibull	(γ, β, α)	H_s	$[-\ln Q]^{1/\alpha}$
Pearson-III	(γ, β, α)	H_s	$G^{-1}(\alpha, P)/\Gamma(\alpha)$

For the two-parameter distributions in Table 22.1, X is shown to be only the function of Q or P and thus the parameters (β, γ) can be directly evaluated with the LS method. The location and scale parameters (γ, β) can be estimated directly as

$$\beta = \frac{\sum_{i=1}^{m} \left(Y_i - \overline{Y}\right)\left(X_i - \overline{X}\right)}{\sum_{i=1}^{m} \left(X_i - \overline{X}\right)^2} \quad \text{and} \quad \gamma = \overline{Y} - \beta\overline{X}, \tag{22.41}$$

where the data (X_i, Y_i) can be generated from the empirical distribution (Q_i, H_i), $\bar{X}$ is the mean of X and $\bar{Y}$ the mean of Y, and i is the ith peak storm wave height ranked in descending order. With the LS method, the two parameters (γ, β) of the FT-I, for example, can are determined explicitly from the empirical distribution (Q, H) as shown in Fig. 22.16, where γ and β are physically represent the intercept and slope of the linear regression line. The goodness of fit may be quantified in terms of the correlation coefficient R^2 of the regression line.

For the three-parameter distributions in Table 22.1, the reduced variable X can't be directly evaluated as the shape parameter α is unknown. However, we may assume a value for α first and then apply the LS method to estimate the rest two parameters (γ, β) and the correlation coefficient R^2. Repeat this procedure until R^2 reaches its maximum. You (2007) extended the LS method to estimate the shape parameter α of three-parameter distributions. Let the sum of squares of the error (SSE) be

$$SSE(H) = \sum_{i=1}^{m} (H_i - H)^2, \tag{22.42}$$

where H_i is the ith peak storm wave height and H is computed from Eq. (22.40). The value of SSE varies with the three parameters (α, β, γ). For a given value of α, the parameters (β, γ) can be uniquely determined from Eq. (22.41) and the value of SSE can be also computed from Eq. (22.42) accordingly. The computed values of (β, γ) and SSE vary with α. The best-fit value of α, which makes SSE minimum, can be uniquely determined as

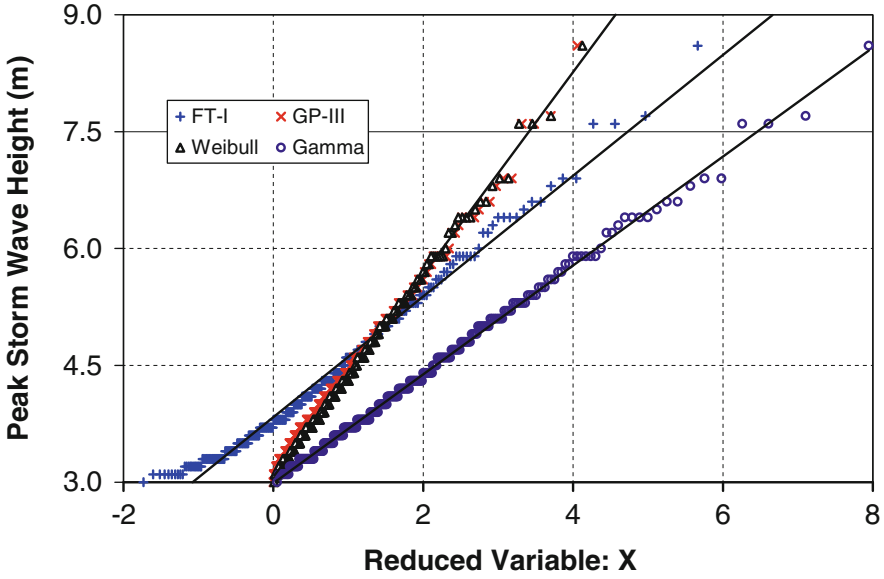

Fig. 22.16 The parameters of the two-parameter FT-I and three-parameter Weibull, GP-III and Pearson-III distributions are estimated with the least-squares method (You 2012)

$$\frac{\partial SSE}{\partial \alpha} = \frac{\partial}{\partial \alpha} \sum_{i=1}^{m} (H_i - \beta X - \gamma)^2 = 0, \tag{22.43}$$

where $H = (\beta X + \gamma)$ is the linear regression line, and β and γ are also the function of α. The shape parameter α of the Weibull, FT-II, FT-III, GP-II and GP-III can be derived from Eq. (22.43) as

$$W = \beta \times \frac{\sum_{i=1}^{m} (X_i^* - \bar{X}^*)(X_i - \bar{X})}{\sum_{i=1}^{m} (X_i^* - \bar{X}^*)(Y_i - \bar{Y})} = 1, \tag{22.44}$$

where $X_i^* = X_i \ln(E_i)$ and $\bar{X}^*$ is the mean of X_i^*, $E_i = -\ln Q_i$ for the Weibull, $E_i = -\ln P_i$ for the FT-II and III, and $E_i = Q_i$ for the GP-II and III.

With this extended LS method, the three parameters of the Weibull and GP-III can be determined from the storm wave data and shown in Fig. 22.16. In order to obtain an accurate estimate of α via Eq. (22.43), the calculated value of $|W-1|$ is proposed to be less than 10^{-4} or $|W-1|^{0.5} < 0.01$. The indicator $|W-1|^{0.5}$ is shown to be more sensitive to the change of α than $|W-1|$. Four different criteria, which are used for the goodness of fit, are compared in Fig. 22.17. The correlation coefficient R^2 of the regression line, which is also equivalent to *SSE*, has been commonly used as an indicator for the goodness of fit for the LS method. It can be seen from Fig. 22.17 that

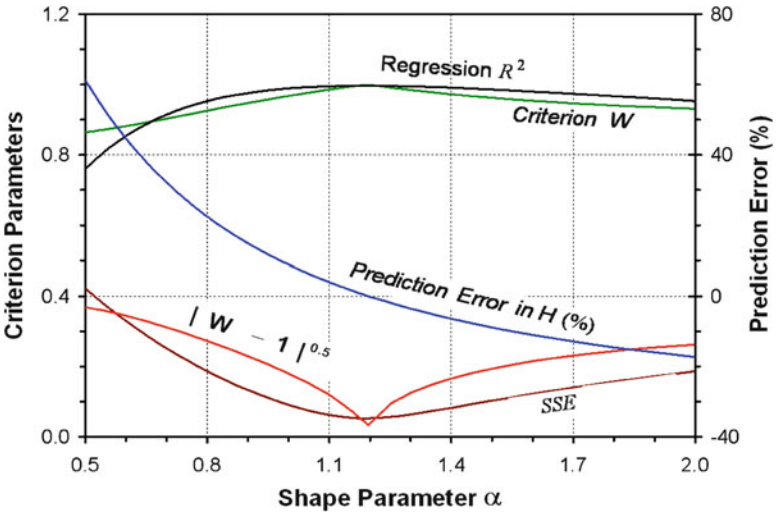

Fig. 22.17 The shape parameter α of the Weibull estimated from four different criteria, W, $|W-1|^{0.5}$, SSE and R^2 based on the storm wave data collected off the coast of Sydney in the Tasman Sea, Australia

the value of R^2 converges slowly around the true value close to $\alpha = 1.2$. In other words, the indicator R^2 becomes insensitive when α is close to its true value. In contrast, the indicator $|W-1|^{0.5}$ is shown to converge much faster than R^2 or SSE and W as illustrated in Fig. 22.17.

22.2.7 Best-Fit Distribution

The Weibull, GP-III and Pearson-III distributions are shown in Fig. 22.16 to give almost equally good fit to the storm wave data. Note the FT-I can also give as the equally good fit to the data as the three-parameter Weibull, GP-III or Peason-III if the upper portion of the empirical distribution is fitted by the FT-I. The ability of manipulating the empirical distribution to achieve a better fit to large wave height data is another advantage of the LS method. Now, the question is which distribution of the FT-I, Weibull, GP-III and Pearson-III should be selected to extrapolate the observed empirical distribution to extreme wave heights in Fig. 22.16. It was proposed by You (2007, 2012) that a best-fit distribution for extrapolation of extreme wave heights should meet following conditions or selection criteria, i.e., unboundedness, goodness of fit, simplicity, and confidence intervals.

The first criterion is unboundedness. The best-fit distribution function must be unbounded at the upper end. Candidate extreme-value distributions with bounded upper ends intend to underestimate extreme wave heights. All the nine distributions in Fig. 22.15 meet this criterion. The second criterion is goodness of fit. The sum of

squares of the error, *SSE* or R^2, for two-parameter distributions and the indicator $|W\text{-}1|^{0.5}$ of You (2007) for three-parameter distributions may be used as a criterion to describe the goodness of fit or how well candidate distributions agree with the empirical distribution, but they may not be sufficient for selection of the best-fit distribution. Caution must be taken when large storm wave heights are not fitted well by candidate distributions even though R^2 is quite large (You 2010). This is because estimates of extreme wave heights will be under/over-calculated if larger wave height data points in the upper portion of the observed empirical distribution can't be fitted well by the "best-fit" distribution. The best way to quantify the goodness of fit is to make a direct comparison between computed and observed return wave heights. The third criterion is simplicity. This includes simplicity in expression of candidate distributions, in estimation of distribution parameters, and in calculation of confidence intervals. In general, simple and explicit candidate distributions may be preferred to complex and implicit ones, two-parameter candidate distributions are preferred to three-parameter ones provided they give an equally good fit to the data. Candidate distributions with $Y = H$ are preferred to those with nonlinear function $Y = f(H)$, e.g. $Y = \ln H$ of the Lognormal distribution provided they were fitted to storm wave data equally well. The last criterion is the confidence interval width. According to the propagation of uncertainty or errors, the confidence interval width of two-parameter distributions is expected to be narrower than that of three-parameter ones provided they give the equally good fit to the storm wave data.

Based on the selection criteria described above, for example, the FT-I of the nine distributions in Fig. 22.15 was selected by You (2007) as the best-fit distribution for estimation of extreme wave heights off the coast of Sydney in the Tasman Sea, Australia. Figure 22.18 shows the comparison of observed return wave heights with those calculated with the FT-I, where the 95% confidence intervals are approximately calculated as

$$H(T_R) = H_R \pm 1.96\left[0.487 + 0.889X + 0.669(X - 0.577)^2\right]^{0.5} \frac{\sigma_H}{\sqrt{m}}, \qquad (22.45)$$

where X is the reduced variable of the FT-I, λ is the average number of storm events per year, T_R is the return period in years, m is the total number of storm events observed over the length of historical wave record and σ_H is the standard deviation of observed peak storm wave heights. Note the confidence intervals computed form the empirical formulae, Eq. (22.45) derived from the moment of method, are assumed to be the same as those from the LS method.

22.2.8 Return Wave Height

Extreme coastal waves are often described in terms of their return height and period. The return period is defined as an average time interval between successive events of a given storm wave height being equalled or exceeded (CEM 2002).

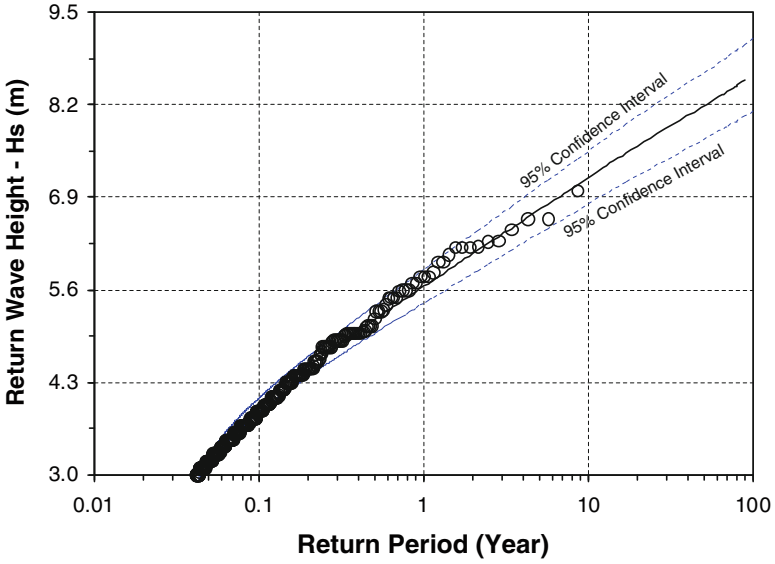

Fig. 22.18 The FT-I of the nine candidate distributions in Table 22.1 is determined to be the best-fit distribution for extrapolation of extreme wave heights from the storm wave data (1988-2009) collected off the coast of Sydney in the Tasman Sea, Australia (You 2007)

For example, there are six peak storm wave heights (H_s = 4.2 m, 4.2 m, 4.8 m, 4.8 m, 6.8 m and 8.6 m) observed over a period of 30 years. According to Eq. (22.31), the return wave heights $H_R \geq$ 4.2 m, 4.8 m, 6.8 m and 8.6 m have $T_R = T/n$ = 5 year, 7.5 year, 15 year and 30 year, respectively, where T is the storm wave record length in years and n is the number of peak storm wave heights being equalled or exceeded. The exceedance probability Q for possible occurrence of extreme wave heights over a period of T_R years may be estimated as

$$Q = \frac{1}{\lambda T_R} \tag{22.46}$$

where λ is the average number of storm events per year, and λT_R is the total number of storm events that may occur in T_R years. For a given return period T_R, the return wave height H_R may be estimated from Eq. (22.40) as

$$H_R = \beta X_R + \gamma, \tag{22.47}$$

except for the Lognormal distribution in Table 22.1. The return wave height data (T_R, H_R) can be generated from the empirical distribution via Eq. (22.31) before the data (T_R, H_R) can be compared with those calculate from Eq. (22.47).

As shown in Fig. 22.14, the return wave height distribution (T_R, H_R) is actually equivalent to the empirical distribution (Q, H), where $T_R = 1/(\lambda Q)$ and λ is the average number of storm events per year. A comparison of the return wave height data from Mazas and Hamm (2011) and those computed from the FT-I, Weibull and

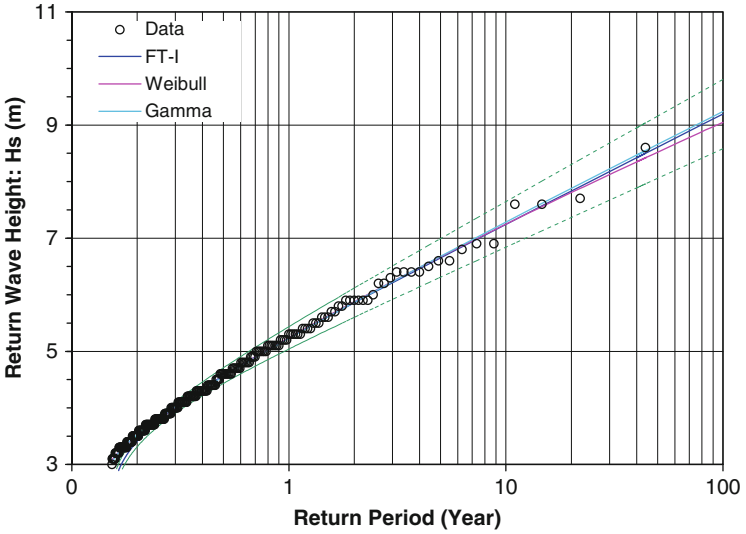

Fig. 22.19 The storm wave data of Mazas and Hamm (2011) are compared with those extrapolated from the FT-I, Weibull and Pearson-III distributions

Pearson-III is presented in Fig. 22.19, where the 95% confidence intervals are computed from Eq. (22.45) of the FT-I. It can be seen that the three distributions give almost equally the best fit to the storm wave data, where the FT-I is fitted only to the upper portion of the empirical distribution with the reduced variable $X \geq 0$.

22.2.9 Mean of Extreme Wave Heights

The n-year return wave height H_{R}, which is estimated from Eq. (22.47) or presented in Fig. 22.19, is the wave height being equalled or exceeded by larger waves, but does not give the upper limit of the larger waves. With the same definition of the mean wave height H_{Q} from Eq. (22.14), the mean $\bar{H}_R$ of extreme wave heights being equal to or larger than H_{R} can be derived from the Weibull distribution, for example, as

$$\begin{aligned}\bar{H}_R &= \beta\left[[\ln(\lambda T_R)]^{1/\alpha} + \frac{1}{\alpha\lambda T_R}\Gamma\left[\tfrac{1}{\alpha}, \ln(\lambda T_R)\right]\right] + \gamma, \\ &= H_R + \frac{\beta}{\alpha\lambda T_R}\Gamma\left[\tfrac{1}{\alpha}, \ln(\lambda T_R)\right] \end{aligned} \tag{22.48}$$

which is similar to Eq. (22.18) for calculation of the mean of n largest wave heights in a set of storm wave data. The difference between H_{R} and $\bar{H}_R$ is equal to

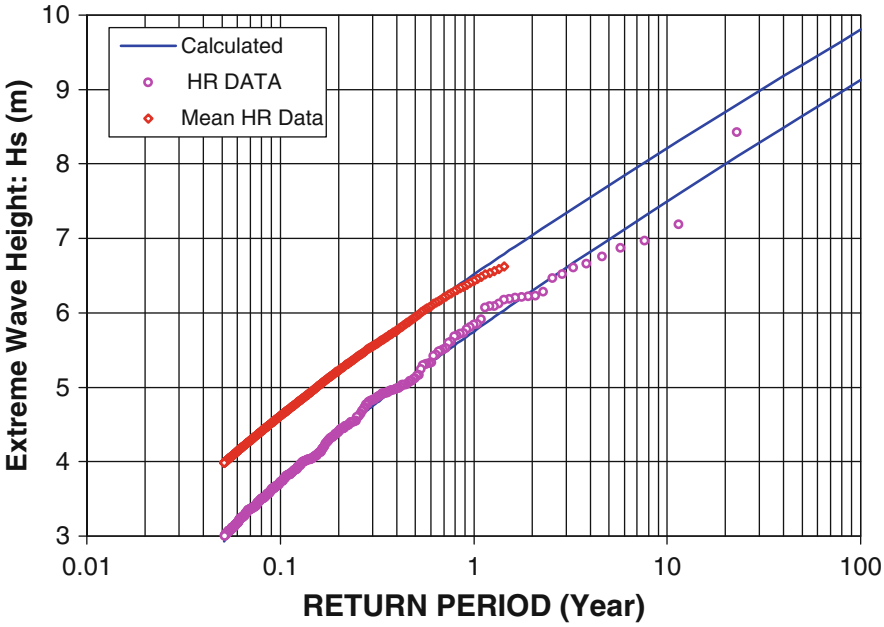

Fig. 22.20 The return wave height H_R and the mean $\bar{H}_R$ of extreme wave heights being equal to or larger than H_R are computed from the Weibull distribution and compared with the storm wave data collected off the coast of Sydney in the Tasman Sea

the second term in Eq. (22.48). In Fig. 22.20, the values of $\bar{H}_R$ computed from Eq. (22.48) are compared with the storm wave data collected off the coast of Sydney in the Tasman Sea, Australia. The measured values of $\bar{H}_R$ at $T_R > 2$ year are not plotted in Fig. 22.20 because of the limit number of data points. The new parameter $\bar{H}_R$ may be a better design parameter than H_R for coastal structure designs.

22.2.10 Uncertainty in Estimates

22.2.10.1 True Distribution Parameters

The confidence intervals for estimates of extreme wave heights in Fig. 22.18, for example, are calculated from the FT-I distribution by Eq. (22.45). This uncertainty is caused due to the unknown true distribution parameters estimated from a single wave record only. If a large number of historical wave records from the same true distribution *might* have been collected simultaneously at the same location, the distribution parameters in Eq. (22.47), which are derived from each of the wave records, are expected to slightly deviate from the true values, resulting in a range of values or intervals for estimates of extreme wave height H_R. The wide intervals may indicate unreliable estimates of extreme wave heights. The confidence intervals are

more easily computed from two-parameter distributions than three-parameter distributions. As a result, the two-parameter distributions are preferred to the three-parameter distributions for estimation of extreme wave heights provided they give the equally best fit to storm wave data. The confidence intervals for the most commonly-used Weibull distribution were approximated by Lawless (1974, 1978). A more general Monte Carlo method is often used to compute the confidence intervals for extreme-value distributions when analytical solutions can't be obtained.

22.2.10.2 Data Sampling Intervals

The data sampling interval is the time period between successive wave segments measured with wave instruments or hindcasted with numerical wave models. The sampling interval, which is used to collect/hindcast a historical time-series wave record, is a key factor causing the uncertainty in estimates of extreme wave heights. In general, extreme wave heights extrapolated from wave records that were collected with longer sampling intervals may be smaller than those with shorter sampling intervals. Storm wave heights of individual storm events with durations less than the sampling interval can't be measured in the wave record. The wave data collected along the NSW coast, for example, were recorded on paper charts for 10 min every 6 h before 1976, and for 17 min every 6 h after digital loggers were introduced in 1976, and for 34 min every 1 h after fully programmable loggers were used in mid 1984 (Webb and Kulmar 1989; Lord and Kulmar 2000). Thus, storm events with their duration less than 6 h could not be recorded in the historical wave records before 1984. As the durations of large coastal storm events are often longer than 1 to 2 h, this uncertain caused by the sampling interval may become insignificant when the data sampling interval is set to be less than 2 h.

22.2.10.3 Wave Record Length

In extreme wave analysis, the return period of estimated extreme wave heights is suggested not to be much longer (e.g. 3 – 4 times) than the length of a historical wave record used for extrapolation of extreme wave heights. The length of wave record is another key factor causing the uncertainty in estimates of extreme wave height. As an example, Fig. 22.21 shows the variation of coastal storm intensity or strength with wave record length (You and Lord 2008). It can be seen that peak storm wave heights vary strongly with time and well correlated with the SOI of El Nino Southern Oscillation (ENSO), a qausiperiodic climate pattern. The SOI is Southern Oscillation Index and a simple measure of the strength and phase of ENSO. The peak storm wave heights are shown to be generally smaller in El Nino years than those in La Nina years. This implies that extreme wave heights extrapolated from the wave data collected in El Nino years are expected to be smaller than those in La Nina years. There are other major oceanographic and meteorological drivers causing the long-term fluctuation of peak storm wave

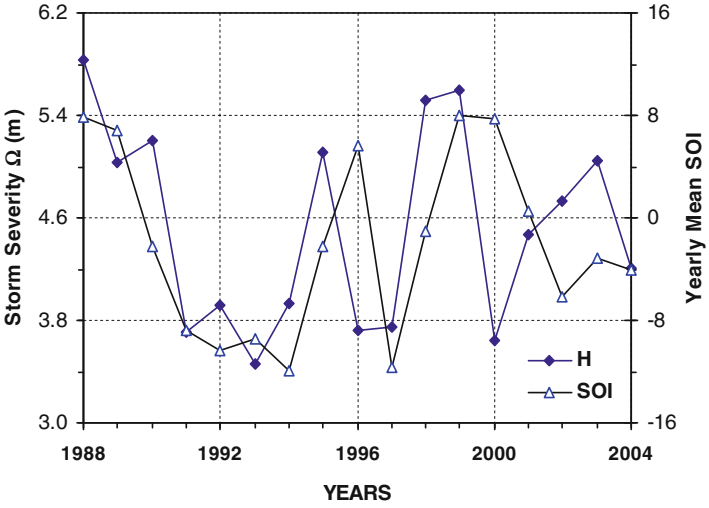

Fig. 22.21 The variation of coastal storm intensity Ω with time measured off the coast of Sydney in the Tasman Sea, Australia (You and Lord 2008)

heights. This uncertainty may be minimised if the length of wave record is longer than the return periods of major oceanographic and meteorological drivers.

22.2.10.4 Missing Storm Data

The missing storm wave data in a historical wave record may be the most important factor causing the uncertainty in estimate of extreme wave heights. For example, the missing wave data, which failed to be collected by waverider buoys on the NSW coast, Australia, are caused by buoy spinning due to vessel impact, mooring failure due to vessel collision or extreme storms, onshore receiving station failure, radio signal interference, power supply failure of the inland receiving station, and buoy submergence due to strong ocean currents. The extreme wave heights extrapolated from the wave dataset of Sydney are compared with those of Byron Bay and shown in Fig. 22.22a. The extreme wave heights extrapolated from the wave record of Byron Bay are shown to be much smaller than those from the wave record of Sydney. The difference between the 100-year return wave heights estimated from the two wave records is about 1.5 m with the same Weibull distribution. This difference is found to be due to the fact the waverider buoy of Byron Bay often failed to collect large storm waves. Whenever possible, hindcast wave data should be used to fill storm wave data gaps in the wave record before it can be extrapolated to extreme wave heights.

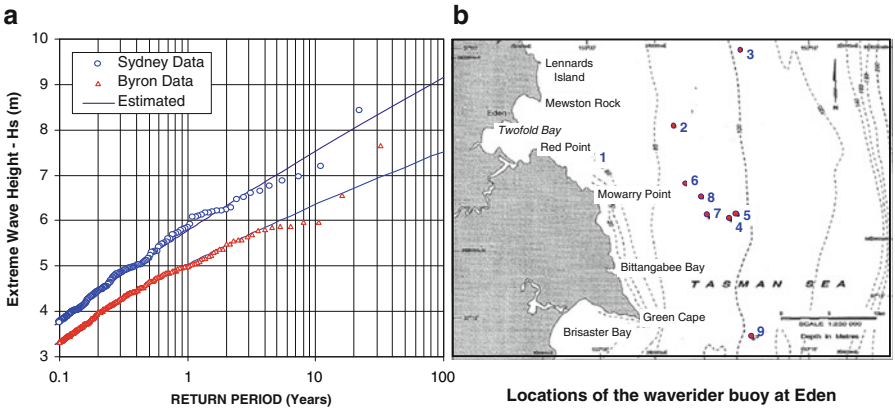

Fig. 22.22 Uncertainty in estimates of extreme wave heights caused by: (**a**) missing storm wave data at Byron Bay and (**b**) changes in locations of the waverider buoys deployed at Eden from 1978 to 1999

22.2.10.5 Relocation of Waverider Buoys

Changes in locations of waverider buoys will also introduce an uncertainty into the wave record. For example, the locations of waverider buoys deployed at seven offshore locations along the NSW coast varied through time when the waverider buoys were lost, replaced with another buoy during routine buoy maintenance work, or repositioned to improve the wave data capture rate. The changes in locations of the waverider buoys deployed at Byron Bay and Eden are found to be more often than those at the other locations. For example, Fig. 22.22b shows the locations of waverider buoys deployed at Eden over the period of 1983–1999. When the waverider buoy was relocated from a deep water of 100 m to an intermediate water of 50 m, for instance, a change in wave height due to wave shoaling may be estimated from wave energy flux conservation as

$$\frac{H}{H_0} = K_D = \left[\tanh(kh)\left(1 + \frac{2kh}{\sinh(2kh)}\right)\right]^{-0.5}, \tag{22.49}$$

of which wave energy loss due to the sea bottom friction is neglected, H_0 is the deepwater wave height, and K_D is the wave shoaling coefficient. In substituting a representative significant wave period $T_s = 10$ s of large storm waves into Eq. (22.49), the relocation of a waverider buoy from one location of $h = 100$ m to another location of $h = 50$ m at Eden, for example, results in a reduction in wave height by 5% or $K_D \approx 0.95$ according to Eq. (22.49) or a higher reduction rate if the seabed friction has been taken into account in intermediate waters Nielsen (1992).

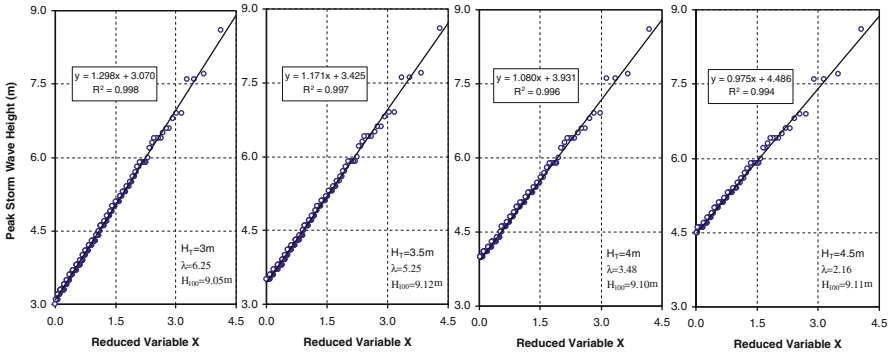

Fig. 22.23 The 100-year return wave heights H_{100} are extrapolated from the same storm wave dataset of Mazas and Hamm (2010), but with four different threshold values of $H_T = 3$, 3.5, 4 and 4.5 m, where the *solid line* is calculated by the Weibull (You 2012)

22.2.10.6 POT Threshold Value

In the POT method, the threshold value H_T is the key parameter for selection of the number of storm events per year. If H_T is set too low, a large number of unwanted small waves and possibly statistically dependent wave heights may be selected and subsequently affect the accuracy of extreme wave heights estimated. On the other hand, if H_T is set too high, there are not enough data points to be generated from the wave record for calculation of extreme wave heights. Figure 22.23 compares the 100-year return wave heights that were calculated from the same storm wave dataset of Mazas and Hamm (2011), but with four different threshold heights of 3 m, 3.5 m, 4 m and 4.5 m. The storm wave dataset was analysed from the 44-year SIMAR-44 hindcast wave data (1958–2011) with a 3 m threshold height. There were 288 peak storm wave heights and the average number of storm events per year is 6.55. The effect of H_T on H_{100} is shown to be insignificant in Fig. 22.23.

Physically, the threshold value H_T should be related to the minimum height of storm waves that may be uniquely determined from synoptic charts of mean sea level atmospheric pressure data. This minimum storm wave height may be used as only the threshold value to generate statistically independent peak storm wave heights from a wave record.

22.3 Ocean Surges

22.3.1 Introduction

Based on Hurricane data from U S coastal areas collected by Irish et al. (2008), Nielsen (2009b) discussed how storm surge height relates to the central pressure Δ_p,

the speed of the weather system c, the size of the weather system given as the radius to maximum wind $R_{\max}$, the slope S of the continental shelf and the angle α of the storm path with the coastline. The relation can be qualitatively derived as

$$\eta_{\max} = \frac{\Delta_p/\rho g}{1 - \frac{c^2}{gh}} S^{-0.33} \left(\frac{R_{\max}}{R_o}\right)^{0.22} g(\alpha), \tag{22.50}$$

which accounts for both the wind and wind driven surges provided the maximum wind stress $\tau_{\max}$ is proportional to Δ_p for a given storm geometry and $R_o = 2$ km. The perhaps surprisingly weak size dependence is explained by the fact that the pressure driven surge is independent of storm size, while the size dependence of the wind driven surge, as explained below, is balanced by its inverse depth dependence through the fact that on a given slope, larger size means greater typical depth.

22.3.2 Weather Systems and Wind Fields

Weather systems can drive surges through the inverse barometer rule (IBR) which predicts 1 cm of surge per hPa of low-pressure and is valid as long as the weather system moves slowly in the sense that $c^2 << gh$. Analysis of data from Macquarie Island, which lies in the southwest corner of the Pacific Ocean, about half-way between Australia and Antarctica, is a clear validation of the IBR. This is to be expected. The Island experiences very strong mid-latitude low pressure systems and, due to the deep surrounding waters, even weather systems travelling at 25 m/s, are slow moving in the above sense because of $c^2 << gh$ at $h \approx 2{,}000$ m.

Holland (1980) developed a clear conceptual model for the wind field of a cyclone without influence from neighbouring high pressure systems. In other words, it is a simple model with circular symmetry. The necessary parameters being the central pressure Δ_p and the radius to maximum wind $R_{\max}$. It is however clear from historical surge data that the enhancing, asymmetrical effects on the wind fields from nearby high pressure systems need to be accounted for. Debris line or runup limit observations also indicate influence from secondary vortices on coastal inundation.

Much of the size effect indicated by Eq. (22.50) can be understood through the fact that the shore-normal wind is a dipole, with the effects of the opposing "poles" cancelling at the far field, see Fig. 22.24 below. The range of the effect of dipoles is proportional to the pole distance. Even if the storm has circular symmetry, the onshore wind stresses will, due to superposition of c, be greater than the offshore ones if the storm is moving towards the coast with speed c. Due to the influence of rainfall, which is usually strongest in front and can transfer wind-momentum downwards, the two sides of the wind dipole often have quite different strengths at sea level. Usually rainfall enhances the ground level winds in front of the storm centre.

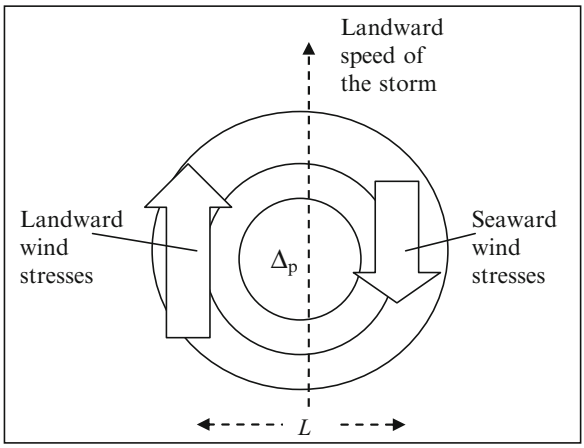

Fig. 22.24 The opposite wind stress on opposite sides of the storm counteract each other less for larger storms, seen from a given distance (Nielsen 2009b)

22.3.3 Wind Stresses

The wind stress τ_w on the sea surface depends on the size, shape and speed of the ocean waves as well as on the wind speed and distribution. Hence, τ_w is expected to be quite different offshore and in the surf zone on a given day. Most of the existing wind stress data have been obtained by measuring wind profiles over deep water and applying the log-law. Deep water data indicates a maximum value of $C_{10,\max} = 0.0025$ for the wind stress coefficient defined by

$$\tau_w = \rho_{air} C_{10} U_{10}^2 \tag{22.51}$$

where U_{10} is the wind speed at 10 m above the sea surface and C_{10} the drag coefficient of the order 2×10^{-3}. Recent reviews on C_{10} were given by Donelan et al. (2004) and Jones and Toba (2001). For the most extreme conditions of wind speeds larger than 33 m/s, Donelan et al. (2004) found $C_{10} \approx 0.0025$, which leads to an extremely small roughness length $k_s \approx 0.1$ m even when the waves would be huge under the extreme conditions.

There is some serious doubt about the small C_{10} values obtained from log-fits to wind profiles over deep water. Firstly, they are too small for numerical models to give enough surge (Stewart et al. 2010). Secondly, different and considerably larger values of C_{10} are obtained, when the momentum flux is measured in a different way. Cavaleri & Zecchetto (1987) measured the Reynolds stresses in the water below the surface and found significantly greater shear stresses than those normally found from measurements in the air above. The small wind stress coefficients measured in deep waters are definitely not representative for surf zones in shallow waters, where the waves have very different shapes and move much more slowly than those in deep waters. However, data on wind stresses over surf zones are not presently available. There is an urgent need for wind stress measurements over surf zones and for Reynolds stress measurements under shallow water waves.

22.3.4 Surge from Steady Onshore Winds

A quantitative description of elevated coastal water levels due to steady onshore winds was given in Fig. 3.2.1 of Nielsen (2009a). With a constant eddy viscosity, a requirement of zero net flow leads to $\tau_b = -0.5\tau_w$, and to the water surface slope

$$\frac{d\overline{\eta}}{dx} = \alpha_v \frac{\tau_w}{\rho g h} = \frac{3}{2}\frac{\tau_w}{\rho g h}. \tag{22.52}$$

With a more general variable eddy viscosity, the factor α_v will range from 1 to 3/2. It is then possible to get a rough estimate of a steady wind generated setup height $\overline{\eta}(h_2)$ at an inshore depth h_2 with the boundary condition of $\overline{\eta}(h_1) = 0$ at the offshore water depth h_1. If the bottom slope is assumed to be constant, Eq. (22.52) can be further reduced to

$$\overline{\eta}(h_2) = \alpha_v \frac{\tau_w}{\rho g}\frac{W}{h_1}\ln\frac{h_1}{h_2}, \tag{22.53}$$

where W is the width of the shelf between the water depths h_1 and h_2.

Hence, the nearshore wind setup has to be evaluated at some arbitrary finite depth. Another problem with it is that the drag coefficients for surf zones are unknown and may very well be greater than the deep water values. Nevertheless, the formula shows the important qualitative fact that "the wider the shelf the greater the wind setup".

22.3.5 Surge from Steady Longshore Winds

If the continental shelf is steep, the effect of steady shore-normal winds is, at most, only a few centimeters as indicated by Eq. (22.53). However, the Coriolis or geostrophic effect on large scale wind-driven longshore currents may in this case cause significant tidal anomalies. The Coriolis acceleration on a water particle with horizontal velocity u is perpendicular to u, to the left in the southern hemisphere and to the right in the northern hemisphere (Alonso and Finn 1968; Le Mehaute 1976), and its magnitude is

$$a_{\text{Coriolis}} = 2\omega_E u \sin\theta \tag{22.54}$$

where $\omega_E = 7.3 \times 10^{-5}$ rad/s is the angular frequency of the Earth's rotation and θ is the latitude. The typical magnitude of the Coriolis acceleration from Eq. (22.54) is about 10^{-4} m/s^2 or 10^{-5} g. This means that the Coriolis acceleration can induce ocean surface slopes of the order $a_{\text{Coriolis}}/g \sim 10^{-5}$ or 1 cm per kilometer when u is of the order 1 m/s. This often becomes significant on the scale of weather systems (>100 km).

22.3.6 Surge from a Moving Wind Field

The scaling and basic dynamics of surges due to moving wind stress fields is illustrated by a simple 1D analytical example, based on the general solution scheme for constant depth (Nielsen 2009a). Subsequently, differences and similarities with 2D scenarios are illustrated and discussed briefly. Consider the wind stress field to be the simple form

$$\tau_w(x,t) = \frac{\tau_{\max}}{\cosh^2[(x-ct)/L]} \quad \text{and} \quad T_w(x,t) = \tau_{\max} L \tanh\left(\frac{x-ct}{L}\right), \tag{22.55}$$

which corresponds to "the stress potential" or $\tau_w = \partial T_w/\partial x$. The steady forced wave solution is then found as

$$\begin{aligned} \eta_{\text{forced}}(x,t) =& A_{\text{forced}} \tanh\left(\frac{x-ct}{L}\right) \\ =& \frac{\tau_{\max} L}{\rho(gh-c^2)} \tanh\left(\frac{x-ct}{L}\right) \\ =& \frac{\frac{\tau_{\max}}{\rho g}}{1-\frac{c^2}{gh}} \frac{L}{h} \tanh\left(\frac{x-ct}{L}\right) \end{aligned} \tag{22.56}$$

The complete solution, including the free waves, for a surge which grows after the onset of the forcing at $t = 0$, is given by (Nielsen 2010):

$$\eta(x,t) = \frac{\tau_{\max} L}{\rho(gh-c^2)} \left(\begin{array}{l} \tanh\left(\frac{x-ct}{L}\right) - \frac{1}{2}\left[1+\frac{c}{\sqrt{gh}}\right] \tanh\left(\frac{x-\sqrt{ght}}{L}\right) \\ -\frac{1}{2}\left[1-\frac{c}{\sqrt{gh}}\right] \tanh\left(\frac{x+\sqrt{ght}}{L}\right) \end{array} \right). \tag{22.57}$$

An example is shown in Fig. 22.25. For these wind stress driven surges, the asymptotic state does not correspond to the forced wave because the free waves have finite surface elevations at $x \to \pm\infty$. The resonant 1D surge takes the shape of $t\sqrt{gh}\frac{\partial}{\partial x}\mathrm{f}(x-ct)$ where f$(x-ct)$ is the shape of the steady, non-resonant forced solution means that at resonance, a wind stress driven 1D surge takes the form of $t\tau_{\mathrm{w}}$ rather than of T_{w}.

The behaviour of a developing 2D wind stress driven surges is different from that of the 1D solution in Fig. 22.25 as illustrated by Nielsen (2009a). That is, the plateaus in front of and behind the stress field are not flat but have elevated edges. In addition we note that that the 2D surge is generally smaller because of radiation in the y-direction. It is also interesting that the 2D solution overshoots at the centre compared with the asymptotic central value. The fact that a wind stress of a given magnitude generates bigger surges in shallower water, cf Eq. (22.57), means that a

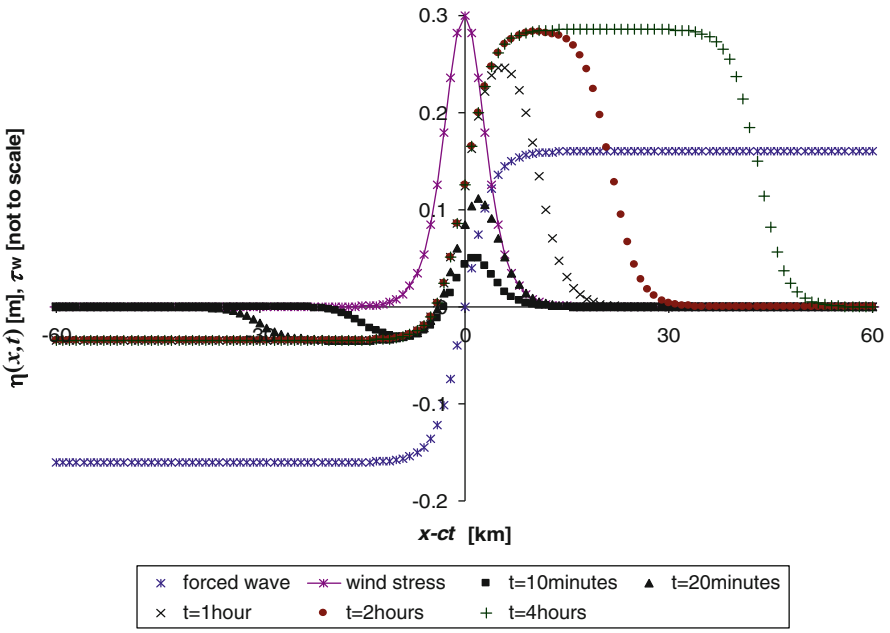

Fig. 22.25 Developing surge driven by a pulse shaped wind stress travelling at speed $c = 11$m/s. $\tau_{\max} = 3$ Pa, $L = 4{,}000$ m, $h = 20$m, $\sqrt{gh} = 14$ m/s,. $A_{\text{forced}} = 0.160$ m, $A^{+}_{\text{free}} = -.143$ m, $A^{-}_{\text{free}} = -.017$ m

surge will grow as it approaches the coast and additional free waves will be associated with this growth. At landfall the shape of fast moving surges will therefore always be transient and perhaps typically resemble the early stages in Fig. 22.25.

22.3.7 Pressure Driven Surges

22.3.7.1 Inverse Barometer Rule

Basic hydrostatic considerations can be used to show that a stationary low pressure system will raise the sea level in a matching shape and with local over-height given by

$$\Delta_\eta = -\Delta_{\text{p}}/\rho g \tag{22.58}$$

which is irrespective of the water depth. This corresponds to the rule of thumb that: For every hPa of low pressure one gets 1 cm of local sea level rise. This rule is often referred to as the *Inverse Barometer Rule, the IBR*.

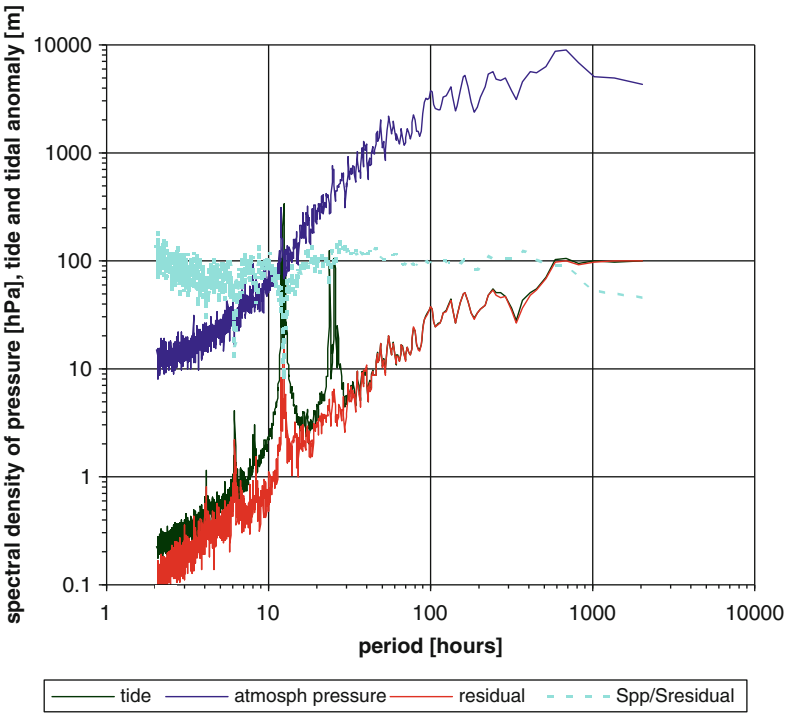

Fig. 22.26 Spectra of atmospheric pressure [hPa], tides and tidal residuals [m] for Macquarie Island 2006

Data from Macquarie Island validate the IBR rule with high accuracy because the waters around the island are so deep ($h > 2{,}000$ m) that the wind driven surge, being inversely proportional to h, is negligible and the amplification factor for all surges due to speed $\left(1 - \frac{C^2}{gh}\right)^{-1}$ is close to unity. The ratio of the spectral ordinates $S_{pp}/S_{residual}$ in Fig. 22.26 has a constant value of 100 corresponding to the IBR throughout the period of 25–700 h, which corresponds to forcing by local weather.

22.3.7.2 Moving Low Pressure System

Interestingly, if the low pressure system moves, one can get considerably more storm surge than the abovementioned 1 cm/hPa. It is also a possible explanation for the response of the continental shelf and river mouth gauges being stronger than the Inverse Barometer Rule (IBR) by a factor 2–3. If a low pressure system propagates with constant but arbitrary form, e g, $p_s(x,t) = P_o f(x-ct)$, this moving pressure system will generate a steady forced wave of the form

$$\eta_{forced}(x,t) = A_{forced} f(x - ct) \quad \text{and} \quad A_{forced} = \frac{-P_o/\rho g}{1 - c^2/gh}, \tag{22.59}$$

22.3.7.3 The Growth of Surges

A slow moving low pressure system ($P_o < 0$ and $c<\sqrt{gh}$) may generate a positive surge, while a fast moving low pressure system generates a negative surge in the steady state (Nielsen 2010). The latter does however not mean that fast systems cannot generate flooding. The flooding is in that case generated by the forward moving free wave $\eta^+(x,t)$, which is borne together with $\eta_{\text{forced}}(x,t)$ at the onset of the forcing. The complete (1D, linear) solution, describing the growth of the storm surge from an ocean which is flat at time zero, can be described as the superposition of three waves:

$$\begin{aligned}\eta(x,t) =&\eta_{\text{forced}}(x,t)+\eta^+_{\text{free}}(x,t)+\eta^-_{\text{free}}(x,t)\,.\\ =&A_{\text{forced}}\text{f}(x-ct)+A^+_{\text{free}}\text{f}\left(x-\sqrt{ght}\right)+A^-_{\text{free}}\text{f}\left(x+\sqrt{ght}\right)\end{aligned} \tag{22.60}$$

When the starting conditions are a flat surface and zero velocity everywhere, the amplitudes of the free waves are given as

$$\left(A^+_{\text{free}},A^-_{\text{free}}\right)=\left(-\frac{A_{\text{forced}}}{2}\left[1+\frac{c}{\sqrt{gh}}\right],-\frac{A_{\text{forced}}}{2}\left[1-\frac{c}{\sqrt{gh}}\right]\right) \tag{22.61}$$

There is no friction so the free shallow-water-waves travel away with constant shape. In this case their speed is $\sqrt{gh}=14$ m/s. The forcing being stationary, the steady amplitude according to (22.50) is $-P_o/\rho g$. In this friction free case the free waves do not decay. Being shallow-water-waves and hence non-dispersive, they also do not disperse.

The unsteady surface profile develops as the steady solution moves with the air pressure field at speed c while the two free waves move with speed $\sqrt{gh}$ in opposite directions. For $0 < c<\sqrt{gh}$, the forward moving free wave increasingly dominates for $c\rightarrow\sqrt{gh}$ but both of $(A^+_{\text{free}},A^-_{\text{free}})$ remain negative. For $c > \sqrt{gh}$, A_{forced} is negative, i e, the forced wave due to a fast moving low pressure system is a surface depression! Eq. (22.61) now shows that the two free waves have opposite signs and A^+_{free} dominates.

For moving low pressure systems in the range $0<c<gh$, the forward moving free wave is largest: $A^+_{\text{free}}>A^-_{\text{free}}$ as was shown in Fig. 22.27. On a shoreline crossed by this system, an observer will see a surface depression of magnitude A^+_{free} arriving before the low pressure system and some time later a larger positive surge of magnitude A_{forced} arriving together with the low pressure. If the low pressure system moves faster than a free wave $c>\sqrt{gh}$, the forced wave is a surface depression, and the free waves both move to the left relative to the forcing. Their amplitudes have opposite signs and the forward moving free wave dominates, see Fig. 22.28. The forward moving free wave now has a greater amplitude than the forced wave. Hence, if friction is negligible, so the free wave does not decay, the inundation sequence at landfall will be a negative surge of magnitude A_{forced} arriving together with the peak low pressure, followed by a larger positive surge of magnitude A^+_{free} (Nielsen et al. 2008).

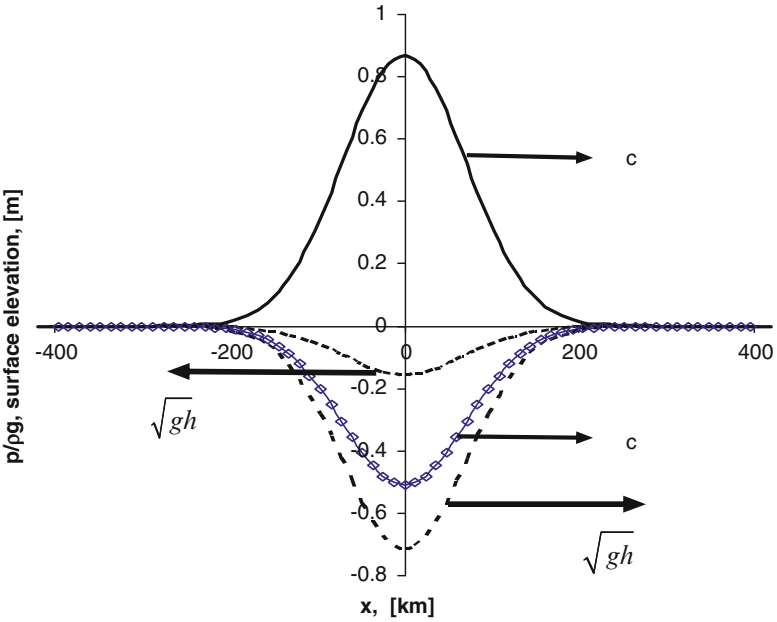

Fig. 22.27 The initial flat surface is seen as the superposition of the steady, forced solution given by Eq. (22.59) and two free waves given by Eq. (22.61), which cancel the forced wave with respect to surface elevations and water velocities at $t = 0$. After Nielsen et al. (2008)

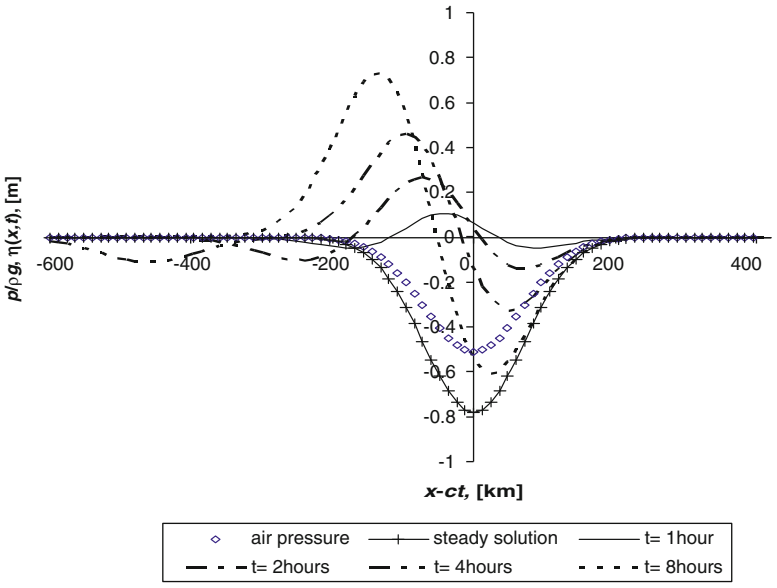

Fig. 22.28 Same low pressure system as in the previous figure but now moving faster than a free wave: $c = 18$ m/s while $\sqrt{gh} = 14$ m/s. $A_{\text{forced}} = -0.78$ m, $\left(A^{+}_{\text{free}}, A^{-}_{\text{free}}\right) = (0.89\text{ m}, -0.11\text{ m})$. After Nielsen et al. (2008)

22.4 Wave Runup

22.4.1 Introduction

Wave runup can reach very large heights given special wave conditions and/or special topography. One of the most extreme recorded events was the fatal event where biologist Hamish Allan Saunders working 45 m, above sea level on Pedra Branca off the South East Cape of Tasmania was washed into the sea by wave runup. Even stronger runup impact at somewhat lower levels: 20–25 m above sea level caused the loss of many houses on the Island of Niue during Cyclone Heta in January 2004, cf Callaghan et al. (2006). Erosion and deposition due to similarly extreme runup events on Scottish islands have been documented by Hansom et al. (2008). On the coast of New South Wales, Australia, a fatality at Tathra during TC Colin in 1972 (or TC Pam in 1974, see Fig. 22.29) was attributed to runup washing a woman off a cliff top possibly at 20 m above sea level. The extreme tropical cyclone Mahina (March 4–5 1899), which made landfall at Bathurst Bay North Queensland stranded dolphins 15 up cliffs and Sharks 40 km inland. This event included a very large surge as well as large waves.

In recognition of the danger of high runup on steep exposed coasts, Japan has recently upgraded their wave runup barrier along the Fuji Coast to 17 m. Debris lines are often found to be of highly irregular elevations, i e varying considerably on scales much shorter than the size of the storm. Some of this variation often has obvious reasons in terms of the nearshore subaqueous topography, which affects shoaling patterns and wave focussing, and/or the slope and roughness of the beach face. However, a significant part of the debris line sinuosity may be caused eye wall eddies in the case cyclones. This is similar to the well known observation of TC wind damage often varying considerably from block to block in build-up areas. While the above mentioned cases of runup hazards are from steep and usually quite

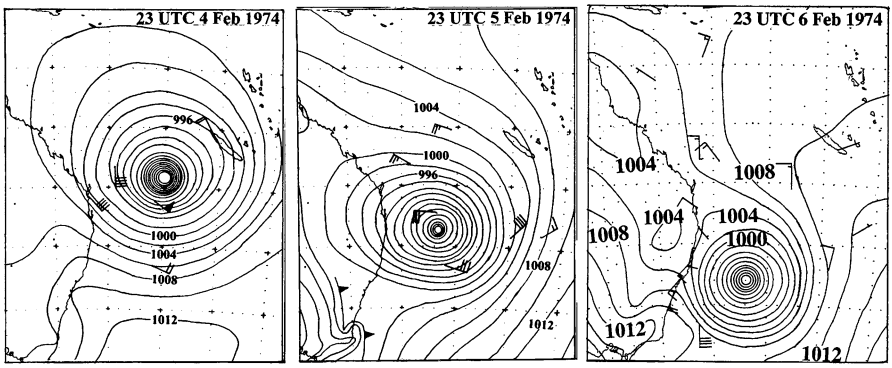

Fig. 22.29 The winds from TC Pam would have caused record waves and corresponding runup along the NSW coas

complex topographies, the following gives a brief introduction to runup hydrodynamics and runup statistics on simple slopes, leading to a new method for estimating the maximum runup on simple topographies during a storm with varying surge level.

22.4.2 Swash Hydrodynamics

The water motion in the area where the beach face is exposed and covered by water on the time scale of individual wind waves is called swash. If the surf similarity parameter is very large ($\sqrt{L_o/H_b}\tan\beta>4$) the waves will not break on the slope but for most natural beaches they will. The swash is then a highly asymmetrical motion where the depth and speed of the uprush is determined by the height and speed of the incoming bores while the backwash is driven by gravity. The sand, onto which the swash is progressing, may be saturated or unsaturated with water depending on the tidal phase and on the strengths of previous uprush events.

If the beach material is coarse ($d_{50} > 1$ mm), the swash may also be asymmetrical with respect to volume. That is, the amount of water running back down the slope is less than what rushed up because a substantial part of the uprush volume seeps into the slope. On very flat beaches where breakers of constant form can dissipate energy fast enough to maintain constant H/h and hence $H\to 0$ for $h\to 0$, there will be no swash. The swash zone can be subdivided into a lower part, where bores and swash lenses may overtake each other, and an upper part without interference, cf Hughes and Moseley (2007). The bore speed equation (e.g. Nielsen 2009a, p. 49):

$$c = \sqrt{\frac{h_1}{h_2} g \frac{h_1 + h_2}{2}} \tag{22.62}$$

blows up when the depth h_2 in front of the bore vanishes. What happens then is that the bore collapses and a smooth swash lens shoots forward from the base of the bore front. This has similarities with a dam break situation and the kinematics of the tip of the swash lens on a slope has been modelled successfully in analogy with dam breaks, using the non-linear shallow water (NLSW) equations. However, bore collapse differs from a dam break in that the water in the bore has initial momentum. This does not affect the kinematics of the tip (at least not in the NLSW solution), but it does affect the depths and flow rates following the tip as described by Guard and Baldock (2007). The boundary layer structure and hence the shear stresses and the resulting sediment transport in the swash are still poorly understood. While some friction as opposed to ideal fluid flow makes a qualitative difference, the difference between a rough porous sand surface and a smooth plastic sheet makes little difference to the swash tip behaviour (Nielsen 2009a).

22.4.3 Regular Wave Runup

When the incoming waves are regular, having fixed height and period, they will all run up to the same height on the beach. In this case it makes sense to talk about *the* runup height R. It turns out that R depends in very different ways on the slope and the wave parameters in the breaking and non-breaking scenarios. Experiments with breaking waves have shown that, the runup height measured from the still water level is proportional to the wave height H just seaward of the slope and to the surf similarity parameter

$$R = H\xi = H\tan\beta_F\sqrt{L_o/H} = \tan\beta_F\sqrt{HL_o} = \tan\beta_F\sqrt{H\frac{gT^2}{2\pi}}. \tag{22.63}$$

In connection with this formula, we note, that the runup height depends more strongly on the wave period than on the height: $R \propto T\sqrt{H}$. Equation (22.63) which is often called Hunt's formula (Hunt 1959) is only valid for breaking waves with $\xi \leq 2$ corresponding to $R \leq 2H$, but this does cover the range of wind waves on natural beaches. For waves that do not break, the motion on the slope can be modelled with the non-linear shallow water equations. The result is stated by Meyer and Taylor (1972), based on the solution of Carrier and Greenspan (1958):

$$\frac{R}{H_o} = \sqrt{\frac{2\pi}{\tan\beta}} \quad \text{for } x>4 \tag{22.64}$$

22.4.4 Irregular Wave Runup

For natural waves with variable heights the maximum heights R_n on the slope reached by the individual swash fronts is variable. A statistical description is therefore required for describing the runup hazard. So far most of the attention has been focussed on the maximum level reached by the waterline as indicated perhaps by lines of light debris (pumice and bits of water weeds). Other statistics related, for example, to the highest levels where the impact forces from the swash can cause structural damage or knock people off balance would also be of interest.

Statistical information may be obtained by tracking instantaneous waterline $(x_w(t),\ z_w(t))$, with runup wires or a video camera. Runup wires are somewhat imprecise in that they have to be a certain distance above the sand surface, and even a video camera cannot always define a receding waterline when the surface remains wet due to seepage. Alternatively, simple transgression statistics can be gathered by counting the number n_i of swash fronts passing stakes at sand levels z_i. The

transgression counts $n_i(z_i)$ define the distribution function for R_n, which is often expected to be a Rayleigh distribution:

$$P\{R_n > x\} = \exp\left[-\left(\frac{x}{L_R}\right)^2\right] \tag{22.65}$$

This hypothesis corresponds to $\left(-\ln\frac{n_i}{N}, z_i\right)$ plotting along a straight line, where N is the total number of waves. The goodness of fit by the Rayleigh distribution, i e, a straight line in Fig. 22.30 is variable. The slight upward convex trend near the runup limit in some of these datasets is perhaps a general feature. What is quite general, is that the best fit straight line does not go through the origin, i e, the point of 100% transgression does not generally coincide with the SWL. The 100% transgression level $Z_{100\%}$ varies quite widely relative to the still water level, e g,

$$z_{100\%}/L_R = -0.31 \pm 0.40 \tag{22.66}$$

for the data of Nielsen and Hanslow (1991). The very low values of $z_{100\%}$ observed on the flattest beaches are not due to swash zone processes. They correspond to bores merging in the inner surf zone on these beaches so that n_i starts to decrease well seaward of the average point of bore collapse. The vertical runup scale L_R, in the Rayleigh runup distribution

$$P\{z_{max} > x\} = \exp\left[-\left(\frac{x - z_{100\%}}{L_R}\right)^2\right] \tag{22.67}$$

depends mainly on the offshore wave parameters and the beach face slope as indicated by Fig. 22.31.

The trend lines indicate that, for fairly steep slopes L_R is approximately 0.6 times the runup height of the rms wave calculated from regular-wave-equation (22.63):

$$L_R = 0.6 \tan\beta_F \sqrt{H_{orms} L_o} \quad \text{for } \tan b_F > 0.1, \tag{22.68}$$

for flatter slopes L_R seems to be independent of β_F and approximately given by

$$L_R = 0.06\sqrt{H_{orms} L_o} \quad \text{for } \tan b_F < 0.1 \tag{22.69}$$

However, this is an artifact of the transgression statistics being influenced by bores merging, and n_i correspondingly decreasing seaward of the bore collapse region on flat beaches. Correspondingly, Stockdon et al. (2006) found the 2% runup level to increase with beach slope throughout the range of slopes. The topography of the outer surf zone will influence the relation between the runup distribution and the offshore wave parameters.

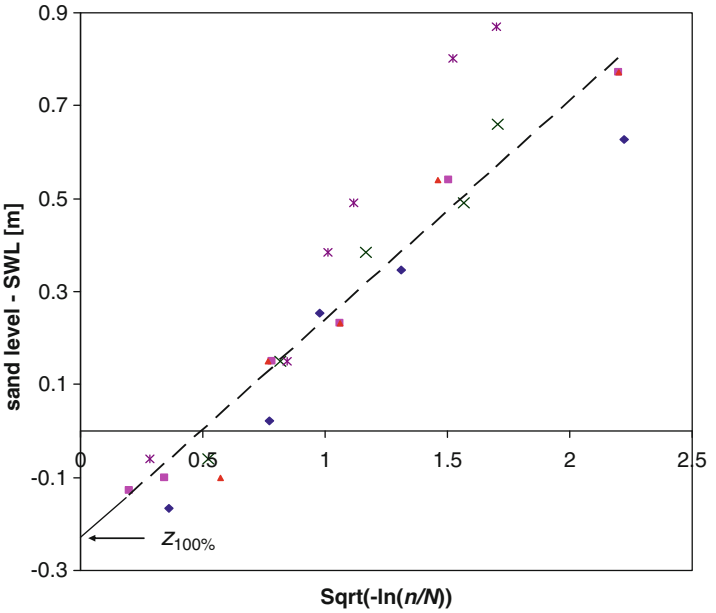

Fig. 22.30 Rayleigh plots of 5 sets of runup data from Moreton Island, 10–11 Dec 2007. $H_{\text{orms}} = 0.9$ m, $T_z = 5.6$ s, $\text{Tan}\beta_F = 0.08$. The trend line corresponds to the data marked ■ . $Z_{100\%}$ is the highest level transgressed by all waves according to the best fit Rayleigh distribution. After Nielsen (2009a)

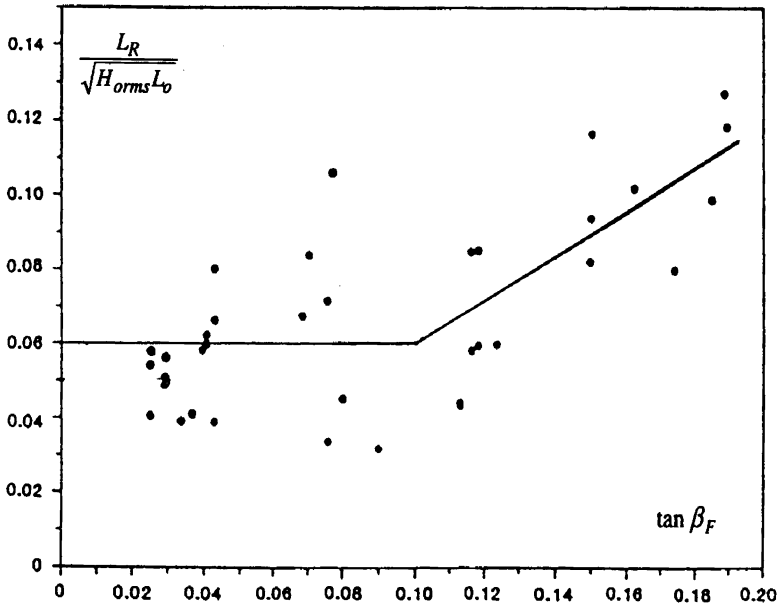

Fig. 22.31 Relationship between the vertical scale L_R in the Rayleigh runup distribution and the ofshore wave parameters. L_o is calculated from $T_{sig} \approx T_z < T_p$. Data from Nielsen and Hanslow (1991)

In analogy with the results for extreme wave heights within a record, the highest of N individual runup heights will under the Rayleigh Distribution, and assuming a constant still water level (SWL), be a stochastic variable with modal value, or maximum likelihood estimate

$$R_{1/N} = L_R\sqrt{\ln N} + z_{100\%} \tag{22.70}$$

and hence, for example, the height exceeded by just 2% of the runups is expected to be

$$R_{2\%} = L_R\sqrt{\ln 50} + z_{100\%} \approx 1.98L_R + z_{100\%} \tag{22.71}$$

22.4.5 Extreme Wave Runup

The question of extreme runup height is more complicated if the SWL is varying due to tide or storm surge or a combination of those. The expected height of the runup limit, will then depend on how rapidly the SWL varies around its peak. Consider the scenario, where a storm tide (= astronomical tide + surge) with arbitrary but fairly smooth shape is superposed by wave runup.

We wish to estimate height of the runup limit RL. This can of course be done for an arbitrary surge shape with Monte Carlo simulation. However, since RL will depend mainly on the maximum storm tide level $\eta_{\max}$ and the radius of curvature of the storm tide near its peak, we will develop a more direct practical estimate. This estimate is based on a Rayleigh runup process with wave period T and vertical scale L_R together with a sinusoidal storm tide with period T_{surge} and amplitude A. We aim for an estimate in the form

$$\mathrm{E}\{RL\} = \eta_{\max} + z_{100\%} + L_R\sqrt{\ln\frac{T_{\mathrm{eff}}}{T}} \tag{22.72}$$

The rationale for the last term in (22.72) is that the expected runup limit for N waves in a steady Rayleigh process (no tide or surge) with vertical scale L_R is E $\{RL\} = L_R\sqrt{\ln N}$ and, T_{eff}/T is the number of waves in an effective time span around the surge peak. The behaviour of T_{eff} based on a sinusoidal surge is, for $0.1 < A/L_R < 10$, well described by

$$\frac{T_{\mathrm{eff}}}{T_{surge}} = 0.18\sqrt{\frac{L_R}{A}} \tag{22.73}$$

which by insertion into (22.72) gives

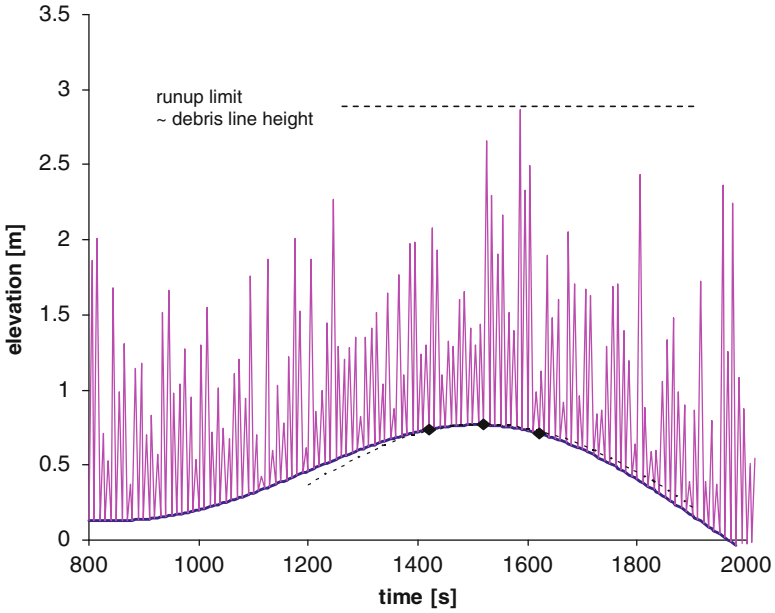

Fig. 22.32 The smooth *solid curve* shows storm tide, on which a Rayleigh runup process with vertical scale $L_R = 1$ m, $z_{100\%} = 0$ and wave period $T = 10$s is superimposed. The time scale of the SWL variation around the peak can be defined as the period of a *sine curve* (*thin dotted curve*), which approximates the shape of the storm tide around its peak

$$\mathrm{E}\{RL\} = \eta_{\max} + z_{100\%} + L_R \sqrt{\ln\left(0.18\sqrt{\frac{L_R}{A}}\frac{T_{\mathrm{surge}}}{T}\right)}. \tag{22.74}$$

To find T_{surge} by approximating a sine curve, we use the fact that $\omega^2 = -y''/y$ for any sine curve $y = A\sin(\omega t - \varphi)$, which can be evaluated using the finite difference approximation with 3 points, of spacing Δ_t around the peak as illustrated in Fig. 22.32:

$$\omega^2_{\mathrm{surge}} = -\frac{\eta(t_{\mathrm{peak}} + \Delta_t) - 2\eta(t_{\mathrm{peak}}) + \eta(t_{\mathrm{peak}} - \Delta_t)}{\Delta_t^2\,\eta(t_{\mathrm{peak}})} \quad \text{and}$$

$$T_{\mathrm{surge}} = \frac{2\pi}{\omega_{\mathrm{surge}}} \tag{22.75}$$

For this example, this procedure gives $T_{\mathrm{surge}} = 1856$s, and with $A = \eta_{\mathrm{peak}} = 0.768$ m, $L_R = 1$ m, $z_{100\%} = 0$ and $T = 10$s, Equation (22.72) gives $\mathrm{E}\{RL\} = 2.68$ m. Perhaps because of the sometimes poor fit of the Rayleigh distribution and the uncertainty about $z_{100\%}$, Stockdon et al. (2006) took the 2% runup level as their

estimate of the extreme runup level. This is perhaps primitive statistics, which is not readily adaptable to runup on top of a time varying surge level, but it has the advantage of being free of assumptions about the type of distribution function.

References

Alonso M, Finn EJ (1968) Fundamental university physics, vol 1, Mechanics. Addison Wesley, Reading, 463 pp

Bretschneider CL (1959) Wave variability and wave spectra for wind-generated gravity waves. Tech. Memo. No.118. Beach Erosion Board, US Army Corps of Engineer, Washington, DC

Callaghan DP, Nielsen P, Cartwright N, Gourlay MR, Baldock TE (2006) Atoll lagoon flushing forced by waves. Coast Eng 53:691–704

Cao B, Wang YG, You ZJ (2006) Comparison of three design wave height calculations. China Ocean Eng 24:6–11

Carrier GF, Greenspan HP (1958) Water waves of finite amplitude on a sloping beach. J Fluid Mech 4:97–109

Carter DJT, Challenor PG (1983) Methods of fitting the Fisher-Tippett Type 1 extreme value distribution. Ocean Eng 10:191–199

Cavaleri L, Zecchetto S (1987) Reynolds stresses under wind waves. J Geophys Res 92:3894–3904

CEM (2002) Coastal engineering manual. Engineer Manual 1110-2-1100, U.S. Army Corps of Engineers, Washington, DC

Cheng RCH, Amin NAK (1983) Estimating parameters in continuous univariate distributions with a shifted origin. J Roy Stat Soc 45:394–403

Cook NJ (2011a) Comments on "Plotting positions in extreme value analysis". J Appl Meteorol Climatol 50:255–266

Cook NJ (2011b) Rebuttal of "Problems in the extreme value analysis". Struct Saf 34:418–423

Cunnane C (1978) Unbiased plotting positions – a review. J Hydrol 37:205–222

Dean RG, Dalrymple RA (1991) Water wave mechanics for engineers and scientists. World Scientific, Singapore, 353 pp

Donelan MA, Haus BK, Reul N, Plant WJ, Stiassnie M, Graber HC, Brown OB, Saltzman ES (2004) On the limiting aerodynamic roughness of the ocean in very strong winds. Geophys Res Lett 31:L18306. doi:10.1029/2004GL019460

Fisher RA, Tippett LHC (1928) Limiting forms of the frequency distribution of the largest or smallest members of a sample. Proc Camb Philos Soc 24:180–190

Forristall GZ (1978) On the statistical distribution of wave heights in a storm. J Geophys Res 83:2353–2358

Fréchet M (1927) Sur la loi de probabilité de l'écart maximum. Ann de la Soc Polonaise de Math 6:93–116

Goda Y (1988) On the methodology of selecting design wave height. Proceedings of the 21st international conference on coastal engineering, ASCE, pp 899–913

Goda Y (2011) Plotting position estimator for the L-moment method and quantile confidence interval for the GEV, GPA and Weibull distributions applied for extreme wave analysis. Coast Eng J 53:111–149

Greenwood JA, Landwehr JM, Matalas NC, Wallis JR (1978) Probability weighted moments: definition and relation to parameters of several distributions expressable in inverse form. Water Resour Res 15:1049–1054

Gringorten II (1963) A plotting rule for extreme probability paper. J Geophys Res 68:813–814

Guard PA, Baldock TE (2007) The influence of seaward boundary conditions on swash zone hydrodynamics. Coast Eng 4:321–331

Gumbel EJ (1958) Statistics of extremes. Columbia University Press, New York, 375 pp

Hansom JD, Barltrop NDP, Hall AM (2008) Modelling the processes of cliff-top erosion and deposition under extreme storm waves. Mar Geol 253:36–50
Holland GJ (1980) An analytical model of the wind and pressure profiles in hurricanes. Mon Wea Rev 108:1212–1218
Holthuijsen LH (2007) Waves in oceanic and coastal waters. Cambridge University Press, Cambridge, p 387
Hosking JRM (1990) L-moments: analysis and estimation of distributions using linear combinations of order statistics. J Roy Stat Soc 52:105–124
Hosking JRM, Wallis JR (1995) A comparison of unbiased and plotting position estimators of L moments. Water Resour Res 31:1049–1064
Hou YJ, Guo PF (2006) Statistical distribution of nonlinear random wave height. Sci China 49:443–448
Hughes MG, Moseley AS (2007) Hydrokinematic regions within the swash zone. Cont Shelf Res 27:2000–2013
Hunt IA (1959) Design of seawalls and breakwaters. Proc A S C E 85:123–152
Irish JL, Resio DT, Ratcliff JJ (2008) The influence of storm size on hurricane surge. J Phys Oceanogr 38:2003–2013
Issacson MS, Mackenzie NG (1981) Long-term distributions of ocean waves: a review. J Waterways Port Coast Ocean Eng 107:93–109
Jones ISF, Toba Y (2001) Wind stress over the ocean. Cambridge University press. J Appl Meteorol Climatol 45:1244–1260
Kamphuis JW (2000) Introduction to coastal engineering and management. World Scientific, Singapore
Lawless JF (1974) Approximations to confidence intervals for parameters in the extreme value and Weibull distributions. Biometrica 61:123–133
Lawless JF (1978) Confidence interval estimation for the Weibull and extreme-value distributions. Technonetrics 20:355–368
Le Mehaute B (1976) An introduction to hydrodynamics and water waves. Springer, New York, p 313
Longuet-Higgins MS (1952) On the statistical distribution of the heights of sea waves. J Mar Res 11:245–266
Longuet-Higgins MS (1962) The distribution of intervals between zeros of random function. Phil Trans Roy Soc Lond Ser A 254:557–599
Longuet-Higgins MS (1963) The effect of non-linearities on statistical distributions in the theory of sea waves. J Fluid Mech 17:459–490
Longuet-Higgins MS (1975) On the joint distribution of the periods and amplitudes of sea waves. J Geophys Res 80:2688–2694
Longuet-Higgins MS (1980) On the distribution of the heights of sea waves: some effects of nonlinearity and finite band width. J Geophys Res 85:1519–1523
Longuet-Higgins MS (1983) On the joint distribution of wave periods and amplitudes in a random wave field. Proc Roy Soc Lond Ser A 389:241–258
Lord D, Kulmar MA (2000) The 1974 storms revisited: 25 years experience in ocean wave measurement along the South-East Australia coast. 27th international conference on coastal engineering, ASCE, Sydney, pp 559–572
Makkonen L (2006) Plotting positions in extreme value analysis. J Appl Meteorol Climatol 45:344–360
Makkonen L (2008) Bringing closure to the plotting position controversy. Commun Stat-Theor Methods 37:460–467
Massel SR, Sobey RJ (2000) Distribution of the highest wave in a record. Coast Eng J 42:153–173
Mazas F, Hamm L (2011) A multi-distribution approach to POT methods for determining extreme wave heights. Coast Eng 58:385–394
McAneney J, Crompton R, Chen K, Hunter L (2007) A century of damage: property losses due to natural perils. J Aus N Z Inst Insur Finance 30:16–22

Mei CC (1991) The applied dynamics of ocean surface waves. World Scientific Pub. Co., Teaneck
Meyer RE, Taylor AD (1972) Runup on beaches. In: Meyer RE (ed) Waves on beaches and the resulting sediment transport. Academic, New York, pp 357–411
Mills GA, Webb R, Davison NE, Kepert J, Seed A, Abbs D (2010) The Pasha Bulker east coast low of 8 June 2007. CSIRO Technical Report No. 023
Muir LR, El-Shaarawi AH (1986) On the calculation of extreme wave heights: a review. Ocean Eng 13:93–118
Nielsen P (1992) Coastal bottom boundary layers and sediment transport. World Scientific, Singapore, 324 pp
Nielsen P (2009a) Coastal and estuarine processes. World Scientific, Singapore, 341 pp
Nielsen P (2009b) How storm size matters for surge height. Coast Eng 56:1002–1004
Nielsen P (2010) Extreme water levels and wave runup with Special emphasis on the coast of New South Wales. Technical Report, University of Queensland, pp 1111
Nielsen P, Hanslow DJ (1991) Wave runup distributions on natural beaches. J Coast Res 7:1139–1152
Nielsen P, Guard PA, Callaghan DP, Baldock TE (2008) Observations of wave pump efficiency. Coast Eng 55:69–72
Ochi MK (1998) Ocean waves: the stochastic approach. Ocean technology series 6. Cambridge University Press, Cambridge, p 319
Rudnick P (1951) Correlograms for Pacific ocean waves. In: Proceedings of 2nd Berkeley Symposium on mathematical statistics and probability, pp 627–638
Song JB, Wu YH (2000) Statistical distribution of water particle velocity below the surface layer for finite water depth. Coast Eng 40:1–19
Stewart JP, Callaghan DP, Nielsen P (2010) Tropical cyclone 'Roger' storm surge assessment, School of Civil Engineering, Research Report CE162, the University of Queensland
Stockdon HF, Holman RA, Howd PA, Sallenger AH (2006) Empirical parameterization of setup, swash and runup. Coast Eng 53:573–588
Sultan NJ, Hughes SA (1993) Irregular wave-induced velocities in shallow water. J Waterway Port Coast Ocean Eng, ASCE 119:429–447
Tayfun MA (1980) Narrow-band nonlinear sea waves. J Geophys Res 85:1548–1552
Tayfun MA (1981) Distribution of crest to trough wave height. J Waterways Port Coastal Ocean Eng, ASCE 107:149–158
Vinje T (1989) The statistical distribution of wave heights in a random seaway. Appl Ocean Res 11:143–152
Webb AT, Kulmar MA (1989) Coastal wave climate of New South Wales – an update. 9th Australasian conference on coastal and ocean engineering, Adelaide, pp 374–379
You ZJ (1994) A simple model for current velocity profiles in combined wave-current flows. Coast Eng 23:289–304
You ZJ (1998) Initial motion of sediment in oscillatory flow. J Waterway Port Coast Ocean Eng, ASCE 124:68–72
You ZJ (2005) Estimation of bed roughness from mean velocities measured at two levels near the seabed. Cont Shelf Res 25:1043–1051
You ZJ (2007) Extrapolation of extreme wave height with a proper probability distribution function. Australasian coasts and ports conference, 17–20 July, Melbourne
You ZJ (2009a) A close approximation of wave dispersion relation for direct calculation of wavelength in any coastal water depth. Appl Ocean Res 30:133–139
You ZJ (2009b) Statistical distribution of nearbed wave orbital velocity in intermediate coastal water depth. Coast Eng 56:844–852
You ZJ (2010) A unified method for calculation of wave spectrum and wave height distribution. AMSA conference, Wollongong
You ZJ (2011) Uncertainty in extrapolating a historical wave record to extreme wave heights. Australasian coasts and ports conference, 28–30 Sep, Perth

You ZJ (2011b) Extrapolation of historical coastal storm wave data with best-fit distribution function. Aust J Civ Eng 9:73–82
You ZJ (2012) Discussion of "a Multi-distribution Approach to POT Methods for Determining Extreme Wave Heights" by Mazas and Hamm. Coast Eng 58:385–394
You ZJ, Hanslow D (2001) Statistical distribution of nearbed wave orbital velocity under irregular waves. Australasian coastal engineering and ports conference, Gold Coast, pp 412–416
You ZJ, Jayewardene I (2003) The occurrence of extreme coastal storms along the NSW coast. Australian national environment conference, Brisbane
You ZJ, Lord D (2008) Influence of the El Nino Southern Oscillation on the NSW coastal storm severity. J Coast Res 24:203–207
You ZJ, Yin BS (2007) Estimation of extreme coastal waves from time series of wave data. China Ocean Eng 20:225–241

Chapter 23
Effects of Stratification on Multi-layered Tsunami Waves

Monzur A. Imteaz, Fatemeh Mekanik, and Amimul Ahsan

Abstract Widely used tsunami warning systems are based on numerical simulations and consider a single layer system, i.e. it is considered that the whole depth of ocean water is having a single density, which is not a realistic approximation. In order to develop a generalized numerical model for multi-layered tsunami wave system, a three-layer system was developed earlier. Six governing equations, two for each layer were derived from Euler equations of motion and continuity for three layers, assuming long wave approximation, negligible friction and interfacial mixing. Developed governing equations were converted to a numerical model using staggered Leap-Frog scheme for the computations of water level and discharge in each layer in one-dimensional propagation. Developed numerical model results were earlier validated (through converting it to a pseudo two- layer model) with a two-layer model, which was rigorously verified by analytical solution. This paper presents effects of stratification on the amplification and water levels of tsunami waves. For the representation of the magnitude of stratification, a new dimensionless number named "stratification number" has been proposed. The model has been simulated for several combinations of layer densities. It is found that with the increase in stratification number magnitude of wave surface level as well as wave amplitude decrease.

M.A. Imteaz (✉) • F. Mekanik
Faculty of Engineering and Industrial Sciences, Swinburne University of Technology, Hawthorn, Melbourne, VIC 3122, Australia
e-mail: mimteaz@swin.edu.au

A. Ahsan
Faculty of Engineering and Industrial Sciences, Swinburne University of Technology, Hawthorn, Melbourne, VIC 3122, Australia

Department of Civil Engineering (Green Engg. & Sust. Tech. Lab, Institute of Advanced Technology), University Putra Malaysia, Selangor, Malaysia

C.W. Finkl (ed.), *Coastal Hazards*, Coastal Research Library 6,

DOI 10.1007/978-94-007-5234-4_23,

23.1 Introduction

Tsunamis can cause widespread coastal hazards including loss of lives, damages to infrastructures, damages to coastal ecosystems and agriculture. On top of that recently occurred tsunami in Japan proved how tsunami havoc can impact on extremely sensitive coastal nuclear establishments and indirectly cause widespread nuclear pollutions. These coastal hazards can be minimized through proper and efficient tsunami warning system. During 2011 Tohoku earthquake (magnitude 9.0) and subsequent tsunami, Japanese tsunami warning system failed to produce accurate predictions (Nature 2011). Widely used tsunami warning systems are based on numerical simulations and consider a single layer system, i.e. it is considered that the whole depth of ocean water is having a single density, which is not a realistic approximation. In order to develop a generalized numerical model for multi-layered tsunami wave system, a three-layer system was developed earlier. Six governing equations, two for each layer were derived from Euler equations of motion and continuity for three layers, assuming long wave approximation, negligible friction and interfacial mixing. Developed governing equations were converted to a numerical model using staggered Leap-Frog scheme for the computations of water level and discharge in each layer in one-dimensional propagation. Developed numerical model results were earlier validated (through converting it to a pseudo two- layer model) with a two-layer model, which was rigorously verified by analytical solution. This chapter presents effects of stratification on the amplification and water levels of tsunami waves. For the representation of the magnitude of stratification, a new dimensionless number named "stratification number" has been proposed. The model has been simulated for several combinations of layer densities. It is found that with the increase in stratification number magnitude of wave surface level as well as wave amplitude decrease.

23.2 Background

Multi-layered flow is related with many environmental phenomena. Thermally driven exchange flows through doorways to oceanic currents, salt water intrusion in estuaries, spillage of the oil on the sea surface, spreading of dense contaminated water, sediment laden discharges into lakes, generation of lee waves behind a mountain range and tidal flows over sills of the ocean are examples of multi-layered flow. In hydraulics, this type of flow is often termed as gravity current. An extensive review on hydrodynamics of various gravity currents was provided by Simpson (1982).

Tsunamis are generated due to disturbances of free surfaces caused by not only seismic fault motion, but also landslide and volcanic eruptions (Imamura and Imteaz 1995). Tsunami waves are also affected by density differences along the depth of ocean. There are some studies on two-layered long waves or flows in the case of underwater landslide generated tsunamis (Hampton 1972; Parker 1982; Harbitz 1991; Jiang and Leblond 1992). Imamura and Imteaz (1995) developed a

linear numerical model on two-layered long wave flow, which was successfully validated by a rigorous analytical solution. Later the linear model was extended to a non-linear model and effects of non-linearity were investigated (Imteaz and Imamura 2001b). Madsen et al. (2002) developed a model of multi-layered flow based on Boussinesq-type equations, which are suitable for shallow depth flow. Lynett and Liu (2004) developed another model of multi-layered flow using piecewise integration of Laplace equation for each individual layer and expanded the model for deep water.

Choi and Camassa (1996) derived two-dimensional non-linear equations for two-layered fluid system and presented some numerical simulations of their model for one-dimensional unidirectional wave propagation. Later Choi and Camassa (1999) further developed governing equations for the unidirectional propagation of internal gravity waves at the interface of two immiscible inviscid fluids. They have compared their numerical results with available experimental data for solitary waves of large amplitude in two-fluid system. Liska and Wendroff (1997) derived one-layer and two-layer classic shallow water equations for flow over topography, as well as one-layer and two-layer non-hydrostatic equations. They have compared their numerical results with the numerical computations obtained by others. Percival et al. (2008) presented a multi-layer extension of Green-Naghdi equations (Green and Naghdi 1976) using a special framework based on the Euler-Poincare theory. Through numerical simulations they have shown that free surface of a multi-layer model can exhibit intriguing differences compared to the results of single layer model. Cotter et al. (2010) modified the multi-layer Green-Maghdi equations to incorporate effects of shear stress. They have presented numerical simulations for the wave propagation and interactions between two layers, with and without shear considerations.

All the above mentioned models, presented their results in two-layer case only. However, interactions within the layers for a two-layer fluid are significantly different than a three (or more) layer fluid. Top surface is having effect from the immediate lower layer only, which is the same for both models; however, intermediate layer is having effects from both the lower and upper layers; and the lower layer is having effects from all the upper layers (Imteaz et al. 2009). Imteaz et al. (2009) provided detailed derivation of multi-layered tsunami wave and flow equations derived from Navier-Stokes equation. Also, properties of multi-layered equations were discussed in details. Finally, based on the developed equations, numerical model for the multi-layered tsunami waves was developed and validated by Imteaz et al. (2011). This chapter presents effects of stratification on the simulations of multi-layered tsunami waves.

23.3 Governing Equation

Figure 23.1 shows the schematic diagram of three layer propagation having different densities and depths. For a three layered one-dimensional propagation, Euler's equations of motion and continuity were converted to simpler continuity and

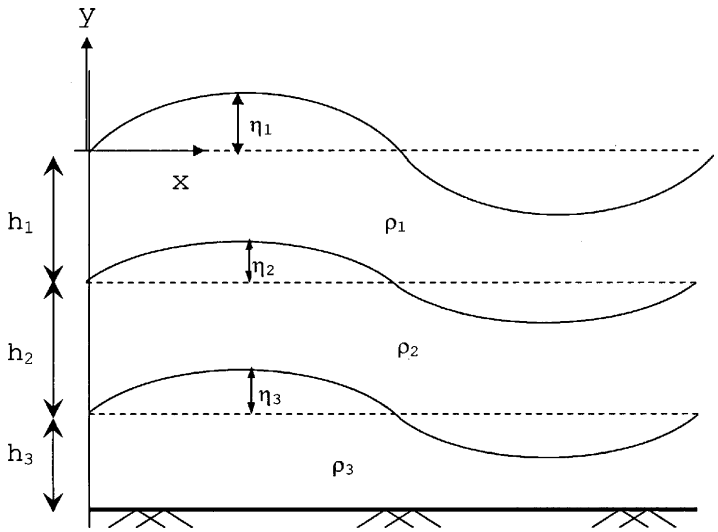

Fig. 23.1 Schematic diagram of three layer profile

momentum equations for each layer through integration and rigorous formulations. In the derivation process a wide channel with non-horizontal bottom was considered. Moreover, a hydrostatic pressure distribution, negligible friction, negligible interfacial mixing, uniform density and velocity distributions (within a layer) were assumed. In this chapter, original derived equations are further simplified ignoring non-linear terms and considering horizontal bottom (i.e. no variations of 'h' along × direction, $\partial h/\partial x = 0$).

Detailed derivations of mathematical equations are described by Imteaz et al. (2009). The equations are as follows:

For the upper layer-

Continuity equation,

$$\frac{\partial M_1}{\partial x} + \frac{\partial(\eta_1 - \eta_2)}{\partial t} = 0 \tag{23.1}$$

Momentum equation,

$$\frac{\partial M_1}{\partial t} + gD_1\frac{\partial \eta_1}{\partial x} = 0 \tag{23.2}$$

For the intermediate layer-

Continuity equation,

$$\frac{\partial M_1}{\partial x} + \frac{\partial(\eta_1 - \eta_2)}{\partial t} = 0 \tag{23.3}$$

Momentum equation,

$$\frac{\partial M_2}{\partial t} + g D_2 \left\{ \frac{\alpha_1}{\alpha_2} \left(\frac{\partial \eta_1}{\partial x} - \frac{\partial \eta_2}{\partial x} \right) + \frac{\partial \eta_2}{\partial x} \right\} = 0 \tag{23.4}$$

For the lower layer-
Continuity equation,

$$\frac{\partial M_2}{\partial x} + \frac{\partial \eta_2}{\partial t} = 0 \tag{23.5}$$

Momentum equation,

$$\frac{\partial M_3}{\partial t} + g D_3 \left\{ \alpha_1 \left(\frac{\partial \eta_1}{\partial x} - \frac{\partial \eta_2}{\partial x} \right) + \frac{\partial \eta_3}{\partial x} + \alpha_2 \left(\frac{\partial \eta_2}{\partial x} - \frac{\partial \eta_3}{\partial x} \right) \right\} = 0 \tag{23.6}$$

Where,

η_1 = Water surface elevation above still water level of layer '1'
η_2 = Water surface elevation above still water level of layer '2'
η_3 = Water surface elevation above still water level of layer '3'
$D_1 = \eta_1 + h_1 - \eta_2$, $D_2 = h_2 + \eta_2 - \eta_3$, $D_3 = h_3 + \eta_3$, $\alpha_1 = \rho_1/\rho_3$, $\alpha_2 = \rho_2/\rho_3$
h_1 = Still water depth of layer '1'
h_2 = Still water depth of layer '2'
h_3 = Still water depth of layer '3'

$$M_1 = \int_{-h_1+\eta_2}^{\eta_1} u_1 dy, M_2 = \int_{-h_1-h_2+\eta_3}^{-h_1+\eta_2} u_2\, dy, M_3 = \int_{-h_1-h_2-h_3}^{-h_1-h_2+\eta_3} u_3\, dy$$

From the derived equations, it is found that momentum equation for upper layer is not affected by the properties of adjacent layer (layer underneath). However, continuity equation of upper layer is affected by surface elevation of intermediate layer. Continuity equation for intermediate layer is affected by the surface elevation of bottom layer. Momentum equation for intermediate layer is affected by density and spatial change of surface elevation of upper layer. Continuity equation for bottom layer is not affected by either uppermost layer or intermediate layer. However, momentum equation of bottom layer is affected by densities and spatial changes in surface elevations of all the layers above it. Properties of

all these equations were described in detailed by Imteaz et al. (2009). Also, wave celerity of each layer was deduced as follows:

$$C_1 = \sqrt{gh_1(1+\alpha_3\beta_1)}, \quad C_2 = \sqrt{gh_2(1-\alpha_3+\beta_2(\alpha_2-\alpha_1))},$$
$$C_3 = \sqrt{gh_3(1-\alpha_2)}$$

where, C_1, C_2 & C_3 are the wave celerities for the layers 1, 2 & 3 respectively. And, $\beta_1 = \frac{h_2}{h_1}$ and $\beta_2 = \frac{h_3}{h_2}$

23.4 Numerical Model

It is found that the developed governing equations are complicated having influence(s) from upper and/or lower layer(s) flow(s). Analytical solutions for such complicated differential equations are yet to be achieved. However, using proper numerical scheme it is possible to solve the governing equations with good accuracy. Numerical models for two layer tsunami waves were validated with analytical solutions for known interface propagation to predict unknown top surface propagation by Imamura and Imteaz (1995) and for known top surface propagation to predict unknown interface propagation by Imteaz and Imamura (2001a). In those validation studies a special numerical scheme named "Staggered Leap-Frog scheme" was used for the numerical simulations. It was found that Staggered Leap-Frog scheme produce very good results for those governing equations. In the current study, same numerical scheme has been used for the development of three-layer model. Figure 23.2 shows the schematic diagram of the staggered Leap-Frog scheme. This scheme is one of the explicit central difference schemes with the truncation error of second order. The staggered scheme considers that the computation points of one variable (η) do not coincide with the computation points of the other variable (M). There are half step differences (½Δt and ½Δx) between computation points of two variables (as shown in Fig. 23.2). Using this scheme, finite difference equations for the derived governing equations are as follows:

For the upper layer-

Continuity equation,

$$\frac{\eta_{1,i}^{n+1/2} - \eta_{1,i}^{n-1/2} - \eta_{2,i}^{n+1/2} + \eta_{2,i}^{n-1/2}}{\Delta t} + \frac{M_{1,i+1/2}^{n} - M_{1,i-1/2}^{n}}{\Delta x} = 0 \tag{23.7}$$

Momentum equation,

$$\frac{M_{1,i+1/2}^{n} - M_{1,i+1/2}^{n-1}}{\Delta t} + g\frac{D_{1,i+1}^{n-1/2} + D_{1,i}^{n-1/2}}{2}\frac{\eta_{1,i+1}^{n-1/2} - \eta_{1,i}^{n-1/2}}{\Delta x} + \tag{23.8}$$

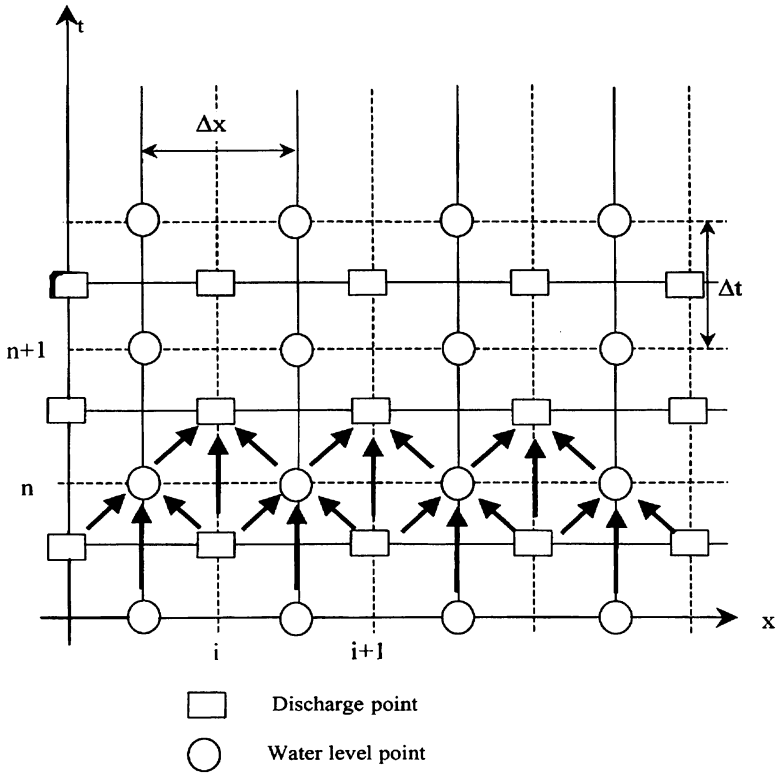

Fig. 23.2 schematic diagram of the staggered Leap-Frog scheme

For the intermediate layer-
Continuity equation,

$$\frac{\eta_{2,i}^{n+1/2}-\eta_{2,i}^{n-1/2}-\eta_{3,i}^{n+1/2}+\eta_{3,i}^{n-1/2}}{\Delta t}+\frac{M_{2,i+1/2}^{n}-M_{2,i-1/2}^{n}}{\Delta x}=0 \tag{23.9}$$

Momentum equation,

$$\begin{aligned}&\frac{M_{2,i+1/2}^{n}-M_{2,i+1/2}^{n-1}}{\Delta t}+g\frac{D_{2,i+1}^{n-1/2}+D_{2,i}^{n-1/2}}{2}\\&\times\left[\frac{\alpha_1}{\alpha_2}\left(\frac{\eta_{1,i+1}^{n-1/2}-\eta_{1,i}^{n-1/2}}{\Delta x}-\frac{\eta_{2,i+1}^{n-1/2}-\eta_{2,i}^{n-1/2}}{\Delta x}\right)+\frac{\eta_{2,i+1}^{n-1/2}-\eta_{2,i}^{n-1/2}}{\Delta x}\right]\\&=0\end{aligned} \tag{23.10}$$

For the lower layer-
Continuity equation,

$$\frac{\eta_{3,i}^{n+1/2}-\eta_{3,i}^{n-1/2}}{\Delta t}+\frac{M_{3,i+1/2}^{n}-M_{3,i-1/2}^{n}}{\Delta x}=0 \tag{23.11}$$

Momentum equation,

$$g\frac{D_{3,i+1}^{n-1/2}+D_{3,i}^{n-1/2}}{2}\left[\alpha_1\left(\frac{\eta_{1,i+1}^{n-1/2}-\eta_{1,i}^{n-1/2}}{\Delta x}-\frac{\eta_{2,i+1}^{n-1/2}-\eta_{2,i}^{n-1/2}}{\Delta x}\right)\right]+$$
$$g\frac{D_{3,i+1}^{n-1/2}+D_{3,i}^{n-1/2}}{2}\left[\frac{\eta_{3,i+1}^{n-1/2}-\eta_{3,i}^{n-1/2}}{\Delta x}+\alpha_2\left(\frac{\eta_{2,i+1}^{n-1/2}-\eta_{2,i}^{n-1/2}}{\Delta x}-\frac{\eta_{3,i+1}^{n-1/2}-\eta_{3,i}^{n-1/2}}{\Delta x}\right)\right]$$
$$+\frac{M_{2,i+1/2}^{n}-M_{2,i+1/2}^{n-1}}{\Delta t}=0 \tag{23.12}$$

where, 'n' denotes the temporal grid points and 'i' denotes the spatial grid points as shown in Fig. 23.2. To calculate 'D' values at the computation points of 'M', the average of four surrounding 'D' values were taken.

In spatial direction all η_1, η_2 and η_3 at step 'n−1/2' and all M_1, M_2 and M_3 at step '(n−1)' are given as initial conditions. For all later time steps at right boundary all values of M_1, M_2 and M_3 are calculated by characteristic method, using the values of previous time step and wave celerity. By using deduced finite difference Momentum equations for upper, intermediate and lower layer all M_1, M_2 and M_3 values at step 'n' are calculated. Then using the latest values of M_3 and deduced finite difference continuity equation for the lower layer all the values of η_3 at step '(n + 1/2)' are calculated. Then using the latest values of η_3, M_2 and deduced finite difference continuity equation for the intermediate layer, all the values of η_2 at step '(n + 1/2)' are calculated. Again, using the latest values of η_2, M_1 and deduced finite difference continuity equation for the upper layer, all the values of η_1 at step '(n + 1/2)' are calculated. Similarly, using new values of η_1, η_2, η_3, M_1, M_2 and M_3 as initial conditions calculations proceeded in time direction up to the desired time step.

As initial condition (i.e. at t = 0) all η_1, η_2, M_1 and M_2 values are taken as zero. For interface (between bottom layer and intermediate layer), assumed initial conditions are shown in Equations 13 & 14, which are based on the initial formation of tsunami wave. Expression of η_3,

$$\eta_3 = a_3\ \mathrm{Sin}\ (kx) = a_3\ \mathrm{Sin}\left(\frac{2\pi}{L}x\right) \tag{23.13}$$

and corresponding discharge,

$$M_3 = \sqrt{(g/h_3)}\,\eta_3\,(h_3+\eta_3) \tag{23.14}$$

where, a_3, k and L are the wave amplitude, wave number and wave length for the interfacial surface of intermediate layer and the bottom layer.

While computing water levels and discharges using Staggered Leap-Frog scheme, it is required to calculate boundary values (right and left boundaries) of water levels and discharges, using appropriate boundary conditions. Imamura and Imteaz (1995) discussed several possible boundary conditions. Among all the possible boundary conditions, it was found that the following provides good results for non-linear model simulations (Imteaz and Imamura 2001b): M_1, M_2 and M_3 at the right boundary are calculated using characteristic method; constant wave celerities (which were estimated using analytical expressions) were used throughout the computational domain. Finally, using periodic condition, water levels at the left boundary were used as the same as the right boundary. However, it is to be noted that for the sake of computational simplicity a periodic boundary condition was assumed, in reality tsunami waves are not periodic.

As the developed three-layer model could not be verified with an analytical solution, it was indirectly compared with an earlier validated two-layer numerical model. Developed model was converted to a pseudo two-layer model by assuming very close densities (1.0 and 0.99) for the intermediate and bottom layers respectively, with an upper layer density of 0.90. This numerical manipulation is supposed to produce similar results with a two-layer model having densities of 0.90 and 1.0 for the upper layer and lower layer respectively, provided depth of upper layer in both the two-layer and three-layer models are the same and total depth of lower layers (intermediate layer and bottom layer) in three-layer model is the same as the bottom layer of the two-layer model. Two separate models (two-layer model and three-layer model) were simulated with the same boundary conditions and it was found that the pseudo three-layer model simulations for water levels (top surface and interface) are very close to the simulations of original two-layer model. Details of the simulations and comparisons are provided in Imteaz et al. (2011). In this chapter, the developed 3-layer numerical model has been used to investigate the effects of stratification on water levels and wave amplitudes of different layers.

23.5 Effects of Stratification

For this investigation, a three-layer (each layer having same height of 10 m) flow system was considered. For the bottom layer, a known wave profile using Equation 13 was applied, with wave amplitude of 2 m. The model simulated wave propagations and amplitudes of intermediate surface and top surface under different stratification/density conditions. To quantify the extent of stratification, a new dimensionless number named “stratification number” has been introduced as follows:

Table 23.1 List of input dataset for model simulations

Variables	Dataset 1	Dataset 2	Dataset 3	Dataset 4	Dataset 5
$\rho_1 =$	1.040	0.95	0.85	0.75	0.65
$\rho_2 =$	1.045	1.00	0.95	0.90	0.85
$\rho_3 =$	1.050	1.05	1.05	1.05	1.05
$S_N =$	0.014	0.15	0.32	0.50	0.71

$$S_N = \frac{\sum_{i=2}^{N} |\rho_i - \rho_{i-1}|/(N-1)}{\sum_{i=1}^{N} \rho_i/N}$$

where, N is the total number of layers and ρ_i is the density of any layer 'i'. Table 23.1 shows the input dataset for different model options. For each case, ΔX and ΔT were considered as 20.0 m and 0.20 s respectively. A wave length of 380 m was considered for all the simulations.

Figure 23.3 shows model simulations for normalized water levels against normalized distance for the top surface, intermediate surface and bottom surface using dataset 3. Computed results are presented at different times (after starting from initial condition) 4, 6 & 8 s. Figure 23.4 shows the effects of stratification number (S_N) on normalized maximum water levels for the top surface, intermediate surface and bottom surface. Water levels were normalized by dividing the 'η' values with the individual layer's depth (which was considered 10 m for each of the layers). Maximum water levels were presented to assess the severity of tsunami waves. It is found that for all the surfaces normalized maximum water levels decreases with the increase in stratification number. Graphs were presented for three simulation periods (4, 6 & 8 s). This finding is in contrary with earlier finding using a two-layer tsunami model, which revealed that wave amplifications gets higher with the increase in stratification. This finding requires further investigations. Figure 23.5 shows the effects of stratification number (S_N) on the absolute wave amplitudes for the top surface, intermediate surface and bottom surface. Similar phenomena were observed for wave amplitudes also, i.e. wave amplitudes for all the layers decreases with the increase in stratification number. An initial known wave amplitude of 2.0 m was considered for the lower layer. It is found that simulated wave amplitudes for the top layer and intermediate layer were within the range of 0.40 m to 1.30 m. So, both the wave amplitude and magnitude of water level (above still water level) for all the layers decreases with the increase in stratification number.

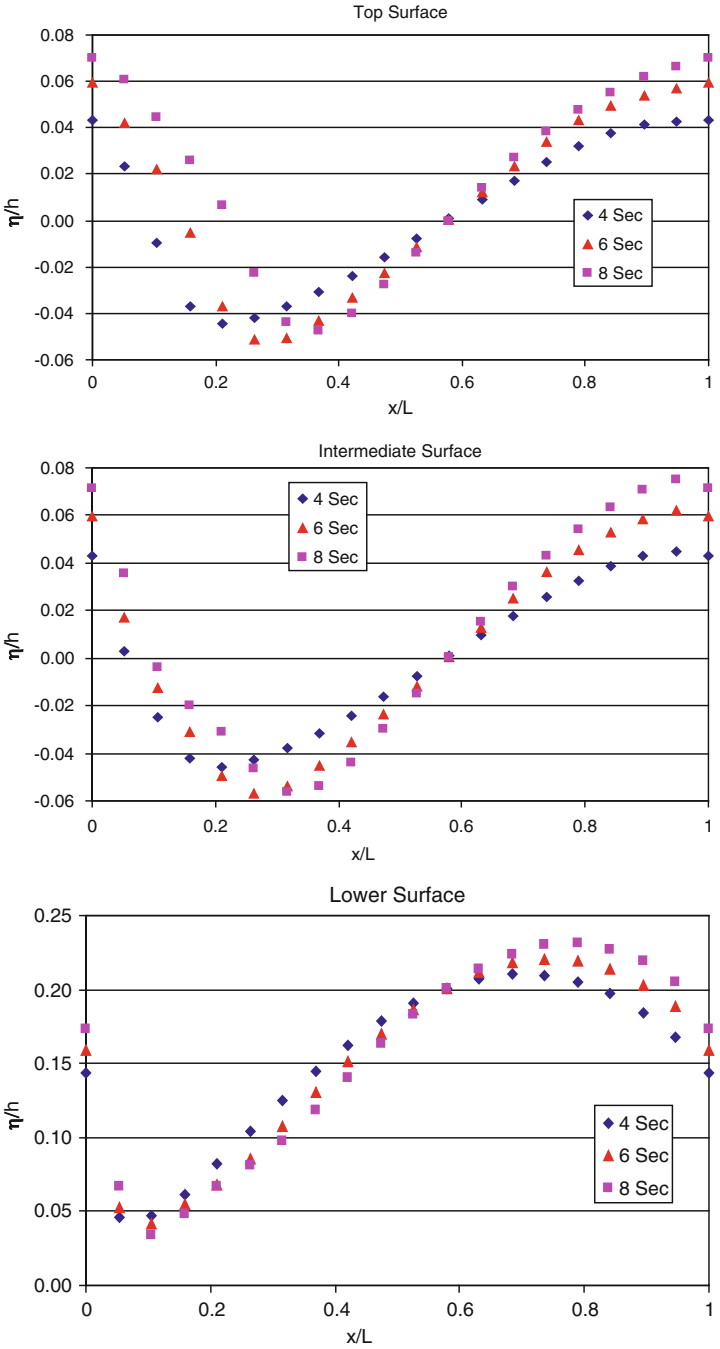

Fig. 23.3 Simulation results for normalized water levels using dataset 3

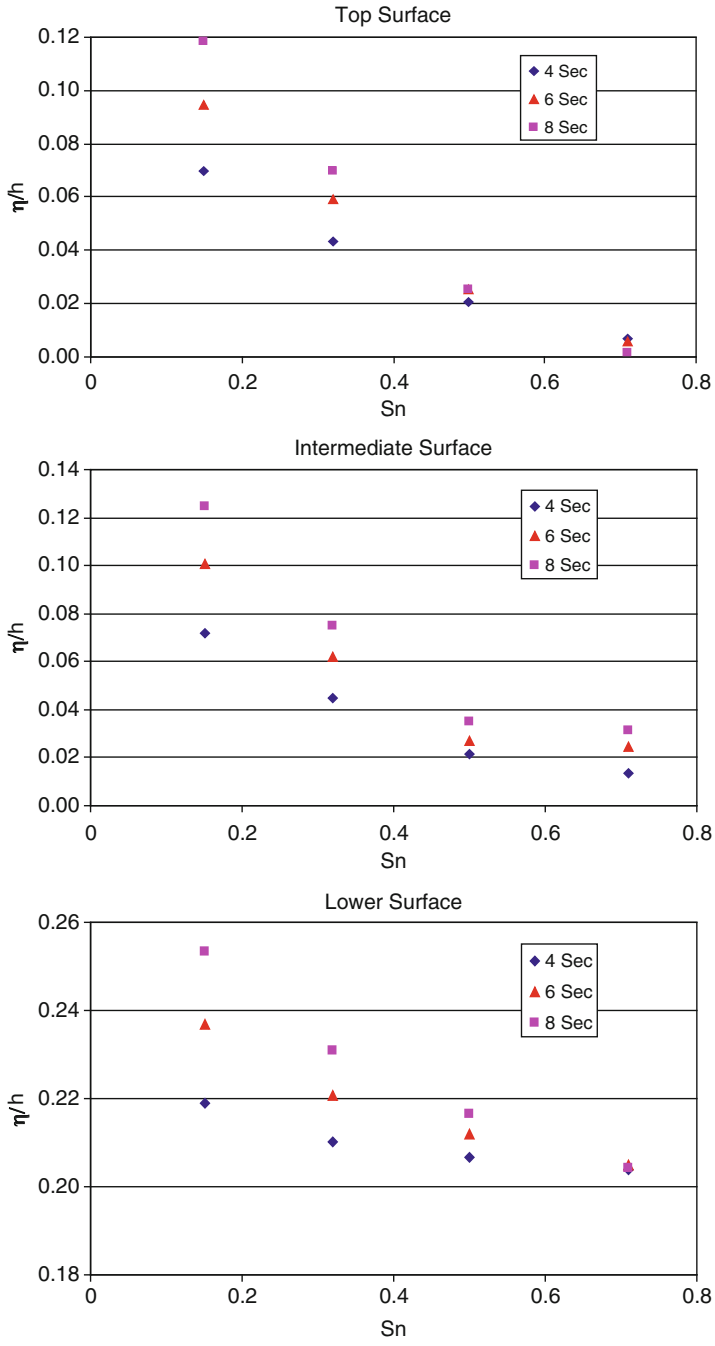

Fig. 23.4 Effects of 'Stratification Number' on normalized water levels

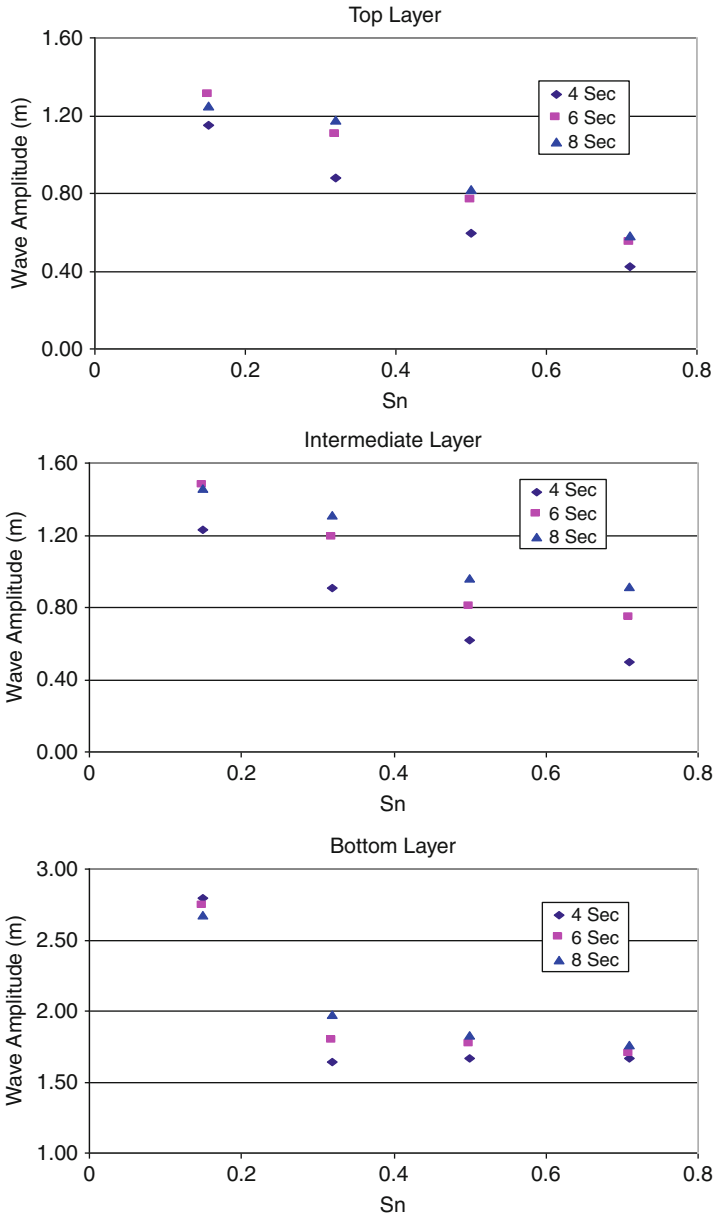

Fig. 23.5 Effects of 'Stratification Number' on wave amplitudes

23.6 Conclusion

Earlier developed governing equations for three layered long waves are complex having several interactions from adjacent/all layers, which make those equations very difficult to solve analytically. Analytical solutions for these sorts of equations are yet to be succeeded. However, in the future if such analytical solution is achieved, numerical results of the current model can be verified analytically.

To achieve a numerical solution, governing equations were transformed into numerical formulations. Original derived equations were simplified considering horizontal bottom (i.e. no variations of 'h' along $\times$ direction, $\partial h/\partial x = 0$). A numerical model was developed using staggered Leap-Frog scheme, as the same scheme produced good results for two layer numerical models. The model was simulated considering three separate layers of constant and equal depth (10.0 m), having different combinations of densities. To quantify the magnitude of stratification a new non-dimensional number named, "stratification number" has been proposed. To analyse the effects of stratification, model outcomes (wave amplitudes and water surface levels) were presented with respect to varying "stratification number".

It is found that with the increase in magnitude of stratification (stratification number), wave amplitudes and water surface levels of upper surfaces decrease. However, results from an earlier two-layer model revealed that with the increase in stratification, wave amplitude and level increase. Current findings with a three-layer model contradict with the earlier findings of a two-layer model. However, current findings are more acceptable compared to earlier findings. In a two-layer model, interaction from only an adjacent (upper/lower) layer was considered, whereas in the current three-layer model, interactions from all the adjacent and upper layers were considered. Latest findings on reductions in wave amplitudes are results of complicated interactions among the stratified layers. However, these findings need further verification.

23.7 Notations

ρ = Density of fluid
M = Discharge per unit width of flow
η = Water surface elevation above still water level
h = Still water depth for a particular layer
D = Total depth of layer
α = Ratio of density of upper layer fluid to lower layer fluid
x = Distance along downstream direction
y = Distance perpendicular to x-direction
u = Uniform velocity over the depth along x-direction
v = Uniform velocity along y-direction

P = Hydrostatic pressure of fluid
β = Ratio of depths of lower layer to upper layer
C = Wave celerity

References

Choi W, Camassa R (1996) Weakly nonlinear internal waves in a two-fluid system. J Fluid Mech 313:83–103
Choi W, Camassa R (1999) Fully nonlinear internal waves in a two-fluid system. J Fluid Mech 396:1–36
Cotter CJ, Holm DD, Percival JR (2010) The square root depth wave equations. Proc Royal Soc A. doi:10.1098/rspa.2010.0124
Green AE, Naghdi PM (1976) A derivation of equations for wave propagation in water of variable depth. J Fluid Mech 78:237–246
Hampton MH (1972) The role of subaqueous debris flow in generating turbidity currents. J Sediment Petrology 42(4):775–793
Harbitz C (1991) Numerical simulations of slide generated water waves. Sci Tsunami Hazards 9 (1):15–23
Imamura F, Imteaz MA (1995) Long waves in two-layers: governing equations and numerical model. Sci Tsunami Hazards 13(1):3–24
Imteaz MA, Imamura F (2001a) Analytical solution and numerical model for the interface in a stratified long wave system. Sci Tsunami Hazards 19(1):39–54
Imteaz MA, Imamura F (2001b) A non-linear numerical model for stratified tsunami waves and its application. Sci Tsunami Hazards 19:150–159
Imteaz MA, Imamura F, Naser J (2009) Governing equations for multi-layered tsunami waves. Sci Tsunami Hazards 28(3):171–185
Imteaz MA, Imamura F, Naser J (2011) Numerical model for multi-layered tsunami waves. In: Mörner N-A (ed) Tsunami threat: research and technology. IN-TECH publishers, Croatia. ISBN 978-953-307-552-5
Jiang L, Leblond PH (1992) The coupling of submarine slide and the surface waves which it generates. J Geophys Res 97(C8):12713–12744
Liska R, Wendroff B (1997) Analysis and computation with stratified fluid models. J Comput Phys 137(1):212–244
Lynett P, Liu PL-F (2004) Linear analysis of the multi-layer model. J Coastal Eng 51:439–454
Madsen PA, Bingham HB, Liu H (2002) A New boussinesq method for fully nonlinear waves from shallow to deep water. J Fluid Mech 462:1–30
Nature (2011) //www.nature.com/news/2011/110811/full/news.2011.477.html, viewed on 22 February 2012
Parker G (1982) Conditions for ignition of catastrophically erosive turbidity currents. Mar Geol 46:307–327
Percival JR, Cotter CJ, Holm DD (2008) A Euler–Poincaré framework for the multilayer Green–Naghdi equations. J Phys A: Math Theoret 41:34
Simpson JE (1982) Gravity currents in the laboratory, atmosphere and ocean. AnnRev Fluid Mech 14:213–234

Part IX
Coastal Marine Pollution

Chapter 24
The Hazards of Beach Litter

A.T. Williams, K. Pond, A. Ergin, and M.J. Cullis

Abstract Marine and beach litter include items that have been made and discarded into the marine environment by people. Over the past few decades concern has been growing regarding the amounts of litter that accumulate on beaches and seas. Litter issues have become very widespread of late due to public awareness and concern for environmental issues. Beach litter is sourced from three areas: marine, industrial and domestic wastes dumped at sea and riverine and beach litter. Such debris mars beach enjoyment, has safety implications (e.g. glass, syringes), needs cultural/attitudinal changes in order to reduce and prevent waste reaching both sea, and beaches. Irrespective of source, litter, the main culprit being plastics, is ubiquitous on global beaches and a perennial problem for any coastal manager. Plastics alone amount to some 265m tonnes worldwide much being recreational litter. Current litter policy must be geared to stopping it at source. Recycling plastics is often seen as a panacea to reducing such waste with many countries pushing for higher targets

A.T. Williams
Built & Natural Environment, Swansea Metropolitan University, Swansea SA1 6ED, Wales, UK

e-GEO Centro de Estudos de Geografia e Planeamento Regional, Faculdade de Ciências Sociais e Humanas, Universidade Nova de Lisboa, Lisbon, Portugal
e-mail: allan.williams@virgin.net

K. Pond
Robens Centre for Public and Environmental Health, University of Surrey, Guildford, UK
e-mail: k.pond@surrey.ac.uk

A. Ergin
Civil Engineering Department, Middle East Technical Univeristy, Ankara, Turkey
e-mail: ergin@metu.edu.tr

M.J. Cullis (✉)
Built & Natural Environment, Swansea Metropolitan University, Swansea SA1 6ED, Wales, UK

University of Surrey, Guildford, UK

Middle East Technical Univeristy, Ankara, Turkey
e-mail: mike.cullis@smu.ac.uk

C.W. Finkl (ed.), *Coastal Hazards*, Coastal Research Library 6,
DOI 10.1007/978-94-007-5234-4_24,

year by year. Current recycling policy is questionable, lacking workable solutions; in effect, a '*knowledge lag*' exists with money being the inevitable forcing function. Figures from the USA show that just 33.4% of plastics are recycled; work done by WRAP in the UK suggest that 45% is achievable. Comparable and reliable methods to evaluate beach plastic litter are currently the weakest point of this particular scientific community. Marine debris can have serious effects on wildlife and their ecosystems; in some instances, such occurrences will be lethal. Clearly, it is essential that beach litter surveys obtain a representative sample by looking at annual litter counts; baseline studies should identify material types. Litter itself constitutes a serious hazard as shown from a number of previous studies, which suggest environmental quality and public health needs to be considered as key indicators. A universal approach inclusive of stringent regulations, particularly for plastic must be developed; incisive, risk-taking innovative technologies, especially in the chemistry of plastics are needed in order to solve the challenges ahead. In essence, to change the way we think about the environment.

24.1 Introduction

A *hazard* – an abstract idea with disaster as its realisation, is a set of circumstances caused by extraneous forces, usually physical environmental elements but sometimes human induced, that could lead to harm i.e. death, injury or an illness of a person and or property. Hazards come in various guises, i.e. natural/anthropogenic, rapid/slow, intense/diffuse; rare/chronic, high/low energy and are functions of risk, exposure and response**.** The *risk* of an event happening is the probability that it will occur due to exposure to a defined hazard degree, i.e. = f (probability of occurrence, vulnerability), or sometimes as =f (hazard, vulnerability) and this causes loss. Risks can vary from negligible – an adverse event occurring at a frequency of >one per million, e.g. asteroid hitting the earth; *via* events such as, bathers stepping on a plank with a nail protruding through it, a syringe etc; to fairly regular events, such as, illness through swimming in contaminated waters.

Although literature relating to beach litter tends to be primarily from the 1990s, the litter issue has become very prevalent of late mainly due to public awareness and concern for environmental issues. The public expect local, national and even international action. Additionally, there appears to be a growth in outdoor activities, tourism, and fish farming activities which in turn has lead to an increase in litigation threats with regards to beach bathing water quality. In the literature, significant quantities of land-sourced debris (litter) have been reported, but knowledge of amounts and distributions are limited (Coe and Rogers 1997; Table 24.1), although a few areas have been looked at in some depth, e.g. Santos et al. (2005); Ivar do Sul and Costa (2007). In the main, beach debris is derived from three main sources: marine (commercial fishing vessels, cruise ships, recreational vessels, stationary platforms (Fig. 24.1), together with industrial and domestic wastes disposed of at sea); riverine; and beach user discards, such as, drink cans from recreation or unauthorised dumping of larger items such as landfill materials – 'land borne litter',

Table 24.1 Litter sources

The main land-based sources of marine litter
Municipal landfills (waste dumps) located on the coast
Riverine transport of waste from landfills or other sources, e.g. fly tipping along rivers and other inland waterways (canals)
Discharge of untreated municipal sewage, including storm water (including occasional overflows)
Industrial facilities: Solid waste from landfills, and untreated waste water
Tourism (recreational visitors to the coast; beach-goers)
The main sea-/ocean-based sources of marine litter
Merchant shipping, ferries and cruise liners, fishing vessels, military fleets and research vessels, pleasure craft, offshore oil and gas platforms, fish farming installations

although the latter could have a riverine origin and be brought to the coast (Corbin and Singh 1993; Rees and Pond 1995a). Litter from any source has the potential to cause damage to people, property and livelihood, e.g. fishing boats and gear, safety risks for people at sea, damage to cooling water intakes, contamination of beaches and harbours, health hazards to people, injuries to grazing cattle etc.

Beach enjoyment is marred by the sight of debris, although perception varies with respect to many parameters, i.e. age, socio-economic status and gender. It is only when a beach is '*severely polluted that visitors perceive (and complain about) it,*' (Silva et al. 2008, 890). Litter studies help raise public awareness of the condition of coastlines so hopefully will show that an attitudinal change is the only guaranteed way of reducing the amount of waste reaching the sea and littering beaches, as *"every individual has a responsibility to contribute to the protection of the environment, in the interests of his or her own health and the health of others"* (WHO 2000).

Before the invention of plastic, the only available mouldable substances were glass, pottery, gum and rubber, but in 1907 Leo Baekeland discovered the first truly synthetic polymer, plastic (termed Bakelite), while researching a substitute for shellac (used in electronic insulation). The plastic was a mixture of phenol (C_6H_5OH) and formaldehyde (HCOH) and was the first material ever produced not based on any material or even molecules found in nature. All plastics are polymers, large molecules of repeating units (each polymer chain has several thousand) of smaller molecules (monomers), chemically bonded repeating units, with the main polymers being composed of carbon and hydrogen alone, or with oxygen, nitrogen, chlorine or sulphur. Common monomers include organic compounds, such as, ethylene, propylene, phenol, formaldehyde, ethylene glycol, acetonitrile, and ones found in marine plastic pellets include polyethylene, polypropylene and polystyrene (Mato et al. 2001). Plastics have extreme versatility and the ability to be tailored to meet very specific technical needs. They are light in weight, 1 tonne of plastic is equivalent to 20,000 two litre drinks bottles or 120,000 carrier bags; are extremely durable, resistant to chemicals, water and impact; are relatively inexpensive to produce, have excellent thermal and electrical insulation properties with good strength and safety, which are important hygienic properties needed for food packaging (www.bpf.co.uk; www.apme.org; www.plasticwaste.co.uk).

Beach litter can constitute a health and safety hazard' as it attracts flies, insects, rats. A series of beach studies over three consecutive years in the UK, showed an apparent fourfold deterioration in environmental quality, where the identified problems of discarded syringes and hypodermic needles, other medical wastes, broken glass and condoms, as well as other non-medical hazardous wastes and litter, helped justify renewed efforts for improved environmental control measures (Philipp 1993; Philipp et al. 1995). As a result of such studies new UK national legislation was introduced: e.g. 6 mm fine-mesh screens on all seawater sewage outfall pipes and removal of screenings for disposal elsewhere; information for the public was distributed which encouraged recreational activities on beaches and healthy behaviour; efforts to protect children against physical hazards such as broken bottles and metal objects by the wearing of footwear on suspect beaches; advice about improving services, such as, the provision of more beach litter bins and their frequent emptying; requests to the public to use the litter bins or take their litter home. Disagreements are current regarding what to do about litter; does one leave it on a beach, as many ecologists would argue, as it provides a rich habitat for a diversity of organisms; or does one go down the mechanical/manual beach cleaning route – see later?

Where many hazards occur in tourist resorts but limited resources exist in which to control them, a priority ranking for the introduction of litter preventive measures should be based on five main questions (Philipp and Hodgkinson 1994):

- How serious is the problem in terms of the likelihood of death, disability, disease, discomfort, or dissatisfaction?
- How many people are likely to be affected during a year?
- To what extent is an intervention technically feasible and likely to relieve or prevent the problem?
- What does an analysis show for the benefits obtained from the risk, adverse effects of the risk, together with the cost implications for different systems of hazard control?
- To what extent is the community likely to accept or adopt the intervention, behaviour or other change required?

24.2 Some Litter Questions That We Currently Only Have Sporadic Answers for

- What are the economic damages/costs associated with litter impact?
- What are the long-term effects of persistent particle breakdown, especially plastics?
- How to prevent litter accumulation, as there is not enough monitored data to source litter items accurately?
- How effective is MARPOL (Annex 5)?

- How marine litter affects populations or whole ecosystems, i.e. how serious is the problem in terms of the likelihood of death, disability, disease, discomfort, or dissatisfaction; how many people/animals are likely to be affected during any time span?

24.3 Litter

There are many definitions of litter, for example, three are:

a. **UNESCO/OSPAR**. Marine litter consists of items that have been made or used by people and deliberately discarded into the sea or rivers or on beaches; brought indirectly to the sea with rivers, sewage, storm water or wind; Accidentally lost, including material lost at sea in bad weather (fishing gear, cargo), or deliberately left by people on shores.
b. **International Convention for the Prevention of Litter from Ships** (MARPOL 1973/1978). Ordinary household waste such as cardboard boxes, empty glass and plastic bottles and other small containers, food waste etc; waste from cargo holds, such as, dunnage, wire straps, and covering material (plastic sheets); non harmful cargo residues; engine room waste which does not come under any other annex; discarded medicinal and sanitary equipment; discarded fishing nets, ropes etc from fishing vessels. More than 78% of the world's shipping are party to this Convention.
c. **UNEP (**2009**)**. Marine litter (debris) includes all objects that do not naturally occur in the marine and coastal environment but are nevertheless found.

Extensive evidence exists that the major source of beach litter is land-borne discharges rather than marine environment pollutants from vessels, oil rigs, etc. (Bean 1987; Faris and Hart 1995). Land-based litter enters the sea through rivers, and/or maybe blown, washed or discharged directly from land. The absence of sewage treatment installations, presence of combined sewer overflows, storm water discharges, runoff from landfills sited by rivers and in coastal areas, absence of waste services or landfills in rural areas, recreational beach users, fly tipping etc. all contribute to beach litter. Irrespective of source, litter, with the main culprit being plastics, is common on global beaches and is a perennial problem for any coastal manager (Derraik 2007; Barnes et al. 2009; Table 2). If one of the main management goals, '*is to reduce the aesthetic effect of litter on beaches.... plastic debris should be the prime target*,'(Widmer and Henneman 2010, 997), as they are ubiquitous, pervasive and unpredictable with new consequences of their presence being discovered all the time. Site specificacy is important, e.g. Silva-Iñiguez and Fisher (2003), found that wood was the main litter found on Baja California beaches; Oigman-Pszczol and Creed (2007), cited paper on Rio de Janeiro beaches.

Table 24.2 Some typical items found on different world beaches: from low water to rear of beach and 50 m width each side of access point

Quilty, Co Clare, Ireland: water bottles, 17, cloth rags 8, pl sheets 1, netting 5 lots of kelp, metal cans 4, tops 8, paper 1, plastic buoy 5, carpets 3, shoes 3, tyre 1 rope 7, plastic pieces 8, cartridge 1, reflector 1, Domestos bottle 1, polyethylene many sweet wrapper 4, plastic cups 5, child's plastic toys 4, straws 2, glass beer bottles 2

Barna, Co Clare, Ireland. Plastic sheets 1, netting 9, rope 16, water bottles 3, green fishing twine 18, caps 3, pl pieces 18, fairy liquid bottle 1, Domestos bottle 1, rubber glove 1, sponge 1, strapping 1, plastic bottles 4, ketchup bottle 1, milk bottle 1, beer cans 8, engine oil cans 4, metal drum lid 1

Hatada, Shirahama, Japan: Plastic forks 12, McDonald cartons 6, shoe, float 8, tennis ball 1 polystyrene many, plastic tops 7, toilet cleaner 2, wood 8, cardboard 1, milk carton 1, tops 5, packing strap 2, lolly sticks 6, plastic bowl and bag 2, light bulb 1, water bottle 1

Irita, Shimoda, Japan: Coca cola 5, beer cans 2, sacks 2, packing straps 6, pl 6, McDonald cartons 12, cloth 1, rope 2, yogurt carton 1, tops 6, plastic shards many, straws 2, polystyrene, 3, rubber straps 5, wood with nails 3

Tojo, Shimoda, Japan: Cig. packet 1, ice cream tub 1, polystyrenes, plastic water bottles 6, straws 3, toilet cleaner 2, glass bottle 1, floats 3, tennis ball 1, plastic bucket 1, large rubber pipe 1, plastic pellets –many

Foster beach, Noyac, Long Island, USA: Beer cans 2, rubber gloves 3, cloth 2, lots of eel grass, plastics 11, netting 6, paper 7, cig butts 2, plastic bottle, straws 2, lolly stick 1

Montauk Point, LI, USA: Balloon 1, Styrofoam cup 1, plastic bag 1, scrap iron (large) 1, coca cola bottle 1, child's pram 1, wood 5, plastic tops 6, socks 3, rubber ball 1, cig. lighters 2, glass bottles 2

Main beach, East Hamptons, LI, USA: Cig. butts 48, paper 11, plastic spoons 2, plastic cups 4, plastic forks 3, tops 3, plastic rope 1, Styrofoam (many), cigar butt 1, 6 dog faeces 7, straws 8, sweet wrappers 5, lolly stick, 2, socks 2, balloons 2, cig. packets 3, plastic bags 2, plastic pieces 19, glass beer bottles 2, beer caps 3

Sagg main beach, Sagaponack, LI, USA: Plastic fork 2, cups 5, bottle1, sand-fence wood 21, Styrofoam 8, tennis ball 1, cartridge case 1, cig. Lighter 1, lolly sticks 5, ropes 3, balloons 2, tops 5, condom 1, dog faeces 4, balloons 3, wood with nails 2

Havens beach, Sag harbour, LI, USA: Fishing twine, string 5, plastic bags 5**,** beer can,, straws 2, plastic pieces 6, paper 6, cig. butts 26, streamers 3, plastic fork 4, balloon 1, plastic pen, cig. lighter 1, cling foil 1, rubber bands 2, fishing twine 6, dog faeces 3, wood 2, cigar holder 1, plastic pellets –many

Alki beach, Seattle, USA: Paper 2, plastics 9, sock 1, newspaper 1, cig. butts 40, glass beer bottle 1, cig foil 8, plastic fork 1, plastic tops 6

Espanosa, Galapagos Islands San Cristobel, Galapagos Islands

2′ by 2′ 2 foot piece of wood 1 m by 30 cm by 20 cm log

2 m by 30 cm 10 cm log 2′ by 2′ by 3 ft log

The above two are 'animal islands' and only certain parties are allowed on them.

Punta Ayora town, Santa Cruz, Galapagos Islands: Bottle tops 12, Plastic bottles (water)15, Paper 10, Light bulb, Milk cartoon, Rope 7, Straws 6, Fishing net parts (green) 7, Netting 8, Wood 3, Glass shards 2dozen plus, Cloth 3, Cig. butts 4, Lolly stick 3, Crisp packets 4, plastic coffee cup 2, Glass bottles 4, sanitary towels 2

Antarctic Peninsula: I ball point pen.

Port Playa, Taquile, Lake Titicaca, Peru: Water bottle 5, plastic bags 4, cig. lighter 1, Dog faeces 6, bottle tops 4

Ramla Bay, Malta: Dog faeces 3, plastic water bottles 16, glass spirit bottles 4, nappies 3, broken glass 7, paper 7, cig. lighters 3, cig. butts 27, tops 16, pens 3, cig. packets 4, plastic bags 5, condom 1

(continued)

Table 24.2 (continued)

Cirali, Turkey: General litter (water bottles, paper, lolly sticks, cans etc.) 135, condom 1, plastic pellets.-many
Paradise Island, Maldives: Two bottle tops
Candolim beach, Goa, India: Typically the general litter was composed of a surprisingly high number of toothbrushes, cosmetic cream holders, glass bottles (unbroken) motor oil containers, polystyrene pieces, shoes, tyres, fishing nets, beer cans, straws, container tops, plastic water bottles, WD 40 cans, plastic bags, shampoo holders, cigarette stubs – 275, Syringes 2, wood with nails 3
West Fiord, Iceland: Cig packet, plastic bottle 2, paper 4
Falkland Islands (Fig. 24.1): Fishing nets 32, planed wood 9, buoys, 6, plastic cups 4, polystyrene pieces many, plastic bags 2, wood with nails 3.plastic pellets – many

(EA/NALG 2000; Source ATW)

24.4 Litter Methodology

Comparable and reliable (calibrated, statistically validated) methods to evaluate beach plastic litter are currently the *weakest* point of this particular scientific community. Questions raised by many beach litter surveys include:

- If litter is there, what is its source and is there a standardised methodology to measure it?
- What are the local perceptions to litter?
- Is litter causing aesthetic/health problems and could these be responsible for any economic losses to the local community?
- Can the effects (if any) be stopped; if so by whom, and what will it cost (Philipp 1993)?

It is essential that all beach litter surveys should obtain a representative sample by looking at annual litter counts, and these baseline studies should identify material types. They are usually carried out by low sampling frequencies over large geographical areas and programme design MUST suit the study aims and objectives and ideally source the litter. Surveys can be on small or large scales (Williams and Simmons 1997) and litter may be categorised according to size (Ribic 1998), weight (YRLMP 1991), or composition (Dixon and Dixon 1981), with the latter being the most favoured. Many organisations exist around the globe which relate to the beach litter problem, *i.e.* Keep Baltic Tidy; Adopt a Beach in California; Marine Education Society of Aetearoa New Zealand; Clean Nova Scotia; Keep Bermuda Beautiful; Coastcare, Australia; Project Aware for divers all over the globe. The USA Ocean Conservancy (OC 2009), co-ordinates the International Coastal Cleanup (ICC), an international network of environmental and civic organizations, government agencies, industries, and individuals working with the objective to remove marine litter and collect valuable information on the amounts and types of litter.

Several guides exist to survey design, such as, Gilbert (1996); Earll et al. (1996), and details needed cover items, such as: site description, map reference, category

Table 24.3 Measurement types

Beach litter survey from water's edge to splash zone
Varying width transects to find the optimum
Transect line quadrats
Strand line counts
Offshore water column
Number of plastic bin bags/trucks etc.
EA/NALG (2000)
USA Ocean Conservancy and UK Marine Conservation Society sourcing approaches

For further information see Williams et al. (2000)

definition, wave, wind, current patterns, site topography and physical characteristics of the beach, measurement units, survey frequency and survey date, all of which need to be identified, and recorded, as well as detailed instructions on how to complete the survey (OC 2009). Table 24.3 is indicative of the many methods researchers utilise, but we would suggest optimising this to the USA Ocean Conservancy (OC 2009) approach which defines 42 litter items relating them to five producing sources, or the similar UK Marine Conservation Society (MCS 2010) sourcing approach, both allied to the beach grading approach of EA/NALG (2000). The EA/NALG (2000), measures litter between the high tide line and back of a beach for a distance of 50 m *either side* of the access point.

Velander and Mocogni (1999) compared strategies looking for the 'best' methodology, and Tudor and Williams (2004) reviewed, for example, the percentage allocation method (Earll et al. 1999); the attribution by litter type method (MCS 2010); sourcing with use of container information, as used by Dixon (1995); use of indicator items (Ribic 1998); matrix scoring method (Whiting 1998) and multivariate analysis (Tudor et al. 2002). Tudor and Williams (2004) described the above methods and highlighted the advantages/disadvantages of each and the reader is referred to the above papers for further details. In summary, a number of methodologies attempt to attribute litter items to a specific source but each method must be considered in the light of the study aims and surveyed area.

24.5 Hazards

24.5.1 Humans

The amount of litter found in recreational water or washed up on world beaches is large, extremely varied in composition and spans coastal areas across the globe. (Table 24.2; Myers 2007). The flotsam/jetsam list – some six million items enters the seas each day, includes items such as crates, palettes, cardboard cartons, newspapers, steel/plastic drums, plastic containers, rubber goods e.g. tyres, bottles (glass/plastic) and metal cans, dead animals, cloth, medical wastes e.g. hypodermic syringes, needles, bottle tops, gloves, shoes, sewage related debris (SRD), cigarette

Table 24.4 World ranking of litter

Rank of debris item	Percentage of total debris items
Cigarettes/cigarette filters	28
Bags (plastic)	12
Food wrappers/containers	8
Caps, lids	8
Beverage bottles (plastic)	6
Bags (paper)	5
Straws, stirrers	4
Plastic cutlery e.g. cups/plates/forks	4
Beverage bottles (glass)	4
Beverage cans	4
Others	17
Top 10 total debris items	**100%**

(Source: OC 2009)

stubs/packets, lighters, glass bulbs, welding gear, matchsticks, fish netting and rope ends, etc. (Table 24.2). A world ranking of litter items is given in Table 24.4 and it is obvious that as far as *homo sapiens* is concerned the main hazardous items here are glass beverage bottles and metal cans.

Beach litter reduction from visual, olfactory and health reasons should be paramount for society and litter should be cut off at source, but in reality this has been found difficult. Potential dangers to beach users' can occur from feet lacertaions by standing on glass or drink ring pull tabs (Olin et al. 1995; Philipp et al. 1995; Williams et al. 2000) and sharps containers have been issued to lifeguards at several beaches (Garrity and Levings 1993). Philipp (1993) has described incidents of 40 needlestick accidents on bathing beaches. Visible litter, e.g. discarded food, dead animals, oil, containers and tyres, that may occur in sea water and beaches, has been associated with gastrointestinal illness after sea bathing, as there is a good chance that high counts of the bacterium *Escherichia* coli can be found, as this is commonly associated with human faecal material (University of Surrey 1987). Where visible beach sewage related debris (SRD) exists, it suggests that adjacent waters are sewage contaminated and this infers the probability to bathers of higher health risk hazards for skin and ear infections (McIntyre 1990). Contact with blood or any other body fluids are less obvious hazards posed by SRD and medical waste, as there exists the potential that these items could be vectors of infectious disease, such as, Hepatitis B and Human-Immuno deficiency virus (Rees and Pond 1995b; Nelson and Williams 1997). Legislation has been shaped by these concerns, e.g. 6mm fine-mesh screens on seawater sewage out-fall pipes for improved environmental control measures, more litter bins, e.g. Nash (1992).

More dangerous litter items have been encountered on beaches e.g munitions, containers of corrosives, pyrotechnics, etc. On a 3 km beach at Sandwich Bay,UK, 11 medium to high hazard rating types of partly used drugs have been found (Dixon and Dixon 1981). Off the French coast in 1993, the ship '*Sherbo*' lost 60,000 bags of a pesticide similar to nerve gas (Olin et al. 1995). A small part of beach debris

Fig. 24.1 Litter on a Falkland island beach – mainly fishing gear

consists of lightstick waste, which is collected by some people who claim the chemicals have beneficial properties, as they contain a chlorinated derivative of salicylic acid, e.g. anti-inflammatory/analgesic activities, insecticide (similar to polychlorinated toxicants such as BHC). Also, hydrocarbons dissolved in the di-*n*-butyl phthalate solvent act as photoreceptors and responds well to tanning, but the downside is that the solvent is toxic and potential cytotoxicity (cell death by apoptosis and/or necrosis), genotoxicity (mutagenicity and/or carcinogenicity), and allergenotoxicity (skin irritation) of such compounds can occur (Bechara and Stevani 2006). Additionally, studies of certain plastic polymers such as PVC (Marcilla et al. 2004), polystyrene (Garrigos et al. 2004) and polycarbonate (von Saal and Hughes 2005), have been shown to release toxic monomers which are linked with cancer and reproductive abnormalities in humans, rodents, and invertebrates.

It is in the economic field that the coastal hazard of marine debris is really felt, as visitors can avoid a beach which is littered with potentially hazardous and unaesthetic items, especially sanitary and medical waste (Hall 1998). Many studies have shown that a clean beach is one of the fundamental characteristics of a seaside resort required by visitors (Oldridge 1992; Williams 2011; McKenna et al. 2011) resulting in a loss of tourist days; damage to leisure/tourism infrastructure dependent on tourism; damage to fishery activities and fishery-dependent activities (Fig. 24.1; lost earnings by Scotish fishermen due to net contamination is Euro 11–13 m/year); damage to the local, national and international image of a resort. A classic study in New Jersey, USA in 1987 and Long Island, USA in 1988, showed that reporting medical waste, such as, syringes, vials and plastic catheters along the

Fig. 24.2 Typical dog waste bin

coastline, resulted in an estimated loss of between 37 and 121 million user days at the beach and between US$1.3 and 5.4 billion in tourism-related expenditure (Valle-Levinson and Swanson 1991). In the UK, coastal tourism brings in Euros 7–11 billion and Beachwatch has shown from surveys undertaken by >5,000 volunteers at 400 beaches, that it costs Euros 18 m/year to clean up beach litter (42% due to visitors; 15% fishing; 5% SRD; 2% shipping; MCS 2010).

A growing hazard to beach users is dog fouling, with *Toxicara canis* being the problem, as the faeces of an infected animal can hold one million eggs, which become infectious some 2–3 week after deposition; but can remain dormant for 3 years. In the UK, some 91% of local councils now employ a dog warden and 600 people were taken to court in 2009, where a maximum fine of Sterling £1,000 can be imposed. Figures 24.2 and 24.3 show some of the signage utilsed plus typical waste bins. Williams and Tudor (2006) showed that residents of social housing and men in general, are more reluctant than females to pick up dog waste and that one is unlikely to get caught.

Beach sediments may also act as a reservoir of micro-organisms or vector of infections but transmission by this route has not been demonstrated in epidimiological studies e.g. Marin et al. (2004). Currently monitoring for epidemiological contamination is not mandatory, but the WHO (2003) have suggested that such monitoring be considered as a precautionary measure for beach user's safety. Higher incidences of micro-organisms seem to occur in sediments rather than adjacent waters and filamentous fungi and yeasts in particular – with a high survival rate due to spore production, seem to owe their occurence to beach user presence. *Candida albicans* and *Microsporum sp. Gruby* (a pathogenic strain possibly

Fig. 24.3 Typical dog fouling sign

due to domestic animal contamination) are able to survive for 1 year in sediment and Williams and Tudor (2001), showed that beach litter can be buried for long time spans and later exhumed by storm activity.

Marin et al. (2004), working on Italian Ligurian coast beaches that complied with the microbiological criteria for EU bathing beaches, found that total coliforms increased in average density from July (30 ± 5 CFU 100 ml) to Sept (232 ± 37 CFU 100 ml); (CFU – colony forming unit) and for the same period, faecal coliforms 9 ± 4 CFU 100 ml to 145 ± 34 CFU 100 ml; faecal streptococci 292 ± 271 CFU 100 ml to 2,848 ± 1,826 CFU 100 ml, with *E. coli* showing no seasonal trend. Maximum filamentous fungi density values were of the order of 524 ± 405 CFU*g^{-1} DW (DW – dry weight) and yeast density ranged from 0 to 6,020 ± 2,384 CFU*g^{-1} DW. It may be suggested that as all the above constitute an hazard, then: not only should litter be removed but also moderate mixing of the superficial beach sand layers be undertaken to enhance the natural anti-microbial action of the UV rays; 'good practices' behaviour should be diffused among users (such as using and lying upon clean towels, do not litter, etc.); domestic animals, mainly dogs, should be banned in the tourist season and their excreta removed by owners. These results show a need to consider these indicators as an environmental quality and public health issue.

In tropical and sub-tropical countries Health Authorities frequently recommend non-accumulation of rubbish in the environment, including beaches (backshore) due to the possibility of their becoming water reservoirs and a breeding ground for mosquitoes. The backshore is close enough to homes, bars and other facilities for people to be exposed to mosquitoe bites and therefore a possibility of becoming infected. It is bad enough if bitten, but a tragedy when people are infected by dengue and other diseases, all common in tropical coastal villages. On large city

beaches which have daily beach and street cleaning, it does not appear to be a major threat, but in smaller communities where the local administraton can not afford beach cleaning efforts for months, rubbish can, and will, accumulate and help proliferate the spread of mosquitoes. These areas are the very pleasant places where people holiday and once infected, they travel with the viruses and spread it to other areas.

Away from tourist destinations, a particular beach site specific hazard exists:

a. Some 50 km, southeast of Bhavnagar on the west coast of the Gulf of Camray, Gujarat state, India, occurs probably the premier world shipbreaking yard, where *circa* 40% of the world's redundant vessels are beached and cut up by >60,000 people. Health and safety regulations are completely absent, the beach strip is extremely hazardous as chemicals, PCBs, asbestos and lead paint together with gas leak explosions, frequently occurs, caused by residual fuels being exposed to welding guns.
b. In Russia e.g. Murmansk, the coastline of the Russian Far East, ex-Soviet nuclear submarines lie rotting, and storage facilities are being built to hold the nuclear reactors from the decommissioned and disintegrating submarines. Radioactive contamination of the surrounding beach and sea areas is a serious hazard, but few tourists are seen.

24.5.2 Wildlife

Marine debris (Table 24.2) affects not only wildlife but their ecosystems (food, shelter, etc.) as winds/currents move debris over the world oceans. Their impacts on wildlife can generally be lethal; are usually sub-lethal; certain populations of bird categories are seriously threatened by plastic ingestion (plus any chemical pollutants) which when regurgitated can be passed on to young birds (Jones 1995; Tanabe et al. 2004; Matsuoka et al. 2005). Therefore marine debris (Table 24.2) affects not only wildlife but their ecosystems (food, shelter, etc.) as winds/currents move debris over the world oceans (Jones 1995; Winston et al. 1997; Tanabe et al. 2004; Matsuoka et al. 2005).

24.5.2.1 Entanglement

Hazards caused by marine debris can include entanglement of scuba divers as well as wildlife. This can cause death by drowning, reduction in the ability to hunt for food, avoid predators etc. Entanglement dangers with respect to marine animals and birds caused by man-made debris have been well documented, e.g. Jones (1995). Emery and Simmonds (1995) reported that the majority of entangled seals have debris wrapped around their heads and necks which can affect ingestion of food and growth restriction/inability to feed. The Ocean Conservancy (2009) survey found that out of 443 animals and birds entangled or trapped by marine debris – 268 were found alive and released. Fish (44%),

including sharks, stingrays, and seahorses, were the most prevalent; Invertebrates, e.g. octopuses, crabs, lobsters, and jellyfish were the second largest category with birds third. Fishing-related items, including line, nets, rope, hooks, and crab/lobster/fish traps, accounted for most entanglements.

Entanglement is particularly prevalent in areas of predominantly heavy maritime traffic or where oceanic currents naturally accumulate surface material, (Walker et al. 1997). Reports exist of a dead sperm whale having 440 lb of fishing gear in its stomach; dead northern fulmar seabirds on Dutch beaches revealed that 98% had plastic in their stomachs; in Florida, 12 stranded dolphins had fishing gear in their stomachs, mouths, or throats, and some had line tangled from their stomachs to their mouths (OC 2009).

A classic study of beach litter and entanglement was carried out by Lucas (1992) who showed that Harbour and Grey seals (6 out of 241) were were entangled in strapping, net, rope, and other items on beaches at Sable Island, Canada. Other examples include seabirds tangled in trawl nets, six-pack yokes and balloon ribbons; a dead beached Sable Island horse had both back legs covered in plastic strapping. Large debris items trap animals and/or can drag animals down. The end result is drowning, death by starvation or predation. Smaller debris items increase drag factor producing increased vulnerability to predators and/or, a decreased ability to forage, ultimately leading to starvation (Loretto 1995).

24.5.2.2 Ingestion

Plastic bags can snag on the sea bed (Goldberg 1997), as well as float and seabirds and turtles appear to confuse litter for food (primary ingestion), or ingest litter within other food (secondary ingestion) and these items can pass to chicks (Loretto 1995). 'Eating plastics' can block/damage digestive tracts and consequently reduce feeding, although fouling organisms and blanketing effects also warrant serious consideration, as much larger proportions of populations ingest marine debris – up to 100% in some seabird species (Loretto 1995). Faris and Hart (1995) showed that there is a large absence of debris from droppings indicating that plastics do not appear to pass through the intestines of seabirds. Plastic ingestion leads to less acute symptoms, but even small amounts can cause death – as the animal can be incapable of feeding and/or have a false sense of fullness, as much plastic remains in an organism's stomach resulting in loss of stomach volume and nutritional 'dilution' of diet (Ryan et al. 1988); McCauley and Bjorndal (1999); Ryan (2008) showed that turtles do not compensate by eating more, leading to slower growth rates, longer developmental periods, depleted energy reserves, reduced reproductive output, and reduced survival rate. Tomas et al. (2002) have suggested that plastics are the largest threat to Leatherback turtles in Mediterranean areas.

Plastic pellets in particular – the raw materials that are melted and moulded to create plastic products, bear close resemblance to fish eggs causing animals to selectively seek out and ingest the pellets (Mato et al. 2001). They come in various

shapes: spherical, ovoid, and cylindrical, typically measuring 1–5 mm in diameter and are made from a variety of polymers, each with different surface structures and therefore different affinities to pollutants. The uptake of particular pellets by different feeding guilds depends on the size, shape and density of the pellets, which dictates their availability and position in the water column. A low-density plastic like polystyrene will float and be available for ingestion by seabirds, whereas high-density plastics such as PVC will tend to sink and accumulate in the sea floor sediment where they are more likely to be ingested by deposit-feeders (Browne et al. 2007). As plastic particles become smaller, their potential for ingestion by animals further down the food chain increases (Browne et al. 2007). Laboratory studies show that amphipods, barnacles and lugworms will readily ingest small PVC fragments and that polychaetes, echinoderms, bryzoans, bivalves and mussels (*Mytilus edulis*) will ingest polystyrene microspheres (Thompson et al. 2004; Ward and Shumway 2004). When ingested by organisms, microplastics are likely to pose an even greater toxic threat than pellets; they have a greater surface area to volume ratio meaning they have greater potential to transport contaminants (Browne et al. 2007). Recently, Browne et al. (2011) have shown that microplastics have been found in sewage sludge, laundry wastewater (on average, >1900 microplastic fibres could be discarded by a synthetic item during one wash) and sewage treatment plant effluent (one fragment of microplastic per litre of wastewater). A pronounced lack of knowledge exists re this topic and work is needed to assess food web accumulation likelihood, as well as methods (ultrafiltration?) to remove microplastics.

An NRC (2008) report stated that plastics collect toxic compounds that move into the bodies of organisms that eat the plastic. Toxicity relates to: additive derived pollutants i.e. plastic polymers contain additives to give the plastic marketable qualities which are able to leach out of the polymer matrix into the environment, e.g. DEHP a phthalate"plasticizers" used nPVC; PBDE used in flame retardants (Browne et al. 2007); and monomer release where certain polymers have been shown to release toxic monomers linked to cancer and reproductive abnormalities in humans, rodents and invertebrates, e.g. PVC, polystyrene, and polycarbonate action (Ivar do Sul et al. 2009). This requires action on a number of fronts and in particular calls for co-ordination of existing activities in order to enhance their effectiveness. It has been shown to work in other fields, e.g. UK drink driving campaigns changed people's behaviour with respect ro driving when under the influence of alcohol

24.5.2.3 Rafting/Aliens

Gregory (2009) suggested that alien species rafted on drifting plastic could pose hazards to the biota of sensitive and/or protected near-shore environments and perhaps the terrestrial ecosystems of small oceanic islands (Winston et al. 1997). These large items of drifting plastics therefore act as rafts for faunal dispersal over large distances (Barnes and Milner 2005). Hard-shelled and crustose organisms,

e.g. barnacles, bryzoans, tube worms, molluscs, foraminifera and coralline algae, as well as some more resistant sponges and hydrozoans, can easily hitch lifts on floating plastic artifacts. Passively drifting islands of plastic and other debris may be a vector for local, regional and transoceanic dispersal of marine organisms and perhaps even some terrestrial ones, e.g. Florida debris carried a previously unrecorded bryozoa (*Thalamoporella* sp.) similar to a Brazilian species (Barnes and Sanderson 2000).

24.6 Beach Clean Ups

Beach surveys are comparatively cheap and give information about the surrounding coast, as debris accumulation represents a function of the source amount, decay rate, burial-exhumation rates, together with the coastal morpho-dynamics. The problem is world-wide, but in developing countries with a huge amount of packaged goods being produced and inefficient waste disposal facilities, the problem is very acute (Uneputty and Evans 1997). Beach cleanups provide a way of collecting data on the types and quantities of marine debris, but cannot permanently solve the problem of marine debris, as they do not reduce quantities at source (Simmons and Williams 1993), even though there is intense pressure to clean a beach, especially by authorities wishing to promote tourism. Clean-ups *per se* do not resolve the problem if they do not address the issues of prevention at source and it is the links to sources that represents the future challenge (Earll et al. 2000; Williams et al. 2000). However, even though they are costly in terms of time and effort, they have their primary value as public participation exercises and as a way of raising public awareness and are a valued educational tool – in most cases to an already conservation biased audience.

Site selection for beach cleans is usually biased towards areas with easy access, tourist locations and depositing beaches. Clean-ups are really only applicable locally; if volunteers are employed, costs are minimal, but are expensive if undertaken by mechanical means as well as being labour intensive**.** At Studland, Dorset, UK, 1.000,000 visitors/year along a 6 km stretch of beach results in a summer weekly collection of 12/13 tonnes of litter at a cost of £36,000 Stirling/annum (Williams et al. 2000). Additionally, if any area is consistently polluted with debris this can lead to falls in property values (Rees and Pond 1995a). UK harbour authorities also pay for the cost of keeping a navigational channel free from litter, e.g. at Lerwick harbour, Shetland, UK, it costs £720 Stirling/annum for harbour clearance (Hall 1998). The cities of Santa Monica and Long Beach in California, USA, each spent more than US$1 million in 1988–1989 to clean their beaches (Kauffman and Brown 1991). Another European example is the Swedish Skagerrack coast where more than 6,000 m^3 of litter was collected in 1993. Approximately 9,000 working days over 4–5 months with a total cost of around £1 million Sterling, gave the fiscal price of clearing marine litter at £156/m^3 (Olin et al. 1995)

In essence, there are two methods of cleaning beach litter:

24.6.1 Mechanical

Involves costly motorised equipment utilising a coarse grained (*circa* 5cm.) sieve effect, which scoops up litter and sand so is not selective, as cigarette stubs and cotton bud sticks pass through. It is carried out either early in the morning (usual) or in late afternoon when tourists have left the beach. The use of mechanical beach cleaners may threaten the stability of some beaches, as removal of organic matter lessens the bond that holds sand grains together. Vehicle vibration also interferes with beach ecology (Llewellyn and Shackley 1996). This method is limited in that it cannot be used on pebble beaches, as these tend to allow smaller litter items, such as, plastic pellets and cotton bud sticks to move downward between voids preventing easy discovery and recording (Williams and Tudor 2001). Such small items are more readily apparant on sand beaches. However, it is speedy and can provide an apparently immaculate large beach. In areas where hazardous or sanitary waste are found, it reduces any potential risk for manual litter pickers.

24.6.2 Manual

The alternative to mechanical methods is manual beach cleaning, often carried out where the expense of a mechanical device is prohibitive, or the substrate is not receptive to such machines. Manual cleans, e.g. organised as community events can clear the many small items missed by mechanical cleans (Pollard 1996). Many surveys (e.g. Coastwatch UK; Beachwatch) give data recording sheets to their field workers which have pre-defined categories of waste. This *can* possibly lead to misidentification or misallocation of litter if categories are not well defined in instruction sheets or adequate training is not given. This will lead to incorrect debris sourcing and therefore can target wrong groups in order to help prevent further pollution. Where volunteers are used litter collection is usually the primary task and item recording is likely to be less of a priority. Rees and Pond (1995a), have shown that volunteers' participating in beach cleans undercounted individual items of debris by 50%, but Williams et al. (1999) showed that volunteers can source debris extremely well. It helps raise community awareness to the litter problem and lends itself to sourcing litter from a scientific perspective rather than scooping it up '*en block*' for landfill site deposition (Earll et al. 1996).

24.7 Discussion

No global figures exist on the scale of the plastic litter problem, but it appears that 265 m tonnes are produced globally each year mainly for the packaging industry creating some 170 m tonnes to be disposed of after usage (Plastics Europe 2011).

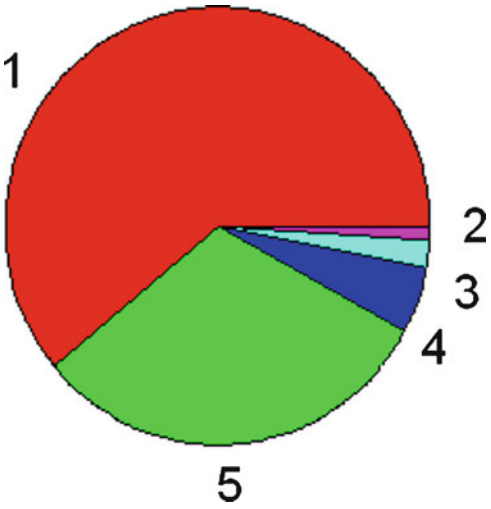

Fig. 24.4 World wide marine debris, International Coastal Cleanup, 2009 (Ocean Conservancy, USA) Nb.Top 10 debris item numbers = 9,507,103; Total worldwide = 11,439,086 (Table 24.2). Key: *1* Recreation, *2* Medical, *3* Dumping, *4* Ocean, *5* Smoking

However, what would be the end result if no plastics were used? Pilz et al. (2010), assessed this matter and found that if wood, glass, tin and cardboard were substituted, it would generate some 3.6 times the packaging mass, take double the energy and generate some 2.7 times higher amounts of greenhouse gases. The substitution of plastics by other materials would need 57% more energy, which represents an energy saving of 53 million tonnes of crude oil (Plastics Europe 2011). The European Packaging and Films (PaFa 2011) has stated that for every tonne of carbon produced in the production of plastics, some 5 tonnes are saved.

As seen from Fig. 24.4, world scale recreational litter seems to be the biggest culprit, but it should be noted that site/regional specificacy is important, as shown in Fig. 24.5 for the UK. Shipping channel areas will have a much higher incidence of shipping related litter than recreational beaches located away from main channels; fishing gear frequently ends up on beaches in Scotland brought over from North America by currents. One fundamental question is how does one cut down on litter left behind by users? The draconian laws of Singapore could be utilsed i.e. deposition of chewing gum on streets etc. means a hefty fine, potential flogging etc. but litter laws in most countries are adequate – it is law enforcement that is the problem. In addition a cultural change needs to be affected; in Australia beach users take their litter home or deposit them in litter bins provided. In Europe, people simply leave massive amounts of litter on the beach. Smoking produces cigarrette stubs on many beaches and authorities try to cut down on this problem by providing recepticles, e.g. cone devices that can be inserted into the sand. Just solving these two matters would cut down beach litter by an order of magnitude.

As noted above, plastics especially those used in recreational pursuits and packaging are ubiquitous on shores, in oceans, and on water surfaces across the globe (Mato et al. 2001; Thompson et al. 2004; Karapanagioti, and Klontza 2008) and by mass 60–80% of marine litter is plastic (Derraik 2007). The world's annual

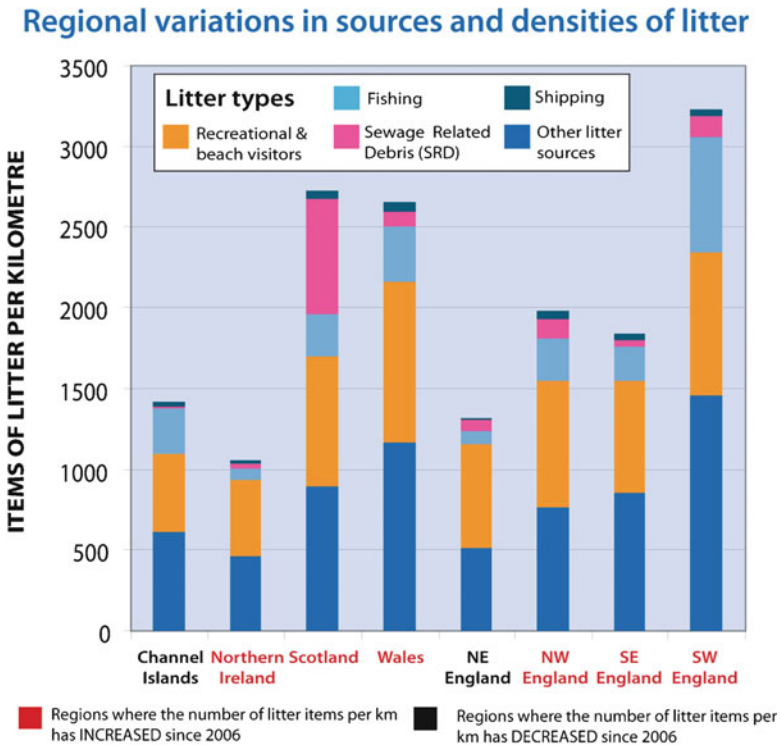

Fig. 24.5 Regional variations in sources and densities of litter (Source: MCS 2010)

consumption of plastic materials has increased 20 times from 5m. tonnes in the 1950s to 100m. tonnes. In the UK alone a total of 4.7 million tonnes of plastic products were used in various economic sectors in 2009, with packaging being the main single factor, it being the material of choice in 56% of all packaged goods (75% from households). This generates an annual UK waste of *circa* three million tonnes of which some 7% is recycled. This is particularly relevant as the world plastic resin pellet consumption is expected to rise from the 2006 figure of £451.9 billion Sterling to £562.2 billion Sterling in 2010. It has been calculated that some 300,000 items of plastic per square kilometre of sea surface exists and 100,000 per square kilometre of seabed (Thompson et al. 2004). One and a half million tonnes of plastic is used for water bottles alone, a US$ 22 billion per year industry. One of the urgent issues that needs resolution, is the extent of harm done by microscopic plastics.

The packaging industry consumes an estimated 35% of all UK plastics and each household uses some 500 bottles per year, of which 130 are recycled (13 bn/year), but 80% of plastics are sent to tips, 8% incinerated, and only 7% recycled. Plastic bags tend to be used for some 20 mn each (once) and can stick around for n − 1 years, as no one can give a decent figure. In 2002 Ireland introduced a Euro 0.15

charge for a plastic bag and demand dropped by 90%; IKEA gave away 32 billion in 2005 and now charges UK10 pence a bag; Italy on Jan 1, 2011 became the first European Union country to ban polythene bags, opting for biodegradable bags which will save 180,000 tonnes of CO_2 emissions; Wales, UK was the first country in the UK to introduce a legal charge (5 pence per single use carrier bag – from October 2011), as part of its efforts to dramatically reduce the volume of carrier bags given out to shoppers. The charge is to encourage people to utilise the bags they already have and is '*estimated as high enough to encourage people to change their shopping habits but not so high that it will deter impulse shopping or place a significant burden on shoppers who have forgotten their reusable bags*' (www.wales.gov.uk). In 2009, people in Wales, UK, took home from major supermarkets alone, an average of 273 carrier bags per household.

Several excellent films relating to plastic bags esist: '*The Plastic Bag*', director Ramin Bahrani, made in the USA in 2009, an 18 min film following the journey of a salmon pink plastic bag from a supermarket checkout to its final resting place in the North Pacific subtropical zone vortex, where debris accumulates as a result of the convergence of four major currents (Moore 2003). The bag has a human voice – that of Wernor Herzog. A similar film, voiced by Jeremy Irons is '*The Magnificent Plastic Bag*', directed by Patrick Jean, made in France in 2010. The Brazilian/British film '*Lixo Extraordinário*', is also striking and was short listed for the US Cinema Academy Awards (Oscar) in 2011. Another award winning movie is '*Ilha das Flores*' (in Portuguese) which deals with the same issues but from a social perspective and has extremely strong images.

The essence of litter avoidance is prevention at source, (it is people who litter), a theoretical ideal but unfortunately in the current world, not yet pragmatic, so that plastics, for example, needs some technological advances, in order to be made more bio-degradable and/or recyclable. Is this achievable? Some 40 years ago, the ITW Hi-Cone company not only reduced by 30%, the plastic amount in six-pack holders, but have since developed a photodegradable version which reduces tensile strength by *circa* 75%, but it should be noted that when these degrade they give off not only CO_2 but also methane which is 24 times more damaging to global heating than CO_2. Biodegradable plastics can also be made from corn, soy etc. which dissolve easily in soil and water and polylactic acid (PLA) can be processed on existing plastics equipment which is a boon to industrialists. Imaginative solutions are needed. One such idea is to utilise sisal, a central American plant with sword-shaped leaves which grows in very dry conditions and is used for cord and rope. Kenya produces some 30,000 tonnes of these stiff fibres per year and theoretically one could substitute this for plastics.

At Dagenham, UK, 'The Closed Loop' recycling plant which takes in 35,000 tonnes of plastic bottles per year is a case in point. Bottles are pulverised to grey granules (the off white colour is due to contaminants in bottle designs), reconstituted and sold at lower prices than virgin plastic. A major stumbling block to current recycling policy is that local authorities operate without any national/international standards or long term view and in general, when mixing recycled plastics and biodegradable bottles is carried out, contamination of the

Fig. 24.6 Reed boat on Lake Titicaca, Peru. The reeds cover >2,000 two litre plastic bottles

whole batch occurs and all is sent to landfill. Additionally, a 'knowledge lag' seemingly exists between innovative design and the latest available recycled material and *'more collaboration is needed between designers, marketers and manufacturers to enable efficient recycling and create demand for recycling through products that contain such materials.'* (Bennett 2010, 17).

However, the over-riding mantra from manufactures is that of costs, money being the inevitable driving factor. On a small scale, Indians on Lake Titicaca, Peru, are *re-using* plastics by making boats out of reeds that have as its centre, some 2,000 two litre plastic bottles (Fig. 24.6). David de Rothschild, built a boat *Plastiki*, kept afloat by a frame of 12,500 discarded plastic bottles (which gives displacement) lashed to its sides, in which srPET – self-reinforced polyethyline terephthalate, recycled plastic formed of layers of cloth like sheets – are the arched supports of the twin hull (www.theplastiki.com). It sailed (2011) to the north Pacific sub-tropical zone 'the eastern garbage patch' which has an area twice the size of Texas and is an 'island' of trashed garbage, north of Hawaii, in order to draw attention to the flood of debris pouring into the oceans each year (c*irca* six million debris items). However, the journey did not stress enough the most important thing of all, which is to *reduce* plastic demand and therefore their chances to reach the marine environment.

Consider recycling. Not nearly enough organisations have dedicated themselves to sorting their recyclables. A significant portion of trash picked up on beaches during cleanup could have been kept out of waterways and the ocean through recycling. The USA Environmental Protection Agency estimates that the equivalent of 4.5 pounds of solid waste per person per day is generated in the USA, yet just 33.4% is recycled, and estimated that Americans use > 90 billion plastic bags a

year, with just a fraction reaching recycling facilities. The UK's, anti-waste body Waste Resources and Action Programme (WRAP), has a vision of 500,000 tonnes of mixed household waste plastics being recycled every year by 2020 (www.WRAP.org.UK). Current UK production is about 1.4 million tonnes per annum with up to 40,000 tonnes collected for recycling. Recycling plastics is difficult due to the many types and contamination issues, but attaining the best UK local authority recycling levels, it could reach 45%. As a stimulus a capital grant competition worth £2 million Sterling has been launched by the UK Government to develop the infrastructure needed, the criteria being that at least 70% of output must replace virgin plastics in end products. Most European recyclers mainly utilise the polyolefin plastic fraction of waste plastics for cement kilns. However, in The Palm Resort, Dubai, recycled plastic artificial reefs are being created and placed along the coastline to replace reefs damaged and/or removed for construction purposes. With respect to the 'reduce, recycle, reuse' mantra, Japan appears to be leading the way in that some 77% (twice that of the UK; *c*/*p* with 20% in the US) of plastics was recycled in 2010. Recycled material is used for textiles, sheeting, industrial materials and household items largely; for the Asian market the success has been because the manufacturers have co-operated well with the waste processing agencies. As an example, 72% of PET bottles in 2010 were re-cycled compared with 48% in Europe and 29% in the US (www.PWMI.org.jp).

Research on devulcanising and re–rubberising old tyres is currently very prevalent, For example, VRTek Operations and the Commonwealth Scientific and Industrial Research Organisation, based in Australia, cut segment tyres into pieces and the resulting powder could make new tyres or be applied to industrial insulation or road surfaces (www.vrtek.com.au). Smithers Rapra, UK, on tests on products made from 100% devulcanized rubber, showed tensile strengths of 18 MPa with an elongation break of 350%.

Establishment of dedicated Plastic Recovery Facilities (PRFs) which have economies of scale (at least 80,000 tonnes/year with a capital cost of £29 million Sterling) to sort waste (including bottles) by polymer type and reprocess them as substitutes for virgin materials, would produce enormous benefits and an integrated PRF and reprocessing facility could have an expected material recovery as high as 60%. Mehta (2009) has indicated that markets (e.g. packaging, refuse bags, pipes, hose reels) exist for >95% of recycled plastics (PET, HDPE, PP, PS, PE film). In films, if clear PET and HDPE are separated at the primary stage, the required capacity would drop to 50,000t per year. However a small amount of PLA entering a recycling stream can have a negative effect on the extruded rPET, such as, molecular weight, making it unfit for further use, e.g. 1% of PLA introduced into 99% of PET produced colour and velocity changes (Asfa-Wossen 2010). Plastics and films can now be removed from waste via the BHS rotary air separator which works like a vacuum and sucks plastics away, transporting and bailing them at a single point in the materials recovery facility (www.sca.com). Additionally, they can be turned into diesel fuel. In 2011, 10 UK plants are scheduled to be operational to covert end of life plastic into fuel and it is estimated that 60,000 tonnes of mixed plastic waste diverted from landfill will produce >4,000,000 litres of diesel fuel (www.sita.co.uk).

At Redcar, UK, Europe's first wholly integrated sorting and recycling facility opened in April, 2011, taking mixed wastes, e.g. tubs trays and bottles, to turn into consumer goods. Magnets/screens/belts first take out contaminants and any useful metals. After washing, a three phase centrifuge separates the mixture by density. The floating phase is composed of polyolefin mixtures (polyethylene [PE] and polypropylene [PP]), while mixtures of the thermoplastic polymer resin of the polyester familly, Polyethylene terephthalate (PET) and other polymers sink to the floor. A tower with near infra red spectroscopy and colour sorters, splits the lighter phase into component parts after which, materials are sorted into polymer types and filtered into a total of eight clear and mixed colour grades. The plastics are supplied from Biffa's Materials Recycling Group facilities plus commercail customers, such as, municipalities, and will initially operate at 20,000 tonnes/annum in 2012 (Redahan 2011). Litter is a trans-boundary issue and in the European context, the current high level Marine Stategy Framework Directive, requires member states to achieve Good Environmental Status by 2020. But what does this mean, as there is little agreement on the subject?

24.8 Conclusions

Litter is an emotive term and is a very large problem on not just beaches but the open sea. Currently many investigative methods are used to research the subject but there appears to be no universal approach. Sourcing is the key and checklists such as OC (2009) and the MCS (2010), allied to a beach grading system (EA/NALG 2000) appears to be the way ahead. Relevant co-ordinating mechanisms are needed to fulfill the aim of reducing litter input and impact, e.g. expand public/private partnership to monitor/reduce debris; community efforts; appoint a Lead Agency and 'General' to look at litter in a holistic manner. Research is badly needed into the economic and ecological impacts of beach litter; the effectiveness of current measures for its control and better enforcement of existing laws; new technology risk assessment tools and contingency valuation techniques, e.g. willingness to pay, etc. as well as on the chemistry of what happens to the many polymer varieties when they enter the marine environment and the digestive systems of organisms.

More stringent regulations are needed on the plastics industry including recycling frameworks and promotion of communication and education to stimulate a more pro-active approach to litter prevention and minimization through collaboration between various stakeholders, e.g. reduce, reuse, recycle. Plastics have become an integral and essential part of life and the threats posed by plastics on the environment cannot be alleviated until consumption viewpoints of the product change. Products are viewed as having a finite lifespan, i.e. they are manufactured, used, breakdown and thrown away. Where does it go – outer space! Plastic does not readily decompose and quietly poisons the environment. Product lifecycle thinking is the way forward, looking for ways in which materials can re-enter the production cycle after their first role has finished. Therefore development of alternate plastic

technologies/or a reduction wherever possible, is needed, that pose less of a threat to the environment when they do escape the production chain, i.e. alternative non-toxic plastics that are more easily broken down and reused. A total change in societal paradigms is unlikely in the short term, but radical changes in our way of thinking and living in this time span can actually be for mankind's own good. To conclude, there are clearly needs for new approaches and the primary approach for the forseeasble future will most probably be further development of biodegradable plastics with significantly reduced and tightly managed disintegration times. UNEP (2009) has implied that any activities that encourage recycling and solid waste reuse plus development of voluntary cleanups are the appropriate ways to go.

References

Asfa-Wossen L (2010) Mixed plastics under the lens. Mater World 18(12):4

Barnes DKA, Milner P (2005) Drifting plastics and its consequences for sessile organism dispersal in the Atlantic Ocean. Mar Biol 146:815–825

Barnes DKA, Sanderson WG (2000) Latitudinal patterns in the colonization of marine debris. In: Proceedings of the 11th international bryozoology conference, Balboa, pp 154–160

Barnes DKA, Galgani F, Thompson RC, Barlaz M (2009) Accumulation and fragmentation of plastic debris in global environments. Philos Trans R Soc B 364:1985–1998

Bean MJ (1987) Legal strategies for reducing persistent plastics in the marine environment. Mar Pollut Bull 18(6B):357–360

Bechara EHH, Stevani CV (2006) Pollution of Brazilian beaches by light stick waste, Outline Research Proposal, Stevani & Stevani Consultores Associados S/C Ltda. R. Manoel Simões da Silva, 47 – Jardim Maria Nazaré, CEP 02354-370, São Paulo, Brasil, 6 pp

Bennett M (2010) Wheels in motion. Mater World 18(11)

Browne MA, Galloway T, Thompson R (2007) Microplastic – an emerging contaminant of potential concern. Integr Environ Assess Manag 3:559–566

Browne MA, Crump P, Niven SJ (2011) Accumulation of microplastic on shorelines worldwide: sources and sinks. Environ Sci Technol 45:9175–9179

Coe JM, Rogers DD (1997) Marine debris sources, impacts and solutions. Springer, New York, 432 pp

Corbin CJ, Singh JG (1993) Marine debris contamination of beaches in St. Lucia and Dominica. Mar Pollut Bull 26(6):325–328

Derraik J (2007) The pollution of the marine environment by plastic debris: a review. Mar Pollut Bull 54:423–433

Dixon TR (1995) Temporal trend assessments of the sources, quantities and types of litter occurring on the shores of the United Kingdom: introduction and methods with results from paired observations 8 and 11 years apart on 63 sampling units in mainland Scotland and the Western isles. Marine Litter Research Programme, Stage 7, The Tidy Britain Group, Wigan, UK

Dixon TJ, Dixon TR (1981) Marine litter distribution and composition in the North Sea. Mar Pollut Bull 14:145–148

EA/NALG (Environment Agency and The National Aquatic Litter Group) (2000) Assessment of aesthetic quality of coastal and bathing beaches. Monitoring protocol and classification scheme, 15 pp

Earll RC, Everard M, Lowe N, Pattinson C, Williams AT (1996) (eds) Measuring and managing litter in rivers, estuaries and coastal waters: a guide to methods, R., Earll Ltd., 78 pp

Earll RC, Moore J, Williams AT, Tudor DT (1999) The measurement of oily waste and garbage disposed of into the marine environment by shipping. A report to the Maritime and Coastguard

Agency. Prepared by Coastal Management for Sustainability, Candle Cottage, Kempley, Glos, UK, 75 pp
Earll RC, Williams AT, Simmons SL, Tudor DT (2000) Aquatic litter, management and prevention – the role of measurement. J Coast Conserv 6(1):67–78
Emery M, Simmonds M (1995) Seal entanglement and rescue options. A report for earthkind. The Conservation Research Group, The University of Greenwich, UK
Faris J, Hart K (1995) Seas of debris: a summary of the third international conference on marine debris, UNC-SG-95-01. North Carolina Sea Grant, Florida, 54pp.
Garrigos MC, Marin ML, Canto A, Sanchez A (2004) Determination of residual styrene monomer in polystyrene granules by gas chromatography–mass spectrometry. J Chromatogr A 1061: 211–216
Garrity SD, Levings SC (1993) Marine debris along the Caribbean coast of Panama. Mar Pollut Bull 26(6):317–324
Gilbert C (1996) The cost to local authorities of coastal and marine pollution – a preliminary appraisal. In: Earll RC (ed) Recent policy developments and the management of coastal pollution. Marine Environmental Management and Training, Candle Cottage, Kempley, Glos, UK, 12–14
Goldberg ED (1997) Plasticizing the sea-floor: an overview. Environ Technol 18:195–202
Gregory MR (2009) Environmental implications of plastic debris in marine settings – entanglement, ingestion, smothering, hangers on, hitch hiking and alien invasions. Philos Trans R Soc B 364:2013–2025
Hall K (1998) Economic and social impacts of marine debris and oil on coastal communities. Stage 1 report, Sept 1998, KIMO and Napier University, UK
Ivar do Sul J, Costa M (2007) Marine debris review for Latin America and the wider Caribbean area, and where do we go from here? Mar Pollut Bull 54(8):1087–1194
Ivar do Sul JA, Rodrigues O, Santos IR, Fillmann G, Matthiensen A (2009) Skin irritation and histopathologic alterations in rats exposed to lightstick contents, UV radiation and seawater. Ecotoxicol Environ Saf 72(7):2020–2024
Jones MM (1995) Fishing debris in the Australian marine environment. Mar Pollut Bull 30(1): 25–33
Karapanagioti HK, Klontza I (2008) Testing phenanthrene distribution properties of virgin plastic pellets and plastic eroded pellets found on Lesvos island beaches (Greece). Mar Environ Res 65(4):283–290
Kauffman J, Brown M (1991) California marine debris action plan. In: Magoon OT, Converse H, Tippie V, Tobin LT Clark D (eds) Coastal zone '91. Proceedings of the 7th symposium on coastal and ocean management. ASCE, Long Beach, California, New York, USA, 8–12 July 1991, pp 3390–3406
Llewellyn PJ, Shackley SE (1996) Effects of mechanical beach-cleaning on invertebrate populations. Br Wildl 7(3):147–155
Loretto C (1995) Impacts of litter on wildlife and ecosystems. In: Earll RC (ed) Coastal and riverine litter: problems and effective solutions, Coastal Management for Sustainability, Candle Cottage, Kempley, Glos, UK, pp 3–4
Lucas Z (1992) Monitoring persistent litter in the marine environment on Sable Island, Nova Scotia. Mar Pollut Bull 24(4):192–199
Marcilla A, Garia S, Garcia-Quesada JC (2004) Study of the migration of PVC plasticizers. J Anal Appl Pyrolysis 71:457–463
Marin V, Misic C, Moreno M, Salvo V-S, Fabiano M (2004) Faecal indicators, bacteria and fungi in beach sediments. In: Micallef A, Vassallo A (eds) Management of coastal recreational resources. First international conference on beaches, yacht marinas and coastal ecotourism, ICOD, University of Malta, pp 107–115
Marpol (1973/1978) The international convention for the prevention of pollution from ships, 1973 as modified by the protocol of 1978, Annex V. Prevention of pollution by garbage from ships, entered into force, 31 Dec 1988

Mato Y, Isobe T, Takada H, Kanehiro H, Ohtake C, Kaminuma T (2001) Plastic resin pellets as a transport medium for toxic chemicals in the marine environment. Environ Sci Technol 35:318–324

Matsuoka T, Nakashima T, Nagaswa N (2005) A review of ghost fishing: scientific approaches to evaluation and solutions. Fish Sci 71:691–702

McCauley SJ, Bjorndal KA (1999) Conservation implications of dietary dilution from debris ingestion: sub-lethal effects in post-hatching loggerhead sea turtles. Conserv Biol 13:925–929

McIntyre AD (1990) Sewage in the sea, Annex XII of state of the marine environment, GESAMP reports and studies no. 39

McKenna J, Williams AT, Cooper JAG (2011) Blue flag: red herring: do beach awards encourage the public to visit beaches? J Tour Manag 32(3):576–588

MCS (Marine Conservation Society) (2010) Beachwatch '09 – nationwide beach clean and survey report, Ross-on-Wye, England, UK, 60 pp

Mehta R (2009) The maze of mixed plastics recycling. Mater World 17(7):10

Moore C (2003) Trashed: across the Pacific Ocean, plastics, plastics, everywhere. Nat Hist 112:46–51

Myers A (2007) What comes around: breaking the cycle of plastics in the ocean. Ocean Conservancy, Autumn

Nash A (1992) Impacts of marine debris on subsistence fishermen – an exploratory study. Mar Pollut Bull 24:150–156

Nelson C, Williams AT (1997) Bathing water quality and health implications. In: Rajar R, Brebbia CA (eds) Water pollution IV. Modelling, measuring and prediction. Computational Mechanics Publications, Southampton, MEDCOAST Secretariat, Middle East Technical Univeristy, pp 175–183

NRC (National Research Council) (2008) Tackling marine debris in the 21st century, Communications on the effectiveness of national and international measures to prevent and reduce marine debris and its impacts

OC (Ocean Conservancy) (2009) A rising tide of ocean debris... and what we can do about it, Ocean Conservancy, 1330, 19th street NW, Washington, DC, 20036, USA, 64 pp

Oigman-Pszczol SS, Creed JC (2007) Quantification and classification of marine litter on beaches along Armãçao dos Búzios, Rio de Janeiro, Brazil. J Coast Res 23(2):421–428

Oldridge S (1992) Bathing water quality: a local authority perspective. In: Kay D (ed) Recreational water quality management, vol 1, Coastal waters. Ellis Horwood Ltd., Chichester, pp 33–47, 220 pp. ISBN ISBN 0-13-770025-3

Olin R, Carlsson B, Stahre B (1995) The west coast of Sweden – the rubbish tip of the North Sea. In: Earll RC (ed) Coastal and riverine litter: problems and effective solutions, Coastal Management for Sustainability, Candle Cottage, Kempley, Glos, UK, pp 12–18

Philipp R (1993) Community needlestick accidents and trends in environmental quality. Public Health 107:363–369

Philipp R, Hodgkinson G (1994) The management of health and safety hazards in tourist resorts. Int J Occup Environ Health 7(3):207–219

Philipp R, Pond K, Rees G (1995) A study of litter and medical waste on the UK coastline. Health Hyg 16:3–8

Pilz H, Brandt B, Fehringer R (2010) The impacts of plastics on life energy consumption and greenhouse gas emissions in Europe, Denkstatt summary report, denkstatt GmbH Hietzinger HauptstraBe 28. 1130 Vienna, Austria, 45 pp

Plastics Europe (2011) Plasticseurope/documents/plastics (accessed 4 Nov 2011); and Plastics; the Facts, 2011. An analysis of European plastic production, demand and recovery for 2011

Pollard S (1996) Beachwatch '96. 1995 Nationwide beach-clean and survey report. The Marine Conservation Society, Ross-on-Wye

Redahan E (2011) Making the most of a mixed bag. Mater World 19(7):9

Rees G, Pond K (1995a) Impacts: aesthetics, health and physical clearance. In: Earll RC (ed) Coastal and riverine litter: problems and effective solutions, Coastal Management for Sustainability, Candle Cottage, Kempley, Glos, UK, pp 5–7
Rees G, Pond K (1995b) Marine litter monitoring programmes – a review of methods with special reference to national surveys. Mar Pollut Bull 30(2):103–108
Ribic CA (1998) Use of indicator items to monitor marine debris on a New Jersey beach from 1991–1996. Mar Pollut Bull 36(11):887–891
Ryan PG (2008) Seabirds indicate changes in the compositiion of plastic litter in the Atlantic and south western Indian oceans. Mar Pollut Bull 56(8):1406–1409
Ryan PG, Connell AD, Gardner BD (1988) Plastic ingestion and PCBs in seabirds: is there a relationship? Mar Pollut Bull 19(4):174–176
Santos IR, Friedrich AC, Barretto FB (2005) Overseas garbage pollution on beaches in northeast Brasil. Mar Pollut Bull 50:778–786
Silva JS, Barbosa SCT, Costa MF (2008) Flag items as a tool for monitoring solid wastes from users on urban beaches. J Coast Res 24(4):890–898
Silva-Iñiguez L, Fisher DW (2003) Quantification and classification of marine litter on the municipal beaches of Ensenada, Baja California. Mar Pollut Bull 46(1):132–138
Simmons SL, Williams AT (1993) Persistent marine debris along the Glamorgan Heritage Coast, UK: a management problem. In: Sterr H, Hofstide J, Plag P (eds) Interdisciplinary discussions of coastal research and coastal management: issues and problems. Peter Lang, Frankfurt, pp 240–250
Tanabe S, Watanabe M, Minh TB, Kunisue T, Nakanishi S, Ono H (2004) PCDFs and coplanar PCBs in albatrosses from the North Pacific and southern oceans: levels, patterns and toxicological implications. Environ Sci Technol 38:403–413
Thompson RC, Olsen Y, Mitchell RP, Davis A, Rowland SJ, John AWG, McGonigle D, Russell AE (2004) Lost at sea: where does all the plastic go? Science 304:838
Tomas J, Guitert R, Mateo R, Raga JA (2002) Marine debris ingestion in loggerhead sea turtles, Caretta caretta, from the western Mediterranean. Mar Pollut Bull 44(3):211–216
Tudor DT, Williams AT (2004) Development of a 'matrix scoring technique' to determine litter sources at a Bristol Channel beach. J Coast Conserv 10(1–2):119–127
Tudor DT, Williams AT, Randerson P, Ergin A, Earll R (2002) The use of multivariate statistical techniques to establish beach debris pollution sources. J Coast Res 36:716–725
UNEP (United Nations Environemnet Programme) (2009) Marine litter a global challenge. www.marine-litter.gpa.unep.org/facts/facts.htm. Accessed 7 Jan 2011
Uneputty P, Evans SM (1997) The impact of plastic debris on the biota of tidal flats in Ambon (Eastern Indonesia). Mar Environ Res 44(3):233–242
University of Surrey (1987) The public health implications of sewage pollution of bathing water. The Robens Institute of Industrial and Environmental Safety, Guildford, England, UK
Valle-Levinson A, Swanson RL (1991) Wind-induced scattering of medically-related and sewage-related flotables. Mar Technol Soc J 25(2):49–56
Velander K, Mocagni M (1999) Beach litter sampling strategies: is there a 'best' method? Mar Pollut Bull 38(12):1134–1140
von Saal FS, Hughes C (2005) An extensive new literature concerning low-dose effects of bisphenol A shows the need for a new risk assessment. Environ Health Perspect 113:926–933
Walker TR, Reid K, Arnould JPY, Croxall JP (1997) Marine debris surveys at Bird Island, South Georgia 1990–1995. Mar Pollut Bull 34(1):61–65
Ward J, Shumway S (2004) Separating the grain from the chaff: particle selection in suspension- and deposit-feeding bivalves. J Exp Mar Biol Ecol 300:83–130
Whiting SD (1998) Types and sources of marine debris in Fog Bay, Northern Australia. Mar Pollut Bull 36(11):904–910
WHO (World Health Organisation) (2000) Monitoring bathing waters. A practical guide to the design and implementation of assessments and monitoring programmes. E&FN Spon, London, UK

WHO (World Health Organisation) (2003) Guidelines for safe recreational water environments, vol 1, Coastal and freshwaters. WHO, Geneva
Widmer WM, Henneman MC (2010) Beach debris in the island of Santa Catarina, south Brazil: spatial patterns, composition and biological aspects. J Coast Res 26(6):993–1000
Williams AT (2011) Definitions and typologies of coastal tourism destinations. In: Andrew J, Phillips M (eds) Disappearing destinations: climate change and future challenges for coastal tourism. CABI, Wallingford, pp 47–66
Williams AT, Simmons SL (1997) Estuarine litter at the river/beach interface in the Bristol Channel, UK. J Coast Res 13(4):1159–1165
Williams AT, Tudor DT (2001) Tudor. Litter burial and exhumation: spatial and temporal distribution on a pocket pebble beach. Mar Pollut Bull 42(11):1031–1039
Williams AT, Tudor DT (2006) The question of dogs on beaches. Shore Beach 74(4):1–5
Williams AT, Pond K, Tudor DT, Jansen H, HongBin Liu (1999) The robustness of litter transect data collection by different survey groups. In: Ozhan E (ed) Proceedings of the MEDCOAST 9 – EMECS 99 Joint conference: land ocean interactions – managing coastal ecosystems, 715–726, MEDCOAST, Middle East Technical University, Ankara, Turkey
Williams AT, Pond K, Phillipp R (2000) Aesthetic aspects, Ch. 12. In: Bartram J, Rees G (eds) Monitoring bathing waters. E&F N Spon, London, Oxon, England, UK, pp 283–311
Winston JE, Gregory MR, Stevens LM (1997) Encrusters, epibionts, and other biota associated with pelagic plastics: a review of biogeographical, environmental and conservation issues. In: Coe JM, Rogers DB (eds) Marine debris: sources, impacts and solutions. Springer, New York, pp 81–97
www.PWMI.or.jp. An introduction to plastic recycling in Japan
www.WRAP.org.UK. Accessed 11 Aug 2011
www.apme.org. Accessed 15 Dec 2010
www.bpf.co.uk. Accessed 15 Dec 2010
www.plasticwaste.co.uk. Accessed 15 Dec 2010
www.sca.com. Accessed 19 Jan 2011
www.sita.co.uk. Accessed 19 Jan 2011
www.pafa.org.uk. Accessed 19 Jan 2011
www.vrtek.com.au. Accessed 15 Dec 2010
www.wales.gov.uk/newsroom/environmentandcountryside/2010/101130carrierbag/?lang=en. Accessed Dec 2010
www.theplastiki.com. Accessed 31 Dec 2010
YRLMP (1991) Yorkshire Rivers Litter Monitoring Project, 1991. Devised by the Tidy Britain group and sponsored by the national rivers authority, 12 pp

Chapter 25
Coastal Hazards from Oil Spills

Erich R. Gundlach

Abstract The transport and utilization of petroleum and its derivatives presents a spill risk in coastal areas. Not only do spills affect coastal and nearshore biota, but can cause severe economic costs due to closure of fisheries areas as well as direct losses due to business disruption. In most countries, compensation is available to assist those damaged by a spill. Often overlooked, spills can also affect the social well-being and health of both residents of the spill area and to workers brought in to assist cleanup. After spill prevention, adequate spill response planning is the best method to reduce potential damages to the ecosystem and to coastal residents.

25.1 Introduction

This chapter examines the risks and potential hazards of oil spills in marine, estuarine, riverine and lacustrine (lake) environments, generically referred to as 'coastal'. First is a review of the likelihood of a coastal spill and a description of factors that influence the potential for shoreline oiling based on spill movement and oil weathering. Once on the shoreline, oil interactions and cleanup requirements are highly influenced by the geomorphology of the affected coastline. Shoreline biota as well as coastal aquaculture facilities and fisheries are all likely to be affected. Coastal oil spills have serious economic, social and health effects on the local population living in the area, and on workers called in to assist the cleanup and recovery operations. Oil spill compensation programs are important to aid the economic recovery of those affected by a spill. The chapter concludes with the principal elements of an oil spill response (contingency) plan which aims to reduce both the risks of a spill as well as its associated hazards.

E.R. Gundlach (✉)
E-Tech International Inc., 15 River Park Drive, New Paltz, NY 12561, USA
e-mail: ErichEti@cs.com

C.W. Finkl (ed.), *Coastal Hazards*, Coastal Research Library 6,
DOI 10.1007/978-94-007-5234-4_25,

The oil spill literature commonly contains both volume and weight units, principally using metric tonnes, cubic meters (m^3), barrels (bbl) and gallons (gal). The exact conversion depends upon the specific gravity of the oil. The specific gravity of light oils is ~0.75 and approaches 1.0 for heavy oils. After weathering, oil may reach greater than 1.0 and potentially sink. Common conversions are shown below:

- 1 tonne (1,000 kg) = 7 barrels (bbl) = 294 U.S. gallons (gal).
- 1 tonne = 1,000 m^3 (Specific Gravity = 1.0).
- 1 barrel (bbl) = 42 U.S. gallons (gal).

The size and location of most oil spill events are catalogued by several major international organizations involved with oil spill response, including NOAA (http://archive.orr.noaa.gov; www.incidentnews.gov), ITOPF (http://www.itopf.com/) and CEDRE (http://www.cedre.fr/index-en.php), as well as other sources (e.g., www.Wikipedia.org). The amount of oil spilled may differ among these sources due to several factors. A common discrepancy occurs when a cargo fire is involved. The amount burned is unknown and therefore the amount spilled may refer to either the total amount lost (including the burned portion) or the amount in the water after burning. Oil spilled from subsea blowouts is another case where the exact quantity lost is unknown. In these cases a range of potential losses is often provided (e.g. the *Deepwater Horizon* blowout; FISG 2010).

25.2 Spill Source, Risk and Size

Coastal oil spills are most commonly caused by accidents associated with the transport of oil by barges, tanker vessels and pipelines. Spillage into coastal waters may also occur during transfer operations at coastal facilities or from leaking storage tanks. However, it is relatively uncommon for a tank spill to reach coastal waters due to containment walls required for each tank. Another major spill source is related to offshore drilling and production, whose performance record was severely tarnished by the *Deepwater Horizon* blowout in the Gulf of Mexico in 2010. Lastly, natural seeps have been noted in coastal waters for centuries. NRC (2003) estimates worldwide natural seepage at 600,000 to 2 million tonnes, and is the largest source of oil input to United States' (U.S.) waters at ~160,000 tonnes.

The amount of oil spilled has dramatically decreased over the last decades in response to industry improvement and government regulations and oversight. The International Tanker Owner's Pollution Fund (ITOPF) keeps records of vessel spills and reports that the worldwide annual quantity of oil spilled by marine transport decreased from >3 million tonnes in the 1970s and 1980s, to 1.137 million tonnes in the 1990s, and then to 211,000 tonnes in the 2000s (ITOPF 2011). This reduction has occurred at the same time that the amount of oil being transported increased from approximately 6,000 billion tonne-miles in 1970 to 10,000 billion tonne-miles in 2010.

Table 25.1 U.S. spillage (tonnes) averaged by decade for activities that may reach coastal waters

	Offshore[a]	Vessels[b]	Pipelines[c]	Cargo[d]	Facilities[e]
(A) 1968/9–1977	4,348	30,060	37,049	149*	8,889**
(B) 1978–1987	725	16,177	25,885	969	6,112
(C) 1988–1997	1,427	9,297	16,900	402	2,151
(D) 1998–2007	557	1,290	10,965	229	604
Change A to D	−87%	−95%	−70%	+54%	−93%

Modified from Etkin 2010
[a]Offshore oil exploration/production, including platforms, related pipelines and vessels
[b]Tank vessels, including ships and barges
[c]Coastal and inland pipelines
[d]Non-tank vessels (*1973–1977)
[e]Coastal facilities, non-refining (**1973–1977)

Table 25.2 U.S. spill rates for activities that may affect coastal waters

	Offshore[a]	Vessels[b]	Pipelines[c]	Cargo[d]	Facilities[e]
1998–2007	1.2	0.008	0.0478	0.16	Not given
Units	Tonnes spilled/ million tonnes produced	Tonnes spilled per million tonne-km oil transport	Tonnes spilled per million tonne-km oil transport	Tonnes spilled per million short tonnes shipped	Storage data for calculation not available

Data from Etkin 2010
[a]Offshore oil exploration/production, including platforms, related pipelines and vessels
[b]Tank vessels, including ships and barges
[c]Coastal and inland pipelines
[d]Non-tank (cargo) vessels (*1973–1977)
[e]Coastal facilities, non-refining (*1973–1977)

Spills in U.S. waters over a four decade period similarly show very large (−70 to −90%) reductions in almost all major categories of oil spills that could affect coastal waters (Table 25.1; Etkin 2010). Only spills from cargo vessels increased, but this is due to exceptionally low spill quantities from 1973 to 1976. (Note that for all other 10-year periods, cargo vessel spills also declined.) The largest source of industrial spillage is from pipelines (coastal and inland), but most onshore pipeline spills are unlikely to reach coastal waters.

The potential amount of oil spilled as a ratio of the total amount transported is shown by category in Table 25.2. For every million tonnes of oil carried by pipeline over a distance of 1 km, a potential loss of 0.0478 tonnes (75 kg) would statistically occur, based on the average decadal loss incurred from 1998 to 2007. Similarly, if a million tonnes comes into a port, then for every 1 km transited, a spillage rate of 0.008 tonnes (16 kg) is indicated. To transport a million tonnes would utilize approximately five *Exxon Valdez* sized vessels. Other sources of spill risk data include NRC (2003), Scanpower (2006) for offshore platforms and CONCAWE (2011) for European pipelines.

Most spills are small and are not publicized. For all U.S. offshore exploration and production spills between 1969 and 2007, 50% were 4 bbl or less and 95% were under 323 bbl. For coastal and inland pipeline spills, 50% were 12 bbl or less, and 95% were 1,260 bbl or less (API 2009). In the United Kingdom, for 259 spills reported from 1989 to 1998, 66% were 35 bbl or less and 95% were under 350 bbl (MCA 2000). Historically, a small number of large incidents dominate the quantity lost. For the decade 1990–1999, 73% of the total lost in spills over 7 tonnes was from just ten incidents. For the 2000s, 44% was from two incidents (ITOPF 2011).

In spite of statistics, a low probability of occurrence and historic improvements in reducing spillages do not guarantee that an oil spill won't occur. Numerous unlikely cases abound, e.g. *Exxon Valdez* leaving the well marked channel and grounding on Bligh Reef in Alaska, two vessels physically breaking apart and sinking (*Erika* and *Prestige*) off western Europe within a period of 3 years, and the statistically unlikely blowout of the *Deepwater Horizon* drilling platform in the Gulf of Mexico in 2010 resulting in the largest spill ever in U.S. waters.

25.3 Oil Transport and Extent of Shoreline Oiling

Transport and weathering processes begin as soon as oil is spilled. Transport is dominated initially by spreading and then by currents and winds. The general rule for calculating spill movement is by using 100% of the current vector and 3% of the wind speed. Weathering processes alter both the chemistry and quantity of oil, and include evaporation, dispersion, dissolution, photo-oxidation, biodegradation and emulsification. Evaporation (particularly of lighter oils where ~40% of the original volume may be removed) and emulsification (generation of a water-in-oil emulsion that may double the spill volume) are the dominant processes within the first days-to-weeks of a spill. Biodegradation gains in importance over the longer term. Weathering and transport processes are described in general terms by API (1999) and ITOPF (2002, 2010a), and for specific spills by Gundlach et al. (1983, *Amoco Cadiz*), Wolfe et al. (1994, *Exxon Valdez*) and FISG (2010, *Deepwater Horizon*).

As shown by several large spills (e.g. *Exxon Valdez* and Ixtoc I), oil in aquatic environments has an uncanny ability to travel great distances. However, the extent of shoreline oiling is not directly related to spill size. Several very large spills had no onshore oiling (Table 25.3, top), due to the distance offshore, current flow and weather (responsible for generating wind-driven currents that transport surface oil away from the shore and increase dispersion into the water column). At the other end of the spectrum, spills with substantial shoreline impacts (Table 25.3 bottom) were influenced by the quantity of oil released coupled with onshore winds and currents that transported oil along shore, oiling beach after beach.

Table 25.3 Variations in the extent of shoreline oiling from large oil spills

Date	Vessel	Tonnes	Oil type	Km oiled	Location	Reference
No shoreline oiling						
15 Dec 1976	*Argo Merchant*	28,000	Fuel oil	0	46 km SE of Nantucket	1
19 Jul 1979	*Atlantic Empress*	287,000	Crude	0	20 km E of Tobago	2
6 Aug 1983	*Castillo de Bellver*	252,000	Crude	0	130 km NW of Cape Town	2
8 Jun 1990	*M/V Megaborg*	14,300	Crude	0	100 km SE Galveston, Texas	3
28 May 1991	*ABT Summer*	260,000	Crude	0	1,300 km off Angola	2
Extensive shoreline oiling						
24 Mar 1989	*Exxon Valdez*	37,000	Crude	2,086	Prince William Sound, Alaska	4
13 Dec 2002	*Prestige*	63,000	Crude	1,900	Offshore, Galicia, Spain	5
20 Apr 2010	*Deepwater Horizon*	700,000 (+/− 10%)	Crude	1,750	Offshore, Gulf of Mexico	6,7

1. NOAA (2012a)
2. White and Baker (1998)
3. NOAA (2012b)
4. Owens (1991)
5. ITOPF (2012)
6. NOAA (2011)
7. Ramseur (2010)

25.4 Oil Impact on Shorelines

Shoreline geomorphology plays a large role in what happens to oil once it comes onshore. Oil interactions and persistence, ecological effects, and difficulty of cleanup are all distilled into the Environmental Sensitivity Index (ESI), which ranks shoreline types on a scale of 1–10, with 10 being the most sensitive (Gundlach and Hayes 1978; IPIECA 1996; NOAA 2002; Table 25.4). The characterization of coastal environments using the ESI is an accepted international standard in oil spill response planning. Maps and wildlife data tables summarize available information on habitats, protection guidance and recommended spill response measures (e.g. NOAA 2010).

25.5 Oil Spill Cleanup and When to Stop

Oil spills and its associated cleanup are a messy, noisy business. Responding to a spill requires significant resources, potentially including surveillance helicopters and fixed-wing aircraft, a flotilla of boats and specially designed oil recovery

Table 25.4 Standard Environmental Sensitivity Index (ESI) shoreline types and interaction with spilled oil

ESI #	Shoreline type	Interaction with oil
1	Exposed rocky cliffs Exposed solid man-made structures	Wave reflection generally keeps oil offshore. If deposited, most oil is rapidly removed by wave action. Heavy, viscous oils are an exception and will persist much longer
2	Exposed wave-cut platforms Exposed scarps and steep slopes in clay	
3	Fine- to medium-grained sand beaches	Sediment-dominated shores: As sediments coarsen, oil penetration and potential oil burial increase. Gravel beaches are particularly prone to deep burial and penetration by oil, show long-term persistence and are among the most difficult to clean
4	Coarse-grained sand beaches	
5	Mixed sand and gravel beaches	
6	Gravel beaches (Granule – to Boulder) riprap	
7	Exposed tidal flats	Limited penetration and burial by oil, but shellfish and other biota may be affected if present
8	Sheltered rocky shores Sheltered scarps in bedrock, mud or clay Sheltered riprap Peat shorelines	Limited penetration into substrate, but biota may be injured where present. Oil may enter openings in riprap, making cleanup very difficult. Peat shorelines may absorb oil
9	Sheltered tidal flats Vegetated low banks Hypersaline tidal flats	Oil tends to persist longer because of sheltered nature and will likely cause ecological damage
10	Marshes (Salt, Brackish and Freshwater) Scrub-shrub wetlands Mangroves Inundated low-lying tundra	High ecological damage is likely and persistence may be long term if heavily oiled and oil is mixed into the underlying sediments

Types and rankings may differ by location and/or country (e.g. for Brazil see MMA 2004). Photographic examples are shown in Fig. 25.1

vessels, various types of equipment including booms, sorbents, skimmers, pumps, generators, and shore-based heavy machinery such as backhoes, front-end loaders and sand-cleaning equipment. The personnel essential for the effort may easily number in the hundreds to many thousands and require substantial support including feeding, shelter, personal protection gear, decontamination facilities, first aid and hospitalization. Personnel trained and working at the *Deepwater Horizon* 2010 spill in the Gulf of Mexico numbered over 45,000 (NIOSH 2010).

A sampling of cleanup activities on different shorelines is provided below in Fig. 25.2. CEDRE (2012) provides web-based information on commonly applied methods. Cleanup operations may be of short duration if a small amount is spilled and oil remains accessible on the beach surface. However, cleanup lasting months and even years may be required for larger spills, particularly if oil penetrates deeply into beach sediments.

Fig. 25.1 Example shoreline types of the Environmental Sensitivity Index (ESI) (Photographs by E.R. Gundlach)

Cleanup activities invariably reach a stage where continued actions may cause more harm than good. The application of a Net Environmental Benefit Analysis (NEBA) enables determination of a scientifically based end point (IPIECA 2000). Other factors, however, may come into play, particularly concerning recreational use issues which require a higher level of cleanup. OSAT-2 (2011) provides a detailed NEBA for oil remaining on sand beaches after the first season of cleanup at the *Deepwater Horizon* incident.

ESI# 5: Mixed Sand and Gravel Beach, oiled to >30 cm the *Metula* spill, Patagonia, Chile, 1976.

ESI# 6: Gravel (Cobble-Boulder) Beach at the *Exxon Valdez* (1989) spill site.

ESI #7: Exposed Tidal Flat, covered with dead and dying shellfish at the 197 *Amoco* 8 *Cadiz* spill site.

ESI #8: Sheltered Rocky Shore, oiled at the 1978 *Amoco Cadiz* spill site.

ESI #9: Sheltered Tidal Flat, Maine, USA.

ESI #10: Marsh; heavily oiled at the 2002 Swanson Creek spill site, Maryland, USA.

Fig. 25.1 (continued)

At large spills, it is nearly impossible to remove all shoreline oil in spite of very significant cleanup actions. The *Exxon Valdez* (1989) spill is the case example: government-required cleanup ended in 1991 after 3 years of intensive effort to remove gross surface oil contamination and to treat heavily oiled subsurface gravels. Continuing cleanup past this point would cause more harm than good: "The consensus and judgment of state and federal agencies involved in the spill response is that additional cleanup would cause unacceptable environmental harm" (Leschine et al. 1993, page 198). However, investigations over more than 20 years show that subsurface oil still persists (although declining) at a limited number of locations (Page et al. 2012). The remaining oil is below the zone of active flushing and nutrient transport, where both physical and biodegradational processes are extremely limited (Li and Boufadel 2011; Pope et al. 2010). Oil sequestered in this manner is unable to cause biological damage (not 'bioavailable', Neff et al. 2006). Other spills showing long-term persistence even after an extensive cleanup include the *Arrow* spill in Nova Scotia, Canada (at least 35 years; Owens et al. 2008) and *Amoco Cadiz* in Brittany, France (at least 23 years; Oudot and Chaillan 2010).

Fig. 25.2 Examples of coastal oil spill response activities (Photographs by E.R. Gundlach)

25.6 Biological Effects

Oil spills can affect biota directly by smothering and indirectly via oil toxicity on the skin or in the water column. Factors influencing the ecological effects of a spill are summarized in Table 25.5. Many references provide descriptions of impacts to birds, fish, marine mammals, marine turtles, shoreline biota and commercial species (e.g. NRC 2003; NOAA 2012c; IPIECA 2012).

Ecological recovery begins soon after first impacts, gaining in strength after cleanup operations are complete. "Recovery" has several meanings related to oil spills. For major shoreline studies of the *Exxon Valdez* spill (summarized in Gundlach et al. 2013), Gilfillan et al. (1995) and Stekoll et al. (1996) found substantial recovery (>70%) within 2 years based on analysis of significant differences (positive or negative) between oiled and unoiled sites for measured biological attributes (e.g. abundance, species richness, diversity, etc.). This assumes that the oiled sites will return to levels equal to the selected control sites. It is widely accepted, however, that a statistical match between reference and oiled sites may

High-pressure, hot-water treatment with chemical additive to remove oil adhered to bedrock/boulder shorelines at the *Tanio* oil spill site, Brittany, France.

Hand cleanup of a boulder-dominated shoreline, Alaska.

Sand washing operation to remove oil spilled from the Jiyah power plant spill, Lebanon.

Decontamination of oiled boom, Texas.

Fig. 25.2 (continued)

never occur considering all the dynamics and interactions possible (e.g. Baker 1990; Sell et al. 1995; Kingston 2002; Laubier et al. 2004). With this understanding, Coats et al. (1999) used a statistical parallelism methodology, finding that recovery on rocky shores at the *Exxon Valdez* site was mostly complete within 2 years and totally complete in 4 years. Parallelism considers that the measured statistical component (e.g. abundance, percent cover) will track in parallel fashion between oil and unoiled sites when recovered, even though they are not equal.

Population statistics as described above may indicate recovery, but other researchers argue that recovery must also consider the habitat (age-class) structure of biota present (Southward 1982; Suchanek 1993; Paine et al. 1996). Using this definition, many more years are likely to be needed for the habitat to regain the same species age and size class structure present before the incident. Along rocky shores at the *Torrey* Canyon (1967) site, heavily affected by the application of chemical detergents in addition to the oil, age-class differences extended nearly 15 years after the incident (Hawkins and Southward 1992).

For coastal habitats, French-McCay (2009) reviews habitat recovery times for use in a bio-effects computer model (Table 25.6). Note that using a 99% level of

Table 25.5 Factors influencing biological effects of an oil spill

Factor	Potential effect
Quantity spilled	Influences potential area covered (surface waters and shoreline) and quantity/thickness in specific locations
Oil type	Lighter oils (gasoline, diesel, light fuel oil) are more toxic. Heavy oils (bunker, heavy fuel oil) persist longer, but are less toxic
Location	Spills near sensitive resources areas (particularly bird rookeries, marsh/mangrove shorelines, seal/turtle habitats) are likely to show greater ecological effects
Season	Influences type and abundance of biota present, particularly related to birds and marine mammals/turtles that occupy locations on a seasonal basis
Weather and sea conditions	Extensive rainfall and rough sea conditions can reduce impacts by washing oil off oiled shorelines and dispersing it into the water column
Protection strategy	Collecting oil offshore and preventing impacts to sensitive areas reduces impact to shoreline and water column organisms. Controlled burning and offshore dispersant application may be used under certain circumstances
Cleanup method	Properly applied cleanup reduces spill quantity and assist ecological recovery. Net Environmental Benefit Analysis (NEBA) determines cleanup termination and when natural recovery can begin
Exposure	Includes both oil concentration and duration of exposure
Species life stage and sensitivity	Young/larval stages show greater sensitivity. Some species show greater or lesser sensitivity due to preening, feeding and/or avoidance

Table 25.6 Estimated recovery times of species found on major shoreline types. Age-class recovery is not included

Habitat	Time to 99% recovery
Rocky shores	3 years – invertebrates
Sand beaches	3 years – benthic invertebrates
Gravel beaches	3 years invertebrates and algae
Mud flats	3 years – benthic invertebrates
Marshes	5 years – invertebrates, 15 years – vegetation
Mangroves	5 years – invertebrates, 20 years – vegetation

Modified from French-McCay (2009)

recovery considers low level effects that might remain even after the vast majority of areas have recovered.

The direct killing of fish by oil toxicity, requiring concentrations >~100 ppm, is uncommon in open waters but is more likely for onshore pipeline and rail spills entering a small creek or stream. Some fish avoidance of oiled sediments may occur (Martin 1992), but it is not clear whether avoidance also occurs in oiled open water conditions (NRC 1985).

Commercial and recreational area fishery closures are common during major spills. The area closed during the *Deepwater Horizon* spill reached over 220,000 km^2 or 37% of federally controlled waters in the Gulf of Mexico (NOAA 2012d). In addition,

state waters (within 4.8 km of the shoreline) also had substantial closures: Alabama (40%), Florida (2%), Louisiana (55%) and Mississippi (95%). The related revenue losses in the Gulf of Mexico are potentially enormous. Using 2008 pre-spill data as a basis, landings from commercial operations were nearly US$ 700 million and recreational fishing (durable equipment and trips in the Gulf) accounted for over US$ 12.5 billion (Upton 2011).

Aquaculture sites, by their location in the nearshore coastal zone where oil concentrations are usually highest, are likely to be affected by spills. Although some purging of contaminants (self cleansing) occurs with shellfish when clean waters are restored, the contaminated harvest is likely to be destroyed in entirety to protect the industry from highly negative publicity that would occur if some contaminated product made it to market.

25.7 Economic Losses and Compensation

The presence of spilled oil degrades the natural environment and reduces human enjoyment of the affected area. The economic impacts of an oil spill may be extensive and far reaching. Direct losses commonly include:

- Salvage, repairs, pollution control, surveillance and cleanup activities.
- Financial value of lost cargo to the owner.
- Property damage (e.g. oiling of boats and gear, damage to roads and piers).
- Lost income or product (e.g. fishers, aquaculture facilities, hotel operators, etc.).
- Government costs (e.g. time spent dealing with spill issues) and revenue losses (e.g. from taxes on hotels or government owned recreational areas).
- Costs of reasonable measures to reinstate a damaged environment.
- Measures to prevent economic loss (e.g. publicity campaigns to increase tourism or verify safety of marketed fish).
- Losses to those who sell goods and services to directly affected industries (e.g. those that make items for shops to sell to tourists or sell fuel to fishing and recreational vessels).

All nations (and their governmental agencies, businesses and individuals) have the ability to access compensation up to approximately US$ 362 million by being national signatories to the 1992 Civil Liability Convention and 1992 Fund Convention. As of 2012, there are 109 national governments (States) as signatories. (www.IOPCFund.org). In addition, following the high costs associated with the *Erika* (1999) oil spill, a Supplementary Fund Protocol was instituted that provides compensation up to approximately US$ 1 billion (28 States are signatories in 2012). A claims manual defines compensable requirements and substantiating documentation (IOPC 2008). Compensable losses must directly link to the location and timing of the spill, and the geographic proximity of the claimant to the spill is important.

Table 25.7 Largest payments through 2009 under the international Fund Conventions

Incident	Location/date	Spilled	Compensation
Antonio Gramsci	Porvoo, Sweden 27 February 1979	5,500 tonnes	US$ 16 million[a]
Tanio	Brittany, France 7 March 1980	8,700 tonnes	US$ 32 million[a]
Haven	Genoa, Italy 11 April 1991	144,000 tonnes*	US$ 52 million[a]
Aegean Sea	La Coruña, Spain 3 December 1992	73,550 tonnes*	US$ 59 million[a]
Braer	Shetland Islands UK 4 January 1993	84,700 tonnes	US$ 81 million[a]
Sea Empress	Milford Haven, UK 15 February 1996	73,000 tonnes	US$ 54 million[a]
Nissos Amorgos	Maracaibo Channel, Venezuela 28 February 1997	3,600 tonnes	US$ 24.4 million[b]
Nakhodka	Japan 2 January 1997	6,240 tonnes	US$ 190 million[a]
Evoikos	Strait of Singapore 15 October 1997	29,000 tonnes	Not all parties signatories. US$ 5.2 million[b]
Erika	Brittany, France 12 December 1999	~19,000 tonnes	US$180 million[c] Max Available: US$ 185 million Settlement ongoing[b]
Prestige	Spain, France, Portugal 13 November 2002	64,000 tonnes	US$73 million[a] Max Available: US$ 192 million

[a]Jacobsson (2005)
[b]IOPC (2010)
[c]ITOPF (2010b)
*Burned and spilled

Examples of compensation released by the Fund are shown in Table 25.7. In the case of the *Prestige* spill, expected claims were over US$ 1.2 billion while the maximum amount available at the time was US$ 192 million. As a result, payments were limited to first 15% of the original claim, and then later increased to 30% (Jacobsson 2005). The Supplementary Fund Protocol, as discussed above, was developed to provide additional compensation to avoid such shortfalls.

The United States is not a signatory to the international Fund Conventions but has its own Oil Spill Liability Trust Fund developed in response to the *Exxon Valdez* incident. Monitored by the U.S. Coast Guard's National Pollution Funds Center (NPFC), it was established to cover spill-associated response and removal costs and damages. The NPFC covers costs above set limits of liability for the vessel based on type and gross tonnage. For example, a double hulled tank vessel greater than 3,000 gross tons has liability limited to US$ 2,000 per gross ton, or $17,088,000 whichever is greater. As vessel and spill size are not directly related to potential economic costs, liability limits may be exceeded, particularly with vessels

having small gross tonnage and high spill costs. In this case the NPFC covers the additional costs above the owner's liability. Funding is principally generated from a tax (raised to US$ 0.08 in 2009) per barrel of petroleum produced in, or imported into, the U.S.

For major events, the responsible party may waive liability limits rather than suffer public and political backlash. The *Exxon Valdez* incident greatly exceeded the liability limits at the time, and Exxon supported over several billion US$ in cleanup costs alone. Similarly, liability in the *Deepwater Horizon* incident was limited by law to US$ 75 million yet BP covered all cleanup activities and additionally set up a US$ 40 billion damage claim fund and a US$ 500 million restoration fund. As of February 2012, over 570,000 claim applications were received, of which over half had received some level of payment for a total of nearly US $6 billion. Terms of a settlement between BP and (non-governmental) plaintiffs reached in March 2012, transferred the remaining funds to a court-appointed overseer with estimated payout of US$ 7.8 billion to fishers and other claimants. Financial penalties (e.g. failure to report a spill, causing death of migratory waterfowl, negligence, etc.) are additional and can be substantial.

Neither the international Fund program nor the U.S. Oil Spill Liability Trust Fund cover scientific studies not specifically related to cleanup or assessment actions, regardless of importance to better understand oil spills.

25.8 Damages to Natural Resources

While both the international Fund Conventions and U.S. programs cover environmental restoration (e.g. replanting oiled marshes, reseeding commercial clam beds), the U.S. compensation program also includes lost-use as part of the restoration requirements. Not only does it consider the restoration of the oiled habitat with all associated organisms but also the duration for which the habitat is taken out of service. Therefore, additional restoration measures ("compensatory restoration") are needed to make up for the time these resources were unavailable in the environment. The U.S. Natural Resource Damage Assessment (NRDA) process includes the following steps:

- Determine and quantify natural resource injury.
- Identify and scale restoration actions (including natural recovery) to re-attain baseline conditions.
- Identify and scale compensatory restorations activities to make up for losses incurred.
- Select a preferred alternative(s) dependent on restoration objectives, likelihood of success, cost and other factors.
- Publish a restoration plan for comments and revise accordingly.
- Implement the selected plan.

Fig. 25.3 Oiled marsh on 2 November 1996 at the Julie N. spill site (*left*) and natural (no cleanup) recovery on 23 July 1997 (*right*) (Photographs by E.R. Gundlach)

Less than 1% of all U.S. oil spills require a NRDA, and then when applied, account for approximately 26% of total spill-related costs (i.e. cleanup, salvage, private payments, etc.) based on analysis of 30 spills from 1986 to 1997 (Helton and Penn 1999).

The *Julie N.* oil spill provides an indication of how the NRDA process works. On 27 September 1996, the vessel struck the south bridge abutment as it transited to its offloading terminal in Portland Harbor, Maine, USA. Two tanks were ruptured, releasing approximately 175,000 gal of fuel oil. A rapidly applied recovery and cleanup operation was successful in collecting 140,976 gal (78%). Oil impacted approximately 12 km of adjacent marshland (10.36 ha in area), 3 km of vertical harbor structures, and lesser quantities of primarily mixed sand and gravel shorelines. Cleanup focused on removal of oil and debris from the harbor structures and allowed oiled marshes to recover naturally (Fig. 25.3). The linkage of oil exposure, resource injury, financial settlement (US$ 1 million) and restoration program is illustrated in Table 25.8. When it comes to NRDA costs, the political and non-scientific nature of these settlements should not be underestimated. It seems not by scientific evaluation or chance that the *Julie N.* restoration program happened to reach an even US $1 million.

25.9 Psychological and Social Impacts

The impact of a spill on the social fabric of people living in the affected area is often overlooked and may be quite severe (Table 25.9).

To date, the *Exxon Valdez* event is the case example where evidence indicates short- and long-term social and psychological effects on individuals, families, and entire communities (Impact Assessment Inc. 2001). Those villages with direct ties to the environment were the hardest hit, showing high chronic stress levels compared to those outside the area (Picou and Gill 1996; Gill et al. 2012). Specific groups include coastal native villagers using biological resources as a major part of their food supply, and commercial fishers whose livelihood depends on the clarity

Table 25.8 Summary of exposure, injuries and application of US$ 1 million settlement at the *Julie N.* spill for natural resource damages

Marine communities (Settlement: US$350,000 for Local Oil and Grease Removal)		
Injured Resource//Service	***Exposure***	
Marine vegetation	106 m^2 and 154 kg cut and removed	
Blue mussels	Total PAH concentration ranged from 27,000 to 290,000 ppb (dry weight)	
Softshell clams	Total PAH concentration ranged from 14,000 to 110,000 ppb (dry weight)	
Vertical wall communities	10,738 m^2 of vertical wall exposed to either heavy oiling and/or hot washing	
Sediments	Four of the 25 sediment samples analyzed contained PAHs attributable to *Julie N.* oil, ranging from 3,600 to 67,000 ppb (dry weight)	
WETLANDS AND BIRDS (Settlement: US$ 475,000 for Wetland/Bird Restoration)		
Injured Resource//Service	***Exposure***	
Wetlands	10.36 ha lightly to heavily oiled	
Birds	27 dead birds and 1,679 cumulative observations of birds with visible oiling	
PUBLIC USE (Settlement: US$ 125,000 for Development of a Local Trail)		
Lost Public Use	***Exposure***	
Ferry boat trips	250 lots ferry trips	2,700 diminished ferry trips
School trail activities	1,280 lost trail activity trips	1,280 diminished trips
Charter boat trips	124 party/charter trips lost	
Recreational boating trips	4,862 lost person-day trips	
Tour boat trips	300 lost tour boat trips	
Whale watching trips	225 lost whale-watching trips	

Modified from MDEP (2000)

Table 25.9 Common concerns and manifestations of stress caused by an oil spill

Sources of concern	Manifestations
Loss of livelihood	Increased use of alcohol, drugs and cigarettes
Loss of way of life	Fighting, domestic violence and child abuse
Loss of control over one's life	Community disturbance/disruption
Need to move family	Anger during public meetings
Long-term health issues	Increased depression, helplessness and anxiety
Break-down of community values	Post-Traumatic Stress Disorder (PTSD)
Uncertainty about the future	Breakdown of social relationships
Workers having long hours and deployments away from home	Apathy – not caring about things
	Feelings of hopelessness
	Not able to function well at work, school or home
	Increased rate of suicide

and productivity of the area's marine waters. Native villages noted changes in their subsistence food species (shellfish, fish and seals, in particular) that, in spite of government assurances of safety, were causes of concern. This in turn increased their (further) distrust of government and feelings of loss of control.

Effects of the *Exxon Valdez* spill on traditional ways of life was still considered by most native households as not recovered 15 years later (Fall 2006). Even financial settlements exacerbated village disharmony (Miraglia 2002). Gill et al. (2012) describe spill-related effects that include increased drug and alcohol use and domestic violence; feelings of helplessness, betrayal, and anger; elevated levels of depression, anxiety, and post traumatic stress disorder; and adoption of avoidance coping strategies. Similarly at the *Sea Empress* spill in the United Kingdom (1996), residents living in oiled areas reported higher rates of physical and psychological (higher anxiety and depression) symptoms than in control areas (Lyons et al. 1999).

A recent survey performed at the *Deepwater Horizon* spill in 2010 showed great similarities to the early stages of the *Exxon Valdez* spill. Moderate to severe stress was found for almost half the respondents (Gill et al. 2012). The strongest predictors of stress were threats to the individual's economic future and family health concerns, economic loss, commercial ties to natural resources, exposure to oil, and age (older people showing greater stress). There has been a dramatic rise in domestic violence, more than doubling from the months just preceding the spill (Olsen, 2010). The *Exxon Valdez* spill followed the Great Alaska Earthquake in the same region, and the *Deepwater Horizon* blowout was 5 years after Hurricane Katrina. The appearance of a second disaster affecting the same residents caused higher anxiety and stress than from a single event alone (Miraglia 2002; Osofsky et al. 2011).

In dealing with these known stresses, it is important to break perceptions of helplessness and hopelessness. For the most part, few government or private services assist affected individuals and communities. The *Deepwater Horizon* event was quite different by including substantial funding to provide additional behavioral health and other social services to the affected states and communities (e.g. SAMHSA (2010) shows BP funding of US$ 52 million). Post-*Prestige* spill studies show that social and economic support can have very positive psychological benefits (Carrasco et al. 2007; Sabucedo et al. 2009).

25.10 Human Health Effects

The effects of a spill on human health are of greatest concern to the public living and working in an oil impacted area. The use of dispersants and/or controlled burning further amplifies concerns. Spill workers, with a higher likelihood of exposure to oil (and possibly oil/dispersant mixtures), are at greatest risk. Some components of crude oil (aromatic hydrocarbons such as benzene, ethyl benzene, toluene and xylenes) are considered human carcinogens.

Table 25.10 Common symptoms of human exposure to components of crude oil

Skin/mucous membranes	Erythema (redness), edema (swelling), irritation, dermatitis (rash, and blisters)
Ocular (eyes)	Redness, soreness, watering and itching
Respiratory	Cough, throat irritation (dry, scratchy, sore), shortness of breath and wheezing
Neurological	Nausea/vomiting, headache, dizziness, irritability, confusion and weakness of extremities

Modified from Sathikumar 2010

There are three exposure pathways for spilled oil and its chemical constituents to affect human health:

- **Inhalation** – Primarily related to the inhalation of Volatile Organic Compounds (VOCs), the lighter components of oil which are particularly present during the first stages of a spill when evaporation is greatest and often clearly noted by the smell of petroleum. As oil weathers, the VOC content declines and inhalation issues decrease. VOCs can also enter the body through the skin and other membranes in addition to the lungs. Warm weather and sunshine can again set off additional evaporation and hydrocarbon odors. High-pressure spraying, as during most cleanup and decontamination activities can volatize even weathered oil and cause respirable airborne droplets. Oil burning can create very small, micron sized particles that can be inhaled. Pollutants from oil combustion, such as sulfur dioxide, benzene, hexane and xylenes, may attach to these particles.
- **Direct contact** – Direct oil contact with skin and eyes may occur in spite of Personal Protection Equipment (PPE), such as during oil recovery or boom placement from a boat, onshore beach cleanup, oily waste collection, and equipment handling during decontamination activities. Skin contact during oil splash up by waves is common for boat operators. Continued use of ruptured or broken PPE by workers may also result in skin contact.
- **Ingestion** – Ingestion of oil may occur by eating oil-tainted food or drinking oil contaminated water. Ingestion of oil tainted fish or shellfish is of major concern to the public and usually monitored by government agencies. Ingestion may also occur accidentally through mouth contact and swallowing of oil-contaminated spray (as during boat movement or high-pressure washing).

The major acute effects of exposure to selected crude oil are shown in Table 25.10. Historically, relatively few studies of spill effects on human health have been done, but are becoming more common place with the increased emphasis on human health as part of understanding the overall environmental effects of a spill. A summary of spills having public health data is shown in Table 25.11 (see also: Aguilera et al. 2010; Goldstein et al. 2011).

In addition to the health issues described above, spill-related injuries are also likely to occur. For a 13 week time period at the *Deepwater Horizon* spill, 46.6% of the 2,099 total cases were illness related while 53.4% were injury related (NIOSH 2010). The total of both averaged 0.6% (range: 0.1–1.0%) of the total work force

Table 25.11 Observed health effects at major oil spills

Spill//Reference	Results
***Brear* (UK)**	Principal health effects on days 1–2 were headache, throat irritation, and itchy eyes. No significant differences between those exposed and controls for any of the biological markers. Six months later, questionnaire results show 7% of exposed people reported poor health compared to 3% of the control group
Campbell et al., (1993)	
Campbell et al., (1994)	
***Sea Empress* (UK)**	Higher self-reported headaches, sore eyes, sore throats and generally ill (24% versus 7.4% for unexposed) for the period 4 weeks after the spill, directly related to spill presence
Lyons et al., (1999)	
***Nakhodka* (Japan)**	Analysis of 282 men and woman expressed symptoms of lower back pain and leg pain, headache and eyes and throat issues after beginning cleanup activities, increasing in occurrence with time involved
Morita et al., (1999)	
***Erika* (France)**	More than half of the 1,465 cleanup workers surveyed reported some malady: backache, headache, skin, eye or respiratory irritations were most common
Schvoerer et al., (2000)	
***Prestige* (Spain, France, Portugal)**	Detailed study of hundreds of 1 day and multiday workers found most common ailments were backache, dizziness, headache, and irritation to throat, eyes and nose
Gestal Otero et al., (2004)	
Zock et al., (2007)	Survey of >6,500 fishermen indicated 33% still had a lower respiratory tract symptom 1–2 years after cleanup. Longer exposure and more tasks showed higher respiratory issues
Carrasco et al.,(2006)	Study of several hundred spill workers showed issues with itchy eyes, nausea/vomiting/dizziness, throat and respiratory problems and headaches; with some significant reduction in symptoms for those informed of health risks and using protective equipment
Rodríguez-Trigo et al., (2010)	Two years after the spill, fishermen in exposed areas (501) compared to those not exposed (177) showed higher (~2–6%) respiratory symptoms, higher exhaled 8-isoprostane levels. Lung function did not significantly differ between the groups. A higher proportion of exposed participants had structural chromosomal alterations, but was not directly tied to the spill
***Tasman Spirit* (Pakistan)**	96% of residents inside spill area showed increases in one or more categories compared to residents 2 km (70%) and 20 km (85%) away relating to eyes, respiratory tract, skin and nervous system, smoking, allergies, beliefs about the effect on their health and anxiety about the health effects
Janjua et al., (2006)	
Meo et al.,(2008)	Significantly impaired lung function in 20 oil spill workers (averaging 13 days on the spill) as compared to 31 unexposed workers; reverted to normal 1 year later
***Hebei Spirit* (Korea)**	Respiratory failure of 66 year old woman may have been induced by hydrocarbon inhalation during oil spill cleanup. The woman recovered with treatment
Kyung et al., (2009)	
Cheong et al., (2011)	42–82% of 288 resident cleanup workers (55% working more than 3 weeks) self-reported physical symptoms; for 60% symptoms were same or increased 2–8 weeks later
	Urine analysis of 154 workers showed a significantly higher VOC metabolite (mandelic acid) with highest levels at weeks 5–6. Other VOC metabolites were higher as well. Those workers having higher VOC metabolite levels reported significantly higher physical symptoms

(continued)

Table 25.11 (continued)

Spill//Reference	Results
***Deepwater Horizon* (USA)** IOM (2010)	State medical surveillance programs showed that most of the illnesses were among rig workers and cleanup workers, with headache, nausea, skin rash and throat irritation being most common. Most symptoms were inhalation related, with dermal contact and ingestion being much less common.
CDC-NIOSH (2010)	Responding to questionnaires (416 persons exposed to oil, 156 exposed to dispersant), 25–33% reported upper respiratory problems compared to 14.4–18.3% for unexposed ($p < 0.01$), 19.5–27% had cough compared to 7.9–10% unexposed ($p < 0.01$), and 12–18% had lower respiratory symptoms compared to 4–4.7% ($p < 0.01$).

Table 25.12 Total reported injury and illness data over a 13 week period during the *Deepwater Horizon* incident (average 26,222 workers per week and includes time of maximum personnel (46,271))

INJURY	First aid	First aid plus[a]	% of total
Burns	51	2	5.0
Traumatic unspecified	93	10	9.8
Bites//Stings	134	14	14.1
Lacerations//Punctures	179	34	20.3
Contusions and hematomas	256	8	25.1
Sprains, muscle and joint pain	187	82	25.6
			100.0
ILLNESS	First aid	First aid plus[a]	% of total
Cardiovascular	15	13	3.7
General symptoms[b]	36	6	5.5
Dermatologic	75	3	10.3
Gastrointestinal	113	9	16.1
Headache/Dizziness	126	1	16.7
Multiple symptoms	148	23	22.5
Heat stress and heat effects	171	21	25.3
			100.0

Data from NIOSH (2010)
[a]Includes missed day of work, restricted duty or medical attention beyond first aid
[b]Not specific; includes malaise, fatigue and non-specified allergic reactions

over the 13 week period. Fluctuations in illnesses were particularly tied to temperature-related heat stress. The type of injury and illnesses reported when known are defined in Table 25.12. Injuries tied to the physical work of cleanup were most common (sprains, contusions, lacerations). Illnesses were most commonly heat related, multiple symptoms, headache/dizziness and gastrointestinal issues. The US$ ~7.8 billion, March 2012 settlement between BP and plaintiffs includes financial remuneration for individuals claiming Gulf spill health effects.

The studies undertaken on the effects of oil spills on human health indicate the following:

- The understanding of the oil exposure on human health is not well understood.
- Exposure to fresh oil (closer to the source) poses greater health risks than does weathered oil.
- Uptake of VOC is illustrated by metabolites in the urine of cleanup workers, increasing with the duration of exposure to spilled oil (e.g. Cheong 2011).
- Those workers showing VOC metabolites in the urine reported significantly higher occurrence of one or more physical impairments (e.g. nasal irritation, nausea and vomiting sensation, fatigue and fever, skin and eye irritation, headache) (Cheong 2011).
- Longer spill exposures show greater heath effects.
- Education regarding potential health effects and the use of protective gear reduces acute and longer-term health issues.
- Although not explicitly studied, VOCs and spill related effects will be greater in children (IOM 2010) and those having existing physical conditions (e.g. reduced lung capacity through smoking or disease).

25.11 Response Planning to Reduce Impacts

When spill prevention fails, spill response planning is the primary method to reduce potential environmental, socio-economic and health-related damages. The International Convention on Oil Pollution Preparedness, Response and Cooperation (OPRC), developed by the International Maritime Organization (IMO), provides guidance on developing a response plan. The OPRC is ratified by individual nations, which then develop the internal legal basis to conform to the Convention. A government agency is designated to oversee oil spill preparedness and response, and is the national contact for reporting a spill and to request international assistance. Responsibilities of government and private companies are designated in the OPRC guidelines, and include pre-positioned response equipment (commensurate with risk), a program of exercises and training, maintenance of detailed response plans and communications pathways, and a management system for coordinating response efforts.

Response planning involves the integration of national and local governments, port and coastal authorities, emergency services, oil transport, production and storage companies, contractors, environmental organizations, and local communities. Typical components of a response plan are outlined in Table 25.13. Importantly, the plan must be continuously tested and updated. Response exercises can be of many varieties, such as testing of specific plan components or the interface between government and industry responders. A full equipment deployment exercise at least once every 2 years is also a critical part of the plan review.

Table 25.13 Principal components of an oil spill response plan

1 - Introduction and scope
1.1 Authorities and responsibilities, coordinating committee
1.2 Statutory requirements, relevant agreements
1.3 Geographical limits of plan
1.4 Interface with other plans/representation at joint control centers
2 - Oil spill risks
2.1 Identification of principal activities and risks
3. Response management structure
3.1 Coordinating structure (Government, Private)
3.2 Incident management roles and responsibilities
4 - Spill response strategy
4.1 Objectives
4.2 Tier 1, 2 and 3 response activities
4.3 Response by location – offshore, nearshore, shoreline, onshore
4.4 Waste transport and management
4.5 Disposal sites
5 - Communications and control
5.1 Incident control room and facilities
5.2 Field communications equipment
5.3 Reports, manuals, maps, charts and incident logs
6 - Training
6.1 Levels and requirements
7 – Media relations
7.1 Coordination
8 – Volunteers
8.1 Use of volunteers + training during spill response
9 – Wildlife capture and rehabilitation
8.1 Methods and procedures
Appendices
Initial procedures
Reporting incident, preliminary estimate of response Tier
Notifying key team members and authorities
Establishing and staffing control room
Collecting information (oil type, sea/wind forecasts, aerial surveillance, beach reports)
Estimating slick fate (24, 48 and 72 h)
Equipment, supplies and services
Type and contact information
Response scenarios (varying by spill size and location)
Material safety data sheets
Common oil types handled
Facility map (with potential flow arrows)
Environmental sensitivity maps
Probable spill movement
High risk locations

With prudent planning and proper attention to spill prevention and risk, the level of spill losses and coastal impacts associated with petroleum-related operations in the coastal zone can be further reduced.

References

Aguilera F, Mendez J, Pisaro E, Laffon B (2010) Review of the effects of exposure to spilled oil. J Appl Toxicol 30:291–301. doi:10.1002/jat.1521

API (1999) Fate of spilled oil in marine waters: where does it go? What does it do? How do dispersants affect it?. American Petroleum Institute, API Publication 4691-1999, Washington, DC, 57 pp

API (2009) Analysis of U.S. oil spillage. API Publication 356, Prepared by Etkin DS. American Petroleum Institute, Washington, DC, 86 pp

Baker JM (1990) Natural recovery of cold water marine environments after an oil spill. In: Arctic and Marine Oilspill Program (AMOP) Technical Seminar, Environment Canada, pp 173–177

Campbell D, Cox D, Crum J, Foster K, Chrístie P, Brewster D (1993) Initial effects of the grounding of the tanker *Braer* on health in Shetland. BMJ 307:1251–1255

Campbell D, Cox D, Crum J, Foster K, Riley A (1994) Later effects of grounding of tanker *Braer* on health in Shetland. BMJ 309:773–774

Carrasco JM, Lope V, Pérez-Gómez B, Aragonés N, Suárez B, López-Abente G, Rodríguez-Artalejo F, Pollán M (2006) Association between health information, use of protective devices and occurrence of acute health problems in the *Prestige* oil spill clean-up in Asturias and Cantabria (Spain): a cross-sectional study. BMC Public Health 6:9. doi:10.1186/1471-2458-6-1 http://www.ncbi.nlm.nih.gov/pmc/articles/PMC1368965/pdf/1471-2458-6-1.pdf. Accessed 1 Mar 2012

Carrasco JM, Pérez-Gómez B, García-Mendizábal MJ, Lope V, Aragonés N, Forjaz MJ, Guallar-Castillón P, López-Abente G, Rodríguez-Artalejo F, Pollán M (2007) Health-related quality of life and mental health in the medium-term aftermath of the *Prestige* oil spill in Galiza (Spain): a cross-sectional study. BMC Public Health 7:245. doi:10.1186/1471-2458-7-245

CDC-NIOSH (2010) Interim report # 9B, health symptom survey findings for response workers assigned to Plaquemines Branch Incident Command System, Louisiana, June 2010. Centers for Disease Control and Prevention – National Institute for Occupational Safety and Health, 6 pp. http://www.cdc.gov/niosh/topics/oilspillresponse/pdfs/report_9.pdf. Accessed 1 Mar 2012

CEDRE (2012) Techniques: what to do. www.cedre.fr/en/response/response-on-land/techniques.php. Accessed 1 Mar 2012

Cheong H-K, Ha M, Lee JS, Kwon H, Ha E-H, Hong Y-C, Choi Y, Jeong W-C, Hur J, Lee S-M, Kim E-J, Im H (2011) *Hebei Spirit* oil spill exposure and subjective symptoms in residents participating in clean-up activities. Environ Health Toxicol 26:9. doi:10.5620/eht.2011.26.e2011007

Coats DA, Imamura EI, Fukuyama AK, Skalski JR, Kimura S, Steinbeck J (1999) In: Shigenaka G, Hoff R, Mearns A (eds) Monitoring the biological recovery of Prince William Sound intertidal sites impacted by the *Exxon Valdez* oil spill, 1997 biological monitoring survey, NOAA technical memorandum NOS OR&R 1. NOAA Office of Response and Restoration, Seattle, WA, 102 pp

CONCAWE (2011) Performance of European cross-country oil pipelines; statistical summary of reported spillages in 2009 and since 1971. Report no. 3/11, Conservation of Clean Air and Water in Europe, Boulevard du Souverain 165, B-1160 BRUSSELS, Belgium, 54 pp

Etkin DS (2010) 40-Year analysis of US oil spillage rates. In: Arctic and Marine Oilspill Program (AMOP) Technical Seminar, Environment Canada, pp 529–554

Fall JA (ed) (2006) Update of the status of subsistence uses in *Exxon Valdez* oil spill area communities, Alaska Department of Fish and Game Division of Subsistence, Anchorage, Alaska 99518 Exxon Valdez Oil Spill Restoration Project Final Report Restoration Project 040471, Final Report l, 739 pp

FISG (2010) Oil budget calculator, *Deepwater Horizon*, technical documentation, Nov 2010. The Federal Interagency Solutions Group, 217 pp. http://www.noaanews.noaa.gov/stories2010/PDFs/OilBudgetCalc_Full_HQ-Print_111110.pdf. Accessed 1 Mar 2012

French-McCay D (2009) State-of-the-art and research needs for oil spill impact assessment modeling. In: Arctic and Marine Oilspill Program (AMOP) Technical Seminar, Environment Canada, pp 601–653

Gestal Otero JJ, Smyth Chamosa E, Figueiras Guzmán A, Montes Martínez A (2004) Recollida e limpeza do Prestige: avaliación da exposición e danos a saúde en voluntarios e traballadores [in Galician: Recovery and cleanup of oil from the *Prestige*: evaluation of exposure and health damages in volunteers and workers] Área de Medicina Preventiva e Saúde Pública da Universidade de Santiago de Compostela, Santiago de Compostela, Spain, 167 pp. www.fundacionarao.xunta.es/P01_gal.pdf. Accessed 1 Mar 2012

Gilfillan ES, Page DS, Harner EJ, Boehm PD (1995) Shoreline ecology program for Prince William Sound, Alaska, following the *Exxon Valdez* oil spill: Part 3 – Biology. In: Wells PG, Butler JN, Hughes J (eds) *Exxon Valdez* oil spill: fate and effects in Alaskan waters, ASTM STP 1219. American Society for Testing and Materials, Philadelphia, pp 398–443

Gill DA, Picou JS, Ritchie LA (2012) The *Exxon Valdez* and BP spills: a comparison of initial social and psychological impacts. Am Behav Sci 56(1):3–23

Goldstein BD, Osofsky HJ, Lichveld MY (2011) The Gulf oil spill. New Engl J Med 364:1334–1348

Gundlach ER, Hayes M (1978) Classification of coastal environments in terms of potential vulnerability to oil spill damage. Mar Technol Soc J 12(4):18–27

Gundlach ER, Boehm PD, Marchand M, Atlas RM, Ward DM, Wolfe DA (1983) Fate of Amoco Cadiz oil. Science 221:122–129

Gundlach ER, Page DS, Neff JM, Boehm PD (2013) Shoreline biota. In: Wiens JA (ed) Oil in the environment: legacies and lessons of the *Exxon Valdez* oil spill, Cambridge University Press, NY (in press). http://www.cambridge.org/gb/knowledge/isbn/item7111920/?site_locale=en_GB

Hawkins SJ, Southward AJ (1992) The *Torrey Canyon* oil spill: recovery of rocky shore communities. In: Thayer GW (ed) Restoring the nation's marine environment. Maryland Sea Grant Book, College Park, pp 583–631

Helton D, Penn T (1999) Putting response and natural resource damage costs in perspective. In: International oil spill conference, American Petroleum Institute, Washington, DC, 9 pp

Impact Assessment Inc (2001) *Exxon Valdez* oil spill, cleanup, and litigation: a collection of social-impacts information and analysis. Final report, vol III Final social factors. Report: Minerals Management Service, Environmental Studies Section, Anchorage, AK, 21 pp. http://www.alaska.boemre.gov/reports/2001rpts/2001_058/volume3.pdf. Accessed 1 Mar 2012

IOM (2010) Assessing the effects of the Gulf of Mexico oil spill on human health: a summary of the June 2010 workshop. Institute of Medicine, National Academies Press, M.A. McCoy and J.A. Salemo (Rapporteurs), Washington, DC, 183 pp

IOPC (2008) Claims manual. December 2008 Edn, International Oil Pollution Compensation Fund 1992, London, 39 pp. www.iopcfund.org/npdf/2008%20claims%20manual_e.pdf. Accessed 1 Mar 2012

IOPC (2010) Incidents involving the IOPC funds. International Oil Pollution Compensation Fund 1992, London, 103 pp

IPIECA (1996) Sensitivity mapping for oil spill response, IMO/IPIECA report series vol one. International Petroleum Industry Environmental Conservation Association, London, 28 pp

IPIECA (2000) Choosing spill response options to minimize damage, Net Environmental Benefit Analysis, IPIECA report series vol ten. International Petroleum Industry Environmental Conservation Association, London, 24 pp

IPIECA (2012) Library: oil spill preparedness. http://www.ipieca.org/library. Accessed 1 Mar 2012
ITOPF (2002) Fate of oil spills. The International Tanker Owners Pollution Federation Limited, London. 8 pp. http://www.itopf.com/marine-spills/fate/weathering-process/documents/tip2.pdf. Accessed 1 Mar 2012
ITOPF (2010a) Fate of oil spills. The International Tanker Owners Pollution Federation Limited, London. http://www.itopf.com/marine-spills/fate/. Accessed 1 Mar 2012
ITOPF (2010b) Cost of spills. http://www.itopf.com/spill-compensation/cost-of-spills/. Accessed 1 Mar 2012
ITOPF (2011) Oil tanker spill statistics, 2010. The International Tanker Owners Pollution Federation Limited, London. 12 pp. http://www.itopf.com/news-and-events/documents/STATSPACK2011.pdf. Accessed 1 Mar 2012
ITOPF (2012) *Prestige* (Spain 2007). http://www.itopf.com/information-services/data-and-statistics/case-histories/plist.html#PRESTIGE. Accessed 1 Mar 2012
Jacobsson M (2005) The international compensation regime and the activities of the international oil pollution compensation funds. ITOPF/INTERTANKO/OCIMF, International Seminar Tanker Safety, Pollution Prevention and Spill Preparedness, Shanghai, People's Republic of China, 16 pp. http://www.itopf.com/_assets/documents/jacobsson05.pdf. Accessed 1 Mar 2012
Janjua NZ, Kasi PM, Nawaz H, Farrooqui SZ, Khuwaja UB, Hassan NU, Jafri SN, Lutfi SA, Kadir MM, Sathiakumar N (2006) Acute health effects of the *Tasman Spirit* oil spill on residents of Karachi, Pakistan. BMC Public Health 6:84. http://www.biomedcentral.com/1471-2458/6/84. Accessed 1 Mar 2012
Kingston PF (2002) Long-term environmental impact of oil spills. Spill Sci Technol Bull 7 (1–2):53–61
Kyung SY, Chon SY, Kim YJ, Lee SP, Park J-W, Jeong SH (2009) A case of respiratory failure after clean-up work of the Hebei Spirit crude oil spill in Taean. Tuberc Respir Dis 67:249–253
Laubier L, Le Moigne M, Flammarion P, Thybaud E, Cossa D (2004) Foreword: the monitoring programme of the ecological and ecotoxicological consequences of the *Erika* oil spill. Aquat Living Resour 17:239–241
Leschine TM, McGee J, Gaunt R, van Emmerik A, McGuire DM, Travis R, McCready R (1993) T/V *Exxon Valdez* oil spill: federal on scene coordinator's report, vol 1, U. S. Coast Guard, Natl. Tech. Inf. Serv., PB94-121845, Washington, DC, 570 pp
Li H, Boufadel M (2011) A tracer study in an Alaskan gravel beach and its implications on the persistence of the Exxon Valdez oil. Mar Pollut Bull 62:1261–1269
Lyons RA, Temple JMF, Evans D, Fone DL, Palmer SR (1999) Acute health effects of the *Sea Empress* oil spill. J Epidemiol Commun Health 53:306–310
Martin D (1992) Response of migrating adult pink salmon to a simulated oil spill. In: Fourth information transfer meeting, MMS, Alaska OCS Region, OCS Study MMS 92-0046, U.S. Department of Interior, Minerals Management Service, Anchorage, AK, pp 131–138
MCA (2000) Information relating to pollution risks in the UK. Maritime and Coastguard Agency, Doc. No.: ST-8782-MI-1-Rev 02. 23 pp. http://www.dft.gov.uk/mca/annex_b-4.pdf. Accessed 1 Mar 2012
MDEP (2000) Restoration plan and environmental assessment for the September 27, 1996 *Julie N.* oil spill. Maine Department of Environmental Protection, Maine Department of Conservation, Maine Department of Inland Fisheries and Wildlife, Maine Department of Marine Resources, National Oceanic and Atmospheric Administration, U.S. Department of Interior, 25 pp
Meo SA, Al-Drees AM, Meo IMU, Al-Saadi MM, Azeem MA (2008) Lung function in subjects exposed to crude oil spill into sea water. Mar Pollut Bull 56(1):88–94. doi:10.1016/j.marpolbul.2007.09.039
Miraglia RA (2002) The cultural and behavioral impact of the *Exxon Valdez* oil spill on the native peoples of Prince William Sound. Alaska Spill Sci Technol Bull 7(1–2):75–87
MMA (2004) Especificações e normas técnicas para elaboração de cartas de sensibilidade ambiental para derramamentos de oleo. Ministério Do Meio Ambiente, Secretaria de

Qualidade Ambiental, Brasil, 107 pp. www.cnpq.br/editais/ct/2011/docs/anexoIII_especificacoes_normas_tecnicas_elaboracao_cartas_sao.pdf. Accessed 1 Mar 2012

Morita A, Kusaka Y, Deguchi Y, Moriuchi A, Nakanaga Y, Iki M, Shigekazui M, Kawahara K (1999) Acute health problems among the people engaged in the cleanup of the *Nakhodka* oil spill. Environ Res Sect A 81:185–194

Neff JM, Bence AE, Parker KR, Page DS, Brown JS, Boehm PD (2006) Bioavailability of PAH from buried shoreline oil residues 13 years after the Exxon Valdez oil spill: a multispecies assessment. Environ Toxicol Chem 25:947–961

NIOSH (2010) NIOSH report of deepwater horizon response/unified Area command illness and injury data (April 23–July 27 2010). U.S. National Institute of Occupational Safety and Health, 17 pp. http://www.cdc.gov/niosh/topics/oilspillresponse/pdfs/NIOSHrot-BPilnessAndInjuryDataApril23-july27-2010.pdf. Accessed 1 Mar 2012

NOAA (2002) Environmental sensitivity index guidelines, Version 3. National Oceanic and Atmospheric Administration, Office of Response and Restoration, Seattle, WA, 192 pp. http://response.restoration.noaa.gov/sites/default/files/ESI_Guidelines.pdf. Accessed 1 Mar 2012

NOAA (2010) Characteristic coastal habitats; choosing response alternatives. National Oceanic and Atmospheric Administration, Office of Response and Restoration, Seattle, WA, 86 pp

NOAA (2011) Stage4ResponseSummaryByState(2011-1105)V3 (1).xlsx. National Oceanic and Atmospheric Administration, Office of Response and Restoration, Seattle, WA, *Deepwater Horizon* Spreadsheet dated 5 Nov 2011

NOAA (2012a) Argo mrchant. http://www.incidentnews.gov/incident/6231. Accessed 1 Mar 2012

NOAA (2012b) M/V Megaborg. http://www.incidentnews.gov/incident/6748. Accessed 1 Mar 2012

NOAA (2012c) Publications. NOAA, Office of Response and Restoration, http://response.restoration.noaa.gov/publications/. Accessed 1 Mar 2012

NOAA (2012d) *Deepwater Horizon*/BP oil spill: size and percent coverage of fishing area closures due to BP oil spill. NOAA Fisheries Service. http://sero.nmfs.noaa.gov/ClosureSizeandPercentCoverage.htm. Accessed 1 Mar 2012

NRC (1985) Oil in the sea: inputs, fates, and effects. National Research Council, National Academies Press, Washington, DC, 602 pp

NRC (2003) Oil in the sea III: inputs, fates, and effects. National Research Council, National Academies Press, Washington, DC, 280 pp. ISBN 0-309-50551-8

Olsen L (2010) Social impact and strategic plan, the *Deepwater Horizon* Gulf oil spill: response, resilience, & recovery. The George Washington University, Institute for Crisis, Disaster and Risk Management, 37 pp. http://www.gwu.edu/~icdrm/publications/PDF/Strategic%20Plan_LauraOlson_NVOAD_Final.pdf. Accessed 1 Mar 2012

OSAT-2 (2011) Summary report for fate and effects of remnant oil in the beach environment. Operational Science Advisory Team, *Deepwater Horizon MC252*. Prepared for Federal On-Scene Coordinator. 36 pp + annexes. www.restorethegulf.gov/release/2011/03/01/osat-2-fate-and-effects-oil-beaches. Accessed 1 Mar 2012

Osofsky HJ, Osofsky JD, Hasel TC (2011) Deepwater Horizon oil spill: mental health effect on residents in heavily affected areas. Dis Med Public Health Prep 5:280–286

Oudot J, Chaillan F (2010) Pyrolysis of aspaltenes and biomarkers for the fingerprinting of the Amoco Cadiz oil spill after 23 years. C R Chim 13:548–552

Owens EH (1991) Shoreline conditions following the *Exxon Valdez* spill as of fall 1990. In: Proceedings of the Arctic and Marine Oilspill Program (AMOP), Environment Canada, pp 579–606

Owens EH, Taylor E, Humphrey B (2008) The persistence and character of stranded oil on coarse-sediment beaches. Mar Pollut Bull 56:14–26

Page DS, Boehm PD, Brown JS, Gundlach ER, Neff JM (2012) Fate of oil on shorelines. Chapter 6, In: Wiens JA (ed) Oil in the environment: legacies and lessons of the *Exxon Valdez* oil spill, Cambridge University Press, NY (in press) http://www.cambridge.org/gb/knowledge/isbn/item7111920/?site_locale=en_GB

Paine RT, Ruesink JL, Sun A, Soulanille EL, Wonham MJ, Harley CDG, Brumbaugh DR, Secord DL (1996) Trouble on oiled waters: lessons from the Exxon Valdez oil spill. Annu Rev Ecol Syst 27:197–235

Picou JS, Gill DA (1996) The Exxon Valdez oil spill and chronic psychological stress. In: Rice SD, Spies RB, Wolfe DA, Wright BA (eds) Exxon Valdez oil spill symposium, vol 18. American Fisheries Society, Cambridge University Press, UPH, Shaftesbury Road, Cambridge CB2 8BS, United Kingdom, pp 879–893

Pope G, Gordon K, Bragg J (2010) Using fundamental practices to explain field observations twenty-one years after the *Exxon Valdez* oil spill. International Oil Spill Conference, American Petroleum Institute, Washington, DC, 13 pp

Ramseur JL (2010) *Deepwater Horizon* oil spill, the fate of the oil. Congressional Research Service, 7–500, R42531, 24 pp

Rodríguez-Trigo G, Zock J-P, Pozo-Rodríguez F, Gómez FP, Monyarch G, Bouso L, Coll MD, Verea H, Antó JM, Fuster C, Barberá JA, the SEPAR (Sociedad Española de Neumología y Cirugía Torácica) – Prestige Study Group (2010) Health changes in fishermen 2 years after clean-up of the *Prestige* oil spill. Annu Intern Med 153(8):489–498. http://www.annals.org/content/153/8/489.full.pdf+html. Accessed 1 Mar 2012

Sabucedo JM, Constantino A, Ferraces MJ, Merino H, Durán M (2009) Psychological impact of the *Prestige* catastrophe. Int J Clin Health Psychol 9(1):105–116

SAMHSA (2010) Newsletter: oil spill response, making behavioral health a top priority. Substance Abuse and Mental Health Service Administration, Department of Health and Human Services, 16 pp. http://www.samhsa.gov/samhsaNewsletter/Volume_18_Number_4/JulyAugust2010.pdf. Accessed 1 Mar 2012

Sathikumar N (2010) Short-term physical effects. In: Assessing the effects of the Gulf of Mexico oil spill on human health: a summary of the June 2010 workshop. National Academy Press, M.A. McCoy and J.A. Salemo (Rapporteurs), Washington, DC, 183 pp

Scandpower (2006) Blowout and well release frequencies – based on SINTEF offshore blowout database, 2005, 44 pp

Schvoerer C, Gourier-Frery C, Ledrans M, Germonneau MP, Derrien J, Prat M, Mansotte F, Guillaumot P, Tual F, Vieuxbled J, Marzin M (2000) Etude épidémiologique des troubles de santé survenus à court terme chez les personnes ayant participé au nettoyage des sites pollutes par le fioul de l'*Erika* [In French: Epidemiological study of short-term health issues with personnel involved in cleanup of sites polluted by oil from the *Erika*] 57 pp. http://www.invs.sante.fr/publications/erika3/rapmaree_dist.pdf. Accessed 1 Mar 2012

Sell D, Conway L, Clark T, Picken GB, Baker JM, Dunnet GM, McIntyre AD, Clark RB (1995) Scientific criteria to optimize oil spill cleanup. International Oil Spill Conference, American Petroleum Institute, Washington, DC, pp 595–610

Southward AJ (1982) An ecologist's view of the implications of the observed physiological and biochemical effects of petroleum compounds on marine organisms and ecosystems. Philos Trans R Soc Vol B 297:241–255

Stekoll MS, Deysher L, Highsmith RC, Saupe SM, Guo Z, Erickson WP, McDonald L, Strickland D (1996) Coastal habitat injury assessment: intertidal communities and the Exxon Valdez oil spill. In: Rice SD, Spies RB, Wolfe DA, Wright BA (eds) Exxon Valdez oil spill symposium, vol 18American Fisheries Society, pp 177–192

Suchanek TH (1993) Oil impacts on marine invertebrate populations and communities. Am Zool 35:510–523

Upton HG (2011) The *Deepwater Horizon* oil spill and the Gulf of Mexico fishing industry. Congressional Research Service 7–5700, 17 pp

White IC, Baker JM (1998) The *Sea Empress* oil spill in context. In: International conference on the *Sea Empress* oil spill, Cardiff, Wales, 33 pp, http://www.itopf.com/uploads/seeec.pdf. Accessed 1 Mar 2012

Wolfe DA, Hameedi MJ, Galt JA, Watabayashi G, Short J, O'Claire C, Rice S, Michel J, Payne JR, Braddock J, Hanna S, Sale D (1994) The fate of the oil spilled from the Exxon Valdez. Environ Sci Technol 28:561–567

Zock JP, Rodriguez-Trigo G, Pozo-Rodriguez F, Barbera JA, Bouso L, Torralba Y, Anto JM, Gomez FP, Fuster C, Verea HS, SEPAR-Prestige Study Group (2007) Prolonged respiratory symptoms in clean-up workers of the Prestige oil spill. Am J Respir Crit Care 176:610–616

Part X
Beach Safety

Chapter 26
Rip Currents

Stephen P. Leatherman

Abstract Rip currents are powerful, channeled currents of water that flow offshore from beaches. These dangerous currents are the most serious hazard that threatens bather safety on the world's surf beaches. In the United States, more people drown in rips annually than are killed by hurricanes, tornadoes or lightning. Florida has the highest loss of life because of its long shoreline and warm waters, followed by other popular states for ocean swimming with many beaches—California and North Carolina. In response to these safety concerns, the science of rip currents has advanced significantly in the past decade. The First International Rip Current Symposium was held in Miami, Florida in 2010 where research advancements through field investigations and modeling were highlighted. These insights are being used to promote more effective public education and develop innovative outreach programs and tools.

26.1 Introduction

Rip currents (rips) are a major coastal hazard, but they receive far less attention than most other coastal hazards; this is largely because rips do not affect houses or infrastructure and relatively few people are lost during each event. Approximately 100 U.S. beachgoers drown annually in these powerful currents (Fig. 26.1). Eighty percent of all lifeguard rescues are the result of rips, which amounts to more than 50,000 people pulled out of the water each year with some requiring medical treatment and hospitalization (www.usla.org). Rip currents are a problem worldwide with other known hot spots being Brazil, Australia and Israel (Short and Hogan 1994; Leatherman and Fletemeyer 2011).

S.P. Leatherman (✉)
Laboratory for Coastal Research and Department of Earth & Environment,
Florida International University, Miami, FL 33199, USA
e-mail: leatherm@hotmail.com

C.W. Finkl (ed.), *Coastal Hazards*, Coastal Research Library 6,
DOI 10.1007/978-94-007-5234-4_26,

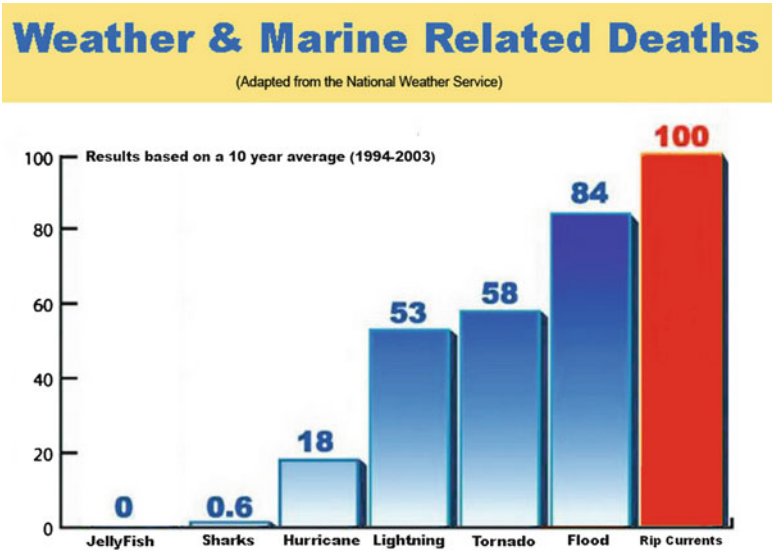

Fig. 26.1 Rip currents cause more deaths on average than lightning, tornados or hurricanes (not counting Hurricane Katrina in 2005) according to the National Weather Service

Rip currents are fairly common on surf (e.g., breaking wave) beaches along oceanic coasts, including the U.S. Atlantic, Pacific and Gulf Coasts as well as the Great Lakes. Beaches are the number one recreational destination for Americans; this fact coupled with the relatively high occurrence of rips and limited knowledge and experience of many beachgoers accounts for the large number of drownings and rescues. These seaward-flowing currents are deceptively dangerous; they sometimes appear as calm water between the whitewater of the breaking waves, and hence appear to be safer places to swim (Leatherman 2003).

These "rivers in the sea" originate in shallow water (Fig. 26.2). The principal driving force is longshore variation in wave height, which is affected by many factors, such as bathymetry and spatially-varying wave fields (Haller et al. 2002; Wright and Short 1984; Sonu 1972). Variability in bar size causes refraction and diffraction, which results in wave height variation along the shore and hence differential water set-up on the beach face (Bowen 1969). Longshore (feeder) currents flow from areas of higher to lower water heights where the rips develop (Voulgaris et al. 2011). Rip currents can possibly be generated by superposition of different wave trains coming from different directions (Dalrymple 1978). Rip currents are maintained and persist once formed because of topographic depressions (e.g., holes in the bar, which are the rip channel) in the surf zone. Rips are also generated by geological and engineering structures on the beach and shoreface.

Rip current magnitude has been shown to increase with increasing wave height, decreasing tidal level and more shore-normal wave approach (Sonu 1972). Mean flow velocities are typically on the order of 0.3–0.8 m/s (Brander and Short 2000).

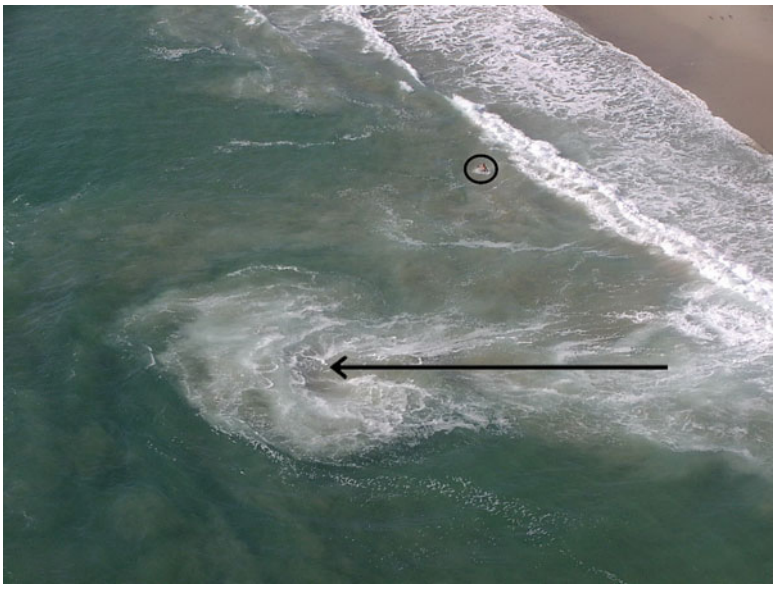

Fig. 26.2 Rip current at Zuma Beach, California is denoted by light brown water moving offshore; note the person in water (Source: Los Angeles County Coastal Monitoring Network, 2002)

Most beachgoers cannot swim against these strong, seaward-flowing currents, and panic quickly ensues, which all too often leads to drowning. Even strong swimmers can panic when caught in a strong rip and try to swim directly onshore, resulting in loss of life. Rips often pulse such that the current suddenly and briefly reaches speeds up to 2 m/s; these rip pulses are probably the cause of mass rescues wherein tens of people are suddenly swept offshore (Short 2007). Mega-rips, which occur on high-energy beaches, also pose a great risk with flow velocities exceeding 2 m/s, but most beachgoers avoid such dangerous conditions because of the threatening nature of the big breaking waves.

Rip currents are called by many names, such as undertow and riptides (Fig. 26.3), which is confusing to the public. Lifeguards along the Florida Atlantic coast often use the term "run-outs" to describe rip currents. Along the South Shore of Long Island, New York, "sea poosies" are sometimes used to describe these currents; this name apparently originated from the indigenous peoples (Slattery et al. 2011).

26.2 Terminology

Undertow, rip current and riptide are common terms used to describe a variety of dangerous currents, all of which have very different characteristics (Table 26.1). However, much of the general public, news media and even dictionary definitions

Fig. 26.3 Warning sign at Lauderdale-by-the-Sea, Florida that uses the word "riptide" instead of rip current (Source: S. P. Leatherman).

confuse and misidentify these ocean hazards (Leatherman 2012a). Many beachgoers use the terms interchangeably, when in fact they are distinct dangers. Undertow, rip currents and riptides occur for different reasons at different locations along the beach. Avoiding each of them or escaping their grip requires different strategies.

26.2.1 Undertow

Breaking waves on surf beaches push water up the beach face, and gravity pulls the water back down the beach as backwash. Big waves breaking on the beach generate a large uprush and backwash; this seaward-flowing water and sand mixture is pulled strongly into the next breaking wave. Waders feel like they are being sucked under the water when the wave breaks over their head—this is undertow (Table 26.1). While bathers can be tumbled around roughly, this return flow only goes a short distance—just to the next breaking wave; it does not pull you offshore into deep water.

Undertow is typically only dangerous for small children who cannot walk up the beach face against the strong backwash flow. In any case, children should always be supervised at the beach, and only experienced swimmers and surfers should enter the water on big wave days.

Table 26.1 Three types of seaward-flowing currents at sandy beaches

	Undertow	Rip currents	Riptides
Description of current	Strong backwash off beach	Strong offshore flow at certain locations	Strong offshore current at inlets
Origin	Big waves breaking on beach face	Longshore variation in wave energy and differential water setup on beach face	Constriction of tidal flow through barrier beaches
Seaward extent of current	Tens of meters or less from shore	100 m offshore in many cases	300+ meters offshore at major inlets
Water depth of occurrence	Centimeters to a meter in most cases	0.6–3 m (but sometimes deeper)	Tens of meters
Danger when caught in current	Knocked around by waves on beach face; generally not life threatening except for small children	Pulled offshore into water over your head	Pulled far offshore by ebbing (falling) tide
Escape from current	Time your escape between breaking waves; walk or crawl up beach	Do not fight the current; swim parallel to the beach or let current take you beyond the breakers while floating and then swim diagonally back to shore	Wave for help to attract attention of fishermen or boaters

Source: Journal of Coastal Research (2012)
Undertow occurs along the entire beach during times of large waves. Rip currents occur periodically at discrete locations along the beach. Riptides occur at inlet areas every day.

26.2.2 Rip Currents

Water piled-up on the beach face by breaking waves must escape back out to the sea as water seeks its own level. Normally the return flow (e.g., backwash) is fairly uniform along the beach so rip currents are not present. Rip currents form where the water can flow back out to sea more easily, such as a break in the sand bar (Table 26.1). Rip currents are generally only 10 m or less in width, but there can be several present at the same time along the shore.

Rip currents are often detected in knee- to waist-high water (e.g., 0.6 m); it can be difficult to walk against these currents in chest-deep water. These strong, offshore-directed currents pull the water, sediment and any unlucky person through the surf zone at all water depths. The current only dissipates offshore of the breaking waves where the water can be quite deep. Moderate waves (e.g., 0.6–1 m high) on sunny days are very appealing to bathers and swimmers, but can sometimes generate life-threatening rip currents.

26.2.3 Riptides

A riptide (or rip tide) is a powerful current caused by the tide pulling water through a constriction, such as an inlet on a barrier beach (Table 26.1). When there is a falling or ebbing tide, the water is flowing strongly through an inlet toward the ocean. These powerful, reversing currents, which are also termed tidal jets by coastal engineers because they carry large quantities of sand that form sand bars in the ocean and bay opposite the inlet channel, can be life threatening. For example, the ebbing tide at Shinnecock Inlet in Southampton, New York extends more than 300 m offshore so that many bathers and swimmers caught in this current will likely not be able to swim back to shore.

26.3 Types and Identification

There are many different types of rip currents (Short 2007; Dalrymple et al. 2011); all coastal scientists and beach safety experts agree on this fact, but the terminology has varied considerably. Leatherman (2012b) suggested using descriptive terminology in order to promote better public understanding. Five rip types are identified and described (Table 26.2): (1) bar-gap rips, (2) cusped-shore rips, (3) structurally-controlled rips, (4) flash rips, and (5) mega-rips.

26.3.1 Bar-Gap Rips

The most common type of rip current at most beaches is the bar-gap rip (Fig. 26.4), which is often called a fixed rip; such rips usually appear as dark, calmer water gaps between areas of whitewater caused by intensely breaking waves (Brander and Short 2000). This type of rip is located at a large depression or hole in the bar and tends to stay in the same location for days, months or until a coastal storm causes major beach profile changes. The term fixed is not descriptive for identification of this type of rip and almost seems like a misnomer in the highly dynamic environment of an oceanic beach. Bar-gap rips tend to be strongest in response to normally-incident waves (e.g., waves approaching perpendicular to shore). Beachgoers often choose to swim in the calmer waters at the bar gap locations because it is thought to be safer (Fig. 26.4). This counter-intuitive thinking makes these rip currents particularly dangerous. Bar-gap rips often occur when the surf is moderate and the weather is ideal, which leads to a larger bather load and hence more rescues and drowning (Table 26.2). These low-energy rips may be the most dangerous because of the lack of strong visual cues (Dalrymple et al. 2011).

Table 26.2 Rip current types and identification

Rip type	Cause	Detection & persistence	Relative threat	Avoidance
Bar-gap	Topographic depression or hole in sand bar	Dark, calmer water; can persist in same location for weeks, months or even years; storms can cause change in sand bar location and dimensions	Probably most dangerous to general public because quite common and can occur during sunny days and moderate wave activity	Use polarizing sunglasses to spot dark channels on beach face and topographic depressions between sand bar; swim in whitewater areas
Cusped-shore	Large, angled sand bars on shoreface that control nearshore circulation	Bow-shaped or meandering shoreline characterized by mega-cusps, which change little in position over time	Dangerous if enter water at embayments in shoreline or step off sand bars into channels when rip currents are present	Swim where waves are breaking on sand bar; avoid calmer areas at shoreline embayments
Structurally-controlled	Rock formations and shore-perpendicular coastal engineering structures on beach and shoreface	Fixed locations for rips because of hard structures; underwater rock formations can be difficult to spot at high tide and/or high surf	Very dangerous to swim near rocky areas and piers, groins, and jetties because of rips and wave action pushing swimmers into structures	Stay at least 30 m from rocky shores and hard structures; seek guidance from lifeguards and surfers regarding underwater rock formations
Flash	Confused sea conditions during strong onshore winds and/or waves with different periods and directions	Difficult to detect because of variable wave breaking and whitewater/ foam; transient both temporarily and spatially	Generally weaker than other rip types, but still dangerous because variable in strength and occurrence	Stay out of water during moderate to high waves and confused sea conditions
Mega-rip	Large waves and usually structurally-controlled	Fixed in location at pocket beaches and by rock formations	Extremely dangerous because so powerful	Avoid swimming during high surf conditions

Shore and Beach (2012); permission to be requested

Fig. 26.4 Bar-gap rips are the most common; the water appears to be the safest at the location of the rip because of the lack of wave action on the Outer Banks of North Carolina (Source: D. Elder)

26.3.2 Cusped-Shore Rips

Cusped-shore rips are found where large transverse bars (e.g., bars angled relative to the shoreline) cause development of megacusps along the shore (Fig. 26.5). Rip currents emanate from the embayments of these megacusps (e.g., shoreline meanders), which is also where most people enter the water because the waves are smaller and conditions appear safer (Houser et al. 2011). The Florida panhandle beaches are characterized by cusped-shore rips, and this popular stretch of shoreline has often been called the "Drowning Capital" of the U.S. by the media. This area has a large number of drownings because rips are so common, and lifeguards are not present along much of this extensive shoreline (Houser et al. 2011).

26.3.3 Structurally-Controlled Rips

Structurally-controlled rips are formed by geological structures such as intertidal/subtidal rocks, headlands and shore-perpendicular coastal engineering structures (Figs. 26.6, 26.7 and 26.8). They are also called permanent rips because their location is topographically and/or bathymetrically controlled; these rip currents are present whenever there is sufficient wave energy (Short 2007). A famous example is the Backpacker Express at Bondi Beach in Sydney, Australia (Fig. 26.7). The name originates from the fact that this is where the tourists (e.g., backpackers) exit the bus and walk down the beach to enter the water. Other examples include Kee Beach in Kauai, Hawaii and the Shell Beach Express at La

Fig. 26.5 Cusped-shore rip at Pensacola Beach, Florida (Source: C. Houser)

Fig. 26.6 The structural control of rock formations that resemble sand bars in shape is apparent at this beach in South Australia (Source: S. P. Leatherman)

Fig. 26.7 The infamous Backpacker Express along the southern headland at Bondi Beach in Sydney, Australia is a structurally-controlled rip current (Source: R. Brander)

Fig. 26.8 A rip current is generated by a groin at Cape Hatteras, North Carolina (Source: S. P. Leatherman)

Fig. 26.9 Flash rips occur frequently at South Florida beaches during persistent, strong onshore winds (Source: J. Fletemeyer)

Jolla Beach in San Diego, California. A powerful rip current is produced in the gap between the intertidal rocks at this Southern California beach. Kee Beach is a small sandy beach that is bounded by a coral reef. A strong rip current is produced near low tide when waves are breaking on the nearly exposed reef; a gap in this rock formation provides a channel for the trapped waters to escape seaward.

Coastal engineering structures, such as groins (Fig. 26.8), jetties and piers, can induce rip currents by acting like a dam to the longshore current, which is deflected offshore. Structurally-controlled rips are particularly strong during times of very oblique wave approach.

26.3.4 Flash Rips

Flash rips are transient in nature, both temporally and spatially. These rips are difficult to spot (Table 26.2) and are usually weaker than their bathymetrically-controlled counterparts (Slattery et al. 2011). They often persist for a few minutes at any location and can migrate downdrift when the incident wave angle is oblique to the shoreline, giving rise to the term traveling rips (Fig. 26.9). Flash rips are hydrodynamically forced by waves with different periods and directions, causing confused sea conditions and variable wave set-up along the beach (Reniers et al.

Fig. 26.10 Mega-rips at Huntington Beach, California can incredibly extend farther offshore than the fishing pier, which is 560 m in length (Source: Huntington Beach Lifeguards)

2009). Therefore, flash rips can occur anywhere along the beach because they are not controlled by bathymetric undulations (e.g., holes or depressions in the bar); this makes them impossible to predict except statistically.

26.3.5 Mega-Rips

Mega-rips are not actually a different type of rip (Table 26.2), but are so-named because they are such extremely powerful rips that extend far offshore. Mega-rips are often associated with structural controls such as the submarine canyon that focuses wave energy at Scripps Pier in La Jolla, California. Mega-rips also occur at Huntington Beach, California during high, long-period wave conditions (Fig. 26.10). Huntington Beach is fully exposed to Pacific Ocean swells and has long been a top surfing beach (e.g., trademarked name of "Surf City USA"). Mega-rips are often generated in small (3–4 km) pocket beaches when large breaking waves quickly flush the embayed surf zone (Dalrymple et al. 2011).

26.4 Prediction and Forecasting

Predictive models of rip currents were first developed by Lushine (1991) for South Florida because onshore winds were responsible for greater rip frequency and many lifeguard rescues and drownings. This National Weather Service forecasting scheme is based on wind speed and direction, wave height and tide level. Strong onshore winds create choppy, confused seas that can catch even informed swimmers by surprise because the tell-tale signs of rips are masked, and the rough conditions can also hide distressed bathers from potential rescuers. Lascody (1998) modified this scheme to account for rip risk due to long-period swells that are particularly important further northward along the Florida Atlantic coast. The National Weather Service's rip current advisory of low, moderate or high risk reaches many beachgoers via local weather reports on TV and by internet; therefore, it has been very effective in increasing public awareness of this coastal hazard.

There are a number of factors that determine the level of risk and outcome (e.g., prevention, rescue or drowning) at surf beaches (Table 26.3). Wave conditions are paramount; the higher the nearshore breaking waves, the more powerful the rip currents. Secondarily, longer wave periods result in stronger rips so that the U.S. Pacific coast is much more rip prone than the Atlantic or Gulf coasts. Rip currents are generally much stronger at low tide as determined by field observations (Brander and Short 2001). At low tide, height of the sand bar relative to water depth is greater, causing water to be concentrated and channeled through holes in the bar at greater speeds. Similarly, higher sand bars can result in stronger rip currents at different beaches with similar wave energy. Therefore, the National Weather Service forecasts should also consider the height of bars at particular beaches (Dean and Thieke 2011). The emplacement of shore-parallel engineering structures, such as offshore breakwaters, can affect the nearshore bathymetry and increase the incidence of rip currents.

Weather is an important consideration; bathers obviously favor calm (e.g., non-storm) conditions when it is sunny and warm (Table 26.3). Warm water also increases bather load albeit some people will swim in chilly waters if the weather is ideal. Beaches are particularly crowded during weekends, especially Sundays, and holidays.

Lifeguards are the most important factor in determining bather safety, but most beaches are unguarded and many beachgoers enter the water after hours. Signs and flags are used on many beaches to warn of dangerous conditions, but some people either do not understand the flags or ignore the signs (Fletemeyer and Leatherman 2010). Public knowledge and awareness of rips is critically important; waves are apparent at surf beaches, but rip currents are often invisible or difficult to spot by beachgoers. Swimming ability is important in terms of being able to escape these powerful currents, but even good swimmers without an understanding of rips have drowned (www.usla.org). Personal behavior is very important. For example, alcohol usage is estimated to account for 25–50 % of adolescent and adult drownings in recreational waters (Howland and Hingson 1988), and many beachgoers are known to drink and swim.

Table 26.3 Factors that determine rip current risk and outcome

Beach and wave conditions		
Wave conditions	Rip activity	Prevention, Rescue or Drowning
Wind speed and direction		
Tide level		
Nearshore bathymetry		
Shore-perpendicular		
Engineering structures		
Weather and timing		
Calm vs. stormy	Bather load	
Water temperature		
Day of week and holidays		
Human factors		
Lifeguards	Safety Precautions	
Signs and flags		
Public knowledge & awareness		
Beachgoer's swimming ability		
Personal behavior		
Pro-active approaches		
Viewing Youtube rip videos		
Testing water for currents		

Pro-active approaches of warning beachgoers of rip dangers at the point of contact (e.g., when beachgoers arrive at the beach) are fundamentally important for prevention of drowning, especially at unguarded beaches (Table 26.3). These approaches are explored in the section on Public Education and Outreach.

26.5 Field Investigations

Many field experiments have been conducted on nearshore circulation and rip currents, but their dynamic nature makes them difficult to study (Sonu 1972; Brander and Short 2000). Rips are extremely variable; they can be fixed in the same location for days or even months (e.g., bar-gap rips) or persist in the same location for only a few minutes (e.g., flash rips). In addition, wave and tidal conditions are always changing. Therefore, field measurements present a logistical problem. Laboratory experiments are often undertaken to clarify relationships because the variables can be carefully controlled and repeatable tests undertaken.

Wave strength affects rip current presence and speed. Field studies have shown that higher energy waves generate more powerful rip currents (Sonu 1972). This is due to larger breaking waves pushing more water up onto the beach as wave set-up, which results in stronger seaward-flowing water when channeled through a hole in the bar or along a headland or shore-perpendicular coastal engineering structure. Wave direction affects rip current presence and strength as well. Shore-normal

Fig. 26.11 Rip current at Pensacola Beach is hooked-shaped because of the longshore current as delineated by tracer dye (Source: C. Sonu)

waves result in much stronger rips, while oblique wave approach generates longshore currents. The flow path of a rip can be hooked in shape due to the influence of longshore currents (Fig. 26.11; Sonu 1972). Strong onshore winds can locally generate waves with large oblique angles of incidence (e.g., wave approach), which can generate very strong longshore currents and suppress rip development as shown by field observations.

Recent field measurements indicate that rip currents are not as simple as first thought (Brander and MacMahan 2011). The classic rip description is an offshore-flowing current that terminates beyond the breaker zone where it diffuses (Fig. 26.12). New studies, utilizing GPS drifters, demonstrate that rips often flow as circulatory eddies. Drifter studies undertaken at many beaches worldwide demonstrate that cellular rip circulation occurs within the surf zone approximately 80 % of the time; only 20 % of the time or less does the water actually exit the surf zone (MacMahan et al. 2010).

These findings have important implications for beachgoers regarding the proper response when caught in a rip current—swim parallel to the shore to escape a rip or stay afloat and let the current bring you back to a nearshore sand bar (Brander and MacMahan 2011). The standard advice found on most websites, such as www.usla.org and www.ripcurrents.com, consists of four main points: (1) do not swim against the current, (2) do not panic, (3) escape the rip by swimming parallel to the shore, and (4) stay afloat and signal for help. There is agreement regarding the first two points, but much debate about the other two.

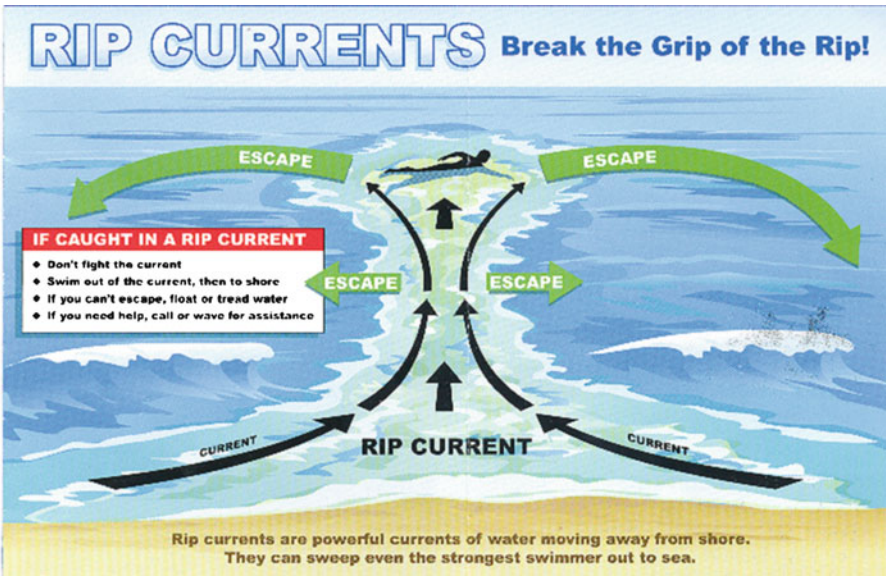

Fig. 26.12 Warning sign of rip current that is posted at many U.S. beaches also shows means of escape (Source: National Weather Service and Sea Grant)

The traditional advice is to swim right or left to escape a rip current. However, swimmers have almost a 50 % chance of swimming in the wrong direction (e.g., against the longshore current) and hence pulled back into the rip. This approach requires physical exertion, which can lead to exhaustion, panic and drowning.

The approach of staying afloat and going with the flow until help arrives is a passive response; many beachgoers will find this strategy difficult to implement as they find themselves being pulled further and further offshore. However, field studies have shown that rip circulation is largely contained within the surf zone so that the current will usually bring floating objects back toward shore within a few minutes (Brander and MacMahan 2011). Therefore, the only real option for poor and non-swimmers is to float and hope to be brought back to the relative safety of a shallow sand bar. Lifeguards note that when many such bathers cannot touch bottom, they panic and try to "climb the ladder" in order to pull themselves out of the water (William MacDonald, Chief of Lifeguards, Miami Beach, Florida, August 2011). Struggling bathers are not able to stay afloat in a vertical position, eventually swallow water and drown if not quickly rescued.

26.6 Laboratory Experiments and Numerical Modeling

Basic understanding of nearshore cell circulation has been greatly improved by laboratory experiments and numerical modeling. A principal focus of this research has involved predicting the formation of rip currents (Haller et al. 2002; Reniers

et al. 2009). As noted earlier, rips are complicated because of wave parameters, wind and tidal conditions, and nearshore bathymetry.

Numerical models can produce reliable results if good information is available on wave and bathymetric conditions. Field drifters are used to calibrate and verify numerical model results. Models cannot predict where the rips are located spatially in the field, but can predict the statistical occurrence of rip currents at particular beaches and hence assist in planning and deployment of beach safety personnel (Voulgaris et al. 2011).

Laboratory experiments allow for controlled conditions, such as generation of monochromatic waves with constant height and period; this is the key to better understanding the flow characteristics of rip currents. In the field, neither the forcing functions nor the beach state can be controlled (Wright and Short 1984).

Field studies require a team of researchers and considerable instrumentation to measure the nearshore circulation pattern. Conditions in the field are constantly changing (e.g., time-varying conditions such as tide level), which affects data collection because the parameters cannot be kept truly constant. Laboratory experiments are undertaken to avoid these problems and permit repetitive experiments under exactly the same conditions. Laboratory studies have their limitations—gravity cannot be scaled and rigid bars and bottom are often used instead of sand. Three-dimensional wave basins provide less boundary constraints than 2D wave tanks, but the cost to operate these indoor facilities is much higher.

26.7 Public Education and Outreach

Rip currents are the most serious hazard that threatens bather safety on the world's surf beaches. Because of inconsistent and often unreliable data collection, the number of rip drownings is not accurately known, but major losses of life are known to occur annually in the U.S. (Lushine 1991), Australia (Short 2007), United Kingdom (Scott et al. 2009), Israel (Hartmann 2006), and Brazil (Klein et al. 2003).

Lifeguards are the obvious answer in terms of bather safety at surf beaches. Lifeguards rescue tens of thousands of beachgoers each year in the U.S. (www.usla.org). The chance of death by drowning on beaches with certified lifeguards is 1 in 18 million (Branche 2001). However, is it impossible to provide lifeguards at every beach because of the high cost. Towers are often spaced every 150–200 m along popular public beaches. The cost of lifeguards can exceed a million dollars per kilometer for year-round coverage (John Fletemeyer, Personal Communication, January 2012).

Flags are often used to warn beachgoers of rip currents. However, the sign colors and systems differ globally, making it a problem for international travelers. Red flags, like red lights, mean to stop, but many beachgoers tend to ignore the flags

because they do not see any problems—rip currents are often invisible or not readily apparent to the public. In addition, red flags are sometimes used to signify other dangers, such as jellyfish. Klein et al. (2003) found that most surf accidents at Brazilian beaches occurred when warning flags were displayed, which indicates a lack of knowledge or respect for the warning system.

Beachgoers are usually warned of rip currents by signage, but such warnings sometimes convey little to no information about these dangerous currents and how to spot them (Fig. 26.3). More recently, warning signs on U.S. beaches have included a diagram that illustrates the flow pattern and how to escape the rip (Fig. 26.12). While this is definitely an improvement in communicating the risk to the public, the problem is that few rips have this classic mushroom shape, and the "telltale signs" vary considerably (Fletemeyer and Leatherman 2010).

The "telltale" signs of rip currents include: (1) persistent change in water color from the surrounding water—lighter color and murkier from bubbles and sediment (Fig. 26.2) or darker because of the depth of the underwater channel where the rip flows (Fig. 26.4), (2) gap in breaking waves where the rip is forcing its way seaward through the surf zone, (3) agitated (choppy) surface water that extends beyond the breaker zone, and (4) floating objects, where present in the surf, moving seaward. Water color is not definitive for delineating rip currents because it spans the range from lighter to darker. Rips can also vary greatly in size and shape according to type and hydrodynamic conditions. Many rips are hard to recognize by the public, and even lifeguards have considerable difficulty making an accurate determination when strong onshore winds are generating confused sea conditions. Consequently, the belief that bathers can be taught to identify rip currents and render judgments about whether or not it is safe to swim is at best problematic if not impossible (Fletemeyer and Leatherman 2010).

A floating dye ball water tracer has been developed by Leatherman (2011), which can be used for rip detection at the point of contact (e.g., when beachgoers first arrive at the beach). This dye can be thrown into the water safely from shore to determine quickly the presence and gauge the strength of any currents, including longshore, tidal and rip currents (Fig. 26.13). The fluorescent dye is very colorful and hence a powerful eye-catching tool to increase public awareness of dangerous currents, especially rip currents. Ballantyne et al. (2005) stated that "Awareness of rips and their potential dangers is worthless without an ability to recognize them, as only the latter can help to avert unsafe behavior." This makes the value of a water tracer apparent.

Improved public education of rip currents is increasingly relying upon the visual media, especially TV weather reports and Youtube videos, which can reach millions of people. Rip current videos on Youtube, such as "Don't get Sucked in by the Rip" by Brander (www.scienceofthesurf.com) and "Beach Rips: Dangerous Currents" by Leatherman (www.ripcurrents.com), are very effective means of conveying the risk of rip currents to beachgoers.

Fig. 26.13 Fluorescent dye, which is non-toxic, biodegradable, and NSF-approved as safe in drinking water (www.hazard.com/msds) in the form of a dye ball can be safely thrown from shore; it quickly dissolves in the water to form a plume that moves with any currents present (Source: S. P. Leatherman)

26.8 Discussion and Conclusions

There have been considerable advances in rip current research in recent years. A book entirely devoted to rip currents was recently published (Leatherman and Fletemeyer 2011), which indicates both the importance of this area of research and the body of work that has already been completed. Clearly the science of rip currents has advanced significantly in recent years, and more studies are currently underway. Beachgoers, especially visitors and tourists from non-coastal areas, have insufficient knowledge and understanding of oceanic conditions. While waves at surf beaches are readily apparent, many visitors do not even know that currents exist, much less that they can be dangerous and even life threatening. The challenge of alerting the public to these dangerous currents is problematic because rips come in many sizes, shapes and strengths. Signs and flags are useful but not sufficient. Lifeguards are the obvious solution, but the cost is high and the U.S. shoreline is very long. Youtube videos that show rip currents in action are vitally important in informing the public about this coastal hazard, especially because they are instantly available via Internet at the point of contact (e.g., before beachgoers enter the water). Other approaches of pro-active beach safety involve testing the water for

currents. Clearly, beachgoers will not drown in rip currents if they do not swim in them; therefore, the best approach to promote rip avoidance is through improved identification and understanding of these coastal hazards.

Acknowledgments The Andrew W. Mellon Foundation is gratefully acknowledged for supporting this rip current research and educational initiative.

References

Ballantyne R, Carr N, Hughes K (2005) Between the flags: an assessment of domestic and international students' knowledge of beach safety in Australia. Tour Manag 26:617–622

Bowen AJ (1969) Rip currents 1. Theoretical investigations. J Geophys Res 74:5467–5478

Branche CM (2001) Lifeguard effectiveness: a report of the working group. Centers for Disease Control and Prevention, Atlanta, 21p

Brander RW, MacMahan J (2011) Future challenges for rip current research and outreach. In: Leatherman SP, Fletemeyer J (eds) Rip currents: beach safety, physical oceanography and wave modeling. CRC Press, New York, pp 1–29

Brander RW, Short AD (2000) Morphodynamics of a large-scale rip current system at Muriwai Beach, New Zealand. Mar Geol 165:27–39

Brander RW, Short AD (2001) Flow kinematics of low-energy rip current systems. J Coast Res 17:468–481

Dalrymple RA (1978) Rip currents and their causes. In: Proceedings of 16th international conference on coastal engineering, ASCE, Hamburg, pp 1414–1427

Dalrymple RA, MacMahan JH, Reniers JHM, Nelko V (2011) Rip currents. Ann Rev Fluid Mech 43:551–581

Dean RG, Thieke RJ (2011) Surf zone hazards: rip currents and waves. In: Leatherman SP, Fletemeyer J (eds) Rip currents: beach safety, physical oceanography and wave modeling. CRC Press, New York, pp 107–123

Fletemeyer J, Leatherman SP (2010) Rip currents and public education. J Coast Res 26:1–3

Haller MC, Dalrymple RA, Svendsen IA (2002) Experimental study of nearshore dynamics on a barred beach with rip currents. J Geophys Res 107:1–21

Hartman D (2006) Drowning and beach safety management along the Mediterranean beaches of Israel: a long-term perspective. J Coast Res 22:1505–1514

Houser C, Caldwell N, Klaus Meyer-Arendt K (2011) Rip current hazards at Pensacola Beach, Florida. In: Leatherman SP, Fletemeyer J (eds) Rip currents: beach safety, physical oceanography and wave modeling. CRC Press, New York, pp 175–197

Howland J, Hingson R (1988) Alcohol as a risk factor for drowning: a review of the literature (1950–1985). Accid Anal Prev 20:19–25

Klein AHF, Santana GG, Diehl FL et al (2003) Analysis of hazards associated with sea bathing: results of five years' work on oceanic beaches of Santa Catarina state, southern Brazil. J Coast Res 35:107–116

Lascody RL (1998) East center Florida rip current program. Natl Weather Dig 22:25–30

Leatherman SP (2003) Dr. Beach's survival guide: what you need to know about sharks, rip currents and more before going into the water. Yale University Press, New Haven, 106p

Leatherman SP (2011) Rip currents: terminology and pro-active beach safety. In: Leatherman SP, Fletemeyer J (eds) Rip currents: beach safety, physical oceanography and wave modeling. CRC Press, New York, pp 259–271

Leatherman SP (2012a) Undertow, rip current and riptide. J Coast Res 28(4):3–5

Leatherman SP (2012b) Rip currents: types and identification. Shore Beach 80(3):5–10

Leatherman SP, Fletemeyer J (2011) Rip currents: beach safety, physical oceanography and wave modeling. CRC Press, New York, 277p
Lushine JB (1991) A study of rip current drowning and related weather factors. Natl Weather Dig 16:13–19
MacMahan J, Brown J, Thornton E et al (2010) Mean Lagrangian flow behavior on an open coast rip-channeled beach: a new perspective. Mar Geol 268:1–15
Reniers A, MacMahan J, Thornton EG et al (2009) Surf zone retention on a rip channeled beach. J Geophys Res 114:C10010. doi:10.1029/2008JC005153
Scott TM, Russell PE, Masselink G et al (2009) Rip current variability and hazard along a macrotidal coast. J Coast Res 56:895–899
Short AD (2007) Australia rip systems: friend or foe? J Coast Res 50:7–11
Short AD, Hogan CL (1994) Rip currents and beach hazards: their impact on public safety and implications for coastal management. J Coast Res SI12:197–209
Slattery MP, Bokuniewicz H, Gayes P (2011) Flash rip currents on ocean shoreline of Long Island, New York. In: Leatherman SP, Fletemeyer J (eds) Rip currents: beach safety, physical oceanography and wave modeling. CRC Press, New York, pp 31–43
Sonu CJ (1972) Field observations of a nearshore circulation and meandering currents. J Geophys Res 77:3232–3247
Voulgaris G, Kumar N, Warner JC (2011) Methodology for prediction of rip currents using a three-dimensional numerical, coupled, wave current model. In: Leatherman SP, Fletemeyer J (eds) Rip currents: beach safety, physical oceanography and wave modeling. CRC Press, New York, pp 87–105
Wright LD, Short AD (1984) Morphodynamic variability of surf zone and beaches. Mar Geol 56:93–118

ERRATUM TO

Chapter 20
Coastal Hazards from Tropical Cyclones and Extratropical Winter Storms Based on Holocene Storm Chronologies

S.M. May, M. Engel, D. Brill, P. Squire, A. Scheffers, and D. Kelletat

DOI 10.1007/978-94-007-5234-4_27

On page 565 Table 20.2 was misprinted. The correct Table should read as follows:

	Air pressure	Wind speed	Duration	Forecast	Storm surge	Inundation	Rain risk	Frequency
Tropical cyclones	<900 hpa	>250 km/h	Several days	Reliable	>7 m	Potentially wide	High	0–12/year
Extratropical winter storms	>950 hpa	150 km/h	Several days	Reliable	3–4 m	Wide (without dikes)	Small	2–6/year

The publisher apologizes for the inconvenience caused.

C.W. Finkl (ed.), *Coastal Hazards*, Coastal Research Library 6,
DOI 10.1007/978-94-007-5234-4_20,

Index

C.W. Finkl (ed.), *Coastal Hazards*, Coastal Research Library 6,
DOI 10.1007/978-94-007-5234-4,